

EFFECT OF CONVERTING NATURAL FORESTS TO PLANTATIONS ON THE SOIL BACTERIAL DIVERSITY IN A SUBTROPICAL MOUNTAINOUS AREA: CASE STUDY IN SOUTHERN CHINA

LU, Q.¹ – FENG, Y. Z.² – LIU, N. Q.¹ – SONG, W.¹ – HUANG, Y.¹ – ZHANG, K.¹ – YU, Y. J.^{2,3*}

¹*Jiangsu Vocational College of Agriculture and Forestry, Jurong 212400, China
(e-mail: luqian@jsafc.edu.cn (Lu, Q.); liunanqing@jsafc.edu.cn (Liu, N. Q.);
songwei@jsafc.edu.cn (Song, W.); huangye010116@163.com (Huang, Y.);
zk781022511@163.com (Zhang, K.))*

²*State Key Laboratory of Soil and Sustainable Agriculture, Institute of Soil Science, Chinese Academy of Sciences, Nanjing 210008, China
(e-mail: yzfeng@issas.ac.cn (Feng, Y. Z.); yjyu@nuist.edu.cn (Yu, Y. J.))*

³*College of Applied Meteorology, Nanjing University of Information Science and Technology, Nanjing 210044, China
(e-mail: yjyu@nuist.edu.cn)*

**Corresponding author
e-mail: yjyu@nuist.edu.cn*

(Received 11th Jan 2022; accepted 2nd May 2022)

Abstract. Although soil bacteria regulate biogeochemical processes, little is known about the response of their distribution and abundance to land-use changes in the subtropical region. In the present study, soil samples from four natural forests and two agricultural plantations were collected from a subtropical mountainous area of southern China. A high-throughput sequencing approach was applied to explore the soil bacterial community composition and diversity. The results showed that dominant bacterial taxa (such as *Acidobacteria*, *α -proteobacteria*, *γ -proteobacteria*, and *Planctomycea*), which accounted for >41% of the bacterial sequences, decreased with the conversion of natural forests to plantations. Structural equation modeling and canonical correspondence analysis indicated that the bacterial community and diversity responded to the decrease in soil carbon and nitrogen contents and the increase in available soil phosphorus content. Multiple statistical analyses, including hierarchical cluster, response ratio, and least discriminate analysis effect size, revealed that the community-level patterns were caused by the responses of a few taxa, particularly *Rhizobiales*, *Bacilli*, *Burkholderiales*, and *Nitrospiraceae*, which are the bacterial indicators of soil nutrient status. Our findings will help better understand the response of soil bacterial communities to reforestation and agricultural management during land-use changes in the subtropical region.

Keywords: *land-use change, soil bacterial community, subtropical acidic soil, high-throughput sequencing, reforestation, soil nutrition*

Introduction

Land-use changes impact carbon balance, nutrient cycling, and global climate change (Cordier et al., 2021; Jovani-Sancho et al., 2021). The conversion of natural forest to agricultural systems, which is the dominant type of land-use change, has been progressing continuously with high rates of 13 million ha per year (Makwinja et al., 2021). The destruction of natural forests causes rapid biomass carbon (C) loss from soil and is a major source of human-induced greenhouse gas emissions (Han and Zhu, 2020; Kim et al., 2021). Soil bacterial communities play a vital role in regulating the cycling, release, and retention of soil C and nitrogen (N) in natural forests and agricultural systems (Burkins

et al., 2001; Liu et al., 2020). However, little is known regarding the response of the taxonomic composition of soil bacteria during land-use changes in subtropical areas despite the fact that the conversion of natural soils to cultivated soils has been expected to progress rapidly in the past and it is still expected to progress in the future in subtropical developing countries, particularly in Asia (Foley et al., 2005; Sheng et al., 2010).

Review of literature

Soil bacterial communities in different land-use patterns have been globally studied via phospholipid fatty acid profiles (Srivastava and Mishra, 2021; Tosi et al., 2021), DNA fingerprinting (Chave et al., 2010; Jangid et al., 2011), or culture-based methods (Ayob and Kusai, 2021), which neither identify bacterial taxonomic groups nor adequately represent the vast diversity of uncultured soil bacteria (Shen et al., 2013). Moreover, environmental and anthropogenic factors associated with the distribution and abundance of soil bacterial groups during land-use changes have been inadequately studied in the subtropical region.

Humid subtropical soils in China cover approximately 0.45 million km², which accounts for approximately 4% of the world's subtropical arable land surface and 37% of China's arable area (Qin et al., 2011). To support the increasing population, many natural forests have been converted to agricultural land (Kan et al., 2021). The soil in these regions is heavily weathered, acidic, and deficient in available nutrients, particularly phosphorus (P) (Han et al., 2022). These characteristics significantly influence certain soil microbial functions, including soil respiration (Sheng et al., 2010) and denitrification (Sünnemann et al., 2021). To predict the comprehensive effects of land-use change on soil microbial functions, an improved understanding of the responses of bacterial communities to land-use changes is required to complement existing knowledge about the bacterial functional groups that control biogeochemical processes. In the present study, the structure and composition of soil bacterial communities in different land-use patterns with long and clear land-use history in southeast China were identified. The studied land-use types contained four natural forests, including *Altingia gracilipes* Hemsl. (ALG), *Cinnamomum chekiangensis* Nakai (CIC), *Castanopsis fargesii* Franch. (CAF), *Tsoongiodendron odorum* Chun (TSO), and two plantations - an adjacent plantation of *Cunninghamia lanceolata* Hook. (Chinese fir) (CUL) and an economic plantation of *Citrus reticulata* (citrus orchard) (ORG). We reported previously that the conversion of natural forests to plantations negatively affects soil microbial community and diversity via phospholipid fatty acid profile, real-time quantitative polymerase chain reaction, and denaturant gradient gel electrophoresis approaches (Yu et al., 2012). Although these methods are indispensable for microbial community studies, they are insufficient for elucidating the diversity. High-throughput sequencing is a revolutionary microbial ecology tool that offers sufficient sequencing depth (Lin et al., 2012). In the present study, we applied high-throughput sequencing to investigate the response of bacterial communities to land-use changes in subtropical soil. We also explored the relationship between soil environmental factors and bacterial communities and diversities, both of which would lead to a better understanding of the ecological effects of land-use changes in subtropical China.

Materials and Methods

Site description and soil sampling

The study area was Wanmulin Nature Reserve in Jian'ou City, Fujian Province, China (118°08'22"–118°09'23"E, 27°02'28"–27°03'32"N) (Fig. 1). This nature reserve was relatively free from human disturbance for approximately 600 years. The soil is classified as red soil in Chinese soil classification (State Soil Survey Service of China, 1998), equivalent to hapludult in USDA Soil Taxonomy (Soil Survey Staff of USDA, 1999). A series of typical land-use types were selected, including ALG, CIC, CAF, TSO, CUL plantation, and ORG plantation. ALG, CIC, CAF, and TSO belong to a natural forest, which was defined as climax vegetation in mid-subtropical China. The CUL plantation developed from a partially abandoned land after the slash-and-burn of the natural forest and regenerated naturally for >20 years in the late 1980s/early 1990s. Moreover, the ORG plantation was converted from the natural forest by reforestation and terraced during the establishment of citrus trees for >15 years. Only the ORG plantation was regularly managed and fertilized primarily with chemical fertilizers. The amounts of N, P, and potassium fertilizers used per year were 310, 115, and 260 kg ha⁻¹, respectively. The soil chemical properties are shown in *Table A1*.

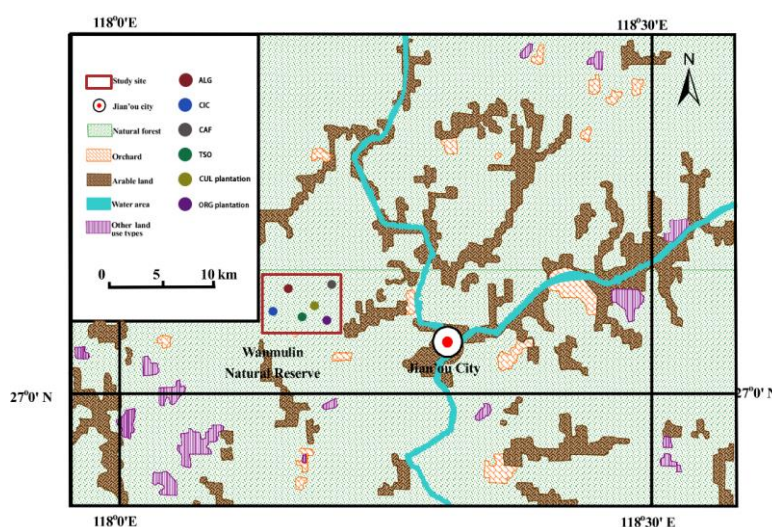


Figure 1. Geographic location and land-use situation of the study area and sampling sites

In September 2018, soil samples were collected from the above six land-use types. Three 45 m × 45 m plots were randomly selected from each type, and each plot had a similar slope with a minimum distance of 100 m. Five subsamples were randomly collected from the 0–20 cm soil layer of each plot, and the minimum distance between the collection points of the subsamples was 15 m. After removing the O layer of each subsample, these subsamples were then mixed into one composite sample. Finally, three discrete soil samples were formed for each land-use type. All the samples were taken to the laboratory immediately. A small portion of each soil sample was stored in a -80 °C freezer for molecular analysis. The remaining fresh soil samples were sieved (<2 mm), and stones and root residues were removed with tweezers. Fresh soils were stored at 4 °C for no more than two weeks before soil microbiological analysis. Afterward, air-dried and sieved soils were used for chemical analyses.

DNA sequencing as well as bacterial composition and diversity analyses

Total DNA was extracted from 0.5 g fresh soil using FastDNA® SPIN Kit for soil (MP Biomedicals, CA, USA) as per the manufacturer's instructions. An aliquot of soil DNA extract (2 µL) was used to partially amplify the bacterial 16S rRNA gene using the barcoded primers 519F and 907R as per the protocol from (Shen et al., 2013). Triplicate reaction mixtures per sample were pooled, purified using QIAquick PCR Purification kit (QIAGEN, Hilden, Germany), and quantified using Agilent 2100 Bioanalyzer (Agilent Technologies, CA, USA) and Qubit 2.0 Fluorometer (Invitrogen, CA, USA). MiSeq (Illumina, CA, USA) coupled with paired-end 250-bp kits were used to generate the sequencing data. Prior to analyses, primer sequences were removed, which resulted in the average sequencing reads of 251 bp. The sequences were processed and analyzed using the Quantitative Insights into Microbial Ecology (QIIME) 1.9.1-dev pipeline with default parameters, unless otherwise noted. In brief, sequences were quality-trimmed (>25 quality score and 200 bp in length) and assigned to soil samples based on unique 5-bp barcodes. Sequences were denoised (Reeder and Knight, 2010) and then binned into operational taxonomic units (OTUs) using *de novo* UCLUST (Edgar, 2010) with a 97% identity threshold. The most abundant sequence from each OTU was selected as the representative sequence for that OTU. Taxonomy was assigned to bacterial OTUs against a subset of the Silva database. OTU representative sequences were aligned using PyNAST via QIIME, and a phylogenetic tree was subsequently constructed using FastTree2 (Price et al., 2009) to support phylogenetic diversity calculations.

The richness of phylotypes was calculated to compare community-level bacterial diversity at a single level of taxonomic resolution. We estimated phylogenetic diversity using Faith's index (Faith, 1992). In this diversity analysis, 1,119,018 bacterial sequences that passed QIIME's quality filtering were included. In total, 9,200–34,353 sequences per sample were obtained (mean = 12,612; median = 12,984). Because an even sampling depth is required for beta diversity calculations, we reduced the datasets to the lowest number available to adjust for differences in survey effort among samples. We calculated both diversity metrics using a randomly selected subset of 9,200 sequences per soil sample. This approach allowed us to compare general diversity patterns among sites, even though it is unlikely that we surveyed the complete diversity in each community (Shaw et al., 2008). Weighted pairwise UniFrac distances (Ramírez et al., 2020) were calculated for community comparisons via QIIME and visualized using nonmetric multidimensional scaling plots as implemented in PRIMER v6.

Statistical analyses

Significant differences in each variable were determined using Tukey's honestly significant difference test at 95% confidence level in SPSS 16.0 (SPSS Inc., IL, USA). Based on the subset of 1,200 16S rRNA gene sequences per soil sample, clustering analysis heatmaps were created in Cluster 3.0 and generated in Java TreeView 1.1. The response ratios of bacterial classes under different land-use soils were analyzed as per the statistical method applied in the literature (Luo et al., 2006). Significant taxonomic differences at the family level were also tested using the least discriminate analysis (LDA) effect size (Segata et al., 2011). This method employs the factorial Kruskal–Wallis sum-rank test ($\alpha = 0.05$) to identify taxa with significant differential abundances among categories (using one-against-all comparisons); this was followed by LDA to estimate the effect size of each differentially abundant feature. Significant taxa were then used to

generate taxonomic cladograms, which illustrated differences among different land-use soils. Canonical correspondence analysis was performed in Canoco 4.5 for Windows. To identify the various species of each bacterial phylum and their discriminating characteristics, similarity percentage (SIMPER) analysis (Clarke, 1993) was performed using the “simper” function of the “vegan” library in R 3.0 software (Dixon, 2003). Structural equation modeling (SEM) was performed in Amos 18.0 (SPSS Inc., IL, USA). The land-use patterns were fit as 1 or 2 to represent natural forests and plantations. Fertilization was fit as 0 or 1 to represent whether fertilization was present in different land-use soils. We tested how effectively the models fit our data using the maximum likelihood chi-square goodness-of-fit test.

Results

The taxonomic distribution of soil bacteria differed among the land-use types (Fig. 2). The dominant phyla across all soil samples included *Acidobacteria*, *Actinobacteria*, and *Proteobacteria*, which accounted for >61% of the bacterial sequences from each of the soils. *Bacteroidetes*, *Chloroflexi*, *Cyanobacteria*, *Firmicutes*, *Gemmatimonadetes*, *Nitrospirae*, and *Planctomycetes* were present in most soils but at relatively low abundances, and some rare bacteria were also identified. The conversion of natural forests to plantations changed the relative abundance of some bacteria; for example, the *Acidobacteria* phylum decreased by ~3.1%, α -*proteobacteria* decreased by ~3.4%, and β - and δ -*proteobacteria* increased by >1.1%.

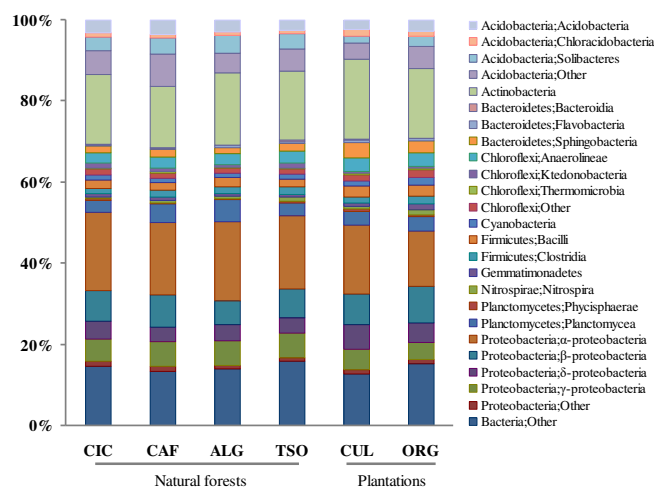


Figure 2. Taxonomic distribution of bacterial communities derived from 16S rRNA genes across different land-use soils. CIC, CAF, ALG, and TSO were four natural forests that represent *Cinnamomum chekiangensis*, *Castanopsis fargesii*, *Altingia gracilipes*, and *Tsoongiodendron odorum*, respectively. CUL and ORG represent the *Cunninghamia lanceolata* and *Citrus reticulata* plantations, respectively

Based on the OTU table at the phylum level, a hierarchical cluster analysis heatmap was created to monitor the responses of bacterial phyla to land-use patterns (Fig. 3). In this figure, color keys represent the deviation from the mean of each OTU number. Less abundant bacterial phyla in different land-use soils are displayed in green, whereas predominant bacterial phyla are shown in red. The six different land-use types were

classified into two major linkage clusters. One cluster comprised CAF, CIC, TSO, and ALG, which were natural forests. The other cluster comprised CUL and ORG, which were plantations. By contrast, bacterial communities were classified into two major clusters. One consisted of *Bacteroidetes*, *Cyanobacteria*, and *Gemmatimonadetes*, which were less dominant in natural forests than in plantations. Other bacterial phyla, including *Chloroflexi*, *Proteobacteria*, *Acidobacteria*, *Planctomycetes*, and other rare bacteria, were clustered together and were more dominant in natural forests than in plantations.

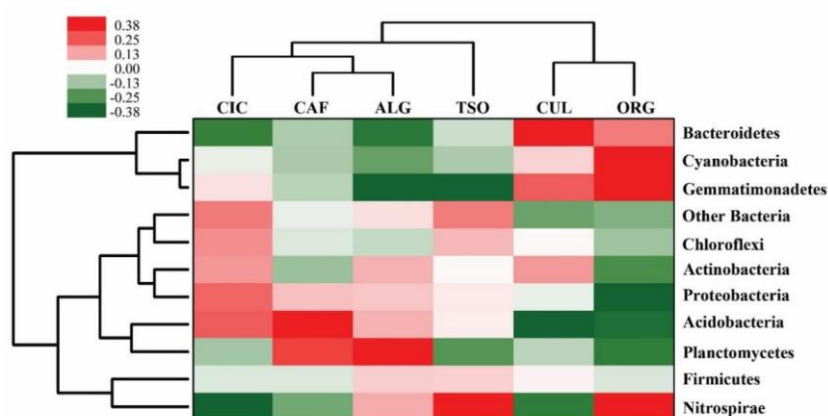


Figure 3. Hierarchical clustering and heatmap display of the relative abundance of the bacteria based on 16S rRNA gene amplicon sequencing in different land-use soils. Color intensity increases with relative abundance. CIC, CAF, ALG, and TSO were four natural forests that represent *Cinnamomum chekiangensis*, *Castanopsis fargesii*, *Altingia gracilipes*, and *Tsoongiodendron odorum*, respectively. CUL and ORG represent the *Cunninghamia lanceolata* and *Citrus reticulata* plantations, respectively

According to the sequence size of each bacterial class, response ratios were calculated to statistically resolve the changed bacterial constituents in response to the conversion of natural forests to CUL and ORG plantations (Fig. 4). The 95% confidence interval (CI) between natural forests and the CUL plantation ranged from 0.07 to -0.01, which overlapped with 0. This suggested that the conversion of natural forests to the CUL plantation did not induce a significant change in the bacterial community composition. While the 95% CI between the natural forests and ORG did not overlap with 0, it indicated that the conversion of natural forests to an ORG plantation significantly influenced the composition of the soil bacterial community. By contrast, most of the dominant bacterial classes, including α -proteobacteria, γ -proteobacteria, *Ktedonobacteria*, *Solibacteria*, *Acidobacteria*, and *Planctomycea*, decreased with the conversion of natural forests to plantations. These decreased bacterial classes accounted for >41% of bacterial sequences across all soil samples. Other bacterial classes, including β -proteobacteria, δ -proteobacteria, *Nitrospira*, *Cyanobacteria*, and *Actinobacteria*, were lower in natural forests than in plantations.

The LDA effect size was performed on the basis of the sequence size at the family level in natural forests and plantations (Fig. 5). This analysis confirmed the observation that the conversion of natural forests to plantations significantly influenced the composition of the bacterial community at the phylum and class levels. Furthermore, the LDA effect size analysis illustrated changes in the bacterial composition at the family level. For example, *Acidobacteriaceae*, *Solibacteraceae*, *Acidimicrobiales*,

Bradyrhizobiaceae, *Rhizobiales*, *Rhodospirillales*, and *Burkholderiales* were more dominant in natural forests than in plantations, whereas *Nocardioidaceae*, *Sphingobacteriales*, *Bacilli*, and *Nitrospiraceae* were less dominant in natural forests.

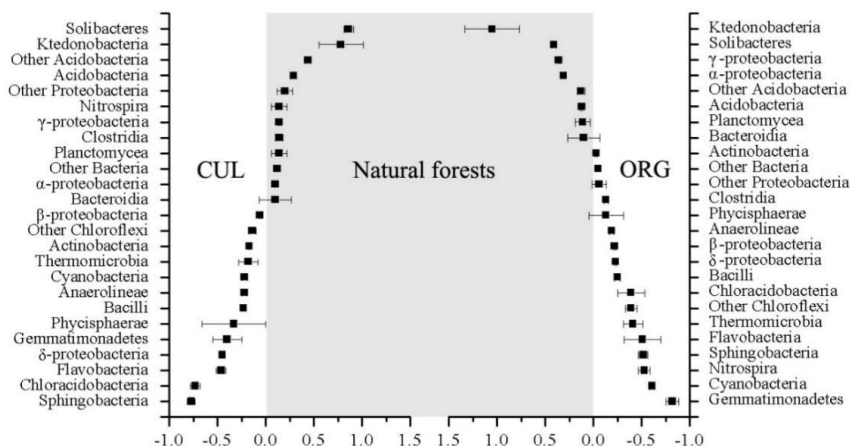


Figure 4. Significant changes in bacterial classes between natural forests and plantations according to the response ratio method at a 95% confidence interval. CIC, CAF, ALG, and TSO were four natural forests that represent *Cinnamomum chekiangensis*, *Castanopsis fargesii*, *Altingia gracilipes*, and *Tsoongiodendron odorum*. CUL and ORG represent the *Cunninghamia lanceolata* and *Citrus reticulata* plantations, respectively

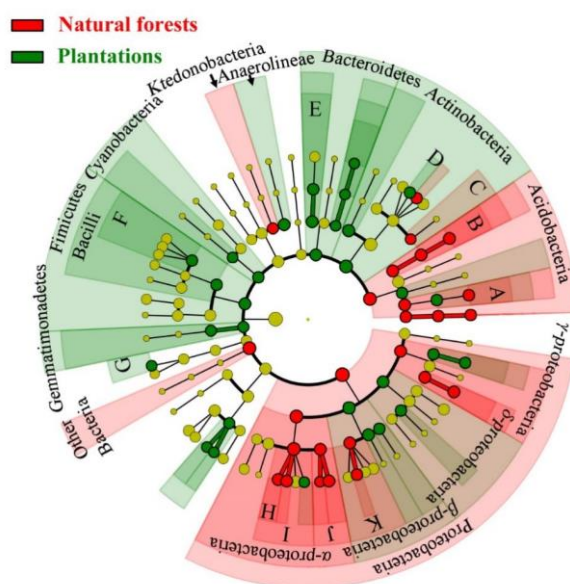


Figure 5. LDA effect size taxonomic cladogram comparing soil bacterial communities between natural forests and plantations. Significantly discriminant taxon nodes are colored, and branch areas are shaded as per the highest-ranked variety of that taxon. For each detected taxon, the corresponding node in the taxonomic cladogram is colored as per the highest-ranked group for that taxon. If the taxon is not significantly differentially represented among sample groups, the corresponding node is colored yellow. Highly abundant and select taxa are indicated as A, *Acidobacteriaceae*; B, *Solibacteraceae*; C, *Acidimicrobiales*; D, *Nocardioidaceae*; E, *Sphingobacteriales*; F, *Bacilli*; G, *Nitrospiraceae*; H, *Bradyrhizobiaceae*; I, *Rhizobiales*; J, *Rhodospirillales*; and K, *Burkholderiales*

Discussion

The conversion of natural forest to agricultural systems is closely associated with the sustainable use of soil resources (Hasan et al., 2020; Kan et al., 2021), and the soil microbial community is well established as the key biological indicator for assessing soil health. Thus, using the high-throughput sequencing method in a subtropical mountainous area of southern China, we investigated how soil bacterial communities are affected by land-use changes. The results showed that the composition and diversity of the bacterial community are significantly negatively influenced by the conversion of natural forests to agricultural plantations.

Soil microbial communities are strongly distributed as per soil chemical properties under different land-use patterns (Srivastava and Mishra, 2021; Tosi et al., 2021). To demonstrate the effects of land-use, fertilization, soil pH, and nutrient concentrations on the diversity of bacterial taxonomic groups, SEM was constructed on the basis of bacterial diversity (*Table A2*) and soil chemical variables (*Table A1*; chi-square = 315, $P < 0.001$) (*Fig. 6*). Bacterial diversity was highly correlated with soil organic C, which accounted for the effects of soil pH, land use, and other chemical variables ($\lambda = 0.981$). The total N, available P, and the C/N ratio had significant effects on the bacterial diversity across different land-use soils. According to canonical correspondence analysis, the soil C and N contents were key factors for classifying natural forests (CIC, CAF, ALG, and TSO) and the CUL and ORG plantations into three main areas (*Fig. 7*). The available P also played an important role in distinguishing between the soil bacterial communities of ORG and other land-use patterns. These results are consistent with those of our previous study (Yu et al., 2012). These differentiations among the soil C, N, and available P between natural forests and the ORG plantation primarily resulted from differences in the nutrient supply. Unlike chemical fertilization in the ORG plantation, the dominant pathway for nutrient return to soil in natural ecosystems is from leaf litterfall, which contains high C and N contents (Price et al., 2009). The CUL plantation, which is a type of coniferous forest, has significantly lower annual litterfall than the natural broad-leaved forests (Yang et al., 2009; Yu et al., 2012). When the soil C and N content decreased as a result of the conversion of natural forests to plantations, the readily decomposable organic C and N were lost preferentially (Qin et al., 2011). These fractions support a majority of the heterotrophic microbial biomasses that have been reported in soils (Degens et al., 2000), and their loss could decrease soil microbial richness and diversity via disproportionate declines in catabolic functions. However, as P is absent in subtropical acidic soil (He et al., 2008), it is reasonable to say that available P plays an important role in separating ORG from other land-use soils.

Multiple statistical analyses, i.e., hierarchical cluster analysis heatmap, response ratio, and LDA effect size, showed that the distribution of the soil bacterial community significantly differed between natural forests and plantations. However, the differences among natural forests, CUL plantation, and ORG plantation were inconsistent. For example, according to the 95% CI, the differences in bacterial communities between natural forests and the ORG plantation were significant, but the difference in bacterial communities between natural forests and the CUL plantation were insignificant (*Fig. 4*). Moreover, the ratio of *Proteobacteria* and *Acidobacteria*, which is a broad indicator of nutrient status (Smit et al., 2001), in the ORG plantation (2.76 ± 0.18) was significantly lower than that in the CUL plantation (3.80 ± 0.27 ; $P < 0.05$). These inconsistent results suggest that certain agricultural practices, such as fertilization, herbicide, and irrigation, in the ORG plantation have a greater effect on the soil bacterial community composition

than on naturally regenerated plantations in the subtropical region (Chave et al., 2010; Sheng et al., 2010). By contrast, the *Proteobacteria* phylum, which was the dominant bacteria in soil ecosystems (Smit et al., 2001; Sheng et al., 2010), made a primary contribution that differentiates the bacterial community of natural forests from that of plantations at the phylum level according to SIMPER analysis (Table A3). A previous study showed that the *Proteobacteria* phylum was associated with C and N cycling in soil ecosystems (Smit et al., 2001). Thus, when the concentration of *Proteobacteria* decreased with the conversion of natural forests to plantations, soil C and N cycling weakened concomitantly. At the class level, *β -proteobacteria* appeared to be less abundant in natural forests than in plantations and were capable of ammonium oxidation, denitrification, and polyphosphate accumulation (Naeem and Wright, 2003), which indicated the important role of this group in soil nutrient cycling in land-use changes. At the family level, the conversion of natural forests to plantations decreased the concentrations of *Acidobacteriaceae*, *Solibacteraceae*, *Acidimicrobiales*, *Bradyrhizobiaceae*, *Rhizobiales*, *Rhodospirillales*, *Burkholderiales*, and others and increased those of *Nocardioidaceae*, *Sphingobacteriales*, *Bacilli*, *Nitrospiraceae*, and others according to LDA effect size (Fig. 5). These bacterial taxa were closely associated with the accumulation and decomposition of soil organic matter, mineralization, and transformation of N and P and other nutrient utilization (Uroz et al., 2010; Knelman et al., 2012; Huang et al., 2013). Therefore, the responses of the soil microbial community to the conversion of natural forests to plantations can influence nutrient cycling and sustainable soil use (Ramírez et al., 2020; Xiao et al., 2021).

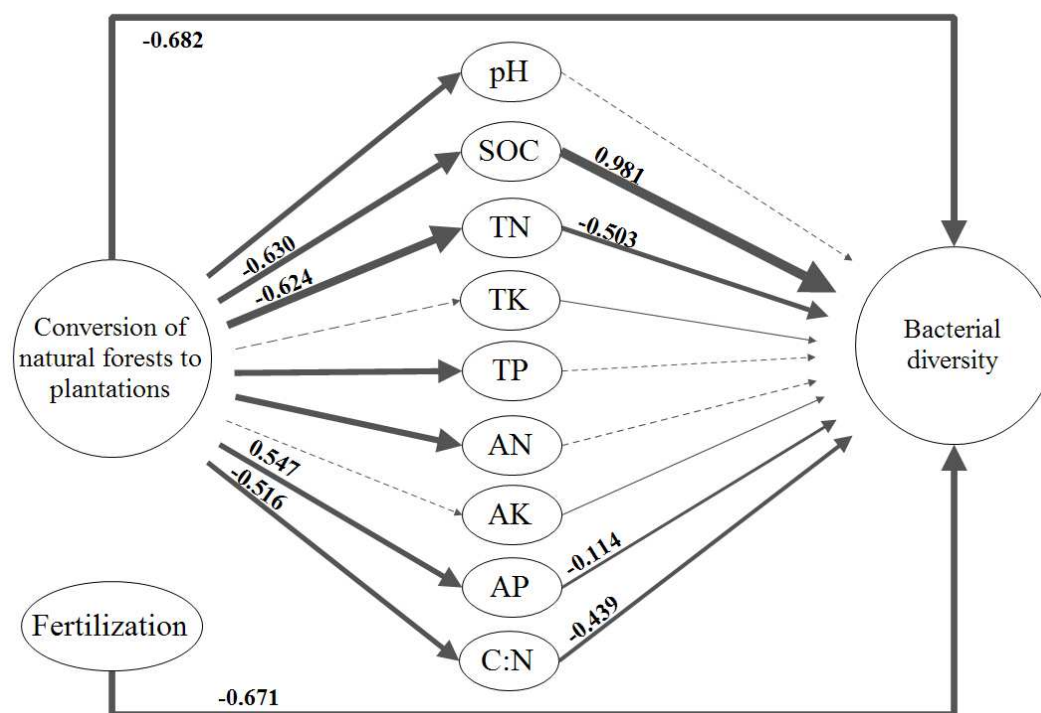


Figure 6. Structural equation model showing the causal influences of natural forests to plantations conversion and soil chemical variables on soil bacterial diversity. The width of arrows indicates the strength of the causal effect. The numbers above the arrows indicate path coefficients (λ), and insignificant pathways are represented by dashed lines ($\lambda \leq 0.05$)

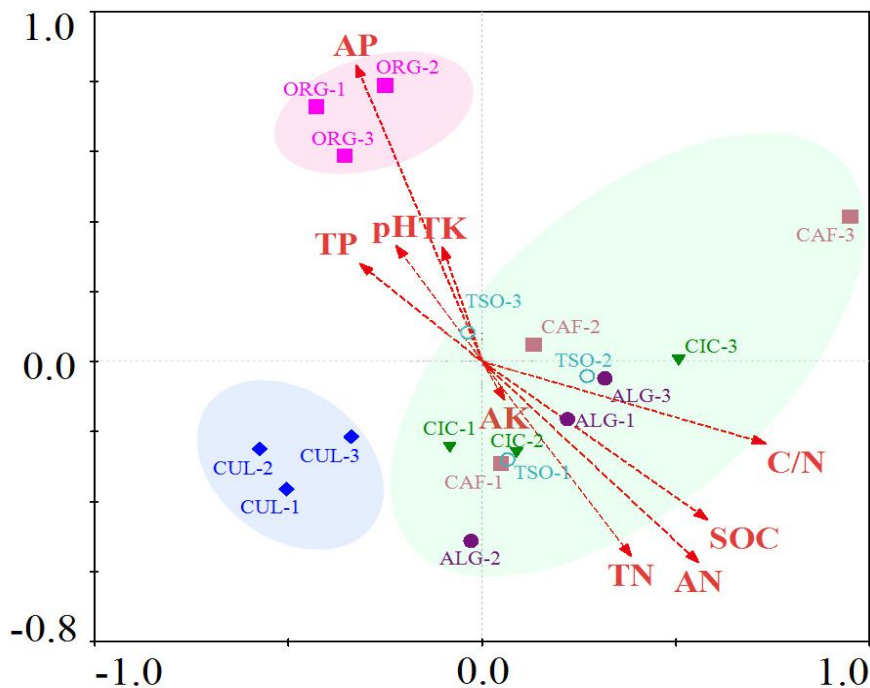


Figure 7. Canonical correspondence analysis relating bacterial sequence patterns and land-use patterns with soil properties such as soil organic C (SOC); total N (TN), P (TP), and K (TK) contents; available N (AN), K (AK), and P (AP) contents; and the C/N ratio. CIC, CAF, ALG, TSO, CUL, and ORG represent *Cinnamomum chekiangensis*, *Castanopsis fargesii*, *Altingia gracilipes*, *Tsoongiodendron odorum*, *Cunninghamia lanceolata*, and *Citrus reticulata* plantation, respectively

Conclusion

In summary, our findings address the lack of knowledge regarding the composition and control over bacterial communities in subtropical China as well as the impact of land-use changes on the bacterial community and diversity. As a result of changes in soil C, N, and available P contents, the conversion of natural forests to plantations alters bacterial community composition and significantly decreases bacterial diversity. The negative responses of soil bacterial communities and the conversion of natural forests to agricultural plantations are not conducive to the conservation of soil nutrition and sustainable use of soil.

In the following research, we will further reveal the driving factors of the dynamic changes in the microbial community structure during this land-use transition, as well as the shift in the feedback patterns generated by the changing microbial communities and vegetation types.

Acknowledgements. This research was funded by the High-end Research Training Project for Professional Leaders of Teachers in colleges in Jiangsu Province, grant number 2020GRFX038, and the investigation was funded by the Youth Support Project in Jiangsu Vocational College of Agriculture and Forestry, grant number 2020kj004.

REFERENCES

- [1] Ayob, Z., Kusai, N. A. (2021): A comparative study of bacterial communities determined by culture-dependent and-independent approaches in oil palm planted on tropical peatland. – *Journal of Oil Palm Research* 33: 588-606.
- [2] Burkins, M. B., Virginia, R. A., Wall, D. H. (2001): Organic carbon cycling in Taylor Valley, Antarctica: quantifying soil reservoirs and soil respiration. – *Global Change Biology* 7: 113-125.
- [3] Chave, J., Navarrete, D., Almeida, S., Álvarez, E., Aragão, L. E., Bonal, D., Châtelet, P., Silva-Espejo, J., Goret, J.-Y., von Hildebrand, P. (2010): Regional and seasonal patterns of litterfall in tropical South America. – *Biogeosciences* 7: 43-55.
- [4] Clarke, K. R. (1993): Non-parametric multivariate analyses of changes in community structure. – *Australian Journal of Ecology* 18: 117-143.
- [5] Cordier, J. M., Aguilar, R., Lescano, J. N., Leynaud, G. C., Bonino, A., Miloch, D., Loyola, R., Nori, J. (2021): A global assessment of amphibian and reptile responses to land-use changes. – *Biological conservation* 253: 108863.
- [6] Degens, B. P., Schipper, L. A., Sparling, G. P., Vojvodic-Vukovic, M. (2000): Decreases in organic C reserves in soils can reduce the catabolic diversity of soil microbial communities. – *Soil Biology and Biochemistry* 32: 189-196.
- [7] Dixon, P. (2003): VEGAN, a package of R functions for community ecology. – *Journal of Vegetation Science* 14: 927-930.
- [8] Edgar, R. C. (2010): Search and clustering orders of magnitude faster than BLAST. – *Bioinformatics* 26: 2460-2461.
- [9] Faith, D. P. (1992): Conservation evaluation and phylogenetic diversity. – *Biological conservation* 61: 1-10.
- [10] Foley, J. A., DeFries, R., Asner, G. P., Barford, C., Bonan, G., Carpenter, S. R., Chapin, F. S., Coe, M. T., Daily, G. C., Gibbs, H. K. (2005): Global consequences of land use science 309: 570-574.
- [11] Han, M., Zhu, B. (2020): Changes in soil greenhouse gas fluxes by land use change from primary forest. – *Global Change Biology* 26: 2656-2667.
- [12] Han, Y., Yi, D., Ye, Y., Guo, X., Liu, S. (2022): Response of spatiotemporal variability in soil pH and associated influencing factors to land use change in a red soil hilly region in southern China. – *CATENA* 212: 106074.
- [13] Hasan, S. S., Zhen, L., Miah, M. G., Ahamed, T., Samie, A. (2020): Impact of land use change on ecosystem services: A review. – *Environmental Development* 34: 100527.
- [14] He, J.-Z., Zheng, Y., Chen, C.-R., He, Y.-Q., Zhang, L.-M. (2008): Microbial composition and diversity of an upland red soil under long-term fertilization treatments as revealed by culture-dependent and culture-independent approaches. – *Journal of Soils and Sediments* 8: 349-358.
- [15] Huang, J., Sheng, X., He, L., Huang, Z., Wang, Q., Zhang, Z. (2013): Characterization of depth-related changes in bacterial community compositions and functions of a paddy soil profile. – *FEMS microbiology letters* 347: 33-42.
- [16] Jangid, K., Williams, M. A., Franzluebbers, A. J., Schmidt, T. M., Coleman, D. C., Whitman, W. B. (2011): Land-use history has a stronger impact on soil microbial community composition than aboveground vegetation and soil properties. – *Soil Biology and Biochemistry* 43: 2184-2193.
- [17] Jovani-Sancho, A. J., Cummins, T., Byrne, K. A. (2021): Soil carbon balance of afforested peatlands in the maritime temperate climatic zone. – *Global Change Biology* 27: 3681-3698.
- [18] Kan, S., Chen, B., Han, M., Hayat, T., Alsulami, H., Chen, G. (2021): China's forest land use change in the globalized world economy: Foreign trade and unequal household consumption. – *Land Use Policy* 103: 105324.

- [19] Kim, H.-S., Noulèkoun, F., Noh, N.-J., Son, Y.-W. (2021): Impacts of the National Forest Rehabilitation Plan and Human-Induced Environmental Changes on the Carbon and Nitrogen Balances of the South Korean Forests. – *Forests* 12: 1150.
- [20] Knelman, J. E., Legg, T. M., O'Neill, S. P., Washenberger, C. L., González, A., Cleveland, C. C., Nemergut, D. R. (2012): Bacterial community structure and function change in association with colonizer plants during early primary succession in a glacier forefield. – *Soil Biology and Biochemistry* 46: 172-180.
- [21] Lin, X., Feng, Y., Zhang, H., Chen, R., Wang, J., Zhang, J., Chu, H. (2012): Long-term balanced fertilization decreases arbuscular mycorrhizal fungal diversity in an arable soil in North China revealed by 454 pyrosequencing. – *Environmental Science & Technology* 46: 5764-5771.
- [22] Liu, T., Wu, X., Li, H., Alharbi, H., Wang, J., Dang, P., Chen, X., Kuzyakov, Y., Yan, W. (2020): Soil organic matter, nitrogen and pH driven change in bacterial community following forest conversion. – *Forest Ecology and Management* 477: 118473.
- [23] Luo, Y., Hui, D., Zhang, D. (2006): Elevated CO₂ stimulates net accumulations of carbon and nitrogen in land ecosystems: A meta-analysis. – *Ecology* 87: 53-63.
- [24] Makwinja, R., Kaunda, E., Mengistou, S., Alamirew, T. (2021): Impact of land use/land cover dynamics on ecosystem service value: A case from Lake Malombe, Southern Malawi. – *Environmental Monitoring and Assessment* 193: 1-23.
- [25] Naeem, S., Wright, J. P. (2003): Disentangling biodiversity effects on ecosystem functioning: deriving solutions to a seemingly insurmountable problem. – *Ecology letters* 6: 567-579.
- [26] Price, M. N., Dehal, P. S., Arkin, A. P. (2009): FastTree: computing large minimum evolution trees with profiles instead of a distance matrix. – *Molecular biology and evolution* 26: 1641-1650.
- [27] Qin, Z., Zhuang, Q., Zhu, X., Cai, X., Zhang, X. (2011): Carbon consequences and agricultural implications of growing biofuel crops on marginal agricultural lands in China. – *Environmental Science & Technology* 45: 10765-10772.
- [28] Ramírez, P. B., Fuentes-Alburquenque, S., Díez, B., Vargas, I., Bonilla, C. A. (2020): Soil microbial community responses to labile organic carbon fractions in relation to soil type and land use along a climate gradient. – *Soil Biology and Biochemistry* 141: 107692.
- [29] Reeder, J., Knight, R. (2010): Rapidly denoising pyrosequencing amplicon reads by exploiting rank-abundance distributions. – *Nature methods* 7: 668-669.
- [30] Segata, N., Izard, J., Waldron, L., Gevers, D., Miropolsky, L., Garrett, W. S., Huttenhower, C. (2011): Metagenomic biomarker discovery and explanation. – *Genome biology* 12: 1-18.
- [31] Shaw, A. K., Halpern, A. L., Beeson, K., Tran, B., Venter, J. C., Martiny, J. B. (2008): It's all relative: ranking the diversity of aquatic bacterial communities. – *Environmental microbiology* 10: 2200-2210.
- [32] Shen, C., Xiong, J., Zhang, H., Feng, Y., Lin, X., Li, X., Liang, W., Chu, H. (2013): Soil pH drives the spatial distribution of bacterial communities along elevation on Changbai Mountain. – *Soil Biology and Biochemistry* 57: 204-211.
- [33] Sheng, H., Yang, Y., Yang, Z., Chen, G., Xie, J., Guo, J., Zou, S. (2010): The dynamic response of soil respiration to land-use changes in subtropical China. – *Global Change Biology* 16: 1107-1121.
- [34] Smit, E., Leeftang, P., Gommans, S., van den Broek, J., van Mil, S., Wernars, K. (2001): Diversity and seasonal fluctuations of the dominant members of the bacterial soil community in a wheat field as determined by cultivation and molecular methods. – *Applied and environmental microbiology* 67: 2284-2291.
- [35] Soil Survey Staff of USDA (1999): *Soil Taxonomy: A Basic System of Soil Classification for Making and Interpreting Soil Surveys*. – Agriculture Handbook No. 436. United States Department of Agriculture (USDA), Natural Resources Conservation Service, Washington, DC.

- [36] Srivastava, M., Mishra, A. K. (2021): Comparative Analysis of Paddy Soil Denitrifying Bacteria with Soil Phospholipid Fatty Acid Profile. – *Geomicrobiology Journal* 38: 404-414.
- [37] State Soil Survey Service of China (1998): *China Soil*. – China Agricultural Press, Beijing. (in Chinese).
- [38] Sünemann, M., Siebert, J., Reitz, T., Schädler, M., Yin, R., Eisenhauer, N. (2021): Combined effects of land-use type and climate change on soil microbial activity and invertebrate decomposer activity. – *Agriculture, Ecosystems & Environment* 318: 107490.
- [39] Tosi, M., Chludil, H. D., Correa, O. S., Vogrig, J. A., Montecchia, M. S. (2021): Long-term legacy of land-use change in soils from a subtropical rainforest: Relating microbiological and physicochemical parameters. – *European Journal of Soil Science* 72: 1054-1069.
- [40] Uroz, S., Buée, M., Murat, C., Frey-Klett, P., Martin, F. (2010): Pyrosequencing reveals a contrasted bacterial diversity between oak rhizosphere and surrounding soil. – *Environmental microbiology reports* 2: 281-288.
- [41] Xiao, E., Wang, Y., Xiao, T., Sun, W., Deng, J., Jiang, S., Fan, W., Tang, J., Ning, Z. (2021): Microbial community responses to land-use types and its ecological roles in mining area. – *Science of The Total Environment* 775: 145753.
- [42] Yang, Y., Xie, J., Sheng, H., Chen, G., Li, X., Yang, Z. (2009): The impact of land use/cover change on storage and quality of soil organic carbon in midsubtropical mountainous area of southern China. – *Journal of Geographical Sciences* 19: 49-57.
- [43] Yu, Y., Shen, W., Yin, Y., Zhang, J., Cai, Z., Zhong, W. (2012): Response of soil microbial diversity to land-use conversion of natural forests to plantations in a subtropical mountainous area of southern China. – *Soil science and plant nutrition* 58: 450-461.

APPENDIX

Table A1. Soil chemical properties under different land-use soils in subtropical China

	CIC	CAF	ALG	TSO	CUL	ORG
pH	4.08(0.19)a	4.65(0.40)b	4.12(0.08)a	4.00(0.42)a	4.60(0.17)b	4.67(0.05)b
Soil organic C (g/kg)	29.3(3.53)b	29.1(14.0)b	63.2(2.71)c	33.3(7.94)b	21.9(5.75)b,c	8.8(0.42)a
Total K (g/kg)	15.6(1.83)b	14.0(4.94)a,b	8.80(0.39)a	13.5(0.92)a,b	10.5(4.82)a,b	16.0(0.55)b
Total P (g/kg)	0.68(0.08)a	0.61(0.43)a	0.49(0.10)a	0.52(0.12)a	1.03(0.48)a	0.93(0.25)a
Total N (g/kg)	2.74(0.34)c	1.77(0.09)b,c	3.80(0.25d)	2.99(0.46)c	2.02(0.42)b	1.36(0.03)a
Available K (mg/kg)	107(23.2)a,b,c	131 (69.4)b,c	55.7(6.78)a,b	37.7(3.31)a	157(78.9)c	64.3(34.4)a,b
Available N (mg/kg)	232(14.1)b,c	209(70.4)b	292(9.6)c	255(28.8)b,c	209(47.7)b	124(7.51)a
Available P (mg/kg)	2.89(0.49)a,b	2.85(1.35)a,b	4.02(0.89)b	3.97(1.36)b	1.94(0.79)a	18.19(0.94)c

The numbers in brackets are standard deviations. Different letters in a line mean significant difference at 5% level. CIC, CAF, ALG, and TSO are four natural forests, representing *Cinnamomum chekiangensis*, *Castanopsis fargesii*, *Altingia gracilipes*, and *Tsoongiodendron odorum*, respectively. CUL and ORG represent *Cunninghamia lanceolata* plantation and *Citrus reticulata* plantation, respectively

Table A2. Bacterial diversity indices

	Average abundance		Average contribution	Ratio	Percent contribution
	Natural forests	Plantations			
<i>Proteobacteria</i>	437	392	1.88	2.54	23.0
<i>Actinobacteria</i>	236	205	1.30	1.44	15.8
<i>Acidobacteria</i>	115	143	1.14	2.15	14.0
<i>Bacteroidetes</i>	55	47	0.57	1.62	6.93
<i>Planctomycetes</i>	50	50	0.48	1.13	5.84
<i>Firmicutes</i>	49	54	0.39	1.40	4.83
<i>Chloroflexi</i>	68	71	0.39	1.46	4.76
<i>Cyanobacteria</i>	16	24	0.33	2.03	4.09
<i>Nitrospirae</i>	7	14	0.28	2.67	3.41
<i>Gemmatimonadetes</i>	12	19	0.26	1.07	3.23

Table A3. SIMPER analysis of dissimilarity

Soil samples		Phylogenetic diversity	Chao1	Shannon
Natural Forests	CIC	109(2.5)c	5904(295)b,c	9.41(0.04)b
	CAF	107(1.4)c	5700(169)b,c	9.43(0.02)b
	ALG	119(1.7)c	6222(569)c	9.54(0.09)b
	TSO	108(1.6)c	5738(109)b,c	9.45(0.03)b
Plantations	CUL	102(1.9)b	5283(140)a,b	9.11(0.06)a
	ORG	93.6(1.1)a	4747(189)a	9.06(0.07)a

All indices were calculated using the subset of 1,200 sequences per soil sample. The numbers in brackets are standard deviations. Different letters in a row mean significant difference at 5% level. CIC, CAF, ALG, and TSO are four natural forests, representing *Cinnamomum chekiangensis*, *Castanopsis fargesii*, *Altingia gracilipes*, and *Tsoongiodendron odorum*, respectively. CUL and ORG represent *Cunninghamia lanceolata* plantation and *Citrus reticulata* plantation, respectively

PREDICTING THE POTENTIAL SUITABLE HABITAT FOR *TAMARIX CHINENSIS* UNDER CLIMATE CHANGE BASED ON CMIP6 IN CHINA

WU, C. W.¹ – XU, X. X.^{1,2*} – ZHANG, G. J.^{1,2} – CHENG, B. B.^{1,2} – HAN, S.¹

¹College of Horticulture Science and Technology, Hebei Normal University of Science & Technology, Qinhuangdao 066600, PR China

²Hebei Key Laboratory of Horticultural Germplasm Excavation and Innovative Utilization, Qinhuangdao 066600, PR China

*Corresponding author
e-mail: xuxingxing0317@126.com

(Received 21st Jan 2022; accepted 2nd May 2022)

Abstract. *Tamarix chinensis* (Tamaricaceae), a halophytic plant, is native to China. *Tamarix chinensis* has shown significant advantages in improving soil desertification and enhancing soil quality in coastal saline lands and can be used for ornamental and medicinal purposes with high scientific, ecological and economic values. The scarcity of information about geographic distribution under global climate change makes it difficult to promote better cultivation of this shrub. For this study, we modeled the current and future suitable growth areas in 2050 and 2070 for *T. chinensis* by the Maxent model using the latest Coupled Model Comparison Program 6 (CMIP6) data set. The results revealed that annual mean temperature, precipitation of wettest quarter, annual mean UV-B and elevation were identified as the most important factors affecting *T. chinensis* distribution. The total suitable potential distribution areas for *T. chinensis* encompassed ca. 191.38×10^4 km², in which the highly suitable areas were mainly distributed in the middle and lower reaches of the Yellow River and the eastern coastal areas in China. Under the Shared Socioeconomic Pathway (SSP) 126 scenario, we predicted an expansion of the suitable habitat range in 2050 followed by a contraction in 2070; however, under the SSP585 scenario, the suitable habitat range of *T. chinensis* would decrease in 2050 and 2070. Overall, *T. chinensis* showed a shift trend in distribution to higher latitudes and elevations with global warming. This study could provide a theoretical guidance for formulating management plans for *T. chinensis* and saline soil rehabilitation in the future.

Keywords: halophyte, environmental factor, species distribution, habitat shift, SSPs

Introduction

Global climate change has already affected ecosystems and biological species (Kozak et al., 2008). According to the report of the Intergovernmental Panel on Climate Change (IPCC), the average global surface temperature has risen by 0.85°C during 1980–2012 (IPCC, 2013). Thus, global warming has become an indisputable fact. A continuous and more rapid warming trend has been simulated by multiple climate models, which predicted that the global surface temperature will increase by 1–6°C by the end of the 21st century, relative to pre-industrial temperature levels (Rogelj et al., 2012). A number of studies have shown that climate change has altered the current habitat suitability and spatial distribution patterns of many species, and even led to the migration and extinction of some organisms (Bertrand et al., 2011; Anderegg et al., 2015; Feng et al., 2021). Therefore, it is very important for predicting the potential distribution of species under global climate change. Understanding the spatial patterns

of species and their dependence on the climate factors is very useful for planning strategies to use resources sustainably in the future (Liu et al., 2018).

To better analyze the frequency and intensity of climate change, the sixth phase of the Coupled Model Comparison Program (CMIP6) has been formulated scientifically based on the scientific gaps learned from CMIP5 in 2021 (Bai et al., 2021). The current CMIP6 models differ from those of CMIP5 due to a new generation of climate models in which a new set of emission scenarios are driven by shared Socioeconomic Pathways (SSPs) for further analysis (Gidden et al., 2019; Liang et al., 2020). CMIP6 models are expected to be more reliable (Eyring et al., 2016; Zhang et al., 2021) because higher transient climate response and climate sensitivity compared to earlier models in CMIP5, with stronger warming in recent decades (Zelinka et al., 2020; Liang et al., 2020). In addition, CMIP6 showed higher accuracy statistics, particularly in annual and seasonal mean temperature and precipitation compared to CMIP5 (Bağçaci et al., 2021). It is of great benefit to researchers and decision makers to provide a guide for the distribution of plantations under the new emission scenarios in the future.

Species distribution models (SDMs) are used as effective tools in analyzing the impact of climate change on the potential distribution of species (Elith et al., 2006; Peterson, 2007). At present, the maximum entropy model (Maxent) has become one of the most frequently used niche models compared to other models, such as biological population growth model (CLIMEX), Domain and genetic algorithm for rule set production (GARP) (Zhang et al., 2018). It builds a prediction model based upon current species distribution records and environmental variables (Elith et al., 2011). Due to its small sample size and superior performance, the Maxent model has become an ideal prediction tool that can meet different research objectives (Phillips and Dudík, 2008; Pearson et al., 2011). For example, numerous studies based on Maxent modeling were conducted on endangered species conservation (Chen et al., 2020; Wei et al., 2020; Lu et al., 2021), invasive species control (Zhang et al., 2021) and planting suitability regionalization (Peng et al., 2019; Xu et al., 2020).

Climate change is considered one of the major contributing factors to soil salinization that leads to environmental degradation (Rogel et al., 2000). Approximately 6.5% of the world's total land area is affected by salinization until 2020 (Munns and Tester, 2008; Litalien and Zeeb, 2020). Soil salinity can strongly affect seed germination and plant growth and directly threat the function of many ecosystems (Santos et al., 2016). Halophytes could not only survive and reproduce in environments where the salt concentration is 200 mM NaCl or more (Flowers and Colmer, 2008) but survive under other harsh conditions, including drought, cold or flooding (Fan, 2020). Therefore, halophytes play an important role in ecological restoration of salt-affected land and minimizing soil degradation (Litalien and Zeeb, 2020).

Tamarix chinensis Lour., is one of the native halophytes usually distributed in China's warm-temperate zone. It is a perennial shrub or small tree with scalelike leaves and racemes of pink flowers (Figure 1a, 1b). In order to adapt to complex hypersaline environments, *T. chinensis* has evolved special salt-secreting structures - salt glands, *T. chinensis* can secrete excess salt out of its body via salt glands to avoid excessive salt absorption (Figure 1c) (Jiang et al., 2012). With properties of strong salt and drought resistance, *T. chinensis* plays a pivotal role in maintaining ecosystem stability in saline lands (Sun et al., 2020). Thus, it is of unique scientific research value and ecological significance. Additionally, *T. chinensis* has high ornamental value and can be used for landscaping applications. Currently, *T. chinensis* is undergoing population declination

and fragmentation due to climate change and human disturbance (Sun et al., 2020). Therefore, it acts as an ideal model species for studying the impact of climate change on species distribution. Predictions of potential distribution of species under global climate change play an instructional role for introduction and sustainable resource use (Peterson et al., 2011; Du et al., 2020). Therefore, *T. chinensis* as a representative species of strong salt and drought resistance plants, Research on *T. chinensis* is urgent and necessary. Predicting the potential distribution of *T. chinensis* under global climate change can provide an important reference for the future introduction and application of *T. chinensis*, maximising the ecological value of the species. However, to my knowledge, there is very limited studies using CMIP6 data set to predict the potential geographic distribution under future climate change scenarios.



Figure 1. Appearance. (a) racemes of pink flowers (b) scale-like leaves (c) Salt glands

In this study, Maxent modeling were used to predict distribution of *T. chinensis* in China based on an extensive collection of geo-referenced occurrence records of *T. chinensis* and associated environmental data for current and future climate scenarios using the current CMIP6 data. The aims of this research were to: (1) identify the main environmental variables affecting the potential distribution of *T. chinensis*; (2) to predict the potential distribution of *T. chinensis* in current and future (2050s and 2070s) climate conditions under the lowest and the highest limits of the Shared Socio-economic Pathways (SSP126 and SSP585); (3) to determine the habitat shift of the core distribution area of *T. chinensis* under 2050s and 2070s climate scenarios. The results will provide a reference for introducing and cultivating *T. chinensis* resources across China.

Material and methods

Species occurrence data for T. chinensis

In this paper, the native records were obtained from three resources: (1) field survey during 2018 in China, (2) the specimen libraries including the Global Biodiversity Information Facility (<https://www.gbif.org/>), the National Specimen Information

Infrastructure (<http://www.nsii.org.cn>) and the Chinese Virtual Herbarium (<http://www.cvh.ac.cn/>), (3) the reports in literatures (Zhang et al., 2019; Sun et al., 2020).

Environmental variables

Initially, 30 environmental variables were chosen to model the current species distribution (*Table S1*). These included 19 bioclimatic variables for the period from 1970 to 2000 obtained from the World Climate Database (WorldClim 2.1 released in January 2020, <http://www.worldclim.org/>) (Fick and Hijmans, 2017). In addition, topographical data were downloaded from the Geospatial Data Cloud (<http://www.gscloud.cn/>) to generate the elevation(Alt), slope (Slop) and aspect (Asp) data layers; soil data (T_OC, T_PH_H₂O, T_TEB and T_USDA_TEX_CLASS) were from the soil characteristics database (<http://globalchange.bnu.edu.cn/research/soil2>) (Shang et al., 2013) and Global ultraviolet-B radiation (UVB 1–4) were from the gIUV database (<http://www.ufz.de/gliv/>) (Beckmann et al., 2014). These environmental variables were extracted from the base map of China that was obtained from the National Fundamental Geographic Information System website (<http://nfgis.nsdi.gov.cn/>) by ArcGIS 10.5 at 2.5 minutes (approximately 5 km²) spatial resolution.

For future climate scenarios, we used BCC-CSM2-MR climate change modeling data (a middle resolution climate system model developed by Beijing) from the new CMIP6 database (Eyring et al., 2016; Jamal et al., 2020). The SSP126 and the SSP585 at 2.5 minutes spatial resolution were used for two future periods: 2041-2060 (2050) and 2061-2080 (2070) (<http://www.worldclim.org/>). The SSP126 represents the low-emission scenario measured by its radiative forcing pathway and predicted a warming inferior to 2°C by 2100. The SSP585 is a high-emission scenario that stabilized radiative forcing at 8.5 W/m² in 2100 (Riahi et al., 2017). The Eleven parameters (three topographical variables, four soil and four UV-B radiation parameters) remained unchanged to predict the influence of future climate changes on the distribution of *T. chinensis*.

To reduce multicollinearity of these variables and overfitting of the Maxent model (Graham, 2003), highly correlated environmental factors ($r \geq 0.80$ Pearson' correlation coefficients) were removed from the prediction models (*Table S2*). Finally, 14 environmental variables were selected by ArcGIS 10.5 (Eris, Redlands California, USA) for the Maxent model. These 14 variables included annual mean temperature (Bio1), temperature annual range (Bio7), precipitation of the driest month (Bio14), precipitation seasonality (Bio15) and precipitation of wettest quarter (Bio16), elevation (Alt), slope (Slop), aspect (Asp), topsoil organic carbon (T_OC), topsoil pH (T_PH_H₂O), topsoil TEB (T_TEB), topsoil USDA texture classification (T_USDA_TEX_CLASS), annual mean UV-B (UVB1) and UV-B seasonality (UVB2) (*Table 1*).

Maxent model processing

The current and future distribution of *T. chinensis* in China was analyzed using the maximum entropy modeling in Maxent v 3.4.1 (Phillips et al., 2020). We ran 20 replicates with randomly 25% of the location points used for model testing and determined logistic probabilities for the output. Other parameter settings were kept as default.

Table 1. The contribution proportions and permutation importance of the 14 environmental variables included in the Maxent models for *T. chinensis*

Code	Environmental variables	Contribution (%)	Permutation importance
Bio1	Annual mean temperature	39.0	42.7
Bio16	Precipitation of wettest quarter	18.8	19.3
UVB1	Annual mean UV-B	10.2	10.8
Alt	Elevation	7.5	15.8
UVB2	UV-B seasonality	7.3	1.2
T_PH_H2O	Topsoil pH (H2O)	5.8	0.3
Bio7	Temperature annual range (BIO5-BIO6)	5.2	1.6
Slop	Slope	2.4	2.1
Bio15	Precipitation seasonality (coefficient of variation)	1.9	1.3
Bio14	Precipitation of driest month	0.6	2.0
T_USDA	Topsoil USDA texture classification	0.5	1.5
Asp	Aspect	0.4	0.6
T_TEB	Topsoil TEB	0.3	0.7
T_OC	Topsoil organic carbon	0.1	0.1

To evaluate the model’s predictive performance, the area under receiver operating characteristic curve (AUC) values were examined. Generally, AUC values between 0.7 and 0.9 were considered to have a very good fit, and higher than 0.9 were considered as a perfectly fitted model (Wei et al., 2020; Xu et al., 2020). The Jackknife test was used to analyze the contribution rate and importance of these environmental variables. Moreover, the most important variables used in the model were analyzed in regard to their response curves.

Determining the environmentally suitable cultivation areas

For further analysis, the outputs of the Maxent models were transformed into raster format predicting the presence of *T. chinensis* (0–1 range) using ArcGIS 10.5. A presence–absence map was produced using the “Maximum training sensitivity plus specificity”. threshold which has been shown to produce highly accurate predictions (Peng et al., 2019; Xu et al., 2019). Finally, we divided the habitat suitability maps into four classes with the “Maximum training sensitivity plus specificity” value of 0.30: unsuitable habitat (0–0.30); poorly suitable habitat (0.30–0.50); moderately suitable habitat (0.50–0.70) and highly suitable habitat (0.70–1.0). For each model, we calculated the suitable habitat area by the proportion of the data set.

The core distributional shifts

The “QuickReclassify to Binary” in the SDMtoolbox v2.4 tool kit (Brown and Barbara, 2014) was used to convert the raster file into a binary file, and then we converted the binary file to the “. asc” file. The “Centroid Changes (Lines)” tool was used to calculate the displacement of the geometric center of current and future suitable areas. Finally, the overall change trend of the distribution area of *T. chinensis* were tracked.

Results

Model performance and major environmental variables

For the current distribution, the average omission rate is close to the predicted omission for the training presence records and the test records (*Figure S1*). In addition, the mean AUC value for the Maxent models was 0.857, it was higher than the AUC value of a random prediction (*Figure S2*). This indicated the model had good predictive accuracy and good performance for modelling the geographic distribution of *T. chinensis* in China.

The importance of the relative contributions of environmental variables to the Maxent model was evaluated using the jackknife test in *Figure 2*. Among the 14 variables, the most important factors affecting the habitat distribution of *T. chinensis* were annual mean temperature (Bio1, 39.0%), precipitation of wettest quarter (Bio16, 18.8%), annual mean UV-B (UVB1, 10.2%), elevation (Alt, 7.5%) and UV-B seasonality (UVB2, 7.3%). The cumulative contributions of these five parameters reached values as high as 82.8% (*Table 1*).

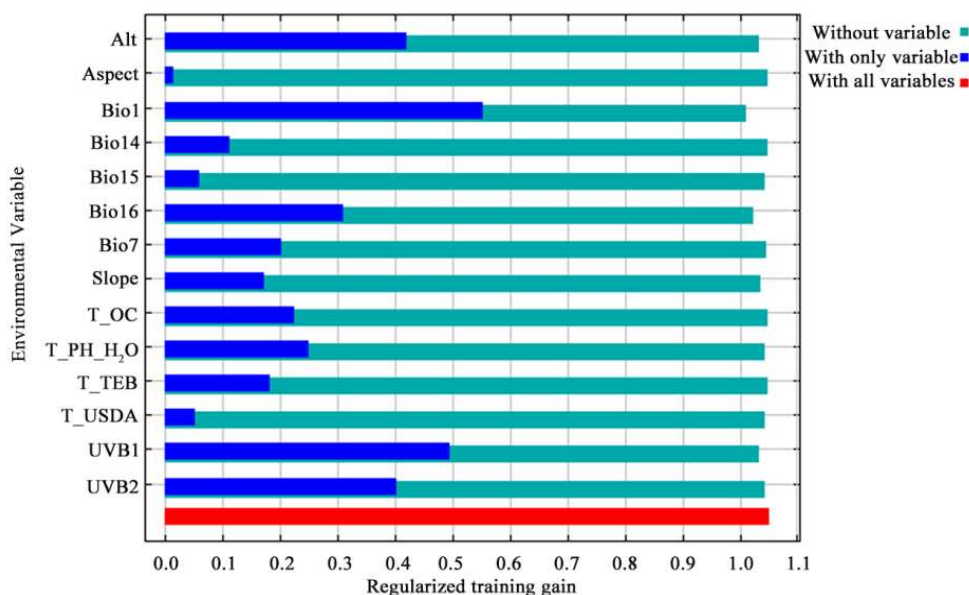


Figure 2. Jackknife test evaluating the relative importance of environmental variables on the distribution of *T. chinensis*

Based on the response curves (*Figure 3*), the thresholds (existence probability > 0.3) of the major ecological factors were obtained: annual mean temperature (Bio1) ranged from 5.6 to 16.7°C, precipitation of wettest quarter (Bio16) ranged from 116 to 860 mm and from 860-1086 mm, UVB1 ranged from 2284 to 3238 J·m⁻²·day⁻¹, UVB2 ranged from 1.27 to 1.75 J·m⁻²·day⁻¹, and elevation (Alt) was from -124m to 2659 m.

Predicted current potential distribution of T. chinensis

In China, *T. chinensis* is naturally distributed in warm-temperate zone, including Hebei, Shandong, Liaoning, Jiangsu provinces (Sun et al., 2020), inhabiting river beds, sandy floodplains, deserts, and coastal tidal flats (Zhang et al., 2019). A total of 381

known occurrences of *T. chinensis* were obtained for constructing the models (Figure 4a). The current potential distribution of *T. chinensis* in China was illustrated in Figure 4b. The results showed that the total suitable area was about 191.38×10^4 km², accounting for 19.94% of the total area of China, and the poor, moderate and high suitable areas accounted for 53.87%, 39.06%, and 7.07% of the total suitable area, respectively (Table 2). The areas with habitats suitability above 30% were mainly distributed in the middle and lower reaches of the Yellow River and the eastern coastal regions. Currently the highly suitable areas were distributed in the Hebei Province, the northeast of Shandong Province, the north of Henan Province, the coastal areas of Tianjin city and Liaoning Province.

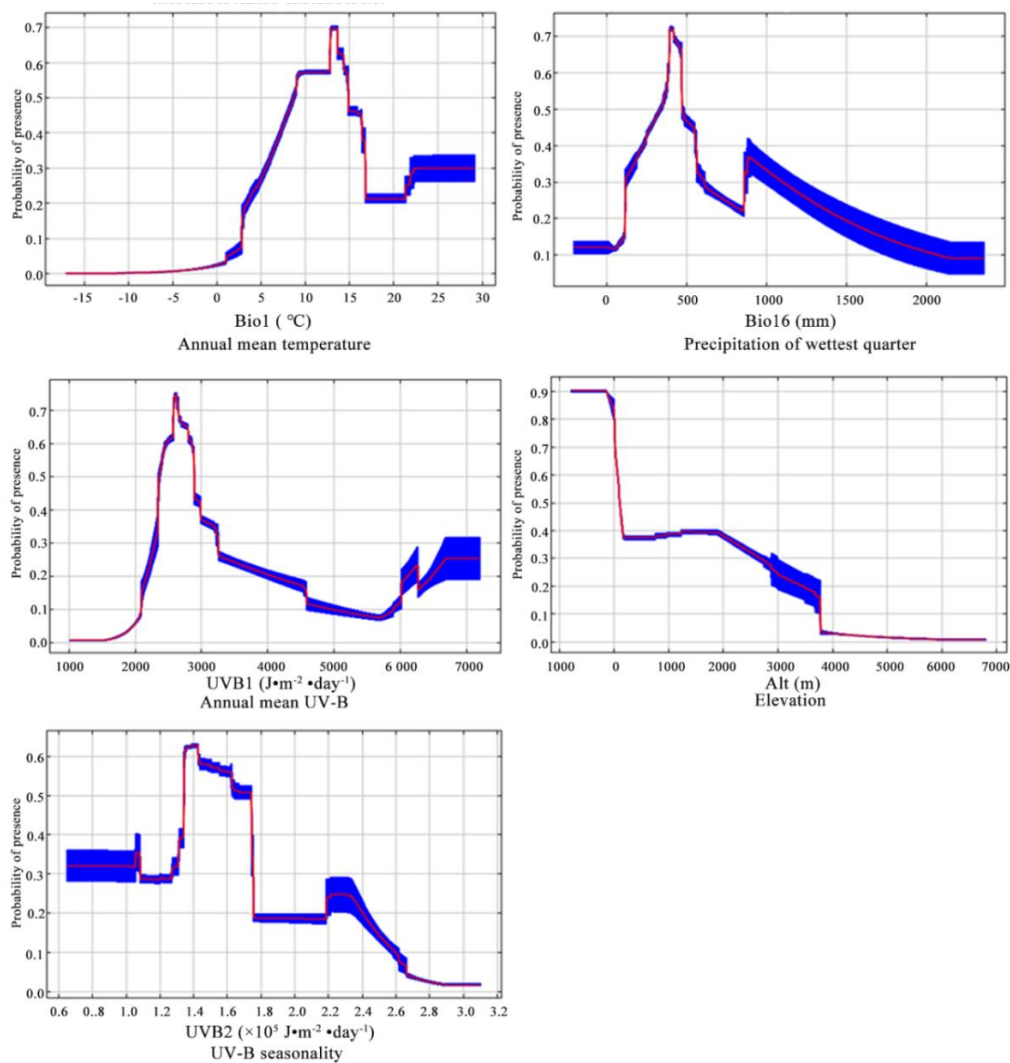


Figure 3. Response curves for important environmental variables affecting the distribution of *T. chinensis* in China. Annual mean temperature (Bio1), precipitation of wettest quarter (Bio16), annual mean UV-B (UVB1), UV-B seasonality (UVB2), and elevation (Alt). The red curves are the averages and blue margins show one standard deviation (SD) calculated over the 20 replicates

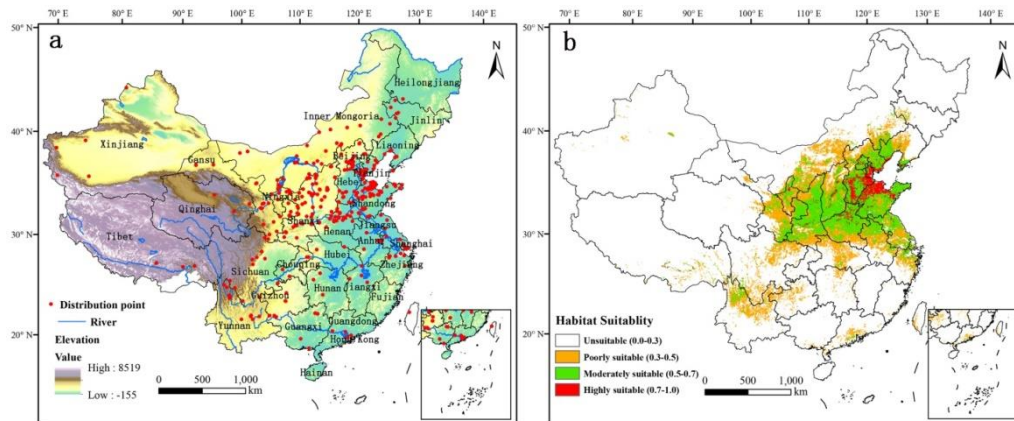


Figure 4. (a) Geographic locations of *Tamarix chinensis* occurrences in China. Red point shows the species occurrence location. (b) The potential distribution of *T. chinensis* under current climate conditions in China using the Maxent model. The red colour indicates areas with a high probability of occurrence for *T. chinensis*, the green colour represents a moderate probability of occurrence, the orange colour represents a low probability of occurrence, and the white colour indicates areas not suitable for *T. chinensis*

Table 2. Suitable areas for *T. chinensis* under different climate change scenarios (10^4 km^2)

Period	Poorly suitable	Moderately suitable	Highly suitable	Total suitable
Current	103.10	74.75	13.54	191.38
2050s, SSP126	105.82	73.90	12.96	192.68
2070s, SSP126	98.90	73.76	14.08	186.74
2050s, SSP585	97.59	75.23	13.05	185.87
2070s, SSP585	97.74	70.98	14.86	183.58

Potentially suitable climatic distributions in the future

We used the Maxent models to predict the suitable distribution areas of *T. chinensis* in China in the future (2050 and 2070) under the lowest and the highest future SSP scenarios (SSP126 and SSP585) (Figure 5). Under the SSP126 climate scenario, the total area of *T. chinensis* increased slightly in the 2050s, amounting to ca. $192.68 \times 10^4 \text{ km}^2$ (Table 2). Maxent estimated that the increased distribution area is $17.89 \times 10^4 \text{ km}^2$, the decreased area is $16.36 \times 10^4 \text{ km}^2$, and the stable area is $169.48 \times 10^4 \text{ km}^2$ (Table 3). The newly suitable habitats mainly appear in the southern sector of Inner Mongolia, the northern Shanxi, Liaoning, as well as in the Yangtze River Basin. Losses in suitable areas appear mainly in northern of Mongolia, Gansu, Yunnan, Hubei, Anhui and Zhejiang Provinces (Figure 5). However, the total area decreased in the 2070s ($186.74 \times 10^4 \text{ km}^2$). Interestingly, in 2070, the highly suitable area was 3.99% higher than the current highly suitable area (Table 2). And the increased area is $10.85 \times 10^4 \text{ km}^2$, the loss area is $15.71 \times 10^4 \text{ km}^2$, and the stable area is $170.48 \times 10^4 \text{ km}^2$ (Table 3).

Under the SSP585 climate scenario, the total area of *T. chinensis* decreased both in the 2050s ($185.87 \times 10^4 \text{ km}^2$) and in the 2070s ($183.58 \times 10^4 \text{ km}^2$) (Table 2). Overall, the increased and decreased habitat stayed generally stable as under SSP126 (Figure 5). In

2050s, the area of increased, decreased and unchanged habitat is $11.88 \times 10^4 \text{ km}^2$, $17.56 \times 10^4 \text{ km}^2$ and $168.28 \times 10^4 \text{ km}^2$, respectively. In 2070, the increased area and the decreased area increase to $14.11 \times 10^4 \text{ km}^2$ and $22.05 \times 10^4 \text{ km}^2$, respectively (*Table 3*).

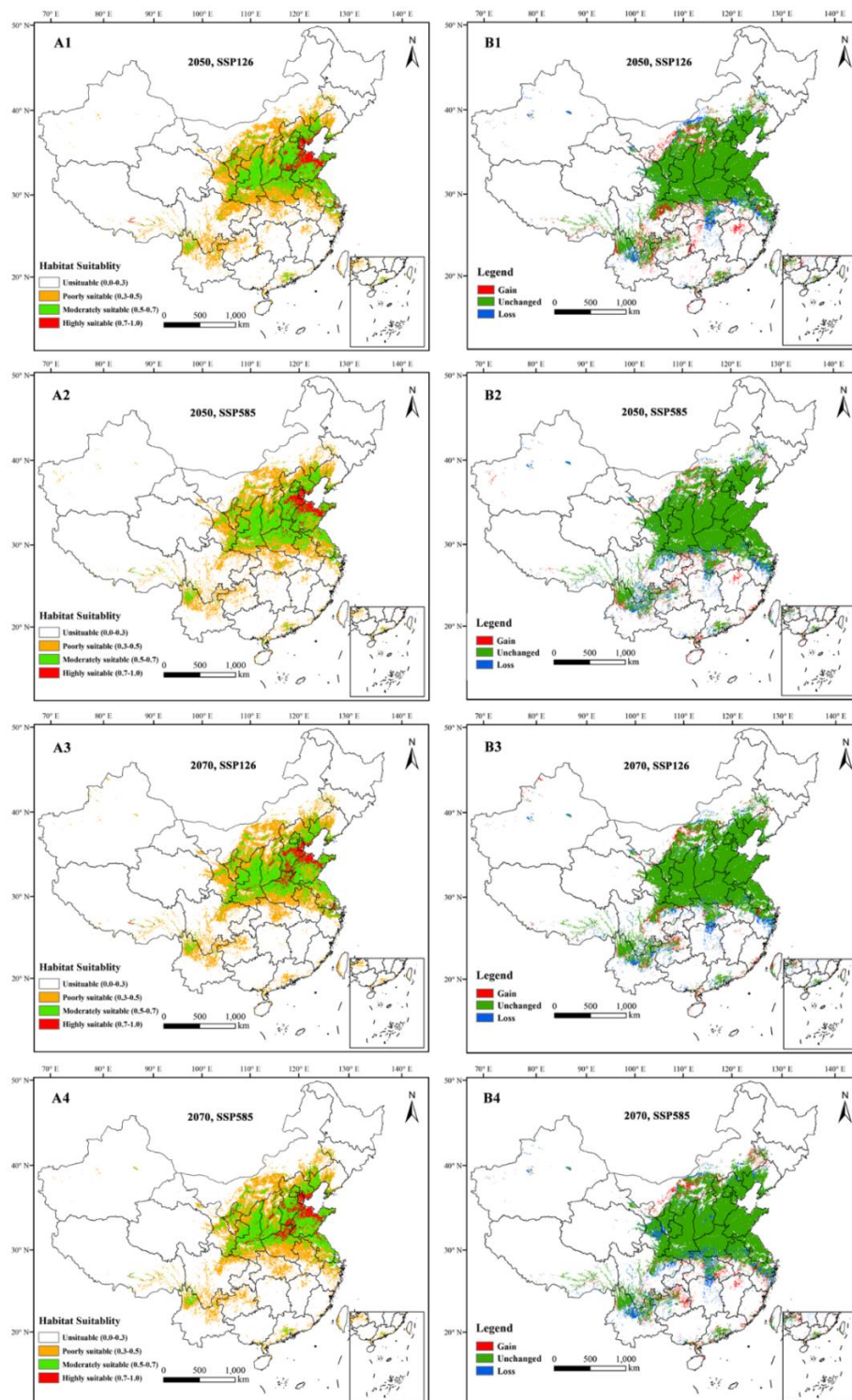


Figure 5. Future species distribution models of *T. chinensis* under climate change scenarios SSP126 and SSP585 in China. A1-A4, future suitable habitats distribution of *T. chinensis*; B1-B4, Comparison between the current and the future climate scenarios

Table 3. Dynamic changes in suitable habitat area for *T. chinensis* under four future climate scenarios (10^4 km^2)

Period	Decreased	Increased	Unchanged
2050s, SSP126	16.36	17.89	169.48
2070s, SSP126	15.71	10.85	170.14
2050s, SSP585	17.56	11.88	168.28
2070s, SSP585	22.05	14.11	163.79

Core distribution shifts

To grasp an overall understanding of distribution shifts, the centroids of both the current and future were calculated and drawn (Figure 6). The centroid of the current habitat of *T. chinensis* was predicted to be located in south Shanxi province (112.267 E and 35.61 N). Under SSP 126, it might shift southwest in 2050 (111.953 E and 35.611 N), but north in 2070 (112.129 E and 35.638 N). Overall, the core distribution of the two climate scenarios under SSP 126 showed a westward-shifting trend. Meanwhile, under SSP 8.5 the centroid of the suitable area was predicted to shift northwest in 2050 (112.192 E and 35.671 N) and then might move east in 2070 (112.524 E and 35.67 N). Overall, the core distribution of the two climate scenarios under SSP 585 showed a northward-shifting trend.

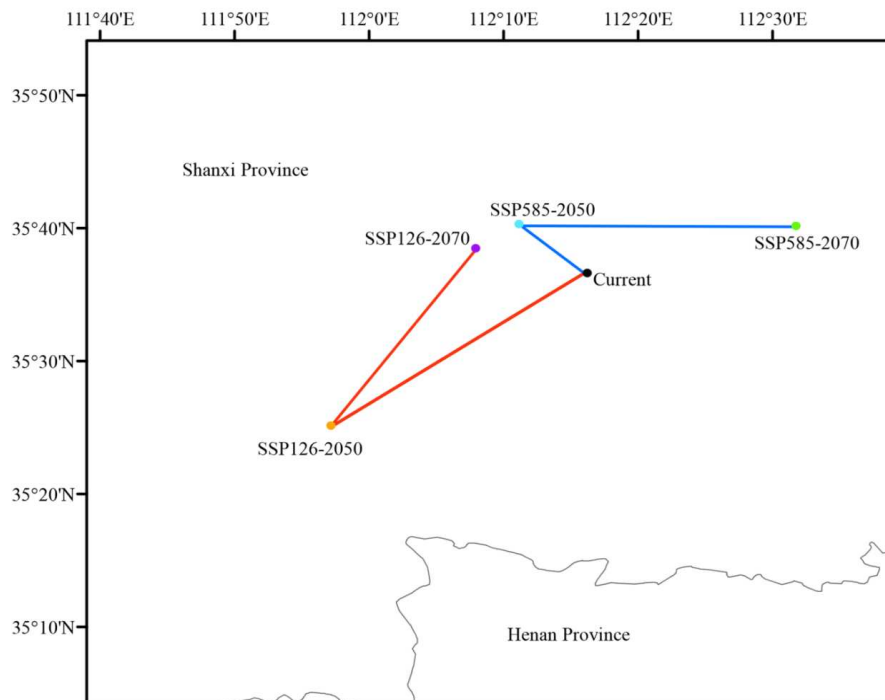


Figure 6. Potential habitats shifts of *T. chinensis* under different climate change scenarios. Black dot indicates the geometric center of suitable area under current climate condition; orange dot and purple dot indicate the geometric centers of future suitable areas of 2050 and 2070 under the climate scenario of SSP126; blue dot and green dots indicate the geometric centers of future suitable areas of 2050 and 2070 under the climate scenario of SSP585

Discussion

Climate change could impact geographical distribution of species (Zhang et al., 2018). *T. chinensis* is one of the most highly salt-tolerant shrub species with 340 Mm NaCl limit (Ye et al., 2020). As a native halophyte, it shows the wide adaptability to different ecological environment such as flooded, salty and arid conditions in China (Zhang et al., 2019). For this study, Maxent and ArcMap software have been used to predict the potential geographic distribution of *T. chinensis* under current and future climate scenarios based on the latest CMIP6 data set which is very important for assessing the suitable cultivation areas and formulating management plans.

The AUC values tested by the Maxent model were more than 0.7, which showed a good fit of the used model (Philips et al., 2006; Wei et al., 2020; Xu et al., 2020). In this study, the mean AUC value for the Maxent models was 0.857, indicating that the model had good predictive accuracy. Moreover, the prediction result and the actual distribution of *T. chinensis* remained consistent in China.

Under the current climate, *T. chinensis* had a wide but sporadic distribution in China. This model was consistent with the previous occurrence records that located in Liaoning, Jiangsu, Shandong, Hebei, Anhui, Henan, and some regions of Shanxi and Gansu etc. (Sun et al., 2020). There are only small differences between the applied scenarios in terms of the predicted area suitable for *T. chinensis* but this could be the reason for the high adaptability of the species. Our results showed that the total potential distribution area of *T. chinensis* was about 191.38×10^4 km² under current climate, in which the highly suitable areas were mainly distributed in the middle and lower reaches of the Yellow River and the eastern coastal regions.

In the current model, according to the contribution proportions of environmental factors and the jackknife test, annual mean temperature, precipitation of wettest quarter, annual mean UV-B and elevation were the most important factors affecting the distribution of *T. chinensis*. Studies have showed that the distribution of *T. chinensis* was largely affected by mean temperature of coldest quarter and precipitation of warmest quarter (Sun et al., 2020). Populations with rich genetic diversity usually existed at lower altitudes, in warmer habitats, and in eastern regions nearer to the sea (Sun et al., 2019). The model species has a wide adaptation capacity. It is confirmed by the wide range of the analysed environmental variables. The maximum acceptable mean temperature is approximately three times higher than the minimum and the differences in the precipitation of the wettest quarter is approximately fourfold.

Temperature affects the seed germination of *T. chinensis*, and it showed that an extremely cold (<5°C) and high temperature (>45°C) were found to be unfavorable for seed germination (Wang et al., 2006). The precipitation of wettest quarter (Bio16) is from 116 to 1086mm, which showed that an extremely dry climate was not suitable for this species. This was consistent with the result of a study that the occurrence of *Tamarix* spp. was positively correlated to precipitation of the warmest quarter (Cord et al., 2010). Previous study has also shown that the soil moisture was the main environmental factor that affected the distribution of *Tamarix gansuensis* (Zhao et al., 2018). Water is a basic requirement for seed. Seeds of *T. chinensis* are light and small, with hairs on the epidermis, making them highly suited to dispersal to different distances by water. In summer, the seeds of *T. chinensis* usually germinate within 24 h in moist soil, even when afloat seedlings could survive submerged for a few weeks (Jiang et al., 2012; Jiao et al., 2021). In addition, the groundwater affects the leaf

photosynthetic efficiency of *T. chinensis* by significantly impacting the soil water content within the distribution range of the root system (Xia et al., 2020).

In this study, the elevation and UV-B radiation were also the important factors affecting the distribution of *T. chinensis*. According to the response curves (existence probability > 0.70), the highly suitable elevation value was from 0 to 171 m. This is in accordance with previous results (Song et al., 2010; Sun et al., 2016), in which populations existed in eastern regions nearer to the sea, where are characterized by low elevation. UV-B radiation has a significant influence on the growth and performance of terrestrial plants (Garcia-Corral et al., 2017; Díaz- Guerra et al., 2019). It may can lead to changes at the cellular and organismal scales, inducing a variety of morphological, physiological, and molecular responses in plants (Valle et al., 2020). However, little is known about how *T. chinensis* respond to UV-B radiation.

With global warming, most species may generally migrate to higher latitudes and elevations (Zhang et al., 2018; Peng et al., 2019). A study in the northeastern United States revealed that the distribution of forests was shifting northward with climate change (Wang et al., 2017). High-alpine species are expanding their range to higher altitudes in respond to climate change (Rumpf et al., 2018). Consistently, the core distribution of *T. chinensis* showed a westward-shifting trend under SSP126 and a northward-shifting trend under SSP585. New suitable habitats would appear in the southern sector of Inner Mongolia, the northern Shanxi and Liaoning. Overall, the centroids of suitable habitat shifted was higher than the current area, which indicated that *T. chinensis* will be able to adapt to climate change.

Under the SSP126 scenario, we predicted suitable habitat range of *T. chinensis* increased in 2050 followed by decreased in 2070. The predicted increase and decrease in the suitable habitat is almost the same, this indicates that the restructuration of the habitats is predicted but large changes in the overall distribution are not expected. Under the SSP 585 scenario, suitable habitat range was predicted to decrease with the increased intensity of global warming, which suggested *T. chinensis* could not benefit from global warming. A continuous rise in temperature might had a negative effect on plants (Xu and Xue, 2013; Zhang, 2018). Losses in suitable areas may be at great risk of soil salinization and aridification under global warming (Sun et al., 2020). The habitat suitability of *T. chinensis* was affected not only by environmental factors, but also by intraspecific facilitation, wind dispersal of seeds and human activities. The intensive dispersal and germination in the short term resulted in habitat fragmentation (Jiao et al., 2021). Additionally, unsustainable land use and management could lead to a decrease in suitable habitat of *T. chinensis*.

Generally, assessment of habitat suitability plays an instructional role for the identification of future suitable areas and cultivation of *T. chinensis*. In this study, the moderate and high suitable areas should be given priority for cultivation of *T. chinensis*. In addition, new habitats in higher latitudes and elevations in the future such as Liaoning province, the southern sector of Inner Mongolia province and north of Shanxi should also be considered as suitable habitats for *T. chinensis* introducing.

Conclusions

To assess the impact of climate change on the distribution of *T. chinensis*, we modeled the current and future potential distribution using the Maxent model based on the latest CMIP6 data. Annual mean temperature, precipitation of wettest quarter,

annual mean UV-B and elevation were the most important factors affecting the distribution of *T. chinensis*. Under the SSP126 scenario, we predicted suitable habitat range of *T. chinensis* increased in 2050 followed by decreased in 2070; however, under the SSP585 scenario, we predicted that the suitable habitat range would decrease with the increased intensity of global warming. Overall, the core distribution of *T. chinensis* showed a westward-shifting trend under SSP 126 and a northward-shifting trend under SSP 585. The predicted spatial and temporal shift patterns of *T. chinensis* will provide a useful reference for assessing the suitable cultivation areas and sustainable resource use of *T. chinensis*.

Declaration of competing interests. The authors declare that they have no known competing financial interests or personal relationships that could have appeared to influence the work reported in this paper.

Acknowledgments. This work was funded by the Doctoral Scientific Research Foundation of Hebei Normal University of Science & Technology (2019YB016), Hebei Provincial Department of Science and Technology Project (21326346D), National Finance Forestry Science and Technology Promotion and Demonstration Project (TG [2020]005), Science and Technology Research Project for Higher Schools in Hebei Province (ZD2022091), Graduate Innovation Project of Educational Committee of Hebei Province of China (CXZZSS2022095).

REFERENCES

- [1] Anderegg, W. R. L., Hicke, J. A., Fisher, R. A., Allen, C. D., Aukema, J., Bentz, B., Hood, S., Lichstein, J. W., Macalady, A. K., McDowell, N., Pan, Y., Raffa, K., Sala, A., Shaw, J. D., Stephenson, N. L., Tague, C., Zeppel, M. (2015): Tree mortality from drought, insects, and their interactions in a changing climate. – *New Phytol* 208: 674-683.
- [2] Bağçacı, S. Ç., Yucel, I., Duzenli, E., Yilmaz, M. T. (2021): Intercomparison of the expected change in the temperature and the precipitation retrieved from CMIP6 and CMIP5 climate projections: A Mediterranean hot spot case, Turkey. – *Atmospheric Research* 256: 105576.
- [3] Bai, H., Xiao, D., Wang, B., Liu, D. L., Feng, P., Tang, J. (2020): Multi-model ensemble of CMIP6 projections for future extreme climate stress on wheat in the North China plain. – *RMetS, International Journal of Climatology* 41(S1): E171-E186. DOI: <https://doi.org/10.1002/joc.6674>.
- [4] Beckmann, M., Vaclavik, T., Manceur, A. M., Sprtova, L., von Wehrden, H., Welk, E., Cord, A. F. (2014): gIUV: A global UV-B radiation data set for macroecological studies. – *Methods Ecol Evol* 5: 372-383.
- [5] Bertrand, R., Lenoir, J., Piedallu, C., Riofrío-Dillon, G., Ruffray, P. D., Vidal, C., Pierrat, J. C., Gégout, J. C. (2011): Changes in plant community composition lag behind climate warming in lowland forests. – *Nature* 479: 517-520.
- [6] Brown, J. L., Barbara, A. (2014): SDMtoolbox: a python-based GIS toolkit for landscape genetic, biogeographic and species distribution model analyses. – *Methods Ecol Evol* 5: 694-700.
- [7] Chen, Q. H., Yin, Y. J., Zhao, R., Yang, Y., Silva, J., Yu, X. N. (2020): Incorporating local adaptation into species distribution modeling of *Paeonia mairei*, an endemic plant to China. – *Front Plant Sci* 10.
- [8] Cord, A., Klein, D., Dech, S. (2010): Remote Sensing Time Series for Modeling Invasive Species Distribution: A Case Study of *Tamarix* spp. in the US and Mexico. – *International Congress on Environmental Modelling and Software* 556.
- [9] Díaz-Guerra, L., Llorens, L., Bell, T. L., Font, J., González, J. A., Verdaguier, D. (2019): Physiological, growth and root biochemical responses of *Arbutus unedo* and *Quercus*

- suber seedlings to UV radiation and water availability before and after aboveground biomass removal. – *Environ Exp Bot* 168: 103861.
- [10] Du, Z. Y., He, Y. M., Wang, H. T., Wang, C., Duan, Y. Z. (2020): Potential geographical distribution and habitat shift of the genus *Ammopiptanthus* in China under current and future climate change based on the Maxent model. – *J Arid Environ* 184: 104328.
- [11] Elith, J., Graham, C. H., Anderson, R. P., Dudik, M., Ferrier, S., Guisan, A., Hijmans, R. J., Huettmann, F., Leathwick, J. R., Lehmann, A., Li, J., Lohmann, L. G., Loiselle, B. A., Manion, G., Moritz, C., Nakamura, M., Nakazawa, Y., Overton, J. M. M., Peterson, A. T., Phillips, S. J., Richardson, K., Scachetti-Pereira, R., Schapire, R. E., Soberón, J., Williams, S., Wisz, M. S., Zimmermann, N. E. (2006): Novel methods improve prediction of species' distribution from occurrence data. – *Ecography* 19: 129-151.
- [12] Elith, J., Phillips, S. J., Hastie, T., Dudik, M., Chee, Y. E., Yates, C. J. (2011): A statistical explanation of MaxEnt for ecologists. – *Divers. Distrib.* 17: 43-57.
- [13] Eyring, V., Bony, S., Meehl, G. A., Senior, C. A., Stevens, B., Stouffer, R. J., Taylor, K. E. (2016): Overview of the Coupled Model Intercomparison Project Phase 6 (CMIP6) experimental design and organization. – *Geosci Model Dev* 9: 1937-1958.
- [14] Fan, D. L., Zhong, H. L., Hu, B., Tian, Z., Sun, L. X., Fischer, G., Wang, X. Y., Jiang, Z. Y. (2020): Agro-ecological suitability assessment of Chinese Medicinal Yam under future climate change. – *Environ. Geochem Health* 42(3): 987-1000.
- [15] Feng, L., Sun, J. J., Wang, T. L., Tian, X. N., Wang, W. F., Guo, J., Guo, H. H., Deng, H. H., Wang, G. B. (2021): Predicting suitable habitats of *Ginkgo biloba* L. fruit forests in China. – *Clim Risk Manag* 34: 100364.
- [16] Fick, S. E., Hijmans, R. J. (2017): WorldClim 2: new 1km spatial resolution climate surfaces for global land areas. – *Int J Climatol* 37: 4302-4315.
- [17] Flowers, T. J., Colmer, T. D. (2008): Salinity tolerance in halophytes. – *New Phytol* 179: 945-963. <https://doi.org/10.1111/j.1469-8137.2008.02531.x>.
- [18] Garcia-Corral, L. S., Holding, J. M., Carrillo-de-Albornoz, P., Steckbauer, A., Pérez-Lorenzo, M., Navarro, N., Serret, P., Duarte, C. M., Agusti, S. (2017): Effects of UVB radiation on net community production in the upper global ocean. – *Glob Ecol Biogeogr* 26: 54-64.
- [19] Gidden, M. J., Riahi, K., Smith, S. J., Fujimori, S., Luderer, G., Kriegler, E., van Vuuren, D. P., van den Berg, M., Feng, L., Klein, D., Calvin, K., Doelman, J. C. (2019): Global emissions pathways under different socioeconomic scenarios for use in CMIP6: A dataset of harmonized emissions trajectories through the end of the century. – *Geosci Model Dev* 12: 1443-1475.
- [20] Graham, M. H. (2003): Confronting multicollinearity in ecological multiple regression. – *Ecology* 84: 2809-2815.
- [21] IPCC (2013): *Climate change 2013: The physical Science Basis*. – Contribution of Working Group I to the Fifth Assessment Report of the Intergovernmental Panel on Climate Change. Cambridge University Press, Cambridge, UK and New York, NY, 1535p.
- [22] Jamal, Z. A., Abou-Shaara, H. F., Qamar, S., Alotaibi, M. A., Khan, K. A., Khan, M. F., Bashirg, M. A., Hannan, A., AL-Kahtani, S. N., Taha, E. A., Anjum, S. I., Attaullah, M., Raza, G., Ansari, M. J. (2020): Future expansion of small hive beetles, *Aethina tumida*, towards North Africa and South Europe based on temperature factors using maximum entropy algorithm. – *J King Saud Univ Sci* 33: 101242.
- [23] Jiang, Z., Chen, Y., Ying, B. (2012): Population genetic structure of *Tamarix chinensis* in the yellow river delta, China. – *Plant Syst Evol* 298: 147-153.
- [24] Jiao, L., Zhang, Y., Sun, T., Yang, W., Shao, D., Zhang, P., Liu, Q. (2021): Spatial analysis as a tool for plant population conservation: a case study of *Tamarix chinensis* in the Yellow River Delta, China. – *Sustainability* 13: 8291.

- [25] Kozak, K. H., Graham, C. H., Wiens, J. J. (2008): Integrating GIS-based environmental data into evolutionary biology. – *Trends in Ecology & Evolution* 23: 141-148. <https://doi.org/10.1016/j.tree.2008.02.001>.
- [26] Liang, Y., Gillett, N. P., Monahan, A. H. (2020): Climate Model Projections of 21st Century Global Warming Constrained Using the Observed Warming Trend. – *Geophysical Research Letters* 47(12): e2019GL086757.
- [27] Litalien, A., Zeeb, B. (2020): Curing the earth: a review of anthropogenic soil salinization and plant-based strategies for sustainable mitigation. – *Sci Total Environ* 698: 134235. <https://doi.org/10.1016/j.scitotenv.2019.134235>.
- [28] Liu, W. S., You, J. L., Zeng, W. B., Qi, D. H. (2018): Prediction of the geographical distribution of *Carex moorcroftii* under global climate change based on MaxEnt model. – *Chin. J. Grassl.* 40(5): 43-49.
- [29] Lu, Y. P., Liu, H. C., Chen, W., Yao, J., Huang, Y. Q., Zhang, Y., He, X. Y. (2021): Conservation planning of the genus *Rhododendron* in Northeast China based on current and future suitable habitat distributions. – *Biodivers. Conserv.* 30: 673-697.
- [30] Munns, R., Tester, M. (2008): Mechanisms of salinity tolerance. – *Annual Review of Plant Biology* 59: 651-681.
- [31] Peng, L. P., Cheng, F. Y., Hu, X. G., Mao, J. F., Xu, X. X., Zhong, Y., Li, S. Y., Xian, H. L. (2019): Modelling environmentally suitable areas for the potential introduction and cultivation of the emerging oil crop *Paeonia ostii* in China. – *Sci Rep* 1: 3213.
- [32] Peterson, A. T. (2007): Ecological niche modelling and understanding the geography of disease transmission. – *Veter Ital* 43: 393-400.
- [33] Peterson, A. T., Soberón, J., Pearson, R. G., Anderson, R. P., Martínez-Meyer, E., Nakamura, M., Araújo, B. (2011): *Ecological niches and geographic distributions*. – Princeton University Press: Princeton, NJ, USA.
- [34] Phillips, S. J., Anderson, R. P., Schapire, R. E. (2006): Maximum entropy modeling of species geographic distributions. – *Ecol Model* 190: 231-259.
- [35] Phillips, S. J., Dudík, M. (2008): Modeling of species distributions with Maxent: new extensions and a comprehensive evaluation. – *Ecography* 31: 161-175.
- [36] Phillips, S. J., Dudík, M., Schapire, R. E. (2020): Maxent software for modeling species niches and distributions. – Version 3.4.1.
- [37] Riahi, K., Vuuren, D. P., Kriegler, E., Edmonds, J., O'Neill, B. C., Fujimori, S., Baue, R. N., Calvin, K., Dellink, R., Fricko, O., Lutz, W. (2017): The Shared Socioeconomic Pathways and their energy, land use, and greenhouse gas emissions implications: An overview. – *Glob. Environ. Chang.* 42: 153-168.
- [38] Rogel, J. A., Ariza, F. A., Silla, R. O. (2000): Soil salinity and moisture gradients and plant zonation in Mediterranean salt marshes of Southeast Spain. – *Wetlands* 20: 357-372.
- [39] Rogelj, J., Meinshausen, M., Knutti, R. (2012): Global warming under old and new scenarios using IPCC climate sensitivity range estimates. – *Nat. Clim. Change* 2: 248-253.
- [40] Rumpf, S. B., Hülber, K., Klöner, G., Moser, D., Schütz, M., Wessely, J., Willner, W., Zimmermann, N. E., Dullinger, S. (2018): Range dynamics of mountain plants decrease with elevation. – *Proc Natl Acad Sci* 115: 1848-1853.
- [41] Santos, J., Al-Azzawi, M., Aronson, J., Flowers, T. J. (2016): eHALOPH a database of salt tolerant plants: helping put halophytes to work. – *Plant Cell Physiol* 57(1): 1-10. <https://doi.org/10.1093/pcp/pcv155>.
- [42] Song, C. Y., Huang, C., Liu, G. H. (2010): Simulating Potential Distribution of *Tamarix chinensis* in Yellow River Delta by Generalized Additive Models. – *Wetland Science* 8: 347-353.
- [43] Sun, L. K., Liu, W. Q., Chen, T., Liu, G. X. (2016): Review on mechanism of habitat adaptability and resource value of *Tamarix* species. – *Journal of Desert of Research* 36: 349-356.

- [44] Sun, L. K., Liu, G. X., Zhang, B. G., Zhang, G. S. (2019): Effects of environmental factors on population genetic diversity of *Tamarix chinensis*. – *Acta Prataculturae Sinica* 28: 178-186.
- [45] Sun, L. K., Liu, G., Lu, Y., Zhang, B., Zhang, G. (2020): Molecular data and ecological niche modelling reveal the phylogeographic pattern of the widespread shrub *Tamarix chinensis* Lour. (Tamaricaceae) in China. – *Kew Bull* 75: 41.
- [46] Valle, J. C. D., Buide, M. L., Whittall, J. B., Valladares, F., Narbona, E. (2020): UV radiation increases phenolic compound protection but decreases reproduction in *Silene littorea*. – *PLoS ONE* 15: e0231611.
- [47] Wang, H. L., Guo, Y. H., Yang, C. J., Chen, Q. L., Yang, T. X., Zhai, Z. X. (2006): Study on Seed Germination Characteristics of *Tamarix chinensis*. – *China Journal of Chinese Materia Medica* 31: 1196-1197.
- [48] Wang, W. J., He, H. S., Thompson, F. R., Fraser, J. S., DiJak, W. D. (2017): Changes in forest biomass and tree species distribution under climate change in the northeastern United States. – *Landsc Ecol* 32: 1399-1413.
- [49] Wei, A. Y., Zhang, L., Wang, J. N., Wang, W. W., Niyati, N., Guo, Y. L., Wang, X. F. (2020): Chinese caterpillar fungus (*Ophiocordyceps sinensis*) in China: current distribution, trading, and futures under climate change and overexploitation. – *Sci Total Environ* 755: 142548.
- [50] Xia, J. B., Lang, Y., Zhao, Q. K., Liu, P., Su, L. (2020): Photosynthetic characteristics of *Tamarix chinensis* under different groundwater depths in freshwater habitats. – *Sci Total Environ* 761: 143221.
- [51] Xu, M. H., Xue, X. (2013): Analysis on the effects of climate warming on growth and phenology of alpine plants. – *J Arid Land Resour Environ* 27: 137-141.
- [52] Xu, X. X., Cheng, F. Y., Peng, L. P., Sun, Y. Q., Hu, X. G., Li, S. Y., Hong, L. X., Jia, K. H., Abbott, R. J., Mao, J. F. (2019): Late Pleistocene speciation of three closely related tree peonies endemic to the Qinling Daba Mountains, a major glacial refugium in Central China. – *Ecology and Evolution* 9: 7528-7548.
- [53] Xu, N., Meng, F. Y., Zhou, G. F., Li, Y. F., Lu, H. (2020): Assessing the suitable cultivation areas for *Scutellaria baicalensis* in China using the Maxent model and multiple linear regression. – *Biochem Syst Ecol* 90: 104052.
- [54] Ye, Y., Wang, J., Wang, W., Xu, L.-A. (2020): ARF family identification in *Tamarix chinensis* reveals the salt responsive expression of TcARF6 targeted by miR167. – *Peer J* 8(4): e8829.
- [55] Zelinka, M. D., Myers, T. A., McCoy, D. T., Po-Chedley, S., Caldwell, P. M., Ceppi, P., Klein, S. A., Taylor, K. E. (2020): Causes of higher climate sensitivity in CMIP6 models. – *Geo physical Research Letters* 47: e2019GL085782.
<https://doi.org/10.1029/2019GL085782>.
- [56] Zhang, K. L., Yao, L. J., Meng, J. S., Tao, J. (2018): Maxent modeling for predicting the potential geographical distribution of two peony species under climate change. – *Sci Total Environ* 634: 1326-1334.
- [57] Zhang, R. H., Wen, Q., Xu, L. A. (2019): Development and characterization of genomic SSR markers for *Tamarix chinensis* (Tamaricaceae). – *Appl Plant Sci* 7: e1219.
- [58] Zhang, H., Song, J. Y., Zhao, H. X., Li, M., Han, W. H. (2021): Predicting the distribution of the invasive species *Leptocybe invasa*: combining MaxEnt and Geodetector models. – *Insects* 12: 92.
- [59] Zhao, L. C., Zhao, C. Z., Wang, X. P., Wen, J. (2018): Interrelations between environmental factors and distribution of *Tamarix gansuensis* in Qinwangchuan wetland. – *Acta Ecologica Sinica* 38: 3422-3431.

APPENDIX

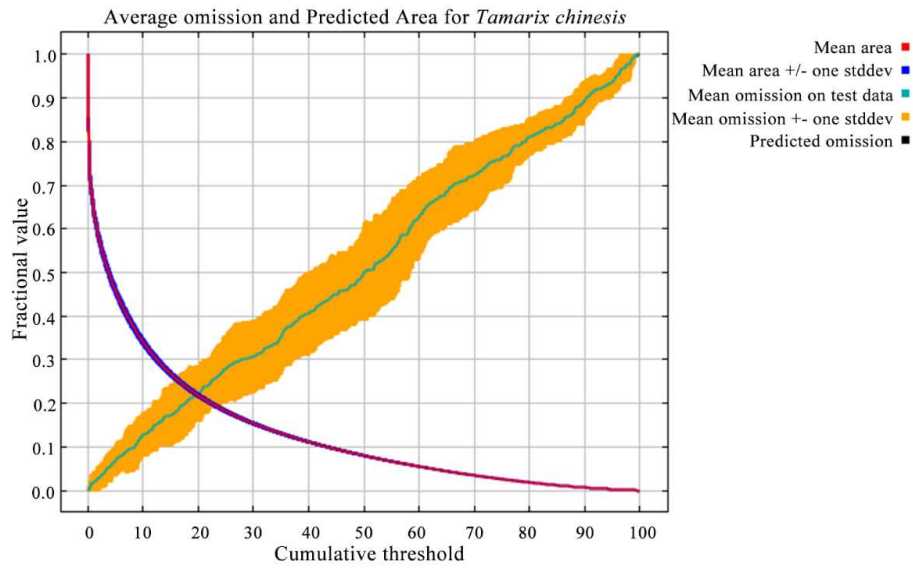


Figure S1. The omission rate for training and test samples, and predicted area as a function of the cumulative threshold

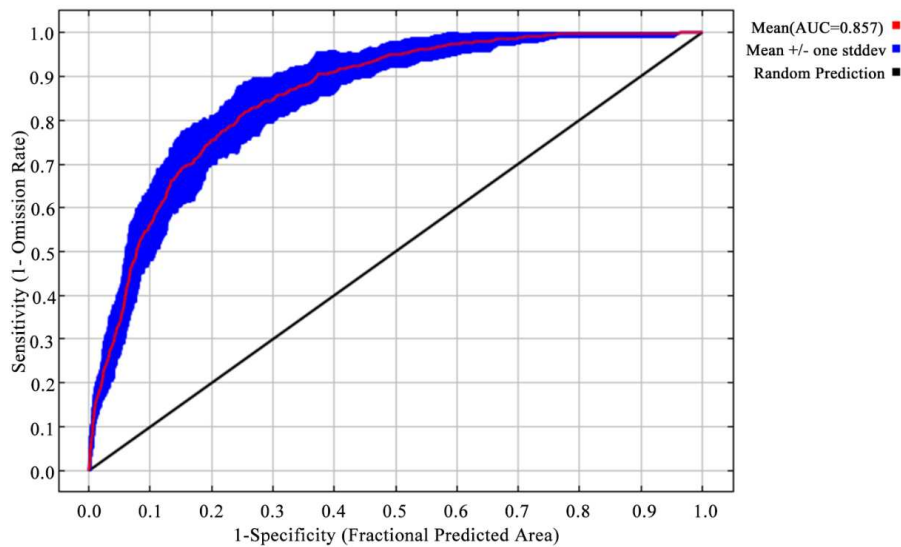


Figure S2. The curve of receiver operating characteristic for the training and test data

Table S1. Environmental variables were chosen to model the potential geographic distribution of *Tamarix chinensis*

Code	Environmental variables	Unit	Source
Bio1	Annual mean temperature	°C	http://www.worldclim.org/
Bio2	Mean diurnal range	°C	http://www.worldclim.org/
Bio3	Isothermality (BIO2/BIO7) (×100)	×100	http://www.worldclim.org/
Bio4	Temperature seasonality (standard deviation ×100)	×100	http://www.worldclim.org/
Bio5	Max temperature of warmest month	°C	http://www.worldclim.org/
Bio6	Min temperature of coldest month	°C	http://www.worldclim.org/
Bio7	Temperature annual range (BIO5-BIO6)	°C	http://www.worldclim.org/
Bio8	Mean temperature of wettest quarter	°C	http://www.worldclim.org/
Bio9	Mean temperature of driest quarter	°C	http://www.worldclim.org/
Bio10	Mean temperature of warmest quarter	°C	http://www.worldclim.org/
Bio11	Mean temperature of coldest quarter	°C	http://www.worldclim.org/
Bio12	Annual precipitation	mm	http://www.worldclim.org/
Bio13	Precipitation of wettest month	mm	http://www.worldclim.org/
Bio14	Precipitation of driest month	mm	http://www.worldclim.org/
Bio15	Precipitation seasonality (coefficient of variation)	mm	http://www.worldclim.org/
Bio16	Precipitation of wettest quarter	mm	http://www.worldclim.org/
Bio17	Precipitation of driest quarter	mm	http://www.worldclim.org/
Bio18	Precipitation of warmest quarter	mm	http://www.worldclim.org/
Bio19	Precipitation of coldest quarter	mm	http://www.worldclim.org/
Alt	Elevation	m	http://www.gscloud.cn/
Slop	Slope	°	http://www.gscloud.cn/
Asp	Aspect	°	http://www.gscloud.cn/
T_OC	Topsoil organic carbon	% weight	http://globalchange.bnu.edu.cn/research/soil2)
T_PH_H2O	Topsoil pH (H2O)	-log(H ⁺)	http://globalchange.bnu.edu.cn/research/soil2)
T_TEB	Topsoil TEB	cmol/kg	http://globalchange.bnu.edu.cn/research/soil2)
T_USDA_TEX_CLASS	Topsoil USDA texture classification	name	http://globalchange.bnu.edu.cn/research/soil2)
UVB1	Annual mean UV-B	J m ⁻² •day ⁻¹	http://www.ufz.de/gluv/
UVB2	UV-B seasonality	J m ⁻² •day ⁻¹	http://www.ufz.de/gluv/
UVB3	Mean UV-B of lightest month	J m ⁻² •day ⁻¹	http://www.ufz.de/gluv/
UVB4	Mean UV-B of lowest month	J m ⁻² •day ⁻¹	http://www.ufz.de/gluv/

Table S2. Correlation matrix between fourteen variables used in ENM test

Variables	BIO1	BIO7	BIO14	BIO15	BIO16	T_OC	PH	TED	USDA	UVB1	UVB2	ALT	aspect	slope
BIO1	1													
BIO7	-0.436	1												
BIO14	0.625	-0.575	1											
BIO15	-0.533	0.3719	-0.601	1										
BIO16	0.586	-0.6599	0.749	-0.267	1									
T_OC	-0.131	-0.1359	0.070	0.015	0.12312	1								
PH	0.005	0.3579	-0.301	0.128	-0.30525	-0.20534	1							
TED	0.033	0.289	-0.199	0.065	-0.24648	0.01339	0.70543	1						
USDA	-0.368	0.2813	-0.442	0.260	-0.44138	-0.19742	0.02345	-0.20844	1					
UVB1	-0.304	-0.5243	-0.060	0.025	-0.06985	0.16508	-0.33669	-0.26159	0.14413	1				
UVB2	-0.684	0.033	-0.469	0.258	-0.57147	0.10392	-0.10055	-0.07518	0.36433	0.77752	1			
ALT	-0.354	-0.098	-0.185	0.132	-0.18525	0.0849	-0.12141	-0.10272	0.15216	0.44031	0.46335	1		
aspect	-0.005	0.001	0.014	-0.017	0.01001	0.00802	-0.0061	0.00805	-0.00922	0.00507	-0.00247	0.00348	1	
slope	-0.03967	-0.02251	-0.01261	-0.00861	-0.00473	0.00144	-0.05172	-0.04079	0.01934	0.0515	0.04312	0.03414	0.09452	1

ASSESSMENT OF CHIKUNGUNYA FEVER (CHIKF) RISK AREAS IN THE SOUTH OF THAILAND BASED ON ENVIRONMENTAL, SOCIO-ECONOMIC AND EPIDEMIOLOGICAL DATA

NUTHAMMACHOT, N.^{1*} – STRATOULIAS, D.²

¹*Faculty of Environmental Management, Prince of Songkla University, P. O. Box 50 Kor-Hong, Hatyai, Songkhla 90112, Thailand*

²*Asian Disaster Preparedness Center, SM Tower, 24th Floor, 979/69 Paholyothin Road, Samsen Nai Phayathai, Bangkok 10400, Thailand
(email: dimitris@adpc.net; phone: +66-22-980-681)*

**Corresponding author
e-mail: narissara.n@psu.ac.th; phone: +66-62-242-3919*

(Received 1st Feb 2022; accepted 2nd May 2022)

Abstract. The south of Thailand is a popular touristic destination and, at the same time, a very high-risk area for a Chikungunya fever (CHIKF) outbreak due to the tropical environment. Therefore, it is essential to monitor and potentially prevent the CHIKF disease outbreak in this area. This research aims to apply synergistically the Geographic Information System (GIS) and Analytic Hierarchy Process (AHP) techniques to evaluate CHIKF risk spatially in the south of Thailand. Five criteria related to the risk of CHIKF disease were selected following the most influential factors: CHIKF patient density data, the number of population density, the household number data, land use/land cover and rainfall data. The importance weight of each criterion was calculated; the consistency ratio (CR) that gives less than 0.1 was considered acceptable. The higher the essential weight of a given factor, the more influence it will have on the final decision. CHIKF risk area in 14 provinces in the south of Thailand was reclassified into five categories (very high, high, moderate, low and very low). The CHIKF risk area map was found to be in agreement with the CHIKF patient number data recorded in the last 10 years. The results can support the government's disease control departments and the Provincial Public Health Office to devise strategies and plans for controlling potential outbreaks efficiently.

Keywords: *analytic hierarchy process, outbreak, geographic information system, multiple criteria decision making, criteria*

Introduction

Chikungunya fever (CHIKF) is a serious disease that has become a major public health concern worldwide. The Chikungunya virus (CHIKV) belongs to the genus Alphavirus and the family *Togaviridae* (Tuanudom et al., 2017; Ramachandran et al., 2012). The CHIKV spreads to people by the bite of infected *Aedes* mosquitoes (Kaslow and Evans, 1997). The symptoms of infection are fever and joint pain including muscle pain, headache, nausea, fatigue or eruption. In the present time, there is no vaccine or medicine against the CHIKV infection, nevertheless, practices to prevent mosquito bites such as wearing neutral-coloured (beige, light grey) clothing and long pants and sleeves, usage of mosquito repellent exist. Outbreaks of CHIKF have occurred in many parts around the world including Europe, Africa and Asia (Garcia et al., 2020). Since the late 1950s, outbreaks of CHIKF have been reported in several Asian countries. In Thailand, CHIKV was found in 1958 (Hammon et al., 1960) and from 1960 to 2000 the disease was reported in several other Asian countries (Cambodia, India, Vietnam Sri Lanka, Philippines, Myanmar and Indonesia) (Chastel,

1963; Sarkar et al., 1964; Dai and Thoas, 1967; Marchette et al., 1978; Slemons et al., 1984). Since October 2018 large outbreaks of CHIKF in Thailand were reported in the southern part of the country (Tuite et al., 2019). *Ae. Albopictus*, commonly named the Asian tiger mosquito, is found in Asia, Africa, America, Australia and Europe (Akiner et al., 2016; Delatte et al., 2010). As the main occupation of inhabitants of the south of Thailand relates to agriculture (rubber trees, fruit and oil palm farms), and the rainy season lasts for 6-8 months per year, there is, therefore, a high risk of CHIKV infection through the bite of infected Asian tiger mosquitoes. The Department of Disease Control, Thailand (2021) have released the data of reported cases of CHIKF in Thailand between 2011-2021. It is evident that many southern provinces had more than 100 cases of CHIKF. Therefore, it is important to address the role and spatial association between CHIKV and risk areas. Moreover, the southern part of Thailand is a touristic region receiving visitors from other parts of Thailand and abroad such as Europe, Singapore, Malaysia etc., and the number of tourists increases every year (Ministry of Tourism and Sports, 2019). The tourists have a high risk in getting exposed to CHIKF as the local weather and environmental conditions are suitable for the CHIKF. Hence, it is very essential to study the hazard and the factors influencing the CHIKF spread in the south of Thailand in order to establish management practices to prevent and control the disease in the risky regions. The application of spatial analyst Geographic Information System (GIS) tool has been proven a powerful tool for performing spatial analysis of managed data. Currently, GIS technique is applied for investigating and monitoring epidemiological surveillance in the tropical countries (Richardson et al., 2013). Therefore, the combination of Multiple Criteria Decision Making (MCDM) and GIS has advanced the multi-criteria decision by integrating geospatial data (Malczewski, 1999). The Analytic Hierarchy Process (AHP), developed by Saaty (1977) is one of the best tools to frame a decision problem based on a set of priorities, namely weightages (Saaty, 1990).

AHP has been applied in Earth Observation synergistically with GIS which is named spatial-AHP (Siddiqui et al., 1996). The capacity of GIS to combine with the AHP technique has been demonstrated in several studies. For example, Ali and Ahmad (2019) applied AHP and GIS to determine a mosquito-borne diseases in Kolkata Municipal Corporation mapping in the Golestan National Park. Ten factors were selected to determine their weight through a pairwise comparison matrix. The results showed that water bodies is a main factor for mosquito-borne diseases. Ahmad et al. (2017) used a Multi-Criteria Approach to study Malaria epidemic for vulnerability zones. Socio-economic, epidemiological and environmental criteria were considered. 59.1% of the study area is vulnerable from high to very high risk of malaria event. Mollalo and Khodabandehloo (2016) used AHP and fuzzy AHP decision-making methods to determine the Zoonotic cutaneous leishmaniasis (ZCL) risk zones in northeastern Iran. They proved that AHP and FAHP techniques are powerful and useful to analyze high risk areas of ZCL. Chaiphongpachara et al. (2017) found that 9% of the total dengue hemorrhagic fever (DHF) areas were in the very high-risk areas, 23.89% in the high-risk areas, 13.14% in the moderate risk areas and 53.97% in the low-risk areas in Samut Songkhram province. Bohra and Andrianasolo (2001) applied GIS in modelling the Dengue risk based on sociocultural data in Rajasthan, India. In this case 5 classes of risk were classified from very low to very high, with 94.5% of validated samples being acceptably classified. Ai-leen and Song (2000) monitored Dengue in Singapore using GIS technique. The previous

studies proposed several main causes of disease outbreak such as socio-economic, epidemiological and environmental factors. The essential environmental criteria set for CHIKF risk area maps were in the order of importance. The most important factor was deemed the CHIKF patient number data and the second and third important factors were the number of population density and the household number data respectively. Land use/land cover and rainfall factors were considered as the fourth and fifth criteria in order of importance.

The main goal of the current study is to develop a map-based system indicating CHIKF risk areas in the south of Thailand. The five factors introduced (CHIKF patient number data, the number of population density, the household number data, land use/land cover and rainfall) are considered and combined using GIS and AHP techniques to categorize fire risk zones and derive a final risk map.

Materials and methods

Study area

The south of Thailand comprises of 14 provinces which are located between Andaman sea and the gulf of Thailand (*Fig. 1*) covering a total area of 71,506 km². Its climate is characterized as a tropical monsoon with 2 alternating seasons, notably the rainy season which lasts from May to December and the dry season lasting from February to April. The average temperature is 27.9 °C, the maximum average temperature is approximately 24.8 °C and the minimum average temperature is around 40.3 °C. The mean rainfall is approximately 2,066.7 mm. The topography of the region is lowlands and the north part of the provinces is high land and mountainous (Thai Meteorological Department, 2019).

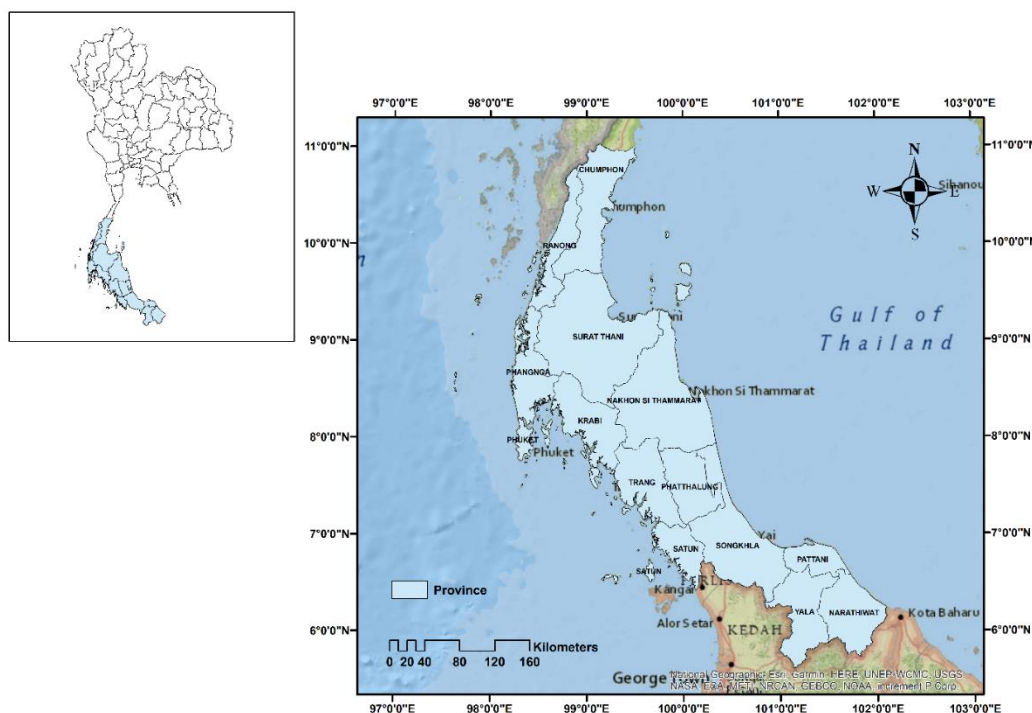


Figure 1. Study area in the south of Thailand

Chikungunya risk factors

Five factors were selected as representative of environmental, socio-economic and epidemiological parameters, which, in sequence of importance based on various research findings, are CHIKF patient number data, population density, the household number data, land use/land cover and rainfall data (Stolerman et al., 2019; Wahid, 2019; Delatte et al., 2010).

Rainfall

The main climatic factor considered to affect Chikungunya transmission is the humidity, which is directly associated to rainfall. As humidity provides suitable conditions for mosquito growth, rainfall impacts mosquito population density. The rainfall data (2019-2021) from the provinces of South Thailand were estimated by the climate data management system (CDMS) method by the Thai Meteorological Department. The average annual rainfall (mm) from 25 stations found in the study area were calculated and used. The kriging interpolation method was selected to build the average annual rainfall map. Then, the rainfall map was classified in five categories (very low, low, moderate, high and very high) as depicted in *Figure 2* (Chaiphongpachara, 2017).

Land use/Land cover (LU/LC)

LU/LC data is an important parameter in support of Chikungunya transmission. Crop cultivation, dense forest, built up and water body areas were considered as possible risk factors for CHIKF outbreak. Falling leaves from plants produce litter with high moisture which provides suitable environment for the mosquito habitats. The LULC data in 2019 were provided by the Land Development Department, Thailand. The LULC map was classified based on satellite imagery from THEOS and Landsat 8 OLI and with ground data. THEOS and Landsat 8 OLI images were selected from 2017-2019. A reclassification was implemented based on five categorical classes. The weight value was set based on the previous scientific findings (Jeefoo and Tripathi, 2011) and is described in *Table 1* and *Figure 2*.

Household density

The number of households considered as a weighted factor in CHIKF outbreak due to the fact that high household density areas provide vital insights into the epidemiology of CHIKF potential risk. Household density was calculated by the number of household in each province per km² area in 2020. The household data were collected from the Official statistics registration systems, The Bureau of Registration Administration (BORA), Thailand. As Choropleth map provides an intuitive display for the spatial distribution of density data, household density data was calculated using Choropleth technique in this study (*Fig. 2*) (Prabhala, 2008).

Population density

Population density is one of the most essential socio-economic factors concerning increasing CHIKF risk. Population data in 2020 were retrieved from Department of Provincial Administration, Thailand. Population density was calculated by population

number in each province per km² area. Subsequently, we used Choropleth map to classify 5 classes ranging from very low to very high (Fig. 2) (Somard et al., 2017).

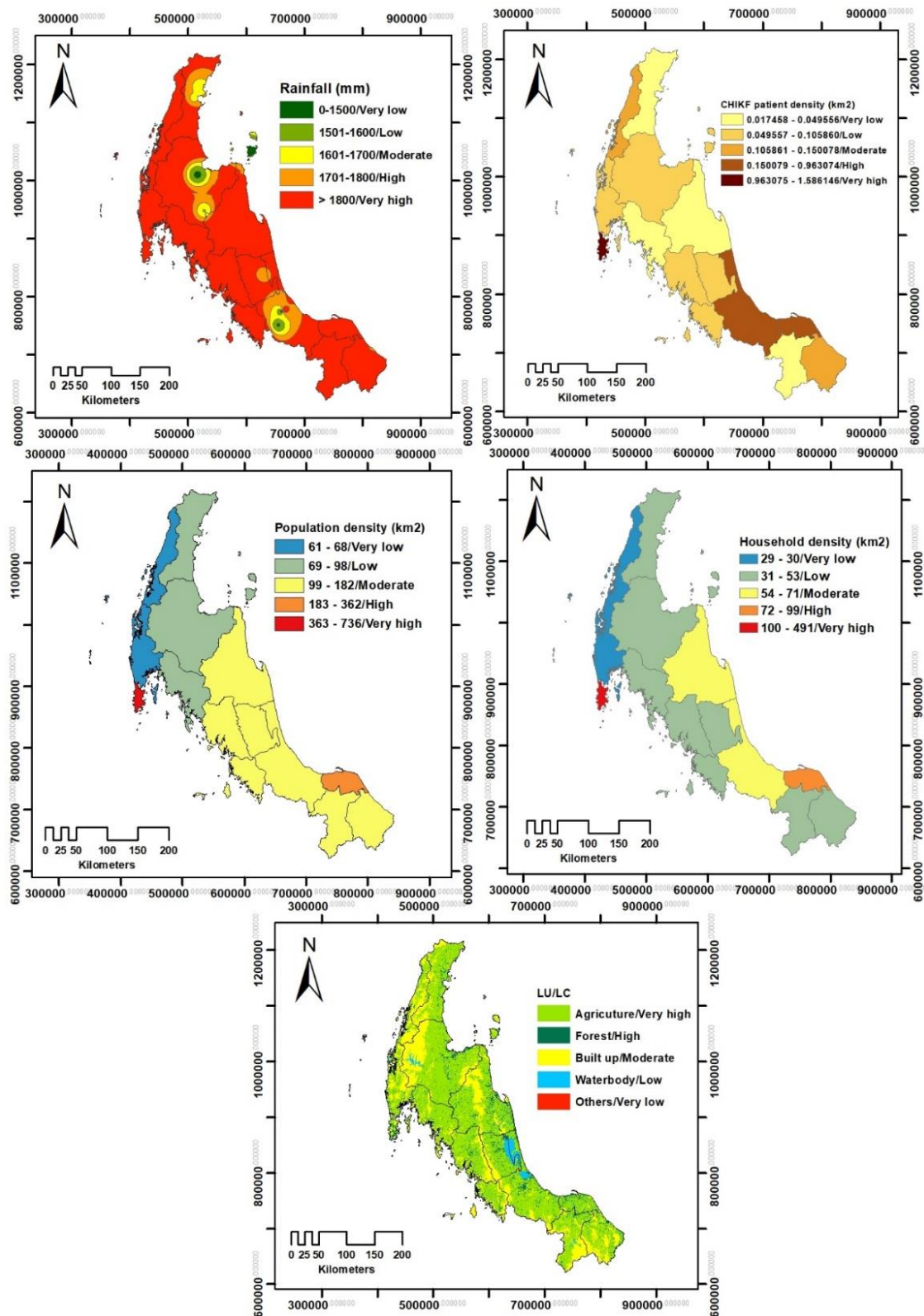


Figure 2. The individual input layers of (a) rainfall (mm), (b) CHIKF patient density (km²), (c) population density (km²), (d) household density (km²) and (e) LU/LC classification

Table 1. Factors, rank and weight for the environmental, socio-economic and epidemiological criteria

Criteria/factor	Class	Range	Weight	Reference
Rainfall (mm)	>1801 1701-1800 1601-1700 1501-1600 0-1500	5 (Very high) 4 (High) 3 (Moderate) 2 (Low) 1 (Very low)	0.07	Chaiphongpachara (2017)
Land use/Land cover	Agriculture Forest Built up Waterbody Others	5 (Very high) 4 (High) 3 (Moderate) 2 (Low) 1 (Very low)	0.11	Jeefoo and Tripathi (2011)
Household density (household number/km ²)	100-491 72-99 54-71 31-53 29-30	5 (Very high) 4 (High) 3 (Moderate) 2 (Low) 1 (Very low)	0.20	Prabphala (2008)
Population density (population number/km ²)	363-736 183-362 99-182 69-98 61-68	5 (Very high) 4 (High) 3 (Moderate) 2 (Low) 1 (Very low)	0.25	Somard et al. (2017)
CHIKF patient density (CHIKF case/km ²)	0.963075 - 1.586146 0.150079 - 0.963074 0.105861 - 0.150078 0.049557 - 0.105860 0.017458 - 0.049556	5 (Very high) 4 (High) 3 (Moderate) 2 (Low) 1 (Very low)	0.36	Somard et al. (2017)

CHIKF patient number data

CHIKF patient number data is the most important factor for analyzing the disease outbreak risk assessment and has been assigned the highest weight value in this multi-criteria model. The data of the DHF patient number in each province from 2019 to 2021 were derived from the Bureau of Epidemiology, Department of Disease Control, MoPH, Thailand. The intensity of CHIKF patient data in each province was calculated by patient number per km² area. For risk area, the intensity of CHIKF patient data in each area was grouped into 5 risk area classes (*Fig. 2*) (Somard et al., 2017).

Analytic hierarchy process (AHP)

We applied the AHP, which was developed by Saaty (1977), to estimate the weight or importance of each individual CHIKF risk factor. A qualitative hierarchy of importance among the five parameters is established by classifying the parameters with a pairwise comparison. The importance of each parameter was defined from the literature review as shown in *Table 1*. The values of each factor were classified into five levels (very low, low, moderate, high and very high). The weights for each factor were calculated by dividing the sum of each row with the total number of factor (*Table 1*). The consistency index (CI) and the consistency ratio (CR) were calculated based on the *Equations 1* and *2*, respectively.

$$CI = \frac{\lambda_{max} - n}{n - 1} \quad (\text{Eq.1})$$

where λ_{max} is the maximum Eigen value of the comparison matrix, n is the dimension of comparison matrix.

$$CR = \frac{CI}{RI} \quad (\text{Eq.2})$$

where RI is the Random Consistency Index and if $CR \leq 0.10$ is considered acceptable.

In this research, CI is 0.04 and RI is 1.12; thus, CR is 0.03 which is less than 0.10. Then the weights calculated are considered acceptable.

The final CHIKF risk map was derived based on the linear combination of five criteria with the weights for each factor from the AHP as *Equation 3*.

$$\text{CHIKF risk} = 0.07 \times \text{Rainfall} + 0.11 \times \text{LULC} + 0.20 \times \text{Household density} + 0.25 \times \text{Population density} + 0.36 \times \text{CHIKF patient data} \quad (\text{Eq.3})$$

Results

The CHIKF risk map was generated based on five factors related to rainfall, LULC, household density, population density and CHIKF patient data. The spatial layer of each factor was reclassified into five risk classes, namely very high, high, moderate, low and very low as presented in *Figure 2*.

Moreover, the percentage and zone of the CHIKF risk map were calculated (*Table 2*). The study area, which covers an area of approximately 71,506.10 km², was categorized as 0.79% of very high class (562.77 km²), 13.23% of high class (9,458.89 km²), 61.59% of moderate class (44,039.27 km²), 24.39% of low class (17,439.26 km²) and 0.01% of very low class (5.91 km²) as presented in *Table 2*. The final CHIKF risk map in the south of Thailand is presented in *Figure 3*. It indicated that very high- and high-risk areas were found in association with environmental, socio-economic and epidemiological parameters. Phuket province is classified as very high CHIKF risk area and Songkhla and Pattani provinces are classified as high CHIKF risk area. The main reason is the highest of CHIKF cases density reported in Phuket, Songkhla and Pattani provinces. Furthermore, the very high- or high-risk areas were calculated where the household density was greater than 72 households/km², population density was more than 183 persons/km² and CHIKF patient density was higher than 0.2 cases/km². Also, agriculture and forest areas of land use and land cover layer were considered as high and very high risk and the quantity of rainfall (mm) was more than 1,701 mm (*Fig. 2*). On the other hand, Krabi, Phangnga and Chumphon provinces were indicated in low CHIKF risk area. Environmental factors such as rainfall (mm) was lower than 1600 mm and waterbody and others (other miscellaneous lands) were considered low and very low classes. For epidemiological parameters, CHIKF patient density (km²) was less than 0.05 case/km². Moreover, the household density was lower than 53 households/km², the population density was less than 98 persons/km² in case of socio-economic factors. Ranong, Surat Thani, Nakorn Si Thammarat, Trang, Phattalung, Satun, Yala and Narathiwat provinces were classified as moderate CHIKF risk areas. The factors were analyzed for moderate class; the quantity of rainfall (mm) factor was the value between 1601-1700 mm; the built-up area was considered for this

level; the household density areas were displayed between 54-71 household number/km²; the population density areas were presented between 99-182 population number/km² and CHIKF patient density areas were showed between 0.11 - 0.15 CHIKF case/km². The Bureau of Epidemiology, Department of Disease Control, Ministry of Public Health, Thailand reported the number of Chikungunya patient cases per province for 14 provinces in the south of Thailand between 2011 and 2021 (Fig. 4). (The Department of Disease Control, Thailand (2021). It was found that Songkhla province had the highest CHIKF patient cases (4,250 cases) while Nakorn Si Thammarat province indicated the lowest CHIKF patient cases (174 cases). Figure 5 indicates that the number of CHIKF disease patients is in strong correlation with the CHIKF disease risk assessment map. For example, Phuket, Songkhla and Pattani provinces have high CHIKF diseased patients which relate to very high and high class CHIKF disease risk assessment map while Chumphon, Phangnga and Krabi provinces identified as low class which related to low CHIKF diseased patients.

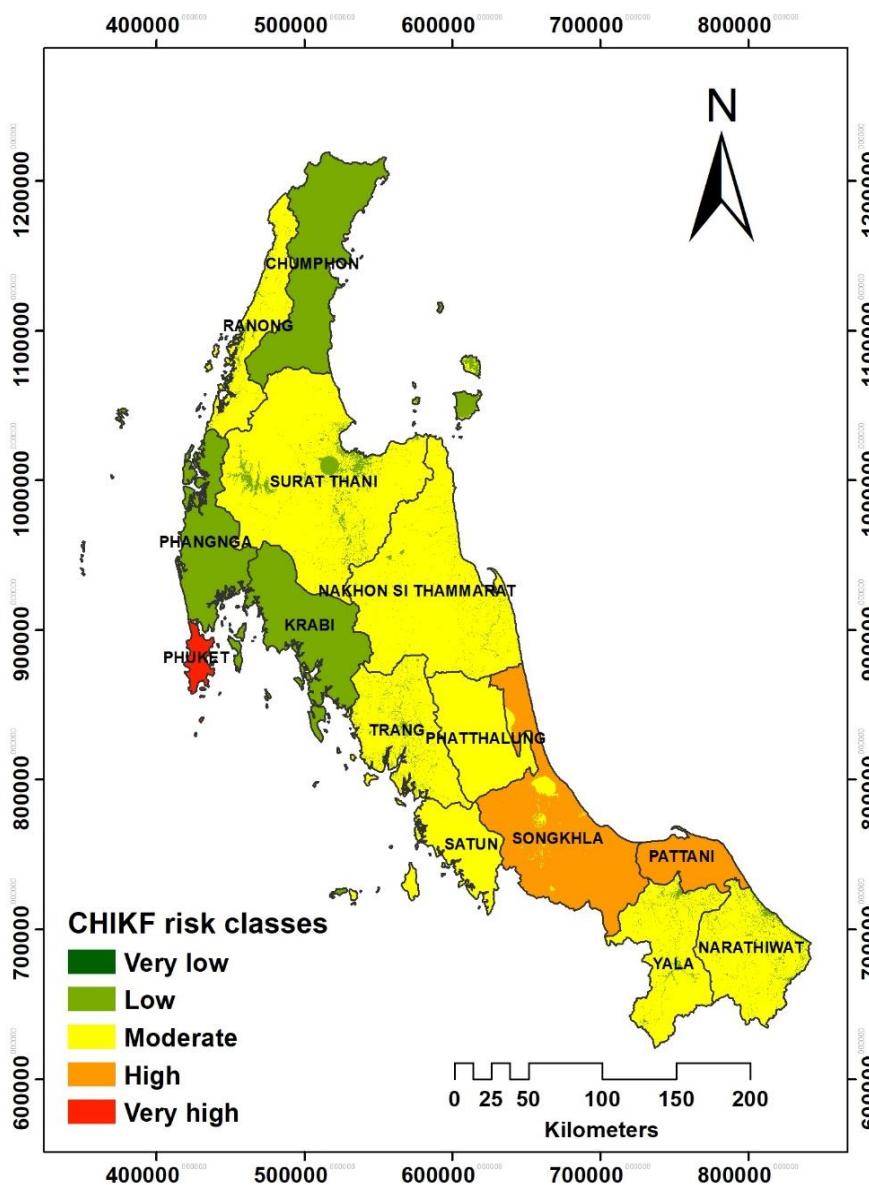


Figure 3. The final CHIKF risk map

Table 2. Percentage and area coverage of the CHIKF risk map

CHIKF class	Area (km ²)	Area (%)
Very high	562.77	0.79
High	9,458.89	13.23
Moderate	44,039.27	61.59
Low	17,439.26	24.39
Very low	5.91	0.01
Total	71,506.10	100

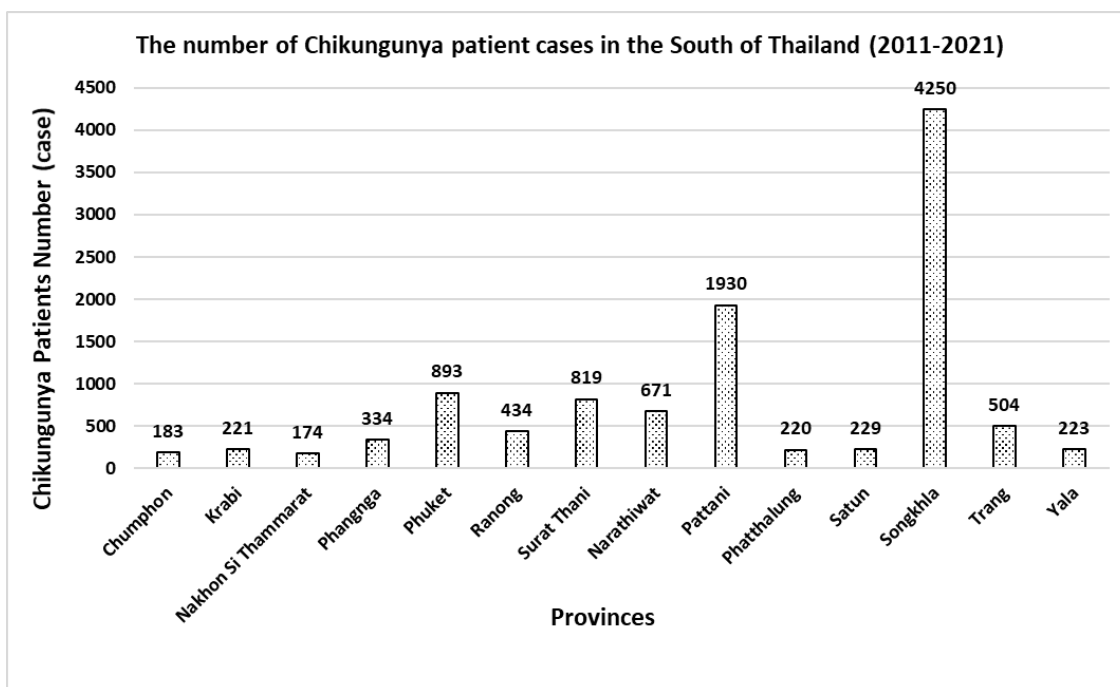


Figure 4. The number of chikungunya patient cases per province for the 14 administrative provinces in the south of Thailand between 2011 and 2021 (The Department of Disease Control, Thailand (2021))

Discussion

In this research, GIS and AHP techniques were selected to analyze five CHIKF-related parameters (namely rainfall, LU/LC, household data, population data and CHIKF patient data) and derive a CHIKF risk map covering 14 provinces in the south of Thailand. The results indicated that the Phuket province is assigned a very high CHIKF risk category and Songkhla and Pattani provinces are classified as high CHIKF risk class (Fig. 3). Interestingly, the same pattern occurs in the assessment of the CHIKF risk based on the number of Chikungunya patient cases in 14 provinces of the south of Thailand. Songkhla, Pattani and Phuket province showed the top three highest cases in the south of Thailand which were 4,250, 1,930 and 893 cases, respectively (Fig. 4). Ranong, Surat Thani, Nakorn Si Thammarat, Trang, Phatthalung, Satun, Yala and Narathiwat provinces were assigned a moderate CHIKF risk areas. Most of them related to the number of Chikungunya patient cases except Nakorn Si Thammarat province. Even though Nakorn Si Thammarat province showed the lowest cases for the

last 10 years, household density (km²) and population density (km²) were classified in moderate groups. Moreover, the south of Thailand receives comparatively higher amounts of rainfall than other parts of Thailand during the rainy season and the inhabitants' main occupation is related to agriculture, therefore Nakorn Si Thammarat province was considered as moderate class based on all factors. Chumphon, Phangnga and Krabi provinces were classified as low CHIKF risk category which concerned on the number of Chikungunya patient cases and household density (km²), population density (km²) and CHIKF cases density were classified low and very low classes.

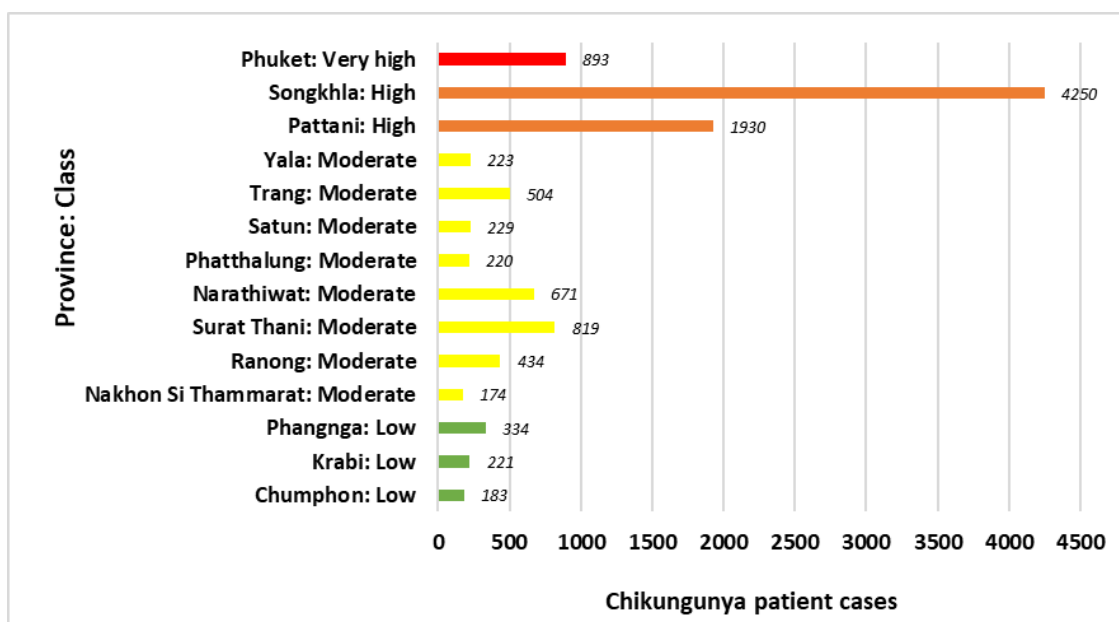


Figure 5. Chikungunya patient cases with the disease risk assessment class in 14 provinces

For the singular input layers, the rainfall data were selected for maintaining the solidity of the methodology in the spatial context. The rainfall data were derived by spatially interpolating the data from 25 Thai Meteorological stations covering 14 provinces in the south of Thailand. As the rainy season lasts for many months from May to December, the amount of rainfall is comparatively higher than other parts of Thailand. Therefore, very high and high classes were classified in the rainfall map for one of the criteria for analyzing CHIKF risk area. LU/LC layer is the fourth most important contributing factor in the overall CHIKF risk area. It is the very high and high risk category of the LU/LC class, mainly agriculture and forest. The three layers related to proximity to epidemiological parameters, CHIKF patient density (km²), population density (km²) and household density (km²). We calculated data in each province related to each area per spatial unit and classified in 5 classes. The higher number of CHIKF patient, population and household have a higher chance of contracting the CHIKF disease. This study using the AHP technique to apply multiple variables to identify CHIKF risk area, which several studies have attempted with similar factors and using AHP tool for analyze the diseases from mosquitoes. Similar results were found by Ali and Ahmad (2018) who applied the AHP and GIS techniques to derive a Dengue risk map in West Bengal, India. Six criteria (population density, household density, water area, LU/LC, temperature and elevation) were selected in this study. The most

important factors were the household and population data. Chaiphongpachara et al. (2017) used population density, household number data for most influential factors to map dengue hemorrhagic risk province in Samut Songkhram province. Last but not least, Dom et al. (2016) proved that GIS-based AHP has a strong ability to predict disease from a mosquito risk map in Subang Jaya, Malaysia. From previous studies and our results we reckon that AHP technique is a powerful tool to help the local government to make a plan for CHIKF disease preparedness and mitigation.

Conclusions

In this research, CHIKF risk was estimated based on the combined application of AHP and GIS techniques based on five individual input layers representative of environmental, socio-economic and epidemiological parameters. Five factors are the main important criteria, either directly or indirectly, related to the occurrence of CHIKF disease risk. The model indicated that the Phuket province has a very high CHIKF risk class while Chumphon, Phangnga and Krabi provinces are classified as low CHIKF risk class. The results are in agreement with the number of CHIKF patients. The AHP application presented that the method is useful and powerful for assessing the CHIKF risk in this specific area. The results can help the people and organizations to create decision making processes. It is envisaged that the AHP technique can be applied in vector-borne diseases such as dengue, malaria etc.

Acknowledgements. This research was supported by National Science, Research and Innovation Fund (NSRF) and Prince of Songkla University (Grant No: ENV6505006S).

Conflict of interests. The authors declare no conflict of interests.

REFERENCES

- [1] Ahmad, F., Goparaju, L., Qayum, A. (2017): Studying malaria epidemic for vulnerability zones: multi-criteria approach of geospatial tools. – *Journal of Geoscience and Environment Protection* 5(5): 30-53.
- [2] Ai-Leen, G. T., Jin Song, R. (2000): The use of GIS in ovitrap monitoring for dengue control in Singapore. – *Dengue Bulletin* 24: 110-116.
- [3] Akiner, M. M., Demirci, B., Babuadze, G., Robert, V., Schaffner, F. (2016): Spread of the invasive mosquitoes *Aedes aegypti* and *Aedes albopictus* in the Black Sea region increases risk of chikungunya, dengue, and Zika outbreaks in Europe. – *PLoS Neglected Tropical Diseases* 10(4): e0004664.
- [4] Ali, S. A., Ahmad, A. (2018): Using analytic hierarchy process with GIS for Dengue risk mapping in Kolkata Municipal Corporation, West Bengal, India. – *Spatial Information Research* 26(4): 449-469.
- [5] Ali, S. A., Ahmad, A. (2019): Mapping of mosquito-borne diseases in Kolkata Municipal Corporation using GIS and AHP based decision making approach. – *Spatial Information Research* 27(3): 351-372.
- [6] Bohra, A., Andrianasolo, H. (2001): Application of GIS in modeling dengue risk based on sociocultural data: case of Jalore, Rajasthan, India. – *Dengue Bulletin* 25: 92-102.
- [7] Chaiphongpachara, T., Pimsuka, S., Ayudhaya, W. S. N., Wassanasompong, W. (2017): The application of geographic information system in dengue haemorrhagic fever risk assessment in samut Songkhram province, Thailand. – *International Journal of GEOMATE* 12(30): 53-60.

- [8] Chastel, C. (1963): Human infections with chikungunya virus or a closely related virus in Cambodia. II. Experimental pathological anatomy. – *Bulletin de la Société de Pathologie Exotique* 56(5): 915-24.
- [9] Dai, V. Q., Thoas, N. T. K. (1967): Enquete sur les anticorps anti-chikungunya chez des enfants Vietnamiens de Saigon. – *Bull. Soc. Pathol. Exot. Filiales* 4: 353-359.
- [10] Delatte, H., Desvars, A., Bouétard, A., Bord, S., Gimonneau, G., Voure'h, G., Fontenille, D. (2010): Blood-feeding behavior of *Aedes albopictus*, a vector of Chikungunya on La Réunion. – *Vector-Borne and Zoonotic Diseases* 10(3): 249-258.
- [11] Department of Disease Control, Thailand (2021): Department of Disease Control Weekly Disease Forecast No.179_Chikungunya. – <https://ddc.moph.go.th/en/> (accessed on 5 Sep 2021).
- [12] Dom, N. C., Ahmad, A. H., Abd Latif, Z., Ismail, R. (2016): Application of geographical information system-based analytical hierarchy process as a tool for dengue risk assessment. – *Asian Pacific Journal of Tropical Disease* 6(12): 928-935.
- [13] Garcia, M., Lipskiy, N., Tyson, J., Watkins, R., Esser, E. S., Kinley, T. (2020): Centers for Disease Control and Prevention 2019 novel coronavirus disease (COVID-19) information management: addressing national health-care and public health needs for standardized data definitions and codified vocabulary for data exchange. – *Journal of the American Medical Informatics Association* 27(9): 1476-1487.
- [14] Hammon, W. M., Rundnick, A., Sather, G. E. (1960): Viruses associated with epidemic hemorrhagic fevers of the Philippines and Thailand. – *Science* 131(3407): 1102-1103.
- [15] Jeefoo, P., Tripathi, N. K. (2011): Dengue risk zone index (DRZI) for mapping dengue risk areas. – *International Journal of Geoinformatics* 7(1): 53-62.
- [16] Kaslow, R. A., Evans, A. S. (1997): Epidemiologic concepts and methods. – In *Viral Infections of Humans*: 3-58.
- [17] Malczewski, J. (1999): *GIS and Multicriteria Decision Analysis*. – John Wiley & Sons, Hoboken, NJ.
- [18] Marchette, N. J., Rudnick, A., Garcia, R., MacVean, D. W. (1978): Alphaviruses in Peninsular Malaysia: I. Virus isolations and animal serology. – *The Southeast Asian Journal of Tropical Medicine and Public Health* 9(3): 317-329.
- [19] Ministry of Tourism and Sports (2019): *Tourism Statistics 2019*. – <https://mots.go.th/index.php> (accessed on 25 Jan 2020).
- [20] Mollalo, A., Khodabandehloo, E. (2016): Zoonotic cutaneous leishmaniasis in northeastern Iran: a GIS-based spatio-temporal multi-criteria decision-making approach. – *Epidemiology & Infection* 144(10): 2217-2229.
- [21] Prabphala, S. (2008): Using geographic information system to identify environmental factors for risk area of dengue hemorrhagic fever infection: a case study in Chaiyaphum province. – *Journal Remote Sensing GIS Association Thailand* 9(3): 24-34.
- [22] Ramachandran, V., Malaisamy, M., Ponnaiah, M., Kaliaperuaml, K., Vadivoo, S., Gupte, M. D. (2012): Impact of chikungunya on health-related quality of life Chennai, South India. – *PLOS one* 7(12): e51519.
- [23] Richardson, D. B., Volkow, N. D., Kwan, M. P., Kaplan, R. M., Goodchild, M. F., Croyle, R. T. (2013): Spatial turn in health research. – *Science* 339(6126): 1390-1392.
- [24] Saaty, T. L. (1977): A scaling method for priorities in hierarchical structures. – *Journal of Mathematical Psychology* 15(3): 234-281.
- [25] Saaty, T. L. (1990): How to make a decision: the analytic hierarchy process. – *European Journal of Operational Research* 48(1): 9-26.
- [26] Sarkar, N., Sarkar, S., Kozloff, L. M. (1964): Tail components of T2 bacteriophage. I. Properties of the isolated contractile tail sheath. – *Biochemistry* 3(4): 511-517.
- [27] Siddiqui, M. Z., Everett, J. W., Vieux, B. E. (1996): Landfill siting using geographic information systems: a demonstration. – *Journal of Environmental Engineering* 122(6): 515-523.

- [28] Slemons, R. D., Haksohusodo, S., Suharyono, W., Harundriyo, H., Laughlin, L. W., Cross, J. (1984): Chikungunya viral disease in Jogjakarta, Indonesia. – In 33rd Annual Meeting of the American Society of Tropical Medicine and Hygiene.
- [29] Somard, J., Suwanlee, S. R., Turnbull, N., Phommat, T. (2017): Analyzing dengue fever risk areas using geographic information systems in Dome Pradis Sub-district, Nam Yuen District, Ubon Ratchathani Province. – *Journal of Medicine and Health Sciences* 24(3): 65-76.
- [30] Stolerman, L. M., Maia, P. D., Kutz, J. N. (2019): Forecasting dengue fever in Brazil: an assessment of climate conditions. – *PloS One* 14(8): p.e0220106.
- [31] Thai Meteorological Department (2019): Climatological Center 2019. – <http://climate.tmd.go.th/> (accessed on 25 Mar 2020).
- [32] Tuanudom, R., Yurayart, N., Tiawsirisup, S. (2017): Effects of Chikungunya virus titers in blood meals on virus infection, dissemination, and transmission in Asian tiger mosquito: *Aedes albopictus* (Diptera: Culicidae). – *The Thai Journal of Veterinary Medicine* 47(2): 233-240.
- [33] Tuite, A. R., Watts, A. G., Khan, K., Bogoch, I. I. (2019): Countries at risk of importation of chikungunya virus cases from southern Thailand: a modeling study. – *Infectious Disease Modelling* 4: 251-256.
- [34] Wahid, B. (2019): Current status of dengue virus, poliovirus, and chikungunya virus in Pakistan. – *Journal of Medical Virology* 91(10): 1725-1728.

ESTIMATION OF ECOLOGICAL ASSET VALUES IN SHANGRI-LA BASED ON REMOTELY SENSED DATA

PAN, J. Y.^{1,2,3} – WANG, J. L.^{1,2,3*} – LIU, G. J.⁴ – GAO, F.⁵

¹*Faculty of Geography, Yunnan Normal University, Kunming 650500, China*

²*Key Laboratory of Resources and Environmental Remote Sensing for Universities in Yunnan, Kunming 650500, China*

³*Center for Geospatial Information Engineering and Technology of Yunnan Province, Kunming 650500, China*

⁴*College of Resources and Environment, Yunnan Agricultural University, Kunming 650201, China*

⁵*Yunnan Minzu University, Kunming 650500, China*

**Corresponding author
e-mail: jlwang@ynnu.edu.cn*

(Received 12th Jun 2021; accepted 3rd Sep 2021)

Abstract. Ecological assets are an important material base of the national economy and sustainable social development. Shangri-La, China is an important area of forest and farmland that has been returned to forest, but the ecological environment is fragile. It is urgent to start to an ecological asset values estimation study. Choosing remote sensing data, meteorological data, surface observations and statistics as the data sources. The results show: (1) From the perspective of ecological assets, adjusting climate and water conservation contribute the most. (2) In the context of single ecological asset value per unit area, the sequence from highest to lowest is the following, water conservation > adjusting climate > soil and water conservation > production of organic matter > nutrient circulation > cultural entertainment. (3) From the perspective of the type of ecological system, forest and shrub grassland contribute the most. (4) From the value of ecological assets per unit area of each ecosystem type, agricultural land > forest > shrub grassland > waters > wetland > artificial land > permanent snow glacier > unutilized land. It is particularly significant for people to make reasonable decisions when exploiting and utilizing natural resources which can be aided by an ecological asset values estimation study.

Keywords: *ecological environment, ecosystem services, CASA model, soil and water conservation, net primary productivity*

Introduction

Ecosystem not only provides humans with the necessary raw materials for life and production, but also the products and services it provides are also important assets that humans rely on for survival and development (Luo, 2008). In the 1970s, scholars such as Holdern (1974) and Westman (1977) began to study global ecosystem services, and the concept of ecological asset value evaluation also came into being. In recent years, China and foreign countries have begun to calculate the value of ecological assets from the perspective of different regional scales (Xu et al., 2012; Chen et al., 2012; Xing, 2020) and different ecosystem types (Han et al., 2000; Yu, 2005). Such as Daily et al. (2009) analyzed the role played by the integration of ecosystem services into decision-making, Richmond et al. (2007) analyzed the contribution of ecological assets to GDP and used this contribution to calculate the empirical price of ecosystem services, Gadaud and Rambolinaza (2010) conduct research on methods and technologies of ecological

asset evaluation, and evaluate the compensation value of fire risk willingness in the Landes area of France, Byeori et al. (2017) use keywords to analyze recent developments in ecological asset research and guide the research direction of future ecosystem asset analysis in Korea. In general, in terms of research content, most foreign countries have made systematic and in-depth estimates for several of the ecosystem services (Daily, 1997; Gómez et al., 2013; Delphin et al., 2016); in China, the main focus is on exploring the concept of ecological assets, constructing an index system for ecological assets, and accounting for the value of ecological assets (Gao et al., 2007; Sun et al., 2008). In terms of research methods, foreign estimation methods mainly include InVEST model, ESR model, ARIES model and SoLVES model (Polasky et al., 2011; Bagstad et al., 2013), Most of these models only account for a single or a few items of ecological service value, and some models are currently only suitable for value evaluation in a very small number of areas. The evaluation methods studied in China mainly include two types. One is to use the unit area value method to estimate ecological assets, for example, Xie et al. (2008) have optimized the value system based on Costanza et al. (1997) and established a value standard system suitable for domestic ecological asset evaluation, and then there have been many related research cases (Ouyang et al., 2013; Liu et al., 2013; Chen, 2021), The disadvantage of this method is that it cannot reflect the temporal and spatial differences of different ecosystems and regions. The other is to obtain different ecological parameters through the establishment of measurement models, and to estimate the value of ecological assets by remote sensing. For example, Zhu et al. (2007) and others have used remote sensing technology to establish an ecological asset calculation model to dynamically assess China's terrestrial ecological assets, but the accuracy of this method is heavily dependent on the established measurement model and the acquired ecological parameters. In general, most of the current studies underestimate the total value of ecological assets and only account for the value of ecosystem services. Although the value of natural resources is included in the very few studies, the results cannot fully reflect the value of natural resources and are related to ecosystems. Some information overlaps in service value accounting (Zhang et al., 2004; Hou et al., 2015; Sun et al., 2017; Wang, 2019). In addition, most of the current researches only carry out static or dynamic estimation of the total amount of ecological assets, and the research scope is limited to the indicator system and accounting methods, and lacks management strategies and suggestions for regional economic and social development and ecological asset conditions.

At the same time, scholars in China and abroad have explored and studied the estimation of ecological assets from various perspectives. However, due to the enormous difficulties in the determination of cost assessment methods and data acquisition, no scholars have been able to complete the resource and environmental accounting in a comprehensive way. For Shangri-La, due to limited data, it is impossible to estimate the value of natural resources, such as mineral resources, biological resources, mobile resources, environmental resources and land resources. In fact, there is a certain relationship between the value of natural resources and the value of ecological services. That is, part of the natural resources is calculated when assessing the value of the ecological services resource value. Therefore, the ecological asset valuation in this study estimated only six values of ecosystem services.

It is of special significance to select Shangri-La in Diqing Prefecture of Northwest Yunnan as the research area to carry out remote sensing estimation of ecological assets. First, Yunnan Province is a high-value area with dense ecological assets in China, while

Northwest Yunnan is the main forest area in Yunnan Province and has high forest coverage. Before the implementation of relevant forestland protection policies in Shangri-La, the main financial revenue of the area came from forestry production. In 1999, Yunnan Province launched the Natural Forest Conservation Project and the Project of Converting Farmland to Forestry and Grassland, and the ecological environment of Yunnan Province has changed accordingly. Second, the study site is located in the middle and upper reaches of the Hengduan Mountains and international rivers, and its ecosystem is fragile. The changes in terrestrial ecosystem assets (especially its forest ecosystem) can reflect global changes to a certain extent. In addition, the study area is located in the hinterland of a World Natural Heritage Site with three parallel rivers in Yunnan Province, which is one of the 20 biodiversity hotspots designated by the WWF. Finally, there is a lack of research on remote sensing measurements of medium-scale ecological assets in Yunnan Province (Liu et al., 2007; Chen et al., 2007; Shi et al., 2009). Therefore, the remote sensing estimation of the ecological assets in Shangri-La and the timely and accurate grasp of the ecological assets in the Northwest Yunnan Converted Farmland to Forest Area can provide a scientific basis for the construction and protection of the ecological environment in the study area, as well as the relevant government decisions.

Materials and Methods

Location and description of the study area

Shangri-La is located in the northwestern part of Yunnan Province, China, which is in the eastern part of Diqing Tibetan Autonomous Prefecture, between 26°52' ~ 28°52' N and 99°22' ~ 100°19' E. It is the location of the "Tea-Horse Ancient Road". Shangri-La is adjacent to Daocheng County and Muli County in Sichuan Province in the east, Lijiang city in Yunnan Province in the south, Lijiang city in Yunnan Province across the river, Deqin County in Diqing Tibetan Autonomous Prefecture and Weixi County in the west, and Derong County and Xiangcheng County in Sichuan Province in the north. The shape of Shangri-La is narrow at both ends and wide in the middle. The widest distance between the east and west is approximately 88 km, and the distance between the north and south is approximately 218 km. Therefore, the shape of Shangri-La is similar to a narrow willow-shaped zone (*Fig. 1*). The total land area of the county is approximately 11613 km², which is the largest county-level city in Yunnan Province (Wang et al., 2004; Yang, 2009). A total of 11 townships are divided into 4 towns and 7 townships. The 4 towns are Jiantang town, Xiaozhongdian town, Jinjiang town and Hutiaoxia town; the seven townships are Nixi township, Dongwang township, Gezan township, Shangjiang township, Sanba Naxi Nationality township and Wujingxiang township.

Shangri-La is located in the north and south of China. The topography is high in the northwest and low in the southeast. The highest point is Balagozhong, with an elevation of 5545 m. The lowest point is Luojihan, with an elevation of 1503 m. The difference between the highest and lowest elevations is 4042 m, and the average elevation of the county is 3459 m (*Fig. 2a*), the data was captured on the geospatial data cloud platform (<http://www.gscloud.cn>). Shangri-La is rich in biological and mineral resources. There are 4 seasons in the mountains and 10 miles in different days. It has a three-dimensional climate pattern and a variety of soil types (*Fig. 2b*). The map of soil types was obtained from 1:200,000 Diqing Soil Distribution Map by geometric correction and vectorization.

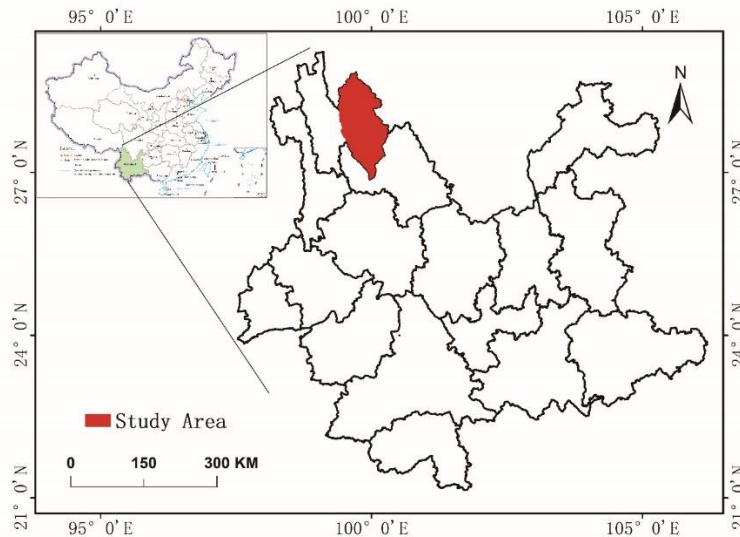


Figure 1. Research Location Map

Note: the map is based on the standard map with drawing review No. GS (2019) 1825 downloaded from the standard map service website of the State Bureau of surveying, mapping, and geographic information of China (<http://bzdt.ch.mnr.gov.cn>), and the base map is not modified.

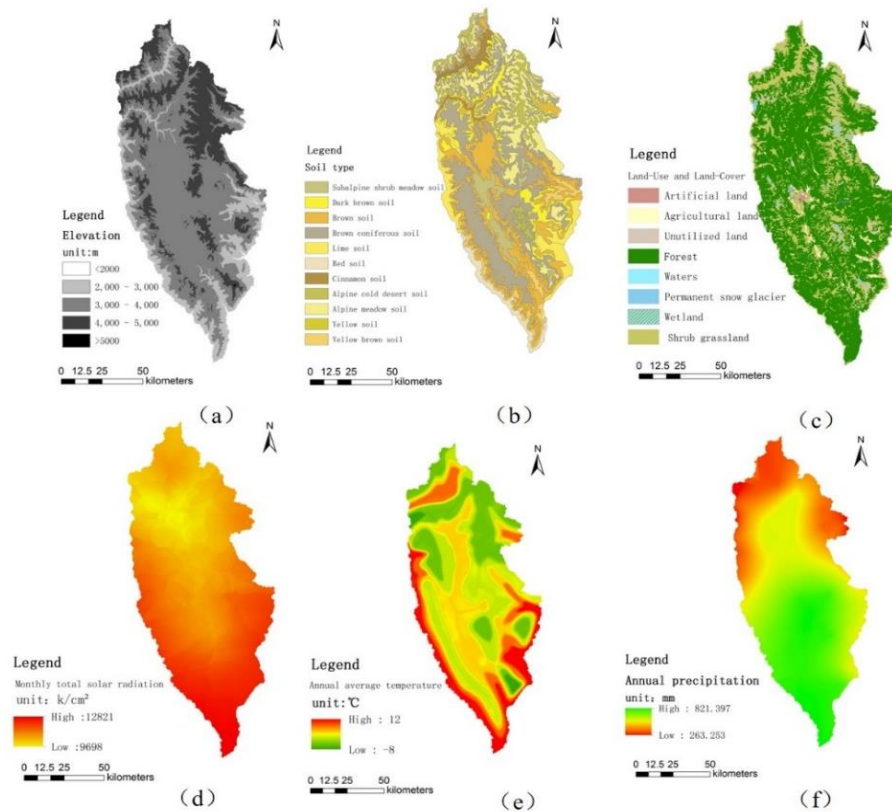


Figure 2. Related images of the study area:(a) Elevation Distribution;(b) Soil Types;(c) Land Use and Land Cover;(d) Monthly Solar Total Radiation Interpolation Chart;(e) Annual Average Temperature;(f) Annual Precipitation

Data sources

Remote sensing image data: The remote sensing data include Terra MODIS (Moderate Resolution Imaging Spectroradiometer, MODIS) MOD09A1 data. Representative MOD09A1 data from July 2013 with a spatial resolution of 500 m × 500 m were selected from the geospatial data cloud, and the Landsat TM (Thematic Mapper, TM) remote sensing images were selected. The date of acquisition was November 12, 2013. The resolution from the geospatial data cloud was 30 m × 30 m. The reason why to choose the images in November is that the image quality in November is the best, however, in June to August is the rainy season in the study area with heavy cloud cover and poor image quality. The MODIS image data and Landsat TM image data were geometrically corrected and tailored. To better analyze and apply the data quantitatively, the MODIS data were resampled to 397 × 946 and then resampled as necessary.

DEM (Digital Elevation Model, DEM): A 1:50,000 DEM with UTM (Universal Transverse Mercator, UTM) projection mode was used.

Meteorological data: The meteorological data included the monthly precipitation, the monthly average temperature and the total monthly solar radiation, and the data were obtained from the Zhongdian County Climate Data. From Zhong Dian County Agricultural Climate Division (Zhongdian County Agricultural Zoning Committee, 1986), we obtain the contour map of the annual average temperature and the annual precipitation contour map of Shangri-La. Finally, in the case of the DEM, the meteorological element raster dataset with the same pixel size, the NDVI (Normalized Difference Vegetation Index, NDVI) data (250 m × 250 m) and the same projection mode was obtained by kriging interpolation. NDVI is derived from MODIS data using the difference between the near-infrared and red bands and the ratio of the sum of the two bands.

$$NDVI = (NIR - R) / (NIR + R) \quad (\text{Eq.1})$$

In the formula, *NIR* is the band of near-infrared, *R* is the band of red.

Other geographic base map data: The 1:200,000 soil type maps of Diqing Tibetan Autonomous Prefecture were scanned, digitized and projected, and the land use classification map of Shangri-La in 2013 was projected by UTM. To facilitate the spatial analysis of relevant data, we unified the coordinate system and projection method of all the above data. The coordinate system was WGS-84; the projection mode was UTM; the Zone was 47; and the spatial unit of measure was meters.

Classification of land use by remote sensing

Landsat TM images were used to classify the three-level classification system into the first-level classification system by means of manual interaction and visual interpretation. The classification system refers to (Table 1). The image interpretation results were verified by field survey sample data and GPS points (Wang and Li, 2004; Wang et al., 2004; Jiang, 2004), with an accuracy of 81.09%, which met the research requirements. The field survey was conducted in all towns and villages of Shangri-La in 2013, including approximately 525 samples of various land use and land cover types like woodland, shrub grassland, water area, agricultural land, artificial land, unused land, wetland and so on.

The main land use classification types in the study area were construction land, traffic land, cultivated land, garden land, natural forest, shrub forest, grassland, inland swamp,

river, lake, reservoir, bare land and permanent snow glacier. And, most of the forest in Shangri-La are natural forests. According to the research needs, the ecosystem types in the study area were classified into 8 categories: forest, shrub grassland, waters, agricultural land, artificial land, unutilized land, wetland and permanent snow glacier (Chen et al., 2001; Du et al., 2004) (Fig. 2c).

Table 1. Land Use/ Land Cover Classification System

Class I	Class II	ClassIII
Artificial land	Land used for building	Urban land use
	Traffic land	Rural residential areas
Agricultural land	Cultivated land	Highway land
	Garden plot	Airport land
	Natural forests	Paddy field
Forest	Natural forests	Dry land
		Orchard
Shrub grassland	Shrub grassland	Deciduous forest
		Evergreen forest
Wetland	Inland wetland	Shrub wood
		Grassland
Waters	Inland waters	Inland marsh
		River
		Lake
Unutilized land	Bare land	Reservoir
		Bare land
		Bare rock
Permanent snow glacier	Sand	River flat
	Permanent snow glacier	Permanent snow glacier

Models and methods

The values of ecological assets are not fixed. Generally, the values will change with time. The total value of ecological services and natural resources provided by all ecosystem types in a region constitutes the total value of the ecological assets. This value will change with changes in ecosystem area and quality.

$$V = \sum V_c \quad (\text{Eq.2})$$

$$V_c = \sum \sum R_{ij} * V_{c_i} * S_{ij} \quad (\text{Eq.3})$$

In the formula, i is the performance of the ecosystem service value of ecosystem type i in ecosystem type C , V_{c_i} is the unit area value of the ecosystem service value of ecosystem type i in ecosystem type C ; j is the total number of pixels in ecosystem type C ; S_{ij} is the spatial resolution, and R_{ij} represents the adjustment coefficient.

Estimation of adjustment coefficient

According to previous research results (Pan et al., 2004), vegetation coverage and NPP (Net Primary Productivity, NPP) are generally used to represent the quality of ecosystems.

$$R_{ij} = \left[\left(\frac{NPP_j}{NPP_{mean}} + \frac{f_j}{f_{mean}} \right) / 2 \right] \quad (\text{Eq.4})$$

In the formula, NPP_{mean} is the average NPP of the ecosystem, f_{mean} is the average vegetation coverage, NPP_j is the NPP of the j pixel, and f_j is the vegetation coverage of the j pixel (Pan, 2004).

Estimation of NPP

NPP refers to the amount of organic matter accumulated by green plants per unit time and area. It is the total amount of organic matter produced by plant photosynthesis minus the remaining part after autotrophic respiration. Traditional NPP measurement methods are easily restricted by natural conditions, and the development of remote sensing technology provides data support for the dynamic estimation of NPP. Among the existing NPP estimation models, the CASA (Carnegie Ames Stanford Approach, CASA) model has attracted attention due to its advantages of fewer parameters and simple calculation process, and has been widely used in global and regional NPP estimation.

Eight different types of ecosystem NPPs, including agricultural land, forest, shrub grassland, wetland, artificial land, waters, unutilized land and permanent snow glacier, were estimated using the experience of previous CASA models. The CASA model is mainly based on remote sensing data, which are driven by vegetation types, soil and soil distribution and meteorological data. This model is a type of light energy utilization model. The NPP value of the model is calculated according to the photosynthetic active radiation, temperature and water stress coefficients and the maximum light energy conversion rate (Potter et al., 1997).

$$NPP(x,y) = APAR(x,y) * \varepsilon(x,y) \quad (\text{Eq.5})$$

Estimation of APAR

Green plants rely on solar radiation energy for photosynthesis. Plants synthesize part of the radiation energy into their own organic matter. PAR (Photosynthetically Active Radiation, PAR) refers to the energy used by vegetation. Its wavelength range is 380-710 nm of visible light. The total amount of solar radiation produced by vegetation and its physiological and ecological characteristics determine the amount of PAR absorbed by vegetation.

$$APAR(x,t) = SOL(x,t) * fPAR(x,t) * 0.5 \quad (\text{Eq.6})$$

In the formula, $SOL(x,t)$ is the total solar radiation at x in the month of image t . These data are interpolated by the kriging spatial interpolation method for many years in Shangri-La (Fig. 2d). $fPAR(x,t)$ indicates the proportion of PAR absorbed by plants. Different vegetation types and seasonal changes will make this value change. A coefficient of 0.5 refers to the ratio of the amount of PAR used by plants to the total amount of solar radiation.

In the model, $fPAR$ is the NDVI and vegetation type, and its maximum value is not more than 0.95.

$$fPAR(x, t) = \min\left[\frac{SR - SR_{\min}}{SR_{\max} - SR_{\min}}, 0.95\right] \quad (\text{Eq.7})$$

In the formula, $SR(x, t)$ is obtained from the $NDVI(x, t)$.

$$SR(x, t) = \left[\frac{1 + NDVI(x, t)}{1 - NDVI(x, t)}\right] \quad (\text{Eq.8})$$

Estimation of light utilization rate

The utilization rate of light energy is the basis and an important parameter for estimating NPP. Generally, the efficiency of photosynthetic radiation absorbed by plants in the transformation to organic carbon is called the utilization rate of light energy. Normally, the utilization rate of plant light energy is large. However, research shows that the utilization rate of light energy is affected by many external conditions. First, it is affected by temperature, and second, it is affected by precipitation.

$$\varepsilon(x, t) = T_{\varepsilon 1}(x, t) * T_{\varepsilon 2}(x, t) * W_{\varepsilon}(x, t) * \varepsilon^* \quad (\text{Eq.9})$$

In the formula, $W_{\varepsilon}(x, t)$ is the influence coefficient of the water stress factor, which refers to the influence of the water factor on the NPP. $T_{\varepsilon 1}(x, t)$ indicates the extent to which the utilization rate is limited when the temperature is high. $T_{\varepsilon 2}(x, t)$ refers to the extent to which the utilization rate is limited when the temperature is low, and ε^* refers to the maximum light utilization rate that can be achieved under ideal conditions.

$$T_{\varepsilon 1}(x, t) = 0.8 + 0.02 * T_{opt}(x) - 0.0005 * [T_{opt}(x)]^2 \quad (\text{Eq.10})$$

In the formula, $T_{opt}(x)$ refers to the monthly mean temperature of the study area at the highest NDVI value. According to the statistics of the NDVI values of Shangri-La in different months of 2013, it is found that the Shangri-La NDVI reached the highest value in July. Through the statistical analysis of the Zhongdian Climate Data, the average temperature of Shangri-La in July is 13°C.

$T_{\varepsilon 2}(x, t)$ refers to the process in which the utilization rate of light energy of plants decreases, that is, when the temperature of the environment increases or decreases slowly and transitions away from the most suitable temperature for vegetation. Its principle is that when the temperature of vegetation is not the most suitable, plant respiration will become stronger, which will naturally lead to an increase in energy consumption, a decrease in photosynthesis and a consequent decrease in the utilization rate of light.

$$T_{\varepsilon 2}(x, t) = \frac{1.184}{\{1 + \exp[0.2 * T_{opt}(x) - 10 - T(x, t)]\}} * \frac{1}{\{1 + \exp[0.3 * (-T_{opt}(x) - 10 + T(x, t))]\}} \quad (\text{Eq.11})$$

In the formula, $T(x, t)$ denotes the temperature at pixel X of the t month. In this paper, the annual mean temperature of Shangri-La (Fig. 2e) and the monthly mean temperature of Shangri-La for many years were used to obtain monthly temperature interpolation maps through spatial interpolation.

$W_{\epsilon}(x,t)$ is the effect of vegetation available water on the change of energy utilization. When the corresponding effective water changes in the environment, the value will change accordingly. Its value is from 0.5 (drought) to 1 (humidity).

$$W_{\epsilon}(x,t) = 0.5 + 0.5 * E(x,t) / E_p(x,t) \quad (\text{Eq.12})$$

In the formula, $E(x,t)$ is the actual regional evapotranspiration, and $E_p(x,t)$ is the potential regional evapotranspiration.

$$E(x,t) = \frac{\{P(x,t) * R_n(x,t) * [P(x,t)^2 + R_n(x,t)^2 + P(x,t) * R_n(x,t)]\}}{\{[P(x,t) + R_n(x,t)] * [P(x,t)^2 + R_n(x,t)^2]\}} \quad (\text{Eq.13})$$

In the formula, $P(x,t)$ is the precipitation (mm) of pixel x in month t . Based on the annual precipitation value of Shangri-La (Fig. 2f) and the monthly average precipitation for many years in Shangri-La, the monthly precipitation interpolation maps are obtained by spatial interpolation (Pan et al., 2014) $R_n(x,t)$ is the net solar radiation.

$$R_n = [E_{p0}(x,t) * P(x,t)]^{0.5} * \{0.369 + 0.589 * [\frac{E_{p0}(x,t)}{P(x,t)}]^{0.5}\} \quad (\text{Eq.14})$$

In the formula, $E_{p0}(x,t)$ can be derived from the Thornthwaite vegetation-climate relationship model (Zhang et al., 1997), which refers to local potential evapotranspiration (mm). The monthly mean is used for the calculation.

$$E_p(x,t) = [E(x,t) + E_{p0}(x,t)] / 2 \quad (\text{Eq.15})$$

Referring to the simulation value of light utilization in the Zhu et al. (2004) model, the value of light utilization factor ϵ^* in this study is shown in Table 2.

Table 2. Value of Light Utilization of Different Ecological Types (unit gCMJ)

Veg. types Month	Forest	Agr. land	Water	Art. land	Unutilized land	Shrub grassland	Wet.	Per. snow glacier
1	0.438	0.268	0.219	0.157	0.168	0.259	0.322	0.219
2	0.365	0.213	0.177	0.124	0.184	0.259	0.306	0.177
3	0.440	0.253	0.228	0.134	0.217	0.280	0.332	0.228
4	0.558	0.292	0.252	0.188	0.218	0.276	0.336	0.252
5	0.681	0.404	0.355	0.221	0.234	0.322	0.328	0.355
6	0.714	0.471	0.383	0.254	0.251	0.400	0.425	0.383
7	0.672	0.473	0.378	0.246	0.239	0.421	0.467	0.378
8	0.696	0.459	0.365	0.242	0.220	0.398	0.410	0.365
9	0.737	0.455	0.386	0.244	0.238	0.374	0.392	0.386
10	0.659	0.352	0.326	0.203	0.202	0.254	0.298	0.326
11	0.565	0.308	0.267	0.199	0.217	0.285	0.341	0.267
12	0.422	0.252	0.216	0.136	0.214	0.266	0.327	0.216
Average value	0.579	0.350	0.296	0.196	0.217	0.316	0.357	0.296

Note: **Veg.:** Vegetation; **Agr.:** Agricultural; **Art.:** Artificial; **Wet.:** Wetland; **Per.:** Permanent

Results and Discussion

Estimated results of ecological assets in Shangri-La

Remote sensing estimation of different types of ecological assets produces different values because of different ecosystem types and ecosystem service functions. For example, forestland is more comprehensive in terms of ecosystem service functions, while urban and unused land are obviously insufficient. And, water conservation mainly means storage the water bodies in local for biological use; water and soil conservation mainly mean the prevention and control of soil erosion and the rational development and utilization of water and soil resources. *Table 3* shows the corresponding relationship between ecosystem types and ecosystem service functions.

Table 3. *Ecosystem Type and Ecological Service Function Relationship Table*

	Water con.	Soil and water con.	Adjusting climate	Nutrient circulation	Pro. of org. matter	Cultural Ent.
Forest	+	+	+	+	+	+
Agricultural land	+	+	+	+	+	-
Waters	+	-	+	-	+	+
Artificial land	+	-	+	+	+	+
Unutilized land	+	+	+	+	+	-
Shrub grassland	+	+	+	+	+	+
Wetland	+	-	+	-	+	+
Permanent snow glaciers	+	-	+	+	+	+

Note: "+" means that the ecosystem has the value of ecological services, while "-" means that it is not or difficult to measure. **con.**: conservation; **Reg.**: Regulating; **Pro.**: Production; **org.**: organic; **Ent.**: Entertainment

Spatial distribution of eco-asset value per unit area

According to the abovementioned relevant models, the value of ecological assets per unit area of the study area can be calculated (*Fig. 3, Table 4*). From the analysis, it can be seen that the highest value of water conservation per unit area of Shangri-La in 2013 is in the water ecosystem, followed by woodland, and the lowest value of water conservation is attributed to unused land. In general, the values of water conservation per unit area of Shangri-La are mostly the same. Among the 8 ecosystem types in Shangri-La, water area, artificial land, wetland and permanent snow glacier have no soil and water conservation value, and the highest value of soil and water conservation per unit area is attributed to agricultural land because the income of agricultural land per square kilometer in the selected model is more than that of woodland. Furthermore, the highest value of regulating climate per unit area is attributed to woodland, followed by shrub and grassland, and the lowest is attributed to water area and permanent snow glacier because the latter two have lower primary productivity values. The highest nutrient cycling value per unit area is in shrub grassland because shrub grassland has a higher N, P, K distribution rate than does woodland, followed by artificial land because the nutrient cycling value of artificial land mainly refers to green grassland and grassland. The value is also affected by shrub and grassland. The lowest cyclic value of nutrients per unit area is in water area and permanent snow glacier because their net primary productivity values are low; the highest value of organic matter per unit area is in woodland, followed by

shrub and grassland, and the lowest value is in permanent snow glacier. The recreational values are the same except for agricultural land and unused land, which is consistent with the model in this paper. Thus, there was a flaw in type selection.

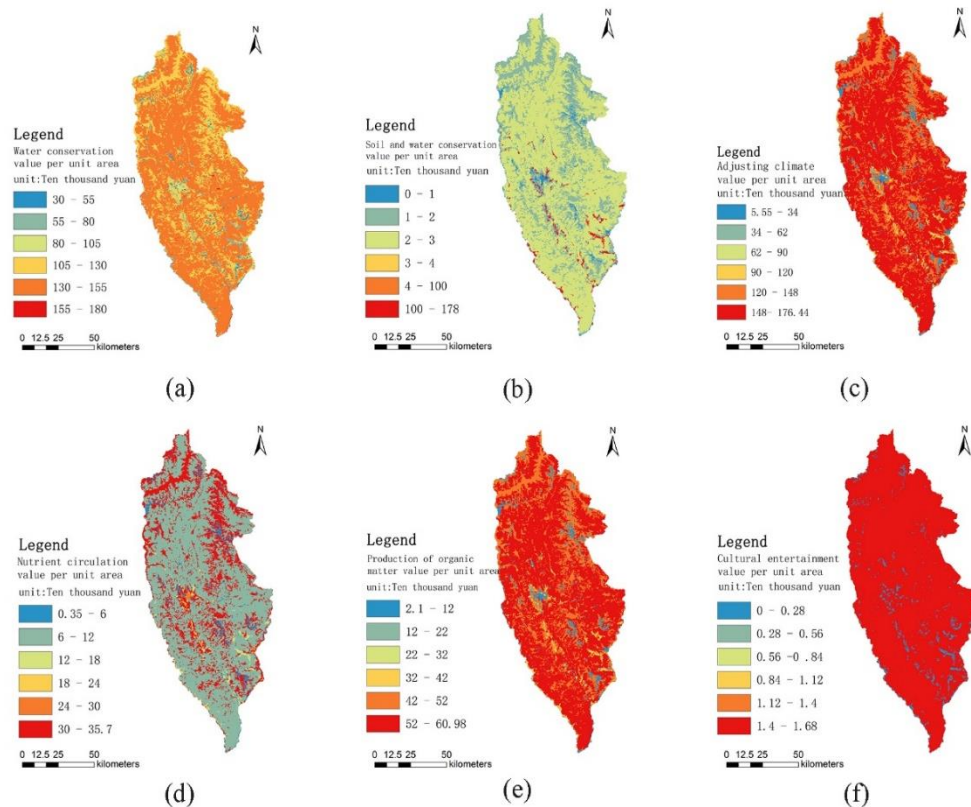


Figure 3. Value of ecological assets per unit area:(a) Water conservation;(b) Soil and water conservation;(c) Adjusting climate;(d) Nutrient circulation;(e) Production of organic matter;(f) Cultural entertainment

Table 4. Value of ecological assets per unit area of various types of ecosystems

	Forest	Agr. land	Unuti. land	Waters	Art. land	Wet.	Shrub gra.	Per. snow glacier	Total value
Water con.	136.000	58.000	30.000	180.000	94.000	120.960	118.440	113.400	850.800
Soil and water con.	2.970	178.000	1.800	0.000	0.000	0.000	1.010	0.000	183.780
Adj. climate	176.440	105.000	18.940	5.550	10.500	38.300	130.440	5.940	491.110
Nutrient cir.	11.180	14.420	3.700	0.350	28.560	2.200	35.700	0.350	96.460
Pro. of org. matter	60.980	36.000	6.550	2.270	3.630	13.240	48.620	2.100	173.390
Cultural ent.	1.680	0.000	0.000	1.680	1.680	1.680	1.680	1.680	10.080
Total value	389.250	391.420	60.990	189.850	138.370	176.380	335.890	123.470	1805.620

Note: **Agr.:** Agricultural; **Unuti.:** Unutilized; **Art.:** Artificial; **Wet.:** Wetland; **gra.:** grassland; **Per.:** Permanent; **con.:** conservation; **Adj.:** Adjusting; **cir.:** circulation; **Pro.:** Production; **org.:** organic; **ent.:** entertainment

From the total value of ecological assets per unit area of each ecological type, the order from high to low is agricultural land, forestland, shrub grassland, water area, wetland, artificial land, permanent snow glacier and unused land. The reason why agricultural land ranks higher than forestland and shrub grassland is that the average income of agricultural land per unit area was relatively high. In addition, the general trend is reasonable.

Spatial distribution of total value of ecological assets in ecosystems

Similarly, using the above model, we can calculate the total value distribution maps of 6 ecological assets in Shangri-La in 2013, including water conservation, nutrient cycling, soil and water conservation, organic matter production, climate regulation and recreational value (Fig. 4, Table 5). The maps and tables show that the highest value of water conservation in the ecosystems of Shangri-La is forestland, accounting for approximately 73% of the total value of water conservation in the whole county, followed by shrub and grassland, accounting for approximately 24%, and other land use types, accounting for a smaller proportion. In the total value of soil and water conservation, agricultural land accounts for a higher value, followed by forestland; in the value of regulating climate, it is still forestland and grassland. The proportion of shrubs and grasslands is larger; among the total value of nutrient cycling, the proportion of shrubs and grasslands and woodlands is the largest, and the smallest is the water ecosystem. The value of organic matter production and recreational value is still dominated by woodlands and shrubs and grasslands. The order of the six values from high to low is adjusting climate value, conserving water source value, producing organic matter value, nutrient cycling value, soil and water conservation value and recreational value. It can be seen that forestland and shrub grassland occupy an important position in the ecological environment, and among all the values of ecological assets, the values of water conservation and climate regulation are particularly important.

Accuracy evaluation and analysis

After estimating the value of an ecosystem's ecological assets, it is necessary to analyze the accuracy of the evaluation results, which repeats the whole estimation process. That is, the process starts over, from the data sources used in this estimation, to the data processing, to the selection and calculation of parameters in the estimation; finally, the use of methods for the estimation and the acquisition of the estimation results must be done. Then, accuracy analysis is carried out.

First, from the point of view of data source acquisition, the TM and MODIS remote sensing data used in this paper were downloaded from authoritative data acquisition website geospatial data clouds, while the meteorological data and related statistical data were extracted from a number of relevant institutions and professions in Shangri-La, and some data processing was also completed through professional software. Although errors are inevitable in these processes, these errors are also within the scope of acceptance.

In addition, in the process of estimating parameters, the parameters in this paper are either calculated based on Shangri-La data or refer to previous research results; moreover, when calculating the NPP and soil conservation of the Shangri-La ecosystems, the parameters involved in estimating the value of individual ecological assets and the statistical parameters involved are calculated based on field data. The accuracy is beyond doubt, and the parameters that refer to the previous research results are also the national average, which may lead to errors in the final results; however, these errors are not very large.

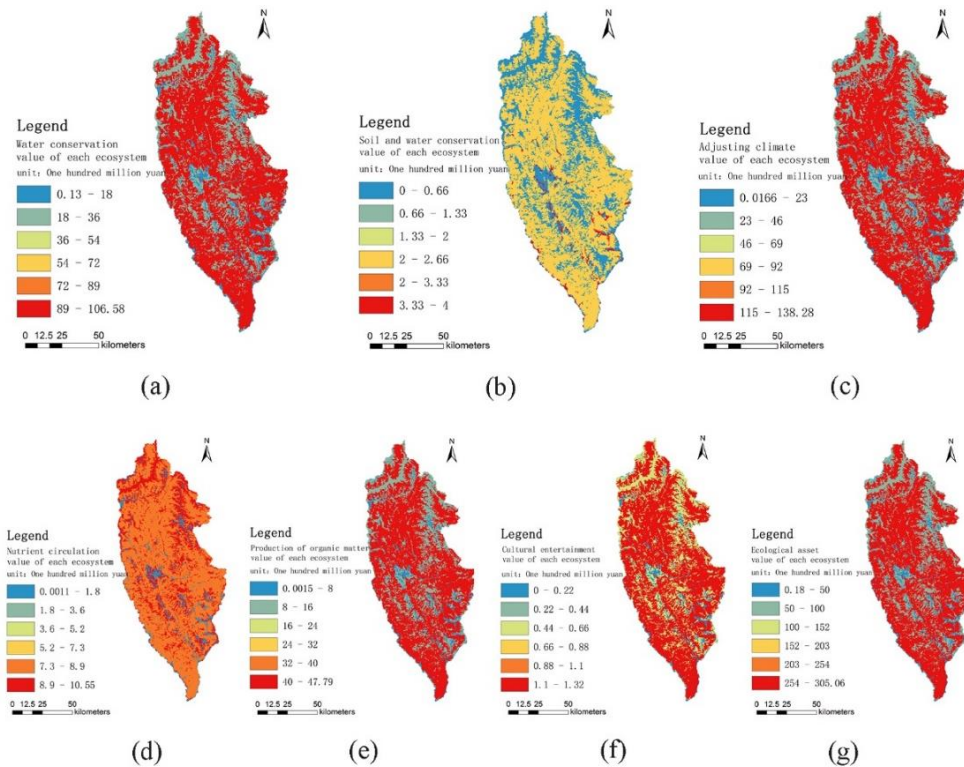


Figure 4. The value of each ecological asset in each ecosystem: (a) Water conservation; (b) Soil and water conservation; (c) Adjusting climate; (d) Nutrient circulation; (e) Production of organic matter; (f) Cultural entertainment; (g) Total ecological asset value

Table 5. The Value of Ecological Assets of Ecosystem (unit:100 million yuan)

	Forest	Agr. land	Unuti. land	Waters	Art. land	Wet.	Shrub gra.	Per. snow glacier	Total value
Water con.	106.580	1.310	0.590	0.540	0.140	0.133	35.000	1.292	145.585
Soil and water con.	2.330	4.000	0.035	0.000	0.000	0.000	0.299	0.000	6.664
Adj. climate	138.280	2.370	0.368	0.017	0.050	0.042	38.540	0.068	179.735
Nutrient cir.	8.760	0.330	0.072	0.001	0.040	0.002	10.550	0.004	19.760
Pro. of org. matter	47.790	0.820	0.127	0.007	0.017	0.002	14.370	0.023	63.156
Cultural ent.	1.320	0.000	0.000	0.005	0.007	0.002	0.496	0.019	1.849
Total value	305.060	8.830	1.192	0.570	0.255	0.181	99.255	1.407	416.749

Note: **Agr.:** Agricultural; **Unuti.:** Unutilized; **Art.:** Artificial; **Wet.:** Wetland; **gra.:** grassland; **Per.:** Permanent; **con.:** conservation; **Adj.:** Adjusting; **cir.:** circulation; **Pro.:** Production; **org.:** organic; **ent.:** entertainment

At the same time, because many basic data and statistics are difficult to obtain, it is difficult to measure the value of ecosystem services in the estimation of the value of ecological assets, such as the scientific research value of ecosystems. However, this paper uses the value of cultural entertainment to supplement these values so that the final results are not too low.

Finally, compare the estimation results of Shangri-La ecological asset value through similar research conducted by domestic and foreign scholars. Costanza et al. (1997) estimated that the average value of the services provided by the global ecosystem is about 33 trillion dollars per year; Pimentel (1997) conducted research on global biodiversity and estimated the value of global ecosystem services to be approximately 2.928×10^{12} dollars; Yu et al. (2006) estimated the total value of ecological assets in Huzhou city, the final result was 20.333 billion yuan; Li (2008) studied Songnen Plain obtained 65.968 billion yuan in total value of ecological assets; Sun (2008) studied in the Yangtze River Delta obtained 17.637 billion yuan in total value; at the same time, Zhang (2004) estimated ecological assets, obtained a result of 39.13 billion yuan in Inner Mongolia. Xie (2010) estimated the total value of Fuzhou's ecological assets, and the total amount he calculated was 23.7 billion yuan. Through the above research, it is found that the total amount of regional ecological assets is positively correlated with area, ecosystem conditions, and geographic conditions, that is, the larger the area, the better the ecosystem conditions, the superior the geographical environment, and the greater the total amount of ecological assets. Comparing the above research results with the estimated result of Shangri-La ecological assets of 41.675 billion yuan, we found that they are consistent in spatial distribution and quantitative trends.

Conclusion

It was found that the models of remote sensing estimation of ecological assets (total regional ecological asset value model and single ecological asset value evaluation model) and the NPP estimation model (CASA) were suitable for Shangri-La. And, the total value of ecological assets in Shangri-La was 41.675 billion yuan, and the total value of ecological assets per unit area was 18.5562 million yuan, among the data, the sequence of the value of various ecological assets in Shangri-La is the following: adjusting climate is 17.97 billion yuan, water conservation is 14.5 billion yuan, production of organic matter is 6.3 billion yuan, nutrient circulation is 1.97 billion yuan, soil and water conservation is 660 million yuan, cultural entertainment is 180 million yuan; the sequence of the value of each ecosystem type is the following: forest is 30.5 billion yuan, shrub grassland is 9.925 billion yuan, agricultural land is 883 million yuan, permanent snow glaciers is 141 million yuan, unutilized land is 119 million yuan, waters is 57 million yuan, artificial land is 25 million yuan, wetland is, and, from the perspective of the proportion of the total value of forest and shrub grassland, vegetation plays an important role in the value of ecological assets; the sequence of the value of single ecological asset value per unit area in Shangri-La is the following: water conservation is 8.508 million yuan, adjusting climate is 4.911 million yuan, soil and water conservation is 1.8378 million yuan, production of organic matter is 1,733,900 yuan, nutrient circulation is 964,600 yuan, cultural entertainment is 100.8 million yuan; the sequence of the value of each ecosystem type per unit area is the following: agricultural land is 3.114 million yuan, forest is 3.895 million yuan, shrub grassland is 3.3589 million yuan, waters is 1.8985 million yuan, wetland is 1.763 million yuan, artificial land is 1.3839 million yuan, permanent snow glaciers is 1.2347 million yuan, unutilized land is 609,000 yuan.

Inevitably, there are some aspects that need to be improved or strengthened in the estimation process. First of all, Shangri-La is a typical mountain and valley area, it is difficult to obtain detailed data of meteorological data and soil data. Although through interpolation analysis, the accuracy still needs to be improved. At the same time, the

selection of ecological asset evaluation index is not perfect, only six indexes were selected, including water conservation, adjusting climate, soil and water conservation, production of organic matter, nutrient circulation and cultural entertainment, but there are more indexes than six (Costanza et al., 1997; Daily, 1997), resulting in a certain difference between the estimated value of ecological assets and the actual value. And, the natural resources do not been separately estimate, in particular, the ecosystem is a dynamic system, so ecological assets are also dynamic, but if the value of ecological assets needs to be dynamically monitored and evaluated (Sun et al., 2017; Wang, 2019; Xing, 2020), it is necessary to ensure that the data is fast and timely, due to the limitations of research materials and technical means, this study did not compare the value of ecological assets on a temporal and spatial scale.

Acknowledgements. This work was supported by Multi-Government International Science and Technology Innovation Cooperation Key Project of National Key Research and Development Program of China grant number 2018YFEO184300; the National Natural Science Foundation of P.R. China, grant number 41961060; the Program for Innovative Research Team (in Science and Technology) in the University of Yunnan Province, IRTSTYN; the Scientific Research Fund Project of the Education Department of Yunnan Province, grant number: 2020J0256; Graduate research and Innovation Fund Project of Yunnan Normal University, grant number: ysdjys2020060.

REFERENCES

- [1] Bagstad, K. J., Semmens, D. J., Waage, S., Winthrop, R. (2013): A comparative assessment of decision-support tools for ecosystem services quantification and valuation. – *Ecosystem Services* 5: 27-39.
- [2] Byeori, K., Jae-Hyuck, L., Hyuksoo, K. (2017): Recent Ecological Asset Research Trends using Keyword Network Analysis. – *Journal of Environmental Impact Assessment* 26(5): 303-314.
- [3] Chen, J., Chen, Y. H., He, C. Y., Shi, P. J. (2001): Subpixel Model of Vegetation Coverage Estimation Based on Land Cover Classification and Its Application. – *Journal of Remote sensing* 5(6): 416-422.
- [4] Chen, Z. L., Wu, Z. F., Xia, N. H. (2007): Research Progress on Ecological Assets Estimation in China. – *Ecological Environment* 16(02): 680-685.
- [5] Chen, M. H., Chen, Y. B., Guo, G. H. (2012): Remote Sensing Quantitative Evaluation of Ecological Assets in Rapid Urbanization Areas-Take Dongguan City, Guangdong Province as an example. – *Journal of Natural Resources* 27(4): 601-613.
- [6] Chen, Q. (2021): Remote Sensing Assessment and Spatiotemporal Evolution Mechanism Analysis of Ecological Assets in Karst Rocky Desertification Area. – Guizhou Normal University.
- [7] Costanza, R., d'Arge, R., Groot, R., Farber, S., Grasso, M., Hannon, B., Limburg, K., Naeem, S., O'Neill, R. V., Paruelo, J., Raskin, R. G., Sutton, P., van den Belt, M. (1997): The value of the world's ecosystem services and natural capital. – *Nature* 387: 253-260.
- [8] Daily, G. C. (1997): *Nature's Services: Societal Dependence on Natural Ecosystems*. – Washington D C: Island Press.
- [9] Daily, G. C., Polasky, S., Goldstein, J., Kareiva, P., Mooney, H. A., Pejchar, L., Ricketts, T., Salzman, J., Shallenberger, R. (2009): Ecosystem Services in Decision Making: Time to Deliver. – *Ecological Society of America* 7(1): 21-28.
- [10] Delphin, S., Escobedo, F. J., Abd-Elrahman, A., Cropper, W. P. (2016): Urbanization as a land use change driver of forest ecosystem services. – *Land Use Policy* 54: 188-199.
- [11] Du, F. L., Tian, Q. J., Xia, X. Q. (2004): Evaluation and Prospect of Remote Sensing Image Classification Method. – *Remote sensing technology and applications* 19(6): 521-525.

- [12] Gadaud, J., Rambonilaza, M. (2010): Amenity values and payment schemes for free recreation services from nonindustrial private forest properties: A French case study. – *Journal of Forest Economics* 16(4): 297-311.
- [13] Gao, J. X., Fan, X. B. (2007): Concepts, characteristics and research trends of ecological assets. – *Environmental Science Research* 20(5): 137-143.
- [14] Gómez, B. E., Barton, D. N. (2013): Classifying and valuing ecosystem services for urban planning. – *Ecological Economics* 86: 235-245.
- [15] Han, W. D., Gao, X. M., Lu, C. Y. (2000): Ecological Value Assessment of Mangrove Ecosystem in China. – *Ecological science* 19(1): 40-46.
- [16] Holdren, J. P., Ehrlich, P. R. (1974): Human population and the global environment. – *American Scientist* 62(3): 282-297.
- [17] Hou, S. T., Zheng, X. L., Di, Y. S. (2015): Remote Sensing Measurement and Evaluation of Ecological Assets in Harbin City. – *Soil and Water Conservation Research* 22(2): 305-309.
- [18] Jiang, Y. F. (2004): Research on High Precision Parallel Supervised Classification of Remote Sensing Images. – National University of Defense Technology.
- [19] Li, Z. Y., Tang, J., Sun, P. A. (2008): Research on Ecological Assets Remote Sensing Measurement and Ecological Regionalization in Songnen Plain. – *Ecological Economy* 5: 122-127.
- [20] Liu, Y., Wu, G., Gao, Z. G. (2007): Assessment of Ecological Assets in Fuxian Lake Basin of Yunnan Province Based on Land Cover/Utilization Model. – *Journal of Ecology* 27(12): 5282-5290.
- [21] Liu, J. F., Sun, H. Q., Zhan, W. F. (2013): Analysis on the Driving Forces of Ecological Assets Changes in the Yangtze River Delta. – *Soil and Water Conservation Research* 20(1): 182-185.
- [22] Luo, X. P. (2008): Estimation and Application of Ecological Assets in Jiangxi Province. – Jiangxi Normal University.
- [23] Ouyang, Z. Y., Zhu, C. Q., Yang, G. B. (2013): Ecosystem GDP accounting: concepts, accounting methods and case studies. – *Acta Ecologica Sinica* 33(21): 6747-6761.
- [24] Pan, Y. Z. (2004): Quantitative Measurement of Ecological Assets of Terrestrial Ecosystem in China by Remote Sensing. – *Chinese Science Series D Geosciences* 4: 375-384.
- [25] Pan, J. Y., Wang, J. L., Gao, F. (2014): Research on Spatial Interpolation Method of Meteorological Elements in Shangri-La. – *The 19th China Remote Sensing Conference*, pp. 1839-1846.
- [26] Pimentel, D., Wilson, C., McCullum, C., Huang, R., Dwen, P., Flack, J., Tran, Q., Saltman, T., Cliff, B. (1997): Economical and environmental benefits of biodiversity. – *BioScience* 47(11): 217-257.
- [27] Polasky, S., Nelson, E., Pennington, D., Johnson, K. A. (2011): The impact of land-use change on ecosystem services, biodiversity and returns to landowners: a case study in the State of Minnesota. – *Environmental and Resource Economics* 48(2): 219-242.
- [28] Potter, C. S., Klooster, S. A. (1997): Global model estimates of carbon and nitrogen storage in litter and soil Pools: response to changes in vegetation quality and biomass allocation. – *Tellus* 49(3): 1-17.
- [29] Richmond, A., Kaufmann, R. K., Myneni, R. B. (2007): Valuing ecosystem services: A shadow price for net primary production. – *Ecological Economics* 64(2): 454-462.
- [30] Shi, P. J., Li, J., Pan, Y. Z. (2009): *Land Use/Coverage and Eco-Assets*. – Beijing: Science Press.
- [31] Sun, H. Q., Deng, L., Jiang, W. G. (2008): Evaluation of Ecological Assets in the Yangtze River Delta. – *Resource Science* 30(9): 1367-1373.
- [32] Sun, X., Li, F. (2017): Assessment method and application of urban ecological assets: a case study in Zengcheng, Guangzhou City. – *Acta Ecologica Sinica* 37(18): 6216-6228.
- [33] Wang, Y. Y., Li, Q. (2004): Summary of Land Use/Cover Classification Methods for Remote Sensing Images. – *Remote Sensing Information* 53-58.

- [34] Wang, J. L., Li, H., Wang, P. (2004): Development, Utilization and Protection of Wetland Resources in Northwest Yunnan Based on 3S Technology.
- [35] Wang, K. H. (2019): The Evaluation of Ecological Assets in Brahmaputra River basins. – China University of Geosciences.
- [36] Westman, W. E. (1977): How much are nature's services worth. – *Science* 197(4307): 960-964.
- [37] Xie, G. D., Zhen, L., Lu, C. X., Xiao, Y., Chen, C. (2008): An Ecosystem Service Valuation Method Based on Expert Knowledge. – *Journal of Natural Resources* 23(5): 911-919.
- [38] Xie, L. (2010): GIS-supported estimation of ecological assets in Fuzhou. – Fujian Normal University.
- [39] Xing, Y. M. (2020): Research on Ecological Asset Value Evaluation of Typical Temperate Forest Nature Reserve - Taking Changbai Mountain Nature Reserve and Taishan Nature Reserve as examples. – Central University for Nationalities.
- [40] Xu, X. B., Chen, S., Yang, G. S. (2012): Spatio-temporal changes of ecological assets in the Yangtze River Delta from 1995 to 2007. – *Acta Ecologica Sinica* 32(24): 7667-7675.
- [41] Yang, L. (2009): Preliminary Study on the Value Change of Ecosystem Services in Shangri-La County Based on 3S Technology. – Yunnan Normal University.
- [42] Yu, Z. B. (2005): Evaluation of Grassland Ecosystem Value and Its Dynamic Simulation. – China Agricultural University.
- [43] Yu, D. Y., Pan, Y. Z., Liu, X., Wang, Y. Y., Zhu, W. Q. (2006): Remote sensing measurement of ecological assets in Huzhou City and its application in social economy. – *Journal of Plant Ecology* 3: 404-413.
- [44] Zhang, X. S., Zhou, G. S., Gao, Q. (1997): Study on the relationship between global change and terrestrial ecosystem in China. – *Frontier of Geosciences (China University of Geosciences, Beijing)* 4(1-2): 137-144.
- [45] Zhang, S. Y., Chen, H. Y., Li, X. B. (2004): Inner Mongolia Ecological Assets Measurement and Ecological Construction Research. – *Resource Science* 26(3): 22-28.
- [46] Zhongdian County Agricultural Climate Division. (1986): Zhongdian County Agricultural Zoning Committee.
- [47] Zhu, W. Q., Chen, Y. H., Pan, Y. Z., Li, J. (2004): Estimation of Vegetation Light Utilization Rate in China Based on GIS and RS. – *Journal of Wuhan University (Information Science Edition)* 8(29): 694-714.
- [48] Zhu, W. Q., Zhang, J. S., Pan, Y. Z., Yang, X. Q. (2007): Ecological Assets Measurement of China's Terrestrial Ecosystem and Analysis of Its Dynamic Changes. – *Journal of Applied Ecology* 18(3): 586-594.

THE COMBINED EFFECT OF ZnO NANO PARTICLES AND TOXICITY OF HEAVY METALS (ARSENIC AND CHROMIUM) ON THE MORPHOLOGICAL, BIOCHEMICAL ATTRIBUTES OF WHEAT (*TRITICUM AESTIVUM* L.) AS WELL AS SOIL AND WATER PROPERTIES

IQBAL, I. – BHATTI, K. H.*

Department of Botany, University of Gujrat, Hafiz Hayat Campus, Gujrat 50700, Pakistan

**Corresponding author
e-mail: khizar.hayat@uog.edu.pk*

(Received 18th Jun 2021; accepted 23rd Nov 2021)

Abstract. This research work was conducted in research area, Department of Botany, University of Gujrat, Pakistan during 2018-2019. The performance of research work was conducted to check the effect of heavy metal Chromium (Cr) and Arsenic (As) on two varieties (Faisalabad, Aas) of wheat and is the foliar application of Zinc oxide nanoparticles helpful to remove the stress effect of heavy metals. Heavy metal (Cr and Ar 10 ppm) were added to plants through the rooting medium. There were 10, 20, 30 levels of ZnO (Zinc oxide) nanoparticles for each heavy metal as applied foliarly after 14 days of germination. Experiments were set up in completely randomized design with four replicates. Heavy metal accumulation in soils is steadily growing, resulting in increased toxicity of this ingredient in a variety of crop plants. While Zn is an important nutrient for plants, some soils are deficient in Zn or have poor Zinc bioavailability. The viability of the project is the subject of this article. Soil amendments containing ZnO nanoparticles (NPs) to increase the amount of Zn in the plant. Results indicated that with the application of ZnO NPs, metal concentrations (As and Cr) declined in morphological, biochemical and gaseous attributes with soil and water properties. This reduction was more prominent in the Faisalabad 2008 variety as compared to Aas 2011. Based on the result we concluded that the foliar application of ZnO nano particles were suitable to boost up the biochemical and morphological characteristics, as well as gas exchange of the studied wheat varieties under heavy metal stress, including soil and water properties. As a result, our findings support the importance of ZnO–NPs in reducing heavy metals toxicity in wheat plants.

Keywords: *chlorophyll, foliar spray, zinc, stress, toxic*

Introduction

Historically, wheat has been the staple grain in western countries. In reality, it is now the world's third-most-produced cereal (after rice and corn) and the second-most-consumed cereal (after rice) for human consumption (Caro et al., 2018). Wheat is the most commonly planted crop on the planet, with annual production in North America, Europe, Asia, Australia, and Africa totaling 600 million tonnes. Wheat supplies 20% of overall protein and calories in human nutrition for millions of people who depend on wheat-based diets, as well as 40% of dietary consumption of essential micronutrients including zinc, iron, manganese, magnesium (Sansaloni et al., 2020).

Soil is one of humanity's most important and precious natural resources. Soil plays a huge role in societal civilization and agricultural sustainability (Mushtaq, 2021). Heavy metal pollution of soil, on the other hand, is a significant danger to humanity and a major global problem. Chromium is a toxic heavy metal which is used in the manufacture of electroplating, garment dyeing, stainless steel, as a radioactive coolant, and in the leather industry (Fu and Xi, 2020). Cr exposure has also been linked to

metabolic changes in wheat, either through direct effects on enzymes or through its ability to produce reactive oxygen species (ROS), which may persuade oxidative stress and increased lipid peroxidation (Wakeel et al., 2020).

Arsenic is a hazardous metalloid and influential toxin that affects living things specially plants. Bio magnification of arsenic is becoming a growing concern around worldwide, especially in Southeast Asian countries. Human and anthropogenic sources also contribute to the metalloid's presence in the environment. Arsenic prevents root proliferation and expansion, while after translocation to the shoot, growth of plant is slowed and productivity as well as reproductive ability are reduced (Sil et al., 2019). Arsenic contamination in plants has been shown to inhibit growth, supplement of nutrients, protein content, photosynthetic pigments as well as biomass accumulation (Farouk and Al-Amri, 2019).

Nanotechnology has risen to prominence as a technological movement in recent years, with potential applications in a variety of fields. Nanoparticles have distinct physicochemical properties when compared to bulk particles and play an important role in transfer of chemical agents in plants to a molecules of targeted cellular organelle (Tripathi et al., 2017). ZnONPs are the most well-known of the many metal nanoparticles that are usually used for industrial purposes. As a result, widespread use of ZnONPs in a variety of materials increases the likelihood of their release into the atmosphere, which may have significant implications for plant productivity (Ifeanyichukwu, 2020).

Under stressful and non-stressful environments, nitric oxide which is a gaseous free radical, affects many physiological as well as biochemical responses in plants. It has been found to efficiently mitigate the toxic effects of various stresses on plants, including ultraviolet rays, salt, heavy metals, sun and light (Tripathi et al., 2017). ZnO NPs induced phytotoxicity in seedlings grown in acid soil, as shown by the inhibition of root elongation in wheat (Watson et al., 2015).

In recent years, the use of nanoparticles (NPs) containing micro- and macronutrients has been promoted as a promising approach for the crop growth and yield (Shang et al., 2017). This nanoparticle supplements may help to minimize nutrient loss and increase crop production in a long-term way. The use of ZnO NPs in agricultural sciences is gaining popularity among metal-based NPs. Despite this, only a few studies have looked into the effects of ZnO–NPs in the soil as well as plant environment. The availability of Zn in soils and the toxicity of ZnO–NPs in plants are influenced by the plant types, soil condition, and soil pH. (Rizwan et al., 2019). Surprisingly, the low abundance of Zn in soils can help foliar application of ZnO–NPs. Many studies have shown that zinc nanoparticle formulations and their use as a foliar spray are effective at reducing heavy metal accumulation in plants (Hussain et al., 2018; Rizwan et al., 2019; Wu et al., 2020).

In the light of above-mentioned literature the main objectives of this research work was to find out the effect of heavy metals and also determine the ZnO nano particles function under heavy metals stressed plant on wheat varieties.

Materials and methods

Pot experiments were carried out in the Botanical Garden, University of Gujrat, Gujrat Pakistan during 2018-2019. Two varieties of wheat were used in these experiments i.e. Aas (2011) and Faisalabad (2008). Heavy metals (Arsenic and

Chromium) and Zinc Oxide Nanoparticles were used. Eleven level of treatment of Ar, Cr and ZnONPs that were:

T0 = Control 0 ppm (As, Cr, ZnO NPs)

T1 = 10 ppm As

T2 = 10 ppm Cr

T3 = 10 ppm ZnONPs

T4 = 20 ppm ZnONPs

T5 = 30 ppm ZnONPs

T6 = 10 ppm ZnONPs + 10 ppm As

T7 = 20 ppm ZnONPs + 10 ppm As

T8 = 30 ppm ZnONPs + 10 ppm As

T9 = 10 ppm ZnONPs + 10 ppm Cr

T10 = 20 ppm ZnONPs + 10 ppm Cr

T11 = 30 ppm ZnONPs + 10 ppm Cr

48 Pots was bought for each variety from market and filled with about 8 kg soil. Eight to ten healthy seeds of both varieties were sown in each pot. After 10th day of germination thinning of the plants was made leaving only 5 plants per pot at equal distance and same height.

After two weeks Chromium in the form of chromium oxide and Arsenic in the form of arsenic oxide were added to plants. Levels of treatments, i.e., 0 (control), 10 ppm by plant rooting medium. ZnO nano particles was added by foliar after a few days of heavy metal stress. Water was supplied on daily basis to keep homeostasis. After 15 days of heavy metals stress ZnO nano particles was applied using a manual sprayer early in the morning. Experiments had four replicates and were set up in a completely randomized system (CRD). Data was collected at vegetative stage for the morphological, biochemical and gaseous exchange parameters such as number of leaves, leaf area, chlorophyll contents and gaseous exchange. Various soil and water analysis parameters were also examined. The number of leaves on each plant was counted first, and then the mean value was determined. To determine the leaf area, Carelton and Foote formula as described in Shahbaz and Ashraf (2008) was used. The formula was:

$$\text{Leaf Area (cm}^2\text{)} = \text{maximum leaf length} \times \text{maximum leaf width} \times 0.75$$

(Correction factor = 0.75)

Chlorophyll a, b and carotenoid contents were calculated by Arnon procedure as described by Nazeer et al. (2020). IRGA (LCA-4 ADC portable infrared gas analyzer (Analytical Production Firm, Hoddeson, England. Model C1-340) was used to estimate the gas exchange parameters such as photosynthetic and transpiration rates, stomatal conductance, and sub-stomatal CO₂ concentration. Data was collected between 10:00am and 02:00pm as mentioned by Khalid et al. (2017). The following adjustments of IRGA were made: leaf surface area (11.35 cm²), leaf chamber temperature (T_{ch}) which may varied from 29.2-37.50 °C, ambient CO₂ concentration (349.12 μmol mol⁻¹), ambient temperature 31-36 °C, gas flow rate of leaf chamber (397 ml min⁻¹), water vapor pressure in chamber 6-9.0 mbar, molar flow of air per unit leaf area (401.06 mol m⁻² s⁻¹), ambient pressure (99.95) KPa, PAR at leaf surface was up to 1515 μmolm⁻².

Water use efficiency was estimated with formula described by Bacon (2009):

$$\text{WUE (g/l)} = (\text{dry wt. of final biomass} - \text{dry wt. of initial biomass}) / \text{Rainfall or water consumed (ml)}$$

Sampling pattern and depth

250 g soil sample in each polyethylene bag were taken within the 8-10-feet radius randomly in order to avoid systematic patterns such as starter or preplant bands from experimental pots of university of Gujrat and analyzed in the Punjab Agriculture Soil Testing Labs Gujrat, Pakistan. Various soil characteristics were determined including soil texture, pH, Electric Conductivity, Organic Matter (%), saturation % and Nitrogen, Phosphorous and potassium in the soils. For the analysis water various water sample were collected from experimental pots of University of Gujrat and examined its physiochemical properties in Punjab Agriculture Water Testing Labs Gujrat, Pakistan. Various water characteristics such as Electric conductivity, Ca + Mg, sodium, HCO₃, Chloride, sodium adsorption ratio, and residual sodium carbonate were determined.

Green synthesis of ZnO nanoparticles

Fresh *Aloe vera* leaves were collected in the area of the University of Gujrat in Pakistan. Tiny fragments of the leaves were chopped. Electrical balancing was used to weigh 35 g of chopped parts. 100 ml purified water was used to boil these leaves. The extracted material was then purified and stored for future use.

To reduce Zinc nitrate into ZnO NPs, *Aloe vera* extract (30 ml) was used as a reducing agent. In *Aloe vera* extract, 3 g of zinc nitrate was added for this reason. After that, the sample was held at 60 °C with magnetic stirring until it dried. To extract moisture, the powder was dried at 400 degrees in a furnace (Singh et al., 2008).

The following methods were used to classify the structural and morphological properties of the sample.

X-ray diffraction analysis

This method was used to characterize nanoparticles and analyze its structure. Each crystalline solid has its own atom structure and powder pattern. Since X-rays interact with the atoms of the lattice planes, the interatomic distance between neighboring atoms is 'd'. Constructive interference happens when the distance length of two rays approaches a whole multiple of the wavelength of radiation used. Bragg's law explains the condition for constructive interference:

$$n\lambda = 2d \sin\theta$$

where 'n' is integral multiple, 'd' is inter atomic spacing, 'λ' the wavelength of X-ray used.

Scanning electron microscopy

A high-resolution image of zinc oxide nano particles with a size of less than 10 nm was obtained using a scanning electron microscope. It specifically tests very small features and artifacts, to put it another way. Nanoparticles range in size from 1 to 100 nm, with an interfacial coating made up mostly of organic and inorganic molecules. The agglomeration mass and irregular shape of nanoparticles is visible in SEM photographs.

Fourier transform infrared spectroscopy

FTIR approach, or a basic failure analysis procedure, can detect molecular motions ranging from two atoms in a diatomic molecule moving in a simple coupled motion to each individual atom in a large poly functional molecule moving. The material knowledge concerning chemical bonding and materials composition can be derived from the research infrared spectra (Griffiths and Haseth, 2007).

Statistical analysis

Data was subjected to two-way variance analysis (ANOVA) for different variables with two factors i.e. variety and treatments using Ministat-C software and means were compared using Tukey 's HSD test at $P \leq 0.05$, with a confidence interval of 95% (Silverman, 2018).

Results

Morphological attributes

Results of ANOVA for morphological parameters was recorded in *Table 1*. ANOVA indicated that the impacts of heavy metals and ZnO nano particles on leaf area and number of leaves of different varieties of wheat (*Triticum aestivum* L.) were highly significant. While effect of varieties showed non-significant results. However, the interaction between treatments and varieties were also highly significant as described in *Table 1*. Highest leaf area was noted at T3 (10 ppm ZnONPs) from Faisalabad variety. Result also narrated that leaf area of both varieties was improved with the foliar spray of 20 ppm ZnONPs. Low leaf area was recorded at 30 ppm ZnONPs + 10 ppm As from both varieties (*Fig. 1A*). Application of ZnONPs at concentration of 30 ppm gave the best result of number of leaves as compare to heavy metal stress at both varieties of wheat. However, control from Faisalabad variety also had high number of leaves as compare to other treatments (*Fig. 1B*).

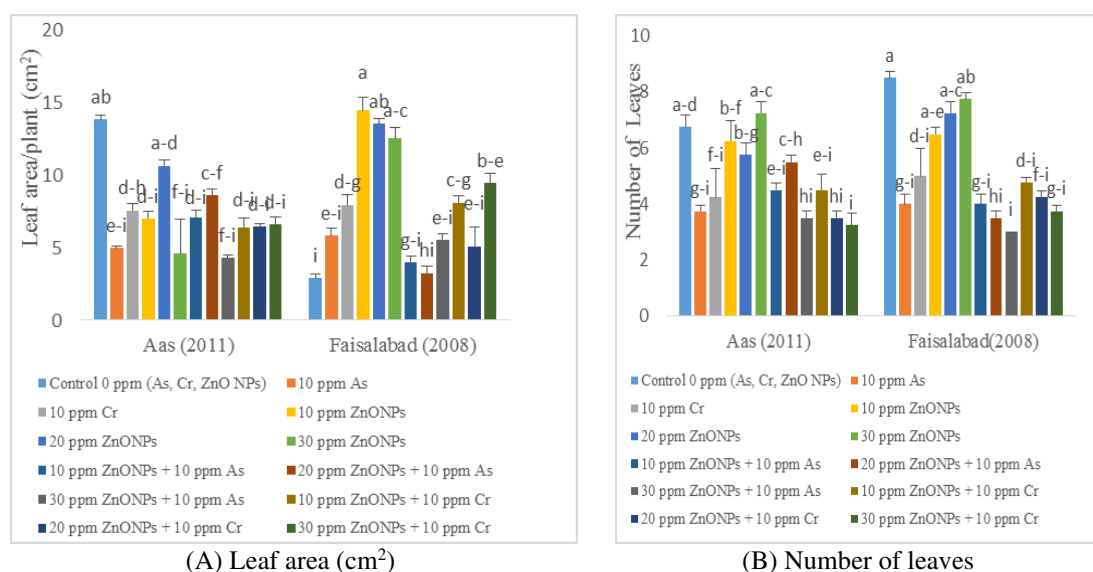


Figure 1. Interactive role of zinc oxide nanoparticles and heavy metals (arsenic and chromium) toxicity on morphological parameters of wheat (*Triticum aestivum* L.)

Biochemical attributes

Analysis of variance ANOVA on biochemical parameters (chlorophyll a, b and carotenoids) was presented in *Table 1*. Results showed that effect of heavy metals and ZnO on chlorophyll and carotenoids content were highly significant with highly significant interaction between treatments and varieties. Graphical representation showed that highest values of chlorophyll and carotenoids content were obtained at combination of 30 ppm ZnONPs + 10 ppm Cr in Faisalabad variety as compare to other treatments. On the other hand, heavy metals (10 ppm Cr and As) stress reduced chlorophyll contents in both varieties of wheat (*Fig. 2A, B, C*).

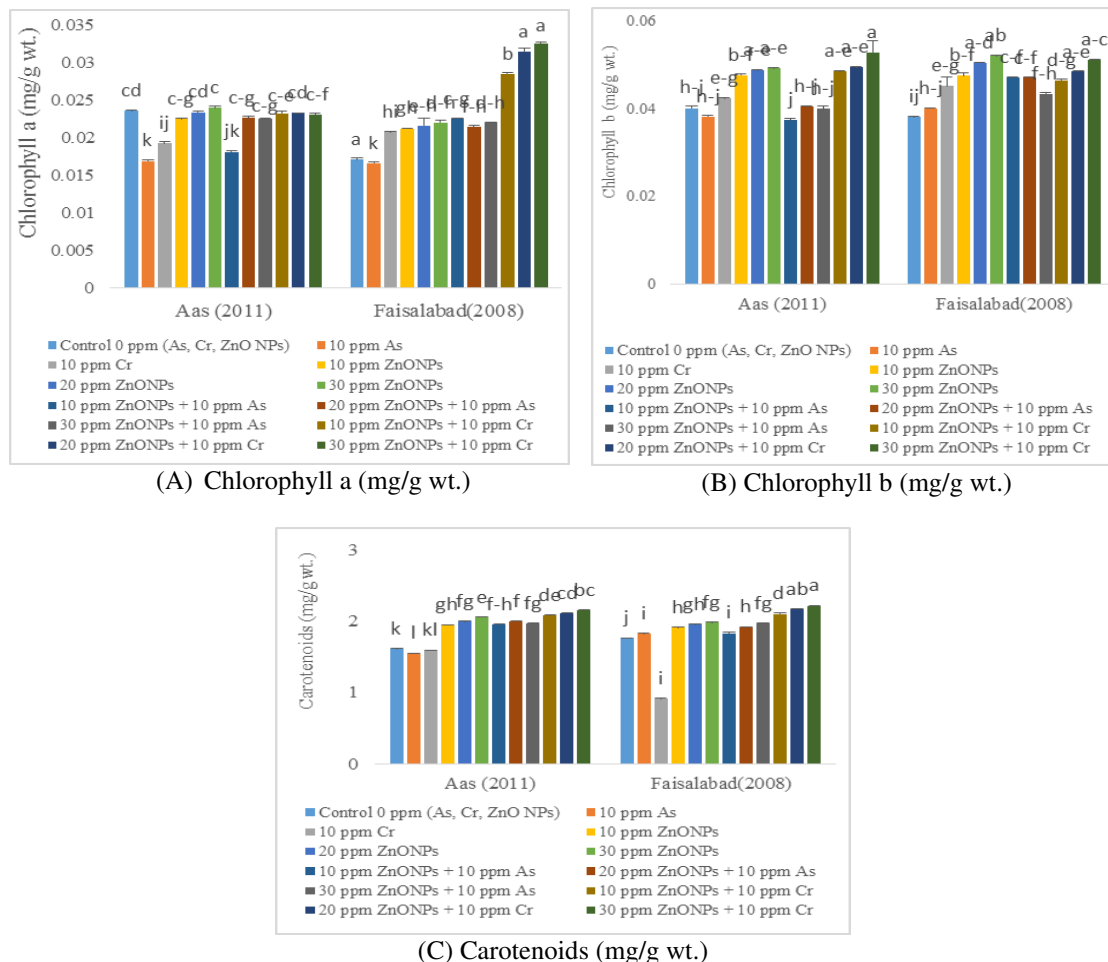


Figure 2. Interactive role of zinc oxide nanoparticles and heavy metals (arsenic and chromium) toxicity on biochemical parameters of wheat (*Triticum aestivum* L.)

Table 1. ANOVA (means squares) for morphological and biochemical parameters of wheat under interactive role of zinc oxide nanoparticles and heavy metals (arsenic and chromium) toxicity

Source	df	Leaf area/plants (cm ²)	Number of leaves/plants	Chlorophyll a (mg/g)	Chlorophyll b (mg/g)	Carotenoids content (mg/g)
Variety	1	3.523ns	2.041ns	0.00003***	0.00008***	0.0404***
Treatment	11	39.526***	19.053***	0.00008***	0.0001***	0.2265***
Variety × treatment	11	54.254***	1.928***	0.00004***	0.00002***	0.0350***
Error	72	2.804	0.652	0.0000	0.00000	0.0003
Total	95	1237.01	279.833	0.0014	0.0023	2.9398

Gaseous exchange attributes

Analysis of variance ANOVA from *Table 2* showed interactive role of heavy metals and ZnO nano particle on gaseous exchange parameters of different varieties of wheat. Varietal effect of photosynthetic, transpiration and stomatal conductance rate were non-significant while, water use efficiency and CO₂ conc. showed highly significant results. However, effect of treatments on all gaseous exchange parameters were highly significant with its interactions except water use efficiency which showed non-significant results. From *Figure 3A* maximum photosynthetic rate was observed in Faisalabad variety at foliar spray of 10 ppm ZnO under As stress as compare to other variety and treatments. Treatment of Cr and As decreased transpiration rate in wheat plants. Application of ZnO concentration 20 ppm gave best results of transpiration rate to overcome heavy metals stress (*Fig. 3B*). It was also concluded from the results that heavy metal stress reduced CO₂ concentration and reduction was greater in Faisalabad (2008) as compare to Aas (2011) (*Fig. 3C*). A significant reduction in the stomatal conductance was noticed when heavy metals (Cr and As) was applied on plants of both varieties (*Fig. 3D*). Graph also demonstrated that Faisalabad (2008) showed less water use efficiency on all treatments it means that there was no effect of heavy metal and ZnO on plants of Aas (2011) (*Fig. 3E*). Foliar spray of ZnO under heavy metal (As) stress gave best results of relative water content at concentration of 10, 20, and 30 ppm in both varieties of wheat as compare to all other treatments (*Fig. 3F*).

Soil analysis attributes

ANOVA results of different soil analysis parameters of two varieties of wheat was recorded in *Table 3*. There was non-significant effect of heavy metals and ZnO on all soil analysis characteristics of wheat varieties. The interaction between variety and treatment also showed non-significant outcomes. Results from *Figure 4A* narrated that heavy metals did not affect soil pH of both varieties of wheat and plants grown under normal condition. Results showed that electric conductivity of soil also did not affect by heavy metals stress as ZnO nano particles enhanced the growth and productivity of plant in the soil. Electric conductivity reached up to normal levels after all treatments of ZnO under heavy metal stress (*Fig. 4B*). Organic matter in soil characteristics also not changed by heavy metals stress and increased growth of plant by ZnO Nano particles application on wheat varieties (*Fig. 4C*). The concentrations of phosphorous and potassium remain same at all treatments of both varieties of wheat as Cr and As not affected the ions concentration in soil of all plants (*Fig. 4D, E*). Saturation in soil also not changed by any kind of treatments (*Fig. 4F*).

Table 2. ANOVA (means squares) for gaseous exchange parameters of wheat under interactive role of zinc oxide nanoparticles and heavy metals (arsenic and chromium) toxicity

Source	df	Photosynthetic rate (μmol/m ² /sec)	Transpiration rate (mmol/m ² /sec)	Inter-cellular CO ₂ concentration (μmol/m ² /sec)	Stomatal conductance rate (mmol/m ² /sec)	Water use efficiency (mmol/mol)	Relative water contents (%)
Variety	1	2.503ns	0.2430ns	25.318***	0.001ns	545930***	179.5ns
Treatment	11	23.854***	0.1529ns	2.958ns	0.002***	26267ns	1450.5***
Variety × treatment	11	32.942***	0.5060***	10.364***	0.0003ns	26158ns	1392.0***
Error	72	3.156	0.1667	2.335	0.0003	26223	234.0
Total	95	854.527	19.4940	339.95	0.0508	3010633	48293.7

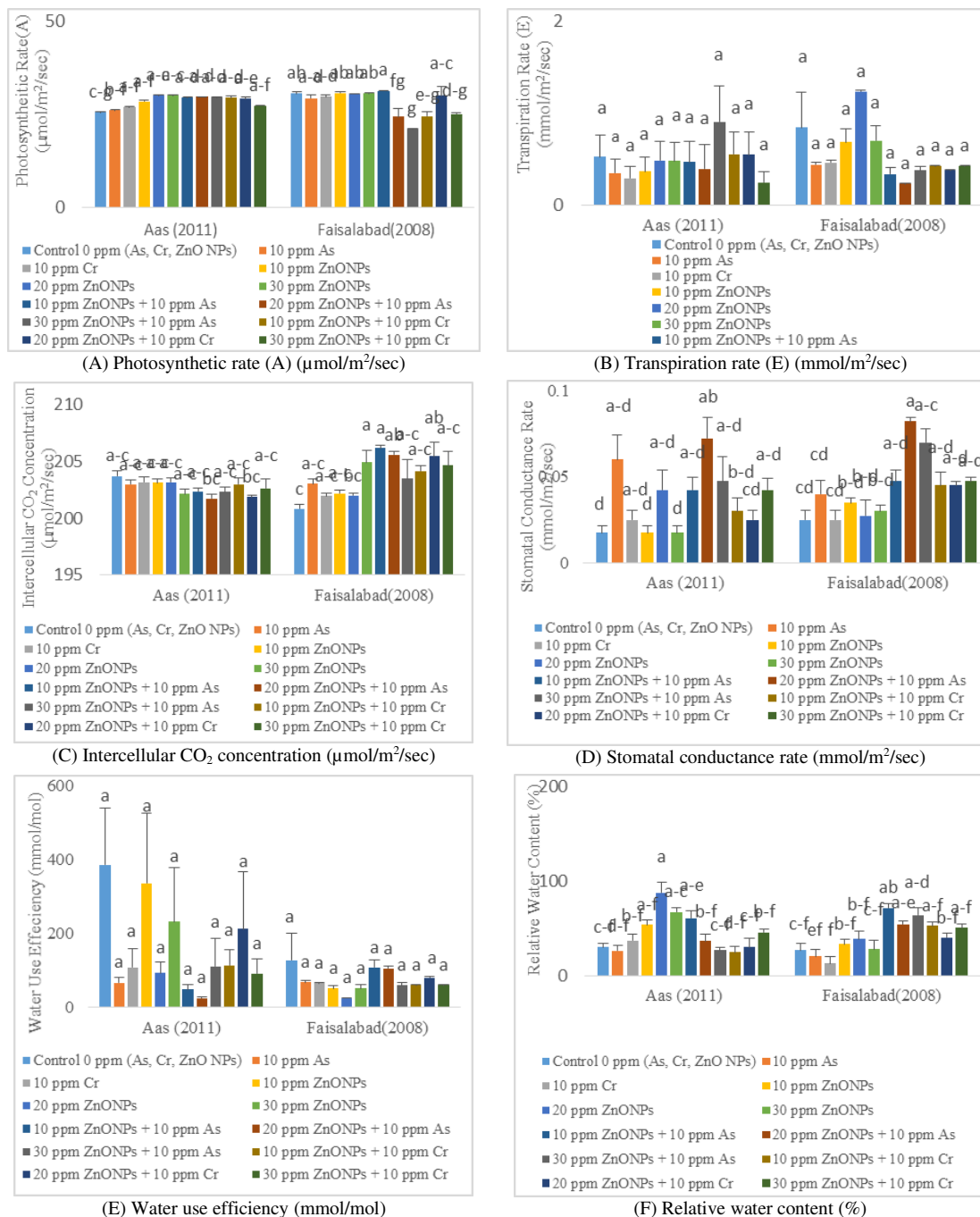


Figure 3. Interactive role of zinc oxide nanoparticles and heavy metals (arsenic and chromium) toxicity on gaseous exchange parameters of wheat (*Triticum aestivum* L.)

Table 3. ANOVA (means squares) for soil analysis parameters of wheat under interactive role of zinc oxide nanoparticles and heavy metals (arsenic and chromium) toxicity

Source	df	Soil pH	Soil E.C	O.M %	Phosphorous (ppm)	Potassium (ppm)	Soil saturation %
Variety	1	0.0001ns	0.063ns	0.003ns	3.840ns	48490208ns	292494ns
Treatment	11	0.0112ns	0.058*	0.002ns	1.646ns	48172515ns	127244ns
Variety × treatment	11	0.0012ns	0.030ns	0.003ns	1.495ns	48214787ns	126842ns
Error	72	0.0101	0.031	0.002	1.629	4818662	140763
Total	95	0.8648	3.341	0.264	153.684	4578187366	13222393

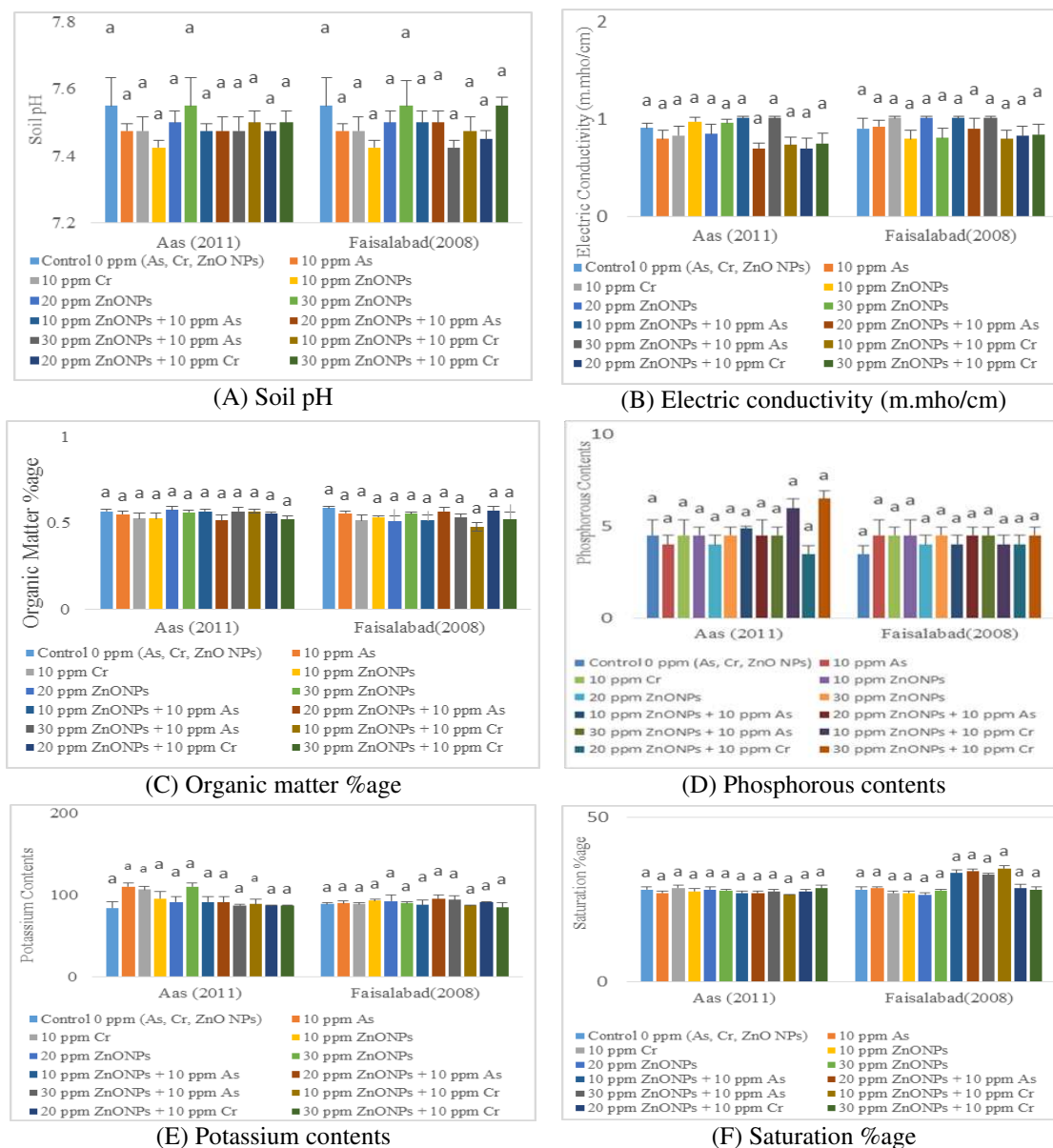


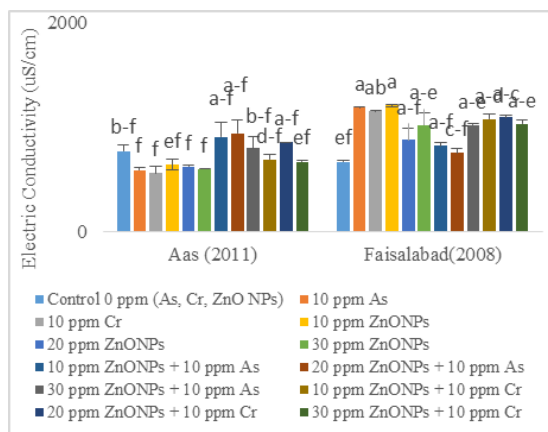
Figure 4. Interactive role of zinc oxide nanoparticles and heavy metals (arsenic and chromium) toxicity on soil analysis parameters of wheat (*Triticum aestivum* L.)

Water analysis attributes

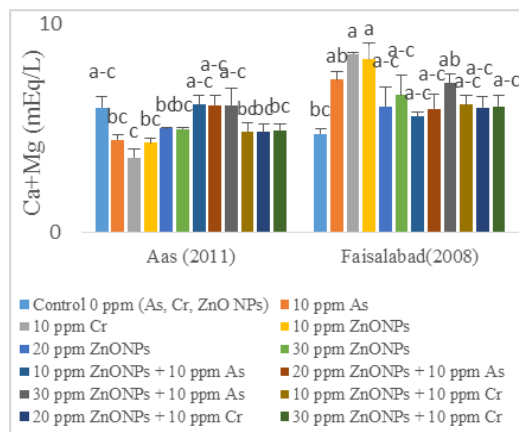
ANOVA results for water analysis parameters of wheat varieties was noted in *Table 4*. Results indicated that the effect of heavy metal and interactive role of ZnO nano particle was highly significant on water characteristics of both varieties of wheat. The interactions between treatments and varieties also showed highly significant results. Results also narrated that water analysis characteristics were highly observed in Faisalabad (2008) as compare to Aas (2011) at all treatments. In Faisalabad (2008), maximum values of water characteristics were detected in plants under heavy metal (Cr and As) stress as there was no effect of heavy metal on water characteristics. From the results of experimental data, it was concluded that heavy metal stress less reduced in water parameters. And this little reduction was more prominent in Faisalabad (2008) as compare to Aas (2011) (*Fig. 5A-G*).

Table 4. ANOVA (means squares) for water analysis parameters of wheat under interactive role of zinc oxide nanoparticles and heavy metals (arsenic and chromium) toxicity

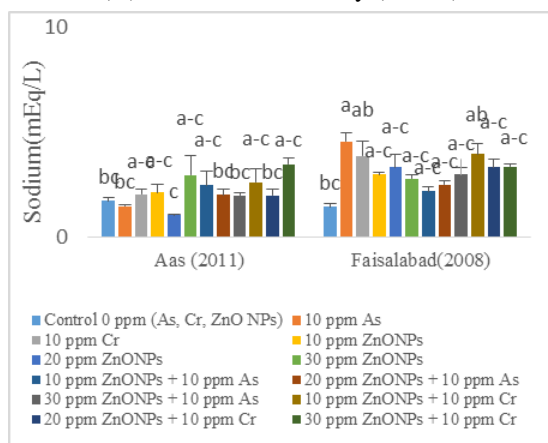
Source	df	EC (uS/cm)	Ca + Mg (mEq/L)	Na (mEq/L)	HCO ₃ (mEq/L)	Cl (mEq/L)	Sodium adsorption ratio	Residual sodium carbonate
Variety	1	1769366***	49.163***	21.5651***	71.760***	2.070***	4.9641***	0.130*
Treatment	11	40289*	1.234 ns	2.0973**	1.049ns	0.041*	0.5374*	0.110***
Variety × treatment	11	147468***	6.372***	2.3631***	5.930***	0.179***	0.6468**	0.068**
Error	72	20987	1.369	0.883	1.439	0.023	0.281	0.034
Total	95	5345770	231.42	134.26	252.15	6.211	38.287	4.5459



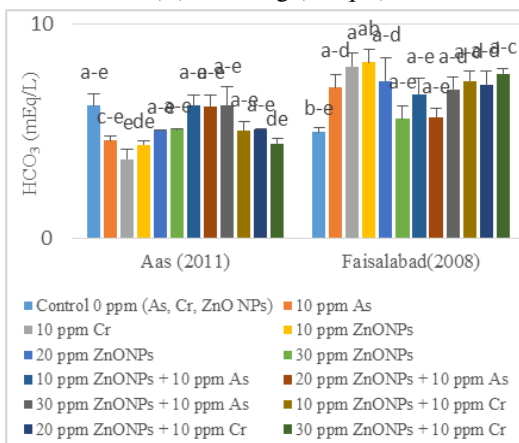
(A) Electric conductivity (uS/cm)



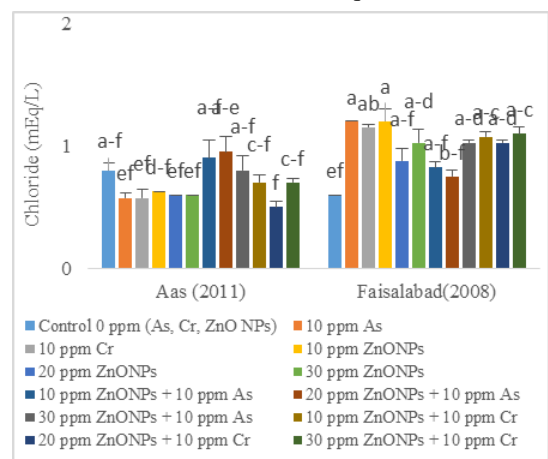
(B) Ca + Mg (mEq/L)



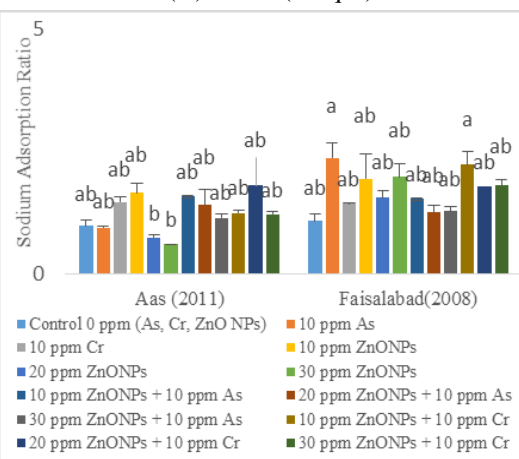
(C) Sodium (mEq/L)



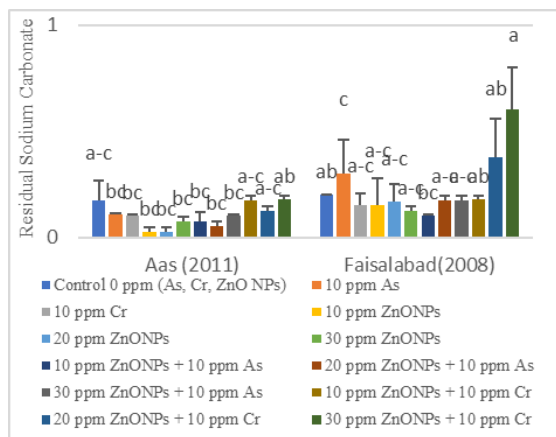
(D) HCO₃ (mEq/L)



(E) Chloride (mEq/L)



(F) Sodium adsorption ratio



(G) Residual sodium carbonate

Figure 5. Interactive role of zinc oxide nanoparticles and heavy metals (arsenic and chromium) toxicity on water analysis parameters of wheat (*Triticum aestivum* L.)

Fourier transform infrared spectroscopy of ZnO nano particles

Figure 6 showed the analysis of ZnO nano particles under heavy metal stress in wheat plants. In order to analyze the structure of the bonds present in the ZnO prepared sample, the FTIR was used. The FTIR spectrum of ZnO nanoparticles was found to be in the 4000-500 cm^{-1} band. The extended modes of ZnO nano particles were defined as the peaks observed in the 500-1000 cm^{-1} region. The hydroxyl group of absorbed H_2O molecules caused the peak around 9705 cm^{-1} . C – O – C and O – H bonds caused the peaks around 14415 and 15523 cm^{-1} . Due to the bound H_2O molecules present on the surface of the ZnO nanoparticles, an extreme peak at 317877 cm^{-1} was assigned to O – H group stretching vibrations.

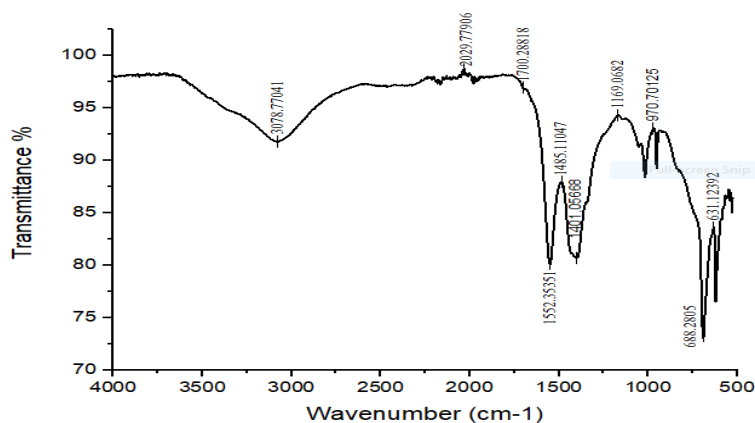


Figure 6. Interactive role of zinc oxide nanoparticles and heavy metals (arsenic and chromium) toxicity on FTIR, of wheat (*Triticum aestivum* L.)

Scanning electron microscopy of ZnO nano particles

Scanning electron microscopy was used to examine the surface morphology of a prepared sample of ZnO nano particles, as seen in Figure 7. The microscopy images clearly showed the homogenous and uniformly distributed ZnO nano particles.

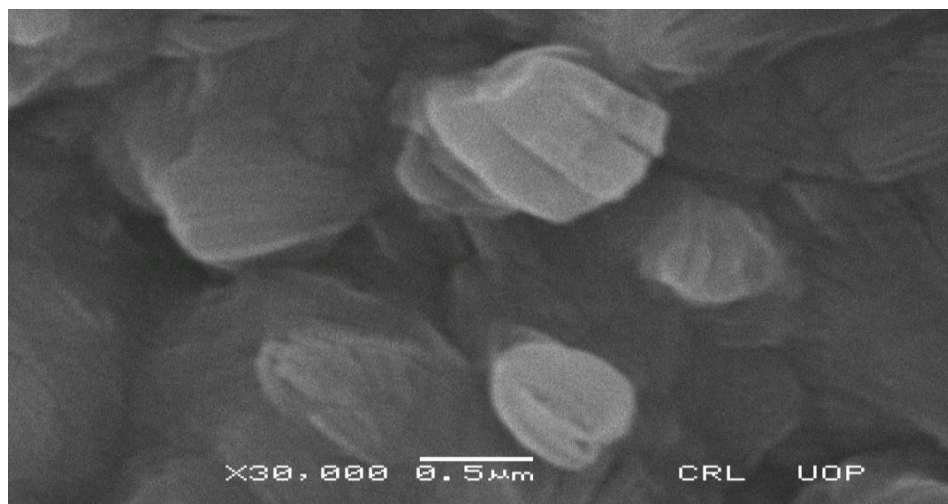


Figure 7. Interactive role of zinc oxide nanoparticles and heavy metals (arsenic and chromium) toxicity on SEM of ZnO nanoparticles of wheat (*Triticum aestivum* L.)

XRD analysis of ZnO nano particles

X-ray diffraction analysis confirmed the phase and crystal structure of ZnO nano particles made with *Aloe vera* extract, and the pattern was reported in the range of 200 to 600, as shown in *Figure 8*. In this pattern the peaks were detected at angles 2θ of 25.3° , 36.1° , 37.5° , 41.5° , 42.3° , 45.2° , 46.1° , 47.2° corresponding to the lattice planes (100), (002), (101), (102), (110), (103), (200), (112), (201), (004) and (202) respectively.

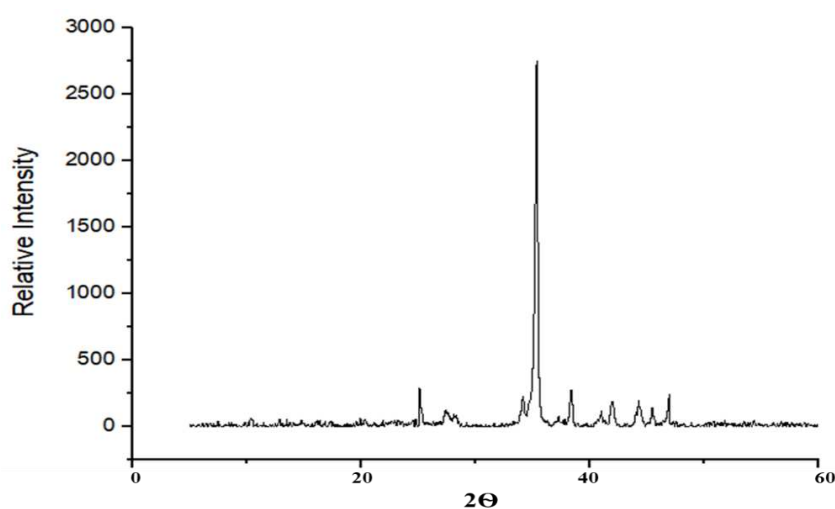


Figure 8. Interactive role of zinc oxide nanoparticles and heavy metals (arsenic and chromium) toxicity on XRD pattern of zinc oxide nanoparticles of wheat (*Triticum aestivum* L.)

Discussion

Arsenic induces oxidative stress in plants by starting a chain reaction that disrupts metabolic processes. Several toxic intermediates released during stress, including superoxide anion, hydroxyl radicals, hydrogen peroxide, and lipid peroxide, disrupt

cellular processes and trigger growth arrest (Majumder et al., 2018). Since it is a key component for auxin synthesis and aggregation, indole-3-acetic acid, which is important for cell division and expansion, ZnO nanoparticles release Zn, which regulates development (Seleiman et al., 2021). Under stress conditions, Zn application preserves membrane integrity by binding to sulfhydryl groups as well as phospholipids, according to Soares et al. (2019). It was also found from the result that Zn is necessary for preserving the structural integrity of plants membranes under salinity stress. In reality, Zn supplementation improves the absorption of micro- and macronutrients that are depleted in stressful situations (Latef et al., 2017).

In our research, however, ZnO–NP supplementation greatly increased the biomass, growth as well as yield of arsenic stressed wheat plants. These findings are similar to those of Rizwan et al. (2017), who found that applying ZnO–NP to Cd-stressed maize plants significantly increased growth. In several other species, including *Leucaena leucocephala*, ZnO–NPs application has been shown to decreased oxidative stress caused by heavy metal (Venkatachalam et al., 2017).

Under As stress, photosynthetic attributes of the soybean plants were found to be reduced. Since arsenic interferes with nitrogen metabolism, it has a lower bioavailability (Rahman et al., 2007). The use of ZnO–nano particles significantly enhanced the amount of chlorophylls in leaves, as well as improving gas exchange attributes. These observations support those of Faizan et al. (2018), who found that applying ZnO–NP to rice plants increased photosynthetic rates. Results from our findings showed that leaf relative water content also reduced in As stressed wheat plants. On the other hand, there was a significant increase in water capacity and RWC of the leaves when arsenic-stressed wheat plants were supplemented with different concentrations of ZnO–NP. This may be attributed to improved water and mineral portion uptake in the vicinity of ZnO–NP (Veza et al., 2018).

Damage to the photosynthetic apparatus caused by arsenate, as well as changes in pigment content and photosynthetic capacity, delayed growth. Increased ROS development under arsenate stress disrupted biochemical and metabolic processes in the test cultivar, resulting in a significant decrease in chlorophyll and carotenoid content and unfavorable associations with applied arsenate (Sil et al., 2019). In Gouan (*Aeluropus littoralis*), replacing Mg^{2+} with arsenic in the chlorophyll structure has been shown to reduce chlorophyll content, lowering photosynthetic rate (Rastgoo and Alemzadeh, 2011). Under arsenate stress, destruction of chloroplasts and photosynthetic apparatus decreased gaseous exchange characters in the cultivar. Heavy metal stress (Cr and As) has been shown to affect various gaseous attributes as well as chlorophyll content of various plants (Gill et al., 2016).

Chromium is more phytotoxic than other metals due to its higher electronegativity (Su et al., 2019). The presence of Cr^{6+} has an effect on plant growth because it prevents seed germination by interfering with amylase activity. Since chromate interfered with stomatal opening and closure, transpiration and stomatal process were also decreased. In the presence of chromium, photosynthesis, transpiration, and water usage efficiency both decreased by up to 31%, 30%, and 29% respectively (Zaheer et al., 2020).

To prevent Zn hidden hunger in humans, higher Zn concentrations in cereal grains are expected (Qaswar et al., 2017). This increased Zn content in cereal grains can be accomplished by a variety of methods, including the use of Zn fertilizers and the production of high Zn accumulating varieties. A level of > 40 mg Zn per kg of grains is

required for Zn biofortification (Cakmak et al., 2017). Higher Zn concentrations can promote wheat growth, resulting in a reduction in heavy metal per unit biomass. Zn NPs and Zn salts were recently confirmed to enhance sorghum growth and nutritional stability with NPK inputs, as well as increase plant nitrogen contents (Dimkpa et al., 2017).

Conclusion

This research shows that ZnO–NPs are effective at reducing heavy metal (As and Cr) toxicity in wheat plants at various concentrations. ZnO–NPs could therefore prove to be an excellent foliar fertilizer in areas vulnerable to heavy metal toxicity if applied at specific doses. Therefore, it was concluded that the use of these nanoparticles will improve system of cropping performance by reducing As and Cr stress and increasing plant growth, yield and soil quality.

Nanotechnology is strengthening the performance and efficiency of common products, making our lives easier. It contributes to a healthy environment by delivering cleaner air and water, as well as clean renewable energy for a long-term future. Nanotechnology has gotten a lot of attention, and top institutions, industries, and organisations are investing more in research and development. Nanotechnology has established itself as a cutting-edge field of science in which extensive research is being conducted in order to put the technology into practice. This study further recommended that Nanotechnology has a bright future because of its efficiency and environmental benefits.

REFERENCES

- [1] Bacon, M. (2009): Water Use Efficiency in Plant Biology. – John Wiley & Sons, CSIRO, Australia.
- [2] Cakmak, I., McLaughlin, M. J., White, P. (2017): Zinc for better crop production and human health. – Plant and Soil 411: 1-4.
- [3] Caro, D., Davis, S. J., Kebreab, E., Mitloehner, F. (2018): Land-use change emissions from soybean feed embodied in Brazilian pork and poultry meat. – Journal of Cleaner Production 172: 2646-2654.
- [4] Dimkpa, C. O., White, J. C., Elmer, W. H., Gardea-Torresdey, J. (2017): Nanoparticle and ionic Zn promote nutrient loading of sorghum grain under low NPK fertilization. – Journal of Agricultural and Food Chemistry 65: 8552-8559.
- [5] Faizan, M., Faraz, A., Yusuf, M., Khan, S. T., Hayat, S. (2018): Zinc oxide nanoparticle-mediated changes in photosynthetic efficiency and antioxidant system of tomato plants. – Photosynthetica 56: 678-686.
- [6] Farouk, S., Al-Amri, S. M. (2019): Exogenous melatonin-mediated modulation of arsenic tolerance with improved accretion of secondary metabolite production, activating antioxidant capacity and improved chloroplast ultrastructure in rosemary herb. – Ecotoxicology and Environmental Safety 180: 333-347.
- [7] Fu, Z., Xi, S. (2020): The effects of heavy metals on human metabolism. – Toxicology Mechanisms and Methods 30: 167-176.
- [8] Gill, R. A., Ali, B., Cui, P., Shen, E., Farooq, M. A., Islam, F., Zhou, W. (2016): Comparative transcriptome profiling of two *Brassica napus* cultivars under chromium toxicity and its alleviation by reduced glutathione. – BMC Genomic 17: 1-25.
- [9] Griffiths, P., De Haseth, J. A. (2007): Fourier Transform Infrared Spectrometry. – John Wiley & Sons, Hoboken, NJ.

- [10] Hussain, A., Ali, S., Rizwan, M., Rehman, M. Z., Javed, M. R., Imran, M., Nazir, R. (2018): Zinc oxide nanoparticles alter the wheat physiological response and reduce the cadmium uptake by plants. – *Environmental Pollution* 242: 1518-1526.
- [11] Ifeanyichukwu, U. L., Fayemi, O. E., Ateba, C. N. (2020): Green synthesis of zinc oxide nanoparticles from pomegranate (*Punica granatum*) extracts and characterization of their antibacterial activity. – *Molecules* 25: 4521.
- [12] Khalid, N., Hussain, M., Hameed, M., and Ahmad, R. (2017): Physiological, biochemical and defense system responses of *Parthenium hysterophorus* to vehicular exhaust pollution. – *Pakistan Journal of Botany* 49: 67-75.
- [13] Latef, A. A. H. A., Alhmad, M. F. A., Abdelfattah, K. E. (2017): The possible roles of priming with ZnO nanoparticles in mitigation of salinity stress in lupine (*Lupinus termis*) plants. – *Journal of Plant Growth and Regulation* 36: 60-70.
- [14] Lin, D., Xing, B. (2007): Phytotoxicity of nanoparticles: inhibition of seed germination and root growth. – *Environmental Pollution* 150: 243-250.
- [15] Majumder, B., Das, S., Mukhopadhyay, S., Biswas, A. K. (2019): Identification of arsenic-tolerant and arsenic-sensitive rice (*Oryza sativa* L.) cultivars on the basis of arsenic accumulation assisted stress perception, morpho-biochemical responses, and alteration in genomic template stability. – *Protoplasma* 256: 193-211.
- [16] Mushtaq, Z., Asghar, H. N., Zahir, Z. A. (2021): Comparative growth analysis of okra (*Abelmoschus esculentus*) in the presence of PGPR and press mud in chromium contaminated soil. – *Chemosphere* 262: 127865.
- [17] Nazeer, A., Hussain, K., Hassain, A., Nawaz, K., Bashir, Z., Ali, S. S., Yasin, G. (2020): Influence of Foliar Applications of IAA, NAA and GA₃ on Growth, Yield and Quality of Pea (*Pisum sativum* L.). – *Indian Journal of Agriculture Research* 54: 699-707.
- [18] Qaswar, M., Hussain, S., Rengel, Z. (2017): Zinc fertilisation increases grain zinc and reduces grain lead and cadmium concentrations more in zinc-biofortified than standard wheat cultivar. – *Science of the Total Environment* 605: 454-460.
- [19] Rahman, M. A., Hasegawa, H., Rahman, M. M., Islam, M. N., Miah, M. M., Tasmen, A. (2007): Effect of arsenic on photosynthesis, growth and yield of five widely cultivated rice (*Oryza sativa* L.) varieties in Bangladesh. – *Chemosphere* 67: 1072-1079.
- [20] Rastgoo, L., Alemzadeh, A. (2011): Biochemical responses of Gouan (*Aeluropus littoralis*) to heavy metals stress. – *Australian Journal of Crop Science* 5: 375.
- [21] Rizwan, M., Ali, S., Ali, B., Adrees, M., Arshad, M., Hussain, A., Waris, A. A. (2019): Zinc and iron oxide nanoparticles improved the plant growth and reduced the oxidative stress and cadmium concentration in wheat. – *Chemosphere* 214: 269-277.
- [22] Sansaloni, C., Franco, J., Santos, B., Percival-Alwyn, L., Singh, S., Petroli, C., Pixley, K. (2020): Diversity analysis of 80,000 wheat accessions reveals consequences and opportunities of selection footprints. – *Nature Communications* 11: 1-12.
- [23] Seleiman, M. F., Almutairi, K. F., Alotaibi, M., Shami, A., Alhammad, B. A., Battaglia, M. L. (2021): Nano-fertilization as an emerging fertilization technique: why can modern agriculture benefit from its use? – *Plants* 10: 2.
- [24] Shahbaz, M., Ashraf, M. (2008): Does exogenous application of 24-epibrassinolide ameliorate salt induced growth inhibition in wheat (*Triticum aestivum* L.)? – *Journal of Plant Growth and Regulation* 55: 51-64.
- [25] Shang, Y., Hasan, M., Ahammed, G. J., Li, M., Yin, H., Zhou, J. (2019): Applications of nanotechnology in plant growth and crop protection: a review. – *Molecules* 24(14): 2558.
- [26] Singh, J., Dutta, T., Kim, K. H., Rawat, M., Samddar, P., Kumar, P. (2018): 'Green' synthesis of metals and their oxide nanoparticles: applications for environmental remediation. – *Journal of Nanobiotechnology* 16(1): 1-24.
- [27] Sil, P., Das, P., Biswas, S., Mazumdar, A., Biswas, A. K. (2019): Modulation of photosynthetic parameters, sugar metabolism, polyamine and ion contents by silicon amendments in wheat (*Triticum aestivum* L.) seedlings exposed to arsenic. – *Environmental Science and Pollution Research* 26: 13630-13648.

- [28] Silverman, B. W. (2018): Density Estimation for Statistics and Data Analysis. – CRC Press, Taylor & Francis Group, Routledge, London.
- [29] Soares, C., Carvalho, M. E., Azevedox, R. A., Fidalgo, F. (2019): Plants facing oxidative challenges—a little help from the antioxidant networks. – Environmental and Experimental Botany 161: 4-25.
- [30] Su, C. Q., Li, L. Q., Yang, Z. H., Chai, L. Y., Qi, L. I. A. O., Yan, S. H. I., Li, J. W. (2019): Cr (VI) reduction in chromium-contaminated soil by indigenous microorganisms under aerobic condition. – Transactions of Nonferrous Metals Society of China 29: 1304-1311.
- [31] Tripathi, D. K., Singh, S., Singh, S., Pandey, R., Singh, V. P., Sharma, N. C., Chauhan, D. K. (2017): An overview on manufactured nanoparticles in plants: uptake, translocation, accumulation and phytotoxicity. – Plant Physiology and Biochemistry 110: 2-12.
- [32] Venkatachalam, P., Jayaraj, M., Manikandan, R., Geetha, N., Rene, E. R., Sharma, N. C., Sahi, S. V. (2017): Zinc oxide nanoparticles (ZnONPs) alleviate heavy metal-induced toxicity in *Leucaena leucocephala* seedlings: a physiochemical analysis. – Plant Physiology and Biochemistry 110: 59-69.
- [33] Vezza, M. E., Llanes, A., Travaglia, C., Agostini, E., Talano, M. A. (2018): Arsenic stress effects on root water absorption in soybean plants: physiological and morphological aspects. – Plant Physiology and Biochemistry 123: 8-17.
- [34] Wakeel, A., Xu, M., Gan, Y. (2020): Chromium-induced reactive oxygen species accumulation by altering the enzymatic antioxidant system and associated cytotoxic, genotoxic, ultrastructural, and photosynthetic changes in plants. – International Journal of Molecular Science 21: 728.
- [35] Watson, J. L., Fang, T., Dimkpa, C. O., Britt, D. W., McLean, J. E., Jacobson, A., Anderson, A. J. (2015): The phytotoxicity of ZnO nanoparticles on wheat varies with soil properties. – Biometals 28: 101-112.
- [36] Wu, F., Fang, Q., Yan, S., Pan, L., Tang, X., Ye, W. (2020): Effects of zinc oxide nanoparticles on arsenic stress in rice (*Oryza sativa* L.): germination, early growth, and arsenic uptake. – Environmental Science and Pollution Research 27(21): 26974-26981.
- [37] Zafar, H., Ali, A., Ali, J. S., Haq, I. U., Zia, M. (2016): Effect of ZnO nanoparticles on Brassica nigra seedlings and stem explants: growth dynamics and antioxidative response. – Frontiers in Plant Science 7: 535.
- [38] Zaheer, I. E., Ali, S., Saleem, M. H., Imran, M., Alnusairi, G. S., Alharbi, B. M., Soliman, M. H. (2020): Role of iron-lysine on morpho-physiological traits and combating chromium toxicity in rapeseed (*Brassica napus* L.) plants irrigated with different levels of tannery wastewater. – Plant Physio. Biochemistry 155: 70-84.

GENETIC VARIABILITY AND HERITABILITY AMONG MANDARIN (*CITRUS RETICULATA* BLANCO) GENOTYPES UNDER INDIAN SUB-TROPICAL CONDITIONS

SINGH, G.^{1*} – RATTANPAL, H. S.¹ – GUPTA, M.¹ – SIDHU, G. S.²

¹*Department of Fruit Science, Punjab Agricultural University, Ludhiana 141004, Punjab, India*

²*School of Agricultural Biotechnology, Punjab Agricultural University, Ludhiana 141004, Punjab, India*

**Corresponding author*

e-mail: gurteg-hort@pau.edu; phone: +91-098-1509-8883

(Received 14th Dec 2021; accepted 2nd May 2022)

Abstract. An effort has been made to study the genotypic variance, heritability, and genetic advance among nineteen mandarin genotypes grown under Indian sub-tropical conditions. The cluster analysis differentiated diverse genotypes which were grouped independently of their geographical origin. Wide variability in morphological characteristics indicated the genetic variability among mandarin genotypes. Rootstock diameter, scion diameter, fruit weight and seed weight showed a higher genotypic coefficient of variance, genetic advance and heritability, and genetic advance percentage of means. However, the phenotypic coefficient of variance was higher than the genotypic coefficient of variance for all the traits under study. The study indicated the existence of diversity in analyzed mandarin accessions. Furthermore, it concluded that the occurrence of additive gene action with low environmental influence is responsible for the determination of rootstock diameter, scion diameter, fruit weight, and seed weight as compared to other traits under study. Fruit yield was strongly correlated with the leaf lamina thickness and fruit weight followed by seed weight, indicating that fruit weight and seed weight can be used as selection criteria in an early year of bearing under crop improvement programme. Principal component analysis (PC1) distinguished positive correlations between fruit weight, fruit diameter, and fruit yield.

Keywords: *citrus, genetic diversity, genetic advance, genotypic variance, phenotypic variance*

Introduction

Citrus is grown extensively in tropical and sub-tropical provinces worldwide. The profitable cultivation of mandarins is concentrated between 40° North and South of the equator (Patil et al., 2012). Citrus is reported to have originated in Southeast Asia, extended up to North Burma, East India, and Southwest of China (Gmitter and Hu, 1990; Soost and Roose, 1996). The maximum citrus germplasm diversity identified in Northeast India including 23 species, one subspecies, and 68 varieties (Sharma et al., 2004). This variation in germplasm might be due to the occurrence of bud sports, natural hybridization, cross-pollination, and the presence of a high percentage of zygotic seedlings (Das et al., 2007; Golein et al., 2011; Singh et al., 2021).

Taxonomic interactions within citrus groups are highly complicated. This complexity in relations might be due to the recurrent occurrence of spontaneous mutants and interspecific hybrids in nature. The crop improvement programs in citrus are mainly based on the depiction of morphological, cytological, and genetic characters of various cultivars (Fatima et al., 2015; Ahmad et al., 2018). The morphological flexibility is considered a major hindrance in the validation of phenotypic diversity. However, the inheritance of agronomic traits of citrus was reported to be governed by multiple genes and evaluated only by their morphological characterization (Liu and Deng, 2007). Morphological

descriptions are the basic passport data of the genotype under the given environmental conditions and that is why they are being used widely (Domingues et al., 1999; Monteverde, 2000; Koehler et al., 2003; Campos et al., 2005; Josan and Kaur, 2006; Lin et al., 2007; Khan et al., 2008, 2014; Kinley and Chinawat, 2011; Dorji and Yapwattanaphun, 2014; Sharma et al., 2015; Baswal et al., 2017; Sunaina et al., 2018; Kaur et al., 2022). The identification of superior genotypes within the collected germplasm is valuable for genetic up-gradation and crop conservation (Clark and Hoy, 2006; Lin et al., 2007; Gaikward et al., 2018; Singh et al., 2022).

The morphological and genetic diversity has been considered as independent from one another (Koehler et al., 2003; Campos et al., 2005; Singh et al., 2017; Rattanpal et al., 2018; Singh et al., 2020). Genetic variability is the basis of any crop improvement program. However, little effort has been made to study the genotypic variance, heritability, and genetic advance among collected accessions. Such a study reveals the nature of inheritance of fruit quantitative and qualitative parameters to design citrus breeding strategies. Moreover, there is a necessity to diversify scion cultivars of citrus for North Indian regions to reduce the new insect-pest load scattering over a narrow genetic pool. Secondly, mandarins represent maximum phenotypic heterozygosity and variation in characters in comparison to other citrus species (Moore, 2001; Faralli et al., 2019).

Thus, the hypothesis for the study is that genetic diversity may be present in mandarin germplasm grown under sub-tropical conditions. Therefore, the present study was carried out to assess the nature and genetic variability in mandarin germplasm.

Materials and methods

Experimental site and climate

The experiment was conducted at the citrus breeding block of Punjab Agricultural University, Ludhiana during 2014 and 2015. This site location is marked at the latitude and longitude 30° 54' N and 75° 48' E, respectively. The climatic zone is subtropical and is situated 247 m above the mean sea level. The mean maximum and minimum monthly temperature for both the years (2014 and 2015) was 40.1 °C and 7.0 °C, respectively. However, the mean maximum monthly relative humidity was 78.2% and the mean minimum monthly relative humidity was 40.75%. The average annual rainfall was 705.8 mm (*Fig. 1*).

Plant material and methodology

A total of 19 mandarin genotypes introduced from the United States of America and different states of India were used in the study (*Table 1*). Fourteen genotypes (CRS-4, Clone-11, Coorg, Darjeeling, Khasi, Mudhkhed Seedless, N-4, N-28, N-34, N-38, N-43, N-51 belonging to *Citrus reticulata* Blanco were introduced from different states of the country while five hybrids (Daisy, Kinnow, Fremont, Nova, and W. Murcott) were introduced from the USA. Rough lemon (*C. jambhiri* Lush.) was used as rootstock for all the genotypes. The age of the studied plants was six years and all the recommended package of practices were followed as per Punjab Agricultural University, Ludhiana, Punjab (India) for citrus cultivation. The morphological descriptors of citrus framed by the International Plant Genetic Resources Institute, Italy (IPGRI, 1999) were used throughout the research period. The number of replication in this experiment was three and each replication included one plant. The total number of plant under study was 57 i.e.

three plants per treatment. The diameter of rough lemon rootstock was measured at 10 cm under graft union; however, scion diameter was noted at 10 cm overhead union. Twenty copiously developed leaves and ten randomly selected fruits were taken for each replication. Leaf quantitative parameter data, viz. leaf lamina length (LLL), leaf lamina width (LLW) and leaf lamina thickness (LLT) and petiolar wing length (PWL) and petiolar wing width (PWW) were measured by using the Vernier's calipers (Mitutoyo Inc., Japan). Fruit parameters data viz. fruit weight, fruit yield, fruit length, fruit diameter, fruit number per tree, seed number per fruit and seed weight were also recorded. The data on total soluble content, as degree Brix, were recorded by using Digital Hand Refractometer. The acidity was estimated as the percentage of citric acid by titrating a well-known volume of juice content against 0.1 N sodium hydroxide (NaOH).

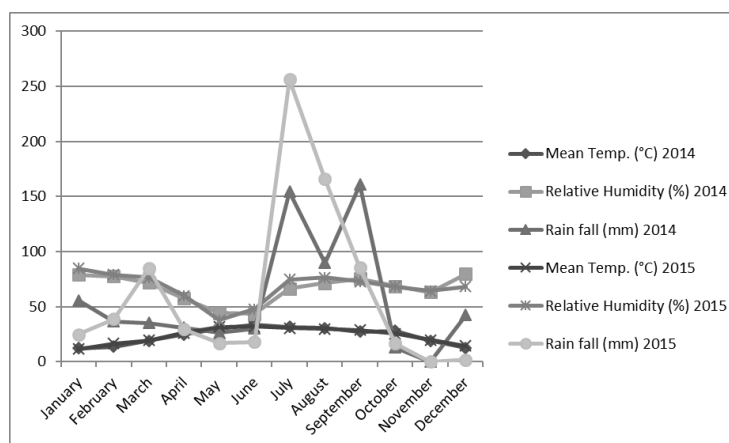


Figure 1. Climatic conditions of the experimental site during the study years 2014 and 2015

Data analysis

The experiment was laid out in Randomized Block Design at the time of planting as described by Gomez and Gomez (2010). Significant differences among genotypes were calculated using one-way ANOVA followed by post hoc Tukey's honestly significant difference (HSD) test at 5% level ($p < 0.05$) for pair wise comparison of genotypes for each of parameters using software version 9.3 (SAS Institute Inc., Cary, NC, USA). The genetic variance (GV) (Eq.1), phenotypic variance (PV) (Eq.2), genotypic coefficient of variance (GCV) (Eq.3) and phenotypic coefficient of variance (PCV) (Eq.4), were computed (Muluaem and Mohammed, 2012).

$$\text{Genotypic variance} = \frac{MSg - MSe}{nr} \quad (\text{Eq.1})$$

$$\text{Phenotypic variance} = \frac{MSg}{nr} \quad (\text{Eq.2})$$

where MSg is genotypic mean square, MSe is error mean square and nr is number of replication.

Table 1. List of mandarin genotypes used in the study

S. No.	Common Name	Latin name	Parentage	Source
1	CRS-4	<i>Citrus reticulata</i> Blanco	Selection	Assam Agricultural University, Tinsukia, Assam
2	Clone-11	<i>Citrus reticulata</i> Blanco	Selection	Central Horticultural Experiment Station, Chettali, Karnataka, India
3	Coorg	<i>Citrus reticulata</i> Blanco	Selection	Central Citrus Research Institute, Nagpur, Maharashtra, India
4	Daisy	<i>Citrus reticulata</i> Blanco	Fortune x Fremont	United States of America
5	Darjeeling	<i>Citrus reticulata</i> Blanco	Selection	Central Citrus Research Institute
6	Fremont	<i>Citrus reticulata</i> Blanco	Clementin mandarin x Ponkan Tangelo	United States of America
7	Khasi	<i>Citrus reticulata</i> Blanco	Selection	Central Citrus Research Institute
8	Kinnow	<i>Citrus nobilis</i> Lourx <i>Citrus deliciosa</i> Tenore	Willow leaf x King Mandarin	United States of America
9	Mudhkhed Seedless	<i>Citrus reticulata</i> Blanco	Selection	Central Citrus Research Institute
10	Nagpur -4	<i>Citrus reticulata</i> Blanco	Nagpur Selection	Central Citrus Research Institute
11	Nagpur -28	<i>Citrus reticulata</i> Blanco	Nagpur Selection	Central Citrus Research Institute
12	Nagpur -34	<i>Citrus reticulata</i> Blanco	Nagpur Selection	Central Citrus Research Institute
13	Nagpur- 38	<i>Citrus reticulata</i> Blanco	Nagpur Selection	Central Citrus Research Institute
14	Nagpur -43	<i>Citrus reticulata</i> Blanco	Nagpur Selection	Central Citrus Research Institute
15	Nagpur-51	<i>Citrus reticulata</i> Blanco	Nagpur Selection	Central Citrus Research Institute
16	Nagpur Seedless	<i>Citrus reticulata</i> Blanco	Nagpur Selection	Central Citrus Research Institute
17	Nagpur	<i>Citrus reticulata</i> Blanco	Selection	Central Citrus Research Institute
18	Nova	<i>Citrus reticulata</i> Blanco	Clementin mandarin x Orlando Tangelo	United States of America
19	W. Murcott	<i>Citrus reticulata</i> Blanco x <i>Citrus sinensis</i>	Murcott and Unknown	United States of America

$$GCV = \frac{\sqrt{VG}}{\text{Grand Mean}} \times 100 \quad (\text{Eq.3})$$

$$PCV = \frac{\sqrt{VP}}{\text{Grand Mean}} \times 100 \quad (\text{Eq.4})$$

Broad sense heritability (h^2) (Eq.5) in percentage was estimated in each character using variance components as described (DeLacy et al., 1996). Genetic advance (GA) and genetic advance percent mean) (GAM) were computed as per Eq.6 and Eq.7, respectively.

$$\text{Heritability } (h^2) = \frac{\text{Genotypic Variance}}{\text{Phenotypic Variance}} \quad (\text{Eq.5})$$

$$\text{Genetic advance} = \sqrt{VP} \times h^2 \times k \quad (\text{Eq.6})$$

where k is the differential selection constant and value for k is 2.06.

$$GAM = \frac{\text{Genetic Advance}}{\text{Grand Mean}} \times 100 \quad (\text{Eq.7})$$

The genetic diversity among the mandarin genotypes was computed based on quantitative data by using the Computer Software DARwin (Perrier and Jacquemoud-Collet, 2006). The data generated dendrogram on subjection to an un-weighted pair group method with arithmetic mean (UPGMA) analysis. The Pearson's Correlation Coefficient method was used to calculate genotypic and phenotypic correlation among important quantitative traits of different mandarin accessions as per the correlation method described by Al-Jibouri et al., 1958. Principle component (PCA) analysis was performed with XLSTAT 14.0 to identify the principal components that contributed the maximum to variability and to identify the association of traits with yield in mandarin germplasm.

Results

Tree traits

All the mandarin genotypes differ significantly in consideration of rootstock diameter (Table 2). The range of rootstock diameter among mandarin genotypes was 36.91 to 124.82. Rootstock diameter (124.82 mm) was the maximum in Darjeeling mandarin and was at par with Nova, Nagpur, Mudhkhed Seedless, Khasi, and Coorg. The maximum scion diameter was observed in Khasi mandarin (97.44 mm) and did not show any significant difference with Nagpur Seedless, Nagpur, Nova, Mudhkhed Seedless, Darjeeling, and Coorg. However, the minimum rootstock diameter (36.91 mm) and scion diameter (27.75 mm) were recorded in the CRS-4 genotype. Scion to rootstock diameter ratio was found to be the maximum in Kinnow (0.90) and was statistically at par with W. Murcott, Nagpur, Nagpur Seedless, Mudhkhed Seedless, Khasi, Fremont, Coorg, and Clone-11. Minimum scion to rootstock diameter ratio (0.69) was observed in N-43 and N-4.

Leaf traits

The data (Table 2, Fig. 2) illustrated significant deviation in quantitative leaf traits amid mandarin genotypes. The maximum mean LLL to width ratio was recorded in Nagpur (2.23) and it was at par with Mudhkhed Seedless, Nagpur Seedless, N-34, N-28, N-4, Khasi, Fremont, Darjeeling, CRS-4, and Coorg. The least average length to width ratio (1.97) of leaf lamina was registered in Kinnow. The maximum mean LLT (0.33 mm) was recorded in Darjeeling and N-43 and both were at par with W. Murcott, N-51, N-28, Kinnow, Daisy, and Coorg. However, the LLT (0.25 mm) was observed to be minimum in Nova genotype. The outcome of the studies depicted that the highest PWL was recorded in N-38 (16.36 mm) which was at par with Nagpur Seedless, Nagpur, N-51, N-43, N-28, and N-4. The least LLW (2.47 mm) was noticed in N-51 that was found statistically at par with N-43, N-38, N-4, Darjeeling, Clone-11, and CRS-4. However, the minimum mean PWL (10.35 mm) and PWW (1.46 mm) were recorded in W. Murcott.

Table 2. Vegetative characters of different mandarin genotypes grown under Punjab conditions (Pooled data 2014 and 2015)

Genotypes	Rootstock Diameter (mm)	Scion diameter (mm)	Scion/Diameter ratio	Leaf lamina length (mm)	Leaf lamina width (mm)	Leaf length/width	Leaf lamina thickness (mm)	Petiole wing length (mm)	Petiole wing width (mm)
CRS-4	36.91 ⁱ	27.75 ⁱ	0.75 ^{de}	68.60 ^{bc}	31.38 ^{efg}	2.19 ^{ab}	0.30 ^{bcd}	13.96 ^{bcd}	2.25 ^{abc}
Clone-11	57.22 ^{gh}	47.69 ^{fgh}	0.83 ^{abcd}	67.71 ^{bc}	32.63 ^{cdefg}	2.08 ^{bcdef}	0.28 ^{efgh}	12.72 ^{def}	2.29 ^{abc}
Coorg	109.04 ^{ab}	92.34 ^{ab}	0.85 ^{abc}	63.81 ^c	30.10 ^g	2.12 ^{abcde}	0.31 ^{abcd}	12.55 ^{defg}	1.80 ^{fg}
Daisy	87.53 ^{cde}	71.35 ^{cd}	0.82 ^{bcd}	74.85 ^a	37.05 ^a	2.02 ^{def}	0.31 ^{abcd}	10.81 ^{gh}	1.83 ^{ef}
Darjeeling	124.82 ^a	94.59 ^{ab}	0.76 ^{de}	71.78 ^{ab}	33.28 ^{bcdefg}	2.16 ^{abcd}	0.33 ^a	13.76 ^{cd}	2.24 ^{abc}
Fremont	74.89 ^{efg}	64.09 ^{de}	0.85 ^{bc}	68.50 ^{bc}	31.58 ^{defg}	2.19 ^{ab}	0.28 ^{efg}	10.96 ^{fgh}	1.47 ^h
Khasi	114.27 ^{ab}	97.44 ^a	0.85 ^{abc}	67.45 ^{bc}	30.85 ^{fg}	2.19 ^{ab}	0.29 ^{def}	12.45 ^{defg}	2.16 ^{bc}
Kinnow	87.18 ^{cde}	78.94 ^{bcd}	0.90 ^a	68.58 ^{bc}	34.75 ^{abcde}	1.97 ^f	0.31 ^{abcd}	11.69 ^{efgh}	2.13 ^{cd}
Mudhkhed	106.01 ^{abc}	87.81 ^{ab}	0.83 ^{abcd}	67.93 ^{bc}	32.65 ^{cdefg}	2.11 ^{abcdef}	0.30 ^{cdef}	13.13 ^{de}	2.09 ^{cde}
Seedless									
N-4	66.11 ^{fg}	45.66 ^{gh}	0.69 ^e	71.13 ^{ab}	34.06 ^{abcdef}	2.12 ^{abcdef}	0.27 ^{fgh}	15.99 ^a	2.31 ^{abc}
N-28	80.48 ^{def}	63.00 ^{def}	0.79 ^{cd}	72.91 ^{ab}	35.00 ^{abcde}	2.08 ^{abcdef}	0.31 ^{abcd}	15.74 ^{ab}	2.13 ^{cd}
N-34	81.18 ^{def}	63.82 ^{de}	0.78 ^{cd}	68.25 ^{bc}	32.75 ^{bcdefg}	2.09 ^{abcdef}	0.30 ^{bcd}	13.94 ^{bcd}	1.84 ^{ef}
N-38	60.01 ^{gh}	49.04 ^{efg}	0.82 ^{bcd}	69.26 ^{bc}	34.40 ^{abcdef}	2.01 ^{def}	0.26 ^{gh}	16.36 ^a	2.41 ^{ab}
N-43	44.31 ^{hi}	32.72 ^{hi}	0.69 ^e	69.62 ^{ab}	33.70 ^{abcdefg}	2.07 ^{bcdef}	0.33 ^{ab}	15.61 ^{abc}	2.23 ^{abc}
N-51	59.93 ^{gh}	44.44 ^{gh}	0.75 ^{de}	71.85 ^{ab}	35.42 ^{abc}	2.04 ^{cdef}	0.31 ^{abcd}	16.22 ^a	2.47 ^a
Nagpur	97.15 ^{bcd}	86.78 ^{abc}	0.89 ^{ab}	69.03 ^{bc}	31.60 ^{defg}	2.19 ^{abc}	0.28 ^{efgh}	15.76 ^{ab}	2.16 ^{bc}
Seedless									
Nagpur	110.61 ^{ab}	94.67 ^{ab}	0.85 ^{abc}	72.63 ^{ab}	32.77 ^{bcdefg}	2.23 ^a	0.29 ^{cdef}	15.56 ^{abc}	1.87 ^{def}
Nova	107.00 ^{ab}	86.81 ^{abc}	0.81 ^{cd}	72.10 ^{ab}	35.12 ^{abcd}	2.05 ^{bcdef}	0.25 ^h	11.68 ^{efgh}	1.55 ^{gh}
W. Murcott	83.03 ^{def}	70.98 ^{cd}	0.86 ^{abc}	71.73 ^{ab}	36.38 ^{ab}	1.98 ^{ef}	0.32 ^{abc}	10.35 ^h	1.46 ^h
Mean	83.56	68.42	0.81	69.88	33.45	2.1	0.3	13.64	2.04
LSD (p≤0.05)	19.13	15.99	0.08	5.5	3.68	0.14	0.03	1.89	0.26
CV	19.97	20.4	8.74	6.88	9.61	6.23	7.86	12.12	11.43

Different alphabets show significant difference among genotypes

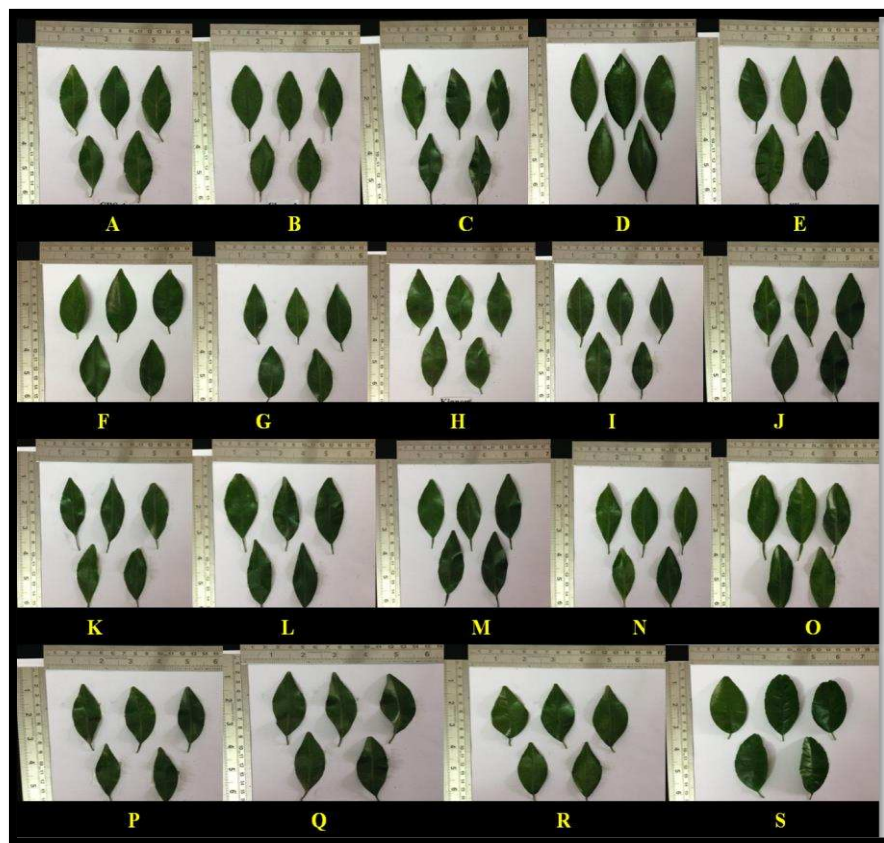


Figure 2. Variation in leaf size of different mandarin genotypes A) CRS-4, B) Clone-11, C) Coorg, D) Daisy, E) Darjeeling, F) Fremont, G) Khasi, H) Kinnow, I) Mudhkhed Seedless, J) N-4, K) N-28, L) N-34, M) N-38, N) N-43, O) N-51, P) Nagpur Seedless Q) Nagpur, R) Nova and S) W. Murcott

Fruit and seed traits

The findings of the study illustrated that significant variation in fruit size and weight existed in mandarin genotypes (Table 3, Fig. 3). Daisy (228.50 g) recorded the maximum mean fruit weight which was at par with W. Murcott, N-34, and Kinnow. However, the minimum fruit weight was measured in N-38 (110.17 g) which was significantly lower than all genotypes except Fremont (112.83 g). Fruit diameter (75.12 mm) and fruit length (65.55 mm) were found to be the highest in Daisy as compared to all other genotypes (Table 2). Mean fruit diameter (56.82 mm) and fruit length (53.37) were recorded minimum in N-38 and Fremont, respectively. The highest fruit number per tree was recorded in Kinnow (403) followed by Mudhkhed Seedless (402) and W. Murcott (365) which was significantly higher than all other genotypes. However, the lowest number of fruits per tree was recorded in Nova (210) mandarin. Daisy recorded the highest fruit yield (74.26 kg/tree) followed by Kinnow (71.06 kg/tree) and W Murcott (62.84 kg/tree) which was significantly higher than all other genotypes. Nova mandarin recorded the lowest fruit yield (28.52 kg/tree). The total soluble solids (9.76 Brix) were recorded maximum in Kinnow that was statistically at par with Daisy, Nova, Fremont, and Darjeeling. The acid content ranged from 0.56 to 0.96 percent among all the genotypes.

Table 3. Fruit characters of different mandarin genotypes grown under Punjab conditions (Pooled data 2014 and 2015)

Genotypes	Fruit weight (g)	Fruit diameter (mm)	Fruit length (mm)	Fruit number per tree	Fruit yield per tree (Kg)	TSS (°Brix)	Acidity (%)	Av. Seed Number/fruit	Av. Seed weight of 20 seeds
CRS-4	133.00 ^{gh}	63.13 ^e	57.72 ^{ghij}	275 ^{fghi}	36.58 ^{fghij}	8.25 ^{def}	0.81 ^{bc}	15.03 ^{bcd}	1.07 ⁱ
Clone-11	135.00 ^{fgh}	66.73 ^{cd}	59.57 ^{defgh}	298 ^{defgh}	40.23 ^{efghij}	9.07 ^{bc}	0.66 ^g	12.80 ^{def}	0.97 ⁱ
Coorg	140.50 ^{efg}	69.70 ^{bc}	64.95 ^a	292 ^{defghi}	41.03 ^{efghij}	7.35 ⁱ	0.63 ^g	13.33 ^{def}	1.81 ^d
Daisy	228.50 ^a	75.12 ^a	65.55 ^a	325 ^{bcde}	74.26 ^a	9.70 ^a	0.56 ^h	18.60 ^a	2.03 ^c
Darjeeling	150.33 ^{de}	69.88 ^{bc}	63.70 ^{ab}	286 ^{defghi}	42.99 ^{efghi}	9.23 ^{ab}	0.80 ^{bc}	14.02 ^{de}	2.14 ^{bc}
Fremont	112.83 ⁱ	61.80 ^e	53.37 ^k	301 ^{defg}	33.96 ^{fghi}	9.45 ^{ab}	0.82 ^b	18.33 ^{ab}	1.49 ^{fg}
Khasi	141.50 ^{efg}	68.23 ^e	61.23 ^{bcde}	352 ^{bc}	49.81 ^{cde}	7.65 ^{hi}	0.71 ^f	11.55 ^{def}	1.73 ^{de}
Kinnow	176.33 ^b	74.03 ^a	59.27 ^{defgh}	403 ^a	71.06 ^{ab}	9.76 ^a	0.73 ^{def}	19.77 ^a	2.30 ^b
Mudhkhed Seedless	146.33 ^{ef}	67.33 ^{cd}	61.53 ^{bcd}	402 ^a	58.82 ^{bcd}	8.17 ^{defgh}	0.92 ^a	12.23 ^{def}	2.11 ^c
N-4	138.50 ^{efgh}	64.22 ^{de}	63.05 ^{abc}	292 ^{defghi}	40.44 ^{efghij}	7.71 ^{ghi}	0.96 ^a	10.78 ^{ef}	1.47 ^{fg}
N-28	144.33 ^{efg}	72.45 ^{ab}	60.22 ^{defg}	312 ^{cdef}	45.03 ^{ef}	7.76 ^{fghi}	0.75 ^{de}	14.58 ^{cd}	1.56 ^{efg}
N-34	161.83 ^{cd}	62.18 ^e	55.55 ^{jk}	252 ^{ghi}	40.78 ^{efghij}	8.21 ^{defg}	0.72 ^{ef}	17.65 ^{abc}	1.72 ^{de}
N-38	110.17 ⁱ	56.82 ^f	55.30 ^{jk}	262 ^{ghi}	28.86 ^j	7.97 ^{efgh}	0.81 ^{bc}	14.25 ^{cde}	2.08 ^c
N-43	126.67 ^h	68.93 ^c	58.23 ^{fghi}	289 ^{defghij}	36.61 ^{fghij}	8.08 ^{efgh}	0.77 ^{cd}	14.10 ^{de}	1.62 ^{ef}
N-51	137.67 ^{efgh}	66.70 ^{cd}	57.00 ^{hij}	248 ^{ij}	34.14 ^{fghij}	7.79 ^{fghi}	0.80 ^{bc}	14.07 ^{de}	1.72 ^{de}
Nagpur Seedless	138.00 ^{efgh}	63.07 ^e	60.65 ^{cdef}	312 ^{cdef}	43.06 ^{efgh}	8.63 ^{cd}	0.76 ^{def}	10.28 ^f	1.25 ^h
Nagpur	135.67 ^{fgh}	68.65 ^c	58.23 ^{fghi}	329 ^{bcd}	44.64 ^{efg}	8.40 ^{de}	0.67 ^g	13.77 ^{def}	1.39 ^{gh}
Nova	135.83 ^{fgh}	74.40 ^a	55.67 ^{ijk}	210 ^j	28.52 ^j	9.59 ^{ab}	0.73 ^{def}	20.62 ^a	2.20 ^{bc}
W. Murcott	172.17 ^{bc}	73.33 ^a	58.70 ^{efgh}	365 ^{ab}	62.84 ^{abc}	9.11 ^{bc}	0.83 ^b	14.60 ^{cd}	3.60 ^a
Mean	145.54	67.72	59.45	305.53	44.93	8.52	0.76	14.76	1.8
LSD (p<0.05)	12.81	3.36	2.63	49.86	13.05	0.54	0.04	3.54	0.17

Different alphabets show significant difference among genotypes

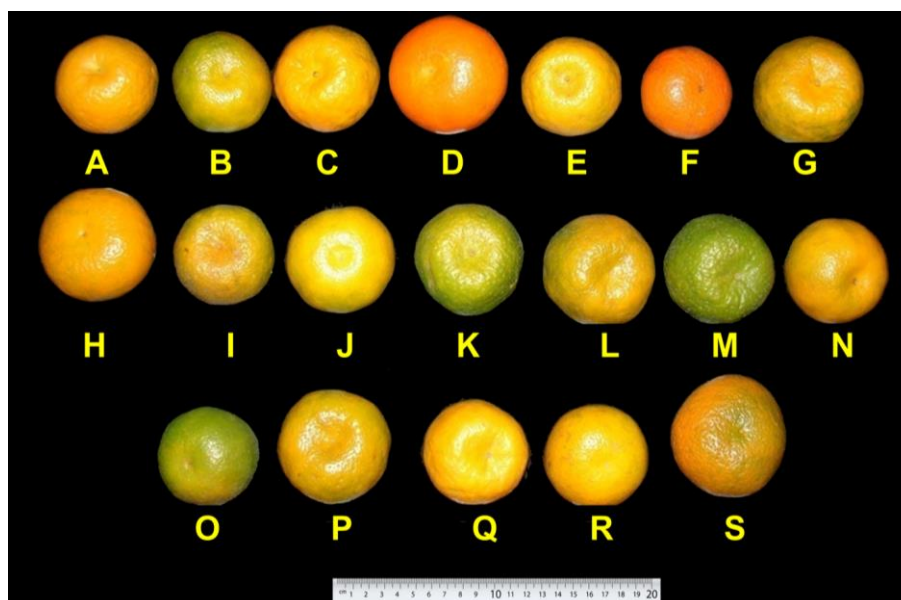


Figure 3. Diversity in fruit size of different mandarin genotypes A) CRS-4, B) Clone-11, C) Coorg D) Daisy, E) Darjeeling, F) Fremont, G) Khasi, H) Kinnow, I) Mudhkhed Seedless, J) N-4, K) N-28, L) N-34, M) N-38, N) N-43, O) N-51, P) Nagpur Seedless Q) Nagpur, R) Nova and S) W. Murcott

The highest (0.96%) and the lowest (0.56%) acid content were recorded in N-4 and Daisy, respectively. The mean seed number per fruit had a significant deviation among all the mandarin genotypes. The number of seeds per fruit varied from 10.28 to 20.62. The maximum number of seeds per fruit was counted (20.62) in Nova while the minimum seed number per fruit was recorded in Nagpur Seedless (10.28). The data illustrated that the maximum number of seeds per fruit was at par with Kinnow, Daisy, Fremont, and N-34. It was evident from the data that the maximum seed weight (3.60 g per 20 seeds) was observed in W. Murcott followed by Kinnow, Nova, Darjeeling, and Mudhkhed Seedless (Fig. 4). However, the minimum mean seed weight was observed in Clone-11 (0.97 g per 20 seeds) which was significantly lower than all genotypes except CRS-4 (1.07 g per 20 seeds).

Genetic variance and heritability

Phenotypic variance for all the important traits was calculated through genotypic variance and genotypic environment variance (Table 4). A wide range of variability was observed for all the entire traits except for LLT and fruit acidity. Phenotypic coefficient of variance which represents total variability in germplasm, was higher for scion diameter (45.9), followed by average seed weight of 20 seeds (45.4), rootstock diameter (42.2), an average number of seeds per fruit (28.3), and fruit weight (25.3) whereas, the genotypic coefficient of variance which represents heritable variability was higher for average seed weight of 20 seeds (45.1), followed by scion diameter (44.3), rootstock diameter (40.6) and fruit weight (24.9). The genetic advance was higher for fruit number per tree (82.21) followed by fruit weight (73.4), rootstock diameter (67.3), and scion diameter (60.4). However, the genetic advance percentage of means was found to be higher for the average seed weight of 20 seeds (92.4) followed by scion diameter (88.3), rootstock diameter (80.5), and fruit weight (50.5).

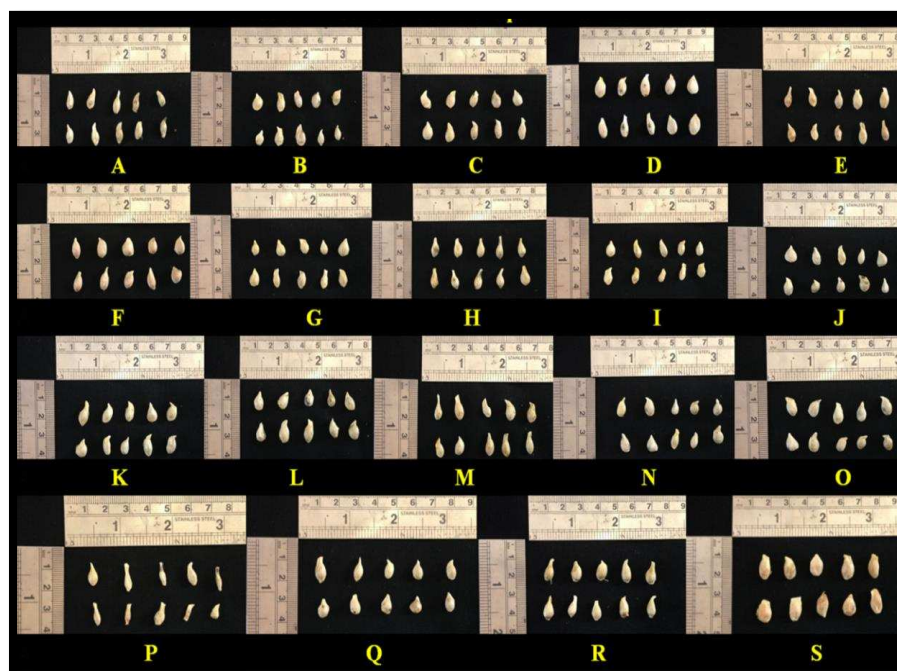


Figure 4. Variation in seed size of different mandarin genotypes A) CRS-4, B) Clone-11, C) Coorg, D) Daisy, E) Darjeeling, F) Fremont, G) Khasi, H) Kinnow, I) Mudhkhed Seedless, J) N-4, K) N-28, L) N-34, M) N-38, N) N-43, O) N-51, P) Nagpur Seedless Q) Nagpur, R) Nova and S) W. Murcott

Table 4. Variability, heritability and genetic advance in mandarin genotypes for 16 traits

Traits	Grand mean	Ranges	GV	PV	PCV	GCV	h ₂	GA	GAM
Rootstock diameter (mm)	83.6	36.91-124.82	1152.9	1245.8	42.2	40.6	0.9	67.3	80.5
Scion diameter (mm)	68.4	27.75-97.44	919.8	984.7	45.9	44.3	0.9	60.4	88.3
Leaf lamina length (mm)	69.9	63.81-74.85	5.5	13.2	5.2	3.4	0.4	3.1	4.5
Leaf lamina width (mm)	33.4	30.10-37.05	3.8	7.2	8.0	5.8	0.5	2.9	8.7
Leaf lamina thickness (mm)	0.3	0.25-0.33	0.0	0.0	8.9	8.9	1.0	0.1	18.3
Petiole wing length (mm)	13.6	10.35-16.22	7.3	8.2	21.0	19.8	0.9	5.2	38.4
Petiole wing width (mm)	2.0	1.46-2.47	0.2	0.2	21.3	20.3	0.9	0.8	39.9
Fruit weight (g)	145.5	110.17-228.50	1311.4	1353.1	25.3	24.9	1.0	73.4	50.5
Fruit diameter (mm)	67.2	56.82-75.12	46.7	49.6	10.5	10.2	0.9	13.7	20.3
Fruit length (mm)	59.4	53.37-65.95	20.9	22.7	8.0	7.7	0.9	9.1	15.2
Fruit number per tree	5810.3	210-403	3281.1	3317.45	7.56	7.51	0.9	82.21	1.41
Fruit yield (kg/tree)	853.6	28.52-74.26	209.54	227.10	5.16	4.95	0.9	21.20	2.48
Average no. of seeds per fruit	14.8	10.28-20.62	14.2	17.4	28.3	25.5	0.8	7.0	47.5
TSS (°Brix)	8.5	7.35-9.76	1.1	1.2	12.9	12.5	0.9	2.1	24.8
Acidity (%)	0.8	0.56-0.96	0.0	0.0	17.9	17.7	1.0	0.3	36.0
Average seed weight of 20 seeds (g)	1.8	0.97-3.60	0.7	0.7	45.4	45.1	1.0	1.7	92.4

Legends: GV = genotypic variance, PV= phenotypic variance, PCV = phenotypic coefficient of variance, GCV = genotypic coefficient of variance, h₂= heritability in broad sense, GA= genetic advance, Genetic advance as percent of the Mean (GAM)

Cluster analysis

Nineteen mandarin genotypes were divided into three major clusters in dendrogram drawn based on UPGMA (Fig. 5). Cluster-I consisted of four genotypes namely N-34, W. Murcott, Daisy, and Kinnow. Likewise, cluster -II included seven genotypes, viz. Nagpur Seedless, Nova, Mudhkhed Seedless, Coorg, Nagpur, Darjeeling, and Khasi. Under cluster -III eight genotypes were grouped (N-28, Fremont, N-4, N-51, Clone-11, N-38, CRS-4, and N-43).

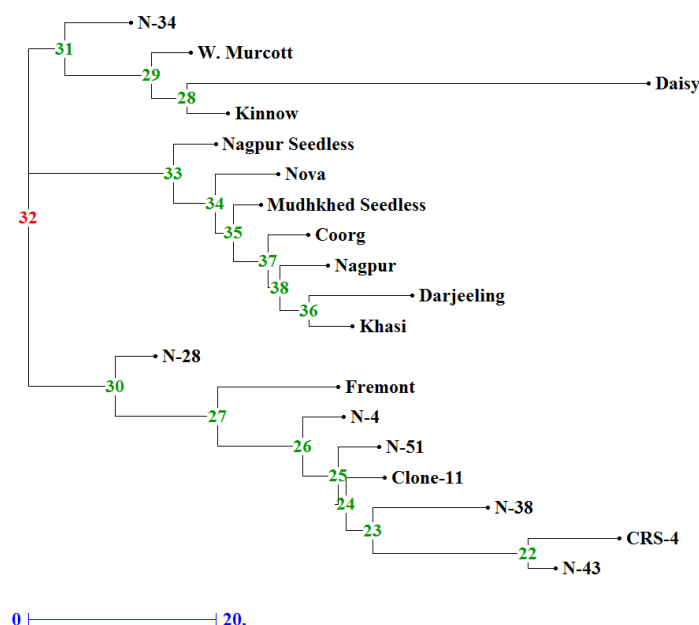


Figure 5. Dendrogram illustrating genetic relationship among 19 mandarin genotypes generated by UPGMA tree analysis based on tree and fruit traits. Cluster -I included N-34, W. Murcott, Daisy, Kinnow, Cluster -II included Nagpur Seedless, Nova, Mudhkhed Seedless, Coorg, Nagpur, Darjeeling, Khasi and Cluster -III included N-28, Fremont, N-4, N-51, Clone-11, N-38, CRS-4, N-43

Correlation studies

Pearson correlation between all the traits was calculated and unrelated traits depicting the highest correlation are represented in Figure 6. Fruit yield was strongly correlated with the fruit weight followed by seed weight, indicating that fruit weight and seed weight can be used as selection criteria during early years of fruit bearing in breeding programs for high yield. Similarly, LLT can give an idea about productivity in the early stages of growth, when trees are not in bearing. Most of the verities are concentrated in 95% confidence interval; some of the values lying outside depict high variability for the combination of traits. Linear fit of traits is shown by a straight line representing the direction of variability.

Principal Component Analysis

PCA simplified 18 parameters into five PC with eigen value > 1 (1.2672 to 5.5204) and cumulative per cent of the variance of 82.6 (Table 5). PC1 had effective parameters like fruit weight (0.356), fruit yield (0.351), and fruit diameter (0.351). PC2 had a high

contribution factor load from the average number of seeds per fruit (0.430), fruit TSS (0.296) and LLL (0.262). PC3 explained the difference with the highest positive factor loads from scion diameter (0.349) and rootstock diameter (0.309) and negative load from leaf lamina width (-0.384) and LLL (-0.333). PC4 explained the highest positive factor load of fruit length (0.236) and LLL (0.186) and negative factor load of fruit acidity (-0.642) and average seed weight of 20 seeds (-0.436). PC5 had highest contribution from rootstock diameter (0.446) and LLL (0.440). PCA allows the reduction of data dimensions (Fig. 7). The two main components of the analysis (herein referred to as PC1 and PC2) explained 34.5% and 17.2% of the total variance of the data, respectively.

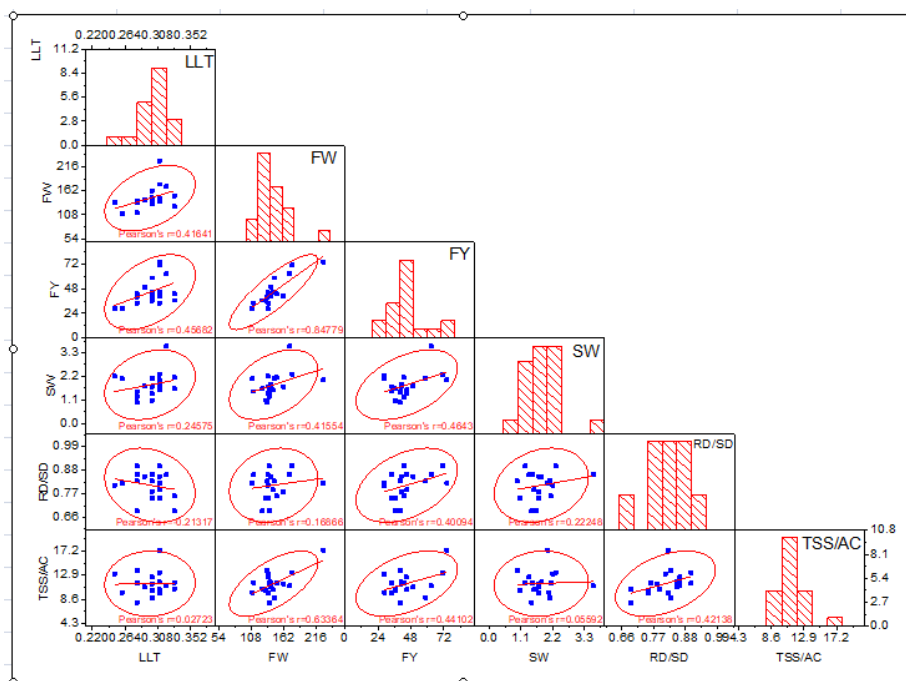


Figure 6. The scatter-matrix, histogram, 95% confidence limit eclipse and Pearson's correlation matrix for leaf lamina thickness (LLT), fruit weight (FW), fruit yield (FY), seed weight (SW), rootstock diameter/scion diameter (RD/SD), and TSS/acidity (TSS/AC)

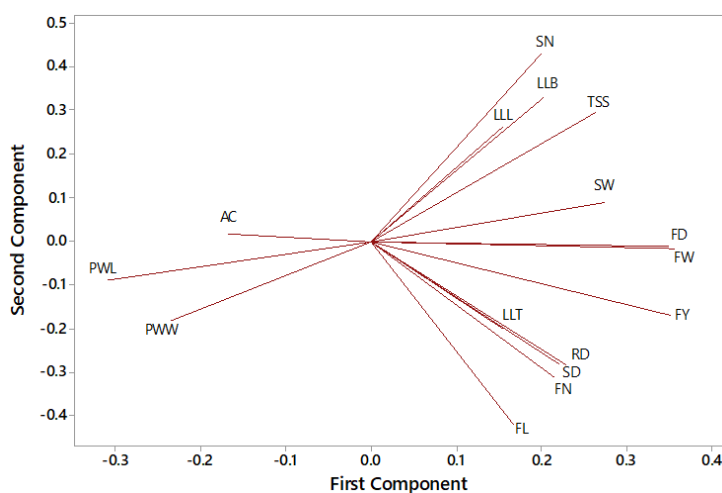


Figure 7. Principal component analysis (PCA) plot of the two principal axes

Table 5. Eigen values, factor and contribution of first five principal components axes in mandarin genotypes for 14 traits

Variables	Eigen values				
	PC1	PC2	PC3	PC4	PC5
Eigenvalue	5.5204	2.7584	2.302	1.3687	1.2672
Proportion	0.345	0.172	0.144	0.086	0.079
Cumulative	0.345	0.517	0.661	0.747	0.826
Rootstock diameter (mm)	0.22	-0.28	0.309	0.096	0.446
Scion diameter (mm)	0.23	-0.283	0.349	0.064	0.365
Leaf lamina length (mm)	0.155	0.262	-0.333	0.186	0.44
Leaf lamina breadth (mm)	0.203	0.33	-0.384	-0.021	0.245
Leaf lamina thickness (mm)	0.154	-0.201	-0.327	-0.025	-0.203
Petiole wing length (mm)	-0.309	-0.089	-0.285	0.162	0.304
Petiole wing width (mm)	-0.234	-0.182	-0.377	0.122	-0.017
Fruit weight (g)	0.356	-0.016	-0.212	0.161	-0.152
Fruit diameter (mm)	0.35	-0.012	-0.093	0.174	0.069
Fruit length (mm)	0.168	-0.419	-0.194	0.236	0.018
Fruit number per tree	0.216	-0.312	-0.08	-0.409	-0.192
Fruit yield per tree	0.351	-0.169	-0.184	-0.144	-0.209
Fruit TSS	0.264	0.296	0.123	-0.011	-0.102
Fruit acidity	-0.167	0.016	-0.145	-0.642	0.27
Av. no of seeds per fruit	0.201	0.43	0.157	0.091	-0.165
Av. seed weight of 20 seeds (g)	0.274	0.09	-0.037	-0.436	0.249

Discussion

The diameter of the rootstock and scion is crucial in determining the degree of compatibility of the stionic relationship between scion and rootstock. A significantly higher mean rootstock diameter was recorded in Darjeeling (124.82 mm) and the lowest was recorded in the CRS-4 (36.91 mm). However, the mean scion diameter was recorded in Khasi (97.44 mm) and the lowest scion diameter was found in genotype CRS-4 (27.75 mm). The maximum scion to rootstock ratio was observed in Kinnow which clearly shows its adaptive suitability under tropical conditions and compatibility with Rough lemon rootstock. The results further showed that Darjeeling, Khasi, Nagpur, Coorg, Nova, and genotype had higher scion to rootstock diameter ratio which indicated better compatibility of these genotypes with Rough lemon rootstock among all genotypes under Punjab conditions whereas, the CRS-4 genotype is not best suited for Rough lemon rootstock under these conditions due to its poor scion to rootstock diameter ratio. The variation in the scion to rootstock diameter ratio might be due to the interaction of genotypes with rootstock and environment. Furthermore, it had been hypothesized that the variation in rootstock diameter of different mandarin genotypes might be due to limited plant growth by bud union resistance to water transport and xylem anatomical characteristics, particularly the number and diameter of vessels and carbohydrate distribution (Martínez-Alcántara et al., 2013; Forner-Giner et al., 2014). Similarly, significant variation in rootstock diameter and scion to rootstock diameter ratio among citrus varieties had already been reported (Sayad et al., 2016; Baswal et al., 2017; Rattanpal et al., 2018; Sunaina et al., 2018; Singh et al., 2022).

The LLL to width ratio showed significant variation in diverse mandarin genotypes. This might be due to the close interaction among genotypes and the environment. It has been observed that variation in leaf characters was due to genotype and environmental factors (Hovenden and Schimanski, 2000; Hovenden, 2001; Gomez et al., 2003). Significant variation has been reported for leaf morphological characters in citrus accessions (Khan et al., 2008; Singh et al., 2010, 2021, 2022; Dorji and Yapwattanaphun, 2011; Sunaina et al., 2018).

The variation in fruit weight among mandarin genotypes ranged from 228.50 g (Daisy) to 110.17 g (N-38). The variation in fruit weight among mandarin genotypes might be due to differential translocation of photosynthates from fully developed leaves to developing fruits. Furthermore, it had been reported that increased pulp tissue caused an increase in fruit weight and fruit size. This can be attributed to cell division during the early stages of fruit development, caused mainly by the thickness of the peel tissue (Dalal et al., 2013). The fruit weight in mandarin genotypes ranged from 59.46 g in Cleopatra to 266.33 g in King, in the studies undertaken by Campos et al. (2005). The highest fruit number per tree was recorded in Kinnow which was significantly higher than all other genotypes except Mudhkhed seedless and W. Murcott. However, Daisy recorded the highest fruit yield (74.26 kg/tree) followed by Kinnow (71.06 kg/tree) and W Murcott (62.84 kg/tree) which was significantly higher than all other genotypes except Kinnow and W Murcott. Nova mandarin recorded the lowest fruit number and fruit yield among all genotypes under study. Significant variation in seed number per fruit among mandarin genotypes was observed during the investigation. Similarly, the variation in the number of bold seeds and the abortive seeds were also observed previously (Altaf et al., 2008; Fatima et al., 2010). Similarly, Kinley and Chinawat (2011) and Dorji and Yapwattanaphun (2011) observed significant variation in fruit number, fruit yield, and seed number in mandarin germplasm.

The maximum TSS was recorded in Kinnow fruits followed by Daisy and Nova. However, the minimum fruit acidity was observed in mandarin genotype Daisy. The variation in fruit TSS and acidity among mandarin genotypes might be due to the seasonal dynamics of carbohydrates and acids in the fruits due to starch hydrolysis during the maturation period. Similarly, in different studies, significant variation in fruit weight, diameter, length, TSS, and acidity had been reported in mandarin genotypes (Khan et al., 2008; Kinley and Chinawat, 2011; Dorji and Yapwattanaphun, 2011; Sunaina et al., 2018; Singh et al., 2022).

A significant variation in morphological characters among mandarin genotypes was observed in this study. The findings are in agreement with the observations made by some other authors (Dorji and Yapwattanaphun, 2011) who reported the highest significant dissimilarity in quantitative traits between 39 mandarin accessions in Bhutan. It has been reported that the mandarin genotypes represented variations of single clones (Dorji and Yapwattanaphun, 2015). Consequently, resemblance among genotypes in our findings also supported the statement that mandarins in the USA and India might occur from a variation of a single clone. The present findings also revealed the fact that the presence of assorted accessions in mandarin genotypes despite accessions exhibited the same morphological qualitative traits. This might be due to the diverse action of evolutionary forces and environmental attributes. In an open field survey, Paudyal and Haq (2008) attributed 40% of variation to environmental factors in pummelo accessions. Similarly, vegetative differences in individual accessions were also reported by Dorji and Yapwattanaphun (2011), they attributed this phenotypic variation to cross-pollination,

natural or induced mutations, and environment interactions. During the current investigation, the high level of significant variation in quantitative vegetative attributes specified the existence of diversity in mandarin germplasm and hence the hypothesis of this study has been accepted. The cluster studies revealed that the mandarin germplasm though collected from the different agro-ecological zones formed sub-groups without clear demarcation by region.

Furthermore, in this study, rootstock diameter, scion diameter, fruit weight, the weight of 20 seeds showed a higher genotypic coefficient of variance, genetic advance, heritability, and genetic advance percentage of means. The phenotypic coefficient of variance was higher than the genotypic coefficient of variance for all the traits under study. High heritability, high genetic advance along higher genotypic coefficient of variance gives good information in terms of selection advance than any parameter alone (Paudyal and Haq, 2008). This suggests the occurrence of additive gene action with low environmental influence for the determination of these traits, compared to other traits, and could be valuable in the phenotypic selection of mandarin genotypes through devising appropriate correlated inheritance breeding strategies (Wera et al., 2014). However, low genetic advance with low heritability observed for leaf characters, fruit juice TSS and acidity indicated the presence of intra and inter allelic interactions. In terms of character scores, PC1 distinguishes positive correlations between fruit weight, fruit diameter, and fruit yield, and negative relationships between petiole wing length and petiole wing width. Similarly, PC2 highlights the positive correlation between seed number per fruit, LLB, LLW, and TSS besides, it contrasts with the highly negatives value of fruit length.

No doubt, quantifying the seed parameters is more complicated than simply measuring the fruit yield directly. However, the positive correlation between yield and other traits can be exploited in early stages of fruit tree breeding. In this study, fruit yield was positively correlated with fruit weight, seed weight, and leaf lamina thickness (LLT). Though high seed weight is undesirable, yet this trait along with fruit weight and LLT will help in selection of genotype during early years of its bearing. It is pertinent to note that hybrid mandarin seedlings come into bearing after 6-7 years. At this stage variety are selected for yield and quality. Though fruit quality potential of seedlings can be assessed in first year of bearing, but for evaluating yield potential of seedlings additional 4 to 6 years are required. These correlations will help in reducing this breeding period.

Conclusion

This study showed that the mandarin genotypes used in the current investigation differ phenotypically. The study concluded that the occurrence of additive gene action with low environmental influence is responsible for the determination of rootstock diameter, scion diameter, fruit weight, and seed weight compared to other traits under study. Furthermore, a strong correlation of fruit yield with LLT, fruit weight and seed weight had been observed in our study, indicating that LLT, fruit weight and seed weight can be used as selection criteria for the genotypes at early years of fruit bearing to shorten the crop improvement programme in mandarin.

Acknowledgments. We are highly thankful to the Project Coordinator, All India Coordinated Research Project on Fruits, ICAR, New Delhi for giving the funds for maintaining the citrus experiments at College orchard, PAU, Ludhiana.

Conflict of interests. The authors declare that they have no conflict of interests in publishing this manuscript.

REFERENCES

- [1] Ahmed, S., Rattanpal, H. S., Singh, G. (2018): Diversity assessment of grapefruit (*Citrus × paradisi*) and tangelo (*Citrus × tangelo*) under Indian conditions using physico-chemical parameters and SSR markers. – *Applied Ecology and Environmental Research* 16: 5343-5358.
- [2] Al-Jibouri, H. W., Miller, P. A., Robinson, H. F. (1958): Genotypic and environmental variances and co-variances in an upland cotton cross of interspecific origin. – *Agronomy Journal* 50: 633.
- [3] Altaf, N., Khan, A. R. (2008): Variation with in Kinnow (*Citrus reticulata*) and Rough Lemon (*Citrus jambhiri*). – *Pakistan Journal of Botany* 40: 589-598.
- [4] Baswal, A. K., Rattanpal, H. S., Uppal, G. S., Gill, K. S. (2017): Assessment on performance and variability in different sweet orange (*Citrus sinensis* Osbeck) cultivars under Punjab conditions. – *Journal of Applied and Natural Sciences* 9: 780-783.
- [5] Campos, E. T., Espinosa, M. A. G., Warburton, M. L., Varela, A. M., Monter, A. V. (2005): Characterization of mandarin (*Citrus* spp.) using morphological and AFLP markers. – *Forum Documentation for Electrical Stimulation (ISO)* 30: 687-93.
- [6] Clark, C. A., Hoy, M. W. (2006): Effects of common viruses on yield and quality of Beauregard sweet potato in Louisiana. – *Plant Disease* 90: 83-88.
- [7] Dalal, R. P. S., Beniwal, B. S., Sehrawat, S. K. (2013): Seasonal variation in growth, leaf physiology and fruit development in Kinnow, a mandarin hybrid. – *Journal of Plant Studies* 2: 72.
- [8] Das, A., Mandal, B., Sarkar, J., Chaudhuri, S. (2007): Occurrence of zygotic twin seedlings in mandarin orange plants of the north eastern Himalayan region. – *Current Science* 92(11): 1488-1489.
- [9] DeLacy, I. H., Basford, K. E., Cooper, M., Bull, J. K., McLaren, C. G. (1996): Analysis of Multi-Environment Trials - An Historical Perspective. – In: Cooper, M., Hammer, G. L. (eds.) *Plant Adaptation and Crop Improvement*. CAB Intl.
- [10] Domingues, E. T., Souza, V. C., Sakuragui, C. M., Pompeu Jr., J., Pio, R. M., Teofilo Sobrinho, J., Souza, J. P. (1999): Morphological characterization of mandarins from the Active Citrus Gene Bank of the Centro de Citricultura Sylvio Moreira/IAC. – *SciAgric* 56: 197-206.
- [11] Dorji, K., Yapwattanaphun, C. (2011): Morphological Identification of Mandarin (*Citrus reticulata* Blanco) in Bhutan. – *Kasetsart Journal* 45: 793-802.
- [12] Dorji, K., Yapwattanaphun, C. (2015): Assessment of genetic variability amongst mandarin (*Citrus reticulata* Blanco) accessions in Bhutan. – *BMC Genetics* 16: 39.
- [13] Faralli, M., Matthews, J., Lawson, T. (2019): Exploiting natural variation and genetic manipulation of stomatal conductance for crop improvement. – *Current Opinion in Plant Biology* 49: 1-7.
- [14] Fatima, B., Usman, M., Khan, I. A., Khan, M. S., Khan, M. M. (2010): Exploring citrus cultivars for underdeveloped and shriveled seeds: A valuable resource for spontaneous polyploidy. – *Pakistan Journal of Botany* 42: 189-200.
- [15] Fatima, B. M., Usman, S., Khan, M. S., Khan, I. A., Khan, M. M. (2015): Identification of citrus polyploids using chromosome counts, morphological and SSR markers. – *Pakistan Journal of Agricultural Sciences* 52: 107-114.
- [16] Forner-Giner, M. A., Rodriguez-Gamir, J., Martínez-Alcántara, B., Quinones, A., Iglesias, D. J., Primo-Millo, E., Forner, J. (2014): Performance of Navel orange trees grafted onto two new dwarfing rootstocks (Forner-Alcaide 517 and Forner-Alcaide 418). – *Scientia Horticulturae* 179: 376-387.
- [17] Gaikwad, K. A., Patil, S. R., Nagree, P. K., Potdukhe, N. R. (2018): Morphological characterization of citrus rootstock genotypes. – *International Journal of Chemical Studies* 6: 516-529.

- [18] Gmitter, J. F. G., Hu, X. (1990): The possible role of Yunnan, China in the origin of contemporary Citrus species (Rutaceae). – *Economic Botany* 44: 267-277.
- [19] Golein, B., Fifaei, R., Ghasemi, M. (2011): Identification of zygotic and nucellar seedlings in citrus interspecific crosses by inter simple sequence repeats (ISSR) markers. – *African Journal of Biotechnology* 10: 18965-18970.
- [20] Gomez, D. C. M., Ruiz, C., Baeza, P., Lissarrague, J. R. (2003): Drought adaptation strategies of four grapevine cultivars (*Vitis vinifera* L.): Modifications of the properties of the leaf area. – *Journal of International des Sciences de la Vigne et du Vin* 37: 731-743.
- [21] Gomez, A. K., Gomez, A. A. (2010): *Statistical Procedures for Agricultural Research*. – John Wiley and Sons; New York, 680p.
- [22] Hovenden, M. J. (2001): The Influence of temperature and genotype on the growth and stomatal morphology of southern beech, *Nothofagus cunninghamii* (Nothofagaceae). – *Australian Journal of Botany* 49: 427-434.
- [23] Hovenden, M. J., Schimanski, L. (2000): Genotypic differences in growth and stomatal morphology of Southern Beech, *Nothofagus cunninghamii*, exposed to depleted CO₂ concentrations. – *Australian Journal of Plant Physiology* 27: 281- 287.
- [24] IPGRI. (1999): *Descriptors of Citrus*. – International Plant Genetic Resource Institute, Rome, Italy. Available from <http://www.cgiar.org/ipgri/>.
- [25] Josan, J. S., Kaur, N. K. (2006): Variability and character association analysis in identified mandarin germplasm. – *Indian Journal of Horticulture* 63: 152-154.
- [26] Kaur, H., Sidhu, G. S., Sarao, N. K., Singh, R., Singh, G. (2022): Assessment of genetic diversity of mandarin cultivars grown in major citrus regions of world using morphological and microsatellite markers. – *Horticulture, Environment, and Biotechnology* published online 21 February, 2022. <https://doi.org/10.1007/s13580-021-00404-4>.
- [27] Khan, M. M., Mumtaz, S., Ahmad, S., Abbas, M., Khan, I. A. (2008): Some studies on the morphology of Kinnow mandarin and Feutrell's Early. – *Pakistan Journal Agricultural Sciences* 45: 424-431.
- [28] Khan, S. N., Shahzadi, S., Rashid, F. S., Zafarullah, A., Ahmad, S. (2014): Molecular characterization and phylogenetic relationship of different citrus varieties of Pakistan. – *Journal of Animal Plant Sciences* 24: 315-320.
- [29] Kinley, D., Chinawat, Y. (2011): Morphological Identification of Mandarin (*Citrus reticulata* Blanco) in Bhutan. – *Kasetsart Journal* 45: 793-802.
- [30] Koehler, S. P., Dornelles, A. L. C., Freitas, L. B. (2003): Characterization of mandarin citrus germplasm from southern Brazil by morphological and molecular analyses. – *Pesquisa Agropecuaria Brasileira* 38: 797-806.
- [31] Lin, K. H., Lai, Y. C., Chang, K. Y., Cheng, Y. F., Hwang, S. Y., Lo, H. F. (2007): Improving breeding efficiency for quality and yield of sweet potato. – *Biochemistry-Botanical Studies* 48: 283-292.
- [32] Liu, Y. Z., Deng, X. X. (2007): *Citrus Breeding and Genetics in China*. – *Asian & Australasian Journal Plant Sciences and Biotechnology* 5: 23-28.
- [33] Martínez-Alcántara, B., Rodríguez-Gamir, J., Martínez-Cuenca, M. R., Iglesias, D. J., Primo-Millo, E., Forner-Giner, M. A. (2013): Relationship between hydraulic conductance and citrus dwarfing by the Flying Dragon rootstock (*Poncirus trifoliata* L. Raft var. *monstruosa*). – *Trees* 27: 629-638.
- [34] Monteverde, E. E., Ruiz, J. R., Rodriguez, M. (2000): Morphological characterization of Caracara orange, vegetative, floral and fruit characteristics. – *Agronomia Tropical (Maracay)* 50: 659-663.
- [35] Moore, G. A. (2001): Oranges and lemons, clues to the taxonomy of Citrus from molecular markers. – *Trends Genetics* 17: 536-540.
- [36] Muluaem, T., Mohammed, H. (2012): Genetic variability and association among yield and yield related traits in Aerial Yam (*Dioscorea bulbifera* L.) accessions at South-western Ethiopia. – *Journal of Natural Sciences and Research* 2(9): 123-129.

- [37] Patil, S. R., Sonkamble, A. M., Waskar, D. P. (2012): Effect of growth regulators and chemicals on germination and seedling growth of Rangpur lime under laboratory conditions. – *International Journal of Agricultural Sciences* 8: 494-497.
- [38] Paudyal, K., Haq, N. (2008): Variation of pomelo (*Citrus grandis* (L.) Osbeck) in Nepal and participatory selection of strains for further improvement. – *Agroforestry System* 72: 195-204.
- [39] Perrier, X., Jacquemoud-Collet, J. P. (2006): DARwin software (online). – Available at: <http://darwin.cirad.fr/darwin>.
- [40] Rattanpal, H. S., Singh, H., Uppal, G. S. (2018): Genetic divergence in trifoliolate citrus rootstocks under sub-tropical conditions of Punjab. – *Journal of Pharmacognosy and Photochemistry* 7: 953-957.
- [41] Sayed, H. A., Ahmed, H. S., ELezaby, A. A. (2016): Morphological and physiochemical characterization of ten lime and lemon accessions and the assessment of their genetic diversity maintained at ISSR marker. – *Journal of Horticultural Science and Ornamental Plants* 8: 200-211.
- [42] Sharma, B. D., Hore, D. K., Gupta, S. G. (2004): Genetic resources of Citrus of north-eastern India and their potential use. – *Genetic Recourses and Crop Evolution* 51: 411-418.
- [43] Sharma, N., Dubey, A. K., Srivastav, M., Singh, B. P., Singh, A. K., Singh, N. K. (2015): Assessment of genetic diversity in grapefruit (*Citrus paradise* Macf) cultivars using physico-chemical parameters and microsatellite markers. – *Australian Journal of Crop Sciences* 9: 62-68.
- [44] Singh, H., Rattanpal, H. S., Sidhu, G. S., Chahal, T. S. (2010): Study on physio-morphological characteristics among six rangpur lime (*Citrus limonia* Osbeck.) strains. – *Journal of Tree Sciences* 29: 48-56.
- [45] Singh, J., Dhaliwal, H. S., Thakur, A., Chhuneja, P., Sidhu, G. S., Singh, R. (2017): Morphological and genetic diversity in citrus genotypes to substantiate rootstock breeding for root rot resistance. – *Indian Journal of Horticulture* 74: 326-333.
- [46] Singh, A., Singh, G., Kalia, A., Rattanpal, H. S., Gupta, M. (2020): Leaf morpho-anatomical diversity analysis in mandarin (*Citrus reticulata* Blanco) genotypes using scanning electron microscopy. – *Genetic Resources and Crop Evolution* 67: 2173-2194.
- [47] Singh, A., Singh, G., Rattanpal, H. S., Monika, G. (2021a): Diversity assessment of mandarin (*Citrus reticulata* Blanco) genotypes under sub-tropical conditions. – *Agricultural Research Journal* 58(6): 1006-1013.
- [48] Singh, J., Singh, R., Thakur, A., Sidhu, G. S., Dhaliwal, H. S., Chhuneja, P. (2021b): Morpho-genetic diversity zygotic populations derived from rough lemon (*Citrus jambhiri* Lush.) and their tolerance against *Phytophthora*. – *Fruits* 76: 236-247.
- [49] Soost, R. K., Roose, M. L. (1996): Citrus. – In: Janick, J., Moore, J. N. (eds.) *Fruit Breeding, Vol. I, Tree and Tropical Fruits*. John Wiley and Sons Inc., New York, Chichester, Brisbane, Toronto, Singapore, pp. 257-323.
- [50] Sunaiana, Gupta, M., Rattanpal, H. S., Sidhu, G. S., Singh, G. (2018): Genetic diversity in sweet orange (*Citrus sinensis* Osbeck) germplasm based on fruit morphological and physiological traits. – *Research on Crops* 19: 425-429.
- [51] Wera, B., Yalu, A., Ramakrishna, A., Deros, M. (2014): Genotypic variability estimates of agronomic traits for selection in a sweet potato (*Ipomoea batatas*) polycross population in Papua New Guinea. – *Journal of Plant Breed and Genetics* 2: 131-136.

RANGELAND DIVERSITY AS A FORAGE RESOURCE FOR WILD UNGULATES IN THE BARSA KELMES NATURE RESERVE (KAZAKHSTAN)

DIMEYEVA, L. A.^{1*} – SALMUKHANBETOVA, Z. K.¹ – MALAKHOV, D. V.² – WUNDERLICH, J.³

¹*Institute of Botany & Phytointroduction, 050040 Almaty, Republic of Kazakhstan*

²*Institute of Zoology, Ministry of Education & Science, 050060 Almaty, Republic of Kazakhstan*

³*Michael, Succow Foundation, Ellernholzstr. 1/3, 17489 Greifswald, Germany*

**Corresponding author*

e-mail: l.dimeyeva@mail.ru; phone: +7-727-394-7642, fax: +7-727-394-8040

(Received 23rd Aug 2021; accepted 2nd May 2022)

Abstract. The nature reserve was founded in 1939 in the limits of the Barsa Kelmes Island (the Aral Sea, Kazakhstan) for the conservation of the saiga antelope (*Saiga tatarica*) and goitered gazelle (*Gazella subgutturosa*). In 1953 kulan from Turkmenistan (*Equus hemionus kulan*) were introduced to the island. The drying up of the Aral Sea led to a junction with the mainland, in the late 1990s. In search of water animals began migrating. For more than 20 years, the rangelands of the former island have not been grazed. A comparative analysis of rangeland productivity between the modern period and the 1970-80s of the last century showed that it has been increased by almost 2 times due to 20 years break of grazing pressure. The natural diet of wild ungulates in the reserve includes 105 species of vascular plants belonging to 26 families and 70 genera. A rangeland map has been compiled based on the interpretation of satellite imagery and field data. The legend to the map contains 16 mapped units. Each mapping unit corresponds to a rangeland type. For each type of rangeland, the total yield is calculated for seasons of the year. The map provides important information for understanding the available forage resources for wild ungulates.

Keywords: *Aral Sea, conservation, mapping, phytomass productivity, desert vegetation*

Introduction

The Barsa Kelmes Nature Reserve in the Aral Sea was established in 1939 to preserve the wild populations of saiga (*Saiga tatarica*, Linnaeus, 1766) and goitered gazelle (*Gazella subgutturosa* Guldendtaedt, 1780). In 1953 the Turkmen kulan (*Equus hemionus kulan*, Boddaort, 1785) was introduced to the island. All of these species are included in the IUCN Red List (IUCN SSC, 2017, 2018; Kaczensky et al., 2020).

The drying up of the Aral Sea led to the fact that in the late 1990s, the territory of the island got connected with the mainland. In search of water sources, the ungulates migrated. In 2006 the former Kaskakulan island and the dry seabed – the territory of the compact habitat of kulans, were added to the reserve. Since then, the total area of the nature reserve increased to 160,826 hectares. There are three artesian wells at the Kaskakulan area, which are important watering sources for animals.

The Barsa Kelmes became the world's first unique scientific center for the research of flora and fauna and got supported by the reserve staff and scientists for studying the ongoing ecological disaster.

Wild ungulates – saigas, gazelles and kulans are well adapted to the harsh desert conditions of the nature reserve and are the flag ship species of the ecosystem. The plant resources of the deserts are the natural forage source for the occurring wild ungulates.

When the Barsa Kelmes Nature Reserve was still an island on an area of 186 sq. km, the number of saigas varied sharply from 50 to 2,000 individuals. The number of goitered gazelles in the 70s ranged from 120 to 400 heads. In 1980 more than 200 kulans were observed in the reserve (Eliseev, 2007; Dimeyeva et al., 2012). Since 2021, it has been estimated that there are 690 kulans, 47 saigas, 171 gazelles in the reserve. Basically, the newly added lands to the reserve are subjected to grazing pressure. There is practically no grazing taking place on the territory of the former island Barsa Kelmes. The level of fresh groundwater has dropped due to the drying up of the sea, and the temporary water reservoirs, which appear during spring in the relief depressions dry up by the beginning of summer. Before the catastrophic decline of the Aral Sea, ungulates could also drink brackish sea water.

As the animals migrated from the former island, the grazing pressure has reduced drastically. Currently, kulans no longer graze at the island, and small groups of saigas and gazelles appear on the territory only in the spring, before the temporary water reservoirs dry.

Numerous investigations on biology, ecology and nutrition of saigas, goitered gazelles and kulans have been published in Kazakhstan (Fadeev and Sludsky, 1982; Sludsky et al., 1983; Grachev and Bekenov, 1993; Sokolov and Zhirnov, 1998; Bekenov et al., 1998; Dieterich and Sarsenova, 2012; Shakula and Khabibrakhmanov, 2014; Zhylkaidarov, 2014; Sapanov, 2017; Kaczensky et al., 2017, 2021 and others). In this paper we pay attention only to the fodder resources.

The diet of the saiga has been studied most. The list of plants eaten by saigas includes at least 85 species (Sludskiy, 1955; Sludskiy et al., 1983; Sokolov and Zhirnov, 1998). Plant species diversity within the entire distribution area of saigas varies, so each given population may feed on 40-60 species. The number of forage plants in one season does not exceed 25-35. Of those, only 10-15 plant species are common and may be referred to as the base of saiga diet (Sludsky et al., 1983).

In early spring (March – mid-April), the saigas of Kazakhstan eat at least 11 species of grasses (Minervin, 1955) and do not visit watering places. The most readily eaten cereals are (up to 45%) *Eremopyrum orientale* (L.) Jaub. & Spach, *E. triticeum* (Gaertn.) Nevski, *Poa bulbosa* L., and also *Rheum tataricum* L.f., *Alyssum desertorum* Stapf, *Bassia prostrata* (L.) Beck, *Limonium gmelinii* (Willd.) Kuntze, *L. suffruticosum* (L.) Kuntze.

The basis of food in summer are cereals (*Agropyron fragile* (Roth) P. Candargy, *Eremopyrum* spp., *Bromus tectorum* L., *Festuca amethystina* L., *Poa bulbosa*), and also *Bassia prostrata*, *Salsola laricifolia* Turcz. ex Litv., *Tanacetum achilleifolium* (M. Bieb.) Sch. Bip., *Achillea micrantha* Willd., *Inula britannica* L., *Artemisia* spp., etc.). In Western Kazakhstan, the summer diet of saigas consist of mainly cereals (up to 80%) with the presence of species from other families (*Bassia prostrata*, *Artemisia* spp., *Astragalus* spp., *Glycyrrhiza* spp.). In autumn, when the cereal component of vegetation becomes dry, saigas feed on saltworts and licorice. However, if the cereal species produce a secondary growth in autumn, saiga consumes cereal vegetation with special attention. Autumn plant composition, consumed by saiga, comprises about 20 species, of those saltworts represent the major part. Seeking for the protein, saiga may feed on lichens (Sludsky et al., 1983). In the Volga-Ural interfluve, in autumn saigas feed on annual and perennial saltworts, *Artemisia* species and *Tanacetum achilleifolium* (Rakov, 1956). In winter, while there is no stable snow cover (December-February), saigas feed on 20 species of plants, and with snow cover – 11 species. In snowless conditions,

Bassia prostrata, *B. scoparia* (L.) A.J. Scott, *Salsola arbuscula* Pall., *Atriplex tatarica* L., *Anabasis salsa* (Ledeb.) Benth. ex Volkens, *Artemisia austriaca* Jacq., *A. terrae-albae* Krasch., *A. pauciflora* Weber ex Stechm., *A. nitrosa* Weber ex Stechm., *A. lessingiana* Besser are most readily eaten. Periods of high and low abundance of Ural population of saiga alternate depending on the productivity of vegetation communities and territorial humidity (the number of watering places) due to climate change (Sapanov, 2017).

The composition of favorite plants is much less, and they mainly belong to the families Amaranthaceae Juss., Asteraceae Giseke, Brassicaceae Burnett, Rosaceae Juss. Russian scientists (Lebedeva, 1959, 1960; Abaturov et al., 2005; Abaturov and Dzhapova, 2015a) found that this list includes not only species preferred by other herbivorous mammals, but also many other plants (*Lactuca serriola* L., *L. tatarica* (L.) C.A. Mey., *Artemisia austriaca*, *Thlaspi arvense* L.), including poisonous species to other animals (*Descurainia sophia* (L.) Webb ex Prantl, *Anabasis aphylla* L.), which indicates the unpretentiousness of saigas. However high density of poisonous plants from Brassicaceae (*Descurainia sophia*, *Lepidium perfoliatum* L., *Lepidium ruderale* L.) and Liliaceae Juss. family especially on abandoned fields became one of the reasons for the death of the Ural saiga population in 2010-2011 (Dieterich and Sarsenova, 2012). The forage ration of saiga inhabiting Kalmykia (Chernye Zemli Reserve, the saiga population of the northwestern Caspian region) is no more than 25 species, where feather grass dominates in vegetation cover, but its participation in the diet of saiga in all seasons is extremely low, not more than 4% (Larionov, 2008). Studies of Russian population of saiga (Abaturov and Dzhapova, 2015b) showed that the forage diet of saiga requires the participation of forbs. Increasing of the proportion of graminoids and decreasing of forbs in steppe rangelands have a negative impact on the nutrition and state of saigas and does not provide the physiological requirements of the animals.

In different range areas of the saigas, the set of forage plants can change markedly. Adolph (1954) mentioned that in Astrakhan steppe the major component of the diet is *Ephedra distachya* L. and its berries, whereas saltworts (*Salsola* spp., *Anabasis* spp.) and cereals (*Agropyron* spp., *Stipa* spp.) are represented components of secondary importance. It is natural that the saiga has a change of food according to the seasons of the year. Under nature conditions, they are characterized by high mobility and moving from one site to another, selectively use plant food resources, consuming primarily only the most nutritious parts of plants.

Turkmen kulan feeds on as much as 109 plant species (14 species of shrubs, 10 species of semi-shrubs, 40 species of perennial and 45 species of annual grasses) (Solomatin, 1977). Spring diet consists of predominately cereals, and other ephemeral species. Animals avoid consuming dry food in spring season. In the summer animal feeds on predominately cereals and sedges. Autumn diet consists of mainly sagebrush and autumn generation of ephemeral plants. Winter diet is based upon green parts of sedges, cereals, sagebrushes and saltworts. If the snow cover become very high (40 cm and more) kulans switch to shrubs (*Haloxylon* spp., saltworts, *Tamarix* spp., etc.). In Altyn Emel National Park (Shakula and Khabibrakhmanov, 2014) kulan feed on about 110 plant species: in spring time – more than 70 species (cereals, sedges, ephemerals); in summer – 29 species including branches of *Tamarix* spp, *Cousinia* spp.; in winter – up to 31 species (saltworts, sagebrush, *Krascheninnikovia ceratoides* (L.) Gueldenst., *Astragalus* spp.).

The forage diet of the Turkmen kulan is similar to that of the Mongolian subspecies (*Equus hemionus* Pallas, 1775). Four major vegetation types: mountain steppe (*Agropyron cristatum* (L.) Gaertn., *Stipa krylovii* Roshev.), desert steppe (*Stipa* spp., *Artemisia* spp.), shrub desert (*Haloxylon ammodendron* (C.A. Mey.) Bunge ex Fenzl, *Stipa* spp., halophytes) and oasis (*Phragmites australis* (Cav.) Trin. ex Steud., *Juncus* spp., *Stipa splendens* Trin.) are feeding places of Mongolian Wild Ass (Hilbig, 1990). In the northern Xinjiang, China, kulan feeds 6 species of plants during the year (Chu et al., 2008; Xu et al., 2012a). Amaranthaceae (*Haloxylon persicum* Bunge, *Krascheninnikovia ceratoides*) and Poaceae Barnhart are major food of kulan during spring. *Stipa caucasica* Schmalh. is preferred in spring and summer; shrubs dominated the kulan's natural diet during autumn and winter.

Goitered gazelle has adapted to feeding on a wide variety of plants, it may use lichens, algae, thrown ashore by storms, grasses, forbs, semi-shrubs and shrubs (Sludsky, 1977). In some range areas, up to 70 plant species are included in the diet of gazelle. They often eat plants that are poisonous for livestock – *Peganum harmala* L., *Dodartia orientalis* L., *Zygophyllum* spp. Study of Chinese researchers (Xu et al., 2012b) implemented in Kalamaili Mountain Ungulate Nature Reserve, Xinjiang, showed that goitered gazelles ate 47 species of plants during the year. Amaranthaceae and Poaceae were major foods, and ephemeral plants were used mostly during spring. *Stipa caucasica* was a major food resource of gazelle throughout the year, *Krascheninnikovia ceratoides* was mainly used in spring and summer, whereas in autumn and winter, gazelles consumed large amounts of *Haloxylon ammodendron* branches. During the dry and hot summer and autumn, succulent plants like *Allium polyrhizum* Turcz. ex Regel, *Zygophyllum rosowii* Bunge, *Salsola subcrassa* Popov were favored by gazelles. In winter, the portion of *Anabasis*, *Stipa splendens* and *Phragmites australis* were evidently higher than in the other seasons.

The forage base of wild ungulates in the Barsa Kelmes Nature Reserve before the catastrophic decline of the Aral Sea was studied by several scientists (Vasenko, 1950; Demchenko, 1950; Rashek, 1974, 1977; Zhevnerov, 1984).

Seasonal preferences of ungulates generally coincide. In spring, they eat ephemerals, especially cereals – *Eremopyrum orientale*, *Bromus tectorum*, *Poa bulbosa* and green shoots of wheatgrass and feather grass (*Agropyron fragile*, *A. desertorum* (Fisch. ex Link) Schult., *Stipa arabica* Trin. & Rupr., *S. caucasica*, *S. lessingiana* Trin. & Rupr.). The most valuable desert cereal is *Eremopyrum orientale*. In spring, in addition to grasses, kulans eat well ephemerals (*Chorispora tenella* (Pall.) DC., *Arabis nova* Vill., *Euclidium syriacum* (L.) R. Br.) and seedlings of annual saltworts. In the midst of spring, goitered gazelles well eat *Calligonum* spp., *Atraphaxis spinosa* L., *Caragana grandiflora* (M. Bieb.) DC. Kulans and gazelles also eat young shoots of *Anabasis salsa* and *Artemisia terrae-albae*. In summer *Atriplex tatarica*, *Ceratocarpus arenarius* L., *Alhagi pseudalhagi* (M. Bieb.) Desv. ex B. Keller & Shap. appear in the diet, gazelles eat the fruits of *Nitraria schoberi* L. and *Ephedra disrachya*. By August, cereals dry up and become very coarse and their importance in the forage ration decreases. From that season on, *Anabasis salsa* and species of *Artemisia* play an increasing role. Most ephemerals do not preserve even in the dry state. Biting by kulans such plants as *Crypsis schoenoides* (L.) Lam., *C. alopecuroides* (Piller & Mitterp.) Schrad., *Lepidium latifolium* L., *Girgensohnia oppositiflora* (Pall.) Fenzl, *Amberboa turanica* Iljin, *Halimocnemis sclerosperma* (Pall.) C. A. Mey., *Halimodendron halodendron* (Pall.) Voss is observed only during this period of the year. The main food of gazelle in the

summer are plants of the Poaceae family (*Agropyron* spp., *Eremopyrum* spp., *Poa bulbosa*, *Aeluropus littoralis* (Gouan) Parl.), Polygonaceae Juss. (*Atraphaxis spinosa*, *Calligonum* spp.), Amaranthaceae (*Haloxylon* spp., *Krascheninnikovia ceratoides*, *Bassia prostrata*, *Anabasis salsa*), Fabaceae Juss. (*Alhagi pseudalhagi*, *Caragana grandiflora*). In dry years in the summer, plants of the Asteraceae family (*Artemisia terrae-albae*, *A. arenaria* DC., *A. quiquiloba* Trautv.) acquire significant importance in nutrition.

In autumn, *Anabasis salsa*, *Frankenia hirsute* L., *Artemisia* spp. are most often eaten, in winter – annual shoots of *Haloxylon ammodendron*, *H. persicum*, *Halocnemum strobilaceum* (Pall.) M. Bieb., *Artemisia terrae-albae*, *Anabasis salsa*. Due to saturation of the annual and perennial saltworts with salts, they are eaten by wild ungulates only from the end of September after rains. By the amount of protein *Anabasis salsa*, *Ceratocarpus arenarius*, *Haloxylon* spp. surpasses cereals (Kurochkina et al., 1986). Their positive quality is also the relatively small amount of fiber.

In winter after frosts wild ungulates eat *Halocnemum strobilaceum*. In December-January, *Artemisia terrae-albae* dominate in the forage ration of the kulans and saigas, in February – *Anabasis salsa*. In winter as compared to other seasons kulans eat well *Haloxylon* spp. Saigas browses *Ephedra distachya* as well. In periods of heavy snow, gazelles eat large quantities of shrubs and large-stemmed grasses, and in low-snow periods – dwarf semi-shrubs and small shrubs; *Halocnemum strobilaceum*, *Ephedra distachya* are the most important among them. *Haloxylon* spp. is especially important during the snowy season.

Forage resources of rangelands vary from year to year and season to season. The study of the productivity of the main plant communities of the Barsa Kelmes Nature Reserve was carried out on ecological sites from 1975 to 1984 during the complex expedition of the Herzen State Pedagogical University of Russia (St. Petersburg). The data of long-term studies were used to assess the forage base of wild ungulates, seasonal dynamics of phytomass accumulation and to determine the average long-term productivity indicators. Yield data of the field research are the basis for compiling maps of forage lands with use of the interpretation of satellite images.

The aim of our research was an inventory of rangeland diversity and mapping of forage resources for wild ungulates in the Barsa Kelmes Nature Reserve.

The following tasks were set to achieve the aim: 1) identification of the species composition of the forage diet of wild ungulates; 2) assessment of rangeland productivity based on field research, retrospective and remote sensing data; 3) development of a rangeland map.

Materials and methods

Study area

The Barsa Kelmes Nature Reserve is located in the northern part of the eastern coast of the former Aral Sea (Kazakhstan) and consists of three cluster areas “Barsa Kelmes”, “Kaskakulan”, including the adjacent territory of the dry seabed, and “Delta”. The research presented in this article is related to cluster area of “Barsa Kelmes” (Fig. 1).

The relief of the former island is divided into two parts: the southern – high plateau and the northern – undulating plain crossing from south to north by valleys of temporary streams (Kuznetsov, 1979). The highest point (108 m asl) is located at the western coast (Butakov cape). The northwestern, northern and eastern coasts are

bordered by belt of sand dunes which are the old Aral marine terraces. The primary marine plain is formed on the dry seafloor with a slightly inclined surface (Dimeyeva et al., 2012).

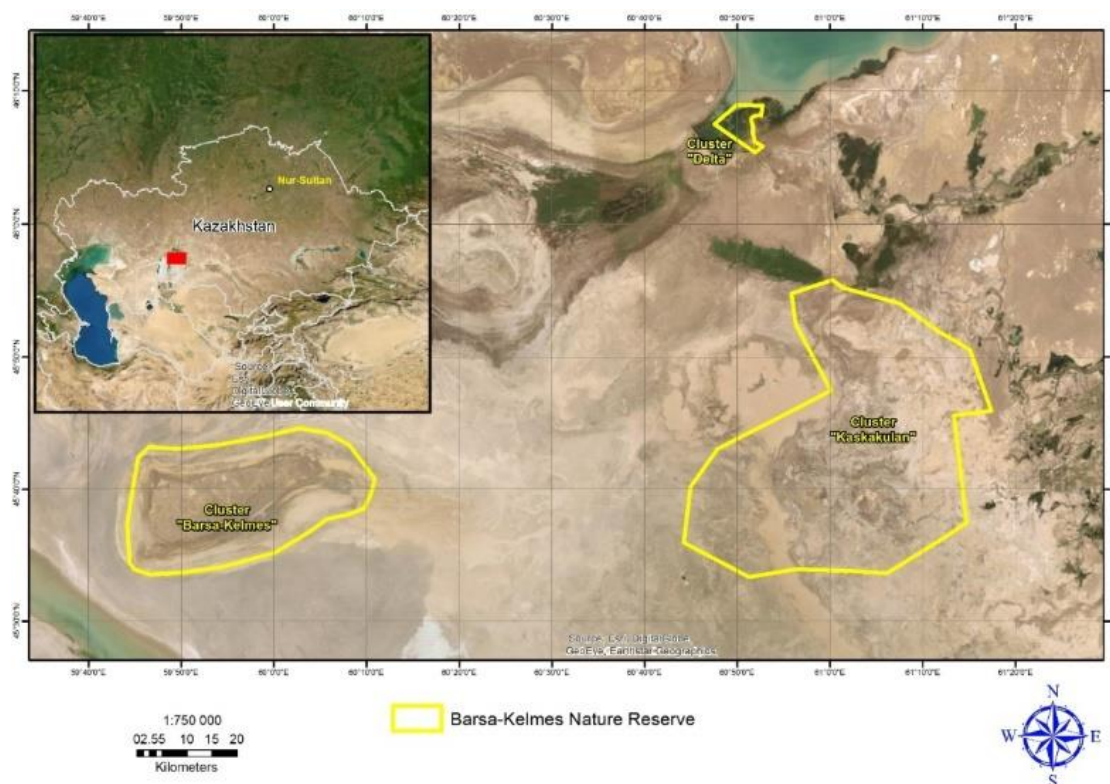


Figure 1. Study area

The climate is temperate with long hot summers, relatively cold winters, and low precipitation that is typical for the temperate deserts of Turan lowland. The average annual precipitation is low (126–128 mm). The average air temperature in July is 25–26 °C; the absolute maximum reaches 42–44 °C. The average air temperature in January is –10–13 °C; the absolute minimum is –34–36 °C with strong winds (the maximum reaches 20–24 m/s) (Dimeyeva et al., 2012).

The light brown desert soils (Calcic Xerosols) of different salinity and texture are represented at the original coast of the former island (Erokhina, 2016). There are also takyr, salt marshes and sandy soils. Within the dry seabed different types of solonchaks are distributed (gleyic, gaplic, degraded, takyr-like), and coastal saline sands.

Vascular flora of the Barsa Kelmes cluster area consists of 264 species, belonging to 42 families and 164 genera. These data are obtained from published papers (Dimeyeva, Alimbetova, 2007; Dimeyeva et al., 2012) taking into account the latest field research data of 2019. Species from Amaranthaceae (49), Asteraceae (32), Brassicaceae (26), Poaceae (27), Polygonaceae (21) families prevail. The most important genera are *Calligonum* (15), *Artemisia* (10), *Atriplex* (7), and *Salsola* (6).

Zonal vegetation is composed by *Artemisia terrae-albae* and *Anabasis salsa* with sparse *Haloxylon ammodendron*. The intrazonal vegetation is distributed on solonchaks with *Halocnemum strobilaceum* and *Limonium suffruticosum* communities. Saltwort

vegetation covers takyr-like solonchaks (*Climacoptera aralensis* (Iljin) Botsch., *C. brachiata* (Pall.) Botsch., *Salsola foliosa* (L.) Schrad. ex Schult., *Halimocnemis sclerosperma*). Communities of *Haloxylon ammodendron*, *H. persicum* dominate in hummocky sand dunes. Plant communities with share of *Atraphaxis spinosa*, *Ephedra distachya*, *Calligonum* spp, *Convolvulus erinaceus* Ledeb. are less significant. Vegetation of the dry seafloor is characterized by a belt distribution parallel to the coastline. Aggregations of *Salicornia europaea* L., *Tamarix hispida* Willd., *Bassia crassifolia* (Pall.) Soldano, *Suaeda acuminata* (C.A. Mey.) Moq., *Halocnemum strobilaceum* are common on coastal salt marshes. The desalinization of the sand and the deflation of surface horizons lead to the formation of psammophytic communities of *Stipagrostis pennata* (Trin.) de Winter, *Eremosparton aphyllum* (Pall.) Fisch. & C.A. Mey, *Astragalus brachypus* Schrenk. The former island Barsa Kelmes is joined to the original eastern coast before 2000s. Vegetation cover between the island and the original coast consists of aggregations of annual saltworts (*Atriplex pratovii* Sukhor., *Bassia hyssopifolia* (Pall.) Kuntze, *Salsola nitraria* Pall.) with *Tamarix laxa* Willd., *Nitraria schoberi*. Lands with a rare plant cover or without plants frequently occur.

Field research was implemented in early June 2019 with the participation of the nature reserve staff. The objects of investigation were plant communities representing desert rangelands. Sites for productivity estimations were defined in areas with typical vegetation cover.

Methods

The vegetation was studied using traditional methods of geobotanic field research, including the geobotanical description of the main vegetation communities and the landscape and ecological profiling with the use of topographic maps and satellite imagery (Bykov, 1957, 1978; Tueller, 1988). Occasionally, geolocation was registered by a GPS device, and the detailed geobotanical description was compiled of the main plant communities representative for the area.

Geobotanical description

For each plant community, coordinates, landscapes, soils, water regime, total projective coverage, layers, degree of transformation were defined; the full floristic composition was given, phenological phases of plant species, vigour (according to a 5-point scale), abundance (by Drude scale), spreading (by Bykov's scale), morphometric parameters (height, habitus) were defined. Description of vegetation is carried out at the vegetation description form. The herbarium was collected. The identification of species was carried out in the office period on the basis of identification keys of 9-volume "Flora of Kazakhstan" (1956-1966) and 2-volume "Illustrated Guide for Identification of the Plants of Kazakhstan" (1969, 1972). The names of plant species, genera, and families were quoted in accordance with summaries by the APG IV system (Chase et al., 2016) and Internet resource of The World Flora Online.

Estimating the amount of standing crop of plant material (economic productivity)

Methods for determining the productivity of pastures are described by Brown (1954), Ramensky et al. (1956), Nechaeva (1957), Bykov (1978), Kurochkina et al. (1986), Ospanov (1995), Smith et al. (2012), etc. The account of yield is made by two basic methods: clipping (usually on square plots) and model bushes (on transects).

Method of clipping (harvest method)

This method involves clipping all the above-ground plant material (standing crop – either current year's growth or total) in a quadrat and weighing it. To determine the standing crop use metal frames (quadrats) of 0.25 sq. m. They were located objectively and preferably with randomization in 12 - fold repetition (3 sq. m). Clipping of plants was carried out separately by species or by economic groups: unpalatable plants (poisonous, weed), ephemerals, herbs (tall grass, legumes, etc.), wormwood/sagebrush (well eaten, poorly eaten) and saltworts (annual, perennial). An approximate percentage of the phytomass eaten on the grazed grass stands is set, after that corrections are made for a certain yield. On desert low grass rangelands, the phytomass is clipped at a height of 1 cm from the soil surface. On semi-shrub and shrub rangelands only young leaves and shoots (annual growth) were cut. The phytomass samples are weighed in the field immediately after clipping, then it is dried to an air-dry basis.

Method of model bushes

It is used to determine the productivity of shrub and semi-shrub vegetation. The method lays transect on which all species are calculated, except for seedlings. The calculation was carried out taking into account the size of plants, which are grouped in 2-3 groups with similar height and diameter. On the transect all specimens were counted in three categories: large, medium, and small. Model plants of each size were selected and annual growth cut off. The yield of bushes of shoots' type was defined by 1 m × 1 m or 2 m × 2 m quadrats (depending on plant height) in 2-fold repetition. All the yield data were recorded in the vegetation description forms, the yields were converted to centners or kilograms per hectare.

Field mapping

Rangeland vegetation mapping was carried out by a combination of detailed-route research and the method of landscape-ecological profiling using the topographic maps and satellite images (Sochava, 1979; Berlyant, 1997). At geolocations defined on the ground by the GPS device, a detailed geobotanical description of the main, predominant in area, plant communities were carried out. Cartographic materials (digital layers of the topographical map, satellite imagery) are reorganized within an ArcGIS software interfaced database.

Remote sensing methods

Remotely sensed data were used to calculate major biophysical parameters of pastures, such as grass cover percentage and biomass production. Satellite data from Landsat OLI sensor (path 160-161 row 028) were obtained from <https://earthexplorer.usgs.gov>. Satellite imagery acquired covers the period from early summer till early autumn of 2019 to provide an adequate understanding of the vegetation dynamics for the year of 2019:

6 June 2019 (LC08_L1TP_160028_20180614_20180703)

8 June 2019 (LC08_L1TP_161028_20190608_20190608)

17 June 2019 (LC08_L1TP_160028_20190617_20190620)

20 August 2019 (LC08_L1TP_160028_20190820_20190903)

27 August 2019 (LC08_L1TP_161028_20190827_20190827)

12 September 2019 (LC08_L1TP_161028_20190912_20190917)

Satellite images were pre-processed with Excelis ENVI 5.3, the pre-processing procedure included the radiometric calibration of raw satellite data and the atmospheric correction of calibrated scenes. We used Excelis ENVI 5.3 to calculate spectral indices, further used to develop map products.

Indices, calculated with satellite data were processed along with ground data to define the better correlations of satellite and ground information. We used Statsoft STATISTICA 12.0 to perform this part of the entire workflow.

We further used ArcGIS 10.5 to process raster data and to visualize resulting maps.

The selection of spectral indices is based upon the previous studies of the spectral parameters and vegetation cover in the desert areas of Kazakhstan (Malakhov and Islamgulova, 2014, 2015). *Table 1* enlists major indices, used in this paper along with meaningful range of the given index values.

Table 1. Spectral indices, used in current study

Index	Expression	Range	Designation
Salinity index	$\sqrt{\frac{blue}{red}}$	> 0.23	Outlining of superficial soil salinization
Water index	$\frac{green - nir}{green + nir}$	> 0.1	Outlining of water bodies
Top soil grain size	$(red - blue) * (red + blue + green)$	0.01-0.025	Differentiation of gravel, sand and clay
Water concentration in green biomass (NDWI)	$\frac{nir - swir}{nir + swir}$	> 0	Calculation of green biomass
Bare soil index	$\left(\frac{nir - green + red}{nir + green + red}\right) * (-1)$	Vary for different soil types	Delineation of areas with depleted or vanished vegetation cover

blue – blue band of satellite image, spectral range 450-520 nm; green – green band of satellite image, spectral range 530-600 nm; red – red band of satellite image, spectral range 630-680 nm; nir – near infrared band of satellite image, spectral range 850-890 nm; swir – short-wave infrared band of satellite image, spectral range 1570-2290 nm

Calculation of green biomass by satellite data

Vegetation Water Content is an important tool for estimating biophysical vegetation parameters (Penuelas et al., 1993). Shortwave infrared reflectance (SWIR) is negatively correlated to the leaf-water content due to the large absorption of water by the leaf (Yilmaz et al., 2008). Gao (1995) proposed a following narrow-band index, describing the water concentration in green biomass, as a tool for estimating vegetation status (*Eq. 1*):

$$NDWI = \frac{(\rho_{857} - \rho_{1241})}{(\rho_{857} + \rho_{1241})} \quad (Eq.1)$$

where ρ_{857} and ρ_{1241} represent the reflectance value in the corresponding band of the satellite image.

It is noticeable that the index operates with the infrared spectrum, only, unlike NIR-RED-based indices. The application of NDWI (Normalized Difference Water Index)

and the high value of its correlations with biophysical vegetation variables explains the physiology of different types of desert vegetation in a better way than NIR-RED-based vegetation indices. The idea of this index is based on the fact, that “Liquid water absorption in the 1.5-2.5 μm region (short-wave infrared, SWIR) for green vegetation is significantly stronger than that of the 0.9-1.3 μm (near infrared, NIR) region” (Gao, 1995).

The index of water concentration in vegetation (NDWI) demonstrated the stable correlation to vegetation cover parameters. Pearson coefficients ($p < 0.05$) are respectively as following 0.78, 0.76 and 0.73 for grass cover, green biomass and productivity.

Seasonal biomass of the Barsa Kelmes pastures was calculated on Landsat data using NDWI and seasonal correction coefficients proposed by Lebed (1989). Production (mass of dry matter) is closely related to green vegetation mass (Malakhov and Islamgulova, 2014), and could be easily estimated from biomass values taken from satellite data.

Results

Forage ration of wild ungulates in the Barsa Kelmes cluster area

The list of forage plants of wild ungulates (*Table A1* in the *Appendix*) has been compiled on a basis of previous publications (Vasenko, 1950; Demchenko, 1950; Rashek, 1974, 1977; Zhevnerov, 1984). It was important for us to compare which species from the local flora of the Barsa Kelmes cluster area are eaten by ungulates, what is common and what are the differences.

The general list of plants eaten by wild ungulates consists of 105 species belonging to 26 families and 70 genera, which is about 40% of the local flora. Among them 35 species are eaten by saigas, 78 – by gazelles, and 71 – by kulans. The preferences of ungulates are similar. In the first place are the Poaceae family, in the second – the species of the Amaranthaceae family, in the third place in the saiga and gazelle ration – Asteraceae, and in the kulan’s ration – Brassicaceae; Fabaceae and Polygonaceae are in fourth and fifth places. 26 species (25% of forage plants) are eaten by all wild ungulates of the reserve (saiga, gazelle, kulan).

Analysis of retrospective studies on productivity dynamics of plant communities in the Barsa Kelmes cluster area

From the beginning of the 70s to the end of the 80s of the last century, students and teachers of the Department of Botany of Herzen University conducted research on the productivity of forage plants of the Barsa Kelmes Island. Only one article was published based on research materials (Romanova et al., 1979). MS theses of students were used for a comparative analysis, which present the results of long-term field observations on the Barsa Kelmes Nature Reserve (Perchatkina, 1979; Galieva, 1980; Kukhtenko, 1989). The studies were carried out on phenoclimatic seasons (Kuznetsov and Burambaev, 1976): early spring (3 decade of March – 1 decade of April, stable temperature transition through 0 °C); full spring (2-3 decade of April – 1 decade of May, the transition of average daily temperatures through +5 °C); early summer (2-3 decades of May – 1-2 decades of June, the transition of average daily temperatures

through +15 °C); hot summer (3 decade of June – July, average daily temperature is above +22-23 °C); late summer (August, September).

Dynamics of the yield of the Artemisia terrae-albae – Agropyron desertorum complex

The vegetation cover of zonal ecosystems is dominated by complexity, where the components are *Artemisia terrae-albae* and *Anabasis salsa* communities, which regularly alternate depending on the microrelief and soil salinity. The ratio of the elements of the complex depends on the position in the landscape. In the undulating plains, the *Artemisia terrae-albae* communities account for about 60% of the area. The rest is occupied by the *Anabasis salsa* communities (Kuznetsov, 2007).

The analysis of regularities of productivity is based on the MS thesis (Galieva, 1980), which discusses the data of 1976-1979. The study of yield was carried out on ecological sites representing the phytocoenotic diversity of the complex within the plain.

Plots (plant communities, i.e. com.) in the central part of the island:

- (I-1) *Artemisia terrae-albae* – *Agropyron desertorum* com.
- (I-2) *Artemisia terrae-albae* com.
- (I-3) *Anabasis salsa* – *Artemisia terrae-albae* com.
- (I-4) *Anabasis salsa* com.
- (II-1) *Anabasis salsa* com.
- (II-2) *Anabasis salsa* – *Artemisia terrae-albae* com.

Plots in the western part of the island:

- (V-1) *Artemisia terrae-albae* com. in a plane
- (V-2) *Anabasis salsa* com.
- (V-3) *Artemisia terrae-albae* com. in a slope
- (V-4) *Artemisia terrae-albae* – *Stipa lessingiana* – *Agropyron desertorum* com. in a ravine

The results of long-term research were carried out for all plots, for some of them which representing the diversity of zonal communities we present diagrams to illustrate the dynamics of the yield (Figs. 2-5).

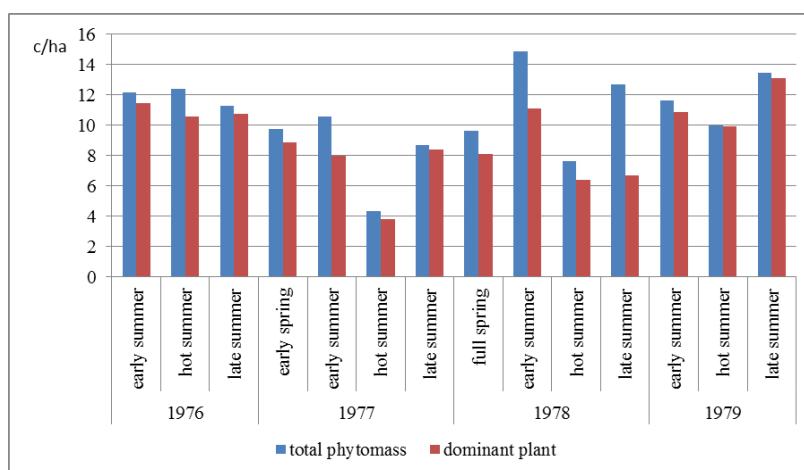


Figure 2. Productivity dynamics of *Artemisia terrae-albae* – *Agropyron desertorum* com. (I-1)

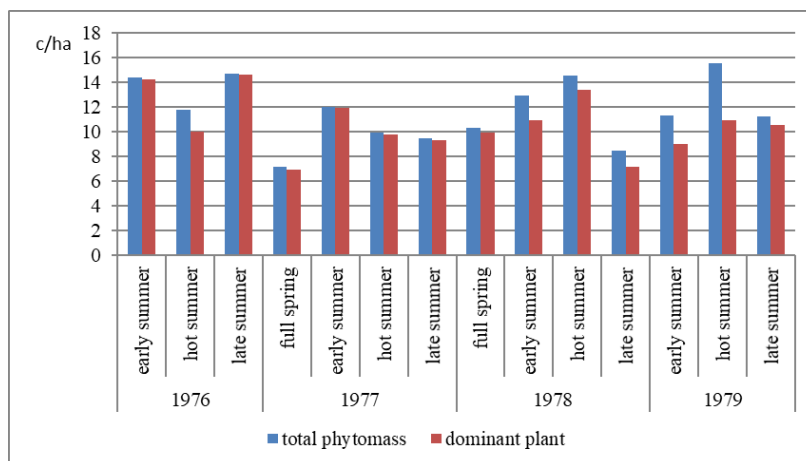


Figure 3. Productivity dynamics of *Artemisia terrae-albae* com. (I-2)

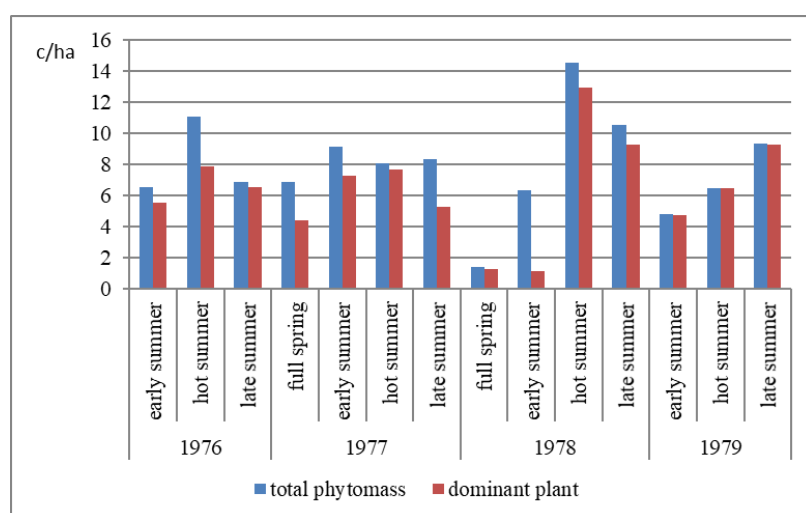


Figure 4. Productivity dynamics of *Anabasis salsa* com. (I-4)

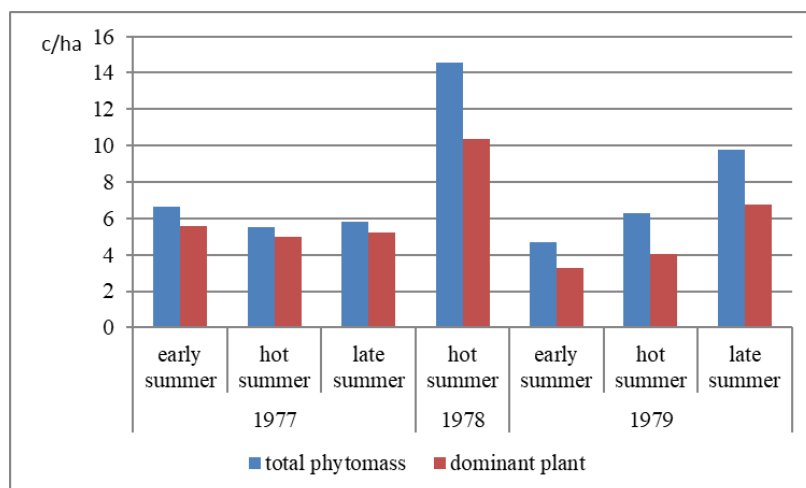


Figure 5. Productivity dynamics of *Artemisia terrae-albae* – *Stipa lessingiana* – *Agropyron desertorum* com. (V-4)

Based on long-term studies it was found that the *Artemisia terrae-albae* communities play a significant role in a complex vegetation, which accumulates on average 11.3 centners per hectare (c/ha) of phytomass during the spring and summer periods. The smaller yield falls on the share of *Anabasis salsa* communities – 7.4 c/ha.

The dynamics of yield in *Artemisia terrae-albae* varies widely in phenoclimatic seasons; the maximum yield is formed more often in early summer and in hot summer. In communities with the participation of subdominants, the seasonal yield is different. In *Artemisia terrae-albae* – *Agropyron desertorum* com. (I-1), the accumulation of the maximum phytomass is mostly confined to the beginning of summer; *Artemisia terrae-albae* – *Stipa lessingiana* – *Agropyron desertorum* com. (V-4) productivity varies from season to season. In *Anabasis salsa* com. (I-4) the development of the maximum yield is noted during the hot summer season, although there may be seasonal fluctuations. In addition, the yield of annual saltworts (*Climacopteraa aralensis*, *Halimocnemis sclerosperma*, *Salsola foliosa*) and perennial saltworts (*Halocnemum strobilaceum*) was determined, which are characterized by high phytomass (from 35.6 to 44.6 c/ha).

An assessment of changes in yield was made depending on the grazing of wild ungulates. For this, plots were defined on the grazed area and within the boundaries of protective fence (Table 2). The yield of ungrazed *Artemisia terrae-albae* com. higher than grazed by 1.3-2 times. In the communities of *Agropyron desertorum* at the beginning of summer, the yield of plots practically does not differ, and in a hot summer in the grazed area it decreases by 2.6 times. In *Anabasis salsa* com. on the grazed area, the phytomass is by 2-2.7 times higher. Average long-term indicators of seasonal yield are presented in Table 2, which was later used in the development of a rangeland map.

Table 2. Average indicators of the productivity of communities in *Anabasis salsa* – *Artemisia terrae-albae* complex

Plant communities/plots	Average yield, c/ha				
	Spring	Early summer	Summer		
<i>Artemisia terrae-albae</i> - <i>Agropyron desertorum</i> com. (I-1)	9.7	12.4	10.8		
<i>Artemisia terrae-albae</i> com. (I-2)	9.1	12.6	12.5		
<i>Anabasis salsa</i> – <i>Artemisia terrae-albae</i> com. (I-3)	6.4	8.4	8.2		
<i>Anabasis salsa</i> com. (I-4)	4.1	6.7	8.5		
<i>Anabasis salsa</i> com. (II-1)	4.1	4.8	7.1		
<i>Anabasis salsa</i> – <i>Artemisia terrae-albae</i> com. (II-2)	3.3	5.2	6.6		
<i>Artemisia terrae-albae</i> com. (V-1)		7.8	11.9		
<i>Anabasis salsa</i> com. (V-2)		9.5	9.2		
<i>Artemisia terrae-albae</i> com. (V-3)		13.9	15.2		
<i>Artemisia terrae-albae</i> – <i>Stipa lessingiana</i> – <i>Agropyron desertorum</i> com. (V-4)		5.7	7.6		
<i>Halimocnemis sclerosperma</i> com.			44.5		
Annual saltwort com. (<i>Salsola foliosa</i> , <i>Climacoptera aralensis</i>)			30.3		
		In the fence	Behind the fence	In the fence	Behind the fence
<i>Artemisia terrae-albae</i> com.		26.5	19.9	26.6	13.8
<i>Anabasis salsa</i> com.		5.1	13.6	5.6	10.9
<i>Agropyron desertorum</i> com.		3.6	3.8	3.9	1.5

Dynamics of the yield of sandy desert vegetation

A sand belt in the island is confined to the old Aral marine terraces, the origin of which is associated with transgressions and regressions of the sea level. The vegetation

cover is dominated by: *Haloxylon ammodendron*, *H. persicum*, *Atraphaxis spinosa*, *Ephedra distachya*, *Calligonum aphyllum* (Pall.) Guerke, *C. caput-medusae* Schrenk, *C. macrocarpum* I.G. Borshch., *C. acanthopterum* I.G. Borshch. From the sea side, the Aral terrace is adjoined by a strip of dunes, which represent a coastal rampart of 1.5-3 m high. The vegetation of the dune is formed by tamarisk (*Tamarix laxa*, *T. ramosissima* Ledeb., *T. hispida*), *Haloxylon ammodendron*, *Calligonum* spp. The analysis of the patterns was carried out on the basis of the MS thesis (Perchatkina, 1979). The study was carried out in 1976-1978 on two ecological sites.

Site IX is located on the northern coast. The productivity of the aboveground phytomass of the following communities were studied:

(IX-1) Psammophytic shrub (*Calligonum aphyllum*, *Atraphaxis spinosa*) with *Tamarix laxa* and *Haloxylon ammodendron* com.

(IX-2) *Aeluropus littoralis* com.

(IX-3) *Ephedra distachya* com. of dense coverage

(IX-4) *Ephedra distachya* com. of sparse coverage

Site X is located at the eastern coast. The following communities were studied:

(X-1) *Haloxylon* spp. with *Calligonum aphyllum*, *Tamarix laxa* com.

(X-2) *Ephedra distachya* – *Haloxylon persicum* com.

(X-3) *Ephedra distachya* – *Calligonum aphyllum* com.

(X-5) *Stipagrostis pennata* com. on hummocks

(X-5a) *Stipagrostis pennata* com. in a beach

In the psammophytic shrub with *Tamarix laxa* and *Haloxylon ammodendron* com. (IX-1) the largest part in the total yield is formed by tamarisk; psammophytic shrubs (*Atraphaxis spinosa*, *Calligonum aphyllum*) and *Haloxylon ammodendron* compose from 5 to 24% of the total phytomass. The highest yield (54.9 c/ha) was formed in the late summer in 1978, and in 1976-1977 the maximum was in early summer (Fig. 6).

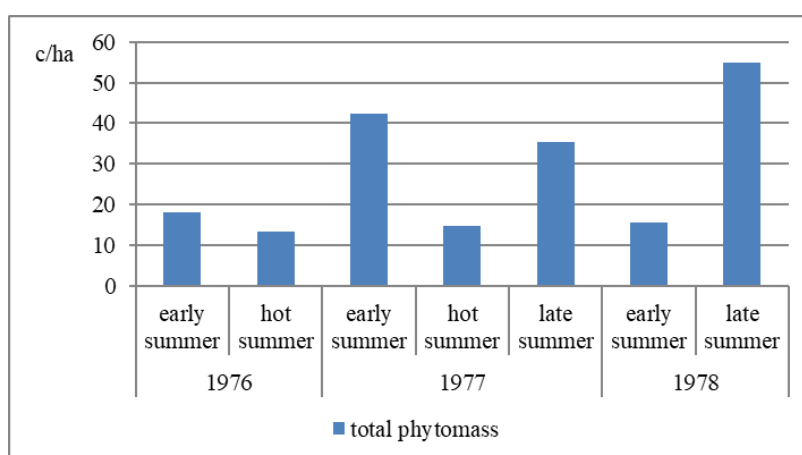


Figure 6. Productivity dynamics of psammophytic shrub with *Tamarix laxa* and *Haloxylon ammodendron* com. (IX-1)

The maximum phytomass of the *Aeluropus littoralis* (IX-2) community accumulates at the early summer (36.9 c/ha in 1977), during the hot summer it is minimal (3.0 c/ha in 1977). The highest phytomass in dense ephedra com. (IX-3) was observed at the

early summer in 1977 (62.6 c/ha), which was also due to a large number of ephemerals. In sparse ephedra com. (IX-4), the maximum yield was noted in the full spring of 1977 (62.9 c/ha), ephemerals accounted for 15% of the total phytomass, during the hot summer the aboveground phytomass was minimal (2.3 c/ha).

In the community of *Haloxylon* spp. with *Calligonum aphyllum* and *Tamarix laxa* com. (X-1), formation of the maximum phytomass is confined to the hot and late summer seasons. The highest productivity of shrubs was in 1977 (67.4 c/ha).

Yield fluctuations of *Ephedra distachya* – *Haloxylon persicum* com. (X-2) are shown in Figure 7. The maximum phytomass was formed at the full spring of 1977 (13.6 c/ha); in other years its accumulation was confined to the early and hot summer seasons.

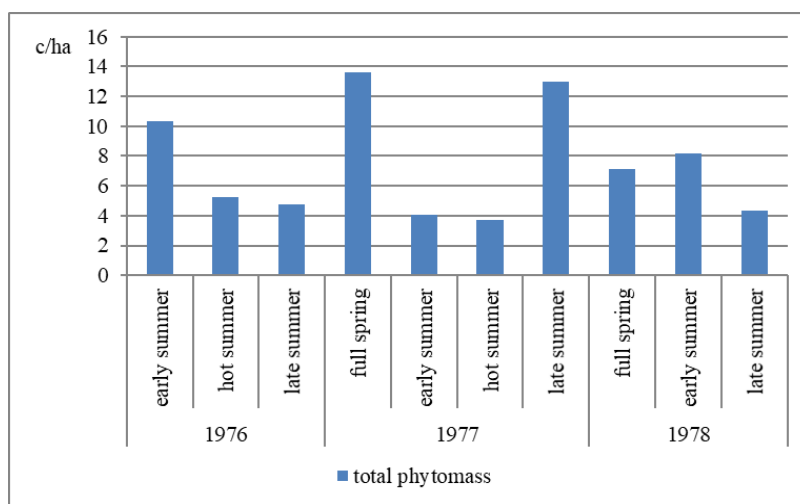


Figure 7. Productivity dynamics of *Ephedra distachya* – *Haloxylon persicum* com. (X-2)

Average long-term indicators of seasonal productivity are presented in Table 3, which were used to develop the rangeland map.

Table 3. Average indicators on productivity of sandy desert communities

Plant communities/plots	Average yield, c/ha	
	Spring	Summer
Psammophytic shrub with <i>Tamarix laxa</i> and <i>Haloxylon ammodendron</i> com. (IX-1)	15.6	30.1
<i>Atraphaxis</i>	0.1	0.1
<i>Calligonum</i>	0.6	0.9
<i>Haloxylon</i>	0.2	0.2
<i>Tamarix</i>	14.7	28.9
<i>Aeluropus littoralis</i> com. (IX-2)	5.3	4.8
<i>Ephedra distachya</i> coms. (IX-3,4)	26.6	17.6
<i>Haloxylon</i> spp. with <i>Calligonum aphyllum</i> , <i>Tamarix laxa</i> com. (X-1)	0.5	34.7
<i>Haloxylon</i>	0.3	7.4
<i>Calligonum</i>	0.2	1.3
<i>Tamarix</i>	-	26.0
<i>Ephedra distachya</i> - <i>Haloxylon persicum</i> com. (X-2)	10.4	5.4
<i>Ephedra distachya</i> – <i>Calligonum aphyllum</i> com. (X-3)	16.4	8.3
<i>Stipagrostis pennata</i> coms. (X-5, 5a)	0.7	4.2

Additional information on productivity of psammophytic vegetation was provided in the MS thesis of Kukhtenko (1989). The work analyzed 10-year data on the dynamics of productivity in the summer (3 phenoclimatic seasons). Six plant communities were selected for the study:

- Haloxylon ammodendron* – *Calligonum aphyllum* – *Ephedra distachya* com.
- Haloxylon* spp. – *Ephedra distachya* com.
- Calligonum aphyllum* – *Ephedra distachya* com.
- Shrub (*Tamarix laxa*, *Haloxylon* spp., *Calligonum aphyllum*) com.
- Stipagrostis pennata* com.
- Atraphaxis spinosa* – *Aeluropus littoralis* com.

Long-term dynamics of productivity for some communities are shown in the graphs (Figs. 8-9).

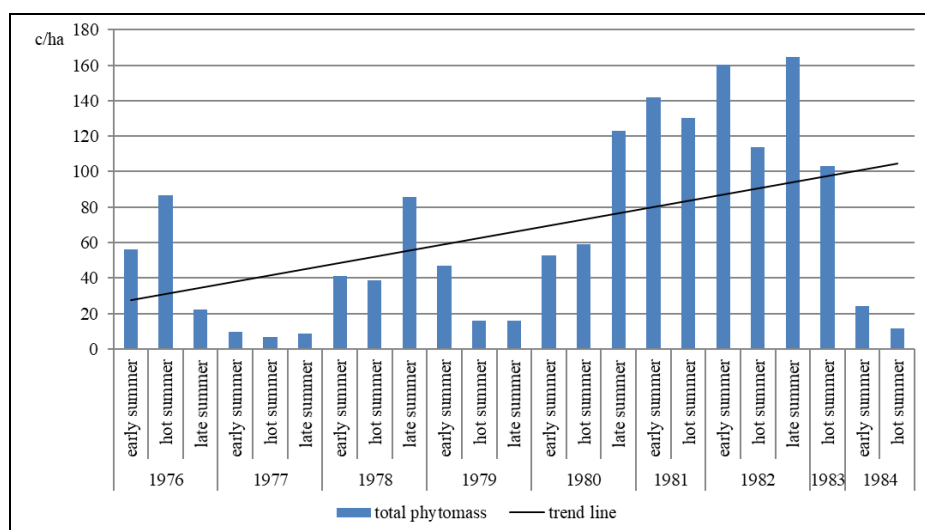


Figure 8. Productivity dynamics of *Haloxylon ammodendron* – *Calligonum aphyllum* – *Ephedra distachya* com.

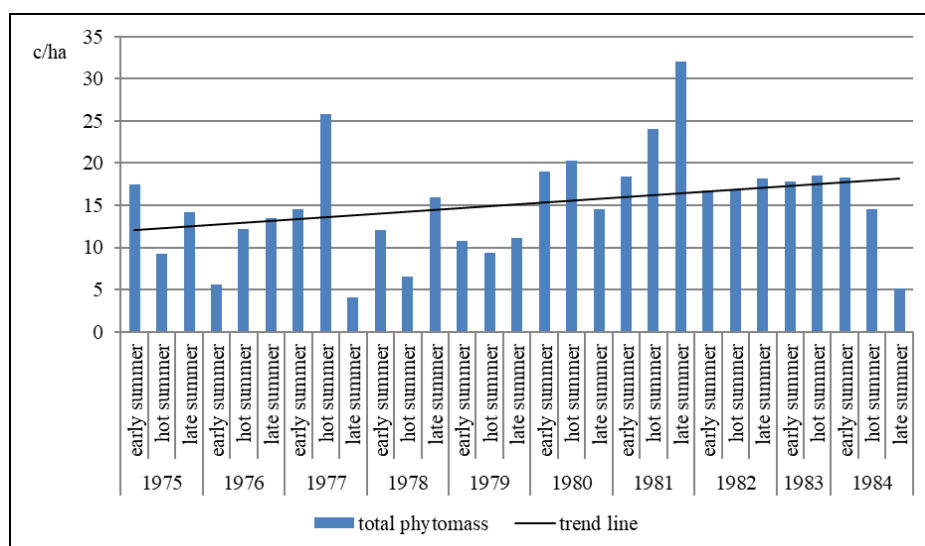


Figure 9. Productivity dynamics of *Haloxylon* spp. – *Ephedra distachya* com.

On the basis of the study, the average indicators for the summer period in long-term dynamics were calculated; the communities are located as the yield decreases: 1) *Haloxylon ammodendron* – *Calligonum aphyllum* – *Ephedra distachya* com. – 66.1 c/ha; 2) shrub (*Tamarix laxa*, *Haloxylon spp.*, *Calligonum aphyllum*) com. – 50.9 c/ha; 3) *Haloxylon spp.* – *Ephedra distachya* com. – 15.1 c/ha; 4) *Calligonum aphyllum* – *Ephedra distachya* com. – 13.9 c/ha; 5) *Atraphaxis spinosa* – *Aeluropus littoralis* com. – 8.2 c/ha; 6) *Stipagrostis pennata* com. – 5.4 c/ha.

The current state of forage resources in the Barsa Kelmes cluster area

Assessment of phytomass accumulation by traditional methods

The study of the accumulation of forage mass was carried out in the first ten days of June 2019 (early summer). The yield was determined by the methods of clipping and model bushes. The sequence of determining the stocks of forage mass included several stages: laying of standard plots (quadrats) or choosing model bushes; clipping off the forage mass; weighing raw phytomass, drying, weighing air dry phytomass; recalculation of the obtained data into centners per hectare. The results are shown in *Table 4*.

Table 4. Yield of forage mass of the Barsa-Kelmes reserve plant communities

Coordinates	Plant community	Coverage %	Number (area) of shrubs per ha	Species	Wet weight, centner per ha	Air dry weight, centner per ha
45°40'56" N 60°10'13" E	<i>Kalidium foliatum</i> (Pall.) Moq.	15-20		Kalidium	18.0	4.3
45°41'59" N 60°08'07" E	<i>Haloxylon ammodendron</i> – <i>Astragalus brachypus</i>	30	1650	Haloxylon	7.1	2.8
			711	Astragalus	0.7	0.2
				Total:	7.8	3.0
45°42'06" N 60°07'31" E	Sparse <i>Haloxylon ammodendron</i> with <i>Nitraria schoberi</i>	15	4400 sq.m	Nitraria	12.1	3.7
45°42'26" N 60°05'33" E	<i>Halocnemum strobilaceum</i>	15-20		Halocnemum	21.0	5.9
45°42'30" N 60°05'20" E	<i>Atraphaxis spinosa</i>	20	3100	Atraphaxis	5.3	3.0
45°42'02" N 60°04'57" E	Sparse <i>Ephedra distachya</i>	5-10	1300 sq.m	Ephedra	1.5	0.6
45°42'05" N 60°04'26" E	<i>Haloxylon ammodendron</i> – <i>Calligonum aphyllum</i> - <i>Ephedra distachya</i> with <i>Tamarix laxa</i>	40	4400	Haloxylon	52.4	15.7
45°40'29" N 59°54'11" E	Complex of <i>Anabasis salsa</i> (70%) and <i>Artemisia terrae-albae</i> (30%) communities	45-50		Anabasis com.:		
				Anabasis	29.0	14.5
				Saltworts	7.2	2.7
				Ephemerals	1.2	0.5
				Total:	37.4	17.7
		60	Artemisia com.:	37.5	23.0	
	Average for the complex:	37.5	20.4			
45°40'39" N 59°54'44" E	Annual saltwort	15-20		Saltworts	16.3	3.3
45°40'39" N 59°54'44" E	Psammophytic shrub with single <i>Haloxylon ammodendron</i>		1600	Calligonum	7.6	1.9
45°38'00" N 59°47'00" E	<i>Anabasis salsa</i> with saltworts and single <i>Haloxylon ammodendron</i>	50		Anabasis	48.7	20.4
				Ceratocarpus	1.3	0.9
				Saltworts	2.0	0.5
				Total:	52.0	21.8

45°37'24" N 59°47'12" E	<i>Artemisia terrae-albae</i> with single <i>Anabasis aphylla</i>	50		Artemisia Ceratocarpus Ephemerals Total:	26.0 1.0 0.3 27.3	16.5 1.0 0.3 17.8
45°42'212" N 60°03'05" E	<i>Artemisia terrae-albae</i> (60%) with microcoenoses of <i>Agropyron fragile</i> , <i>Stipa lessingiana</i> (10%) and single <i>Haloxylon ammodendron</i>	70		Artemisia Agropyron Stipa Ceratocarpus Ephedra Total:	6.0 10.3 3.8 2.3 0.8 23.2	3.8 6.2 2.2 2.3 0.3 14.8
45°41'45" N 59°58'60" E	<i>Calligonum acanthopterum</i> - <i>Ammodendron conollyi</i> Boiss. with <i>Artemisia quinqueloba</i>	50	700 800	Artemisia Calligonum Total:	1.1 3.6 4.7	0.4 1.0 1.4
45°41'11" N 60°02'40" E	Grass (<i>Stipa lessingiana</i> , <i>Agropyron desertorum</i>) with <i>Ephedra distachya</i> , <i>Rhaponticum repens</i> (L.) Hidalgo	90		Grass Ephedra Rhaponticum Total:	15.0 1.2 0.5 16.7	9.6 0.3 0.1 10.0
45°41'33" N 59°58'40" E	<i>Tamarix laxa</i>	60-70	1600	Tamarix	10.6	4.2

Assessment of forage mass accumulation by remote sensing methods

Landsat OLI images were used to calculate seasonal yield.

The temporal coverage (early summer - mid-autumn) of these data allowed reliably assessing the dynamics of soil-vegetation cover and calculating the main seasonal biophysical parameters of rangelands (biomass and dry weight). The use of the author's methodology (Malakhov and Islamgulova, 2014, 2015) and seasonal correction factors (Lebed, 1989) allowed to compile a series of maps of rangeland productivity in the Barsa Kelmes Nature Reserve for different seasons (*Fig. 10*).

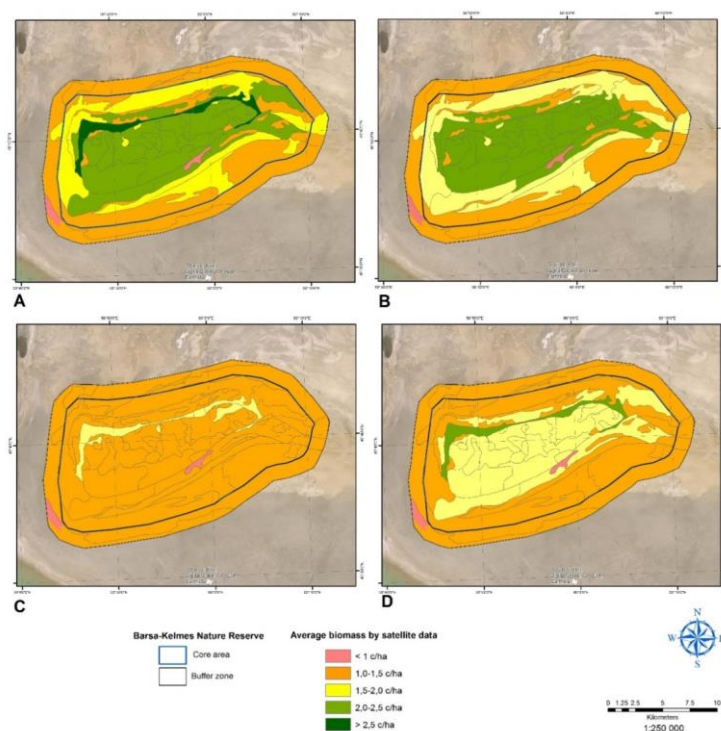


Figure 10. Yield of rangelands for different seasons: A – spring, B – summer, C – autumn, D – winter

Rangeland map of the Barsa Kelmes cluster area

The stages of the rangeland map (Fig. 11) compilation included: systematization of geobotanical descriptions, interpretation of the Landsat OLI satellite image, drawing up a contour map, and developing a legend for the map. The available cartographic materials were analyzed to create the map: Map of forage lands of Kazakhstan (Scale 1:2 000 000) (Bakanach et al., 1978); Vegetation map of Kazakhstan and Central Asia (within the limits of desert zone) (Scale 1:2 500 000) (Rachkovskaya, 1995); Vegetation map of Kyzylorda region (Scale 1:1 500 000) (Dimeyeva, 2020); Map of soils (Scale 1:1 350 000) (Erokhina, 2016); Map of vegetation (Scale 1:1 350 000) (Rachkovskaya and Egemberdieva, 2016), and some archive materials of the Barsa Kelmes Nature Reserve.

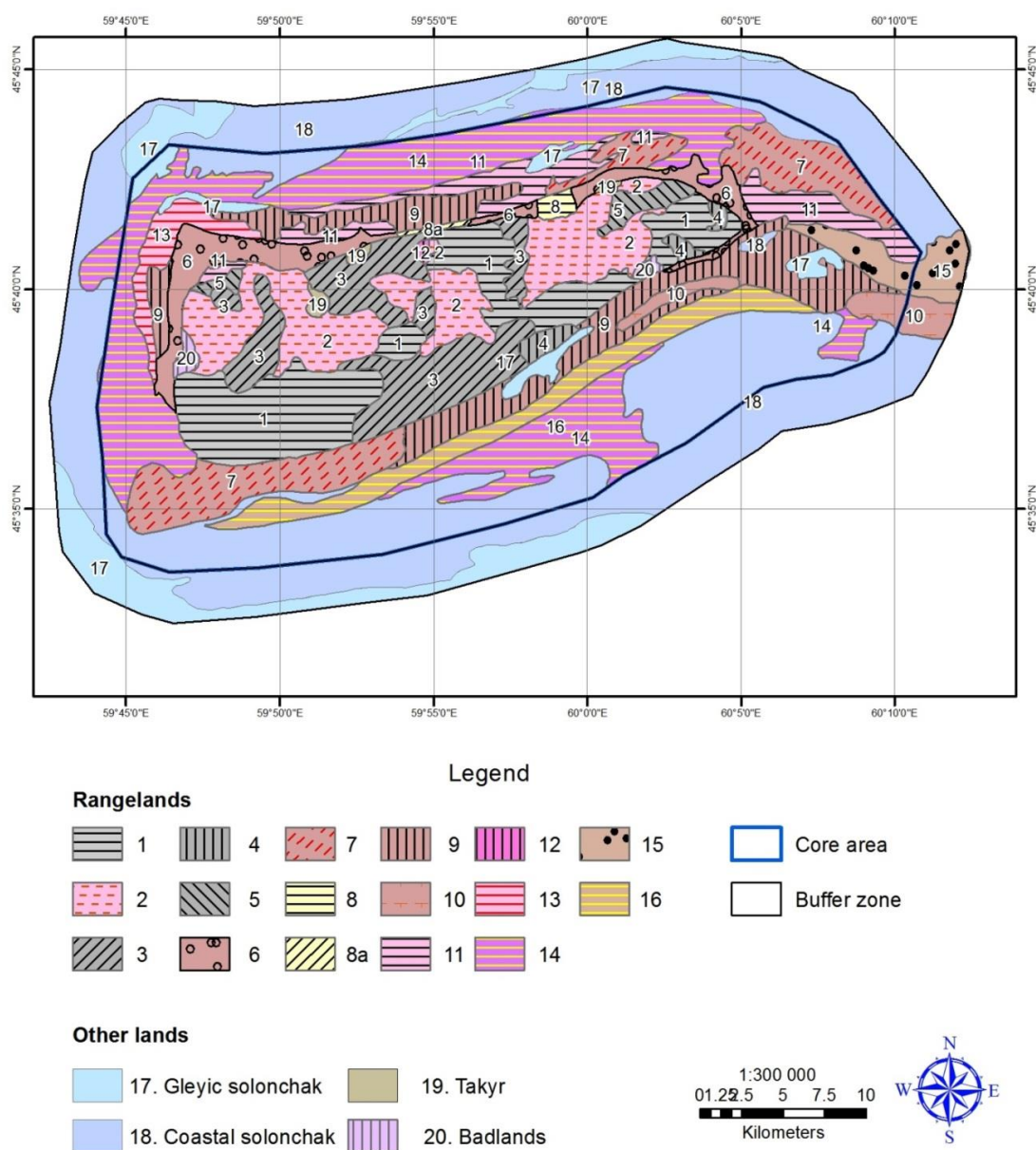


Figure 11. Rangeland map of the Barsa Kelmes cluster area

Seasonal yield maps (Fig. 10) were used to highlight the contours. The structure of the legend to the map is based on the principles of the Map of forage lands of Kazakhstan (1978), where each mapping unit shows the yield for seasons (spring, summer, autumn, winter). Seasonal yield was calculated on a basis of the coefficients (Osmanov, 1995) (Table 5). For plants that are not on the list, the coefficients were calculated using other sources (Dimeyeva, 1990, 1994).

Table 5. Coefficients for the dynamics of growth and preservation of the phytomass for one-year growth, %

Plant name	Seasons of a year			
	Spring	Summer	Autumn	Winter
<i>Stipa lessingiana</i>	80	100	70	60
<i>Agropyron desertorum</i>	70	100	80	60
<i>Stipagrostis pennata</i>	80	100	90	80
<i>Aeluropus litoralis</i>	80	100	60	50
<i>Phragmites australis</i>	50	100	80	70
<i>Eremopyrum orientale, Bromus tectorum</i>	100	60	30	20
<i>Poa bulbosa</i>	100	50	40	20
<i>Alhagi pseudalhagi</i>	30	100	90	70
<i>Ephedra distachya</i>	50	100	90	60
<i>Calligonum aphyllum</i>	100	80	30	10
<i>Haloxylon ammodendron</i>	40	100	80	50
<i>Artemisia terrae-albae</i>	80	100	90	60
<i>Artemisia quinqueloba</i>	60	100	90	60
<i>Anabasis salsa</i>	50	100	90	60
<i>Halostachys belangeriana</i> (Moq.) Botsch., <i>Kalidium foliatum</i>	40	100	80	70
<i>Halocnemum strobilaceum</i>	30	100	90	60
<i>Ceratocarpus arenarius</i>	30	100	80	30
<i>Climacoptera aralensis</i>	50	100	90	70
<i>Salsola nitraria</i>	40	100	80	60

The legend to the rangeland map (Table 6) is a system of titles to which the mapped units are subordinated. Each mapping unit of the legend corresponds to the type of rangeland that are combined by relief. The headings of the first and second rank reflect the confluence of vegetation to zonal conditions for the formation of forage lands (desert rangelands) and life forms of dominant plants. The total yield for different year seasons is given for each mapping unit, which is the sum of the aboveground phytomass of the community species. In mapping units with complex vegetation, the total yield is the average of its constituent components.

Table 6. Legend to the rangeland map of the Barsa Kelmes cluster area

No	Mapping unit	Rangeland aboveground phytomass (dry weight, centner per ha)			
		Spring	Summer	Autumn	Winter
Desert rangelands					
Sagebrush and Anabasis dwarf semi-shrub rangelands					
1	Ephemeroid – sagebrush, sagebrush – anabasis, sagebrush – bulbous bluegrass (<i>Artemisia terrae-albae</i> , <i>Anabasis aphylla</i> , <i>Poa bulbosa</i> , <i>Tulipa biflora</i> Pall., <i>Rheum tataricum</i>) on plateau and undulating plain	9.4	11.6	10.4	7.0

2	Anabasis, annual saltwort, ephemeral – anabasis (<i>Anabasis salsa</i> , <i>Climacoptera brachiata</i> , <i>Eremopyrum orientale</i> , <i>Lepidium perfoliatum</i>) on plateau and undulating plain	4.1	8.3	7.5	5.0
3	Complex of sagebrush – anabasis, anabasis – sagebrush (<i>Artemisia terrae-albae</i> , <i>Anabasis salsa</i> , <i>Anabasis aphylla</i>) with feather grass (<i>Stipa lessingiana</i>) on plateau and undulating plain	6.8	10.0	9.0	6.0
4	Sagebrush, ephemeroïd – anabasis, salsola (<i>Artemisia terrae-albae</i> , <i>Anabasis salsa</i> , <i>Allium decipiens</i> Fisch. ex Schult. & Schult.f., <i>Ferula canescens</i> (Ledeb.) Ledeb., <i>Salsola orientalis</i> S. G. Gmel.) in combination with bulbous bluegrass – sagebrush, wheat grass – aeluropus, feather grass (<i>Artemisia schrenkiana</i> Ledeb., <i>A. nitrosa</i> , <i>A. scopiformis</i> Ledeb., <i>Poa bulbosa</i> , <i>Agropyron desertorum</i> , <i>Aeluropus littoralis</i> , <i>Stipa lessingiana</i>) on eroded slopes of plateau and ravines	7.4	10.3	8.3	5.7
5	Sagebrush with feather grass, bulbous bluegrass and haloxyton (<i>Artemisia terrae-albae</i> , <i>Stipa lessingiana</i> , <i>Poa bulbosa</i> , <i>Haloxyton ammodendron</i>) on pre-sand plain	6.0	7.6	6.8	4.6
Haloxyton woodland rangelands					
6	Haloxyton, ephemeral – haloxyton with psammophytic shrubs, microcoenoses of ephedra and aeluropus (<i>Haloxyton ammodendron</i> , <i>Calligonum</i> spp., <i>Atraphaxis spinosa</i> , <i>Eremopyrum orientale</i> , <i>Poa bulbosa</i> , <i>Lepidium perfoliatum</i> , <i>Ephedra distachya</i> , <i>Aeluropus littoralis</i>) on the hummocky sands of the old Aral marine terrace	3.4	8.6	6.9	4.3
7	Haloxyton, annual saltwort – haloxyton with tamarisk and psammophytic shrubs (<i>Haloxyton ammodendron</i> , <i>Tamarix laxa</i> , <i>Astragalus brachypus</i> , <i>Calligonum aphyllum</i> , <i>Atraphaxis spinosa</i> , <i>Salsola nitraria</i> , <i>Atriplex pratovii</i>) on a slightly hummocky primary marine plain	1.1	3.0	2.4	1.5
Psammophytic shrub rangelands					
8	Psammophytic wormwood – psammophytic shrub with ephedra and tamarisk (<i>Ammodendron conollii</i> , <i>Calligonum</i> spp., <i>Artemisia arenaria</i> , <i>A. quinqueloba</i> , <i>Ephedra strobilacea</i> Bunge, <i>E. distachya</i> , <i>Tamarix laxa</i>) on the hummocky sands of the old Aral marine terrace	3.6	5.6	4.2	2.4
8a	Psammophytic shrub with ephedra, tamarisk and haloxyton (<i>Calligonum</i> spp., <i>Atraphaxis spinosa</i> , <i>Ephedra distachya</i> , <i>Tamarix laxa</i>) on the hummocky sands of the old Aral marine terrace	3.2	6.4	5.2	3.0
9	Psammophytic shrub in combination with tamarisk (<i>Astragalus brachypus</i> , <i>Calligonum aphyllum</i> , <i>Eremosparton aphyllum</i> , <i>Tamarix laxa</i>) on hummocky sands of a primary marine plain	3,0	4,9	4,0	2,5
10	Rare aggregations of psammophytic shrubs, haloxyton, stipagrostis (<i>Calligonum aphyllum</i> ,	1.8	4.0	3.1	2.1

	<i>Atraphaxis spinosa</i> , <i>Haloxylon ammodendron</i> , <i>Stipagrostis pennata</i>) on a primary marine plain				
Saltwort rangelands					
11	Perennial saltwort with halophytic herbs (<i>Halocnemum strobilaceum</i> , <i>Kalidium foliatum</i> , <i>Salsola paulsenii</i> Litv., <i>Frankenia hirsuta</i> L., <i>Limonium otolepis</i> (Schrenk) Kuntze) on a hummocky primary marine plain	1.8	5.1	4.4	4.4
12	Annual saltwort with anabasis and ephemerals (<i>Halimocnemis karelinii</i> Moq., <i>Climacoptera brachiata</i> , <i>Anabasis salsa</i> , <i>Lepidium perfoliatum</i>) on flat depressions of takyr	1.7	3.3	3.0	2.3
13	Orach with single tamarisk (<i>Atriplex pratovii</i> , <i>Tamarix laxa</i>) on a slightly undulating primary marine plain	1.7	2.9	2.3	1.7
14	Rare aggregations of orach and sea blite (<i>Atriplex pratovii</i> , <i>Suaeda acuminata</i>) on a slightly undulating primary marine plain	< 1	< 1	< 1	< 1
Nitrebush, tamarisk shrub rangelands					
15	Nitrebush and tamarisk with psammophytic shrubs, haloxylon, annual saltworts (<i>Nitraria schoberi</i> , <i>Tamarix laxa</i> , <i>Astragalus brachypus</i> , <i>Haloxylon ammodendron</i> , <i>Salsola nitraria</i> , <i>Atriplex pratovii</i>) on a hummocky primary marine plain	1.8	4.6	3.8	2.3
16	Rare aggregations of tamarisk and annual saltworts (<i>Tamarix laxa</i> , <i>T. hispida</i> , <i>Atriplex pratovii</i> , <i>Suaeda acuminata</i>) on a slightly undulating primary marine plain	< 1	< 1	< 1	< 1

Discussion

Comparative analysis of the food ration of wild ungulates in the Barsa Kelmes Nature Reserve and other populations both in Kazakhstan and beyond its borders showed that the species composition of the reserve's forage plants is extensive, despite the limited size of the former island (186 sq. km) and the relatively low species composition of plants (264 species).

Of the total diversity, 105 species are food for wild ungulates (40%). Geographical distribution and species diversity determine food preferences. For saiga inhabiting Kazakhstan, 85 species of plants are forage, in the Barsa Kelmes – 35 species.

For Turkmen kulan, 109 species are fodder plants throughout its distribution (Solomatin, 1977). The studies in the Altyn Emel National Park (Shakula and Khabibrakhmanov, 2014) revealed an extensive list of edible species for kulan (110). It is worth noting that the kulan population was formed from 20 heads removed from the Barsa Kelmes at the end of the 80s last century. Forage ration of the Barsa Kelmes kulan includes 71 species.

According to literary sources, the gazelle in Kazakhstan eats about 70 species of plants (Sludskiy, 1977), in Xinjiang – 47 species (Xu et al., 2012b), detailed studies of Zhevnerov (1984) in the Barsa Kelmes revealed 78 species.

The forage ration in different habitats of wild ungulates may differ. But similarities can be seen in seasonal preferences. In spring, ungulates prefer young shoots of cereals,

ephemerals, sedges. In summer, annual and perennial saltworts appear in the diet, such as *Atriplex tatarica*, *Ceratocarpus arenarius*, *Bassia prostrata*. In autumn, the share of juicy saltworts and sagebrush species increases. In winter, the forage ration consists of annual shoots of haloxylon, shrubs, and dwarf semi-shrubs.

For the wild ungulates of the Barsa Kelmes, it is worth noting that in winter they can feed on the shoots of *Halocnemum strobilaceum*; saiga and gazelle – of ephedra. The berries of ephedra and nitrebush are eaten by gazelles in summer. *Krascheninnikovia ceratoides* is eaten by gazelles in the Barsa Kelmes and in Xinjiang. Kulans of the Barsa Kelmes usually do not eat tamarsk, but in Altyn Emel National Park they feed young twigs. Young shoots of feather grass willingly eat all reserve ungulates in spring, but do not use them in other seasons. We can compare with populations of kulan and gazelle in Xinjiang, where they eat *Stipa caucasica* in spring and summer, and gazelles – throughout the year. Saigas of the northwestern Caspian region use feather grass to a minimum in their forage diet.

The rangeland productivity in the Barsa Kelmes cluster area in 2019 turned out higher compared to the retrospective data of the last century. This is due to a long absence of grazing.

According to the data of the 70s and 80s, the productivity of *Anabasis salsa* communities at the early summer on the island varied from 2.7 to 12.6 c/ha, and in 2019 this indicator increased to 14.5-21.8 c/ha. Also, in 2019 a high yield of the *Artemisia terrae-albae* community was noted – 17.8-23.0 c/ha, and in retrospective data it was 7.8-14.3 c/ha.

Figure 12 shows comparative data on the yield of *Artemisia terrae-albae* and *Anabasis salsa* communities at ecological sites in the early summer season.

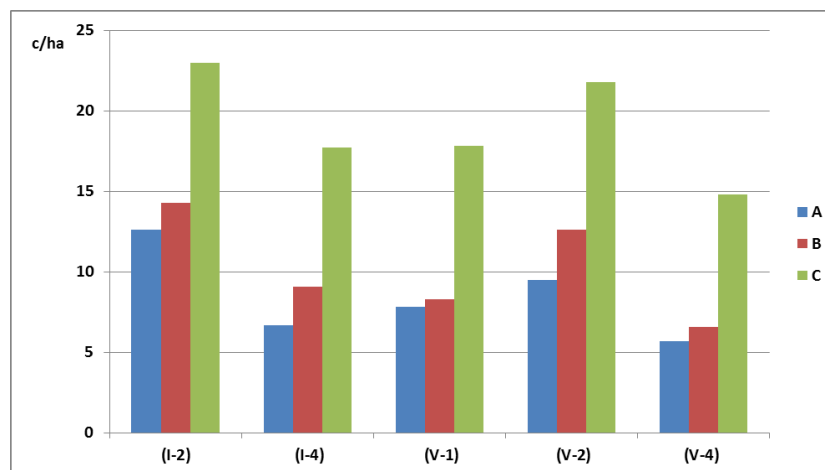


Figure 12. Comparative characteristics of the aboveground phytomass productivity of zonal communities in the Barsa Kelmes cluster area (early summer season): A – average yield (1976-1979), B – maximum yield (1976-1979), C – yield in 2019; communities: (I-2) *Artemisia terrae-albae*; (I-4) *Anabasis salsa*; (V-1) *Artemisia terrae-albae*; (V-2) *Anabasis salsa*; (V-4) *Artemisia terrae-albae – Stipa lessingiana – Agropyron desertorum*

Phytomass in *Artemisia terrae-albae* communities increased by 38-55% compared to retrospective data, which correlates with the earlier conclusions about an increase in yield by 1.3-2 times in the absence of grazing. In *Anabasis salsa* communities, the yield

increased by 42-49% compared to the maximum indicators for this season in the 70s. The previously put forward assumption about the decrease of phytomass in *Anabasis salsa* communities in the absence of grazing does not coincide with the indicators obtained in 2019. Most likely this is due to the very long (20 years) period of the rangeland rest.

In 2019, the productivity of haloxyton in *Haloxylon ammodendron* - *Calligonum aphyllum* - *Ephedra distachya* with *Tamarix laxa* com. on the sands in the early summer season was 15.7 c/ha. Indicators of accumulation of haloxyton phytomass in different communities of the sandy desert in the 70s varied from 1.0 to 5.4 c/ha in the same season, the long-time average productivity of haloxyton in early summer over 10 years (70-80s) was 4.7 c/ha (from 0.8 to 7.8 c/ha). The lack of grazing has led to the fact that the sands of the old Aral marine terrace are 90-100% overgrown with desert moss (*Tortula desertorum* Broth.), which usually prevent the regrowth of haloxyton. However, this did not prevent an increase in the productivity of phytomass and it is associated with an increase in the average size of model bushes. On the other hand, *Haloxylon ammodendron* is developing new sandy areas of the dry seabed, where its yield is still low – 2.8 c/ha.

The newly developed rangeland map clearly shows the distribution of rangeland types and their seasonal productivity. The map is an important tool for understanding the scale and structure of rangeland vegetation, predicting habitats for wild ungulates, and modeling the succession status of vegetation under climate change in conditions of zonal ecosystems and the dry seabed. The map also provides data to estimate the extent of carbon sequestration. At last, it provides important information for understanding the available forage resources for wild ungulates, which is the basis for wildlife and rangeland management in particular.

Conclusions

Research has been carried out that summed up the study of the forage resources of wild ungulates in the Barsa Kelmes Nature Reserve. They were carried out 20 years after the ungulates left the island after its association with the mainland. Over a long period of rest, the rangelands have fully recovered and increased their productivity.

On the basis of previous studies, the species composition of the forage ration of wild animals of the Barsa Kelmes Nature Reserve was determined. The general list of plants consists of 105 species, which belong to 26 families and 70 genera. Among them 35 species are eaten by saigas, 78 by gazelles, 71 by kulans. 26 species are eaten by all wild ungulates of the reserve (saiga, gazelle, kulan), i.e. 25% of forage plants. In terms of consumption in the first place are the Poaceae species, in the second – species of the Amaranthaceae (Chenopodiaceae) family, in the third place in the saiga and gazelle forage ration – Asteraceae, and in the kulan ration – Brassicaceae; Fabaceae and Polygonaceae are in fourth and fifth places.

Seasonal feed preferences of wild ungulates generally coincide throughout the habitat. In spring they eat ephemerals, especially cereals, green shoots of feather grass and sedges. In summer *Krascheninnikovia ceratoides* and fruits of *Nitraria schoberi* and *Ephedra distachya* appear in the diet. In autumn saltworts and sagebrush are most often eaten, in winter – annual shoots of *Haloxylon* spp., perennial saltworts and sagebrush.

A comparative analysis of rangelands productivity in recent times and researches in the 70-80s last century showed increasing phytomass in 2019 by more than 2 times. This is due to the lack of grazing on rangelands. On the dry seafloor *Haloxylon*

ammodendron forms a phytomass of 2.8 c/ha, *Nitraria schoberi* – 3.7, *Kalidium foliatum* – 4.3, *Atraphaxis spinosa* – 3.0, *Ephedra distachya* – 0.6 c/ha.

Ground and remote sensing data were used to assess the seasonal yield of rangelands.

A rangeland map of the Barsa Kelmes cluster area has been compiled in a medium scale basing at the interpretation of satellite imagery, field data, and retrospective research. The legend to the map contains 16 mapped units (rangeland types) for which the total yield was calculated for year seasons.

Our research has shown changes in the productivity of rangelands as a result of a long absence of grazing in a specially protected area. Rangeland resources have increased. Ecosystems develop under the influence of natural factors, which must consist of all ecosystem components, including ungulates. An experiment was inadvertently set up, where the ecosystem has no influence of large herbivores on rangelands. Future actions should be aimed at restoring water sources for the balanced functioning of the reserve's ecosystems.

On the other hand, estimating grazing capacity is necessary for successful pasture management in order to balance stocking rates of grazing animals with the ability of the rangeland to provide forage on a sustainable basis. Grazing capacity is a function of the kind and amount of vegetation produced on the rangeland, topographic characteristics of the landscape, and availability of water resources (Smith et al., 2012). Determination of grazing capacity is therefore a complex process that needs to explicitly consider all these components. Estimating grazing capacity will be the future task connected with availability of water resources.

Acknowledgements. This study was funded by the Michael Succow Foundation (Greifswald, Germany) through Association of Biodiversity Conservation of Kazakhstan and International Fund for saving the Aral Sea in the Republic of Kazakhstan.

Conflict of interests. The authors declare no conflict of interests.

REFERENCES

- [1] Abaturov, B. D., Larionov, K. O., Kolesnikov, M. P., Nikonova, O. A. (2005): Condition and supply of saigas (*Saiga tatarica*) with food on pastures with different types of vegetation. – Zoological Journal 84(3): 377-390.
- [2] Abaturov, B. D., Dzhapova, R. R. (2015a): Forage availability to saigas (*Saiga tatarica*) and their state on steppe pastures with a different ratio of graminoid plants and forbs. – Biology Bulletin 42: 163-170. <https://doi.org/10.1134/S1062359015020028>.
- [3] Abaturov, B. D., Dzhapova, R. R. (2015b): State and food sufficiency of saiga (*Saiga tatarica*) in steppe rangelands with different correlation of grasses and forbs. – News of Russian Academy of Sciences, Biology series 2: 207-214. DOI: 10.7868/S0002332915020022.
- [4] Adolf, T. A. (1954): Some data on saiga biology in the Astrakhan steppes. Scientific notes of the Moscow City Pedagogical Institute named after V. P. Potemkin. – Zoology 28(2): 247-256.
- [5] Bakanach, E. I., Podolskiy, L. I., Terekhov, V. I. (eds.) (1978): Map of Forage Lands of Kazakhstan. Scale 1:1 500 000. – Complex Department of “Kazgiprozem”, Alma-Ata.
- [6] Bekenov, A. B., Grachev, J. A., Milner-Gulland, E. J. (1998): The ecology and management of the Saiga antelope in Kazakhstan. – Mammal Review 28: 1-52.
- [7] Berlyant, A. M. (1997): Geoinformational Mapping. – Moscow State University, Moscow.

- [8] Brown, D. (1954): *Methods of Surveying and Measuring Vegetation Hardcover*. – Commonwealth Bureau of Pastures and Field Crops Bulletin, Hurley, Berks.
- [9] Bykov, B. A. (1957): *Geobotany*. – Nauka, Alma-Ata.
- [10] Bykov, B. A. (1978): *Geobotany*. – Nauka, Alma-Ata.
- [11] Chase, M. W., Christenhusz, M. J. M., Fay, M. F., Byng, J. W., Judd, W. S., Soltis, D. E., Mabberley, D. J., Sennikov, A. N., Soltis, P. S., Stevens, P. F. (2016): An update of the Angiosperm Phylogeny Group classification for the orders and families of flowering plants: APG IV. – *Botanical Journal of the Linnean Society* 181(1): 1-20. <https://doi.org/10.1111/boj.12385>.
- [12] Chu, H.-J., Jiang Zh., Lan, W.-X., Wang Ch., Tao, Y.-Sh., Jiang, F. (2008): Dietary overlap among kulan *Equus hemionus*, goitered gazelle *Gazella subgutturosa* and livestock. – *Acta Zoologica Sinica* 54(6): 941-954.
- [13] Demchenko, L. A. (1950): Vegetation of Barsa-Kelmes Island as forage reserve for ungulate animals. – *Proceedings of Nature reserve Barsa-Kelmes* 1: 6-37.
- [14] Dieterich, T., Sarsenova, B. (2012): Examination of the forage basis of saiga in the Ural population on the background of the mass death in May 2010 and 2011 in the Ural population. – In: *Materials of the II International Scientific Conference “Biological Diversity of Asian Steppes.”* Kostanay, Kazakhstan.
- [15] Dimeyeva, L. A. (1990): Productivity and Chemistry. – In: Kurochkina, L. Y., Shabanova, L. V. (eds.) *Complex Characteristics of Pastures in the Desert Zone of Kazakhstan*. Nauka. Alma-Ata.
- [16] Dimeyeva, L. A. (1994): Dynamics of productivity of phytocoenoses of the dry seabed of the Aral Sea. – *News of National Academy of Sciences Republic of Kazakhstan, Biology Series* 5: 17-24.
- [17] Dimeyeva, L. A. (2020): Vegetation map of Kyzylorda region. Scale 1: 1 500 000. – Web Atlas of Kyzylorda region. <http://isca.kz/ru/analytics-ru/3122> (accessed 25.04.2022).
- [18] Dimeyeva, L. A., Alimbetova, Z. Z. (2007): Analysis of flora of nature reserve “Barsa Kelmes”. – *Proceedings of Nature reserve Barsa Kelmes* 2: 11-34.
- [19] Dimeyeva, L. A., Ogar, N. P., Alimbetova, Z. Z., Breckle, S-W. (2012): Nature Conservation in the Aral Sea Region: Barsa-Kelmes as an Example. – In: Breckle, S-W., Wucherer, W., Dimeyeva, L. A., Ogar, N. P. (eds.) *Aralkum - a Man-Made Desert: The Desiccated Floor of the Aral Sea (Central Asia)*. Springer, Heidelberg. https://doi.org/10.1007/978-3-642-21117-1_14.
- [20] Eliseev, D. O. (2007): Modern state of vertebrates' fauna in Barsakelmes island and their dynamics during last 50 years. – In: *Proceedings of Nature Reserve Barsa Kelmes* 2: 107-128.
- [21] Erokhina, O. G. (2016): Soils. – In: *Atlas of Functional Zoning of the Aral District of Kyzylorda Region*. – UNDP Kazakhstan, Astana.
- [22] Fadeev, V. A., Sludsky, A. A. (1982): *Saigak in Kazakhstan*. – Nauka, Alma-Ata.
- [23] *Flora of Kazakhstan (1956-1966)*: 1-9. – Nauka, Alma-Ata.
- [24] Galieva, L. A. (1980): Dynamics of the productivity of the aboveground phytomass of the *Anabasis salsa-Artemisia terrae-albae* complex. – MS Thesis, Herzen State Pedagogical Institute, Leningrad, Russia.
- [25] Gao, B. (1995): Normalized difference water index for remote sensing of vegetation liquid water from space. In: – *Proceedings of SPIE* 2480: 225-236. <https://doi.org/10.1117/12.210877>.
- [26] Grachev, I. A., Bekenov, A. B. (1993): The present state of Saiga populations in Kazakhstan. – *Zoological research in Kazakhstan* 2: 165-189.
- [27] Hilbig, W. (1990): *Pflanzengesellschaften der Mongolei*. – In: Schuh, J., Schubert, R., Batsuur, D., Stubbe, M., Hilbig, W., Dorn, M., Dawaa, N., Schamsran, Z. (eds.) *Erforschung Biologischer Ressourcen der Mongolischen Volksrepublik* 8: 5-146. Martin-Luther-Universität, Halle-Wittenberg.

- [28] Illustrated Guide for Identification of the Plants of Kazakhstan (1969-1972): 1-2. – Nauka, Alma-Ata.
- [29] IUCN SSC Antelope Specialist Group (2017): *Gazella subgutturosa*. – The IUCN Red List of Threatened Species 2017: e.T8976A50187422. <https://dx.doi.org/10.2305/IUCN.UK.2017-2.RLTS.T8976A50187422.en> (accessed 19 March 2021).
- [30] IUCN SSC Antelope Specialist Group. (2018): *Saiga tatarica*. – The IUCN Red List of Threatened Species 2018: e.T19832A50194357. <https://dx.doi.org/10.2305/IUCN.UK.2018-2.RLTS.T19832A50194357.en> (accessed 19 March 2021).
- [31] Kaczensky, P., Doldin, R., Enke, D., Linnell, J. D. C., Lukanovsky, O., Salemgareyev, A. R., Sidorova, T. V., Sklyarenko, S., Kisebaev, T., Walzer, C., Ward, S., Zuther, S. (2017): Feasibility study for kulan (*Equus hemionus kulan*) reintroduction into the central steppe of Kazakhstan. – NINA Report 1366.
- [32] Kaczensky, P., Lkhagvasuren, B., Pereladova, O., Hemami, M., Bouskila, A. (2020): *Equus hemionus* (amended version of 2015 assessment). – The IUCN Red List of Threatened Species 2020: e.T7951A166520460. <https://dx.doi.org/10.2305/IUCN.UK.2020-1.RLTS.T7951A166520460.en> (accessed 19 March 2021).
- [33] Kaczensky, P., Salemgareyev, A., Linnell, J. D. C., Zuther, S., Walzer, Ch., Huber, N., Petit, Th. (2021): Post-release Movement Behaviour and Survival of Kulan Reintroduced to the Steppes and Deserts of Central Kazakhstan – *Frontiers in Conservation Science* 2: Article 703358. <https://doi.org/10.3389/fcsc.2021.703358>.
- [34] Kukhtenko, M. Y. (1989): Dynamics of the productivity of aboveground phytomass in plant communities of the coastal sands of Barsa-Kelmes Island. – MS Thesis, Herzen State Pedagogical Institute, Leningrad.
- [35] Kurochkina, L. Y., Osmanova, L. T., Karibaeva, K. N. (1986): Forage Plants of Deserts of Kazakhstan. – Kainar, Alma-Ata.
- [36] Kuznetsov, L. A. (1979): Physico-Geographical Outline of Barsakelmes Island. – In: Kuznetsov, L. A. (ed.) *Stationary Studies of Ecosystems in the Northern Aral Sea Region*. Publishing House of Leningrad State Pedagogical Institute Named After A.I. Herzen, Leningrad.
- [37] Kuznetsov, L. A. (2007): Once again about the zonal vegetation of Barsa Kelmes. – *Proceedings of Barsa Kelmes Nature Reserve* 2: 35-44.
- [38] Kuznetsov, L. A., Burambaev, K. (1976): Observations of the Seasonal Development of Desert Vegetation in the Barsa-Kelmes Island. – In: *Systematics, Ecology and Anatomy of Plants in the Asian Part of the USSR*. Publishing House of Leningrad State Pedagogical Institute Named After A.I. Herzen, Leningrad.
- [39] Larionov, K. O. (2008): Nutrition and availability of *Saiga tatarica* forage, depending on the characteristics of vegetation in rangelands. – PhD Thesis, Severtsov Institute of Ecology and Evolution of RAS, Moscow.
- [40] Lebed, L. V. (1989): Recommendations for the Organization and Conduct of Aerial Photometric Surveys of Agricultural Lands in Kazakhstan. – Kazgidromet, Alma-Ata.
- [41] Lebedeva, L. S. (1959): *Saiga* feeding on the right bank of the Volga River. – *Bulletin of Moscow Society of Naturalists, Biology Series* 64(5): 27-35.
- [42] Lebedeva, L. S. (1960): Materials for the study of spring forages and pastures of saigas on the right bank of the Volga River. – *Zoological Journal* 39(9): 1438-1442.
- [43] Malakhov, D. V., Islamgulova, A. F. (2014): Parametric interpretation of pasture images: experience with low and medium resolution remote sensing data. – *Optics of the Atmosphere and Ocean* 27(7): 587-592.
- [44] Malakhov, D. V., Islamgulova, A. F. (2015): Calculation of seasonal forage reserves in the Altyn-Dala nature reserve based on Landsat satellite data. – In: *Materials of the VII International Symposium “Steppes of Northern Eurasia”*. Orenburg, Russia.

- [45] Minervin, V. N. (1955): Pasture and Watering Regime of Sheep in the Desert. – Publishing House of Turkmenistan, Ashgabat.
- [46] Nechaeva, N. T. (1957): Methodology of Accounting Feed Stock in Desert Rangelands. – Publishing House of Turkmenistan, Ashgabat.
- [47] Ospanov, B. S. (Ed) (1995): Instructions for Conducting Large-Scale (S 1: 1000 – 1: 100 000) Geobotanical Surveys of Natural Forage Lands of the Republic of Kazakhstan. – Research and Production Center of Land Resources and Land Management, Almaty.
- [48] Penuelas, J., Filella, I., Biel, C., Serrano, L., Save, R. (1993): The reflectance at the 950-970 nm region as an indicator of plant water status. – *International Journal of Remote Sensing* 14: 1887-1905.
- [49] Perchatkina, M. N. (1979): Productivity dynamics of sandy deserts in the North Aral Sea region. – MS Thesis, Herzen State Pedagogical Institute, Leningrad.
- [50] Rachkovskaya, E. I. (ed.) (1995): Vegetation Map of Kazakhstan and Middle Asia (Desert Zone). Scale 1:2 500 000. – Komarov Botanical Institute, Russian Academy of Sciences, Saint Petersburg.
- [51] Rachkovskaya, E. I., Egemberdieva, K. B. (2016): Vegetation. – In: Atlas of Functional Zoning of the Aral District of the Kyzylorda Region. UNDP Kazakhstan, Astana.
- [52] Rakov, N. V. (1956): Saiga antelope in Western Kazakhstan. – In: Proceedings of the Institute of Zoology of the Academy of Sciences of the Kazakh SSR 6: 28-60.
- [53] Ramensky, L. G., Tsatsenkin, I. A., Chizhikov, O. N., Antipin, N. A. (1956): Ecological Evaluation of Natural Grasslands on Vegetation Cover. – Publishing House of Agricultural Literature, Moscow.
- [54] Rashek, V. L. (1974): Winter in the Life of Saigas on Barsa-Kelmes Island. – In: Hunting-Commercial Animals. VINITI, Moscow.
- [55] Rashek, V. A. (1977): Seasonal eating habits of the kulans on the Barsa-Kelmes island. – Bulletin of the Moscow Society of Naturalists, Biology Series 82(2): 8-16.
- [56] Romanova, N. N., Kasatkina, N. S., Sharina, G. A., Kuznetsov, L. A. (1979): To the Characteristic of Artemisia Terrae-Albae - Anabasis Salsa Ecosystem Productivity. – In: Kuznetsov, L. A. (ed.) Stationary Studies of Ecosystems in the Northern Aral Sea Region. – Publishing House of Leningrad State Pedagogical Institute Named After A. I. Herzen, Leningrad.
- [57] Sapanov, M. K. (2017): The Influence of natural and climatic factors on the number of Saiga (*Saiga tatarica* Pall.) (Bovidae, Artiodactyla) between the Volga and Ural Rivers. – *Biology Bulletin* 44: 1302-1307. <https://doi.org/10.1134/S1062359017100132>.
- [58] Shakula, V. F., Khabibrakhmanov, R. M. (2014): To ecology of Turkmen Kulan in National Park "Altyn Emel". – In: Proceedings of Int. Science-Applied Conference "Conservation of biodiversity and perspectives of sustainable development of Aral region and Barsa-Kelmes Nature reserve." Aral, Kazakhstan.
- [59] Sludskiy, A. A. (1955): Saiga antelope in Kazakhstan. – Proceedings of Institute of Zoology of the Academy of Sciences of the Kazakh SSR 4: 18-56.
- [60] Sludskiy, A. A. (1977): Gazelle. – In: Hoofed Animals. Forest Industry, Moscow, pp. 28-61.
- [61] Sludskiy, A. A., Bekenov, A., Zhevnerov, V. V., Kapitonov, V. I., Fadeev, V. A., Fedosenko, A. K. (1983): Artiodactyla (Bovidae). – In: Gvozdev, E. V., Kapitonov, V. I. (eds.) Mammals of Kazakhstan 3(3). Nauka, Alma-Ata.
- [62] Smith, L., Ruyle, G., Dyess, J., Meyer, W., Barker, S., Williams, S. M., Maynard, J. L., Bell, D., Stewart, D. (2012): Guide to Rangeland Monitoring and Assessment: Basic Concepts for Collecting, Interpreting, and Use of Rangeland Data for Management Planning and Decisions. – Arizona Grazing Lands Conservation Association, Tucson.
- [63] Sochava, V. B. (1979): Vegetation Cover in Thematic Maps. Nauka, Novosibirsk.
- [64] Sokolov, V. E., Zhirnov, L. V. (eds.) (1998): Saiga: Filogeny, Taxonomy, Ecology, Protection and Utilization. – Russian Agricultural Academy, Moscow.
- [65] Solomatin, A. O. (1977): Kulan. Hoofed Animals. – Forest Industry, Moscow.

- [66] The World Flora Online. <http://www.worldfloraonline.org>. – Accessed 4 April 2022.
- [67] Tueller, P. T. (ed.) (1988): *Vegetation Science Applications for Rangeland Analysis and Management* 14. – Kluwer Academic Publishers, Dordrecht.
- [68] Vasenko, E. P. (1950): Ecology and distribution of saiga. – *Proceedings of Nature Reserve Barsa Kelmes* 1: 38-115.
- [69] Xu, W., Xia, C., Yang, W., Blank, D. A., Qiao, J., Liu, W. (2012a): Seasonal diet of Khulan (Equidae) in Northern Xinjiang, China. – *Italian Journal of Zoology* 79(1): 92-99. <https://doi.org/10.1080/11250003.2011.620635>.
- [70] Xu, W., Xia, C., Lin, J., Yang, W., Blank, D. A., Qiao, J., Liu, W. (2012b): Diet of *Gazella subgutturosa* (Güldenstaedt, 1780) and food overlap with domestic sheep in Xinjiang, China. – *Folia Zoologica* 61(1): 54-60. <https://doi.org/10.25225/fozo.v61.i1.a9.2012>.
- [71] Yilmaz, M. T., Hunt, E. R., Jackson, T. J. (2008): Remote sensing of vegetation water content from equivalent water thickness using satellite imagery. – *Remote Sensing of Environment* 112: 2514-2522.
- [72] Zhevnerov, V. V. (1984): Goitred gazelle of the Barsa-Kelmes Island. – Nauka, Almaty.
- [73] Zhylkaidarov, A. B. (2014): The population of gazelles in the Barsa Kelmes reserve. – In: *Proceedings of the International Scientific and Practical Conference “Biodiversity Conservation and Prospects for Sustainable Development of the Aral Sea Region and Barsa Kelmes Nature Reserve.”* Aral, Kazakhstan.

APPENDIX

Table A1. List of forage species of wild ungulates in the Barsa Kelmes cluster area

Families/species	Eaten species by ungulates		
	Saiga	Gazelle	Kulan
Amaranthaceae Juss.			
<i>Anabasis aphylla</i> L.	-	+	+
<i>A. salsa</i> (C. A. Mey.) Benth. ex Volkens (Ledeb.) Benth. ex Volkens	+	+	+
<i>Atriplex cana</i> C. A. Mey. Ledeb.	-	-	+
<i>A. ornata</i> Iljin	-	+	-
<i>A. sagittata</i> Borkh.	-	-	+
<i>A. tatarica</i> L.	+	+	+
<i>Bassia prostrata</i> (L.) Beck	+	+	+
<i>Ceratocarpus arenarius</i> L.	+	+	+
<i>Climacoptera aralensis</i> (Iljin) Botsch.	-	-	+
<i>C. brachiata</i> (Pall.) Botsch.	+	+	-
<i>C. crassa</i> (M. Bieb.) Botsch.	+	-	+
<i>Girgensohnia oppositiflora</i> (Pall.) Fenzl	-	+	+
<i>Halimocnemis karelinii</i> Moq.	-	-	+
<i>H. sclerosperma</i> (Pall.) C. A. Mey.	-	-	+
<i>Halocnemum strobilaceum</i> (Pall.) M. Bieb.	+	+	+
<i>Haloxylon ammodendron</i> (C.A. Mey.) Bunge ex Fenzl	+	+	+
<i>H. persicum</i> Bunge	+	+	+
<i>Krascheninnikovia ceratoides</i> (L.) Gueldenst.	-	+	-
<i>Salsola arbuscula</i> Pall.	-	+	-
<i>S. nitraria</i> Pall.	-	-	+
<i>S. orientalis</i> S. G. Gmel.	-	+	-
Apiaceae Lindl.			
<i>Ferula lehmannii</i> Boiss.	+	+	-
Asparagaceae Juss.			
<i>Asparagus breslerianus</i> Schult. & Schult. f.	-	+	-
<i>A. persicus</i> Baker			+
Asteraceae Giseke			
<i>Amberboa turanica</i> Iljin	-	-	+
<i>Artemisia arenaria</i> DC.	-	+	+
<i>A. pauciflora</i> Weber ex Stechm.	+	+	+
<i>A. quinqueloba</i> Trautv.	-	+	-
<i>A. terrae-albae</i> Krasch.	+	+	+
<i>A. tomentella</i> Trautv.	-	+	-
<i>Rhaponticum repens</i> (L.) Hidalgo (= <i>Acroptilon repens</i> (L.) DC.)	+	-	+
<i>Takhtajianantha pusilla</i> (Pall.) Nazarova	-	+	+
<i>Taraxacum bicorne</i> Dahlst.	+	+	+
<i>Tragopogon ruber</i> S. G. Gmel.	-	+	-
Boraginaceae Juss.			
<i>Asperugo procumbens</i> L.	-	-	+
Brassicaceae Burnett			
<i>Alyssum linifolium</i> Stephan ex Willd. (= <i>Meniocus linifolius</i> (Steph.) DC.)	-	+	+
<i>Chorispora tenella</i> (Pall.) DC.	-	+	+
<i>Descurainia sophia</i> (L.) Webb ex Prantl	-	+	+
<i>Euclidium syriacum</i> (L.) R. Br.	-	-	+
<i>Goldbachia laevigata</i> (M. Bieb.) DC.	-	-	+
<i>Lepidium appelianum</i> Al-Shehbaz	-	-	+
<i>L. perfoliatum</i> L.	-	+	+
<i>Leptaleum filifolium</i> (Willd.) DC.	-	-	+

<i>Litwinowia tenuissima</i> (Pall.) Woronow ex Pavl.	-	-	+
Capparaceae Juss.			
<i>Capparis spinosa</i> L.	+	+	-
Convolvulaceae Juss.			
<i>Convolvulus erinaceus</i> Ledeb.	-	-	+
Cyperaceae Juss.			
<i>Bolboschoenus maritimus</i> (L.) Palla	-	+	+
<i>Carex stenophylla</i> subsp. <i>stenophylloides</i> (V.I. Krecz.) T.V. Egorova (= <i>C. dimorphothecca</i> Stshegl.)	-	+	-
<i>C. pachystylis</i> J. Gay	-	-	+
Ephedraceae Dumort.			
<i>Ephedra distachya</i> L.	+	+	-
<i>E. intermedia</i> Schrenk & C. A. Mey	-	+	-
<i>E. strobilacea</i> Bunge	-	+	-
Fabaceae Juss.			
<i>Alhagi pseudalhagi</i> (M. Bieb.) Desv. ex B. Keller & Shap.	+	+	+
<i>Astragalus ammodendron</i> Bunge	+	+	+
<i>A. brachypus</i> Schrenk	+	+	+
<i>A. lasiophyllus</i> Ledeb.	-	-	+
<i>Caragana grandiflora</i> (M. Bieb.) DC.	-	+	+
<i>Eremosparton aphyllum</i> (Pall.) Fisch. & C.A. Mey.	-	+	-
Frankeniaceae Desv.			
<i>Frankenia hirsuta</i> L.	+	+	+
<i>F. pulverulenta</i> L.			+
Geraniaceae Juss.			
<i>Geranium linearilobum</i> DC.	-	-	+
Juncaceae Juss.			
<i>Juncus jaxarticus</i> V.I. Krecz. & Gontsch.	+	-	+
Liliaceae Juss.			
<i>Gagea reticulata</i> (Pall.) Schult. & Schult. f.	+	+	-
<i>Tulipa biflora</i> Pall. (= <i>Tulipa buhseana</i> Boiss.)	-	+	+
Nitrariaceae Lindl.			
<i>Nitraria schoberi</i> L.	-	+	-
Orobanchaceae Vent.			
<i>Orobanche cernua</i> Loefl.	-	+	-
Plumbaginaceae Juss.			
<i>Limonium otolepis</i> (Schrenk) Kuntze	-	+	+
<i>L. suffruticosum</i> (L.) Kuntze	+	+	+
Poaceae Barnhart			
<i>Aeluropus littoralis</i> (Gouan) Parl.	+	+	+
<i>A. lagopoides</i> (L.) Thwaites (= <i>A. repens</i> (Desf.) Parl.)	+	-	+
<i>Agropyron desertorum</i> (Fisch. ex Link) Schult.	+	+	+
<i>A. fragile</i> (Roth) P. Candargy	+	+	+
<i>Bromus lanceolatus</i> Roth	-	+	-
<i>B. oxyodon</i> Schrenk	-	+	-
<i>B. tectorum</i> L.	+	+	+
<i>Calamagrostis epigejos</i> (L.) Roth	-	+	+
<i>Crypsis schoenoides</i> (L.) Lam.	-	+	+
<i>C. alopecuroides</i> (Piller & Mitterp.) Schrad.	-	-	+
<i>Eremopyrum orientale</i> (L.) Jaub. & Spach	+	+	+
<i>E. triticeum</i> (Gaertn.) Nevski	-	+	-
<i>Leymus racemosus</i> (Lam.) Tzvel.	-	+	+
<i>Phragmites australis</i> (Cav.) Trin. ex Steud.	-	+	+
<i>Poa bulbosa</i> L.	+	+	+
<i>Puccinellia gigantea</i> (Grossh.) Grossh.	-	+	-
<i>Secale sylvestre</i> Host	-	+	-

<i>Stipa arabica</i> Trin. & Rupr. (=S. <i>caspia</i> C. Koch)	+	+	+
<i>S. caucasica</i> Schmalh.	+	+	+
<i>S. lessingiana</i> Trin. & Rupr.	+	+	+
<i>Stipagrostis pennata</i> (Trin.) de Winter	-	+	+
<hr/>			
Polygonaceae Juss.			
<i>Atraphaxis spinosa</i> L.	+	+	+
<i>Calligonum acanthopterum</i> I.G. Borshch.	-	+	-
<i>C. aphyllum</i> (Pall.) Guerke	-	+	-
<i>C. platyacanthum</i> I.G. Borshch.	-	+	-
<i>Rheum tataricum</i> L.f.	+	+	+
<hr/>			
Ranunculaceae Juss.			
<i>Ceratocephala testiculata</i> (Grantz.) Besser	-	+	-
<i>Clematis orientalis</i> L.	-	+	-
<i>Thalictrum isopyroides</i> C. A. Mey.	-	-	+
<hr/>			
Rosaceae Juss.			
<i>Rosa persica</i> Michx. ex Juss. (=Hulthemia <i>persica</i> (Michx. ex Juss.) Bornm.)	-	+	+
<hr/>			
Rubiaceae Juss.			
<i>Galium aparine</i> L.	-	+	-
<hr/>			
Solanaceae Adans.			
<i>Lycium ruthenicum</i> Murr.	-	-	+
<hr/>			
Tamaricaceae Link			
<i>Tamarix elongata</i> Ledeb.	-	+	-
<i>T. hispida</i> Willd.	-	+	-
<i>T. laxa</i> Willd.	-	+	-
<i>T. ramosissima</i> Ledeb.	-	-	+
<hr/>			
Zosteraceae Dumort			
<i>Zostera noltii</i> Hornem.	-	+	-

HEAVY METAL CONTENT AND HEALTH RISK ASSESSMENT OF FISH IN 4 RESERVOIRS OF DALIAN

CHEN, B. J.^{1,2} – SUN, X.^{1,2} – WANG, H. J.^{1,2} – ZHANG, Z.^{1,2} – GU, Y. X.^{1,2} – LUO, J.^{1,2,3} –
WANG, W.^{1,2*}

¹Key Laboratory of applied biology and aquaculture of northern fishes in Liaoning Province,
Dalian 116023, China

²College of Fisheries and Life Sciences, Dalian Ocean University, Dalian 116023, China

³Dalian Sun Asia Tourism Holding Co. Ltd, Dalian 116023, China
(phone: +86-151-0407-4555)

*Corresponding author
e-mail: wangwei@dlou.edu.cn; phone: +86-134-7840-8956

(Received 15th Oct 2021; accepted 23rd Dec 2021)

Abstract. Reservoir is an important water source for residents, and heavy metal pollution as a common pollution factor has also attracted much attention. In the three seasons of spring (March), summer (August), and autumn (October) in 2018, 2019 and 2020, the fish resources in 4 reservoirs (Zhuanjiaolou Reservoir, Yingnahe Reservoir, Zhuweizi Reservoir, and Songshu Reservoir) were investigated, the species composition, distribution characteristics and growth of the catch were analyzed, and the inductively coupled plasma mass spectrometry (ICP-MS) was used to determine the heavy metals (Cr, Cd, Pb, Hg, As) content. The results of the study showed that a total of 758 fishes were collected, belonging to 4 orders, 16 families and 24 genera. The fish importance index (IRI) analysis results showed that the main dominant species in Zhuanjiaolou Reservoir are *Carassius auratus*, *Cyprinus carpio*, *Zacco platypus*, *Rhodeinae*, *Pelteobagrus fulvidraco*. The main dominant species in Yingnahe Reservoir are *Cyprinus carpio*, *Carassius auratus*, *Pelteobagrus fulvidraco*, *Silurus asotus*, *Hemiculter leucisculus*, *Opsariichthys bidens*, *Rhodeinae*, *Culter alburnus* and *Acheilognathus macropus*. The main dominant species in Zhuweizi Reservoir are *Cyprinus carpio*, *Carassius auratus*, *Rhodeinae*, *Zacco platypus*, *Hemiculter leucisculus*, *Acheilognathus macropus* and *Opsariichthys bidens*. The main dominant species of Songshu Reservoir are *Hypophthalmichthys molitrix*, *Opsariichthys bidens*, *Pelteobagrus fulvidraco*, *Acheilognathus macropus*, *Culter alburnus* and *Carassius auratus*. The tissues of various dominant fish species have been contaminated by heavy metals. The pollution value of As in Zhuweizi Reservoir is the highest (1.836 mg/kg), but it does not exceed the standard value. The comprehensive pollution indexes of the 4 reservoirs were 1.266, 1.712, 1.536, 1.003 and 1.976, respectively. The exposure risk assessment results showed that *Pelteobagrus fulvidraco* had the highest Cr exposure coefficient, and other species were of lower risks.

Keywords: Dalian, reservoir, fish, heavy metals, health risk assessment

Introduction

Reservoir is an important water source for residents, and the artificial adjustment upon it makes it significantly different from natural water bodies in terms of hydraulic retention time and pollutant dilution and diffusion capacity. Heavy metal pollutants will be deposited in large quantities in the reservoir area as the water flow slows down, posing a threat to the safety of aquatic ecosystems. Fish as higher consumers in the reservoir ecosystem, has a close interaction relationship with the environment (Kominkova et al., 2007; Lü et al., 2011; Chang et al., 2021). After the water body is seriously polluted by heavy metals, the accumulation and enrichment of heavy metals exceeds the fish's bearing capacity, thus bringing toxic hazards (Yu et al., 2013) to it reproducing (Wang et

al., 2019), development (Shi et al., 2019), growth (Da Silva Cardoso et al., 2021) and physiological function (Niu et al., 2015), etc.

The rapid development of China's social economy has accelerated the progress of industrialization and urbanization. The discharge of pollutants accumulates every day, leading to a large amount of heavy metals in surface water bodies, such as reservoirs and rivers. The environmental problem of heavy metal pollution is becoming more and more serious (Xiao et al., 2019). With the improvement of living standards, people have higher requirements for food safety. However, when the living environment such as water bodies and bottom mud are polluted by heavy metals, fish exposed to the environment will accumulate heavy metals through feeding or breathing during the growth process, and those heavy metals cannot be discharged (Yao et al., 2014). When human consume contaminated fish, the heavy metals in it accumulate and are enriched in human body, causing corresponding damage to health (Ma et al., 2018), forming chronic poisoning (Monroy et al., 2014; Chen et al., 2019; Zeng et al., 2021), and it is not easy to be excreted (Lu et al., 1995; Tu et al., 2017).

Once heavy metals enter the human body through human breathing, daily diet and direct contact, the normal functions of the body will be greatly damaged. The heavy metals in the liver cannot be excreted from the body, and they are easily retained in the brain, kidneys and other organs. When their content exceeds the standard, they can easily cause gene mutations, endanger cell inheritance, and even lead to teratogenesis and cancer (Jian et al., 2015). With the development of urbanization and the extremely rapid improvement of living standards, water has been polluted by the increased human activities of mining, smelting, processing, etc. As the result, heavy metals such as Pb, Hg, and Cd enter the environment, causing serious pollution. And once that happens, they stay and further cause harm. For example, heavy metals can be concentrated in algae and bottom sludge even if there was little of them in discharged wastewater. Fish and other lives absorb and condense them in the food chain, which leads to risks (Ma al., 2014).

Chu et al. (2021) took *Carassius auratus* and *Pseudorasbora parva* as the research objects, which are common *Carassius auratus* in two lakes of Dajiu Lake, Shennongjia, Hubei Province. The contents of 7 heavy metals, Cu, Cd, Cr, Pb, As and Hg, were detected and analyzed. The results showed that the content of Zn, Cd, Cr, and Hg in the muscle of *Pseudorasbora parva* was significantly higher than that in the muscle of *Carassius auratus*. Liu et al. (2018) analyzed and concluded that the average content of heavy metals in the fish from Songhua River ranks as: Zn>Pb>Cr>Cu>Cd; Cd and Cr are enriched in carnivorous fish, and Pb pollution is the most serious; (Li et al., 2019) found that the Cd and Cr content of most fish samples in the collected areas exceeded the standard, and the heavy metal pollution of fish collected in some locations has caused a great health risk to human, thus it was recommended to reduce the consumption of fish from those areas; Lin et al. (2018) found through experimental testing that muscle tissue is the least affected part of a fish, and the safe concentration of fish contaminated by heavy metals for Cu, Zn, Cd and Cr are 0.009 mg/kg, 0.59 mg/kg, 24.41 mg/kg and 2.23 mg/kg, respectively. Zhang et al. (2017) discovered the phenomenon that heavy metals reach the fish body through the gills, the digestive tract, and the absorption through the body surface. In water bodies, heavy metal becomes harmful to fish once a certain amount is reached, and it also has an impact on fish respiration. Wu et al. (1999) conducted a difference test on *Branchiostoma* with different doses of heavy metals and found that low concentrations of heavy metals can accelerate the growth of *Branchiostoma*, while death will occur when the concentration is higher than a certain level.

Alidadi et al. (2019) collected 140 water samples from the treated drinking water in Masad City, Iran, and conducted chemical analysis and tests on them with three methods including hazard quotient (HQ), hazard index (HI) and carcinogenic risk (Cr). The results showed that the value of heavy metals is below the safety level for adults, but for children, HI is relatively high, which may cause cancer through ingestion and skin routes. Okogwu et al. (2019) conducted heavy metal pollution investigation and risk exposure assessment on four important fishes and water bodies in Nigeria's trans-river ecosystem, and found that the heavy metal content in the water exceeded the allowable limit. Except Pb, the values of the other four heavy metals (Fe, Mn, Hg, Cr) were all lower than the allowable intake value. Although the risk factor is lower than 1, the total risk factor and carcinogenic risk of all fishes were higher than acceptable, which should be paid more attention to. Kaus et al. (2017) investigated the exposure of fish to heavy metals in the Hara River Basin in Mongolia. Ever since the beginning, gold mining in the Hara River Basin of Mongolia has been identified as the main cause of heavy metal pollution, where heavy metal pollutants such as Cr, Zn, As, Cd, Hg, Cu, Ni and Pb are found with enrichment potential. The results showed that the amount of As and Hg in the tributaries exceeded the national allowable limits for drinking water. The heavy metals Cr, As, Hg, and Pb were of high content in the muscles of fishes collected in the middle and lower reaches, while Zn was high in that of fishes from upstream tributaries. The accumulation of Cr, Cu, Hg and Pb will increase with the higher level in food chain. Among the heavy metals, the enrichment of Hg poses the greatest threat to human health. In the study, 10.7% of fish samples exceeded the internationally recommended Hg level for consumption, which may cause chronic heavy metal poisoning.

The health risk assessment was carried out by detecting the heavy metal content of fish in 4 reservoirs of Dalian. At the same time, the composition of the catch was investigated. So far, there has not been a comprehensive and systematic survey of fish resources in the 4 reservoirs. This study plays an important role in the protection of ecological environment and the effective preservation of fish resources. It provides scientific basis to better help the residents of Dalian to understand the pollution of heavy metals in the reservoir water.

Materials and Methods

Overview of the research locations

The 4 reservoirs in Dalian (Zhuanjiaolou Reservoir, Zhuweizi Reservoir, Yingnahe Reservoir and Songshu Reservoir) are rich in biological species, and fish resources there are particularly important. The following 23 locations (*Figure 1*) were chosen for fish sample collection in three seasons (spring in March, summer in August, autumn in October) between 2018-2020. See *Table 1* for latitude and longitude (*Table 1*).

The Yingnahe Reservoir is located on the main stream of the Yingna River, with a drainage area of 1004 km² and a total storage capacity of 287 million m³. It is a big Type II reservoir mainly for Dalian's urban water supply, and flood control, agricultural irrigation, and freshwater aquaculture on the side (Shan et al., 2014).

The Zhuanjiaolou Reservoir is located on the west tributary of the Huli River in Zhuanghe City, with a total storage capacity of 140 million m³. Its control basin covers an area of about 146 km² and integrates multiple functions such as irrigation, water supply, flood control, and fish farming (Zhao et al., 2009). The water area is about

15.48 km², which can provide daily water supply for several thousand hectares of paddy fields in four nearby towns.

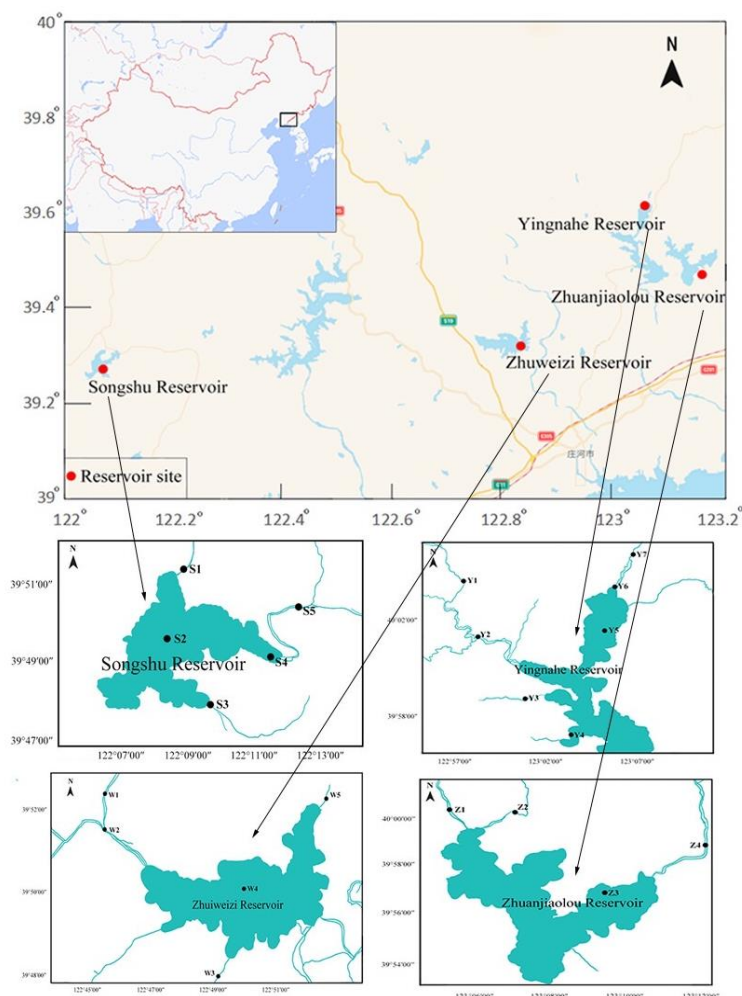


Figure 1. Distribution map of sampling points in the study area

Zhuweizi Reservoir is located on the west tributary of Taipingling Township, Zhuanghe City, with approximately 9,300 hectares of irrigated area and approximately 9,420 hectares of fish farming area. It is a large-scale reservoir that focuses on flood control and urban water supply (Liu et al., 2017), and takes into account the comprehensive utilization of irrigation, fish farming, and power generation. It is the only reservoir that's both the water source for the Zhuanghe Power Plant in Zhuanghe City and also a backup water source for Dalian City (Yang et al., 2018).

The Songshu Reservoir is located in the Fuzhou River Basin in Songshu Town, Wafangdian City. It is a big type II reservoir that's response of flood control, irrigation, and urban water supply, as well as fish farming and power generation. The water area is about 302.4 km², the total storage capacity is about 186 million m³, the irrigation area is about 1.08 million hectares, and fish farming area is about 460 hectares. There are many ports in the reservoir area, and the flow is long and narrow, winding 5 km from east to west (Lin et al., 2018).

Table 1. The sampling stations and coordinates four reservoirs in Dalian area

Sampling sites	Latitude (N)	Longitude (E)
Z1	40°0'1.2"	123°6'54.7"
Z2	40°0'7.9"	123°7'55.2"
Z3	39°56'19.9"	123°8'54.7"
Z4	39°58'50.6"	123°12'2.18"
Y1	40°2'20.9"	122°57'4.9"
Y2	40°0'28.9"	122°55'2.6"
Y3	39°58'48.6"	123°1'54.9"
Y4	39°57'14.2"	123°3'23.3"
Y5	40°0'52.9"	123°4'0.9"
Y6	40°3'2.9"	123°4'56.6"
Y7	40°4'36.4"	123°5'38.6"
W1	39°52'58.0"	122°45'33.8"
W2	39°52'43.4"	122°45'7.7"
W3	39°49'21.8"	122°49'31.2"
W4	39°50'47.9"	122°50'50.4"
W5	39°52'0.00"	122°52'9.9"
S1	39°50'47.4"	122°8'28.5"
S2	39°49'24.3"	122°7'47.2"
S3	39°48'1.5"	122°9'25.6"
S4	39°49'33.9"	122°10'16.8"
S5	39°50'29.7"	122°12'48.9"

Sampling and examination

Inductively coupled plasma mass spectrometry (ICP-MS) was used to determine the heavy metal content in the dominant fish species. After the heavy metals were digested, a 0.45 µm filter membrane was used. In order to eliminate the influence of sampling, transportation and other reasons on the water samples, quality control such as blanks, transportation blanks and parallel double sample collection were set up during the collection process. When the number of quality control was less than one, at least one quality control sample was set up to perform high-quality control on the collection, transportation and other processing steps. "National Food Safety Standard Determination of Total Arsenic and Inorganic Arsenic in Foods" (GB5009.11-2014), "National Food Safety Standard Determination of Total Mercury and Organic Mercury in Foods" (GB5009.17-2014), etc. were referred to.

The method of sampling fish in the reservoir was through net catching. In the tributary of the reservoir, the electrofishing method was used, which takes electric current as a tool to catch fish. By using a DC power supply and a wire, a strong electric field is formed around the electrode to coronate fishes in flowing water, which are then collected by a net. In local reservoirs, local fishermen or reservoir staff helped to obtain fish samples. It was done by a double-strap 32-tube ultrasonic electrofishing gear in water less than 1.5 m. The unit output is 16.7 ms, and 12.5% of the working area produces a voltage of 220-380V (depending on the water Conductivity). One person controlled the electric fishing device, while the other used an insulated net to catch fish from five points that evenly distributed about 100 m from the sampling point, covering habitats of different

features, such as strong current, little current, various sediments, and rich with aquatic plants. The sampling time of each sampling point is about 30 minutes. In water deeper than 1.5 m, a net was used for fishing, which is about 200 m long with a diameter of 1.5-3 cm. The sampling time was 30 minutes (Liu et al., 2018), and all collected samples were checked regarding amount, weight, ovulation, abnormalities (deformities, lesions, tumors, fin tail erosion, etc.). Fish specimens were decided according to "Liaoning Zoology" (Liaoning Zoology, 1985) and "Chinese Economic Fishes" (Yang et al., 1963) etc., and all the fishes collected in the watershed with a body length greater than 20 mm were classified to the level of species (or subspecies).

Data analysis

The relative importance index (IRI) was used in the analysis of the dominance of the reservoir catch, expression (Chen et al., 2012) is as below:

$$IRI = (W + N) \times F \quad (\text{Eq.1})$$

where W represents the ratio of the weight of a certain species to the total weight, N represents the ratio of the number of a certain species to the total number, and F represents the frequency of occurrence of a certain species.

The basis for the division of dominance is: rare species $IRI < 1$; general species $1 \leq IRI < 10$; common species: $10 \leq IRI < 100$; main species $100 \leq IRI < 1000$; dominant species: $IRI \geq 1000$.

The comprehensive pollution index method (Liu et al., 2017) can show the pollution degree of heavy metals in a certain fish in an all-round way. The calculation formula is as follows:

$$P_{comp} = \sqrt{(p_{2imax}^2 + p_{2iavg}^2) / 2} \quad (\text{Eq.2})$$

where P_{imax} represents the maximum value of the single-factor pollution index of all heavy metals in the same fish, and P_{iavg} represents the average value of the single-factor pollution index of heavy metals in the same fish. $P_{comp} > 1.0$ is regarded as light pollution, $P_{comp} < 1.0$ is regarded as no pollution.

The target hazard quotient method (Zhang et al., 2018; Wang et al., 2019; Xue et al., 2020) is a pollutant evaluation method proposed by the US Environmental Protection Agency USEPA. It is extremely suitable for evaluating the health risks of food that people can come into contact with in daily life. The formula is as follows:

$$THQ = C \times E_F \times E_D \times E_{IR} / R_{FD} \times T_A \times W_{AB} \times 10^{-3} \quad (\text{Eq.3})$$

where C is the concentration of heavy metals in fish (mg/g), E_F is the exposure frequency (365 day/year), E_D is the exposure duration (year), E_{IR} is the intake reference of fish (g/day), R_{FD} is the reference amount of heavy metals (mg/(kg·d)), T_A is the average time of non-carcinogenic exposure (d), and W_{AB} is the average weight of an adult (kg). Among them, E_F is 365, E_D is 30, E_{IR} is 55, R_{FD} is the reference amount of heavy metals (mg/(kg·d)); T_A is 10950, W_{AB} is 60 kg. When $THQ < 1$, there is no health risk to the exposed population; When $THQ > 1$, there is a health risk to the exposed population. The greater the value of THQ, the greater the health risk (Table 2).

Table 2. standard limit of heavy metals in fish

	Cr (mg/kg)	As (mg/kg)	Cd (mg/kg)	Pb (mg/kg)	Hg (mg/kg)
CHINA	2.00	0.10	0.10	0.50	1.00
CAC	-	-	0.05	0.30	0.50

Results

List and distribution of catches in 4 reservoirs

A total of 758 fishes were collected in this survey, belonging to 4 orders, 7 families, 23 genera and 25 species (Table 3). *Cypriniformes* are the most numerous, with 19 species, 18 genera and 2 families, accounting for 76% of the total species. *Salmoniformes* are the least, with 1 family, 1 genus and 1 species, accounting for 4% of the total number of species. Among them, plankton feeding fishes accounted for 28%; herbivorous fishes accounted for 4%; omnivorous fishes accounted for 48%; carnivorous fishes accounted for 20%. The nine species that are found in all four reservoirs are *Hypophthalmichthys molitrix*, *Aristichthys nobilis*, *Cyprinus carpio*, *Carassius auratus*, *Pseudorasbora parva*, *Barbatula barbatula nuda*, *Phoxinus lagowskii*, *Opsariichthys bidens*, *Acheilognathus maCropterus*.

Fish dominance

Through the analysis of the dominance of the catch (Table 4), we can conclude that in the Zhuanjiaolou Reservoir, the IRI values of 9 fish species (*Carassius auratus*, *Phoxinus lagowskii*, *Pseudobagrus fulvidraco*, *Hypophthalmichthys molitrix*, *Rhodeinae*, *Abbottina rivularis*, *Hypomesus*, *Zacco platypus*, *Pseudorasbora parva*) are 896.4, 91.9, 147.7, 782.5, 184.6, 59.1, 76.4, 492.4 and 56.1. Among them, *Carassius auratus*, *Pseudobagrus fulvidraco*, *Hypophthalmichthys molitrix*, *Rhodeinae*, *Zacco platypus* are the main species, and *Phoxinus lagomesus*, *Abbottina rivularis*, *Hypomesus* and *Pseudorasbora parva* are common species. There is no rare species or dominant species.

In the Yingnahe Reservoir, the IRI values of 10 fish species (*Silurus asotus*, *Hemiculter leucisculus*, *Carassius auratus*, *Pseudobagrus fulvidraco*, *Opsariichthys bidens*, *Cyprinus carpio*, *Rhodeinae*, *Pseudorasbora parva*, *Culter alburnns*, *Acheilognathus maCropterus*) are 130.7, 430, 787.6, 226, 330.2, 453, 161.2, 85.5, 129.9 and 312.4. Among them, *Silurus asotus*, *Hemiculter leucisculus*, *Carassius auratus*, *Pseudobagrus fulvidraco*, *Opsariichthys bidens*, *Cyprinus carpio*, *Rhodeinae*, *Culter alburnns* and *Acheilognathus maCropterus* are main species, and *Pseudorasbora parva* is common species. There is no rare species or dominant species.

In the Zhuweizi Reservoir, the IRI values of 8 fish species (*Cyprinus carpio*, *Carassius auratus*, *Rhodeinae*, *Hemiculter leucisculus*, *Acheilognathus maCropterus*, *Zacco platypus*, *Opsariichthys bidens*, *Cultrichthys erythropterus*) are 384.5, 265.9, 535.2, 914.8334.4, 303.2, 224.4 and 81.4. Among them, *Cyprinus carpio*, *Carassius auratus*, *Rhodeinae*, *Zacco platypus*, *Hemiculter leucisculus*, *Acheilognathus maCropterus* and *Opsariichthys bidens* are main species, *Cultrichthys erythropterus* is common species. There is no rare species or dominant species.

Table 3. Catalogue of catches from 4 reservoirs in Dalian

Order	Family	Genus	Species	Zhuanjiaolou Reservoir	Yingnahe Reservoir	Zhuweizi Reservoir	Songshu Reservoir
Cypriniformes	Cyprinidae	<i>Hypophthalmichthys</i>	<i>Hypophthalmichthys molitrix</i>	+	+	+	+
		<i>Aristichthys</i>	<i>Aristichthys nobilis</i>	+	+	+	+
		<i>Carassius</i>	<i>Carassius auratus</i>	+	+	+	+
		<i>Cyprinus</i>	<i>Cyprinus carpio</i>	+	+	+	+
			<i>Cyprinus carpio</i>		+		
		<i>Pseudorasbora</i>	<i>Pseudorasbora parva</i>	+	+	+	+
		<i>Rhodeus</i>	<i>Rhodeinae</i>	+	+		+
		<i>Phoxinus</i>	<i>Phoxinus lagowskii</i>	+	+	+	+
		<i>Opsariichthys</i>	<i>Opsariichthys bidens</i>	+	+	+	+
		<i>Zacco</i>	<i>Zacco platypus</i>	+		+	+
		<i>Hemiculter</i>	<i>Hemiculter leucisculus</i>	+		+	+
		<i>Acheilognathus</i>	<i>Acheilognathus macropterus</i>	+	+	+	+
		<i>Culterichthys</i>	<i>Cultrichthys erythropterus</i>	+		+	+
		<i>Hemibarbus</i>	<i>Hemibarbus labeo</i>	+		+	
	<i>Culter</i>	<i>Culter alburnus</i>				+	
	<i>Megalobrama</i>	<i>Megalobrama amblycephala</i>				+	
	Cobitidae	<i>Misgurnus</i>	<i>Misgurnus anguillicaudatus</i>	+			+
		<i>Barbatula</i>	<i>Barbatula barbatula nuda</i>	+	+	+	+
		<i>Paramisgurnus</i>	<i>Paramisgurnus dabryanus</i>	+	+		
Perciformes	Gobiidae	<i>Rhinogobius</i>	<i>rhinogobius giurinus</i>	+		+	
	Eleotridae	<i>Hypseleotris</i>	<i>Hypseleotris swinhonis</i>		+	+	+
		<i>Perccottus</i>	<i>Perccottus glehni</i>	+	+		
Siluriformes	Siluridae	<i>Silurus</i>	<i>Silurus asotus</i>		+		
	Bagridae	<i>Pelteobagrus</i>	<i>Pseudobagrus fulvidraco</i>	+	+		+
Salmoniformes	Osmeridae	<i>Hypomesus</i>	<i>Hypomesus olidus</i>	+			

Table 4. Dominance of catches in 4 reservoirs

	Species name	W value	N value	F value	IRI value
Zhuanjiaolou Reservoir	<i>Carassius auratus</i>	15.73%	29.09%	20	896.4
	<i>Phoxinus lagowskii</i>	1.92%	7.27%	10	91.9
	<i>Pseudobagrus fulvidraco</i>	5.68%	9.09%	10	147.7
	<i>Hypophthalmichthys molitrix</i>	72.8%	5.45%	10	782.5
	<i>Rhodeinae</i>	0.17%	9.09%	20	184.6
	<i>Abbottina rivularis</i>	0.23%	5.45%	10	59.1
	<i>Hypomesus</i>	0.37%	7.27%	10	76.4
	<i>Zacco platypus</i>	2.8%	21.82%	20	492.4
	<i>Pseudorasbora parva</i>	0.16%	5.45%	10	56.1
Yingnahe Reservoir	<i>Silurus asotus</i>	8.72%	4.35%	10	130.7
	<i>Hemiculter leucisculus</i>	8.46%	13.04%	20	430
	<i>Carassius auratus</i>	21.99%	17.39%	20	787.6
	<i>Pseudobagrus fulvidraco</i>	2.26%	8.7%	20	226
	<i>Opsariichthys bidens</i>	4.92%	11.59%	20	330.2
	<i>Cyprinus carpio</i>	39.50%	5.80%	10	453
	<i>Rhodeinae</i>	1.63%	14.49%	10	161.2
	<i>Pseudorasbora parva</i>	1.30%	7.25%	10	85.5
Zhuweizi Reservoir	<i>Cyprinus carpio</i>	33.69%	4.76%	10	384.5
	<i>Carassius auratus</i>	17.07%	9.52%	10	265.9
	<i>Rhodeinae</i>	7.71%	19.05%	20	535.2
	<i>Hemiculter leucisculus</i>	20.34%	25.40%	20	914.8
	<i>Acheilognathus maCrouterus</i>	4.02%	12.70%	20	334.4
	<i>Zacco platypus</i>	4.05%	11.11%	20	303.2
	<i>Opsariichthys bidens</i>	9.74%	12.70%	10	224.4
	<i>Cultrichthys erythropterus</i>	3.38%	4.76%	10	81.4
Songshu Reservoir	<i>Opsariichthys bidens</i>	8.69%	19.23%	20	558.4
	<i>Pseudobagrus fulvidraco</i>	5.00%	15.38%	10	203.8
	<i>Acheilognathus maCrouterus</i>	1.51%	15.38%	10	168.9
	<i>Culter alburnrs</i>	6.66%	15.38%	10	202.4
	<i>Hypophthalmichthys molitrix</i>	64.62%	11.54%	10	761.6
	<i>Carassius auratus</i>	13.53%	23.08%	20	732.2

In Songshu Reservoir, the IRI values of 6 fish species (*Opsariichthys bidens*, *Pseudobagrus fulvidraco*, *Acheilognathus maCrouterus*, *Culter alburnrs*, *Hypophthalmichthys molitrix*, *Carassius auratus*) are 558.4, 203.8, 168.9, 202.4, 761.6 and 732.2. Among them, *Opsariichthys bidens*, *Pseudobagrus fulvidraco*, *Acheilognathus maCrouterus*, *Culter alburnrs*, *Hypophthalmichthys molitrix* and *Carassius auratus* are main species. There is no rare species, common species or dominant species.

Heavy metal content of fish in 4 reservoirs in Dalian

The heavy metal content in the muscles of the four fishes *Carassius auratus*, *Hypophthalmichthys molitrix*, *Rhodeinae* and *Pseudobagrus fulvidraco* in Zhuanjiaolou Reservoir is shown in Figure 2. The Cr contents are all lower than the standard value of 2.0, ranking from high to low as: *Carassius auratus* > *Rhodeinae* > *Hypophthalmichthys molitrix* > *Pseudobagrus fulvidraco*. The Cd contents are all lower than the standard value of 0.01, ranking from high to low as: *Pseudobagrus fulvidraco* > *Rhodeinae* > *Hypophthalmichthys molitrix* > *Carassius auratus*. The Pb contents are all lower than the standard value of 0.5, ranking from high to low as: *Carassius auratus* > *Rhodeinae* > *Pseudobagrus fulvidraco* > *Hypophthalmichthys molitrix*. The Hg contents are all lower than the standard value of 1.0, ranking from high to low as: *Hypophthalmichthys molitrix* > *Pseudobagrus fulvidraco* > *Carassius auratus* > *Rhodeinae*. The As contents are all lower than the standard value of 0.10, ranking from high to low as: *Rhodeinae* > *Hypophthalmichthys molitrix* > *Carassius auratus* > *Pseudobagrus fulvidraco*. The highest content of the five heavy metals is the As in *Rhodeinae*, and the lowest is the Cd in *Carassius auratus*.

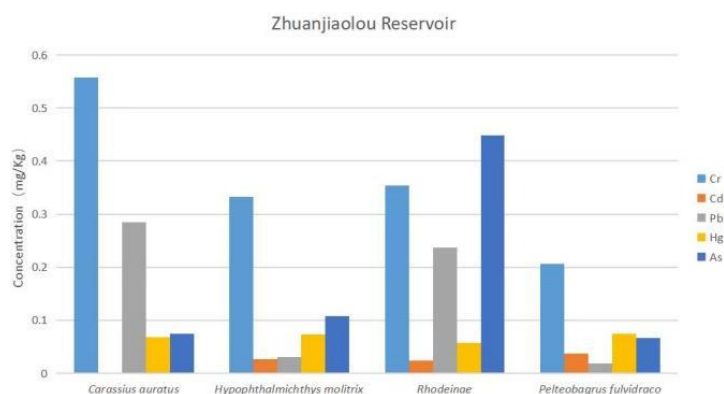


Figure 2. Heavy metal content of fish in Zhuanjiaolou Reservoir

The heavy metal content in the muscles of the four fishes *Carassius auratus*, *Opsariichthys bidens*, *Cyprinus carpio* and *Hemiculter leucisculus* in Yingnahe Reservoir are shown in Figure 3. According to the standard limit of heavy metal in fish, we can know that the Cr contents in the muscles of the four fishes are all lower than the standard value of 2.0, ranking from high to low as: *Cyprinus carpio* > *Carassius auratus* > *Hemiculter leucisculus* > *Opsariichthys bidens*, the Cd contents in the fish muscles are all lower than the standard value of 0.10, ranking from high to low as: *Hemiculter leucisculus* > *Cyprinus carpio* > *Opsariichthys bidens* > *Carassius auratus*, the Pb contents in the fish muscles are all lower than the standard value of 0.5, ranking from high to low as: *Cyprinus carpio* > *Hemiculter leucisculus* > *Opsariichthys bidens* > *Carassius auratus*, the Hg contents in the fish muscles are all lower than the standard value of 1.0, ranking from high to low as: *Carassius auratus* > *Cyprinus carpio* > *Opsariichthys bidens* > *Hemiculter leucisculus*, the As contents in the fish muscles are all lower than the standard value of 0.10, ranking from high to low as: *Hemiculter leucisculus* > *Opsariichthys bidens* > *Carassius auratus* > *Cyprinus carpio*. The highest content of the five heavy metals is the Cr in *Cyprinus carpio*, and the lowest is the Pb in *Carassius auratus*.

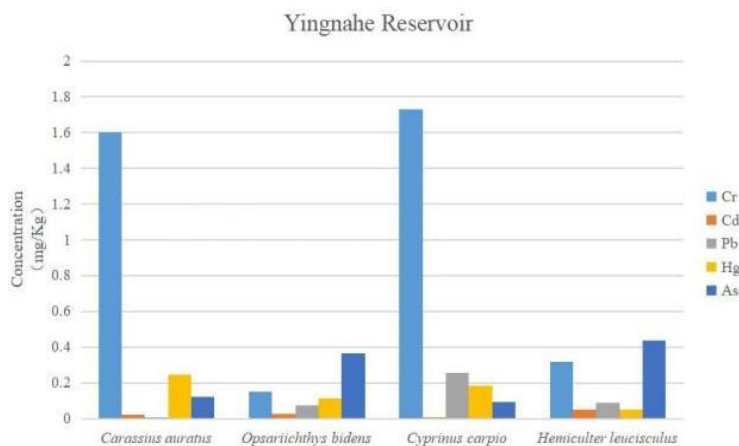


Figure 3. Heavy metal content of fish in Yingnahe Reservoir

The heavy metal content in the muscles of the four fishes *Rhodeinae*, *Carassius auratus*, *Cyprinus carpio* and *Hemiculter leucisculus* in Zhuweizi Reservoir are shown in Figure 4. According to the standard limit of heavy metal in fish, we can know that only the Cr content in the muscles of *Hemiculter leucisculus* is above the standard value of 2.0, while none of the others do, ranking from high to low as: *Hemiculter leucisculus* > *Rhodeinae* > *Carassius auratus* > *Cyprinus carpio*, the Cd contents in the fish muscles are all lower than the standard value of 0.10, ranking from high to low as: *Rhodeinae* > *Hemiculter leucisculus* > *Carassius auratus* > *Cyprinus carpio*, the Pb contents in the fish muscles are all lower than the standard value of 0.5, ranking from high to low as: *Rhodeinae* > *Carassius auratus* > *Hemiculter leucisculus* > *Cyprinus carpio*, the Hg contents in the fish muscles are all lower than the standard value of 1.0, ranking from high to low as: *Rhodeinae* > *Hemiculter leucisculus* > *Carassius auratus* > *Cyprinus carpio*, the As contents in the muscles of *Rhodeinae* and *Hemiculter leucisculus* are above the standard value of 0.5 while others don't, ranking from high to low as: *Hemiculter leucisculus* > *Rhodeinae* > *Carassius auratus* > *Cyprinus carpio*. The highest content of the five heavy metals is the Cr in *Hemiculter leucisculus*, and the lowest is the Cd in *Cyprinus carpio*.

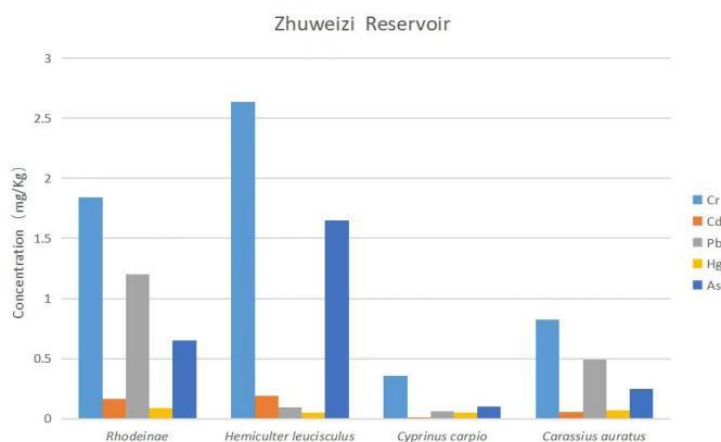


Figure 4. Heavy metal content of fish in Zhuweizi Reservoir

The heavy metal content in the muscles of the four fishes *Carassius auratus*, *Opsariichthys bidens*, *Hypophthalmichthys molitrix* and *Pseudobagrus fulvidraco* in Songshu Reservoir are shown in Figure 5. According to the standard limit of heavy metal in fish, we can know that only the Cr content in the muscles of *Pseudobagrus fulvidraco* is above the standard value of 2.0, while none of the others do, ranking from high to low as: *Pseudobagrus fulvidraco* > *Hypophthalmichthys molitrix* > *Opsariichthys bidens* > *Carassius auratus*, the Cd contents in the fish muscles are all lower than the standard value of 0.10, ranking from high to low as: *Pseudobagrus fulvidraco* > *Opsariichthys bidens* > *Hypophthalmichthys molitrix* > *Carassius auratus*, the Pb content in the muscles of *Hypophthalmichthys molitrix* is above the standard value of 0.5, while the rest don't, ranking from high to low as: *Hypophthalmichthys molitrix* > *Opsariichthys bidens* > *Pseudobagrus fulvidraco* > *Carassius auratus*, the Hg contents in the fish muscles are all lower than the standard value of 1.0, ranking from high to low as: *Opsariichthys bidens* > *Pseudobagrus fulvidraco* > *Hypophthalmichthys molitrix* > *Carassius auratus*, the As contents in the muscles of *Pseudobagrus fulvidraco* and *Carassius auratus* are above the standard value of 0.10, while the rest don't, ranking from high to low as: *Carassius auratus* > *Pseudobagrus fulvidraco* > *Opsariichthys bidens* > *Hypophthalmichthys molitrix*. The highest content of the five heavy metals is the Cr in *Pseudobagrus fulvidraco*, and the lowest is the Pb in *Carassius auratus*.

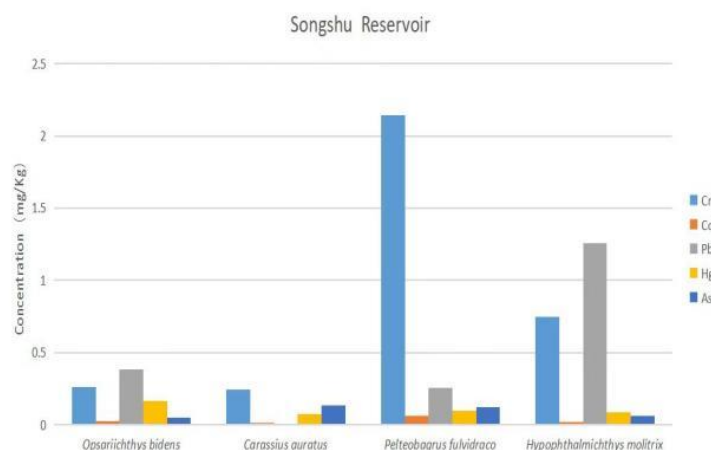


Figure 5. Heavy metal content of fish in Songshu Reservoir

Health risk assessment of heavy metals in fishes in 4 reservoirs of Dalian

The calculation results of the comprehensive pollution index (Table 5) showed that in Zhuanjiaolou Reservoir, the order of the comprehensive pollution index of the four fishes from high to low is: *Rhodeinae* > *Carassius auratus* > *Hypophthalmichthys molitrix* > *Pseudobagrus fulvidraco*. Among them, the index of *Pseudobagrus fulvidraco* is the lowest ($P_{comp}=0.501$), the index of *Rhodeinae* is the highest ($P_{comp}=1.266$), indicating light pollution. The indices of the other three fishes are below 1, indicating no pollution; In Yingnahe Reservoir, the order of the comprehensive pollution index of the four fishes from high to low is: *Opsariichthys bidens* > *Hemiculter leucisculus* > *Carassius auratus* > *Cyprinus carpio*. Among them, the index of *Cyprinus carpio* is the lowest ($P_{comp}=0.774$), the index of *Opsariichthys bidens* is the highest ($P_{comp}=1.712$), indicating light pollution. The index of *Hemiculter leucisculus* is above 1, indicating light pollution. While the

indices of *Carassius auratus*, *Cyprinus carpio* are below 1, indicating no pollution; In Zhuweizi Reservoir, the order of the comprehensive pollution index of the four fishes from high to low is: *Rhodeinae* > *Hemiculter leucisculus* > *Cyprinus carpio* > *Carassius auratus*. Among them, the index of *Carassius auratus* is the lowest ($P_{comp}=0.384$), the index of *Rhodeinae* is the highest ($P_{comp}=1.976$), indicating light pollution. The index of *Hemiculter leucisculus* is above 1, indicating light pollution. And the indices of *Carassius auratus*, *Cyprinus carpio* are above 1, indicating no pollution; In Songshu Reservoir, the order of the comprehensive pollution index of the four fishes from high to low is: *Pseudobagrus fulvidraco* > *Hypophthalmichthys molitrix* > *Carassius auratus* > *Opsariichthys bidens*. Among them, the index of *Opsariichthys bidens* is the lowest ($P_{comp}=0.597$), the index of *Pseudobagrus fulvidraco* is the highest ($P_{comp}=0.997$), the indices of all are over 1, indicating no pollution; Among the 16 fish species in the four reservoirs, *Rhodeinae* of Zhuweizi Reservoir has the highest comprehensive pollution index ($P_{comp} = 1.976$) and *Carassius auratus* of Zhuweizi Reservoir has the lowest pollution index ($P_{comp} = 0.384$). Fish with a comprehensive pollution index of non-polluting accounted for 68.75% of the total.

Table 5. Comprehensive pollution index of dominant fish species in 4 reservoirs in Dalian

Location	Species name	P_{comp}
Zhuanjiaolou Reservoir	<i>Carassius auratus</i>	0.815
	<i>Hypophthalmichthys molitrix</i>	0.656
	<i>Pseudobagrus fulvidraco</i>	0.501
	<i>Rhodeinae</i>	1.266
Yingnahe Reservoir	<i>Carassius auratus</i>	0.943
	<i>Opsariichthys bidens</i>	1.712
	<i>Cyprinus carpio</i>	0.774
	<i>Hemiculter leucisculus</i>	1.536
Zhuweizi Reservoir	<i>Cyprinus carpio</i>	0.549
	<i>Carassius auratus</i>	0.384
	<i>Hemiculter leucisculus</i>	1.003
	<i>Rhodeinae</i>	1.976
Songshu Reservoir	<i>Opsariichthys bidens</i>	0.597
	<i>Carassius auratus</i>	0.625
	<i>Pseudobagrus fulvidraco</i>	0.997
	<i>Hypophthalmichthys molitrix</i>	0.643

The *THQ* values of Cr, Cd, Pb, Hg and As in the muscle tissues of dominant fish species from 4 reservoirs in Dalian are as shown in *Table 6*. In Zhuanjiaolou Reservoir, the health risk values of heavy metal Cr in the four fishes range from high to low as: *Carassius auratus* > *Hypophthalmichthys molitrix* > *Rhodeinae* > *Pseudobagrus fulvidraco*, the health risk values of heavy metal Cd in the four fishes range from high to low as: *Carassius auratus* > *Hypophthalmichthys molitrix* > *Pseudobagrus fulvidraco* > *Rhodeinae*, the health risk values of heavy metal Pb in the four fishes range from high to low as: *Rhodeinae* > *Carassius auratus* > *Hypophthalmichthys molitrix* > *Pseudobagrus fulvidraco*, the health risk values of heavy metal Hg in the four fishes range from high to low as: *Carassius auratus* > *Pseudobagrus fulvidraco* > *Rhodeinae* > *Hypophthalmichthys molitrix*, the health risk values of heavy metal As in the four fishes range from high to low as: *Rhodeinae* > *Carassius auratus* > *Pseudobagrus fulvidraco* > *Hypophthalmichthys*

molitrix. The highest *THQ* value of the five heavy metals in the four fishes is Cr in *Carassius auratus*, and the lowest value is Hg in *Hypophthalmichthys molitrix*. All *THQ* values are less than 1, which means that the heavy metal content in the edible muscle tissue of the four fishes has no obvious effect on human health.

Table 6. *THQ* values of different heavy metals in 16 fished from 4 reservoirs in Dalian

Location	Species name	Cr	Cd	Pb	Hg	As
Zhuanjiaolou Reservoir	<i>Carassius auratus</i>	0.57136	0.01547	0.15431	0.00494	0.04161
	<i>Hypophthalmichthys molitrix</i>	0.41467	0.01262	0.09021	0.00342	0.00979
	<i>Pseudobagrus fulvidraco</i>	0.16302	0.00546	0.02928	0.00475	0.03941
	<i>Rhodeinae</i>	0.28014	0.00490	0.29042	0.00367	0.08837
Zhuweizi Reservoir	<i>Rhodeinae</i>	0.40676	0.00597	0.86890	0.00563	0.08113
	<i>Hemiculter leucisculus</i>	0.18834	0.04934	0.13216	0.00355	0.10897
	<i>Cyprinus carpio</i>	0.44316	0.00217	0.40913	0.00532	0.04178
	<i>Carassius auratus</i>	0.58086	0.00886	0.46136	0.00595	0.02202
Yingnahe Reservoir	<i>Carassius auratus</i>	1.26459	0.00783	0.00554	0.01545	0.01413
	<i>Opsariichthys bidens</i>	0.37194	0.01506	0.99157	0.00861	0.07864
	<i>Cyprinus carpio</i>	1.56056	0.00783	0.26985	0.00374	0.04718
	<i>Hemiculter leucisculus</i>	0.11237	0.01690	0.42417	0.01323	0.06677
Songshu Reservoir	<i>Opsariichthys bidens</i>	0.28172	0.01377	0.24770	0.01418	0.04523
	<i>Carassius auratus</i>	0.88790	0.03913	0.06885	0.00728	0.02659
	<i>Pseudobagrus fulvidraco</i>	1.69509	0.02394	0.40043	0.00627	0.06101
	<i>Hypophthalmichthys molitrix</i>	0.84200	0.00249	0.12345	0.00987	0.06048

In Zhuweizi Reservoir, the health risk values of heavy metal Cr in the four fishes range from high to low as: *Carassius auratus* > *Cyprinus carpio* > *Rhodeinae* > *Hemiculter leucisculus*. The health risk values of heavy metal Cd in the four fishes range from high to low as: *Hemiculter leucisculus* > *Carassius auratus* > *Rhodeinae* > *Cyprinus carpio*, the health risk values of heavy metal Pb in the four fishes range from high to low as: *Rhodeinae* > *Carassius auratus* > *Cyprinus carpio* > *Hemiculter leucisculus*, the health risk values of heavy metal Hg in the four fishes range from high to low as: *Carassius auratus* > *Rhodeinae* > *Cyprinus carpio* > *Hemiculter leucisculus*, the health risk values of heavy metal As in the four fishes range from high to low as: *Hemiculter leucisculus* > *Rhodeinae* > *Cyprinus carpio* > *Carassius auratus*. The highest *THQ* value of the five heavy metals in the four fishes is Pb in *Rhodeinae*, and the lowest value is As in *Carassius auratus*. All *THQ* values are less than 1, which means that the heavy metal content in the edible muscle tissue of the four fishes has no obvious effect on human health.

In Yingnahe Reservoir, the health risk values of heavy metal Cr in the four fishes range from high to low as: *Cyprinus carpio* > *Carassius auratus* > *Opsariichthys bidens* > *Hemiculter leucisculus*. The health risk values of heavy metal Cd in the four fishes range

from high to low as: *Hemiculter leucisculus* > *Opsariichthys bidens* > *Cyprinus carpio* = *Carassius auratus*, the health risk values of heavy metal Pb in the four fishes range from high to low as: *Opsariichthys bidens* > *Hemiculter leucisculus* > *Cyprinus carpio* > *Carassius auratus*, the health risk values of heavy metal Hg in the four fishes range from high to low as: *Carassius auratus* > *Hemiculter leucisculus* > *Opsariichthys bidens* > *Cyprinus carpio*, the health risk values of heavy metal As in the four fishes range from high to low as: *Opsariichthys bidens* > *Hemiculter leucisculus* > *Cyprinus carpio* > *Carassius auratus*. The highest *THQ* value of the five heavy metals in the four fishes is Cr in *Cyprinus carpio*, and the lowest value is Pb in *Carassius auratus*. All *THQ* values are above 1, except for that of Cr in *Carassius auratus* and *Cyprinus carpio*, which are slightly higher than 1. That means that the heavy metal content in the edible muscle tissue of those two fishes has a slight impact on human health, and the rest have no obvious impact.

In Songshu Reservoir, the health risk values of heavy metal Cr in the four fishes range from high to low as: *Pseudobagrus fulvidraco* > *Carassius auratus* > *Hypophthalmichthys molitrix* > *Opsariichthys bidens*. The health risk values of heavy metal Cd in the four fishes range from high to low as: *Carassius auratus* > *Pseudobagrus fulvidraco* > *Opsariichthys bidens* > *Hypophthalmichthys molitrix*, the health risk values of heavy metal Pb in the four fishes range from high to low as: *Pseudobagrus fulvidraco* > *Opsariichthys bidens* > *Hypophthalmichthys molitrix* > *Carassius auratus*, the health risk values of heavy metal Hg in the four fishes range from high to low as: *Pseudobagrus fulvidraco* > *Opsariichthys bidens* > *Hypophthalmichthys molitrix* > *Carassius auratus*, the health risk values of heavy metal As in the four fishes range from high to low as: *Opsariichthys bidens* > *Hypophthalmichthys molitrix* > *Carassius auratus* > *Pseudobagrus fulvidraco*. The highest target hazard quotient value of the five heavy metals in the four fishes is Cr in *Pseudobagrus fulvidraco*, and the lowest value is Hg in *Pseudobagrus fulvidraco*. Only the *THQ* value of Cr in *Pseudobagrus fulvidraco* are above 1, means that the heavy metal content in the edible muscle tissue of that fish has a slight impact on human health, and the rest have no obvious impact.

Discussion

Characteristics of fish communities in 4 reservoirs of Dalian

As an important part of the aquatic ecosystem, fish promotes the energy flow and material conversion in the aquatic ecosystem. The stability of its community structure reflects the health of the aquatic ecosystem to a certain extent, and dominance level is one of the characteristics that affect the structure of fish communities (Wang et al., 2014). With the rapid development of social economy, in order to meet the needs of modern agricultural production development, irrigation, flood control, etc., reservoirs, as the water body connecting the upper and lower water surfaces, are important feeding grounds and habitats for fish (Yuan et al., 2015; Liu et al., 2016; Zheng et al., 2017; Yi et al., 2021). In the investigation, it was found that the fish community diversity index can reflect the stability of the community structure to a certain extent, and has a close relationship with the surrounding environment of the habitat. The complexity of habitat will affect the diversity of fish communities, and the diversity of fish communities can reflect the stability of the community structure. The richer the species in the community, the more even the distribution of individuals of various types. Similarly, the higher the richness index and uniformity index, the more stable the community structure (Bai et al.,

2020). That may be related to the different fish dominance distribution at different points in the reservoir. The living environments of the upper and lower reaches of the reservoir are different, and the results of fish community diversity research are affected by the survey methods, which may be slightly biased, thus further research is needed (Liani et al., 2018).

Analysis of characteristics of heavy metal content in fish

Heavy metal pollution mainly refers to the harm to the environment caused by heavy metal compounds such as Hg, Cd, Zn, Cr, As, Zn and Cu that enter the environment through various channels. Heavy metal elements have a long residual poison time and are accumulative. They can be enriched in organisms and transmitted or amplified through the food chain, so that organisms that originally provide people with protein and other nutrients, such as fish, shrimp, crabs, shells, etc., become concentrates of toxic metals, which can affect or potentially affect human health (Xu et al., 2013).

Heavy metals are important pollutants in water bodies, and they can be enriched in fish through respiration, ingestion, and adsorption (Zhang et al., 2017; Li and Liu, 2019; Lin et al., 2018). It has been found from related studies that the level of heavy metals in fish tissues is mainly related to the environment. Fishes of different types have different heavy metal content, and fishes of the same type living in different environments also have different heavy metal content (Tchounwou et al., 2012). The four fishes with the highest IRI values in the four reservoirs and water bodies of Dalian were selected for heavy metal content testing. It was found that some fish have higher Cr values. That may be due to the discharge of wastewater from surrounding factories and enterprises, which caused heavy metal pollution in the water, and further lead to heavy metal enrichment in the fish through food chain.

The harm of heavy metal content in fish to human body

The risk exposure assessment of heavy metals refers to the qualitative or quantitative analysis of the heavy metal intake from food, that is, the estimation of the heavy metal intake according to people's dietary consumption pattern and dietary consumption amount of heavy metals (Duan et al., 2009). With the gradual acceleration of China's industrialization, there will be more and more pollutants of heavy metals in water bodies. For example, if the concentration of heavy metals in the well-loved *Procambarus clarkii* deepens, the total amount of heavy metals entering people's bodies will also increase, which can become harmful to health (Yang et al., 2020). There are many risk exposure assessment methods for heavy metals. For example, point assessment is a method of expressing population risk through a single value. This method is simple and clear. Zhou et al. (2018) used it to assess the risk of *Procambarus clarkii*. If the residents of Hubei Province consume one serving a day, the results indicate that they are at a safe level; The simple distribution assessment estimates based on the distribution of food intake. Considering the variability of consumption, heavy metal is a fixed reference value, which can also be seen as the highest level of heavy metal pollution.

The analysis of the comprehensive fish heavy metal pollution index can more comprehensively show the heavy metal pollution of 16 types of fishes in 4 reservoirs of Dalian. Among them, *Rhodeinae* in Zhuanjiaolou Reservoir, *Hemiculter leucisculus* in Yingnahe Reservoir and *Hemiculter leucisculus* and *Rhodeinae* in Zhuweizi Reservoir showed light pollution, with values above 1, and all others showed no pollution. *Rhodeinae* in Zhuweizi Reservoir had the highest value, which may be because that,

compared with other fishes, *Rhodeinae* prefers to live in places with a lot of water and grass and close to the shore, making it easier for heavy metals to accumulate.

The method of health risk assessment adopted in this paper is the same as that used by Luo et al. (2021) and Xu et al. (2020) on the determination of heavy metal content in wild fish, the determination of heavy metal content in three cultured freshwater fish and the health risk assessment. Through the health risk assessment of the heavy metal elements of 16 fish species in 4 reservoirs of Dalian, the results showed that most of the fishes have no obvious health risks to human, except for *Pseudobagrus fulvidraco* in Songshu Reservoir, which has a slightly high value, indicating minor impact on human health.

Analysis of causes of changes in fish resources and protective measures

Biological invasion is already one of the global environmental problems today. The loss of global biodiversity and the destruction of global ecosystems are both extremely serious (Liu et al., 2019). The invasion of alien species will seriously harm the community structure, leading to the decline of indigenous fishes, and different fishes distributed in different locations will be different in size and quality (Andrzej et al., 2008; Liu et al., 2016).

Most of the exotic fishes such as *Pseudorasbora parva* have strong survival tolerance, and can adapt to the changes in the living environment quickly, change the structure of fish communities, and compete with indigenous fishes, which may pose threat to other fishes (Wang et al., 2016).

River water conservancy will also cause the reduction of fish species and changes in community composition, which will affect the structure, growth, reproduction and habitat environment of fish populations (Yang et al., 2013; Huang et al., 2015; Cao et al., 2017). The original hydrological environment was changed when 4 reservoirs were built and expanded, and the reservoir water being used for irrigation reduced the living space of fish (Wang et al., 2021).

Exotic fish should be strictly controlled and monitored regularly; fish habitats should be protected; fishery management should be strengthened and publicity should be strengthened; excessive fishing need to be strictly prohibited, proliferation and release should be actively carried out, and fish germplasm resources and gene banks should be established (Ma et al., 2014; Cheng et al., 2017; He et al., 2021; Wang et al., 2021; Liao et al., 2021).

Conclusion

Through the investigation of fish in 4 reservoirs of Dalian, a total of 758 fishes were collected in this survey, belonging to 4 orders, 7 families, 23 genera and 25 species. Among them, *Cypriniformes* are the most, with 2 families, 18 genera and 19 species, accounting for 76% of the total species. It was found from the comprehensive pollution index results that *Rhodeinae* in Zhuanjiaolou Reservoir, *Opsariichthys bidens* and *Hemiculter leucisculus* in Yingnahe Reservoir, *Hemiculter leucisculus* and *Rhodeinae* in Zhuweizi Reservoir have relatively high values. From the exposure risk assessment results of the four reservoirs, it can be found that the exposure coefficient of Cr in *Pseudobagrus fulvidraco* is the highest, indicating a certain exposure risk, while the risks of other types are low. We should fully implement the concept of ecological priority in the new era, strengthen the management and protection of the reservoir environment, rationally use the water suitable for fishing, explore a new model of high-quality

development of green fisheries, and ensure the sustainable development of reservoir fishery resources.

Acknowledgements. This study was supported by The Special Agricultural Finance Project "Investigation of Fishery Resources and Environment in Key Waters in Northeast China", Liaoning important marine fish high-efficiency green production model research and development and demonstration project (2020JH1/10200002). The authors are grateful to the people that helped in the experiment.

REFERENCES

- [1] Alidadi, H., Sany, S. B. T., Oftadeh, B. Z. G., Mohamad, T., Shamszade, H., Fakhari, M. (2019): Health risk assessments of arsenic and toxic heavy metal exposure in drinking water in northeast Iran. – *Environmental health and preventive medicine* 24: 59.
- [2] Bai, J. P., Huang, G., Jiang, C. J., Zhang, W. C., Wang, Q. D., Yao, L. G. (2020): The characteristics and historical changes of fish communities in Danjiangkou Reservoir. – *Biodiversity* 28(10): 1202-1212.
- [3] Cheng, L., Ma, B. J. (2017): Health Risk Assessment of Heavy Metal Pollution in the Water Environment of Xiaolangdi Reservoir. – 2017 Science and Technology Annual Conference Proceedings of Chinese Society for Environmental Sciences (Volume 4).
- [4] Chang, T., Duan, Z. H., Li, M. Z. (2021): Dynamics of early fish resource agglomeration in the Yichang section of the middle reaches of the Yangtze River after the impoundment of the Three Gorges Reservoir. – *Resources and Environment in the Yangtze River Basin* 30(01): 137-146.
- [5] Chen, W. J., Zhang, Y. P., Zhao, C. L., Wang, C. L. (2012): Composition and diversity of fish communities in the Yangtze River Estuary in recent years. – *Resources and Environment in the Yangtze Basin* 21(06): 684-691.
- [6] Cao, N., Mao, Z. P. (2017): Countermeasures and suggestions for fish protection in hydropower development on the main stream of the Dadu River. – *Water Resources and Hydropower Technology* 48(01): 116-121.
- [7] Chu, L. J., Yang, X. J., Liu, J. L. (2021): Analysis of heavy metal pollution of two carps in Dajiu Lake, Shennongjia. – *Journal of Water Ecology*
- [8] Chen, M. Y., Zhou, Y. Q., Huang, J. Y. (2019): Study on the enrichment of heavy metals in aquatic organisms. – *Journal of Food Safety and Quality Inspection* 10(08): 2085-2091.
- [9] Duan, X. L., Nie, J., Wang, Z. S. (2009): Overview of domestic and foreign research on human exposure parameters in health risk assessment. – *Journal of Environment and Health* 26(04): 370-373.
- [10] Da Silva Cardoso, A. J., dos Santos, W. V., Gomes, J. R., Martins, M. T. S., Coura, R. R., et al. (2021): Ginger oil, *Zingiber officinale*, improve palatability, growth and nutrient utilisation efficiency in Nile tilapia fed with excess of starch. – *Animal Feed Science and Technology* 272: 114756.
- [11] GB 5009.11-2014 (2014): National Food Safety Standard, Determination of Total Arsenic and Inorganic Arsenic in Food.
- [12] GB 5009.17-2014 (2014): National Food Safety Standard, Determination of Total Mercury and Organic Mercury in Food.
- [13] He, Y., Hong, X., Bi, X. Y. (2021): Pollution characteristics and source analysis of heavy metals in the water environment of Jiuzhou River Basin. – *Environmental Chemistry* 40(01): 240-253.
- [14] Huang, G. M., Wang, H. L., Wang, W. Y., Chen, H., Ding, C. Z. (2015): Practice of fish habitat protection in the Lancang River Basin. – *Journal of Water Ecology* 36(06): 86-92.

- [15] Jian, M. F., Li, L. Y., Yu, H. P., Xiong, J. Q., Yu, G. J. (2015): Poyang Lake wetland water and sediment heavy metal pollution and its impact on submerged plant communities. – *Journal of Ecological Environment* 24(01): 96-105.
- [16] Kapusta, A., Bogacka-Kapusta, E., Czarnecki, B. (2008): The Significance of Stone Moroko, *Pseudorasbora Parva* (Temminck and Schlegel), in the Small-Sized Fish Assemblages in the Littoral Zone of the Heated Lake Licheńskie. – *Archives of Polish Fisheries* 16(1): 49-62.
- [17] Kaus, A., Schaffer, M., Karthe, D., Büttner, O., Von Tümpling, W., Borchardt, D. (2017): Regional patterns of heavy metal exposure and contamination in the fish fauna of the Kharaa River basin (Mongolia). – *Regional Environmental Change* 17(7): 2023-2037.
- [18] Kominkova, D., Nabelkova, J. (2007): Effect of urban drainage on bioavailability of heavy metals in recipient. – *Water Science & Technology* 56(9): 43-50.
- [19] Liu, B. J., Liu, Q. X., Jia, Z. Z. (2021): Distribution, distribution characteristics and influencing factors of heavy metals in Modaomen waters of the Pearl River Estuary. – *Marine Environmental Science* 40(01): 8-15.
- [20] Liu, F., Liu, P. C., Li, M. Z., Gao, X., Wang, C. L., Liu, H. Z. (2019): Current status of fish resources in the Yangtze River Basin and protection strategies. – *Journal of Hydrobiology* 43(S1): 144-156.
- [21] Lu, J. M., Lin, Y. H., Li, H. M. (1995): Study on the toxicity of heavy metals to grass carp embryos and carp fry. – *Journal of Fisheries Science* 1995(01): 55-62.
- [22] Liu, J. L., Li, H. L., Tang, Y. J., Xie, L. N., Zhong, J. Y. (2017): Current status of heavy metal pollution in mangrove wetlands on Qi'ao Island in Zhuhai and analysis of human health risks. – *Ecological Science* 36(05): 186-195.
- [23] Liu, K., Jing, L., Chen, Y. J., Xu, D. P. (2016): Evaluation of growth, death and utilization status of wheat earfish in Taihu Lake. – *Journal of Dalian Ocean University* 31(04): 368-373.
- [24] Li, J. F., Liu, N. N. (2019): Risk assessment of heavy metal pollution in fish at the confluence of Huangweiluo Three Rivers. – *Journal of Fisheries Science* 32(04): 50-54.
- [25] Liaoning Zoology (1987): Liaoning Science and Technology Press, Editorial Committee of Liaoning Provincial Science and Technology Commission.
- [26] Lin, L. L., Liu, H. J., Yuan, H. Y. (2018): The impact of heavy metal pollution on fish. – *Henan Fisheries* 1: 2-4.
- [27] Liu, B. L., Mei, Y. C., Gao, X. A. (2018): Heavy metal pollution characteristics and health risk assessment of fish in Songhua River. – *Journal of Northeast Normal University (Natural Science Edition)* 50(04): 142-147.
- [28] Lü, Z. B., Li, F., Xu, B. Q., Wang, B. (2011): Fish community diversity during spring and autumn in the Yellow Sea off the coast of Shandong. – *Journal of Fisheries of China* 35(5): 692-698.
- [29] Liu, W. F. (2017): Resource environmental protection, utilization and development prospects of Yingna River Basin. – *Liaoning Urban and Rural Environmental Science and Technology* 17(4): 56-57.
- [30] Lin, Q. (2018): Discussion on abnormal factors of manganese content in Dalian Songshu Reservoir. – *Water Science and Engineering Technology* 2018(02): 73-75.
- [31] Luo, Q. (2021): Comparison of the fatty acid quality of Australian freshwater lobster muscle under three culture modes. – *Journal of Northwest A&F University (Natural Science Edition)* 9: 1-8.
- [32] Liu, W., Zhang, Y., Gao, X., Jia, X. B., Ma, S. Q., Liu, S. S. (2016): Analysis of fish community and water ecological health changes in the Hunhe River Basin from 2010 to 2014. – *Journal of Hydrobiology* 40(05): 968-977.
- [33] Liu, Y., Chen, K., Cai, Y. J., Yin, H. B., Yan, Y. Z. (2018): Application of fish integrity index F-IBI to assess the health of major rivers in the Chaohu Lake Basin. – *China Environmental Monitoring* 34(06): 73-83.

- [34] Lian, Y. X., Li, C., Ye, S. W., Li, W., Liu, J. S., Li, Z. J. (2018): The spatial distribution pattern of fish in Yudong Reservoir on the Yunnan Plateau and its main influencing factors. – *Journal of Lake Science* 30(06): 1755-1765.
- [35] Monroy, M., Maceda-Veiga, A., de Sostoa, A. (2014): Metal concentration in water, sediment and four fish species from Lake Titicaca reveals a large-scale environmental concern. – *Science of the Total Environment* 487: 233-244.
- [36] Ma, X. L., Tan, Y. C., Lin, J. H. (2018): Comparative analysis of heavy metal content in crucian carp and mud carp in different waters of Huizhou City. – *Journal of Huizhou University* 38(03): 29-36.
- [37] Ma, Y. Q., Shi, Y., Qin, Y. W., Zheng, B. H., Zhao, Y. M., Zhang, L. (2014): Spatial and temporal distribution and pollution evaluation of heavy metals in the water environment of the upper reaches of the Hunhe River (Qingyuan section), northeast China. – *Environmental Science* 35(01): 108-116.
- [38] Niu, J. Y., Liu, Z. C. (2015): Talking about the influence of environmental stress on the growth performance of fish. – *Fujian Agriculture* 2015(02): 124.
- [39] Okogwu, O. I., Nwonumara, G. N., Okoh, F. A. (2019): Evaluating Heavy Metals Pollution and Exposure Risk Through the Consumption of Four Commercially Important Fish Species and Water from Cross River Ecosystem, Nigeria. – *Bulletin of Environmental Contamination and Toxicology* 102(6): 867-872.
- [40] Shan, G. (2014): Preliminary study on the ecological environment protection plan of Yingnahe reservoir group. – *Science and Technology Vision* 2014(34): 305+326.
- [41] Shi, N. (2019): Study on the Spatio-temporal Characteristics of Fishes in the National Aquatic Germplasm Resources Conservation Zone of the Four Major Family in Chongqing Section of the Yangtze River. – Chongqing Normal University.
- [42] Tu, Z. C., Pang, J. J., Zheng, T. T. (2017): Enrichment and safety evaluation of fish heavy metals in Poyang Lake Nature Reserve, Wucheng. – *Journal of Hydrobiology* 41(04): 878-883.
- [43] Wang, S. X., Gao, C. X., Tian, S. Q., Dai, X. J. (2014): Composition and diversity analysis of pelagic fish communities in Qingcaosha Reservoir. – *Journal of Shanghai Ocean University* 23(04): 594-601.
- [44] Wang, W. J., Yi, Y. J., Zhang, S. H., Yang, Y. F. (2019): Heavy metal pollution and health risk assessment of fish in the middle and lower reaches of the Yangtze River. – *Water Resources and Hydropower Technology* 50(02): 8-13.
- [45] Wang, X. J., Guo, X. (2021): Research on Comprehensive Evaluation Index System of Water Environment Quality in Qiantang River Basin. – *Jiangsu Science and Technology Information* 38(05): 76-80.
- [46] Wu, X. H., Jiang, X. J., Zhang, B. L. (1999): The effects of several heavy metals on the toxicity and growth of Qingdao Amphioxus. – *Ocean and Limnology* 6: 604-608.
- [47] Wang, D. Q., Gao, L., Duan, X. B. (2019): Preliminary Analysis of the Fish Larvae and Eggs and the Effects of the Eco-operation of Cascade Reservoirs on Fish Propagation in the Lower Hanjiang River. – *Resources and Environment in the Yangtze River Basin* 28(08): 1909-1917.
- [48] Wang, Y. P. (2016): Study on the growth and feeding characteristics of *Pseudorasbora parva*. – Xinyang Normal University.
- [49] Wang, Z., Liu, M., Lin, L. (2021): Spatiotemporal distribution and pollution evaluation of heavy metals in the middle and lower reaches of the Hanjiang River. – *Yangtze River Science News*: 1-9 [2021-03-10].
- [50] Xu, Q. (2013): Distribution characteristics and health risk assessment of heavy metal pollution in freshwater fish in different water bodies. – Shanghai University.
- [51] Xiao, X., Long, J., Zhang, R.Y., Chen, J.A., Zou, Y.H., Wu, Q.S., Wu, J.N. (2019): Diffusion fluxes of heavy metals at the sediment-water interface during summer and winter from AHA Reservoir, Guiyang. – *Chinese Journal of Ecology* 38(05): 1508-1519.

- [52] Xu, C. X., Yang, R. Q., Ba, J. W. (2020): Heavy metal content and health risk assessment of main wild fish in Caohai, Weining, Guizhou Province. – *Southern Journal of Agricultural Science* 51(12): 3040-3048.
- [53] Xue, G. (2020): Distribution and health risk assessment of heavy metals in fish in Taiyuan section of Fenhe River. – Shanxi University.
- [54] Yang, G. R. (1963): Freshwater economic fishes in my country-a brief introduction to the book "Chinese Economic Animal History-Freshwater Fishes". – *Bulletin of Biology* 1963(03): 24.
- [55] Yu, Y. (2013): Study on Heavy Metal Pollution in Fishes at the Initial Stage of the Three Gorges Reservoir. – China Institute of Water Resources and Hydropower Research.
- [56] Yang, Y. R., Yang, X. Y., Li, S. D. (2020): Research progress in exposure assessment of heavy metal pollution in crayfish. – *Agriculture and Technology* 40(17): 129-130.
- [57] Yang, G. M., Wu, G. F., Wang, S. (2018): Countermeasures and suggestions on the protection of water source areas in Dalian - Taking Biliuhe Reservoir and Yingnahe Reservoir as examples. – *Journal of Dalian University* 39(03): 98-101+124.
- [58] Yuan, J. L., Li, M., Yang, Y. J., Xin, J. M., Liu, J. D., Gu, Z. M. (2015): Analysis of fish community diversity and growth characteristics of silver carp and bighead carp in Yankou Reservoir, Yiwu City, Zhejiang Province. – *Journal of Shanghai Ocean University* 24(05): 754-764.
- [59] Yang, J. X., Pan, X. F., Chen, X. Y., Wang, X. A., Zhao, Y. P. (2013): Current status of artificial propagation and release of freshwater fish in China. – *Zoological Research* 34(04): 267-280.
- [60] Yi, X. X., Cai, Z. J., Qin, Z. j., Bao, B. L., Chen, L. J., Gong, X. L. (2021): Interannual changes in fish community structure in Qingcaosha Reservoir, Shanghai. – *Journal of Shanghai Ocean University* 30(04): 664-674.
- [61] Yao, Q. H., Yan, S. A., Lin, Q. (2014): Heavy metal enrichment rules and risk assessment of aquatic products. – *Fujian Journal of Agriculture* 29(05): 498-504.
- [62] Zheng, S. C., Wu, Z. Q., Huang, L. L., Feng, W. L., Shi, R. D., Ding, Y., Chang, X. Z. (2017): Analysis of fish species composition and diversity in Qingshitan Reservoir, Guilin, Guangxi. – *Southern Fisheries Science* 13(02): 36-42.
- [63] Zhao, W., Yin, X. W. (2009): Fishery ecology survey of Yingnahe Reservoir. – *Journal of Dalian Fisheries University* 24(3): 221-222.
- [64] Zhang, X. L., Wang, J. J., Zhao, Y. J., Liu, Y. (2018): Characteristics of heavy metal residues in the muscles of cultured fish on the south bank of the Yellow River in Zhengzhou. – *China Environmental Science* 38(06): 2363-2370.
- [65] Zhou, Y., Wen, S., Chen, M. (2018): Cadmium content and dietary exposure assessment of crayfish sold in Hubei Province. – *Public Health and Preventive Medicine* 29(02): 52-54.
- [66] Zeng, H., Zhang, H., Xiong, X.Y. (2021): Characteristics of heavy metal content and health risk assessment of fish in the interlaced area of Poyang Lake. – *Acta Scientiae Circumstantiae* 41(02): 649-659.
- [67] Zhang, C. (2017): The harm of heavy metals to fish and the prevention and control of pollution. – *Journal of Science & Technology Economics* 11: 114.

IMPACT OF SEASONAL VARIABILITY ON PHENOLOGICAL DEVELOPMENT AND PRODUCTIVITY OF MUNGBEAN (*VIGNA RADIATA* (L.) R. WILCZEK) IN ARID CLIMATIC CONDITION

HUSSAIN, F.^{1,2*} – KHAN, E. A.¹ – BALOCH, M. S.¹ – ULLAH, A.² – KHAKWANI, A. A.¹ – ULLAH, Q.¹

¹*Department of Agronomy, Gomal University of Agriculture, D. I. Khan, Pakistan*

²*Directorate of Agronomy, Ayub Agricultural Research Institute, Faisalabad, Pakistan*

**Corresponding author
e-mail: fiazaari1981@gmail.com*

(Received 4th Dec 2021; accepted 21st Mar 2022)

Abstract. Mungbean is an important legume in arid regions that is under threat due to changing rainfall conditions and temperature fluctuations in the region. These risks can be addressed by optimizing sowing time and selecting the right mungbean cultivars. Therefore, the present study was conducted during summer seasons of 2018 and 2019 to reveal the best sowing time for mung bean genotypes. Experiment was comprised of two factors i.e., sowing dates; 1st April, 15th April, 1st May and 15th May, and genotypes, Bahawalpur-mung-2017, NIAB-mung-2016 and AZRI-mung-2006. NIAB-mung-2016 sown at 1st April during 2018 and 2019 took higher days to complete the phenological stages as well as gave higher viable pollens (79.63 and 73.40%), chlorophyll contents (50.11 and 47.04 $\mu\text{g cm}^{-2}$) number of pods/plant (38.13 and 30.32), number of seed/pod (14.20 and 11.67), 1000-seed weight (53.21 g), grain yield (1856 and 1585 Kg ha^{-1}), biological yield (5940 and 5335 Kg ha^{-1}) and harvest index (31.45 and 28.04%). Likewise higher heat use efficiency, heat thermal unit, relative temperature depression were also recorded when mungbean was sown at 1st April during 2018 and 2019. Hence it is concluded that NIAB-mung-2016 sown at 1st April had the potential to increase mungbean productivity under arid conditions.

Keywords: *mungbean, genotypes, heat stress, phenological stages, productivity*

Introduction

Among all pulses, mungbean (*Vigna radiata* (L.) R. Wilczek) is the crucial legume crop. Its seed contains a variety of nutrients, including 60.4% carbohydrates, 24.20% protein, and 1.30% fat (Imran et al., 2015). Its roots have great ability to capture atmospheric nitrogen which can be fixed in the soil for next crop and helpful for increasing the fertility of soil (Basu et al., 2016; Abdi et al., 2021). In Pakistan, annually 231 thousand hectares area remains under its cultivation and produced 204.5 thousand tons grains with an average production of 0.88 tons ha^{-1} (Government of Pakistan, 2020-21). Punjab is the most prominent mungbean growing province where its cultivation is generally carried out in rainfed zones of thal (arid) region that alone accounted for 88% area and its contribution towards production is 85% of the total mungbean production (Anonymous, 2019). The crop has greater potential, but the average grain yield is very low to its actual potential. The effect of high aerial temperature is the primary cause of low yield in mungbean at the time of flowering and seed setting which lead to flower abortion, poor grain filling. The growing of unapproved mungbean varieties without an optimum sowing time is another reason of low grain yield in mungbean.

Temperature is the most critical variable of climate change effecting mungbean yield. The optimal temperature for mungbean reproductive growth and development is 25-30 °C (Wahid et al., 2007). Rise in 1 °C temperature affects growth (Ullah et al.,

2019) and yield of mungbean and disturbs photosynthetic function in leaves (Hussain et al., 2011). Photosynthesis is halted as a result of decreased chlorophyll production in leaves, and assimilation of carbon fixation slowed as a result of heat stress (Sinsawat et al., 2004). Increase in temperature speed up the phenology period resulting low yield especially at the grain filling stage (Ullah et al., 2018). The mungbean plant produces flowers in cluster of 10-20 on top terminal racemes and various flushes of flower appeared during the cropping season. The mungbean plant loss huge number of flowers under normal situations (Kumari and Varma, 1983) which is exacerbated to high temperature (Tickoo et al., 1996). The growth behavior is indeterminate type and various flushes appeared during its growth cycle but unfortunately rate of flowers abortion increased due to elevated temperature which may rise to 40-45 °C (in late April-May) (Malaviarachchi et al., 2015). The reproductive stage is highly susceptible to high temperatures, leading to the loss of buds, flowers, and pods, all of which have negative impact on seed yield (Awasthi et al., 2014; Kaushal et al., 2013). The effect of increasing temperature can be minimized through variations in sowing times and heat tolerant genotypes of mungbean. Therefore, appropriate sowing time and selection of high potential mungbean cultivars are the best agronomic approaches for enhancing mungbean production under hot and arid environments.

Sowing time is considered as one of the important limiting factors that affect the plant performance and ultimately crop yield (Sadeghipour, 2008). Sowing time influences the productivity of mungbean in terms of growth, production and yield (Soomro and Khan, 2003). Too early mungbean seeding causes poor germination, while too late sowing lowers yields because of unfavorable growth and development environment (Hussain et al., 2004) particularly during reproductive phase. In addition, the infestation of insect pests is also higher in both early and late sowing than in the middle. Therefore, optimum time of sowing plays crucial role for enhancing grain yield of timely sown crop (Rathore et al., 2010). Optimal sowing time confirms greater balance and relationship between the weather and plant, resulting in a higher seed yield.

The plants dry matter production is not only dependent on the sowing atmosphere, but also on the genetic potential of varieties, with few varieties having a greater response to translocate assimilates towards the economic part of the plant due to differential potential of various varieties (Reddy, 2009). Economic yield and crop phenology may influence due to variation in sowing times and genotypes. Each variety has own time of sowing period and regional variability also present due to inimitable agro-ecological conditions (Sarkar et al., 2004). To get greater seed yield, specific sowing times may vary for various mungbean genotypes (Reddy, 2009). Therefore, determination of optimum sowing time is inevitable for mungbean crop which may differ from season to season and variety to variety due to difference in agroecological conditions which determines the vegetative, reproductive and maturity periods (Soomro and Khan, 2003).

At present, in major production region (Punjab) early sowing of mungbean lead to excessive vegetative growth and poor germination due to low temperature coinciding rainfall in spring season, while delay in planting reduces the maturity period due to increasing temperature (Hussain et al., 2004). The key reasons for this crop's low yield include improper sowing time and the use of tradition low potential cultivars (Ansari et al., 2000). So, there is dire need to guide mungbean growers for ideal time of sowing and suitable genotypes to get higher yield. Mungbean yield can be increased to a greater

extent by optimization of newly high yielding varieties that can be planted at the right time. Therefore, the present study was conducted to find out optimum sowing time and suitable mungbean cultivar under arid conditions. Different agrometeorological indices provide a reliable forecast for crop yield (Prakash et al., 2017). Thus, specific objective of the study was to optimize mungbean cultivars with specific sowing environment to increase productivity of mungbean.

Materials and methods

Experimental site and weather

The field experiments were conducted at Agronomic Research Station, Karor Lal Eason-Layyah, Pakistan during summer season 2018 and 2019. It is situated at longitude 70°58 E, latitude 31°13', North, with an altitude of 158 meters above sea level. The climate of the region is very hot and temperature reached at peaks in summer, the maximum temperature (46.0 °C, 45.5 °C) and in winter temperature goes to (2.5 °C and 2.6 °C) during the growing year 2018 and 2019 respectively. The mean maximum (40.31 °C and 40.50 °C) and mean minimum temperature was 19.44 °C and 19.20 °C during both seasons respectively. The total rainfall of 117.0 mm and 166.7 mm was received during the cropping season of 2018 and 2019, respectively (Fig. 1).

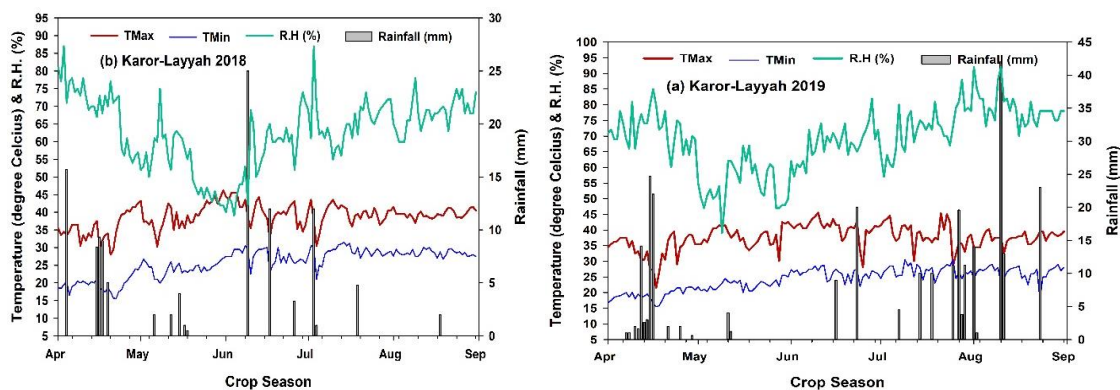


Figure 1. Seasonal daily weather conditions during the crop season 2018 and 2019

Soil properties

The soil samples were taken with the help of soil twist drill up to 15 and 30 cm soil layers for physic-chemical properties (Table 1). The soil of the study area was sandy loam in texture having (pH = 8.5), low in organic carbon, medium in total nitrogen, phosphorus, and potassium and low in organic matter less than 0.5% (Table 1).

Experimental design and treatments

Three mungbean varieties (Bahawalpur (BWP)-mung-2017, NIAB-mung (NM) - 2016 and AZRI-mung-2006) and four sowing dates (1st April, 15th April, 1st May, 15th May) were laid out in split plot design having three replications. In the main plots, the varieties were randomized, while the sowing dates were divided into sub-plots. The mungbean seed was sown with maintaining a spacing of 10 cm between the plants and 30 cm between rows. The individual experimental plot size was 6 m × 1.8 m having an

area of 10.8 m² with 6 rows (lines). Seed rate of 30 kg ha⁻¹ was used for sowing the experiment and total number of plants were 400000 ha⁻¹. After successful stand establishment thinning was done to maintain healthy plants whereas plant and row spacing was maintained 10 cm and 30 cm, respectively. In each line there were 60 plants and a total of 360 plants per plot were maintained after thinning.

Table 1. Soil characteristic of experimental sites

Year	Depth (cm)	Sand %	Silt %	Clay %	SOC* %	Ec** dSm ⁻¹	pH 1:1	***SAR	Texture	N**** gkg ⁻¹	P***** ppm	K***** ppm
2018	0-15	51.3	31.5	14.6	0.48	0.30	8.3	1.16	Sandy loam	0.38	13.26	106
	15-30	50.2	30.5	15.2	0.40	0.35	8.5	1.18	Sandy loam	0.36	8.16	82
2019	0-15	52.4	31.0	14.4	0.46	0.38	8.2	1.04	Sandy loam	0.40	7.82	113
	15-30	52.2	31.2	15.0	0.35	0.42	8.5	1.06	Sandy loam	0.37	5.10	77

*Soil organic carbon, **Electrical conductivity, ***Sodium absorption ratio, ****Nitrogen, *****Phosphorus, *****Potash

Crop husbandry

Before the sowing of the experiment, land was prepared with one rotavator followed by two cultivations. Pre-soaking irrigation was applied to attain suitable moisture for sowing. The recommended dose of nitrogen and phosphorus at rate of 22-57-0 NPK kg ha⁻¹ in the form of urea and diammonium phosphate (DAP) was given to the crop before sowing at the time of seed bed preparation. The soil was not deficient in K; so potash was not applied. The post sowing irrigation was given when required especially at critical stages of the crop at flowering, pods, and grain formation stages. Pre-emergence weedicide S-metachlor at rate of 2.0 L ha⁻¹ was applied and two hoeings with an intervals of 20 and 40 days after sowing were done to keep the plots weed free during the entire crop growth period. For plant protection measures, one application of imidacloprid (Confidor) insecticide at rate of 625 ml ha⁻¹ against sucking insects and two application of Perfenophos and Cypermethrein (Polytrin-C) at rate of 1.5 L ha⁻¹ were sprayed against chewing insects. The crop was harvested when 80-90% pods were fully matured and turned their color from green to dark black.

Observations

Crop phenology

Data regarding various phenological stages (days to emergence, days to 50% flowering, pod formation and maturity of mungbean crop) were observed based on visual observations. Ten plants were tagged and observed on daily basis. Each stage was considered and recorded when 50 percent of ten tagged plants reached that stage.

Agro-meteorological indices

The various temperature base meteorological indices such as Growing degree days (GDD), Helio-Thermal Unit (HTU), Photo-Thermal Unit (PTU), Relative Temperature Depression (%) and Temperature base Use Efficiency (HUE) were calculated by adopting the procedures mentioned by Rajput et al. (1987) and

Nuttonson (1955). The various agrometeorological indices were determined by following methods.

1. Growing degree days (degree days hours)

Growing degree days (GDD) were premeditated by considering 10 °C as base temperature by using *Equation 1*:

$$GDD = \frac{(T_{max} + T_{min})}{2} - T_b \quad (\text{Eq.1})$$

where T_b = Base temperature, T_{max} = Temperature maximum, T_{min} = Temperature minimum.

2. Helio-thermal unit (degree-days hours)

Helio-thermal unit was calculated on the basis of growing degree days (GDD) and actual sunshine hours by *Equation 2*:

$$HTU = GDD \times \text{Duration of sunshine hours} \quad (\text{Eq.2})$$

where GDD = Growing degree days

3. Heat use efficiency (kg ha⁻¹ degree days)

Heat use efficiency was calculated with the help of seed yield (kg ha⁻¹) per growing degree days (GDD) with the help of *Equation 3*:

$$HUE = \text{Seed yield (kg ha}^{-1}\text{)} / GDD \quad (\text{Eq.3})$$

4. Relative temperature depression (%)

Relative temperature depression was calculated using *Equation 4*:

$$RTD = \sum \frac{T_{max} - T_{min}}{T_{mean}} \quad (\text{Eq.4})$$

where T_{max} = Temperature maximum, T_{min} = Temperature minimum.

Yield and yield traits

At harvest, data regarding plant height, number of branches per plant, and pods per plant were collected from ten randomly selected plants in each plot and averaged. Pod length was measured by selecting twenty randomly selected pods per plot and averaged. Twenty pods per plot were selected to record data on grains per pod. When crop attained 90 percent physiological maturity, whole plants from the six central rows of net plot area (6 m × 1.8 m = 10.8 m²) were manually harvested, sundried for 24 h and weighed for biological yield. Sundried plants were threshed to calculate grain yield, and harvest index was calculated by dividing grain yield into biological yield. From the grains produced in each plot, 1000-seeds were counted and weighed to express 1000-seed weight.

Pollen viability (%)

On 21 days after flowering, pollen viability was determined using Iodine Starch Test method (Chang et al., 2014). For each treatment, pollen was collected between 9:00 and 11:00 a.m. from four to five fresh flowers from three tagged plants. The percentage of viable and non-viable pollen grain were determined as described by Patriyawaty et al. (2017).

Chlorophyll contents ($\mu\text{g cm}^2$)

Chlorophyll contents were measured in each plot on three fully expanded leaves of three randomly selected plants at 20 days after flowering in each treatment. The chlorophyll meter (Minolta SPAD-502 meter) was used to determine chlorophyll density in the leaves.

Statistical analysis

The parameters under investigation were statistically analyzed using a split-plot design with three replications. The various variables of sowing dates and genotypes were statistically analyzed using Fisher's analysis of variance techniques. The variations between treatment means were compared using the Honest Significant Difference (HSD) test at a 5% probability level (Steel et al., 1997). Statistix version 8.1 software computer base was used to done the statistical analysis (Statistix, analytical Software, USA, 1985- 2003).

Results

Phenological parameters

Phenology parameters (days to maturity, days taken to 50% flowering, days to 50% podding, days to emergence) were significantly influenced by sowing dates and genotypes during both years of study. There was significant reduction in all phenology parameters with delayed sowing of mungbean from April 15th up to May 15. Early sown mungbean (1st April) took significantly higher number of days to physiological maturity, days taken to 50% flowering and podding stages i.e. (75.0-77.0, 49.0-50.33 and 39.0-42.27) respectively, during 2018 and 2019, while delay in sowing (15th of May) took 6.7 and 9.0% less number of days to complete all phenological stages during 2018 and 2019 respectively, as compared to early sowing. Variation in all phenological stages were found significant among genotypes. In case of genotypes, the variety AZRI-mung-2006 took higher number of days taken to maturity, days to 50% flowering and days to 50% podding stages i.e. (75.0-76.0, 39.0-43.0 and 49.0-50.0) during both period of study respectively, while variety BWP-mung-2017 took least number of days to maturity, days to 50% flowering and podding stages due to early maturing behaviour (Table 2).

Agrometeorological indices

The agrometeorological indices (GDD, HTU, HUE, RTD) were significantly affected by sowing times and genotypes. The results of various agrometeorological indices elucidated that sowing of mungbean crop on 15th May accumulated the highest GDD (1684 and 1545) than that of May 1st, April 15th and April 1st up to maturity

during the year 2018 and 2019. The sowing of crop on May 1st showed higher GDD as compared to the April 15th and April 1st sowing during both periods of study. The May 15th sowing accumulated (5.3, 7.9 and 10.5%) and (1.2, 3.3 and 5.7%) higher GDD as compared to 1st May, 15th April and 1st April sowing respectively, during both years. This may be due to progressive increase in temperature with delayed sowing (*Table 1*). Similarly, the grain heat use efficiency (HUE) was the highest for April 1st sowing followed by April 15th but significantly higher than sowing on 1st and 15th May and minimum heat use efficiency was recorded in May 15 sowing during both years. It might be due to less grain yield under late sowing. The HTU available to the crop was the highest for April 1st sown crop which was significantly higher than sowing of crop on 15th April, May 1st and May 15 sowing whereas lowest HTU was recorded in 15th May sown crop during the year 2018 and 2019. On the basis of 2-year data, the HTU recorded in April 1st sowing crop were (12.5, 29.8 and 35.3%) and (0.1, 15.5 and 27.7%) higher than April 15th, May 1st and May 15 sowing, respectively. Likewise, higher relative temperature depression 8.1% was noted in 1st April sown crop which was significantly greater than remaining three sowing dates whereas minimum RTD was recorded in 15th May sown crop i.e. 4.6% during the period 2019 and results for the year 2018 was non-significant.

Table 2. Impact of temperature variability and genotypes on phenological stages of summer mungbean

Treatment	Days to emergence		Days taken to 50% flowering		Days taken to 50% podding		Days taken to maturity	
	2018	2019	2018	2019	2018	2019	2018	2019
Sowing dates								
1 st April	12a	11a	39.00a	42.27a	49.00a	50.33a	75a	77a
15 th April	11a	10ab	37.44ab	41.00a	47.00ab	48.30b	73ab	74b
1 st May	10b	10b	36.00bc	39.00b	45.11b	46.00c	72b	71bc
15 th May	9b	9c	34.00c	37.11b	43.00c	44.00c	70b	70c
SEm ±	0.44	0.35	0.77	0.59	0.64	0.56	0.87	0.85
Tukey HSD (P = 0.05)	1.24	0.99	2.16	1.66	1.80	1.57	2.46	2.40
Genotypes								
BWP-2017	9 b	10 b	33.25 c	36.00 c	43.00 c	44.25 c	70 c	69 c
NM-2016	10 a	11 a	37.00 b	40.25 b	46.00 b	47.42 b	72 b	73 b
AZRI-2006	11 a	12 a	39.00 a	43.17 a	49.00 a	50.00 a	75 a	76 a
SEm ±	0.26	0.18	0.44	0.30	0.51	0.42	0.17	0.81
Tukey HSD (P = 0.05)	0.92	0.66	1.56	1.05	1.79	1.51	0.59	2.89
Interaction	NS	NS	NS	NS	NS	NS	NS	NS

In case of genotypes, the higher GDD up to maturity (1613 and 1546), and HTU (14154 and 13619) was showed by genotype AZRI-mung-2006 and minimum GDD and HTU was recorded in genotypes BWP-mung-2017 respectively during 2018 and 2019. Similarly, the greater HUE (0.88 and 0.85 kg ha⁻¹) was shown in NIAB Mung-2016 as compared to other genotypes. The lower HUE (0.56 and 0.54 kg ha⁻¹) was recorded in

BWP-mung-2017. The genotypes showed non-significant results in case of relative temperature depression (Table 3).

Table 3. Impact of temperature variability and genotypes on accumulated growing degree days (GDD), helio-thermal unit (HTU), heat use efficiency (HUE), relative temperature depression (RTD) on mungbean

Treatment	GDD (°C days) Up to maturity		HTU (°C days) Up to maturity		HUE (kg ha ⁻¹)		RTD (%)	
	2018	2019	2018	2019	2018	2019	2018	2019
Sowing dates								
1 st April	1507	1457	13877	14382	0.93	0.89	5.76	8.1
15 th April	1550	1494	12130	14361	0.79	0.74	5.78	7.3
1 st May	1595	1526	9733	12142	0.68	0.65	5.67	6.3
15 th May	1684	1545	8973	10396	0.57	0.57	5.22	4.6
SEm ±	16.90	25.43	1643.0	1273.3	0.023	0.024	0.43	0.81
HSD at 5%	35.50	53.42	3451.8	2675.1	0.04	0.05	NS	1.7
Genotypes								
BWP-2017	1540	1450	8527	11637	0.56	0.54	5.81	6.7
NM-2016	1598	1520	10221	13206	0.88	0.85	5.51	6.4
AZRI-2006	1613	1546	14154	13619	0.78	0.75	5.01	6.6
SEm ±	8.27	14.86	2081.0	860.5	0.022	0.021	0.32	0.45
HSD at 5%	22.97	41.26	5777.9	NS	0.062	0.059	NS	NS
Interaction	NS	NS	NS	NS	NS	NS	NS	NS

Yield and yield attributes

Sowing dates and genotypes markedly influenced seed yield, biological yield and all yield components of mungbean during both period of experimental study (Table 4). However, the interactive effect was also significant in all yield related attributes except in plant height and number of pods bearing branches (Table 5). In case of interaction results, the significant reduction was noted in seed yield with delayed sowing from 15th April upto 15th May. Early sowing (1st April) of NIAB-mung 2016 produced higher seed yield (1856 and 1585 kg ha⁻¹) during 2018 and 2019 followed by sowing on 15th April with same variety during both growing seasons and its particular increase over 15th of April, 1st of May and 15th of May sowing were 22.18, 37.58 and 81% during 2018, whereas during 2019 the corresponding values were 17.84, 40.63 and 64.24% respectively. However, lowest seed yield (773.3 and 681.8 kg ha⁻¹) was obtained with BWP-mung-2017 on 15th May during 2018 and 2019 seasons respectively. Significant variation in biological yield was seen among sowing time and different varieties during both years of study as 1st April NIAB-mung 2016 sown produced highest biological yield (5904 and 5335 kg/ha, during 2018 and 2019 respectively) than that of biological yield of other sowing dates and varieties. The 15th May sowing of BWP-mung-2017 gave minimum biological yield i.e. 3477 and 3144 kg ha⁻¹ during 2018 and 2019, with a decrease of 23.4 and 24.8% over 1st April sowing of BWP-mung-2017 during both year respectively.

Table 4. Impact of temperature variation and genotypes on yield and yield attributes of mungbean

Treatment	Plant height at harvest (cm)		Branches plant ⁻¹ (Nos.)		Pods plant ⁻¹ (Nos.)		Seed pods ⁻¹ (Nos.)		Pod length (cm)		1000-seed. wt (g)		Harvest index (%)		Biological yield (kg ha ⁻¹)		Seed yield (kg ha ⁻¹)		
	2018	2019	2018	2019	2018	2019	2018	2019	2018	2019	2018	2019	2018	2019	2018	2019	2018	2019	
Sowing Dates																			
1 st April	62.00 a	54.67 a	11.83 a	9.43a	30.92 a	26.13 a	12.26 a	9.47a	9.11 a	8.19 a	48.16 a	46.50 a	28.32 a	26.0 a	5305 a	4879 a	1512.9 a	1340 a	
15 th April	59.16 ab	53.13 ab	9.97 b	8.59 b	27.67 ab	24.12ab	10.20 b	8.37 b	8.36 b	7.57 b	46.06 ab	44.69 a	27.16 a	24.15 ab	4817.23 b	4482 b	1309.5 b	1130 b	
1 st May	57.10 ab	51.28 b	9.48 bc	7.73 c	26.98 ab	21.77 bc	9.53 bc	7.61 bc	7.81 c	7.39 b	43.57 b	39.18 b	24.39 b	22.61 bc	4582.05 c	4229 bc	1129.4 c	1030 b	
15 th May	56.00 b	51.16 b	8.44 c	7.06 d	23.68 b	20.12 c	8.48 c	6.94 c	7.69 c	6.37 c	40.69 c	37.12 b	22.50 c	21.28 c	4161.68 d	3978 c	934.3 d	896 c	
SEm ±	1.70	1.14	0.35	0.18	1.80	0.95	0.46	0.31	0.35	0.17	0.92	0.97	0.88	1.11	163.9	105.6	37.53	34.44	
Tuckey HSD at 5 %	4.84	3.22	1.29	0.51	5.07	2.69	1.30	0.45	0.26	0.48	2.59	3.0	1.21	2.32	228.70	221.76	102.00	106.88	
Genotypes																			
BWP-2017	65.60 a	59.33 a	8.09 c	7.11 c	20.91b	18.37 c	8.10 c	6.45 c	7.16 c	6.51c	36.95b	36.69 c	23.21 b	20.78 b	4011.87 c	3539 c	979.50 c	828 c	
NM-2016	59.00 b	50.82 b	11.94 a	9.38 a	33.38 a	26.86 a	12.50 a	9.98 a	9.23 a	8.02 a	51.0 a	47.07 a	26.95 a	25.18 a	5285.48 a	4979 a	1437.42 a	1310 a	
AZRI-2006	52.47 c	47.53 b	9.76 b	8.13 b	27.65 a	23.52 b	9.80 b	7.88 b	8.35 b	7.63 b	45.88 c	41.85 b	25.62 ab	24.57 a	4852.84 b	4657 b	1247.71 b	1159 b	
SEm ±	1.36	1.46	0.66	0.09	1.76	0.61	0.32	0.35	0.31	0.07	0.50	1.09	0.68	0.80	106.4	67.98	36.61	37.81	
Tuckey HSD at 5%	4.80	5.20	0.78	0.30	6.26	2.18	1.13	0.65	0.23	0.23	1.77	3.46	1.68	2.22	134.95	188.74	130.5	123.0	

Table 5. Interactive effects of temperature variation and genotypes on yield and yield attributes of mungbean

Treatment	Pods plant ⁻¹ (Nos.)		Seed pods ⁻¹ (Nos.)		Pod length (cm)		1000-seed. wt (g)		Harvest index (%)		Biological yield (kg ha ⁻¹)		Seed yield (kg ha ⁻¹)	
	2018	2019	2018	2019	2018	2019	2018	2019	2018	2019	2018	2019	2018	2019
Interaction SD×V														
V1×SD1	23.55 bc	20.45 cdef	9.77 bc	7.40 de	7.53 d	7.53 bcd	37.08 ef	39.36 bcd	26.19 cd	23.08 def	4538.5 e	4178.0f	1188.4 def	1087.5 c
V1×SD2	19.33 c	18.97 def	8.27 c	6.50 efg	7.20 de	6.83 de	36.81 ef	37.92 cd	27.13 bc	21.00 fg	4246.3 f	3564.8 g	1151.0 efg	888.2 d
V1×SD3	21.11 bc	18.56 ef	8.00 c	6.13 fg	7.00 e	6.20 ef	39.58 def	35.14 d	21.27 f	19.99 gh	3785.7 g	3273.1gh	805.3 h	739.4 e
V1×SD4	19.66 c	16.93 f	7.13 c	5.77 g	6.93 e	5.47 f	34.35 f	34.35 d	22.25 ef	18.99 h	3477.0 h	3144.7 h	773.3 h	681.8 e
V2×SD1	38.13 a	30.32 a	14.20 a	11.67 a	10.40 a	8.70 a	53.21 a	53.21 a	31.46 a	28.04 a	5904.9 a	5335.8 a	1856.0 a	1585.8 a
V2×SD2	34.50 ab	28.29 ab	13.47 a	10.30 b	9.00 bc	8.27 ab	57.03 a	52.46 a	28.95 b	26.54 abc	5246.9 bc	5122.5 ab	1519.2 b	1345.4 b
V2×SD3	32.46 abc	25.37 abc	12.41 ab	9.47 bc	8.80 c	8.00 abc	47.26 b	42.31 bcd	25.98 cd	24.76 cd	5197.4 c	4881.2 bc	1349.2 cd	1127.9 c
V2×SD4	28.45 abc	23.48 bcde	9.60 bc	8.50 cd	8.70 c	7.10 cde	46.62 bc	40.31 bcd	21.40 ef	21.32 efg	4792.8 d	4571.6 cd	1025.3 fg	965.0 d
V3×SD1	31.10 abc	27.64 ab	12.97 a	9.33 bc	9.41 b	8.33 ab	54.20 a	46.93 ab	27.31 bc	26.77 ab	5474.6 b	5126.3 ab	1494.3 bc	1487.7 a
V3×SD2	29.15 abc	25.09 abcd	9.40 bc	8.30 cd	8.91 c	8.23 ab	44.35 bcd	43.70 bc	25.39 cd	25.01 bcd	4958.5 d	4753.7 cd	1258.3 de	1147.3 c
V3×SD3	27.41 abc	21.38 cdef	8.69 c	7.33 def	7.63 d	7.34 bcd	43.89 bcd	40.08 bcd	25.91 cd	23.37 d	4763.0 de	4533.9 de	1233.9 de	1128.4 c
V3×SD4	22.94 bc	19.96 cdef	8.67 c	6.53 efg	7.47 d	6.60 de	41.09 cde	36.70 cd	23.84 de	23.25 de	4215.2 f	4221.9 ef	1004.3 g	950.6 d
Tukey HSD (p = 0.05)	11.60	6.15	2.98	1.02	0.46	1.10	5.92	7.08	2.10	3.24	224.65	326.27	146.38	137.60

V1: BWP-mung-2017, V2: NIAB-mung-2016, V3: AZRI-mung-2006, SD1: 1st April, SD2: 15th April, SD3: 1st May, SD4: 15th May

Variation among all yield attributes regarding sowing times and genotypes found to be significant in mungbean during both period of years (Table 4). However, the interactive effect of sowing time and genotypes was also significant during both study period (Table 5). The NIAB-mung-2016 sown on 1st April recorded significantly higher number of pods/plants (38.13 and 30.32), number of seeds/pod (14.20 and 11.67), pod length (10.40 and 8.70 cm), 1000 seed weight (53.21 g in both seasons) and harvest index (31.46 and 28.04%) during 2018 and 2019 respectively. Sowing of NIAB-mung-2016 on 15th April also gave higher yield components values than that of AZRI-mung-2006 and BWP-mung-2017 compared to other sowing dates. Furthermore, sowing of BWP-mung-2017 on 15th May produced significantly lower pod length (6.93 and 5.47 cm), pods per plant (19.66 and 16.93), seeds per pod (7.13 and 5.77), 1000-seed weight (34.35 g in both seasons), and harvest index (22.25 and 18.99) during 2018 and 2019 respectively as compared to other sowing dates and genotypes.

Physiological parameters

Pollen viability (%)

The results presented in Figure 2 revealed that pollen viability percentage statistically differed between sowing dates, genotypes and their interaction during 2018. The maximum viable pollen percentage (79.63%) was found in 1st April sowing by variety NM-2016 followed by AZRI-mung-2006 that produced 78.75% which was statistically at par with 15th April and 1st May date of sowing. The minimum pollen viability (45.47%) was recorded in BWP-mung-2017 which was sown on 15th May. During the second year 2019 (Fig. 3), the pollen viability was significantly influenced by varieties and sowing dates. In case of sowing dates, early sown crop gave maximum pollen viability (73.40%) followed by 15th April that produced (66.90%) viable pollen. The minimum (57.68%) pollen viability was recorded when crop was sown on 15th May under late sowing date. Among varieties, the variety NIAB Mung-2016 gave maximum pollen viability (75.71%) and lowest value (51.38%) were observed by variety BWP- mung-2017.

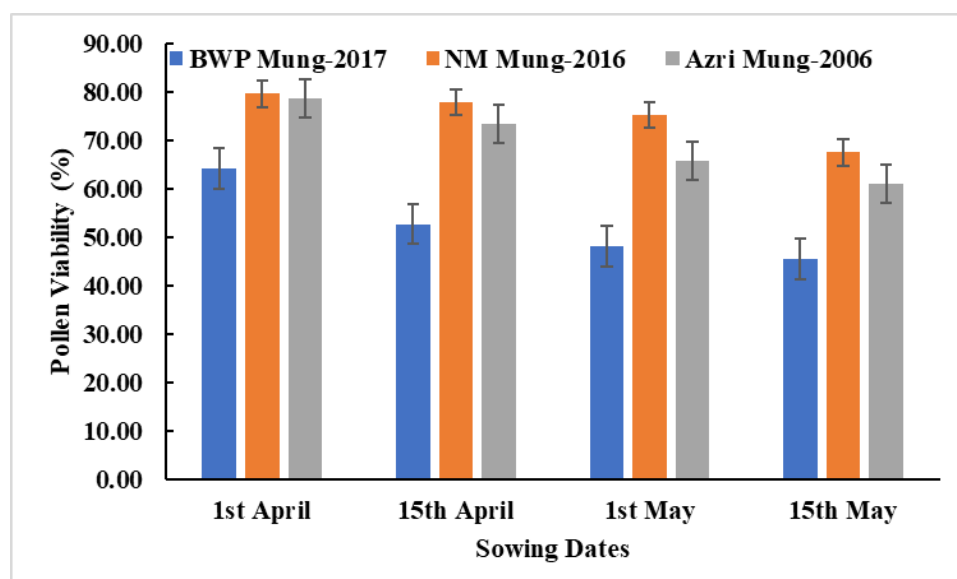


Figure 2. Impact of sowing dates on pollen viability of mungbean cultivars during 2018 growing season

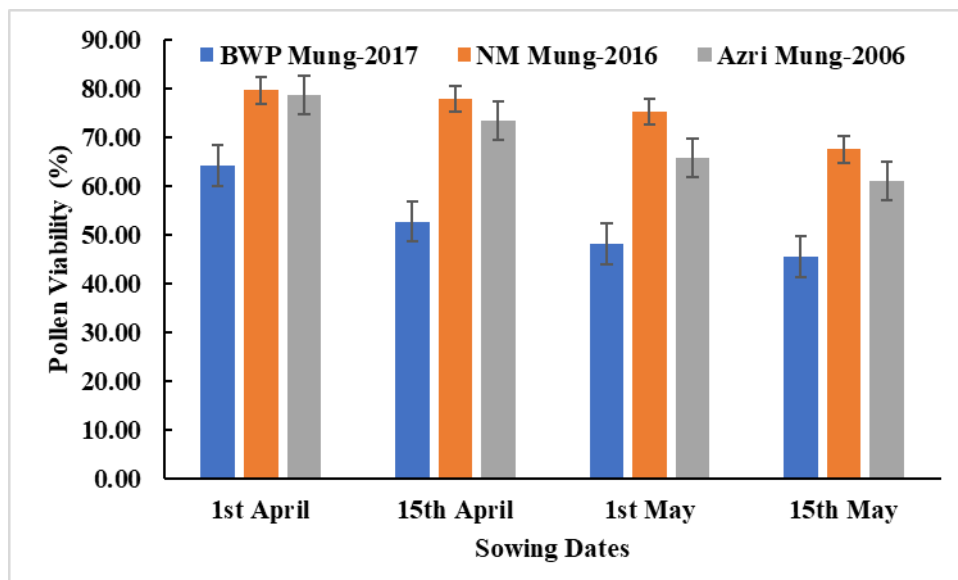


Figure 3. Impact of sowing dates on pollen viability of mungbean cultivars during 2019 growing season

SPAD chlorophyll contents ($\mu\text{g cm}^2$)

It is evident from *Figures 4 and 5* that significant variations among genotypes, date of sowings as well as their interaction was recorded regarding chlorophyll contents during both period of study. The results for the year 2018 and 2019 showed that the greater chlorophyll contents (50.11 and 47.04) were noted in variety NIAB Mung-2016 followed by variety AZRI-mung-2006 when sown on 1st April and decline in chlorophyll content was seen due to elevated temperature in late sowing. While, lowest value of chlorophyll contents (42.44 and 41.92) were recorded in BWP-mung-2017 with sowing date of 15th May.

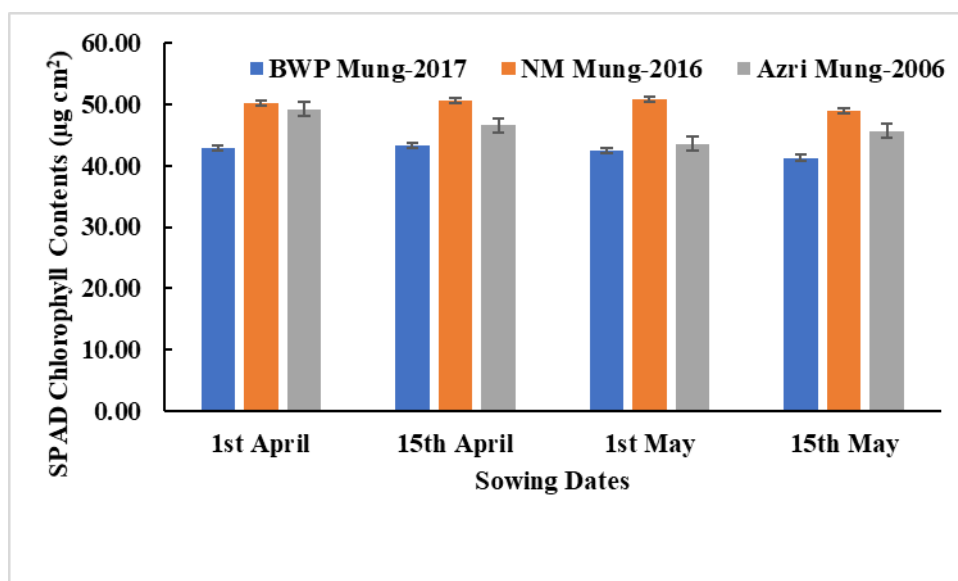


Figure 4. Impact of sowing dates on chlorophyll contents of mungbean cultivars during 2018 growing season

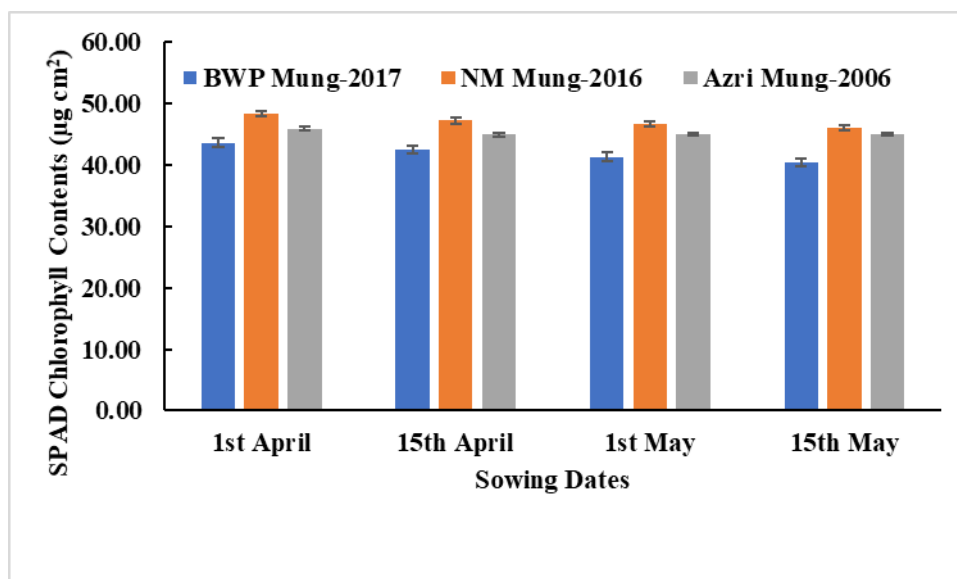


Figure 5. Impact of sowing dates on chlorophyll contents of mungbean cultivars during 2019 growing season

Discussion

Results of the two years study confirmed our hypothesis that sowing dates and genotypic variations have remarkable impact on mungbean phenological development, yield, and yield attributes. The total time available for plants to complete various phenophases in life, and morphological and physiological improvements in plants are greatly affected by temperature and photoperiod which are directly correlated with sowing time variations (Ullah et al., 2020). Mungbean sown on 15th May had minimum time to complete phenological traits due to accumulation of highest growing degree days (GDD) for crop growth because of rise in temperature (*Fig. 1; Table 3*). Similar findings were also observed by Singh et al. (2019) who stated that reduction in duration of green gram due to late sowing might be because of early fulfillment of thermal unit requirement due to increase in temperature (*Table 2*). Whereas 1st April sown mungbean had maximum time to reach at phenological stages because of lowest accumulation of GDD. Among mungbean cultivars, BWP-mung-2017 had least time to attain crop developmental stages and in AZRI-mung-2006 increased time to reach each crop phenological stage was due to their genetic make-up (Miah et al., 2009; Singh and Singh, 2015).

Thermal indices such as Helio thermal unit, Heat use efficiency, Relative temperature depression were highest in 1st April sown mungbean and were lowest in 15th May crop because of long duration to attain maturity (*Table 3*) and relatively low temperature (*Fig. 1*) compared with each succeeding late in sowing with reduced thermal indices requirement (Singh and Singh, 2015). Significantly higher HTU with early sown mungbean were also reported by Kiran and Bains (2007), Sheoran and Pal (2007) and Singh et al. (2010).

The reason for significantly higher seed yield with early sown crop (1st April) was probably due to greater plants height, maximum number of pods/plants, seed/pod and 1000 seed weight compared to other sowing times (*Table 4*). High expression of growth and yield parameters in early planted crop was due to favorable environment for growth

(Singh and Sekhon, 2007; Singh et al., 2010; Singh and Singh, 2015) which enhanced physiological activities such as percent increase in chlorophyll contents (Figs. 4 and 5) and increased pollen viability (Figs. 2 and 3). Therefore, early sown crop utilized best temperature and produced greater viable pollen percentage with yield advantage as compared to delayed sowing.

Similarly, highest growth and yield parameters in NIAB-Mung-2016 were because of high chlorophyll concentration (Figs. 4 and 5) and increased pollen viability (Figs. 2 and 3), which revealed that NIAB-Mung-2016 has the potential to perform under stress environment. Kaur et al. (2015) also revealed variation in chlorophyll concentration and pollen viability in mungbean genotypes under stress or elevated temperatures. Similar variation among mungbean genotypes in respect of yield attributes was also confirmed by Miah et al. (2009), Sarkar et al. (2004), Sadeghipour (2008), Singh et al. 2019 and Dhaka et al. (2018). Variation in sowing dates and genotypes was found to be significant regarding pollen viability under normal and delay planting in mungbean (Chand et al., 2018).

Conclusion

It can be concluded from the findings that grain yield, yield attributes, phenology and yield based on thermal indices significantly affected on early and late planting of mungbean cultivars. The early sowing (1st of April) produced higher grain yield and physiologically performed well. Under delayed sowing of mungbean after 1st May, crop maturity might overlap with high temperature and early monsoon which ultimately resulted in less grain yield. The genotype NIAB-Mung-2016 was found more suitable due to significantly higher yield and high heat use efficiency as compared to BWP-Mung-2017 and AZRI-mung-2006. Therefore, it is recommended that for getting higher grain yield and better thermal energy utilization, mungbean genotype NIAB-Mung-2016 can be sown during 1st and 3rd week of the April in arid climatic conditions. However, detailed studies are required to investigate the root architecture, genetic expression and other biochemical parameters of mungbean crop in arid conditions.

REFERENCES

- [1] Abdi, N., Labuschagne, M., Ullah, A., Hemissi, I., Biljon, A. V., Hachana, A., Sifi, B. (2021): Legume-rhizobia symbiosis under abiotic constraints: performance system. – *Agrociencia* 55(2): 37-61.
- [2] Anonymous (2019): Pakistan Economic Survey, 2018-19. – Finance Division Government of Pakistan, Islamabad.
- [3] Ansari, A. H., Kakar, A. A., Tareen, A. B., Barecht, A. R., Kakar, G. M. (2000): Planting pattern and irrigation level effects on growth, yield components and seed yield of soybean (*Glycine max* L.). – *Pakistan Journal of Agricultural Science* 4: 37-61.
- [4] Awasthi, R., Kaushal, N., Vadez, V., Turner, N. C., Jens Berger, J., Siddique, K. H. M., Nayyar, H. (2014): Individual and combined effects of transient drought and heat stress on carbon assimilation and seed filling in chickpea. – *Functional Plant Biology* 41: 1148-1167.
- [5] Basu, P. S., Singh, U., Kumar, A., Praharaj, C. S. (2016): Climate change and its mitigation strategies in pulses production. – *Indian Journal of Agronomy* 61: 71-82.

- [6] Chand, G., Nandwal, A. S., Kumar, N., Devi, S., Khajuria, S. (2018): Yield and physiological responses of mungbean *Vigna radiata* (L.) Wilczek genotypes to high temperature at reproductive stage. – *Legume Research* 41(4): 557-562.
- [7] Chang, F., Zhang, Z., Jin, Y., Ma, H. (2014): Cell Biology Analyses of Anther Morphogenesis and Pollen Viability Arabidopsis and Rice. – In: Riechmann, J. I., Wellmer, F. (Eds.), *Flower Development: Methods and Protocols, Methods in Molecular Biology*. Springer Science + Business Media, New York, pp. 203-216.
- [8] Dhaka, A. K., Singh, K., Kumar, S., Singh, B., Bhatia, J. K., Kumar, N. (2018): Thermal energy utilization in mungbean (*Vigna radiata* L.) as influenced by sowing times and genotypes. – *Legume Research* 1-6. DOI: 10.18805/LR-3993.
- [9] Govt. of Pakistan (2020-21): *Economic Survey of Pakistan 2020-21*. – Ministry of Food, Agriculture and Livestock, Finance Division. Economic Advisor Wing, Islamabad, Pakistan.
- [10] Hussain, A., Khalil, S. K., Khan, S., Khan, H. (2004): Effect of sowing time and variety on grain yield mungbean. – *Sarhad Journal of Agriculture* 20: 481-484.
- [11] Hussain, F., Malik, A. U., Haji, M. A., Malghani, A. L. (2011): Growth and yield response of two cultivars of mungbean (*Vigna radiata* L.) to different potassium levels. – *Journal of Animal and Plant Sciences* 21(3): 622-625.
- [12] Imran, H., Khattak, I., Rehman, A., Ahamd, U., Zada, F., Naveed, S. (2015): Roots nodulation, yield and yield contributing parameters of mungbean cultivars as influenced by different phosphorous level in Swat-Pakistan. – *Journal of Pure and Applied Biology* 4: 557-567.
- [13] Kaur, R., Bains, T. S., Bindumadhava, H., Harsh, N. (2015): Responses of mungbean (*Vigna radiata* L.) genotypes to heat stress, effects on reproductive biology, leaf function and yield traits. – *Journal of Scientia Horticulturae* 197: 527-541.
- [14] Kaushal, N., Awasthi, R., Gupta, K., Gaur, P., Siddique, K. H. M., Nayyar, H. (2013): Heat-stress induced reproductive failures in chickpea (*Cicer arietinum* L.) are associated with impaired sucrose metabolism in leaves and anthers. – *Functional Plant Biology* 40: 1334-1349.
- [15] Kiran, R., Bains, G. S. (2007): Thermal time requirement and heat use efficiency in summer green gram. – *Journal of Agrometeorology* 9(1): 96-99.
- [16] Kumari, P., Varma, S. K. (1983): Genotypic differences in flower production/shedding and yield in mungbean (*Vigna radiata* L.). – *Indian Journal of Plant Physiology* 26: 402-405.
- [17] Malaviarachchi, M. A. P. W. K., DeCosta, W. A. J. M., Kumara, J. B. D. A. P., Suriyagoda, L. D. B., Fonseka, R. M. (2015): Response of mung bean (*Vigna radiata* L.) to an increasing natural temperature gradient under different crop management systems. – *Journal of Agronomy and Crop Science* 202(1): 51-68.
- [18] Miah, M. A. K., Anwar, M. P., Begum, M., Juraimi, A. S., Islam, M. A. (2009): Influence of sowing date on growth and yield of summer mungbean varieties. – *Journal of Agriculture and Social Sciences* 5-3: 73-76.
- [19] Nuttonson, M. Y. (1955): *Wheat Climatic Relationship and Use of Phenology in Ascertaining the Thermal and Photo Thermal Requirements of Wheat*. – American Institute of Crop Ecology, Washington, DC.
- [20] Patriyawaty, R., Rachaputi, C. N. R., George, Douglas, C. (2017): Genotypic Variation for Tolerance to High Temperature Stress During Reproductive Phase in Mungbean (*Vigna radiata* L.). – Queensland Alliance for Agriculture and Food Innovation, The University of Queensland, Australia.
- [21] Prakash, V., Mishra, J. S., Kumar, R., Kumar, R., Kumar, S. K., Dwivedi, K. K., Bhatt, B. P. (2017): Thermal utilization and heat use efficiency of sorghum cultivars in middle Indo-Gangetic Plains. – *Journal of Agrometeorology* 19(1): 29-33.

- [22] Rajput, R. P., Deshmukh, M. R., Paradker, V. K. (1987): Accumulated heat units and phenology relationship in wheat as influenced by planting dates under late sown conditions. – *Journal of Agronomy and Crop Science* 159: 345-349.
- [23] Rathore, S. S., Dshora, L. N., Kaushik, M. K. (2010): Effect of sowing time and fertilization on productivity and economic of urdbean genotypes. – *Journal of Food Legumes* 23: 154-155.
- [24] Reddy, A. A. (2009): Pulses production technology, status and way forward. – *Economic & Political Weekly* 44: 73-80.
- [25] Sadeghipour, O. (2008): Response of mungbean varieties to different sowing dates. – *Pakistan Journal of Biological Sciences* 11(16): 2048-2050.
- [26] Sarkar, M. A. R., Kabir, M. H., Begum, M., Salam, M. A. (2004): Yield performance of mungbean as affected by planting density, variety and planting date. – *Journal of Agronomy* 3(1): 18-24.
- [27] Sheoran, P., Pal, S. (2007): Thermal indices for prediction of mungbean phenology under varying irrigation schedules. – *Journal of Agrometeorology* 9(2): 247-252.
- [28] Singh, G., Sekhon, H. S. (2007): Effect of sowing date on growth and yield of mungbean varieties during Kharif season. – *Journal of Food Legume* 20: 59-61.
- [29] Singh, H., Singh, G. (2015): Growth, phenology, and thermal indices of mungbean as influenced by sowing time, varieties and planting geometry. – *Indian Journal Agriculture Research* 49(5): 472-475.
- [30] Singh, G., Sekhon, H. S., Ram, H., Gill, K. K., Sharma, P. (2010): Effect of date of sowing on nodulation, growth, thermal requirement, and grain yield of Kharif mungbean genotypes. – *Journal of Food Legume* 23: 132-134.
- [31] Singh, R. P., Dhillon, B. S., Sidhu, A. S. (2019): Productivity of summer mungbean as influenced by different sowing dates and varieties. – *Journal of Pharmacognosy and Phytochemistry* 8(3): 781-784.
- [32] Sinsawat, V., Leipner, J., Stamp, P., Fracheboud, Y. (2004): Effect of heat stress on the photosynthetic apparatus in maize (*Zea mays* L.) grown at control or high temperature. – *Environmental and Experimental Botany* 52: 123-129.
- [33] Soomro, N. A., Khan, H. R. (2003): Response of mungbean genotypes to different sowing dates in Kharif season under rain-fed conditions. – *Asian Journal of Plant Sciences* 2: 377-379.
- [34] Steel, R. G. D., Torrie, J. H., Dickey, D. A. (1997): Principles and Procedure of Statistics. – McGraw Hill, New York, pp. 178-182.
- [35] Tickoo, J. L., Gajraj, R., Matho, M. C. (1996): Plant Type in Mungbean (*Vigna radiata* L.) – In: Asthana, A. N., Kim, D. H. (eds.) Proceedings Recent Advances in Mungbean Research, Indian Society of Pulses Research and Development. Indian Institute of Pulses Research, Kanpur, India, pp. 197-213.
- [36] Ullah, A., Salehnia, N., Kolsoumi, S., Ahmad, A., Khaliq, T. (2018): Prediction of effective climate change indicators using statistical downscaling approach and impact assessment on pearl millet (*Pennisetum glaucum* L.) yield through Genetic Algorithm in Punjab, Pakistan. – *Ecological Indicators* 90C(2018): 569-576.
- [37] Ullah, A., Ahmad, I., Ahmad, A., Rahman, M. H., Khaliq, T., Saeed, U., Hoogenboom, G. (2019): Assessing climate change impacts on pearl millet under contrasting environments using system analysis approach. – *Environmental Science and Pollution Research* 26(7): 6745-6757.
- [38] Ullah, A., Ahmad, I., Rahman, M. H., Waseem, M., Waqas, M. M., Bhatti, M. A., Ahmad, A. (2020): Evaluation of management options through empirical modeling to improve pearl millet production in semi-arid and arid regions of Punjab Pakistan. – *Sustainability* 12(18): 7715.
- [39] Wahid, A., Gelani, S., Ashraf, M., Foolad, M. (2007): Heat tolerance in plants. – *Environmental and Experimental Botany* 61: 199-223.

EFFECT OF CLIMATE CHANGE ON STEM BIOMASS AND CARBON STOCK OF MONGOLIAN SCOTS PINE (*PINUS SYLVESTRIS* VAR. *MONGOLICA*) PLANTATION FORESTS IN HORQIN SANDY LAND, CHINA

KHAN, D.¹ – KOUASSI, C. J. A.¹ – ZHANG, K.^{1*} – ZHANG, X.² – SHI, Z.² – UDDIN, S.³ – HAYAT,
M.⁴ – KHAN, M. A.⁵ – SHAH, S.⁶ – GULL, S.⁷ – YANG, X. H.^{2*}

¹*School of Soil and Water Conservation, Beijing Forestry University, Beijing 100083, China
(e-mail: Dilawarafri333@hotmail.com – D. Khan; anoma@bjfu.edu.cn – C. J. A. Kouassi)*

²*Institute of Desertification Studies, Chinese Academy of Forestry, Beijing 100091, China
(e-mail: Zhangxiao978@caf.ac.cn – X. Zhang; Shizj@caf.ac.cn – Z. Shi)*

³*School of Biological Sciences and Technology, Beijing Forestry University, Beijing 100083,
China
(e-mail: saleemkhan86@hotmail.com)*

⁴*School of Environment and Energy, Peking University Shenzhen Graduate School, Shenzhen
518055, China
(e-mail: muhammadhayat66@gmail.com)*

⁵*Ministry of Education, Key Laboratory of Silviculture and Conservation, Beijing Forestry
University, Beijing 100083, China
(e-mail: Asifkhanbaluch@yahoo.com)*

⁶*Institute of Agriculture Sciences and Forestry, University of Swat, Charbagh, District Swat,
KP, Pakistan
(e-mail: s.shah@uswat.edu.pk)*

⁷*Department of Horticulture and Plant Protection, Yangzhou University, Yangzhou, China
(e-mail: sadiagull137@yahoo.com)*

**Corresponding authors*

e-mail: ctccd@126.com; yangxh@caf.ac.cn; phone: +86-133-6665-5775

(Received 7th Dec 2021; accepted 17th Mar 2022)

Abstract. Mongolian Scots pine has been used for vegetation restoration and windbreaks in Horqin Sandy land, Northern China, where climate change is the principal factor limiting tree survival and growth. To investigate the effect of annual precipitation and annual temperature variables on stem biomass and carbon stock of Mongolian Scots pine healthy (HP), sub healthy (SHP), stress (STP), and shrink (SRP) plantation. We used climate sensitive allometric model to find out accurate biomass along climatic factors from 1965 to 2019. The result show that, stem biomass and carbon stock of Mongolian Scots pine, HP, SHP, STP and SRP plantation, have strong correlations with annual PP and annual (T_{max}) ($R^2 = 0.88$, $R^2 = 0.84$, $R^2 = 0.82$, $R^2 = 0.61$) and ($R^2 = 0.86$, $R^2 = 0.82$, $R^2 = 0.72$, $R^2 = 0.60$). While, annual average (T_{mini}) and annual (T_{mean}) have a slightly positive correlations with the Mongolian Scots pine, HP and SHP, plantation ($R^2 = 0.73$, $R^2 = 0.70$) and ($R^2 = 0.76$, $R^2 = 0.71$). However, negative correlations ($R^2 = 0.49$, $R^2 = 0.29$) and ($R^2 = 0.40$, $R^2 = 0.39$) were found with STP, and SRP, plantation. Mongolian Scots pine, afforestation on reclamation sites brings important environmental and production benefits. Mongolian Scots pine has a strong adaptive nature with climate change and hence can survive under stress conditions of Horqin sandy land China.

Keywords: *Pinus sylvestris* var. *mongolica*, stem biomass, carbon stock, global warming, afforestation

Introduction

It is universally admitted that climate change is influencing forest ecosystems. There is enough evidence that indicating the potential downfall in amazon rainforest, related to climate change (Pecl et al., 2017; Zhu et al., 2019; Ayanlade et al., 2020). Due to water deficiency, barren soil, and scattered vegetation, desert ecosystems, may be particularly exposed to climate change (Seddon et al., 2016; Zhu et al., 2019; Jordaan et al., 2020). It has been considered that soil degradation caused by desertification influences one-quarter of the world's land cover, including one fifth of the world's community, mostly living in emerging countries (D'Odorico et al., 2013; Turan et al., 2019). This amount will extensively increase in the coming decades, given the forecasted rise in aridity linked to climate change (Huang et al., 2016, 2017). Precise understanding the influence of climate change on desert ecosystems, therefore, its essential and integral to their stability (Vogt et al., 2011). Furthermore, in past decades, climatic changes have deeply affected the composition and of territorial ecosystems, driving to uncertainties concerning ecological rehabilitation in desert areas (Zhou et al., 2015). Assumed these climatic changes, studying trees dynamics and its relationship with climatic factors is necessary for understanding how the changing climate alters the dry ecosystems (Wang et al., 2013).

As an active component of ecosystems, forests links the soil and atmosphere through energy and mass transport; thus, it is a sensitive indicator of environmental change (Piao et al., 2006). Monitoring Stem biomass and carbon stock dynamics and analysing their responses to climatic variations are popular approaches to studying global climate change (Virtanen et al., 2010; Svenning and Sandel, 2013; Yin et al., 2016). Mongolian Scots pine, growth can be endorsed by increased precipitation and temperature in northern and upper areas where production is cold-limited (Kullman and Kjällgren, 2006; Briffa et al., 2008). However, evidence indicates that cold-constrained sites also influence Mongolian Scots pine growth due to aggravated soil moisture deficit, linked to increasing demand for evapotranspiration during the growing season (Lloyd and Bunn, 2007; Dũthorn et al., 2016). The influence of minimum temperature and mean temperature brings uncertainty to tree growth and vigor throughout the range, specifically in cold-dry climates (Matías and Jump, 2012). Moreover, other dry environments, particularly warmer areas of Mediterranean, where Mongolian Scots pine also exposed to winter and responsive atmosphere (Camarero et al., 2015; Marqués et al., 2018). In this concern, the comparison of low temperature and warm atmosphere has a simultaneous effect on Mongolian Scots pine growth, which is of particular interest to predict the climate change influences on conifer species (Babst et al., 2017; De Andres et al., 2017).

Mongolian Scots pine was introduced for afforestation in the 1950s to Horqin Sandy Land, China. Now it has become the most commonly used tree species for creating shelterbelt plantations, condense to soil water conservation, and increase sand fixation in Horqin Sandy land China (Zhu et al., 2005). Since the early 1990s, Mongolian Scots pine plantations began to decline due to dieback, the absence of natural regeneration, low growth rates, and mortality (Shuren, 2001; Zheng et al., 2012). There is a remarkable expansion in desertification across Mongolia due to climate warming at a global scale, and it has potential influence on plantations in current years (Sternberg, 2008; Gerelbaatar and Baatarbileg, 2011). Because of this decline, a large number of studies have been conducted from many perspectives, including water use strategy, decreasing groundwater, hydraulic architecture, and

differences in plant nutrients and soil microbes among origin regions (Song et al., 2016; Liu et al., 2018; Zhang et al., 2019b). However, its impact on the carbon sink is minimal. Basic research has been conducted to evaluate the response of potential biomass changes and carbon storage *Pinus sylvestris* var. *mongolica* plantations to climate change.

In this paper, we studied Mongolian Scots pine plantations forests stem biomass and carbon stock along with the climatic factors in Horqin Sandy Land, China. Our main objective of this study was to find out a correlations of climatic variables, including annual precipitation and annual temperature variables, with the stem biomass and carbon stock of Mongolian Scots pine plantations, to investigate tree growth survival in drought conditions. It is anticipated that the results of this study might be helpful for the management of forest plantations concerning the growth conditions of Mongolian Scots pine.

Materials and methods

Study area

The present study was conducted at the Liaoning Province Sand-Fixation and Afforestation Research Institute, which is located above sea level (42°42' N, 122°29' E, 220.67 m) in Horqin sandy land, Northeast China (Fig. 1). The Horqin Sandy Land is the major sandy land of the country and an important section of the Three North Shelterbelt regions. The whole region is characterized by a moderate, semi-humid monsoon climate, with annual average temperature and precipitation in this region from (1965-2019) were 7.7 °C and 500 mm, respectively, with nearly 67.0% of the precipitation occurring from June to August and the annual frost-free period is 150 to 160 days. The geomorphology is characterized by staggered distributions between oval or round sand dunes and low-lying land caused by wind erosion. The primary soil type is Aeolian sandy soil, accounting for 89.4% of soil, and other soil types include meadow soil, peat soil, and paddy soil.

Mongolian Scots pine is naturally distributed in the mountainous region of northeast China (Zhu et al., 2006). Because of its strong drought tolerance and fast growth, this species was first introduced successfully to Horqin sandy land in the 1950s, under the project of Three-North Shelterbelt regions during the past few decades (Zhu et al., 2016). It has become the main tree species widely used for afforestation in water-limited sandy lands of China. There are a large number of Mongolian Scots pine plantation stands of different ages and densities. Other woody plants in this region include *Pinus tabuliformis* Carr. *Populus L.* and *Ulmus pumila L.* The main understory herbaceous plants have *Digitaria sanguinalis (L.) Scop.* *Setaria viridis (L.) Beauv.* *Chloris virgate Sw.* *Cleistogenes squarrosa (Trin.) Keng.* *Eragrostis pilosa (L.) Beauv.* *Geranium wilfordii Maxim.* *Elymus dahuricus Turcz.* *Euphorbia pekinensis Rupr.* *Portulaca oleracea L.*, and *Axyris amaranthoides L.*

Field data collection

A field survey was conducted in 2019 to collect data from the study area Zhanggutai region. Trees of different growth states of Mongolian Scots pine, healthy, sub-healthy, stress, and shrink plantation were chosen from 5 location as a target tree to investigate the Stem biomass and carbon stock (Fig. 2). Recorded the location information such as

geographic coordinates and altitude (*Table 1*), as well as the basic information of individual trees such as diameter at breast height, tree height. Within each plot, tree diameter at the breast (DBH) of each tree measured by caliper, while tree height was measured by concern indicator (NIKON 550S, TOKYO, JAPAN).

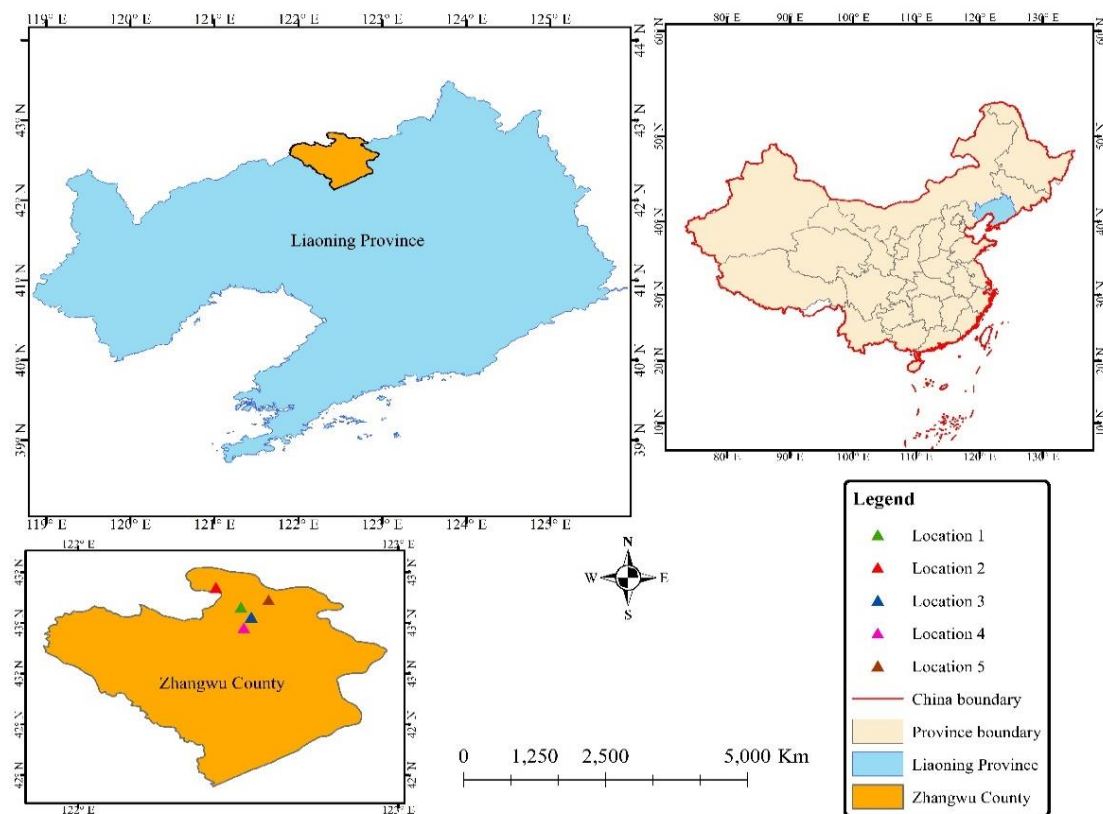


Figure 1. Sketch sites map of geographic division of Horqin Sandy land, Liaoning Province, Northern China

Scots pine (*Pinus Sylvestris* var. *mongolica*) plantation



Figure 2. Mongolian Scots pine (*Pinus sylvestris* var. *mongolica*) plantation health condition

Table 1. Description of study site of *Pinus sylvestris* var. *mongolica*, health condition, and samples

Mongolian Scots pine	Health status	Longitude	Latitude	Altitude (m)	Number of sampled trees
1	Healthy	122°25'49"	42°47'3"	252	150
2	Sub healthy	122°30'4"	42°43'7"	90	140
3	Stress	122°32'57"	42°40'57"	199	141
4	Shrink	122°34'31"	42°41'28"	86	146
Total					577

Climatic data collection

The climatic data, such as annual maximum temperature, annual minimum temperature, annual mean temperature, and annual precipitation, were collected from 1965 to 2019 (Fig. 3). KNMI Climate Explorer (<https://climexp.knmi.nl>) was used to download the (0.5°) grid data of these parameters. These selected climate stations were consistently assigned in the northeastern region of Inner Mongolia, China. The global positioning system (GPS) was used to download the Climatic data of each sample plot from its coordinate and to extract geographical data of each sample plot. We used regression analysis between interpolated and measured temperature variables and precipitation to calculate the accuracy of interpolated values. Climatic factors such as Temperature variables were divided into three main seasons, such as summer (July, August, September, October), winter (November, December, January, and February), and mid-season (March, April, May, and June).

Stem biomass

Researchers have developed several allometric equations to estimate biomass of diverse tree species using many variables as predictors or independent variables. For estimation of tree biomass, a standard variable such as DBH, total height, density, volume, basal area, and crown radius are mainly used (Chave et al., 2005; Mandal et al., 2013; Goodman et al., 2014). In forest ecological system the biomass is an important part. Quantifying accurate tree biomass is necessary to investigate the carbon storage and the effect of climatic factors such as precipitation and temperature variables (Clark et al., 2001; Wang et al., 2017). Although measuring the actual weight of tree constituents such as stem, root, foliage and branches the suitable method, however, it is time-consuming, costly and destructive. Therefore, to estimate tree biomass the stem biomass model is supposed to be the finest method (Bi et al., 2004; Dong et al., 2015). Recommended components such as height of the tree (H) and diameter at the breast height should be used to measure stem biomass (Chave et al., 2006). Minimum standard error (SRR) is used for a tree model and is accounted realistic if it yields evaluate on it, throughout the range of data the minimum sum if the square of the residual error (SSE) does not give negative estimates and does not exhibit a reduction in biomass with an escalation in height or diameter. Whereas minimum standard error (SEE) is used for a tree model and considered reasonable if it yields estimates on it, the minimum sum of the square of the residual error (SSE) during the range of data, does not give negative estimate (Ali et al., 2016). The following allometric equation was used, which was developed by (Cheng and Li, 1989):

$$\text{Biomass Equation } W_s = 0.0134(D^2 H) 1.02 \quad (\text{Eq.1})$$

The coefficient of determination of (R^2) is 0.0134. Where (W_s) indicated stem biomass, (D) indicated tree diameter at breast height, and (H) indicated tree height, respectively. To measure, the total stem biomass per plot was summed for all plots to average carbon stock and biomass of the separate plot, subsequently converted to tons per hectare (ton/ha). To convert the value to its carbon equivalent biomass fraction analysis was carried out. Carbon stock was measured as the corresponding biomass of the individual tree and product of the carbon sink.

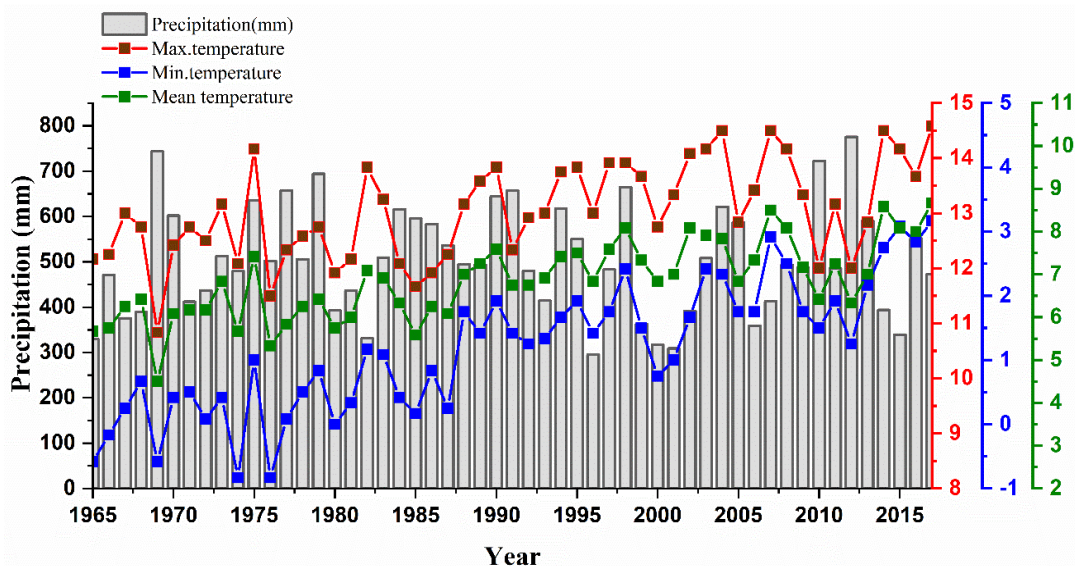


Figure 3. Yearly climate diagram for annual precipitation, annual maximum temperature, annual minimum temperature, and annual mean temperature from 1965 to 2019 from the sampling plots for Mongolian Scots pine (*Pinus sylvestris* var. *mongolica*), in Horqin Sandy Land, China

Data analyses

The relative change rate of biomass was used as the dependent variable, and climatic variables were used as the independent variables for stepwise regression analysis. Correlation's analysis was used to determine the association among two variables. Climatic factors such as annual temperature and annual precipitation affect the relative change rate of biomass were achieved with the following regression equation:

$$B = \beta_0 + \beta_i P_i \quad (\text{Eq.2})$$

where b is the relative change rate of biomass, β_0 is a constant, and β_i is the coefficient estimates of effecting factor i .

Estimated biomass was as

$$B = \frac{\beta_i P_j}{x_i} X_i + B_j(1 + \beta_0 - \beta_i) \quad (\text{Eq.3})$$

where B_j is the measured value of biomass in adjacent land, the positive and negative effects of biomass variation with climatic factors have the same positive and negative

effects of biomass as their corresponding factors of the forest, but the coefficient estimates are different. To detect the effect on biomass and stand age with climatic factors such precipitation and temperature changes, Stepwise regression analysis was carried out in which the stem biomass was taken as dependent variables while climatic factors were independent variables. To uncover the relation between variables and to detect the statistical differences among climatic factors and biomass, such as precipitation and temperature (Origin 2018) was used to detect these differences. The level of significance ($R^2 = 0.05$) and level of probability ($P \leq 0.05$) were evaluated in the analysis of variance (ANOVA). To check the variable relationship accuracy, we used linear regression analysis. All statistical analyses were done with Origin 2018 on Windows 10.

Results

Mongolian Scots pine, healthy plantation, amount of stem biomass, and carbon stock with climatic factors

Climatic factors significantly influence stem biomass and carbon stock of Mongolian Scots pine healthy plantation. The average stem biomass 46.5 ± 17.3 (ton/ha), variation from minimum to maximum 20 ± 80 (ton/ha) was measured. Simultaneously, the total average stem biomass of 164 (ton/ha) was recorded. Carbon stock was measured at 23.2 ± 8.6 to 10 ± 40 (ton/ha) with, total average carbon stock of 82 (ton/ha) in the study area. The total average precipitation of 382 (mm) was recorded with the range of 479 ± 109.1 (mm) along, variation from minimum to maximum 280 ± 660 (mm). Maximum temperature range was 11.9 ± 3.3 to 7 ± 18 ($^{\circ}\text{C}$) with a total average of 10 ($^{\circ}\text{C}$), While minimum temperature was noted at the range of -2.7 ± 1.3 ($^{\circ}\text{C}$) to -5 ± 0 ($^{\circ}\text{C}$), total average -2 ($^{\circ}\text{C}$) and 6.7 ± 1.7 to 4 ± 10 ($^{\circ}\text{C}$) total average mean temperature -2 ($^{\circ}\text{C}$) were found. The maximum and minimum values of stem biomass and carbon stock of healthy plantation beside with climatic factors are described in *Table 2*.

Table 2. Mean and SD of stem biomass, carbon stock, annual precipitation (PPT), and annual (T_a) temperature variables of Mongolian Scots pine healthy, plantation in Horqin sandy land, China

Mongolian Scots pine	Statistical variables	Biomass (ton/ha)	Carbon stock (ton/ha)	PPT (mm)	Max Tm ($^{\circ}\text{C}$)	Mini Tm ($^{\circ}\text{C}$)	Mean Tm ($^{\circ}\text{C}$)
Healthy	Mean	46.5	23.2	479	11.9	-2.7	6.7
	SD	17.3	8.6	109.1	3.3	1.3	1.7
	Minimum	20	10	280	7	-5	4
	Maximum	80	40	660	18	0	10
	Total	164 ton/ha	82 ton/ha	382 mm	10 $^{\circ}\text{C}$	-2 $^{\circ}\text{C}$	6 $^{\circ}\text{C}$

Correlations of climatic factors with stem biomass and temperature variables with Scot pine, healthy, sub healthy, stress, and shrink plantation

Mongolian Scots pine healthy (HP), sub healthy (SHP), stress (STP) and shrink (SRP) plantation stem biomass correlations with precipitation, temperature variables 1965-2019. To determine the correlations with climatic factors showed the strongest coefficient correlations ($p < 0.05$). Stem biomass response of Mongolian Scots pine along annual precipitation (PP), was as follows: Annual (PP) has the strongest

correlations with (HP), plantation ($R^2 = 0.88$), (SHP), plantation ($R^2 = 0.84$), and (STP), plantation ($R^2 = 0.84$). while, slightly positive correlations were found with (SRP), plantation ($R^2 = 0.61$), in the study area of Horqin sandy land, as shown in *Figure 4a-d*. (HP), plantations and (SHP), plantations a positive correlations with annual maximum temperature ($R^2 = 0.88$), ($R^2 = 0.82$). While, slightly positive correlated ($R^2 = 0.72$) with (STP), plantation. However, significant correlations ($R^2 = 0.60$) was found with (SRP), plantation in Horqin sandy land China, as shown in *Figure 5a-d*.

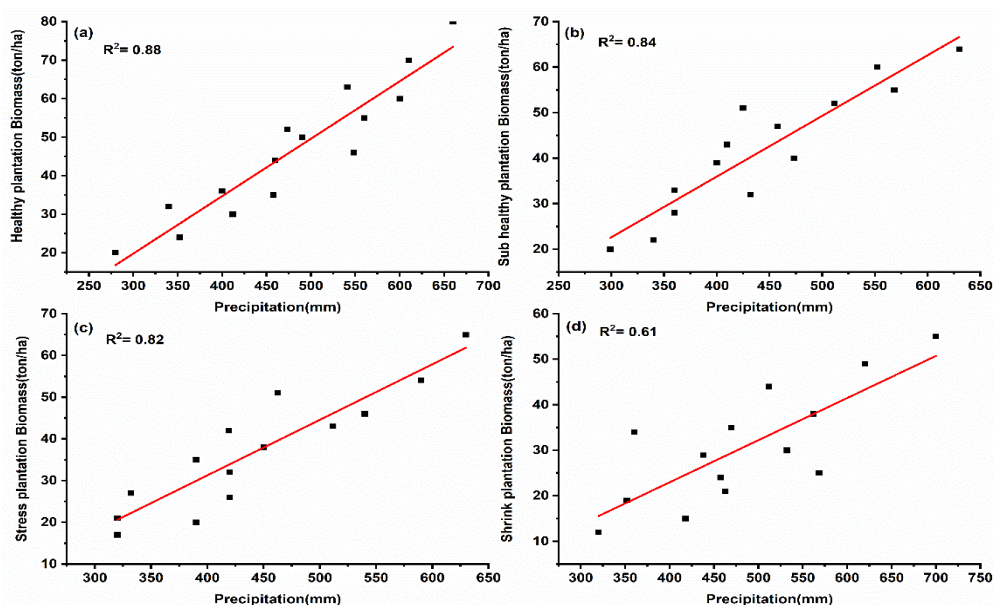


Figure 4. Association between *Pinus Sylvestris* var. *mongolica*, stem biomass along with annual precipitation from 1965 to 2019: (a) healthy; (b) sub healthy; (c) stress; (d) shrink plantation

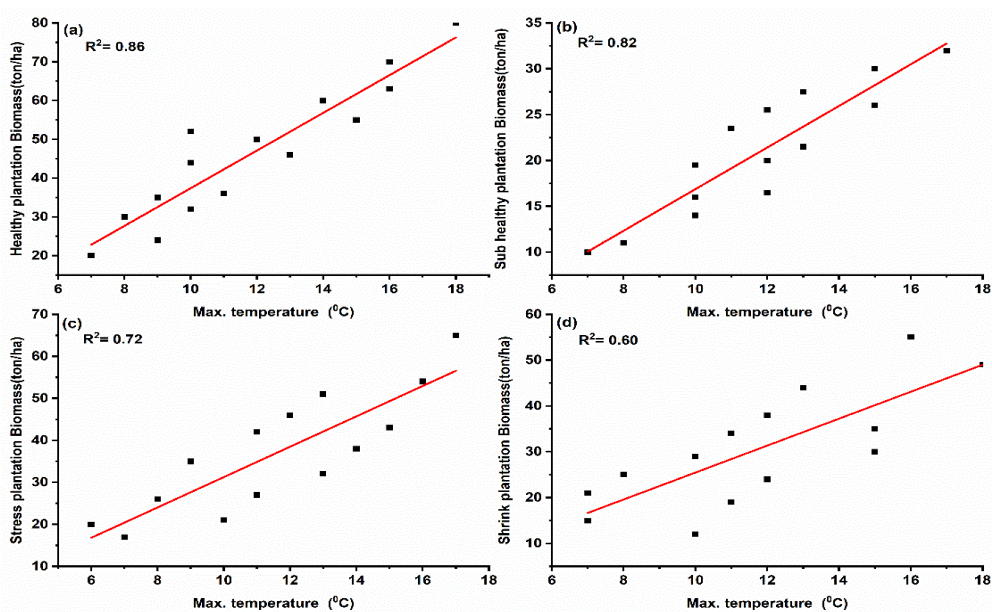


Figure 5. Relationship between *Pinus sylvestris* var. *mongolica*, stem biomass along with annual maximum temperature from 1965 to 2019: (a) healthy; (b) sub healthy; (c) stress; (d) shrink plantation

Although, Mongolian Scots pine correlations result with annual minimum temperature is not the same. Stem biomass of (HP), and (SHP), plantation response positively correlated ($R^2 = 0.73$), ($R^2 = 0.70$), while negative correlations were observed with (STP), and (SRP), plantation with annual minimum temperatures ($R^2 = 0.49$), ($R^2 = 0.29$), respectively (Fig. 6a-d).

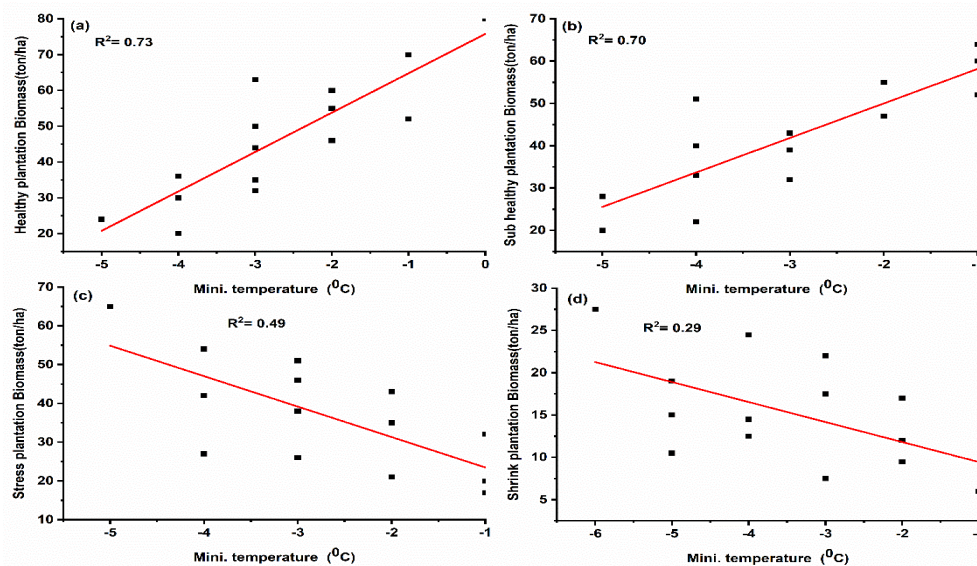


Figure 6. Relationship between *Pinus Sylvestris* var. *mongolica*, stem biomass along with annual minimum temperature from 1965 to 2019: (a) healthy; (b) sub healthy; (c) stress; (d) shrink plantation

In addition to the correlations with an annual mean temperature of Mongolian Scots pine, (HP), (SHP), (STP), and (SRP), plantation were different (Fig. 7a-d). The annual mean temperature was positively correlated ($R^2 = 0.76$) with a (HP) plantation (Fig. 7a), while significant positive correlations ($R^2 = 0.71$) with a (SHP), plantation (Fig. 7b). However, negative correlations were found for stem biomass of Mongolian Scots pine (STP), and (SRP), plantation ($R^2 = 0.40$) ($R^2 = 0.39$) with annual mean temperature in Horqin sandy land China (Fig. 7c, d).

Pinus sylvestris var. *mongolica*, sub healthy plantation cumulative stem biomass, carbon stock with climatic parameters

Stem biomass and carbon stock of *Pinus mongolica* sub healthy plantation with climatic parameters presented enormous differences in their carbon stock and biomass. The average stem biomass is 41.9 ± 13.7 (tons/ha), variation started of sample from minimum to maximum 20.0 ± 64.0 (ton/ha), although the average 140 (ton/ha) of stem biomass was calculated. Carbon stock was measured at the range of 20 ± 6.9 to 10.0 ± 32.0 (ton/ha) with a total average of 70 (ton/ha) carbon stock in the study area. The total average precipitation of 367 (mm) was recorded with the range of 444.2 ± 94.9 (mm) along with variation from minimum to maximum 299.0 ± 630.0 (mm). Maximum temperature range 11.8 ± 2.8 to 7.0 ± 17.0 ($^{\circ}\text{C}$) with a 10 ($^{\circ}\text{C}$) of the total average temperature. Minimum temperature, noted at the range of -3.0 ± 1.4 ($^{\circ}\text{C}$) to -5.0 ± -1.0 ($^{\circ}\text{C}$), with total average minimum temperature -2 ($^{\circ}\text{C}$)

respectively. Mean temperature varies from 5.3 ± 2.1 ($^{\circ}\text{C}$) to 2.0 ± 9.0 ($^{\circ}\text{C}$), with total average of 5 ($^{\circ}\text{C}$). The maximum and minimum values of stem biomass and carbon stock of sub-healthy plantation were found along with climatic variables in study area, which are presented in *Table 3*.

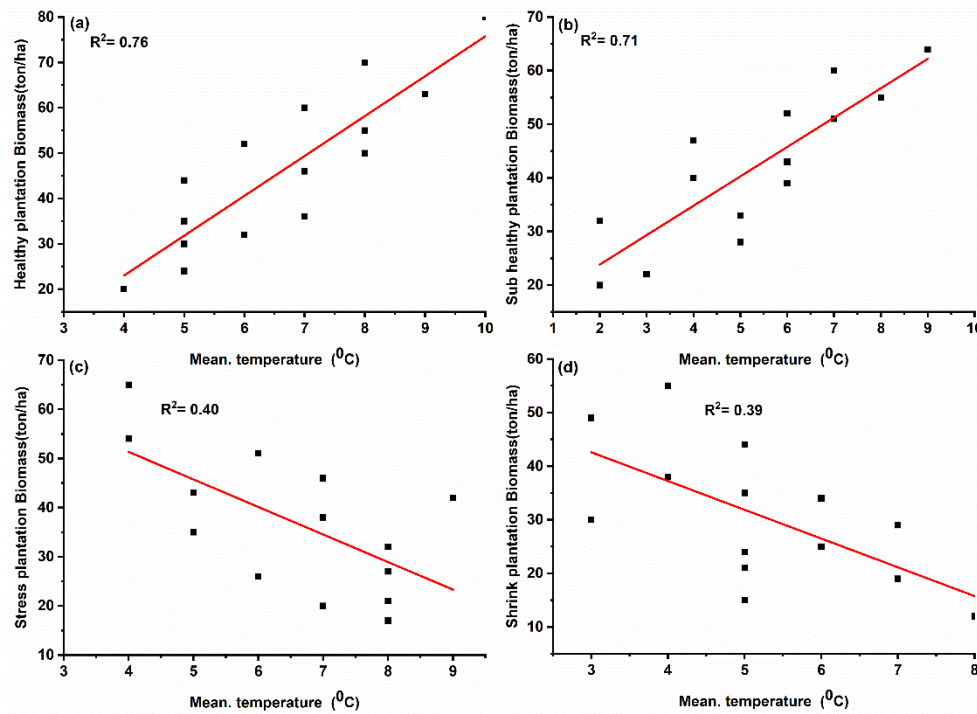


Figure 7. Relationship between *Pinus Sylvestris* var. *mongolica*, stem biomass along with annual mean temperature from 1965 to 2019: (a) healthy; (b) sub healthy; (c) stress; (d) shrink plantation

Table 3. Mean (*M*) and standard deviation (*SD*) of stem biomass, carbon stock, annual precipitation (*PP*), and annual temperature (*T_a*) variables of Mongolian Scots pine sub healthy plantation in of Horqin Sandy Land, China

Mongolian Scots pine	Statistical variables	Biomass (ton/ha)	Carbon stock (ton/ha)	PP (mm)	Max Tm ($^{\circ}\text{C}$)	Mini Tm ($^{\circ}\text{C}$)	Mean Tm ($^{\circ}\text{C}$)
Sub healthy	Mean	41.9	20.9	444.2	11.8	-3	5.3
	SD	13.7	6.9	94.9	2.8	1.4	2.1
	Minimum	20	10	299	7	-5	2
	Maximum	64	32	630	17	-1	9
	Total	140 ton/ha	70 ton/ha	367 mm	10 $^{\circ}\text{C}$	-2 $^{\circ}\text{C}$	5 $^{\circ}\text{C}$

Pinus sylvestris var. *mongolica*, stem biomass and carbon stock with stand age

It is comparatively easy to predict stand stem wood biomass with stand age. This relationship is quite similar to that between stem wood biomass, carbon stock, and stand volume. Most investigations indicate that stem biomass increases in with stand increment (Ilvesniemi and Liu, 2001; Jagodzinski and Kalucka, 2008), besides that, some additional studies exhibited a variation even later; for example, “the second

maximum” can be found at a stand age of 40 to 50 years (Makarenko, 1985). Also, some investigations show that stem biomass increases slowly up to maturity (Mikšys et al., 2007; Burrascano et al., 2013). Carbon capture by biomass growth and the duration of carbon in biomass resulted in carbon stocks of forests (Körner, 2017) described that “rather than growth rate tree endurance controls the carbon capital of forests.” He further elaborated, that the size of an ecosystem’s carbon pool and its carbon turnover is “normally not correlated” and hypothesizes that a system’s carbon residence time must be prolonged to reserve carbon fluxes from the atmosphere to the forest biomes. The traditional perspective of sustainable forest management fails when carbon residence in a forest ecosystem is considered, which focuses on the balance of increment and fellings. Even when the forest ecosystem perspective is widened to a forest sector perspective, the forest carbon loss induced by logging activities in tropical forests can often not be compensated by accounting for the carbon pool in harvested wood products and the carbon substitution effects by timber utilization (Butarbutar et al., 2016). A previous study (Brienen et al., 2015; Huang et al., 2021) described a declining trend of carbon accumulation during the past decade for the Mongolian Scots pine plantation. Our result also elaborated that stem biomass and carbon stock increase in *Pinus sylvestris* healthy, sub-healthy plantation with age. At the same time, the sudden decline was observed in stress and shrink plantation in Horqin sandy land in *Figures 8 and 9a-d*. In addition, the decline is a consequence of the limitation of carbon resistance time due to increased mortality and growth rates that level off. Although carbon stock dynamics occur in significantly huge areas, they can be recognized as individual tree collectives’ dynamics. High biomass carbon stocks reduce shifts in size distributions towards trees with larger dimensions necessary (Körner, 2006, 2017). Stand level dynamics determine by large trees (Newbery and Ridsdale, 2016), they play an essential role in minor-scale carbon storage and accumulation. Declines in carbon accumulation can be limited in time.

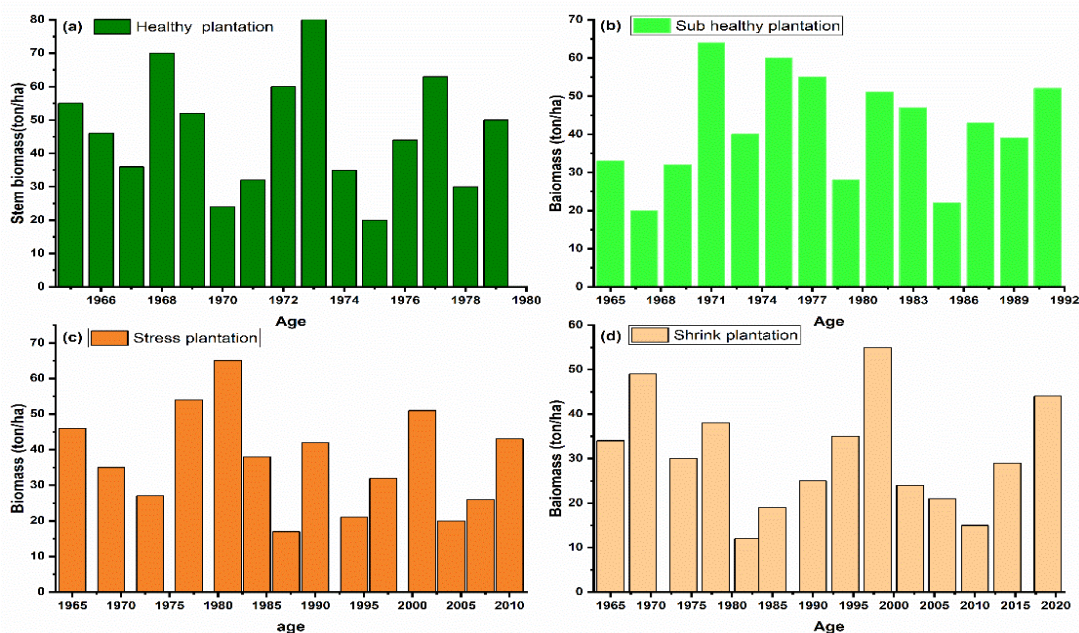


Figure 8. Accumulation of *Pinus Sylvestris* var. *mongolica*, stem biomass of (a) healthy (b) sub healthy (c) stress and shrink plantation at different age from 13, 26, 39, and 54-year-old stands in Horqin Sandy Land China

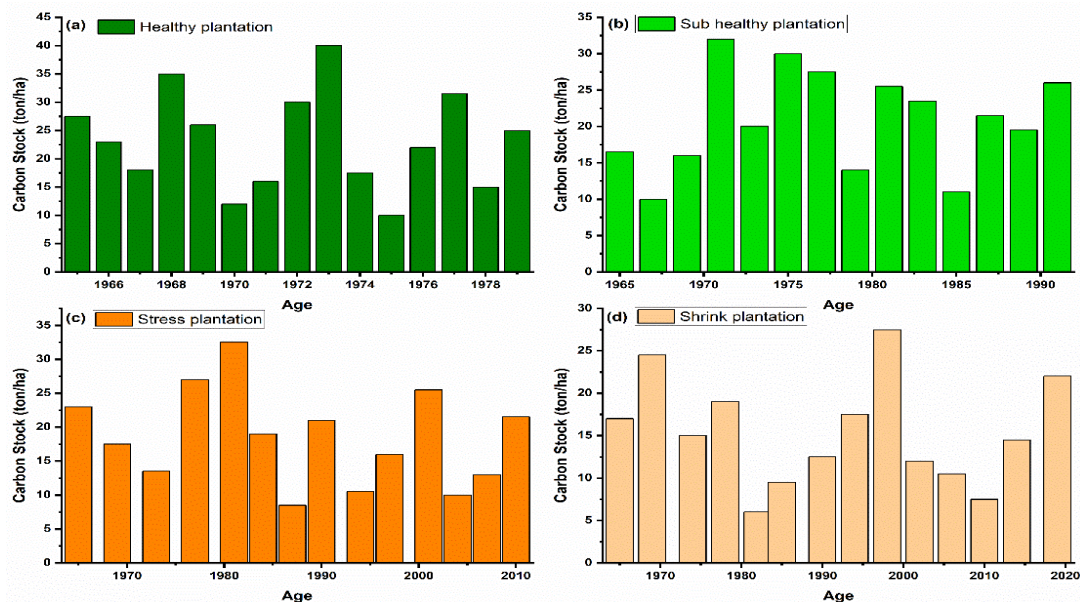


Figure 9. Accumulation of *Pinus Sylvestris* var. *mongolica*, carbon stock of (a) healthy (b) sub healthy (c) stress and shrink plantation at different age from 13, 26, 39, and 54-year-old stands in Horqin Sandy Land China

Mongolian Scots pine stress plantation, amount of stem biomass, and carbon stock with climatic variables

With climate factors, Mongolian Scots pine stress plantation, stem biomass and carbon stock displayed a vast difference. The average stem biomass 36.9 ± 14.2 (ton/ha), through minimum to maximum 17.0 ± 65.0 (ton/ha) was recorded. While the total average 133 (ton/ha) stem biomass was recorded. Carbon stock ranged from 18.5 ± 7.1 to 8.5 ± 32.5 (ton/ha) with, total average of 67 (ton/ha) carbon stock was found. However, Total annual precipitation 372 (mm) was recorded with the range of 442.5 ± 96.5 (mm), with a minimum to maximum 320.0 ± 630.0 (mm). Furthermore, the maximum temperature ranged from 11.6 ± 3.3 to 6.0 ± 17.0 ($^{\circ}\text{C}$) with a total average temperature of 9 ($^{\circ}\text{C}$). Minimum temperature was noted from -2.7 ± 1.3 ($^{\circ}\text{C}$) to -5.0 ± -1.0 ($^{\circ}\text{C}$), with total average minimum temperature of -2 ($^{\circ}\text{C}$). On the other hand, Mean temperature varied from 6.3 ± 1.8 to 4.0 ± 9.0 ($^{\circ}\text{C}$) with a total average mean temperature of 5 ($^{\circ}\text{C}$). We found that stress plantation statistics values of stem biomass and carbon stock and climatic factors are described in Table 4.

Table 4. Mean (M) and standard deviation (SD) of stem biomass, carbon stock, annual precipitation (PP), and annual temperature (T_a) variables of Mongolian Scots pine stress plantation in Horqin Sandy Land, China

Mongolian Scots pine	Statistical variables	Biomass (ton/ha)	Carbon stock (ton/ha)	PP (mm)	Max Tm ($^{\circ}\text{C}$)	Mini Tm ($^{\circ}\text{C}$)	Mean Tm ($^{\circ}\text{C}$)
Stress	Mean	36.9	18.5	442.5	11.6	-2.7	6.3
	SD	14.2	7.1	96.5	3.3	1.3	1.8
	Minimum	17	8.5	320	6	-5	4
	Maximum	65	32.5	630	17	-1	9
	Total	133 ton/ha	67 ton/ha	372 mm	9 $^{\circ}\text{C}$	-2 $^{\circ}\text{C}$	5 $^{\circ}\text{C}$

Mongolian Scots pine Shrink plantation, amount of carbon stock and stem biomass, with climatic variables

Carbon stock and stem biomass of Mongolian Scots pine, shrink plantation with climate parameters presented a significant difference in their carbon stock and biomass. In the current study, we measured 30.7 ± 12.7 (tons/ha) average stem biomass, variation started from minimum to maximum of 12 ± 55 (ton/ha), even if the filled average of stem biomass 110 (ton/ha) were documented. Whereas, Carbon stock was verified at 15.4 ± 6.3 to 6 ± 27.5 (ton/ha) with, total average carbon stock of 55 (ton/ha). Additionally, annual precipitation 403 (mm) was recorded with the range of 483.7 ± 107.1 (mm), alongside a minimum to maximum 320 ± 700 (mm). Furthermore, maximum temperature range from 12.3 ± 3.4 to 8 ± 18 (°C) with a total average temperature of 10 (°C) and minimum temperature, noted at the range of 10 ± 1.5 (°C) to -6 ± -1 (°C), with total average minimum temperature -2 (°C) respectively. However, mean temperature varies from 5.2 ± 1.5 (°C) to 3 ± 8 (°C), with total average of 4 (°C). Statistical values of carbon stock and stem biomass of *Pinus sylvestris* var. *mongolica*, shrink plantation with climatic factors are presented in *Table 5*.

Table 5. Mean (M) and standard deviation (SD) of stem biomass, carbon stock, annual precipitation (PP), and annual temperature (T_a) variables of Mongolian Scots pine shrink plantation in Horqin Sandy Land, China

Mongolian Scots pine	Statistical variables	Biomass (ton/ha)	Carbon stock (ton/ha)	PP (mm)	Max Tm (°C)	Mini Tm (°C)	Mean Tm (°C)
Shrink	Mean	30.7	15.4	483.7	12.3	-3.5	5.2
	SD	12.7	6.3	107.1	3.4	1.5	1.5
	Minimum	12	6	320	8	-6	3
	Maximum	55	27.5	700	18	-1	8
	Total	110 ton/ha	55 ton/ha	403 mm	10 °C	-2 °C	4 °C

Discussion

Mongolian Scots pine is often used in the afforestation of sandy land and reclamation areas (Kuznetsova et al., 2010; Pietrzykowski and Socha, 2011; Jagodziński et al., 2019). Mongolian Scots pine is an extremely drought-tolerant species and drought stress is thought to be the main climate limitation for its radial growth in semi-arid or arid regions, such as in the Mongolia Plateaus and north eastern Horqin sandy land China (Liu et al., 2009; Pederson et al., 2013; Bao et al., 2015). Previous studies suggest that the radial growth of Mongolian Scots pine is sensitive to precipitation, temperature (Bao et al., 2015). In these areas, the radial growth of Mongolian Scots pine usually has a typical climatic response pattern with a positive tree growth response to increasing precipitation and a negative response to increasing temperature (Davi et al., 2006; Martínez-Sancho et al., 2018). This typical climate factors response pattern is usually found in other drought or wetland tree ring reconstructions (Liu et al., 2017).

Our results depicted the positive correlations with annual maximum temperature and annual precipitation with stem biomass of Mongolian Scots pine (*Figs. 4 and 5*). Our results are consistent with the previous investigations (Qian and Qin, 2006). Recognizing the beneficial role of precipitation and temperature in tree growth. The carbon storage and stem biomass concentration was not comparable to climatic factors

in Mongolian Scots pine, healthy (HP), sub healthy (SHP), stress (STP), and shrink (SRP), plantation. Ultimately caused inconsistency in the development of the tree health condition. The highest positive effect on tree growth was observed in terms of annual precipitation and annual maximum temperature. Similarly, (Vacek et al., 2017) showed that precipitation and temperature are the essential variables for pine tree growth during the growing season. Our study confirmed that annual precipitation and the maximum temperature had the highest effect on stem biomass of Mongolian Scots pine plantation. Such findings were also confirmed by other studies dealing with the tree growth of pine forests (Vacek et al., 2016, 2019). It is caused by the climatic conditions when the fastest xylem formation and radial increment were recorded (Mäkinen et al., 2003; Putalová et al., 2019). The photosynthesis rate is increasing during long and sunny summer days, which positively affects the tree biomass. In addition, increases in the rate of decomposition and nitrogen mineralization by increasing temperature and precipitation, improving nutrient availability (Huang et al., 2010; Zhang et al., 2010). The annual precipitation has affected the soil and air quality, while temperature increases influence the soil and water content via evaporation (Zheng and Hoefs, 1993). Therefore, It demonstrates positive relationship between annual maximum temperature, annual precipitation, and stem biomass (Usoltsev et al., 2020).

We further analyzed that the annual mean and minimum temperatures had a positive correlations with Mongolian Scots pine, (HP), and (SHP), plantation in *Figures 6* and *7a, b*. While, negative correlations were found with (STP) and (SRP) plantation in *Figures 6* and *7c, d*. The negative relationship for (STP), and (SRP), plantation of the (*Pinus sylvestris* var. *mongolica*) may be attributed to the potential effect of other factors, such as local environmental and physiological conditions (Freire et al., 2019; Wang et al., 2019). Mainly, during the cold and short seasons, tree growth also affects across climatic variables. We further highlighted that the annual minimum and mean temperature during the cold season were the key components limiting Mongolian Scots pine stress and shrinking plantation growth. Our findings are consistent with the previous reports (Qian and Qin, 2006). Moreover, It was also studied that biomass was well regulated by the amount of storage compounds and the current soil moisture regime (Fritts et al., 1965; Huang et al., 2010). The most sensitive physiological responses to water deficit are decreased turgor, slowed down elongation tree growth, and impaired protein metabolism, which ultimately represses cell division by inhibiting mitosis (Oberhuber et al., 1998; Kutschera and Niklas, 2013). Similarly, the utilization of stored carbohydrates increases when the temperature starts rising at the end of hot winter months (Su et al., 2015). Therefore, the present study emphasized that wet winter's annual mean and minimum temperatures have a comparatively weak adverse impact on Mongolian Scots pine (STP), and (SRP), biomass (*Figs. 6* and *7c, d*). The possible explanation this plantation had fewer leaves; they could not do proper photosynthesis and respiration in the high snowfall weather during the winter season, which prolonged the snow melting process affecting tree development and biomass (Vaganov et al., 1999). It might be because the mean temperature and quantity of precipitation in the humid climatic region are very appropriate for tree development in the drought-resistant tree species, predominantly in the wettest quarter of the growing season (Fu et al., 2017; Khan et al., 2019). Previously it was reported that tree height decreases the inconstancy of stem biomass estimation (Feldpausch et al., 2012; Zhang et al., 2019a). The natural change of soil, species composition, solar radiations, and humidity and also affect biomass growth (Nascimbene et al., 2013; Hu et al., 2019).

A high amount of precipitation in the growing season and has the maximum annual temperature of the moistened season is moderately high. It sustains tree growth as well and has an effective relationship with tree biomass (Fu et al., 2017). *Pinus sylvestris* var. *mongolica* is a naturally drought-resistant tree species cultivated in northeastern China (Zhu et al., 2006; Fu et al., 2017). Therefore, it can smoothly maintain its survival at maximum precipitation and temperatures. Such conditions cannot restrain the tree and stem biomass (Hao et al., 2021). Besides, the loss of nutrients overflow has been affected by the high quantity of precipitation and humidity (Chen et al., 2015). Incorporating various stand levels of the tree and climatic variables could be better for more accurate precision of tree biomass prediction (Zeng and Tang, 2012; Dong et al., 2016). For this reason, in the current study, we determined only a simple tree biomass model together with climatic factors for conclusive stem biomass prediction.

Conclusion

This study was conducted in Horqin sandy land China, to find out impact of climatic variables on stem biomass and carbon stock of Mongolian Scots pine different health conditions from 1965-2019. Mongolian Scots pine healthy (HP), Sub healthy (SHP), Stress (STP), and Shrink (SRP), plantations have a strong correlations with annual precipitation (PP), and maximum temperature (T_{max}). Meanwhile, annual minimum temperature (T_{mini}) and mean temperature (T_{mean}), significantly correlated with (HP), and (SHP), plantations, but, negative correlations were found for (STP), and (SRP), plantations. Even though the melting of snow and high exposure to strong winds at the end of winter, it could be possible to slow down the growth of Mongolian Scots pine, (STP), and (SRK), plantation. Various parameters such as tree height, age, water, drought, nutrients, and competition among individuals tree also influence tree growth. In the future, to study the tree growth, one should consider some factors that highly affect the tree growth. Conclusively, the analyses highlighted that Mongolian Scots pine has a promising adaptability potential to the climate factors and stress condition of Horqin sandy land China. As a result of its uncomplicated nature, Mongolian Scots pine has been recommended for afforestation of reclamation sites, mainly on poor and dry sandy soils, exacerbated by the ongoing climate change.

Acknowledgment. We are thankful to the Beijing Forestry University and Chinese Academy of Forestry, China for supporting our work. This work was supported by International (Regional) Cooperation and Exchange Program of The National Natural Science Foundation of China (32061123005) and the National Natural Science Foundation of China (41971061).

REFERENCES

- [1] Ali, A., Iftikhar, M., Ahmad, S., Muhammad, S., Khan, A. (2016): Development of allometric equation for biomass estimation of *Cedrus deodara* in dry temperate forests of Northern Pakistan. – *Journal of Biodiversity and Environmental Sciences* 9: 43-50.
- [2] Ayanlade, A., Sergi, C. M., Di Carlo, P., Ayanlade, O. S., Agbalajobi, D. T. (2020): When climate turns nasty, what are recent and future implications? Ecological and human health review of climate change impacts. – *Current Climate Change Reports* 6: 55-65.

- [3] Babst, F., Poulter, B., Bodesheim, P., Mahecha, M. D., Frank, D. C. (2017): Improved tree-ring archives will support earth-system science. – *Nature Ecology & Evolution* 1: 1-2.
- [4] Bao, G., Liu, Y., Liu, N., Linderholm, H. W. (2015): Drought variability in eastern Mongolian Plateau and its linkages to the large-scale climate forcing. – *Climate Dynamics* 44: 717-733.
- [5] Bi, H., Turner, J., Lambert, M. J. (2004): Additive biomass equations for native eucalypt forest trees of temperate Australia. – *Trees* 18: 467-479.
- [6] Brienen, R. J., Phillips, O. L., Feldpausch, T. R., Gloor, E., Baker, T. R., Lloyd, J., Lopez-Gonzalez, G., Monteagudo-Mendoza, A., Malhi, Y., Lewis, S. L. (2015): Long-term decline of the Amazon carbon sink. – *Nature* 519: 344-348.
- [7] Briffa, K. R., Shishov, V. V., Melvin, T. M., Vaganov, E. A., Grudd, H., Hantemirov, R. M., Eronen, M., Naurzbaev, M. M. (2008): Trends in recent temperature and radial tree growth spanning 2000 years across northwest Eurasia. – *Philosophical Transactions of the Royal Society B: Biological Sciences* 363: 2269-2282.
- [8] Burrascano, S., Keeton, W. S., Sabatini, F. M., Blasi, C. (2013): Commonality and variability in the structural attributes of moist temperate old-growth forests: a global review. – *Forest Ecology and Management* 291: 458-479.
- [9] Butarbutar, T., Köhl, M., Neupane, P. R. (2016): Harvested wood products and REDD+: looking beyond the forest border. – *Carbon Balance and Management* 11: 1-12.
- [10] Camarero, J. J., Gazol, A., Sancho-Benages, S., Sangüesa-Barreda, G. (2015): Know your limits? Climate extremes impact the range of Scots pine in unexpected places. – *Annals of Botany* 116: 917-927.
- [11] Chave, J. r., Andalo, C., Brown, S., Cairns, M. A., Chambers, J., Eamus, D., Fölster, H., Fromard, F., Higuchi, N., Kira, T. (2005): Tree allometry and improved estimation of carbon stocks and balance in tropical forests. – *Oecologia* 145: 87-99.
- [12] Chave, J., Muller-Landau, H. C., Baker, T. R., Easdale, T. A., Steege, H. t., Webb, C. O. (2006): Regional and phylogenetic variation of wood density across 2456 neotropical tree species. – *Ecological Applications* 16: 2356-2367.
- [13] Chen, Y., Song, X., Zhang, Z., Shi, P., Tao, F. (2015): Simulating the impact of flooding events on non-point source pollution and the effects of filter strips in an intensive agricultural watershed in China. – *Limnology* 16: 91-101.
- [14] Cheng, Y. X., Li, Z. X. (1989): A study on biomass of three main forest types in *Larix gmelinii* forest. – *Inner Mongolia Forestry Investigation and Design* 4: 89-100.
- [15] Clark, D. A., Brown, S., Kicklighter, D. W., Chambers, J. Q., Thomlinson, J. R., Ni, J. (2001): Measuring net primary production in forests: concepts and field methods. – *Ecological Applications* 11: 356-370.
- [16] D’Odorico, P., Bhattachan, A., Davis, K. F., Ravi, S., Runyan, C. W. (2013): Global desertification: drivers and feedbacks. – *Advances in Water Resources* 51: 326-344.
- [17] Davi, N. K., Jacoby, G. C., Curtis, A. E., Baatarbileg, N. (2006): Extension of drought records for central Asia using tree rings: West-central Mongolia. – *Journal of Climate* 19: 288-299.
- [18] De Andres, E. G., Seely, B., Blanco, J. A., Imbert, J. B., Lo, Y. H., Castillo, F. J. (2017): Increased complementarity in water-limited environments in Scots pine and European beech mixtures under climate change. – *Ecohydrology* 10: e1810.
- [19] Dong, L., Zhang, L., Li, F. (2015): Developing additive systems of biomass equations for nine hardwood species in Northeast China. – *Trees* 29: 1149-1163.
- [20] Dong, L., Zhang, L., Li, F. (2016): Developing two additive biomass equations for three coniferous plantation species in Northeast China. – *Forests* 7: 136.
- [21] DÜthorn, E., Schneider, L., Günther, B., Gläser, S., Esper, J. (2016): Ecological and climatological signals in tree-ring width and density chronologies along a latitudinal boreal transect. – *Scandinavian Journal of Forest Research* 31: 750-757.

- [22] Feldpausch, T. R., Lloyd, J., Lewis, S. L., Brien, R. J., Gloor, M., Monteagudo Mendoza, A., Lopez-Gonzalez, G., Banin, L., Abu Salim, K., Affum-Baffoe, K. (2012): Tree height integrated into pantropical forest biomass estimates. – *Biogeosciences* 9: 3381-3403.
- [23] Freire, J. A., Rodrigues, G. C., Tomé, M. (2019): Climate change impacts on *Pinus pinea* L. silvicultural system for cone production and ways to contour those impacts: a review complemented with data from permanent plots. – *Forests* 10: 169-198.
- [24] Fritts, H. C., Smith, D. G., Cardis, J. W., Budelsky, C. A. (1965): Tree-ring characteristics along a vegetation gradient in northern Arizona. – *Ecology* 46: 393-401.
- [25] Fu, L., Sun, W., Wang, G. (2017): A climate-sensitive aboveground biomass model for three larch species in northeastern and northern China. – *Trees* 31: 557-573.
- [26] Gerelbaatar, S., Baatarbileg, N. (2011): Growth of scotch Pine (*Pinus sylvestris* L.) plantation in Northern Mongolia. – *Journal of Agricultural Science and Technology B* 1: 111-116.
- [27] Goodman, R. C., Phillips, O. L., Baker, T. R. (2014): The importance of crown dimensions to improve tropical tree biomass estimates. – *Ecological Applications* 24: 680-698.
- [28] Hao, B., Hartmann, H., Li, Y., Liu, H., Shi, F., Yu, K., Li, X., Li, Z., Wang, P., Allen, C. D. (2021): Precipitation gradient drives divergent relationship between non-structural carbohydrates and water availability in *Pinus tabulaeformis* of Northern China. – *Forests* 12: 133.
- [29] Hu, P., Zhang, W., Xiao, L., Yang, R., Xiao, D., Zhao, J., Wang, W., Chen, H., Wang, K. (2019): Moss-dominated biological soil crusts modulate soil nitrogen following vegetation restoration in a subtropical karst region. – *Geoderma* 352: 70-79.
- [30] Huang, J., Tardif, J. C., Bergeron, Y., Denneler, B., Berninger, F., Girardin, M. P. (2010): Radial growth response of four dominant boreal tree species to climate along a latitudinal gradient in the eastern Canadian boreal forest. – *Global Change Biology* 16: 711-731.
- [31] Huang, J., Yu, H., Guan, X., Wang, G., Guo, R. (2016): Nature Climate Change. – Accelerated dryland expansion under climate change 6: 166-171.
- [32] Huang, J., Li, Y., Fu, C., Chen, F., Fu, Q., Dai, A., Shinoda, M., Ma, Z., Guo, W., Li, Z. (2017): Dryland climate change: recent progress and challenges. – *Reviews of Geophysics* 55: 719-778.
- [33] Huang, Z., Cui, Z., Liu, Y., Wu, G. L. (2021): Carbon accumulation by *Pinus sylvestris* forest plantations after different periods of afforestation in a semiarid sandy ecosystem. – *Land Degradation & Development* 32: 2094-2104.
- [34] Ilvesniemi, H., Liu, C. (2001): Biomass distribution in a young Scots pine stand. – *Boreal Environment Research* 6: 3-8.
- [35] Jagodzinski, A. M., Kalucka, I. (2008): Age-related changes in leaf area index of young Scots pine stands. – *Dendrobiology* 59: 57-65.
- [36] Jagodziński, A. M., Dyderski, M. K., Gęsikiewicz, K., Horodecki, P. (2019): Effects of stand features on aboveground biomass and biomass conversion and expansion factors based on a *Pinus sylvestris* L. chronosequence in Western Poland. – *European Journal of Forest Research* 138: 673-683.
- [37] Jordaan, K., Lappan, R., Dong, X., Aitkenhead, I. J., Bay, S. K., Chiri, E., Wieler, N., Meredith, L. K., Cowan, D. A., Chown, S. L. (2020): Hydrogen-oxidizing bacteria are abundant in desert soils and strongly stimulated by hydration. – *Msystems* 5: e01131-01120.
- [38] Khan, D., Muneer, M. A., Nisa, Z.-U., Shah, S., Amir, M., Saeed, S., Uddin, S., Munir, M. Z., Lushuang, G., Huang, H. (2019): Effect of climatic factors on stem biomass and carbon stock of *Larix gmelinii* and *Betula platyphylla* in Daxing'anling Mountain of Inner Mongolia, China. – *Advances in Meteorology* 2019.
- [39] Körner, C. (2006): Plant CO₂ responses: an issue of definition, time and resource supply. – *New Phytologist* 172: 393-411.

- [40] Körner, C. (2017): A matter of tree longevity. – *Science* 355: 130-131.
- [41] Kullman, L., Kjällgren, L. (2006): Holocene pine tree-line evolution in the Swedish Scandes: recent tree-line rise and climate change in a long-term perspective. – *Boreas* 35: 159-168.
- [42] Kutschera, U., Niklas, K. J. (2013): Cell division and turgor-driven stem elongation in juvenile plants: a synthesis. – *Plant Science* 207: 45-56.
- [43] Kuznetsova, T., Mandre, M., Klõšeiko, J., Pärn, H. (2010): A comparison of the growth of Scots pine (*Pinus sylvestris* L.) in a reclaimed oil shale post-mining area and in a Calluna site in Estonia. – *Environmental Monitoring and Assessment* 166: 257-265.
- [44] Liu, Y., Bao, G., Song, H., Cai, Q., Sun, J. (2009): Precipitation reconstruction from Hailar pine (*Pinus sylvestris* var. *mongolica*) tree rings in the Hailar region, Inner Mongolia, China back to 1865 AD. – *Palaeogeography, Palaeoclimatology, Palaeoecology* 282: 81-87.
- [45] Liu, Y., Zhang, X., Song, H., Cai, Q., Li, Q., Zhao, B., Liu, H., Mei, R. (2017): Tree-ring-width-based PDSI reconstruction for central Inner Mongolia, China over the past 333 years. – *Climate Dynamics* 48: 867-879.
- [46] Liu, Y. Y., Wang, A. Y., An, Y. N., Lian, P. Y., Wu, D. D., Zhu, J. J., Meinzer, F. C., Hao, G. Y. (2018): Hydraulics play an important role in causing low growth rate and dieback of aging *Pinus sylvestris* var. *mongolica* trees in plantations of Northeast China. – *Plant, Cell & Environment* 41: 1500-1511.
- [47] Lloyd, A. H., Bunn, A. G. (2007): Responses of the circumpolar boreal forest to 20th century climate variability. – *Environmental Research Letters* 2: 045013.
- [48] Makarenko, A. (1985): Aboveground biomass of young Scots pine stands in Kazakhstan. – *Lesovedenie* 3: 11-19.
- [49] Mäkinen, H., Nöjd, P., Saranpää, P. (2003): Seasonal changes in stem radius and production of new tracheids in Norway spruce. – *Tree Physiology* 23: 959-968.
- [50] Mandal, R. A., Yadav, B. K. V., Yadav, K. K., Dutta, I. C., Haque, S. M. (2013): Development of allometric equation for biomass estimation of eucalyptus *camaldulensis*: a study from Sagarnath Forest, Nepal. – *Int J Biodiv Ecosyst* 1: 1-7.
- [51] Marqués, L., Madrigal-González, J., Zavala, M. A., Camarero, J. J., Hartig, F. (2018): Last-century forest productivity in a managed dry-edge Scots pine population: the two sides of climate warming. – *Ecological Applications* 28: 95-105.
- [52] Martínez-Sancho, E., Dorado-Liñán, I., Gutiérrez Merino, E., Matiu, M., Helle, G., Heinrich, I., Menzel, A. (2018): Increased water-use efficiency translates into contrasting growth patterns of Scots pine and sessile oak at their southern distribution limits. – *Global Change Biology* 24: 1012-1028.
- [53] Matías, L., Jump, A. S. (2012): Interactions between growth, demography and biotic interactions in determining species range limits in a warming world: the case of *Pinus sylvestris*. – *Forest Ecology and Management* 282: 10-22.
- [54] Mikšys, V., Varnagiryte-Kabasinskiene, I., Stupak, I., Armolaitis, K., Kukkola, M., Wójcik, J. (2007): Above-ground biomass functions for Scots pine in Lithuania. – *Biomass and Bioenergy* 31: 685-692.
- [55] Nascimbene, J., Benesperi, R., Brunialti, G., Catalano, I., Vedove, M. D., Grillo, M., Isocrono, D., Matteucci, E., Potenza, G., Puntillo, D. (2013): Patterns and drivers of β -diversity and similarity of *Lobelia pulmonaria* communities in Italian forests. – *Journal of Ecology* 101: 493-505.
- [56] Newbery, D., Ridsdale, C. (2016): Neighbourhood abundance and small-tree survival in a lowland Bornean rainforest. – *Ecological Research* 31: 353-366.
- [57] Oberhuber, W., Stumboeck, M., Kofler, W. (1998): Climate-tree-growth relationships of Scots pine stands (*Pinus sylvestris* L.) exposed to soil dryness. – *Trees* 13: 19-27.
- [58] Pecl, G. T., Araújo, M. B., Bell, J. D., Blanchard, J., Bonebrake, T. C., Chen, I.-C., Clark, T. D., Colwell, R. K., Danielsen, F., Evengård, B. (2017): Biodiversity redistribution under climate change: impacts on ecosystems and human well-being. – *Science* 355.

- [59] Pederson, N., Leland, C., Nachin, B., Hessler, A., Bell, A., Martin-Benito, D., Saladyga, T., Suran, B., Brown, P., Davi, N. K. (2013): Three centuries of shifting hydroclimatic regimes across the Mongolian Breadbasket. – *Agricultural and Forest Meteorology* 178: 10-20.
- [60] Piao, S., Mohammat, A., Fang, J., Cai, Q., Feng, J. (2006): NDVI-based increase in growth of temperate grasslands and its responses to climate changes in China. – *Global Environmental Change* 16: 340-348.
- [61] Pietrzykowski, M., Socha, J. (2011): An estimation of Scots pine (*Pinus sylvestris* L.) ecosystem productivity on reclaimed post-mining sites in Poland (central Europe) using of allometric equations. – *Ecological Engineering* 37: 381-386.
- [62] Putalová, T., Vacek, Z., Vacek, S., Štefančík, I., Bulušek, D., Král, J. (2019): Tree-ring widths as an indicator of air pollution stress and climate conditions in different Norway spruce forest stands in the Krkonoše Mts. – *Lesnický Casopis* 65: 21-33.
- [63] Qian, W., Qin, A. (2006): Spatial-temporal characteristics of temperature variation in China. – *Meteorology and Atmospheric Physics* 93: 1-16.
- [64] Seddon, A. W., Macias-Fauria, M., Long, P. R., Benz, D., Willis, K. J. (2016): Sensitivity of global terrestrial ecosystems to climate variability. – *Nature* 531: 229-232.
- [65] Shuren, J. (2001): Report on the causes of the early decline of *Pinus sylvestris* var. *mongolica* shelterbelt and its preventative and control measures in Zhang Gutai of Liaoning Province. – *Scientia Silvae Sinicae* 37: 131-138.
- [66] Song, L., Zhu, J., Li, M., Zhang, J., Lv, L. (2016): Sources of water used by *Pinus sylvestris* var. *mongolica* trees based on stable isotope measurements in a semiarid sandy region of Northeast China. – *Agricultural Water Management* 164: 281-290.
- [67] Sternberg, T. (2008): Environmental challenges in Mongolia's dryland pastoral landscape. – *Journal of Arid Environments* 72: 1294-1304.
- [68] Su, H., Axmacher, J. C., Yang, B., Sang, W. (2015): Differential radial growth response of three coexisting dominant tree species to local and large-scale climate variability in a subtropical evergreen broad-leaved forest of China. – *Ecological Research* 30: 745-754.
- [69] Svenning, J. C., Sandel, B. (2013): Disequilibrium vegetation dynamics under future climate change. – *American Journal of Botany* 100: 1266-1286.
- [70] Turan, Í. D., Dengiz, O., Özkan, B. (2019): Spatial assessment and mapping of soil quality index for desertification in the semi-arid terrestrial ecosystem using MCDM in interval type-2 fuzzy environment. – *Computers and Electronics in Agriculture* 164: 104933.
- [71] Usoltsev, V. A., Lin, H., Shobairi, S. O. R., Tsepordey, I. S., Ye, Z. (2020): Are there differences in the reaction of the light-tolerant subgenus *Pinus* spp. biomass to climate change as compared to light-intolerant genus *Picea* spp.? – *Plants* 9: 1255.
- [72] Vacek, S., Vacek, Z., Bílek, L., Simon, J., Remeš, J., Hůnová, I., Král, J., Putalová, T., Mikeska, M. (2016): Structure, regeneration and growth of Scots pine (*Pinus sylvestris* L.) stands with respect to changing climate and environmental pollution. – *Silva Fennica* 50: 1564.
- [73] Vacek, S., Vacek, Z., Remeš, J., Bílek, L., Hůnová, I., Bulušek, D., Putalová, T., Král, J., Simon, J. (2017): Sensitivity of unmanaged relict pine forest in the Czech Republic to climate change and air pollution. – *Trees* 31: 1599-1617.
- [74] Vacek, S., Vacek, Z., Bílek, L., Hůnová, I., Bulušek, D., Král, J., Brichta, J. (2019): Stand dynamics in natural Scots pine forests as a model for adaptation management? – *Dendrobiology*.
- [75] Vaganov, E., Hughes, M., Kirilyanov, A., Schweingruber, F., Silkin, P. (1999): Influence of snowfall and melt timing on tree growth in subarctic Eurasia. – *Nature* 400: 149-151.
- [76] Virtanen, R., Luoto, M., Rämä, T., Mikkola, K., Hjort, J., Grytnes, J. A., Birks, H. J. B. (2010): Recent vegetation changes at the high-latitude tree line ecotone are controlled by geomorphological disturbance, productivity and diversity. – *Global Ecology and Biogeography* 19: 810-821.

- [77] Vogt, J., Safriel, U., Von Maltitz, G., Sokona, Y., Zougmore, R., Bastin, G., Hill, J. (2011): Monitoring and assessment of land degradation and desertification: towards new conceptual and integrated approaches. – *Land Degradation & Development* 22: 150-165.
- [78] Wang, F., Pan, X., Wang, D., Shen, C., Lu, Q. (2013): Combating desertification in China: past, present and future. – *Land Use Policy* 31: 311-313.
- [79] Wang, X., Bi, H., Ximenes, F., Ramos, J., Li, Y. (2017): Product and residue biomass equations for individual trees in rotation age *Pinus radiata* stands under three thinning regimes in New South Wales, Australia. – *Forests* 8: 439.
- [80] Wang, Z., Yang, H., Wang, D., Zhao, Z. (2019): Spatial distribution and growth association of regeneration in gaps of Chinese pine (*Pinus tabulaeformis* Carr.) plantation in northern China. – *Forest Ecology and Management* 432: 387-399.
- [81] Yin, G., Hu, Z., Chen, X., Tiyyip, T. (2016): Vegetation dynamics and its response to climate change in Central Asia. – *Journal of Arid Land* 8: 375-388.
- [82] Zeng, W.-s., Tang, S.-z. (2012): Modeling compatible single-tree aboveground biomass equations for masson pine (*Pinus massoniana*) in southern China. – *Journal of Forestry Research* 23: 593-598.
- [83] Zhang, X., Cui, M., Ma, Y., Wu, T., Chen, Z., Ding, W. (2010): *Larix gmelinii* tree-ring width chronology and its responses to climate change in Kuduer, Great Xing'an Mountains. – *Ying yong sheng tai xue bao = The Journal of Applied Ecology* 21: 2501-2507.
- [84] Zhang, R., Zhou, X., Ouyang, Z., Avitabile, V., Qi, J., Chen, J., Giannico, V. (2019a): Estimating aboveground biomass in subtropical forests of China by integrating multisource remote sensing and ground data. – *Remote Sensing of Environment* 232: 111341.
- [85] Zhang, X., Zhang, X., Han, H., Shi, Z., Yang, X. (2019b): Biomass accumulation and carbon sequestration in an age-sequence of Mongolian pine plantations in Horqin sandy land, China. – *Forests* 10: 197.
- [86] Zheng, Y.-F., Hoefs, J. (1993): Effects of mineral precipitation on the sulfur isotope composition of hydrothermal solutions. – *Chemical Geology* 105: 259-269.
- [87] Zheng, X., Zhu, J., Yan, Q., Song, L. (2012): Effects of land use changes on the groundwater table and the decline of *Pinus sylvestris* var. *mongolica* plantations in southern Horqin Sandy Land, Northeast China. – *Agricultural Water Management* 109: 94-106.
- [88] Zhou, D., Zhao, X., Hu, H., Shen, H., Fang, J. (2015): Long-term vegetation changes in the four mega-sandy lands in Inner Mongolia, China. – *Landscape Ecology* 30: 1613-1626.
- [89] Zhu, J., Zeng, D., Kang, H., Wu, X., Fan, Z. (2005): *Decline of Pinus Sylvestris Var. Mongolica Plantation Forests on Sandy Land*. – China Forestry Publishing House, Beijing.
- [90] Zhu, J., Kang, H., Tan, H., Xu, M. (2006): Effects of drought stresses induced by polyethylene glycol on germination of *Pinus sylvestris* var. *mongolica* seeds from natural and plantation forests on sandy land. – *Journal of Forest Research* 11: 319-328.
- [91] Zhu, J., Zheng, X., Yan, Q. (2016): *Assessment of Impacts of the Three-North Protective Forest Program on Ecological Environments by Remote Sensing Technology-Launched after 30 Years (1978–2008)*. – Science Press, Beijing.
- [92] Zhu, Y., Zhang, J., Zhang, Y., Qin, S., Shao, Y., Gao, Y. (2019): Responses of vegetation to climatic variations in the desert region of northern China. – *Catena* 175: 27-36.

PROTOCOL FOR IN VITRO MASS PRODUCTION OF *NEPHROLEPIS EXALTATA* SCHOTT (BOSTON FERN)

NOFAL, E. M. S.¹ – SAYED, S. S.² – HASSAN, H. H. M.^{2*}

¹Hort. Dept., Fac. Agric, Kafr El-Sheikh Univ., Kafr El-Sheikh, Egypt

²Ornamental Plants Res. Dept., Hort. Res. Inst., Agric Res. Center, Giza, Egypt

*Corresponding author

e-mail: heba.khder456@gmail.com

(Received 27th Dec 2021; accepted 17th Mar 2022)

Abstract. This study was carried out in the Tissue Culture Laboratory of Horticulture Research Institute (HRI), Agricultural Research Center, Giza, Egypt during the years of 2020 and 2021 on Boston fern (*Nephrolepis exaltata* Schott cv. *Bostoniensis*) to find a commercial method for in vitro mass production in the shortest time possible. The statistical analysis revealed that the ideal time for the sterilization of explants with 0.1% mercuric chloride (MC) was 15 min, which resulted in the highest survival rate and the lowest contamination percentage of explants (66.66 and 77.77%, respectively). For the multiplication stage, the highest shootlet number and leaf number were recorded for explants culture in MS medium supplemented with 1.0 mg/l BAP with 1 g/l AC (35.17 shootlet/explant and 5.17 leaf/shootlet). For rooting stage, full MS medium supplemented with 0.5 mg/l NAA and 1 g/l AC produced the highest rooting percentage, root number/plantlet, and longest root length (100.0%, 29.4 root/shootlet and 4.5 cm, respectively). Culturing plants in peat moss recorded the longest plant, also the greatest leaf number and the longest root (4.01 cm, 8.75 leaf/number and 1.97 cm, respectively).

Keywords: mercuric chloride, MS medium, cytokinins, auxins, activated charcoal

Introduction

Boston fern (*Nephrolepis exaltata* Schott cv. *Bostoniensis*) is an ornamental foliage plant considered today as one of the most marketable indoor pot plants (Hagiabad et al., 2007). *Nephrolepis exaltata* belongs to the Nephrolepidaceae family. It is native to North, Central, and South America (Karmakar et al., 2020).

Due to its improved ornamental value and higher tolerance to indoor environmental conditions, the mutant was named as *N. exaltata* 'Bostoniensis' and quickly gained its popularity as Boston fern (Schall et al., 2018).

Nephrolepis exaltata propagates usually asexually through long thin and green runners, (also through spores) and is a common houseplant commercially found in florist shops (Popovici, 2018). Due to the restriction of conventional propagation methods, mass propagation of this plant has increased through in vitro culture techniques (Hagiabad et al., 2007) and exploited as a common commercial method (Shafiei, 2008).

The efficient plant in vitro culture processes start with an optimal sterilization technique. The choice of time period and chemical agents depend on the sensitivity of the explant to be sterilized (Örge et al., 2018). There are a lot of common sterilants for the surface sterilization of plant material. Popular disinfectants are sodium hypochlorite, ethanol, mercuric chloride, calcium hypochlorite, silver nitrate, hydrogen peroxide, bromine water, and Tween 20 (Ishfaq, 2016).

Growth optimal of tissues may vary for different plants according to their nutritional requirements. Additionally, tissues from diverse parts of plants may have different

requirements for satisfactory growth (Sulaiman et al., 2020). Cytokinins and auxins are the most widely used plant growth regulators in in vitro plant culture and are usually used together. The ratio between cytokinins to auxins determining the type of culture was established or regenerated. In general auxins promote both cell division and cell growth while cytokinins promote cell division. A high auxin to cytokinin ratio generally favours root formation, while a high cytokinin to auxin ratio favours shoot formation. An intermediate ratio favours callus production (Sulaiman et al., 2020). Activated charcoal is commonly added to tissue culture media.

The effects of activated charcoal may be due to establishing a darkened environment; adsorption of undesirable/inhibitory substances; adsorption of growth regulators and other organic compounds, or the release of growth promoting substances present in or adsorbed by activated charcoal (Pan and Van Staden, 1998). Peat moss is one of the most important constituents of mixture media due to its capacity in affecting plant growth either indirectly or directly. Indirectly it improves the physical conditions of mixture media by enhancing aggregation, aeration (8%) and water retention (77%), thereby creating a suitable environment for root growth (Sensi and Loffredo, 1999). The aim of this research was to find commercial method for in vitro mass production for *Nephrolepis exaltata* Schott.

Materials and methods

This study was performed in the Tissue Culture Laboratory of Horticulture Research Institute (HRI), Agricultural Research Center; Giza, Egypt during the years 2020 and 2021 to find commercial method for in vitro mass production for *Nephrolepis exaltata* Schott.

Plant material

The plant sample of *Nephrolepis exaltata* Schott was obtained from the greenhouse of Al Zohriya Garden, Agricultural Research Center (*Fig. 1*).

Culture medium and incubation condition

The explants were cultured on 250 ml/jar containing 25 ml of MS (Murashige and Skoog, 1962) basal medium enriched with 25 g/l sucrose and solidified with 7 g/l agar. The pH medium was adjusted to 5.7 ± 0.1 with NaOH or HCl before sterilization by autoclaving at 121 °C for 20 min. The Plant growth regulators (PGR) were used according to the experimental stage: benzylaminopurine (BAP), 6-Furfuryl-aminopurine (kinetin or kin), isopentenyl adenine (2 ip) and naphthalene acetic acid (NAA). All cultures were stored in room chamber at 24 ± 1 °C, under fluorescent illumination of 2000-2500 lux at 16 \8 day\night fluctuation.

Sterilization stage

Runners of *N. exaltata* Schott were used as explants for in vitro cultures. Pieces of the runners were removed, thoroughly washed with soap and water for 15 min, rinsed under a running water for 1 h and then taken inside the laminar air flow cabinet for further sterilization. These segments were disinfected by soaking in either clorox at 5% (v/v) or mercuric chloride HgCl₂ (MC) at 0.1% each for (10, 15 or 20 min) with a few drops of Tween-20, then rinsed 3 times by a distilled sterilized water. These segments

were chopped to (1.0 cm) long segments (explants) before being put individually in - MS medium free hormones for three weeks. Each treatment included nine explants for three replicates. At the end of the sterilization period percentages of contamination-free, and surviving explants were calculated. Contamination-free and surviving explants were taken for multiplication stage.



Figure 1. *Nephrolepis exaltata* Schott (Boston fern)

Multiplication stage

The survived contamination- free explants were inoculated on MS medium fortified with BAP, kin or 2 ip at 0.0, 0.5, 1.0 or 1.5 ppm) with or without activated charcoal (AC) at (1 g/l). Each treatment was done in three replications with nine explants kept for two months (two subcultures). At the end of the second subculture data were noted [shootlet number/explant, leaf number/shootlet, shootlet length (cm), fresh weight (g), total chlorophyll and carotenoids (mg/g fw)]. For pigments determination, according to Saric et al. (1967) the ethanolic extractions were subjected to define the colour density to measure chlorophyll and carotenoids against the blank methanol.

Rooting stage

The multiplied shootlets were transferred to different MS strength (full, $\frac{3}{4}$, $\frac{1}{2}$ or $\frac{1}{4}$ strength) without or with NAA 0.5 ppm. All previous treatments with or without activated charcoal. Each treatment included nine shootlets in three replicates. After six weeks of culturing, rooting percentage, root number/plantlet, root length (cm) were recorded.

Acclimatization stage

After eight weeks, the rooted plantlets were carefully removed out of the jars and the roots were washed under running water. They were then cultured in plastic pots containing peat moss, peat moss: perlite (1:1 v/v), peat moss: perlite (2:1 v/v), peat moss: sand (2:1 v/v), or peat moss: sand: perlite (1:1:1 v/v/v). These pots were covered with polyethylene bags and maintained in a greenhouse for eight weeks to acclimatize. The polythene bags were progressively, taken away to expose the plantlets to the outer environment. Each treatment contained nine plantlet for three replicates. Data recorded at the end of acclimatization period were plantlet height (cm) leaf number/plantlet, root number/plantlet, root length (cm).

Statistical analysis

All experiments were factorial, except for the acclimatization experiment, which has one factor. The experiments were designed in complete randomized design. Least Significant Differences (L.S.D.) at $p \leq 0.05$ were used for the comparison of means according to Steel and Torrie (1980).

Results and discussion

Sterilization stage

Effects of various types, times and their interactions with sterilization agents on contamination-free% and survival% of Nephrolepis exaltata Schott.

The results on the effect of exposure to clorox and mercuric chloride (MC) for different times and their interaction are displayed in *Table 1*. The highest percentage of survival and contamination-free explants (70.37% and 81.48%, respectively) was obtained by treating the explants with 0.1% MC, while the reverse was observed with clorox, where it gave 59.25 survival% and 7.41% contamination-free explants.

Table 1. *Effect of various types, times and their interactions with sterilization agents on contamination-free % and survival % of Nephrolepis exaltata Schott.*

	Survival %			Free contamination %		
	5% Clorox	0.1% MC	Mean A	5% Clorox	0.1% MC	Mean A
10 min	77.77	88.89	83.33	0.00	66.66	33.33
15 min	55.55	66.66	61.11	11.11	77.77	44.44
20 min	44.44	55.55	50.00	11.11	100.0	55.56
Mean B	59.25	70.37		7.41	81.48	
LSD _{0.05}	A = 19.87 B = 24.34 A × B = 34.42			A = 11.07 B = 13.56 A × B = 19.18		

L.S.D. at 0.05 = least significant different at 0.05 level of probability

For the different immersing times, the maximum survival percentage (83.33%) was obtained in explants treated with sterilization agent for 10 min but this time decreased contamination-free explants to the lowest percentage (33.33%). The suitable time for survival and contamination free (61.11 and 44.44%) was recorded when immersing explants for 15 min in a disinfectant solution.

For the interaction between disinfections and time the results were as follows, exposure of explants for 10 min, in 0.1% MC increased survival % to 88.88% and contamination-free explants to 66.66%, while using 5% clorox gave the lowest percentage of contamination-free in all cases.

Our results on sterilization of explants are in line with Ali et al. (2004) showing that 60-75% contamination free cultures of sugarcane were derived after treatment with 0.1% HgC12 for 10 min. Yadav et al. (2017) on banana cv. Grand Naine, Guaranna et al. (2017) on *Punica granatum* reported that, the best results with lower contamination and higher explants survival % were recorded with 0.1% MC.

Multiplication stage

Effects of PGR, activated charcoal (AC) and their interactions on shootlet number/explant and shoot length (cm) of Nephrolepis exaltata Schott.

Data presented in Table 2 revealed the effects of PGR and activated charcoal (AC). For Shootlet number, the highest shootlet number was observed on MS medium supplemented with 1.0 mg/l BA, with an average number of 29.00 shoots per explants, On the other hand, kin at 1.0, 1.5 mg/l gave the lowest shootlet number (12.5 shootlets). Using AC increased shootlet number to 23.47 shootlet/explant compared to medium without AC which decreased shootlet number to 11.23 shootlet/explant. For the interaction between PGR and AC, the highest number of shootlets was a result of using 1.0 mg/l BAP with 1 g/l AC which recorded 35.67 shootlets, while applying of 1.5 mg/l kin without AC gave the lowest values (3.67 shootlets).

Table 2. *Effects of PGR, activated charcoal (AC) and their interactions on shootlet number/explant and Shoot length (cm) of Nephrolepis exaltata Schott.*

	Shootlet number/explant			Shoot length (cm)		
	Without AC	With AC	Mean A	Without AC	With AC	Mean A
Control	14.00	15.00	14.50	0.80	1.00	1.15
0.5 mg/l BAP	15.00	30.00	22.50	0.75	1.60	1.18
1.0 mg/l BAP	22.03	35.67	29.00	0.65	1.67	1.16
1.5 mg/l BAP	11.67	34.33	23.00	0.38	1.53	0.96
0.5 mg/l Kin	6.00	28.00	17.00	0.77	1.87	1.32
1.0 mg/l Kin	5.67	19.33	12.50	0.83	2.57	1.70
1.5 mg/l Kin	3.67	21.33	12.50	0.71	2.23	1.47
0.5 mg/l 2 iP	12.67	14.33	13.50	0.79	2.97	1.88
1.0 mg/l 2 iP	12.33	15.33	13.80	0.87	2.83	1.85
1.5 mg/l 2 iP	9.00	21.33	15.17	0.71	3.07	4.89
Mean B	11.23	23.47		0.726	2.183	
LSD _{0.05}	A = 3.454 B = 1.545 A×B = 4.885			A = 0.1811 B = 0.08098 A×B = 0.2561		

L.S.D. at 0.05 = least significant different at 0.05 level of probability

For shootlet length (cm), the longest shootlet was achieved for culturing explants on medium containing 2 iP at 0.5, 1.0 or 1.5 mg/l (1.88, 1.85, and 4.89 cm, respectively), while the shortest shootlets were recorded for culturing explants on MS medium free PGR (control) which gave 1.15 cm. For AC, MS medium supplemented with 1 g/l AC recorded the longest shootlet (2.183 cm), compared to the medium without AC which gave shortest shootlets (0.726 cm). For the interaction between PGR and AC, using 2 iP at 1.5 mg/l with AC gave rise to the longest shootlet (3.07 cm). The shortest shootlets were observed for BAP at 1.5 mg/l without AC (0.38 cm).

In this concern, Datta et al. (2006) on *Taxus wallichiana* and Stojicic et al. (2012) on *Pinus peuce* reported the lengthening effect of AC on internodes in plants. The use of activated charcoal in the intergeneric hybrid of orchid *Laeliocattleya amber* x *Brassocattleya pastoral* resulted in the greatest number of shoots (Villa et al., 2014). Souza et al. (2021) on *Cattleya crispata* revealed that adding activated charcoal after

ninety days of culture for in vitro multiplication of orchid *C. crispata* gave the longest and greatest number of shooting.

Effects of PGR, activated charcoal (AC) and their interactions on leaf number/shootlet and fresh weight (g) of Nephrolepis exaltata Schott.

Data presented in Table 3 showed significant differences between PGR, activated charcoal (AC) and their interactions. For leaf number, the effect of PGR, medium free PGR (control) resulted in the largest number of leaves (4.67 leaves), compared to other treatments. For AC, the medium containing AC recorded the greatest values of leaf number (4.063 leaf/shootlet) while the lowest values in the same interest were a result of using MS medium without AC (3.377 leaf/shootlet). For the interaction between PGR and AC, the greatest number of leaves was obtained by BAP at 1.0 mg/l with AC which produced (5.17 leaf/shootlet). The lowest values in the same concern were results of using BAP at 1.0 or 1.5 mg/l without AC (1.00 leaf/shootlet).

Table 3. *Effects of PGR, activated charcoal (AC) and their interactions on leaf number/shootlet and fresh weight (g) of Nephrolepis exaltata Schott.*

	Leaf number/shootlet			Fresh weight (g)		
	Without AC	With AC	Mean A	Without AC	With AC	Mean A
Control	4.90	4.43	4.67	0.70	1.80	1.25
0.5 mg/l BAP	1.17	5.03	3.10	0.82	2.43	1.63
1.0 mg/l BAP	1.00	5.17	3.08	0.79	1.93	1.36
1.5 mg/l BAP	1.00	4.63	2.82	0.52	2.10	1.31
0.5 mg/l Kin	4.33	4.27	4.30	0.84	2.57	1.71
1.0 mg/l Kin	4.23	3.87	4.05	0.83	1.60	1.22
1.5 mg/l Kin	3.93	4.33	4.13	0.77	1.83	1.30
0.5 mg/l 2 iP	4.87	2.97	3.92	1.53	1.57	1.55
1.0 mg/l 2 iP	4.27	2.73	3.50	1.40	1.27	1.33
1.5 mg/l 2 iP	4.07	3.20	3.63	1.03	1.90	1.47
Mean B	3.377	4.063		0.925	1.900	
LSD _{0.05}	A = 0.4262 B = 0.1906 A×B = 0.6028			A = 0.2123 B = 0.09495 A×B = 0.3003		

L.S.D. at 0.05 = least significant different at 0.05 level of probability

For fresh weight, the heaviest fresh weight of shootlet were obtained when 0.5 mg/l kin was used (1.71 g), while using kin at 1.0 mg/l or medium free PGR (control) gave the lightest fresh shootlet (1.22 and 1.25 g, respectively). For AC, MS medium supplemented with AC gave the heaviest fresh weight (1.90 g) than without AC (0.93 g). For the interaction, using 0.5 mg/l kin with AC resulted in the heaviest fresh weight (2.57 g). The lightest shootlets resulted when BAP without AC was applied which gave 0.52 g.

In this respect, Moraes et al. (2003) noticed that the best results for the plant fresh weight of Brazilian native orchids were observed with MS media supplemented with 1 g/l of activated charcoal (AC). Moreover, Lajayer et al. (2011) reported that the maximum shoot fresh weight was devoted to plantlets of potato grown on medium supplemented with 0.5% of AC in addition to the fresh weight of shoot increased with

ABA at 1 and 4 μM . An et al. (2021) showed that the fresh weight of orchid species *Sedirea japonica* shootlet cultured in MS and 1/2 MS medium with activated charcoal and BAP was approximately 6 times higher than that of shootlet grown in MS and 1/2 MS medium without activated charcoal and BAP.

Effects of PGR, activated charcoal (AC) and their interactions on total chlorophyll (mg/g fw) and carotenoids (mg/g fw) of Nephrolepis exaltata Schott.

As shown in Table 4 there were significant correlations of PGR, activated charcoal (Ac) and their interactions. For total chlorophyll, the highest total chlorophyll content was a result of using kin at 1.0 mg/l, which recorded 1.59 mg/g fw, while the lowest one was obtained upon using BAP at 1.5 mg/l (0.88 mg/g fw). For the effect of AC, medium including AC induced more total chlorophyll content (1.52 mg/g fw) compared to medium without AC which gave 1.03 mg/g fw. For the interaction, medium fortified with 1.0 mg/l kin with AC produced the highest content of total chlorophyll (1.95 mg/g fw) compared with using 1.5 mg/l BAP which recorded 0.47 mg/gfw.

Table 4. *Effects of PGR, activated charcoal (AC) and their interactions on total chlorophyll (mg/g fw) and carotenoids (mg/g fw) of Nephrolepis exaltata Schott.*

	Total chlorophyll (mg/g fw)			Carotenoids (mg/g fw)		
	Without AC	With AC	Mean A	Without AC	With AC	Mean A
Control	1.31	1.71	1.50	0.16	0.31	0.24
0.5 mg/l BAP	0.97	1.37	1.17	0.14	0.22	0.18
1.0 mg/l BAP	0.87	1.38	1.12	0.20	0.23	0.21
1.5 mg/l BAP	0.47	1.29	0.88	0.08	0.28	0.18
0.5 mg/l Kin	0.75	1.19	0.97	0.15	0.37	0.24
1.0 mg/l Kin	1.23	1.95	1.59	0.17	0.41	0.29
1.5 mg/l Kin	1.14	1.48	1.31	0.15	0.51	0.33
0.5 mg/l 2 iP	1.25	1.72	1.48	0.25	0.44	0.35
1.0 mg/l 2 iP	1.27	1.67	1.47	0.30	0.48	0.39
1.5 mg/l 2 iP	1.03	1.42	1.22	0.26	0.43	0.34
Mean B	1.03	1.52		0.19	0.36	
LSD _{0.05}	A = 0.3447 B = 0.1542 A×B = 0.4875			A = 0.08265 B = 0.03696 A×B = 0.1169		

L.S.D. at 0.05 = least significant different at 0.05 level of probability

Regarding carotenoids, applying 2 iP at 1.0 mg/l resulted in the highest content of carotenoids (0.39 mg/g fw) while the lowest carotenoids content was observed with BAP at 0.5 mg/l (0.18 mg/g fw). For AC, MS medium with AC produced more carotenoids content (0.36 mg/g fw) than without AC (0.19 mg/g fw). For the effect of the interaction between PGR and AC, kin at 1.5 mg/l with AC resulted in the highest carotenoids content (0.51 mg/g fw), while the lowest content (0.08 mg/g fw) was induced by BAP at 1.5 mg/l without AC.

These results coincided with the earlier data found by Tung Ming Sung (1997) on *Cucumis sativus* and Gao et al. (2000) on *Carthamus tinctorius*. They showed that the different concentrations of cytokinins had a significant effect on the chlorophylls and carotenoids formation capacity.

Rooting stage

Effects of MS strength medium, activated charcoal (AC) and their interactions on rooting percentage, root number/shootlet and root length (cm) of Nephrolepis exaltata Schott.

The illustrated values in Table 5 showed significant differences resulted for MS strength medium and AC and their interactions. For rooting percentage, the highest rooting percentage was achieved in $\frac{3}{4}$ MS with or without 0.5 mg/l NAA or full MS plus 0.5 NAA (94.44%), while the lowest values resulted from $\frac{1}{2}$ MS strength plus 0.5 NAA (72.22%). For the effect of AC, the highest rooting percentage was obtained from MS with AC (94.44%), while MS without AC the lowest rooting ratio (79.16%) was achieved. The interaction between MS strength and AC resulted in greater percentage of rooting in most of the treatments, with a percentage ranging between 100, 88.89 and 77.77% while the lowest rooting percentage (44.44%) resulted when $\frac{1}{2}$ MS plus 0.5 NAA without AC was used.

Table 5. *Effects of MS strength medium, activated charcoal (AC) and their interactions on rooting percentage, root number/shootlet and root length (cm) of Nephrolepis exaltata Schott.*

	Rooting %			Root number/shootlet			Root length (cm)		
	Without AC	With AC	Mean A	Without AC	With AC	Mean A	Without AC	With AC	Mean A
Full MS	77.77	100.0	88.89	10.54	23.20	16.87	0.65	1.13	0.89
$\frac{3}{4}$ MS	88.89	100.0	94.44	11.23	16.10	13.67	0.65	0.91	0.78
$\frac{1}{2}$ MS	77.77	77.77	77.77	3.78	3.77	3.78	0.36	0.27	0.32
$\frac{1}{4}$ MS	88.89	77.77	83.33	6.88	7.89	7.39	0.75	0.65	0.70
Full + 0.5NAA	88.89	100.0	94.44	11.53	29.40	20.47	0.59	4.50	1.05
$\frac{3}{4}$ + 0.5NAA	88.89	100.0	94.44	10.33	16.57	13.45	0.58	1.46	1.02
$\frac{1}{2}$ + 0.5NAA	44.44	100.0	72.22	2.44	7.44	4.94	0.28	0.76	0.52
$\frac{1}{4}$ + 0.5NAA	77.77	100.0	88.89	4.33	10.53	7.43	0.57	0.99	0.78
Mean B	79.16	94.44		7.634	14.36		0.554	0.958	
LSD _{0.05}	A = 20.77 B = 10.38 A×B = 29.37			A = 1.315 B = 0.658 A×B = 1.860			A = 0.348 B = 0.172 A×B = 0.486		

L.S.D. at 0.05 = least significant different at 0.05 level of probability

For root number, it was noticed that the highest root number recorded by using full MS plus 0.5 mg/l NAA which recorded 20.47 roots, while the lowest number of roots resulted from using $\frac{1}{2}$ MS without or with 0.5 mg/l NAA (3.78 or 4.94 roots, respectively). For AC, it was observed that MS with AC gave more roots (14.36 roots) than MS without AC (7.63 roots). For the interaction between MS strength medium and AC, applying full MS plus 0.5 NAA with AC gave rise to the highest number of roots (29.40 roots). The lowest value in the same concern was obtained when $\frac{1}{2}$ MS plus 0.5 NAA without AC was applied (2.44 roots).

For root length, it was observed that the longest root (1.05 cm) was observed by using full MS plus 0.5 mg/l NAA, while the shortest roots resulted when using $\frac{1}{2}$ MS without NAA (0.32 cm). In respect to AC, MS with AC gave longer roots (0.958 cm) than MS without AC (0.554 cm). For the interaction between MS strength and AC, the

longest root (4.50 cm) was recorded from cultured shoots on full MS plus 0.5 mg/l NAA, while, the shortest roots were a result from using ½ MS with AC (0.27 cm).

A wide survey of the obtained data indicated that the shoots of *Fortunella crassifolia* were obtained from epicotyl explants, that recorded maximum rooting (75%) on ½ MS medium supplemented with NAA, kin and AC (Yang et al., 2006). Haddad and Bayerly (2014) remarked that during rooting of the fern *Asplenium nidus*, the maximum root length was observed when NAA was added at 0.5 mg/l. Dev et al. (2015) found that supplementing with AC was important not only for promoting the rooting frequency, but also for improving overall root quality, essential for subsequent ex vitro survival. Seleem and Taha (2021) reported that half strength MS medium with 0.5 mg L-1 NAA gave the lowest values of rooted shoots percentage, number of roots/shoot, and average root length (cm) (75%, 4.0, 3.8 cm, respectively).

Acclimatization stage

Effects of various substrate types on acclimatization for plant behaviour of Nephrolepis exaltata Schott.

Data presented in Table 6 showed significant differences between the effects of various substrates on vegetative growth (plantlet length and leaf number/plantlet), while non significant differences on root growth (root length and root number/plantlet). The plantlets acclimatized in peat moss alone gave the longest plant and greatest leaf number (4.01 cm and 8.75 leaf/plant, respectively). On the other hand, acclimatized plants in Peat moss + Sand (1:1 v: v) produced the shortest plants (2.78 cm), while the lowest number of leaves was obtained from using peat moss + sand (2:1 v: v) which gave 6.17 leaf/plantlet.

Table 6. *Effects of various substrate types on acclimatization for plant behaviour of Nephrolepis exaltata Schott.*

	Plantlet length (cm)	Leaf number/plantlet	Root length (cm)	Root number/plantlet
Peat moss	4.01	8.75	1.97	6.33
Peat moss + Perlite (1:1)	3.00	7.70	1.43	7.67
Peat moss + Perlite (2:1)	2.93	8.55	1.33	7.67
Peat moss + Sand (1:1)	2.78	6.75	1.10	6.33
Peat moss + Sand (2:1)	3.15	6.17	1.70	6.67
Peat moss + Perlite + Sand (1:1:1)	3.71	7.75	1.27	7.67
LSD _{0.05}	1.214	1.581	NS	NS

L.S.D. at 0.05 = least significant different at 0.05 level of probability (NS: Non significant differences)

In this concern, Kurtar et al. (2010) transplanted plantlets of winter squash (*Cucurbita maxima*) to soil, sand, perlite and peat moss, to decide the growth media effects on growth and survival of in vitro plantlets during acclimatization stage. They found that the highest survival % and plant height were recorded from peat moss as a potting medium while the lowest values were resulted when sand was used, in the same request. Abbas et al. (2011) reported that the in vitro derived plantlets of *Zingiber officinale* were acclimatized in plastic trays including different soil mixture. They revealed that the highest survival% (100%) was observed when only peat moss was used. Other mixtures, i.e. peat moss: sand (1:1), peatmoss: sand: perlite (1:1:1) and peat

moss: sand: vermiculite (1:1:1) recorded 80, 80 and 60% survival percentage, respectively. Wang et al. (2013) remarked that survival ratio of *Cymbidium lowianum* plantlets (Orchidaceae) was up to 92 percent in peat moss after 1 month of acclimatization. Taha et al. (2018) acclimatized plantlets of *Dillenia indica* successfully in peat moss alone or a mixture of peat moss + perlite + sand.

Conclusion

Data in *Figure 2* revealed that, sterilization explant with 0.1% mercuric chloride (MC) for 15 min the suitable time and disinfection for survival and free contamination explant percentage. For multiplication stage, the greatest shootlet number and leaf number were recorded in explants culture in MS medium supplemented with 1.0 mg/l BAP with 1 g/l AC. On rooting stage, full MS medium supplemented with 0.5 mg/l NAA and 1.0 g/l AC produced the highest rooting percentage, root number/plantlet, and the longest root length. Culturing plantlet in peat moss recorded the longest plant, the greatest leaf number and the longest root.

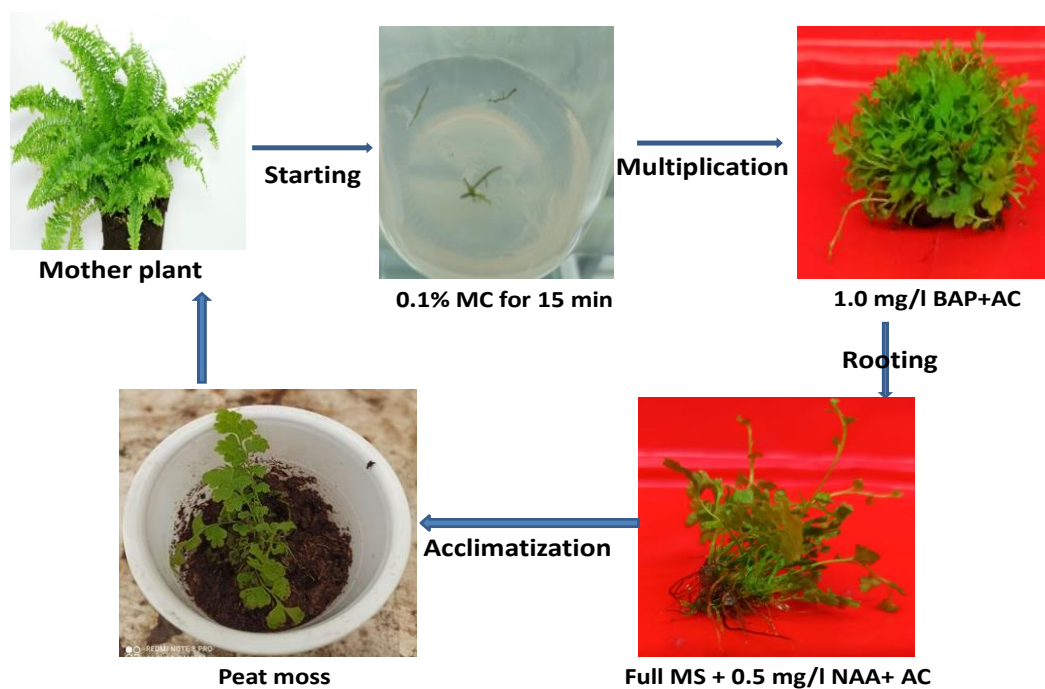


Figure 2. Different stages on micropropagation of *Nephrolepis exaltata* Schott.

REFERENCES

- [1] Abbas, M. S., Taha, H. S., Aly, U. I., El-Shabrawi, H. M., Gaber, E. S. I. (2011): In vitro propagation of ginger (*Zingiber officinale* Rosco). – Journal of Genetic Engineering and Biotechnology 9(2): 165-172.
- [2] Ali, S., Hassan, S. W., Razi-ud-Din, S., Shah, S., Zamir, R. (2004): Micropropagation of sugarcane through bud culture. – Sarhad J. Agric. 20(1): 79-82.

- [3] An, J., Kim, P. B., Park, H. B., Kim, S., Park, H. J., Lee, C. W., Lee, B. D., Kim, N. Y., Hwang, J. E. (2021): Effects of different growth media on in vitro seedling development of an endangered orchid species *Sedirea japonica*. – *Planta* 10(6): 1193.
- [4] Datta, M. M., Majumder, A., Jha, S. (2006): Organogenesis and plant regeneration in *Taxus wallichiana* (Zucc.). – *Plant Cell Reports* 25: 11-8.
- [5] Dev, R., Singh, S. K., Singh, A. K., Verma, M. K. (2015): Comparative in vitro multiplication of some grape (*Vitis vinifera*) genotypes. – *Ind. J. Agr. Sci.* 85: 1477-1483.
- [6] Dharishini, M. P., Moorthy, M. K., Balasubramanian, K. (2015): Effects of plant growth regulators and activated charcoal on regeneration and plantlet development in Neer Brahmi (*Bacopa monnieri*). – *J Acad Ind Res* 4: 69-74.
- [7] Gao, W. Y., Fan, L., Paek, K. Y. (2000): Yellow and red pigment production by cell cultures of *Carthamus tinctorius* in a bioreaction. – *Plant Cell, Tissue & Organ Culture* 60(2): 95-100.
- [8] Guaranna, P., Hosamani, I., Sathyanarayana, R., Hegdeand, R., Hipparagi, K. (2017): Micropropagation in pomegranate (*Punica granatum* L.) cv. 'Bhagwa' through Indirect Organogenesis and assessment of genetic fidelity by RAPD marker. – *Biotechnology Journal International* 20: 1-8.
- [9] Haddad, S., Bayerly, R. (2014): In vitro propagation of ferns (*Asplenium nidus*) via spores culture. – *Jordan J. Agric. Sci.* 10(1): 144-153.
- [10] Hagiabad, M. S., Hamidoghli, Y., Gazvini, R. F. (2007): Effects of different concentrations of mineral salt, sucrose and benzyladenine on Boston fern (*Nephrolepis exaltata* Schott cv. *Bostoniensis*) runner tips Initiation. – *JWSS-Isfahan University of Technology* 11(40): 137-146.
- [11] Ishfaq, S., Ahmed, S. D., Shah, H. A., Khan, R. T., Bukhari, S. M. F., Hameed, I., Mubeen, H., Awan, N., Abbas, S. R., Raza, S. (2016): In-vitro optimization protocol of wheat cultivars in newly established lab of plant culture, *Muzaffarad*. – *Euro J Pharma and Med Res* 3(3): 477-479.
- [12] Joshi, P., Dhawan, V. (2007): Assessment of genetic fidelity of micropropagated *Swertia chirayita* plantlets by ISSR marker assay. – *Biol. Plant.* 51: 22-26.
- [13] Karmakar, B., Chakrabarty, S., Hayat, A., Bagchi, S. (2020): Processing of *Nephrolepis exaltata* with glycerine to enhance shelf life by drying. – *Int. J. Curr. Microbiol. App. Sci.* 9(3): 348-356.
- [14] Kurtar, E. S., Balkaya, A., Özbek, N. (2010): Effects of polymers and growth media on in vitro plantlets of winter squash (*Cucurbita maxima* Duch. ex Lam.) and pumpkin (*Cucurbita moschata* Duch. ex Poir.) in acclimatization. – *Annals of Biological Research* 1(2): 148-154.
- [15] Lajayer, H. M., Esmailpour, B., Chamani, E. (2011): Hinokitiol and activated charcoal influence the microtuberization and growth of potato (*Solanum tuberosum* cv. *Agria*) plantlets in vitro. – *Australian Journal of Crop Science* 5(11): 1481-1485.
- [16] Moraes, L. M., Faria, R. T., Cuquel, F. L. (2003): Activated charcoal for in vitro propagation of Brazilian orchids. – *V International Symposium on New Floricultural Crops* 683: 383-390.
- [17] Murashige, T., Skoog, F. (1962): A revised medium for rapid growth and bio-assay with tobacco tissue culture. – *Physiolgia Plantarum* 15: 473-497.
- [18] Öргеç, M., Karakaş, F. P., Şahin, G., Ferdi, A. Ğ. I. L., Zencirci, N. (2018): Einkorn (*Triticum monococcum* ssp. *monococcum*) in vitro propagation sterilization protocol. – *Inter. J. of Secondary Metabolite* 5(2): 67-74.
- [19] Pan, M. J., Van Staden, J. (1998): The use of charcoal for in vitro culture. A review. – *Plant Growth Regulation* 26(3): 155-163.
- [20] Popovici, P. C., Ancuceanu, V. R., Oлару, T. O., Stoicescu, C. S., Dinu, M., Ancuceanu, V. R. (2018): Toxicity assessment of *Nephrolepis exaltata* (L.) Schott, Fam. Nephrolepidaceae. – *Acta Biologica Marisiensis* 1(1): 26-35.

- [21] Saric, M.; Kostrori, R.; Cupina, T., Geric, I. (1967): Chlorophyll determination. – Univ. Noven Sadu Praktikum is kiziologize Bilijaka Beogard, Haucana, Anjiga.
- [22] Schall, W., Huo, H., Chen, J. (2018): Cultural Guidelines for Commercial Production of Boston fern (*Nephrolepis exaltata* ‘Bostoniensis’). – EDIS 2018(1).
- [23] Seleem, E., Taha, Z. K. (2021): Effect of plant growth regulators on in vitro direct organogenesis of *Paulownia tomentosa* plant. – Scien. J. of Agric. Sci. 3(1): 111-118.
- [24] Sensi, N., Loffredo, E. (1999): The Chemistry of Soil Organic Matter. – In: Spark, D. L. (ed.) Soil Physical Chemistry. CRC Press, Boca Raton, FL, pp. 239-370.
- [25] Shafiei, H. M., Hamidoughli, Y., Fotouhi, G. R., Fatahi, M. J. (2008): The effects of different nutrient media on shoot proliferation of boston fern (*Nephrolepis exaltata* Schott cv. Bostoniensis). – Iranian Journal of Horticultural Science and Technology 2(9): 139-152.
- [26] Souza, D. M. S. C., Fernandes, S. B., Molinari, L. V., Avelar, M. L. M., Brondani, G. E. (2021): Activated charcoal application for the micropropagation of *Cattleya crispata* (Thunb.) – Van den Berg. Nativa 9(4): 352-358.
- [27] Steel, R. G. D., Torrie, J. H. (1980): Principles of Statistics. A Biometrical Approach. 2nd Ed. – Mc Graw-Hill Kogakusha, Kawasaki.
- [28] Stojicic, D., Janosevic, D., Uzelac, B., Cokesa, V., Budimir, S. (2012): Micropropagation of *Pinus peuce*. – Biologia Plantarum 56: 362-364.
- [29] Sulaiman, S., Yusuf, N. A., Awal, A. (2020): Effect of plant growth regulators on in vitro culture of pineapple (*Ananas comosus* L. Merr) MD2 variety. – Food Research 4(5): 110-114.
- [30] Taha, L. S., Sayed, S. S., Farahat, M. M., El-Sayed, I. M. (2018): In vitro culture and bulblets induction of Asiatic hybrid lily ‘Red Alert’. – J. Biol. Sci. 18: 84-91.
- [31] Tung Ming Sug, S. (1997): Cytokinins-efficiently enhanced pigment production in detached cotyledons of dark-grown cucumber seedlings. – Jour. of Agric. & Forest. 46(2): 85-91.
- [32] Villa, F., Pasqual, M., Silva, E. F. (2014): Micropropagation of orchid hybrids in Knudson culture medium with addition of vitamins of MS culture medium, benzilaminopurine and activated charcoal. – Semina: Ciências Agrárias 35(2): 683-694.
- [33] Wang, Y., Li, Z., Huang, L., Su, J. (2013): In vitro mass scale propagation of wild *Cymbidium lowianum* with a rare and endangered plant. – American Journal of Plant Sciences (4): 1500-1507.
- [34] Yadav, A. K., Prasad, Y., Prakash, S., Chand, P., Singh, B. S. G., Singh, G. (2017): Effects of surface sterilization agents on in vitro plant growth in BAPbnana cultivar “Grand Naine”. – IJCS 5(4): 1744-1747.
- [35] Yang, L., Xu, C. J., Hu, G. B., Chen, K. S. (2006): Direct shoot organogenesis and plant regeneration in *Fortunella crassifolia*. – Biol. Plant. 50: 729-732.

DYNAMIC COMPLEX NETWORK ANALYSIS OF PM_{2.5} IN HENAN PROVINCE OF CHINA

LIU, L. – LI, H. – LI, W. W.* – SUI, Q. L. – ZHU, Y. H.

Shandong University of Science and Technology, Qingdao, China

**Corresponding author
e-mail: liwanwuqd@126.com*

(Received 18th Jan 2022; accepted 2nd May 2022)

Abstract. At present, air pollution has become a major environmental problem threatening human health. PM_{2.5} concentration is an important indicator to measure air pollution. Studying the distribution and interaction of PM_{2.5} concentration between cities can provide a scientific basis for air quality monitoring, air pollution control, and the formulation of collaborative strategy for economy and environment in Henan Province of China. According to the PM_{2.5} concentration data of each prefecture-level city in 2018, we analyze the correlation of PM_{2.5} concentration between cities in Henan Province of China. Further, we construct a directed complex network of PM_{2.5} interaction based on Granger causality to explore the directivity of the impact between cities in Henan Province of China. Then, we introduce the “trophic coherence” method in biology to infer the hierarchical structure and stability of the network. The research indicates: (1) there are the evident of seasonal differences in PM_{2.5} concentration in Henan Province of China. The mean of PM_{2.5} concentration in the four seasons shows different trends, and there is the relatively obvious holiday effect. (2) In different seasons, the cross-correlation of PM_{2.5} concentration between cities is different. The cross-correlation between cities in spring and summer shows obvious spatial heterogeneity, and PM_{2.5} concentration between cities in autumn and winter shows higher spatial embeddedness. (3) The impact of PM_{2.5} concentration between cities in Henan Province of China has obvious causal directivity. The trophic coherence of the PM_{2.5}-directed network is the smallest in autumn, with the most stable structure, while is with the largest vulnerability in summer.

Keywords: *air pollution, PM_{2.5} network, cross-correlation analysis, Granger causality test, trophic coherence*

Introduction

With the development of industrialization level in China, energy consumption continues to accelerate, resulting in increasingly serious PM_{2.5} pollution problems. PM_{2.5} refers to fine particles with a diameter of less than or equal to 2.5 microns. The main sources are anthropogenic emissions, including pollution particles directly generated by the combustion of fuels such as coal and gasoline, and the gas pollutants emitted by the chemical industry which are converted into PM_{2.5} in the air. Other sources include road dust, industrial dust, kitchen fumes, etc. PM_{2.5} can penetrate into the human lungs and increase the risk of people suffering from various heart and respiratory diseases. Some have pointed out that PM_{2.5} causes more than 4 million deaths worldwide each year (Apte et al., 2015). Therefore, it is particularly urgent to carry out research on the spatial-temporal distribution, transmission and pollution prevention of PM_{2.5}, which is of great significance for reducing respiratory and cardiovascular diseases and protecting human health.

The existing researches on PM_{2.5} mainly focus on the spatial distribution analysis, temporal evolution characteristics and influencing factor exploration of PM_{2.5} concentration, and the quantitative calculation, prediction and simulation of PM_{2.5} concentration in specific spatial-temporal dimensions. The methods used mainly include two categories: one is traditional spatial-temporal statistics and GIS spatial analysis, the other is machine learning algorithm. The former includes autoregressive analysis,

geographic weighting analysis, spatial correlation analysis, GIS interpolation, etc., and the latter includes decision tree, random forest, etc.

Lin et al. (2015) proposed an observation-based algorithm which considers the effect of the main aerosol characteristics, and used this method to quantitatively analyze PM_{2.5} distribution in China. Ye et al. (2018) explored the distribution rule and the change in the standard-reaching rate of PM_{2.5} on different time scales, and analyzed its spatial hotspots. Song et al. (2018) conducted a quantitative research on the seasonal differences of NO₂ and PM_{2.5} in Foshan City, and described the spatial variation for daily concentration of NO₂ and PM_{2.5} by geographical semi-variogram function. Yang et al. (2018) studied the spatial distribution, temporal change and evolutionary relationships of PM_{2.5} based on PM_{2.5} concentration data. Ye et al. (2019) proposed a new multi-scalar framework based on spatial-temporal integration to better describe the evolving trajectories and characteristics of PM_{2.5} on different spatial-temporal scales. Yun et al. (2019) used spatial statistical analysis and geographic detector model to reveal the spatial distribution and the change characteristics of PM_{2.5} and analyze the main influencing factors in the Yangtze River Delta from 2005 to 2015. Hinojosa-Baliño et al. (2019) modeled the spatial distribution of PM_{2.5} air pollution caused by 37 personal exposures in Mexico City, and used GIS, spatial analysis, and Land Use Regression (LUR) to generate the final prediction model and the spatial distribution map. Guo et al. (2020) studied the spatial distribution of PM_{2.5} of the complex terrain in Jincheng of China using Weather Research and Forecast (WRF) model/California Puff Model (CALPUFF) modeling system. Wang et al. (2020) used exploratory spatial data analysis and geographically weighted method to analyze the spatial distribution characteristics of PM_{2.5} pollution and the spatial heterogeneity of its influencing factors. Wang et al. (2020) used spatiotemporal autoregressive (STAR) model to quantify the short-term dynamic change process of PM_{2.5}. Tan et al. (2020) developed an eigenvector spatial filtering based spatially varying coefficient (ESF-SVC) model to estimate PM_{2.5} concentration of the ground. Wang et al. (2020) collected PM_{2.5} samples from three representative locations in Yantai City, and analyzed mass concentration and chemical composition characteristics of these samples. Then they used Chemical Mass Balance (CMB) model to perform the source apportionment on environmental air receptors, and analyzed the spatial distribution characteristics of PM_{2.5}. Li et al. (2021) evaluated the sparse PM_{2.5} measurement values captured at decentralized monitoring sites using dynamically constrained interpolation methodology (DCIM) to simulate the nationwide PM_{2.5} spatial distribution. Wang et al. (2021) combined Kriging spatial interpolation technology, geographic detectors and other methods with GIS platform to analyze the characteristics of temporal change, spatial distribution and influencing factors of PM_{2.5} concentration in Changsha City. Wang et al. (2020) proposed a framework of joint prevention and collaborative governance of PM_{2.5} pollution based on data mining technology.

With the development of artificial intelligence (AI), methods related to machine learning are applied to the research of the distribution and prediction for PM_{2.5} concentration. Zhan et al. (2019) inferred and analyzed the two periods of the spatial-temporal distribution of PM_{2.5} in winter in Wuhan City using a machine learning method, Gradient Boost Decision Tree (GBDT). Wang et al. (2019) constructed a Random Forest (RF) model and estimated actual exposure level of the population to PM_{2.5}. Wu et al. (2019) used optimized ensemble learning method to highlight the most important meteorological and surface variables related to PM_{2.5} concentration, and examined these variables through multiple linear regression models to provide physical mechanistic

insights into the morphology of the PM_{2.5} annual cycles. Lin et al. (2020) believed that comparing with other land use types, industrial land has a greater impact on PM_{2.5} concentration. Wang et al. (2021) developed a workflow to predict PM_{2.5} concentration by the long short-term memory (LSTM) model, predicted the PM_{2.5} concentration in the next year, and generated a high-resolution spatial distribution map of PM_{2.5} concentration.

Since the small-world model proposed by Stogatz and Watts and the scale-free network model proposed by Barabasi and Albert (Watts et al., 1998; Barabasi et al., 1999), the complex network had become the focus of system science research and had been widely used in many fields, such as finance and trade (Liu et al., 2020; Zhang et al., 2020), population migration (Zhao et al., 2018; Shen et al., 2020) and transportation (Xu et al., 2020; Gao et al., 2018). However, in environmental science, especially in the research of PM_{2.5} pollution between cities, the complex network analysis method is in its infancy. A small number of scholars used the complex network analysis method to research the spatial-temporal distribution of PM_{2.5}. Zhang et al. (2014) used the algorithm of the shortest augmenting chain to build a capacity network model of urban PM_{2.5} diffusion based on the complex network theory, which realized the exploration for the physical process of PM_{2.5} regional diffusion. Fan et al. (2016) used the correlation coefficient method to construct a complex network and analyzed the topological characteristics of air quality data. Xue et al. (2015) constructed a weighted network based on PM_{2.5} concentration between cities, and used the Girvan Newman (GN) algorithm for community division, aiming to obtain the regional spatial distribution of PM_{2.5}. Ma et al. (2018) constructed an undirected weighted network based on PM_{2.5} concentration between cities, and used indicators such as node degree, clustering coefficient, network efficiency and vulnerability to measure the importance of nodes. Zhang et al. (2018) established a correlation model for complex network, and used long-term PM_{2.5} concentration data to divide highly relevant regions within China. Xiao et al. (2019) applied the complex network method to the research of air pollution index PM_{2.5}, and the analysis showed that the method can effectively analyze the main polluted cities. Li et al. (2019) used discrete wavelet transform, GARCH-BEKK model and complex network to construct an overflow network of multi-time scale. Wang et al. (2019) built a directed weighted network model using the transfer entropy method based on complex network to study the interaction of smog between cities. Zhang et al. (2020) carried out the study of structure characteristic for smog pollution based on complex network analysis methods.

Traditional methods, such as mathematical statistical analysis, geostatistical analysis and GIS interpolation (e.g. Kriging interpolation), are used to research the spatial-temporal distribution of PM_{2.5} concentration. Although these methods can excavate the spatial-temporal heterogeneity of PM_{2.5} in detail, they still consider the spatial-temporal distribution of PM_{2.5} concentration as a static characteristic to investigate, which lacks the exploration of the dynamic distribution and evolution of PM_{2.5} from the perspective of interaction. PM_{2.5} pollution presents the characteristics such as high frequency, wide spread, long duration and difficulty in governance (Ning et al., 2020), and has regional mobility. The PM_{2.5} concentration in a region are not only affected by the emission of local pollution sources, but also transmitted and exchanged with the pollutants around the regions. This is the basis for using the complex network method to research PM_{2.5}. The concentration distributions of PM_{2.5} in different regions will affect each other, so as to form a complex network relationship. The existing researches on PM_{2.5} based on complex network mainly analyze the distribution characteristics of PM_{2.5} from the

perspective of complex network structure, such as analyzing the individual characteristics of node cities in the network and dividing local communities. There is a lack of relevant research on the interaction of PM_{2.5} distribution between cities from the perspective of the whole region, and a lack of exploration and explanation of the causal directivity of relevant impacts.

Aiming at the above problems, based on the PM_{2.5} concentration data of 17 prefecture-level cities in Henan Province in 2018 from China National Environmental Monitoring Station, we use Cross-correlation analysis method to analyze the correlation of PM_{2.5} between prefecture-level cities, and adopt Granger causality test to determine the causal directivity of the interaction of PM_{2.5} between the cities. On this basis, we construct a PM_{2.5}-directed network between prefecture-level cities in Henan Province, and analyze the PM_{2.5} interaction relationship between cities in Henan Province and the dynamic characteristics of each city node. Further, we introduce the trophic consistency index in biology to explore the hierarchical structure and stability of the PM_{2.5} network in Henan Province, and then excavate the spatial-temporal heterogeneity of the PM_{2.5} concentration distribution in Henan Province and the causal directivity of interaction between prefecture-level cities, which is expected to provide a scientific basis for air environment governance in Henan Province. This research analyzes the correlation of PM_{2.5} concentration between cities in Henan Province from the perspective of complex network, and then gives causal directivity of the PM_{2.5} network between the prefecture-level cities in Henan Province through the results of Granger causality test, which provides a new technical way for the dynamic characteristic analysis and interaction relationship of each city node. It is helpful to clarify the causal mechanism of the complex interaction relationship of PM_{2.5} between the prefecture-level cities in Henan Province, which can provide scientific basis for air quality monitoring, air pollution governance and even the formulation of collaborative strategy for economy and environment in Henan Province.

Study area and data

Study area

The research area is Henan Province in central China (E110°21' ~ 116°39', N31°23' ~ 36°22'), and the terrain is high in the west and low in the east. It has 17 prefecture-level cities, with a total area of 16.7×10^4 km². Henan Province is located at the junction of coastal open regions and the central and western regions and is the middle zone of Chinese economic development from east to west.

Data source

The research data, the concentration data of PM_{2.5} in the 17 prefecture-level cities in Henan Province, comes from the real-time release platform of national urban air quality of CNEMC (China National Environmental Monitoring Centre). The timing interval of data is an hour, and the distribution of air monitoring stations is shown in *Figure 1*. In the research, the seasonal timescale is divided into 4 windows: the first window (spring) from March 1st to May 31st, 2018, the second window (summer) from June 1st to August 31st, 2018, the third window (autumn) from September 1st to November 30st, 2018, the fourth window (winter) from December 1st, 2018, to February 28st, 2019. We perform preprocessing such as integration, cleaning, etc. on the data to prepare for further research.



Figure 1. The distribution of air monitoring stations

Methodology

Cross-correlation analysis

Cross-correlation analysis is a measure that examines the change of two or more sets of time series data relative to each other (Davis et al., 2002). For two time series x and y , the cross-correlation is:

$$r_m = \frac{\sum(x_i - \bar{x})(y_{i-m} - \bar{y})}{\sqrt{\sum(x_i - \bar{x})^2 \sum(y_{i-m} - \bar{y})^2}} \quad (\text{Eq.1})$$

In the equation, m is the time lag coefficient. For positive lag, x is compared with y which has delayed m samples. Therefore, the high correlation value of positive lag means that the characteristic in y takes the lead, while the characteristic in x lags behind. For negative lag, the characteristic in x takes the lead. In the research, the two time series in the cross-correlation analysis are aligned, that is, the time lag coefficient is 0. The range of r_m is $[-1.0, 1.0]$. The closer the value of r_m is to 1, the stronger the correlation between series data is.

In order to compare the similarity of PM_{2.5} concentration time series of each pair of cities in the current research, the hourly based cross-correlation of PM_{2.5} concentration of all stations (136 pair of cities) in the four season windows of spring, summer, autumn and winter is calculated according to the above equation to examine the impact of seasons on the correlation of PM_{2.5} time series.

Granger causality test

Granger causality test is used to determine whether the historical information of one time series is helpful to predict the current value of another time series, which measures the ability for a prior value of one time series to predict the value of another time series. By testing the causality of city pairs, the research infers whether a city will have an impact on PM_{2.5} of the target cities, so as to mine the dynamic causality of PM_{2.5}

between cities. In order to test whether there is Granger causality between PM_{2.5} time series of the two city nodes X and Y in Henan Province, the following time series are constructed:

$$X_t = \sum_{k=1}^m \beta_{1k} X_{t-k} + \sum_{k=1}^n \theta_{1k} Y_{t-k} + \varepsilon_{1t} \quad (\text{Eq.2})$$

$$Y_t = \sum_{k=1}^p \beta_{2k} X_{t-k} + \sum_{k=1}^q \theta_{2k} Y_{t-k} + \varepsilon_{2t} \quad (\text{Eq.3})$$

In the equation, $\{X_t\}$ and $\{Y_t\}$ are respectively PM_{2.5} time series of city nodes X and Y. β and θ are respectively regression coefficients of $\{X_t\}$ and $\{Y_t\}$, and ε is the residual term. m , n , p and q are the maximum lag orders.

If $\theta_{11} = \theta_{12} = \dots = \theta_{1n} = 0$ in the above equation (Eq. 2), the time series $\{Y_t\}$ is the Granger cause of the $\{X_t\}$, that is, PM_{2.5} concentration of city Y effects on city X. In Equation 3, if $\beta_{11} = \beta_{12} = \dots = \beta_{1n} = 0$, the time series $\{X_t\}$ is the Granger cause of the $\{Y_t\}$, that is, the PM_{2.5} concentration of city X effects on city Y. If both equations (Eqs. 2 and 3) hold, it shows that there is two-way Granger causality between the $\{Y_t\}$ and $\{X_t\}$ time series.

It is worth noting that a precondition for Granger causality test is that the time series must be stationary, otherwise may arise the problem of false regression. Because the time series of PM_{2.5} are not stationary, it is necessary to detrend the data before using Granger causality test. After detrending, it is necessary to conduct Augmented Dickey Fuller (ADF) test for the time series. If ADF test concludes that contain a unit root in the time series, the series is not stable. Then it is necessary to make further difference for the time series data until the series is stable.

To maintain the stability of the model, the research chooses the optimal lag coefficient to be 7 based on Akaike Information Criterion (AIC). It performs Granger causality test for each pair of cities in undirected correlation networks of different seasons, then, when the p -value is below the α level (5%), the original hypothesis is denied. The direction of Granger causality is determined by the side with the lower value of p . For example, the p -value of PM_{2.5} concentration in Xinxiang City affecting that in Luoyang City in autumn is $p_1 = 6 \times 10^{-16}$ in the research, while the p -value of PM_{2.5} concentration of Luoyang City affecting that of Xinxiang City is $p_2 = 1 \times 10^{-12}$. Since $p_1 < p_2$, it is believed that the PM_{2.5} concentration in Xinxiang City will have an impact on Luoyang City.

The research calculates Granger causality of each city pair on the basis of the undirected network, and constructs the direction of the network link of city pairs according to Granger causality, then upgrades the PM_{2.5} network from undirected network to directed network. According to this, the causal directivity between city nodes in PM_{2.5} network of Henan Province can be analyzed.

Trophic coherence analysis

The research introduces trophic coherence (Moutsinas et al., 2019) of biology to reconstruct the grade structure of PM_{2.5}-directed network and mark the grade levels. The trophic level comes from the food chain and predator level and it has been proved to be an index that infers the stability of large-scale directed network in the absence of clear definitions of input and output (Pagani et al., 2019). To define trophic coherence in a direct causality network, we should first define the basal nodes. We define the nodes

with a low trophic level as the basal nodes, that is, the pollution affects the cause node in relationship, and define the nodes with a high trophic level as the nodes affected by pollution. When basal nodes and affected nodes are difficult to determine due to the complicated directional relationship between nodes, the basal nodes are the nodes with more outward directional relationships. The trophic level (s_i) of node i is defined as the average trophic level of adjacent nodes pointing to i plus one:

$$s_i = 1 + \frac{1}{k_i^{in}} \sum_j a_{ij} s_j \quad (\text{Eq.4})$$

In the equation, a_{ij} is the adjacency matrix, $k_i^{in} = \sum_j a_{ij}$ is the number of nodes pointing to i , the nodes where $k_i^{in} = 0$ are defined as the basal nodes, representing the cause nodes that affect other nodes in PM_{2.5} transmission. The trophic level is set to $s_i = 1$ for the basal nodes. The trophic level of the non-basal nodes in the network is the average trophic level of all the monitoring stations from which it receives PM_{2.5} pollutants plus one.

The trophic difference is the difference in trophic level between two nodes connected by an edge in the network, defined as:

$$x_{ij} = s_i - s_j \quad (\text{Eq.5})$$

$p(x)$ represents the distribution of network trophic difference, with a mean value of 1. The standard deviation of $p(x)$ is called as the trophic non-coherence parameter, and the parameter q is used to measure the trophic coherence of the network:

$$q = \sqrt{\frac{1}{L} \sum_{ij} a_{ij} x_{ij}^2 - 1} \quad (\text{Eq.6})$$

In the equation, $L = \sum_{ij} a_{ij}$ is the number of connected edges between nodes of the network. The smaller the q -value, the stronger the trophic coherence of the network, the more unstable the network, and the greater the vulnerability.

Experimental results and analysis

Time distribution characteristics of PM_{2.5} in Henan Province

Temporal distribution characteristics

The mean of PM_{2.5} concentration of 4 seasons in various cities is counted, and the characteristics of time distribution for PM_{2.5} in Henan Province from March 2018 to February 2019 are examined on a seasonal scale, as shown in *Figure 2*. The mean of PM_{2.5} concentration of each prefecture-level city in Henan Province in winter is apparently higher than that in the other three seasons. The PM_{2.5} pollution of winter is the most serious, and the PM_{2.5} concentration is higher than the threshold of 75ug/m³ for the second-level air quality (good) specified in the national standard (GB3095-2012). Among them, Anyang City has the highest mean of PM_{2.5} concentration in winter that reaches 132.3 ug/m³ and is higher than the threshold of 115ug/m³ for the third-level air quality (lightly polluted), so it is more polluted than the other cities. Thus,

it can be seen that Henan Province should place the focus on PM_{2.5} prevention in winter and strengthen the treatment measures for regions with high PM_{2.5} pollution in winter, such as Anyang City. In spring and autumn, the mean of PM_{2.5} in various cities is similar, between 50ug/m³ and 70ug/m³, which is higher than the threshold for the first-level and lower than the threshold for the second-level specified in the national air quality standard. Among them, the concentration difference in Zhoukou City is the largest, reaching 14.9 ug/m³, indicating that the fluctuation of PM_{2.5} pollution in Zhoukou City is relatively large. The mean of PM_{2.5} concentration of all cities in summer is the lowest and fluctuates around 30 ug/m³. The air quality of most cities is within the range of the first-level threshold, which indicates that PM_{2.5} pollution is the least and air quality is the best in summer of all cities in Henan Province.

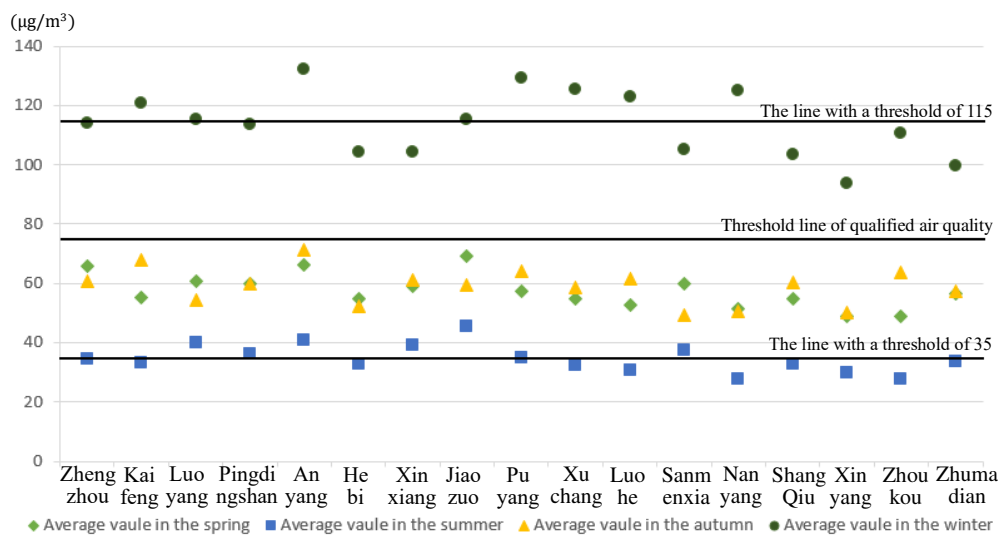


Figure 2. PM_{2.5} concentration change in four seasons in various prefecture-level cities of Henan Province

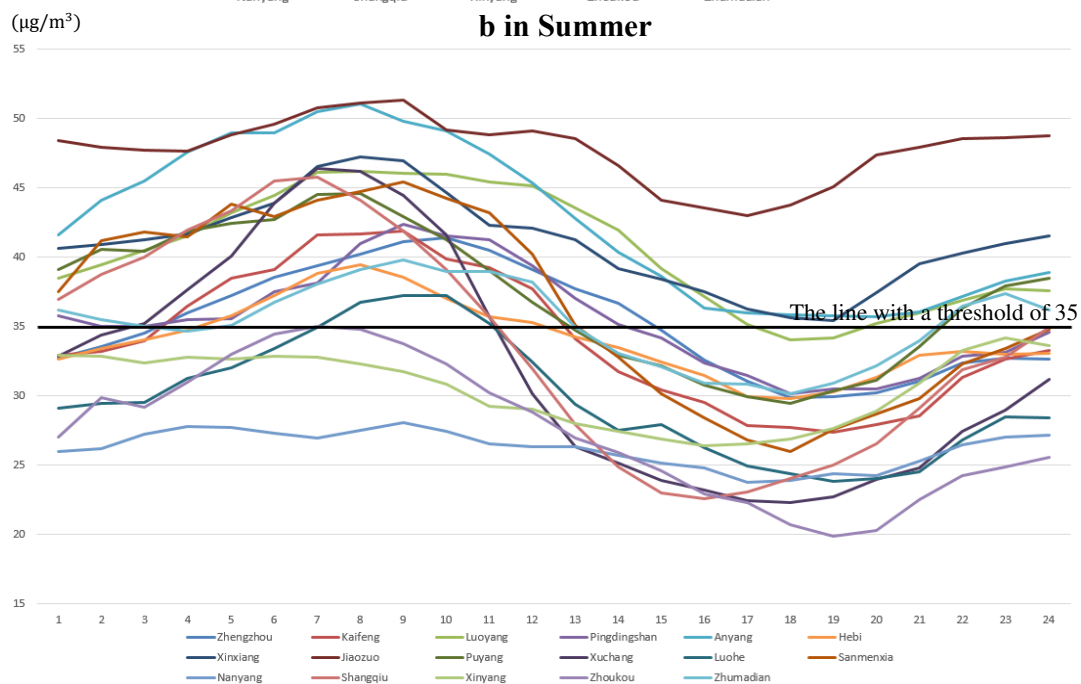
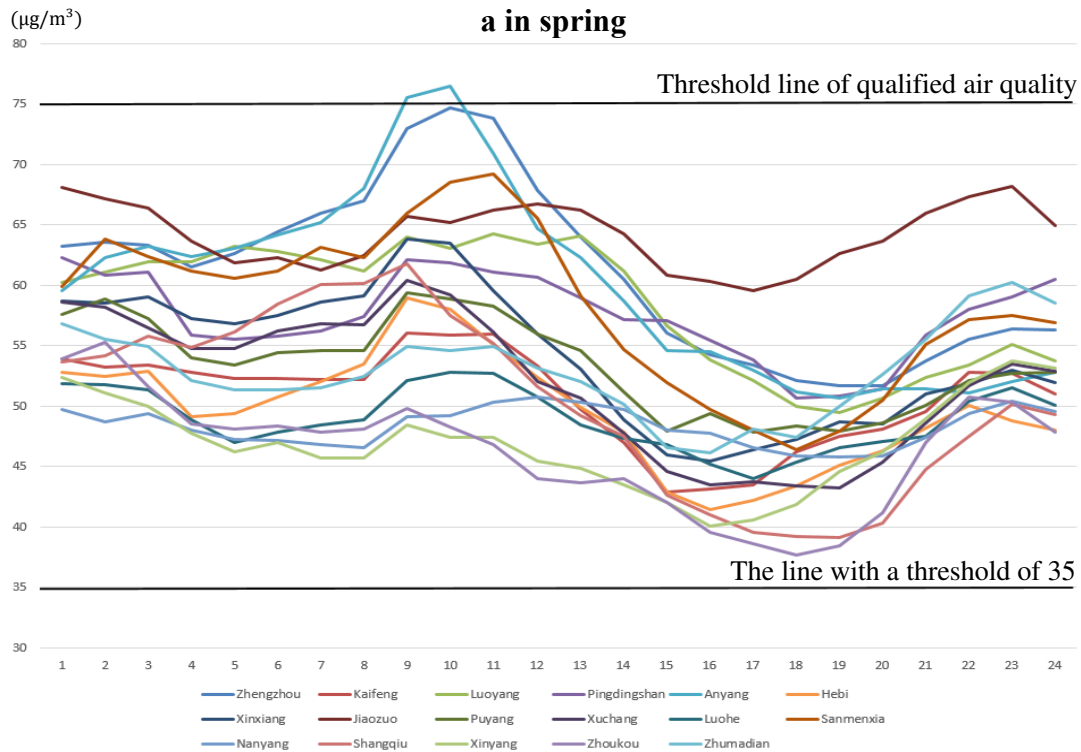
The time scale is further subdivided on the seasonal scale, and the change in the mean of hourly PM_{2.5} concentration of each season in each prefecture-level city is calculated, as shown in Figure 3. It can be seen from the figure that the changing rule of PM_{2.5} concentration in various cities as follows:

(1) In winter, the range of hourly mean concentrations of various cities in Henan Province is the highest, and the overall range is between 80 ug/m³ and 150 ug/m³. The pollution level is the third level, and the pollution degree is significantly higher than that in other three seasons. In spring and autumn, the range of hourly mean concentrations in various cities is basically the same, most of which are within 30-80 ug/m³, and the grade of air quality is good. The mean of hourly concentration of each city in summer is between 20 ug/m³ and 50 ug/m³, and the grades of air quality are excellent and good.

(2) The trend in various cities in autumn is the same. Except for the obvious deviation of the mean of PM_{2.5} concentration between Anyang City and other cities from 7 o'clock to 17 o'clock, the overall deviation in autumn from 1 to 24 h in each city is small. It indicates that the fluctuation of air quality is small in autumn. The maximum

deviation appears at 4 o'clock, reaching 29.9 $\mu\text{g}/\text{m}^3$, and the minimum deviation appears at noon, reaching 19.4 $\mu\text{g}/\text{m}^3$.

(3) The change of PM_{2.5} concentration in various prefecture-level cities in winter from 1 to 24 h is consistent with the trend in autumn. The PM_{2.5} concentration of them all develop in a steady state from 1 to 11 h. After 12 o'clock, the mean of PM_{2.5} concentration shows an obvious downward trend and reaches the lowest point from 17 to 19 o'clock. Then, PM_{2.5} concentration begin to show an upward trend after 19 o'clock.



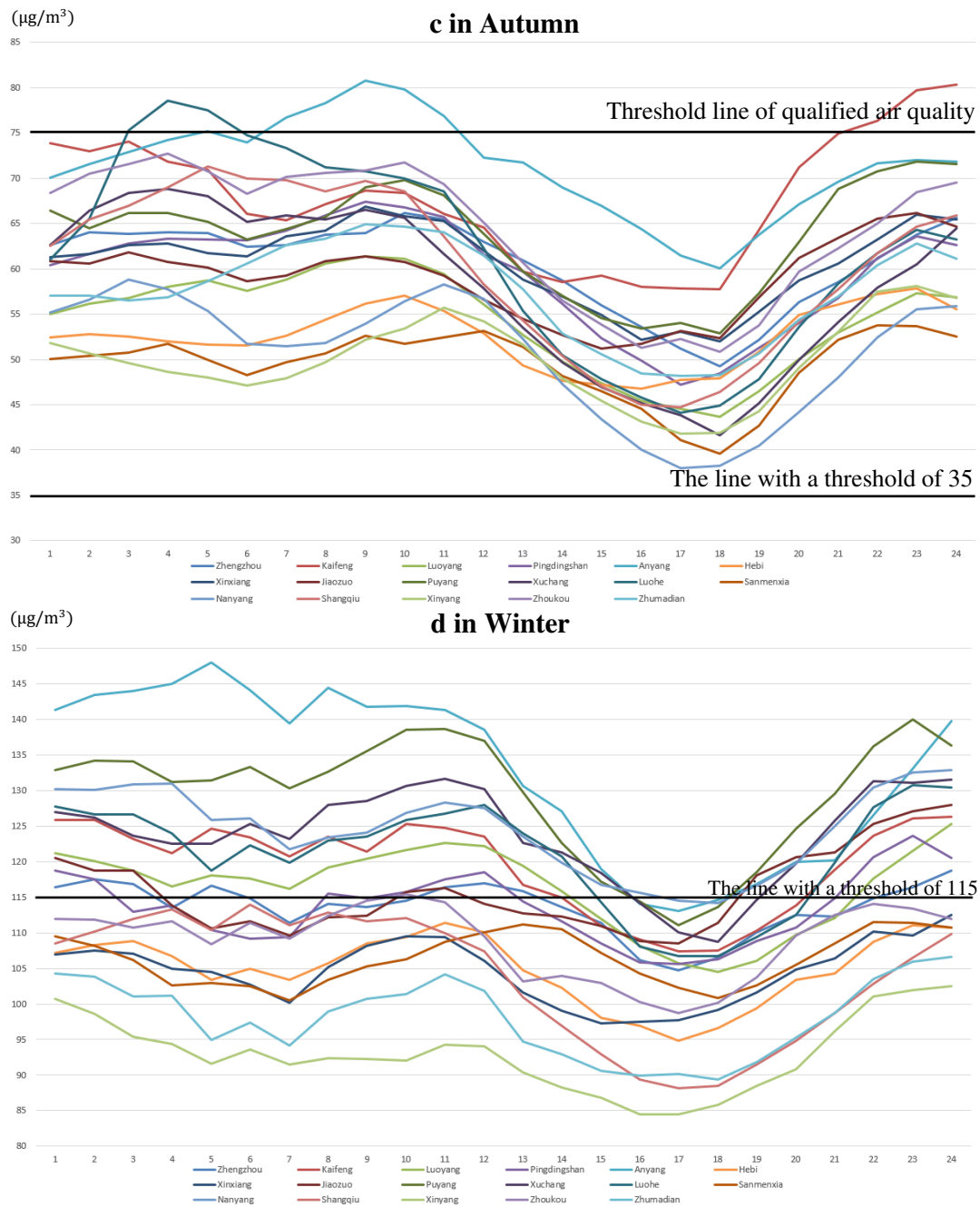


Figure 3. Hourly mean change of PM_{2.5} concentration in various prefecture-level cities of Henan Province in the four seasons

(4) The concentration in spring generally presents a more obvious double-peaks trend. PM_{2.5} concentration in various prefecture-level cities shows a significant upward trend from 8 o'clock to 9 o'clock and is at the peak value from 9 o'clock to 12 o'clock. The mean of PM_{2.5} concentration decreases significantly after 12 o'clock and reaches a trough position from 18 o'clock to 20 o'clock. While the mean shows an upward trend again after 20 o'clock in the evening and reaches a small peak until 23 o'clock.

(5) There is a big difference in the mean change of hourly PM_{2.5} concentration of various cities in summer. For example, the mean change of hourly PM_{2.5} concentration

is relatively small and basically tends to be flat in Nanyang City and other cities. While it is in a reclining “Z” type word in Shangqiu City and other cities, the mean of hourly PM_{2.5} concentration has evident changes.

Monthly distribution characteristics

The mean of monthly PM_{2.5} concentration in each city is calculated, as shown in Figure 4. In spring, the mean of PM_{2.5} concentration in each city is higher in March and is all lower from May to September. Compared with other months, the mean of PM_{2.5} concentration in January and February in various cities is significantly higher. Among them, the cumulative mean of PM_{2.5} concentration in Anyang City is the highest throughout the year and is the lowest in Xinyang City. It shows that even in the same season, there are still difference of different degrees between different months.

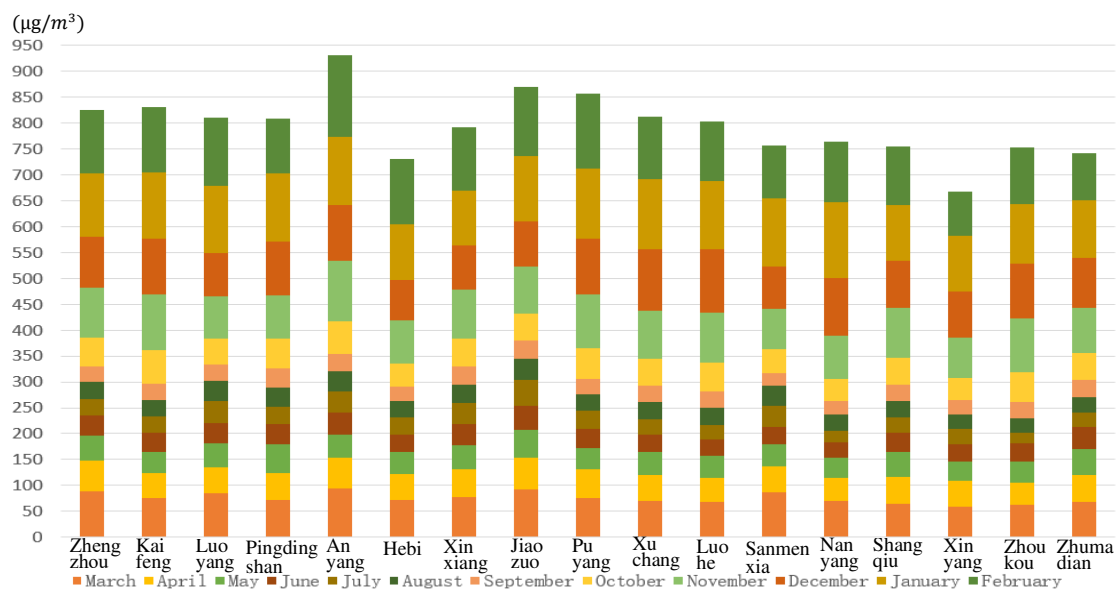


Figure 4. Monthly mean change of PM_{2.5} concentration in various prefecture-level cities of Henan Province

National Day holiday effect

In order to examine whether there is holiday effect in the change of PM_{2.5} concentration of holidays, three periods are respectively taken from September 25, 2018 to September 30, 2018, October 1, 2018 to October 7, 2018, and October 8, 2018 to October 12, 2018. These periods are regarded as three research intervals before, during and after National Day, excluding three non-working days of September 24, October 13 and 14. The mean of PM_{2.5} concentration of each city in Henan Province during these periods is counted, and the visualization analysis is carried out by combining the inverse distance interpolation method, as shown in Figure 5. The mean of PM_{2.5} concentration of each prefecture-level city in Henan Province before National Day is in a lower position in general, and the highest mean of PM_{2.5} concentration is no more than 20 $\mu\text{g}/\text{m}^3$ in this period, that is, the air quality is the first-level (excellent). The mean of PM_{2.5} concentration during and after National Day is apparently higher than that before National Day. The air quality in almost all regions exceeds the threshold for the second-

level, and some reaches the third-level. And the holiday effect of National Day is relatively apparent.

During National Day, multi-factors such as the large population flow and large traffic volume cause the significant increase of PM_{2.5} concentration in each city. The regions with high PM_{2.5} concentration during National Day are mainly located in Kaifeng City, Luohe City and other regions in the east and Puyang City in the northeast. After National Day, the mean of PM_{2.5} concentration is still high in the whole province, and PM_{2.5} concentration in some cities is even higher than that during National Day. Combined with the weather conditions around National Day in Henan Province in 2018, the weather was relatively good. In addition to a few regions with sporadic light rain in some periods, the weather was mainly sunny, and the whole region was mainly breeze without strong wind weather. During this period, the atmosphere was stable and this situation did not effectively settle and dilute the PM_{2.5} particles generated during the National Day. Therefore, the PM_{2.5} concentration in all cities in Henan Province still remains high after the National Day.

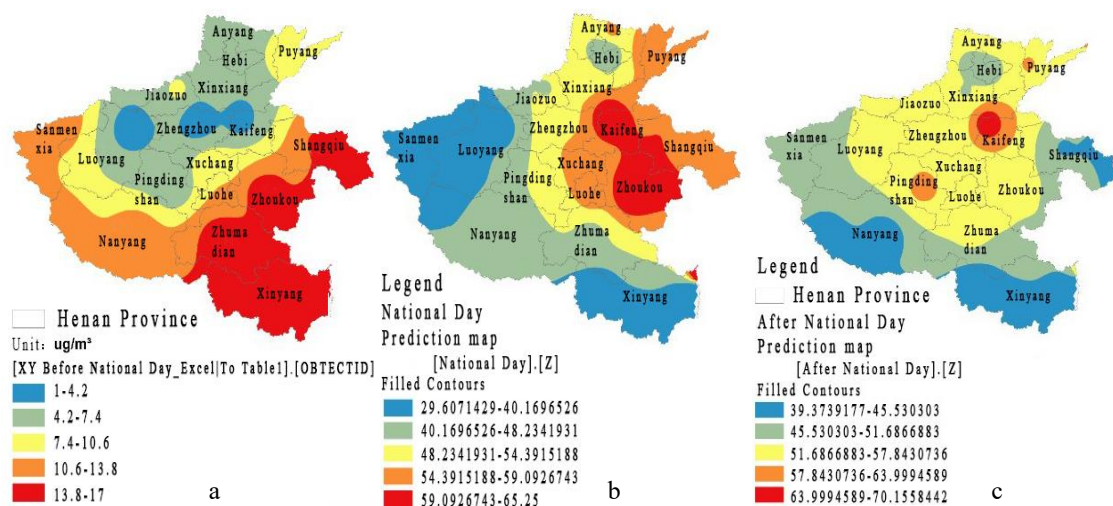


Figure 5. Changes in the mean of PM_{2.5} concentration during the National Day holiday and the periods before and after the National Day holiday in various prefecture-level cities in Henan Province

Construction and analysis of PM_{2.5}-undirected cross-correlation network

According to Equation 1 in “Methodology,” the cross-correlation degree of each city pair in Henan Province is calculated, among them, the results in winter are shown in Table 1.

There are 17 prefecture-level cities in Henan Province. According to the PM_{2.5} time-series cross-correlation between the prefecture-level cities calculated above, it is judged whether there is a correlation between city pairs. The cross-correlation threshold of the city pair is set to 0.7 (Gehrig et al., 2003). When the cross-correlation value between the two cities is greater than the threshold, there is a correlation between the two cities and can establish an edge relationship. Taking the city pairs with correlation as nodes, we construct the undirected correlation network of each season in Henan Province. The four PM_{2.5}-undirected correlation networks constructed according to different seasons are shown in Figure 6.

Table 1. The cross-correlation between cities in the winter in Henan Province

	Kai feng	Luo yang	Pingdingshan	An yang	Hebi	Xin xiang	Jiao zuo	Pu yang	Xu chang	Luo he	San menxia	Nan yang	Shang qiu	Xin yang	Zhou kou	Zhuma dian
Zheng zhou	0.86876	0.79472	0.72145	0.74304	0.76559	0.85062	0.8474	0.73987	0.77497	0.62787	0.61831	0.56799	0.6171	0.35001	0.58352	0.5121
Kai feng		0.7194	0.69291	0.72847	0.73709	0.81475	0.74946	0.78452	0.83312	0.68919	0.53475	0.60197	0.70771	0.38473	0.66762	0.55783
Luo yang			0.79762	0.60343	0.64077	0.72413	0.80122	0.60578	0.7012	0.64094	0.73044	0.66192	0.61439	0.43484	0.5759	0.56273
Pingdingshan				0.52018	0.51792	0.59738	0.65391	0.53211	0.82189	0.81599	0.67467	0.80397	0.64911	0.55437	0.72293	0.71604
An yang					0.92359	0.83871	0.72412	0.81108	0.60245	0.46662	0.46667	0.44264	0.59469	0.22222	0.45795	0.31298
Hebi						0.87519	0.79214	0.81152	0.58063	0.4494	0.48246	0.43385	0.58597	0.21772	0.43775	0.31286
Xin xiang							0.85986	0.77937	0.67669	0.54469	0.54285	0.50356	0.6115	0.30475	0.52772	0.42171
Jiao zuo								0.66674	0.66071	0.5713	0.61474	0.55852	0.61621	0.34846	0.53669	0.47354
Pu yang									0.63975	0.53624	0.44437	0.50222	0.61512	0.298	0.51034	0.39928
Xu chang										0.84717	0.54952	0.71051	0.73768	0.51275	0.76577	0.69019
Luohe											0.53274	0.79169	0.74863	0.6918	0.87985	0.86112
San menxia												0.60275	0.43378	0.45549	0.46752	0.50646
Nan yang													0.63765	0.72861	0.73986	0.80328
Shang qiu														0.46287	0.77087	0.60453
Xin yang															0.65583	0.82897
Zhou kou																0.80642

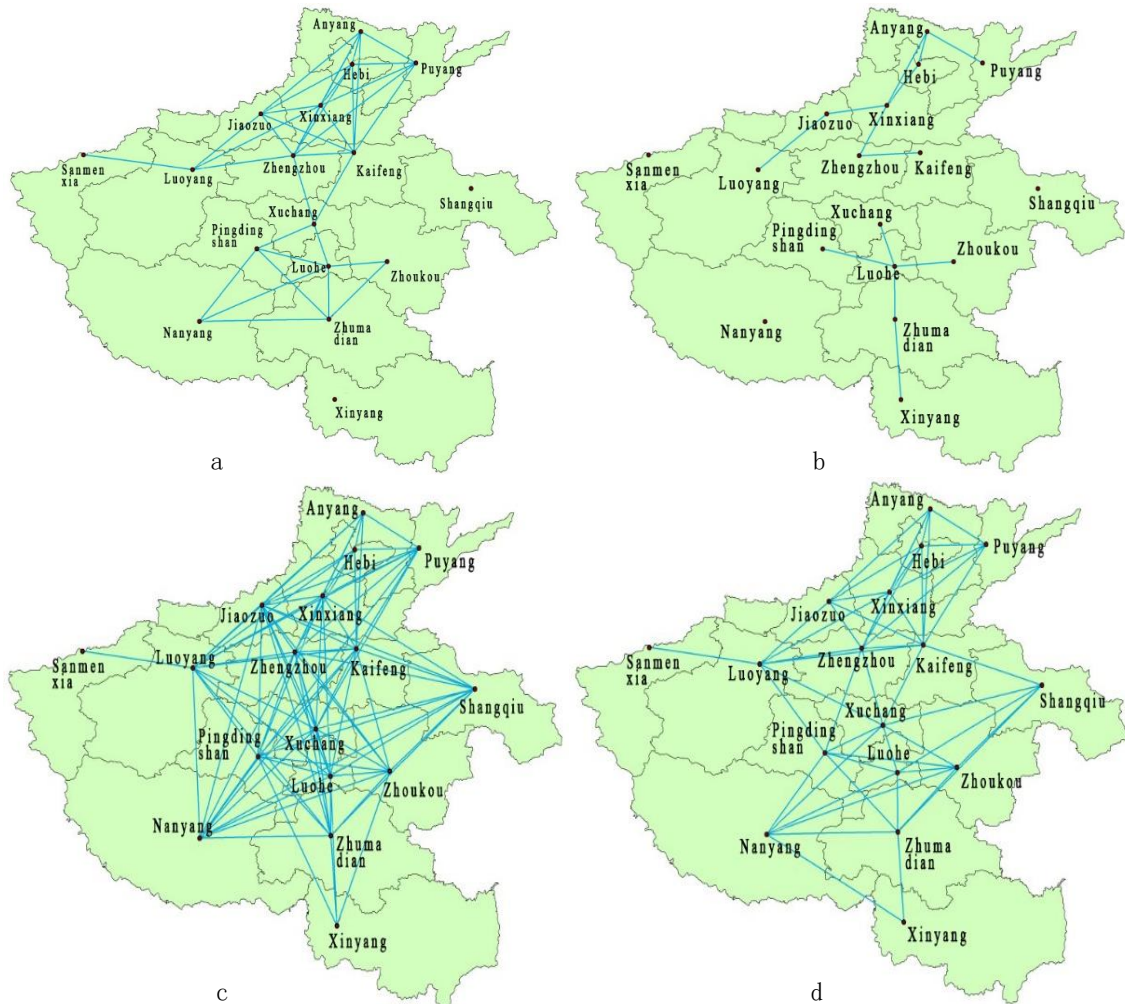


Figure 6. The PM_{2.5}-undirected network in Henan Province: a spring window, b summer window, c autumn window, d winter window

It can be seen that the 17 prefecture-level cities in Henan Province present a relatively obvious spatial characteristic of north-south division. Therefore, they are divided into two groups, the southern Henan and the northern Henan. The northern Henan group includes Anyang City, Hebi City, Xinxiang City, Sanmenxia City, Jiaozuo City, Puyang City, Kaifeng City, Zhengzhou City, Luoyang City and Shangqiu City. The southern Henan Group includes Xuchang City, Luohe City, Nanyang City, Zhoukou City, Pingdingshan City, Zhumadian City, and Xinyang City. The cross-correlation relationship of PM_{2.5} concentration for prefecture-level cities in Henan province is different in different seasons. Among them, the southern and northern Henan groups have obvious identification in spring and summer. In spring, compared with the southern Henan group, the cross-correlation between the cities in the northern Henan group is closer. In autumn and winter, the correlation between the cities is still very high within the two groups, but the number of city pairs, composed of two cities in different groups, with high correlation becomes larger.

Since the influence of the spatial distance between cities on the change of PM_{2.5} concentration between regions cannot be ignored, the research studies the spatial embeddedness of the cross-correlation network of PM_{2.5} concentration between the

various cities in Henan Province. To quantify the level of spatial embedding, the pairs of cross-correlated cities are divided into three groups based on the linear distance between two cities (<100 km, <200 km and >200 km). *Table 2* shows the relationship of the cross-correlation and the distance of each city pair (*Table 2*).

Table 2. The relationship between cross-correlation (XCROSS) of the hourly value of PM_{2.5} and the city distance in Henan Province

Distance	Total city pairs	City pairs of the northern Henan	City pairs of the southern Henan	Outliers (city pairs outside the group)
Spring				
< 100 Km	19 (53%)	11 (58%)	6 (32%)	2 (11%)
< 200 Km	36 (100%)	24 (67%)	10 (28%)	2 (6%)
> 200 Km	0	0	0	0
Summer				
< 100 Km	13 (100%)	8 (62%)	5 (38%)	0
< 200 Km	13 (100%)	8 (62%)	5 (38%)	0
> 200 Km	0	0	0	0
Autumn				
< 100 Km	21 (29%)	11 (52%)	8 (38%)	2 (10%)
< 200 Km	72 (79%)	32 (44%)	19 (26%)	21 (29%)
> 200 Km	19 (21%)	4 (21%)	2 (11%)	13 (68%)
Winter				
< 100 Km	21 (43%)	11 (52%)	8 (38%)	2 (10%)
< 200 Km	49 (96%)	27 (55%)	15 (31%)	7 (14%)
> 200 Km	2 (4%)	1 (50%)	1 (50%)	0

The spatial embedding degree of the network is very high in all seasons when the distance is smaller than 100 km, and it decreases when the distance increases to over 200 km. In spring, autumn and winter, the number of city pairs with a distance of 100 to 200 km is more than that of city pairs with a distance less than 100 km in the northern Henan group. The proportion of city pairs with a distance less than 100 km in the southern Henan group is respectively 60%, 100%, 38% and 50% in spring, summer, autumn and winter. In spring and summer, the number of city pairs with a distance more than 200 km in the southern and northern Henan groups is both 0.

Construction and analysis of PM_{2.5}-directed causality network

Construction of Granger causality network

On the basis of the above undirected cross-correlation network of PM_{2.5}. *Equations 2 and 3* in “Methodology” is used to carried out Granger causality test for cross-correlated city pairs. It is found that *p*-value of corresponding Granger causality of city pairs with high cross-correlation is low (less than 5%). According to the calculation results, in spring, the PM_{2.5} concentration in Zhengzhou City can affect that in Luoyang City, corresponding to $p = 7 \times 10^{-17}$, that is, the PM_{2.5} concentration time series in Zhengzhou City can predict that in Luoyang City, the PM_{2.5} concentration in Pingdingshan City can affect that in Luohe City, corresponding to $p = 9 \times 10^{-14}$. In

summer, the PM_{2.5} concentration in Luohe City can affect that in Zhumadian City, and the *p*-value is 6×10^{-16} . In winter, the PM_{2.5} concentration in Zhoukou City can affect that in Xuchang City, and the *p*-value is 6×10^{-17} . The PM_{2.5} concentration in the prefecture-level cities of Henan Province shows different interaction relationships in each season.

Based on the Granger causality test results, we determine the causal directivity of the impact between city nodes. According to this, we construct a directed Granger causality network for PM_{2.5} in Henan Province and further excavate the causal relationship of PM_{2.5} concentration between cities. The specific method is to define the 17 prefecture-level cities as network nodes, if the PM_{2.5} concentration at city node *i* can impact the PM_{2.5} concentration at city node *j*, then a directed edge relationship is established between the two nodes, that is, the directed edge from node *i* to *j*. The constructed PM_{2.5}-directed causal network in Henan Province is shown in *Figure 7*.

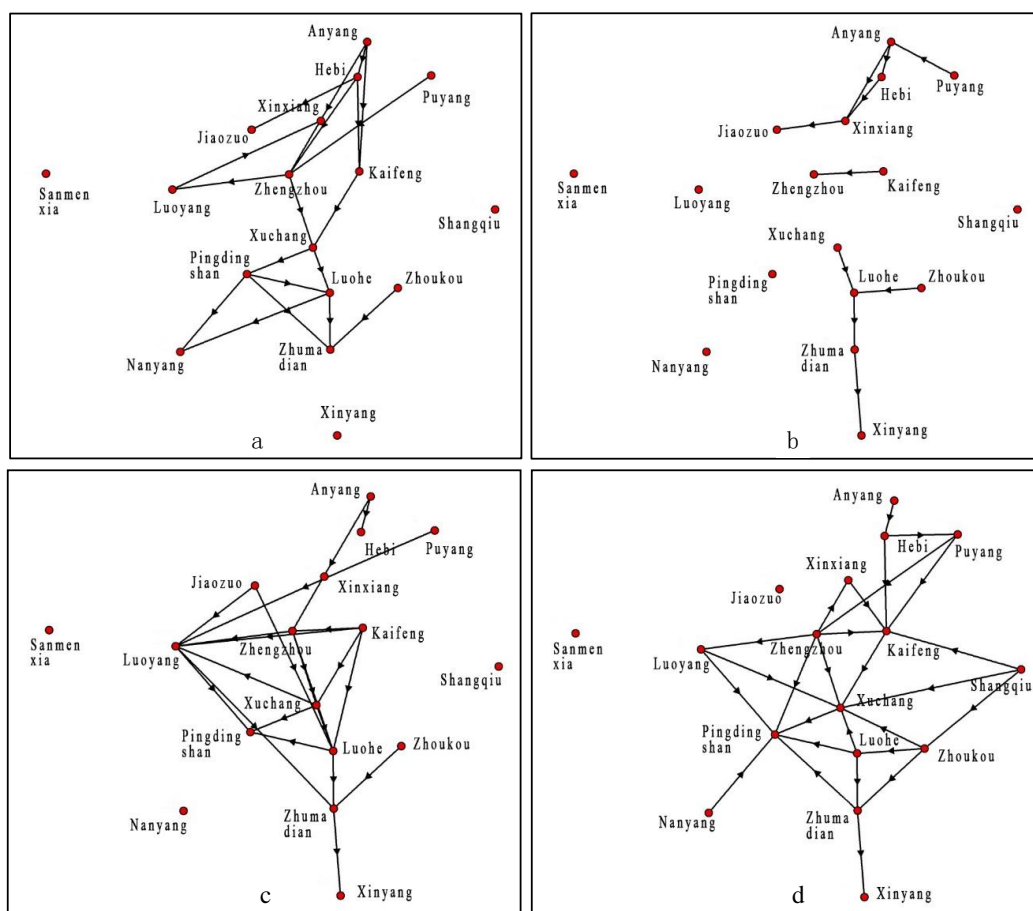


Figure 7. The directed causality network of PM_{2.5} in Henan Province: a spring window, b summer window, c autumn window, d winter window

As shown in *Figure 7*, there are more independent nodes in summer and the interaction relationship of PM_{2.5} between prefecture-level cities is weaker. The PM_{2.5} concentration values are generally lower in summer, and due to more precipitation, the scouring of rainwater further weakens the interaction of PM_{2.5} between regions. In the four seasons, Sanmenxia City exists as an independent node, which is neither affected

by the PM_{2.5} of other cities nor any effect on them. This is mainly due to the fact that Sanmenxia City is located in the junction of the eastern extension of the Qinling Mountains, the Funiu Mountains, Xionger Mountains and Xiao Mountains, with an average altitude of 300 to 1500 m. The landforms are mainly mountainous and mostly covered with vegetation, which is not conducive to the accumulation of PM_{2.5} particles, and makes the local PM_{2.5} pollution degree in Sanmenxia less obvious. At the same time, the straight-line distance between Sanmenxia City and the rest of the prefecture-level cities in Henan Province is more than 100 km, which is relatively far away, and makes it difficult for Sanmenxia City to have an interaction with the other cities on PM_{2.5}.

Analysis of network trophic coherence

In order to further clarify the mechanism and hierarchical structure of PM_{2.5}-directed network, we use the trophic coherence method in “Methodology” to divide the hierarchical structure of directed network. On the basis of Granger causality directed network in the four seasons, the nodes with the in-degree of 0 are defined as the basal nodes, and the trophic level is 1. The trophic levels of other nodes in the four seasons are calculated according to *Equation 4*, as shown in *Table 3*.

Table 3. *The trophic levels of each prefecture-level city in four seasons in Henan Province*

Season	Trophic levels of prefecture-level cities in Henan Province (in ascending order)
Spring	Zhoukou(1), Anyang(1), Puyang(1), Hebi(2), Zhengzhou(2.33), Kaifeng(2.5), Jiaozuo(3), Luoyang(3.33), Xuchang(3.33), Pingdingshan(4.33), Xinxiang(4.33), Zhumadian(4.39), Luohe(4.83), Nanuang(5.58)
Summer	Zhoukou(1), Kaifeng(1), Puyang(1), Xuchang(1), Anyang(2), Luohe(2), Zhengzhou(2), Zhumadian(3), Hebi(3), Xinxiang(3.5), Xinyang(4), Jiaozuo(4.5)
Autumn	Zhoukou(1), Anyang(1), Kaifeng(1), Jiaozuo(1), Zhengzhou(2), Hebi(2), Luoyang(2.5), Xuchang(2.5), Luohe(2.625), Zhumadian (3.04), Pingdingshan(3.54), Xinyang (4.04)
Winter	Nanyang(1), Shangqiu(1), Anyang(1), Zhoukou(2), Hebi(2), Kaifeng(3), Luohe(3), Puyang(3), Zhengzhou(3), Zhumadian(3.5), Xuchang(3.67), Xinxiang (4), Luoyang(4), Pingdingshan(4.03), Xinyang(4.5)

According to the trophic coherence principle, in the PM_{2.5}-directed network of Henan Province, the cities with low trophic level are the basal nodes, that is, the city nodes that have an impact on PM_{2.5} in other cities. While the cities with high trophic level are more affected by PM_{2.5} in other cities. In the PM_{2.5}-directed network, the causal directivity is from the city nodes with low trophic level to that with high trophic level. As can be seen in *Table 3* that the highest trophic level in spring is Nanyang City, reaching 5.58, far higher than the highest trophic level in the other three seasons. It shows that the PM_{2.5} distribution of Nanyang City is affected by many other cities. According to the directivity of the network, its PM_{2.5} is affected by cities such as Pingdingshan and Luohe. In spring, the trophic levels for city nodes of the southern Henan group is generally higher than that of the northern Henan group. It is thus clear that the source regions of PM_{2.5} pollution in spring are mainly concentrated in the cities of the northern Henan group, for which we should consider strengthening the prevention of PM_{2.5}. In summer, the overall trophic level of Henan Province is the lowest, among them, Jiaozuo City has the highest trophic level of 4.5. In autumn, there are the most basal nodes, that

is, the cities that play the role of pollution source are the most. While the PM_{2.5} in Xinyang City is most affected by other cities, and its trophic level of 4.04 is the highest. In winter, there are 3 basal nodes, that is, there are 3 cause nodes that act as PM_{2.5} transmission sources. Xinyang City is still at the highest trophic level of 4.5 in winter, which indicates that PM_{2.5} in Xinyang City is more seriously affected by other cities. Its pollution control should not only control itself, but also control the output cities combining the causal directivity in the directed network.

By calculating the trophic level, PM_{2.5}-directed networks are further divided into different hierarchical structure, as shown in *Figure 8*. In the figure, based on the parameter definition, the basal nodes with low trophic level represent PM_{2.5} transmission source nodes, while the nodes with high trophic level are receptors in the causality network.

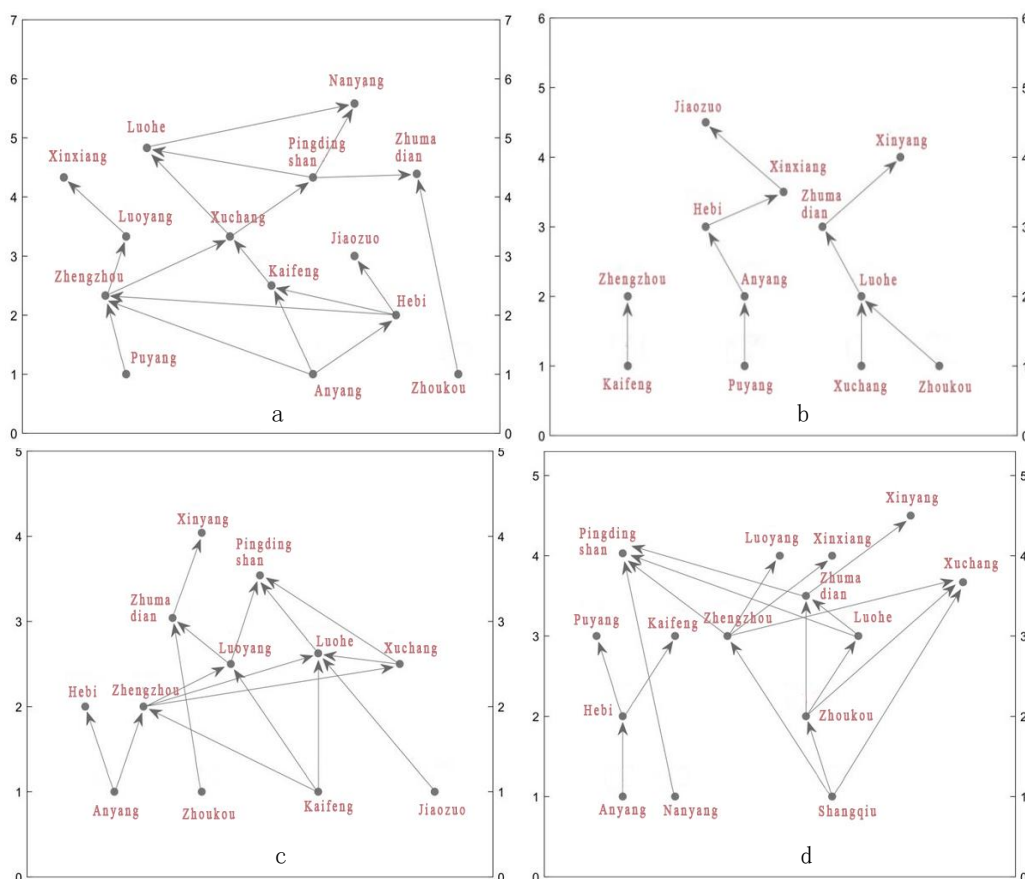


Figure 8. The hierarchical structure of PM_{2.5} causality network in Henan Province: a. spring window, b. summer window, c. autumn window, d. winter window

It can be seen from *Figure 8* that Anyang City and Puyang City with low trophic level are classified as PM_{2.5} transmission sources in spring, and Nanyang City and Shangqiu City are classified as PM_{2.5} transmission sources in winter. Among them, in addition to being at the second trophic level in summer, Anyang City is located in the basal nodes of the first trophic level in spring, autumn and winter. That is, its PM_{2.5} pollution is serious and affects the distribution of PM_{2.5} in other cities. Geographically, Anyang City borders the haze-prone Hebei province and is close to Handan City. As a

result, Anyang is highly susceptible to the impact of PM_{2.5} concentration in Hebei Province, which can then develop into a pollution source of in Henan Province. Further considering its industrial structure, Anyang is an important industrial production base in Henan Province and has initially formed an industrial system dominated by metallurgy, electronics, machinery, chemicals and others. The industrial structure dominated by industry is bound to increase PM_{2.5} pollution emissions. Anyang City is always located in the pollution source position of the first trophic level as a result of internal and external causes. In response to this situation, Anyang City should actively optimize the industrial structure and proactively accept high-tech industries to reduce PM_{2.5} emissions.

Using Equation 6 in “Methodology,” the standard deviation q of the network trophic difference distribution $p(x)$ is calculated. Then, the consistency results of seasonal causality networks are obtained, as shown in Table 4.

Table 4. The standard deviation for trophic difference of seasonal directed networks in current research

The directed network	The standard deviation (q)
Spring	0.87
Summer	0.23
Autumn	0.97
Winter	0.71

The larger the q , the weaker the trophic coherence of the network and the more stable the network. The results in Table 4 show that the season with the weakest trophic coherence in Henan Province is autumn, the q -value is 0.97, and the stability of the PM_{2.5} network is the strongest (Table 4). The season with the strongest trophic coherence is summer, the q -value is 0.23, and the vulnerability of the PM_{2.5} network is the largest. Precipitation in Henan Province is mainly in summer, and the scouring effect of rainwater can effectively reduce the PM_{2.5} concentration in the air, so the vulnerability of the PM_{2.5} network in summer of Henan Province is the largest. While because of the relatively small precipitation and the northeasterly and northerly winds in autumn, pollutants from north China and northwest China are hoarded over Henan Province. At the same time, rising temperature is likely to cause stable weather and gradually form the inversion layer, and the meteorological conditions are gradually stabilized, which is adverse to the deposition and diffusion of PM_{2.5}, so the stability of the PM_{2.5} network in autumn of Henan Province is the strongest. It can provide decision support for the pollution prevention of PM_{2.5} in Henan Province through the above differences obtained in the stability and vulnerability of the network in different seasons by the trophic coherence of the PM_{2.5} network in Henan Province.

Discussion and conclusion

Discussion and suggestion

According to the above research results, we discuss the spatial-temporal distribution of PM_{2.5} in Henan Province as follows, and put forward the suggestion on the pollution prevention of PM_{2.5}.

(1) The results of cross-correlation and Granger causality test show that there is a certain causal relationship for the PM_{2.5} concentration between cities in Henan Province. Therefore, the problem for the pollution prevention of PM_{2.5} cannot be viewed in isolation. The idea of joint prevention and collaborative governance of PM_{2.5} pollution in the region should be established, so as to achieve the common governance and prevention of the air environment.

(2) The trophic coherence analysis for the PM_{2.5}-directed network of Henan Province shows that the pollution situation in different seasons within the province is different, and the vulnerability of the PM_{2.5} network is also different. Henan Province should focus on the strengthening the pollution prevention in autumn and winter, and carry out pollution prevention work of PM_{2.5} in a targeted manner based on the situation of trophic levels of each prefecture-level city in the four seasons.

(3) The calculation results of trophic levels for the PM_{2.5}-directed network of Henan Province show that the prefecture-level cities that are located at the transmission source of PM_{2.5} include Anyang, Puyang, Zhoukou, Kaifeng, Xuchang, Jiaozuo, Nanyang, and Shangqiu. In these cities, it is necessary to establish joint supervision departments for key regions to emphatically strengthen the pollution prevention work of PM_{2.5} in basic node cities. It should strengthen the intensity of supervision and actively optimize the industrial structure to reduce the probability of PM_{2.5} pollution emissions.

Conclusion

According to PM_{2.5} concentration data from seventeen prefecture-level cities in Henan Province in 2018, the research analyzes the characteristics of the temporal distribution of PM_{2.5} concentration using descriptive statistics and inverse distance interpolation method. The result shows that there are significant seasonal differences in PM_{2.5} concentration in Henan Province, with the highest in winter and the lowest in summer, and the means in spring and autumn are similar. The hourly mean of PM_{2.5} concentration shows different trends for each season, and PM_{2.5} concentration between different months within the same season is not completely consistent. At the same time, by analyzing and visualizing the mean of PM_{2.5} concentration in three research periods around the National Day holiday, we find that the mean of PM_{2.5} concentration within the province during and after National Day is significantly higher than that before National Day, and there is a relatively significant holiday effect caused by human activities.

We further analyze the correlation of PM_{2.5} concentration between prefecture-level cities in Henan Province using the methods such as cross-correlation and Granger causality test, and construct a directed network based on Granger causality to excavate the directivity of the interaction of PM_{2.5} concentration between cities. Meanwhile, we introduce the trophic coherence to explore the hierarchical structure and stability of the PM_{2.5} network in Henan Province. The research shows that the cross-correlation of PM_{2.5} concentration between the prefecture-level cities of Henan Province in each season is different. In spring and summer, the cross-correlation between the cities within the province has significantly spatial differentiation, showing two groups, namely, southern and northern Henan. In autumn and winter, the cross-correlation of PM_{2.5} of city pairs within the province is closer, with higher spatial embeddedness. In the four seasons, the impact of PM_{2.5} concentration between the cities within Henan province has significant causal directivity. The trophic coherence of the PM_{2.5}-directed network is the smallest in autumn, with the most stable structure, while is with the largest vulnerability in summer.

The research uses the complex network analysis method to analyze the causal directivity relationship of PM_{2.5} interaction between the prefecture-level cities in Henan Province from the perspective of data, in order to provide a scientific basis for the air environment governance in Henan Province. In the future, combined with advanced technologies such as geographic information technology and remote sensing, the relevant departments can conduct real-time monitoring and forecasting for fixed and mobile emission sources, and build relevant cloud platforms to realize the sharing of air quality information and the timely warning, so as to provide a decision-making basis for regional policy making. Further research work can use meteorological parameters to evaluate the prediction network based on the PM_{2.5} time series.

Acknowledgements. This study was supported by the Natural Science Foundation of Shandong Province (NO.ZR2019MD034) and the Education Reform Project of Shandong Province (M2020266).

REFERENCES

- [1] Apte, J. S., Marshall, J. D., Cohen, A. J. (2015): Addressing global mortality from ambient PM_{2.5}. – *Environmental Science & Technology* 49(13): 8057-8066.
- [2] Barabasi, A. L., Albert, R. (1999): Emergence of scaling in random networks. – *Science* 286(5439): 509-512.
- [3] Davis, J. C. (2002): *Statistics and Data Analysis in Geology*. 3rd Ed. – Library of Congress, New York.
- [4] Fan, X., Wang, L., Xu, H. (2016): Characterizing air quality data from complex network perspective. – *Environmental Science and Pollution Research* 23(4): 3621-3631.
- [5] Gao, T. Z., Chen, K. M., Li, F. L. (2018): Topology analysis of urban rail transit network. – *Journal of Chang'an University (Natural Science Edition)* 38(03): 97-106.
- [6] Gehrig, R., Buchmann, B. (2003): Characterising seasonal variations and spatial distribution of ambient PM₁₀ and PM_{2.5} concentrations based on long-term Swiss monitoring data. – *Atmospheric Environment* 37(19): 2571-80.
- [7] Guo, D., Wang, R., Zhao, P. (2020): Spatial distribution and source contributions of PM_{2.5} concentrations in Jincheng, China. – *Atmospheric Pollution Research* 11(8): 1281-1289.
- [8] Hinojosa-Baliño, I., Infante-Vázquez, O., Vallejo, M. (2019): Distribution of PM_{2.5} air pollution in Mexico City: spatial analysis with land-use regression model. – *Applied Sciences* 9(14): 2936.
- [9] Li, H., Qi, Y., Li, C. (2019): Routes and clustering features of PM_{2.5} spillover within the Jing-Jin-Ji region at multiple timescales identified using complex network-based methods. – *Journal of Cleaner Production* 209.
- [10] Li, N., Xu, J., Lv, X. (2021): Application of dynamically constrained interpolation methodology in simulating national-scale spatial distribution of PM_{2.5} concentrations in China. – *Atmosphere* 12(2): 272.
- [11] Lin, C., Li, Y., Yuan, Z. (2015): Using satellite remote sensing data to estimate the high-resolution distribution of ground-level PM_{2.5}. – *Remote Sensing of Environment* 156: 117-128.
- [12] Lin, Y., Yuan, X., Zhai, T. (2020): Effects of land-use patterns on PM_{2.5} in China's developed coastal region: exploration and solutions. – *Science of the Total Environment* 703: 135602.
- [13] Liu, C., Guo, Y. D. (2020): An empirical study on contagion effect and co-movement behavior of financial crisis in stock markets. – *Operations Research and Management Science* 29(10): 198-211.

- [14] Ma, Y. B., Gao, G. K. (2018): Research on haze pollution network of Beijing-Tianjin-Hebei region based on node importance evaluation. – *Acta Scientiae Circumstantiae* 38(06): 2287-2296.
- [15] Moutsinas, G., Shuaib, C., Guo, W. (2019): Graph hierarchy and spread of infections. – arXiv preprint arXiv 1908.04358.
- [16] Ning, Z. X., Yin, Y., Li, Q. (2020): Analysis of the influencing factors of China's inter-provincial haze pollution based on the spatial dubin model. – *Modern Business Trade Industry* 41(26): 44-46.
- [17] Pagani, A., Mosquera, G., Alturki, A. (2019): Resilience or robustness: identifying topological vulnerabilities in rail networks. – *Royal Society Open Science* 6: 181301.
- [18] Shen, S. J., Shen, G. C. (2020): Analysis on the spatial structure of inter-provincial migrant in China. – *Population Journal* 42(04): 103-112.
- [19] Song, W., Jia, H., Li, Z. (2018): Using geographical semi-variogram method to quantify the difference between NO₂ and PM_{2.5} spatial distribution characteristics in urban areas. – *Science of the Total Environment* 631: 688-694.
- [20] Tan, H., Chen, Y., Wilson, J. P. (2020): An eigenvector spatial filtering based spatially varying coefficient model for PM_{2.5} concentration estimation: a case study in Yangtze River Delta region of China. – *Atmospheric Environment* 223: 117205.
- [21] Wang, H. Q., Gu, C. G. (2019): Research on the importance of city nodes in the smog network of the Yangtze River Delta based on complex network theory. – *China Water Transport* 19(01): 92-94.
- [22] Wang, M., Wang, H. (2020): Spatial distribution patterns and influencing factors of PM_{2.5} pollution in the Yangtze River Delta: empirical analysis based on a GWR model. – *Asia-Pacific Journal of Atmospheric Sciences* 1-13.
- [23] Wang, H., Li, J., Gao, Z. (2019): High-spatial-resolution population exposure to PM_{2.5} pollution based on multi-satellite retrievals: a case study of seasonal variation in the Yangtze River Delta, China in 2013. – *Remote Sensing* 11(23): 2724.
- [24] Wang, X. J., Chen, Q., Dong, S. N. (2020a): Spatial distribution characteristics and source apportionment of PM_{2.5} in Yantai City. – *Environmental Monitoring in China* 36(04): 53-60.
- [25] Wang, X., Sun, W., Zheng, K. (2020b): Estimating hourly PM_{2.5} concentrations using MODIS 3km AOD and an improved spatiotemporal model over Beijing-Tianjin-Hebei, China. – *Atmospheric Environment* 222: 117089.
- [26] Wang, Y., Liu, Z., Huang, L. (2020c): Development and evaluation of a scheme system of joint prevention and control of PM_{2.5} pollution in the Yangtze River Delta region, China. – *Journal of Cleaner Production* 275: 122756.
- [27] Wang, C. M., Wan, D. J., Wang, K. X. (2021a): Spatial-temporal distribution and influencing factors of PM_{2.5} concentration in Changsha City. – *Science Technology and Engineering* 21(12): 5157-5165.
- [28] Wang, Z., Zhou, Y., Zhao, R. (2021b): High-resolution prediction of the spatial distribution of PM_{2.5} concentrations in China using a long short-term memory model. – *Journal of Cleaner Production* 297: 126493.
- [29] Watts, D., Strogatz, S. (1998): Collective dynamics of 'small-world' networks. – *Nature* 393: 440-442.
- [30] Wu, D., Lary, D. J., Zewdie, G. K. (2019): Using machine learning to understand the temporal morphology of the PM_{2.5} annual cycle in East Asia. – *Environmental Monitoring and Assessment* 191(2): 1-14.
- [31] Xiao, Q., Lu, Y. T. (2019): Application of the complex network in the PM_{2.5} analysis of air pollution in regions. – *Journal of Technology* 19(01): 77-83.
- [32] Xu, J., Song, S. X., Zhai, H. Y. (2020): Analysis of network development of Beijing subway based on complex network. – *Urban Rapid Rail Transit* 33(05): 88-93.
- [33] Xue, A., Geng, E. Z. (2015): Region division study of PM_{2.5} pollution in cities of China based on complex networks. – *Journal of Basic Science and Engineering* 23(S1): 68-78.

- [34] Yang, D., Ye, C., Wang, X. (2018): Global distribution and evolvement of urbanization and PM_{2.5} (1998–2015). – *Atmospheric Environment* 182: 171-178.
- [35] Ye, W. F., Ma, Z. Y., Ha, X. Z. (2018): Spatial-temporal patterns of PM_{2.5} concentrations for 338 Chinese cities. – *Science of the Total Environment* 631: 524-533.
- [36] Ye, C., Chen, R., Chen, M. (2019): A new framework of regional collaborative governance for PM_{2.5}. – *Stochastic Environmental Research and Risk Assessment* 33(4): 1109-1116.
- [37] Yun, G., He, Y., Jiang, Y. (2019): PM_{2.5} spatiotemporal evolution and drivers in the Yangtze River Delta between 2005 and 2015. – *Atmosphere* 10(2): 55.
- [38] Zhan, Q., Fan, Z., Yan, S. (2019): New MAIAC AOD product based high resolution PM_{2.5} spatial-temporal distribution change at urban scale. – 10th International Workshop on the Analysis of Multitemporal Remote Sensing Images (MultiTemp). IEEE 1-4, Wuhan, China.
- [39] Zhang, X. Y., Wang, Z. J. (2014): The study of diffusion networks model of about PM_{2.5} in urban areas. – *Environmental Monitoring in China* 30(6): 130-132.
- [40] Zhang, N., Ma, F., Qin, C. (2018): Spatiotemporal trends in PM_{2.5} levels from 2013 to 2017 and regional demarcations for joint prevention and control of atmospheric pollution in China. – *Chemosphere* 210.
- [41] Zhang, H., Wang, S. H., Guo, X. (2020a): Structure learning of region feature of haze pollution. – *Journal of Shaanxi Normal University (Natural Science Edition)* 48(02): 117-124.
- [42] Zhang, S. L., Liu, H. H., Yin, H. (2020b): Quantitative research on international petroleum trade relations based on complex networks. – *Journal of Southwest Petroleum University (Science & Technology Edition)* 42(06): 187-196.
- [43] Zhao, L. T., Cao, W. D., Wei, Z. (2018): A study on population flow network and its characteristics in Pan-Yangtze River Delta. – *Resources and Environment in the Yangtze Basin* 27(04): 705-714.

LEAF POSITION AND LEAF AREA EFFECTS ON THE DIVERSITY OF FOLIICOLOUS LICHENS ASSOCIATED WITH *STENANONA FLAGELLIFLORA* (ANNONACEAE)

FIGUEROA-CASTRO, D. M.* – PÉREZ-PÉREZ, R. E.

Facultad de Ciencias Biológicas, Benemérita Universidad Autónoma de Puebla, Blvd. Valsequillo y Av. San Claudio s/n, Edif. 112-A, Ciudad Universitaria, Col. Jardines de San Manuel, C.P. 72570, Puebla, Puebla, México

**Corresponding author
e-mail: figgery@gmail.com*

(Received 19th Jan 2022; accepted 2nd May 2022)

Abstract. Follicolous lichens grow on the surface of alive leaves of vascular plants and are highly diverse in tropical habitats. Their taxonomy and ecology are relatively well known; however, there are no studies on the within-individual variation in the diversity and composition of the communities growing on single leaves. We describe the diversity of follicolous lichens associated with leaves of *Stenanona flagelliflora* (Annonaceae) of different sizes and within-canopy position at Los Tuxtlas, Veracruz, Mexico. Species composition, richness, cover, and the Shannon-Wiener diversity index of the lichen communities growing on each leaf were determined. The community of follicolous lichens associated with *S. flagelliflora* is highly diverse: 94 follicolous lichen species from 12 families were recorded. *Porina karnatakensis* (Porinaceae) was the dominant species across leaves at different positions. Species richness, lichen cover, and diversity index were not significantly affected by leaf area nor by leaf position, but both of these factors influenced community composition. We discuss the importance of within-phorophyte microclimate variation, competitive interactions, and environmental requirements of each lichen species as the main drivers of the differences found in the assemblage of lichens. More studies on the factors that determine the diversity of the communities of organisms within the phylloplane are needed.

Keywords: *phylloplane, phyllosphere, Shannon-Wiener diversity index, Sørensen similarity index, species composition, species richness – area relationship*

Introduction

Plant leaves are a harsh habitat exposed to diverse sources of environmental stress (Lindow and Brandl, 2003). Leaves are an ephemeral habitat exposed to UV radiation, desiccation, rainfall, nutrient limitation, and frequent fluctuations in temperature and relative humidity (Gomes et al., 2018; Hirano and Upper, 2000; Lindow and Brandl, 2003; Thapa and Prasanna, 2018). In spite of this, numerous epiphyte microorganisms such as bacteria, fungi, protozoa, yeasts, algae, and nematodes (Lindow and Brandl, 2003; Thapa and Prasanna, 2018), as well as follicolous lichens (Lücking, 2001; Lücking and Cáceres, 2002) colonize and establish successfully on the phylloplane.

Diverse studies have documented the existence of spatial variation in the communities of phylloplane organisms within the phorophyte and the factors that might explain such variation. These studies have shown that the diversity, abundance, and composition of phylloplane bacteria, fungi, and yeast communities vary within a single host according to canopy position (Andrews et al., 1980; Carroll, 1979; Harrison et al., 2016; Hermann et al., 2021; Izuno et al., 2016; Laforest-Lapointe et al., 2016; Leff et al., 2015; Nguyen, 2017; Stone and Jackson, 2019), leaf age, leaf region (Carroll, 1979) tissue and organ type (Leff et al., 2015), leaf orientation (Andrews et al., 1980; Nguyen, 2017), and microclimate (temperature, vapor pressure deficit, humidity and precipitation; Al-Ashhab et al., 2021).

In contrast, only one study has documented the existence of within-individual variation in the diversity of the communities of foliicolous lichens (Sipman, 1997). This study shows that lichen diversity decreases from the top to the bottom part of the phorophyte, such that the lowest lichen diversity is found in the most shaded region of the phorophyte. This pattern of vertical variation on the diversity of foliicolous lichens was explained by the differential incidence of light along the phorophyte (Sipman, 1997).

In this study, we describe the intra-individual variation in the diversity and composition of the communities of foliicolous lichens associated with the phorophyte *Stenanona flagelliflora* T. Wendt & G. E. Schatz (Annonaceae). Particularly, we were interested in finding out if the communities of lichens vary as a function of leaf area and leaf position within the phorophyte. We hypothesized that: i) the diversity of lichens will increase with leaf area, as it has been demonstrated for numerous groups of organisms (Brunet and Medellín, 2001; Feinstein and Blackwood, 2012; Flores-Palacios and García-Franco, 2006; Kohn and Walsh, 1994; Löfgren and Jerling, 2002; Lyons et al., 2010), and ii) the composition, abundance and diversity of the communities of lichens will vary across leaves with different positions within an individual phorophyte as it has been documented for different groups of organisms within the phylloplane (Andrews et al., 1980; Carroll, 1979; Harrison et al., 2016; Hermann et al., 2021; Izuno et al., 2016; Laforest-Lapointe et al., 2016; Leff et al., 2015; Nguyen, 2017; Sipman, 1997).

Methods

Phorophyte species

Stenanona flagelliflora (Annonaceae) is a tree of 1–4.5 m in height, that produces inflorescences on specialized branches (i.e., flagelliflorous) with up to 3 m in length on the surface of the ground. Leaves are membranaceous, bright medium glossy green above and paler beneath when fresh, elliptic, 9–18 cm in length and 2.6–6.5 cm width, getting narrower towards the tip (Schatz and Wendt, 2004). *Stenanona flagelliflora* has been recorded in the southern part of the Uxpanapa region of extreme southern Veracruz and the adjacent part of the Chimalapa region on eastern Oaxaca (Schatz and Wendt, 2004). A population at Los Tuxtlas, Veracruz, where the present study took place, has also been recorded (Xicohténcatl-Lara et al., 2016).

Study site

The study took place at the Los Tuxtlas Biosphere Reserve, in the Lic. Adolfo López Mateos locality (18°26'19.60"N, 94°57'53.16"; 219 m a.s.l.; Morteo, 2011), in the State of Veracruz, Mexico (Fig. 1). Vegetation at the locality is an evergreen rainforest (Miranda and Hernández, 1963). Climate is hot and humid, with an average annual temperature of 22–26 °C (Cruz, 2009) and a mean annual precipitation of 2000–2500 mm (Cruz, 2009; Guevara et al., 1999).

The community of foliicolous lichens associated with Stenanona flagelliflora

In March 2013, we collected 63 leaves from 12 individuals of *Stenanona flagelliflora* [Annonaceae; 1–7 leaves per individual plant, depending upon the availability of leaves without (or very low) damage by herbivores]. Although leaves were collected on a specific time of the year, community patterns of foliicolous lichens might be similar at other times because: (i) the lifespan of leaves in tropical forests is between 1–3 years;

(ii) within few months after their establishment, foliicolous lichens reproduce assuring their prevalence in the habitat (Lücking 2008a); (iii) *Stenanona flagelliflora* is a perennial plant, its leaves are available for colonization throughout the year. We chose *S. flagelliflora* to conduct the study because most of the foliar surface is covered by foliicolous lichens and because it has a relatively short height [1–4.5 m according with Schatz and Wendt (2004); but a maximum of 2.2 m in the sampled population), which facilitates the collection of leaves at different heights within each individual. At the locality of study, the species is distributed close to the edge of the forest, but where a canopy layer is well developed. Leaves were collected from individual phorophytes selected randomly but at a distance of 1.5-2 m from each other. In order to have represented foliicolous species from different positions within the phorophyte, leaves were collected from the top (>150 cm in height; N = 21), base (<70 cm in height; N = 21) and middle (70 – 150 cm in height; N = 21) regions of each individual plant. Collected leaves were pressed and dried using standard herbarization procedures. Specimens were deposited in the Lichen collection of the Biological Sciences Department at Autonomous University of Puebla. Identification of the foliicolous lichen species growing on the adaxial surface of each leaf was conducted under a NIKON SMZ645 stereoscopic microscope. Species identification at the lowest taxonomic level was conducted using Lücking and Cáceres (2002) guide and Lücking (2008b).

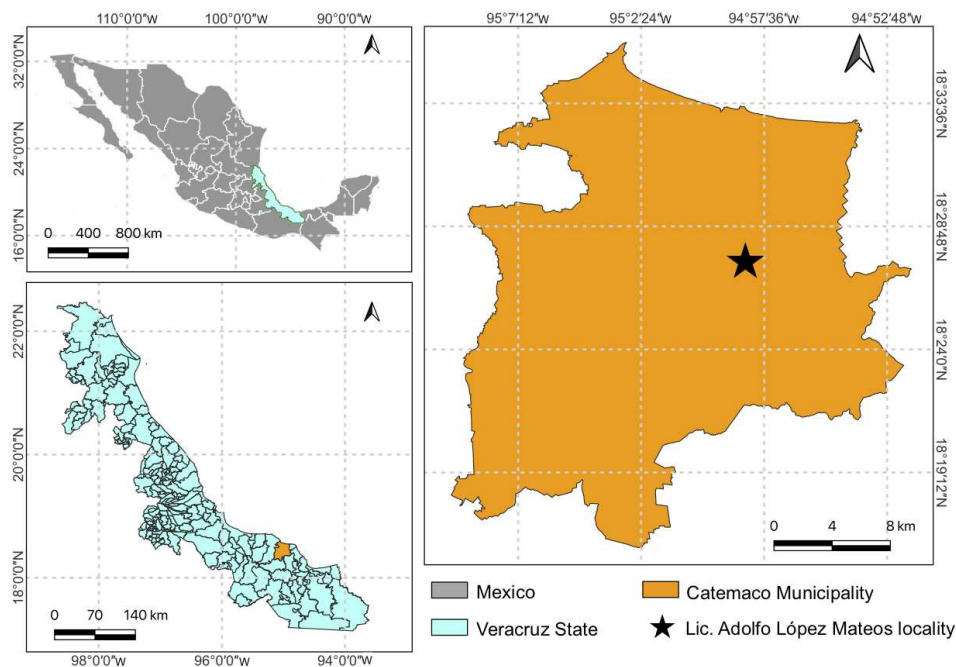


Figure 1. Location of the area of study

Lichen abundance was estimated as the area covered by each lichen species within each leaf (Löhmus and Löhmus, 2001). To do this, dry leaves were scanned in a HP Scanjet G2410 at 300 pixels per inch. Then, using the free software ImageJ (Rasband, 1997-2018), we determined the total area covered by each lichen species within each leaf as well as the total area of each collected leaf. Shannon-Wiener (H') diversity index was estimated as $H' = -\sum p_i \ln p_i$, where p_i is the relative cover of each foliicolous

species in relation to the total cover of foliicolous lichens growing on each leaf (Lõhmus and Lõhmus, 2001). The importance of leaf position (i.e., top, middle, and base) on species richness and relative lichen cover were analyzed with one-way ANOVA tests. Species richness was transformed logarithmically, whereas relative lichen cover was transformed as arcsine $(p)^{1/2}$ (Zar, 2010). The effect of leaf position on the diversity index was tested with a non-parametric Kruskal-Wallis analysis. Finally, Spearman correlation analyses were used to test the relationship between leaf area and the community parameters estimated (species richness, relative lichen cover, and diversity index). Analyses were conducted in PAST v. 2.17 (Hammer et al., 2001).

Rank-abundance curves (James and Rathbun, 1981) were constructed to compare the dominant foliicolous lichen species among leaves with different positions. Relative abundance was estimated as n_i/N , where n_i = relative cover of the i th foliicolous lichen species, and N = relative cover from all the lichen species including all leaf positions. Relative abundance was plotted on a \log_{10} scale against the rank from the most to the least common species.

Differences in species composition among leaves of different size and position were analyzed with two ordination methods. Using a matrix of species relative cover on each collected leaf, we first conducted a non-metric multidimensional scale (NMDS) analysis to determine if the communities of foliicolous lichens grouped together according with leaf position. The NMDS analysis is widely used in community studies (Arcos-Pulido and Gómez-Prieto, 2006; Ruíz-Pineda et al., 2016). The stress value obtained in the analysis is a measure of fit of the similarity among samples in the two-dimensional space (Clarke et al., 2014). In addition, an analysis of similarities (ANOSIM) was conducted. The ANOSIM test shows the existence of differences among groups according to the value of the statistic R . If $R = 1$ there is low similarity among groups, whereas if $R = 0$, the groups are rather similar (Clarke et al., 2014). The NMDS analysis was conducted using the Bray-Curtis similarity index and the foliicolous lichen species collected in at least five sampled leaves. The analysis was performed in the program PAST v. 4.03 (Hammer et al., 2001). In addition, we conducted two canonical correspondence analyses (CCA) to evaluate the effects of both leaf area and leaf position on the composition of the communities of foliicolous lichens. Leaves collected in different positions were classified as 1 for those collected on the base, 2 on the middle, and 3 when they were collected from the top part of the tree. A first CCA analysis was conducted at the species level (using relative cover data of the lichen species found in at least five sampled leaves), whereas the second one was conducted at the family level (using relative cover data pooled across all lichen species within each family). CCA analyses were conducted in the software MVSP v. 3.21 (Kovach, 2004).

Results

The community of foliicolous lichens

A total of 94 foliicolous lichen taxa were identified growing on the adaxial surface of the leaves of *Stenanona flagelliflora* (Table 1; Fig. 2). Most taxa (90, 95.7%) were identified to the genus (51 species, 54.3%) or the species level (39 species, 41.5%). The remaining 4 taxa (4.3%) were distinguished only as morphospecies, determination at family level was not even possible for them. Porinaceae was the richest family (41 species, 43.6%; Table 1). The other 11 families were represented by 1–8 foliicolous lichen species: Gomphillaceae (8), Arthoniaceae, Pilocarpaceae, Roccellaceae (7

species each), Strigulaceae (6), Microthelipsidaceae (4), Coenogoniaceae, Lyrommataceae (3 species each), Monoblastiaceae (2), Ramalinaceae, and Thelotremaaceae (1 species each; Table 1; Fig. 2). Three species, *Coenogonium luteum* (Dicks.) Kalb & Lücking, *Trichotelium pauciseptatum* Vězda, and *Strigula obducta* (Müll. Arg.) R.C. Harris represent new records for Mexico.

Table 1. List of foliicolous lichens growing on the adaxial surface of the leaves of *Stenanona flagelliflora* (Annonaceae) at Los Tuxtlas, Veracruz, Mexico. Relative cover (mean \pm s.e.) across the 63 sampled leaves of *Stenanona flagelliflora* and number of leaves with different position on which each lichen species was registered are shown

Family Species	Lichen cover (%)	Top	Middle	Base
Arthoniaceae				
<i>Arthonia accolens</i> Stirt.	0.46 \pm 0.3	1	3	3
<i>Arthonia lecythidicola</i> (Bat. & H. Maia) Lücking & Sérus	1.75 \pm 0.88	1	3	3
<i>Arthonia</i> sp. 1	2.15 \pm 0.91	8	9	10
<i>Arthonia</i> sp. 2	0.05 \pm 0.04	1	1	0
<i>Arthonia</i> sp. 3	0.098 \pm 0.098	1	0	0
<i>Arthonia</i> sp. 4	0.012 \pm 0.012	1	0	0
<i>Arthonia</i> sp. 5	0.25 \pm 0.2	0	3	0
Coenogoniaceae				
<i>Coenogonium luteum</i> (Dicks.) Kalb & Lücking	0.92 \pm 0.92	1	0	0
<i>Coenogonium</i> sp. 1	2.63 \pm 1.6	3	2	5
<i>Coenogonium</i> sp. 2	0.73 \pm 0.73	0	0	1
Gomphillaceae				
<i>Aulaxina microphana</i> (Vain.) R. Sant.	0.024 \pm 0.017	0	0	2
<i>Aulaxina</i> sp. 1	0.31 \pm 0.16	6	6	4
<i>Aulaxina</i> sp. 2	0.001 \pm 0.001	1	0	0
<i>Gyalectidium filicinum</i> Müll. Arg.	0.04 \pm 0.03	1	1	0
<i>Gyalectidium</i> sp. 1	0.003 \pm 0.002	0	0	2
<i>Gyalectidium</i> sp. 2	0.009 \pm 0.009	1	0	0
<i>Tricharia</i> sp. 1	0.002 \pm 0.001	0	2	0
<i>Tricharia</i> sp. 2	0.001 \pm 0.001	1	0	0
Lyrommataceae				
<i>Lyromma nectandrae</i> Bat. & H. Maia	0.01 \pm 0.01	0	1	0
<i>Lyromma</i> sp. 1	0.22 \pm 0.15	0	1	3
<i>Lyromma</i> sp. 2	0.22 \pm 0.22	0	0	1
Microthelipsidaceae				
<i>Microtheliopsis</i> sp. 1	0.41 \pm 0.25	1	1	3
<i>Microtheliopsis</i> sp. 2	0.2 \pm 0.2	0	0	1
<i>Microtheliopsis uleana</i> Müll. Arg.	0.24 \pm 0.14	0	3	1
<i>Microtheliopsis uniseptata</i> Herrera-Campos & Lücking	1.18 \pm 1.18	0	0	1
Monoblastiaceae				
<i>Anisomeridium foliicola</i> R. Sant. & Tibell	0.065 \pm 0.065	1	0	0
<i>Anisomeridium</i> sp. 1	0.89 \pm 0.89	0	0	1
Not determined family				
Sp. 1	8.53 \pm 2.66	13	12	13
Sp. 2	0.64 \pm 0.64	1	0	0
Sp. 3	1.79 \pm 1.24	2	3	5
Sp. 4	0.69 \pm 0.63	1	0	2

Table 1. Continued

Family Species	Lichen cover (%)	Top	Middle	Base
Pilocarpaceae				
<i>Bapalmuia</i> sp. 1	0.24 ± 0.22	0	1	1
<i>Byssolecania fumosonigricans</i> (Müll. Arg.) R. Sant.	0.26 ± 0.16	1	2	0
<i>Byssolecania</i> sp. 1	0.87 ± 0.87	0	1	0
<i>Byssoloma</i> sp. 1	1.95 ± 1.35	1	2	1
<i>Calopadia</i> sp. 1	1.45 ± 1.13	0	0	2
<i>Lasioloma</i> sp. 1	0.04 ± 0.04	0	1	0
<i>Sporopodium</i> sp. 1	0.18 ± 0.17	1	0	0
Porinaceae				
<i>Porina alba</i> (R. Sant.) Lücking	4.44 ± 2.31	9	10	7
<i>Porina atrocoerulea</i> Müll. Arg.	0.11 ± 0.07	2	0	2
<i>Porina atropunctata</i> Lücking & Vezda	0.61 ± 0.61	0	0	1
<i>Porina epiphylla</i> (Fée) Fée	2.65 ± 1.56	4	10	2
<i>Porina karnatakensis</i> Makhija, Adawadkar & Patwardhan	51.82 ± 4.48	18	20	20
<i>Porina limbulata</i> (Kremp.) Vain.	0.02 ± 0.01	0	2	0
<i>Porina monocarpa</i> (Kremp.) F. Schill.	0.02 ± 0.02	1	0	0
<i>Porina nitidula</i> Müll. Arg.	0.04 ± 0.04	1	0	0
<i>Porina octomera</i> (Müll. Arg.) F. Schil	0.07 ± 0.04	3	1	1
<i>Porina rubentior</i> (Stirt.) Müll. Arg.	2.32 ± 0.47	14	18	13
<i>Porina rubescens</i> (Lücking) Hafellner & Kalb	0.04 ± 0.03	3	0	1
<i>Porina rufula</i> (Kremp.) Vain.	0.04 ± 0.03	2	0	0
<i>Porina</i> sp. 1	1.19 ± 1.04	2	2	1
<i>Porina</i> sp. 2	0.02 ± 0.02	0	1	0
<i>Porina</i> sp. 3	0.11 ± 0.11	0	1	0
<i>Porina</i> sp. 4	0.19 ± 0.19	1	0	0
<i>Porina</i> sp. 5	0.05 ± 0.05	1	0	0
<i>Porina</i> sp. 6	0.06 ± 0.06	1	0	0
<i>Porina</i> sp. 7	0.04 ± 0.04	1	0	0
<i>Porina</i> sp. 8	0.02 ± 0.02	1	0	0
<i>Porina</i> sp. 9	0.003 ± 0.003	0	1	0
<i>Porina</i> sp. 10	0.002 ± 0.002	1	0	0
<i>Porina</i> sp. 11	0.1 ± 0.096	0	2	1
<i>Porina</i> sp. 12	0.006 ± 0.006	0	1	0
<i>Porina</i> sp. 13	0.06 ± 0.06	0	1	0
<i>Porina</i> sp. 14	0.34 ± 0.22	2	0	1
<i>Porina</i> sp. 15	0.04 ± 0.04	1	0	0
<i>Porina</i> sp. 16	0.002 ± 0.002	0	1	0
<i>Porina</i> sp. 17	0.03 ± 0.03	1	0	0
<i>Porina tetramera</i> (Malme) R. Sant.	2.11 ± 1.03	5	8	5
<i>Trichothelium epiphyllum</i> Müll. Arg.	0.33 ± 0.17	3	4	5
<i>Trichothelium intermedium</i> Herrera-Campos & Lücking	0.01 ± 0.01	1	0	0
<i>Trichothelium longisporum</i> Lücking	0.009 ± 0.009	1	0	0
<i>Trichothelium minus</i> Vain.	0.07 ± 0.04	3	2	0

Table 1. Continued

Family Species	Lichen cover (%)	Top	Middle	Base
<i>Trichothelium mirum</i> Lücking	0.1 ± 0.04	7	4	2
<i>Trichothelium pallidesetum</i> Lücking	0.004 ± 0.004	1	0	0
<i>Trichothelium pauciseptatum</i> Vézda	0.09 ± 0.04	1	4	1
<i>Trichothelium</i> sp. 1	0.16 ± 0.06	4	5	6
<i>Trichothelium</i> sp. 2	0.04 ± 0.03	0	0	2
<i>Trichothelium</i> sp. 3	0.01 ± 0.01	1	0	0
<i>Trichothelium</i> sp. 4	0.009 ± 0.009	1	0	0
Ramalinaceae				
<i>Bacidina</i> sp. 1	0.005 ± 0.004	0	1	1
Roccellaceae				
<i>Enterographa</i> sp. 1	0.01 ± 0.01	1	0	0
<i>Mazosia melanophthalma</i> (Müll. Arg.) R. Sant.	0.29 ± 0.21	4	2	2
<i>Mazosia phyllosema</i> (Nyl.) Zahlbr.	0.02 ± 0.02	1	0	0
<i>Mazosia rotula</i> (Mont.) A. Massal.	0.14 ± 0.06	5	2	4
<i>Mazosia</i> sp. 1	0.05 ± 0.03	1	3	2
<i>Mazosia</i> sp. 2	0.03 ± 0.03	1	0	0
<i>Opegrapha</i> sp. 1	0.12 ± 0.05	0	3	5
Strigulaceae				
<i>Phyllobathelium firmum</i> (Stirt.) Vézda	0.02 ± 0.02	1	0	0
<i>Phyllobathelium</i> sp. 1	0.01 ± 0.01	1	0	0
<i>Strigula nitidula</i> Mont.	0.18 ± 0.09	1	1	4
<i>Strigula obducta</i> (Müll. Arg.) R.C. Harris	0.44 ± 0.27	2	0	1
<i>Strigula phyllogena</i> (Müll. Arg.) R.C. Harris	0.35 ± 0.21	1	2	1
<i>Strigula platypoda</i> (Müll. Arg.) R.C. Harris	1.46 ± 0.66	2	3	3
Thelotremaaceae				
<i>Chroodiscus coccineus</i> (Leight.) Müll. Arg.	0.006 ± 0.006	1	0	0

A single leaf of *S. flagelliflora* had a mean area of 44.99 ± 2.01 cm² (range: 19.82–94.26 cm²) and supported a community of $7.94 \pm$ s.e. 0.44 species of foliicolous lichens (range: 1–17 species) in average. Likewise, mean lichen cover on a single leaf was 11.75 ± 0.81 cm² (range: 0.04–30.5 cm²). Mean diversity index on the leaves of *S. flagelliflora* was 0.83 ± 0.06 . The highest diversity index across all sampled leaves was 1.89; whereas the lowest one was 0, on a leaf on which a single lichen species was growing.

Frequency of each foliicolous lichen species on the sampled leaves of *S. flagelliflora* was highly variable (range: 1–58 leaves). *Porina karnatakensis* Makhija, Adawadkar & Patwardhan (Porinaceae) was the most frequent species, being identified in 92.1% of the leaves. Other species with high frequency were *P. rubentior* (Stirt.) Müll. Arg. (45 leaves, 71.43%), *P. alba* (R. Sant.) Lücking (Porinaceae) (26 leaves, 41.27%), *Arthonia* sp. 1 (Arthoniaceae) (27 leaves, 42.86%), and the unidentified morphospecies 1 (38 leaves, 60.32%). In contrast, 45 species were present in only one out of the 63 leaves sampled (Table 1).

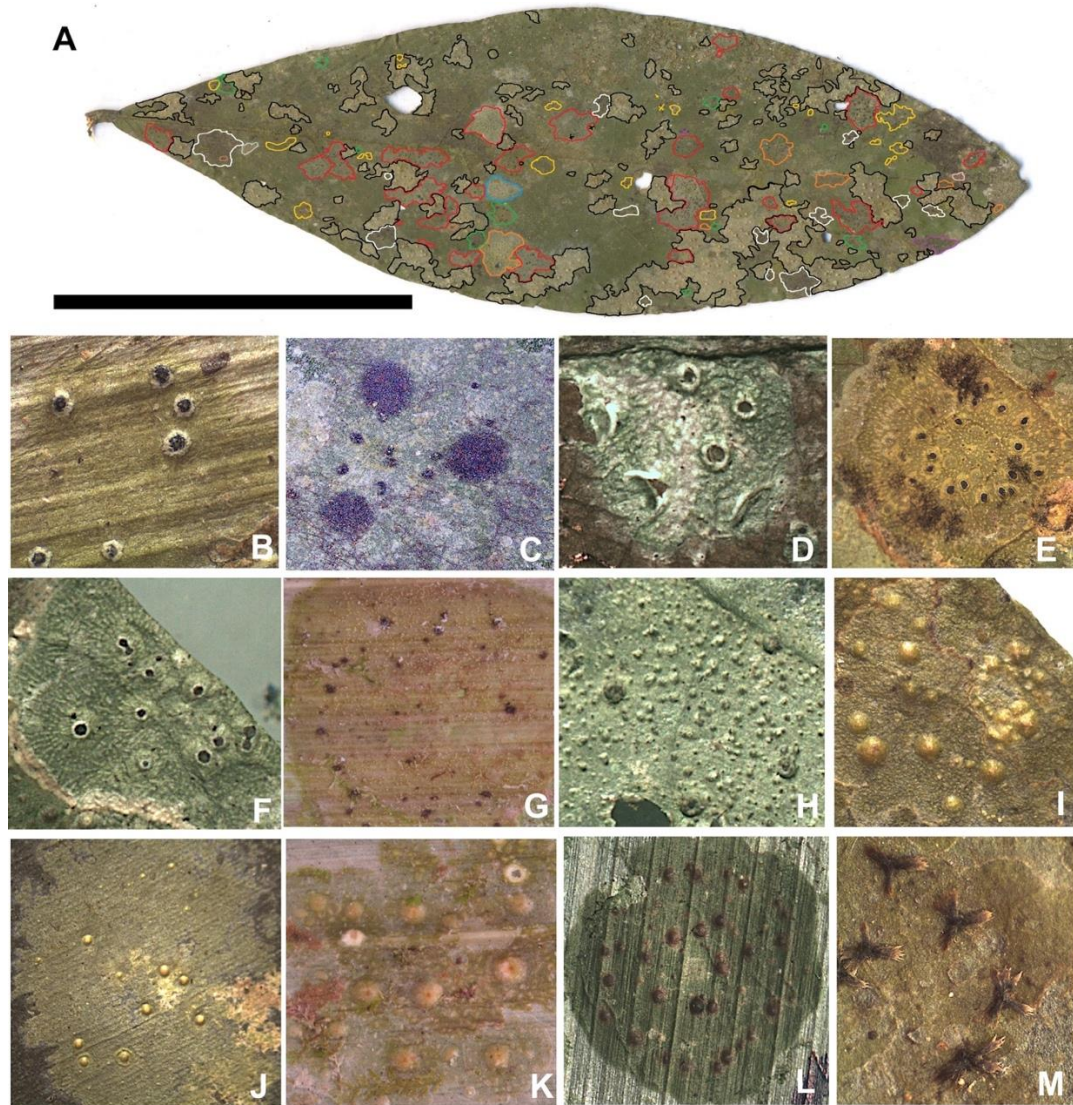


Figure 2. Foliicolous lichens growing on the leaves of *Stenanona flagelliflora*. (A) The community of foliicolous lichens on a single leaf. Scale bar = 5 cm. (B) *Anisomeridium foliicola* (Monoblastiaceae), (C) *Arthonia lecythidicola* (Arthoniaceae), (D) *Gyalectidium filicinum* (Gomphillaceae), (E) *Mazosia melanophthalma* (Roccellaceae), (F) *Mazosia rotula* (Roccellaceae), (G) *Microtheliopsis uniseptata* (Microthelipsidaceae), (H) *Phyllobathelium firmum* (Strigulaceae), (I) *Porina alba* (Porinaceae), (J) *Porina epiphylla* (Porinaceae), (K) *Porina karnatakensis* (Porinaceae), (L) *Porina rubentior* (Porinaceae), (M) *Trichothelium epiphyllum* (Porinaceae). B-M photographs were taken with a microscope Nikon DXM 1200

Mean relative cover of lichen species per leaf varied between $0.001 \pm 0.001\%$ and $51.82 \pm 4.48\%$ (Table 1). Lichen species with the highest relative cover per leaf were *Porina karnatakensis* ($51.82 \pm 4.48\%$), the unidentified morphospecies 1 ($8.53 \pm 2.66\%$), *P. alba* ($4.44 \pm 2.31\%$), *P. epiphylla* (Fée) Fée ($2.65 \pm 1.56\%$), *Coenogonium* sp. 1 ($2.63 \pm 1.6\%$), *P. rubentior* ($2.32 \pm 0.47\%$), *Arthonia* sp. 1 ($2.15 \pm 0.91\%$), and *P. tetramera* (Malme) R. Sant. ($2.11 \pm 1.03\%$; Table 1). In contrast, *Tricharia* sp. 2, and *Aulaxina* sp. 2 had the lowest relative cover per leaf ($<0.0016\%$).

Effect of leaf area and leaf position on the community of foliicolous lichens

Overall, top leaves were colonized by a total of 66 foliicolous lichen species; whereas middle and basal leaves represented a substrate for 48 and 47 species, respectively (Table 1). Leaf-area was not significantly different among leaves from different positions (base: $44.71 \pm 3.16 \text{ cm}^2$, middle: $49.02 \pm 3.74 \text{ cm}^2$, top: $41.25 \pm 3.49 \text{ cm}^2$; $F_{2,60} = 1.26$, $P = 0.291$).

Relative cover of foliicolous lichens in top, middle, and basal leaves was $24.5 \pm 3.3\%$, $30.78 \pm 2.22\%$, and $25.5 \pm 3.21\%$, respectively. Rank-cover curves showed a strong dominance of a few foliicolous lichen species within the communities growing on leaves from all positions (Fig. 3). *Porina karnatakensis* was the most dominant (Fig. 3) and frequent species in leaves of all positions (top: 18 leaves, middle and basal: 20 leaves each). Moreover, *P. karnatakensis* had the highest relative cover across all leaf positions (top: $14.8 \pm 0.03\%$, middle: $20.3 \pm 0.03\%$, basal: $12.8 \pm 0.03\%$). Leaf position did not have a significant effect on the relative cover of *P. karnatakensis* ($F_{2,60} = 2.4$, $P = 0.099$). The unidentified morphospecies 1 was the second and third dominant species in leaves of all positions; whereas *P. alba* was the third and second dominant species in middle and top leaves. *Coenogonium* sp. 1 was the third most dominant species on basal leaves. In contrast, 42 (63.64%), 17 (35.42%), and 18 (38.3%) species were found in only one top, middle, and basal leaf, respectively. In top leaves, *Tricharia* sp. 2, and *Aulaxina* sp. 2 had the lowest mean relative cover per leaf ($<0.01 \text{ cm}^2$, $<0.005\%$). Likewise, *Porina octomera* (Müll. Arg.) F. Schil in middle leaves, as well as *Bacidina* sp. 1 and *Porina* sp. 14 in basal leaves, had the lowest mean relative cover per leaf ($<0.004\%$).

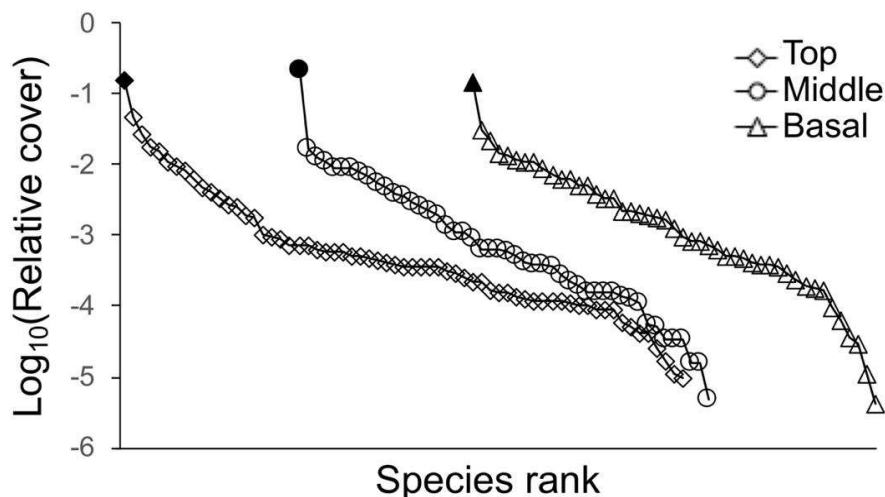


Figure 3. Mean relative cover-rank curve of the foliicolous lichen species recorded in top, middle, and basal leaves of *Stenanona flagelliflora*. Relative cover is plotted on a \log_{10} scale and the horizontal axis corresponds to the rank from the most to the less common species (James and Rathbun, 1981). Black symbols correspond to the cover of *Porina karnatakensis* (*Porinaceae*)

Lichen species richness, relative cover, and the Shannon-Wiener diversity index did not differ significantly among leaves with different position (Table 2). Likewise, none

of the three variables were significantly affected by leaf area (species richness: $r_s = 0.215$, $df = 63$, $P = 0.09$; lichen cover: $r_s = -0.16$, $df = 63$, $P = 0.21$; diversity: $r_s = 0.047$, $df = 63$, $P = 0.714$).

Table 2. Species richness, relative cover, and Shannon-Wiener diversity index (mean \pm s.e.) of the communities of foliicolous lichens associated to *Stenanona flagelliflora* leaves with different position. Results of statistical tests (ANOVA for species richness and relative cover; and Kruskal-Wallis for diversity) are shown. $n = 63$ leaves (21 from each position)

Community parameter	Leaf position			Statistical results
	Base	Middle	Top	
Species richness	7.57 \pm 0.65	8.24 \pm 0.71	8.0 \pm 2.56	$F_{2, 60} = 0.18$, $P = 0.83$
Relative cover (%)	25.5 \pm 3.21	30.78 \pm 2.22	24.5 \pm 3.3	$F_{2, 60} = 1.672$, $P = 0.197$
Shannon diversity index	0.888 \pm 0.102	0.825 \pm 0.09	0.802 \pm 0.37	$H_2 = 0.51$, $P = 0.774$

The communities of foliicolous lichens associated with leaves on different positions within the plant were fairly similar. The communities of middle and basal leaves had a similarity index of 67.37%. Similarity index between the communities of lichens on top and middle leaves was 52.63%, whereas between top and basal leaves it was 54.87%. Out of the 94 lichen species distinguished, 26 (27.6%) were recorded in all leaf positions (Table 1). In contrast, 31 (33% out of the total; 47% from the species recorded in top leaves), 12 (12.8% out of the total; 25% from the species recorded in the middle position), and 10 (10.6% out of the total; 21.3% from the species observed on basal leaves) taxa were unique to top, middle, and basal leaves, respectively (Table 1).

Porinaceae was the richest family at all leaf positions (top: 31; middle: 20; base: 17). Out of the 12 families of foliicolous lichens identified across all leaves, 10 were registered on top and middle leaves, and 11 in basal leaves. Species from the Lyrommataceae and Ramalinaceae families were not observed on top leaves (Table 1). Likewise, taxa from the Monoblastiaceae were not recorded in leaves from middle positions; whereas Thelotremaaceae was not found in both middle and basal leaves. All other families were found in leaves from all positions (range: 1–6 lichen species per family; Table 1).

The stress value obtained in the NMDS analysis was 0.1091, indicating that the ordination is adequate for interpretation (Clarke et al., 2014). Results from the NMDS show that there is not a clear grouping of the communities of foliicolous lichens according with leaf position (Fig. 4). Results of the ANOSIM confirmed the lack of significant differences among lichen communities collected on leaves with different position ($R = 0.026$; $P = 0.067$).

At the species level, the CCA analysis showed that axes 1 and 2 explained 52.3% and 33.1% of the total variation on lichen cover, respectively. Most of the lichen species were not associated with either leaf area or leaf position. However, *M. melanophthalma*, *P. tetramera*, *P. alba*, *P. octomera*, *M. rotula*, and *P. rubentior* showed some association with leaf position, in a gradient that goes from the top to the basal leaves within the tree (Fig. 5A). At the family level, axis 1 and 2 explained 46.1% and 19.7% respectively, of the total variation in lichen cover. Strigulaceae showed an association with small leaves (Fig. 5B). Porinaceae, Roccellaceae, and Thelotremaaceae were associated with leaf position (from the base towards the top, respectively; Fig. 5B).

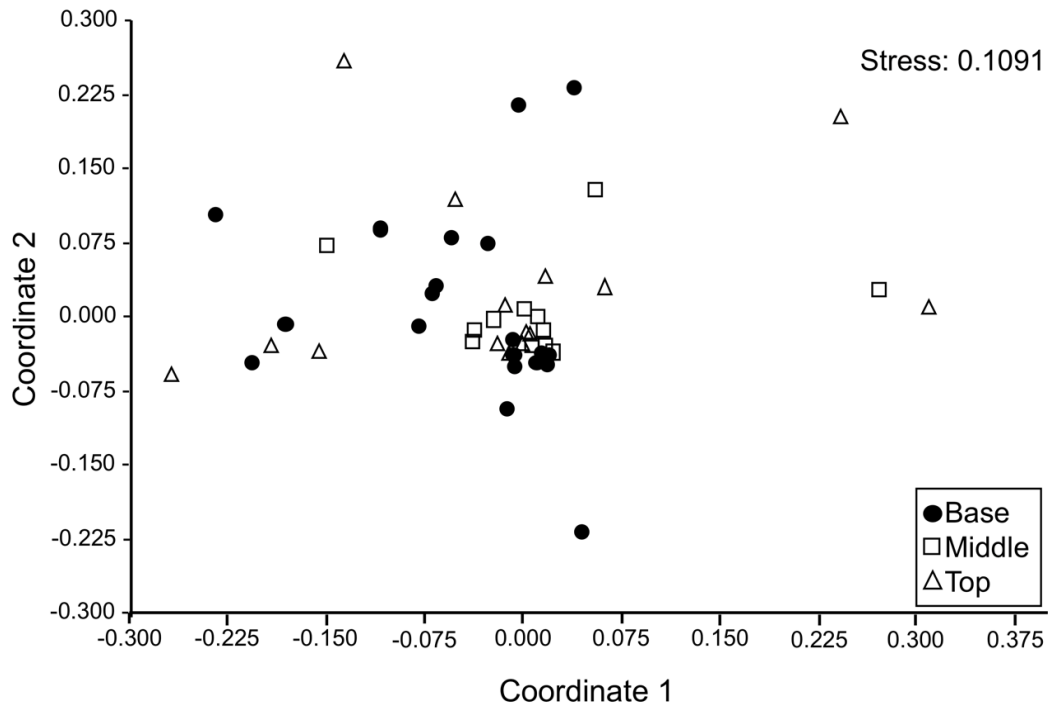


Figure 4. Non-metric multidimensional scaling (N-MDS) scatterplot of the communities of foliicolous lichens growing on leaves with different position within the phorophyte *Stenanona flagelliflora*

Discussion

Our results showed that *Stenanona flagelliflora* supports a community of foliicolous lichens characterized by its high species richness and high dominance. Previous studies at Los Tuxtlas have recorded between 157 and 191 species of foliicolous lichen species (Bárceñas-Peña, 2007; Martínez-Colín, 2016). Accordingly, *Stenanona flagelliflora* supports between 32.6% and 59.8% of the total richness of foliicolous lichens recorded at the locality.

In contrast, species richness on a single leaf of *S. flagelliflora* was rather poor (1-17 species). Other studies have recorded a species richness of between 30 and 81 species per leaf (Lücking, 1995, 2008b; Lücking and Bernecker-Lücking, 2002; Lücking and Matzer, 2001). Thus, although *S. flagelliflora* supports a relatively rich community of foliicolous lichens, only 1 to 18% of the complete community is represented on each leaf. This suggests that there is a high variation in the composition of foliicolous lichens within each leaf (Lücking, 1995).

Leaf position and leaf area did not affect species richness, abundance (estimated as relative lichen cover) and diversity of the communities of foliicolous lichens, but they did have important effects on species composition. Likewise, the effect of leaf position on species composition has been documented for communities of other microorganisms of the phylloplane (Harrison et al., 2016; Hermann et al., 2021; Izuno et al., 2016; Laforest-Lapointe et al., 2016; Leff et al., 2015; Nguyen, 2017; Stone and Jackson, 2019). Vertical variation in species composition within a single tree might be determined by microclimate factors that influence the colonization and establishment of each species (Leff et al., 2015). Particularly, the colonization and establishment of lichens are influenced by fluctuations in UV radiation, desiccation, rainfall, nutrient

limitation, temperature and relative humidity (Gomes et al., 2018; Hirano and Upper, 2000; Lindow and Brandl, 2003; Thapa and Prasanna, 2018) commonly experienced by leaves (and the phylloplane communities on them; Lücking, 1998, 1999). Moreover, colonization and establishment of lichens on leaves might be determined by the dispersion patterns of each species (Stone and Jackson, 2019), leaf structure (Lücking, 1998, 1999); leaf age (Carroll, 1979) and the successional processes associated with it; interactions with other microorganisms, leaf orientation (Andrews et al., 1980; Nguyen, 2017), and horizontal intra-phorophyte position (Andrews et al., 1980; Stone and Jackson, 2019). Although *S. flagelliflora* is a short tree, vertical microclimate differences seem to explain the differences in species composition of follicolous lichens among leaves. Undoubtedly, detailed studies at a small spatial scale are needed in order to determine the relative importance of each factor on the composition of the communities of follicolous lichens.

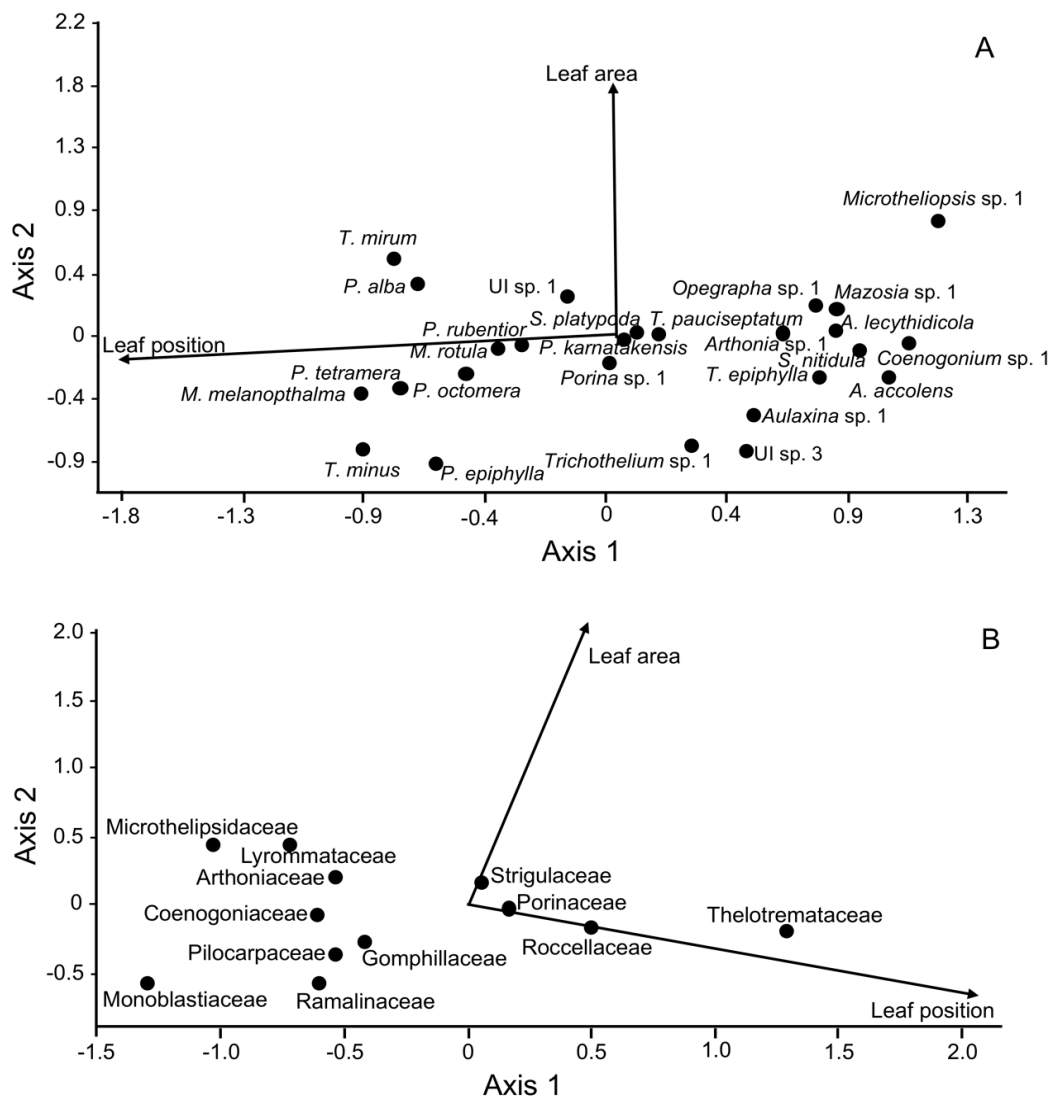


Figure 5. Canonical correspondence analyses on the relative cover of follicolous lichens in response to leaf area and leaf position (1 = base, 2 = middle, 3 = top) within individual plants of the phorophyte *Stenanona flagelliflora*. (A) Analysis at the species level, using the follicolous species recorded in at least five leaves; (B) analysis at the family level

Finally, three not mutually exclusive phenomena might explain the lack of significant effects of leaf position and leaf area on species richness, abundance, and diversity of foliicolous lichens. First, there might be a low microclimate variation across a short plant inhabiting the understory as *S. flagelliflora*, whose maximum height at the study site is 2.2 m. Significant vertical variation in communities of bacteria, fungi, microorganisms, and lichens of the phylloplane has been documented in phorophytes of between 4 - 108 m in height (Andrews et al., 1980; Carroll, 1979; Harrison et al., 2016; Hermann et al., 2021; Izuno et al., 2016; Leff et al., 2015; Nguyen, 2017; Sipman, 1997; Stone and Jackson, 2019). Second, *S. flagelliflora* leaf size (14.2 - 94.3 cm²) might be too small to provide sufficient habitat heterogeneity that favors the establishment of a high number of species (Connor and McCoy, 2001; Kohn and Walsh, 1994). Last, the community dynamics within a single leaf (colonization and extinction) might be regulated by competitive interactions (Lindow and Brandl, 2003). In the leaves of *S. flagelliflora*, the communities of foliicolous lichens are strongly dominated by a few species (i.e., strong competitors), which might prevent the establishment of others (i.e., weaker competitors). Particularly, small leaf size and the existence of competitive interactions might be important in determining a not significant species richness-leaf area relationship in small-sized organisms such as molds, yeasts (Andrews et al., 1987), liverworts (Aranda et al., 2014), bryophytes (Kimmerer and Driscoll, 2000; Aranda et al., 2014), fungi (Kinkel et al., 1987; Feinstein and Blackwood, 2012), bacterioplankton (Logue et al., 2012), and foliicolous lichens (this study).

Conclusion

The leaves of *Stenanona flagelliflora* host a highly diverse community of lichens, whose richness, abundance (estimated as relative lichen cover) and diversity are not determined by both leaf area and leaf position. Instead, community composition seems to be associated with both of those factors. These patterns seem to be explained by the existence of microclimate variation within the canopy of *S. flagelliflora*, strong competitive interactions regulated by the dominant species within the communities, and particular environmental requirements needed for the colonization and establishment of each lichen species. Undoubtedly, more studies on the importance of organisms within the phylloplane and the factors that determine their diversity are needed.

Acknowledgments. We thank to the community of Lic. Adolfo López Mateos for allowing us to conduct this study in their locality, especially Mr. Israel Medina Mena and Mr. Antonio Mena Velazco. L. Xicohténcatl-Lara helped during the collection of leaves. P. Martínez-Colín and A. Aptroot were very helpful identifying the foliicolous lichen species. Equipment for lichen photographs was provided by A. Burgos. U. Campos-Pineda and I. L. Castillo-Sánchez were very supportive scanning the leaves and estimating lichen cover.

REFERENCES

- [1] Al-Ashhab, A., Meshner, S., Alexander-Shani, R., Dimerets, H., Brandwein, M., Bar-Lavan, Y., Winters, G. (2021): Temporal and spatial changes in phyllosphere microbiome of acacia trees growing in super arid environments. – *Frontiers in Microbiology* 12: 656269.

- [2] Andrews, J. H., Kenerley, C. M., Nordheim, E. V. (1980): Positional variation in phylloplane microbial populations within an apple tree canopy. – *Microbial Ecology* 6: 71-84.
- [3] Andrews, J. H., Kinkel, L. L., Berbee, F. M., Nordheim, E. V. (1987): Fungi, leaves, and the theory of island biogeography. – *Microbial Ecology* 14: 277-290.
- [4] Aranda, S. C., Gabriel, R., Borges, P. A. V., Santos, A. M. C., Brito de Azevedo, E., Patiño, J., Hortal, J., Lobo, J. M. (2014): Geographical, temporal and environmental determinants of bryophyte species richness in the Macaronesian islands. – *PLoS One* 9: e101786.
- [5] Arcos-Pulido, M. P., Gómez-Prieto, A. C. (2006): Microalgas perifíticas como indicadoras del estado de las aguas de un humedal urbano: Jaboque, Bogotá D. C., Colombia. – *Nova* 4: 60-79.
- [6] Bárcenas-Peña, A. (2007): Comparación de la zonación altitudinal de los líquenes folícolos de los volcanes San Martín Tuxtla y Santa Marta, Veracruz, México. – M.Sc. Thesis, Universidad Nacional Autónoma de México, Mexico.
- [7] Brunet, A. K., Medellín, R. A. (2001): The species-area relationship in bat assemblage of tropical caves. – *Journal of Mammalogy* 82: 114-1122.
- [8] Carroll, G. C. (1979): Needle microepiphytes in a Douglas fir canopy: biomass and distribution patterns. – *Canadian Journal of Botany* 57: 1000-1007.
- [9] Clarke, K. R., Gorley, R. N., Somerfield, P. J., Warwick, R. M. (2014): *Change in Marine Communities: An Approach to Statistical Analysis and Interpretation*. – Primer-e, Plymouth.
- [10] Connor, E. F., McCoy, E. D. (2001): Species - Area Relationships. – In: Levin, S. A. (ed.) *Encyclopedia of Biodiversity*. Academic Press, Cambridge.
- [11] Cruz, L. A. M. (2009): Diversidad alfa, beta, y abundancia relativa de vertebrados voladores del ejido Lic. Adolfo López Mateos, Catemaco, Veracruz. – BSc. Thesis, Universidad Veracruzana, Veracruz, Mexico.
- [12] Feinstein, L., Blackwood, C. B. (2012): Taxa-area relationship and neutral dynamics influence the diversity of fungal communities on senesced tree leaves. – *Environmental Microbiology* 14: 1488-1499.
- [13] Flores-Palacios, A., García-Franco, J. G. (2006): The relationship between tree size and epiphyte species richness: testing four different hypotheses. – *Journal of Biogeography* 33: 323-330.
- [14] Gomes, T., Pereira, J. A., Benhadi, J., Lino-Nieto, T., Baptista, P. (2018): Endophytic and epiphytic phyllosphere fungal communities are shaped by different environmental factors in a Mediterranean ecosystem. – *Microbial Ecology* 76: 668-679.
- [15] Guevara, S. D., Larborde, D. J., Sánchez, R. G. (1999): La Reserva de la Biosfera Los Tuxtlas, México. – Documento de trabajo No. 29. ONU and MAB-UNESCO, Paris.
- [16] Hammer, Ø., Harper, D. A. T., Ryan, P. D. (2001): PAST: Paleontological statistics software packaged for education and data analysis. – *Palaeontologia Electronica* 4: 1-9.
- [17] Harrison, J. G., Forister, M. L., Parchman, T. L., Koch, G. W. (2016): Vertical stratification of the foliar fungal community in the world's tallest trees. – *American Journal of Botany* 103: 2087-2095.
- [18] Hermann, M., Geesink, P., Richter, R., Küsel, K. (2021): Canopy position has a stronger effect than tree species identity on phyllosphere bacterial diversity in a floodplain hardwood forest. – *Microbial Ecology* 81: 157-168.
- [19] Hirano, S. S., Upper, C. D. (2000): Bacteria in the leaf ecosystem with emphasis on *Pseudomonas syringae* - a pathogen, ice nucleus, and epiphyte. – *Microbiology and Molecular Biology Reviews* 64: 624-653.
- [20] Izuno, A., Kanzaki, M., Artchawakom, T., Wachrinrat, C., Isagi, Y. (2016): Vertical structure of phyllosphere fungal communities in a tropical forest in Thailand uncovered by high-throughput sequencing. – *PLoS ONE* 11: e0166669.

- [21] James, F. C., Rathbun, S. (1981): Rarefaction, relative abundance, and diversity of avian communities. – *Auk* 98: 785-800.
- [22] Kimmerer, R. W., Driscoll, M. J. L. (2000): Bryophyte species richness on insular boulder habitats: the effect of area, isolation, and microsite diversity. – *Bryologist* 103: 748-756.
- [23] Kinkel, L. L., Andrews, J. H., Berbee, F. M., Nordheim, E. V. (1987): Leaves as islands for microbes. – *Oecologia* 71: 405-408.
- [24] Kohn, D. D., Walsh, D. M. (1994): Plant species richness - the effect of island size and habitat diversity. – *Journal of Ecology* 82: 367-377.
- [25] Kovach, W. L. (2004): MVSP. A MultiVariate Statistical Package for Windows. Ver. 3.21. – Kovach Computing Services, Pentraeth, Wales, UK.
- [26] Laforest-Lapointe, I., Messier, C., Kembel, S. W. (2016): Tree phyllosphere bacterial communities: exploring the magnitude of intra- and inter-individual variation among host species. – *PeerJ* 4: e2367.
- [27] Leff, J. W., Del Tredici, P., Friedman, W. E., Fierer, N. (2015): Spatial structuring of bacterial communities within individual *Ginkgo biloba* trees. – *Environmental Microbiology* 17: 2352-2361.
- [28] Lindow, S. E., Brandl, M. T. (2003): Microbiology of the phyllosphere. – *Applied and Environmental Microbiology* 69: 1875-1883.
- [29] Löfgren, A., Jerling, L. (2002): Species richness, extinction and immigration rates of vascular plants on islands in the Stockholm archipelago, Sweden, during a century of ceasing management. – *Folia Geobotanica* 37: 297-308.
- [30] Logue, J. B., Langenheder, S., Andersson, A. F., Bertilsson, S., Drakare, S., Lanzén, A., Lindström, E. S. (2012): Freshwater bacterioplankton richness in oligotrophic lakes depends on nutrient availability rather than on species-area relationships. – *The ISME Journal* 6: 1127-1136.
- [31] Lõhmus, P., Lõhmus, A. (2001): Snags, and their lichen flora in old Estonian peatland forests. – *Annales Botanici Fennici* 38: 265-280.
- [32] Lücking, R. (1995): Biodiversity and Conservation of Follicolous Lichens in Costa Rica. – In: Scheidegger, C., Wolseley, P. A., Thor, G. (eds.) *Conservation Biology of Lichenized Fungi*. Herausgeber Eidgenössische Forschungsanstalt für Wald, Schnee und Landschaft, Birmensdorf.
- [33] Lücking, R. (1998): Ecology of follicolous lichens at the “Botarrama” trail (Costa Rica), a neotropical rain forest site. Part II. Patterns of diversity and area cover, and their dependence on microclimate and phorophyte species. – *Ecotropica* 4: 1-24.
- [34] Lücking, R. (1999): Ecology of follicolous lichens at the ‘Botarrama’ trail (Costa Rica), a neotropical rainforest. IV. Species associations, their salient features and their dependence on environmental variables. – *Lichenologist* 31: 269-289.
- [35] Lücking, R. (2001): Lichens on Leaves in Tropical Rainforests: Life in a Permanently Ephemeral Environment. – In: Gottsberger, G., Liede, S. (eds.) *Life Forms and Dynamics in Tropical Forests*. *Dissertationes Botanicae*, Berlin.
- [36] Lücking, R. (2008a): Follicolous Lichenized Fungi. *Flora Neotropica Monograph* 103. – New York Botanical Garden Press, New York.
- [37] Lücking, R. (2008b): Follicolous lichens as model organisms to study tropical rainforest ecology: background, data, and protocols. – *Sauteria* 15: 335-362.
- [38] Lücking, R., Bernecker-Lücking, A. (2002): Distance, dynamics, and diversity in tropical rainforests: an experimental approach using follicolous lichens on artificial leaves. I. Growth performance and succession. – *Ecotropica* 8: 1-13.
- [39] Lücking, R., Cáceres, M. (2002): Follicolous Lichens of the World. Part 1. Genera and Selected Species I (Introduction). – The Field Museum, Chicago.
- [40] Lücking, R., Matzer, M. (2001): High follicolous lichen alpha-diversity on individual leaves in Costa Rica and Amazonian Ecuador. – *Biodiversity and Conservation* 10: 2139-2152.

- [41] Lyons, M. M., Ward, J. E., Gaí, H., Hicks, R. E., Drake, J. M., Dobbs, F. C. (2010): Theory of island biogeography on a microscopic scale: organic aggregates as islands for aquatic pathogens. – *Aquatic Microbial Ecology* 60: 1-13.
- [42] Martínez-Colín, P. (2016): Análisis de la estructura de la comunidad de los líquenes folícolas en la Estación de Biología Tropical Los Tuxtlas, Veracruz, México. – BSc. Thesis, Universidad Nacional Autónoma de México, Mexico.
- [43] Miranda, F., Hernández, X. E. (1963): Los tipos de vegetación de México y su clasificación. – *Boletín de la Sociedad Botánica de México* 28: 29-179.
- [44] Morteo, M. O. (2011): Abandono de tierras y el desarrollo de la vegetación secundaria en dos ejidos de la Sierra de Santa Marta. – BSc. Thesis, Universidad Veracruzana, Veracruz, Mexico.
- [45] Nguyen, E. Q. (2017): Spatial variation of bacterial communities on the leaves of a southern *Magnolia* tree. – Honors Theses, University of Mississippi.
- [46] Rasband, W. S. (1997-2018): ImageJ, U.S. National Institutes of Health, Bethesda, Maryland, USA. – <https://imagej.nih.gov/ij/>.
- [47] Ruíz-Pineda, C., Suárez-Morales, E., Gasca, R. (2016): Copépodos planctónicos de la Bahía de Chetumal, Caribe Mexicano: variaciones estacionales durante un ciclo anual. – *Revista de Biología Marina y Oceanografía* 51: 301-316.
- [48] Schatz, G. E., Wendt, T. (2004): A new flagelliflorous species of *Stenanona* (Annonaceae) from Mexico, with a review of the phenomenon of flagelliflory. – *Lundellia* 7: 28-38.
- [49] Sipman, H. J. M. (1997): Observations on the follicolous lichen and bryophyte flora in the canopy of a semi-deciduous tropical forest. – *Abstracta Botanica* 21: 153-161.
- [50] Stone, B. W. G., Jackson, C. R. (2019): Canopy position is a stronger determinant of bacterial community composition and diversity than environmental disturbance in the phyllosphere. – *FEMS Microbiology Ecology* 95: fiz032.
- [51] Thapa, S., Prasanna, R. (2018): Prospecting the characteristics and significance of the phyllosphere microbiome. – *Annals of Microbiology* 68: 229-245.
- [52] Xicohténcatl-Lara, L., Figuroa-Castro, D. M., Andrés-Hernández, A. R., Campos-Villanueva, A. (2016): Aspects of the reproductive biology of *Stenanona flagelliflora* (Annonaceae). – *Pakistan Journal of Botany* 48: 211-221.
- [53] Zar, J. H. (2010): *Biostatistical Analysis*. – Prentice Hall, Upper Saddle River.

ENDOPHYTIC BACTERIA OF COMMON TAMARISK (*TAMARIX GALLICA* L.) AND ALKALI SEEPWEED (*SUAEDA FRUTICOSA* (L.) FORSSK.) AS POTENTIAL BIOCONTROL AND PLANT GROWTH-PROMOTING AGENTS IN ARID ENVIRONMENTS

BAKELLI, A.^{1,2,3*} – AMRANI, S.¹ – BOURI, M.³ – KALAYCI, S.³ – SAHIN, F.³

¹Laboratoire de Biologie et de Physiologie des Organismes, Faculté des Sciences Biologiques, Université des Sciences et de la Technologie Houari Boumediene (USTHB), BP32 El-Alia, 16111 Bab Ezzouar, Algiers, Algeria

²Département de Biologie, Faculté des Sciences de la Nature et de la Vie et Sciences de la Terre, Université de Ghardaia, BP 455, Ghardaïa 47000, Algeria

³Yeditepe University, Faculty of Engineering, Department of Genetics and Bioengineering, Kayisdagi St., 34755 Istanbul, Turkey

*Corresponding author

e-mail: bakelliaissa@gmail.com; phone: +213-21-24-72-17; fax: +213-21-24-79-50

(Received 21st Jan 2022; accepted 2nd May 2022)

Abstract. In this study, fifty-two endophytic halotolerant bacteria from *Tamarix gallica* L. and *Suaeda fruticosa* (L.) Forssk. growing in the M'Zab valley (Southern Algeria) were isolated to test their ability to reduce salt stress in barley (*Hordeum vulgare* L.), and tomato (*Solanum lycopersicum* L.) seeds. Identification by Gas Chromatography (GC) and matrix-assisted laser desorption ionization-time of flight (MALDI-TOF) confirmed the presence of strains belonging mainly to the genera *Bacillus* followed by *Pseudomonas*, *Pantoea*, *Klebsiella* and *Providencia*. All isolates were characterized for their antagonistic activities against some plant pathogenic bacteria and fungi. In addition, isolates were screened for their *in vitro* plant growth promotion (PGP) abilities, including ACC-deaminase activity, inorganic phosphate solubilization and production of indole-3-acetic acid (IAA), siderophores and lytic enzyme activity. Four isolates that expressed interesting PGP capabilities were tested for their efficacy in modulating salt stress and promoting the growth of barley and tomato seedlings in Petri dish experiments. The strain TE7 showed interesting performances under salt stress for tomato seedlings while strains SE5 and SE19 produced positive results for barley seedlings under normal conditions. The results of this study suggest that endophytic bacteria from natural plants in saline habitats present an interesting source for the isolation of salt-tolerant PGP bacteria that can be used in plant cultivation under normal and saline conditions.

Keywords: endophytes, halophytes, PGPB, Algeria, crops, seed enhancement

Introduction

Soil salinity and drought are among the most prevalent abiotic stresses limiting production and yield, especially in arid and semi-arid regions, causing a decrease in cultivable areas and threatening food balance (Shrivastava and Kumar, 2015).

Plants that grow in regions facing prolonged exposure to different abiotic stresses may have been adapted and developed specific physiological and molecular stress responses that allow them to grow and thrive (Ma et al., 2020). Furthermore, these plants may also select particular root-associated bacteria capable of helping the plants to cope with unfavourable growth conditions (Oleńska et al., 2020). These adapted bacteria can possess potential Plant Growth-Promoting (PGP) abilities which make them very attractive for research purposes as they can support plant growth, health and resistance to

different abiotic stresses (salt, drought, etc.) (Souza et al., 2015; Compant et al., 2019; Leontidou et al., 2020). The PGP endophytic bacteria associated with different plant species have been largely documented in many areas of the world (Souza et al., 2015; ALKahtani et al., 2020). Many of them have been identified from various genera of which *Pseudomonas* and *Bacillus* are most extensively studied (Santoyo et al., 2016). The plant-associated bacteria can directly or indirectly influence the plant growth by fixing atmospheric nitrogen, solubilizing various minerals (P, K, etc.), producing siderophores, HCN, phytohormones as well as ACC deaminase activity which mitigate the effects of various stresses in plants (Souza et al., 2015; Leontidou et al., 2020).

Algeria's flora contains plenty of halophytic plant species of multiple interests. *Tamarix gallica* L. (*Tamaricaceae*) and *Suaeda fruticosa* (L.) Forssk. (*Amaranthaceae*) are among halophyte trees or shrubs that occur in arid and semi-arid regions (Chenchouni, 2012; Baameur et al., 2015). These plants can grow under various environmental conditions such as high temperatures, drought and especially salinity (Chekroun-Bechlaghem et al., 2019; Bencherif et al., 2019). In addition, *T. gallica* L. and *S. fruticosa* (L.) Forssk. are two salt-tolerant plants that are potentially useful in traditional medicine (Ksouri et al., 2009, 2012; Aslam and Ali, 2018; Fellah et al., 2018).

To our knowledge, there are no reports on endophytes from *T. gallica* L., and only one recent paper has been published on endophytes isolated from different species of *Suaeda* including, *S. fruticosa* (L.) Forssk. (Alishahi et al., 2020). However, most researchers have been focusing on the study of the rhizospheric bacteria associated with *S. fruticosa* (L.) Forssk. roots (Goswami et al., 2014a,b; Ullah and Bano, 2015; Aslam and Ali, 2018). Thus, these plants can be valuable for plant-associated bacteria research and the selection of potential PGP Bacteria (PGPB) for agricultural uses.

For the purpose of targeting bacterial endophytes from *T. gallica* L. and *S. fruticosa* (L.) Forssk. with a promising potential for biocontrol and plant growth enhancement, we explored the diversity of the associated bacteria isolated from an arid environment in Algeria (Ghardaïa Province). The obtained bacteria were identified by MALDI-TOF analysis, Gas Chromatographic analysis of Fatty Acid Methyl Esters (GC-FAME), evaluated for their antagonistic potential toward different plant pathogens and their PGP abilities.

Materials and Methods

Sample collection

Samples that were collected from the edges of the M'Zab valley (N 32°26'39" E 3°45'33") in Ghardaïa Province (Northern Algerian Sahara) consisted of three individual plants of *T. gallica* L. and *S. fruticosa* L. (Forssk.) each, collected aseptically in September 2018 and were put in an icebox and directly transferred to the laboratory for analysis.

Isolation, growth conditions and conservation of endophytic bacteria

Parts of the root systems from the three individuals of each plant were surface sterilized by dipping in a solution of 5.25% calcium hypochlorite (CaCl_2O_2) for 5 min, then 70% ethanol for 1 min followed by three times washing with sterilized distilled water (Coombes and Franco, 2003). The sterilization procedure was checked by spreading 100 μL of the

last washing water on Tryptic Soy Agar (TSA) medium (GranuCult™, Merck KGaA Germany).

One gram (1g) of the sterilized roots was then macerated with 9 ml of a 0.9% physiological saline solution and subjected to serial dilutions (up to 10^{-6}). The resulting dilutions were spread in triplicate plates on TSA medium amended with 0%, 3%, 6% and 10% of NaCl (w/v) and a 0.45 μ m sterilized solution of cycloheximide (50 mg/L) (AppliChem GmbH, Darmstadt, Germany). Plates were incubated at $30\pm 2^{\circ}\text{C}$ for one week and Colony-Forming Units (CFU) per gram of root weight were counted.

Based on colony morphology characteristics for example: form, elevation, margin, surface, opacity and pigmentation, only bacterial colonies were hand-picked and further purified by multiple streaking. Twenty-six endophytic bacterial colonies from plant roots were randomly selected, cultured on TSA medium and stored at -20°C in 2 mL cryotubes filled with Tryptic Soy broth (TSB) (GranuCult™, Merck KGaA Germany) and 30% glycerol.

Identification of endophytic bacteria

Identification by MALDI-TOF MS system

Endophytic bacteria were identified using a matrix-assisted laser desorption ionization-time of flight mass spectrometry systems: Microflex LT (Bruker Daltonics, Bremen, Germany) equipped with a 337 nm wavelength UV laser MBT Compass software (Sauget et al., 2017). According to the manufacturer's recommendations, sample preparation was carried out on fresh bacterial cultures. Briefly, bacterial colonies were streaked on the polished steel plate MSP 96 target (BC), covered with formic acid (1 μ L, 70%) and air-dried. The samples were sprayed with 1 μ L cyano-4-hydroxycinnamic acid in an organic solution (50% acetonitrile and 2.5% trifluoroacetic acid) (Bruker Daltonics, Bremen, Germany). The target plate was then submitted to the MALDI-TOF analyzer.

The spectra were recorded by Flex Control software in linear positive mode over a mass range between 2 and 20 kDa at an acceleration voltage of 20 kV. Spectra were analyzed using Bruker Biotyper automation control, the Biotyper software (MBT Compass and Explorer 4.1.80) with the Bruker database (7311 MSP available).

Identification of endophytic bacteria by Gas Chromatography (GC)

The identification of the endophytic bacteria from both plants by Gas Chromatography was based on the analysis of Fatty Acid Methyl Esters (FAME) (Oates et al., 2017; Miura et al., 2017). To proceed with the FAME analysis, samples were processed according to the recommendations as-signed by MIDI Corporation (Sasser, 2001). Fresh bacterial cultures (24-48 h) replicas were subjected to several saponification, methylation and extraction treatments. The prepared samples were stored at -20°C until they were analyzed. The FAMES were analyzed using a 6890 Plus Agilent gas chromatograph (Agilent Technologies, Palo Alto, CA, USA), including a 7683 auto-injector, a splitless inlet with Merlin Microseal septum (Merlin Instrument, Half Moon Bay, CA, USA). The system was controlled by Chemstation (Agilent) and Sherlock (MIDI) software. Fatty acid identities were determined by using the TSBA 40 method with a microbial identification system (MIDI) version Sherlock 6.1.

Tolerance of endophytic bacteria to salt stress

All isolated bacteria were tested for their ability to tolerate different salt concentrations. Bacterial isolates were inoculated on TSA plates containing 0%, 3%, 6%, 12%, 15%, 18% and 22% of NaCl, and their growth was monitored and scored as + for growth and – for no growth after ten days of culture (Ramadoss et al., 2013).

Antimicrobial activity

Bacterial strains were screened *in vitro* for their antimicrobial activity by the agar disc diffusion method (Bonev et al., 2008). The antimicrobial activity was conducted on several phytopathogenic microorganisms obtained from the collection of the Laboratory of Biology of Microbial Systems (LBSM, Ecole Normale Supérieure de Kouba, Algiers, Algeria) and the Laboratory of Microbiology (Department of Genetics and Bioengineering, Yeditepe University, Istanbul-Turkey). The phytopathogenic bacterial species used in this study were: *Agrobacterium tumefaciens*, *Pseudomonas syringae*, *Xanthomonas campestris* pv. *vesicatoria* and *Erwinia amylovora*, while the used phytopathogenic fungal strains were: *Clavibacter michiganensis* subsp. *insidiosus*, *Clavibacter flaccumfaciens*, *Aspergillus carbonarius*, *Aspergillus niger*, *Aspergillus ochraceus*, *Fusarium culmorum* and *Umbelopsis ramanniana*.

Briefly, Tryptic Soy Agar (TSA) disc (6 mm in diameter) from the fresh culture of each bacterial isolate was placed on semi-solid TSA and PDA plates streaked with the phytopathogenic bacteria and fungi, respectively. Sterile TSA agar discs were used as negative controls. The plates were incubated at 30±2°C and checked for inhibition zones after 24 h and 72 h against phytopathogenic bacteria and fungi, respectively.

In vitro characterization of PGP traits

Nitrogen fixation

The nitrogen (N) fixation activity was tested on NFb semi-solid medium containing malic acid (Döbereiner, 1980). The bacterial strains were tested in a solid medium containing 0.5% bromothymol blue as a pH indicator. Blue-colored colonies were considered positive for nitrogen fixation. Positives tests were confirmed after inoculation on tubes containing semi-solid NFb medium incubated at 30±2°C for seven days and strains that formed a pellicle were considered positive for nitrogen fixation.

Phosphate solubilization

For phosphate solubilization, all bacterial strains were inoculated onto plates of NBRIP (Nautiyal, 1999) and Pikovskaya (PKV) (Pikovskaya, 1948) agar medium containing 5 g.L⁻¹ tricalcium phosphate (Ca₃PO₄). After 72 h of incubation at 30±2°C, a clear zone around the colony indicated phosphate solubilization activity. For quantitative estimation of inorganic phosphate solubilization by the isolates, after ten days of incubation at 30±2°C in liquid Pikovskaya medium, the concentration of the soluble phosphate was estimated from the supernatant by stannous chloride method (King, 1932).

Potassium solubilization

To test potassium solubilization capacity, the isolates were transferred to the Aleksandrov agar medium (HiMedia Laboratories GmbH, Germany) and incubated at

30±2°C for 48 h (Aleksandrov et al., 1967). Inorganic potassium solubilization activity was checked by the appearance of clear zones around the bacterial colonies.

Calcium solubilization

Bacterial strains were separately grown on Henderson's culture medium (Henderson and Duff, 1963) at 30±2°C for seven days. Calcium solubilization activity was displayed by clear halos around the bacterial colonies (Saleh et al., 2019).

Siderophore production

Siderophore production by bacterial isolates was performed according to the method described by Schwyn and Neilands (1987) by using blue indicator dye and chrome azurol S (CAS) agar. After inoculation of 1 µl of bacterial suspensions in plates containing (CAS) and incubation at 30±2°C for five days, the production of siderophores by bacteria was visualized by a color change of the medium from blue to orange/yellow color.

Ammonia production

For the ammonia production test, all bacterial strains were grown in peptone water (10 g/L peptone and 5 g/L sodium chloride) for 48 h at 30±2°C. Nessler reagent (K₂HgI₄; 1.4%) was added to the tubes containing suspensions in a 2:1 ratio. The development of a brown to yellow color was recorded as a positive reaction for ammonia production. A faint yellow color indicates a small amount of ammonia and deep yellow to brownish color indicates maximum ammonia production. Optical density was measured at 450 nm using a spectrophotometer (JASCO V-530, USA). The concentration of ammonia was estimated using the standard curve of ammonium sulfate (Cappuccino and Sherman, 1992).

Indole-3-Acetic Acid (IAA) production

Production of IAA was carried out by the method of Patten and Glick (2002), with some modifications. The bacterial isolates were cultured in Luria Bertani (LB) medium (Sigma Aldrich, Germany) supplemented with L-tryptophan (500 µg.mL⁻¹). After four days of incubation at 30±2°C, bacterial suspensions were centrifuged (10000 g, 5 min at 4°C). A 2 mL of the cell-free supernatants were mixed with 4 mL of Salkowski's reagent in the ratio of 2:4 (containing 150 mL of pure H₂SO₄, 250 mL of H₂O and 75 mL of 0.5 M FeCl₃ × 6H₂O) and 150 µL of 10mM phosphoric acid (H₃PO₄) and incubated at room temperature in the dark for 25 min. The development of a pink color indicated the production of IAA, which was quantitatively estimated by the absorbance of supernatant mixtures at 530 nm compared to the standard curve of IAA (Gordon and Weber, 1951).

1-aminocyclopropane-1-carboxylate (ACC) deaminase activity

Based on the modified method of Glick et al. (1995), all bacterial strains were screened for 1-aminocyclopropane-1-carboxylate (ACC) deaminase activity on a DF (Dworkin and Foster) salts minimal medium containing 3 mM ACC as the only nitrogen source (Dworkin and Foster, 1958). ACC deaminase activity was considered positive if bacterial growth was recorded on the medium after 48 h of incubation at 30±2°C.

***In vitro* characterization of PGP traits**

Cellulase activity

To study the cellulase production, the bacterial strains were transferred in a basal solid medium supplemented with Carboxy Methyl Cellulose (CMC; 10 g/L) as the only carbon source and incubated for 72 h at $30\pm 2^{\circ}\text{C}$. The cellulolytic activity of bacteria was revealed by adding Congo red (0.1%) to the medium for 30 min and then discoloring with sodium chloride (1M) solution for 15 min. The formation of clear halos around colonies indicated positive degradation of CMC (Teather and Wood, 1982).

Amylolytic activity

One microliter (1 μL) of each bacterial suspension was transferred on plates containing nutrient agar medium enriched with 0.5% soluble starch and incubated at $30\pm 2^{\circ}\text{C}$ for 48 h (Akpan et al., 1999). The coloring reagent solution (0.254 g iodine and 4.0 g potassium iodide in 1 L) was poured on the surface of the medium, and the apparition of a clear halo around colonies denotes a positive amylolytic activity of the strains (Raj et al., 2009).

Protease activity

Protease activity was tested on Skim Milk Agar medium (Loper and Schroth, 1986). After incubation at $30\pm 2^{\circ}\text{C}$ for 24 h, plates were examined for the development of clear halos around the bacterial colonies.

***In vitro* characterization of PGP traits**

Barley (*Hordeum vulgare*; cultivar Yakamoz) and tomato (*Solanum lycopersicum* L.; cultivar Aicha) seeds were used in the experiments. Seeds were immersed in 70% ethanol for 1 min, then surface sterilized by 2% sodium hypochlorite (NaOCl) solution for 3 min, followed by rinsing and continuous agitation with sterile distilled water.

Active fresh suspensions of bacterial isolates cultured in TSB medium for 24 h at $30\pm 2^{\circ}\text{C}$ under shaking conditions (150 rpm) were prepared. After centrifugation at 15000 g for 10 min, approximately 10^8 CFU/mL in 3 mL of Phosphate Buffered Saline (PBS) solution were prepared, added to the seeds and gently agitated for 10 minutes. Twenty pre-germinated seeds were placed in Petri dishes (90 mm diameter) within sterile Whatman filter papers; the experiments were realized in three replicates and performed in controlled environmental conditions with three replicates without any bacterial isolates were used as a negative control group. The Petri dishes were maintained in growth room conditions with a temperature of $25\pm 2^{\circ}\text{C}$, 16 h light/8 h dark photoperiod and relative humidity of 70%.

The germination rate was determined after three days for barley seeds and five days for tomato seeds. The growth morpho-physiological parameters: stem and root lengths and fresh and dry weights were determined after ten days for both germinated seeds.

Statistical analysis

The bacterial diversity was performed in triplicates, the mean and Standard Deviation (SD) were calculated using Microsoft Excel 2016. All data of tomato and barley growth parameters (in triplicate) obtained from plant growth promotion assay were analyzed by one-way ANOVA at $P = 0.05$ followed by Tukey's test. In addition, a Principal Component Analysis (PCA) was performed with R v3.5.1 using the Rcmdr package and

FactoMine R function. This analysis was carried out with the objective of the selection of the best bacterial strain in terms of growth promotion for tomato and barley cultured in the presence and absence of salt stress.

Results

Density of endophytic bacteria

The diversity of cultivable endophytic bacteria associated with *S. fruticosa* (L.) Forssk. and *T. gallica* L. was assessed on TSA supplemented with different concentrations of NaCl (0, 3, 6 and 10%) (Fig. 1). Overall, with and without NaCl supplementation, bacterial growth was noticed in all the Petri-dishes. Several colonies were observed in all the salt levels for samples from *S. fruticosa* (L.) Forssk. compared to those from *T. gallica* L. We noticed important bacterial populations in the roots of both studied plants with a high abundance of the halotolerant population, whereas bacteria that can grow in high salinity concentrations, in our case 10% NaCl were detected.

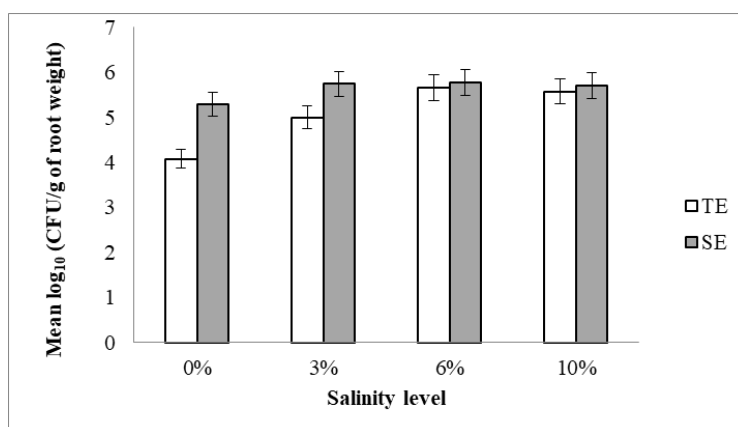


Figure 1. Cultivable bacterial endophytes abundance from the roots of *Tamarix gallica* L. and *Suaeda fruticosa* (L.) Forssk. on TSA medium without and with different NaCl concentrations. Error bars represent the standard deviation ($n = 3$). TE: *Tamarix* Endophytes, SE: *Suaeda* Endophytes

Identification of endophytic bacteria

In order to identify the fifty-two endophytic isolates from *T. gallica* L. (26 isolates) and *S. fruticosa* (L.) Forssk. (26 isolates), we used the MALDI-TOF as well as GC analyses. All the isolates showed characteristic MALDI-TOF MS spectra after comparison to the reference database however, several gave a No Reliable Identification (NRI) by GC analysis (Table 1).

In this study, the MALDI-TOF generated more secure results at genus and species levels with (5.8%) and (94.2%), respectively. Strains collected from *T. gallica* L. identified by MALDI-TOF were assigned to *Pseudomonas* sp. (1 strain), and the remaining twenty-five strains (25) were identified as *Bacillus* species (17 *B. cereus*, 6 *B. subtilis*, 1 *B. megaterium* and 1 *Bacillus* sp.). The twenty-six endophytes isolated from the roots of *S. fruticosa* (L.) Forssk. were affiliated to five genera with *Bacillus* as the predominant genus (20 strains), followed by *Providencia* and *Pantoea* with two strains each and only one strain of *Pseudomonas aeruginosa* and *Klebsiella aerogenes* each.

Table 1. MALDI-TOF, GC (FAME-MIDI) and salt tolerance of endophytic bacterial isolates from *Tamarix gallica* L. and *Suaeda fruticosa* (L.) Forssk

Plant	Strain code	MALDI-TOF species match	Score	GC (FAME-MIDI) species match	SI	Phylum	Salt tolerance (% NaCl)							
							0	3	6	9	12	15	18	22
<i>Tamarix gallica</i> L.	TE1	<i>Bacillus subtilis</i>	2.13	<i>Bacillus subtilis</i>	0.820	Firmicutes	+	+	+	+	+	+	+	+
	TE2	<i>Bacillus subtilis</i>	2.06	NRI	-	Firmicutes	+	+	+	+	+	+	+	+
	TE3	<i>Bacillus subtilis</i>	2.17	<i>Bacillus subtilis</i>	0.731	Firmicutes	+	+	+	+	+	+	+	+
	TE4	<i>Bacillus subtilis</i>	2.07	<i>Bacillus subtilis</i>	0.825	Firmicutes	+	+	+	+	+	+	+	+
	TE5	<i>Bacillus subtilis</i>	2.02	<i>Bacillus subtilis</i>	0.821	Firmicutes	+	+	+	+	+	+	+	+
	TE6	<i>Bacillus subtilis</i>	2.20	NRI	-	Firmicutes	+	+	+	+	+	+	+	+
	TE7	<i>Pseudomonas</i> sp.	1.98	NRI	-	Gammaproteobacteria	+	+	+	+	+	+	+	-
	TE8	<i>Bacillus cereus</i>	2.16	NRI	-	Firmicutes	+	+	+	+	+	+	-	-
	TE9	<i>Bacillus cereus</i>	2.05	NRI	-	Firmicutes	+	+	+	+	+	+	+	-
	TE10	<i>Bacillus cereus</i>	2.02	NRI	-	Firmicutes	+	+	+	+	+	+	+	+
	TE11	<i>Bacillus cereus</i>	2.17	NRI	-	Firmicutes	-	+	+	+	+	+	+	+
	TE12	<i>Bacillus cereus</i>	2.24	NRI	-	Firmicutes	-	+	+	+	+	+	+	+
	TE13	<i>Bacillus megaterium</i>	2.42	NRI	-	Firmicutes	-	+	+	+	+	+	+	+
	TE14	<i>Bacillus cereus</i>	2.10	NRI	-	Firmicutes	-	+	+	+	+	+	+	+
	TE15	<i>Bacillus cereus</i>	2.21	NRI	-	Firmicutes	-	+	+	+	+	+	+	+
	TE16	<i>Bacillus cereus</i>	2.18	NRI	-	Firmicutes	-	+	+	+	+	+	+	+
	TE17	<i>Bacillus cereus</i>	2.35	NRI	-	Firmicutes	-	+	+	+	+	+	+	+
	TE18	<i>Bacillus cereus</i>	2.05	NRI	-	Firmicutes	-	+	+	+	+	+	+	+
	TE19	<i>Bacillus cereus</i>	2.24	NRI	-	Firmicutes	-	+	+	+	+	+	+	+
	TE20	<i>Bacillus cereus</i>	2.12	NRI	-	Firmicutes	-	+	+	+	+	+	+	+
	TE21	<i>Bacillus cereus</i>	2.21	NRI	-	Firmicutes	-	+	+	+	+	+	+	+
	TE22	<i>Bacillus cereus</i>	2.21	NRI	-	Firmicutes	-	+	+	+	+	+	+	+
	TE23	<i>Bacillus cereus</i>	2.18	NRI	-	Firmicutes	-	+	+	+	+	+	+	+
	TE24	<i>Bacillus cereus</i>	2.01	NRI	-	Firmicutes	-	+	+	+	+	+	+	+
	TE25	<i>Bacillus</i> sp.	1.98	NRI	-	Firmicutes	-	+	+	+	+	+	+	+
	TE26	<i>Bacillus cereus</i>	2.14	NRI	-	Firmicutes	-	+	+	+	+	+	+	+

Plant	Strain code	MALDI-TOF species match	Score	GC (FAME-MIDI) species match	SI	Phylum	Salt tolerance (% NaCl)							
							0	3	6	9	12	15	18	22
<i>Suaeda fruticosa</i> (L.) Forssk.	SE1	<i>Bacillus cereus</i>	2.08	<i>Bacillus cereus</i>	0.655	Firmicutes	+	+	+	+	-	-	-	-
	SE2	<i>Bacillus cereus</i>	2.04	<i>Bacillus cereus</i>	0.656	Firmicutes	+	+	+	+	-	-	-	-
	SE3	<i>Bacillus cereus</i>	2.01	<i>Bacillus cereus</i>	0.657	Firmicutes	+	+	+	+	-	-	-	-
	SE4	<i>Bacillus cereus</i>	2.08	<i>Bacillus cereus</i>	0.658	Firmicutes	+	+	+	+	-	-	-	-
	SE5	<i>Providencia rettgeri</i>	2.47	NRI	-	Gammaproteobacteria	+	+	+	+	-	-	-	-
	SE6	<i>Klebsiella aerogenes</i>	2.34	NRI	-	Gammaproteobacteria	+	+	+	+	+	+	-	-
	SE7	<i>Bacillus subtilis</i>	2.26	<i>Bacillus subtilis</i>	0.872	Firmicutes	+	+	+	+	+	+	-	-
	SE8	<i>Bacillus subtilis</i>	2.09	<i>Bacillus subtilis</i>	0.745	Firmicutes	+	+	+	+	+	+	-	-
	SE9	<i>Bacillus subtilis</i>	2.17	<i>Bacillus pumilis</i>	0.659	Firmicutes	+	+	+	+	+	-	-	-
	SE10	<i>Bacillus subtilis</i>	2.09	NRI	-	Firmicutes	+	+	+	+	-	-	-	-
	SE11	<i>Bacillus subtilis</i>	2.23	<i>Bacillus subtilis</i>	0.765	Firmicutes	+	+	+	+	-	-	-	-
	SE12	<i>Providencia rettgeri</i>	2.47	NRI	-	Gammaproteobacteria	+	+	+	+	-	-	-	-
	SE13	<i>Bacillus subtilis</i>	2.17	<i>Bacillus subtilis</i>	0.789	Firmicutes	+	+	+	+	+	-	-	-
	SE14	<i>Bacillus subtilis</i>	2.08	NRI	-	Firmicutes	+	+	+	+	+	-	-	-
	SE15	<i>Bacillus subtilis</i>	2.18	<i>Bacillus subtilis</i>	0.890	Firmicutes	+	+	+	+	+	-	-	-
	SE16	<i>Bacillus subtilis</i>	2.20	<i>Bacillus subtilis</i>	0.856	Firmicutes	+	+	+	+	+	+	+	+
	SE17	<i>Bacillus subtilis</i>	2.05	<i>Bacillus subtilis</i>	0.842	Firmicutes	+	+	+	+	+	+	+	+
	SE18	<i>Bacillus</i> sp.	1.70	<i>Bacillus</i> sp.	0.481	Firmicutes	+	+	+	+	-	-	-	-
	SE19	<i>Pantoea agglomerans</i>	2.20	NRI	-	Gammaproteobacteria	+	+	+	+	-	-	-	-
	SE20	<i>Pantoea agglomerans</i>	2.34	NRI	-	Gammaproteobacteria	+	+	+	+	+	-	-	-
	SE21	<i>Bacillus licheniformis</i>	2.08	<i>Bacillus</i> sp.	0.459	Firmicutes	+	+	+	+	+	+	+	+
	SE22	<i>Bacillus subtilis</i>	2.34	<i>Bacillus subtilis</i>	0.931	Firmicutes	+	+	+	+	+	+	+	+
	SE23	<i>Bacillus subtilis</i>	2.19	<i>Bacillus subtilis</i>	0.889	Firmicutes	+	+	+	+	+	+	+	+
	SE24	<i>Bacillus subtilis</i>	2.06	<i>Bacillus subtilis</i>	0.890	Firmicutes	+	+	+	+	+	+	+	+
	SE25	<i>Pseudomonas aeruginosa</i>	2.39	<i>Pseudomonas aeruginosa</i>	0.721	Gammaproteobacteria	+	+	+	+	+	-	-	-
	SE26	<i>Bacillus subtilis</i>	2.20	<i>Bacillus subtilis</i>	0.892	Firmicutes	+	+	+	+	+	+	+	+

NRI: No Reliable Identification, -: No growth, +: Growth. SI: Similarity index. For MALDI-TOF: +++, score value 2.300–3.000, highly probable species identification; ++, score value 2.000–2.299, secure genus identification and probable species identification; +, score value 1.700–1.999, probable genus identification, - score value < 1.700 no reliable species identification. For GC- FAME: samples with an SI of 0.500 or higher and with a separation of 0.100 between the first and second choice are considered good library comparisons

Furthermore, isolates affiliated with the genera *Bacillus* were assigned to four species with *Bacillus subtilis* (14 strains) as the predominant, followed by four *B. cereus* strains (4) and one strain of *B. licheniformis* and *Bacillus* sp. each.

Salt tolerance profile of endophytic bacteria

All the endophytic bacterial isolates were tested for their growth at different salt concentrations (0, 3, 6, 9, 12, 15, 18% and 22% NaCl). The obtained results show that twenty-six strains from the roots of *S. fruticosa* (L.) Forssk. were found to be 100% halotolerant, whereas the strains associated with *T. gallica* L. were divided into 38.46% of halotolerant bacteria (10 strains) and 61.54% of halophiles (16 strains) which were able to grow only at NaCl concentrations $\geq 3\%$.

Antimicrobial properties of endophytic bacteria

The antagonistic activity of the fifty-two strains selected from the endophytic bacterial population associated with *T. gallica* L. and *S. fruticosa* (L.) Forssk. were tested against some phytopathogenic bacteria and fungi (Table 2).

Six strains associated with *T. gallica* L. showed moderate to high antibacterial activities against all the tested phytopathogenic bacteria, while no antagonistic activity was recorded within isolates from *S. fruticosa* (L.) Forssk except for SE23 and SE25. The anti-bacterial activity was limited to the *Bacillus* genus only, whereas the antifungal activity was also detected in other genera such as *Providencia*, *Klebsiella* and *Pseudomonas* associated with *S. fruticosa* (L.) Forssk. Further, no antifungal activities were observed within the strains isolated from *T. gallica* L.

Plant growth-promoting traits of endophytic bacteria

The PGP traits of the fifty-two endophytic bacteria were screened according to their nitrogen fixation ability, phosphate, potassium and calcium solubilization, siderophore, ammonia and IAA production, and ACC deaminase activity (Table 3).

The results showed that seven strains (7/52) were able to fix atmospheric nitrogen with one strain from *T. gallica* L. and six strains from *S. fruticosa* (L.) Forssk.

Phosphate solubilization ability was measured in solid and liquid media. Based on NBRIP and PKV solid media results, one strain for both media from *T. gallica* L. and 13 strains from *S. fruticosa* (L.) Forssk. were phosphate solubilizers. For the quantification results, the phosphate solubilization activity was limited within endophytic bacteria associated with *T. gallica* L. to only *Pseudomonas* sp. TE7 with $23 \mu\text{g.mL}^{-1}$ while 13 strains gave positive results with the maximum, was obtained by strain *Providencia rettgeri* SE12.

The potassium solubilization ability was detected for only one strain from *T. gallica* L. (TE7) and SE12, SE20 and SE21, three strains isolated from *S. fruticosa* (L.) Forssk. On the other hand, two strains (SE19 and SE20) that were isolated from the roots of *S. fruticosa* (L.) Forssk were able to solubilize calcium.

Furthermore, a total of ten isolates out of fifty-two were able to produce siderophores with the majority (9/10) isolated from *T. gallica* L. For ammonia production, all the bacterial strains showed positive ammonia production. Variable quantities that ranged from $6.56 \mu\text{g.mL}^{-1}$ to $122.01 \mu\text{g.mL}^{-1}$ and the maximum given by strain SE13 were obtained.

Table 2. Antimicrobial activity of endophytic bacterial isolates from *Tamarix gallica* L. and *Suaeda fruticosa* (L.) Forssk.

Plant	Strain code	Species	Bacteria						Fungi				
			GRAM-			GRAM+			Ac	An	Ao	Fc	Ur
			Ag	Ps	Xv	Ea	Cf	Cm					
<i>Tamarix gallica</i> L.	TE1	<i>Bacillus subtilis</i>	28	22	14	12	22	30	0	0	0	0	0
	TE2	<i>Bacillus subtilis</i>	28	22	15	12	22	30	0	0	0	0	0
	TE3	<i>Bacillus subtilis</i>	30	22	14	12	22	30	0	0	0	0	0
	TE4	<i>Bacillus subtilis</i>	26	22	14	12	22	30	0	0	0	0	0
	TE5	<i>Bacillus subtilis</i>	28	22	14	12	22	30	0	0	0	0	0
	TE6	<i>Bacillus subtilis</i>	24	22	14	12	22	30	0	0	0	0	0
	TE7	<i>Pseudomonas</i> sp.	0	0	0	0	0	0	0	0	0	0	0
	TE8	<i>Bacillus cereus</i>	0	0	0	0	0	0	0	0	0	0	0
	TE9	<i>Bacillus cereus</i>	0	0	0	0	0	0	0	0	0	0	0
	TE10	<i>Bacillus cereus</i>	0	0	0	0	0	0	0	0	0	0	0
	TE11	<i>Bacillus cereus</i>	12	0	0	0	0	0	0	0	0	0	0
	TE12	<i>Bacillus cereus</i>	13	0	0	0	0	0	0	0	0	0	0
	TE13	<i>Bacillus megaterium</i>	15	0	0	0	0	0	0	0	0	0	0
	TE14	<i>Bacillus cereus</i>	16	0	0	0	0	0	0	0	0	0	0
	TE15	<i>Bacillus cereus</i>	14	0	0	0	0	0	0	0	0	0	0
	TE16	<i>Bacillus cereus</i>	14	0	0	0	0	0	0	0	0	0	0
	TE17	<i>Bacillus cereus</i>	13	0	0	0	0	0	0	0	0	0	0
	TE18	<i>Bacillus cereus</i>	13	0	0	0	0	0	0	0	0	0	0
	TE19	<i>Bacillus cereus</i>	14	0	0	0	0	0	0	0	0	0	0
	TE20	<i>Bacillus cereus</i>	0	0	0	0	0	0	0	0	0	0	0
	TE21	<i>Bacillus cereus</i>	12	0	0	0	0	0	0	0	0	0	0
	TE22	<i>Bacillus cereus</i>	12	0	0	0	0	0	0	0	0	0	0
	TE23	<i>Bacillus cereus</i>	13	0	0	0	0	0	0	0	0	0	0
	TE24	<i>Bacillus cereus</i>	15	0	0	0	0	0	0	0	0	0	0
	TE25	<i>Bacillus</i> sp.	14	0	0	0	0	0	0	0	0	0	0
	TE26	<i>Bacillus cereus</i>	15	0	0	0	0	0	0	0	0	0	0

Plant	Strain code	Species	Bacteria						Fungi					
			GRAM-			GRAM+			Ac	An	Ao	Fc	Ur	
			Ag	Ps	Xv	Ea	Cf	Cm						
<i>Suaeda fruticosa</i> (L.) Forssk.	SE1	<i>Bacillus cereus</i>	0	0	0	0	0	0	0	0	0	0	0	12
	SE2	<i>Bacillus cereus</i>	0	0	0	0	0	0	0	0	0	0	0	12
	SE3	<i>Bacillus cereus</i>	0	0	0	0	0	0	0	0	0	0	0	12
	SE4	<i>Bacillus cereus</i>	0	0	0	0	0	0	0	0	0	0	0	12
	SE5	<i>Providencia rettgeri</i>	0	0	0	0	0	0	0	0	20	14	20	
	SE6	<i>Klebsiella aerogenes</i>	0	0	0	0	0	0	0	0	22	24	25	
	SE7	<i>Bacillus subtilis</i>	0	0	0	0	0	0	0	0	25	20	34	
	SE8	<i>Bacillus subtilis</i>	0	0	0	0	0	0	0	0	22	0	26	
	SE9	<i>Bacillus subtilis</i>	0	0	0	0	0	0	0	0	30	20	30	
	SE10	<i>Bacillus subtilis</i>	0	0	0	0	0	0	0	0	21	0	25	
	SE11	<i>Bacillus subtilis</i>	0	0	0	0	0	0	0	0	20	26	29	
	SE12	<i>Providencia rettgeri</i>	0	0	0	0	0	0	0	0	19	0	0	
	SE13	<i>Bacillus subtilis</i>	0	0	0	0	0	0	0	0	20	0	0	
	SE14	<i>Bacillus subtilis</i>	0	0	0	0	0	0	0	0	0	0	0	
	SE15	<i>Bacillus subtilis</i>	0	0	0	0	0	0	0	0	18	20	25	
	SE16	<i>Bacillus subtilis</i>	0	0	0	0	0	0	0	0	24	25	26	
	SE17	<i>Bacillus subtilis</i>	0	0	0	0	0	0	0	0	20	0	32	
	SE18	<i>Bacillus</i> sp.	0	0	0	0	0	0	0	0	0	0	0	
	SE19	<i>Pantoea agglomerans</i>	0	0	0	0	0	0	0	0	0	0	0	
	SE20	<i>Pantoea agglomerans</i>	0	0	0	0	0	0	0	0	0	0	0	
	SE21	<i>Bacillus licheniformis</i>	0	0	0	0	0	0	0	0	0	0	15	
	SE22	<i>Bacillus subtilis</i>	0	0	0	0	0	0	0	0	0	0	18	
	SE23	<i>Bacillus subtilis</i>	22	0	0	0	0	0	0	0	0	0	24	
	SE24	<i>Bacillus subtilis</i>	0	0	0	0	0	0	0	0	0	0	20	
	SE25	<i>Pseudomonas aeruginosa</i>	18	0	0	0	0	0	22	22	25	16	27	
	SE26	<i>Bacillus subtilis</i>	0	0	0	0	0	0	0	0	0	0	0	

Ag: *Agrobacterium tumefaciens*, Ps: *Pseudomonas syringae*, Xv: *Xanthomonas campestris* pv. *vesicatoria*, Ea: *Erwinia amylovora*, Cm: *Clavibacter michiganensis*, Cm: *Clavibacter michiganensis* subsp. *insidiosus*, Cf: *Clavibacter flaccumfaciens*, Ac: *Aspergillus carbonarius*, An: *Aspergillus niger*, Ao: *Aspergillus ochraceus*. Fc: *Fusarium culmorum*, Ur: *Umbelopsis ramanniana*. Inhibition zone values are given including the disc (10 mm). <10 mm: Low activity, 10-20 mm: Medium activity, 20-30: High activity, >30: very strong activity

Table 3. Plant growth promotion traits of endophytic bacterial isolates from *Tamarix gallica* L. and *Suaeda fruticosa* (L.) Forssk.

Plant	Strain code	Species	PGP traits										Enzymatic activity		
			N ₂ -fixation	Phosphate solubilization			Potassium solubilization	Calcium solubilization	Siderophore production	Amonia production (µg.ml ⁻¹)	IAA (µg.ml ⁻¹)	ACC deaminase	Cellulase	Amylase	Protease
			NRBIP	PKV	PKV (µg.ml ⁻¹)										
<i>Tamarix gallica</i> L.	TE1	<i>Bacillus subtilis</i>	-	-	-	0	-	-	-	84.87	0.0	-	-	+	+
	TE2	<i>Bacillus subtilis</i>	-	-	-	0	-	-	-	61.30	0.0	-	-	+	+
	TE3	<i>Bacillus subtilis</i>	-	-	-	0	-	-	-	54.87	0.0	-	-	+	+
	TE4	<i>Bacillus subtilis</i>	-	-	-	0	-	-	-	59.16	0.0	-	-	+	+
	TE5	<i>Bacillus subtilis</i>	-	-	-	0	-	-	-	20.84	0.0	-	-	+	+
	TE6	<i>Bacillus subtilis</i>	-	-	-	0	-	-	-	68.44	0.0	-	-	+	+
	TE7	<i>Pseudomonas</i> sp.	+	+	+	23	+	-	+	54.87	53.5	+	-	-	-
	TE8	<i>Bacillus cereus</i>	-	-	-	0	-	-	-	79.87	0.0	-	-	+	+
	TE9	<i>Bacillus cereus</i>	-	-	-	0	-	-	-	25.59	0.0	-	-	+	+
	TE10	<i>Bacillus cereus</i>	-	-	-	0	-	-	-	47.73	0.0	-	-	+	+
	TE11	<i>Bacillus cereus</i>	-	-	-	0	-	-	-	53.44	0.0	-	-	+	+
	TE12	<i>Bacillus cereus</i>	-	-	-	0	-	-	-	75.59	0.0	-	-	+	+
	TE13	<i>Bacillus megaterium</i>	-	-	-	0	-	-	-	19.87	0.8	-	-	+	+
	TE14	<i>Bacillus cereus</i>	-	-	-	0	-	-	-	27.73	7.2	-	-	+	+
	TE15	<i>Bacillus cereus</i>	-	-	-	0	-	-	-	44.16	3.1	-	-	+	+
	TE16	<i>Bacillus cereus</i>	-	-	-	0	-	-	-	45.59	0.0	-	-	+	+
	TE17	<i>Bacillus cereus</i>	-	-	-	0	-	-	-	18.44	0.0	-	-	+	+
	TE18	<i>Bacillus cereus</i>	-	-	-	0	-	-	-	47.73	0.0	-	-	+	+
	TE19	<i>Bacillus cereus</i>	-	-	-	0	-	-	+	64.16	1.9	-	-	+	+
	TE20	<i>Bacillus cereus</i>	-	-	-	0	-	-	+	75.59	3.2	-	-	+	+
	TE21	<i>Bacillus cereus</i>	-	-	-	0	-	-	+	36.30	2.8	-	-	+	+
	TE22	<i>Bacillus cereus</i>	-	-	-	0	-	-	+	42.01	6.8	-	-	+	+
	TE23	<i>Bacillus cereus</i>	-	-	-	0	-	-	+	59.16	4.5	-	-	+	+
	TE24	<i>Bacillus cereus</i>	-	-	-	0	-	-	+	51.30	74.5	-	-	+	+
	TE25	<i>Bacillus</i> sp.	-	-	-	0	-	-	+	44.87	0.8	-	-	+	+
	TE26	<i>Bacillus cereus</i>	-	-	-	0	-	-	+	47.73	0.2	-	-	+	+

Plant	Strain code	Species	PGP traits									Enzymatic activity				
			N ₂ -fixation	Phosphate solubilization		Potassium solubilization	Calcium solubilization	Siderophores	Amonia production (µg.ml ⁻¹)	IAA (µg.ml ⁻¹)	ACC deaminase	Cellulase	Amylase	Protease		
				NRBIP	PKV	(µg.ml ⁻¹)										
<i>Suaeda fruticosa</i> (L.) Forssk.	SE1	<i>Bacillus cereus</i>	-	-	-	0.0	-	-	-	64.09	0.0	-	-	+	+	
	SE2	<i>Bacillus cereus</i>	-	-	-	0.0	-	-	-	106.30	0.0	-	-	+	+	
	SE3	<i>Bacillus cereus</i>	-	-	-	0.0	-	-	-	100.59	0.0	-	-	+	+	
	SE4	<i>Bacillus cereus</i>	-	-	-	0.0	-	-	-	100.59	0.0	-	-	+	+	
	SE5	<i>Providencia rettgeri</i>	+	+	+	31	-	-	+	114.87	174.5	+	-	+	+	
	SE6	<i>Klebsiella aerogenes</i>	+	+	+	12	-	-	-	42.01	101.7	-	-	+	+	
	SE7	<i>Bacillus subtilis</i>	-	+	+	16	-	-	-	64.87	0.0	-	-	+	+	
	SE8	<i>Bacillus subtilis</i>	-	+	+	13	-	-	-	47.01	0.0	-	-	+	+	
	SE9	<i>Bacillus subtilis</i>	-	+	+	15	-	-	-	53.44	0.0	-	-	+	+	
	SE10	<i>Bacillus subtilis</i>	-	+	-	0.0	-	-	-	89.87	0.0	-	+	+	+	
	SE11	<i>Bacillus subtilis</i>	-	+	-	0.0	-	-	-	84.87	0.0	-	+	+	+	
	SE12	<i>Providencia rettgeri</i>	+	+	+	35	+	-	-	99.16	39.9	+	+	+	+	
	SE13	<i>Bacillus subtilis</i>	-	+	+	0.5	-	-	-	122.01	30.8	+	-	+	-	
	SE14	<i>Bacillus subtilis</i>	-	+	+	12	-	-	-	6.56	33.5	+	+	+	+	
	SE15	<i>Bacillus subtilis</i>	-	+	-	0.0	-	-	-	20.84	0.0	-	+	+	+	
	SE16	<i>Bacillus subtilis</i>	-	+	-	0.0	-	-	-	13.70	0.0	-	+	+	+	
	SE17	<i>Bacillus subtilis</i>	-	+	-	0.0	-	-	-	7.73	0.0	-	+	+	+	
	SE18	<i>Bacillus</i> sp.	-	+	-	0.0	-	-	-	108.44	0.0	-	+	+	+	
	SE19	<i>Pantoea agglomerans</i>	-	+	+	29	-	+	-	106.30	0.0	+	+	+	-	
	SE20	<i>Pantoea agglomerans</i>	+	+	+	14	+	+	-	55.59	0.0	+	+	+	-	
	SE21	<i>Bacillus licheniformis</i>	+	+	-	0.0	+	-	-	41.30	0.0	-	+	+	+	
	SE22	<i>Bacillus subtilis</i>	-	+	-	0.0	-	-	-	59.16	49.9	-	-	+	+	
	SE23	<i>Bacillus subtilis</i>	-	+	+	14	-	-	-	54.87	0.0	-	-	+	+	
	SE24	<i>Bacillus subtilis</i>	-	+	+	12	-	-	-	61.30	0.0	-	-	+	+	
	SE25	<i>Pseudomonas aeruginosa</i>	-	+	+	18	-	-	-	84.87	0.0	+	-	+	+	
	SE26	<i>Bacillus subtilis</i>	+	-	-	0.0	-	-	-	77.01	0.0	-	+	+	+	

PKV: Pikovskaya medium, NBRIP: National Botanical Research Institute's phosphate growth medium, +: Positive reaction, -: Negative reaction

The results presented in *Table 3* show that seventeen strains were IAA producers with 12 strains were isolated from *T. gallica* L. and six strains from *S. fruticosa* (L.) Forssk. The recorded range of concentrations of IAA were $0.2 \mu\text{g}\cdot\text{mL}^{-1}$ to $174.5 \mu\text{g}\cdot\text{mL}^{-1}$ with the strain SE5 as the biggest producer. Out of fifty-two (52) tested strains, only one strain *Pseudomonas* sp. TE7 obtained from the roots of *T. gallica* L. and seven strains (SE5, SE12, SE13, SE14, SE19, SE20, and SE25) isolated from *S. fruticosa* (L.) Forssk. roots had positive ACC deaminase activity.

Plant growth-promoting traits of endophytic bacteria

Each of the cellulase, amylase and protease production by the fifty-two strains was verified in specific media with the overview of the results is shown in *Table 3*. No cellulose degradation activity was noticed for the strains isolated from *T. gallica* L. while several strains (12) isolated from *S. fruticosa* (L.) Forssk. were positive for cellulase activity. The majority of the strains had positive amylase activity, with only the strain TE7 did not show any amylase production. For protease activity, most of the strains were positive with only the strain (TE7) that was isolated from *T. gallica* L. and the three strains SE13, SE19 and SE20 that were isolated from *S. fruticosa* (L.) Forssk. were negative producers of proteases (*Table 3*).

Petri-dishes experiment

From the endophytes collection of our study, we selected four strains, namely: TE7, SE5, SE12 and SE19 that showed salt tolerance and ACC-deaminase activity and many of the PGP traits for a Petri dish experiments for both tomato and barley plants under salt stress control (*Figs. 2 and 3*).

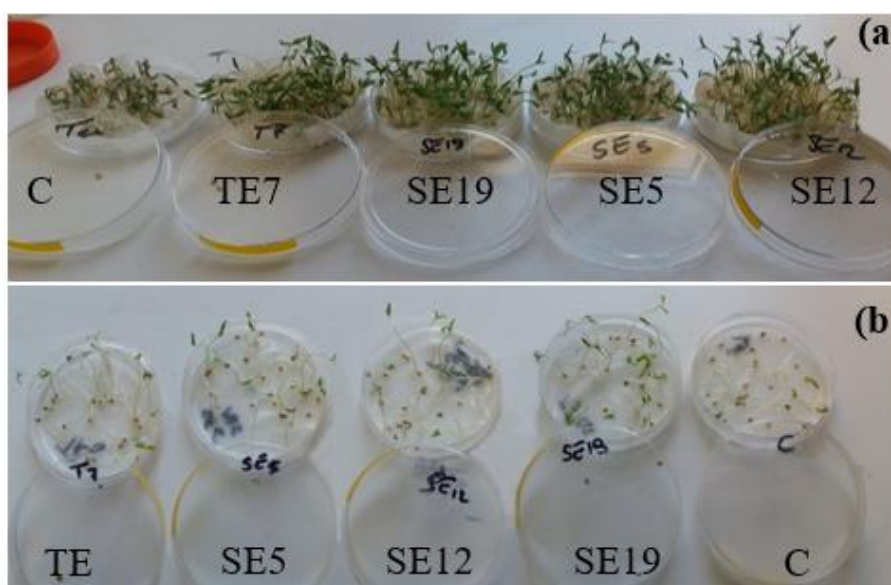


Figure 2. Morphological appearance of tomato seedlings ten days after sowing. (a) Uninoculated seeds without salt stress (C), Inoculated seeds with TE7, SE19, SE5 and SE12. (b) Tomato seeds subjected to salt stress (150 Mm NaCl), (C) Uninoculated seeds, seeds inoculated with strains TE7, SE5, SE12 and SE19

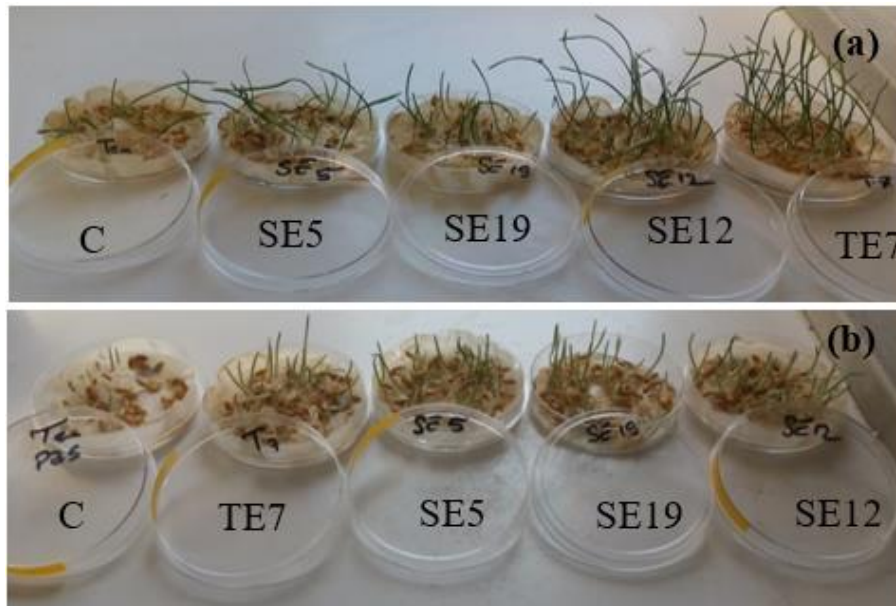


Figure 3. Morphological appearance of barley seedlings ten days after sowing. (a) Uninoculated seeds without stress (C), Inoculated seeds with SE5, SE19, SE12 and TE7. (b) Barley seeds subjected to salt stress (150 Mm NaCl), (C) Uninoculated seeds, seeds inoculated with strains TE7, SE5, SE19 and SE12

A reduction in the germination percentage, fresh and dry weights and seedling lengths of tomato and barley plants were observed at 150 mM of salt concentration compared to the control groups (Figs. 4 and 5). It seems that tomato and barley plants were affected by salt. The tomato and barley seeds that were inoculated by the four selected bacterial endophytes showed growth promotion for both plants by increasing germination percentage, dry weight and seedling lengths at 0 and 150 mM NaCl compared to the uninoculated seeds.

The germination percentage of the inoculated tomato seeds by the strains TE7, SE5 and SE12 were significantly higher than the control and the other tested strain SE19 in 0 Mm NaCl concentration. There was no significant difference in the fresh weight of the inoculated and uninoculated tomato seeds compared to the dry weight. The seedling lengths of the inoculated tomato seeds by all four strains were significantly higher than the control group.

On the other hand, the inoculation with TE7, SE5 and SE12 significantly ameliorated the germination percentage, fresh and dry weights as well as seedling lengths for barley seeds under normal conditions (0 mM NaCl) whereas, all the strains used as bioinoculants showed a positive impact on all the recorded parameters under 150 mM of NaCl.

In order to determine the best bacterial strains that promoted tomato and barley growth under normal and saline conditions, we conducted a PC analysis. As shown in Fig. 6a, the first axis (Dim 1) and a second axis (Dim 2) accounted for 96.83% of the total variability exhibited by the analyzed parameters taken into consideration (germination percentage, fresh and dry weight and seedling length). Four clusters were obtained with the two clusters of SE5 and TE7 (cluster 1) and SE12 and SE19 (cluster 2) showed notable plant growth-promoting ability in the absence of salt stress (0 mM NaCl). In the presence of 150 mM of NaCl, the strain TE7 clustered in a group with the control group of non-saline condition (negative control, cluster 3). Thus, the strain SE7 seemed to efficiently

mitigate salt stress permitting plant performance to be equivalent to those obtained in non-saline control conditions. The remaining fourth cluster was composed of the four strains that were used as bioinoculants under the tested salt stress condition (150 mM of NaCl). The inoculation with the four strains TE7, SE5, SE12 and SE19 exhibited performances closer to those expected by the positive control group (cluster 4) making the results less interesting.

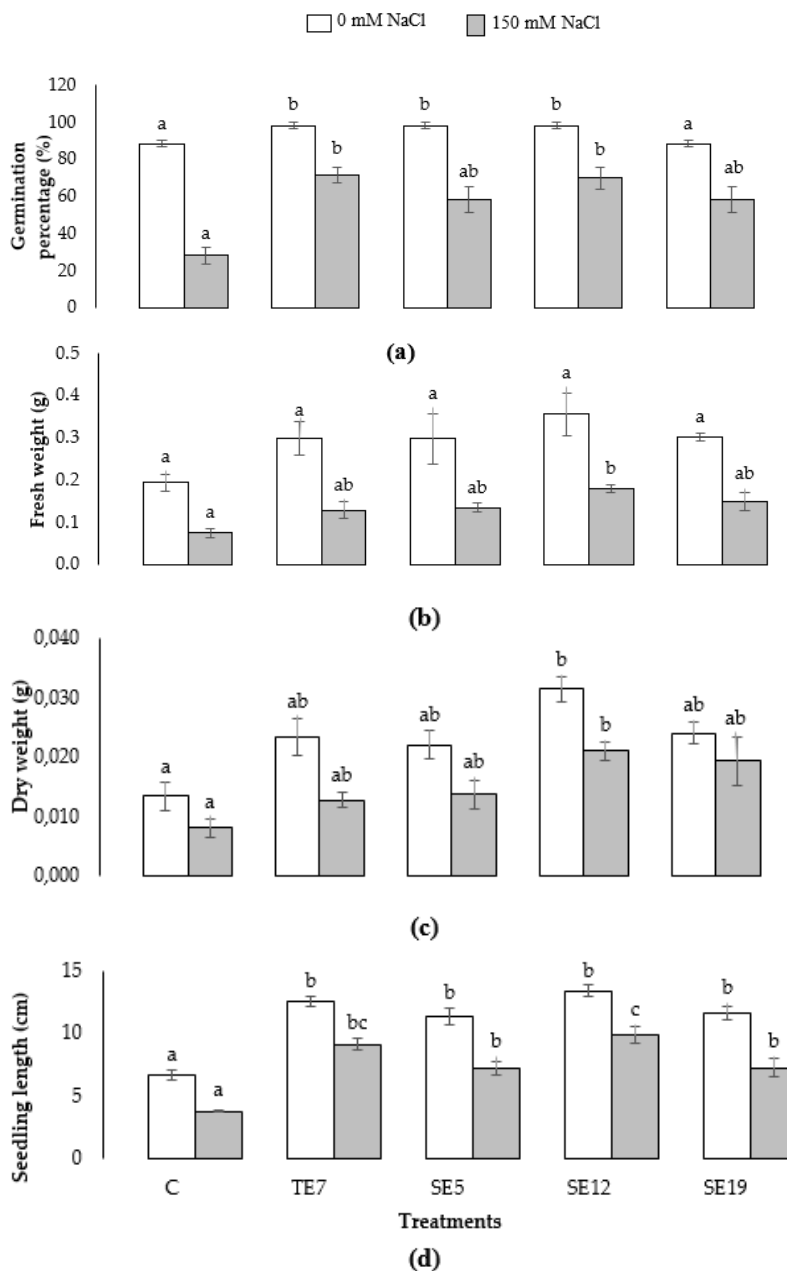


Figure 4. Effect of seed bacterization with endophytic bacteria on plant growth promotion of tomato. (a) Germination percentage, (b) Fresh weight, (c) Dry weight, (d) Seedling length. Evaluation was made 10 days after sowing. Bars represent mean \pm SD of three replicates. Different letters on bars indicate significant differences between white columns treatments (0mM NaCl) or grey columns treatments (150 mM NaCl), Tukey test at P= 0.05

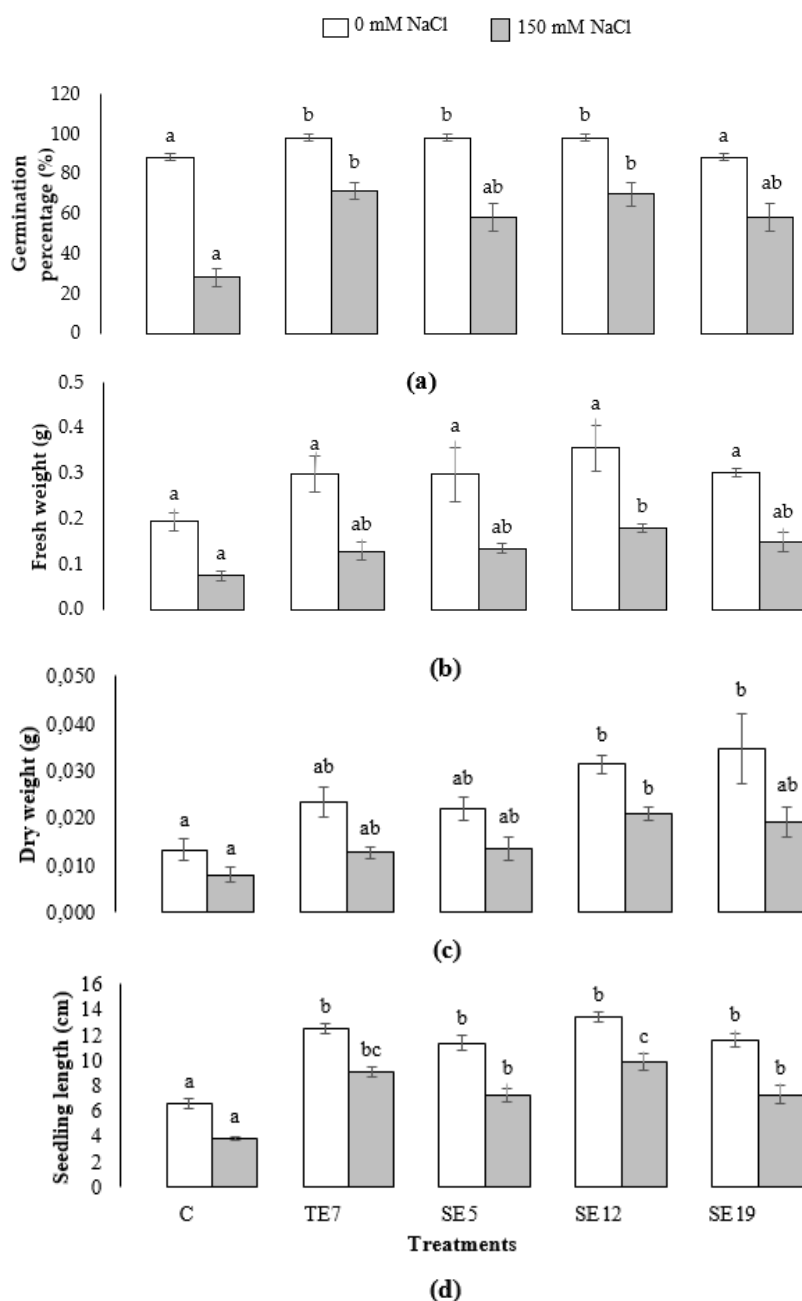


Figure 5. Effect of seed bacterization with endophytic bacteria on plant growth promotion of barley. (a) Germination percentage, (b) Fresh weight, (c) Dry weight, (d) Seedling length. Evaluation was made 10 days after sowing. Bars represent mean ± SD of three replicates. Different letters on bars indicate significant differences between white columns treatments (0mM NaCl) or grey columns treatments (150 mM NaCl), Tukey test at P= 0.05

For the barley Petri-dish experiment and the results obtained in Fig. 6b, the two axes (Dim 1 and Dim 2) accounted for 90.00% of the total variability exhibited by the analyzed parameters taken into consideration (germination percentage, fresh and dry weight and seedling growth).

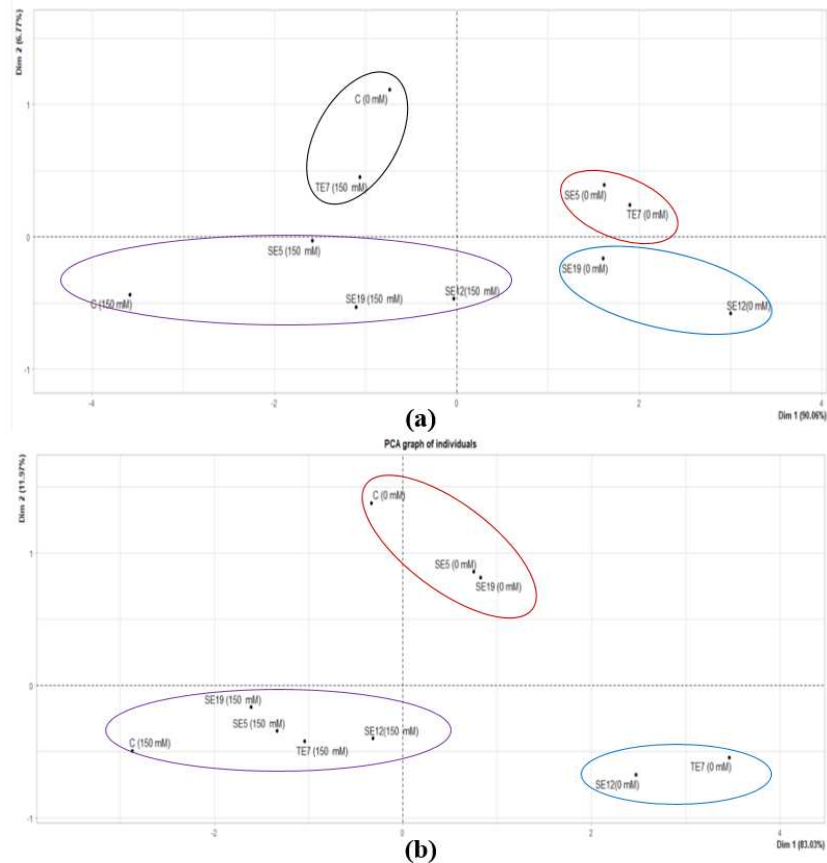


Figure 6. Principal Component Analysis (PCA) plots (PC1 and PC2) to show the efficacy of endophytic bacterial strains (TE7, SE5, SE12 and SE19) for their growth-promoting effect on tomato (a) and barley (b) seedlings in the absence (0 Mm NaCl) and presence of salt stress (150 Mm NaCl)

This time, we distinguished only three clusters. The first cluster was formed by the strains SE5 and SE19 and the negative control while the second cluster was formed only by strains TE7 and SE12 in which both of them were grown in the absence of salt stress (0 mM NaCl). These two strains performed close to that of negative control which make them the most interesting ones. The last cluster was formed by all the tested strains under 150 mM of NaCl that exhibited growth performances closer to the positive control group.

Discussion

Many researchers have been studying the bacterial communities from the endosphere of naturally occurring plants which can potentially have PGP traits that can be useful to plants that are grown under plant-limiting environments like saline soils or even when facing biological attackers (Etesami and Beattie, 2018; Fadiji and Babalola, 2020).

Two halophytes that thrive in arid rangelands of Algeria and are known for their medicinal properties are *T. gallica* L. (*Tamaricaceae*) and *S. fruticosa* (L.) Forssk. (*Amaranthaceae*). From literature in Algeria, these two plants have never been the subject of research on their associate endophytes which make them good candidates for searching

for bacteria that can promote plant growth under plant-limiting environments as the case for saline conditions.

Many researchers are seeking to develop fast and efficient methods with moderate cost that can be applied to identify and classify microorganisms, including bacteria. One of the methods of choice is the matrix-assisted laser desorption/ionization time-of-flight mass spectrometry (MALDI-TOF MS) that is based on analyzing proteins for the identification and is used in clinical studies (Croxatto et al., 2012; Sauget et al., 2017). Further, The MIDI MIS technique is based on fatty acid methyl ester analysis by gas chromatography (GC-FAME) and has been used to identify microorganisms isolated from clinical and environmental samples (Slabbinck et al., 2009). When comparing the two different methods for taxonomic identification, it seems that MALDI-TOF gave a better identification percentage when compared to GC FAME MIDI identification. This latter gave only four reliable identifications similar to those obtained by MALDI-TOF of the twenty-six isolates of *T. gallica* L. In addition, more than 70% of the isolates were identified by GC FAME MIDI with only two differences from the MALDI-TOF results. The MIDI MIS system and MALDI-TOF analysis are two methods used for the identification of bacterial species by many authors (Adams et al., 2005; Fykse et al., 2015). In our case, the difference between the MIDI MIS and MALDI-TOF results can be explained by the difference in the databases as suggested by Fykse et al. (2015). We did not perform the 16S rDNA sequencing method, which is time-consuming and more laborious compared to the other two methods. Still, we stipulate that MALDI -TOF results can be accurate, as suggested by Fykse et al. (2015) and Dybwad et al. (2012). From the roots of the studied plants in our study, endophytes were isolated with a total of twenty-six per plant. The obtained identification-based results showed the dominance of *Bacillus* genera in both studied plants. Many researchers reported the dominance of *Bacillus* as endophytes in many plant species (maize, cacao, vanilla orchids and rice (White et al., 2014; Bodhankar et al., 2017; Lu et al., 2021). *Bacillus* species have been reported to have PGP traits that help the plants, especially under limiting environments and bio-control of plant diseases (Yu et al., 2011; Lim et al., 2013; Chowdhury et al., 2015).

In addition to *Bacillus*, other minor species were isolated and belonged to *Pseudomonas*, *Pantoea*, *Klebsiella* and *Providencia* that have also been implicated in the positive effects on many host plants (Naz et al., 2016; Pavlova et al., 2017; Lu et al., 2021). The use of halotolerant bacteria and halophiles is one of the strategies used by the scientific community for crops grown in stress conditions (Dodd and Perez-Alfocea, 2012; Etesami and Beattie, 2018).

Antagonistic activity of the isolated endophytes tested was tested toward different phytopathogenic bacteria and fungi. All the endophytes isolated from *T. gallica* L. showed no antifungal activity against all the tested fungi, while the majority (23/26 strains) of endophytes isolated from *S. fruticosa* (L.) Forssk. showed antifungal activity against at least one tested-fungi. Six *Bacillus subtilis* strains (TE1, TE2, TE3, TE4, TE5 and TE6) out of the twenty-six isolated from the roots of *T. gallica* L. have shown antibacterial activity towards all the tested bacterial phytopathogens whereas, only *Bacillus subtilis* SE23 and *Pseudomonas aeruginosa* SE25 presented antibacterial activity for *Agrobacterium tumefaciens* only for isolated from *S. fruticosa* (L.) Forssk. Many *Bacillus* strains are known for their antimicrobial activities as reported by many authors (Chowdhury et al., 2015; Foldes et al., 2000; Lu et al., 2021). Foldes et al. (2000) showed that from the results of 25 *Bacillus* tested isolates; only one (4%) has shown activity towards phytopathogens.

In general, PGPB's help the plants to have the efficient acquisition of nutrients through nitrogen fixation activity increased availability of minerals such as phosphate and potassium, or production of siderophores (iron acquisition). *Pseudomonas* sp. TE7, *Providencia rettgeri* SE5 and SE12, *Klebsiella aerogenes* SE6, *Pantoea agglomerans* SE20 and *Bacillus licheniformis* SE21 are the only isolates to fix nitrogen. Members of the genera *Klebsiella*, *Bacillus* and *Pseudomonas* are capable of fixing atmospheric nitrogen as reported in James (2000).

As *Pseudomonas* sp. TE7, *Providencia rettgeri* SE5 and SE12 as well as *Pantoea agglomerans* SE19 were found to possess many PGPB activities we chose them for *in vitro* pot experiments. Our results were in accordance with those reported by Li et al. (2020) from which *Providencia rettgeri* P2 had IAA, nitrogen fixation, P-solubilization and biocontrol activity.

Many bacteria producing ACC-deaminase are able to facilitate plant growth under salt stress. They are able to promote root elongation and plant growth by lowering ethylene levels in the roots, as stated by Suárez et al. (2008). Our results revealed that a number of the tested strains were ACC deaminase positive, from which TE7, SE5 and SE12 had an interesting ACC deaminase activity. The plants inoculated with these bacteria ameliorated their germination rate in the presence and absence of NaCl for both tomato and barley. These results are in accordance with the work of Damodaran et al. (2013) who reported that endophytes improved germination of plants when facing salt stress. One of the mechanisms that can explain this effect is the production of auxins such as IAA by our strains. This could have triggered the activity of specific enzymes that promoted early germination (Chiwocha et al., 2005). The present study that compared inoculated and uninoculated seeds with PGP endophytes under normal (0 mM NaCl) and salt stress conditions (150 mM NaCl) showed maximum seedling lengths. Furthermore, the inoculation with SE12 gave the best results followed by TE7 and SE9, whereas a minimum was recorded in the control group. Several authors obtained similar results for maize by Shaharouna et al. (2006) and tomato by Neelam and Meenu (2010) and Masmoudi et al. (2021).

Conclusion

Bacteria act as important components in agriculture. They can promote plant growth potential by controlling external abiotic adverse effects. The current study highlights the beneficial plant-microbe interactions between the tested bacterial halophytes on tomato and barley seeds exposed to one salt level. The tested strains had multiple PGP properties that helped alleviate salt stress on the used plants, making them attractive for further field experiments with the use of the four strains alone or as a small synthetic community as bioinoculants.

Acknowledgments. The authors acknowledge both, the Ministry of Higher Education and Scientific Research (MESRS) of Algeria for funding and Yeditepe University, Faculty of Engineering, Department of Genetics and Bioengineering, Istanbul (Turkey) for having kindly welcomed Aissa Bakelli in their laboratories.

REFERENCES

- [1] Adams, D. J., Gurr, S., Hogge, J. (2005): Cellular Fatty-acid Analysis of *Bacillus thuringiensis* var. *kurstaki* Commercial Preparations. – Journal of Agricultural and Food Chemistry 53(3): 512-517.
- [2] Akpan, I., Bankole, M. O., Adesemowo, A. M. (1999): A Rapid Plate Culture Method for Screening of Amylase Producing Microorganisms. – Biotechnology Techniques 13: 411-413.
- [3] Aleksandrov, V. G., Blagodyr', R. N., Il'ev, I. P. (1967): Zvil'nennia sylikatnymi bakteriiamy fosfornoj kysloty z apatytu [Phosphorus Acid isolation from Apatite Produced by Silicate Bacteria]. – Mikrobiologichnyi Zhurnal 29(2): 111-114.
- [4] Alishahi, F., Alikhani, H. A., Khoshkholgh-Sima, N. A., Etesami, H. (2020): Mining the Roots of Various Species of the Halophyte *Suaeda* for Halotolerant Nitrogen-Fixing Endophytic Bacteria with the Potential for Promoting Plant Growth. – International Microbiology 23(3): 415-427.
- [5] AlKahtani, M. D., Fouda, A., Attia, K. A., Al-Otaibi, F., Eid, A. M., Ewais, E. E., Hijri, M., St-Arnaud, M., Hassan, S. E., Khan, N., Hafez, Y. M., Abdelaal, K. A. (2020): Undefined Isolation and Characterization of Plant Growth Promoting Endophytic Bacteria from Desert Plants and Their Application as Bioinoculants for Sustainable Agriculture. – Agronomy 10(9): 1325.
- [6] Aslam, F., Ali, B. (2018): Halotolerant Bacterial Diversity Associated with *Suaeda fruticosa* (L.) Forssk. Improved Growth of Maize Under Salinity Stress. – Agronomy 8(8): 131.
- [7] Baameur, M., Abdelguerfi, Daddi, B. M., Saadi, H., Ould, E. H. (2015): Distribution Study of Some Species of Spontaneous Flora in Two Saharan Regions of the North-East of Algeria (Ouargla and Ghardaia). – International Journal of Biodiversity and Conservation 7(1): 41-47.
- [8] Bencherif, K., Djaballah, Z., Brahimi, F., Boutekrabt, A., Dalpè, Y., Lounès-Hadj Sahraoui, A. (2019): Arbuscular Mycorrhizal Fungi Affect Total Phenolic Content and Antimicrobial Activity of *Tamarix gallica* in Natural Semi-Arid Algerian Areas. – South African Journal of Biology 125: 39-45.
- [9] Bodhankar, S., Grover, M., Hemanth, S., Reddy, G., Rasul, S., Yadav, S. K., Desai, S., Mallappa, M., Mandapaka, M., Srinivasarao, C. (2017): Maize Seed Endophytic Bacteria: Dominance of Antagonistic, Lytic Enzyme-producing *Bacillus* spp. – 3 Biotech 7(4): 232.
- [10] Bonev, B., Hooper, J., Parisot, J. (2008): Principles of Assessing Bacterial Susceptibility to Antibiotics using the Agar Diffusion Method. – Journal of Antimicrobial Chemotherapy 61: 1295-1301.
- [11] Cappuccino, J. G., Sherman, N. (1992): Biochemical Activities of Microorganisms. – In: Microbiology, A Laboratory Manual. The Benjamin/Cummings Publishing Co. California, USA.
- [12] Chekroun-Bechlaghem, N., Belyagoubi-Benhammou, N., Belyagoubi, L., Gismondi, A., Nanni, V., Di Marco, G., Canuti, L., Canini, A., El Hacı, I. A., Atik Bekkara, F. (2019): Phytochemical Analysis and Antioxidant Activity of *Tamarix africana*, *Arthrocnemum macrostachyum* and *Suaeda fruticosa*, Three Halophyte Species from Algeria. – Plant Biosystems 153(6): 843-852.
- [13] Chenchouni, H. (2012): Diversité Floristique d'un Lac du Bas-Sahara Algérien: Flora Diversity of a Lake at Algerian Low-Sahara. – Acta Botanica Malacitana 37: 33-44.
- [14] Chiwocha, S. D. S., Cutler, A. J., Abrams, S. R., Ambrose, S. J., Yang, J., Ross, A. R. S., Kermode, A. R. (2005): The *etr1-2* mutation in *Arabidopsis thaliana* Affects the Abscisic Acid, Auxin, Cytokinin and Gibberellin Metabolic Pathways during Maintenance of Seed Dormancy, Moist-Chilling and Germination. – Plant Journal 42: 35-48.

- [15] Chowdhury, S. P., Hartmann, A., Gao, X., Borriss, R. (2015): Biocontrol Mechanism by Root-associated *Bacillus amyloliquefaciens* FZB42 - A Review. – *Frontiers in Microbiology* 6: 780.
- [16] Compant, S., Samad, A., Faist, H., Sessitsch, A. (2019): A Review on the Plant Microbiome: Ecology, Functions, and Emerging Trends in Microbial Application. – *Journal of Advanced Research* 19: 29-37.
- [17] Coombs, J. T., Franco, C. M. (2003): Isolation and Identification of Actinobacteria from Surface-Sterilized Wheat Roots. – *Applied and Environmental Microbiology* 69(9): 5603-5608.
- [18] Croxatto, A., Prod'hom, G., Greub, G. (2012): Applications of MALDI-TOF Mass Spectrometry in clinical diagnostic microbiology. – *FEMS Microbiology Reviews* 36(2): 380-407.
- [19] Damodaran, T., Mishra, V. K., Sharma, D. K., Jha, S. K., Verma, C. L., Rai, R. B., Kannan, R., Nayak, A. K., Dhama, K. (2013): Management of Sub-soil sodicity for Sustainable Banana Production in Sodic Soil - An Approach. – *International Journal of Current Research* 5(7): 1930-1934.
- [20] Döbereiner, J. (1980): Forage Grasses and Grain Crops. – In: Bergersen, F. J. (ed.) *Methods for Evaluating Biological Nitrogen*. John Wiley & Sons Ltd. New York, pp. 535-555.
- [21] Dodd, I. C., Perez-Alfocea, F. (2012): Microbial Amelioration of Crop Salinity Stress. – *Journal of Experimental Botany* 63(9): 3415-3428.
- [22] Dworkin, M., Foster, J. (1958): Experiments with Some Microorganisms Which Utilize Ethane and Hydrogen. – *Journal of Bacteriology* 75: 592-603.
- [23] Dybwad, M., Granum, P. E., Bruheim, P., Blatny, J. M. (2012): Characterization of Airborne Bacteria at an Underground Subway Station. – *Applied and Environmental Microbiology* 78: 1917-1929.
- [24] Etesami, H., Beattie, G. A. (2018): Mining Halophytes for Plant Growth-Promoting Halotolerant Bacteria to Enhance the Salinity Tolerance of Non-halophytic Crops. – *Frontiers in Microbiology* 9: 148.
- [25] Fadji, A. E., Babalola, O. O. (2020): Elucidating Mechanisms of Endophytes used in Plant Protection and other Bioactivities with Multifunctional Prospects. – *Frontiers in Bioengineering and Biotechnology* 8: 467.
- [26] Fellah, O., Hameurlaine, S., Gherraf, N., Zellagui, A., Ali, T., Abidi, A., Altun, M., Demirtas, I., SahinYaglioglu, A. (2018): Anti-proliferative Activity of Ethyl Acetate Extracts of *Tamarix gallica* L. Grown at Different Climatic Conditions in Algeria. – *Acta Scientifica Naturalis* 5(2): 23-31.
- [27] Foldes, T., Banhegyi, I., Herpai, Z., Varga, L., Szigeti, J. (2000): Isolation of *Bacillus* Strains from the Rhizosphere of Cereals and *In Vitro* Screening for Antagonism Against Phytopathogenic, Food-borne Pathogenic and Spoilage Micro-organisms. – *Journal of Applied Microbiology* 89: 840-846.
- [28] Fykse, E. M., Tjärnhage, T., Humppi, T., Eggen, V. S., Ingebretsen, A., Skogan, G., Olofsson, G., Wästerby, P., Gradmark, P., Larsson, A., Dybwad, M., Blatny, J. M. (2015): Identification of Airborne Bacteria by 16S rDNA Sequencing, MALDI-TOF MS and the MIDI Microbial Identification System. – *Aerobiologia (Bologna)* 31(3): 271-281.
- [29] Glick, B. R., Karaturovic, D. M., Newell, P. C. (1995): A Novel Procedure for Rapid Isolation of Plant Growth Promoting Pseudomonads. – *Canadian Journal of Microbiology* 41: 533-536.
- [30] Gordon, S. A., Weber, R. P. (1951): Colorimetric Estimation of Indole Acetic Acid. – *Plant Physiology* 26: 192-195.
- [31] Goswami, D., Dhandhukia, P., Patel, P., Thakker, J. N. (2014a): Screening of PGPR from Saline Desert of Kutch: Growth Promotion in *Arachis hypogea* by *Bacillus licheniformis* A2. – *Microbiological Research* 169(1): 66-75.

- [32] Goswami, D., Pithwa, S., Dhandhukia, P., Thakker, J. N. (2014b): Delineating *Kocuria turfanaensis* 2M4 as a Credible PGPR: A Novel IAA-producing Bacteria Isolated from Saline Desert. – *Journal of Plant Interactions* 9(1): 566-576.
- [33] Henderson, M. E. K., Duff, R. B. (1963): The Release of Metallic and Silicate Ions from Minerals, Rocks, and Soils by Fungal Activity. – *Soil Science Society of America Journal* 14: 236-246.
- [34] James, E. (2000): Nitrogen Fixation in Endophytic and Associative Symbiosis. – *Field Crops Research* 65: 197-209.
- [35] King, J. E. (1932): The Colorimetric Determination of Phosphorus. – *Biochemistry Journal* 26: 292-297.
- [36] Ksouri, R., Falleh, H., Megdiche, W., Trabelsi, N., Mhamdi, B., Chaieb, K., Bakrouf, A., Magné, C., Abdelly, C. (2009): Antioxidant and Antimicrobial Activities of the Edible Medicinal Halophyte *Tamarix gallica* L. and Related Polyphenolic Constituents. – *Food and Chemical Toxicology* 47(8): 2083-2091.
- [37] Ksouri, R., Ksouri, W. M., Jallali, I., Debez, A., Magné, C., Hiroko, I., Abdelly, C. (2012): Medicinal Halophytes: Potent Source of Health Promoting Biomolecules with Medical, Nutraceutical and Food Applications. – *Critical Reviews in Biotechnology* 32(4): 289-326.
- [38] Leontidou, K., Genitsaris, S., Papadopoulou, A., Kamou, N., Bosmali, I., Matsi, T., Madesis, P., Vokou, D., Karamanoli, K., Mellidou, I. (2020): Plant Growth Promoting Rhizobacteria Isolated from Halophytes and Drought-Tolerant Plants: Genomic Characterisation and Exploration of Phyto-beneficial Traits. – *Scientific Reports* 10(1): 14857.
- [39] Li, H., Qiu, Y., Yao, T. (2020): Effects of PGPR Microbial Inoculants on the Growth and Soil Properties of *Avena sativa*, *Medicago sativa*, and *Cucumis sativus* Seedlings. – *Soil and Tillage Research* 199: 104-577.
- [40] Lim, J. H., Kim, S. D. (2013): Induction of Drought Stress Resistance by Multi-Functional PGPR *Bacillus licheniformis* K11 in Pepper. – *Plant Pathology Journal* 29: 201-208.
- [41] Loper, J. E., Schroth, M. N. (1986): Influence of Bacterial Sources of Indole-3-Acetic Acid on Root Elongation of Sugar Beet. – *Phytopathology* 76: 386-389.
- [42] Lu, L., Chang, M., Han, X., Wang, Q., Wang, J., Yang, H., Guan, Q., Dai, S. (2021): Beneficial Effects of Endophytic *Pantoea ananatis* with Ability to Promote Rice Growth Under Saline Stress. – *Journal of Applied Microbiology* 131(4): 1919-1931.
- [43] Ma, Y., Dias, M. C., Freitas, H. (2020): Drought and Salinity Stress Responses and Microbe-Induced Tolerance in Plants. – *Frontiers in Plant Science* 2020: 11.
- [44] Masmoudi, F., Tounsi, S., Dunlap, C. A., Trigui, M. (2021): Endophytic Halotolerant *Bacillus velezensis* FMH2 Alleviates Salt Stress on Tomato Plants by Improving Plant Growth and Altering Physiological and Antioxidant Responses. – *Plant Physiology and Biochemistry* 165: 217-227.
- [45] Miura, T., Makoto, K., Niwa, S., Kaneko, N., Sakamoto, K. (2017): Comparison of Fatty Acid Methyl Ester Methods for Characterization of Microbial Communities in Forest and Arable Soil: Phospholipid Fraction (PLFA) Versus Total Ester Linked Fatty Acids (EL-FAME). – *Pedobiologia* 63: 14-18.
- [46] Nautiyal, C. (1999): An Efficient Microbiological Growth Medium for Screening Phosphate Solubilizing Microorganisms. – *FEMS Microbiology Letters* 170(1): 265-270.
- [47] Naz, I., Ahmad, H., Khokhar, S. N., Khan, K., Shah, A. H. (2016): Impact of Zinc Solubilizing Bacteria on Zinc Contents of Wheat. – *American-Eurasian Journal of Agricultural & Environmental Sciences* 16: 449-454.
- [48] Neelam, T., Meenu, S. (2010): Salinity-Resistant Plant Growth Promoting Rhizobacteria Ameliorates Sodium Chloride Stress on Tomato Plants. – *Journal of Plant Interaction* 5(1): 51-58.
- [49] Oates, L. G., Read, H. W., Gutknecht, J., Duncan, D. S., Balsler, T. B., Jackson, R. D. A. (2017): Lipid Extraction and Analysis Method for Characterizing Soil Microbes in Experiments with Many Samples. – *Journal of Visualized Experiments* 125: 55310.

- [50] Oleńska, E., Małek, W., Wójcik, M., Swiecicka, I., Thijs, S., Vangronsveld, J. (2020): Beneficial Features of Plant Growth-Promoting Rhizobacteria for Improving Plant Growth and Health in Challenging Conditions: A Methodical Review. – *Science of the Total Environment* 2020: 140682.
- [51] Patten, C. L., Glick, B. R. (2002): Role of *Pseudomonas putida* Indole Acetic Acid in Development of the Host Plant Root System. – *Applied and environmental microbiology* 68(8): 3795-3801.
- [52] Pavlova, A., Leontieva, M., Smirnova, T., Kolomeitseva, G., Netrusov, A., Tsavkelova, E. (2017): Colonization Strategy of the Endophytic Plant Growth-promoting Strains of *Pseudomonas fluorescens* and *Klebsiella oxytocaon* the Seeds, Seedlings and Roots of the Epiphytic Orchid, *Dendrobium nobile* Lindl. – *Journal of Applied Microbiology* 123(1): 217-232.
- [53] Pikovskaya, R. I. (1948): Mobilization of Phosphorus in Soil in Connection with the Vital Activity of Some Microbial Species. – *Mikrobiologiya* 17: 362-370.
- [54] Raj, S. V., Raja, A. K., Vimalanathan, A. B., Tyagi, M. G., Shah, N. H., Johnson, J., Santhos, B. I., Sathiyaseelan, K. (2009): Study of Starch Degrading Bacteria from Kitchen Waste Soil in the Production of Amylase by using Paddy Straw. – *Recent Research in Science and Technology* 1(1): 008-013.
- [55] Ramadoss, D., Lakkineni, V. K., Bose, P., Ali, S., Annapurna, K. (2013): Mitigation of Salt Stress in Wheat Seedlings by Halotolerant Bacteria Isolated from Saline Habitats. – *Springerplus* 2(1): 6.
- [56] Saleh, D., Jarry, J., Rani, M., Aliferis, K., Seguin, P., Jabaji, S. (2019): Diversity, Distribution and Multi-Functional Attributes of Bacterial Communities Associated with the Rhizosphere and Endosphere of Timothy (*Phleum pratense* L.). – *Journal of Applied Microbiology* 127(3): 794-811.
- [57] Santoyo, G., Moreno-Hagelsieb, G., del Carmen Orozco-Mosqueda, M., Glick, B. R. (2016): Plant Growth-Promoting Bacterial Endophytes. – *Microbiological Research* 18: 92-99.
- [58] Sasser, M. (2001): Identification of Bacteria by Gas Chromatography of Cellular Fatty Acids. – *MIDI Technical Note* 101.
- [59] Sauget, M., Valot, B., Bertrand, X., Hocquet, D. (2017): Can MALDI-TOF Mass Spectrometry Reasonably Type Bacteria? – *Trends in Microbiology* 25(6): 447-455.
- [60] Schwyn, B., Neilands, J. B. (1987): Universal Chemical-assay for the Detection and Determination of Siderophore. – *Analytical Biochemistry* 160: 47-56.
- [61] Shaharoon, B., Arshad, M., Zahir, Z. A., Khalid, A. (2006): Performance of *Pseudomonas* spp. Containing ACC-deaminase for Improving Growth and Yield of Maize (*Zea mays* L.) in the Presence of Nitrogenous Fertilizer. – *Soil Biology and Biochemistry* 38: 2971-2975.
- [62] Shrivastava, P., Kumar, R. (2015): Soil Salinity: A Serious Environmental Issue and Plant Growth Promoting Bacteria as One of the Tools for its Alleviation. – *Saudi Journal of Biological Sciences* 22(2): 123-131.
- [63] Slabbinck, B., De Baets, B., Dawyndt, P., De Vos, P. (2009): Towards Large-scale FAME-based Bacterial Species Identification using Machine Learning Techniques. – *Systematic and Applied Microbiology* 32(3): 163-176.
- [64] Souza, R. D., Ambrosini, A., Passaglia, L. M. (2015): Plant Growth-Promoting Bacteria as Inoculants in Agricultural Soils. – *Genetics and Molecular Biology* 38(4): 401-419.
- [65] Suárez, R., Wong, A., Ramírez, M., Barraza, A., Orozco, M. D. C., Cevallos, M. A., Lara, M., Hernández, G., Iturriaga, G. (2008): Improvement of Drought Tolerance and Grain Yield in Common Bean by Overexpressing Trehalose-6-phosphate Synthase in *Rhizobia*. – *Molecular Plant-Microbe Interactions* 21: 958-966.
- [66] Teather, R. M., Wood, P. J. (1982): Use of Congo red-polysaccharide Interactions in Enumeration and Characterization of Cellulolytic Bacteria from the Bovine Rumen. – *Applied and Environmental Microbiology* 43(4): 777-780.

- [67] Ullah, S., Bano, A. (2015): Isolation of Plant-Growth-Promoting Rhizobacteria from Rhizospheric Soil of Halophytes and their Impact on Maize (*Zea mays* L.) Under Induced Soil Salinity. – Canadian Journal of Microbiology 61(4): 307-313.
- [68] White, J. F., Torres, M. S., Sullivan, R. F., Jabbour, R. E., Chen, Q., Tadych, M., Irizarry, I., Bergen, M. S., Havkin-Frenkel, D., Belanger, F. C. (2014): Occurrence of *Bacillus amyloliquefaciens* as a Systemic Endophyte of Vanilla Orchids. – Microscopy research and technique 77(11): 874-885.
- [69] Yu, X., Ai, C., Xin, L., Zhou, G. (2011): The siderophore-producing Bacterium, *Bacillus subtilis* CAS15, has a Biocontrol Effect on *Fusarium* Wilt and Promotes the Growth of Pepper. – European Journal of Soil Biology 47: 138-145.

EXTREMELY HALOPHILIC ARCHAEA FROM ALGERIAN SALT LAKES: ISOLATION, PHYLOGENETIC IDENTIFICATION AND BIOPROSPECTION OF HYDROLYTIC ENZYMES

KHELFAOUI, M. E. A.¹ – LENCHI, N.^{2,3*} – KEBBOUCHE-GANA, S.³ – GANA, M. L.⁴ – MEDHKOUR, H.⁵
– GRINE, G.⁵ – KHEMILI-TALBI, S.³ – AKMOUSSI-TOUMI, S.³

¹ *Laboratoire de recherche Conservation et Valorisation des Ressources Biologiques, Faculté des Sciences, Université M'Hamed Bougara de Boumerdes, Independence Avenue, Boumerdes 35000, Algeria*

² *Department of Natural and Life Sciences, Faculty of Sciences, University Algiers 1 BenYoucef Benkhedda, Algiers, Algeria*

³ *Bioinformatics, Applied Microbiology and Biomolecules Laboratory, Faculty of Sciences, University M'Hamed Bougara of Boumerdès, Boumerdès, Algeria*

⁴ *Research and Development Center, SONATRACH, Independence Avenue, Boumerdes 35000, Algeria*

⁵ *Aix Marseille University, MEPHI, IHU Fondation Méditerranée Infection, 19-21 Boulevard Jean Moulin, 13005 Marseille, France*

**Corresponding author*

*e-mail: n.lenchi@univ-alger.dz ; phone: +213-555-975-420
m.khelfaoui@univ-boumerdes.dz*

(Received 25th Jan 2022; accepted 2nd May 2022)

Abstract. Hyper-saline aquatic ecosystems are among the most inhospitable habitats where life can be found; Chotts and sebkhas constitute a model of extreme environments where lives a halophilic microflora adapted to these conditions. These habitats are not sufficiently studied in Algeria and this research has been carried out on four distant and different sebkhas where the salt reaches more than 300 g/L. The physical-chemical analysis showed that these waters contain numerous minerals, of which the chlorides are the most dominants. The study of the microflora revealed the presence of an important morphologic, physiologic, metabolic and phylogenetic diversity, including archaeal species. Twelve strictly halophilic archaea (XA1, XC1, XC2, XE1, XE2, WA1, WC1, YA1, YA2, YF2, ZC1 and ZD1) were selected for further characterization. The growth occurred between 15 and 30% (w/v) NaCl with an optimum at 20% (w/v) NaCl. 16S rRNA gene sequencing revealed that the strains belonged to *Halorubrum sp*, *Natribaculum sp*, *Haloarcula sp*, *Natrinema sp*, *Halostagnicola sp*, *Haloferax sp* and *Haloterrigena sp* genera. Noting that these halophilic *Archeae* are capable of producing different enzymes at high salt concentrations (20% NaCl). The production yields obtained are very promising for applications in the biotechnology and industrial microbiology.

Keywords: *extreme environments, halophiles archaea, phylogenetic diversity, enzymes*

Introduction

A certain number of particular ecosystems have been formed, following climatic and geophysical changes, in the course of the evolution of the earth (Henriet et al., 2014). These so-called “extreme” ecosystems are special habitats whose physicochemical conditions are, not very favorable to the development of life, characterized by the absence of several life forms and by a distinct microbial diversity (McGenity and Grant, 1995). The organisms found there must have particular properties to be able to

proliferate under these hostile conditions (Kebbouche-Gana et al., 2009). Among the extreme environments, ecosystems with high or low pH values, high or low temperatures or high content of salt can be found in many parts of the world (Antranikian and Egorova, 2007). This is the case of the hyper-saline aquatic environments that contain in their solutions mineral salts that can reach saturation; usually referred to as sebkha or over-salted mediums.

Arid and Saharan habitats (North-Western Algerian Sahara), characterized by a saline and gypsum-saline substrate, occupy small areas. This type of habitat corresponds to depressions known as Chott or Sebkh. Geologically and topographically, Sebkh are depression in the form of basins, periodically flooded, in which an accumulation of salt occurs. They function as evaporation tanks, which after drying, reveal a layer of salt whose concentration is maximum in the center and decreases towards the periphery, hence a composition of the vegetation according to the degree of salinity. These media have a dissolved salt content higher than that of seawater (Baliga et al., 2004). When one exceeds 100 g/l in salt, the media becomes extreme and inhibits the growth of a large majority of microorganisms (Antranikian and Egorova, 2007).

In hyper-saline environments, *Halobacteria* (members of the halophilic *Archaea*) are the dominant organisms. The halophilic *Archaea* are associated with prokaryotes (Antranikian and Egorova, 2007). They are cells without nucleus, very diverse in morphology as well as in physiology (Menasria et al., 2018). In addition to their gene sequences coding for ribosomal RNAs, they are distinguished from the other two kingdoms by many points concerning the structure and chemistry of the wall, the structure of membrane lipids and certain metabolic pathways (Castillo et al., 2006).

In Algeria, the hyper-saline Chotts and Sebkh aquatic ecosystems have been few studied; they are still rich in divers microorganisms (Kharroub et al., 2014; Quadri et al., 2016; Lenchi et al., 2020). Genera that have been retrieved are: *Halorubrum*, *Halobacterium* and *Haloterrigena* isolated by Menasria et al. (2018); the genera *Haloarcula* and *Halovivax* isolated by Kebbouche-Gana et al. (2009); the genera *Haloarcula*, *Halorubrum*, *Natrialba*, *Halovivax* and *Haloferax* are isolated by Quadri et al. (2016) and Imadalou-Idres et al. (2013) and the species *Haloferax mediterranei* isolated by Akmoussi-Toumi et al. (2018). These halophilic microorganisms have different biotechnological applications such as, pigments for food coloring, extracellular polysaccharides (EPS), poly-hydroxyalkanoate used in the production of biodegradable plastic, the production of fermented foods, compatible solutes and hydrolytic enzymes (Bajpai et al., 2015). The reports on the diversity of halophilic microorganisms producing hydrolytic enzymes in hypersaline habitats, such as solar salt marshes, salt lakes, salt deserts and salt deposits are sparse (Makhdoumi-Kakhki et al., 2011).

Due to its biotechnological potential and industrial applications, the detection and isolation of hydrolytic enzymes produced by extreme halophiles is an interesting research field. These enzymes, including amylase, lipase, protease, gelatinase and cellulase, are the most used in the industrial field such as the process of biosynthesis, environmental bioremediation and food processing (Makhdoumi-Kakhki et al., 2011; Delgado-García et al., 2012). They tend to be very stable in organic solvents that allow their use in green chemistry (Oztetik and Cakir, 2014). These microorganisms considered non-pathogenic are found in hyper-saline lakes, the Dead Sea (Jordan), Salt Marshes (Spain) and in large, extremely saline alkaline lakes such as Oued Natron in Egypt, Lake Magadi in Kenya, ponds in solar distillation and Salt Lake City (USA) (Menasria et al., 2018).

To our knowledge, except the sebkha of Tinsilt in Oum el Bouaghi, there is no study on the diversity of the Archean communities living in the Sebkhass of El Outaya in Biskra, Ain Beida and Oum Reneb in Ouargla in the Algerian Sahara Desert. The main purpose of this research was to isolated halophilic archaeal strains from different salt lakes of Algerian desert and characterize them with respect to some phenotypic and phylogenetic characteristic, with a view to screening for enzymes of an industrial and biotechnological interest.

Materials and methods

Geographical location

The sampling study was carried out in Sebkhass El Outaya (Biskra), Tinsilt (Oum el Bouaghi), Ain Beida and Oum Reneb (Ouargla) in January 2020. Biskra location is in the north-east of the Algerian Sahara. This sebkha is characterized by a depth of 150 cm and an area of 50 m²; it is located 28 km north of the city of Biskra (35°01' North, 5°44' East and Altitude 282 m). The location of Oum El Bouaghi is in northeast Algeria. This sebkha is characterized by a depth of 50 cm and an area of 2.15 ha; it is located in the region of Ain M'Lila 5 km from the Commune of Souk-Naâmane and 17 km south of the city of Aïn-M'lila (35°53'14" Nord, 06°28'44" East and Altitude 792 m). Ouargla's location is in south-eastern Algeria. the sebkha of Ain Beida is characterized by a depth of 60 cm and an area of 6.85 hectares; it is located east of the wilaya of Ouargla (6 km) and near the town of Ain El Beida (31°59'2" North, 5°21'52" East and Altitude 139 m) and the sebkha of Um Reneb is characterized by a depth of 70 cm and an area of 7.15 hectares; it is located to the north of the wilaya of Ouargla (10 km) and in the municipality of Sidi Khouiled (32°01'31" North, 5°21'51" East and Altitude 150 m) (see *Fig. 1*). The geographical position of the study areas, the Aurès Mountains in the north, and the Sahara in the south, gives it an unstable arid climate with frankly Saharan tendencies. Climate is influenced relatively by the cold weather especially in winter and by the high temperatures due to the winds blowing from the south in summer and the sirocco. Therefore, the vegetation is spontaneous and governed by both climatic conditions and degradations from anthropogenic causes. Apart from the irrigated areas, the reliefs are practically devoid of vegetation.

Sample collection

Water samples are obtained from three different points in the shape of a triangle; on the surface and at a depth of 20 cm. The three samples were mixed in order to obtain a representative sample of 200 ml (American Public Health Association, 2005). Water was collected in sterile jerry cans, completely filled after three overflows and sealed directly with screw caps to avoid contamination. The samples were immediately transported at ambient temperature to the laboratory and stored at 4 °C until analyses. Samples were treated within 24 h after collection. Temperature, pH, electrical conductivity (Cs) and salinity were measured *in situ* using a multi-parameter probe (SimpHony, VWR).

Water samples analysis

The physico-chemical analyzes of water samples are carried out at the Research and Development Center (CRD) according to standard methods 4500-S⁻² F (American

Public Health Association, 2005). The chemical and physical properties included estimates of the composition of Na^+ , Ca^{2+} and K^+ by spectrophotometry with DR 2000 flame ionization. Mg^{2+} by a complexometry method using ethylene diaminetetraacetic acid and EDTA. Cl^- at 497 nm, multi-ray spectrophotometry (DR2000). CO_3^- and HCO_3^- by colorimetry at 497 nm. Nitrates by colorimetry at 520 nm. SO_4^- by colorimetry at 495 nm and salinity by electrochemistry (NF EN 27-888 (1994)). The different characteristics are given in *Table 1*.



Figure 1. Location of sampling sites

Enrichment and halophilic archaea isolation

Cultivation of the halophilic species requires a stage of reactivation and enrichment (Oren, 2008). A specific medium for aerobic, neutrophilic and alkalophilic halophilic microorganisms given by Oren (2008), has been used, it is used both for enrichment, isolation, and also for physiological identification tests, containing (per liter); 250 g of NaCl, 6 g of KCl, 29 g of $\text{MgSO}_4 \cdot 7\text{H}_2\text{O}$, 19.5 g of $\text{MgCl}_2 \cdot 6\text{H}_2\text{O}$, 1.1 g of $\text{CaCl}_2 \cdot 6\text{H}_2\text{O}$, 0.8 g of NaBr, 0.2 g of NaHCO_3 and 5 g of yeast extract, adjusted to pH 7 with HCl. The sodium chloride and sodium bicarbonate are sterilized separately in 250 ml bottles.

They are added extemporaneously to the other components of the medium (in order to avoid precipitation of the salt). Enrichments are made in 250 ml Erlenmeyer flasks autoclaved at 120 °C for 20 min, filled with 100 ml of culture medium then inoculated 1/10 with the water sample and the various dilutions prepared. Incubation of the cultures takes place in a shaker incubator at 40 °C with a stirring speed of 120 rpm, this temperature promotes the growth of most *Halobacteriaceae* (Oren, 2008). So, and dilutions of 10^{-1} to 10^{-4} were made on the same agar medium solidified with 20 g of agar. After 7-10 days of incubation at 40 °C, the pigmented colonies were picked and sub-cultured several times to obtain a pure culture.

Physiological and biochemical morphological characterization of isolates

The identification of *Halobacteria* is based on the study of phenotypic, physiological, biochemical and phylogenetic characteristics according to several recommendations (Amoozegar, 2017; Joint, 2010; Oren, 2008). The macroscopic study of colonies is considered the first step that guides the progress of strain identification. Macroscopic examination of the colonies obtained on the solid medium based on morphological characters observed with the naked eye such as colony shape, pigmentation, diameter, elevation and opacity. The study of micro-morphological characters allows to have an observation of the isolates in the fresh state in the absence of any fixation or staining in a saline solution (20%). The modified Gram stain applied to the halophilic microflora was performed by samples fixed with acetic acid as described by Kebbouche-Gana et al. (2009). To study certain classification criteria, liquid enrichment media have undergone modifications by varying the concentration of NaCl (%) (5, 10, 15, 20, 25, 30, and 35) (p/v), pH (4.0, 6.0, 7.0, 8.0 and 9.0) and temperature (10, 25, 32, 37, 42, 50 and 60 °C). This study is carried out by varying one of the parameters while the other two are kept constant, the latter being inoculated with archaeal cultures aged 72 H in 100 ml Erlenmeyer flasks containing 20 ml each of medium or it is isolated, in the presence of controls (tubes containing the unseeded sterile culture medium) (Kebbouche-Gana et al., 2009). The growth in anaerobiosis is affected by the use of another acceptor of electrons such as nitrate. The enzymatic activities of oxidase and catalase were tested using standard procedures (Oren and Ventosa, 2000). The reduction of nitrates was tested using the liquid enrichment medium supplemented with 0.1% KNO₃ (w/v) (Oren, 2008). The TSI medium confirms the fermentation of glucose and the attack of lactose and sucrose, the production of H₂S and the gas, using Kligler-Hajna medium supplemented with 25% (w/v) NaCl, in incubating at 40 °C for 7 days. The indole formation was tested after 7 days of incubation at 40 °C in a liquid medium in the presence of tryptone (Oren, 2008). Some strains have the ability to use different sources of carbon to grow; this source is sometimes a sugar (glucose, sucrose, lactose, arabinose and rhamnose), an alcohol (inositol, sorbitol and mannitol) or an organic acid (citrate). To study this capacity, we performed the various tests given by Oren (2008). The other phenotypic characteristics were tested using API 20E (Biomérieux Kit), Modified by adding sterile NaCl. The study of antibiotic susceptibility is a criterion for the classification of strains. The test consists of determining the resistance or sensitivity of isolated archaeal strains to certain antibiotics: Nalidixic acid, 30 µg; Ofloxacin, 5 µg; Penicillin G, 6 µg; Ampicillin and derivatives, 10 IU; Amoxicillin + clavulamic acid, 20/10 µg; Erythromycin, 15 µg; Pristinamycin, 15 µg; Trimethoprim, 1.25/23.75 µg; Furans, 30 µg; Gentamicin, 30 µg; Chloramphenicol/Thiamphenicol, 5 µg; Tetracycline, 30 µg; Oxacillin, 5 µg;

Cefotaxime, 30 µg; Cefalexin, 30 µg; Novobiocin, 30 µg; Streptomycin, 300 µg; Bacitracin, 200 µg. The test is performed on solid medium, inoculated with young archaeal cultures and cultured with the presence of antibiotic discs, then incubated at 40 °C for one week (Kebbouche-Gana et al., 2009).

16S rRNA gene sequencing of the isolates

The extraction of the DNA from each strain tested is carried out with the PCI method (phenol/chloroform/isoamyl alcohol) (Baliga, 2004; Castillo, 2007; Quadri, 2016). The gene coding for the 16S RNA is amplified by PCR from the previously extracted genomic DNAs. The partial 16S rRNA gene was amplified using broad-spectrum *Archaea* primers SDArch0333aS15 (5'-TCCAGGCCCTACGGGG-3') and SDArch0958aA19 (5' YCCGGCGTTGAMGCCGATTCCAATT-3') (Tamura, 2013). In order to verify the presence of DNA and the size of the fragments of the PCR products, agarose gel electrophoresis is performed (Tamura, 2013). The amplicon was sequenced using the Sanger method at the laboratory Microbes, Evolution, Phylogeny and Infection (MEPHI) (Marseille-France). The alignment of the sequences for the homology search with the closest sequences set to the database was carried out using the program: the Basic Local Alignment Search Tool (BLAST) on the NCBI (National Center for Biotechnology Information; www.ncbi.nlm.nih.gov). The sequences are then deposited in GenBank data base and an accession number is obtained for each strain. Phylogenetic tree construction based on strains sequences and database sequences was constructed using the Neighbor-Joining algorithm implemented in MEGA 7.0 (Tamura, 2013).

Screening of extracellular hydrolytic enzymes

The search for halophilic enzymes is such an important criterion. The search for enzymatic activity was carried out on agar plates using a drop technique after incubation at 40 °C for 7 days. The cultures used for the enzymatic screening were obtained by cultivating the halophilic microorganisms in 10 ml of enrichment media supplemented with 20% NaCl while stirring at 120 revolutions per minute for approximately one week. A sample of (10 µl) of liquid culture from each test culture was identified on an appropriate medium. The subsequent experimentation was carried out in duplicate according to the standard protocols described below (Akmoussi-Toumi et al., 2018; Menasria et al., 2018).

Amylase activity

The detection of the amylase is carried out by cultivating the strains to be tested on a solid culture medium supplemented with 0.1% of the starch; the presence of amylase activity was confirmed by the appearance of a clear halo zone around the colonies after staining with Gram's iodine solution (Abd-Elhalem et al., 2015; Akmoussi-Toumi et al., 2018; Menasria et al., 2018).

Cellulase activity

The presence of cellulase is examined on enrichment medium containing 0.5% (w/v) Carboxy-Methyl Cellulose (CMC) (Saxena et al., 2007). The results were expressed by the appearance of clarification zones around the archeal colony (Latorre et al., 2016).

Lipolytic activity

The search for lipase is carried out on a medium supplemented with 0.1% Tween 80 indicator. An opaque halo around the colonies indicated the positive lipolytic activity (Ghanem, 2007).

Gelatine hydrolysis

The detection of gelatinase is carried out on a solid medium supplemented with 0.1% of gelatin indicator, the appearance of a clear zone around the colony indicated gelatinase positive (Delgado-García et al., 2012).

Caseine hydrolysis

The presence of caseinase is achieved by adding to the double-agar isolation medium the same volume of milk containing no fat. The positive reaction results in zones of clarification around the spots (Delgado-García et al., 2012).

Results and discussion

Water analysis

In the purpose of isolating and characterizing of the halophilic *Archaea* present in the studied Sebkhas, the physicochemical analysis of water samples was firstly performed. Besides studying its salinity and ionic composition, *Table 1* presents the results of the salt analyzes in the sample compared to other hyper-saline ecosystems. The hyper-salinity of the studied sebkhas, located in the North-East of the Algerian Sahara, comes from the dissolution of salts of continental origin; these waters are classified as athalassohaline. This is the case of the Pink Salt Lake in Senegal and most sebkhas located in semi-arid and arid zones (Atanasova et al., 2013; Liu et al., 2015; Roussel et al., 2008). These environments have a saline ionic composition different from that of seawater (Litchfield and Dalmat, 2009). The day of the sampling; the water temperature was 10 °C. This average temperature is explained by a sampling carried out in winter (January). The waters are alkaline with a pH value of 8.07. We noted that these pH values are close to that of the Great Salt Lakes in the USA (Grant et al., 2011) and higher than that of the Dead Sea (5.9 - 6.3) but remains well below that of Wadi Natrun of Egypt (pH 11) (Quadri et al., 2011). The waters analyzed are highly mineralized, in which the salinity equal 374 g per liter and Na⁺ and Cl⁻ ions are dominant, such as those found in the large salt lakes (USA) and Lake Natrun in Egypt and the Dead Sea in Jordan (Madigan and Martinko, 2006). The concentration of Na⁺ ion is much higher than that of the Dead Sea. On the other hand, the high chloride content is also noted in the Dead Sea in Jordan (Madigan and Martinko, 2006). As for sulfate ions (SO₄⁻), it is also observed that they are present in relatively high concentration. Sulphate is the most oxidized form of sulfur. It plays an essential role in the life cycle, thus promoting the development of sulphate-reducing bacteria (Gana et al., 2010). In addition, the total alkalimetric titre (HCO₃⁻) of the two samples is low, close to that of the Dead Sea (0.2 g/l). These ions are used as a carbon source by the halophilic autotrophic (Grant et al., 2006). These waters have a considerable content of Mg⁺⁺ ion and a mean concentration of Ca⁺⁺ and K⁺ ions. In fact, these trace elements act as cofactors or enzymatic activators (Amoozegar et al., 2017; Madigan and Martinko, 2006; Oren,

2008). In particular, Mg⁺⁺ions, which promote the proliferation of extreme halophilic flora, Ca⁺⁺ ions are necessary for the bacterial metabolism (Grant et al., 2011; Madigan and Martinko, 2006; Oren, 2008).

Table 1. Chemical properties of the studied salt lakes of the North Algerian Sahara compared to other hyper-saline and marine ecosystems

Ecosystems	Chemical properties								
	pH	Na ⁺	K ⁺	Mg ²⁺	Ca ²⁺	Cl ⁻	SO ₄ ²⁻	HCO ₃ ⁻	Salinity
Chott of Biskra (Algeria)	8.7	190	7.41	2.16	0.5	207	69	0.21	374
Chott of Oum Bouaghi (Algeria)	7.9	157	1	6.45	0.7	180	45	0.95	324
Chott of Ain Beida (Algeria)	8.07	120	0.21	2.74	0.1	124	66	0.16	224
Chott of Oum Reneb (Algeria)	8.10	117	0.19	2.62	0.13	184	66	0.15	332
Caspienne Sea ¹	8.3	3.18	0.09	0.73	0.34	5.33	3.0	0.4	12.8
Aral Sea ¹	8.2	2.2	0.08	0.55	0.51	3.47	3.2	0.07	10.2
Great Salt Lake (USA) ¹	7.7	105	6.7	11.1	0.3	181	27	0.72	333
Lake Natrun (Egypt) ¹	11	142	2.3	UD	UD	155	22.6	67	394
Lake Magadi (Kenya) ¹	11.5	46	0.06	0.8	0.62	14	nd	34.9	277
Salt Lake El Goléa (Algeria) ²	9	107	nd	0.3	0.4	198	nd	nd	296
Chott of Ouargla (Algeria) ²	8.57	37.33	1.71	4.04	5.63	64.68	41.22	0.43	128

Salinity and ions are represented as g per liter. nd., not determined. UD., undetectable. References for abiotic features of other hypersaline and marine habitats were as follows:

¹Grant et al. (2011)

²Boutaiba et al. (2011)

Isolation and identification of the microorganisms

Among the 43 strains isolated from the water of these Sebkhass, twelve distinct strictly halophilic strains: (XA1, XC1, XC2, XE1 and XE2) from Biskra, (WA1 and WC1) from Oum El Bouaghi, (YA2, YA3 and YF2) from Ain Beida and (ZC1 and ZC2) from Oum Reneb were chosen for further characterization. These twelve isolates were unable to grow in the absence of NaCl and required at least 10% NaCl to grow, which showed their strict halophilic character (Oren et al., 2008). The isolates were morphologically, biochemically, and physiologically characterized (Table 2). Pure orange and red colonies (Fig. 2) were isolated from Sebkhass waters with a population density of 6.1×10^4 CFU g⁻¹. Growth under aerobic conditions was noticed between 25 and 50 °C, with an optimum temperature of 40 °C. A pH range of 6 to 9 was tested at 40 °C, with an optimal pH of 8. No growth noted at 0% and 5% NaCl, with slight growth to 10% NaCl, go up to 30% and a growth optimum of 25%. The isolated strains are immobile and Gram negative. Microscopic observation shows pleomorphic or cocci forms. Glucose is assimilated by all the strains, only the XA1 and WA1 strains use lactose, others use mannitol (XA2 and ZC1) and two others use xylose (NE1 and ZD1). Sucrose, fructose, arabinose, rhamnose, ribose and sorbitol are not assimilated by all the strains isolated. All the strains studied are sensitive to Novobiocin and Bacitracin, this is a major criterion of halophilic *Archaea* (Atanasova et al., 2013). The majority of strains are resistant to antibiotics generally active on bacteria (Penicillin, Ampicillin, Amoxicillin, Erythromycin, Pristinamycin and Streptomycin) which is an important feature for the description of halophilic *Archaea*. Resistance to penicillin G, ampicillin, amoxicillin, clavulamic acid, oxacillin, cefotaxime, cefalexin, cefixime and fosfomycin that inhibit cell wall synthesis can be explained by a very different biochemical composition of the *Archaea* wall (Atanasova et al., 2013; Imadalou-Idres, 2013). Likewise, *Archaea*-dependent DNA RNA polymerase is insensitive to rifampicin, which inhibits the bacterial enzyme at very low concentrations. In addition, the protein synthesis of *Archaea* is not affected by the usual antibiotics, chloramphenicol and

streptomycin; tetracycline is also a weak inhibitor although it inhibits the protein synthesis of Bacteria and eukaryotes (Klingl, 2014). The pH ranges investigated varies from 6 to 10, the pH above 11 and below 6 are inhibitory for all strains. On the other hand, all strains can grow relatively well at pH 7 and 8, they are therefore neutro-alkalophilic strains. So, Castillo et al. (2006), report that 55% of the known halophilic *Archaea* species have a pH optimum of 7-8, the rest of the halophilic *Archaea* species are alkalophilic (optimal pH 9). In this study, the temperature range explored varies from 25 to 50 °C. The temperature above 50 °C and below 25 °C inhibited the isolates obtained but grew optimally at 35 and 40 °C. Castillo et al. (2006), report that 63% of the known halophilic *Archaea* species have a temperature optimum of 38-40 °C. Furthermore, the rest of the *Archaea* halophilic species are either thermo-tolerant (optimal temperature equal 50 °C) or mesophilic (28 and 35 °C). Oren (2008), report that several obligate alkalophilic *Archaea* species have been isolated from Magadi Lake and Rift Valley, Kenya, *Natronobacterium gregoryi*, *Halorubrum vacuatum*, *Natrialba magadii*, *Natronomonas pharaonis* and *Natronococcus amylocticus*; each of these microorganisms has a pH optimum of 9.0 or higher. Of all the known extreme halophilic *Archaea*, only two species are extremely halophilic, necessarily alkalophilic and thermophilic and called poly-extremophiles, *Natrialba hulunbeirensis*, which has an optimum (Na^+) of 3.4 M, an optimum pH of 9.0, and an optimum temperature equal 50 °C. So, *Natronolimnobius aegytiacus* has an optimum of 4.5 M (Na^+), a pH optimum of 9.5 and an optimum temperature of 55 °C (Liu and al., 2015; Oren and Ventosa, 2000). It should also be noted that with the exception of glucose, with an acid production for all strains, our isolates have shown a low assimilable fermentative power of most sweet compounds tested. Although there are species using carbohydrates, such as *Haloferax mediterranei*, *Haloarcula mamarismortui* and *Halococcus sacharolyticus*, which catabolize hexoses (glucose, fructose), pentoses (arabinose, xylose), sucrose and lactose, other halophilic *Archaea* such as *H. salinarum* are not able to degrade them (Oren, 2008). Species that do not use carbohydrates degrade amino acids and compounds typical of hypersaline habitats. *Haloferax volcanii*, for example, is able to grow on glycerol and organic acids excreted by halophilic algae *Dunaliella salina* and *Microcoleus chthonoplasts*, respectively (Akmoussi-Toumi et al., 2018; Cuadros-Orellana et al., 2012; Henriot et al., 2014; McGenity and Grant, 1995).

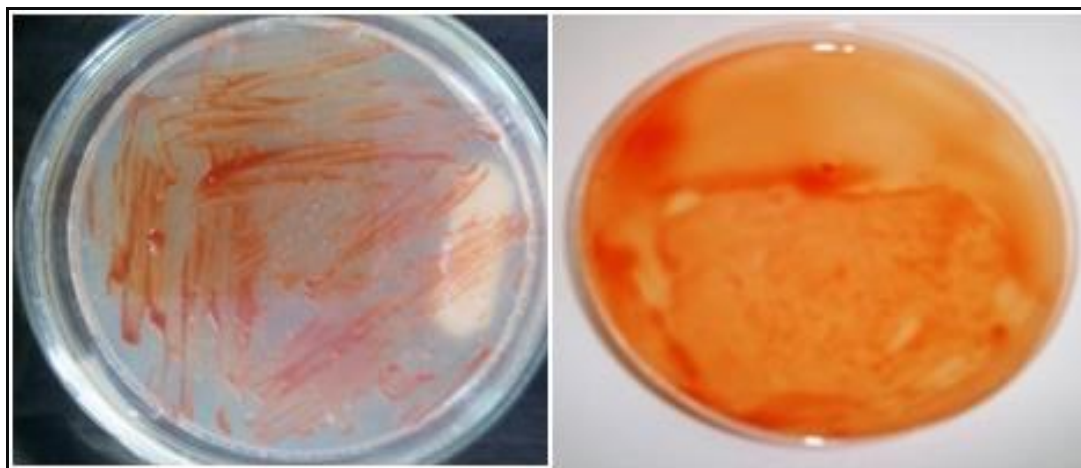


Figure 2. Colony of strain XA2 obtained on enrichment agar medium, after 7-10 days of incubation at 40°C.

Table 2. Phenotypic, biochemical and physiological characters of the isolates

Characteristics	Isolated strains											
	XA1	XA2	XC1	XC2	XE1	WA1	WC1	YA2	YA3	YF2	ZC1	ZD1
Pigmentation	Brick red	Orange red	Red	Orange	Light red	Red	Dark red	Light red	Orange red	Orange	Orange	Orange red
Cells shape	P	P	C	C	P	P	C	P	C	C	C	C
Gram staining	-	-	-	-	-	-	-	-	-	-	-	-
NaCl range (%)	10- 30	20- 30	20- 30	15- 30	15- 30	20-30	15-30	20-30	15-30	15-30	20-30	15-30
pH range	7- 9	6- 9	7- 8	7- 9	7- 9	6-9	7-9	7-8	7-9	7-9	6-9	6-9
T° range (°C)	30- 50	25- 50	30- 50	30- 50	30- 50	30-60	30-50	30-60	30-50	30-50	30-50	30-50
Acid production from												
Glucose	+	+	+	+	+	+	+	+	+	+	+	+
Lactose	+	-	-	-	-	+	-	-	-	-	-	-
Mannitol	-	+	-	-	-	-	-	-	-	-	+	-
Saccharose	-	-	-	-	-	-	-	-	-	-	-	-
Xylose	-	-	-	-	+	-	-	-	-	-	-	+
Fructose	-	-	-	-	-	-	-	-	-	-	-	-
Arabinose	-	-	-	-	-	-	-	-	-	-	-	-
Rhamnose	-	-	-	-	-	-	-	-	-	-	-	-
Ribose	-	-	-	-	-	-	-	-	-	-	-	-
Sorbitol	-	-	-	-	-	-	-	-	-	-	-	-

P, Pleomorph, C, Cocci, +, Positive; -, Negative

Phylogenetic studies based on the partial 16S rRNA gene are the main tool for delineating hierarchical relationships between different organisms (Amoozegar et al., 2017; Grant et al., 2011). The phylogenetic tree based on the gene encoding the partial 16S rRNA of the isolated identified strains is shown in *Figure 3*. The phylogenetic characteristics of isolated halophilic *Archaea* are given in *Table 3*. After DNA isolation, amplification and sequencing of 16S rRNA, partial sequence analysis from the Archaeal strain library indicated that the isolated strains were related to the order *Halobacteriales*. Partial sequencing showed a high degree of similarity with the closest species, with significant phylogenetic diversity (*Tables 3* and *4*).

The sequencing allowed us to identify strains isolated from seven different Archean genera belonging to *Halobacteriaceae*: for Biskra sebkha; *Halorubrum sp.* strain XA1, *Natribaculum sp.* strain XC1, *Haloarcula sp.* strains XC2 and XE1 and *Natrinema sp.* strain XE2. Their partial 16S rDNA gene sequences have been deposited in GenBank under the accession numbers: MN393054, MN393056, MN393057, MN393058 and MN393086, respectively (*Fig. 3*). The partial 16S rDNA sequence of the isolated strain XA1 (559 bp) gave 94.29% match with *Halorubrum terrestre* (KY129965), *Halorubrum litoreum* (LN649886), *Halorubrum chaoviator* (LN649850) and *Halorubrum distributum* (NR_113475). The partial 16S rDNA sequence of the XC1 strain (567 bp) showed a correspondence of 99.47% with *Natribaculum longum* (KF739019) and 99.12% with *Natribaculum breve* (KF739011). However, the phylogenic position of this strain places it in the genus *Natribaculum*. The partial 16S rDNA sequence of strain XC2 (547 bp) has 93.20% sequence identity with *Haloarcula hispanica* (NR112194). The partial 16S rDNA sequence of the halophilic isolate XE1 (560 bp) gave a match of 99.64% with *Haloarcula amylolytica* (KY411772), *Haloarcula argentinensis* (LC198790), *Haloarcula janonica* (LC085249), *Haloarcula hispanica* (LN649974), *Haloarcula tradensis* (KF962648) and *Haloarcula salaria* (KF962645). Finally, the partial 16S rDNA sequence of the halophilic isolate XE2

(571 bp) gave a match of 99.88% with *Natrinema altunense* (MK490895), *Natrinema pallidum* (LC331311), *Natrinema salaciae* (AB935413), *Natrinema gari* (JF802154) and *Natrinema ajinwuensis* (AY570917).

Table 3. Phylogenetic characterization of the isolated strictly halophilic *Archaea* strains (Biskra and Oum Bouaghi sebkhas)

Strain ID	Strain name (accession number)	Sequence length	Closely related validly published taxa	Similarity of 16S rRNA gene sequence (%)
XA1	<i>Halorubrum sp.</i> (MN393054)	559 bp	<i>Halorubrum terrestre</i> (KY129965)	94.29
			<i>Halorubrum litoreum</i> (LN649886)	94.29
			<i>Halorubrum chaoviator</i> (LN649850)	94.29
			<i>Halorubrum distributum</i> (NR_113475)	94.29
XC1	<i>Natribaculum sp.</i> (MN393056)	567 bp	<i>Natribaculum longum</i> (KF739019)	99.47
			<i>Natribaculum breve</i> (KF739011)	99.12
XC2	<i>Haloarcula sp.</i> (MN393057)	547 bp	<i>Haloarcula hispanica</i> (NR112194)	93.20
XE1	<i>Haloarcula sp.</i> (MN393058)	560 bp	<i>Haloarcula amylolytica</i> (KY411772)	99.64
			<i>Haloarcula argentinensis</i> (LC198790)	99.64
			<i>Haloarcula janonica</i> (LC085249)	99.64
			<i>Haloarcula hispanica</i> (LN649974)	99.64
			<i>Haloarcula tradensis</i> (KF962648)	99.64
			<i>Haloarcula salaria</i> (KF962645)	99.64
XE2	<i>Natrinema sp.</i> (MN393086)	571 bp	<i>Natrinema altunense</i> (MK490895)	94.88
			<i>Natrinema pallidum</i> (LC331311)	94.88
			<i>Natrinema salaciae</i> (AB935413)	94.88
			<i>Natrinema gari</i> (JF802154)	94.88
			<i>Natrinema ajinwuensis</i> (AY570917)	94.88
WA1	<i>Halorubrum sp.</i> (MN393054)	590 bp	<i>Halorubrum xinjiangense</i> (JF261094)	99.83
			<i>Halorubrum trapanicum</i> (NR_112869)	99.83
			<i>Halorubrum terrestre</i> (KY129965)	99.66
			<i>Halorubrumchaoviator</i> (LN649850)	99.66
			<i>Halorubrum litoreum</i> (HM748596)	99.66
WC1	<i>Haloarcula sp.</i> (MN392906)	569 bp	<i>Haloarcula amylolytica</i> (KJ499812)	93.10
			<i>Haloarcula marismortui</i> (AY994193)	93.10
			<i>Haloarcula vallismortis</i> (LC198794)	92.92
			<i>Haloarcula salaria</i> (NR_116666)	92.74
			<i>Haloarcula hispanica</i> (DQ089682)	92.74

For Oum El Bouaghi sebkha; *Halorubrum sp.* strain WA1, *Haloarcula sp.* strain WC1. Their partial 16S rDNA gene sequences have been deposited in GenBank under the accession numbers: MN393054 and MN392906, respectively (Fig. 3). The partial 16S rDNA sequence of the isolated strain WA1 (590 bp) gave 99.83% match with *Halorubrum xinjiangense* (JF261094), *Halorubrum trapanicum* (NR_112869), 99.66% match with *Halorubrum terrestre* (KY129965), *Halorubrum chaoviator* (LN649850) and *Halorubrum litoreum* (HM748596). The partial 16S rDNA sequence of the isolated strain WC1 (569 bp) gave 93.10% match with *Haloarcula amylolytica* (KJ499812) and *Haloarcula marismortui* (AY994193), 92.92% match with *Haloarcula vallismortis* (LC198794) and 92, 74% match with *Haloarcula salaria* (NR_116666) and *Haloarcula hispanica* (DQ089682).

For Ain Beida Sebkha; *Halostagnicola sp.* strain YA2, *Haloferax sp.* strain YA3 and *Halorubrum sp.* strain YF2. Their partial sequences of the 16S rDNA gene have been deposited in GenBank under the accession numbers: MN393084, MN393084 and

MN393087 respectively (Fig. 3). The partial 16S rDNA sequence of the isolated strain YA2 (568 bp) gave 99.82% match with *Halostagnicola larsenii* (NR_028169), 98.40% match with *Halostagnicola kamekurae* (KF650665), 98.23% match with *Halostagnicola alkaliphila* (MN713677) and 97.88% match with *Halostagnicola bangensis* (NR_134744). The partial 16S rDNA sequence of the isolated strain YA3 (576 bp) gave 99.82% match with *Haloferax lucentense* (MH062946), 99.66% match with *Haloferax sulfurifontis* (MG213726), 99.65% match with *Haloferax volcanii* (JX646768) and *Haloferax alexandrinus* (JX646752) and 99.30% match with *Haloferax prahovense* (NR_028165). The partial 16S rDNA sequence of the isolated strain YF2 (565 bp) gave 99.82% match with *Halorubrum xinjiangense* (NR_113491) and *Halorubrum trapanicum* (NR_112869) and 99.29% match with *Halorubrum terrestre* (KY129965), *Halorubrum litoreum* (LN649886) and *Halorubrum chaoviator* (LN649850).

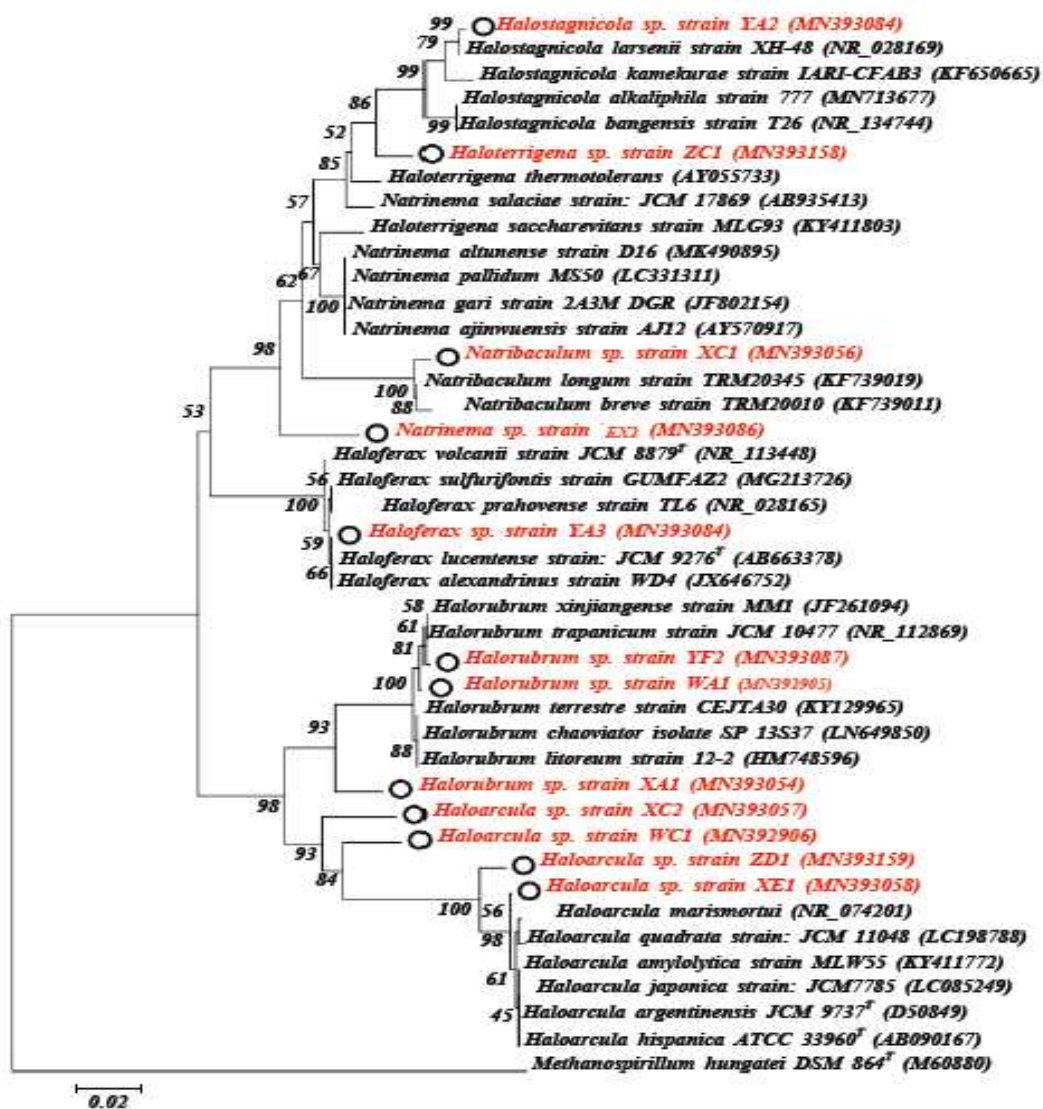


Figure 3. Phylogenetic tree based on the gene encoding 16S rRNA showing the result of the phylogenetic identification of identified and isolated strains of studied sebkhas. The tree is obtained using the software MEGA.7. Rooting was performed using the ribosomal sequence of Archaea *Methanospirillum hungatei*

Table 4. Phylogenetic characterization of the isolated halophilic *Archaea* strains (Ain Beida and Oum Reneb sebkhas)

Strain ID	Strain name (Accession number)	Sequence length	Closely related validly published taxa	Similarity of 16S rRNA gene sequence (%)
YA2	<i>Halostagnicola sp.</i> (MN393084)	568 bp	<i>Halostagnicola larsenii</i> (NR_028169)	99.82
			<i>Halostagnicola kamekurae</i> (KF650665)	98.40
			<i>Halostagnicola alkaliphila</i> (MN713677)	98.23
			<i>Halostagnicola bangensis</i> (NR_134744)	97.88
YA3	<i>Haloferax sp.</i> (MN393084)	576 bp	<i>Haloferax lucentense</i> (MH062946)	99.82
			<i>Haloferax sulfurfontis</i> (MG213726)	99.66
			<i>Haloferax volcanii</i> (JX646768)	99.65
			<i>Haloferax alexandrinus</i> (JX646752)	99.65
			<i>Haloferax prahovense</i> (NR_028165)	99.30
YF2	<i>Halorubrum sp.</i> (MN393087)	565 bp	<i>Halorubrum xinjiangense</i> (NR_113491)	99.82
			<i>Halorubrum trapanicum</i> (NR_112869)	99.82
			<i>Halorubrum terrestre</i> (KY129965)	99.29
			<i>Halorubrum litoreum</i> (LN649886)	99.29
			<i>Halorubrum chaoviator</i> (LN649850)	99.29
ZC1	<i>Haloterrigena sp.</i> (MN393158)	582 bp	<i>Haloterrigena thermotolerans</i> (AY055733)	96.20
			<i>Halostagnicola alkaliphila</i> (MN713677)	95.68
			<i>Haloterrigena saccharevitans</i> (KY411803)	95.68
ZD1	<i>Haloarcula sp.</i> (MN393159)	588 bp	<i>Haloarcula vallismortis</i> (KR866136)	98.62
			<i>Haloarcula marismortui</i> (NR_074201)	98.62
			<i>Haloarcula californiae</i> (LC198792)	98.45
			<i>Haloarcula amylytica</i> (KY411772)	98.28
			<i>Haloarcula argentinensis</i> (LC198790)	98.28
			<i>Haloarcula quadrata</i> (LC198788)	98.28
			<i>Haloarcula japonica</i> (LC085249)	98.28
			<i>Haloarcula tradensis</i> (KJ875316)	98.28

For Oum Reneb sebkha; *Haloterrigena sp.* strain ZC1 and *Haloarcula sp.* strain ZD1. Their partial sequences of the 16S rDNA gene have been deposited in GenBank under the accession numbers: MN393158 and MN393159 respectively (Fig. 3). The partial 16S rDNA sequence of the isolated strain ZC1 (582 bp) gave 96.20% match with *Haloterrigena thermotolerans* (AY055733), 95.68% match with *Halostagnicola alkaliphila* (MN713677) and *Haloterrigena saccharevitans* (KY411803). The partial 16S rDNA sequence of the isolated strain ZD1 (588 bp) gave 98.62% match with *Haloarcula vallismortis* (KR866136) and *Haloarcula marismortui* (NR_074201), 98.45% match with *Haloarcula californiae* (LC198792), 98.28% match with *Haloarcula amylytica* (KY411772), *Haloarcula argentinensis* (LC198790), *Haloarcula quadrata* (LC198788), *Haloarcula japonica* (LC085249) and *Haloarcula tradensis* (KJ875316). Obviously, more extensive analysis, as well as sequencing of the total 16S rDNA genes and DNA/DNA hybridation, are required in order to determine the correct phylogenetic position of the halophilic isolated strains. So, the genus *Halorubrum* was proposed in 1995 by Mc Genity and Grant (1995), the genus *Haloarcula* was created by Torreblanca et al. cited by Baliga et al. (2004). The genus *Natribaculum* was created by Liu et al. (2015) and the genera cited by Oren and Ventosa (2000). Finally, identification of a part of a DNA sequence, usually then related to the full-length sequence by alignment. The determinations of the phylogenetic relationships of some of these obligatorily inter and intracellular organisms are essential and a DNA-

DNA hybridization study is needed to confirm. The complete 16S rRNA gene sequence analysis can better identify poorly described, rarely isolated, or phenotypically aberrant strains, can be used for identification of halobacteria. So far, only a few reports have been produced on isolation, the characterization of *Archaea* halophiles isolated from the Algerian saline ecosystem. These studies focused mainly on saline lakes (Akmoussi-Toumi et al., 2018; Boutaiba et al., 2011; Imadalou-Idres et al., 2013; Kebbouche-Gana et al., 2009; Quadri et al., 2016; Makhdoumi-Kakhki et al., 2011; Menasria et al., 2018). Kharroub et al. (2014) reported the isolation of ten strains of Oum Bouaghi sebkha. These strains are related to four genera of halophilic *Archaea* (*Halorubrum*, *Halobacterium*, *Haloarcula*, *Haloferax* and *Haloterrigena*). Quadri et al. (2016) isolated eighteen strains from the Ouargla sebkha belonging to genera (*Natrialba*, *Halovivax* and *Haloferax*). Imadalou-Idres (2013) isolated six strains of *Archaea* halophilic from the sebkha of Oran description of four strains of *Haloarcula* and two strains of *Halorubrum*. Moreover, to the best of our knowledge, our study remains the first report of the presence of *Natribaculum* in the salt lakes of the Algerian Sahara.

Screening of enzyme producing strains

Halophile enzymes, useful in biotechnology, represent the main industrial interest, because they can function at salinity within the limits of life. The low level of contamination in their culture media due to the high salt concentration is another advantage for the industrial application of halophilic enzymes (Antranikian and Egorova, 2007; Bajpai et al., 2015; Delgado-García et al., 2012; Menasria et al., 2018). The extreme adaptation of halophilic *Archaea* has attracted the attention of scientific researchers because of their capacity to produce active enzymes and pigments with important biotechnological applications (Antranikian and Egorova, 2007; Bajpai et al., 2015; Delgado-García et al., 2012; Klingl, 2014; Menasria et al., 2018).

In the present study, the screening of twelve isolates of *Archaea* for active extracellular halophilic enzymes showed that our isolates produced at least one hydrolytic enzyme apart from the YA3 *Haloferax* sp strain (Tables 5 and 6; Fig. 4). The halophilic *Archaea* strains tested exhibit significant enzymatic potential, reflected by their ability to hydrolyze gelatin and casein (*Natribaculum* sp “XC1”, *Haloarcula* sp “XC2, XE1, ZD1 and WC1”, *Halorubrum* sp “WA1” and *Haloterrigena* sp “ZC1”), to produce lipase (*Haloarcula* sp “XE1”, *Halostagnicola* sp “YA2” and *Haloterrigena* sp “ZC1”) and degrades cellulose (*Haloterrigena* sp “ZC1” and *Haloarcula* sp “ZD1”). However, the isolates (*Halorubrum* sp “XA1 and YF2”, *Haloarcula* sp “XC2 and XE1” and *Haloterrigena* sp “ZC1”) showed extracellular amylase activity. It is important to note that all these enzymatic activities occurred at high salt concentration (20% NaCl). Furthermore, Kharroub et al. (2014), reported that the most degraded substrate by the strains tested, is starch, while several strains had gelatinase, amylase and lipase. The diversity of extreme halophilic archaea producing different hydrolases isolated from salt lakes, concluding that *Halorubrum* and *Haloarcula* are the dominant haloarchaeon genera with high-throughput enzyme production, including amylase and lipase (Makhdoumi-Kakhki et al., 2011). The diversity of hydrolytic enzymes in halophilic *Archaea* strains isolated from Salt Lake in Iran has shown that the genera *Halorubrum*, *Haloarcula* and *Natrinema* contain the largest number of strains with enzymatic activity (Delgado-García et al., 2012). *Archaea* are an important source of enzymes, including proteases, for applied research as well as basic enzymology. Protease activities of the *Haloferax* and *Natrialba*

species have been the subject of previous studies (Grant et al., 2012). Hyper-saline environments represent a source of potentially interesting hydrolytic enzymes, whose haloarchaeon strains isolated from these environments could generate a number of viable economic applications (Antranikian and Egorova, 2007; Henri et al., 2014; Oztetik and Cakir, 2014). The catalytic properties of these halophilic enzymes have applications in different fields such as the food industry and biotechnological processes as additives in detergents (Antranikian and Egorova, 2007; Amoozegar et al., 2017; Henri et al., 2014; McGenity and Grant, 1995).

Table 5. Screening result of enzyme producing strains

Hydrolysis of	Isolated strains						
	XA1	XC1	XC2	XE1	XE2	WA1	WC1
	<i>Halorubrum sp</i>	<i>Natribaculum sp</i>	<i>Haloarcula sp</i>	<i>Haloarcula sp</i>	<i>Natrinema sp</i>	<i>Halorubrum sp</i>	<i>Haloarcula sp</i>
Starch	+	-	+	+	+	-	-
Gelatin	-	+	+	+	-	+	+
Casein	-	+	+	+	-	+	+
Tween 80	-	-	-	+	-	-	-
Cellulose	-	-	-	-	-	-	-

+, positive; -, negative

Table 6. Screening result of enzyme producing strains (continued)

Hydrolysis of	Isolated strains				
	YA2	YA3	YF2	ZC1	ZD1
	<i>Halostagnicola sp</i>	<i>Haloferax sp</i>	<i>Halorubrum sp</i>	<i>Haloterrigena sp</i>	<i>Haloarcula sp.</i>
Starch	-	-	+	-	+
Gelatin	-	-	-	+	+
Casein	-	-	-	+	+
Tween 80	+	-	-	+	-
Cellulose	-	-	-	+	+

+, positive; -, negative

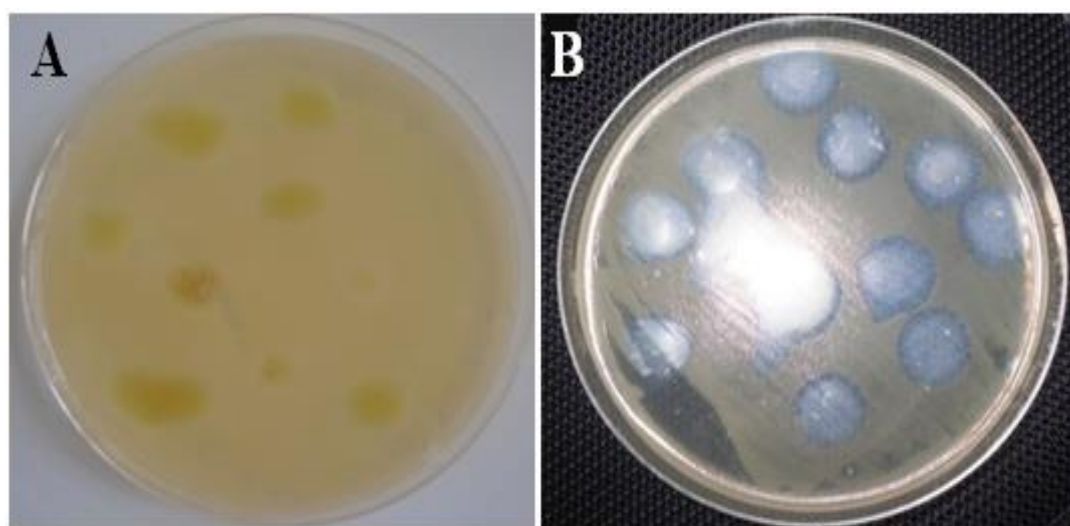


Figure 4. Screening of halophilic active enzymes (*XE1* strain) using a drop spot technique. (A) Amylase; (B) Lipase

Conclusion

The physicochemical analysis study of the waters of the sebkhas studied located in the north-east of the Algerian Sahara, and their comparison with other aquatic super-saline ecosystems of the world, in particular their alkalinity and salinity, was studied for the first time. The microbiological study showed a remarkable morphological, physiological and metabolic diversity of the isolated strains. We have new access to an archaeal diversity including extremely halophilic alkalo-thermotolerant strains belonging to the order *Halobacteriales* : *Halorubrum sp*, *Natribaculum sp*, *Haloarcula sp*, *Natrinema sp*, *Halostagnicola sp*, *Haloferax sp* and *Haloterrigena sp*, until now isolated for the first time in the hyper-saline environments of northern Algerian Sahara. The hyper-saline environments represent a source of potentially interesting bioactive molecules, whose haloarchaeal strains isolated from these environments could generate a number of viable economic applications. As most of the currently used enzymes are known mainly for their instability and fragility under extreme conditions, the search for new, more stable enzymes has therefore become a property. In the present study, many isolates showed several combined hydrolytic activities mainly the ZD1 strain affiliated with *Haloarcula*. The *Haloterrigena* affiliated ZC1 strain also displays interesting hydrolytic activities. Complementary work on these two strains is planned for the study of the other enzymes of biotechnological interest and secondary metabolites with novel therapeutic activities (e.g. anti-cancer effect).

Acknowledgments. We thank Pr Idir BITAM and Pr Michel DRANCOURT Michel, the members of MEPHI (Aix-Marseille France) for their technical assistance, and the access to the laboratories. Also, to DGRSDT for the support provided to the research.

Disclosure statement. No potential conflict of interests was reported by the authors.

REFERENCES

- [1] Abd-Elhalem, B. T., El-Sawy, M., Gamal, R. F., Abou-Taleb, K. A. (2015): Production of amylases from *Bacillus amyloliquefaciens* under submerged fermentation using some agro-industrial by-products. – *Ann AgricSci* 60: 193-202.
- [2] Akmoussi-Toumi, S., Khemili-Talbi, S., Kebbouche-Gana, S., Ferrioune, I. (2018): Purification and characterization of an organic solvent-tolerant and detergent stable lipase from *Haloferax mediterranei* CNCMM 50101. – *International Journal of Biological Macromolecules* 116: 817-830.
- [3] American Public Health Association. (2005): *Standard Methods for the Examination of Water and Wastewater*. 21st Ed. – American Water works Association and Water Pollution Control Federation, Baltimore, MD.
- [4] Amoozegar, M. A., Siroosi, M., Atashgahi, S., Smidt, H., Ventosa, A. (2017): Systematics of haloarchaea and biotechnological potential of their hydrolytic enzymes. – *Microbiology* 163: 623-645.
- [5] Antranikian, G., Egorova, K. (2007): Extremophiles a Unique Resource of Biocatalysts for Industrial Biotechnology. – In: Gerday, C., Glansdorff, N. (eds.) *Physiology and Biochemistry of Extremophile*. Wiley, Hoboken, NJ.
- [6] Atanasova, N. S., Pietila, M. K., Oksanen, H. M. (2013): Diverse antimicrobial interactions of halophilic archaea and bacteria extend over geographical distances and cross the domain barrier. – *Microbiol* 2(5): 811-825.

- [7] Bajpai, B., Chaudhary, M., Saxena, J. (2015): Production and characterization of alpha-amylase from an extremely halophilic archaeon, *Haloferax* sp. HA10. – Food Technology and Biotechnology 53: 11-17.
- [8] Baliga, N. S., Bonneau, R., Facciotti, M. T., Pan, M., Glusman, G. et al. (2004): Genome sequence of *Haloarcula marismortui*: a halophilic archaeon from the Dead Sea. – Genome Research 14: 2221-2234.
- [9] Boutaiba, S., Hacène, H., Bidle, K. A., Maupin-Furlow, J. A. (2011): Microbial diversity of the hypersaline SidiAmeur and Himalatt Salt Lakes of the Algerian Sahara. – Arid Environments 75(10): 909-916. <https://doi.org/10.1016/j.jaridenv.2011.04.010>.
- [10] Castillo, A. M., Gutiérrez, M. C., Kamekura, M., Ma, Y., Cowan, D. A. et al. (2006): *Halovivax asiaticus* gen. nov., sp. nov., a novel extremely halophilic archaeon isolated from Inner Mongolia, China. – International Journal of Systematic and Evolutionary Microbiology 56: 765-770.
- [11] Cuadros-Orellana, S., Pohlschroder, M., Grossman, M. J., Durrant, L. R. (2012): Biodegradation of aromatic compounds by a halophilic archaeon isolated from the Dead Sea. – Chemical Engineering Transactions 27: 3-18.
- [12] Delgado-García, M., Valdivia-Urdiales, B., Aguilar-González, C. N., Contreras-Esquível, J. C., Rodríguez-Herrera, R. (2012): Halophilic hydrolases as a new tool for the biotechnological industries. – J. Sci. Food Agric 92: 2575-2580.
- [13] Gana, M. L., Kebbouche-Gana, S., Touzi, A., Pauss, A., Lounici, H. et al. (2010): Antagonistic activity of *Bacillus* sp. obtained from an Algerian oilfield and chemical biocide THPS against Sulfate-reducing bacteria consortium inducing corrosion in the oil industry. – Journal of Industrial Microbiology and Biotechnology 38(3): 391-404.
- [14] Ghanem, A. (2007): Trends in lipase-catalyzed asymmetric access to antiomerically pure/enriched compounds. – Tetrahedron 63(8): 1721-1754.
- [15] Grant, W. D., Pagaling, E., Marquez, M. C., Gutiérrez, M. C., Cowan, D. A. et al. (2011): The Hypersaline Lakes of Inner Mongolia. – In: Ventosa, A., Oren, A., Yanhe, M. (eds.) Halophiles and Hypersaline Environments. Springer-Verlag, Berlin, pp. 65-107.
- [16] Henriot, O., Fourmentin, J., Delincé, B., Mahillon, J. (2014): Exploring the diversity of extremely halophilic archaea in food-grade salts. – International Journal of Food Microbiology 191: 36-44.
- [17] Imadalou-Idres, N., Carré-Mlouka, A., Vandervennet, M., Yahiaoui, H., Peduzzi, J. et al. (2013): Diversity and antimicrobial activity of cultivable halophilic archaea from three Algerian sites. – Journal of Life Sciences 7: 1057-1069.
- [18] Joint, I., Mühling, M., Querellou, J. (2010): Culturing marine bacteria an essential prerequisite for biodiscovery. – Microb. Biotechnol 3: 564-575.
- [19] Kebbouche-Gana, S., Gana, M. L., Khemili, S., Fazouane-Naimi, F., Bouanane, N. A. et al. (2009): Isolation and characterization of halophilic Archaea able to produce biosurfactants. – Journal of Industrial Microbiology & Biotechnology 36(5): 727-738.
- [20] Kharroub, K., Gomri, M. A., Aguilera, M., Monteoliva-Sanchez, M. (2014): Diversity of hydrolytic enzymes in haloarchaea isolated from Algerian sabkhas. – African Journal of Microbiology Research 56: 1583-1588.
- [21] Klingl, A. (2014): S-layer and cytoplasmic membrane – exceptions from the typical archaeal cell wall with a focus on double membranes. – Frontiers in Microbiology 5: 624-2. DOI: 10.3389/fmicb.2014.00624.
- [22] Latorre, J. D., Hernandez-Velasco, X., Wolfenden, R. E., Vicente, J. L., Wolfenden, A. D., et al. (2016): Evaluation and selection of *Bacillus* species based on enzyme production, antimicrobial activity, and bio-film. – Front Vet Sci. DOI: 10.3389/fvets.2016.00095.
- [23] Lenchi, N., Kebbouche, S., Khelifaoui, M. L., Laddada, B., Khemili, S., Gana, M. L., Akmoussi, S., Ferioune, I. (2020): Phylogenetic characterization and screening of halophilic bacteria from Algerian salt lake for the production of biosurfactant and

- enzymes. – World Journal of Biology and Biotechnology 5(2).
<https://doi.org/10.33865/wjb.005.02.0294>.
- [24] Litchfield, B., Dalmat, S. (2009): Microbial diversity in hypersaline environments. – Proceedings of the 2nd International Conference on the Ecological Importance of Solar Saltworks (CEISSA2009). Merida, Yucatan, Mexico, pp. 26-29.
- [25] Liu, Q., Ren, M., Zhang, L. L. (2015): *Natribaculum* breve gen. nov., sp. nov. and *Natribaculumlongum* sp. nov., halophilic archaea isolated from saline soil. – Int J Syst Evol Microbiol 65(Pt 2): 604-608.
- [26] Madigan, M. T., Martinko, J. M. (2006): Brock Biology of Microorganisms. 11th Ed. – Pearson Prentice Hall, Upper Saddle River, NJ.
- [27] Makhdoumi-Kakhki, A., Amoozegar, M. A., Mahmodi-Khaledi, E. (2011): Diversity of hydrolytic enzymes in haloarchaeal strains isolated from Salt Lake. – Int. J. Environ. Sci. Technol 8: 705-714.
- [28] McGenity, T. J., Grant, W. D. (1995): Transfer of *Halobacterium* *saccharovorum*, *Halobacterium* *sodomense*, *Halobacterium* *trapanicum* NRC 34021 and *Halobacterium* *lacusprofundito* the genus *Halorubrum* gen. nov., as *Halorubrum* *saccharovorum* comb. nov., *Halorubrum* *sodomense* comb. nov., *Halorubrum* *trapanicum* comb. nov., and *Halorubrum* *lacusprofundi* comb. nov. – Syst Appl Microbiol 18: 237-243.
- [29] Menasria, T., Aguilera, M., Hocine, H., Benammar, L., Ayachi, A. et al. (2018): Diversity and bioprospecting of extremely halophilic archaea isolated from Algerian arid and semi-arid wetland ecosystems for halophilic-active hydrolytic enzymes. – Microbiological Research 207: 289-298.
- [30] Oren, A. (2008): Microbial life at high salt concentrations: phylogenetic and metabolic diversity. – Saline Systems 4: 2.
- [31] Oren, A., Ventosa, A. (2000): International Committee on Systematic Bacteriology Subcommittee on the taxonomy of Halobacteriaceae. Minutes of the meetings, 16 August 1999, Sydney, Australia. – Int. J. Syst. Evol. Microbiol 50: 1405-1407.
- [32] Oztetik, E., Cakir, A. (2014): New Food for an old mouth: new enzyme for an ancient Archaea. – Enzyme and Microbial Technology 55: 58-64.
- [33] Quadri, I., Hassani, I., Chalopin, M., Hacene, H., Jebbar, M. (2016): Characterization and antimicrobial potential of extremely halophilic archaea isolated from hypersaline environments of the Algerian Sahara. – Microbiological Research 186-187: 119-3.
- [34] Roussel, E. G., Cambon Bonavita, M. A., Querellou, J., Cragg, B. A., Webster, G., et al. (2008): Extending the subsea-floor biosphere. Science 320(5879): 1046. *Salinicoccusiranensis* sp. nov., a novel moderate halophile. – Int J Syst Evol Microbiol 58: 178-183.
- [35] Saxena, K. R., Dutt, K., Agarwal, L., Nayyar, P. (2007): A highly and thermostable alkaline amylase from a *Bacillus* sp. PN5. – Bio-resource Techno 198: 260-265.
- [36] Tamura, K., Nei, M., Kumar, S. (2004): Prospects for inferring very large phylogenies by using the neighbor-joining method. – Proc Natl AcadSci USA 101: 11030-11035.

EFFECTS OF PYOCYANIN PIGMENT ON THE CHEMICAL AND PHYSICAL CHARACTERISTICS OF AGRICULTURAL SOILS

KIKI, M. J.

*The University of Jeddah, College of Science, Department of Biology, Jeddah, Saudi Arabia
e-mail: mjiki@uj.edu.sa*

(Received 27th Jan 2022; accepted 2nd May 2022)

Abstract. The widespread use of agricultural chemicals, such as pesticides and fertilizers, has caused imbalances in agricultural soil. The use of several alternative methods (such as bio-fertilizers) has been suggested. Recent studies have focused on the application of microbial products instead of microbial cells to enhance plant growth. The present study aimed to investigate the effects of pyocyanin (produced as a secondary metabolite by *Pseudomonas aeruginosa*) on the chemical and physical properties of agricultural soil. Two plants, *Lens culinaris* and *Eruca sativa*, were utilized in the study. Based on the results, soil treatment with pyocyanin caused significant increase in some nutrients and minerals such as magnesium, chlorine, and iron, levels of which rose gradually with increasing pyocyanin concentration in the soil from both plants. In contrast, a gradual decline in levels of certain heavy metals, such as copper, lead, manganese, and boron, were observed, and the highest concentrations were reported in the control samples. Positive correlation was observed between electrical conductivity and hydrogen ion concentration in the soil, both of which decreased gradually with increasing pyocyanin concentration in the soil from both plants. Moreover, the *P. aeruginosa* strain studied herein showed significant antimicrobial activity against plant pathogenic fungi and bacteria. Overall, the study proved the positive interplay between pyocyanin and environmental factors that affect the development of plants, making it an ideal target for extended future research according to its environmental and agricultural significance.

Keywords: *Pseudomonas aeruginosa*, bio-fertilizers, heavy metals, essential elements

Introduction

Soil nutrients are essential for plant development and crop production because they control many plant processes. Mineral nutrition has also been identified as an important component in plant disease management and nutrient availability through soil modification (Moreira et al., 2015). While nutrients may be available in the soil, their chemical properties may hinder plants from using them. There are several techniques for supplying plants with essential nutrients, including chemical and biological approaches (Miransari et al., 2014).

Plant growth-enhancing microorganisms, such as rhizobia, mycorrhizae, and plant growth promoting bacteria, have been found to increase plant development under both stressed and non-stressed condition, influencing micronutrient solubility in the soil and subsequently, absorption thereof by plants (Lim et al., 2019). Although these bacteria are naturally found in the rhizosphere and plant tissue, they are frequently insufficient to provide the desired effects. Resultantly, it is recommended to isolate and prepare them as a microbial inoculum (Bender et al., 2016). This employment of microorganisms by inoculation is known as bio-fertilization, which can influence soil nutrient availability and hence, plant development (Hirel et al., 2011).

Many studies have examined the capacity of microbial cells to inhibit plant diseases and alleviate the effects of abiotic stress on plants, with encouraging results (Lim et al., 2019). Recent research has suggested that microbial compounds can be utilized successfully, rather than microbes that cannot survive in harsh environments and even if they do, their effectiveness may be diminished. Further, compounds are less susceptible

to abiotic stress, and if the microorganisms are facultative pathogens, microbial compounds may be a preferable alternative (Compant et al., 2019).

Pseudomonas aeruginosa (*P. aeruginosa*); is a versatile bacterium found in a variety of aquatic and terrestrial habitats (Streeter and Katouli, 2016). Some strains are classified as rhizobacteria because they may colonize root surfaces and promote plant development (Anjaiah et al., 2003) whereas, other strains are capable of degrading environmental pollutants (Hasanuzzaman et al., 2004). It is also a notable opportunistic bacterium that may cause a range of diseases, including nosocomial infections (Del Barrio-Tofiño et al., 2020). Additionally, it has been reported as an effective agent in a variety of applications, including bio-control (Anjaiah et al., 2003) and bioremediation programs (Vieta et al., 2021). Moreover, it may produce several extracellular secondary metabolites, including pyocyanin pigment; this blue-green, water-soluble, nitrogen-containing, heterocyclic phenazin has enjoyed special interest due to its capacity to generate reactive oxygen species (Hassani et al., 2012). Pyocyanin has been used in biosensors as a redox chemical for electron transfer between enzyme molecules and electrode materials; these biosensors are intended for use in different arenas, including the environment, agriculture, and medicine (Priyaja et al., 2014). It also plays a role in the control of phytopathogens (Sudhakar et al., 2013).

Most previous studies involved the use of microorganisms as bio-fertilizers. However, current research is tending towards investigation the potential of microbial products as important plant growth regulators. Recently, pyocyanin has received considerable attention due to its beneficial properties and applications in several different fields. Accordingly, the present study was designed to determine the effects of pyocyanin pigment on the chemical and physical properties of agricultural soil. Two plants, *Eruca sativa* and *Lens culinaris* which are known as arugula and lentil, respectively, were employed in obtaining the research results. These two plants were selected regarding to their high nutritional value and their widespread around the world as agricultural crops.

Materials and methods

Isolation and cultivation of bacteria

The *P. aeruginosa* strain used in this research was isolated and identified in a previous study (Al-Zahrani, 2012), based on the cultural, morphological, and biochemical characteristics described by Schaad et al. (2001). It was cultured and preserved at 4 °C on cetrinide slant agar.

Antimicrobial activity of bacteria

The antimicrobial activity of the *P. aeruginosa* strain was tested using the agar plate diffusion technique described by Lim et al. (2019), against the pathogenic microorganisms *Rhizoctonia solani*, *Fusarium oxysporium*, *Staphylococcus aureus* and *Escherichia coli*. Screening was performed in triplicate using potato-dextrose-agar (PDA) medium for the fungi and Muller-Hinton medium for the bacteria. Growth inhibition of bacteria and fungi was measured after 24 h and 6 d, respectively.

Production of pyocyanin pigment

Selected colonies of *P. aeruginosa* were transferred from cetrimide agar to King's B broth medium to prepare the inoculums for pyocyanin pigment production, as described by Özyürek et al. (2016).

The effect of pyocyanin on soil

Digestion of soil samples

The soil that was used in this study is a mixture of peat-moss and sandy soil (2:1) obtained from the local market in Jeddah, in the west of Saudi Arabia. A known weight (0.5 g) of air-dried soil samples was used for digestion, following the procedure reported by Da-Silva (2013). Samples were placed in glass containers in the refrigerator at 4 °C, until use. All digestions were performed in triplicate.

Estimation of elements in the soil

Level of essential elements and heavy metals in digested dry soil samples, were estimated following the procedure reported by Cottenie et al. (1982). Additionally, hydrogen ion concentration (pH) and electrical conductivity (EC) were measured according to the procedure of Corwin and Yemoto (2020). All samples were analyzed thrice.

Soil treatment with pyocyanin

The effect of pyocyanin pigment on the chemical and physical properties of agricultural soil was studied using a crude solution of pigment, made up to different concentrations (5, 15, and 25%, respectively) by adding sterilized distilled water. *E. sativa* and *L. culinaris* seeds were grown in pots (30 diameter × 40 height) and irrigated every other day using pyocyanin solution. One month later, soil samples from the two plants were collected and analyzed to measure levels of essential elements, heavy metals, along with the pH and EC. All experiments were performed in triplicate.

Statistical analysis

All collected data were analyzed to determine the mean and standard deviation (SD) at $P \leq 0.05$, using SPSS software.

Results

Antimicrobial activity

The selected *Pseudomonas* strain was re-cultured on King's B medium and confirmed as *P. aeruginosa*, which was gram-negative, oxidase and catalase positive, did not ferment lactose, emitted a grape-like odor and produced blue-green pigment (*Fig. 1*).

The strain was tested for antimicrobial activity against different bacteria and fungi. The results are shown in *Table 1* and indicate antimicrobial activity against all tested microorganisms. The highest activity levels were reported against the fungi *R. solani* and *F. oxysporium*, with an average inhibition zone of 32 and 30 mm, respectively.

Antibacterial activity was monitored against both gram-positive and negative bacteria. The lowest activity level (inhibition zone diameter: 15 mm) was detected against *E. coli*,

whereas higher activity was perceived against gram-positive *S. aureus*, with an average diameter of the inhibition zone, of 28 mm.



Figure 1. Cultural characteristics of *Pseudomonas aeruginosa* and pyocyanin production on King's B agar, after 48 h at 37 °C

Table 1. Antimicrobial activity of *Pseudomonas aeruginosa* against tested microorganisms

Tested microorganisms	Inhibition zone diameter (mm) ± SD
<i>Rhizoctonia solani</i>	32 ± 0.03
<i>Fusarium oxysporium</i>	30 ± 0.00
<i>Staphylococcus aureus</i>	28 ± 0.04
<i>Escherichia coli</i>	15 ± 0.02

Essential elements in soils treated with pyocyanin

The results in Tables 2 and 3 reveal the response of some essential elements (Mg, Ca, N, Cl, Na, K, and P), which are present in the growing soil of *L. culinaris* and *E. sativa*, before and after exposure to different concentrations of pyocyanin. It was observed that magnesium content in the soil increased gradually with increasing pyocyanin concentration, for both plants. The highest magnesium concentration observed were 46% for *L. culinaris* and 45% for *E. sativa*, at pyocyanin concentration of 25%.

Table 2. Essential elements in *Lens culinaris* soil irrigated with different concentrations of pyocyanin

Pyocyanin conc.	Essential elements (%) ± SD						
	Cl	Na	Mg	Ca	K	P	N
Control	317.9 ± 0.02	0.13 ± 0.01	0.36 ± 0.01	0.20 ± 0.01	0.10 ± 0.00	0.02 ± 0.01	0.10 ± 0.01
5%	320.4 ± 0.01	0.11 ± 0.03	0.40 ± 0.03	0.12 ± 0.02	0.11 ± 0.01	0.02 ± 0.01	0.09 ± 0.02
15%	324.2 ± 0.01	0.12 ± 0.01	0.44 ± 0.05	0.11 ± 0.04	0.11 ± 0.01	0.02 ± 0.02	0.08 ± 0.02
25%	341.4 ± 0.04	0.12 ± 0.07	0.46 ± 0.02	0.10 ± 0.06	0.10 ± 0.02	0.01 ± 0.04	0.05 ± 0.01

Table 3. Essential elements in *Eruca sativa* soil irrigated with different concentrations of pyocyanin

Pyocyanin conc.	Essential elements (%) ± SD						
	Cl	Na	Mg	Ca	K	P	N
Control	248.5 ± 0.01	0.14 ± 0.01	0.30 ± 0.04	0.20 ± 0.02	0.10 ± 0.05	0.01 ± 0.01	0.15 ± 0.01
5%	267.5 ± 0.09	0.11 ± 0.03	0.36 ± 0.04	0.16 ± 0.05	0.10 ± 0.02	0.02 ± 0.02	0.13 ± 0.02
15%	280.5 ± 0.06	0.12 ± 0.01	0.38 ± 0.01	0.15 ± 0.02	0.11 ± 0.01	0.02 ± 0.00	0.09 ± 0.01
25%	284.4 ± 0.05	0.13 ± 0.03	0.45 ± 0.01	0.14 ± 0.00	0.12 ± 0.01	0.01 ± 0.01	0.06 ± 0.03

Similarly, soil treated with 25% pyocyanine exhibited the highest concentrations of chlorine, levels of which increased gradually in the soil of both plants, with increasing pyocyanin concentrations. Compared to the controls that reflected the lowest chlorine concentrations of 317.9% and 248.5% for *L. culinaris* and *E. sativa*, respectively. The highest concentrations were 314.4% for *L. culinaris* and 284.5% for *E. sativa* at 25% pyocyanin exposure.

In contrast, as pyocyanin concentration increased, the calcium and nitrogen content decreased. The lowest percentages of both elements were reported in soil treated with 25% pyocyanin, for both plants. No significant differences were observed in the levels of sodium, potassium, and phosphorus in soil treated with different concentrations of pyocyanin, compared to the control, for either plants.

Heavy metals in soils treated with pyocyanin

The data in Tables 4 and 5 reflect the heavy metal contents (Fe, Pb, B, Cu, Zn, and Mn) in the growing soil of *L. culinaris* and *E. sativa*, before and after treatment with different concentrations of pyocyanin. The iron concentration was highest in the soil samples before treatment, followed by manganese, while copper levels were the lowest. The results show different values of heavy metals in the soil when treated with different concentrations of pyocyanins, for both plants.

Table 4. Heavy metals in *Lens culinaris* soil irrigated with different concentrations of pyocyanin

Pyocyanin conc.	Heavy metals (ppm) ± SD					
	Pb	B	Cu	Zn	Mn	Fe
Control	27.7 ± 0.01	18.1 ± 0.00	13.6 ± 0.01	31.4 ± 0.02	105.4 ± 0.01	753.4 ± 0.02
5%	27.2 ± 0.02	15.1 ± 0.01	13.1 ± 0.01	42.9 ± 0.03	93.9 ± 0.01	760.7 ± 0.07
15%	22.3 ± 0.01	10.2 ± 0.06	12.0 ± 0.00	36.4 ± 0.05	92.3 ± 0.04	761.7 ± 0.03
25%	22.1 ± 0.04	5.5 ± 0.05	11.2 ± 0.01	35.5 ± 0.02	90.5 ± 0.02	774.7 ± 0.03

Table 5. Heavy metals in *Eruca sativa* soil irrigated with different concentrations of pyocyanin

Pyocyanin conc.	Heavy metals (ppm) ± SD					
	Pb	B	Cu	Zn	Mn	Fe
Control	24.7 ± 0.01	29.5 ± 0.01	15.3 ± 0.01	25.0 ± 0.01	100.1 ± 0.02	615.4 ± 0.05
5%	23.0 ± 0.01	18.5 ± 0.01	15.0 ± 0.02	30.6 ± 0.06	97.8 ± 0.02	761.7 ± 0.03
15%	21.4 ± 0.02	13.9 ± 0.05	13.0 ± 0.01	35.5 ± 0.05	87.8 ± 0.01	762.6 ± 0.07
25%	19.7 ± 0.02	10.4 ± 0.03	11.8 ± 0.04	33.5 ± 0.03	85.9 ± 0.05	775.7 ± 0.04

A gradual increase in iron level was observed with increasing pyocyanin, with the highest concentrations reported at 25% pyocyanin exposure; values were 774.7 ppm in *L. culinaris* soil and 775.7 ppm in *E. sativa* soil, compared to the control which 753.4 and 615.4 ppm were recorded for the two plants as mentioned above, respectively. Concerning zinc, the results showed varying values, with the highest concentration in *L. culinaris* being 42.9 ppm at 5% pyocyanin, and the highest concentration in *E. sativa* being 35.5 ppm at 15% pyocyanin.

The remaining heavy metals (lead, boron, copper, and manganese) concentrated in the control samples of growing soil of both plants, and gradually decreased with increasing pyocyanin concentration. The lowest values of all these elements were reported at 25% pyocyanin in the soil of both plants.

Soil electrical conductivity and pH

The EC of a soil solution is often used to determine the concentration of soluble salts in the soil. Herein, the EC of growing soil of *L. culinaris* and *E. sativa* was measured before and after treatment with different concentrations of pyocyanin. The results in Table 6 show that the highest rate of EC appeared in the control samples for both plants. It is notable that the EC rate decreased gradually with increasing pyocyanin in treatment, with the lowest values recorded as 0.56 and 0.44 dSm⁻¹, respectively at 25% pyocyanine.

Table 6. Electrical conductivity of soil treated with different concentrations of pyocyanin

Pyocyanin conc.	Electrical conductivity (dSm ⁻¹) ± SD	
	<i>Lens culinaris</i>	<i>Eruca sativa</i>
Control	1.38 ± 0.03	1.84 ± 0.01
5%	1.24 ± 0.01	1.01 ± 0.01
15%	1.02 ± 0.02	0.74 ± 0.02
25%	0.56 ± 0.06	0.44 ± 0.04

Table 7 illustrates the soil pH values before and after treatment with different concentrations of pyocyanin. The results revealed that soil pH decreased gradually with increasing pyocyanin concentrations, with the lowest values recorded as 8.75 and 8.81, respectively, at 25% pyocyanin.

Table 7. Hydrogen ion concentration of soil treated with different concentrations of pyocyanin

Pyocyanin conc.	Hydrogen ion concentration (pH) ± SD	
	<i>Lens culinaris</i>	<i>Eruca sativa</i>
Control	9.12 ± 0.00	9.35 ± 0.01
5%	9.11 ± 0.01	9.20 ± 0.02
15%	8.81 ± 0.02	9.13 ± 0.04
25%	8.75 ± 0.02	8.81 ± 0.03

Discussion

Antimicrobial activity

The relevant *P. aeruginosa* strain was tested for antimicrobial activity against different bacteria and fungi, as illustrated in *Table 1*. The results revealed higher inhibitory activity against fungi than bacteria. This finding supports the study outcomes of El-Fouly et al. (2015), who concluded that pyocyanin could modify and stop the electron transport chain in fungi, resulting in the formation of free oxygen radicals with antifungal properties. Moreover, Navarros et al. (2019) found that *Pseudomonas* species generate various phenazine chemicals with variable effectiveness against fungi.

Consistent with the findings of Özyürek et al. (2016), the present study showed that pyocyanin has a much stronger effect on gram-positive than gram-negative bacteria. According to a previous study by Das and Manefield (2012), variations in the lipid composition of the cell walls of gram-positive and negative bacteria may be responsible for this variance in pyocyanin sensitivity.

Essential elements in soils treated with pyocyanin

Tables 2 and *3* reflect the essential elements content of soil from both plants, treated with different concentrations of pyocyanin during this study. It is clearly shown that magnesium levels increased with increasing pyocyanin concentration. This result is significant since magnesium is a vital nutrient in plant physiology, as it is required for photosynthesis and involved in the chlorophyll structure (Moreira et al., 2015). Further, it can alleviate the symptoms of 22 different plant diseases (Huber and Jones, 2012).

The same observation was made regarding chlorine, which also increased with increasing pyocyanin concentrations in soil from both plants. According to several previous studies, chlorine is one of the elements of which large amounts can be detected in soil. It is involved in the regulation of cytoplasmic enzyme activities, turgor pressure and pH, along with photosynthesis, and contributes to stabilization of the membrane potential (Baetz et al., 2016). Chlorine deficiency is uncommon because its levels in soil are often high and plants only require minimal quantities (White and Broadley, 2001). Moreover, it has been observed that chlorine homeostasis in plants is strongly connected to salt tolerance (Vatansever et al., 2016).

However, the percentages of calcium and nitrogen, were shown to decrease with increasing pyocyanin in soil from both plants. Previous studies suggest that nitrogen which is more mobile under humid circumstances is susceptible to processes such as leaching and denitrification, reducing its availability to the plant (Miransari et al., 2014).

In general, this study clearly indicated that pyocyanin influences the availability of several crucial nutrients and changes the soil characteristics. These findings are consistent with those of previous research, (Gupta et al., 2015; Naamala and Smith, 2020), which suggested that the addition of microbial products to soil as bio-fertilizer, could improve the availability and absorption of critical plant nutrients.

Heavy metals in soils treated with pyocyanin

Tables 4 and *5* illustrate the heavy metal content in the soil samples from both plants, before and after treatment with pyocyanin. A gradual rise in iron concentration was observed with increasing exposure to pyocyanin. This result may be explained by the findings of Cox (1986), which indicated that pyocyanin can be involved in solubilizing and releasing iron. Additionally, another study (Jayaseelan et al., 2013) found that

pyocyanin is involved in iron metabolism and contributes to a process capable of reducing and releasing iron.

Zinc showed varying responses to different concentrations of pyocyanin, as illustrated by the results. According to Vatansever et al. (2016), zinc is a vital element for plant development and crop production, and it is influenced by soil microbial activity. Another study (He et al., 2010) indicated that zinc-tolerant bacterial strains such as *P. aeruginosa* can enhance zinc availability in soil and resultantly, its absorption by plants which is also important in bioremediation. The results also revealed a gradual decrease in the concentrations of other heavy metals (lead, boron, copper, and manganese) with increasing pyocyanin concentration. This observation clearly indicated that pyocyanin has a positive effect on reducing heavy metals and their toxic effects in soil, since heavy metal contamination is a significant issue of concern for natural ecosystems, in general. This finding agrees with majority of previous studies, observing that microbes have developed mechanisms to deal with metal toxicity, one of which is the production of different functional molecules (Teitzel et al., 2006; Hesse et al., 2018).

Soil electrical conductivity and pH

It is clearly shown in *Table 6* that the salt concentration in the soil decreased when treated with pyocyanin. This finding could be helpful in agriculture to reduce the problem of desertification resulting from the unsuitability of lands for cultivation, due to high salinity. Many previous studies, such as that by Corwin and Yemoto (2020), have proven the impact of salinity on plant production, which includes limiting plant water intake by lowering osmotic potential and altering soil permeability, making it more difficult for the plant to absorb water.

The soil pH was also measured in this study as shown in *Table 7*, a noticeable decrease in pH was observed in soil treated with pyocyanin. Soil acidity is a significant determinant of metal solubility and toxicity (Hesse et al., 2018). It has been demonstrated by Naamala and Smith (2020) that alkalinity affects and limits the availability of some metals, while toxicity is linked to low pH. Some studies have confirmed that the concentration of metals in, and the acidity of, soil are closely related to the types of microorganisms present in the soil and their production of certain extracellular microbial compounds (Hesse et al., 2018). Further, Miransari et al. (2014) proposed that some microbial products can alter the pH and activity of microorganisms in the rhizosphere, thereby influencing soil nutrient availability.

Conclusion

The results of this study revealed the effects of pyocyanin on the nutrients and minerals in soil. It was observed that levels of some important elements such as magnesium, chlorine, and iron had gradually increased when soil was treated with pyocyanin; the highest concentrations of all mentioned elements were recorded at a 25% pyocyanin concentration. In contrast, levels of some elements, such as calcium and nitrogen, had gradually decreased in the soil treated with pyocyanin, whereas, some elements were not affected. The gradual decrease in levels of certain heavy metals, in soil when treated with different concentrations of pyocyanin, was especially noteworthy. It is remarkable, that the gradual decrease in EC and soil pH after treatment with different concentrations of pyocyanin, can improve the properties of soil and make it more suitable for agricultural use. Moreover, the study has shown the ability of pyocyanin-producing bacteria to

suppress plant pathogenic fungi and bacteria. The antimicrobial effect is stronger against fungi than bacteria, on the one hand, and against gram-positive over negative bacteria, on the other. The findings of this study have important implications for the application of pyocyanin to agricultural soil, which is of economic and environmental importance. Further research is required on the different products of the phytomicrobiome, such as pyocyanin, and their potential effects in reducing the adverse conditions that could affect plant growth, both under laboratory conditions and in the field.

REFERENCES

- [1] Al-Zahrani, S. H. (2012): Bacteria isolated from contact and non-contact lens and antibiotic susceptibility patterns of isolated *Pseudomonas aeruginosa*. – *African Journal of Microbiology Research* 6(47): 7350-7356.
- [2] Anjaiah, V., Cornelis, P., Koedam, N. (2003): Effect of genotype and root colonization in biological control of fusarium wilts in pigeonpea and chickpea by *Pseudomonas aeruginosa* PNA1. – *Canadian Journal of Microbiology* 49(2): 85-91.
- [3] Baetz, U., Eisenach, C., Tohge, T., Martinoia, E., De Angeli, A. (2016): Vacuolar chloride fluxes impact ion content and distribution during early salinity stress. – *Plant Physiology* 172(2): 1167-1181.
- [4] Bender, S. F., Wagg, C., Van der Heijden, M. G. (2016): An Underground Revolution: Biodiversity and Soil Ecological Engineering for Agricultural Sustainability. – *Trends Ecology and Evolution* 31(6): 440-452.
- [5] Compant, S., Samad, A., Faist, H., Sessitsch, A. (2019): A review on the plant microbiome: Ecology, functions and emerging trends in microbial applications. – *Journal of Advance Research* 19: 29-37.
- [6] Corwin, D. L., Yemoto, K. (2020): Salinity: Electrical conductivity and total dissolved solids. – *Soil Science Society of American Journal* 84(5): 1442-1461.
- [7] Cottenie, A., Verloo, M., Kiekens, L., Velghe, G., Camerlynck, R. (1982): *Chemical Analysis of Plants and Soils*. Laboratory of Analytical and Agrochemistry. – State University, Ghent, Belgium.
- [8] Cox, C. D. (1986): Role of Pyocyanin in the Acquisition of Iron from Transferrin. – *Infection and Immunity* 52(1): 263-270.
- [9] Da Silva, Y., Do Nascimento, C., Biondi, C. M. (2013): Comparison of USEPA digestion methods to heavy metals in soil samples. – *Environmental Monitoring and Assessment* 186(1): 47-53.
- [10] Das, T., Manefield, M. (2012): Pyocyanin promotes extracellular DNA release in *Pseudomonas aeruginosa*. – *PLoS ONE* 7(10): e46718.
- [11] Del Barrio-Tofiño, E., López-Causapé, C., Oliver, A. (2020): *Pseudomonas aeruginosa* epidemic high-risk clones and their association with horizontally-acquired β -lactamases: 2020 update. – *International Journal of Antimicrobial Agents* 56(6): e106196.
- [12] El-Fouly, M., Sharaf, A. M., Shahin, A. A., El-Bialy, H. A., Omara, A. M. (2015): Biosynthesis of pyocyanin pigment by *Pseudomonas aeruginosa*. – *Journal of Radiation Research and Applied Science* 8(1): 36-48.
- [13] Gupta, G., Parihar, S. S., Ahirwar, N. K., Snehi, S. K., Singh, V. (2015): Plant growth promoting rhizobacteria (PGPR): Current and future prospects for development of sustainable agriculture. – *Journal of Microbial Biochemical Technology* 7: 96-102.
- [14] Hasanuzzaman, M., Umadhay-Briones, K., Zsiros, S., Morita, N., Nodasaka, Y., Yumoto, I., Okuyama, H. (2004): Isolation, identification, and characterization of a novel oil-degrading bacterium, *Pseudomonas aeruginosa* T1. – *Current Microbiology* 49: 108-114.
- [15] Hassani, H., Hasan, H., Al-Saadi, A., Ali, A., Muhammad, M. (2012): A comparative study on cytotoxicity and apoptotic activity of pyocyanin produced by wild type and mutant

- strains of *Pseudomonas aeruginosa*. – *European Journal of Experimental Biology* 2: 1389-1394.
- [16] He, C. Q., Tan, G. E., Liang, X., Du, W., Chen, Y. L., Zhi, G. Y., Zhu, Y. (2010): Effect of Zn-tolerant bacterial strains on growth and Zn accumulation in *Orychophragmus violaceus*. – *Applied Soil Ecology* 4(1): 1-5.
- [17] Hesse, E., O'Brien, S., Tromas, N., Bayer, F., Luján, A. M., Van Veen, E. M., Hodgson, D., Buckling, A. (2018): Ecological selection of siderophore producing microbial taxa in response to heavy metal contamination. – *Ecology Letter* 21(1): 117-127.
- [18] Hirel, B., Tétu, T., Lea, P. J., Dubois, F. (2011): Improving nitrogen use efficiency in crops for sustainable agriculture. – *Sustainability* 3(9): 1452-1485.
- [19] Huber, D. M., Jones, J. B. (2012): The role of magnesium in plant disease. – *Plant Soil* 368(2): 73-85.
- [20] Jayaseelan, S., Ramaswamy, D., Dharmaraj, S. (2013): Pyocyanin: production, applications, challenges and new insights. – *World Journal of Microbiological Biotechnology* 30(4): 1159-1168.
- [21] Lim, S. H. J., Zainual, N. S. M., Samahah, N. (2019): Isolation of potential fluorescent pseudomonads from Kuini (*Mangifera odorata*) planted soil and their potential as bio-fertilizer. – *Microbiology Research* 10(1): e7844.
- [22] Miransari, M., Omidi, H., Korde, N., Amini, M., Maleki, S. (2014): Soil Microbes and Soil Nutrients. – In: Miransari, M. (ed.) *Soil Nutrients*. Nova, USA, pp. 297-309.
- [23] Moreira, W. R., Bispo, W. M., Rios, J. A., Debona, D., Nascimento, C. W., Rodrigues, F. Á. (2015): Magnesium-induced alterations in the photosynthetic performance and resistance of rice plants infected with *Bipolaris oryzae*. – *Scientific Agriculture Journal* 72(4): 328-333.
- [24] Naamala, J., Smith, D. (2020): Relevance of plant growth promoting microorganisms and their derived compounds, in the face of climate change. – *Agronomy* 10(8): e1179.
- [25] Navarro, M. O. P., Piva, A. C. M., Simionato, A. S., Spago, F. R., Modolon, F., Emiliano, J., Azul, A. M., Chryssafidis, A. L., Andrade, G. (2019): Bioactive compounds produced by bio-control agents driving plant health. – In: Kumar, V., Prasad, R., Kumar, M., Choudhary, D. (eds.) *Microbiome in Plant Health and Disease*. Springer, Singapore, pp. 337-374.
- [26] Özyürek, S. B., Gür, S. D., Bilkay, I. S. (2016): Investigation of Antimicrobial Activity of Pyocyanin Produced by *Pseudomonas aeruginosa* Strains Isolated from Different Clinical Specimens. – *Hacettepe Journal of Biology and Chemistry* 44(1): 1-6.
- [27] Priyaja, P., Jayesh, P., Correya, N., Sreelakshmi, B., Sudheer, N., Philip, R., Singh, I. (2014): Antagonistic effect of *Pseudomonas aeruginosa* isolates from various ecological niches on *Vibrio* species pathogenic to crustaceans. – *Journal of Coastal Life Medicine* 2(1): 76-84.
- [28] Schaad, N. W., Jones, B., Chun, W. (2001): *Laboratory Guide for Identification of Plant Pathogenic Bacteria*. – APS Press, St. Paul, MN, USA.
- [29] Streeter, K., Katouli, M. (2016): *Pseudomonas aeruginosa*: A review of their pathogenesis and prevalence in clinical settings and the environment. – *Infection Epidemiology and Microbiology* 2(1): 25-32.
- [30] Sudhakar, T., Karpagam, S., Shiyama, S. (2013): Analysis of pyocyanin compound and its antagonistic activity against phytopathogens. – *International Journal of Chemtech Research* 5(3): 1101-1106.
- [31] Teitzel, G. M., Geddie, A., De Long, S. K., Kirisits, M. J., Whiteley, M., Parsek, M. R. (2006): Survival and growth in the presence of elevated copper: transcriptional profiling of copper-stressed *Pseudomonas aeruginosa*. – *Journal of Bacteriology* 188(20): 7242-7256.
- [32] Vatanserver, R., Ozyigit, I., Filiz, E. (2016): Essential and beneficial trace elements in plants, and their transport in roots: a Review. – *Applied Biochemistry and Biotechnology* 181(1): 464-482.

- [33] Vieto, S., Rojas-Gätjens, D., Jiménez, J. I., Chavarría, M. (2021): The potential of *Pseudomonas* for bioremediation of oxyanions. – *Environmental Microbiology Report* 13(6): e12999.
- [34] White, P. J., Broadley, M. R. (2001): Chloride in soils and its uptake and movement within the plant: a review. – *Annals of Botany* 88(6): 967-988.

EXPLORING THE SPECIES AND PHYLOGENETIC DIVERSITY, PHYLOGENETIC STRUCTURE OF MIXED COMMUNITIES ALONG THE COASTAL GRADIENT. A CASE STUDY IN A SUBTROPICAL ISLAND, CHINA

ZHENG, J. M.^{1,2,3*} – ZHENG, Y. S.²

¹College of Civil Engineering, Putian University, Putian 351100, PR China

²College of Landscape Architecture, Fujian Agriculture and Forestry University, Fuzhou 350002, PR China

³Fujian University Engineering Research Center for disaster prevention and mitigation of engineering structures along the southeast coast, Putian University, Putian 351100, PR China

*Corresponding author
e-mail: zjm1991@foxmail.com

(Received 28th Jan 2022; accepted 2nd May 2022)

Abstract. To better understand the effect of distance from seashore on the pattern of species diversity, phylogenetic diversity, and phylogenetic structure, four sample sites on Dongshan Island, China with varied distances to seashore were selected, the soil and species composition of *Casuarina equisetifolia* and *Dendrocalamus minor* var. *amoenus* mixed communities were investigated, and species diversity, phylogenetic diversity, and phylogenetic structure were analyzed. The result showed that there are existed 44 taxa in the communities, 18.8% of which were exotic species. Species diversity and phylogenetic diversity exhibited an increasing trend with shorter distance. The EC (Electrical conductivity) and SOC (Soil organic matter) determined the species diversity and phylogenetic diversity. The phylogenetic structure does not change with distance from the seashore, which may be caused by human disturbance and niche competition that has altered the environmental filtering effect.

Keywords: sandy coast, distance to seashore, species richness, phylogenetic structure, phylogenetic diversity, bamboo

Introduction

Almost all coasts in Fujian Province, China are sandy, except for a few bedrocks and muddy coasts (Kong, 1999). The windbreak constructed in sandy coasts serves to protect the manmade environment from sandy dust by wind blowing and alleviate the damage caused by salt spray to plants or crops. In the harsh environment of coastal sandy zones, there are few suitable species, such as *Casuarina equisetifolia* and *Pinus elliottii*. More than 20 years ago, many bamboo species were introduced to Dongshan Island, Fujian Province, China to build a mixed community of windbreak in the coast, which has contributed to better soil quality and higher community stability (Zheng et al., 2020; Zheng et al., 2021b). Bamboo-dominated patches facilitate species coexistence and promote species richness and phylogenetic diversity (Schweizer et al., 2017). Phylogenetic diversity and phylogenetic structure were selected to evaluate the priority of conservation of plant communities and animals (Liu et al., 2017a; Gumbs et al., 2020). Therefore, it is meaningful to study the species diversity, phylogenetic diversity, and phylogenetic structure of windbreak.

Plant diversity is the result of responses to environmental filtering (Faith, 1992; Japhet et al., 2009). Species richness was changed with soil pH and precipitation

(Palpurina et al., 2017). The soil texture and nutrients influenced the distribution of plant communities (Ahmed and Shawky, 2017). Huang et al. (2020) suggested that the species component and seed bank were highly correlated along a center-to-edge gradient. The phylogenetic structure might change with the distance to coast in an island. In the Kunlun Mountains, habit filtering has a higher impact on plant diversity and its ecological process (Du and Hesp, 2020). Anthropogenic changes in the environment have a subsequent impact on plant diversity and evolution (Tilman and Lehman, 2001). The phylogenetic structure of communities varies with spatial distance (Cavender-Bares et al., 2006), slope and aspect (Kitagawa et al., 2015), and elevation (Qian et al., 2014), and so on. Nevertheless, the pattern that the relationship between species diversity, phylogenetic structure with the distance to coast needs to be explored.

In this study, the typically mixed communities of *Casuarina equisetifolia* and *Dendrocalamus minor* var. *amoenus* were selected as objects in Dongshan Island, China. It is meaningful that *Casuarina equisetifolia* and *Dendrocalamus minor* var. *amoenus* mixed communities distributed widely with strong adaptability. Four sample plots with varying distances to the coast were sampling, the species diversity, phylogenetic diversity, and phylogenetic structure were analyzed to evaluate the health of ecosystem, find out the determining factors of environmental stress, and reveal the mechanism of species co-exist in sandy coast. This study would provide proposal for the windbreak forest management, and conversation of coastal vegetation.

Materials and Methods

Study site

The study site is located at Dongshan Island (23°40'N, 118°18'E) in Zhangzhou City, Fujian Province, China (Fig. 1). The study area has a subtropical maritime monsoon climate. The mean annual precipitation is 1113.9 mm and the mean annual evaporation is 2013.2 mm. The temperature ranged from 13.1~27.3 °C (Kong, 1999). Typhoons usually occurred from July to August. The windbreak is dominated by *Casuarina equisetifolia* on the sandy coast.

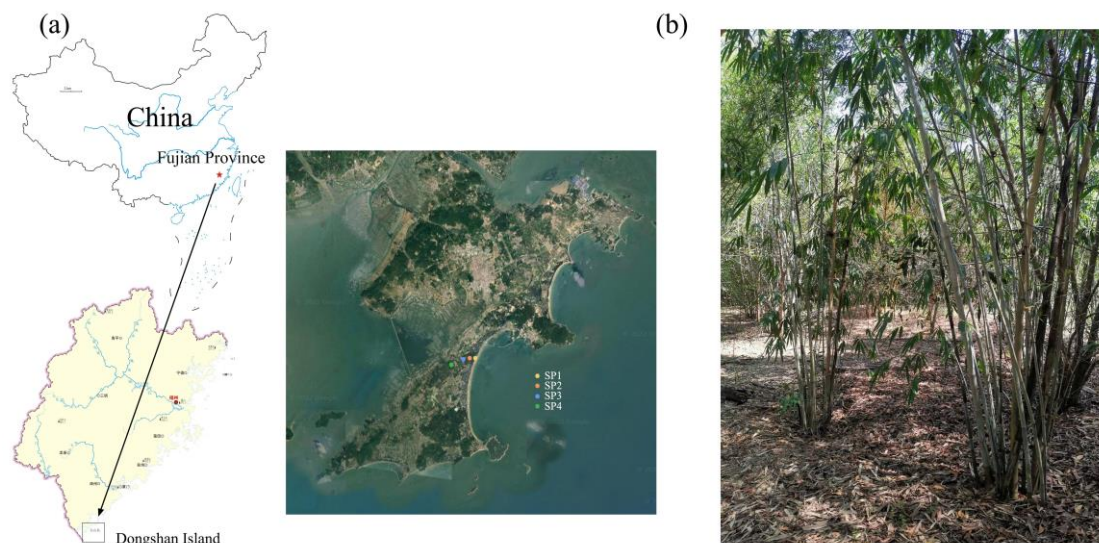


Figure 1. The location of study area (a), and the situation of sample plots (b)

Sampling and investigation

The sampling and investigation were conducted from August to October 2020. According to the distribution and size of mixed communities of *Casuarina equisetifolia* and *Dendrocalamus minor* var. *amoenus*, Four plots with different distances from coastline vertical to inland (SP1. 50~60 m, SP2. 60~200 m, SP3. 200~600 m, SP4. 600~1200 m) were selected. Four subplots of 20 m × 20 m were randomly selected at each sample plot. The species name and number of individual species were recorded. The latitude, longitude, elevation, slope, and canopy density of the sample plots were also recorded (Table 1).

Table 1. The situations of *Dendrocalamus minor* var. *amoenus*

Sample plot	Elevation/m	Slope/°	Canopy density/%	Distance to seashore/m
SP1	0~10	3~10	40~50	50~60
SP2	3~11	4~8	45~60	60~200
SP3	2~12	5~7	45~65	200~600
SP4	1~11	3~12	55~65	600~1200

The species diversity determined

Species richness (SR), Simpson's index, Shannon-Wiener's index, and Pielou's evenness index were selected to assess the species diversity of the *Casuarina equisetifolia* and *Dendrocalamus minor* var. *amoenus* mixed community. The formulae of these indicators were followed by Greig-Smith (1983), as follow:

Species richness, SR

$$SR=S \quad (\text{Eq.1})$$

Simpson index, D

$$D = 1 - \sum_{i=1}^S P_i^2 \quad (\text{Eq.2})$$

Shannon-Wiener's index, H'_e

$$H'_e = -\sum_{i=1}^S P_i \ln P_i \quad P_i = \frac{n_i}{N} \quad (\text{Eq.3})$$

Pielou index, J_e

$$J_e = \frac{H'_e}{H'_{\max}} \quad H'_{\max} = \ln S \quad (\text{Eq.4})$$

where n_i – the number of individuals of i species; n – the total number of samples plots. S – the number of all species, N – the total number of individuals of all species, $i=1,2,3,\dots,n$.

The phylogenies of communities constructed

The information of all species and their phylogeny were entered into Phylomatic Version 3.0 (Webb et al., 2008), and selected the evolutionary tree skeleton followed by Zanne et al. (2014), then the phylogenetic tree with branch lengths was selected to construct.

The phylogenetic diversity and phylogenetic structure calculated

The Faith Phylogenetic diversity (PD) was selected to assess phylogenetic diversity (Faith, 1992), representing the sum of the shortest branch lengths connecting species within a sample plot to a phylogenetic tree. Net related index (NRI) and nearest taxon index (NTI) represent the phylogenetic structure of the community (Webb et al., 2008). NRI is based on mean phylogenetic distance (MPD), which estimates the mean relatedness between possible pairs of taxa. NTI is based on the mean nearest taxon distance (MNTD), which estimates the mean relatedness between each taxon and its nearest relative (Qian et al., 2014).

Species attribute query

The invasiveness of plants in the communities was referred to the Chinese Invasive Alien Species Database (<http://www.iplant.cn/ias/protlist>) (Ma, 2013; Yan et al., 2014), and classified into five classes, namely Class I, malignant invasive; Class II, severely invasive; Class III, locally invasive; Class IV, generally invasive; and Class V, yet to be observed.

The soil sampling and determined

Soil samples were collected from two soil layers, 0-20 cm and 20-40 cm, at five points in the sample plot for mixing and processing, and the soil samples were brought back to the laboratory for air-drying to determine the physicochemical properties of the soil. The soil sample were sieved through 2 mm sieve and 0.149 mm sieve to get sub-samples. Soil pH was measured using the potentiometric method (LYT 1239-1999). Soil organic matter was measured by the potassium dichromate - external heating method (LYT 1237-1999), soil total nitrogen was evaluated by the semi-micro Kjeldahl method (LYT 1228-1999) and total phosphorus was determined by the molybdenum antimony colorimetric method (LYT 1232-1999). Soil water content was measured by the ring knife method (LY/T 1215-1999) and hydrolysis nitrogen was estimated by the alkaline diffusion method (LY/T 1229-1999). Quick-acting potassium was determined by the ammonium acetate leaching - flame photometric method (LY/T 1236-1999). Effective phosphorus was evaluated by leaching with hydrochloric acid and sulphuric acid solution (LY/T 1233-1999). The EC value (Electrical conductivity) of the soil leachate at 25 °C was used as the soil water-soluble salt content (LY/T 1251-1999). The details of determination of soil physical and chemical parameters were described by Bao (2005) and Tu (2014).

Data analysis

Data were collected and analyzed using Excel 2013. The Plantlist package in R 3.6.0 was used to search for species scientific names, ICUN Red List, and Chinese endemics (Zhang, 2018). Phylogenetic trees were drawn using Figtree Version 1.4.4. The difference of species diversity, phylogenetic diversity, and phylogenetic structure at

different distances was analyzed for One-way ANOVA and Tukey multiple comparisons (Tukey HSD). The Redundant analysis (RDA) of species diversity, phylogenetic diversity and phylogenetic structure and environmental factors were performed by Canoco 5.0, *P*-value was corrected by Bonferroni method. Values presented in the tables are means \pm SD. The statistics were performed on the R 3.6.1 with Ape package, Vegan package, Spaa package.

Results

Species composition

There are a total of 44 taxa in mixed communities (Fig. 2), including eight invasive alien species, accounting for 18.18% of the total, *Bidens pilosa*, *Lantana camara*, *Mimosa bimucronata*, *Malvastrum coromandelianum*, *Panicum repens*, *Casuarina equisetifolia*, *Ageratum conyzoides*, *Acacia confusa*, respectively.

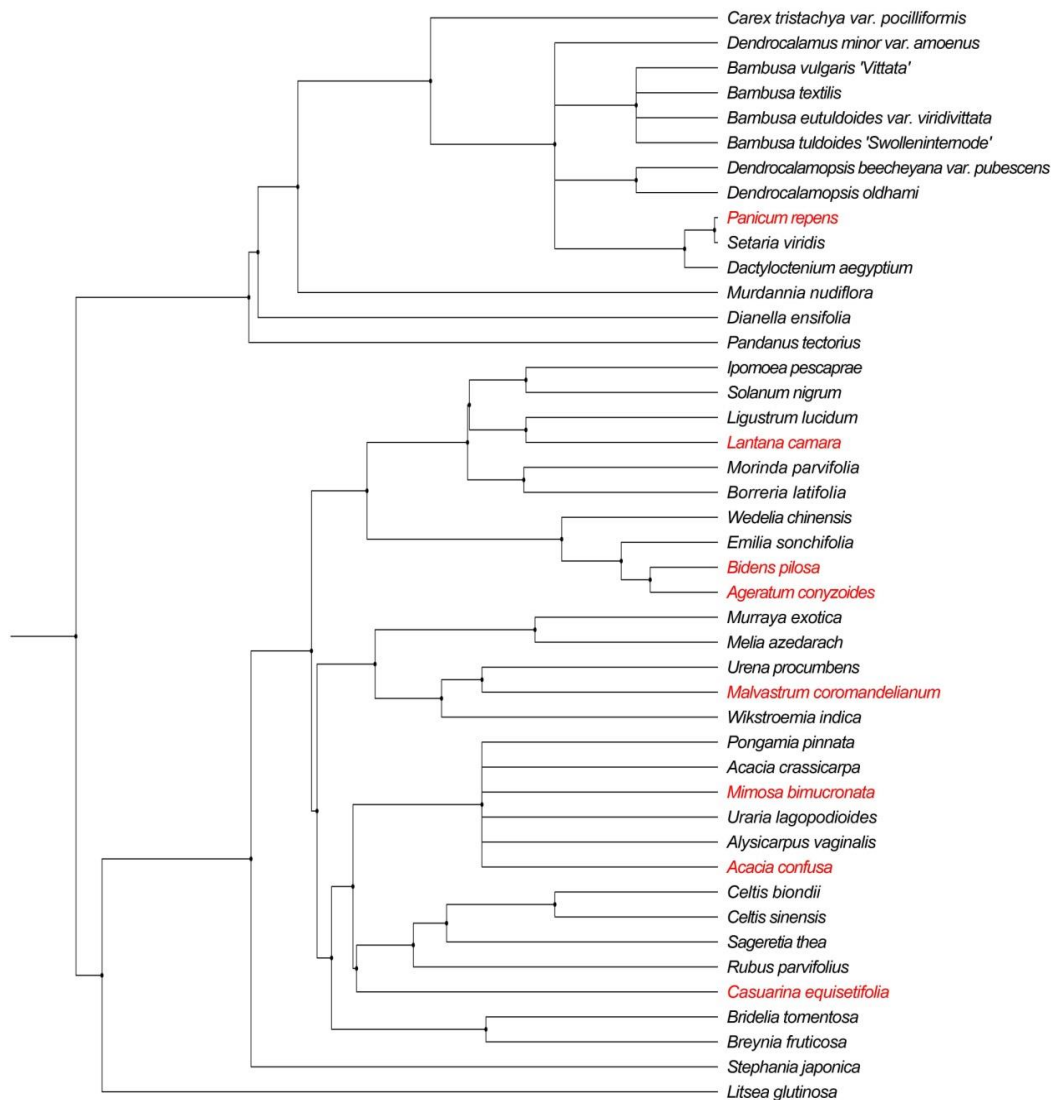


Figure 2. Phylogenetic tree of forty-four angiosperms species

Species diversity

The Shannon-Wiener diversity index and Pielou index were not significantly different among the four sample plots ($P > 0.05$, Fig. 3). The Simpson index in SP3 was significantly higher than that in SP1 ($P < 0.05$). The species richness in SP4 was significantly higher than that in SP1 ($P < 0.05$).

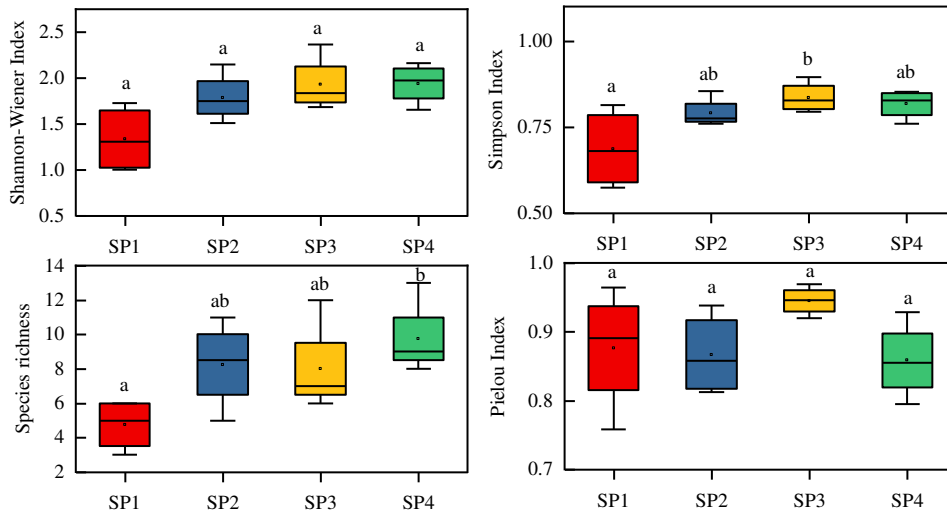


Figure 3. The species diversity plot showing the difference of species richness, species diversity and phylogenetic diversity in various distance to seashore. * Different lowercase letters indicate that the index is significantly different at $P < 0.05$

Phylogenetic diversity and phylogenetic structure

The phylogenetic diversity of SP4 was the highest at 1371.91 and the lowest at 871.01 for SP1 (Fig. 4). the NRI and NTI values for SP1 were both more than 0, indicating that the phylogenetic structure of SP1 tended to be clustering. The NRI and NTI values for SP2 and SP3 were less than 0, indicating that the phylogenetic structure tended to be over-dispersion.

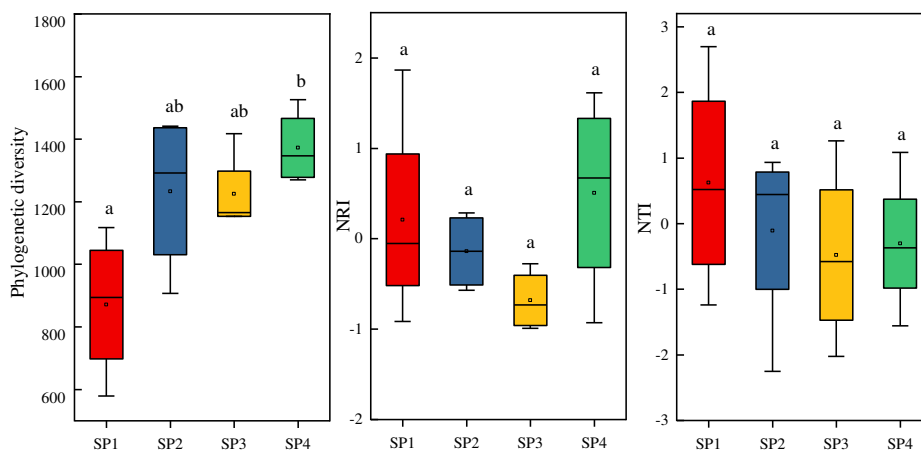


Figure 4. The phylogenetic diversity and phylogenetic structure plot showing the difference of phylogenetic diversity and phylogenetic structure in various distance to seashore. * Different lowercase letters indicate that the index is significantly different at $P < 0.05$

Soil environment

Water content in SP1 is higher than in other sample plots ($P < 0.05$, Table 2). The soil organic matter, total nitrogen, and pH were the highest in SP4 at $14.50 \text{ g}\cdot\text{kg}^{-1}$, $0.49 \text{ g}\cdot\text{kg}^{-1}$, and 6.59 , respectively. SP1 had the highest EC value of $117.31 \mu\text{S}\cdot\text{cm}^{-1}$.

Table 2. Soil environmental factors

Sample plot	WC (%)	SOC (g/kg)	TN (g/kg)	TP (g/kg)	TK (g/kg)	AN (mg/kg)	AK (mg/kg)	AP (mg/kg)	pH	EC ($\mu\text{S}\cdot\text{cm}^{-1}$)
SP1	6.39±0.50b	5.62±0.33a	0.21±0.01a	0.15±0.05ab	51.75±3.59c	10.87±0.76b	29.51±1.79c	9.79±1.59b	5.40±0.03a	117.31±1.46d
SP2	4.50±0.25a	10.40±0.51c	0.25±0.02b	0.13±0.01a	50.63±0.84bc	5.71±0.82a	21.51±0.75a	7.62±0.53a	5.39±0.02a	24.92±0.30c
SP3	5.14±0.23a	8.03±0.21b	0.19±0.02a	0.20±0.01b	45.65±1.07ab	6.88±0.42a	24.51±2.23ab	6.43±0.89a	5.64±0.05b	19.15±0.47b
SP4	5.09±0.29a	14.50±2.15d	0.49±0.03c	0.18±0.01ab	40.78±3.94a	11.94±0.73b	26.80±2.01bc	11.86±0.72b	6.59±0.02c	15.96±0.53a

*Different letters in the same column indicate that the same index has significant differences between different plots at $P < 0.05$; WC. Soil water content; SOC. Soil organic matter; TN. Soil total nitrogen; TP. Soil total phosphorus; TK. Soil total potassium; AN. Soil available nitrogen; AP. Soil available phosphorus; AK. Soil available potassium; pH. Hydrogen ion concentration; EC. Soil electric conductivity

The relationship between environment and species diversity, phylogenetic diversity and phylogenetic structure

Environmental factors explained 61.7% of species diversity, phylogenetic diversity, and phylogenetic structure (Figure 5). EC was negatively correlated with SR and PD. EC was negatively correlated with SOC, TN, and pH.

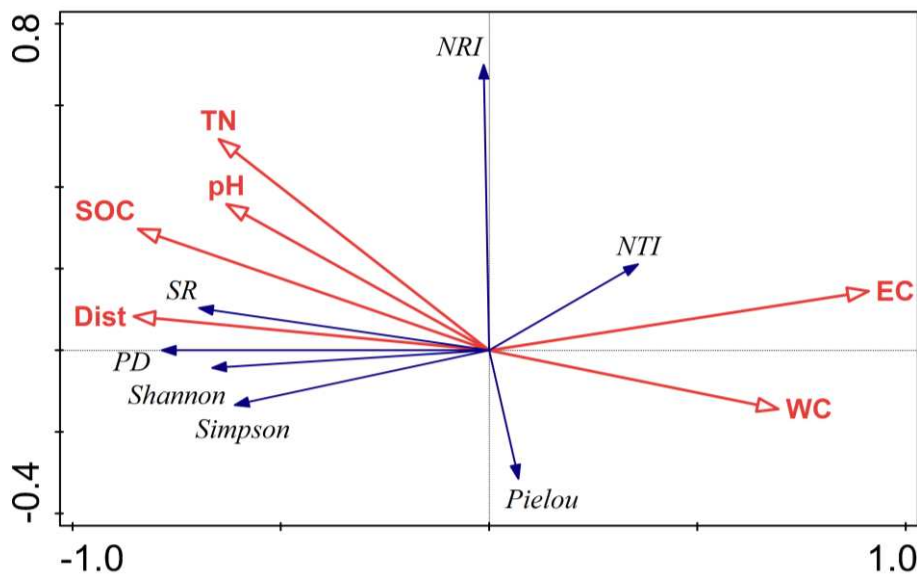


Figure 5. Redundancy analysis biplot showing the the relationship between species diversity, phylogenetic diversity and phylogenetic structure and environmental factors. Where EC. Soil electric conductivity; WC. Soil water content; SOC. Soil organic matter; TN. Soil total nitrogen, pH. Hydrogen ion concentration; Dist. distance

EC, Dist, and SOC have a significant impact on species diversity, phylogenetic diversity, and phylogenetic structure ($P < 0.05$, Table 3), the explain rate is 51.2%, 5.7%, 0.6%, respectively. The EC, Dist, and SOC were the determining factors influencing species diversity, phylogenetic diversity, and phylogenetic structure.

Table 3. Explanation rate of environmental factors on species diversity, phylogenetic diversity and phylogenetic structure under coastal gradients

Environmental Factors	Explains %	F-value	P	P _{adj}
EC	51.2	14.7	0.004	0.024
Dist	5.7	11.4	0.006	0.036
SOC	0.6	10.9	0.008	0.048
WC	2.3	5.9	0.020	0.120
TN	1.7	4.9	0.040	0.240
pH	0.2	4.6	0.050	0.300

Correlation analysis

The distance was significantly and positively correlated with the Shannon-Wiener index, Simpson diversity index, PD, and SR ($P < 0.05$, Table 4). The correlation between distance and NRI and NTI was not significant ($P > 0.05$). Species richness was significantly positively correlated with phylogenetic diversity ($r = 0.963$, $P < 0.01$).

Table 4. Spearman correlation analysis of species diversity, phylogenetic diversity, and phylogenetic structure

	Distance	Shannon-Wiener	Pielou	Simpson	PD	SR	NRI
Shannon-Wiener	0.620*						
Pielou	0.045	0.322					
Simpson	0.586*	0.955**	0.502*				
PD	0.670**	0.880**	-0.093	0.775**			
SR	0.614*	0.911**	-0.031	0.768**	0.924**		
NRI	0.045	-0.151	-0.104	-0.240	-0.170	0.015	
NTI	-0.273	-0.140	0.173	-0.174	-0.423	-0.056	0.421

SR:species richness, PD:phylogenetic diversity, NRI:net related index, NTI. nearest taxon index
*: $P < 0.05$, **: $P < 0.01$ (two-tails)

Discussion

Species composition

The species composition of *Casuarina equisetifolia* and *Dendrocalamus minor* var. *amoenus* mixed communities existed coastal native species, such as *Ipomoea pes-caprae*, *Pandanus tectorius* and *Pongamia pinnata*, which have a strong adaptive capacity to coastal stress. However, there are a high proportion of exotic species in the communities, accounting for 18.18% of the total number of species. It indicating that the invasive exotic species can adapt to the harsh coastal environment. The harsh habitat can accommodate a great number of invasive alien species (Hope et al., 2006; Liu et al.,

2017a). These species can colonize harsh habitats, such as roadsides and rock crevices. *Lantana camara* spreads rapidly and widely, posing a threat to the local ecosystem and can reduce agricultural productivity (Ranjan, 2019). This species is a potential ecological threat to native and endemic species in the sandy coast. It had been proved that *Lantana camara* has a highly positive interspecific association with *Dendrocalamus minor*, resulting in unstable communities of *Casuarina equisetifolia* and *Dendrocalamus minor* var. *amoenus* (Zheng et al., 2021a). *Casuarina equisetifolia* is an introduced exotic species for the protection of windbreak forests, and it is irreplaceable with strong colonization ability in the coastal zone (Lin et al., 2017). *Casuarina equisetifolia* is a potential threat to native tree species, but the severity is yet to be proven.

The effect of distance on the species diversity and phylogenetic diversity

Distance is an important factor influencing species composition (Abdelaal et al., 2019; Valli et al., 2019). The species diversity and habitat changed with the distance to seashore (Chen et al., 2015). The species diversity increased with the distance increased (Liu, 2009). The similarity of vegetation increased from the center to the edge of the island (Huang et al., 2020). These results consist with this study, the Simpson index in SP3 is significantly higher than in SP1 ($P>0.05$). The species diversity reflects the environment of communities. “Luxury effect” means the environment with a rich resource can live more species than the poor environment (Liu et al., 2017b). The species richness is highly correlated with phylogenetic diversity ($r=0.963$, $P<0.01$). The Simpson index, species richness, and phylogenetic diversity increased with distance increased (Fig. 4), which suggested that further the distance from shore, the sample plot was more stable and resource-rich. Distance to seashore showed a certain environmental gradient (Liu et al., 2017a), which is supported by the findings of this study. Soil organic matter and soil total nitrogen in SP4 were highest, while soil total phosphorus, effective phosphorus, and hydrolytic nitrogen were also relatively high than other sample plots (Table 2), This also demonstrating that soil quality in SP4 were better than other sample plots.

The effect of distance on the phylogenetic structure

The phylogenetic structure was correlated with environmental factors (Qian et al., 2014). In this study, the phylogenetic structure has not significantly relationship with distance from shore (Fig. 4), indicating that phylogenetic structure would not change along with the distance to the seashore. The environmental gradients related to distance to the seashore caused the species richness and diversity to change, but it has a low impact on the phylogenetic structure.

The NRI and NTI values in SP2 and SP3 were both less than 0, which indicated that the competition of communities caused the phylogenetic structure tended to be over-dispersion. The NRI and NTI values in SP1 are both more than 0, indicating that the phylogeny of the community tended to be clustering due to environmental filtering. The NRI and NTI were opposite in SP4, which suggested that the determining factors of phylogenetic structure are random or the combination of habitat filtering and species competition. Our result is consistent with previous studies (Kress et al., 2009; Liu et al., 2017a). The differences in phylogenetic structure are related to the environmental factors, local species pool, and the seed bank associated with land use (Stadler et al., 2017).

The determining factors of species diversity, phylogenetic diversity, and phylogenetic structure

In this study, EC, distance and SOC are the determining factors affecting species diversity, phylogenetic diversity, and the phylogenetic structure of communities under coastal gradients. Plant lived on the coast suffered salt damage mainly caused by salt spray (Li, 2017). Salt spray is blown from sea to inland, settles on the leave and soil surface, and salt spray decreased with increasing distance to seashore (Du and Hesp, 2020), resulting in an increase in species richness and phylogenetic diversity with decreasing distance from shore. Soil organic matter facilitates carbon uptake and tissue growth by plants and it is closely related to other nutrient contents. The communities in site further to seashore would attract large numbers of seabirds, and seabird feces are supplied to the soil nutrient pool, and large amounts of litter also lead to an increase in soil organic matter (Huang et al., 2020). As a result, differences in soil organic matter along the coastal gradient lead to changes in species diversity and phylogenetic diversity. Habitat environment, human disturbance and ecological niche competition combined to constrain community phylogenetic structure (Liu et al., 2017a). There are no differences of NRI and NTI among sample plots with varying distances to the seashore ($P>0.05$). The phylogenetic structure in SP1 is clustering, and the phylogenetic structure in SP2 and SP3 is over-dispersion. The phylogenetic structure in SP4 tends to be random. These results suggested that distance had some influence on the phylogenetic structure, but the differences were not significant among sample sites. The same with previous studies, the phylogenetic structure is not statistically significantly different across distinct topographic variation (Kitagawa et al., 2015). This result may be related to the short spatial distance to the seashore with small elevational variation, thus having a weaker effect on phylogenetic structure. It is probably that the greater influence of human disturbance and niche competition on phylogenetic structure covered the effect of habitat filtering.

Conclusions

The species composition *Casuarina equisetifolia* and *Dendrocalamus minor* var. *amoenus* mixed communities existed endemic species and exotic species under coastal gradients. The species richness, phylogenetic diversity, Simpson index, and Shannon-Wiener index showed a decreasing trend with decreasing distance from shore. The determining factors of species diversity, phylogenetic diversity are EC and SOC. The phylogenetic structure did not change with distance from shore. Future research can focus on revealing the patterns and determining factors (i.e. soil types, growth habits, and elevations) of phylogenetic structure in the coastal area.

Acknowledgements. This project was jointly supported by the Introduction of Talents Project of Putian University of Science & Technology Grant (No. 2021074); Fujian Province educational research project of young and middle-aged teachers (No. JAT210386); Special project of scientific research and innovation of Putian University (No. 2021ZP02); Fujian Province Regional Development Program (2015N3015). Foundation for scientific and technological innovation of Fujian agriculture and forestry university (CXZX2017089); Fujian University Engineering Research Center for disaster prevention and mitigation of engineering structures along the southeast coast (No. JDGC03).

Author contributions. ZJM conceived of the research idea, wrote the manuscript and conducted the fieldwork. ZYS supervised the experiment. Both authors discussed the results and comments on the manuscript.

REFERENCES

- [1] Abdelaal, M., Ahmed, D., Fois, M., Fenu, G., Bacchetta G. (2019): Floristic patterns and ecological drivers of sand dune ecosystem along the Mediterranean coast of Egypt. – *Arid Land Research and Management* 33(4): 388-411.
- [2] Ahmed, A. A. E., Shawky, R. A. (2017): Plant species diversity of some wadis at Red Sea Coast, Egypt. – *Environment, Resource and Ecology Journal* 1(1): 1-14.
- [3] Bao, B. D. (2005): *Analysis of soil agricultural chemistry*. – Beijing: Higher Education Press.
- [4] Cavender-Bares, J., Keen, A., Miles, B. (2006): Phylogenetic structure of Floridian plant communities depends on taxonomic and spatial scale. – *Ecology* 87(7): 109-122.
- [5] Chen, X. X., Li, Y., Ru, Z. Z. (2015): Community structure and diversity of *Heritiera littoralis* in Baguang of Shenzhen. – *Chinese Journal of Ecology* 6: 17-28. (In Chinese with English abstract).
- [6] Du, J., Hesp, P. A. (2020): Salt Spray Distribution and Its Impact on Vegetation Zonation on Coastal Dunes: A Review. – *Estuaries and Coasts* 43(8): 1885-1907.
- [7] Faith, D. P. (1992): Conservation evaluation and phylogenetic diversity. – *Biological Conservation* 61(1): 1-10.
- [8] Greig-Smith, P. (1983): *Quantitative plant ecology*. – Blackwell Science Publications, Oxford.
- [9] Gumbs, R., Gray, C. L., Böhm, M., Hoffmann, M., Grenyer, R., Jetz, W., Meiri, S., Roll, U., Owen, N. R., Rosindell, J. (2020): Global priorities for conservation of reptilian phylogenetic diversity in the face of human impacts. – *Nature Communications* 11(1): 2016.
- [10] Hope, D., Gries, C., Casagrande, D., Redman, C. L., Grimm, N. B., Martin, C. (2006): Drivers of Spatial Variation in Plant Diversity Across the Central Arizona-Phoenix Ecosystem. – *Society & natural resources* 19(2): 101-116.
- [11] Huang, Y., Ren, H., Wang, J., Liu, N., Jian, S., Cai, H., Hui, D., Guo, Q. (2020): Relationships between vegetation and soil seed banks along a center-to-edge gradient on a tropical coral island. – *Ecological Indicators* 117: 106689.
- [12] Japhet, W., Zhou, D., Zhang, H., Zhang, H., Yu, T. (2009): Evidence of phenotypic plasticity in the response of *Fagopyrum esculentum* to population density and sowing date. – *Journal of Plant Biology* 52(4): 303-311.
- [13] Kitagawa, R., Mimura, M., Mori, A. S., Sakai, A. (2015): Topographic patterns in the phylogenetic structure of temperate forests on steep mountainous terrain. – *AoB Plants* 7: 1-12.
- [14] Kong, F. (1999): *Island vegetation of Fujian*. – Fujian science press, Fuzhou. (In Chinese).
- [15] Kress, W. J., Erickson, D. L., Jones, F. A., Swenson, N. G., Perez, R., Sanjur, O., Bermingham, E. (2009): Plant DNA barcodes and a community phylogeny of a tropical forest dynamics plot in Panama. – *Proceedings of the National Academy of Sciences, PNAS* 106(44): 18621-18626.
- [16] Li, Q. Q. (2017): Relationships between spatiotemporal distribution of saltspray deposition and growth status of coastal greeningplants -a case study at Gulei Peninsula. – Xiamen University Master Thesis. (In Chinese with English abstract).
- [17] Lin, Y., Li, J., Bakker, J. D., Lin, H., Chen, C., Hong, W., Fisher, L., Wu, C., Hong, T., Deng, H., Zhang, G., Du, K. (2017): Wind and salt spray alter tree shape and dry mass density in *Casuarina equisetifolia* L. – *Trees* 31(1): 15-26.

- [18] Liu, F. Q. (2009): Study on Community Diversity and Physical and Chemical Property of Soil of Interlace Zone of Sandy Coastal in Shandong. – Shandong Agricultural University Master Thesis. (In Chinese with English abstract).
- [19] Liu, M. L., Pan, X., Chen, Q. H. (2017a): Significance of Phylogenetic Diversity and Phylogenetic Structure in Conservation of Island Plant Communities. A Case of Wuzhizhou Island. – *Journal of Tropical and Subtropical Botany* 25(05): 419-428. (In Chinese with English abstract).
- [20] Liu, J., Yu, M., Tomlinson, K., Slik, J. W. F. (2017b): Patterns and drivers of plant biodiversity in Chinese university campuses. – *Landscape and Urban Planning* 164: 64-70.
- [21] Ma, J. S. (2013): The Checklist of the Chinese Invasive Plants. – Higher Education Press, Beijing. (In Chinese with English abstract).
- [22] Palpurina, S., Wagner, V., von Wehrden, H., Hájek, M., Horsák, M., Brinkert, A., Hölzel, N., Wesche, K., Kamp, J., Hájková, P., Danihelka, J., Lustyk, P., Merunková, K., Preislerová, Z., Kočí, M., Kubešová, S., Cherosov, M., Ermakov, N., German, D., Gogoleva, P., Lashchinsky, N., Martynenko, V., Chytrý, M. (2017): The relationship between plant species richness and soil pH vanishes with increasing aridity across Eurasian dry grasslands. – *Global Ecology and Biogeography* 26(4): 425-434.
- [23] Qian, H., Hao, Z., Zhang, J. (2014): Phylogenetic structure and phylogenetic diversity of angiosperm assemblages in forests along an elevational gradient in Changbaishan, China. – *Journal of Plant Ecology* 7(2): 154-165.
- [24] Ranjan, R. (2019): Deriving double dividends through linking payments for ecosystem services to environmental entrepreneurship: The case of the invasive weed *Lantana camara*. – *Ecological Economics* 164: 1-15.
- [25] Schweizer, D., Rother, D. C., Muler, A. E., Rodrigues, R. R., Pizo, M. A., Brancalion, P. H. S. (2017): Effects of bamboo dominance and palm-heart harvesting on the phylogenetic structure of the seed and seedling communities in an old-growth Atlantic Forest. – *Journal of Tropical Ecology* 33(5): 309-316.
- [26] Stadler, J., Klotz, S., Brandl, R., Knapp, S. (2017): Species richness and phylogenetic structure in plant communities: 20 years of succession. – *Web Ecology* 17(2): 37-46.
- [27] Tilman, D., Lehman, C. (2001): Human-caused environmental change: Impacts on plant diversity and evolution. – *Proceedings of the National Academy of Sciences* 98(10): 5433.
- [28] Tu, Z., Chen, L., Yu, X., Zheng, Y. (2014): Rhizosphere soil enzymatic and microbial activities in bamboo forests in southeastern China. – *Soil Science and Plant Nutrition* 60(2): 134-144.
- [29] Valli, A. T., Kougioumoutzis, K., Iliadou, E., Panitsa, M., Trigas, P. (2019): Determinants of alpha and beta vascular plant diversity in Mediterranean island systems: The Ionian islands, Greece. – *Nordic Journal of Botany* 37(1): e02156.
- [30] Webb, C. O., Ackerly, D. D., Kembel, S. W. (2008): Phylocom: software for the analysis of phylogenetic community structure and trait evolution. – *Bioinformatics* 24(18): 2098-2100.
- [31] Yan, X., Liu, Q., Shou, H., Zeng, X., Zhang, Y., Chen, L., Liu, Y., Ma, H., Qi, S., Ma, J. (2014): The categorization and analysis on the geographic distribution patterns of Chinese alien invasive plants. – *Biodiversity Science* 22(5): 667-676. (In Chinese with English abstract).
- [32] Zanne, A. E., Tank, D. C., Cornwell, W. K., Eastman, J. M., Smith, S. A., FitzJohn, R. G., McGlenn, D. J., O'Meara, B. C., Moles, A. T., Reich, P. B., Royer, D. L., Soltis, D. E., Stevens, P. F., Westoby, M., Wright, I. J., Aarssen, L., Bertin, R. I., Calaminus, A., Govaerts, R., Hemmings, F., Leishman, M. R., Oleksyn, J., Soltis, P. S., Swenson, N. G., Warman, L., Beaulieu, J. M. (2014): Three keys to the radiation of angiosperms into freezing environments. – *Nature* 506(7486): 89-92.

- [33] Zhang, J. (2018): Plantlist: Looking up the status of plant scientific names based on The Plant List Database. – R package version 0.5.3.
- [34] Zheng, J. M., Chen, X. Y., Chen, L. G., He, T. Y., Rong, J. D., Lin, Y., Zheng, Y. S. (2020): Comprehensive evaluation of soil quality at different stand densities of *Dendrocalamus minor* var. *amoenus* plantations. – *Applied ecology and environmental research* 18(4): 5985-5996.
- [35] Zheng, J. M., Li, M., Zhang, M., Tarin, M. W. K., He, T., Chen, L. Y., Chen, L. G., Hong, X. L., Zheng, Y. S. (2021a): Interspecific Association and Niche of Mixed Forest Communities of *Casuarina equisetifolia* and *Dendrocalamus minor* var. *amoenus* in the Windbreak of Sandy Coast. – *Journal of Tropical and Subtropical Botany* 5(29): 465-473. (In Chinese with English abstract).
- [36] Zheng, J. M., Tarin, M. W. K., Jiang, D., Li, M., Zhang, M., Chen, L., He, T., Hong, X., Zheng, Y. (2021b): Various distances and orientations influenced the branching traits of *Dendrocalamus minor* var. *amoenus* in Dongshan Island, China. – *Global Ecology and Conservation* 26: 1-9.

EFFECTS OF EXOGENOUS CaCl₂ ON THE PHOTOSYNTHETIC FUNCTION AND ACTIVE OXYGEN METABOLISM OF *SALIX VIMINALIS* LEAVES UNDER PB STRESS

NING, W. – ZHU, S. Q. – NIAN, H. – YIN, J. H.* – AN, B. Y.*

College of Horticulture, Jilin Agricultural University, Changchun 130118, China

*Corresponding authors
e-mail:6325695@qq.com; jlnabya2020@126.com

(Received 9th Aug 2021; accepted 3rd Dec 2021)

Abstract. In order to provide some basic data for revealing the mechanism of exogenous CaCl₂ on improving drought resistance of *Salix viminalis* seedlings. The experimental results showed that: Spraying exogenous of different CaCl₂ concentrations significantly alleviated the damage degree of *S. viminalis* seedlings leaves caused by heavy metal stress, and the effect of 30 μmol·L⁻¹ CaCl₂ was the most significant. Spraying exogenous CaCl₂ could regulate stomatal limitation of *S. viminalis* seedlings leaves under heavy metal stress, which was beneficial to water holding capacity of *S. viminalis* seedlings leaves under heavy metal stress, and enhanced photosynthetic carbon assimilation capacity of leaves under heavy metal stress; Spraying exogenous CaCl₂ can reduce the energy pressure of PSII reaction center by increasing the non-photochemical quenching (NPQ) of leaves of *S. viminalis* seedlings, alleviate the photoinhibition of PSII, and promote the electron transfer process, especially on the receptor side of PSII; Spraying exogenous CaCl₂ effectively reduced the production of reactive oxygen species in leaves of *S. viminalis* seedlings, as well as the degree of membrane peroxidation, which was also one of the important reasons for alleviating the inhibition of photosynthetic capacity.

Keywords: heavy metals, *S. viminalis*, PSII, reactive oxygen, antioxidants

Introduction

Heavy metal stress is an important limiting factor in agricultural production, and the yield of crops caused by heavy metal stress alone exceeds the sum of all pathogens. Lead (Pb) is one of the most harmful heavy metals in the environment. In recent years, with the rapid development of economy, mining, agriculture and recycling of waste metals have significantly increased the concentration of Pb in the soil, and the damage dealt by Pb pollution to the environment has gradually intensified, and the impact on human health has become a hot topic (Soffianian et al., 2014; Sauliutė and Svecėvičius, 2015). The majority of Pb enters the human body through the soil-plant-human pathway and causes harm. To a certain extent, Pb in the soil will have a series of adverse effects on plant physiological metabolism, such as the increase of cell membrane permeability, the accumulation of reactive oxygen species, and the aggravation of membrane lipid peroxidation, and even lead to plant death in severe cases (Shu et al., 2012; Ogbomida et al., 2018).

Plant photosynthesis is one of the most sensitive processes to heavy metals. Persistent heavy metal stress will cause irreversible damage to plant photosynthetic apparatus (Zhang et al., 2018a), such as inhibition of photosynthetic pigment degradation (Albert et al., 2011; Guadagno et al., 2017; Chen et al., 2018; Zhang et al., 2018), photosynthetic phosphorylation and electron transport. Oxidative stress caused by oxidative stress in plant cell membrane caused by oxidative stress (Gill et al., 2010; Wang et al., 2017). Plant photosystem II (PSII) is one of the sensitive parts to heavy metal stress. A series of

photosynthetic physiological processes such as light energy absorption, water photolysis and electron transfer are closely related to PSII (Allahverdiyeva et al., 2013; Chen et al., 2017). To ensure the stability of photosynthetic function, especially PSII function, of plant leaves under heavy metal stress plays an important role in maintaining the normal growth of plants and improving the stress resistance of plants.

Calcium is not only an essential mineral nutrient element for plants, but also a second messenger for intracellular physiological and biochemical reactions. Therefore, the stress resistance of plants can be improved by stabilizing cell wall and cell membrane structures and inducing the expression of specific genes (Ryan and Kochian, 1993; Larkindale and Huang, 2004). At present, there are a lot of reports about CaCl₂ can protect the normal physiology of PSII and increase the content of antioxidant enzymes in plant leaves under stress. *S. viminalis* is a *Salix* plant of *Salix family*. *S. viminalis* has the advantages of rapid growth, high biomass and strong ability to accumulate heavy metals is widely used in phytoremediation and biomass energy development in heavy metal contaminated soil areas, and has certain ecological and economic value (Zhai et al., 2016). Therefore, improving the resistance of *S. viminalis* seedlings to heavy metal stress is the key to ensure the survival and growth of seedlings after transplanting. However, the regulation of exogenous CaCl₂ on physiological function of *S. viminalis* seedlings under heavy metal stress, especially the regulation mechanism of PSII function, was less studied. In this experiment, the effects of spraying different concentrations of exogenous CaCl₂ on PSII function of *S. viminalis* leaves under heavy metal stress were studied, in order to provide some basic data for improving the drought resistance ability of *S. viminalis*.

Materials and methods

Test materials and treatment

The experiment was conducted in the laboratory of soil science of Jilin Agricultural University (Changchun, Jilin Province, China) from March to June 2019. The annual seedlings were raised by cutting. The culture substrate was fully mixed with peat soil and quartz sand; the ratio was 2:1 (V / V). It was cultured in an artificial climate box with temperature of 25/23 °C (light / dark), light intensity of 400 μmol·m⁻²·s⁻¹, photoperiod of 12/12 h (light/dark), and relative humidity of about 75%. After the seedlings had long functional leaves, 1/2 of Hoagland nutrient solution was irrigated once a week. When the seedlings grow to six leaves and one heart, they are transplanted. Before transplanting, the seedlings are irrigated once to make the relative water content of the soil basically reach saturation. The seedlings are transplanted into a cultivation bowl with a diameter of 12 cm and a height of 15 cm, and one plant is planted in each pot.

After transplanting, the seedlings with the same growth were selected as the experimental seedlings. The treatment group was sprayed with CaCl₂ solution with concentration of 15 and 30 μmol·L⁻¹ (PH=7), and the control group was sprayed with water (CK). The foliar spray was carried out at 4:00 p.m., and the front and back sides were evenly sprayed until the solution on the leaves formed fine mist like uniform droplets ready to drop, after the water on the leaf surface evaporates naturally and the CaCl₂ solution is completely absorbed, repeat spraying 1 time with the same amount each time. 10 plants in each treatment were repeated. After spraying CaCl₂, the water on the surface of leaves is naturally evaporated. In order to fully absorb the spraying CaCl₂ on the leaf surface, after the CaCl₂ solution on the leaf surface evaporates, spray once more, and the usage and dosage are the same as the first time. The content of Pb in the test

matrix was set at 200 mg·kg⁻¹. On the 15th day after treatment, the physiological indexes were determined after the results showed obvious differences among different treatments.

Determination parameters and methods

The growth parameters were determined: Vernier caliper was used to measure plant height and leaf area was measured by leaf area meter.

Photosynthetic gas exchange parameters were measured: A CIRAS-2 portable photosynthesis system (PPsystem Company, UK) was used to determine the net photosynthetic rate (P_n), stomatal conductance (G_s), transpiration rate (T_r), and intercellular CO₂ concentration (C_i) of the second fully expanded functional leaf of the penultimate leaf of *S. viminalis* seedlings was selected. The CO₂ concentration was fixed at 400 μl·L⁻¹ in a CO₂ cylinder. The light intensity PFD was set to 1000 μmol·m⁻²·s⁻¹ with the light source built in the instrument. The net photosynthetic rate (P_n), stomatal conductance (G_s), transpiration rate (T_r) and intercellular CO₂ concentration (C_i) of *S. viminalis* leaves under different treatments were measured. Repeat 5 times.

Chlorophyll fluorescence parameters were measured: The electron transfer rate (ETR) and non-photochemical quenching (NPQ), the maximum photochemical efficiency (F_v/F_m) and the actual photochemical efficiency (Φ_{PSII}) of PSII reaction center under light acclimation were measured by FMS-2 (Hansatech company, UK) for 5 times.

The chlorophyll fluorescence kinetic curve and its parameters were determined: After 30 min dark adaptation, the OJIP curve of leaves after dark adaptation was measured by handy pea (Hansatech compan, UK). According to Strasser et al.'s method (1995), the OJIP curves were standardized by $V_{O-P}=(F_t-F_o)/(F_m-F_o)$ and $V_{O-J}=(F_t-F_o)/(F_J-F_o)$ respectively. The relative variable fluorescence (V_J and V_K) of J point at 2 ms and K point at 0.3 ms were obtained, respectively. The differences between the standardized V_{O-P} and V_{O-J} curves of different treatments and the control were calculated, expressed as V_{O-P} and V_{O-J} , respectively. The measured OJIP curve was analyzed by JIP test. The maximum photochemical efficiency (F_v/F_m) of PSII and the photosynthetic performance index (PI_{ABS}) based on absorbed light energy were measured.

Determination of ROS metabolism and other physiological indices: The rate of production of O₂[·] was measured using the method of Zhang et al. (2007), The malondialdehyde (MDA) content was determined using the thiobarbituric acid method. The conductivity was measured by DDS-11C. Relative conductivity was used to express the electrolyte leakage rate. The content of superoxide dismutase activity (SOD) was determined using the NBT method. The activity unit (U) was 50% of the enzyme that inhibited the photochemical reduction of NBT in 1 ml of reaction solution in 1 h. The activity of ascorbic acid peroxidase (APX) was determined as described by Shen et al. (1996). An activity unit (U) is defined as the amount of enzyme that catalyzes 1 μmol ascorbic acid oxidation in one minute. Each index was measured five times.

Data and analysis

Excel and SPSS software (Version. 22) were used to conduct statistical analyses on the measured data. The data in the figure was denoted as mean ± standard deviation (SE). One-way ANOVA and least significant difference (LSD) were used to compare the differences among different data groups.

Results and analysis

*Effects of exogenous CaCl_2 on leaf growth of *S. viminalis* seedlings under Pb Stress*

Under Pb stress, the leaf growth of *S. viminalis* seedlings changed significantly, and the increase of leaf area of *S. viminalis* seedlings without spraying exogenous CaCl_2 was significantly delayed (Fig. 1). Compared with CK, the plant height of *S. viminalis* seedlings was decreased by 20.36% ($P < 0.01$), reaching a very significant difference level. However, spraying different concentrations of exogenous CaCl_2 significantly alleviated the reduction of leaf area of *S. viminalis* seedlings under heavy metal stress, of which 15 and 30 $\mu\text{mol}\cdot\text{L}^{-1}$ were sprayed under heavy metal stress. The leaf area of *S. viminalis* seedlings treated with 30 $\mu\text{mol}\cdot\text{L}^{-1}$ exogenous CaCl_2 was 26.51% ($P < 0.05$) and 37.21% ($P < 0.05$), respectively.

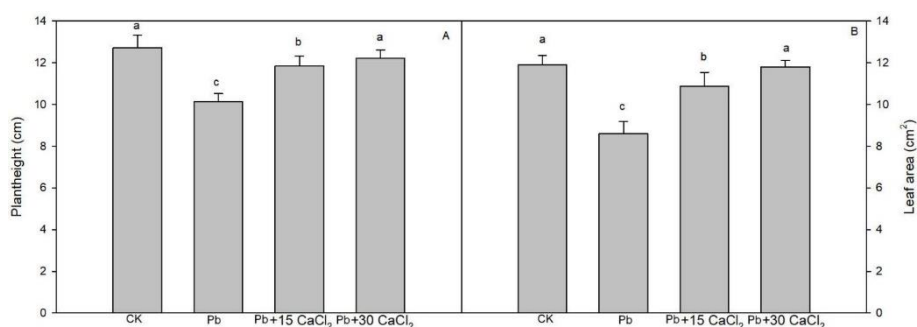


Figure 1. Effects of CaCl_2 on leaf growth of *S. viminalis* seedlings under Pb Stress. CK: CK + 0 CaCl_2 contents; + CaCl_2 : CK + different amounts of CaCl_2 contents. Note: Data in the figure are the mean \pm SD; values followed by different lowercase letters indicate a significant difference ($p < 0.05$)

*Effects of exogenous CaCl_2 on Photosynthetic gas exchange parameters of *S. viminalis* seedlings under Pb Stress*

Compared with CK, P_n , G_s and T_r of *S. viminalis* seedlings leaves under Pb stress were significantly decreased, but spraying different concentrations of exogenous CaCl_2 significantly alleviated the reduction range of P_n , G_s and T_r . Except that there was no significant difference between spraying different concentrations of exogenous CaCl_2 and spraying CaCl_2 under heavy metal stress, spraying 15 and 30 $\mu\text{mol}\cdot\text{L}^{-1}$ in leaves of *S. viminalis* seedlings leaves Under CaCl_2 Treatment, P_n and G_s in leaves of *S. viminalis* seedlings were significantly increased compared with those without CaCl_2 treatment. It can be seen from Fig. 2D that spraying different concentrations of exogenous CaCl_2 also significantly alleviated the C_i reduction of *S. viminalis* seedlings under heavy metal stress, but there was no significant difference between the C_i of *S. viminalis* seedling leaves treated with 30 $\mu\text{mol}\cdot\text{L}^{-1}$ exogenous CaCl_2 and that without spraying exogenous CaCl_2 .

*Effects of exogenous CaCl_2 on F_v/F_m , Φ_{PSII} , ETR and NPQ of *S. viminalis* seedlings under Pb stress*

Under Pb stress, F_v/F_m , Φ_{PSII} and ETR of *S. viminalis* seedlings decreased significantly, while NPQ increased significantly (Fig. 3). However, spraying different concentrations of CaCl_2 significantly alleviated the decrease of F_v/F_m , Φ_{PSII} and ETR of *S. viminalis* seedlings leaves, especially under heavy metal stress, when spraying

30 $\mu\text{mol}\cdot\text{L}^{-1}$ exogenous CaCl₂, the Φ_{PSII} of *S. viminalis* seedlings leaves increased by 73.24% ($P<0.01$). There was no significant difference in F_v/F_m , Φ_{PSII} and ETR between different concentrations of CaCl₂. Spraying different concentrations of CaCl₂ increased NPQ of *S. viminalis* seedlings leaves under heavy metal stress, but there was no significant difference among different concentrations of CaCl₂. However, NPQ of *S. viminalis* seedlings under 30 $\mu\text{mol}\cdot\text{L}^{-1}$ CaCl₂ treatment was significantly higher than that under Pb stress.

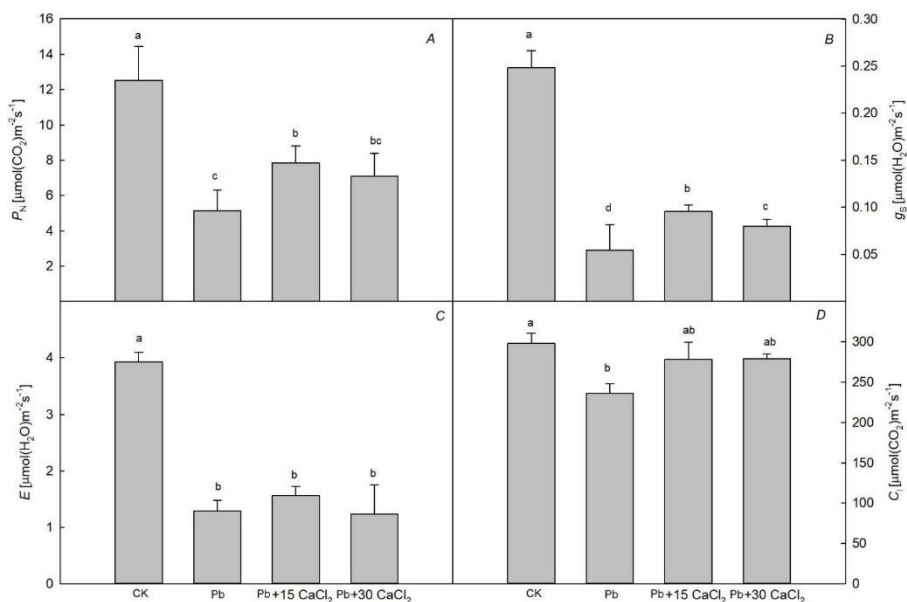


Figure 2. Effects of different concentrations of exogenous CaCl₂ on net photosynthetic rate (a), stomatal conductance (b), transpiration rate (c) and intercellular CO₂ concentration (d) of *S. viminalis* seedlings under Pb Stress. CK: CK + 0 CaCl₂ contents; +CaCl₂: CK + different amounts of CaCl₂ contents. Note: Data in the figure are the mean \pm SD values followed by different lowercase letters indicate a significant difference ($p<0.05$)

Effects of exogenous CaCl₂ on OJIP curve of *S. viminalis* seedlings under Pb stress

Compared with CK, the relative fluorescence intensity of O point and J point had no significant change under Pb stress, while the relative fluorescence intensity of I and P decreased significantly, especially that of P point (Fig. 4). However, spraying different concentrations of exogenous CaCl₂ could significantly reduce the change range of OJIP curve of *S. viminalis* seedlings under heavy metal stress.

Effects of exogenous CaCl₂ on standardized O-P curve, V_J and V_I of *S. viminalis* seedlings under heavy metal stress

Compared with CK, the relative variable fluorescence (V_J) of each point on the V_{O-P} curve of *S. viminalis* seedlings leaves under Pb stress increased significantly with the relative variable fluorescence V_I of J point at 2 ms (Fig. 5). the increase range of V_J in leaves of *S. viminalis* seedlings treated with different concentrations of exogenous CaCl₂ was significantly less than that of no CaCl₂ treatment. At 0.3 ms, the change range of K point relative to variable fluorescence V_K was small, and it was not significantly affected by spraying CaCl₂.

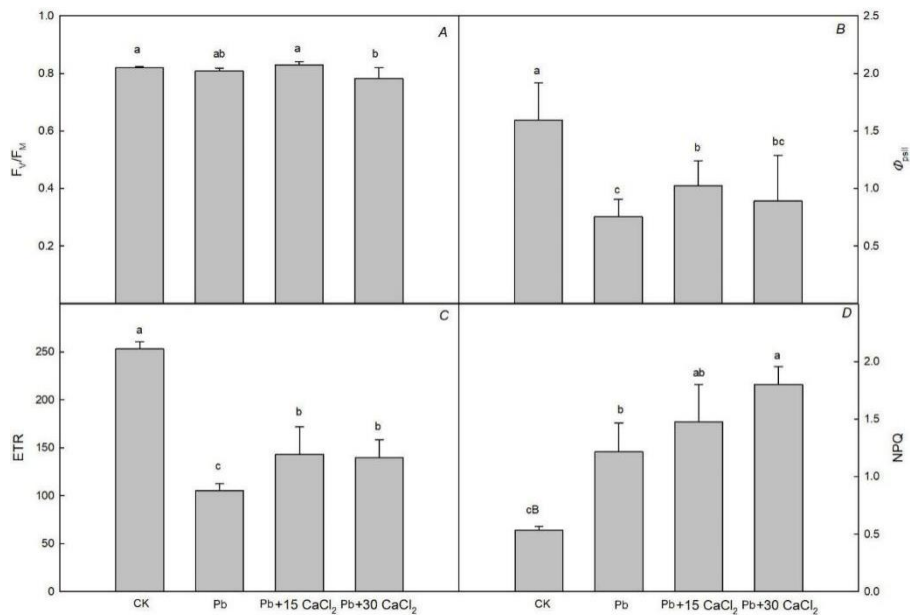


Figure 3. Effects of different concentrations of exogenous CaCl₂ on the maximum photochemical efficiency (F_v/F_m) and the actual photochemical efficiency (Φ_{PSII}) of PSII reaction center electron transfer rate (ETR) and non-photochemical quenching (NPQ) in leaves of *S. viminalis* seedlings under Pb Stress. CK: CK + 0 CaCl₂ contents; +CaCl₂: CK + different amounts of CaCl₂ contents. Note: Data in the figure are the mean \pm SD values followed by different lowercase letters indicate a significant difference ($p < 0.05$)

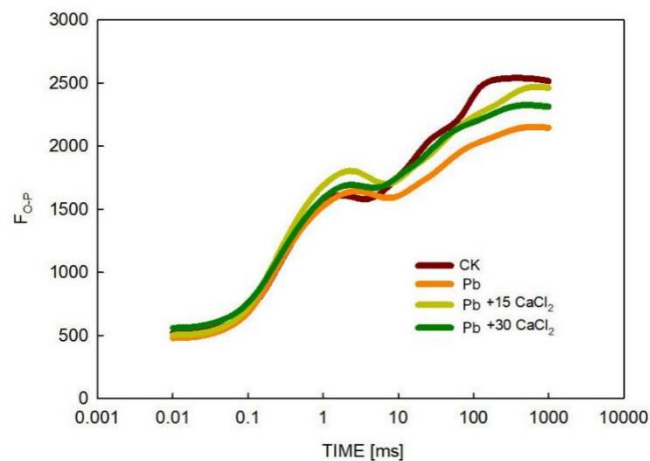


Figure 4. Effects of different concentrations of exogenous CaCl₂ on OJIP curve of *S. viminalis* seedlings under Pb Stress. CK: CK + 0 CaCl₂ contents; +CaCl₂: CK + different amounts of CaCl₂ contents

The results of quantitative analysis of V_J and V_K showed that the V_J of *S. viminalis* seedling leaves under Pb stress increased by 24.63% ($P < 0.05$), while the V_J of leaves of *S. viminalis* seedlings treated with 15 and 30 $\mu\text{mol}\cdot\text{L}^{-1}$ CaCl₂ increased by 21.77% ($P < 0.05$) and 18.44% ($P < 0.05$), respectively. Under Pb stress, the V_K of *S. viminalis* seedlings leaves had no significant change compared with CK, and spraying different concentrations of CaCl₂ did not significantly change the V_K of *S. viminalis* seedlings leaves.

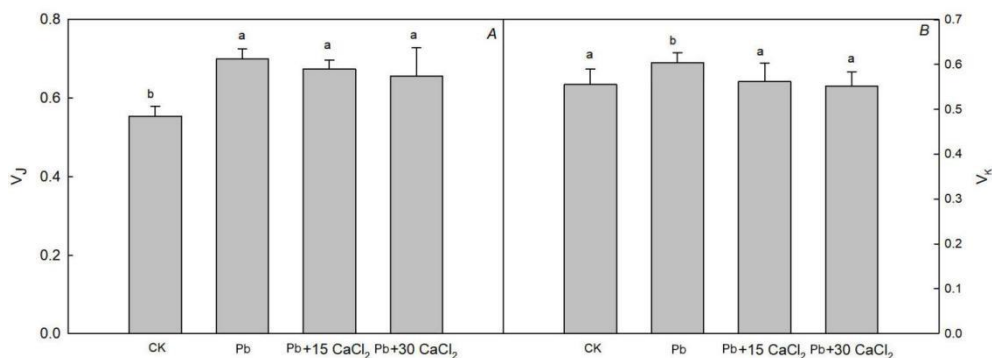


Figure 5. Effects of different concentrations of exogenous CaCl₂ on V_j (a) and V_k (b) in leaves of *S. viminalis* seedlings under Pb Stress. CK: CK + 0 CaCl₂ contents; +CaCl₂: CK + different amounts of CaCl₂ contents. Note: Data in the figure are the mean ± SD; values followed by different lowercase letters indicate a significant difference ($p < 0.05$)

Effects of exogenous CaCl₂ on reactive oxygen species and membrane peroxidation of *S. viminalis* seedlings under Pb Stress

Compared with CK, the results showed that the treatment of 30 μmol·L⁻¹ exogenous CaCl₂ had the most obvious effect, and the O₂^{·-} production rate and H₂O₂ content decreased by 25.83% ($P < 0.05$) and 32.22% ($P < 0.05$), respectively, which resulted in the decrease of MDA content and electrolyte leakage rate of membrane lipid peroxidation by 21.43% ($P < 0.05$) and 25.14% ($P < 0.05$), respectively (Fig. 6).

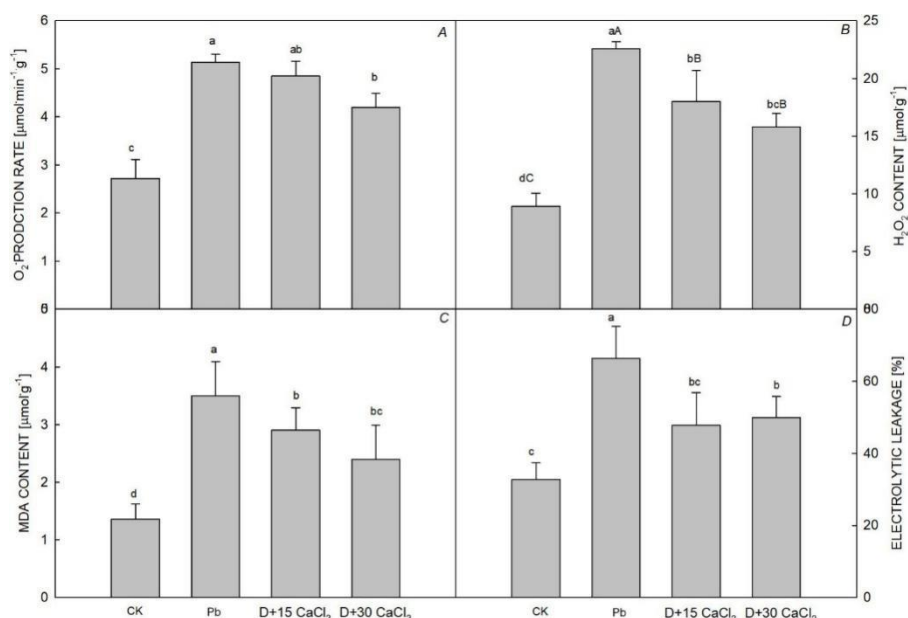


Figure 6. Effects of different concentrations of exogenous CaCl₂ on O₂^{·-} production rate (a), H₂O₂ Content (b), MDA content (c) and electrolyte leakage rate (d) in leaves of *S. viminalis* seedlings under Pb Stress. CK: CK + 0 CaCl₂ contents; +CaCl₂: CK + different amounts of CaCl₂ contents. Note: Data in the figure are the mean ± SD; values followed by different lowercase letters indicate a significant difference ($p < 0.05$)

Discussion

Pb is a kind of non-essential element for plant growth, which has different effects on different plants when it enters into plants. Many studies have shown that low concentrations of Pb can stimulate plant growth, moderate concentrations of Pb can cause plant metabolic disorders and inhibit growth, while heavy concentrations of Pb can cause plant death (Del et al., 1999a,b; Dong et al., 2008), CaCl₂ could alleviate the growth inhibition of heavy metals on plants (Saradhi et al., 2001; Li et al., 2011; Zhang et al., 2014). In this study, Pb significantly reduced the growth rate of plant height and leaf area; Application of CaCl₂ after Pb stress could reduce the inhibition of Pb on leaf area and plant height growth of *S. viminalis*.

Under Pb stress, the photosynthetic carbon assimilation capacity of *S. viminalis* seedlings leaves was limited, which was mainly manifested in the decrease of P_n , along with the decrease of G_s , T_r and C_i . According to Farquhar's photosynthetic stomatal factor analysis theory (Farquhar et al., 2003), the reason for the decrease of photosynthetic carbon assimilation capacity of *S. viminalis* seedlings under heavy metal stress was directly related to the decrease of stomatal conductance. Although the decrease of water loss can effectively prevent the loss of water, it also directly reduces the supply of carbon assimilation material (CO₂), which limits its carbon assimilation capacity. In this experiment, spraying different concentrations of exogenous CaCl₂ increased P_n in different degrees, which was similar to the change of G_s , and accompanied by the increase of C_i , indicating that spraying exogenous CaCl₂ could improve the photosynthetic capacity of *S. viminalis* seedlings by improving stomatal limitation.

Under Pb stress, the dark response of plant leaves was inhibited, and the accumulation of assimilative capacity (ATP and NADPH) would feedback inhibit the light response process, resulting in the excess of electrons in the photosynthetic electron transport chain (Li et al., 2000; Liu et al., 2006). In addition, the decrease of PSII activity also inhibited the process of light energy absorption and electron transfer. In this experiment, although F_v/F_m , ETR and, Φ_{PSII} of *S. viminalis* seedlings were significantly decreased under Pb stress. F_v/F_m and, Φ_{PSII} were important indexes reflecting the photochemical activity of PSII, and the sensitivity of Φ_{PSII} was significantly higher than that of F_v/F_m (Kalaji et al., 2016). Therefore, the results showed that the photochemical activity of PSII in leaves of *S. viminalis* seedlings was inhibited under heavy metal stress, and the process of PSII electron transport was hindered. However, the decrease of PSII photochemical activity was alleviated by spraying different concentrations of exogenous CaCl₂, especially 30 $\mu\text{mol}\cdot\text{L}^{-1}$. The results showed that exogenous CaCl₂ could alleviate the photoinhibition of *S. viminalis* seedlings under heavy metal stress and promote electron transfer. NPQ was positively correlated with heat dissipation dependent on xanthophyll cycle. Under Pb stress, NPQ in leaves of *S. viminalis* seedlings increased significantly, which means that the excess excitation energy in PSII could be dissipated by increasing NPQ under Pb stress, so as to reduce the pressure of PSII reaction center. The NPQ of *S. viminalis* seedlings leaves treated with different concentrations of exogenous CaCl₂ increased to varying degrees. Ivanov et al. (1995) found that CaCl₂ treatment enhanced the xanthophyll cycle in barley seedlings, which enhanced the opening degree of photosystem II reaction center and promoted the utilization rate of light energy. Therefore, the reason why spraying exogenous CaCl₂ to alleviate the decrease of PSII in leaves of *S. viminalis* seedlings under heavy metal stress may be related to the mechanism of energy dissipation dependent on xanthophyll cycle induced by CaCl₂.

Under stress conditions, the blocking sites of photosynthetic electron transfer often occur on the electron donor side and receptor side of PSII reaction center, especially the transfer of Q_A to Q_B is the main inhibition site (Zhang et al., 2018a). The increase of J point relative to variable fluorescence V_J at 2 ms on the normalized O-P curve indicated that the electron transfer from Q_A to Q_B was blocked in the photosynthetic electron transport chain (Zhang et al., 2017; Zhang, 2018b). The increase of relative variable fluorescence V_K at 0.3 ms on the normalized O-J curve was considered as a specific marker of damage to OEC activity of PSII electron donor side oxygen complex (Zhang et al., 2012, 2016). In this experiment, the V_J of *S. viminalis* seedlings leaves increased significantly under Pb stress, but the V_K did not change significantly, which indicated that the reason for the decrease of PSII photosynthetic electron transfer rate under Pb stress mainly occurred in PSII receptor side. However, the change of V_K was not only affected by the donor side injury of PSII, but also by the receptor side injury of PSII. When the injury degree of the recipient side was greater than that of the donor side, the V_K did not increase significantly (Xu et al., 2018; Zhang et al., 2018c). Therefore, in this study, the effect of heavy metal stress on the donor side of PSII may be due to the insensitivity of OEC to Pb stress, or it may be due to the excessive damage on the receptor side. However, spraying different concentrations of exogenous CaCl₂ significantly alleviated the increase of V_J, but the effect on V_K was not significant, which indicated that exogenous CaCl₂ could promote the electron transfer from Q_A to Q_B in PSII receptor side of *S. viminalis* seedlings under Pb stress.

Pb usually leads to excessive reduction of photosynthetic electron transport chain in plants, and produces a large number of ROS in chloroplasts and mitochondria (Ramachandra et al., 2004; Asada, 2009; Ahmed et al., 2009). Excessive ROS breaks the redox balance in plants, causes membrane peroxidation, damages membrane system, and causes oxidative damage to cell components and structures (Jiang and Zhang, 2004; Gill et al., 2010). Under normal conditions, the production and elimination of intracellular free radicals are in a dynamic equilibrium state. When the concentration of exogenous Pb²⁺ reaches a certain level, this dynamic balance will be broken, resulting in membrane lipid peroxidation and osmotic stress (Amhed et al., 2009; Li and Li, 2011). The results also showed that under Pb stress, the relative permeability of cell membrane increased, the production rate of O₂^{•-} and the content of MDA increased, which caused lipid peroxidation in the inner membrane of *S. viminalis*. Under Pb stress, O₂^{•-} production rate and H₂O₂ content were significantly increased, MDA content and electrolyte leakage rate were also significantly increased, which indicated that excessive ROS caused membrane system peroxidation and increased membrane permeability. However, spraying different concentrations of exogenous CaCl₂ significantly alleviated ROS production and membrane lipid peroxidation of *S. viminalis* seedlings, especially the treatment of 30 μmol·L⁻¹ CaCl₂ was the most effective, which was consistent with the change of photosynthetic parameters of *S. viminalis* seedlings. Spraying exogenous CaCl₂ could alleviate ROS production by enhancing photosynthetic capacity and reducing PSII damage degree of *S. viminalis* seedlings, and the decrease of ROS production could also alleviate the photoinhibition of *S. viminalis* seedlings leaves under heavy metal stress.

Conclusion

The photosynthetic capacity of *S. viminalis* seedlings was decreased under Pb stress, mainly due to stomatal factors, and also related to the decrease of PSII photochemical

activity and the damage of membrane system caused by ROS. Under Pb stress, spraying different concentrations (15 and 30 $\mu\text{mol}\cdot\text{L}^{-1}$) of exogenous CaCl₂ promoted the photosynthetic capacity of *S. viminalis* seedlings, especially 30 $\mu\text{mol}\cdot\text{L}^{-1}$ CaCl₂. The main reason is that exogenous CaCl₂ can effectively reduce the energy pressure of PSII reaction center in leaves of *S. viminalis* seedlings under Pb stress by inducing the increase of NPQ, thus alleviating the photoinhibition degree of PSII under Pb stress, promoting the electron transfer rate, especially the electron transfer ability of PSII receptor side. Under Pb stress, spraying exogenous CaCl₂ could also effectively reduce ROS production in leaves of *S. viminalis* seedlings and alleviate the degree of membrane lipid peroxidation. Therefore, the inhibition of ROS production by spraying CaCl₂ under heavy metal stress is not only related to the enhancement of photosynthetic capacity, but also to the increase of enzymatic or non-enzymatic related ROS scavenging system induced by CaCl₂, but this needs further study.

Funding. This study was financially supported by Jilin Provincial Natural Science Foundation No. YDZJ202101ZYTS113.

REFERENCES

- [1] Ahmed, C. B., Rouina, B. B., Sensoy, S., Boukhris, M., Abdallah, F. B. (2009): Changes in gas exchange, proline accumulation and antioxidative enzyme activities in three olive cultivars under contrasting water availability regimes. – *Environmental & Experimental Botany* 67(2): 345-352.
- [2] Albert, K. R., Mikkelsen, T. N., Michelsen, A., Ropoulsen, H., Leon, V. D. L. (2011): Interactive effects of drought, elevated CO₂ and warming on photosynthetic capacity and photosystem performance in temperate heath plants. – *Journal of Plant Physiology* 168(13): 1550-1561.
- [3] Allahverdiyeva, Y., Suorsa, M., Rossi, F., Pavesi, A., Kater, M. M., Antonacci, A., Tadini, L., Pribil, M., Schneider, A., Wanner, G., Leister, D., Aro, E. M., Barbato, R., Pesaresi, P. (2013): Arabidopsis plants lacking PsbQ and PsbR subunits of the oxygen-evolving complex show altered PSII supercomplex organization and short-term adaptive mechanisms. – *Plant Journal* 75(4): 671-684.
- [4] Asada, K. (2006): Production and scavenging of reactive oxygen species in chloroplasts and their functions. – *Plant Physiology* 141(2): 391-396.
- [5] Chen, E., Zhang, C. M., Su, Y. Q., Ma, J., Zhang, Z. W., Yuan, M., Zhang, H. Y., Yuan, S. (2017): Responses of photosystem II and antioxidative systems to high light and high temperature co-stress in wheat. – *Environmental & Experimental Botany* 135(3): 45-55.
- [6] Chen, Z. F., Wang, Z., Yang, Y. G., Li, M., Xu, B. C. (2018): Abscisic acid and brassinolide combined application synergistically enhances drought tolerance and photosynthesis of tall fescue under water stress. – *Scientia Horticulturae* 228(26): 1-9.
- [7] Del, V. C., Barea, J. M., Azcon-Aguilar, C. (1999a): Diversity of arbuscularmycorrhizal fungus populations in heavy-metal-contaminated soils. – *Applied Environmental Microbiology* 65(2): 718-723.
- [8] Del, V. C., Barea, J. M., Azcon-Aguilar, C. (1999b): Assessing the tolerance to heavy metals of arbuscular mycorrhizal fungi isolated from sewage sludge-contaminated soils. – *Applied Soil Ecology* 11(2-3): 261-269.
- [9] Dong, Y., Zhu, Y. G., Smith, F. A., Wang, Y., Chen, B. (2008): Arbuscular mycorrhiza enhanced arsenic resistance of both white clover (*Trifolium repens* Linn.) and ryegrass (*Lolium perenne* L.) plants in an arsenic-contaminated soil. – *Environmental Pollution* 155(1): 174-181.

- [10] Farquhar, G. D. F., Sharkey, T. D. (2003): Stomatal Conductance and Photosynthesis. – Annual Review of Plant Physiology and Plant Molecular Biology 33(33): 317-345.
- [11] Gill, S. S., Tuteja, N. (2010): Reactive oxygen species and antioxidant machinery in abiotic stress tolerance in crop plants. – Plant Physiology & Biochemistry 48(12): 909-930.
- [12] Guadagno, C. R., Ewers, B. E., Speckman, H. N., Aston, T. L., Huhn, B. J., DeVore, S. B., Ladwig, J. T., Strawn, R. N., Weinig, C. (2017): Dead or alive? Using membrane failure and chlorophyll fluorescence to predict mortality from drought. – Plant Physiology 175(1): 223-234.
- [13] Hu, Y. B., Sun, G. Y., Wang, X. C. (2007): Induction characteristics and response of photosynthetic quantum conversion to changes in irradiance in mulberry plants. – Journal of Plant Physiology 164(8): 959-968.
- [14] Ivanov, A. G., Krol, M. D., Huner, N. P. (1995): Abscisic acid induced protection against photoinhibition of PSII correlates with enhanced activity of the xanthophyll cycle. – Febs Letters 371(1): 61-64.
- [15] Jiang, M. Y., Zhang, J. H. (2004): Abscisic acid and antioxidant defense in plant cells. – Acta Botanica Sinica 46(1): 1-9.
- [16] Kalaji, H. M., Schansker, G., Ladle, R. J., Goltsev, V., Bosa, K., Allakhverdiev, S. I., Brestic, M., Bussotti, F., Calatayud, A., Dabrowski, P., Elsheery, N. I., Ferroni, L., Guidi, L., Hogewoning, S. W., Jajoo, A., Misra, A. N., Nebauer, S. G., Pancaldi, S., Penella, C., Poli, D., Pollastrini, M., Romanowska-Duda, Z. B., Rutkowska, B., Serodio, J., Suresh, K., Szulc, W., Tambussi, E., Yanniccari, M., Zivcak, M. (2014): Frequently asked questions about in vivo chlorophyll fluorescence: practical issues. – Photosynthesis Research 122(2): 121-58.
- [17] Larkindale, J., Huang, B. R. (2004): Thermotolerance and antioxidant systems in *Agrostis stolonifera*: involvement of salicylic acid, abscisic acid, calcium, hydrogen peroxide, and ethylene. – Journal of Plant Physiology 161(4): 405-413.
- [18] Li, X. P., Bjorkman, O., Shi, C., Grossman, A. R., Rosenquist, M., Jansson, S., Niyogi, K. K. (2000): A pigment-binding protein essential for regulation of photosynthetic light harvesting. – Nature 403(6768): 391-395.
- [19] Li, Y. Q., Li, T. L. (2011): Regulations of Calcium and Calcium Inhibitors on the Low Light Tolerance in Tomato. – Acta Agriculturae Boreali-Occidentalis Sinica.
- [20] Liu, W. J., Yuan, S. N. H., Lei, T., Duan, H. G., Liang, H. G., Lin, H. H. (2006): Effect of water stress on photosystem 2 in two wheat cultivars. – Biologia Plantarum 50(4): 597-602.
- [21] Ogbomida, E. T., Nakayama, S. M. M., Bortey-Sam, N., Oroszlany, B., Tongo, I., Enuneku, A. A., Ozekeke, O., Ainerua, M. O., Fasipe, I. P., Ezemonye, L. I., Mizukawa, H., Ikenaka, Y., Ishizuka, M. (2018): Accumulation patterns and risk assessment of metals and metalloids in muscle and offal of free-range chickens, cattle and goat in Benin City. – Ecotoxicology and Environmental Safety 151: 98-108.
- [22] Ramachandra, R. A., Chaitanya, K. V., Vivekanandan, M. (2004): Drought-induced responses of photosynthesis and antioxidant metabolism in higher plants. – Journal of Plant Physiology 161(11): 1189-1202.
- [23] Ryan, P. R., Kochian, L. V. (1993): Interaction between aluminum toxicity and calcium uptake at the root apex in near-isogenic lines of wheat (*Triticum aestivum* L.) differing in aluminum tolerance. – Plant Physiology 102(3): 975-982.
- [24] Saradhi, P. P., Suzuki, I., Katoh, A., Sakamoto, A., Sharmila, P., Shi, D. J. (2000): Protection against the photo-induced inactivation of the photosystemII complex by CaCl₂ cistic acid. – Plant Cell Environment 23(7): 711-718.
- [25] Sauliutė, G., Svecevičius, G. (2015): Heavy metal interactions during accumulation via direct route in fish: a review. – Zoology & Ecology 25(1): 77-86.
- [26] Shen, W. B., Xu, L. L., Ye, M. B., Zhang, R. X. (1996): Study on determination of ASP activity. – Plant Physiology Communications 32(3): 203-205.

- [27] Shu, X., Yin, L. Y., Zhang, Q. F., Wang, W. B. (2012): Effect of Pb toxicity on leaf growth, antioxidant enzyme activities, and photosynthesis in cuttings and seedlings of *Jatropha curcas* L. – *Environmental Science and Pollution Research* 19(3): 893-902.
- [28] Soffianian, A., Madani, E., Arabi, M. (2014): Risk assessment of heavy metal soil pollution through principal components analysis and false color composition in Hamadan Province, Iran. – *Environmental Systems Research* 3(1): 1-14.
- [29] Strasser, R. J., Srivastava, A., Govindjee (1995): Polyphasic chlorophyll a fluorescence transient in plants and cyanobacteria. – *Photochemistry and Photobiology* 61(1): 32-42.
- [30] Wang, Y. G., Peng, C. X., Zhan, Y. N., Yu, L. H., Li, M., Li, J., Geng, G. (2017): Comparative proteomic analysis of two sugar beet cultivars with contrasting drought tolerance. – *Journal of Plant Growth Regulation* 36(3): 1-13.
- [31] Xu, N., Zhang, H. H., Zhong, H. X., Wu, Y. N., Li, J. B., Li, X., Yin, Z. P., Zhu, W. X., Qu, Y., Sun, G. Y. (2018): The response of photosynthetic functions of F1 cutting seedlings from *Physocarpus amurensis* Maxim (♀) × *Physocarpus opulifolius* “Diabolo” (♂) and the parental leaves to salt stress. – *Frontiers in Plant Science*, DOI: 10.3389/fpls.00714.
- [32] Zhai, F. F., Mao, J. M., Liu, J. X., Peng, X., Han, L., Sun, Z. Z. (2016): Male and female subpopulations of *S. viminalis* present high genetic diversity and high long-term migration rates between them. – *Frontiers in Plant Science* 7: 330.
- [33] Zhang, F. Q., Wang, Y. S., Luo, Z. P., Dong, J. D. (2007): Effect of heavy metal stress on antioxidative enzymes and lipid peroxidation in leaves and roots of two mangrove plant seedlings (*Kandeliacandel* and *Bruguieragymnorhiza*). – *Chemosphere* 67(1): 44-50.
- [34] Zhang, Z., Li, G., Gao, H., Zhang, L. T., Yang, C., Liu, P., Meng, Q. W. (2012): Characterization of photosynthetic performance during senescence in stay-green and quick-leaf-senescence *Zea mays* L. inbred lines. – *Plos One* 7(8): e42936.
- [35] Zhang, G. H., Liu, Y. F., Ni, Y., Meng, Z. J., Lu, T. (2014): Exogenous Calcium Alleviates Low Night Temperature Stress on the Photosynthetic Apparatus of Tomato Leaves. – *Plos One* 9(5): e97322.
- [36] Zhang, H. H., Zhong, H. X., Wang, J. F., Xu, N. (2016): Adaptive changes in chlorophyll content and photosynthetic features to low light in *Physocarpus amurensis* Maxim and *Physocarpus opulifolius* “Diabolo”. – *Peer J* 4(3): e2125.
- [37] Zhang, H. H., Xu, N., Li, X., Jin, W. W., Tian, Q., Sun, G. Y., Gu, S. Y. (2017): Overexpression of 2-Cys Prx increased salt tolerance of photosystem II in tobacco. – *International Journal of Agriculture and Biology* 19(4): 735-745.
- [38] Zhang, H. H., Xu, N., Sui, X., Long, J. H., Wu, Y. N., Li, J. B., Wang, J. F., Qu, Y., Sun, G. Y. (2018a): Arbuscular mycorrhizal fungi (*Glomus mosseae*) improves growth, photosynthesis and protects photosystem II in leaves of *Lolium perenne* L. under cadmium contaminated soil. – *Frontiers in Plant Science*, DOI: 10.3389/fpls.01156.
- [39] Zhang, H. H., Feng, P., Yang, W., Sui, X., Li, W., Zhang, R. T., Gu, S. Y., Xu, N. (2018b): Effects of flooding stress on the photosynthetic apparatus of leaves of two *Physocarpus* cultivars. – *Journal of Forest Research* 39(4): 1049-1059.
- [40] Zhang, H. H., Xu, N., Sui, X., Yin, Z. P., Zhu, W. X., Li, X., Sun, G. Y. (2018c): Photosystem II function response to drought stress in leaves of two alfalfa (*Medicago sativa*) varieties. – *International Journal of Agriculture and Biology* 20(5): 1012-1020.

ECOLOGICAL WISDOM CONTAINED IN THE BELIEF IN WATER GOD ALONG THE ANCIENT SILK ROAD

MENG, F. L. – WANG, Y.*

*School of Literature and Art, Shihezi University, No. 225, No. 31 Beishi Road, Shihe-Zi 832003,
Xinjiang, China*

**Corresponding author*

e-mail: 1076435664@qq.com; phone: +86-137-5310-3709

(Received 31st Aug 2021; accepted 6th Dec 2021)

Abstract. With the increasing scarcity of potable freshwater resources worldwide, the protection and utilization of water resources in the current ecological civilization society should be more scientific and accurate. This paper takes the belief in the water god as the research object, focusing on the ecological ethics, ecological aesthetics, and moral concern of “harmony between human and water” along the ancient Silk Road with frequent cultural exchanges and trade under the triple vision of belief, culture and aesthetics. From the aspects of artistic dissemination, regional resources (humanities and nature), and technological exchanges, this paper excavates the water wisdom of ancient society in daily production and life. It adopts the methods of historical carding, category study, and case analysis. This paper attempts to reveal the development value and application of cross-regional ecological aesthetics and ecological wisdom in the cultural exchange between the East and the West under the artistic form and spatial distribution of water god worship along the ancient Silk Road. This paper discusses the construction method of sustainable development of water culture under the concept of “harmony between human and water.”

Keywords: *mutual learning among civilizations, spiritual belief, artistic image, mutual proof of picture and text, ecological aesthetics*

Introduction

Due to the global ecological crisis, water resources are scarce, and water disasters occur frequently. As a result, modern people try to find the wisdom to solve problems from the ancient people’s view of nature and life, and the result is that the thought of “unity of man and nature” in the East rises all boats. From the western perspective, the charm of the natural view of “the unity of man and nature” lies in the harmonious symbiosis between man and nature. In oriental culture, man and nature are not the relationships of opposition and mutual conquest. Man is a part of natural life, and nature is the object of awe. With the deepening of people’s understanding of it, water has changed from the “deified” resources worshipped and feared by the ancients to the modern “materialized” development of economic resources and then to the protection and rational utilization under the current ecological background. Because the belief in Water God has a robust regional color, different geographical environments, humanistic atmosphere, and social politics will give birth to different belief contents and expressions. The unique geographical environment and folk cultural atmosphere of the areas along the Silk Road make it very different from other regional artistic circles. As different from the water god belief culture in the Humid zone, the water god belief culture in the arid area along the Silk Road is not only the product of regional cultural characteristics but also has a particular influence on the exchange of ideas, culture, and folk customs along the Silk Road.

This study attempts to take the ancient Silk Road as cultural space and geographical space, to study the relationship between folk belief and artistic expression, to explore

the regional water culture type research centered on the creative image of the water god, and to reveal the ecological wisdom in production, life, and spiritual belief through the mutual evidence between written and non-written materials and the value expression of water god belief culture. Studying the belief in water gods from regional culture along the ancient Silk Road is of great value for us to understand the folk culture, belief culture, and artistic aesthetics in the old Silk Road.

Journals reviewed

The research on the belief of water god along the Silk Road is “minimal at home and abroad.” The study and exposition of the art image of the water god are even less, and there is a lack of research on the integrity, origin, and generality of water god worship. Reading the literature shows that the worship of water gods is primarily concentrated in water-rich areas and coastal areas of rivers and seas. At the same time, there is little research on the worship of water gods in arid regions. In terms of discipline, there are many types of research on water god worship in national water culture, flood myth, water conservancy project, etc. Still, the content of analyzing water god worship by artistic image is more diminutive. As a branch of nature worship, water god worship embodies human ecological consciousness from primitive society to the present. The research on the belief culture of Water God mainly includes the following aspects:

Water god worship is a branch of nature worship in folk culture, and the protection of water resources has been a hot issue in academic circles. Generally speaking, the concept of “water culture” has been integrated into social production and daily life discourse. The eco-theological movement in the West has developed considerably since the 1960s. Many theologians pay attention to the ecological crisis from different angles. The famous German theologian, Jurgen Moltmann, emphasizes the secular nature of belief in his theology. His research is closely related to contemporary social problems. However, most Western countries pay attention to the study of the ecological concept of nature, and the systematic analysis on the water god is less. The water belief in the areas along the Silk Road is even more lacking. In China, water god worship has a long history as a branch of folk belief under genuine conviction, and Chinese academic circles have studied it for a long time. The earliest research on water god is Mr. Huang Zhigang. His book *Chinese Water God* (Huang, 1998) makes a comparative analysis of many myths, summarizes, combs, and discusses the situation of water gods in various parts of China based on ancient books and legends. In his book *Water worship in China* (Xiang, 1996), Xiang Baisong studied the basis of belief in water gods, the original connotation and development of water mythology, water worship, constituent factors, water worship objects, water worship rituals, and the influence of water worship on Chinese culture and history. Wu Bingen makes a comprehensive study of Chinese folk beliefs in his book *Chinese Folk beliefs* (Wu, 1996), in which he briefly expounds on the worship of water and water gods and introduces the primary worship of water gods of each nation. In the article *Research on Water God worship in pre-Qin, Qin, and Han dynasties* (Cai, 2013), Cai Honghua mainly expounds on the influence of water god worship on the historical and cultural society at that time from the scope of water god worship, the change of function, the personification of water god and so on. In his article on *Water God worship in the Tang Dynasty* (Wang, 2006), Wang Yong Ping systematically enumerated the objects and types of water god worship in the Tang Dynasty and then described the development of water god-belief from two aspects: temples and rivers and lakes.

Ethnology, folklore, history, human geography, literature and art, and other different disciplines are involved in the study of water god belief. In Shen Songbai's study of *Wu Yue Folk Water God belief* (Shen, 2009), the author takes the Wu Yue area as the research scope and uses the knowledge of folklore, sociology, and anthropology to theoretically analyze and summarize the water god-belief from the perspectives of life and folklore. Still, there is little discussion on the performance carrier and characteristics of water god belief. In Hu Mengfei's study of *Water God belief along the Beijing-Hangzhou Canal in Ming and Qing dynasties* (Hu, 2015), the author macroscopically grasps the composition and distribution of water god belief in Beijing-Hangzhou Canal from the perspective of history, analyzes the reasons and conditions for the rise and spread of water god belief in Beijing-Hangzhou Canal from both natural and social aspects, and expounds the influence of water god belief on the national water control activities in Ming and Qing dynasties and the social life of local people along the coast. In the above article, the biased regional research on the transmission and change of the image is not comprehensive in the systematic and holistic examination of the research content. In Tang Fei's study on *Custom characteristics of Water Temple frescoes in Guangsheng Temple, Shanxi Province* (Tang, 2016), the author explores the artistic and historical value of Guangsheng Temple frescoes and the influence of the custom characteristics of murals on the latest creation and makes contributions to the case study of water gods belief with the research method of fine arts. Still, the analysis of artistic images mainly focuses on the case analysis of murals. There is not much discussion on the influence of the regional scope on his artistic image.

According to the author's data of water god belief, most of the existing discussions are about the description and nature analysis of water god Noumenon and its historical origin, evolution process, cultural connotation, cultural history significance, and rain praying ceremony process. The research on water worship mainly focuses on the connotation, object, regional sacrificial activities, the cultural and historical influence of water worship. At the same time, there are few studies on the artistic image and aesthetic analysis, regional art image characteristics, and evolution of water worship. Further research is needed.

Based on the research results, the author puts forward the necessity of this research. Water culture is a research field with many contents, so multi-disciplinary research methods and theoretical knowledge will be used in the research and discussion. Due to the lack of academic research on the reclaimed water culture in the area along the Silk Road, especially on the artistic image of the water culture. Therefore, this paper takes the relevant theoretical knowledge of art as a starting point and studies water culture from artistic aesthetics and ecology. Therefore, this paper uses the original data about Xinjiang water culture, based on text materials, to study the remaining visual image data to carry out the image analysis and research of "using pictures to prove the history."

Research methods and data

Different geographical environments and cultural atmospheres will give birth to other belief contents. In the historical development process of cultural and economic exchanges, artistic images, as "historical evidence," together with written materials, will become materials for analyzing and corroborating history and culture. In the way of interpretation, this paper will make a comprehensive analysis from three visual fields: space, text, and image.

First of all, from the perspective of space, the origin of civilization is closely related to climatic conditions and has an essential impact on the development of types of society. Geographical environment and climatic conditions determine the basic style and features of national culture, and the birthplaces of major civilizations are directly related to water. As the central area of the ancient Silk Road, Xinjiang has a sensitive ecological environment and weak self-recovery ability (Fig. 1). Many civilizations have disappeared under the influence of natural habitats and manufactured. Some scholars believe that rapid climate change (especially severe cold and dry events) is crucial for the decline of an ancient civilization on the regional scale (Buckley et al., 2010). Some scholars believe that the unreasonable development of the environment is an essential factor leading to the decline of ancient civilization in arid and semi-arid regions of the earth. In the 1990s, some Chinese scholars have noticed the relationship between climate change and the rise and fall of the Silk Road since 2000 (Du, 1996), but there is a little detailed discussion on the relationship between the formation of the Silk Road and climate change. In 1907, when Joseph Widney, an American scholar, proposed to explore the origin of Indo-Europeans from the perspective of “border people,” he mentioned the persistent drought in Central Asia and the resulting reduction of grassland area (Mallory, 1973). In 2007, Craig G. R. Benjamin, an American scholar, analyzed written, monetary and archaeological evidence and explored the relationship between culture and politics in ancient Central Asia when explaining the relationship between the origin of Le Zhi and several Chinese dynasties, among which climate change was one of the reasons for their migration.

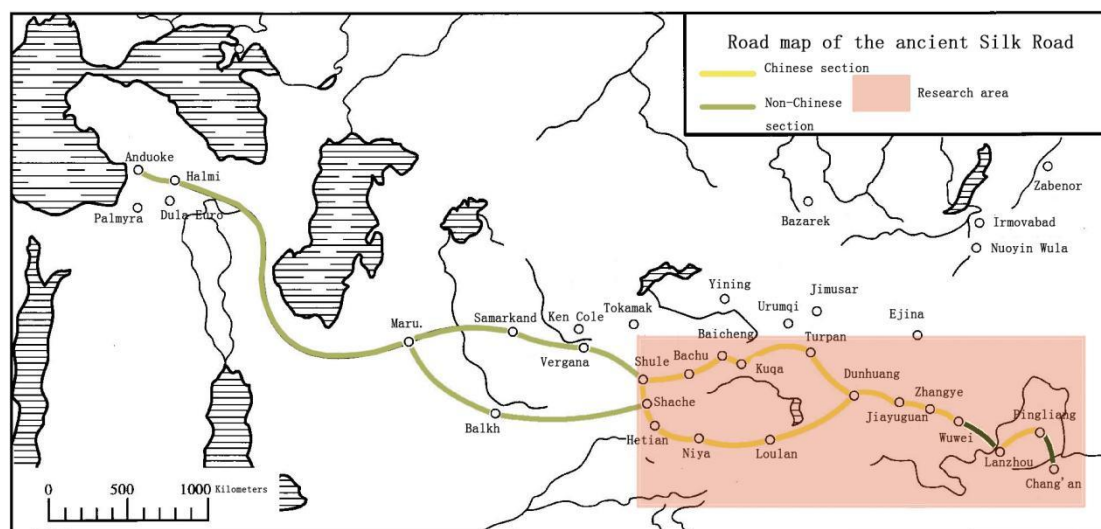


Figure 1. A schematic map of the route of the ancient Silk Road. Figure source network, Redraw <http://www.onegreen.net/jingdianditu/HTML/60920.html>

Secondly, it is explained from the text that this paper mainly combs the relevant literature in the essential context of Chinese traditional cultural ecology based on local chronicles, archives, documents, and other historical materials. This paper studies the regional water culture along the Silk Road from theory, belief, aesthetics, and reality through the research materials of agricultural civilization, natural geographical environment, survival purpose, folklore, and cultural blending. This paper summarizes the cultural implication, spiritual core, folk customs, and unique value orientation in the

water worship culture. As a natural element closely related to human life activities, water must be restored to a more specific, vivid, and perceptual cultural situation to dig out the objective and actual water archetypal image from the root. Yeruyad believes that the invisible “water of life” can be biochemical and tangible, and water symbolizes all primitive matter in form. As the initial form of culture, water in mythology is the sublimation of man’s authentic experience of water. Going back to the source of the thought of water worship, by excavating the inherent genes of water in the region’s mythology along the ancient Silk Road, the ideological similarities and differences of water worship in a large area are compared (*Table 1*).

Table 1. Comparison of world flood myths

Area	Reason	Disaster attribute	Solution	Protagonist image	Life extension
Ancient China	Gonggong (Water God) cannot hit Zhoushan	Tribal war	The female harness is used to control the water	<ul style="list-style-type: none"> • Co-worker: human face and snake body • Nu WA: human face and snake body 	Nu WA pinches people with loess and water
	Flooding of the Yellow River	Natural disaster	King yu combating the flood	<ul style="list-style-type: none"> • No spirit • Man triumphs over nature 	
Ancient Babylon	Human sin	Divine punishment	The water god told me in advance that the ship was built	Enki: there are two streams of water on the shoulders in statues and murals	Return home after escaping
Ancient Greece	Human sin	Divine punishment	Prometheus told me that shipbuilding	God and man	
Ancient India	Flood	Natural disaster	Animals return the favor and build ships	Fish and man	

Third, from the image to explain, through artistic anthropology, folklore, iconology, and other research methods, the ancients how to express water worship through art, embody the thought of heavy water (water worship concept, water control spirit), give full play to the function of art and other aspects. It is devoted to revealing the artistic characteristics of the origin and transplantation of water worship across regions along the Silk Road. It analyzes the creative attributes of folk culture and art images constructed by the concept of water worship in visual images and text display and the expression of the ecological value of water gods worship to today. In the post-industrial era, the traditional oasis water conservancy system and living environment in ancient Iran, Xinjiang, and other regions have changed significantly. They are going through the inheritance process, which is called water cultural heritage in the modern context. At present, the well-preserved aquatic cultural heritage, as a typical underwater cultural heritage, has been concerned by the academic circles and has become the object of protection and development (*Table 2*).

Results

The meeting of belief and aesthetics—faith in water god and folk art

Human development and the natural environment are the unity of mutual influence and interaction in the construction of human history. Without exception, the splendid ancient civilization was born and developed from the river basin. The earlier the period of social development, the greater the dependence of human beings on the environment;

the lower the level of productivity, the more significant the impact of environmental factors on human beings. The Silk Road was the most crucial land passage for East-West communication in Eurasia from the 2nd century BC to the 16th century AD. It was also regarded as the center of world civilization in that period (Frankopan, 2015). As the core area of the ancient Silk Road, Xinjiang of China is the intersection area of Eurasian civilization evolution and the cultural exchange focus of the convergence and integration of Eastern and Western cultural elements.

Table 2. *Water related important agricultural cultural heritage in the context of World Heritage*

Serial number	Name	Type	Approval time	Region	Value characteristics
1	Ningar Waterway Bridge	Water diversion and transportation hybrid water conservancy and transportation facilities	1985	France	Pont du Gard is an excellent example of highly developed water conservancy construction technology in ancient Rome
2	Segovia ancient city and its waterway	Historical buildings and infrastructure	1985	Madrid, Spain	The ancient city and the ancient Roman water bridge are the models of the times
3	Assa oasis: an evolving cultural landscape	Oasis cultural landscape	2018	Saudi Arabia	Oasis cultural landscape is a model for human beings to get along with the environment
4	Jujube planting system in Elche	Oasis cultural landscape	2000	Spain	Good at using water, poor land created a miracle of oasis agricultural production
5	Afraja irrigation system	Oasis cultural landscape	2006	Oman	Irrigation systems in extremely dry areas are the best way to solve the problem of livelihood
6	Shushtar's ancient water conservancy system	water conservancy facilities	2009	Iran	Excellent solution to urban water supply, mill, irrigation, inland transportation, defense system diversity of uses
7	Aien cultural site	Oasis cultural landscape	2011	The United Arab Emirates	Typical oasis human settlements in evolution
8	Persian Karez	Oasis cultural landscape	2016	Iran	In the arid area, the natural water resources are skillfully utilized, controlled and mastered the wisdom of water cycle

Xinjiang, eastern Iran, and five Central Asian countries belong to the arid region of central Asia, which is the largest non-zonal dry area in the world and essential oasis agriculture and landscape distribution area in the world. The water resources change significantly, and the oasis ecosystem is fragile. Many famous ancient civilizations (such as the Loulan Ancient Kingdom and the Qiuci Ancient Kingdom) developed and flourished in the arid areas of central Asia but were finally lost in the long history. Climate change may be one of the essential factors leading to the decline and decline of ancient civilizations in this region.” Historical Records” was written by Sima Qian in 104 BC and was written in 91 BC. Xuan Zang returned to Chang’an in 645 AD. During these 700 years, “Loulan unearthed jade, plants are rich in Reed, Tamarix, Populus euphratica and white grass,” as recorded in the Historical Records. Residents living by the water source to live animal husbandry life “turned into Loulan,” which Xuanzang returned from the scriptures to see that “the city building is still there, but there is no human figure.” This tragic change is believed by some scholars to be caused by the rapid deterioration of the environment and severe drought due to the quicksand

blockage of the lower reaches of the Tarim River flowing into Lop Nur after the 3rd century AD, and some scholars believe that it is the influence of human activities.

Xinjiang's particular geographical pattern and climatic environment make the natural distinction of a regional culture different from that of Rain Water. Because of the bad natural environment, drought, and little rain, based on the need for a living environment and psychological thirst for water, under the influence of primitive religion, shamanism, Zoroastrianism, Taoism, and other ideas of "animism," the primitive nomadic people's belief in water gods gradually formed. Animism is the early result of the primitive ancestors' cognition of natural and social phenomena under the deterrence of nature. Edward Taylor, a British philosopher, is an authoritative interpreter of animism. He believes that animism is the basis of religious philosophy. Under the exchange and collision of various national cultures, the belief in water gods in the areas along the Silk Road is influenced by folk beliefs, traditional cultural thoughts, regional environment, and other comprehensive factors, which is characterized by practicality and utilitarianism. "useful" folk belief culture, which is closely related to production and life, is reflected in myths and legends, arts and crafts, grotto murals and so on. Folk art is rooted in the ecology of folk culture and studies the relationship between folk art and the spiritual belief of "humans." It is the cognition, experience, and psychology formed by people in understanding, development, and survival, and the folk cultural ecology based on these cognition, experience, and psychology. The needs of survival belief and life emotion determine the ways and methods of folk art, so the function of folk art not only expresses the people's feelings but also becomes a symbol of the spiritualization of belief worship and is an essential carrier for the study of cultural characteristics.

People have different ways of expression to symbolize the aesthetic ideal of water culture in different periods, influenced by the social mode of production, social, ideological cognition, the degree of social and cultural development, and other factors at that time. At the same time, it is also influenced by folk customs. The primitive ancestors' cognitive expression of water was mainly totem worship. Nowadays, in the archaeological discoveries along the Silk Road, the pottery unearthed is painted with water ripple, vortex pattern, fish pattern, frog pattern, grid pattern, etc. These are the initial expressions of the early primitive ancestors' prayers and worship for water. These objects have become the physical "evidence" of the early water worship with the combination of practicality and utilitarianism. After the social development, in the period of agricultural society, under the influence of social culture, religious culture, political education, and other factors, the object of water worship has developed from primitive water worship, water-related animal totem worship to water control figures, animal deification, dragons and other worship objects.

From artistic image to folk intention: "mutual proof of picture and text" in the belief of water god

The area's topography along the Chinese section of the Silk Road is complex, including high mountains, basins, Pingchuan, deserts, and the Gobi, especially in Xinjiang and Gansu. For the ancestors who lived along the Silk Road in ancient times, as a necessary factor for survival, water gave rise to natural worship related to water, such as asking for water and praying for rain. Socrates believes that "art imitates nature," and the creation of art is the exertion of imitation instinct. Croce believes that "art is intuition," the source of intuition is emotion, and art is the expression of emotion. Taylor believes that primitive art originates from primitive witchcraft, which is rooted in the animistic

worldview. I think the emergence and development of the art of water belief are that the ancient ancestors generated intuition from the cognition of water-based on imitating nature and formed the water belief culture under the idea of animism in practice.

The belief of water god in the spiritual level

In thousands of years of Chinese cultural history, water belief, as a deep-rooted folk traditional spiritual belief, is not uncommon in the images and text materials along the Silk Road. In collecting data, the author found that although the East and the West are far apart in terms of content expression and image form, there are many similarities in the belief and expression of water. First of all, take fairy tales as an example. The creation myths and heroic myths of the East and the West are mostly related to water. The artistic image of Water God is an image expression symbol based on symbolic semantics, a kind of social, cultural consensus, and folk art based on the interpretable image connotation under the general psychological structure of the people.

The outstanding feature of the art image in the water god belief culture is that it reflects the belief support, ideal needs, emotional comfort, and even psychological dependence of the people. This awe, worship, and demand for water can also be seen through well-known myths, such as the Chinese creation myth Pangu Kai Heaven and Nu WA made man. The myths and legends of various ethnic groups in the area along the Silk Road, such as the mythological motif of the Tatar Qingniuding Earth, in which there is an endless sea below the earth, there is a big fish in the sea, and a green cow is standing on the board of the fish. The horns of the green cattle support the whole earth. If the green cow is tired, change a horn to support it, and there will be an earthquake. In the Kazak creation mythology, the universe is separated from the darkness to give birth to a new world; from the boiling mixture, water, earth, sun, and stars are produced, and the rain-seeking ceremony “Tasatek” is recorded; in Uygur mythology, it was evident that “crops cannot be cultivated because the river is cut off,” killing sheep and offering sacrifices to the god of rain, such as Akhtihan, and other plots with water as elements.

Fuxi Nu WA in Chinese mythology, Naga and Naji in Indian mythology, Isis and Serapis in ancient Greek mythology all appear in the human head and snake tail in legends and images. Fu Xi Nu WA is a figure in ancient Chinese legends. It is said that Nu WA created human beings in the form of loess and water. In Hindu mythology, Naga and Najib are the guardians of Buddhism and the guardians of the river, which can make rain and bring bumper harvests and natural disasters. Enki is the water god of Sumeria, whose central city is near the Persian Gulf, symbolized by a goat and a fish. From the perspective of flood myths and legends in the world, the general formula of the story is human sin-flood punishment-human rebirth.

Through the comparison of the above stories, we can find that the difference between Chinese God and the West is that God is not in the leading position of absolute authority, but more reflects the unity of God and man, and there is an equal and friendly relationship between God and man. This is quite different from the dominant position of the gods in the West and the contractual relationship between people. Take Dayu flood control in China and Noah’s ark in the West as examples to understand the different concepts of water between the two civilizations. It is also for the flood Noah relied on the revelation of God through the ark to escape the disaster that God brought to the people. At the same time, Dayu regarded it as a natural phenomenon, through his summary and thinking of previous experience, followed the laws of nature to overcome the flood. Noah enabled human beings to continue to reproduce. Still, at the same time,

it also provided a precedent for human beings to repent to God, while Dayu left the idea of “the unity of man and nature” that human beings transform nature based on following the laws of nature. In China, people generally regard the origin and development of the universe as an ongoing natural process, and man is an organic part of it. People want to adapt to nature and the unity of man and nature.

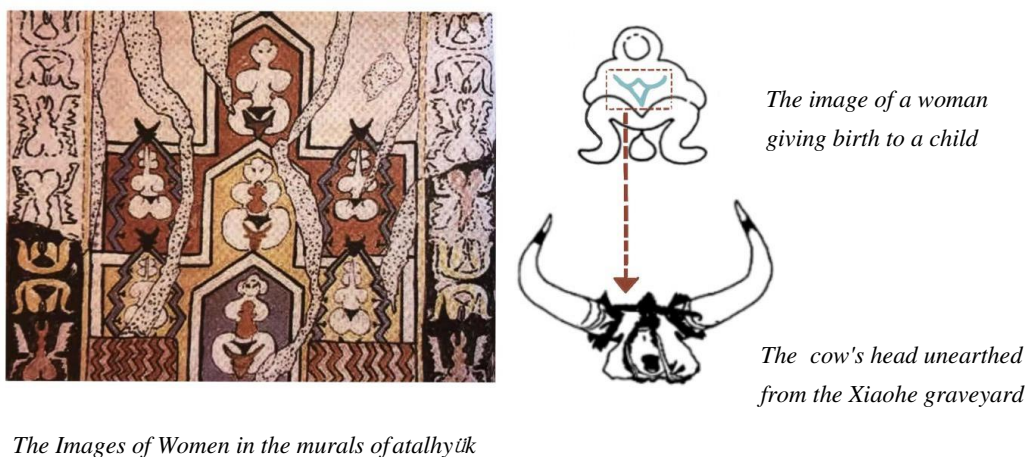
From the grid pattern and fish pattern in the pottery unearthed from Yangshao Culture in Shaanxi, China, to the vortex pattern and frog pattern in the painted pottery relics unearthed in Majiayao in Gansu Province, and the water ripple, fishing net, and vortex patterns in the painted pottery unearthed in Xinjiang, as well as the waves, water vortex patterns, grid patterns, fish patterns, ox head patterns, tortoise patterns, snake patterns and so on unearthed from the Qiogamish site in Iran. The appearance of similar ornamentation in different areas of the ancient Silk Road proves to a certain extent that the development of early human art comes from the understanding and understanding of the world and is related to its own needs. The art image comes from the imitation and abstract generalization of things. It is the imitation of objective things and the processing of subjective emotions (Mao, 2017). The Qiogamish site in present-day Khuzestan province in southwestern Iran is an agricultural, cultural site, which should be a farming group while domesticating dogs, cattle, sheep, and other animals, and fishing is also one of its economic models. The belief system of the agricultural nation is generally closely related to the themes of high yield, barren, life, and production. Thick lines, repeated grids, fishing and hunting energy, and simple drawing pursue survival and life. Ornamentation has become a symbol of the vitality of these themes, and it is normal for water belief elements to appear.

Bulls and horns have been unearthed in the Xiaohe graveyard in Xinjiang. Chinese scholar Xu Feng connects the Xiaohe cemetery with the site of atalhyük in death and Rebirth: a glimpse of the burial customs of the Creek Cemetery in Xinjiang (Xu, 2011). He believes that the form of cattle remains (cattle heads and horns) seen at the Chattar site is similar to that seen in the Xiaohe graveyard, giving people a very marginal, ferocious, and primitive feeling (*Fig. 2*). A room was excavated in the Katai mound in south-central Turkey (ancient Anatolia), apparently used to hold religious rituals related to birth. They painted the room red, which some scholars think is the color of blood, and red is the color of life. The figures painted on the wall show the woman in childbirth, and the circular and wavy lines painted next to them may symbolize the uterus, umbilical cord, and amniotic fluid.

The image of the uterus similar to the ox’s head represents life, and the water ripple is the element of amniotic fluid, that is, the carrier of life. We can infer that the spiritual world of the ancestors at that time believed that water, Horn, and goddess were the beginning of life. Human life originated in the waters of the womb.

Therefore, according to analogy, the goddess is the source of all life, including human beings, animals, and plants, so a large number of female images have been unearthed in many archaeological sites, highlighting reproductive features. This represents that water worship is an element of nature worship and an element of reproductive worship. Mellaart, a former excavator at the site of Chattar Hugh, once briefly pointed out that the bull is the symbol of the male god. At the same time, the leopard has the attribute of a goddess. Ms. Gimbutas believes that the bull symbolizes the seasonal function of the water of life, the inherent vitality of the bull can be proved by the artistic expression of flowers and plants on the bull, through the sacrifice of the bull, the concept of regeneration can be dramatically understood as the birth of new life

(Gimbutas, 1991). From the above discussion, it can be concluded that the bull represents regeneration and is the symbol of the water of life. In the sacrificial activities in ancient China, cattle are also often used animals, so in the archaeological discoveries in China, cattle remains are common and appear in various forms. As an object that has been stored for a long time and is easy for secondary processing, Horn has become a symbolic representation in sacrificial activities.



The Images of Women in the murals of atalhytk
Figure 2. The image relationship between cattle and water. Photo source: epainting of the relics of Xu, 2011

To sum up, the belief in water gods at the spiritual level is all over the ancient Silk Road, and the material needs are transformed into spiritual needs related to fish, frogs, and snakes directly associated with water. And later developed into a symbolic form of worship of cattle. The influence of water on spiritual belief in the East is imperceptible. As a necessary element of life, it is often associated with the origin of the world. Religious belief in water can be found that water plays a role in preventing misfortune and purification. In ancient times, water always played an essential role in the process from birth to death, and bathing before ancient sacrifices and religious ceremonies embodied the purification role of water.

The belief of water god in the material level

The folk art in the Silk Road has the cultural characteristics of multi-ethnic and multi-regional communication and integration. The folk art resources attached to the trade exchanges and derivatives along the Silk Road are integrated with “text, images, and rituals.” The artistic expression always revolves around the aesthetic phenomenon of production, life, and trade in the Silk Road, the aesthetic activities created, and the resulting aesthetic emotion, aesthetic consciousness, aesthetic concept, and aesthetic thought. The artistic image of water worship exists in all aspects of society, from clothing, food, housing, transportation, related festival customs, belief taboos, etc. Although the opening of the Silk Road started with Zhang Qian’s mission from Chang’an to the Western regions, the folk culture of water belief emerged as early as the primitive Yangshao culture. At that time, people had a preliminary understanding of water. After their expectations and demand, they drew abstract and straightforward patterns with symbolic connotations in daily necessities, sacrifices, and funerary objects

according to the limitations of technology and technology at that time. From the grid patterns and fish patterns in pottery unearthed in Yangshao culture in Shaanxi to the vortex patterns and frog patterns in painted pottery relics unearthed in Majiayao, Gansu Province, these patterns appear. It is the ancient human's initial worship of water, extending to the worship of the dragon king and the river god. The worship of water belief in the artifacts unearthed in Yangshao culture, whether witchcraft or worship, embodies the primitive ancestors' preliminary understanding of nature and displays and develops its practical function and aesthetic consciousness to a certain extent (Wang, 2017). Similarly, among the painted pottery relics unearthed in Xinjiang, water ripples, net fishing patterns, vortex patterns, and further understanding and worship of water in Xinjiang. Although the artistic image of Water God has different ways of expression according to varying objects of belief, through the collection and arrangement of the creative manifestation of Water God along the Silk Road, the artistic image of Water God takes water Noumenon, animal image, character image and consciousness image as the main body of creative expression. At the same time, clouds, rain, thunder, electricity, and other images related to precipitation also exist in the depiction image.

The belief in the god of water has a prominent position in the Chinese folk belief system. People transform their awe and fear of water into the consciousness of religious belief, "endow water with supernatural fantasy power," thus providing a conscious basis for the personification and deification of water. Before Zhang Qian's mission to the Western regions, there had been exchanges between the Central Plains and the Western regions. After Zhang Qian's mission to the Western provinces, sales in economic, cultural, ideological, and other fields became more frequent and profound. The area along the Silk Road has always been where nomadic civilization and agricultural civilization collide and merge. Xinjiang and Gansu belong to oasis agrarian areas. Although mobile agriculture is not highly developed, exchanges with the Central Plains, especially after the Han Dynasty attacked Xiongnu, Jiuquan County, and Dunhuang County. After the Han people moved to Gansu and other areas, they brought advanced farming techniques and production tools. Oasis agriculture has significantly been developed. The worship of water comes from the critical significance of water to life, from the nomadic people living after water plants to the development of agricultural areas that irrigate water sources, the shortage of water resources will inevitably lead to the contradiction of water used to maintain stability, the government supports the water god belief and puts the water belief into the national sacrifice, and appropriately regulates the folk water conservancy activities. As a result, the water belief in Xinjiang and Gansu has become a water belief culture in arid areas, which is different from the water-rich regions.

The feudal official sacrificial policy promoted the development of the belief in water gods. Based on the needs of social reality, the continuous implementation of the sacrifice system has objectively promoted the development of the belief in the water god. In Cave 25 of the Yulin Grottoes in Dunhuang Mogao Grottoes, a yellow and black dragon will be at the top of the murals, with red clouds and auspicious clouds on its feet. (Fig. 3) in the period of Emperor Xuanzong of the Tang Dynasty, the Zhao Temple Longchi set up altar officials to offer sacrifices to the Dragon King. As a result, the function of Dragon King Siyu was established and was believed in among the people. The Asura in the sea on the west wall of Mogao Grottoes 249 stands in the sea, and the traditional Chinese images of Fengshen and Thor are painted on both sides, a combination of Chinese and Western water gods (Fig. 4). Xinjiang is an arid agricultural area, and the prerequisite for

agricultural planting is the availability and quantity of irrigation water sources. The shortage of water resources will inevitably lead to contradictions in water use, and civil water conservancy disputes continue to emerge. To maintain stability, the Qing government supported the construction of Longwang Temple and appropriately regulated non-governmental water conservancy activities. Longwang Temple is no longer only a sacred place for officials and people to sacrifice but also plays a religious role in the irrigation activities to maintain regional water conservancy order. According to Xinjiang Tu Zhi, more than 30 Longwang temples were built during the reign of the Qing Dynasty and formed regional and cultural characteristics different from those in the mainland. The first difference is that the Longwang Temple in Xinjiang is mainly built on riverbanks, springs, and water dividers. Not all the Longwang temples in the mainland are built by the water. The second difference is that Longwang Temple has evolved from the function of “seeking rain” in the Central Plains to the position of “seeking water” and “dividing water” in Xinjiang.



Figure 3. *The Middle Tang Dynasty in Cave 25 of Yulin Grottoes. Photo from the official Weibo of Dunhuang Grottoes*



Figure 4. *Mogao Grottoes Cave 249 Sea Asura. Photo from the official Weibo of Dunhuang Grottoes*

From the perspective of the areas along the ancient Silk Road, the belief in water gods has common or similar characteristics. From the above, it can be concluded that the belief in the water god along the ancient Silk Road can be divided into the worship

of the original water body, the regeneration of the water worship function of the ox horn, and the establishment of the image of the dragon god (Fig. 5). Most of the ancient civilizations originated in the river basin. Still, civilization has never been a single generation, and various civilizations continue to learn from and learn from each other in the process of communication. The ancient Silk Road promoted the development and spread of civilization, and the interaction and communication between regions is a necessary process of the evolution of society. The class has similar needs in the relative time range, and human beings have the same psychological function in a similar social state. Therefore, the same or similar belief culture can be produced under the same or similar geographical conditions, and water is a necessary element of life on earth. Understandably, similar water god beliefs, totem worship, and technical systems appear along the Silk Road, which is also the reality of close communication between global and regional perspectives. There is a wide range of areas along the ancient Silk Road, the differences in different regions, landforms, climate and other natural factors, the differences in the needs of the people, as well as the differences in subjective factors such as concepts, methods, skills and other personal factors adopted in the transformation of nature. There are different restrictions on the image shape and style of the water god, making the created social and cultural tradition have apparent regional characteristics. Thus resulting in the difference and diversity in the modeling characteristics of folk art.

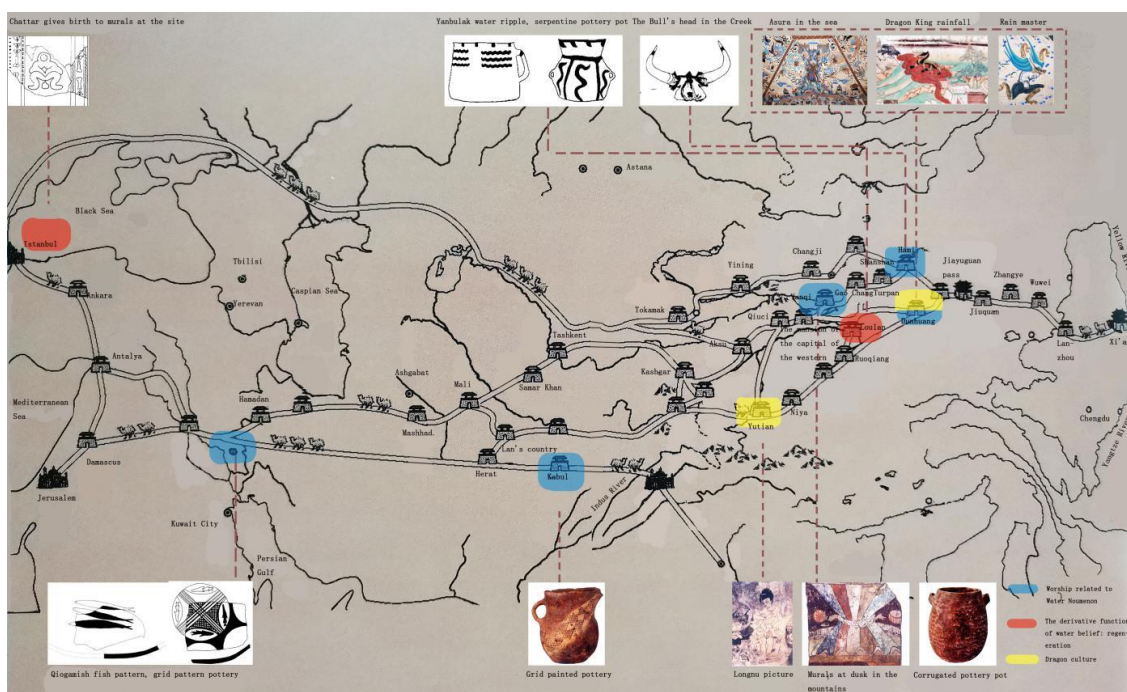


Figure 5. Schematic diagram of belief in water gods along the ancient Silk Road. Photo source: repainting of the relics of the Northwest of the Silk Road

The unity of knowledge and practice in response to the times: the contemporary value of ecological wisdom in the belief of water god

In the historical process of development, the ancient ancestors along the Silk Road took the opening of the Silk Road as an opportunity, the interweaving of nomadic

farming civilization as a link, and the needs of the development of oasis agriculture and animal husbandry in arid areas. It created a regional water culture, which represented the development level of productive forces at that time and adapted to the external living environment. Including climate, temperature difference, topography, natural disasters, and so on. This kind of pioneering, enterprising, and adaptability in the face of nature and poor living conditions is the content we need to inherit and learn when our current social living conditions are superior.

Construction of social order

In the past, the belief in Water God played a role in calming the people's hearts, organizing and mobilizing to a certain extent, and had the responsibility of promoting ethics and educating the people. The water god sacrifice space conveys the official sacrifice idea through worshipping the water god to achieve the goal of harmony in the countryside and thick customs. Generally speaking, the belief in Water God pursues the realm of "harmony." In Confucianism, it puts more emphasis on the harmony between man and society and the unity of emotion and reason; in Taoism, it puts more emphasis on the connection between man and nature and the unity of heart and thing; in Zen Buddhism, it puts more emphasis on the harmony between man and people and the pursuit of spiritual purity. The belief in Water God pursues the harmony between man and nature and runs through the connection between man and people, man and society (Wu and Li, 2021). Such harmony is connected from individual to society, from humanities to art, heaven, and earth to the whole universe. In other words, heaven, man, and literature are the same, all run through and. The harmonious beauty of the unity of man and nature is the highest pursuit of Chinese traditional art. Chinese aesthetics requires the unity of beauty and goodness. Although Confucianism and Taoism have different views on the so-called highest realm of excellence, in the end, they all regard "the unity of man and nature" as the highest realm, and the so-called "unity of man and nature" is also a kind of aesthetic realm, a realm of the unity of truth, goodness, and beauty.

Inheritance of ecological wisdom

At present, the rise of ecological civilization construction is a worldwide revolution involving the transformation of the mode of production, way of life, and even values (Berleant, 2010). Promoting the promotion of public environmental awareness is an inevitable requirement in the development and construction. Judging from the content reflected in the culture of belief in God in Sheung Shui, the folk culture that has been worshipping and protecting water for thousands of years has continued to develop. The pace of the times has not stopped. In today's economic development, social development, and scientific and technological development, the protection consciousness has become relatively thin. The ancient people already have the concept of ecological environment consciousness is still the cultural treasure that we need to take its essence today. In the formulation of relevant environmental laws and regulations, we should attach importance to water resources from the perspective of moral and emotional constraints to educate the concept of getting along with nature in harmony with nature. In the year when festivals, folk customs, and other traditional folk culture to play the role of art imperceptibly, teaching in fun. In today's economic globalization, ecological globalization is also an important issue we are facing. We

should use the ecological wisdom exchange, blending, and communication of the water gods in the ancient Silk Road to deal with the practice of human community with a shared future in culture, ecology, and social construction in different periods. We should pay more attention to the ecological quality education of the people, strive to build a cultural atmosphere of environmental protection awareness, enhance the information access channels of public awareness of environmental protection, and improve and develop the construction of an ecological education system.

Aesthetic value of art

Morality, art, and science are the three pillars of human culture, and the belief in Water God is included in these three pillars. The aesthetic value embodied in the traditional ecological wisdom in the ancient Silk Road can be used for reference to the construction of contemporary environmental aesthetics. Many categories of Chinese traditional aesthetics and art appear in the form of unity of opposites, such as “rigidity and softness,” “emptiness and reality,” “movement,” “form and spirit,” “cultural quality,” “reason,” “scene,” “image,” “artistic conception” and so on. Among them, the spiritual side is more dominant in the unity of contradictions, such as “spirit” in “form and spirit,” “emotion” in “situation,” and so on. “meaning” in “image” and so on. In the artistic images of belief in water gods, the relationship between “form and spirit” and “image,” which is dominated by the expression of spirituality, provides a reference and guidance for the development and aesthetics of our art today (Zhang, 2021). This dialectical thinking shines with the rational wisdom of the Chinese nation, which has a significant influence on Chinese traditional art and aesthetic thought and forms the analytic harmony view full of national characteristics in classic Chinese art and aesthetic opinion.

Summary and discussion

The development of human society is rooted in the ecological environment, and it is an inevitable requirement to promote the environmental awareness of the public (Carlson and Lintott, 2008). At present, saving water has not become the conscious behavior of human beings in daily life. Understand the worship of water gods, learn ecological wisdom, and make water saving, water use, and water management become the conscious behavior of the people from the heart. The ancient people’s understanding of water and life already had a simple, universal, and strong sense of protection and measures from the contents reflected in the above materials. This is reflected in the relevant environmental laws and regulations and moral regulations. Dunhuang Mengshu has attached importance to the education of the concept of living in harmony with nature since childhood; the karez in Turpan, the development of human society, and the progress of civilization are based on a healthy ecological environment. The change of ecological environment has its regularity and regionality, and the formation and development of ecological civilization also have corresponding frequency, regionality, and nationality. In the face of today’s ecological problems, we should learn their ecological wisdom from the belief in ancient water gods. We inherit the past and the future from the water belief culture, and what we want to take from its essence and discard its dross is to integrate the new needs into the present era scene. Inherit the belief of respect for water, the protection and utilization of water, with the concept of ecological, green, and sustainable development. The ancient ancestors could not control

the amount of water and used the method of sacrifice to please the gods in charge of the water. The space places, image texts, and behavior rituals of its sacrifice together form the belief culture of water gods. Its sacrificial activities are inseparable from “etiquette and music civilization.” The order and etiquette formed in the sacrificial activities of this belief have become the moral laws that restrict the behavior. In the sacrifice to the water god, the rights, obligations, and daily norms of conduct of the members of the society are stipulated. After receiving the grace, the ancestors will be grateful, restrain their behavior, and internalize their beliefs into moral laws that people consciously abide by.

With the rapid development of the economy and society, the belief in Water God seems to have become a lost folk belief. The current eco-environmental problems have not received enough attention. Similarly, in natural science, the research on the ecological environment is mainly focused on the current situation, spatial cognition, efficiency assessment, risk assessment, and other biological factors, but behind the rapid social development is the pollution and abuse of water resources. In the “regional social relations system with water conservancy as the center,” the maintenance of water conservancy order, protection, and rational use of water resources should not be based on the destruction of natural resources. The relationship between man and water profoundly impacts the past and the present and will continue to shape the future. Nowadays, the widespread problems of water shortage, water environment pollution, and flood disasters affect the long-term and effective utilization of water resources and the realization of sustainable development of human society. We should pick up “water worship” and even “nature worship” again, not to worship unknown gods, but to have awe of nature and restrain ourselves from our behavior, to establish natural moral restraint norms at the social level of the masses. Attaching importance to and strengthening the study of ancient ecological thoughts plays a positive role in enriching and building today’s ecological civilization.

Acknowledgements. Support from the National Social Science Foundation of China: “Study on Landscape Protection of Oasis Historic and Cultural Villages and Towns” (14G126) and “Study on the Cooperative Mechanism of Water Cultural Heritage Protection and Rural Revitalization in Xinjiang Section of the Silk Road” (19XMZ046).

REFERENCES

- [1] Berleant, A (2010): *Sensibility and Sense: The Aesthetic Transformation of the Human World* (St Andrews Studies in Philosophy and Public Affairs 6). – Imprint Academic, Charlottesville.
- [2] Buckley, B. M., Anchukaitis, K. J., Penny, D., Fletcher, R., Cook, E. R., Sano, M., Nam, L. C., Wichienkeo, A., Minh, T. T., Hong, T. M. (2010): Climate as a contributing factor in the demise of Angkor, Cambodia. – *Proceedings of the National Academy of Sciences of the United States of America* 107(15): 6748-6752.
- [3] Cai, H. H. (2013): *A Study on the Worship of Water God in the pre-Qin, Qin and Han Dynasties*. – Guangxi Normal University, Guilin.
- [4] Carlson, A., Lintott, S. (2008): *Nature, Aesthetics, and Environmentalism: From Beauty to Duty*. – Columbia University Press, New York.
- [5] Du, Z. (1996): The East-West differentiation of climate change in China in the past two millennia and its impact on the rise and fall of the Silk Road. – *Geography of Arid Areas* 3.

- [6] Frankopan, P. (2015): *The Silk Roads. A New History of the World.* – Bloomsbury Publishing, London.
- [7] Gimbutas, M. (1991): *The Language of the Goddess. Unearthing the Hidden Symbols of Western Civilization.* – Harper, San Francisco.
- [8] Hu, M. F. (2015): *A Study on the Belief in Water Gods Along the Beijing-Hangzhou Canal in the Ming and Qing Dynasties.* – Nanjing University, Nanjing.
- [9] Huang, Z. (1988): *The Water God of China.* – Shanghai Literature and Art Publishing House, Shanghai.
- [10] Mallory, J. (1973): A short history of the Indo-European problem. – *Journal of Indo-European Studies* 1(1): 21-64.
- [11] Mao, N. (2017): *The Discovery and Integration of the Art Ideal of Going to the Folk and the Folk Tradition (1919-1945).* – China Central Academy of Fine Arts, Beijing.
- [12] Shen, S. B. (2009): *A Study on the Belief of Water God in Wu Yue Folk.* – Wen Zhou University, WenZhou.
- [13] Tang, F. (2016): *A Study on the Custom Characteristics in the Murals of the Water Temple in Guangsheng Temple.* – North China University of Technology, Shanxi Province.
- [14] Wang, Y. P. (2006): On the worship of water god in Tang Dynasty. – *Journal of Capital Normal University (Social Science Edition)* 2006(04): 12-17.
- [15] Wang, S. (2017): The imprint of Silk Road in Xixia Art Image. – *Xixia Studies* 2017(04): 50-57.
- [16] Wu, B. (1996): *Chinese Folk Letters.* – Shanghai People's Publishing House, Shanghai.
- [17] Wu, Y. H., Li, F. L. (2021): Change and Cohesion: Water Beliefs and Legends and Their Social Functions in Dali Erhai Basin. – *Journal of Honghe University* 19(02): 58-63.
- [18] Xiang, B. (1996): *Chinese Water Worship.* – Shanghai Sanlian Publishing House, Shanghai.
- [19] Xu, F. (2011): Death and rebirth: a glimpse of the burial custom of Xiaohe graveyard in Xinjiang. – *National Art* 2011(04): 58-64.
- [20] Yuan, I., Zhang, X. L., Xue, Z. Y., Jiang, X. (2021): The influence of the change of minority water culture on water environment pollution. A case study of Miaolan Village in Southeast Guizhou Province. – *Rural Economy and Science and Technology* 32(07): 30-32.
- [21] Zhang, H. (2021): Symbol and situation: a study on the interpretation model of visual art based on art history. – *Journal of Qiqihar University (Philosophy and Social Sciences Edition)* 2021(02): 23-27.

EFFECTS OF ARBUSCULAR FUNGI ON GROWTH INDEXES AND PHOTOSYNTHETIC APPARATUS OF *SALIX VIMINALIS* IN Pb CONTAMINATED SOIL

WEI, N. – HAO, N. A. – ZHU, S. Q. – YIN, J. H.[†] – AN, B.^{†*}

College of Horticulture, Jilin Agricultural University, Changchun 130118, China

[†]*These authors contributed equally to this work.*

^{*}*Corresponding author
e-mail: jlnbya@126.com*

(Received 29th Oct 2021; accepted 21st Mar 2022)

Abstract. The effects of arbuscular mycorrhizal fungi *Funneliformis mosseae* on the growth, chlorophyll content, photosynthetic parameters and chlorophyll fluorescence characteristics of *Salix viminalis* growing on Pb contaminated soil (0, 50, 200 and 400 mg·kg⁻¹) were studied. The results show that: In Pb contaminated soil, the root activity of *Salix viminalis*, and the content of chlorophyll, especially chlorophyll-a, decreased significantly with the increase of Pb content. The mycorrhizal infection rate of *Salix viminalis* roots was 50-70% after inoculation with *F. mosseae*. The root activity of *Salix viminalis* was increased and the chlorophyllin degradation of *Salix viminalis* leaves in Pb contaminated soil was alleviated. The infection of *F. mosseae* could improve the photosynthetic electron transfer ability of PSII in *Salix viminalis* leaves under Pb stress. It could promote the activity of OEC of PSII donor side and the electron transfer ability of Q_A to Q_B of PSII receptor side in *Salix viminalis* leaves, which ensured that the leaves of *Salix viminalis* had relatively high PSII activity in Pb soil. Therefore, the inoculation of *F. mosseae* could improve the tolerance to Pb and reduce the toxicity of Pb to *Salix viminalis*.

Keywords: *Salix viminalis*, AMF, Pb, photosystem, photosynthesis

Introduction

Lead is one of the most harmful elements in heavy metal pollutants. The pollution in soil mainly comes from industrial production and transportation (Soffianian et al., 2014; Sauliutė and Svecevičius, 2015). Pb stress inhibited the growth and development of plants, especially the root. Pb toxicity may cause swelling, bending, thickening and shortening of plant roots (Hall, 2002; Chen and Zhao, 2009; Pallara et al., 2013; Chen et al., 2017a,b,c). The toxic effect of Pb depends on the stress time and heavy metal concentration. In addition, different plants have different tolerance to Pb. For example, hyperaccumulators are more resistant to Pb than sensitive plants (Ogbomida et al., 2018). For example, Jiang and Liu (2010) studied the effect of Pb stress on the cellular defense system of garlic meristems. The results showed that after Pb treatment for 48-72 hours, the mitochondria swelled; the cristae disappeared; the endoplasmic reticulum and Golgi humoral bubbled; the plasmalemma was damaged, and the color of nucleus deepened. The high concentration of Pb can reduce the biomass of rice plant varieties, such as *Najas indica*, guixiang zhang, and nongxiang-18. In addition, Pb stress leads to fewer smaller, and more fragile leaves or leaves with dark purple patches on their surface (Gupta et al., 2010).

Arbuscular mycorrhizal fungi (AMF) exist in soil of most ecosystems, even if it is contaminated soil. AMF can form symbiotic arbuscular consortium with plant roots, which can accelerate the phytoremediation process, improve the remediation efficiency

and increase the stability of heavy metals (Zhang et al., 2007; Xue and Gao, 2017). The toxicity also has a growth deceleration or damaging impact on the photosynthetic apparatus. The toxic effect of Pb depends on the amount of time the organism is subjected to it and the concentration. In addition, different plants vary in their level of tolerance to Pb. For example, hyperaccumulating plants have a stronger tolerance to Pb than sensitive plants (Arena et al., 2017). When the concentration of heavy metals increased, the host's uptake of heavy metals increased as well, resulting in a negative effect on plant growth. Under heavy metal stress, AMF promotes plant growth, alleviates the toxicity of heavy metals to plants or has no effect on plant growth. Therefore, it has important theoretical value and practical significance to study the mechanism of AMF combined with plants to perform and accelerate the remediation of heavy metal contaminated soils (Qu et al., 2009; Rozpádek et al., 2016; Xue and Gao, 2017; Rizwan et al., 2017).

Salix viminalis grows rapidly, has large biomass, and has strong ability to accumulate heavy metals, *Salix viminalis* has the advantages of rapid growth, high biomass and strong ability to accumulate heavy metals, which is widely used in phytoremediation and biomass energy development in heavy metal contaminated soil areas, and has certain ecological and economic value (Zhai et al., 2016). Therefore, improving the resistance of *Salix viminalis* seedlings to heavy metal stress is the key to ensure the survival and growth of seedlings after transplanting. At present, there are a lot of studies on arbuscular mycorrhizal fungi can improve the resistance of plants to heavy metals, but there are few studies on arbuscular mycorrhizal fungi on the growth index and photosynthetic characteristics of *Salix viminalis* in Pb contaminated soil. In this study, the effects of arbuscular mycorrhizal fungi *F. mosseae* on the growth, photosynthetic gas exchange parameters and chlorophyll fluorescence parameters of *Salix viminalis* under Pb contaminated soil were studied from the perspective of plant photosynthesis mechanism, in order to provide some basic data for suggesting the mechanism of arbuscular mycorrhizal fungi to improve the resistance of *Salix viminalis* to Pb stress.

Materials and methods

Test materials and treatment

The experiment was conducted in the laboratory of soil science of Jilin Agricultural University (Changchun, Jilin Province, China) from March to June 2019. The substrate was composed of organic fertilizer, perlite and yellow soil (6.0: 3.0 : 0.5 : 0.5). The substrate was sterilized at high temperature (121 °C) for 2 h in an autoclave to kill the indigenous mycorrhiza and other microorganisms in the soil. The mycorrhizal strain used in the experiment was *F. mosseae*, and the inoculum was purchased from the China Arbuscular Mycorrhizal Fungi Germplasm Resource Bank and was numbered "BGXJ01". The mycorrhizal agent used for inoculation contained spores, hyphae and mycorrhizal segments, and each gram of mycorrhizal agent contained 40-50 spores. The plants that were tested materials were approximately 20 cm tall. The physicochemical properties of sterilization matrix were determined to be pH 7.66 (soil / water = 1:2.5, w v), organic matter 16.85 g·kg⁻¹, ammonium nitrogen 7.37 mg·kg⁻¹, nitrate nitrogen 25.77 mg·kg⁻¹, available phosphorus 11.48 mg·kg⁻¹, available potassium 108.96 mg·kg⁻¹, and total Pb 3.58 mg·kg⁻¹. Before transplanting, the seedlings are irrigated once to make the relative water content of the soil basically reach saturation.

The seedlings are transplanted into a cultivation bowl with a diameter of 12 cm and a height of 15 cm, and one plant is planted in each pot.

A two factor test AMF×Pb was arranged in a completely randomized block. The appropriate amount of Pb(NO₃)₂ solution was added to the substrate and evenly mixed, so that the Pb content in the soil Pb test medium was established at 4 gradients of 0, 50, 200 and 400 mg·kg⁻¹. The control group was treated with the same amount of distilled water, and each Pb level was treated with inoculation of *F. mosseae* (+AMF) and no inoculation of arbuscular mycorrhizal fungi (CK). The mycorrhizal fungi were inoculated by adding 50 g of soil containing fungi per kilogram of substrate, and the treatment of non-inoculation of mycorrhizal fungi involved the addition of same amount of sterilized soil. *Salix viminalis* cuttings with the same growth status were selected (the number of leaves, height, number of new roots and length were close to each other), and then the cuttings were fixed by filling holes with substrate. Each treatment was repeated in five pots for a total of 40 pots. The pot was cultured in an incubator with temperature of 25 °C, light intensity of 1200 μmol·m⁻²·s⁻¹, a photoperiod of 12 / 12 h (light/dark) and relative humidity of approximately 75%.

The pots were watered regularly and managed at the seedling stage. Fresh 0.25 × Hoagland's nutrient solution (35 ml pot⁻¹) was cultured for one month, and the relevant data were measured when the seedlings were approximately 25-35 cm high. Hoagland's nutrient solution was used [10 μM H₃BO₃, 6mM KNO₃, 8M Ca(NO₃)₂, 1M NH₄H₂PO₄, 2.6M MgSO₄, 0.5mM CuSO₄, 1.0M ZnSO₄, 1.6μM MnSO₄, (NH₄)MoO₂PO₄, 2μM Fe-EDTA, pH 6.0±0.5], Na₂EDTA, DTE, sucrose, Tris HCl (50 mm, pH 7.5).

Determination items and methods

The growth parameters were determined: After measuring the plant height, the plant was taken out from the substrate, and the root length of single plant was measured after washing the substrate on the surface of root system. After the water on the surface of root system was dried with absorbent paper, the aboveground and underground parts were put into aluminum box to kill (105 °C, 30 min) and dried (60 °C, 30 h) to constant weight, and then the biomass of each plant was calculated. Repeat 5 times.

Mycorrhizal infection rate, chlorophyll content and root activity were measured: The infection rate of mycorrhiza was determined by section staining. The root system was rinsed with tap water, put into 1n KOH solution at 80 °C for 1h, then washed with distilled water, put it into 20% H₂O₂ solution for 30min, and then put in 1n HCl for 2 min. Finally, it was stained with 0.5% acid fuchsin and pressed into tablets. The number of cells stained was observed under the microscope. Soil organic matter content was determined by k₂cro₇-h₂so₄ oxidation method, soil pH value was determined by electrode method, and soil field water holding capacity was determined by drying method. Mycorrhizal infection rate (%) = root segments forming clumps / number of measured root segments × 100; Root activity was measured by TTC method (Shao et al., 2009).

Determination of Pb Content in the Underground and Aboveground Parts: The collected aboveground and underground samples were rinsed with tap water and deionized water for several times to remove dust and residues on the surface as far as possible. The samples were placed in an oven at 80 °C for at least 48 h until they reached a constant weight, and the dry weight was recorded. The dried plant samples were then placed in a micro grinder to make a uniform powder. 0.5 g powder samples of roots, stems and leaves were weighed, nitric acid and perchloric acid (4:1 in volume

ratio) were added and placed for 12 h, digested until the solution was transparent, filtered, and the volume was fixed to 50 ml. Lead content was measured by atomic absorption spectrophotometer. Repeat 5 times.

Determination of photosynthetic gas exchange parameters: The net photosynthetic rate (P_n), stomatal conductance (G_s), transpiration rate (T_r) and intercellular CO_2 concentration (C_i) of the second fully expanded functional leaf of *Salix viminalis* from top to bottom were measured by Li-6800 photosynthetic measurement system (Licor company, USA) from 9:00 am to 11:00 am. The concentration of CO_2 was fixed at $400 \mu L \cdot L^{-1}$ in a CO_2 cylinder. The net photosynthetic rate (P_n), stomatal conductance (G_s), transpiration rate (T_r) and intercellular CO_2 concentration (C_i) of *S. viminalis* leaves under different treatments were measured. Repeat 5 times.

The OJIP curve of chlorophyll fluorescence was determined: After 30 min dark adaptation, the OJIP curve of leaves after dark adaptation was measured by handy PEA (PPsystem Company, UK). According to Strasser et al.'s (1995) method, the OJIP curves were standardized by $V_{O-P}=(F_t-F_o)/(F_m-F_o)$ and $V_{O-J}=(F_t-F_o)/(F_J-F_o)$, respectively. The relative variable fluorescence (V_J and V_K) of J point at 2 ms and K point at 0.3 ms were obtained, respectively. The differences between the standardized V_{O-P} and V_{O-J} curves of different treatments and the control were calculated, expressed as V_{O-P} and V_{O-J} , respectively. The measured OJIP curve was analyzed by JIP test Strasser et al. (1995).

Chlorophyll content were measured: Chlorophyll a (Chl a), chlorophyll b (Chl b), total chlorophyll (Chl a+b) and chlorophyll a/b (Chl a/b) were calculated respectively (Shao et al., 2009).

Data processing methods

Excel and SPSS software (Version. 22) were used to conduct statistical analyses on the measured data. The data in the figure was denoted as mean \pm standard deviation (SD). Two-way ANOVA was used to detect the significant differences of heavy metal concentration, AMF inoculation and their interaction on all variables.

Results and analysis

Effects of arbuscular mycorrhizal fungi (F. mosseae) on the growth characteristics of Salix viminalis in Pb contaminated soil

With the increase of Pb content in soil, the plant height, root length and biomass of *Salix viminalis* decreased significantly. However, when the Pb content was $50 \text{ mg} \cdot \text{kg}^{-1}$, the root length of *Salix viminalis* decreased, but the plant height and biomass of different parts did not change significantly, even the ratio of root to shoot increased. The plant height, root length and biomass of *Salix viminalis* inoculated with *F. mosseae* were higher than those without inoculation under different soil Pb contents. When the Pb content in soil was $400 \text{ mg} \cdot \text{kg}^{-1}$, the inoculation of *F. mosseae* increased the plant height, root length and biomass (Fig. 1). The root length, aboveground biomass and underground biomass of *F. mosseae* treatment were 18.07% ($P < 0.05$), 32.32% ($P < 0.05$), 21.33% ($P < 0.05$) and 32.51% ($P < 0.05$), respectively.

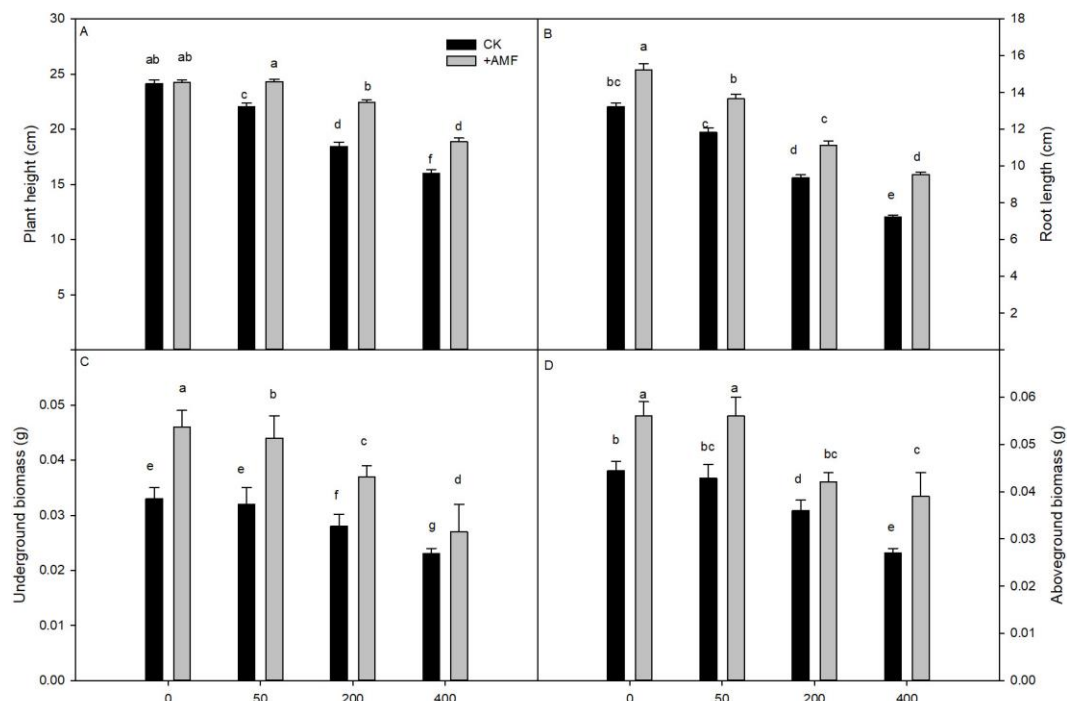


Figure 1. Growth characteristics of *Salix viminalis* mycorrhizae in Pb contaminated Soil. The aboveground parts were placed in aluminum boxes and killed by treatment at 105°C for 30 min, dried to a constant weight at 60°C for 30 h, and the biomass was weighed; Underground biomass was treated as the aboveground biomass. CK: CK + 0AMF contents; +AMF: CK + different amounts of arbuscular mycorrhizal fungi (AMF). Note: Data in the figure are the mean \pm SD values followed by different lowercase letters indicate a significant difference ($p < 0.05$)

Effects of *F. mosseae* inoculation on the Pb content in the underground and aboveground parts

Figure 2A,B show that both the Pb contents in the underground and aboveground parts of *Salix viminalis* represented significant increasing tendencies with the increasing Pb content in soil, and the Pb content in the underground part of *Salix viminalis* was higher than in the aboveground plant parts. Inoculation with *F. mosseae* significantly improved the absorption of Pb in *Salix viminalis* roots. The Pb content in the underground plant parts in the +AMF treatment were significantly higher than the plants not inoculated, except in the treatments without Pb, as there was no significant difference found in the absorption of Pb in *Salix viminalis*, the Pb content in the aboveground part of *Salix viminalis* in the +AMF treatment was not significantly different from the Pb content in the aboveground part of the non-inoculated *Salix viminalis*.

Effects of arbuscular mycorrhizal fungi (*F. mosseae*) on mycorrhizal infection rate and root activity of *Salix viminalis* in Pb contaminated soil

The mycorrhizal infection rate of *Salix viminalis* roots inoculated with *F. mosseae* decreased significantly with the increase of Pb content in soil. When the Pb content in soil reached 400 mg·kg⁻¹, the infection rate of roots decreased by 45.51 % ($P < 0.05$) (Fig. 3A). Although the root activity of *Salix viminalis* also decreased with the increase

of Pb content in soil, the root activity of *Salix viminalis* was increased in different degrees under different soil Pb contents due to the infection of *F. mosseae* (Fig. 3B).

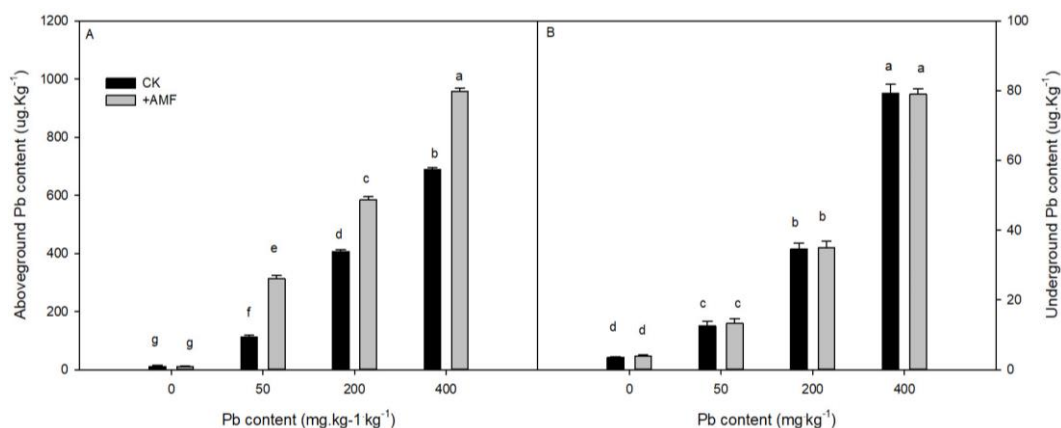


Figure 2. The Pb Content in the Underground and Aboveground Parts. A: Aboveground Pb Content; B: Underbeyond Pb Content. CK: CK + AMF contents; +AMF: CK + different amounts of arbuscular mycorrhizal fungi (AMF). Note: Data in the figure are the mean \pm SD; values followed by different lowercase letters indicate a significant difference ($p < 0.05$)

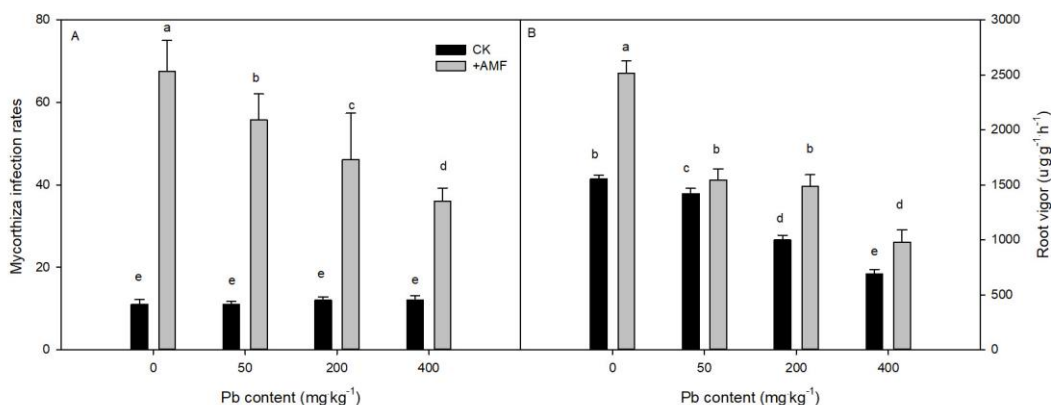


Figure 3. Infection rate and the Pb Content in the mycorrhizal infection rate and root activity. A: mycorrhizal infection rate; B: Root vigor. CK: CK + AMF contents; +AMF: CK + different amounts of arbuscular mycorrhizal fungi (AMF). Note: Data in the figure are the mean \pm SD; values followed by different lowercase letters indicate a significant difference ($p < 0.05$)

Effects of arbuscular mycorrhizal fungi (*F. mosseae*) on chlorophyll content of *Salix viminalis* leaves in Pb contaminated soil

With the increase of Pd content in soil, the contents of chlorophyll a, chlorophyll b and total chlorophyll in *Salix viminalis* leaves decreased significantly, and the decrease degree of chlorophyll a content was greater than that of chlorophyll b, which showed that the chlorophyll a/b value also decreased with the increase of Pb content in soil (Fig. 4D). Under different soil Pb content, there was no significant difference in chlorophyll b content between the treatment of *F. mosseae* and the control, but there was significant difference between chlorophyll a and total chlorophyll.

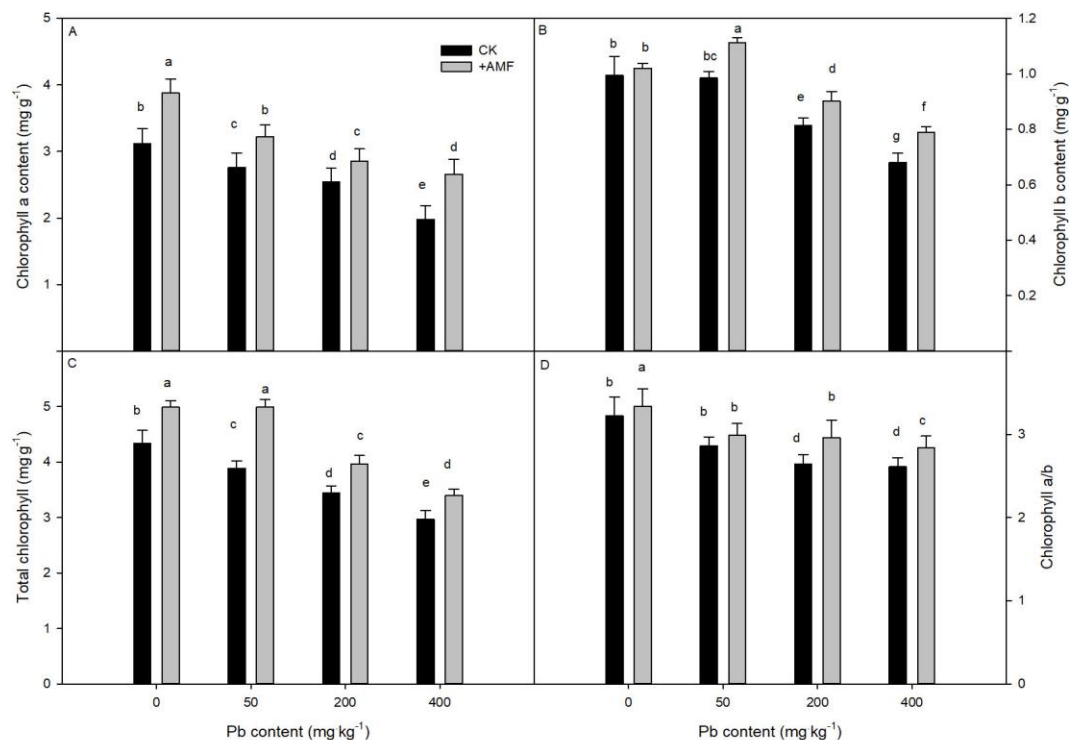


Figure 4. Effect of *F. mosseae* on the chlorophyll content of *Salix viminalis* leaves in Pb-contaminated soil. A: Chlorophyll a content; B: Chlorophyll b content C: Total chlorophyll content: chlorophyll a content+ chlorophyll b content; D: Chlorophyll a/b content: chlorophyll a content/chlorophyll b content; AMF, arbuscular mycorrhizal fungi. CK: CK +0 AMF contents; +AMF: CK + different AMF contents. Note: Data in the figure are mean \pm SD; values followed by different lowercase letters indicate a significant difference ($p < 0.05$)

Effects of arbuscular mycorrhizal fungi (*F. mosseae*) on photosynthetic characteristics of *Salix viminalis* leaves in Pb contaminated soil

With the increase of Pb content in soil, P_n , G_s and T_r of *Salix viminalis* leaves decreased. When the Pb content in soil increased to $400 \text{ mg} \cdot \text{kg}^{-1}$, P_n , and t_r increased by 31.33% ($P < 0.05$), and 13.55% ($P > 0.05$), respectively (Fig. 5).

Effects of inoculation of arbuscular mycorrhizal fungi (*F. mosseae*) on OJIP curve of *Salix viminalis* leaves in Pb contaminated soil

With the increase of Pd content in soil, the relative fluorescence intensity of o point increased significantly, while the relative fluorescence intensity of P point decreased significantly, especially F_m (Fig. 6B). The change range of OJIP curve of *Salix viminalis* leaves inoculated with *F. mosseae* was significantly less than that without inoculation. The results of quantitative analysis of the relative fluorescence intensity (F_o and F_m) of O and P points showed that when the soil Pb content was 0 and $50 \text{ mg} \cdot \text{kg}^{-1}$, there was no significant difference between the treatments inoculated with *F. mosseae* and those without inoculation. However, when the soil Pb content was 200 and $400 \text{ mg} \cdot \text{kg}^{-1}$, the f_o content of *Salix viminalis* leaves inoculated with *F. mosseae* was significantly lower than that without inoculation.

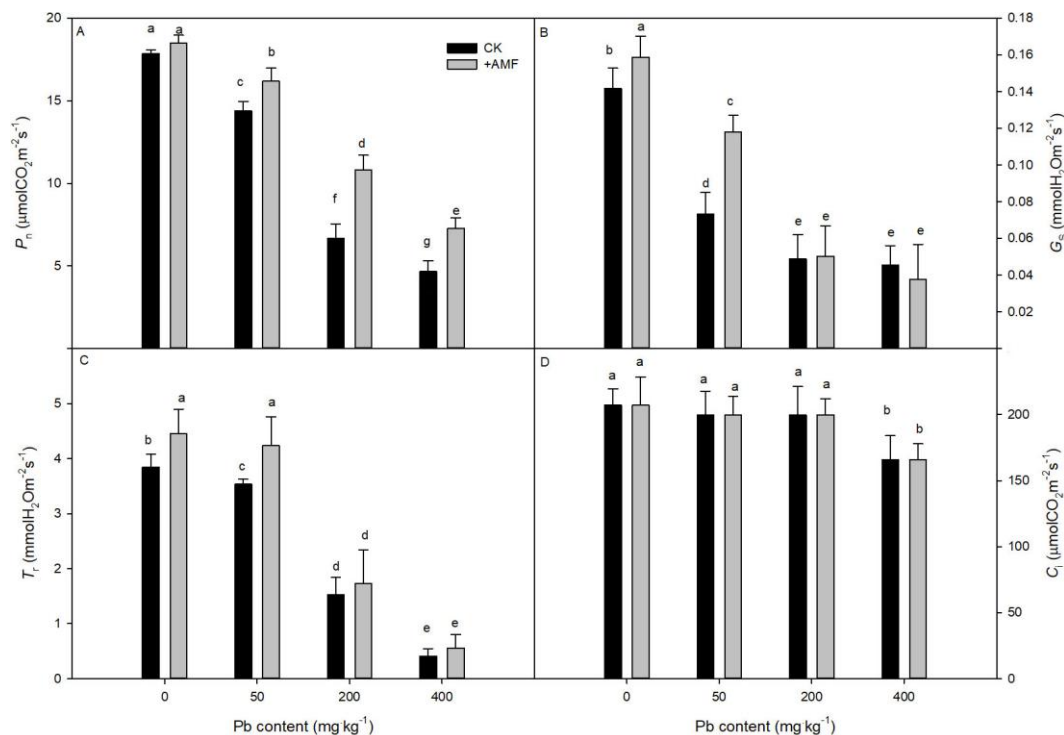


Figure 5. The photosynthetic characteristics of *Salix viminalis* leaves in Pb contaminated soil. CK: CK + 0 AMF contents; +AMF: CK + different AMF contents. A: P_n : Net photosynthetic rate; B: G_s : Stomatal conductance; C: T_r : Transpiration rate; D: C_i : Intercellular CO_2 ; AMF, arbuscular mycorrhizal fungi. Note: Data in the figure are mean \pm SD; values followed by different lowercase letters indicate a significant difference ($p < 0.05$)

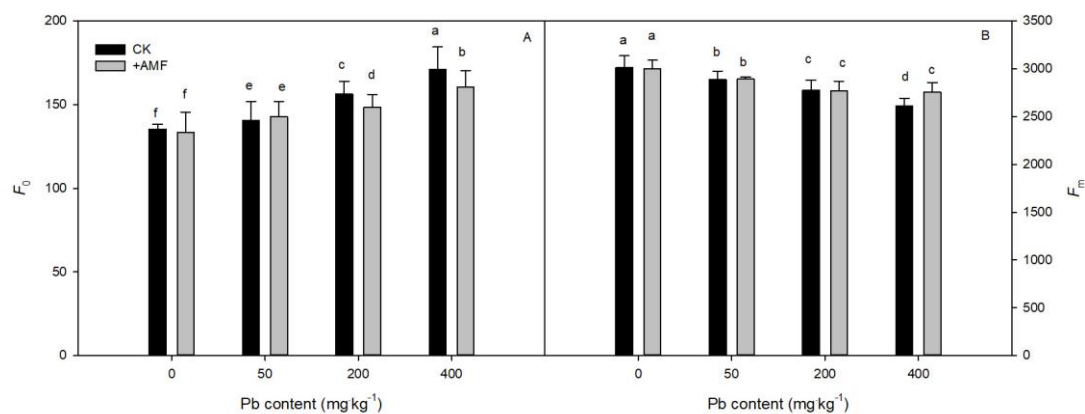


Figure 6. The F_o and F_m of *Salix viminalis* mycorrhiza in soil contaminated with Pb. CK: CK + 0 AMF contents; +AMF: CK + different AMF contents. A: F_o : Quantitative analysis of the changes of the relative fluorescence intensity of o-point; B: F_m : Quantitative analysis of the changes of the relative fluorescence intensity P-point; AMF, arbuscular mycorrhizal fungi. Note: Data in the figure are represented as mean \pm SD; values followed by different lowercase letters indicate a significant difference ($p < 0.05$)

Effects of inoculation with *F. mosseae* on electron transport of PSII donor and acceptor side in Pb contaminated soil

The relative variable fluorescence V_J of J point at 2 ms on the standardized OJIP curve of *Salix viminalis* leaves increased most significantly, but the increase range of V_J in the treatment of inoculating *F. mosseae* was significantly lower than that of non-inoculation treatment (Fig. 7). The results of quantitative analysis of V_J and V_K showed that with the increase of soil Pb content, V_J and V_K increased significantly, and the increase range of V_J was significantly greater than that of V_K . Under different soil Pb contents, V_J and V_K of *Salix viminalis* leaves inoculated with *F. mosseae* were significantly lower than those without inoculation, and the V_J of *Salix viminalis* leaves inoculated with *F. mosseae* was significantly lower than that of non-inoculation treatment under different soil Pb contents, while V_K reached significant difference level only when soil Pb content was 200 mg·kg⁻¹ and 400 mg·kg⁻¹.

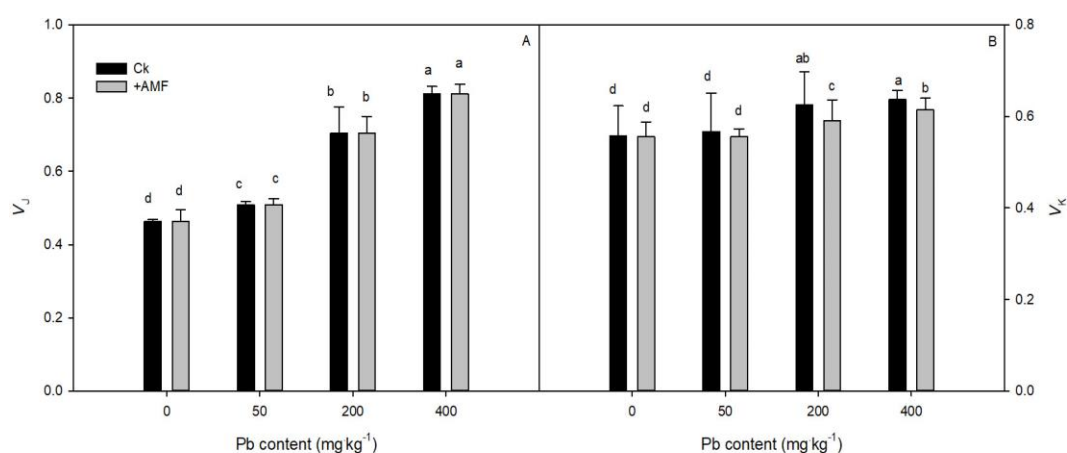


Figure 7. The PSII and PSI photochemical activity of *Salix viminalis* leaves in Pb contaminated soil. CK: CK + 0 AMF contents; +AMF: CK+ different AMF contents. A: V_J , the relative variable fluorescence transient at point J (2 ms); B: V_K : the relative variable fluorescence transient at point K (0.3 ms); AMF, arbuscular mycorrhizal fungi. Note: Data in the figure are represented as mean \pm SD; values followed by different lowercase letters indicate a significant difference ($p < 0.05$)

Effects of arbuscular mycorrhizal fungi (*F. mosseae*) on PSII photochemical activity of *Salix viminalis* leaves in Pb contaminated soil

With the increase of Pb concentration, the Φ_{PSII} of *Salix viminalis* leaves showed a decreasing trend, and the decreasing range was greater than 200 mg·kg⁻¹ at 400 mg·kg⁻¹. The increase of ETR in *Salix viminalis* leaves under Pb stress was significantly lower than that of CK, especially at the concentration of 400 mg·kg⁻¹ Pb (Fig. 8B). Under 400 mg·kg⁻¹ Pb stress, NPQ of *Salix viminalis* leaves increased significantly compared with CK (Fig. 8D). In the soil without Pb pollution, the PI_{ABS} of *Salix viminalis* leaves inoculated with *F. mosseae* was 17.28 % higher than that without inoculation ($P < 0.05$). With the increase of Pb content in soil, the PI_{ABS} of *Salix viminalis* leaves decreased significantly.

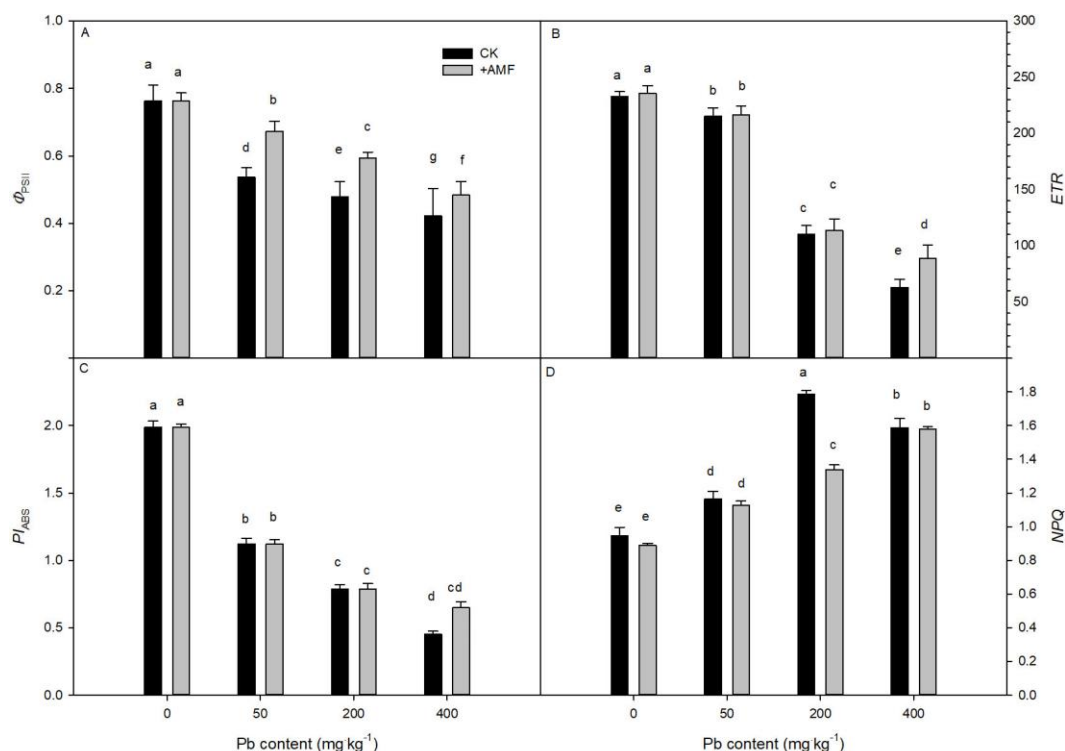


Figure 8. The PSII photochemical activity of *Salix viminalis* leaves in Pb contaminated soil. CK: CK + 0 AMF contents; +AMF: CK+ different AMF contents. A: Φ_{PSII} : actual photochemical efficiency; B: ETR: electron transfer rate; C: PI_{ABS} : absorption-based photosynthetic performance index; D: NPQ: non-photochemical quenching. Note: Data in the figure are represented as mean \pm SD; values followed by different lowercase letters indicate a significant difference ($p < 0.05$)

Discussion

Pb can significantly inhibit the growth of plants. In order to maintain normal growth and dry matter accumulation, plants must adapt to the stress environment in terms of external morphological characteristics and physiological functions, so as to ensure that the roots can normally absorb water and Photosynthesis and other physiological processes under adverse conditions (Del et al., 1999a,b; Dong et al., 2008). In this experiment, the growth of *Salix viminalis* in Pb contaminated soil was obviously inhibited, and its plant height, root length, biomass and accumulation decreased significantly with the increase of Pb content in soil, indicating that the growth and development of *Salix viminalis* roots would be hindered by Pb in soil, which may be due to the accumulation of Pb in *Salix viminalis* roots. The effect on the growth of aboveground was also studied. The infection level of arbuscular mycorrhizal fungi (*F. mosseae*) on the roots of *Salix viminalis* was relatively high. Under the influence of its infection, the root activity of *Salix viminalis* L. inoculated with *F. mosseae* under different Pb pollution levels was significantly higher than that without inoculation, which increased the root length and root biomass of *Salix viminalis* under Pb pollution.

Pb can also cause disordered grana stacking in chloroplasts, matrix lamellae disappearing and chloroplast function decreasing. Pb stress can also limit the photosynthetic carbon assimilation capacity of plants (Romanowska et al., 2006; Tukaj et al., 2007; Marmioli et al., 2013). Some studies have found that heavy metal stress

can increase the activities of carbon assimilation related enzymes such as Rubisco (Kalaji et al., 2016; Liu et al., 2017). However, a large number of studies have shown that heavy metal ions such as Pb^{2+} can combine with functional groups of some enzymes (such as sulfhydryl, -SH) to replace the essential elements in metalloproteins, which will change the conformation of biological macromolecules and inhibit their activities, resulting in the decrease of photosynthetic capacity (Li et al., 2000; Malecka et al., 2001; Qureshi et al., 2007; Skórzyńska-Polit et al., 2010). In this experiment, with the increase of soil Pb content, P_n , G_s and T_r decreased significantly. Inoculation with *F. mosseae* significantly improved stomatal limitation of *Salix viminalis* leaves, and then increased T_r and P_n , which was conducive to the accumulation of assimilates. When Pb content in soil increased to $200\text{ mg}\cdot\text{kg}^{-1}$, C_i of *Artemisia argyi* leaves inoculated with *F. mosseae* continued to decrease, while C_i of leaves without inoculation increased compared with that of $200\text{ mg}\cdot\text{kg}^{-1}$. The results showed that Pb content of $\text{mg}\cdot\text{kg}^{-1}$ destroyed the photosynthetic mechanism of *Salix viminalis* leaves, which was related to the decrease of CO_2 utilization capacity. Even with the decrease of stomatal conductance, C_i was forced to increase. However, C_i in leaves of *Salix viminalis* inoculated with *F. mosseae* was lower than that without inoculation when Pb content reached $200\text{ mg}\cdot\text{kg}^{-1}$, indicating that inoculation with *F. mosseae* could protect the physiological function of photosynthetic apparatus and increase the ability of CO_2 assimilation. In conclusion, inoculation with *F. mosseae* could improve photosynthetic capacity by increasing stomatal opening and the tolerance of photosynthetic apparatus to Pb. According to Farquhar et al. (1982), it can be concluded that the decrease of photosynthetic capacity of *Salix viminalis* leaves caused by Pb stress is the result of both stomatal and non-stomatal factors.

The content of chlorophyll directly affects the photosynthetic capacity and growth of plants. Under Pb stress, the number of chloroplast decreased or the structure of chloroplast was destroyed, which accelerated the degradation of chlorophyll and affected the photosynthetic capacity (Al-aghaby et al., 2005; Mani et al., 2015). In this experiment, Chla and Chlb decreased significantly with the increase of Pb concentration, especially Chla was more sensitive to Pb, which led to the decrease of Chl a/b with the increase of Pb concentration, which was consistent with the results of sheet, Vajpayee and Paiva who found that Chla was more sensitive to heavy metals than Chlb. Pb stress not only reduced the light energy capture ability of *Salix viminalis* leaves, but also reduced the light energy utilization capacity. The results showed that the chlorophyll a/b ratio of *Salix viminalis* leaves inoculated with *F. mosseae* was higher than that without inoculation. Therefore, inoculation with *F. mosseae* had a higher chlorophyll a/b ratio than that without inoculation. *F. mosseae* not only ensured the light energy capture ability of *Salix viminalis* leaves in Pb contaminated soil, but also increased the activity of reaction center to ensure the normal progress of photosynthesis.

Chlorophyll fluorescence technology is one of the important means to study the photosynthetic mechanism, especially the function of PSII (Zhang et al., 2019a,b). In this experiment, with the increase of Pb content in soil, F_o on OJIP curve of *Salix viminalis* leaves increased significantly, while F_m showed a decreasing trend. F_v/F_m and piabs parameters reflecting PSII photochemical activity of *Salix viminalis* leaves were significantly decreased. However, the decrease range of F_v/F_m and piabs of *Salix viminalis* leaves inoculated with *F. mosseae* were significantly lower than those without inoculation, indicating that inoculation with *F. mosseae* could significantly reduce the decrease of F_v/F_m and piabs. *F. mosseae* treatment could alleviate the decrease of PSII

photochemical activity in *Salix viminalis* leaves. In order to further analyze the reason why the inoculation of *F. mosseae* could relatively improve the photochemical activity of PSII in *Salix viminalis* leaves under Pb stress, we standardized the OJIP curves of *Salix viminalis* leaves under different treatments. The results showed that compared with the soil Pb content of 0 (CK), J point at 2 ms and 0.3 m on the OJIP curve of *Salix viminalis* leaves under different Pb stress were compared. The relative variable fluorescence V_J and V_K of K point at MS were significantly increased. Many studies have found that under stress conditions, the blocking sites of photosynthetic electron transfer often occur on the electron acceptor side and electron donor side of PSII reaction center (Xu et al., 2018; Zhang et al., 2018). The transfer of Q_A (primary electron receptor of photosystem II electron transport chain) to Q_B (secondary electron receptor of photosystem II electron transport chain) is the main inhibition site, and the activity of OEC on electron donor side is also observed is one of the sensitive parts to adversity. The relative variable fluorescence V_J at 2 ms on the OJIP curve can reflect the accumulation of Q_A^- that is, the enhancement of V_J indicates that the electron transfer from Q_A to Q_B on the PSII receptor side is blocked. The increase of V_K is considered as a specific marker for the damage of OEC activity on the side of PSII electron donor. Rashid et al. Showed that Pb^{2+} competitively inhibited the binding site of Ca^{2+} and Cl^- on 23kd protein in the exoxygenation complex, and affected the activity of 23K protein, thus inhibiting the activity of exoxygenation complex. Yao et al. (2009) also found that the photoinhibition of PSII in *Maize* Leaves under Pb stress was mainly related to the damage of OEC. Therefore, the decrease of photochemical activity of PSII in leaves of *Salix viminalis* was mainly due to the inhibition of electron transfer from Q_A to Q_B and the decrease of OEC activity of PSII donor side. However, the increase of V_J and V_K in *Salix viminalis* leaves inoculated with *F. mosseae* were significantly lower than those without inoculation, which indicated that the PSII activity of *Salix viminalis* leaves could be improved by stabilizing the electron transport of PSII receptor side and donor side.

Conclusion

Both 200 mg·kg⁻¹ and 400 mg·kg⁻¹ Pb stress resulted in the decrease of chlorophyll (especially Chla) degradation and photosynthetic capacity of *Salix viminalis* leaves. The reduction of photosynthetic carbon assimilation capacity of *Salix viminalis* leaves was limited by both stomatal and non-stomatal factors. The decrease of PSII activity and carboxylation efficiency and the oxidative damage of ROS were important non stomatal factors. The results showed that PSII was more sensitive to Pb stress than PSI, and the damage of PSII donor side was greater than that of PSII receptor side.

Soil Pb pollution first affected the root system of *Salix viminalis*, resulting in the decrease of root activity and underground biomass accumulation, as well as the decrease of chlorophyll content and photosynthetic capacity of leaves. *F. mosseae* could infect the roots of *Salix viminalis*. By inoculating *F. mosseae*, the root activity and chlorophyll content of *Salix viminalis* in Pb contaminated soil were significantly increased. In addition, the photosynthetic carbon assimilation capacity and PSII photochemical activity of *Salix viminalis* leaves were also improved in different degrees. Therefore, inoculation with *F. mosseae* could improve the Pb tolerance of *Salix viminalis* from morphological characteristics and photosynthetic function. Our future study aims to reveal the toxicological effect of Pb on the mechanisms underlying the anti-Pb response in tobacco.

REFERENCES

- [1] Al-aghaby, K., Zhu, Z. J., Shi, Q. H. (2005): Influence of silicon supply on chlorophyll content, chlorophyll fluorescence, and antioxidative enzyme activities in tomato plants under salt stress. – *Journal of Plant Nutrition* 27(12): 2101-2115.
- [2] Arena, C., Figlioli, F., Sorrentino, M. C., Izzo, L. G., Capozzi, F., Giordano, S., Sapgnuolo, V. (2017): Ultrastructural, protein and photosynthetic alterations induced by Pb and Cd in, *Cynaracardunculus* L. and its potential for phytoremediation. – *Ecotoxicology and Environmental Safety* 145: 83-89.
- [3] Chen, X. H., Zhao, B. (2009): Arbuscular mycorrhizal fungi mediated uptake of nutrient elements by Chinese milk vetch (*Astragalussinicus* L.) grown in lanthanum spiked soil. – *Biology & Fertility of Soils* 45(6): 675-678.
- [4] Chen, M., Yang, G., Sheng, Y., Li, P. Y., Qiu, H. Y., Zhou, X. T., Chao, Z., Huang, L. Q. (2017a): *Glomusmosseae* inoculation improves the root system architecture, photosynthetic efficiency and flavonoids accumulation of liquorice under nutrient stress. – *Frontiers in Plant Science* 8: 931.
- [5] Chen, M., Yang, G., Liu, D. H., Li, M. H., Qiu, H. Y., Guo, L. P., Huang, L. Q., Chao, Z. (2017b): Inoculation with *Glomusmosseae* improves the growth and salvianolic acid b accumulation of continuously cropped *Salvia miltiorrhiza*. – *Applied Sciences* 7(7): 692.
- [6] Chen, S., Zhao, H., Zou, C., Li, Y. S., Chen, Y. F., Wang, Z. H., Jian, Y., Li, A. R., Zhao, P. Y., Wang, M. M., Ahammed, G. J. (2017c): Combined inoculation with multiple arbuscular mycorrhizal fungi improves growth, nutrient uptake and photosynthesis in cucumber seedlings. – *Frontiers in Microbiology* 8: 2516.
- [7] Del, V. C., Barea, J. M., Azcon-Aguilar, C. (1999a): Diversity of arbuscularmycorrhizal fungus populations in heavy-metal-contaminated soils. – *Applied Environmental Microbiology* 65(2): 718-723.
- [8] Del, V. C., Barea, J. M., Azcon-Aguilar, C. (1999b): Assessing the tolerance to heavy metals of arbuscular mycorrhizal fungi isolated from sewage sludge-contaminated soils. – *Applied Soil Ecology* 11(2-3): 261-269.
- [9] Dong, Y., Zhu, Y. G., Smith, F. A., Wang, Y., Chen, B. (2008): Arbuscular mycorrhiza enhanced arsenic resistance of both white clover (*Trifoliumrepens* Linn.) and ryegrass (*Loliumperenne* L.) plants in an arsenic-contaminated soil. – *Environmental Pollution* 155(1): 174-181.
- [10] Farquhar, G. D., Sharkey, T. D. (1982): Stomatal conductance and photosynthesis. – *Annual Review of Plant Physiology* 33(33): 317-345.
- [11] Gupta, D. K., Huang, H. G., Yang, X. E., Bam, H. N. R., Masahiro, I. (2010): The detoxification of lead in *Sedum alfredii* H. is not related to phytochelatins but the glutathione. – *Journal of Hazardous Materials* 1: 437-444.
- [12] Hall, J. L. (2002): Cellular mechanisms for heavy metal detoxification and tolerance. – *Journal of Experimental Botany* 53(366): 1-11.
- [13] Kalaji, H. M., Jajoo, A., Oukarroum, A., Brestic, M., Zivcak, M., Samborska, I. A., Cetner, M. D., Łukasik, I., Goltsev, V., Ladle, R. J. (2016): Chlorophyll a, fluorescence as a tool to monitor physiological status of plants under abiotic stress conditions. – *Acta Physiologiae Plantarum* 38(4): 102.
- [14] Li, X. P., Bjorkman, O., Shi, C., Grossman, A. R., Rosenquist, M., Jansson, S., Niyogi, K. K. (2000): A pigment-binding protein essential for regulation of photosynthetic light harvesting. – *Nature* 403(6768): 391-395.
- [15] Liu, M., Sun, J., Li, Y., Xiao, Y. (2017): Nitrogen fertilizer enhances growth and nutrient uptake of *Medicago sativa* inoculated with *Glomustortuosum* grown in Cd-contaminated acidic soil. – *Chemosphere* 167: 204-211.
- [16] Malecka, A., Jarmuszkiewicz, W., Tomaszewska, B. (2001): Antioxidative defense to lead stress in subcellular compartments of pea root cells. – *Acta Bioquimica Polonica* 48(3): 687-698.

- [17] Mani, D., Kumar, C., Patel, N. K. (2015): Hyperaccumulator oilcake manure as an alternative for chelate-induced phyto remediation of heavy metals contaminated alluvial soils. – *International Journal of Phytoremediation* 17(3): 256-263.
- [18] Marmiroli, M., Imperiale, D., Maestri, E., Marmiroli, N. (2013): The response of *Populus* spp. to cadmium stress: chemical, morphological and proteomics study. – *Chemosphere* 93(7): 1333-1344.
- [19] Pallara, G., Todeschini, V., Lingua, G., Camussi, A., Racchi, M. L. (2013): Transcript analysis of stress defence genes in a white poplar clone inoculated with the arbuscular mycorrhizal fungus *Glomus mosseae*, and grown on a polluted soil. – *Plant Physiology & Biochemistry* 63(4): 131-139.
- [20] Qu, Y. P., Fang, Y. L., Liu, Y. L., Song, S. R., Zhang, A., Zhou, G. R. (2009): Effects of AM fungal on the secondary metabolites of grape under cadmium stress. – *Journal of Northwest Forestry University* 24(5): 101-105.
- [21] Qureshi, M. I., Abdin, M. Z., Qadir, S., Iqbal, M. (2007): Lead- induced oxidative stress and metabolic alterations in *Cassia angustifolia* Vahl. – *Biologia Plantarum* 51(1): 121-128.
- [22] Rizwan, M., Ali, S., Hussain, A., Asma, M. (2017): Effect of zinc-lysine on growth, yield and cadmium uptake in wheat (*Triticum aestivum* L.) and health risk assessment. – *Chemosphere* 187: 35-42.
- [23] Romanowska, E., Wróblewska, B., Drozak, A., Siedlecka, M. (2006): High light intensity protects photosynthetic apparatus of pea plants against exposure to lead. – *Plant Physiology and Biochemistry* 44(5-6): 387-394.
- [24] Rozpądek, P., Rapałkożik, M., Wężowicz, K., Grandin, A., Karlsson, S., Wazny, R. (2016): Arbuscular mycorrhiza improves yield and nutritional properties of onion (*Allium cepa*). – *Plant Physiology & Biochemistry* 107: 264-272.
- [25] Sauliutė, G., Svecevičius, G. (2015): Heavy metal interactions during accumulation via direct route in fish: a review. – *Zoology & Ecology* 25(1): 77-86.
- [26] Shao, X. J., Yang, H. Q., Qiao, H. T., Zhang, L., You, S. Z., Shao, X. J., Yang, H. Q., Qiao, H. T., Zhang, L., You, S. Z. (2009): Effects of CdCl₂ on grape root mitochondrial characteristics and root activity. – *Chinese Journal of Applied Ecology* 20(6): 1390-1394.
- [27] Soffianian, A., Madani, E., Arabi, M. (2014): Risk assessment of heavy metal soil pollution through principal components analysis and false color composition in Hamadan Province, Iran. – *Environmental Systems Research* 3(1): 1-14.
- [28] Strasser, R. J., Srivastava, A., Govindjee (1995): Polyphasic chlorophyll a fluorescence transient in plants and cyanobacteria. – *Photochem. Photobiol* 61: 32-42.
- [29] Tukaj, Z., Bascik-Remisiewicz, A., Skowronski, T., Tukaj, C. (2007): Cadmium effect on the growth, photosynthesis, ultrastructure and phytochelatin content of green microalga *Scenedesmus armatus*: a study at low and elevated CO₂ concentration. – *Environmental & Experimental Botany* 60(3): 291-299.
- [30] Xu, N., Zhang, H. H., Zhong, H. X., Wu, Y. N., Li, L. B., Li, X., Yin, Z. P., Zhu, W. X., Qu, Y., Sun, G. Y. (2018): The response of photosynthetic functions of F₁ cutting seedlings from *Physocarpus amurensis* Maxim (♀) × *Physocarpus opulifolius* “Diabolo” (♂) and the parental leaves to salt stress. – *Frontiers in Plant Science* 9: 714.
- [31] Xue, Z. C., Gao, H. Y. (2017): The difference of photosynthetic responses to the cadmium stress between a wild soybean (*Glycine soja* Sieb. et Zucc.) and a cultivated soybean. – *Bulletin of Environmental Contamination & Toxicology* 99(3): 1-6.
- [32] Yang, Y., Han, X., Yan, L., Amit, G., Jie, C., Ming, T. (2015): The combined effects of arbuscular mycorrhizal fungi (AMF) and lead (Pb) stress on Pb accumulation, plant growth parameters, photosynthesis, and antioxidant enzymes in *Robinia pseudoacacia* L. – *PLoS ONE* 10(12): e145726.
- [33] Yao, G., Gao, H. Y., Wang, W. W., Zhao, L. T., Bu, J. W. (2009): The effects of Pb-stress on functions of photosystems and photosynthetic rate in maize seedling leave. – *Acta Ecologica Sinica* 29(3): 1162-1169.

- [34] Zhai, F. F., Mao, J. M., Liu, J. X., Peng, X., Han, L., Sun, Z. (2016): Male and female subpopulations of *Salix viminalis* present high genetic diversity and high long-term migration rates between them. – *Frontiers in Plant Science* 7: 330.
- [35] Zhang, F. Q., Wang, Y. S., Luo, Z. P., Dong, J. D. (2007): Effect of heavy metal stress on antioxidative enzymes and lipid peroxidation in leaves and roots of two mangrove plant seedlings (*Kandeliacandel* and *Bruguieragymnorrhiza*). – *Chemosphere* 67(1): 44-50.
- [36] Zhang, H. H., Xu, N., Wu, X. Y., Wang, J. R., Ma, S. L., Li, X., Sun, G. Y. (2018): Effects of 4 kinds of sodium salt stress on plant growth, PSII and PSI function in leaves of Sorghum. – *Journal of Plant Interaction* 13(1): 506-513.
- [37] Zhang, H. H., Shi, G. L., Shao, J. Y., Li, X., Li, M. B., Meng, L., Xu, N., Sun, G. Y. (2019a): Photochemistry and proteomics of mulberry (*Morusalba* L.) seedlings under NaCl and NaHCO₃ stress. – *Ecotoxicology and Environmental Safety* 184: 109624.
- [38] Zhang, H. H., Xu, N., Teng, Z. Y., Wang, J. R., Ma, S. L., Wu, X. Y., Li, X., Sun, G. Y. (2019b): 2-Cys Prx plays a critical role in scavenging H₂O₂ and protecting photosynthetic function in leaves of tobacco seedlings under drought stress. – *Journal of Plant Interaction* 14(1): 119-128.

THE GROSS ALPHA AND GROSS BETA ACTIVITIES OF HOLOCENE MARINE SEDIMENTS AND THE RELATIONSHIP OF THESE ACTIVITIES WITH RADIONUCLIDES IN THE WESTERN MARMARA SEA, TURKEY

YÜMÜN, Z. Ü.^{1*} – YENTÜR, M. M.² – ASLIYÜKSEK, H.³ – KAM, E.⁴

¹*Namık Kemal University, Çorlu Engineering Faculty, Environmental Engineering Department, 59860 Çorlu, Tekirdağ, TURKEY
(e-mail: zyumun@nku.edu.tr)*

²*Istanbul Sabahattin Zaim University, Küçükçekmece/ Istanbul, TURKEY
(e-mail: myentur@hotmail.com)*

³*Istanbul University-Cerrahpaşa Institute of Forensic Medicine and Forensic Sciences, Büyükçekmece/Istanbul, TURKEY
(e-mail: doktorhizir@gmail.com)*

⁴*Yıldız Technical University, Faculty of Arts and Sciences, Physics Department, Davutpaşa Campus, 34220 Esenler/ İstanbul, TURKEY
(e-mail: erolkam@yildiz.edu.tr)*

**Corresponding author
e-mail: zyumun@nku.edu.tr*

(Received 14th Nov 2021; accepted 2nd May 2022)

Abstract. The aim of this study is to analyze the gross alpha and gross beta activities of Holocene marine sediments and to determine the relationship of these activities with radionuclides in the west of Marmara Sea (Turkey). Background and anthropogenic ionizing radiations are the main sources of environmental radioactivity human beings are exposed to. Background radiation occurs as a result of cosmogenic and terrestrial radiation, while anthropogenic refers to man-made radiation. In this context, gross alpha and beta activity of sea sediment samples collected at 29 different stations in the research region were analyzed using the low-background counter (Berthold, LB 770, 10- channel α - β low-level counter). Also, the relation between abundance of radioactive isotopes and alpha and beta activity were discussed in this paper. As a result, the average gross alpha and beta activities were determined as 223.18 ± 14.9 Bq kg⁻¹ and 572.00 ± 23.9 Bq kg⁻¹, respectively. The results obtained can be used as a data base for Holocene marine sediments.

Keywords: radionuclide, radioactivity, radioactivity pollution, Chernobyl accident K-40, Sr-90, Cs-137, Marmara Sea

Introduction

Ionizing radiation pollution which is mainly caused by background and anthropogenic radiations is one of the recent environmental problems. Background radiation originates from cosmogenic and terrestrial radiations, while anthropogenic means man-made. The recent increase in the levels of environmental ionizing radiation pollution is directly related with the industrialization such as the use of fossil fuels, phosphate industry and wrong and excessive use of fertilizers (Topcuoğlu et al., 2010). The radioactive elements are found in magmatic rocks, in phosphate rocks, in sedimentary masses such as clay and shale, and in granitic rocks in high amounts. But

these elements are found in small quantities in Sedimentary rocks such as sand-gravel, sandstone, and limestones with crack (Kumru et al., 2002). The source of radioactivity in the aquatic environment is water pollution which occurs with particles and minerals present in water. The geological structure of the area where the water deposit is located is also a determinant of natural radioactivity. It differs in radioactivity levels according to the quality of the rocks forming the Earth's crust (Karaman, 2003). The knowledge of environmental natural radioactivity is very important in terms of determining where the nuclear accidents and industrialization pollute the environment (Degerlier, 2007). For example, after the Chernobyl accident, anthropogenic radionuclides entered the marine environment. The atmospheric sediments spread from the nuclear weapon tests in the countries around the Black Sea reached the Marmara Sea through the Bosphorus (Topcuoğlu, 2001).

The alpha particle is a helium nucleus with an electric charge (+2). Due to its large mass, it is unlikely to penetrate into matter. Alpha particles are emitted from natural radioactive isotopes such as polonium, thorium, radium, uranium, which are formed in nature and have large atomic weights. The ionization betting that the alpha rays bring into the matter is relatively high. The gross alpha radioactivity consists of U-238, Th-232, Ra-226, Rn-222 and their alpha emitter nuclei. The gross beta radioactivity is due to fission and activation products such as natural long-lived K-40, Sr-90, Cs-137, Co-60 and I-125 (Varol, 2011). Beta particles are negatively charged and have smaller mass than alpha particle. As soon as one of the neutrons in the nucleus of the isotope changes, beta degradation occurs immediately. As it carries ionizing properties, it has harmful effects on living organisms (Varol, 2011). The sediments play an important role in the aquatic environment, because of their geological and chemical structure, which provides the flow system between land, sea and atmosphere (Kurt et al., 2016). Determination of radioactivity in sediment samples provide information on the level of sea water radioactivity the sediment is receiving. One of the most commonly used methods for determining environmental radiation is gross alpha and gross beta measurements, which are the result of quick access and low cost (Bunz and Kracke, 1998). Numerous studies have been conducted in the past years on the identification of environmental radioactivity and the monitoring of pollution using heavy metals and radioactivity in marine environments (Taskin, 2006; Bozkurt et al., 2007; Varol, 2011; Agbalagba et al., 2013; Cam et al., 2013; Kaya et al., 2016; Kurt et al., 2016; Yümün, 2016; Kam et al., 2016; Yümün et al., 2016, 2017; Yümün and Önce, 2017).

In the studies given in the above paragraph, gross alpha and beta activity measurements were performed for groundwater and drinking waters and also radionuclides in sediments were examined. In this study, gross alpha and beta activity of sea sediment samples collected from 29 different stations in the Western Marmara Sea (Recent marine sediments) were analyzed and environmental radioactivity concentration values were determined. Also, the traces of nucleotides, such as Cs-137, which gave rise greatly to the pollution of marine environments, was discussed.

Material and Methods

The sampling stations were between Silivri (Istanbul) - Bandırma (Balıkesir) in Western Marmara Sea which is at the west part of Turkey (*Fig. 1*). The bathymetry of the study area varies between 20.00 m and 35.00 m in core samples. Core samples from 29 locations were used in the study. The samples were taken between 15-20.10.2015

and the coordinates and depth information of the samples are given in *Table 1*. Because the samples are obtained from about 30 m, the samples are in the form of fine-grained, sandy-silty clay (Yümün, 2017). Sediment samples were immediately taken in a nylon bag and protected from atmospheric moisture. Later, the samples were taken to the laboratory, where they were removed from the nylon bags and dried in room temperature.

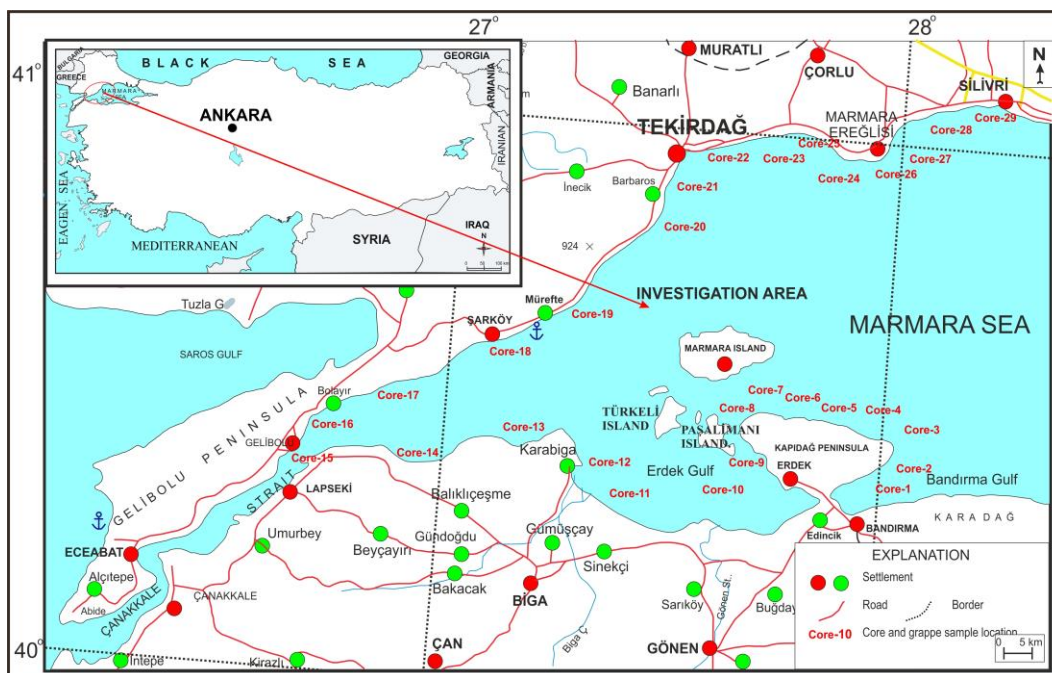


Figure 1. Location map of investigation area and sample's locations

The dried sediment samples were ground in granite bowls and sieved with a stainless-steel sieve to remove the portion that came to the size of the powder. Approximately 100 mg of each sample was weighed on a precision scale and placed in an empty aluminum bowl. Distilled pure water has been used to homogeneously distribute the samples in the bowl. The specimens were dried for 2 hours at 105 °C, then left in the desiccator to cool to room temperature without drawing any moisture. Then, the prepared samples were homogenized with distilled water and placed in the oven. This process is important to determine the amount of residue. If the amount of the residue is more than 400 mg, the self-absorption effect of the alpha particles increases. In this way, fewer particles will reach the detector, causing the results to be erroneous (Taskin, 2006). Finally, the gross alpha and gross beta activity rates of all samples were measured using two low-level LLB 770-PC 10-channel alpha-beta counting systems in two cycles of 500 minutes each. LLB 770-PC 10-channel alpha-beta counting systems have been produced by Contact Berthold Technologies GmbH & Co. in Germany. Each analysis was repeated twice and the arithmetic mean of these measurements was used. The samples were taken from the sea using a boat and the gravity core method. The diameter of the samples (54 mm) and the sampling depths are given in *Table 1*.

Table 1. Gross alpha and beta activity concentration of sediments collected from Western Marmara Sea

Sample No	Gross Alpha (Bq/kg)	Uncertainty (±)	Gross Beta (Bq/kg)	Uncertainty (±)	Geographic Position (WGS-84)		Sample Depth (m)
					Y	X	
CORE-1	311.76	17.6	900.41	30	0581459	4474677	30,
CORE-2	259.45	16.1	585.45	24.1	0584985	4476692	29
CORE-3	135.2±11	11	338.19	18.3	0588105	4481639	30
CORE-3b	265.58	16.2	768.23	27.7	0586229	4482780	35
CORE-4	240.88	15.4	38.38	6.1	0582393	4483551	30
CORE-4b	286.8	16.9	848.05	29.1	0582260	4483937	32
CORE-4c	119.12	10.9	456.56	21.3	0579835	4485462	35
CORE-5	282.76	16.7	640.28	25.2	0577401	4485335	38
CORE-6	309.42	17.5	875.06	29.5	0566840	4486334	40
CORE-7	149.43	12.2	344.29	18.5	0562101	4486810	48
CORE-8	32.23	5.6	154.99	12.4	0558197	4484862	39,5
CORE-9	184.99	13.5	658.76	25.6	0558282	4480129	28
CORE-9b	269.92	16.4	667.47	25.8	055 83 61	4479791	32
CORE-10	253.39	15.9	613.51	24.7	0556281	4463687	19
CORE-11	152.24	12.3	475.71	21.7	0542436	4464634	26
CORE-12	608.41	24.6	1320.14	36.3	0528796	4470648	18
CORE-13	121.04	11	496.28	22.7	0514452	4478784	46
CORE-14	307.22	17.5	753.74	27.4	0490282	4473347	29
CORE-15	137.53	11.7	563.11	23.7	0473914	4469971	41
CORE-16	178.87	13.3	150.33	12.2	0472908	4472487	30
CORE-17	158.37	12.5	591.22	24.3	0488099	4481025	33
CORE-18	166.42	12.8	374.49	19.3	0511008	4494809	32
CORE-19	134.78	11.5	459.08	21.4	0540197	4522435	30
CORE-20	347.03	15.6	970.66	31.1	0542591	4530386	32
CORE-21	164.15	11.3	447.84	21.1	0546815	4533986	33
CORE-22	106.34	18.1	117.65	11.8	0560139	4536953	33
CORE-23	104.22	14.6	212.23	12.2	0569767	4535792	32
CORE-24	127.64	14.7	307.82	26.5	0579050	4532627	30
CORE-25	419.99	20.4	321.19	28.6	0581005	4534924	33
CORE-26	66.34	8.1	115.65	10.8	0585198	4539137	32
CORE-27	114.3	10.6	252.93	11.8	0588549	4541739	30
CORE-28	167.64	12.9	707.82	16.5	0596407	4543970	31
CORE-29	419.99	20.4	821.19	18.6	0604571	4544155	35

Gross Alpha and Beta concentration obtained from analysis results have been analyzed by Kriging method (*Figures 2 and 3*). The Kriging method is an interpolation method that estimates the optimal values of the data at one point using the data from the other known points (Inal et al., 2002). Kriging method is a technique in which the estimation of spatial changes in not sampled points is made optimally using semi variogram structural properties (Trangmar et al., 1985). The activities were obtained using the following formulas:

$$Activity() = \frac{NetCounting}{60 Efficiency Mass(kg)} \quad (Eq.1)$$

$$Activity() = \frac{N() B(crosstalk)}{60 Efficiency Mass(kg)} \quad (Eq.2)$$

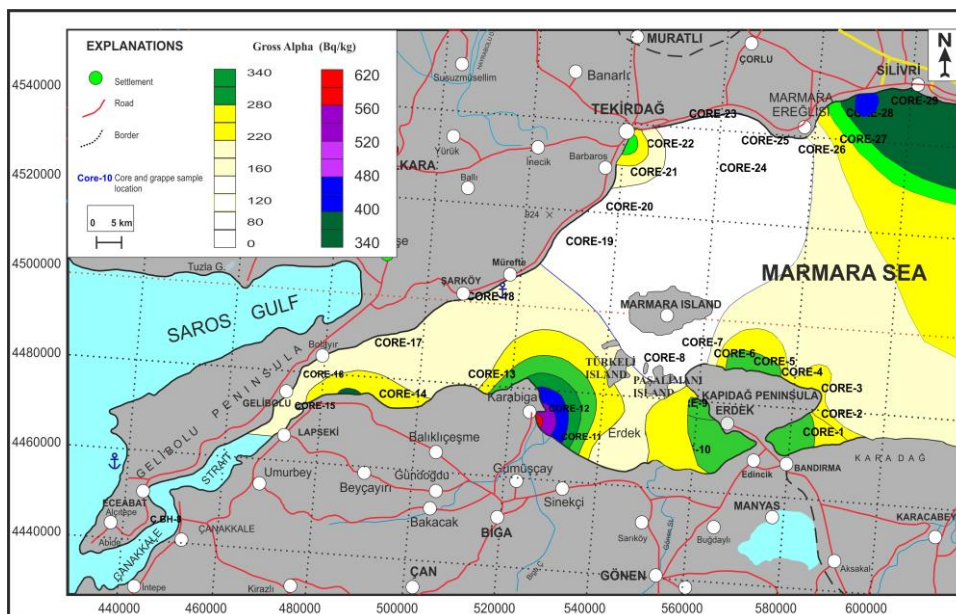


Figure 2. Map of gross alpha distribution of investigation area (Western Marmara Sea)

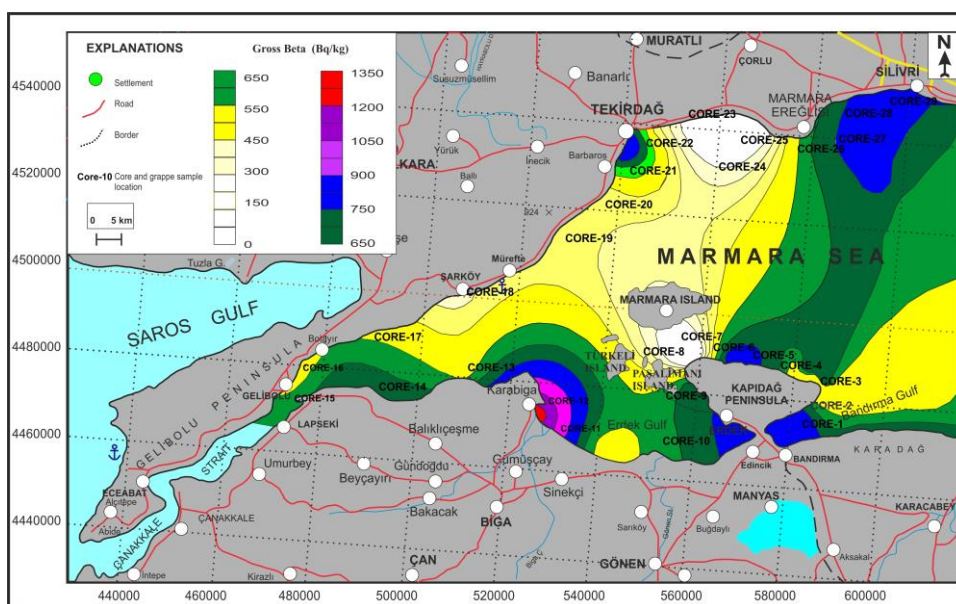


Figure 3. Map of Gross Beta distribution of investigation area (Western Marmara Sea)

Low level counting system is commonly used for measuring environmental samples with low natural radiation. Its calibration has been carried out with standard solutions, which contained known activities of ^{241}Am for alphas and ^{90}Sr for betas which are similar to the sample geometry (Currie, 1968). Gross alpha radioactivity is composed of radionuclides (U-238, Th-232, Ra-226, Rn-222) and their alpha emitting nuclei, Gross beta radioactivity is of natural long-lived radionuclides (K-40, Sr-90, Cs-137, Co-60 and I-125) are known to originate from fission and activation products (Table 2). For this reason, the causes of Gross alpha and Gross Beta activities were evaluated by taking the radionuclide values of the samples of this study.

Table 2. Results of gamma spectrometric analyses of core samples (Yümin and Kam, 2020)

Sample	Radionuclide	Activity ± Bq/kg	Gross Alpha (Bq/kg)	Gross Beta (Bq/kg)	Sample	Radionuclide	Activity ± Bq/kg	Gross Alpha (Bq/kg)	Gross Beta (Bq/kg)		
CORE-1	⁴⁰ K	490	311.76	900.41	CORE-13	²³² Th	45	269.92	667.47		
	¹³⁷ Cs	2.5				²²⁶ Ra	25.7				
	²²⁶ Ra	30				¹³⁷ Cs	2.2				
	²³² Th	42				⁹⁵⁺ Zr	0.27				
CORE-2	¹³⁷ Cs	1.9	259.45	585.45	CORE-14	⁴⁰ K	470	253.39	613.51		
	²²⁶ Ra	19.8				²³² Th	36				
	²³² Th	27.1				²²⁶ Ra	25.2				
CORE-3	²²⁶ Ra	25	135.2	338.19	CORE-15	¹³⁷ Cs	3.2	152.24	475.71		
	²³² Th	28				²²⁶ Ra	19.5				
CORE-4	⁴⁰ K	24.4	265.58	768.23	CORE-16	²³² Th	36	608.41	1320.14		
	¹³⁷ Cs	1.4				⁴⁰ K	600				
	²³² Th	21.6				¹³⁷ Cs	4.7				
	⁵⁴ Mn	0.71				²²⁶ Ra	24.9				
CORE-5	⁴⁰ K	470	240.88	38.38	CORE-17	²³² Th	37	121.04	496.28		
	¹³⁷ Cs	1.8				¹³⁷ Cs	1.6				
	²²⁶ Ra	21.5				²²⁶ Ra	18.9				
	²³² Th	30				²³² Th	26				
CORE-6	⁴⁰ K	450	286.8	848.05	CORE-18	¹³⁷ Cs	4.8	307.22	753.74		
	¹³⁷ Cs	1.3				²²⁶ Ra	29				
	²²⁶ Ra	27				²³² Th	36				
	²³² Th	26				⁴⁰ K	650				
CORE-7	¹³⁷ Cs	1.1	119.12	456.56	CORE-19	¹³⁷ Cs	2.3	137.53	563.11		
	²²⁶ Ra	24				²²⁶ Ra	27.9				
	²³² Th	39				²³² Th	39				
	⁹⁵⁺ Zr	0.2				⁴⁰ K	630				
CORE-8	¹³⁷ Cs	1.1	282.76	640.28	CORE-20	¹³⁷ Cs	9.4	178.87	150.33		
	²²⁶ Ra	18.6				²²⁶ Ra	20.5				
	²³² Th	30				²³² Th	35				
CORE-9	⁴⁰ K	470	309.42	875.06	CORE-21	¹³⁷ Cs	3.7	158.37	591.22		
	¹³⁷ Cs	0.9				²²⁶ Ra	20.6				
	²²⁶ Ra	19				²³² Th	30				
	²³² Th	33				¹³⁷ Cs	5.1				
CORE-10	¹³⁷ Cs	3.5	149.43	344.29	CORE-22	²²⁶ Ra	27	166.42	374.49		
	²²⁶ Ra	50				²³² Th	20.7				
	²³² Th	86				¹³⁷ Cs	1.7				
	¹⁵⁵ Eu	3.2				²²⁶ Ra	13.7				
CORE-11	⁴⁰ K	670	32.23	154.99	CORE-23	²³² Th	18.9	134.78	459.08		
	²³² Th	57				CORE-24	²²⁶ Ra			10	
	²²⁶ Ra	34					²³² Th			21	
	¹³⁷ Cs	3.8					CORE-25			⁴⁰ K	550
	⁵⁴ Mn	1.1								¹³⁷ Cs	1
²³² Th	49	²²⁶ Ra	22								
CORE-12	²²⁶ Ra	28.2	184.99	658.76	CORE-26	²³² Th	38	164.15	447.84		
	¹³⁷ Cs	4.9				⁹⁵⁺ Zr	0.19				
	⁴⁰ K	480				CORE-28	⁴⁰ K			580	
²³² Th	24	¹³⁷ Cs	1								
²²⁶ Ra	19.2	²²⁶ Ra	18.1								
¹³⁷ Cs	0.8	²³² Th	24.8								
CORE-27	¹³⁷ Cs	1.3	114.3	252.93	CORE-29	²²⁶ Ra	20.9	419.99	821.19		
	²²⁶ Ra	16.1				CORE-29	²³² Th			31	
	²³² Th	21.7									

Results and Discussion

The gross alpha and gross beta concentration of the obtained sediments are given in *Table 1* and the position of the sample stations are given in *Fig. 1*. According to the analysis results, gross beta values were found higher than gross alpha values at all locations except M5. The lowest and highest gross alpha and gross beta values are 32, 23-608, 41 Bq/kg (average value: 223, 18 Bq/kg) and 38, 38-1320, 14 Bq/kg (average value: 572, 00 Bq/kg), respectively. The lowest concentration of gross alpha is in M11, M26, while Beta is in M5. However, M16 is the region with the highest gross alpha and beta intensities.

Since there is no regulatory standard for radiological pollutants in sediments, the results obtained in this study are compared with those in different countries in *Table 3* and gross alpha and gross beta activity concentration of sediment samples are shown in *Figure 4*. According to *Table 3*, the gross alpha concentration of the study is higher than that in Los Alamos and Sir Dam Pond. The gross beta concentration of the western Marmara sea samples is considerably lower than the values for the Bendimahı River, but higher than the data for other locations referenced in the manuscript. Although the gross alpha and gross beta concentrations in studies conducted in other countries are close to the average value, the concentrations obtained in this study have very large ranges. This is due to the high concentration of environmental pollutants in some locations in this region. According to the locations where the samples are taken, there are differences in the analysis results. Core samples have a fine-grained, sandy-silty clayey composition, because they have been taken from areas, where higher than 30 m depth. Concentrations of radionuclides vary depending on sediment particle size, mineral composition, local pollution and organic matter content (Papaeftymiou et al., 2007).

Table 3. Gross alpha and gross beta activity concentration values compared to similar studies (1: (Pentreath, 1984), 2: (Wallove et al., 2016), 3: (Zorer, 2009), 4: (Pentreath, 1984))

Stations	Gross α (Bq/kg)	Gross β (Bq/kg)	References
<i>Pentreath, 1984</i> : Western Marmara, Turkey	32.23-608.41 (average: 223,18)	38.38-1320.14 (average: 572,00)	Present study
Los Alamos, New Mexico	55,5	55.5	<i>Wallove et al., 2016</i>
Bosna River, Bosnia	215-610 (average: 460,7)	495-628 (average: 539,1)	<i>Wallove et al., 2016</i>
Bendimahı River (May)	782-4596 (average: 2000)	482-10372 (average: 4635)	<i>Zorer, 2009</i>
Sir Dam Pond (May)	34.8-229 (average: 101)	144.1-419.3 (average: 234,3)	<i>Pentreath, 1984</i>

In this study the results generally have high values compared to similar studies which are generally referred to. K-40 is the most abundant natural radioisotope in the earth's crust and soluble in abundant amounts in seawater (Peterson, 2007). The areas where the Nilüfer and Gönen Streams flow into the Marmara Sea and the sea areas adjacent to the coasts where the settlements are located are the most polluted areas of the Marmara Sea. It has been observed that K40 values in these locations are higher than the world average values.

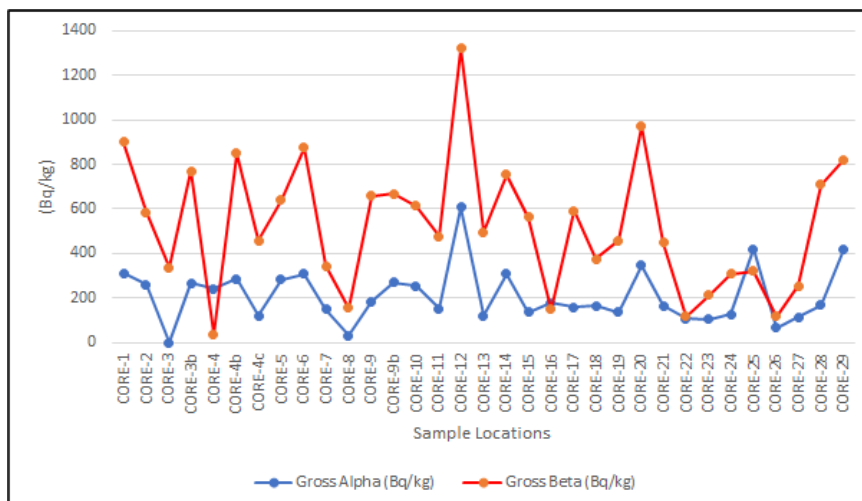


Figure 4. The gross alpha and gross beta activity concentration of sediment specimens in the Western Marmara Sea

In the graph given in *Figure 4*, it is seen that gross alpha and gross beta concentrations decreased and increased similarly in each location. In *Table 2*, gross alpha and gross beta activities were also compared with radionuclides (^{40}K , ^{137}Cs , ^{226}Ra , ^{232}Th , ^{95}Zr , ^{54}Mn) of the same samples. It is seen that gross alpha and gross beta values increase in locations where radionuclide concentrations increase, and decrease in locations where radionuclide concentrations decrease. It is thought that domestic and industrial wastes, agricultural activities and ship wastes are among the reasons for the very high concentrations of gross alpha and gross beta, especially in settlements, agricultural areas, piers and ports. Another important reason why the gross alpha and beta concentrations are generally high is that the fertilizers used in agriculture contain uranium, thorium and their decomposition products and natural potassium-40 (NCRP, 1987).

This study shows that fertilizer and agricultural pesticide residues from the soil carried by Kocasu, Gönen and Biga streams in the areas where agricultural activities are concentrated cause radioactive pollution (Kam et al., 2016). Another contribution to gross beta results is the Chernobyl nuclear reactor accident and nuclear weapon trials. Radioactive nuclei of ^{137}Cs , ^{90}Sr , ^{131}I , ^{132}Te and ^{239}Pu are spread from the nuclear reactor accident and nuclear weapon tests. The points where Gross alpha and Gross Beta activity values are high are the locations close to Çanakkale. The locations with low activity values were obtained in the samples taken near the Kapıdağ Peninsula. The high activity values may be related to the geological structure and pollution. In part, it could be the effects of the Chernobyl accident. Especially high Cs values may be due to weapon trials. After the Chernobyl accident, the vertical velocity of ^{134}Cs and ^{137}Cs in the soil was found to be 0.2-0.3 cm/hour (Bunz and Kracke, 1988).

Especially ^{137}Cs (half-life 30 years) and ^{90}Sr (half-life 29, 12 years) radionuclides have quite long half-lives. For this, background levels should be determined for the individual radionuclides that may create the potential pollution cause of the regions. The radionuclide potential of marine sediments from the same locations where this study was conducted was determined (Yümün and Kam, 2020). International average values of radionuclides are ^{232}Th : 30 Bq/kg, ^{226}Ra : 35 Bq/kg, ^{40}K : 400 Bq/kg (UNSCEAR,

2000). The radionuclide potential obtained from the study is given in *Table 2*. In *Table 2*, gross alpha and gross beta values are presented together with radionuclides and correlations are made. When the values given in *Table 2* are examined, it is seen that the gross alpha radioactivity consists of radionuclides (U-238, Th-232, Ra-226, Rn-222) and their alpha emitter cores. Again in *Table 2* it was seen that gross beta radioactivity resulted from fission and activation products such as natural long-lived radionuclides (K-40, Sr-90, Cs-137, Co-60 and I-125). However, in most of the sediment samples taken in this study, it is seen that the radionuclides are above the world average values. The high radionuclide concentrations seen here are responsible for the high gross alpha and gross beta activities. These analyses can be applied to water and sediment samples, as well as to foodstuffs (Pintilie et al., 2017) such as bread (Pintilie et al., 2018).

Conclusion

The main purpose of this study was to determine the natural radioactivity of the region by examining the gross alpha and gross beta concentrations of sediment samples from the Western Marmara Sea. In addition, studies have been carried out to define the relationship of gross alpha and gross beta activities with radionuclides. As a result, beta activity has been found to be significantly higher than alpha activity at all locations. Natural radioactivity depends directly on the regional geology, weather conditions and physicochemical variability of the water. The fact that the agricultural activities of the study area is high and is in the leading region of the country in terms of population and industry, strongly influences radioactive pollution.

Gross alpha radioactivity consists of U-238, Th-232, Ra-226, Rn-222 and their alpha emitting nuclei. The gross beta radioactivity is due to fission and activation products of natural long-lived radionuclides (K-40, Sr-90, Cs-137, Co-60 and I-125) (Varol, 2011). According to the values given in *Table 2*, Gross alpha and gross beta concentrations are also high in locations where K40 and other radionuclides are high. In addition, the presence of Cs-137, which cannot occur in the natural environment, in many locations in this study area, is thought to be a result of the Chernobyl Nuclear accident. In addition, there may have been nuclear weapon tests carried out by some countries recently. This is an important issue and needs to be taken seriously.

The data published in this paper can be the base data which also will be used to evaluate future changes. In future studies to determine the radioactive pollution of the Marmara Sea, sea water and sea sediment samples should be sampled at more frequent intervals.

REFERENCES

- [1] Agbalagba, E. O., Avwiri, G. O., Chadumoren, Y. E. (2013): Gross and Activity Concentration and Estimation of Adults and Infants Dose intake in Surface and Ground. – TSpace, University of Toronto.
- [2] Bozkurt, A., Yorulmaz, N., Kam, E. (2007): Environmental Radioactivity Measurements in Harran Plain of Sanliurfa, Turkey. – Sixth International Conference of the Balkan Physical Union.
- [3] Bunz, K., Kracke, W. (1988): Cumulative deposition of ^{137}Cs , ^{238}Pu , $^{239+240}\text{Pu}$ and ^{241}Am from global fallout in soils from forest, grassland and arable land in Bavaria (FRG). – *Journal of Environmental Radioactivity* 8: 1-14.

- [4] Çam, H., Dogru, M., Kucukonder, A., Karatepe, S. (2013): Seasonally gross alpha and beta activity concentration in surface water and sediments in Sir Dam Pond. – *Kerntechnik* 78: 431-436.
- [5] Currie, L. A. (1968): Limits for Qualitative Detection and Quantitative Determination. Application to Radiochemistry. – *Analytical Chemistry* 40: 586-93.
- [6] Degerlier, M. (2007): Determination of Environmental Natural Radioactivity of Adana and Surrounding Area and Finding the Annual Effective Dose Equivalence of Natural Radiation. – Ph.D. Thesis, Çukurova University. Institute of Natural and Applied Sciences.
- [7] Gorcia-Leon, M., Madurga, G. (1991): Low Level Measurements of Man-Made Radiations in the Environment. – World Scientific, 484p.
- [8] Inal, C., Turgut, B., Yigit, C. Ö. (2002): Comparison of Interpolation Methods Used in Determination of Geoid Ondulations in Local Areas. – Selcuk University 30th Year Symposium in Geodesy and Photogrammetry Engineering Teaching, Konya. (In Turkish).
- [9] Kam, E., Once, M. (2016): Pollution Potential of Heavy Metals in the Current Sea Sediments Between Bandirma (Balikesir) and Lapseki (Canakkale) in the Marmara Sea. – *Journal of Engineering Technology and Applied Science* 1: 141-148.
- [10] Kapdan, E., Taskin, H., Kam, E., Osmanoglu, A. E., Karahan, G., Bozkurt, A. (2011): A Study of Environmental Radioactivity Measurements for Çankırı, Turkey. – *Radiation Protection Dosimetry* 150(3): 398-404.
- [11] Karaman, E. S. (2003): Determination of Gross Alpha and Gross Beta Radioactivity Levels of Different Turkish Marble Species. – İstanbul Technical University, Energy Institute, Master Thesis.
- [12] Kaya, A., Karabidak, S. M., Kaya, S. (2016): Radioactivity Measurement of Natural Water Sources in the Area of Bahcecik Village/Gumushane-Turkey. – *GUFBED/GUSTİJ* 6: 13-22.
- [13] Kumru, M. N., Aydin, B., Bakac, M. (2002): Determination of Natural Radioactivity (Radium) in the Aegean Sea from Gediz River. – *Ecology Environment Magazine* 10: 22-25.
- [14] Kurt, D., Kam, E., Yumun, Z. U. (2016): Distribution of Gamma Radiation Levels in Core Sediment Samples in Gulf of İzmir: Eastern Aegean Sea, Turkey. – *International Journal of Environmental, Chemical, Ecological, Geological and Geophysical Engineering* 10: 375-379.
- [15] National Council on Radiation Protection and Measurements (1987): Radiation exposure of the U.S. population from consumer products and miscellaneous sources. – NCRP report no. 95, Washington DC.
- [16] Papaefthymiou, H., Papatheodorou, G., Moustakli, A., Christodoulou, D., Geraga, M. (2007): Natural radionuclides and ¹³⁷Cs distributions and their relationship with sedimentological processes in Patras Harbour, Greece. – *Journal of Environmental Radioactivity* 94: 55-74.
- [17] Pentreath, R. J. (1984): Alpha-emitting nuclides in the marine environment. – *Nuclear Instruments and Methods in Physics Research* 223: 493-501.
- [18] Peterson, J., MacDonell, M., Haroun, L., Monette, F. (2007): Radiological and Chemical Facts Sheets to Support Health Risk Analyses for Contaminated Areas. – Argonne National Laboratory Environmental Science Division.
- [19] Pintilie, V., Ene, A., Georgescu, L. P., Moraru, D. I. (2017): Gross Alpha, Gross Beta and 40k Activities and Daily Effective Dose Due to Natural Radionuclides from Food Supplements. – *Romanian Journal of Physics* 62: 703.
- [20] Pintilie, V., Ene, A., Georgescu, L. P., Moraru, D. I., Pintilie, A. (2018): Determination of Gross Alpha, Gross Beta, and Natural Radionuclides (²¹⁰Po, ²¹⁰Pb, ²³⁸U, ²³²Th and ⁴⁰K) Activity Concentrations in Bread and Their Contribution to the Effective Dose. – *Romanian Journal of Physics* 63: 801.

- [21] Taskin, H. (2006): Identification and Mapping of Fundraising of Kirklareli Province in Terms of Human Health and Environmental Pollution. – Master's thesis, Marmara University. Health Sciences Institute. Public Health Department, İstanbul.
- [22] Topcuoğlu, S. (2001): Bioaccumulation of cesium-137 by biota in different aquatic environments. – *Chemosphere* 44: 691-695.
- [23] Topcuoğlu, S., Ergue, H. A., Belivermis, M., Kilic, O. (2010): Monitoring of radionuclide concentrations in marine algae, mussel and sediment samples from the Turkish marine environment during the period of 2001-2009. – *J. Black Sea/Mediterranean Environment* 16: 285-293.
- [24] Trangmar, B. B., Yost, R. J., Wehara, G. (1985): Application of Geostatistic to Spatial Studies of Soil Properties. – *Advances in Agronomy* 38: 65-91.
- [25] UNSCEAR (2000): Sources and Effects of Ionizing Radiation. – United Nations Scientific Committee on the Effects of Atomic Radiation. Report to General Assembly with Scientific Annexes, United Nations, New York, 659p.
- [26] Varol, S. (2011): Gross Alfa and Beta Radioactivity in Underground Waters. – *Journal of Engineering and Design* 1: 101-106. (In Turkish).
- [27] Wallova, G., Kulichova, Z., Rajczykova, E., Makovinska, J. (2016): Survey of radioactivity along the Bosna River. – *J Radiation Nucl. Chem. Hungary* 307: 247-252.
- [28] Yümün, Z. U. (2016): The Effects of Heavy Metal Concentrations In the Canakkale Strait (Turkey): Morphological Differences In the Holocene Foraminiferal Assemblages. – *Journal of Engineering Technology and Applied Sciences* 1: 77-88.
- [29] Yümün, Z. U., Meriç, E., Avsar, N., Nazik, A., Barut, I. F., Yokeş, B., Sagular, E. K., Yildiz, A., Eryilmaz, M., Kam, E., Bassari, A., Sonuvar, B., Dincer, F., Baykal, K., Kaya, S. (2016): Meiofauna, Microflora and Geochemical Properties of The Late Quaternary (Holocene) Core Sediments in The Gulf of İzmir (Eastern Aegean Sea, Turkey). – *Journal of African Earth Sciences* 124: 383-408.
- [30] Yümün, Z. U. (2017): The Effect of Heavy Metal Pollution on Foraminifera in the Western Marmara Sea (Turkey). – *Journal of African Earth Science* 129: 346-365.
- [31] Yümün, Z. U., Once, M. (2017): Monitoring Heavy Metal Pollution in Foraminifera from The Gulf of Edremit (Northeast Aegean Sea) Between İzmir, Balıkesir And Canakkale (Turkey). – *Journal of African Earth Sciences* 130: 110-124.
- [32] Yümün, Z. U., Kam, E. (2017): Effects of Radionuclides on the Recent Foraminifera from the Clastic Sediments of the Canakkale Strait-Turkey. – *Journal of African Earth Sciences* 131: 179-182.
- [33] Yümün, Z. Ü., Kam, E. (2020): Radionuclide Potential of Holocene Sediments in the West of Marmara Sea (Turkey). – *JOTCSA* 7(2): 517-524.
- [34] Zorer, S., Ceylan, H., Dogru, M. (2009): Gross alpha and beta radioactivity concentration in water, soil and sediment of the Bendimahı River and Van Lake (Turkey). – *Environ Monit Assess* 148: 39-46.

PATTERNS OF LEAF STOICHIOMETRY DURING PLANT (*DEYEUZIA ANGUSTIFOLIA* KOM.) ENCROACHMENT IN THE ALPINE TUNDRA OF THE CHANGBAI MOUNTAIN, CHINA

NI, B.^{1,2} – LIU, C.³ – ZUO, X. H.^{1,2} – YOU, J.^{1,2} – HE, Y. X.^{1,2} – LI, Y. L.^{1,2} – ZHAO, W.^{1,2} – DU, Y. D.² – CHEN, X.^{1,2*}

¹National & Local United Engineering Laboratory for Chinese Herbal Medicine Breeding and Cultivation, Jilin University, Changchun 130012, China

(e-mails: nibiao1991@163.com – B. Ni, zuoxianghua626@163.com – X. H. Zuo, jianyou@jlu.edu.cn – J. You, hyx19930910hyx@163.com – Y. X. He, 15575119483@163.com – Y. L. Li, cbs1981@163.com – W. Zhao, chenxiajlu@163.com – X. Chen; phone: +86-043-185-1552; fax: +86-043-185-1552)

²School of Life Sciences, Jilin University, Changchun 130012, China
(e-mail: duyinda@jlu.edu.cn; phone: +86-138-4301-9360)

³Changchun Institute of Biological Products Co., Ltd., Changchun 130012, China
(e-mail: lc6699_2001@126.com; phone: +86-186-4310-2770)

*Corresponding author

e-mail: chenxiajlu@163.com; phone: +86-0431-8515-5284; fax: +86-0431-8515-5284

(Received 26th Nov 2021; accepted 20th May 2022)

Abstract. Alpine tundra ecosystems are experiencing great changes due to plant encroachment under the influence of global change, yet our understanding of the patterns of encroachment plant leaf stoichiometry is limited. This study aimed to determine the dynamic characteristics of leaf stoichiometry and the driving factors during species encroachment in the alpine tundra ecosystems. C, N, and P concentration of leaf of encroachment species as well as soil physicochemical properties and enzyme activities at different encroachment levels along an elevation gradient in the alpine tundra of the Changbai Mountain, China, were measured. The results showed that leaf stoichiometry of *D. angustifolia* and the soil properties were separated significantly by encroachment degree, and varied considerably among elevations and plant types. Differences in nutrient contents and stoichiometries in *D. angustifolia* leaves were mainly determined by soil moisture, available phosphorus, total nitrogen, and alkaline phosphatase. Results of leaf N:P ratios showed that the growth of *D. angustifolia* in the study area was mainly limited by phosphorus. Findings from this study may be useful to improve our insight on the protection of the alpine tundra ecosystems and provide a scientific basis for predicting the response of the alpine tundra ecosystem to climate change.

Keywords: global change, species encroachment, alpine tundra, ecological stoichiometry, soil factors

Introduction

Global climate change and human activities are altering the distributions of organisms worldwide (Collins et al., 2020; Du et al., 2017; Scheffers et al., 2016). High-latitude or/and high-elevation ecosystems have been a hotspot in plant range expansion research, owing to their high vulnerability to climate warming (Álvarez-Garrido et al., 2019; Ramirez et al., 2019; Shi et al., 2020). It is reported that global change is restructuring alpine tundra ecosystems via local plant encroachment (Krab et al., 2019; Løkken et al., 2020). Studies have shown that plant encroachment will cause serious consequences, including affecting aboveground productivity (usually increased), threatening biodiversity, and degradation of ecosystem functions (Alexander et al., 2016; Dukes et al., 2016). Although the effects of plant encroachment on aboveground and belowground

have been well documented (Bialic-Murphy et al., 2021; DeMarco et al., 2014; Ricciardi et al., 2017), relatively little research has been done on the patterns of leaf ecological stoichiometry of encroachment plant during the process of encroachment.

Ecological stoichiometry tries to analyze the balance of numerous elements and energy in ecosystems by combining the fundamental principles of biology, chemistry, and physics. It is a powerful resource for determining the nutrient cycling and dynamic functions of terrestrial ecosystems (Hessen et al., 2013; Moe et al., 2005; Schindler, 2003). Carbon (C), nitrogen (N), and phosphorus (P) are the three main nutritional components required for plant growth and development (Vitousek et al., 2010), thus they have always been the focus of plant stoichiometry research (Bai et al., 2012; Cao et al., 2020; Finzi et al., 2011). C:N:P stoichiometry has become increasingly popular in recent decades for studying the relationship between aboveground and belowground parts of ecosystems (Bai et al., 2019; Cao et al., 2020; Shi et al., 2021). Plant nutrient limits, nutrient cycling, and plant responses to climate change and ecological circumstances can be studied using leaf stoichiometry (Baxter and Dilkes, 2012; Tie et al., 2020; Zhu et al., 2020). At the same time, the study of leaf stoichiometric characteristics and driving factors in terrestrial ecosystems has been widely discussed at the local, regional, and global scales (Agren and Weih, 2012; Xia et al., 2014; Xiao et al., 2021). Leaf N:P ratio usually serves as a useful indicator of plant nutrient limitation (Koerselman and Meuleman, 1996). Specifically, if leaf N:P < 14, indicates that plant growth is limited by nitrogen; if leaf N:P > 16, indicates that plant growth is limited by phosphorus; and if $14 < \text{leaf N:P} < 16$, indicates that plant growth is limited by both nitrogen and phosphorus (Shi et al., 2021; Xiao et al., 2021).

Many factors can affect the stoichiometric characteristics of plant leaves, including geographical location, climate, soil characteristics, altitude, slope aspect, etc (Cao et al., 2020; Xiao et al., 2021; Zhao et al., 2018). There are extensive relationships between plant and soil stoichiometric characteristics. For example, changes in plant species abundance can alter soil nutrient stoichiometry, and soil C:N:P ratios may change with plant community dynamics (Ding et al., 2019; Pellegrini et al., 2014; Zhou et al., 2018b). Meanwhile, the status of soil resources will further affect the composition of specific plant communities and the abundance of plant species (Bell et al., 2014).

In recent years, ecological stoichiometry has been gradually applied to the study of species encroachment (Ding et al., 2019; Gao et al., 2021). Studies have shown that species encroachment can alter soil nutrient status and soil stoichiometry characteristics, but so far there is no clear conclusion (Ding et al., 2019; Feng and Bao, 2018). For example, species encroachment could reduce soil nutrient levels (Guidi et al., 2014; Jackson et al., 2002), while soil nutrient levels increased with species encroachment (Blaser et al., 2014; Ding et al., 2020; Pellegrini et al., 2014). It is also found that the trend of soil carbon, nitrogen, and phosphorus is not synchronized with species encroachment (Zhou et al., 2018b). In addition to effects on soil nutrient content and stoichiometry, plant chemical composition and stoichiometry would also change during the encroachment process (Blaser et al., 2014; Urbina et al., 2020; Wang et al., 2021), so it is often used to study plant nutrient requirements and material cycling. Encroachment plants have a high demand for phosphorus (Vitousek et al., 2002, 2010), but this nutrient limitation is often alleviated or reduced with the encroachment process (Blaser et al., 2014).

Dramatical changes has happened in the alpine tundra ecosystem (2000-2200 m) of Changbai Mountain in recent decades as a result of climate warming and atmospheric nitrogen deposition, one of which is the extensive encroachment of the local low-altitude

plant *Deyeuxia angustifolia* Kom. (*D. angustifolia*) (Zong et al., 2016). *D. angustifolia*, a herbaceous plant, was once one of the dominant plants in the Changbai Mountains' low altitude birch forest belt. Natural disasters, nutritional features, adaptability, and genetic variation are elements contributing to *D. angustifolia*'s upward expansion (Li et al., 2017; Ni et al., 2021; Zong et al., 2016). However, the dynamic changes in leaf and soil ecological stoichiometry during the encroachment of *D. angustifolia* have not yet been discussed so far. *D. angustifolia* encroachment can be divided into different stages according to its relative abundance (Catford et al., 2012), which provides a unique opportunity to study the changing patterns in leaf ecological stoichiometry during plant encroachment. Understanding leaf stoichiometry and its driving factors during species expansion are essential for understanding nutrient cycling processes and predicting ecosystem response to climate change (Cao et al., 2020; Sistla and Schimel, 2012).

Our purpose was to understand the pattern of leaf ecological stoichiometry during plant encroachment and to determine the main soil properties that affect leaf stoichiometry. Therefore, we conducted our study across different *D. angustifolia* encroachment degrees and along three elevations in the alpine tundra of Changbai Mountain. We hypothesized that: (1) leaf C, N, and P stoichiometry will differ significantly across elevations as small elevation changes will lead to huge changes in the alpine environment, (2) leaf C, N, and P stoichiometry will differ significantly across encroachment levels due to changes in community composition, and (3) changes in leaf stoichiometry may be driven by soil properties as soil conditions varied significantly across elevations and plant encroachment levels. These findings will assist in our knowledge of the nutritional condition and growth status of encroachment species, as well as provide useful information for the conservation and restoration of the alpine tundra ecosystem.

Materials and methods

Study area

Changbai Mountains National Nature Reserve (41°41' 49"–42°25' 18" N, 127°42' 55"–128°16' 48" E), located in Jilin province, northeast China, has been managed for environmental conservation for nearly six decades, making it one of the few well-preserved natural ecosystems on the planet (He et al., 2005). Vertical vegetation zones on Changbai Mountain are clearly outlined: deciduous broad-leaved forest (below 500 m), mixed deciduous broad-leaved/conifer forest (500–1,100 m), dark coniferous forest (1,100–1,700 m), betula ermine forest (1,700–1,950 m), and tundra (>1,950 m) (Li et al., 2017). Our research site is on the western slope of the alpine tundra (41°53'–42°04'N, 127°57'–128°11'E; 2,050–2,250 m), where *D. angustifolia* encroachment occurs (Fig. 1). Freezing temperatures, significant precipitation, as well as a short growing season characterize the alpine tundra climate (Zong et al., 2016). In this study, we focused on the soil properties and leaf stoichiometry of *D. angustifolia* in the two main vegetation types: shrubs and herbaceous plants.

Field sampling

In July 2018, during the plant growing season, fresh leaf samples from healthy *D. angustifolia* plants were collected within the elevation of 2,075 m (Group A: 41°59'24.78"N, 128°0'15.48"E), 2,157 m (Group B: 41°59'26.40"N, 128°0'34.80"E),

and 2,240 m (Group C: 41°59'33.66"N, 128°0'58.56"E). The soil types of these three elevations are tundra soil, which has a thin soil layer, and has more gravel and less soil and low fertility. We studied two common and contrasting plant community types where *D. angustifolia* encroachment typically occurs in the alpine tundra, one shrubs (S) and one herbaceous (H). In each of the two plant community types, we established a replicated sampling design on three encroachment levels during the process of *D. angustifolia* encroachment, which are low encroachment level (L, 10% ≤ plant cover of *D. angustifolia* ≤ 40%), medium encroachment level (M, 40% ≤ plant cover of *D. angustifolia* ≤ 70%), and high encroachment level (H, plant cover of *D. angustifolia* ≥ 70%), respectively. In each level, we collected three replicates and set a total of 54 sampling plots (1 m × 1 m, 3*2*3*3 = 54). We collected a total of 54 leaf and soil samples: 3 elevations × 2 plant community types (*D. angustifolia* encroachment occurs) × 3 encroachment levels × 3 replicates. Surface plants and litter layers were removed from each plot, and soils (top 10 cm) were collected using a soil drill (diameter 5 cm). Each sample contains 5 drillings, and the soil was mixed evenly. After collection, the samples were transported to the laboratory in an icebox, sieved (<2 mm), and removed the plant roots.

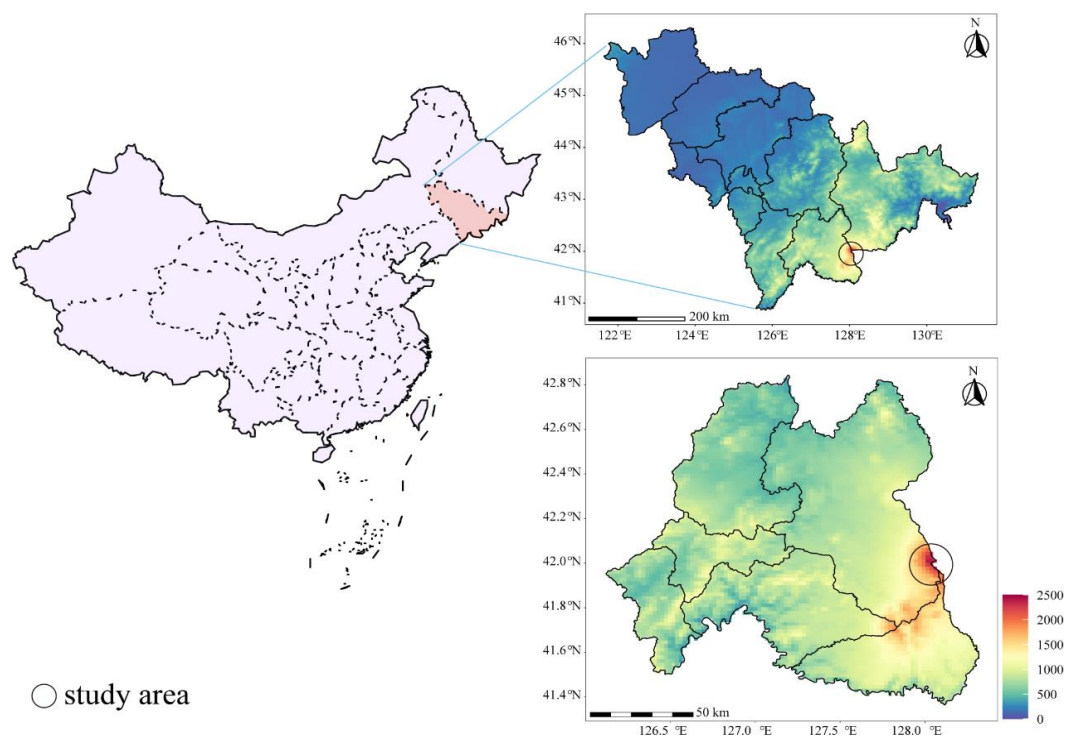


Figure 1. Location of the study area in the alpine tundra of the Changbai Mountain, China

Determination of soil properties and leaf stoichiometry

Leaf samples were oven-dried at 65 °C for 48 h, and the dried plant samples were ground to a fine powder using a mill. Leaf carbon (LC) was determined using the external heating method. Soil total organic carbon (TC) was determined by the potassium dichromate - concentrated sulfuric acid oxidation method (Li et al., 2017). Leaf nitrogen (LN) and soil total nitrogen (TN) were quantified on an automatic Kjeldahl nitrogen meter K1306 (Sonnen, Shanghai, China). Ammonium nitrogen

($\text{NH}_4^+\text{-N}$) and nitrate nitrogen ($\text{NO}_3^-\text{-N}$) were extracted with 2 M KCl, and $\text{NH}_4^+\text{-N}$ was determined by indophenol blue colorimetric method, while $\text{NO}_3^-\text{-N}$ was determined by ultraviolet spectrophotometry (SP-1900UV, Shanghai, China). Leaf phosphorus (LP) was determined colorimetrically using the molybdate method (Xu et al., 2016). Available phosphorus (AP) was determined colorimetrically based on the Olsen method. Soil pH was measured on a 1:5 (w/v) ratio in distilled water using a pH meter (MODEL828, ORION, USA). Soil moisture was determined after drying at 105 °C to a constant mass (Qin et al., 2019). The soil C:N was calculated as the TC to TN ratio. The LC:LN was calculated as the LC to LN ratio, LC:LP was calculated as the LC to LP ratio, and LN:LP was calculated as the LN to LP ratio.

The activity of catalase, alkaline phosphatase (ALP), and urease were quantified. Catalase activity was measured using the potassium permanganate titration method. ALP activity was determined spectrophotometrically at 660 nm using the p-nitrophenyl phosphate salt method. Urease activity was determined spectrophotometrically at 578 nm (Zhang et al., 2020).

Statistical analyses

Statistical analyses were performed using SPSS20.0 (IBM, Chicago, USA) and R software (version 4.0.2, <http://www.r-project.org>). Preliminary permutation multivariate analysis of variance (PERMANOVA) revealed significant differences ($P = 0.001$) between shrubs and herbaceous samples for both soil properties and leaf stoichiometry of *D. angustifolia* (Table A1); therefore, data analyses on shrubs and herbaceous samples were performed separately. Using SPSS 20.0, One-way ANOVA followed by least significant difference (LSD) was performed to test the significance of the effect of elevation and *D. angustifolia* encroachment on soil properties and leaf stoichiometry, and all statistical differences in this study were considered significant at $P < 0.05$. The R platform was used to run the following analyses and to generate plots using the “ggplot2” package. PERMANOVA was employed to assess the significance of the influential factors that differentiate plant leaf stoichiometry and soil properties (package: “vegan”, adonis function) (Taş et al., 2018; Xue et al., 2016) followed by Bray-Curtis distance. Principal component analysis (PCA) was performed to compare the differences in plant leaf stoichiometry and soil properties based on Bray-Curtis distance metric. Clustering heatmap was performed in the “pheatmap” package to reveal the differences in leaf stoichiometry and soil properties in different samples. The correlation between soil properties and plant leaf stoichiometry was estimated using Mantel tests in the “vegan” package with 9999 permutations based on Pearson’s product-moment correlation. Pearson coefficients were calculated in the “corrplot” package and used to reveal correlations between leaf stoichiometry and soil properties. Redundancy analyses (RDA) were performed by Canoco5 to determine soil properties significantly driving leaf stoichiometry of *D. angustifolia*.

Results

Effects of elevation, encroachment and their interaction on leaf stoichiometry of D. angustifolia

In shrubs communities, LN and LP at group BS were lower than that at group AS and CS, but the LC, LC:LN, LC:LP, and LN:LP were higher than those at group AS and

CS (Fig. 2). Leaf stoichiometry of *D. angustifolia* varied strongly with encroachment levels, but interestingly, the changes of most indexes were different across elevations. The LC and LC:LN increased at group BS and CS but decreased at group AS with *D. angustifolia* encroachment (Fig. 2a, d; Table A2); the LN and LP increased at group AS but decreased at group CS with *D. angustifolia* encroachment (Fig. 2b, c; Table A2); the LC:LP increased at group CS but decreased at group AS with *D. angustifolia* encroachment (Fig. 2e; Table A2); the LN:LP decreased at group CS with *D. angustifolia* encroachment (Fig. 2f; Table A2). PERMANOVA showed that elevation, encroachment, and their interaction had significant effects on the leaf stoichiometry of *D. angustifolia*, except for leaf nitrogen content ($P < 0.05$, Table 1).

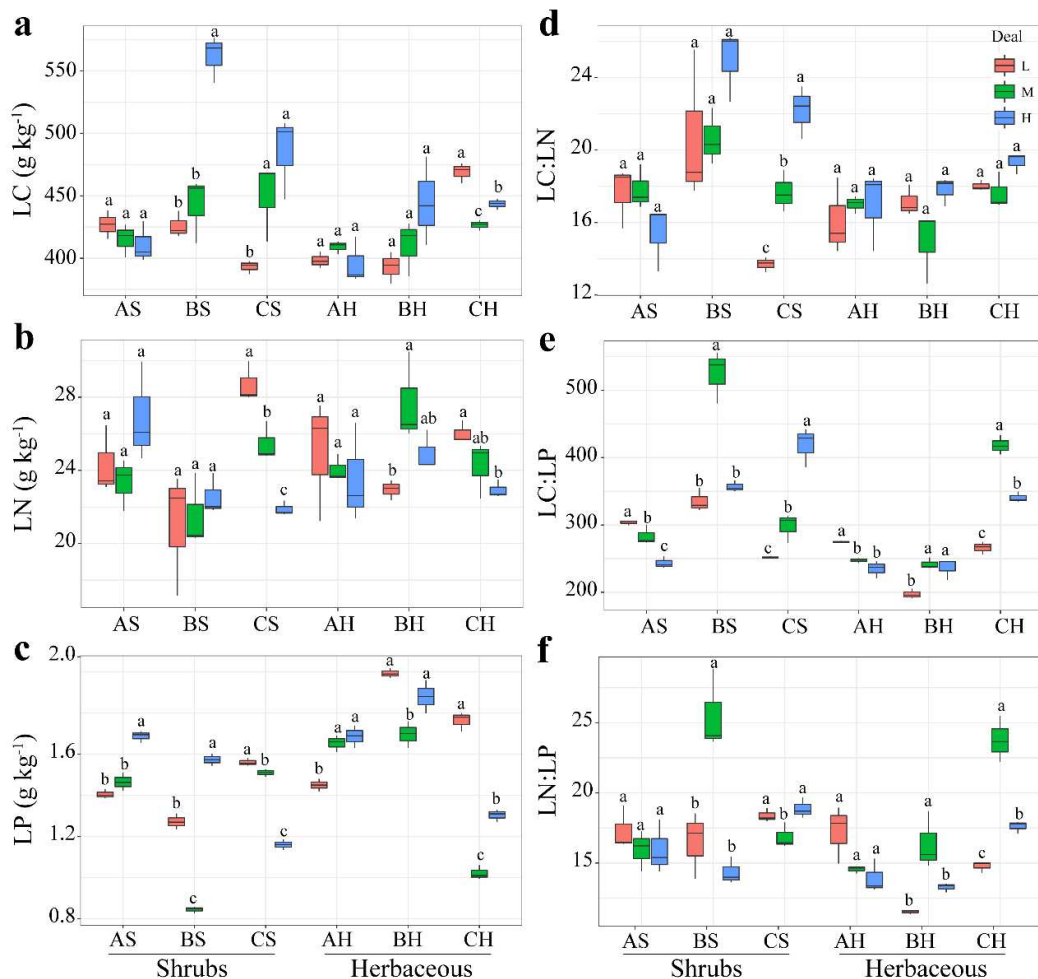


Figure 2. Leaf stoichiometry of *D. angustifolia* across encroachment levels and elevations within the study area. LC = leaf carbon concentration, LN = leaf nitrogen concentration, LP = leaf phosphorus concentration, LC:LN = LC to LN ratio, LC:LP = LC to LP ratio, LN:LP = LN to LP ratio. Different lowercase letters represent significant differences among encroachment levels within a group ($P < 0.05$)

In herbaceous communities, LC, LC:LN, LC:LP, and LN:LP at group CS were higher than that at group AS and BS; LN and LP at group BS were higher than that at group AS and CS (Fig. 2). Similar to these results in shrubs communities, leaf stoichiometry of *D. angustifolia* differed across encroachment levels and elevations.

The LC increased at group BH with *D. angustifolia* encroachment; the LN decreased at group AH and CH with *D. angustifolia* encroachment; the LP and LC:LN increased but the LC:LP and LN:LP decreased at group AH with *D. angustifolia* encroachment (Fig. 2; Table A2). In addition, LC in CHL was significantly higher than that in CHM and CHH (ANOVA: $P < 0.05$; Fig. 2a); LP in BHL and CHL was significantly lower, while LN:LP was significantly higher than the other two levels within group BH and CH, respectively (ANOVA: $P < 0.05$; Fig. 2c, f). PERMANOVA showed that elevation had significant effects on the LC, LP, LC:LN, LC:LP, and LN:LP; while encroachment significantly influenced LP, LC:LP, and LN:LP ($P < 0.05$; Table 1). The interaction between elevation and encroachment had significant effects on LC, LN, LP, LC:LP, and LN:LP ($P < 0.05$; Table 1).

Table 1. The effects of elevation and *D. angustifolia* encroachment on leaf stoichiometry of *D. angustifolia* based on PERMANOVA

	Shrubs						Herbaceous					
	Elevation		Encroachment		Elevation × encroachment		Elevation		Encroachment		Elevation × encroachment	
	R ²	P	R ²	P	R ²	P	R ²	P	R ²	P	R ²	P
LC (g kg ⁻¹)	0.222	0.001	0.334	0.001	0.322	0.001	0.450	0.002	0.032	0.293	0.292	0.005
LN (g kg ⁻¹)	0.310	0.001	0.025	0.506	0.350	0.004	0.041	0.508	0.089	0.222	0.347	0.041
LP (g kg ⁻¹)	0.244	0.001	0.124	0.001	0.625	0.001	0.473	0.001	0.156	0.001	0.355	0.001
LC:LN (ratio)	0.352	0.001	0.150	0.007	0.316	0.001	0.223	0.038	0.136	0.127	0.149	0.278
LC:LP (ratio)	0.400	0.001	0.100	0.001	0.466	0.001	0.626	0.001	0.117	0.001	0.234	0.001
LN:LP (ratio)	0.089	0.025	0.135	0.008	0.583	0.001	0.370	0.001	0.214	0.001	0.334	0.001

LC = leaf carbon concentration, LN = leaf nitrogen concentration, LP = leaf phosphorus concentration, LC:LN = LC to LN ratio, LC:LP = LC to LP ratio, LN:LP = LN to LP ratio. Values with $P < 0.05$ are in bold

Principal component analysis (PCA) showed that in shrubs and herbaceous communities, the leaf stoichiometry of *D. angustifolia* among elevations was separated along the first axis of the principal component, and the samples with different encroachment levels were distributed along the second axis of the principal component within each elevation. The first two principal components explained 94.78% (PC1 67.04% and PC2 27.74%, Fig. 3a) and 94.89% (PC1 81.29% and PC2 13.6%, Fig. 3b) of the total variation, respectively. Clustering heatmap showed that in shrubs communities, all samples can be clustered into two large branches, in which the composition of the samples of group AS and CS were similar, and both were separated from the samples of group BS. Samples with different *D. angustifolia* encroachment levels showed obvious separation within each group (Fig. A2a). In herbaceous communities, all samples could also be clustered into two large branches, and the separation in samples was not obvious among elevations, but the sample composition showed obvious separation across encroachment levels within each group (Fig. A2b). The above results showed that the leaf stoichiometry of *D. angustifolia* appeared significant heterogeneity across elevations and encroachment levels.

D. angustifolia encroachment shaped soil physicochemical properties and enzyme activities

In shrubs communities, the soil TN, NH₄⁺-N, NO₃⁻-N, AP, and moisture increased but C:N, ALP, and catalase decreased with rising elevation. Additionally, TC and urease at

group BS were higher than that at group AS and CS, and pH at group AS was higher than that at group BS and CS (Table A3). Soil properties differed among *D. angustifolia* encroachment levels, and their variation trend was different among elevations. The soil TC, NH₄⁺-N, and AP increased at group CS with *D. angustifolia* encroachment; the NO₃⁻-N and catalase increased at group BS with *D. angustifolia* encroachment. The soil C:N decreased while the urease increased at group AS and BS with *D. angustifolia* encroachment. The soil moisture increased at group CS but decreased at group BS with *D. angustifolia* encroachment (Table A3). PERMANOVA showed that elevation, encroachment, and their interaction had significant effects on the soil physicochemical properties and enzyme activities, except for soil ALP ($P < 0.05$, Table 2).

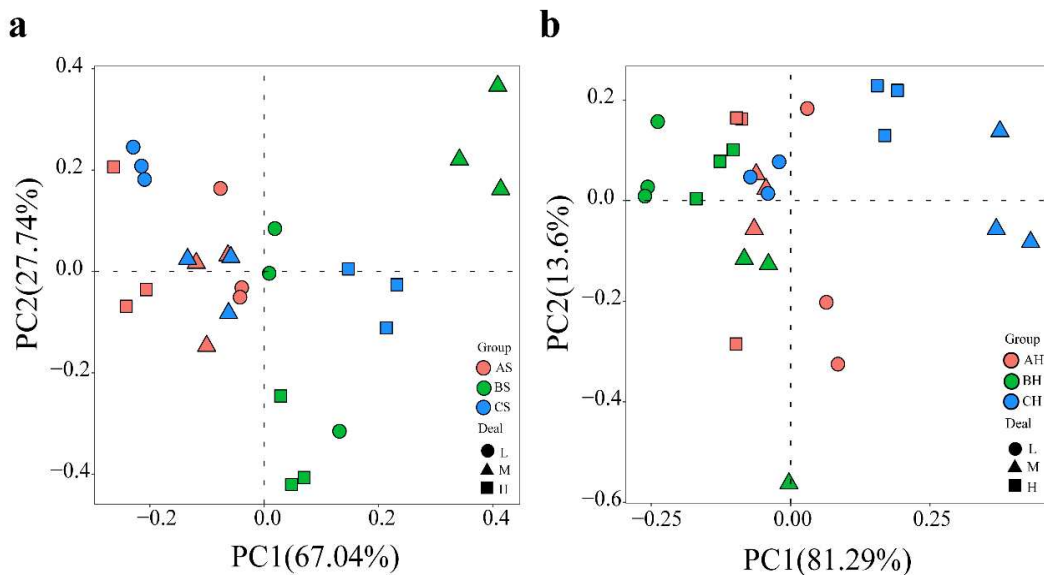


Figure 3. Principal component analysis (PCA) of leaf stoichiometry of *D. angustifolia* in shrubs (a) and herbaceous (b) communities

Table 2. The effects of elevation and *D. angustifolia* encroachment on soil properties based on PERMANOVA

	Shrubs						Herbaceous					
	Elevation		Encroachment		Elevation × encroachment		Elevation		Encroachment		Elevation × encroachment	
	R ²	P	R ²	P	R ²	P	R ²	P	R ²	P	R ²	P
TC (g kg ⁻¹)	0.656	0.001	0.055	0.001	0.252	0.001	0.118	0.001	0.261	0.001	0.593	0.001
TN (g kg ⁻¹)	0.808	0.001	0.052	0.001	0.112	0.001	0.260	0.001	0.095	0.001	0.594	0.001
C:N (ratio)	0.930	0.001	0.015	0.031	0.021	0.047	0.356	0.001	0.059	0.145	0.330	0.007
NH ₄ ⁺ -N (mg kg ⁻¹)	0.697	0.001	0.111	0.001	0.182	0.001	0.340	0.001	0.172	0.001	0.464	0.001
NO ₃ ⁻ -N (mg kg ⁻¹)	0.538	0.001	0.268	0.001	0.167	0.001	0.367	0.001	0.053	0.001	0.563	0.001
AP (mg kg ⁻¹)	0.570	0.001	0.257	0.001	0.073	0.034	0.605	0.001	0.102	0.016	0.115	0.043
Moisture	0.669	0.001	0.066	0.001	0.264	0.001	0.018	0.622	0.137	0.006	0.571	0.001
pH	0.204	0.003	0.319	0.001	0.302	0.001	0.224	0.001	0.227	0.001	0.483	0.001
Catalase	0.902	0.001	0.010	0.044	0.063	0.001	0.895	0.001	0.041	0.001	0.035	0.008
ALP	0.932	0.001	0.007	0.098	0.035	0.004	0.976	0.001	0.002	0.167	0.009	0.031
Urease	0.617	0.001	0.117	0.001	0.195	0.001	0.602	0.001	0.099	0.003	0.191	0.001

TC: total organic carbon, TN: total nitrogen, C:N: TC to TN ratio, NH₄⁺-N: ammonium nitrogen, NO₃⁻-N: nitrate nitrogen, AP: available phosphorus, Moisture: water content, ALP: alkaline phosphatase. *P* is the significance level. Values with $P < 0.05$ are in bold

In herbaceous communities, the soil AP increased but C:N, ALP, and urease decreased with rising elevation. Additionally, TC, TN, moisture, pH, and catalase at group BH were higher than that at group AH and CH; $\text{NH}_4^+\text{-N}$ was higher in group CH, while $\text{NO}_3^-\text{-N}$ was higher in group AH (Table A3). Similar to these results in shrubs communities, soil properties differed across *D. angustifolia* encroachment levels and elevations. The soil $\text{NO}_3^-\text{-N}$ increased at group AH but decreased at group CH with *D. angustifolia* encroachment; AP increased at group AH with *D. angustifolia* encroachment. The soil TN and pH decreased at group AH with *D. angustifolia* encroachment, while $\text{NH}_4^+\text{-N}$ decreased at group CH with *D. angustifolia* encroachment (Table A3). PERMANOVA showed that elevation, encroachment, and their interaction had significant effects on the soil physicochemical properties and enzyme activities, except for soil C:N, moisture, and ALP ($P < 0.05$, Table 2).

Principal component analysis (PCA) showed that in shrubs communities, the soil properties among elevations were separated along the first axis of the principal component, and the samples with different encroachment levels were distributed along the second axis of the principal component within each elevation. In herbaceous communities, samples among elevations and encroachment levels were distributed along the first axis of the principal component, and the first two principal components explained 85.99% (PC1 74.07% and PC2 11.92%, Fig. 4a) and 72.00% (PC1 52.36% and PC2 19.64%, Fig. 4b) of the total variation, respectively. Clustering heatmap showed that in shrubs communities, all samples can be clustered into two large branches, in which group AS was clustered into one branch, and group BS and CS were clustered into one another branch and separated from each other. Samples with different *D. angustifolia* encroachment levels showed obvious separation within each group (Fig. A3a). In herbaceous communities, all samples can also be clustered into two large branches. Unlike shrubs communities, the separation of samples at different groups was not obvious, but the composition of samples within each group showed obvious separation (Fig. A3b). The above results showed that the soil properties showed significant heterogeneity across elevations and encroachment levels.

Relationships between leaf stoichiometry and soil properties

Redundancy analyses (RDA) showed that soil properties could explain 60.04% of *D. angustifolia* leaf stoichiometric variation, among which RDA1 and RDA2 explained 52.02% and 8.02% of the total variation, respectively (Fig 5a). Soil moisture, C:N, pH, AP, and Urease had significant effects on leaf stoichiometry ($P < 0.05$, Table A4). In addition, $\text{NH}_4^+\text{-N}$ and ALP also had strong effects on leaf stoichiometry. Mantel tests showed that there was a positive correlation between soil properties and leaf stoichiometry of *D. angustifolia* (Mantle: $R = 0.073$, $P = 0.132$). Further analysis showed that soil TN, $\text{NH}_4^+\text{-N}$, AP, moisture, ALP, and urease significantly affected leaf stoichiometry (Mantle: $P < 0.05$; Fig. 5b).

Pearson correlation analysis showed that LN was positively correlated with soil $\text{NH}_4^+\text{-N}$, AP, moisture, and negatively correlated with pH and ALP. LN was negatively correlated with soil TC and moisture. LP was negatively correlated with soil TN, AP, and moisture, and positively correlated with ALP. LC:LN was positively correlated with soil AP and moisture, and negatively correlated with ALP. LC:LP and LN:LP were positively correlated with soil TN, and negatively correlated with ALP. In addition, LC:LP was positively correlated with AP and moisture ($P < 0.05$, Fig. 6). Together, these results suggested that soil properties had a great impact on the variation of leaf stoichiometry of *D. angustifolia*.

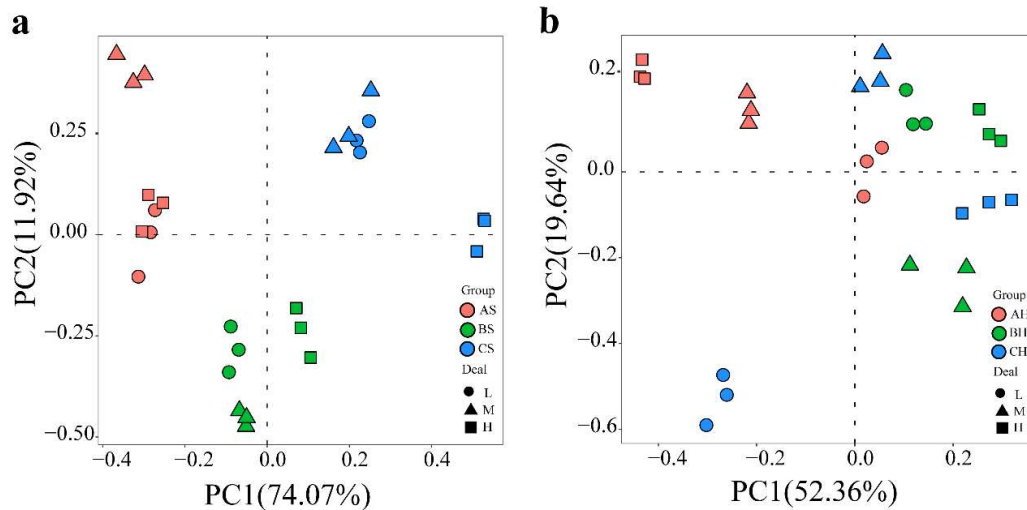


Figure 4. Principal component analysis (PCA) of soil properties in shrubs (a) and Herbaceous (b) communities

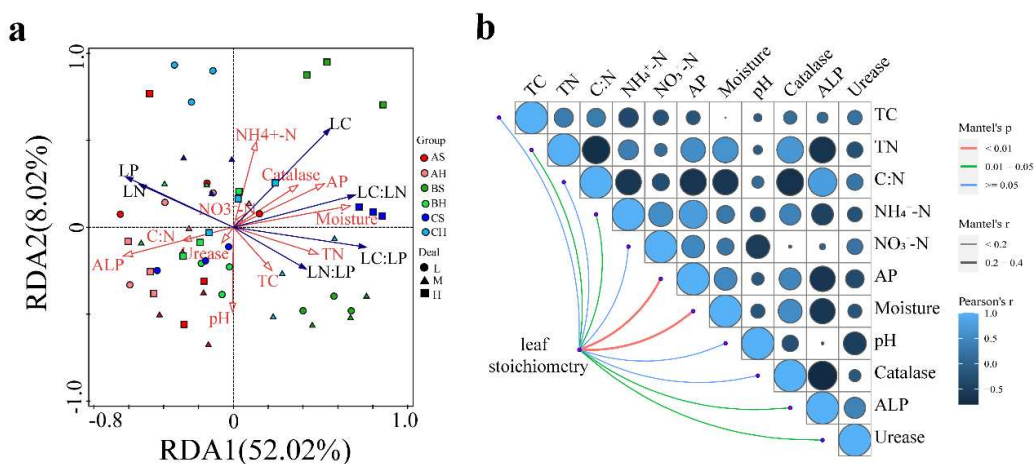


Figure 5. Redundancy analysis (RDA) (a) and Mantel tests (b) analysis of leaf stoichiometry of *D. angustifolia* and soil properties. Edge width corresponds to Mantel's r value, and the edge color denotes the statistical significance. Pairwise correlations of these variables are shown with color gradient denoting Pearson's correlations coefficients. * indicates significant differences ($P < 0.05$)

Discussion

Dynamic of leaf stoichiometry of *D. angustifolia*

Elevation had a significant effect on *D. angustifolia* leaf stoichiometry (PERMANOVA, $P = 0.001$; Table A1). Leaf C, N, P and their ratios varied with elevation, except for leaf nitrogen content in herbaceous communities ($P < 0.05$; Table 1, A2), which supported our first hypothesis. Other studies have also reported that plant leaf stoichiometry changed along elevation gradients (Cao et al., 2020; Li et al., 2018), part of which can be attributed to spatial variation of the soil environment, such as the redistribution of water and heat balance caused by topographic change, and changes in soil C, N, and P supply (Cao et al., 2020; Reich and Oleksyn, 2004).

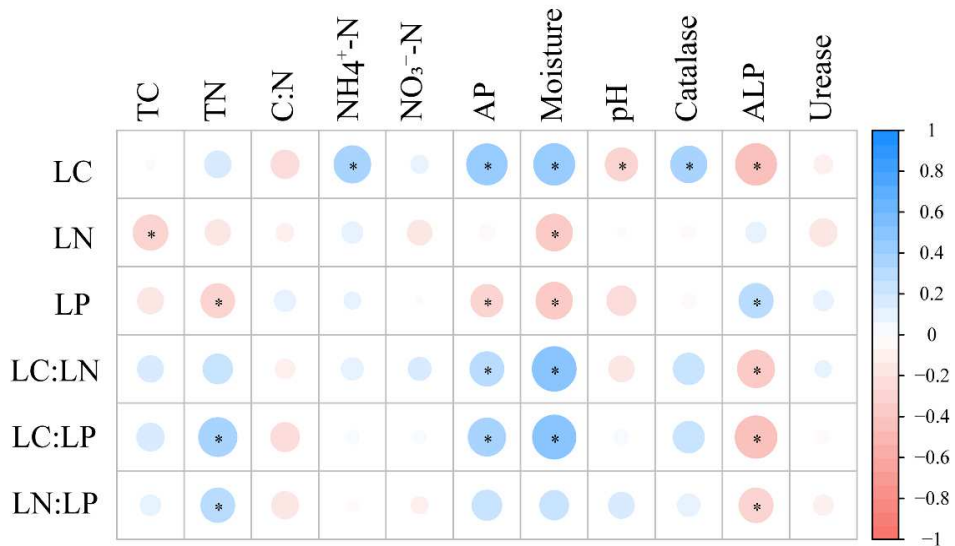


Figure 6. Pearson coefficients between leaf stoichiometry characteristics of *D. angustifolia* and soil properties. Pairwise correlations of these variables are shown with color gradient denoting Pearson's correlations coefficients. * indicates significant differences ($P < 0.05$)

Encroachment levels had a significant effect on *D. angustifolia* leaf stoichiometry (PERMANOVA, $P = 0.001$; Table A1). PCA and cluster analysis showed that there was a significant separation of leaf stoichiometric characteristics at each elevation (Figs. 3 and A2), which supported our second hypothesis. Interestingly, leaf C, N, P, and their ratios increased, decreased, or did not change significantly with the increase of *D. angustifolia* encroachment level, which depended on the elevation and vegetation community type encroached by *D. angustifolia* (Fig. 2). *D. angustifolia* leaf stoichiometry showed significant heterogeneity in elevations and encroachment levels, which indicated the adaptability of *D. angustifolia* to different environments, and has also been confirmed in the study of *Spartina alterniflora* (Zuo et al., 2021). Nutrient patterns reflect plants' adaptation to the environment. Plants must change their absorption and storage of nutrient elements to adapt to the differences in element availability, which can change within a distance of a few meters (Baxter and Dilkes, 2012). In addition, the significant heterogeneity of *D. angustifolia* leaf stoichiometry across encroachment levels may be caused by the competition with the original vegetation in the tundra zone. It is found that the interspecific competition alters the leaf stoichiometry of the encroachment plants (Zhu et al., 2020).

Responses of soil properties to *D. angustifolia* encroachment

Our results showed that *D. angustifolia* encroachment significantly affected most soil index (PERMANOVA, $P < 0.05$; Table 2), indicating that *D. angustifolia* encroachment significantly affected soil nutrient conditions, which was consistent with other studies results (Gao et al., 2021; Yang and Liu, 2019). However, this effect depended on the encroachment level, elevation, and the vegetation community type encroached by *D. angustifolia* (Figs. 4 and 5). It is reported that changes in plant species abundance had an effect on the soil nutrient characteristics, and soil nutrient contents changed with plant community dynamics (Blaser et al., 2014; Ding et al., 2019; Pellegrini et al., 2014; Zhou et al., 2018b). Given the importance of plant

functional features in soil biological processes, changes in C:N:P stoichiometry in plant tissues during encroachment are expected to have comparable effects on soil properties (Zhou et al., 2018a).

Soil nutrient concentration usually shows vertical zonal distribution characteristics, which have been widely observed on the regional scale (Cui et al., 2019; Tong et al., 2021). Our results showed that elevation significantly affected soil properties (PERMANOVA, $P = 0.001$; *Table A1*), and soil properties were significantly separated among elevations (*Fig. 4*), which was consistent with previous research results (Byars et al., 2007; Cui et al., 2019). In addition, the researchers found that the soil physicochemical characteristics of wetland ecosystems also changed significantly under small-scale elevation gradients (Li et al., 2018). These results suggest that the influence of elevation should be considered in future research to have a more comprehensive understanding of ecological stoichiometric characteristics.

Dominant factors influencing leaf stoichiometry of *D. angustifolia*

In this study, soil moisture and AP were the two most important ecological factors affecting *D. angustifolia* leaf stoichiometry in the tundra of Changbai Mountain (RDA, Mantel; *Fig. 5*). Soil moisture mainly affects the transformation and availability of soil nutrients by controlling various biogeochemical processes, thus affecting leaf stoichiometry (Anderson and Lockaby, 2011). Soil moisture was positively correlated with leaf LC, LC:LN, and LC:LP ($P < 0.05$, *Fig. 6*). The relationship between soil moisture and LC is consistent with previous reports (Cao et al., 2020), but other studies have found contrary results (Lin et al., 2019; Liu et al., 2020). For LC, it is because soil water content contributes to plant photosynthesis and growth (Li et al., 2018), and our previous results also showed that the water environment in the tundra zone of Changbai Mountain is favorable for the survival of *D. angustifolia* (Ni et al., 2021). Soil moisture was significantly negatively correlated with LN and LP ($P < 0.05$, *Fig. 6*), which is consistent with the results that soil moisture has a negative correlation on leaf nutrient content on a global scale (Ordonez et al., 2009). These results suggest that the effect of water conditions on plant stoichiometry may vary due to the selected environmental scale and species type. Soil AP was another important factor affecting leaf stoichiometry (RDA, Mantel; *Fig. 5*), as soil AP was positively correlated with LC, LC:LN, and LC:LP ($P < 0.05$, *Fig. 6*). Liu et al. also found that there was a positive correlation between soil AP and LC (Liu et al., 2020), which may be due to the fact that phosphorus is required for photosynthesis and plays a direct role in biological processes such as photophosphorylation and carbon assimilation. AP may indirectly affect the relationship between LC:LN and LC:LP through its effect on soil TC. There is a significant negative correlation between soil AP and LP ($P < 0.05$, *Fig. 6*), which is contrary to the previous results (Liu et al., 2020). Most plants obtain phosphorus through roots, and the supply of soil phosphorus can determine the concentration of plant phosphorus, thus soil AP is a factor affecting the content of phosphorus in the leaves of *D. angustifolia* (Li et al., 2018, 2014; Yan et al., 2015).

Nitrogen and phosphorus are the main limiting elements in the terrestrial ecosystem, as they play important roles in the physiology and metabolism of plant growth (Mao et al., 2016). In this study, soil TN took essential parts in the formation of *D. angustifolia* leaf stoichiometry (RDA, Mantel; *Fig. 5*), mainly by affecting LP, LC:LP, and LN:LP ($P < 0.05$, *Fig. 6*). Soil ALP significantly affected *D. angustifolia* leaf stoichiometry

(RDA, Mantel; *Fig. 5*), as ALP was negatively correlated with *D. angustifolia* LC, LC:LN, LC:LP, and LN:LP, and positively correlated with LP ($P < 0.05$, *Fig. 6*). Soil enzyme is the key to controlling the biogeochemical cycle and soil nutrient concentration (Aragon et al., 2014). The significant positive correlation between soil ALP and LP is that high phosphatase activity enables roots to obtain phosphorus in organic form in soil (Blaser et al., 2014; Venterink, 2011; Zhou et al., 2018a). The relationship between ALP and *D. angustifolia* leaf stoichiometry may be due to the influence of root phosphorus uptake on the balance of leaf nutrients. These results showed that in addition to soil moisture and AP, soil TN and ALP also play important roles in the leaf stoichiometry of *D. angustifolia*.

Elements limiting D. angustifolia growth

LN:LP plays a more important role in evaluating plant nutritional limitations than the concentration of N and P alone (Koerselman and Meuleman, 1996; Li et al., 2018; Zhu et al., 2020). In terrestrial ecosystems, when $LN:LP > 16$, plants growth is limited by P; when $14 < LN:LP < 16$, plant growth is limited by N and P, and when $LN:LP < 14$, plants is limited by N (Blaser et al., 2014; Koerselman and Meuleman, 1996). Our results showed that *D. angustifolia* LN:LP was significantly affected by the elevation, encroachment level, and their interaction (PERMANOVA: $P < 0.05$; *Table 1*). *D. angustifolia* LN:LP was between 11.52 and 25.53, indicating that the growth of *D. angustifolia* was limited by N and P during the encroachment process. However, the average $LN:LP = 16.82$ and > 16 at most sample sites (*Fig. 2f*; *Table A2*) indicated that the growth of *D. angustifolia* was mainly limited by phosphorus rather than nitrogen in the tundra of Changbai Mountain. This was consistent with other researchers' results (Cao et al., 2020; Zhou et al., 2018a) that it may be due to the high phosphorus demand of encroachment species (Binkley et al., 2003; Vitousek et al., 2002).

Conclusion

This study revealed the leaf stoichiometry and driving factors of *D. angustifolia* at different elevations and encroachment levels and is helpful for us to understand its nutritional and growth status. Elevation and encroachment degree significantly affected *D. angustifolia* leaf stoichiometry. Leaf carbon, nitrogen, and phosphorus and their ratios showed significant heterogeneity across elevations and encroachment levels, indicating the adaptability of *D. angustifolia* to different environments. Soil properties had important effects on *D. angustifolia* leaf stoichiometry, and soil moisture, AP, TN, and ALP were the main factors affecting *D. angustifolia* leaf stoichiometry in the alpine tundra of Changbai Mountain. Phosphorus was the main factor limiting the growth of *D. angustifolia* in the process of upward expansion. Results of this study improve our understanding of C:N:P stoichiometry of encroachment species, and are critical for predicting the responses of ecosystems to environmental changes.

Acknowledgments. This study was supported by the Natural Science Foundation of Jilin province, China (20190201298JC). The authors thank Yulin Wang, Yuanbo Ni, Jiahua Pang, Jianan San, and Xiangyu Zhang for their assistance with the field sampling, lab experiments, and data processing.

REFERENCES

- [1] Agren, G. I., Weih, M. (2012): Plant stoichiometry at different scales: element concentration patterns reflect environment more than genotype. – *New Phytologist* 194: 944-952.
- [2] Alexander, J. M., Lembrechts, J. J., Cavieres, L. A., Daehler, C., Haider, S., Kueffer, C., Liu, G., McDougall, K., Milbau, A., Pauchard, A., Rew, L. J., Seipel, T. (2016): Plant invasions into mountains and alpine ecosystems: current status and future challenges. – *Alpine Botany* 126: 89-103.
- [3] Álvarez-Garrido, L., Viñepla, B., Hortal, S., Powell, J. R., Carreira, J. A. (2019): Distributional shifts in ectomycorrhizal fungal communities lag behind climate-driven tree upward migration in a conifer forest-high elevation shrubland ecotone. – *Soil Biology and Biochemistry* 137.
- [4] Anderson, C. J., Lockaby, B. G. (2011): Foliar nutrient dynamics in tidal and non-tidal freshwater forested wetlands. – *Aquatic Botany* 95: 153-160.
- [5] Aragon, R., Sardans, J., Penuelas, J. (2014): Soil enzymes associated with carbon and nitrogen cycling in invaded and native secondary forests of northwestern Argentina. – *Plant and Soil* 384: 169-183.
- [6] Bai, X., Wang, B., An, S., Zeng, Q., Zhang, H. (2019): Response of forest species to C:N:P in the plant-litter-soil system and stoichiometric homeostasis of plant tissues during afforestation on the Loess Plateau, China. – *Catena* 183.
- [7] Bai, Y., Wu, J., Clark, C. M., Pan, Q., Zhang, L., Chen, S., Wang, Q., Han, X. (2012): Grazing alters ecosystem functioning and C:N:P stoichiometry of grasslands along a regional precipitation gradient. – *Journal of Applied Ecology* 49: 1204-1215.
- [8] Baxter, I., Dilkes, B. P. (2012): Elemental profiles reflect plant adaptations to the environment. – *Science* 336: 1661-1663.
- [9] Bell, C., Carrillo, Y., Boot, C. M., Rocca, J. D., Pendall, E., Wallenstein, M. D. (2014): Rhizosphere stoichiometry: are C:N:P ratios of plants, soils, and enzymes conserved at the plant species-level? – *New Phytol* 201: 505-517.
- [10] Bialic-Murphy, L., Smith, N. G., Voothuluru, P., McElderry, R. M., Roche, M. D., Cassidy, S. T., Kivlin, S. N., Kalisz, S. (2021): Invasion-induced root-fungal disruptions alter plant water and nitrogen economies. – *Ecology Letters* 13724.
- [11] Binkley, D., Senock, R., Cromack, K. (2003): Phosphorus limitation on nitrogen fixation by *Facaltaria* seedlings. – *Forest Ecology and Management* 186: 171-176.
- [12] Blaser, W. J., Shanungu, G. K., Edwards, P. J., Venterink, H. O. (2014): Woody encroachment reduces nutrient limitation and promotes soil carbon sequestration. – *Ecology and Evolution* 4: 1423-1438.
- [13] Byars, S. G., Papst, W., Hoffmann, A. A. (2007): Local adaptation and cogradient selection in the alpine plant, *Poa hiemata*, along a narrow altitudinal gradient. – *Evolution* 61: 2925-2941.
- [14] Cao, J., Wang, X., Adamowski, J. F., Biswas, A., Liu, C., Chang, Z., Feng, Q. (2020): Response of leaf stoichiometry of *Oxytropis ochrocephala* to elevation and slope aspect. – *Catena* 194.
- [15] Catford, J. A., Vesk, P. A., Richardson, D. M., Pyšek, P. (2012): Quantifying levels of biological invasion: towards the objective classification of invaded and invulnerable ecosystems. – *Global Change Biology* 18: 44-62.
- [16] Collins, C. G., Spasojevic, M. J., Alados, C. L., Aronson, E. L., Benavides, J. C., Cannone, N., Caviezel, C., Grau, O., Guo, H., Kudo, G., Kuhn, N. J., Mullerova, J., Phillips, M. L., Pombubpa, N., Reverchon, F., Shulman, H. B., Stajich, J. E., Stokes, A., Weber, S. E., Diez, J. M. (2020): Belowground impacts of alpine woody encroachment are determined by plant traits, local climate, and soil conditions. – *Global Change Biology* 26: 7112-7127.

- [17] Cui, Y., Bing, H., Fang, L., Wu, Y., Yu, J., Shen, G., Jiang, M., Wang, X., Zhang, X. (2019): Diversity patterns of the rhizosphere and bulk soil microbial communities along an altitudinal gradient in an alpine ecosystem of the eastern Tibetan Plateau. – *Geoderma* 338: 118-127.
- [18] DeMarco, J., Mack, M. C., Bret-Harte, M. S. (2014): Effects of arctic shrub expansion on biophysical vs. biogeochemical drivers of litter decomposition. – *Ecology* 95: 1861-1875.
- [19] Ding, L., Wang, P., Zhang, W., Zhang, Y., Li, S., Wei, X., Chen, X., Zhang, Y., Yang, F. (2019): Shrub encroachment shapes soil nutrient concentration, stoichiometry and carbon storage in an abandoned subalpine grassland. – *Sustainability* 11.
- [20] Ding, L., Wang, P., Zhang, W., Zhang, Y., Li, S., Wei, X., Chen, X., Zhang, Y., Yang, F. (2020): Soil stoichiometry modulates effects of shrub encroachment on soil carbon concentration and stock in a subalpine grassland. – *Iforest-Biogeosciences and Forestry* 13: 65-72.
- [21] Du, H., Liu, J., Li, M. H., Büntgen, U., Yang, Y., Wang, L., Wu, Z., He, H. S. (2017): Warming-induced upward migration of the alpine treeline in the Changbai Mountains, northeast China. – *Global Change Biology* 24: 1256-1266.
- [22] Dukes, J. S., Lawler, J. J., Olden, J. D., Blumenthal, D. M., Gonzalez, P., Grosholz, E. D., Ibañez, I., Miller, L. P., Sorte, C. J. B., Tatem, A. J. (2016): Global threats from invasive alien species in the twenty-first century and national response capacities. – *Nature Communications* 7.
- [23] Feng, D., Bao, W. (2018): Shrub encroachment alters topsoil C:N:P stoichiometric ratios in a high-altitude forest cutover. – *Iforest-Biogeosciences and Forestry* 11: 594-598.
- [24] Finzi, A. C., Austin, A. T., Cleland, E. E., Frey, S. D., Houlton, B. Z., Wallenstein, M. D. (2011): Responses and feedbacks of coupled biogeochemical cycles to climate change: examples from terrestrial ecosystems. – *Frontiers in Ecology and the Environment* 9: 61-67.
- [25] Gao, X.-l., Li, X., Zhao, L., Kuzyakov, Y. (2021): Shrubs magnify soil phosphorus depletion in Tibetan meadows: conclusions from C:N:P stoichiometry and deep soil profiles. – *Science of the Total Environment* 785.
- [26] Guidi, C., Vesterdal, L., Gianelle, D., Rodeghiero, M. (2014): Changes in soil organic carbon and nitrogen following forest expansion on grassland in the Southern Alps. – *Forest Ecology and Management* 328: 103-116.
- [27] He, H. S., Hao, Z. Q., Mladenoff, D. J., Shao, G. F., Hu, Y. M., Chang, Y. (2005): Simulating forest ecosystem response to climate warming incorporating spatial effects in north-eastern China. – *Journal of Biogeography* 32: 2043-2056.
- [28] Hessen, D. O., Elser, J. J., Sterner, R. W., Urabe, J. (2013): Ecological stoichiometry: an elementary approach using basic principles. – *Limnology and Oceanography* 58: 2219-2236.
- [29] Jackson, R. B., Banner, J. L., Jobbagy, E. G., Pockman, W. T., Wall, D. H. (2002): Ecosystem carbon loss with woody plant invasion of grasslands. – *Nature* 418: 623-626.
- [30] Koerselman, W., Meuleman, A. (1996): The Vegetation N:P Ratio: a New Tool to Detect the Nature of Nutrient Limitation. – *Journal of Applied Ecology* 33: 1441-1450.
- [31] Krab, E. J., Monteux, S., Weedon, J. T., Dorrepaal, E. (2019): Plant expansion drives bacteria and collembola communities under winter climate change in frost-affected tundra. – *Soil Biology & Biochemistry* 138.
- [32] Li, L., Zerbe, S., Han, W., Thevs, N., Li, W., He, P., Schmitt, A. O., Liu, Y., Ji, C. (2014): Nitrogen and phosphorus stoichiometry of common reed (*Phragmites australis*) and its relationship to nutrient availability in northern China. – *Aquatic Botany* 112: 84-90.
- [33] Li, L., Xing, M., Lv, J., Wang, X., Chen, X. (2017): Response of rhizosphere soil microbial to *Deyeuxia angustifolia* encroaching in two different vegetation communities in alpine tundra. – *Scientific Reports* 7.

- [34] Li, F., Hu, J., Xie, Y., Yang, G., Hu, C., Chen, X., Deng, Z. (2018): Foliar stoichiometry of carbon, nitrogen, and phosphorus in wetland sedge *Carex brevicuspis* along a small-scale elevation gradient. – *Ecological Indicators* 92: 322-329.
- [35] Lin, Y., Chen, A., Yan, S., Rafay, L., Du, K., Wang, D., Ge, Y., Li, J. (2019): Available soil nutrients and water content affect leaf nutrient concentrations and stoichiometry at different ages of *Leucaena leucocephala* forests in dry-hot valley. – *Journal of Soils and Sediments* 19: 511-521.
- [36] Liu, D., Zhang, J., Biswas, A., Cao, J., Xie, H., Qi, X. (2020): Seasonal dynamics of leaf stoichiometry of *Phragmites australis*: a case study from Yangguan Wetland, Dunhuang, China. – *Plants* 9.
- [37] Løkken, J. O., Evju, M., Söderström, L., Hofgaard, A., Kikvidze, Z. (2020): Vegetation response to climate warming across the forest–tundra ecotone: species-dependent upward movement. – *Journal of Vegetation Science* 31: 854-866.
- [38] Mao, R., Chen, H.-M., Zhang, X.-H., Shi, F.-X., Song, C.-C. (2016): Effects of P addition on plant C:N:P stoichiometry in an N-limited temperate wetland of Northeast China. – *Science of the Total Environment* 559: 1-6.
- [39] Moe, S. J., Stelzer, R. S., Forman, M. R., Harpole, W. S., Daufresne, T., Yoshida, T. (2005): Recent advances in ecological stoichiometry: insights for population and community ecology. – *Oikos* 109: 29-39.
- [40] Ni, B., You, J., Li, J., Du, Y., Zhao, W., Chen, X. (2021): Genetic and Epigenetic Changes during the Upward Expansion of *Deyeuxia angustifolia* Kom. in the Alpine Tundra of the Changbai Mountains, China. – *Plants* 10.
- [41] Ordonez, J. C., van Bodegom, P. M., Witte, J.-P. M., Wright, I. J., Reich, P. B., Aerts, R. (2009): A global study of relationships between leaf traits, climate and soil measures of nutrient fertility. – *Global Ecology and Biogeography* 18: 137-149.
- [42] Pellegrini, A. F. A., Hoffmann, W. A., Franco, A. C. (2014): Carbon accumulation and nitrogen pool recovery during transitions from savanna to forest in central Brazil. – *Ecology* 95: 342-352.
- [43] Qin, Y., Adamowski, J. F., Deo, R. C., Hu, Z., Cao, J., Zhu, M., Feng, Q. (2019): Controlling factors of plant community composition with respect to the slope aspect gradient in the Qilian Mountains. – *Ecosphere* 10.
- [44] Ramirez, K. S., Snoek, L. B., Koorem, K., Geisen, S., Bloem, L. J., Ten Hooven, F., Kostenko, O., Krigas, N., Manrubia, M., Caković, D., van Raaij, D., Tsiafouli, M. A., Vreš, B., Čelik, T., Weser, C., Wilschut, R. A., van der Putten, W. H. (2019): Range-expansion effects on the belowground plant microbiome. – *Nature Ecology & Evolution* 3: 604-611.
- [45] Reich, P. B., Oleksyn, J. (2004): Global patterns of plant leaf N and P in relation to temperature and latitude. – *Proceedings of the National Academy of Sciences of the United States of America* 101: 11001-11006.
- [46] Ricciardi, A., Blackburn, T. M., Carlton, J. T., Dick, J. T. A., Hulme, P. E., Iacarella, J. C., Jeschke, J. M., Liebhold, A. M., Lockwood, J. L., MacIsaac, H. J., Pyšek, P., Richardson, D. M., Ruiz, G. M., Simberloff, D., Sutherland, W. J., Wardle, D. A., Aldridge, D. C. (2017): Invasion science: a horizon scan of emerging challenges and opportunities. – *Trends in Ecology & Evolution* 32: 464-474.
- [47] Scheffers, B. R., De Meester, L., Bridge, T. C. L., Hoffmann, A. A., Pandolfi, J. M., Corlett, R. T., Butchart, S. H. M., Pearce-Kelly, P., Kovacs, K. M., Dudgeon, D., Pacifici, M., Rondinini, C., Foden, W. B., Martin, T. G., Mora, C., Bickford, D., Watson, J. E. M. (2016): The broad footprint of climate change from genes to biomes to people. – *Science* 354.
- [48] Schindler, D. W. (2003): Ecological stoichiometry: the biology of elements from molecules to the biosphere. – *Nature* 423: 225-226.
- [49] Shi, H., Zhou, Q., Xie, F., He, N., He, R., Zhang, K., Zhang, Q., Dang, H. (2020): Disparity in elevational shifts of upper species limits in response to recent climate

- warming in the Qinling Mountains, North-central China. – *Science of the Total Environment* 706.
- [50] Shi, L., Li, Q., Fu, X., Kou, L., Dai, X., Wang, H. (2021): Foliar, root and rhizospheric soil C:N:P stoichiometries of overstory and understory species in subtropical plantations. – *Catena* 198.
- [51] Sistla, S. A., Schimel, J. P. (2012): Stoichiometric flexibility as a regulator of carbon and nutrient cycling in terrestrial ecosystems under change. – *New Phytologist* 196: 68-78.
- [52] Taş, N., Prestat, E., Wang, S., Wu, Y., Ulrich, C., Kneafsey, T., Tringe, S. G., Torn, M. S., Hubbard, S. S., Jansson, J. K. (2018): Landscape topography structures the soil microbiome in arctic polygonal tundra. – *Nature Communications* 9.
- [53] Tie, L., Zhang, S., Penuelas, J., Sardans, J., Zhou, S., Hu, J., Huang, C. (2020): Responses of soil C, N, and P stoichiometric ratios to N and S additions in a subtropical evergreen broad-leaved forest. – *Geoderma* 379.
- [54] Tong, R., Zhou, B., Jiang, L., Ge, X., Cao, Y. (2021): Spatial patterns of leaf carbon, nitrogen, and phosphorus stoichiometry and nutrient resorption in Chinese fir across subtropical China. – *Catena* 201.
- [55] Urbina, I., Grau, O., Sardans, J., Ninot, J. M., Penuelas, J. (2020): Encroachment of shrubs into subalpine grasslands in the Pyrenees changes the plant-soil stoichiometry spectrum. – *Plant and Soil* 448: 37-53.
- [56] Venterink, H. O. (2011): Legumes have a higher root phosphatase activity than other forbs, particularly under low inorganic P and N supply. – *Plant and Soil* 347: 137-146.
- [57] Vitousek, P. M., Cassman, K., Cleveland, C., Crews, T., Field, C. B., Grimm, N. B., Howarth, R. W., Marino, R., Martinelli, L., Rastetter, E. B., Sprent, J. I. (2002): Towards an ecological understanding of biological nitrogen fixation. – *Biogeochemistry* 57: 1-45.
- [58] Vitousek, P. M., Porder, S., Houlton, B. Z., Chadwick, O. A. (2010): Terrestrial phosphorus limitation: mechanisms, implications, and nitrogen-phosphorus interactions. – *Ecological Applications* 20: 5-15.
- [59] Wang, R., Lu, L., Cao, Y., Sardans, J., Liu, H., Li, B., Zhang, Y., Penuelas, J., Dijkstra, F. A., Jiang, Y. (2021): Stability of elemental content correlates with plant resistance to soil impoverishment. – *Plant and Soil* 467: 213-226.
- [60] Xia, C., Yu, D., Wang, Z., Xie, D. (2014): Stoichiometry patterns of leaf carbon, nitrogen and phosphorus in aquatic macrophytes in eastern China. – *Ecological Engineering* 70: 406-413.
- [61] Xiao, L., Bi, Y., Du, S., Wang, Y., Guo, C., Christie, P. (2021): Response of ecological stoichiometry and stoichiometric homeostasis in the plant-litter-soil system to revegetation type in arid mining subsidence areas. – *Journal of Arid Environments* 184.
- [62] Xu, W., Liu, L., He, T., Cao, M., Sha, L., Hu, Y., Li, Q., Li, J. (2016): Soil properties drive a negative correlation between species diversity and genetic diversity in a tropical seasonal rainforest. – *Scientific Reports* 6.
- [63] Xue, K., Yuan, M. M., Shi, Z. J., Qin, Y., Deng, Y., Cheng, L., Wu, L., He, Z., Nostrand, J. D. V., Bracho, R., Natali, S., Schuur, E. A. G., Luo, C. (2016): Tundra soil carbon is vulnerable to rapid microbial decomposition under climate warming. – *Nature Climate Change* 6: 595-600.
- [64] Yan, K., Duan, C., Fu, D., Li, J., Wong, M. H. G., Qian, L., Tian, Y. (2015): Leaf nitrogen and phosphorus stoichiometry of plant communities in geochemically phosphorus-enriched soils in a subtropical mountainous region, SW China. – *Environmental Earth Sciences* 74: 3867-3876.
- [65] Yang, Y., Liu, B. (2019): Effects of planting *Caragana* shrubs on soil nutrients and stoichiometries in desert steppe of Northwest China. – *Catena* 183.
- [66] Zhang, H.-Y., Goncalves, P., Copeland, E., Qi, S.-S., Dai, Z.-C., Li, G.-L., Wang, C.-Y., Du, D.-L., Thomas, T. (2020): Invasion by the weed *Conyza canadensis* alters soil nutrient supply and shifts microbiota structure. – *Soil Biology and Biochemistry* 143.

- [67] Zhao, H., Xu, L., Wang, Q., Tian, J., Tang, X., Tang, Z., Xie, Z., He, N., Yu, G. (2018): Spatial patterns and environmental factors influencing leaf carbon content in the forests and shrublands of China. – *Journal of Geographical Sciences* 28: 791-801.
- [68] Zhou, Y., Boutton, T. W., Wu, X. B. (2018a): Soil C:N:P stoichiometry responds to vegetation change from grassland to woodland. – *Biogeochemistry* 140: 341-357.
- [69] Zhou, Y., Boutton, T. W., Wu, X. B. (2018b): Soil phosphorus does not keep pace with soil carbon and nitrogen accumulation following woody encroachment. – *Global Change Biology* 24: 1992-2007.
- [70] Zhu, D., Hui, D., Wang, M., Yang, Q., Yu, S. (2020): Light and competition alter leaf stoichiometry of introduced species and native mangrove species. – *Science of The Total Environment* 738.
- [71] Zong, S., Jin, Y., Xu, J., Wu, Z., He, H., Du, H., Wang, L. (2016): Nitrogen deposition but not climate warming promotes *Deyeuxia angustifolia* encroachment in alpine tundra of the Changbai Mountains, Northeast China. – *Science of the Total Environment* 544: 85-93.
- [72] Zuo, X., Cui, L., Li, W., Lei, Y., Dou, Z., Liu, Z., Cai, Y., Zhai, X. (2021): *Spartina alterniflora* Leaf and Soil Eco-Stoichiometry in the Yancheng Coastal Wetland. – *Plants-Basel* 10.

APPENDIX



Figure A1. Landscape photography of different vegetation types of *Deyeuxia angustifolia* Kom. (*D. angustifolia*) encroachment

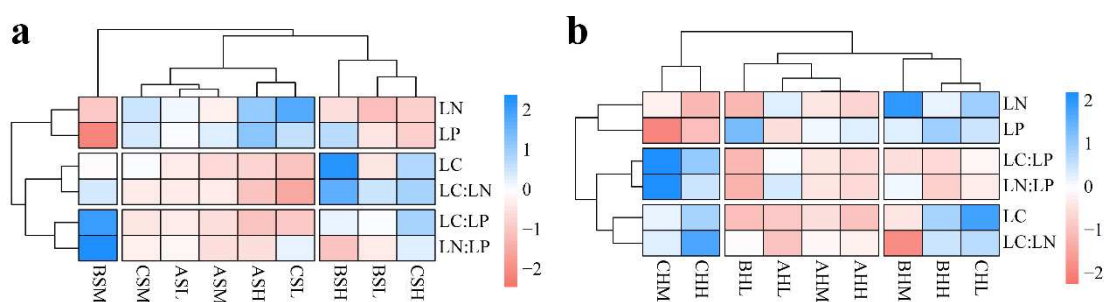


Figure A2. Clustering heatmap of leaf stoichiometry of *D. angustifolia* in different sampling sites. a, shrub ; b: herbaceous. LC: leaf carbon concentration, LN: leaf nitrogen concentration, LP: leaf phosphorus concentration, LC:LN = LC to LN ratio, LC:LP = LC to LP ratio, LN:LP = LN to LP ratio

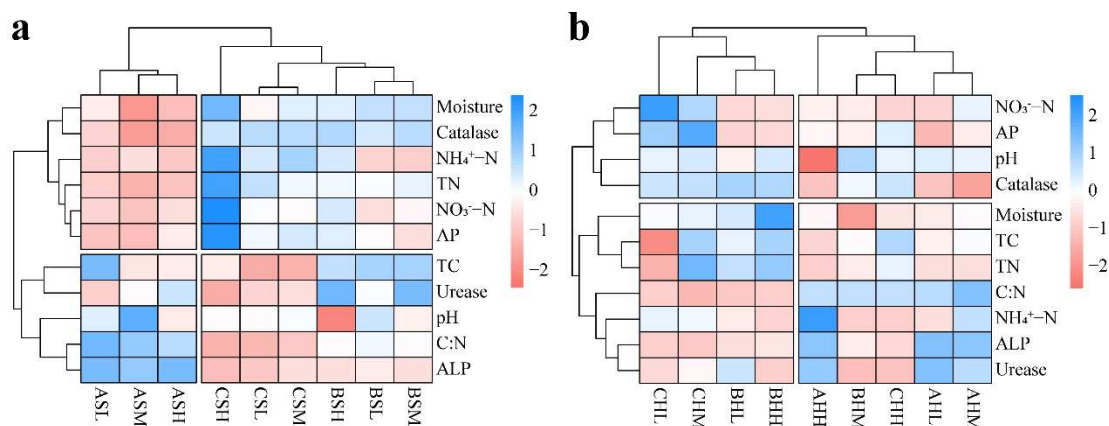


Figure A3. Clustering heatmap of soil properties in different sampling sites. *a*, shrubs ; *b*: herbaceous. TC: total organic carbon, TN: total nitrogen, C:N: TC to TN ratio, $\text{NH}_4^+\text{-N}$: ammonium nitrogen, $\text{NO}_3^-\text{-N}$: nitrate nitrogen, AP: available phosphorus, Moisture: water content, ALP: alkaline phosphatase

Table A1. Effects of plant type, elevation, and *D. angustifolia* encroachment on leaf stoichiometry of *D. angustifolia* and soil properties based on PERMANOVA

	Leaf stoichiometry		Soil properties	
	R ²	P	R ²	P
Elevation	0.134	0.001	0.429	0.001
Plant type	0.134	0.001	0.062	0.001
Encroachment	0.113	0.001	0.025	0.001
Elevation × plant type	0.223	0.001	0.108	0.001
Elevation × encroachment	0.187	0.001	0.110	0.001
Plant type × encroachment	0.028	0.001	0.104	0.001
Elevation × plant type × encroachment	0.121	0.001	0.125	0.001

P is the significance level. Values with $P < 0.05$ are in bold

Table A2. Leaf stoichiometry of *D. angustifolia* across encroachment levels and elevations within the study area

Vegetation types		LC (g kg ⁻¹)	LN (g kg ⁻¹)	LP (g kg ⁻¹)	LC:LN (ratio)	LC:LP (ratio)	LN:LP (ratio)
Shrubs	ASL	427.03 ± 11.42a	24.33 ± 1.87a	1.41 ± 0.02b	17.64 ± 1.69a	303.77 ± 3.67a	17.32 ± 1.54a
	ASM	415.23 ± 13.28a	23.35 ± 1.42a	1.47 ± 0.04b	17.83 ± 1.22a	283.61 ± 14.37b	15.97 ± 1.44a
	ASH	411.10 ± 16.27a	26.89 ± 2.74a	1.69 ± 0.03a	15.40 ± 1.81a	243.65 ± 8.76c	15.96 ± 1.91a
	BSL	425.96 ± 10.51b	21.06 ± 3.43a	1.27 ± 0.04b	20.69 ± 4.23a	335.21 ± 17.32b	16.52 ± 2.38b
	BSM	442.59 ± 26.38b	21.53 ± 2.01a	0.84 ± 0.02c	20.63 ± 1.56a	524.5 ± 39.20a	25.53 ± 2.88a
	BSH	561.65 ± 18.65a	22.56 ± 1.11a	1.57 ± 0.03a	24.96 ± 1.98a	356.95 ± 8.33b	14.35 ± 0.96b
	CSL	393.20 ± 5.31b	28.70 ± 1.09a	1.56 ± 0.02a	13.71 ± 0.41c	251.90 ± 1.52c	18.38 ± 0.48a
	CSM	449.88 ± 31.42a	25.46 ± 1.06b	1.51 ± 0.02b	17.68 ± 1.15b	297.91 ± 21.57b	16.86 ± 0.90b
	CSH	485.49 ± 33.34a	21.89 ± 0.40c	1.16 ± 0.02c	22.18 ± 1.46a	418.59 ± 29.48a	18.88 ± 0.74a
Herbaceous	AHL	398.27 ± 6.61a	25.03 ± 3.35a	1.45 ± 0.03b	16.10 ± 2.11a	274.76 ± 1.42a	17.24 ± 2.06a
	AHM	409.11 ± 5.12a	24.05 ± 0.73a	1.65 ± 0.04a	17.02 ± 0.48a	247.64 ± 3.71b	14.55 ± 0.26a
	AHH	395.95 ± 18.47a	23.53 ± 2.73a	1.69 ± 0.05a	16.99 ± 2.23a	234.91 ± 12.88b	13.93 ± 1.21a
	BHL	393.10 ± 12.54a	22.95 ± 0.54b	1.99 ± 0.02a	17.14 ± 0.84a	197.34 ± 7.29b	11.52 ± 0.15b
	BHM	410.47 ± 22.11a	27.67 ± 2.45a	1.70 ± 0.06b	14.95 ± 2.00a	241.99 ± 8.49a	16.36 ± 2.04a
	BHH	444.59 ± 35.32a	24.95 ± 1.09ab	1.88 ± 0.08a	17.80 ± 0.79a	236.50 ± 15.91a	13.27 ± 0.32b
	CHL	468.99 ± 8.05a	26.02 ± 0.60a	1.76 ± 0.04a	18.02 ± 0.28a	266.14 ± 9.38c	14.76 ± 0.40c
	CHM	426.61 ± 4.08c	24.25 ± 1.56ab	1.02 ± 0.03c	17.63 ± 1.01a	418.23 ± 14.10a	23.77 ± 1.65a
	CHH	443.42 ± 4.34b	22.93 ± 0.48b	1.30 ± 0.03b	19.35 ± 0.57a	340.50 ± 8.02b	17.61 ± 0.44b

Different lowercase letters represent significant differences among encroachment levels within group ($P < 0.05$)

Table A3. Soil properties and enzyme activities across encroachment levels and elevations within the study area

		TC (g kg ⁻¹)	TN (g kg ⁻¹)	C:N	NH ₄ ⁺ -N (mg kg ⁻¹)	NO ₃ ⁻ -N (mg kg ⁻¹)	AP (mg kg ⁻¹)	Moisture (%)	pH	Catalase	ALP	Urease
2075 m	ASL	113.14 ± 7.57a	5.66 ± 0.33a	20.10 ± 2.42a	32.53 ± 2.96b	13.97 ± 1.59ab	87.14 ± 10.17a	0.38 ± 0.00a	4.88 ± 0.02ab	0.76 ± 0.01a	0.12 ± 0.00ab	0.50 ± 0.03c
	ASM	82.34 ± 1.38b	4.48 ± 0.33c	18.45 ± 1.21a	40.03 ± 1.44a	11.75 ± 1.09b	86.42 ± 8.95a	0.24 ± 0.00c	5.05 ± 0.03a	0.7 ± 0.02b	0.12 ± 0.00b	0.62 ± 0.02b
	ASH	84.59 ± 1.85b	5.12 ± 0.13b	16.54 ± 0.45a	29.92 ± 1.84b	15.25 ± 0.99a	103.49 ± 4.09a	0.31 ± 0.00b	4.81 ± 0.18b	0.72 ± 0.01b	0.13 ± 0.01a	0.71 ± 0.05a
2157 m	BSL	104.87 ± 2.98a	7.81 ± 0.38a	13.44 ± 0.47a	33.64 ± 1.51b	15.76 ± 0.67c	110.72 ± 8.07ab	0.47 ± 0.00a	4.91 ± 0.02a	0.83 ± 0.00a	0.08 ± 0.00a	0.64 ± 0.08b
	BSM	106.05 ± 2.98a	8.40 ± 0.17a	12.64 ± 0.59a	33.46 ± 1.36b	18.90 ± 0.70b	99.41 ± 4.14b	0.47 ± 0.00a	4.82 ± 0.02b	0.85 ± 0.01a	0.08 ± 0.01a	0.85 ± 0.06a
	BSH	101.25 ± 5.89a	7.96 ± 0.29a	12.72 ± 0.56a	62.40 ± 1.85a	23.15 ± 1.51a	121.02 ± 7.86a	0.45 ± 0.00b	4.59 ± 0.01c	0.86 ± 0.01a	0.08 ± 0.00a	0.87 ± 0.07a
2240 m	CSL	66.72 ± 1.85b	9.36 ± 0.84b	7.18 ± 0.74a	62.23 ± 1.39c	20.45 ± 0.88b	116.91 ± 10.20b	0.40 ± 0.01c	4.84 ± 0.02a	0.85 ± 0.01a	0.07 ± 0.00b	0.52 ± 0.03a
	CSM	66.81 ± 3.90b	8.06 ± 0.80b	8.37 ± 1.32a	72.13 ± 0.62b	19.67 ± 0.81b	122.66 ± 11.28b	0.45 ± 0.01b	4.85 ± 0.04a	0.85 ± 0.01a	0.08 ± 0.00a	0.54 ± 0.06a
	CSH	83.80 ± 4.08a	12.52 ± 0.29a	6.69 ± 0.20a	96.05 ± 2.32a	40.08 ± 0.43a	167.84 ± 4.45a	0.56 ± 0.01a	4.84 ± 0.01a	0.84 ± 0.01a	0.07 ± 0.00b	0.42 ± 0.02b
2075 m	AHL	99.33 ± 0.81b	6.75 ± 0.76a	14.84 ± 1.67a	51.21 ± 3.91c	17.57 ± 0.79c	92.21 ± 2.14b	0.35 ± 0.01b	4.82 ± 0.03a	0.78 ± 0.00a	0.13 ± 0.00a	0.95 ± 0.03a
	AHM	105.55 ± 0.41a	6.60 ± 0.34a	16.02 ± 0.86a	65.16 ± 1.18a	32.92 ± 1.64b	106.01 ± 7.07a	0.36 ± 0.00a	4.81 ± 0.04a	0.75 ± 0.01b	0.13 ± 0.00a	0.86 ± 0.07ab
	AHH	88.00 ± 0.80c	6.00 ± 0.06a	14.68 ± 0.22a	57.88 ± 1.58b	52.52 ± 1.09a	109.68 ± 9.53a	0.36 ± 0.01a	4.59 ± 0.04b	0.78 ± 0.01a	0.13 ± 0.00a	0.92 ± 0.06b
2157 m	BHL	110.44 ± 4.43b	9.54 ± 0.37b	11.60 ± 0.88a	52.07 ± 2.61b	19.73 ± 0.69a	100.60 ± 10.89a	0.38 ± 0.00ab	4.77 ± 0.03b	0.88 ± 0.01a	0.09 ± 0.00a	0.82 ± 0.05a
	BHM	103.78 ± 3.81b	7.14 ± 0.62c	14.65 ± 1.81a	57.55 ± 1.61a	14.50 ± 1.60b	108.54 ± 6.29a	0.30 ± 0.01b	4.85 ± 0.02a	0.84 ± 0.01b	0.10 ± 0.00a	0.58 ± 0.09b
	BHH	127.11 ± 9.60a	10.71 ± 0.16a	11.87 ± 0.87a	54.28 ± 1.08b	15.74 ± 1.22b	101.68 ± 4.53a	0.45 ± 0.10a	4.82 ± 0.01a	0.87 ± 0.01a	0.10 ± 0.00a	0.62 ± 0.02b
2240 m	CHL	56.72 ± 3.03b	4.83 ± 0.53c	11.84 ± 1.24b	92.95 ± 1.85a	27.78 ± 0.84a	128.88 ± 14.43a	0.37 ± 0.01ab	4.81 ± 0.01a	0.86 ± 0.02a	0.09 ± 0.00a	0.65 ± 0.03b
	CHM	126.1 ± 6.37a	11.59 ± 1.26a	11.00 ± 1.73b	73.85 ± 1.71b	27.07 ± 1.05a	142.00 ± 6.52a	0.37 ± 0.00a	4.82 ± 0.01a	0.86 ± 0.01a	0.09 ± 0.00a	0.73 ± 0.02a
	CHH	125.02 ± 9.79a	8.54 ± 0.31b	14.64 ± 0.95a	51.65 ± 0.68c	14.22 ± 1.39b	118.21 ± 3.18a	0.35 ± 0.01b	4.81 ± 0.02a	0.86 ± 0.00a	0.09 ± 0.00a	0.59 ± 0.04b

Different lowercase letters represent significant differences among encroachment levels within group ($P < 0.05$)

Table A4. The explained variance of soil properties and their significant analysis in redundancy analysis (RDA)

Soil abiotic factor	Explains %	Contribution %	F	P**
Moisture	23.5	39.2	16	0.002
C:N (ratio)	9.7	16.2	7.8	0.002
pH	4.2	7	4.2	0.026
AP (mg kg ⁻¹)	4.2	6.9	3.5	0.034
Urease	4.1	6.9	3.9	0.048
NH ₄ ⁺ -N (mg kg ⁻¹)	4.1	6.8	3.6	0.052
ALP	4.2	7	3	0.064
Catalase	2.1	3.5	2.2	0.112
TN (g kg ⁻¹)	2.1	3.4	2.2	0.126
NO ₃ ⁻ -N (mg kg ⁻¹)	1.9	3.1	1.9	0.152
TC (g kg ⁻¹)	< 0.1	< 0.1	< 0.1	0.974

**Indicates the variance of each soil abiotic factor significantly contributed to the total variance. Significant values are in bold

ASSESSMENT OF THE IMPACTS OF URBAN EXPANSION ON AGRICULTURAL LAND-USE INTENSITY IN ETHIOPIA, THE CASE OF ADDIS ABABA

ARGAIE, S. T. – WANG, K. X. – ABDULLAH, M. – LAN, J.*

*College of Public Administration, Nanjing Agricultural University, Nanjing 210095, China
(e-mails: 2019109079@stu.njau.edu.cn – S. T. Argaie; 2019109046@stu.njau.edu.cn – K. X. Wang; 2019209030@stu.njau.edu.cn – M. Abdullah)*

**Corresponding author
e-mail: lanjing@njau.edu.cn*

(Received 14th Dec 2021; accepted 2nd May 2022)

Abstract. Unplanned urban expansion is one of the challenging problems faced by developing countries, such as Ethiopia. Therefore, this study was conducted to assess the impact of urbanization on the land-use intensity in Addis Ababa by taking advantage of modern techniques, such as Geographic Information Systems (GIS) and Remote Sensing (RS). The research used multi-spatiotemporal Landsat OLI images of 2010, 2015, and 2020 with a 30 m resolution. Maximum likelihood-based supervised classification was employed to extract the study area's leading land use/land cover (LULC) classes. Six land cover classes were identified: built-up land, water bodies, woodland, grassland, arable land, and unused lands. Results revealed that 11.87% of the arable land was converted into built-up land over the study period (2010-2020). Interestingly, urbanization showed adverse trends, occupying 30.63%, 39.03%, and 46.62% of the entire study area in 2010, 2015, and 2020, respectively. Of all the classes, arable land was the most affected category, as 78.65% (86.282 km²) of the land encroached upon by urbanization belonged to arable land. Therefore, the aggressive and rapid encroachment of built-up land was a significant factor in the severe degradation of agricultural land, significantly impacting agricultural land-use intensity.

Keywords: *Addis Ababa, land use, land cover, urban expansion, urbanization, urban growth*

Introduction

Urban areas in developing countries have been experiencing rapid expansion due to the increased inflow of people to the cities searching for better employment opportunities. This rapid growth of the urban regions poses vast opportunities and challenges for sustainable development in a country's future (Terfa et al., 2019; Busho et al., 2021). Large cities are expected to provide increased wealth and drive innovation. They also need more flexible infrastructural and service resources than small cities—this evolution requires energy and material from remote and nearby ecosystems, including the nearby agricultural lands (Balogun et al., 2011). In Africa, most cities face multiple challenges due to poor urban planning and uncontrolled urban population growth; informal settlements become part of urban ecosystems (Balogun et al., 2011; Lamson-Hall et al., 2019; Uddin and Anjuman, 2013). According to a report by the United Nations, more than 54% of the world's population lives in urban areas (Lark et al., 2020). The spatial expansion of urbanization plays an essential role in the loss of arable land as it modifies biogeochemistry, habitat, and land cover (Eregata et al., 2019; d'Amour et al., 2017). The population in Addis Ababa has also increased from 3,126,000 in 2010 at 4.34% to 5,228,000 in 2022 at 4.43%. Notably, the rapid population growth in African cities, including Addis Ababa, drives urban expansion as local authorities build more residential areas to accommodate the people living in the city and support business operations (Xu et al., 2019). With more people migrating from

rural areas to the city, the government and communities must protect farmland by strictly controlling urban land expansion and population movement.

Ethiopia has experienced rapid urban growth during the past several decades, reflected in its demographic composition and large-scale urban landscape expansion. Satellite imagery shows that Ethiopia's urban areas increased by almost 25% in 2009 (Terfa et al., 2019). Urban land cover is expanding at rates faster than the growth of the urban population (Berhanu et al., 2017). This has resulted in a massive loss of cultivated land in the coastal and central provinces and expansion into other regions, especially Addis Ababa (Anees et al., 2019; Busho et al., 2021). Although the exact figures on the loss in total cultivated land area in Ethiopia remain controversial, experts agree that the newly reclaimed cultivated land is less fertile than the converted land (Johnson et al., 2014; Koroso et al., 2020). Given the decline of cultivated land, the level of inputs and outputs or frequency of cultivation against constant land, or intensity of agricultural land use, is vital for maintaining the food production capacity (Anees et al., 2019; Balogun et al., 2011). However, urban expansion and economic development can lead to a rise in off-farm opportunities resulting in a labor shortage in the agricultural sector (Fitton et al., 2019).

The declined intensity in agricultural land use and farmland abandonment have been documented for many regions and different crops. This has posed additional challenges to food security and ecosystem conservation (Fitton et al., 2019). Notably, urban expansion on agricultural land and increased land-use intensity have adverse impacts on the agricultural productivity in Ethiopia (Arsiso et al., 2018; Shiferaw et al., 2017). More importantly, the nature and magnitude of their relationship can directly affect a country's food provision and may further influence a nation's agricultural land patterns (d'Amour et al., 2017). Understanding the relationship between urban expansion and agricultural land-use intensity is critical to formulating appropriate policies to balance the pressure between urban growth and agricultural land use and preservation not only in Ethiopia but also in other parts of the world, including in America, Europe, India, and China, where urbanization has heightened over the years (Güneralp et al., 2020; Wu et al., 2021; Zhang, 2001; Zhong et al., 2018). Besides, a decrease in agricultural land-use intensity implies more future farmland expansion at the expense of other ecosystems (Addis, 2020; Balogun et al., 2011). Therefore, understanding how urban land expansion affects agricultural land-use intensity will better examine the environmental impacts of farmland expansion and the sustainability of land resource utilization.

In Addis Ababa, urban development has taken over agricultural lands, which form the primary source of foodstuff and the backbone of the Economy of Ethiopia (Arsiso et al., 2018; Busho et al., 2021; d'Amour et al., 2017). With urban expansion threatening local and regional sustainable development, the study on the impacts of urbanization on agricultural land-use intensity is crucial. This research will inform effective urban planning, urban ecological construction, and sustainable development. Urbanization policies adopted by urban officials are usually for purely industrial purposes, without giving much attention to the livelihood of surrounding smallholder farmers (Lark et al., 2020; Mohammed et al., 2020; Uddin and Anjuman, 2013). These farmers could be exposed to severe economic issues that lead to impoverishment (Fitton et al., 2019). Such behavior may force farmers in rural and semi-urban areas to displace due to financial barriers (Johnson et al., 2014). This, in turn, directly affects the agricultural land-use intensity, which is an extra economic issue for the country. There is little

evidence showing the effects of urbanization on agricultural land use in Addis Ababa and Ethiopia entirely. Therefore, with the increasing urbanization in Addis Ababa and surrounding areas, it is imperative to explore urbanization's effects on agricultural land use within the administrative border of the city.

To our best knowledge, this study is the first to attempt to address this specific issue. One of the main effects of the uncontrolled expansion of urban areas is the shrinking of cultivated territories through encroachment on fertile agricultural lands, such as civil infrastructures and governmental projects (Addis, 2020; Artmann et al., 2019; Johnson et al., 2014). Therefore, this study's primary goal is to discover the nature and extent of agricultural land-use intensity in Addis Ababa between 2010 and 2020 and identify the factors responsible. Six land-use/land-cover (LULC) classes are mapped over the capital city of Ethiopia, spread over 539.04 kilometers squared (km²) of the study area. These classes are Arable land, Woodland, Grassland, Built-up land, Water-body, and Unused land. Therefore, the main contribution of this paper is the following:

- To investigate and assess current urban development policies regarding agricultural land-use intensity in Addis Ababa regional state between 2010 and 2020
- To identify the significant factors contributing to urban sprawl in Addis Ababa state in which agricultural land-use intensity is directly reduced
- To analyze the prime effects of the urban expansion on agricultural land-use intensity during the study period
- To highlight the importance of agricultural land-use intensity for the country's economy and provide suggestions and recommendations to government bodies and policymakers responsible for preserving farmland and managing it sustainably

The findings of this study could provide the information required to contribute to the protection of agricultural land-use intensity and the improvement of urbanization issues. Hence, this study would help urban planners and government agencies to anticipate growth patterns and plan infrastructure projects accordingly. It will also explore remotely sensed satellite imagery for the analysis section.

The remainder of this paper is organized as follows: Section 2 presents the materials and methods used to conduct the study, including data analysis techniques. Section 3 illustrates and discusses the results. Finally, Section 4 concludes the work and briefly provides recommendations that have conclusive remarks.

Materials and methods

Study area description

This study was conducted in Addis Ababa, as depicted in *Figure 1*, the capital city of the Republic of Ethiopia. The city's total area is about 539.04 km², with a total population of approximately 3,433,999 residents as of 2017 (Ethiopian Central Statistical Agency). However, consistent with many African cities, the population seasonally fluctuates as people move from agricultural to urban areas (Eregata et al., 2019). Addis Ababa is the country's social, economic, and political center. It is the largest city in the country, and its population growth is due to both in-migration and natural population increase.

Based on the UTM coordinate system, Addis Ababa is located between 465,000 m and 485,000 m E, 980,000 m, and 100,500 m N (Berhanu et al., 2017). It has an altitude between 3,000 m in the Entoto Mountains in the North and 2,100 m at Akaki Kaliti in the South. This characterizes Addis Ababa as the highest capital city in Africa. Addis Ababa is administratively divided into ten counties, as shown in *Figure 1*. It is characterized by an average temperature of 16 °C, which shows no remarkable variation throughout the year. It has two rainy seasons. According to local standards, the first season is from June to mid-September, the most extended rainy season, characterized by cool days and nights. The second rainy season is from March to mid-April, characterized by moderately warm days and cool nights. Addis Ababa has hot and dry months from April to May, characterized by warm to hot days and cool nights (Eregata et al., 2019).

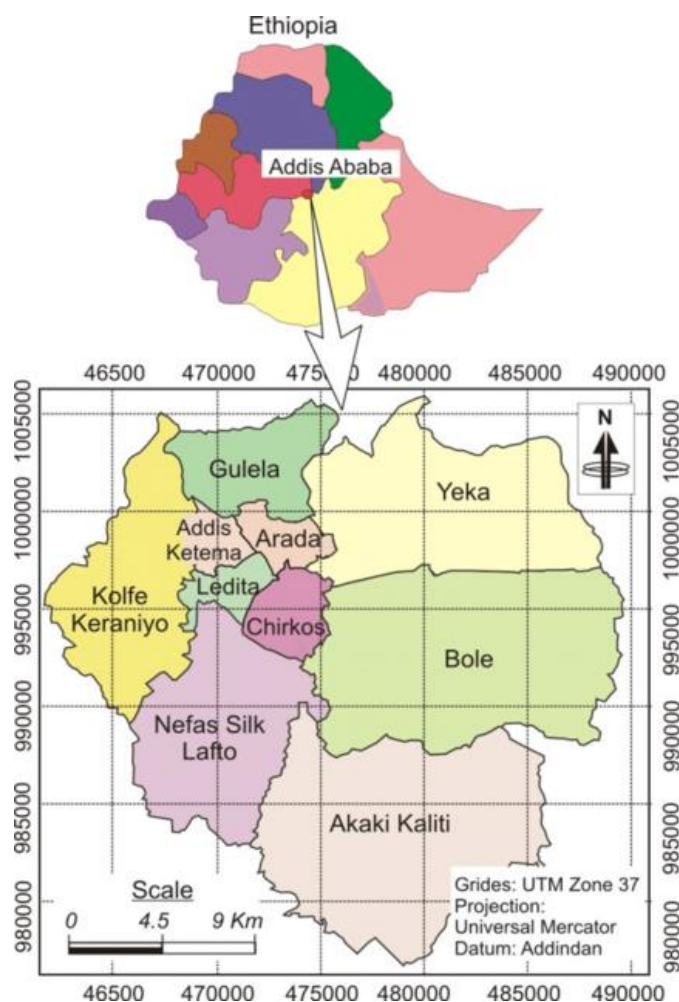


Figure 1. Addis Ababa location map (Berhanu et al., 2017)

Data collection and analysis

The paper employed a descriptive (observational method) research design to make an intensive investigation of the extent of urban expansion and its implications on land use in the town. Hence, to maintain triangulation in its findings, the design manifested the basic features of both qualitative and quantitative research. Two types of data were used.

Primary data

Data used in this paper was collected by different means. Semi-structured interviews between urban farmers and selected vital informants will be conducted to identify the effect of Addis Ababa's urbanization on their agricultural practices. A semi-structured interview is a research tool used in the social sciences. It was adopted in this study because it is versatile and allows new questions to be asked during the interview based on the interviewees' responses.

Moreover, observation is a data collection technique in which a trained person observes the actual processing associated with a device or walks through it. The analysis appreciated observation as an integral approach for gathering data on urbanization and agricultural land-use phenomena. Observation on the spot also helps chart the ongoing urban agriculture activities, plot use, and research settlement coverage. This also helped define the actual agricultural activities in Addis Ababa. At the same time, this approach assisted in gathering original data. It also secures data that participants might neglect, thinking it is not relevant.

Finally, subjects seem easier to embrace an observational intrusion than respond to questioning. Besides, The Focus Group Discussion (FGD) is a rapid evaluation method of semi-structured data collection. A carefully chosen set of participants meet to address issues and concerns based on a list of critical topics prepared by the researcher/facilitator (Uddin and Anjuman, 2013). FGD allowed communication between groups and defined the typical construction of meaning created by individuals related to the concepts under investigation. Tape recorders helped in information management. Local people were also involved in the discussion, particularly urban farmers, key informants, and the elderly. With five urban farmers and five older people, FGDs were held, and the selection was made randomly regardless of gender.

Secondary data

Secondary data were also extracted from satellite images characterized by multi-temporal and multispectral. It was also collected by reviewing documents, including published and unpublished scientific research papers, reports, books, and aerial photographs obtained from topographic maps, Google Earth. The collected data were integrated to present a solid background to the research and provide comprehensive insights into urbanization dynamics, causes, consequences, forms, and challenges of urban mobility and urbanization infrastructural services. The secondary data about infrastructure, environmental profile and states, existing land-use patterns, and trends of the study area were obtained primarily from administrative organs within Addis Ababa's jurisdiction. We utilized both quantitative and qualitative methods.

The application of quantitative methods includes the usage of the GIS and RS data to generate maps of 2010, 2015, and 2020 and the calculation of the rate of urban expansion within Addis Ababa from the Landsat-based classified images. GIS-enabled techniques allowed us to reclassify land cover data into classes fitting for the objectives of this research, studying urban expansion and its effects on agricultural land use. Moreover, the ArcGIS tools helped conduct a land use's thematic change analysis. The matrix of the relative change detection is calculated based on the changes from one class to another.

This report used three satellite images obtained from United States Geological Survey (USGS) databases. The satellite images were geo-referenced using the Universal

Transverse Mercator (UTM) projection with the datum World Geodetic System (WGS) 1984 UTM. The collected satellite images were converted into Tiff format to simplify processing. *Table 1* lists the properties of each image. Landsat Operational Land Imager (OLI) and Thermal Infrared Sensor (TIRS) are characterized by suitability for urban land-use change detection applications. The process correction level of the tree collected images is Terrain Precision Correction (L1TP). To analyze the urbanization expansion effects on land-use intensity, we used three images obtained by Landsat 8 & 5 imageries captured in 2010, 2015, and 2020. The spatial resolution of the collected images is 30 m. These images are conductively compared for urban expansion during the last ten years.

Table 1. *The characteristics of satellite imageries of 2010, 2015, and 2020*

Satellite	Acquisition time	Resolution	Path/Row	Collection category	Source
Landsat 8-OLI/TIRS (Data 3)	26/03/2020	30 m	168/054	Tier 1	USGS
Landsat 8- OLI/TIRS (Data 2)	10/03/2015	30 m	168/054	Tier 1	USGS
Landsat 5- OLI/TIRS (Data 1)	09/12/2010	30 m	168/054	Tier 1	USGS

Results

This section presents and discusses the results of the classified Landsat images and field survey conducted at Addis Ababa and its urban fringes. As introduced in Section 2, Six LULC classes are mapped over the area within the administrative borders of the capital city of Ethiopia, spread over 539.04 km² of the study area. The following subsections provide a detailed explanation.

Spatiotemporal urban extension in Addis Ababa between 2010 and 2020

Maximum Likelihood Estimation (MLE) helped to classify Landsat images. Land-cover maps were generated based on the MLE results, as shown in *Figures 2, 3, and 4*. These spatiotemporal images (from 2000 to 2020) were obtained by analyzing the multispectral and multitemporal Landsat images. The study area was subjected to different spatial and temporal land-use intensities as illustrated in the ground truth data and classified Landsat images for the specified period. As shown in the percentages in *Table 2*, there is a gradual growth in the built-up areas of the study area with values of 30.63%, 39.03%, and 46.62% in 2000, 2015, and 2020, respectively. On the other hand, there is a continuous shrinkage in the arable land of the study area with values of 47.33%, 39.72%, and 35.46% in 2000, 2015, and 2020, respectively. *Table 2* presents the aggregate statistics of spatiotemporal urban extension experienced in ten years as extracted from the thematic maps.

The spatial distribution of land-use intensity within the area and the Normalized Difference Vegetation Index (NDVI) of Addis Ababa from 2010 are shown in *Figure 2* and *Table 2*. Agricultural land consisting of rainfed and irrigated arable lands, farming, cropland with permanent crops, and fallow fields occupied the largest area of 255.15 km², ascribed to the fact that the land was widely cultivated with majority ownership.

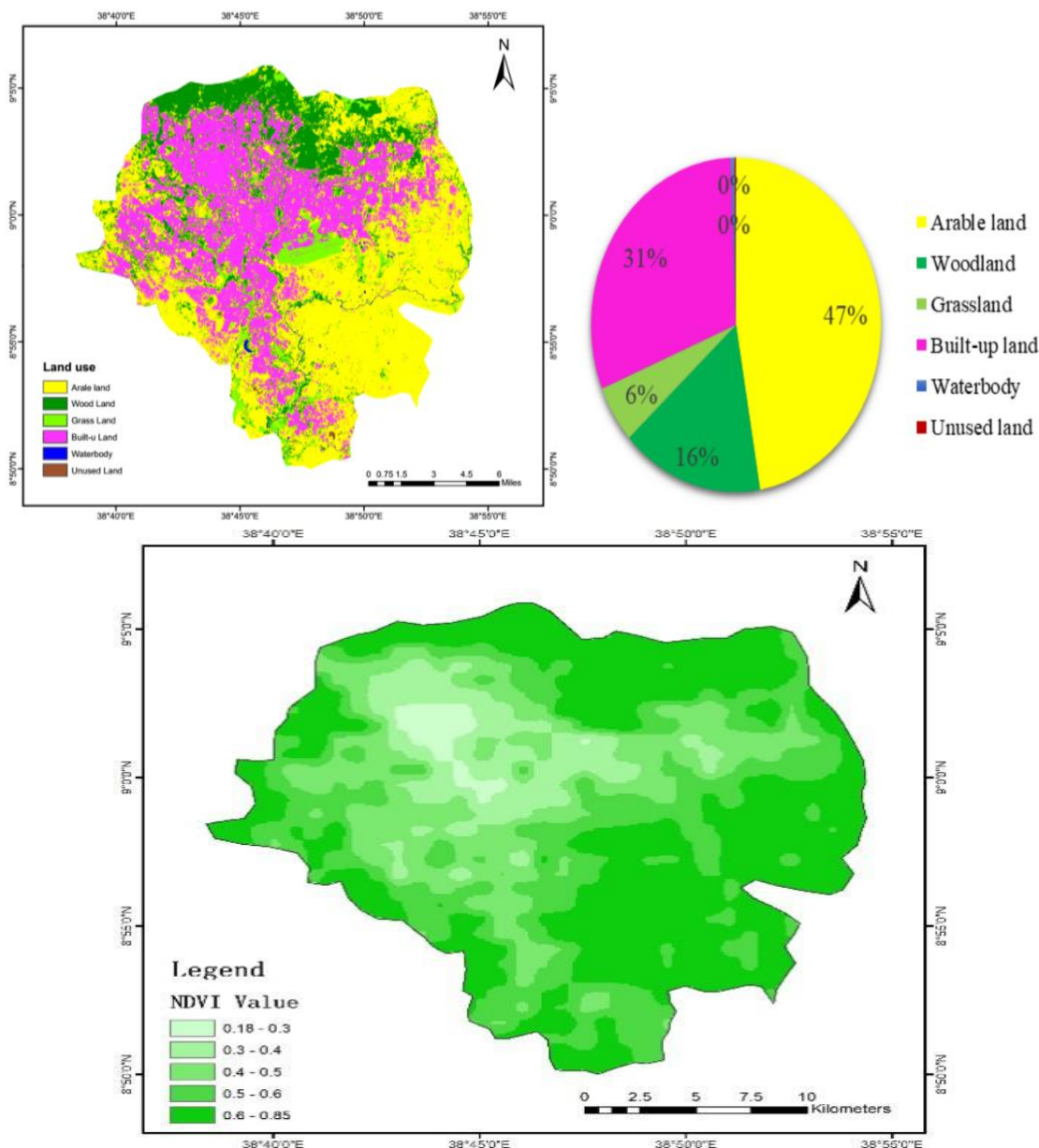


Figure 2. Land-use and land-cover map for 2010. Normalized difference vegetation index (NDVI) of Addis Ababa for 2010. (Source: adapted from Landsat 5-OLI/TIRS image for 2010)

In 2010, large agricultural production was the mainstay of the capital's economy, and its condition had to be maintained to protect the economy. *Figure 2* shows a gradual loss of arable land cover to more brown spaces (building and road construction) as expressed in the NDVI values (0.18 to 0.3) for 2010. This shows that the vegetation cover suitable for crop farming is lost to real estate construction. This may have repercussions for smallholder farmers who depend on crop farming. The built-up area comes in second place, with a much smaller inhabited area of arable land, 165.13 km², 36.63% of the total area. Built-up land consisting of industrial, commercial, and residential units within 165.13 km² is mainly due to the lack of development and increased agricultural activities. This comparison reflects the early stages of growth in the 2010s with a small compact metropolitan area. This signalizes that Addis Ababa

was a predominantly agricultural area when urban development was in its infancy stages in that period. Woodland is also making a considerable impact, occupying 85.52 km², 15.87% of Addis Ababa's total area. The area covered by grassland has more minor effects on the agricultural land-use intensity, where it occupies about 30 km² of the area from the capital city. The area under the waterbody, including dams and rivers, covers only 2.35 km². Similarly, Unused land is unoccupied by any human activity, including unfilled spaces, rocky areas, and sands. This class occupied only 0.87 km², the smallest area among all classes in 2010, attributed to the removal of farmland in the preparatory planting season.

In 2015, the arable land in the study area covered 214.12 km², as listed in *Table 2*, a decline from the 255.15 km² recorded in 2010. Arable land has been continuously shrunk and converted to civilian activities in the urbanization process according to the Normalized Difference Vegetation Index (NDVI) of Addis Ababa from 2015. Although arable land remains the dominant land class in the study area, it is also evident that there has been a continuous decline in arable land; it had decreased from 47.33% in 2010 to 39.72% in 2015 (see *Figs. 2 and 3*). Due to the consecutive reduction of agricultural land-use intensity, built-up areas increased intensively in the study periods (five years). This horizontal extension of urbanization led to the complete expropriation of agricultural land or the downsizing of the farm.

Table 2. Areas of land-use classes and spatiotemporal urban extension in the study period

Class	2010		2015		2020	
	Area (km ²)	Percentage (%)	Area (km ²)	Percentage (%)	Area (km ²)	Percentage (%)
Arable land	255.15	47.33	214.12	39.72	191.15	35.46
Woodland	85.52	15.87	83.29	15.45	71.62	13.29
Grassland	30.02	5.57	28.18	5.23	22.64	4.20
Built-up land	165.13	30.63	210.40	39.03	251.29	46.62
Water-body	2.35	0.44	2.31	0.43	1.92	0.36
Unused land	0.87	0.16	0.74	0.14	0.42	0.08
Total	539.04	100.00	539.04	100.00	539.04	100.00

Source: adapted from analysis of Landsat images for the years 2010, 2015, and 2020

Oppositely, the built-up area was expanded in 2015 and inhabited 39.03 km², increasing from 30.63 km² in 2010. In just half a decade (from 2010 to 2015), land-cover change analysis disclosed that built-up areas of Addis Ababa disclosed a persistent increase (8% every five years), as shown in *Figure 3*. It is well known that increased demand for urbanization is likely to impact urban and rural marginal areas. Cities worldwide are randomly expanding, depleting arable land in the peri-urban areas, reducing their economic prospects, and hampering positive growth (Wegedie, 2018; Wubie et al., 2021). This is the primary reason for the ongoing construction of commercial and residential buildings for various community activities while ignoring the importance of agricultural benefits to the community itself. Another study shows that the continued growth in urban area coverage is due to clearing farmland for the planting season and its clarification through clearing arable land to pave the way for urban developments, especially governmental bodies, housing, and infrastructure (Addis, 2020).

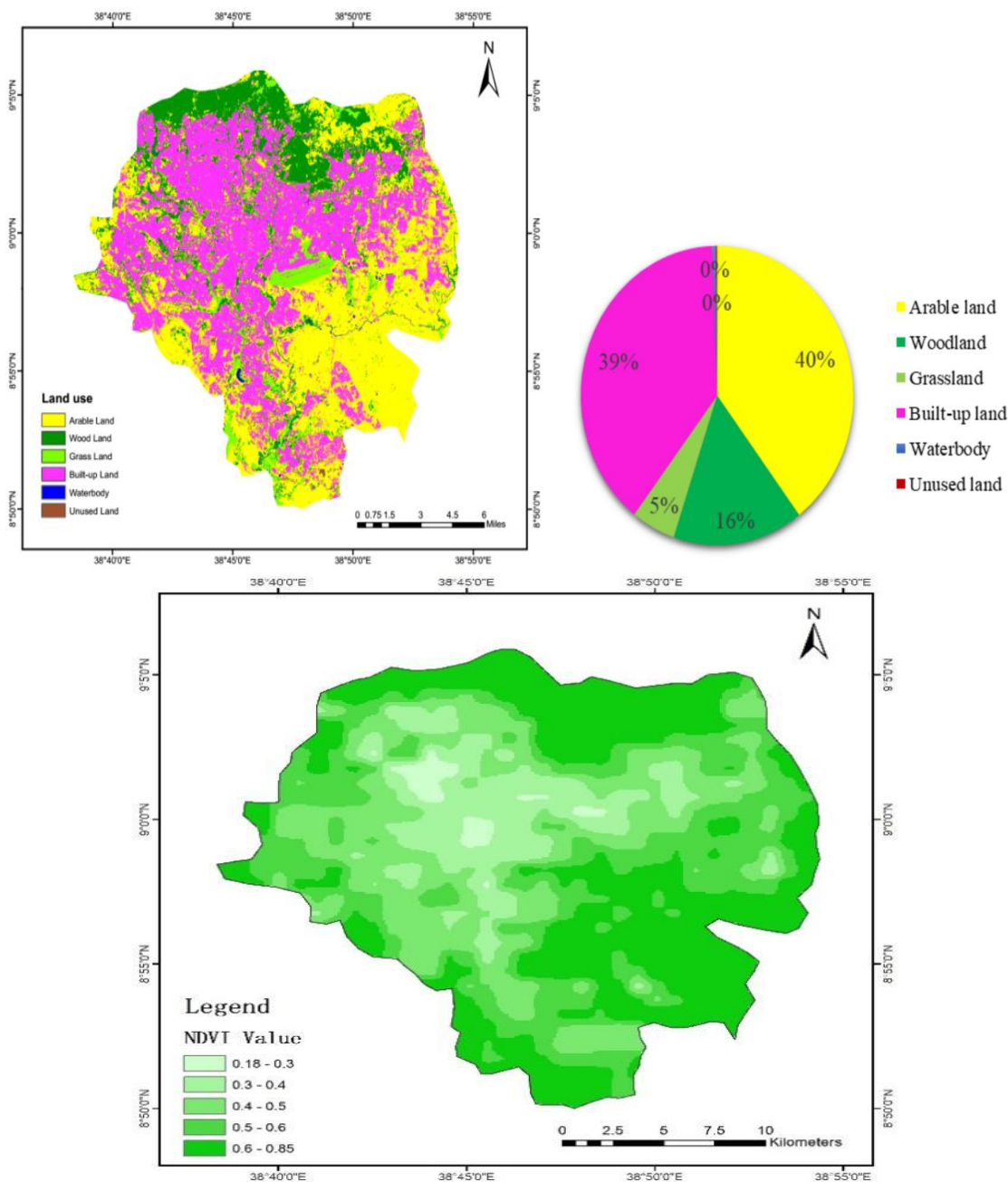


Figure 3. Land-use and land-cover map for 2015. Normalized difference vegetation index (NDVI) of Addis Ababa for 2015. (Source: adapted from Landsat 8-OLI/TIRS image for 2015)

Interestingly, the area covered by Woodlands did not change much between 2010 and 2015, occupying 85.52% and 83.29 km², respectively. A similar situation occurred in grasslands that inhabited 30.02 km² in 2010 and 28.18 km² in 2015. This means that the percentages of Woodlands and grasslands decreased by only about 1% each in five years. The water bodies and unused lands remained less than 0.5% in the study period, indicating the minimal impact on the agricultural use-land intensity. *Figure 3* exhibits the spatial distribution of land uses in Addis Ababa in 2015. As seen from the LULC map (*Fig. 3*), there is no doubt that the built-up land has increased compared to 2010. It is scattered in the east, southeast, and west of the study area.

In 2020, the area covered by arable land had shrunk further from 214.12 km² (39.72% of the total study area) to 191.15 km² (35.46% of the entire study area). In contrast, built-up land had broadened, reaching 251.29 km², gaining more than 40 km² of land in just five years, 47% of the land area in the study area. This points out that the bulk of urban extension took place in the town's center and areas surrounding the city (on the fringes), as shown in *Figure 4* (see the purple scattering). Unexpectedly, the area covered by Woodlands shrank by about 10% compared to the percentage was in 2015 when it covered 83.29 km² and decreased to 71.62 km² in 2020. The aforementioned urban expansion also directly impacted the area under the Grassland, where it declined to about 22.64 km² compared to 28.18 km² in 2015. Moreover, the areas under water bodies and unused lands continue dropping their shares to less than 0.36% and 0.08%, respectively. The spatial distribution of the LULC map in 2020 is shown in *Figure 3*.

By taking a closer look at *Figure 4*, we can note that the area covered by arable land was on the descent. Between 2010 and 2015 exhibits a minimal descent in area coverage of arable land where it inhabited 255.15 and 214.12 km², respectively, a descent of 41.03 km². This trend was strong between 2015 and 2020, in which arable land further dropped, to an area of 191.15 km² in 2020, a descent of 22.97 km². This urban expansion had swept land used for agriculture, mainly arable land.

In a decade (from 2010 to 2020), the study of LULC change revealed that waterbody areas occupied the least space, less than 0.5%, as shown in *Figures 2, 3, and 4*. Also, during the same period, the area covered by unused land occupied the least area, which is less than 0.15% each year. Even worse, the statistics demonstrate decreasing trends in both classes. This implies that Addis Ababa has no areas naturally wasted by waterbody or unused land. Nevertheless, the urban extension could be the biggest threat to agricultural land-use intensity as it shows a continuous occupation of approximately 8% of the agricultural land every five years.

Assessment of the classification accuracy

The classification of remotely sensed images cannot be 100% accurate. Land-cover maps are classified from images remotely sensed by imaging satellites. Thus, they usually include some errors. Therefore, it is necessary to identify these errors to ensure the reliability and user-friendly land-cover maps. As the accuracy governs the obtained classification results, it must be evaluated. After the classified image is inserted in the GIS, it plays the role of a fundamental source of information for both researchers and urban planners. The standard confusion matrix helped assess the classification accuracy of a classified map. After calculating the elements of this confusion matrix by Equation, *Table 3* illustrates the accuracy assessment of this study. Then, the Kappa coefficient was calculated to measure the difference between the actual agreement and the change agreement, as shown in *Table 4*. The assessment suggests that the accuracy of our classification was acceptable.

Rates and trends analysis for land-cover and land-use intensity

Understanding general trends of LULC classes is a necessary part of the decision-making process for agricultural land-use intensity. The change in spatial trend is affected by the evolution of the built-up area, which in turn influences all other land classes. The general trends show a sprawling direction of urbanization to the east, southeast, and west. This can be inferred from LULC maps (*Figs. 2, 3, and 4*).

However, for an in-depth analysis, the trends and rates of land-use intensity that occurred in Addis Ababa for each land class in km² and percentage are presented in Table 5.

Table 3. Accuracy and kappa statistics for the classifications

The study year	2010	2015	2020
Overall accuracy (%)	90	88	90.54
Overall kappa coefficient (%)	87.56	84.83	87.96

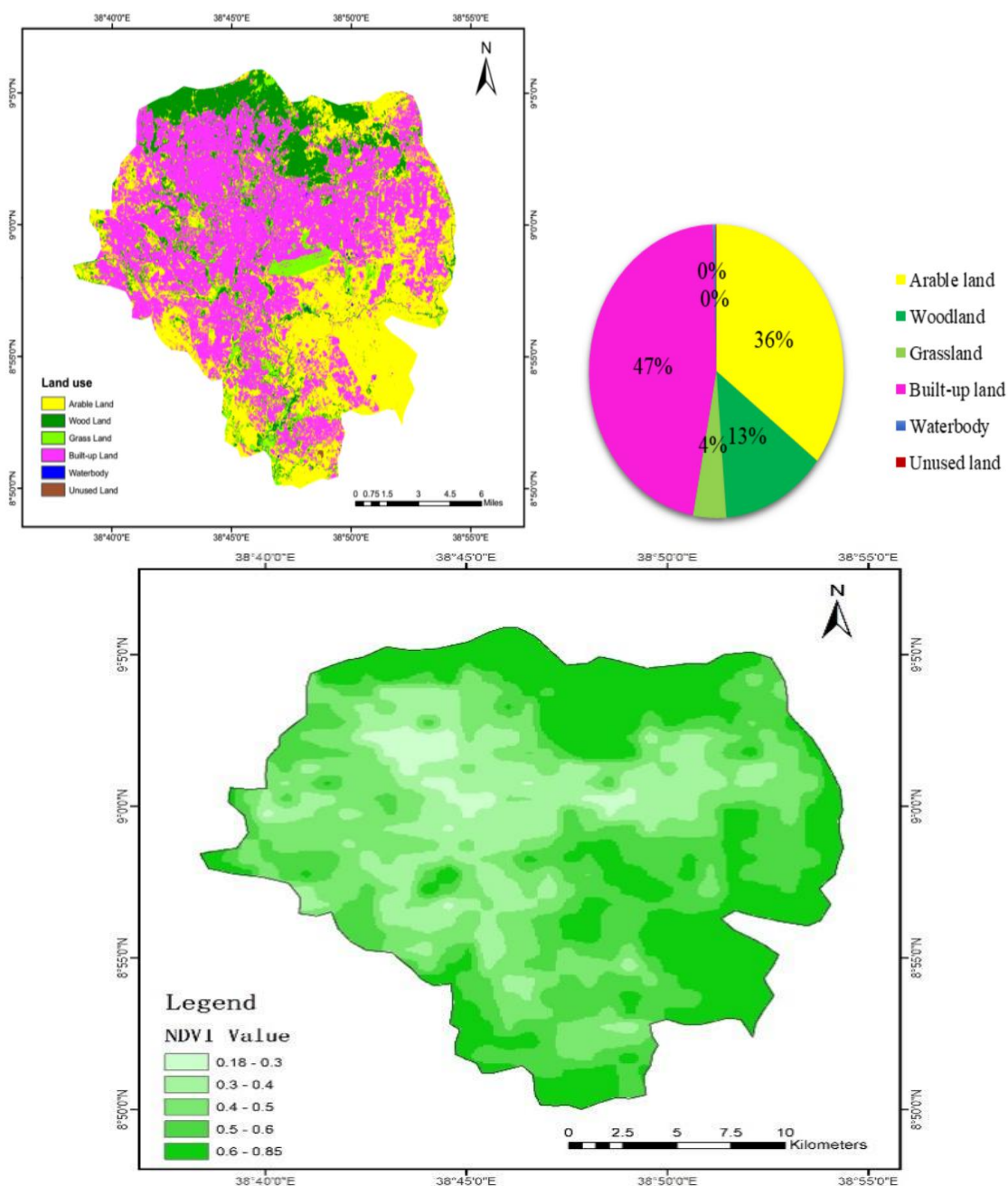


Figure 4. Land-use and land-cover map for 2020. Normalized difference vegetation index (NDVI) of Addis Ababa for 2020. (Source: adapted from Landsat 8-OLI/TIRS image for 2020)

Table 4. Producer and user accuracy for individual LULC classes

Year	2010 (%)		2015 (%)		2020 (%)	
	Producer accuracy	User accuracy	Producer accuracy	User accuracy	Producer accuracy	User accuracy
Arable land	90	86	85	80.95	95.00	79.17
Wood land	100	83	100	88.24	100.00	93.75
Grass land	100	91	100	83.33	80.00	88.89
Built-up land	85	94	80	94.12	89.47	100.00
Water-body	70	100	80	100.00	80.00	100.00
Unused land	100	100	80	100.00	80.00	100.00

As shown in *Table 5*, all land classes have experienced massive land loss except for the built-up class. The results demonstrate that significant changes have occurred in the land-use and land-cover intensity over the past decade (between 2010 and 2020). Surprisingly, areas under agricultural land (arable land, woodland, and grassland) show a constant area loss, where they decreased by -25% (-64 km²), -16% (-13 km²), and -24% (-7.38 km²) at an annual rate of -6.4 km², -1.39 km², and -0.738 km²/year, respectively. This is a clear sign that farmland is trending downward. In contrast, the built-up land increased by more than twice its area in just a decade, where it rose by +52.17% (+86.16 km²) at an annual rate of +8.616 km² per year. For this study period (2010-2020), the capital city's experienced significant land-use changes. Converting about 65% of agricultural land to other uses within ten years could seriously threaten agricultural land-use intensity. Although the water body and unused land usually cover small areas in Addis Ababa, their area sizes have also decreased significantly during these ten years due to the aggressive effect of urbanization. Thus, we can notice that the water body and unused land have lost -18.6% and -51.72%, respectively. This trend corresponds to the trend mentioned above, which indicates a significant downtrend.

By comparing the two study periods (2010-2015) and (2015-2020), the results indicate that in the first period, arable land demonstrated a more significant decline than in the following five-year period, where 16% (41.03 km²) of the areas covered by arable land have been converted to urbanization activities (see *Table 5*). On the other hand, the urban area expanded by 9% (45.27 km²) in the first period of the study and 8.18% (40.89 km²) in the second period.

Table 5. Trends and rates in land classes for three time periods of 2010, 2015 and 2020

Period	2010 to 2015			2015 to 2020			2010 to 2020		
	Annual rate of change in (km ²)	Change in percentage (%)	Change in (km ²)	Annual rate of change in (km ²)	Change in percentage (%)	Change in (km ²)	Annual rate of change in (km ²)	Percentage (%)	Change in (km ²)
Arable land	-41.03	-8.206	-16.0807	-22.97	-4.594	-10.7276	-64.00	-6.4	-25.0833
Woodland	-2.23	-0.446	-2.60758	-11.67	-2.334	-14.0113	-13.90	-1.39	-16.2535
Grassland	-1.84	-0.368	-6.12925	-5.54	-1.108	-19.6593	-7.38	-0.738	-24.5836
Built-up land	+45.27	+9.054	27.41476	+40.89	+8.178	+19.43441	+86.16	+8.616	+52.17707
Water-body	-0.04	-0.008	-1.70213	-0.39	-0.078	-16.8831	-0.43	-0.043	-18.2979
Unused land	-0.13	-0.026	-14.9425	-0.32	-0.064	-43.2432	-0.45	-0.045	-51.7241

Source: adapted from analysis of Landsat images for the years 2010, 2015, and 2020
 The positive sign (+) indicates an increase in the areal range. The negative sign (-) indicates a decrease in the areal range

Volume and rate of built-up area expansion (2010-2020)

Since the results of the spatiotemporal analysis indicated urbanization as the main issue facing agricultural land, it is vital to analyze the volume and rate of built-up land. In this subsection, we compared the built-up area in the study period of 10 years from 2010 to 2020 to identify the changes (expansion amounts) that were taking place (Fig. 5 and Table 6). The time interval between 2010 and 2015 revealed that the city's urban sprawl was 45.27 km², representing an expansion of 27.144%, and the annual growth rate was also 9.045% per year (Table 6). In the following period (2015-2020), the results of the classified images demonstrated that the area covered by built buildings continued to expand to reach 40.89 km², which represented an expansion of 19.434%, and the annual growth rate was also 8.178% per year. These findings draw attention to Addis Ababa's rapid growth in built-up land, diminishing other lands and agricultural land in particular.

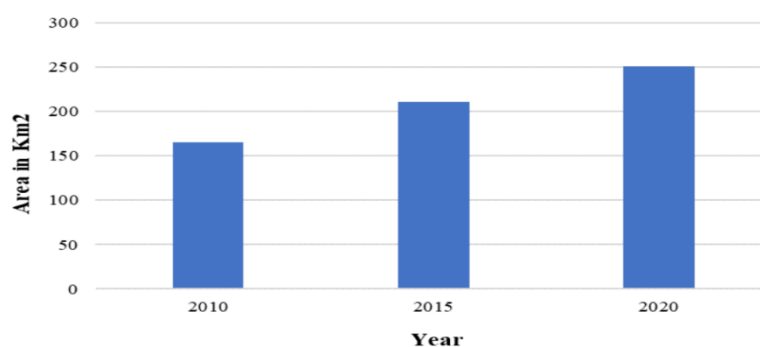


Figure 5. Addis Ababa built-up area expansion (2010, 2015, and 2020). (Source: author's analysis)

Table 6. Volume and rate of built-up area expansion in Addis Ababa (2010-2020)

Study period	Built-up area in (km ²)	Expansion (km ²)	Expansion (%)	Annual rate of growth (ha)
2010	165.13	0	0	0
2015	210.4	45.27	27.414	9.045
2020	251.29	40.89	19.434	8.178

Change detection analysis

To understand the agricultural land-use intensity, we have to successfully analyze land-use change detection, which identifies, describes, and quantifies differences between images of the same scene under different circumstances or times. One of these circumstances and arguably the most influential is the time difference, which can cause scenes from the same region to appear differently. Therefore, a multi-date post-classification comparison change detection was performed to investigate the land-cover change in the study area from 2010 to 2020. Six classes were identified through the supervised approaches of classification; Arable land, Woodland, Grassland, Built-up land, Water-body, and Unused land.

The outcomes of classifications in 2010, 2015, and 2020 were used as inputs to calculate the land transition matrix (Tables 6, 7, and 8). Note that the land covers is not

separated from any change were the ground covers, which changed by comparing the three thematic layers. It was observed that the same types of land cover for the three specified study periods did not change, while different types of land cover did. Thus, this change detection analysis generated a change in each of the six land classes.

It is worth noting that the area of each land-cover classification for the previous year (e.g., 2010) will be subtracted from the following year (e.g., 2015) to calculate the thematic change detection for that period (between 2010 to 2015). The diagonal values highlighted in grey from the cross-tabulation matrix (Tables 7, 8, and 9) demonstrate land cover and land use that did not change in the corresponding years.

Table 7. Land-cover/land-use transition matrix (km²) from 2010 to 2015

	2015							
	Class	Arable land	Woodland	Grassland	Built-up land	Water-body	Unused land	Grand total
2010	Arable land	209.2933	1.477761	0.223469	43.98759	0.068333	0.016897	255.147
	Woodland	1.600387	80.16911	0.091318	3.587176	0.02334	0.023112	85.521
	Grassland	0.68103	0.614046	27.69732	0.852138	0.172062	0.00311	30.024
	Built-up land	1.688013	0.353432	0.040076	163.0335	0.003272	0.000563	165.125
	Water-body	0.159222	0.079417	0.026063	0.045111	2.040997	4.03E-05	2.3514
	Unused land	0.15264	0.023778	0.001561	0.023724	0	0.671346	0.8731
	Grand total	213.6429	82.73841	28.08296	211.5345	2.308308	0.715084	539.042
	Total change	-41.5042	-2.78289	-1.94124	46.4096	-0.04309	-0.158	

Source: Landsat maps of 2010 and 2015

Table 8. Land-cover/land-use transition matrix (km²) from 2015 to 2020

	2020							
	Class	Arable land	Woodland	Grassland	Built-up land	Waterbody	Unused land	Grand total
2015	Arable land	183.124	1.08749	0.06417	29.196	0.05146	0.0511	213.643
	Woodland	1.18633	68.2305	0.02096	13.2389	0.01537	0.02547	82.7384
	Grassland	2.85877	1.56607	22.4246	1.15454	0.07469	0.00118	28.0829
	Built-up land	3.3727	0.48386	0.07065	207.6	0.00154	0.00022	211.535
	Water-body	0.30143	0.19402	0.04214	0.07633	1.69409	0	2.3083
	Unused land	0.22739	0.03891	0.01134	0.09171	0.0016	0.34413	0.71508
	Grand total	191.149	71.6245	22.6373	251.37	1.8393	0.4221	539.042
	Total change	-22.494	-11.114	-5.4457	39.8355	-0.469	-0.293	

Source: Landsat maps of 2015 and 2020

Table 9. Land-cover/land-use transition matrix (km²) from 2010 to 2020

	2020							
	Class	Arable land	Woodland	Grassland	Built-up land	Water-body	Unused land	Grand total
2010	Arable land	187.2446	0	0	67.8563	0	0.0462	255.1471
	Woodland	0.0083	69.345	0.0002	16.1477	0	0.0201	85.5213
	Grassland	3.2255	2.0235	22.555	2.0423	0.1766	0.0013	30.0242
	Built-up land	0	0	0.0369	165.088	0	0	165.1249
	Water-body	0.3275	0.2113	0.0333	0.1182	1.6611	0	2.3514
	Unused land	0.3429	0.0447	0.0119	0.1175	0.0016	0.3545	0.8731
	Grand total	191.1488	71.6245	22.6373	251.37	1.8393	0.4221	539.042
	Total change	-63.9983	-13.8968	-7.3869	86.2451	-0.5121	-0.451	

Source: Landsat maps of 2010 and 2020

By looking at *Table 7*, from the area of 255.14 km² that was recognized for arable land in 2010, only 209.19 km² remained unchanged. There was a significant change in 2015 for built-up land of about 43.60 km². Also, 1.478 km² of arable land has been changed to Woodland. The rest of the changes for this class are insignificant, where each of the Grassland, Water-body, and Unused land have gained less than 0.25 km² from arable land. The Woodland areas exhibited moderate change, with about 3.59 km² out of 85.52 km² converted to built-up land as the largest change, and only 1.6 km² of the same classification changed to arable land. At the same time, the rest of the classes have shown minimal gain from this class. Grassland class did not demonstrate any significant changes, where it lost less than 2.4 km², distributed among the other categories.

Interestingly, about 99% of the built-up land remained unchanged from 2010 to 2015, where 163.033 km² out of 165.124 km² were untouched. However, it was constantly increasing by occupying areas from every other land class. Waterbody and Unused land also experienced some changes, where they got converted into other land classes, 0.16 km² and 0.15 km² were converted to arable land, respectively. Although these were the only changes in which arable land exceeded the proportion of land converted by built-up land at the same time slot, they were minor and insignificant.

For the second period (2015-2020), arable land showed a similar trend in changes as the previous period (2010-2025), in which built lands took the largest share of arable land (more than 29 km²). This represents about 96% of the area lost in arable land because it lost 30.51 km² in total (183.124 out of 213.643 km² was unchanged), as presented in *Table 8*. Woodland did not seem to agree with similar trends, showing decisive changes compared to its previous five years. From an area of 82.73 km² recognized as Woodland in 2015, 68.23 km² remained unchanged, losing more than 13 km² in 2020 for built-up land. The Grassland class also encountered more significant changes than in its previous period. However, the most substantial part of the land lost was converted to other agricultural uses (2.86 km² for arable land and 1.7 km² for Woodland). Again, unsurprisingly, built-up land preserved its area unchanged, 207.6 km² out of 211.53 km² has not seen a change, and 3.37 km² (about 85%) of the area was lost by built-up land went for arable land. Although this change was insignificant, it is the largest area of arable land obtained from other lands, indicating the most significant change in positive agricultural land-use intensity during these five years.

For the entire period under the area studied (2010-2020), it is evident that the area covered by agricultural uses, especially arable land, is gradually dwindling through other land uses, mainly through the aggressive encroachment of built-up land (*Table 9*). We can notice that of 255.1471 km² of cultivable land in 2010, 167.8563 km² were converted to built-up land, apparently to prepare and equip for the built-up area (*Table 9*). At the same time, zero km² of arable land was converted to Woodland and Grassland. In addition, Woodland was converted to arable land, but only 0.0083 km² supported this purpose, while 16.147 km² was converted to buildings, proving the loss of agricultural land for non-recoverable uses. Moreover, the built-up area was maintained without a change in these ten years, of which 165.1249 out of 165.088 km² remained unchanged. From *Tables 7, 8, and 9*, it can be concluded that the findings demonstrate that substantial areas that were under agricultural use have been converted to urban activities.

Table 10 presents the LULC factors that contributed to the continuing expansion in the built-up area. According to land-cover/land-use change statistics, between 2010 and 2015, 43.987 km² (90.7% of total conversion) of arable land, 7.397 km² of Woodland, and 1.757 km² of Grassland were converted to built-up area. Between 2015 and 2020, the total amount of agricultural land taken by urbanization was not much different from the previous period, 48.49 versus 43.75 km². However, Woodland in 2020 lost area nearly twice as much as it was in 2015 for built-up areas, 13.24 versus 7.39 km², respectively. Also, 78.65% and 18.71% of the arable land and Woodland were converted to urban activities in just ten years. The change detection results (post-classification comparison) conclude that cultivable land is facing a severe decline due to urbanization. A total of 86.282 km² of farmland land has been converted for buildings and construction uses within a decade (*Table 10*). The consequence of these aggressive and rapid changes in land use is a steep descent in the area belonging to agricultural land.

Table 10. Land-cover/land-use class conversion to built-up area in km²

Land use/land cover	2010-2015		2015-2020		2010-2020	
	Area (km ²)	Area (%)	Area (km ²)	Area (%)	Area (km ²)	Area (%)
Arable land to built-up	43.987	90.704	29.196	66.72	67.8563	78.65
Woodland to built-up	3.587	7.3969	13.238	30.25	16.1477	18.71
Grassland to built-up	0.8521	1.75714	1.154	2.63	2.0423	2.367
Water-body to built-up	0.0451	0.09302	0.076	0.17	0.1182	0.137
Unused land to built-up	0.0237	0.0489	0.092	0.21	0.1175	0.136
Total	48.49	100	43.75	100	86.282	100

Source: adapted from analysis of Landsat images of 2010, 2015, and 2020

Discussion

Urban development, which is defined as the spatial expansion of an urban area on the outskirts, and urban sprawl, which is defined as scattered and uneven development on non-urban land (i.e., new lots) leading to land fragmentation, are both included in the growth of the built land cover in this context. The built-up land cover increased significantly across the country during the study period. Because population expansion has a significant impact on the need for food and fiber, settlements, water, forests, and other natural resources, successful sustainable development programs must be multi-faceted and interconnected. The city also must foster empowered government institutions.

Based on the literature, inadequate execution of existing regulations has been identified as a concern in managing Addis Ababa's resources. Government agencies must have the authority to implement current laws efficiently. In addition, if required, legislation should be amended in conjunction with stakeholders to accommodate evolving demands. Where stakeholder involvement is inadequate, new policies should be designed using stakeholder input. The built-up land cover is now dominant, and it is anticipated to become much more so in locations where population expansion is expected. Hence, the need for better land-use planning in urban areas cannot be overlooked. According to popular views, land use planning in Addis Ababa looks to be broken. It is embroiled in a slew of problems and hence is not performing as expected.

The most pressing issues are poor implementation of legal restrictions, customary land tenure, citizen disengagement in the planning process, and institutional bottlenecks. In Addis Ababa, ensuring the independence of land management organizations can assist streamline policy difficulties, reduce duplication and conflicting tasks, and improve the long-term sustainability of urban regions.

Touching on the current urban development policies regarding agricultural land-use intensity, it is clear that many nations have conducted research and assessments of their land sectors' performance in the last two decades and developed new reform strategies. Algeria, Libya, Egypt, and Tunisia are examples of North African countries; Benin, Mali, Niger, and Ghana are examples of West African countries; Burkina Faso is an example of Central Africa; Rwanda and Tanzania are examples of East African countries; and Botswana, Malawi, Mozambique, Namibia, South Africa, Zambia, and Zimbabwe are examples of Southern African countries (Southern Africa). Mauritania (North Africa); Sierra Leone and Liberia (West Africa); Angola, Lesotho, Madagascar, and Swaziland (Southern Africa); and Kenya, Southern Sudan, and Uganda (East Africa) are among the nations actively reviewing their land policies. Although many countries not mentioned here have not conducted comprehensive or systematic reviews in the last two decades, they have undertaken significant reforms or enacted land laws that reflect their overall policy priorities in their various land sectors. As a result, there is little question that an evaluation of policy problems in the land sector is required to guide land-related legislation or institution-building throughout Africa. The following vision statement proposes a set of boundaries based on developing best practices, within which new or revised land policies, legislation, and institutions should be developed comprehensively and methodically.

Apart from agriculture, land plays an important role in Africa's economy by contributing to other industries and employment. South Africa, Mauritius, Kenya, Egypt, Tunisia, and Morocco have diversified their economies to include tourism, manufacturing, and services. In contrast, Sudan, Angola, Libya, and the Democratic Republic of the Congo have become increasingly reliant on oil and mineral earnings. Nature conservancies and woods account for a significant amount of land in other nations such as Zimbabwe, Namibia, and Botswana.

The implications of urbanization due to massive demographic dynamics and artificial built-up conurbation are enormous. In fact, urban regions account for the least percentage of overall land usage of any location. It accounts for approximately 11% of the region's general area. However, environmental consequences are linked to the magnitude of land conversion and the kind of land lost to urban areas. The growth of Addis Ababa has resulted in the loss of a substantial quantity of agricultural and forest areas. This form of settlement consequently utilizes natural resources greater than their regeneration rate.

On the other hand, the rapid rise of the built environment, or impermeable surfaces, drastically alters the area's relative land surface temperature compared to the hinterlands. It may also have an impact on the area's hydrological features. Such urban-related activities produce a variety of by-products that degrade the city's environmental quality and its environs. About 63% of the land in the planning region is dedicated to the street network, transportation, housing, infrastructure, and other built-ups, which emit massive amounts of undesired contaminants into the natural system.

The study region's current and anticipated LULC dynamics are marked by growing urbanization at the expense of ecologically significant green zones. This high built-up

expansion also contradicts population dynamics, as seen by the disparity between population and built-up densities per unit area. The population density of the region is decreasing with time in comparison to the built-up density. The issue may be summed up by the tendency of suburbanization, which develops larger conurbations in neighboring districts and small towns, resulting in haphazard land development congestion and mobility/transport issues. As a result of these processes, the region became dispersed, resulting in new neighbourhoods and isolated properties in the hinterlands, as well as uncontrolled built-up growth fragmenting different ecosystems, resulting in the degradation of important mountain forest landscapes, watershed, and riparian ecosystems, and a significant loss of prime cultivated land.

Although the African continent is still in the early phases of urbanization, with just 38% of the population living in cities, the pace of change in this transition is ongoing. It will continue to be the greatest in the world for several decades. By 2050, half of Africa's population, or at least 1.2 billion people, will be living in cities, accounting for a quarter of the global urban population. Much of this expansion will be seen in Africa's capital cities, which frequently house more than 10% of the urban population of most nations. Although the extent of urbanization will continue to vary by country, with South Africa, Zambia, Mauritius, Gabon, and Egypt already having between 40 and 58% of their total population in urban areas and others having less than 20%, urbanization in Africa is still primarily driven by large-scale migration from the countryside as a result of a variety of factors including poverty, famine, drought, disaster, conflict, and the general pessimism. However, it is vital to remember that African urbanization will continue to be defined by informal settlement developments, which already house over 60% of urban dwellers. This tendency will exacerbate inequalities in access to development resources in these places. This feature directly influences social and economic stability, particularly in capital cities, which are significant economic forces.

In terms of the region's spatial characteristics, the following main aspects could be expressed:

- In terms of location, the region has undergone several geological processes that have shaped the current environment, giving Addis Ababa and the surrounding area a moderate temperate temperature with a diversified flora cover, abundant groundwater, and fertile soil.
- Economically, the region is attracting more demand from the rest of the country. Addis Ababa, for example, accounts for approximately half of the country's GDP.
- By coincidence, the city is the country's first cultural destination. There are also government offices and buildings; the country's overall culture is represented and designated as the nation's cosmopolitan metropolis.

Africa is experiencing increasing urbanization creates unique issues that necessitate rigorous local planning, housing (or shelter), and service delivery. As a result, a key goal is to work toward interventions that include, among other things, the provision of affordable and legally secure land and housing (or shelter) rights, as well as access to complimentary services such as water and electricity, in well-planned communities, regardless of tenure or structure status. This will encompass a variety of interventions aimed at responding to the diverse nature of African urban settlements, rationalizing public sector management, lowering entry costs, and improving the overall quality of

life, such as the design of adaptable development control requirements, the implementation of property taxes (where necessary), and proper and socially inclusive urban governance. These actions will be crucial for Addis Ababa and the peri-urban regions, where the most unplanned change occurs, frequently on high-potential agricultural land.

Conclusion

This paper has been conducted to assess and analyze the impact of urbanization expansion on the land-use intensity in Addis Ababa, Ethiopia. Land use in Addis Ababa has changed drastically from agriculture to real estate construction. The rate of the loss of arable land has intensified in the last twelve years because of urbanization, as shown by the NDVI data. This change has resulted in the scarcity of land for farming. This has also affected the farm size. Thus, this research has employed GIS and RS to explore the urban expansion impact on pre-urban land use, especially on agricultural lands. Three Landsat-based imageries of the study area were acquired for 2010, 2015, and 2020 to detect changes in urban LULC in the last ten years. Based on the findings of this study, most of the LULC changes seen throughout the research period appear to be impacted by agricultural operations and urbanization, both of which are bolstered by population expansion. The study also indicated that changes in various land coverings differed during the periods studied. This shows that the driving variables' strength or cumulative influence is also changing. This insight paves the way for a better understanding of the dynamics of these factors and informs more timely responses to unfavorable trends.

The spatiotemporal urban extension analysis concluded that land-use intensity encountered significant changes and trends during the ten years explored in the research. In this study, six land classes were defined: Arable land, Woodland, Grassland, Built-up land, Water-body, and Unused land. Results showed that arable land occupied 47.33% of the entire area in 2010, 39.72% in 2015, and 35.46% in 2020. These clear trends show that 11.87% of cultivable land experienced a conversion to other land uses in just a decade. Meanwhile, the built-up land took the opposite trends, occupying 30.63%, 39.03%, and 46.62% in the same given periods, respectively. These findings indicate that the aggressive and rapid encroachment of built-up land was the primary factor for the sharp decline of farmland in 2020.

Moreover, Post-classification comparison results confirm that agricultural land faces severe degradation due to urbanization. A total of 86.282 km² of farmland land has been converted to built-up land within a decade (see *Table 9*). Cultivable land is the most impacted among all land classes, where 78.65% of the land has been converted into urban or metropolitan areas. Nonetheless, with proper management and planning, government officials at regional and local levels can balance urban development and population growth in Addis Ababa more efficiently and effectively. With the continuous urbanization and the ever-changing population dynamics, further studies are also necessary to explore the effects of urban expansion on land use intensity and agricultural activities in Addis Ababa and other cities in Ethiopia.

Recommendations

The study recommends balancing physical urban and population growth in Addis Ababa through appropriately planned strategies. The authorities can use this research to

understand the change needed, the rate of urban growth, demographic pressure, and the capabilities of the available services. Building a comprehensive GIS database and information systems to sustainably regulate the development of urban areas, especially in Addis Ababa, is also essential to accomplish this objective. Accordingly, supplying the public services and the needed infrastructures to cope with the future urban expansion can be considerably managed. Using satellite imagery with powerful tools for mapping the changes in the urban and pre-urban areas will enable appropriate monitoring and effective urban planning for the city. Consequently, the authorities can control and reduce the unplanned housing and the associated agricultural land loss.

Adaptation of Environmental Impact Assessment strategies for practical urban developments and involving public participation in decision-making will assist in assessing the prospective impacts of urban expansion on the surrounding ecosystems. Since the urban expansion is ignited by the growth of the urban population caused by rural-urban migration, establishing a conducive environment by providing employment opportunities and social services in rural areas will mitigate the rapid population growth of the urban areas. A well-functioning land management system can help address the existing fragmented and haphazard pattern of urban growth. An advanced operating system can also help cities shift to a more compact and vertical development pattern, making urban expansion more sustainable and limiting further engulfment of peri-urban environments. Green areas or green belts, drainage infrastructure, and green technology should be included in this shift.

Acknowledgments. The authors are indebted to thank the National Natural Science Foundation of China (Fund No.72074114), Fundamental Research Funds for the Central Universities (SKYC2019003), and the Ministry of Education of China for financial support and encouragement in conducting this study. We are also grateful to thank the anonymous reviewers for their helpful comments and suggestions on an earlier draft of this manuscript.

REFERENCES

- [1] Addis, T. L. (2020): Environmental sustainability of squatter settlements in Yeka Sub City, Addis Ababa, Ethiopia. – *Journal of Urban Development Studies* 1: 1-19.
- [2] Anees, M. M., Sajjad, S., Joshi, P. K. (2019): Characterizing urban area dynamics in historic city of Kurukshetra, India, using remote sensing and spatial metric tools. – *Geocarto International* 34: 1584-1607.
- [3] Arsiso, B. K., Tsidu, G. M., Stoffberg, G. H., Tadesse, T. (2018): Influence of urbanization-driven land use/cover change on climate: The case of Addis Ababa, Ethiopia. – *Physics and Chemistry of the Earth, Parts A/B/C* 105: 212-223.
- [4] Artmann, M., Kohler, M., Meinel, G., Gan, J., Ioja, I. C. (2019): How smart growth and green infrastructure can mutually support each other. A conceptual framework for compact and green cities. – *Ecological Indicators* 96: 10-22.
- [5] Balogun, I. A., Adeyewa, D. Z., Balogun, A. A., Morakinyo, T. E. (2011): Analysis of urban expansion and land use changes in Akure, Nigeria, using remote sensing and geographic information system (GIS) techniques. – *Journal of Geography and Regional Planning* 4: 533-541.
- [6] Berhanu, M., Raghuvanshi, T. K., Suryabhadgavan, K. (2017): Web-based GIS approach for tourism development in Addis Ababa city, Ethiopia. – *Malays J Remote Sens GIS* 6: 13-25.

- [7] Busho, S. W., Wendimagegn, G. T., Muleta, A. T. (2021): Quantifying spatial patterns of urbanization: growth types, rates, and changes in Addis Ababa City from 1990 to 2020. – *Spatial Information Research* 29(5): 699-713.
- [8] d'Amour, C. B., Reitsma, F., Baiocchi, G., Barthel, S., Güneralp, B., Erb, K. H., Haberl, H., Creutzig, F., Seto, K. C. (2017): Future urban land expansion and implications for global croplands. – *Proceedings of the National Academy of Sciences* 114: 8939-8944.
- [9] Eregata, G. T., Hailu, A., Memirie, S. T., Norheim, O. F. (2019): Measuring progress towards universal health coverage: national and subnational analysis in Ethiopia. – *BMJ Global Health* 4: e001843.
- [10] Fitton, N., Alexander, P., Arnell, N., Bajzelj, B., Calvin, K., Doelman, J., Gerber, J. S., Havlik, P., Hasegawa, T., Herrero, M., others. (2019): The vulnerabilities of agricultural land and food production to future water scarcity. – *Global Environmental Change* 58: 101944.
- [11] Güneralp, B., Reba, M., Hales, B. U., Wentz, E. A., Seto, K. C. (2020): Trends in urban land expansion, density, and land transitions from 1970 to 2010: a global synthesis. – *Environmental Research Letters* 15: 044015.
- [12] Johnson, J. A., Runge, C. F., Senauer, B., Foley, J., Polasky, S. (2014): Global agriculture and carbon trade-offs. – *Proceedings of the National Academy of Sciences* 111: 12342-12347.
- [13] Koroso, N. H., Zevenbergen, J. A., Lengoiboni, M. (2020): Urban land use efficiency in Ethiopia: an assessment of urban land use sustainability in Addis Ababa. – *Land Use Policy* 99: 105081.
- [14] Lamson-Hall, P., Angel, S., DeGroot, D., Martin, R., Tafesse, T. (2019): A new plan for African cities: the Ethiopia urban expansion initiative. – *Urban Studies* 56: 1234-1249.
- [15] Lark, T. J., Spawn, S. A., Bougie, M., Gibbs, H. K. (2020): Cropland expansion in the United States produces marginal yields at high costs to wildlife. – *Nature Communications* 11: 1-11.
- [16] Mohammed, I., Kosa, A., Juhar, N. (2020): Economic linkage between urban development and livelihood of peri-urban farming communities in Ethiopia (policies and practices). – *Agricultural and Food Economics* 8: 1-17.
- [17] Shiferaw, A. (2017): Productive capacity and economic growth in Ethiopia. – United Nations, Department of Economics and Social Affairs, New York.
- [18] Terfa, B. K., Chen, N., Liu, D., Zhang, X., Niyogi, D. (2019): Urban expansion in Ethiopia from 1987 to 2017: Characteristics, spatial patterns, and driving forces. – *Sustainability* 11: 2973.
- [19] Uddin, M., Anjuman, N. (2013): Participatory rural appraisal approaches: an overview and an exemplary application of focus group discussion in climate change adaptation and mitigation strategies. – *International Journal of Agricultural Research, Innovation, and Technology* 3: 72-78.
- [20] Wegedie, K. T. (2018): Communities in peri-urban area of Bahir Dar City Amahara, Ethiopia. – *Communities* 9.
- [21] Wu, W., Zhao, S., Zhu, C., Jiang, J. (2015): A comparative study of urban expansion in Beijing, Tianjin and Shijiazhuang over the past three decades. – *Landscape and Urban Planning* 134: 93-106.
- [22] Wubie, A. M., de Vries, W. T., Alemie, B. K. (2021): Synthesizing the dilemmas and prospects for a peri-urban land use management framework: evidence from Ethiopia. – *Land Use Policy* 100: 105122.
- [23] Xu, G., Dong, T., Cobbinah, P. B., Jiao, L., Sumari, N. S., Chai, B., Liu, Y. (2019): Urban expansion and form changes across African cities with a global outlook: spatiotemporal analysis of urban land densities. – *Journal of Cleaner Production* 224: 802-810.
- [24] Zhang, T. (2001): Community features and urban sprawl: the case of the Chicago metropolitan region. – *Land Use Policy* 18: 221-232.

- [25] Zhong, T., Qian, Z., Huang, X., Zhao, Y., Zhou, Y., Zhao, Z. (2018): Impact of the top-down quota-oriented farmland preservation planning on the change of urban land-use intensity in China. – *Habitat International* 77: 71-79.

EFFECTS OF SOIL PROPERTIES ON THE PERFORMANCE OF BLACK LOCUST (*ROBINIA PSEUDOACACIA*) IN A RECLAMATION AREA

GUO, C. Y.^{1,2*} – ZHANG, J. H.^{1,2} – WU, Y. Z.^{1,2} – CAO, Y. G.³ – QIN, H.⁴

¹*Department of Biological Science and Technology, Jinzhong University, Jinzhong 030619, China*

²*Shanxi Characteristics Plant Resources Application Research Center, Jinzhong University, Jinzhong 030619, China*

³*School of Land Science and Technology, China University of Geosciences, Beijing 100083, China*

⁴*School of Statistics, Shanxi University of Finance and Economics, Taiyuan 030006, China*

**Corresponding author
e-mail: swsgcy@163.com*

(Received 5th Jan 2022; accepted 20th May 2022)

Abstract. In this research, we investigated nine black locust (*Robinia pseudoacacia* L.) plantations in a reclamation area of an opencast coal mine in Shuozhou, Shanxi, China. One hundred individuals of black locust in each of plantations were randomly selected, and variables related to growth and nutritional status were recorded. In addition, soil physiochemical and biological properties were analyzed. Results showed that there were significant differences ($P < 0.05$) in the growth variables and leaf nutrient concentrations of black locust and soil properties among the nine plantations. According to the principal component analysis (PCA), Field moisture capacity, soil water content, number of fungi, urease activity and bulk density were the main soil influencing factors. During the multidimensional scaling (MDS) analysis, soil water content, bulk density, soil fungi and catalase affected the highest values of diameter at breast height (DBH) and top height (H) of black locust, and soil alkaline phosphatase affected crown diameter (CD). There was no significant relationship between death rate (DR) and soil properties. Among the factors, soil water content, soil bulk density and soil fungi had important effects on performance of black locust. Therefore, attention must be paid to the soil water content of black locust plantations in the reclamation area and ensure that each individual plant can absorb necessary water. At the same time, suitable soil bulk density and fungal inoculation may promote black locust's growth. The results will contribute to the cultivation and management of black locust.

Keywords: *ecological rehabilitation, plantation, growth variables, soil characteristics, black locust*

Introduction

Black locust (*Robinia pseudoacacia* L.) is a medium-sized deciduous tree native to subtropical and temperate regions of North America. In the early 17th century, it was introduced to Europe, and at the end of the 19th century, it was introduced to Qingdao, China by Germans (Xun et al., 2014). The applications and studies of black locust vary in different countries. American scientists have carried out several studies on expansion characteristics of black locust and the relationship between biomass and climate, soil conditions, and other external variables (Converse et al., 1995). In Greece and other Mediterranean countries, black locust is used as local auxiliary feed for livestock. Accordingly, cultivation and breeding are the main research topics. In Hungary, black locust is used for its excellent timber quality, and research has mainly focused on genetic

improvement, plantation management, and resource development (Redei et al., 2001). In western and southern Europe, black locust is an important tree species for afforestation; therefore, research has focused mainly on breeding and cultivation modalities. In Bulgaria, black locust is used as the main tree species for revegetation to combat the serious pollution caused by the coal industry (Filcheva et al., 2000). In some other European countries and in South Korea, black locust is considered to be an invasive alien species, and research has mainly focused on the impact of black locust on native species and other ecological effects (Chang-Seok et al., 2003). As black locust has a wide ecological amplitude, fast growth, sand fixation capacity, soil conservation capacity, and notable ability to fix nitrogen, it has been widely planted as a revegetation and afforestation pioneer species in China (Zhao et al., 2018).

We studied black locust plantations in a reclamation area of an opencast coal mine in Shuozhou, Shanxi, China more than 20 years. With the extension of reclamation time, the incidences of shoot blight and tree death in black locust have gradually increased, however, the reasons for these increases are still not well understood. There is a close relationship between plants and soil. On the one hand, plants improve soil structure and fertility. On the other hand, soil provides nutrients and moisture for plants growth, so the growth, productivity, and reproductive capacity of plants are largely determined by soil properties (van der Putten et al., 2013). Although many studies have documented that black locust greatly improves the maturation of reclaimed soil, information about the impact of maturing soil on the performance of this species is lacking. Therefore, the objective of this study was to determine the main soil factors affecting the performance of black locust, providing a scientific basis for vegetation restoration.

Materials and Methods

Study area

The study area is situated in the reclamation area of Antaibao opencast coal mine (39°23'–39°37'N, 112°10'–113°30'E), which is located in Shuozhou, Shanxi, China. This district is located in the northern temperate and belongs to semi-arid continental monsoon climate, including windy weather during the winter and spring. The annual rainfall is 428–449 mm, which mainly falls between June and September; however, the annual evaporation is 1786–2598 mm, which is approximately five times greater than the amount of rainfall. The annual average temperature is 4.8–7.8°C, with extreme maximum and minimum temperatures of 37.9°C and –32.4°C, respectively, and the daily temperature difference is 18–25°C. The frost-free period is between 115 and 130 days. There are northwest winds, with a maximum wind speed of 20 m s⁻¹ and annual average wind of 3.4 m s⁻¹ (Guo et al., 2020). In addition, this district is also on the Loess Plateau and belongs to a typical ecologically fragile area. The vegetation is scattered with low coverage, and the zonal vegetation is steppe ecosystems. The soil type falls between Castanozems and Castano-cinnamon soils. Soil erosion and wind erosion are severe, and gullies have a roughly north-south dendritic distribution, with average cutting depths of 30–50 m, with mostly “V”-shaped channels, forming a typical Loess Plateau landscape. Mining-stripped soil was stacked as dump in the reclamation area, forming a stepped terrain with a platform-slope alternated distribution. The relative height of dump is 100–150 m, with a step height of 20–40 m and a slope angle of more than 30° (Cao et al., 2015). This structure increases the proneness for geological environmental disasters, such as collapse, landslides, and debris flows.

Experimental design

Nine plots of black locust plantations with different altitude, age, and stand density were selected in present study (Table 1, Fig. 1). In each plot, 100 individuals of black locust were randomly selected and several variables related to black locust growth were investigated in August during 2015-2017. Leaves of black locust and soil samples were collected simultaneously. Three parallel studies were performed for the measurements of soil properties and leaf nutrition properties. One-way ANOVA analyzed the significant differences in soil and black locust properties; principal component analysis (PCA) analyzed the main soil properties; multidimensional scaling (MDS) explored the similarities among soil and black locust properties.

Table 1. Basic characteristics of the sample plots. Initial planting conditions: black locust was 1-year-old and 30 cm high

Plot	Vegetation Types	Age (a)	Altitude (m)	Stand Density (per 100 m ²)	Soil Texture	Terrain	Area (ha)	Geographical Location
1	black locust	22	1360	30	sandy loam	platform	0.3	39°27.651'N 112°20.041'E
2	black locust	22	1360	27	sandy loam	platform	0.3	39°27.710'N 112°20.011'E
3	black locust	22	1360	28	sandy loam	platform	0.3	39°27.667'N 112°20.032'E
4	black locust	20	1420	19	sandy loam	platform	0.3	39°27.670'N 112°19.859'E
5	black locust	20	1420	21	sandy loam	platform	0.3	39°27.615'N 112°19.867'E
6	black locust	20	1420	20	sandy loam	platform	0.3	39°27.654'N 112°19.877'E
7	black locust	18	1500	22	sandy loam	platform	0.3	39°27.634'N 112°19.675'E
8	black locust	18	1500	25	sandy loam	platform	0.3	39°27.606'N 112°19.663'E
9	black locust	18	1500	23	sandy loam	platform	0.3	39°27.577'N 112°19.646'E

Physiochemical and biological characterization of the soil

Ten randomly soil subsamples along “S” shape that were collected using an auger at 0–20 cm depths in each plot, mixing them as a soil sample. The samples were put in cloth bags and sent to laboratory for analysis. After removing the roots and plant residues, half of the soil samples were dried in natural air and sieved through a 40-mesh sieve for measuring the chemical properties and the other half of the soil samples were refrigerated at 4°C for measuring the biological properties. Soil physical properties were measured using soil samples collected with cutting rings into the aluminum boxes.

All physiochemical properties were measured using regular methods: soil water content by oven drying method, field moisture content and bulk density by cutting ring method (Rayment and Higgingson, 1992), Soil organic carbon by potassium dichromate oxidation and ferrous sulfate titration, total nitrogen content by the Kjeldahl method (Parkinson and Allen, 1975), available nitrogen by steam distillation (Liu et al., 2019),

available phosphorus by spectrophotometry (Evolution 260 Bio; Thermo Scientific, USA), total phosphorus by colorimetry (Hu et al., 2019), soil pH by portable pH meter (Sartorius PB-21, Germany).



Figure 1. (a) *Robinia pseudoacacia* plantation in plot 1-3. (b) *Robinia pseudoacacia* plantation in plot 4-6. (c) *Robinia pseudoacacia* plantation in plot 7-9

For biological properties, four soil enzymes were measured by spectrophotometry, sucrase activity at 508 nm (Schinner and von Mersi, 1990), urease activity at 660 nm (Kandeler and Gerber, 1988), Polyphenol oxidase activity at 420 nm (Guan, 1986), alkaline phosphatase activity at 412 nm. Catalase activity was determined by potassium permanganate titration method. Spread plate counting method (Mallavarapu et al., 1998) was used for soil microbiological analysis. The following media were used for the culturing of soil microorganisms: bacteria: beef extract-peptone agar medium; fungi: Martin agar medium; actinomycetes: Gause's agar medium; nitrogen-fixing bacteria: Ashbey's nitrogen-free agar medium; denitrifying bacteria: denitrifying bacteria culture medium. The number of colony forming units was determined per 1 g of soil dry matter.

Growth variables and leaf nutritional status

One-hundred black locust trees were chosen randomly in every sample plot of 0.3 ha. For each tree, diameter at breast height (DBH, diameter at 1.3 m), top height (H), crown diameter (CD) and death rate (DR) were recorded. In each plot, healthy leaves were taken randomly from 20 black locust trees in plastic bags for nutritional analysis. The leaves were dried at 80°C for 48 h and milled to a powder. The concentration of leaf C was determined by potassium dichromate oxidation and ferrous sulfate titration, leaf N by sulfuric acid digestion and hydrochloric acid titration (Parkinson and Allen, 1975), leaf P and K by sulfuric acid and peroxide digestion, leaf P by spectrophotometry and leaf K by atomic absorption (PinAAcle 800; PerkinElmer, USA), leaf Ca, Mg, Fe, Mn, Cu, and Zn by dry combustion method (Melgar et al., 2006).

Statistical analysis

Normality of the data was tested by the Kolmogorov-Smirnov and the Brown-Forsythe test for homogeneity of variance. Significant differences in soil and black locust properties among plots were analyzed by one-way ANOVA (F-test). The significance of results at the $P < 0.05$ level was tested using Duncan's test. All results were given as mean \pm standard deviation ($n=3$). In addition, correlations were computed using the Pearson correlation coefficient. The similarities among physicochemical and biological properties of the soil, leaf nutrient concentrations, and growth variables were explored by MDS (Proxscal). These statistical analyses were performed using the SPSS 17.0 statistical package (SPSS Inc., Chicago, IL, USA). Soil physicochemical and biological properties were subjected to PCA using Canoco 4.5 to identify the main soil properties of plots.

Results

Physiochemical and biological properties of the soil

Soil physiochemical and biological properties were significantly ($P < 0.05$) different among nine plots (Table 2). The range of physiochemical properties was wider than those of the biological properties. Available nitrogen ranged from 21.27 in plot 6 to 68.91 mg kg⁻¹ in plot 8. The values of soil organic carbon in different plots varied greatly and ranged from 19.22 to 50.27 g kg⁻¹. Soil water content and bulk density were higher in plot 1 to plot 6 and lower in plot 7 to plot 9, while field moisture capacity was on the contrary, the percentage of which did not exceed 21%. Soil organic carbon, pH, and soil total phosphorus were highest in plot 1 to plot 3 and lowest in plot 7 to plot 9. Available phosphorus and available nitrogen were higher in plot 7 to plot 9, but the lower values of available phosphorus were in plot 1 to plot 3 and available nitrogen was lower in plot 4 to plot 6. Overall, soil enzyme activity and the number of microorganisms were higher in plot 7 to plot 9 and lower in plot 4 to plot 6. However, the number of fungi and catalase and alkaline phosphatase activity were higher in plot 4 to 6, while the number of nitrogen-fixing bacteria and alkaline phosphatase activity were lower in plot 1 to 3.

PCA was applied to the soil physiochemical and biological properties to analyze similarities among the plots and to identify the main properties in each plot (Fig. 2). Most of the soil properties were clearly associated with the first axis that explained 68% of the total variation.

Table 2. Physicochemical and biological properties of the soil in the different plots. Data are shown as the mean \pm SE, $n = 3$. a, b, c, and d indicate that there is a significant difference between the nine plots ($P < 0.05$). Abbreviations: SWC soil water content, FMC field moisture capacity, BD bulk density, SOC soil organic carbon, TP total phosphorus, AP available phosphorus, TN total nitrogen, AN available nitrogen, POP polyphenol oxidase, ALP alkaline phosphatase, ACT actinomycetes, NFB nitrogen-fixing bacteria, DEB denitrifying bacteria

Soil property	Plot								
	1	2	3	4	5	6	7	8	9
SWC (%)	9.25 \pm 0.18b	8.97 \pm 0.46b	9.00 \pm 0.48b	8.77 \pm 0.19b	8.79 \pm 0.20b	9.00 \pm 0.08b	5.26 \pm 0.03a	5.33 \pm 0.05a	5.32 \pm 0.06a
FMC (%)	5.76 \pm 0.21a	5.87 \pm 0.13a	5.63 \pm 0.12a	5.86 \pm 0.22a	5.20 \pm 0.54a	5.25 \pm 0.58a	20.42 \pm 0.80b	20.73 \pm 0.57b	19.81 \pm 0.37b
BD (g cm ⁻³)	1.53 \pm 0.03b	1.53 \pm 0.03b	1.55 \pm 0.01b	1.48 \pm 0.03b	1.56 \pm 0.08b	1.57 \pm 0.06b	1.20 \pm 0.07a	1.25 \pm 0.04a	1.17 \pm 0.05a
pH	8.48 \pm 0.01c	8.49 \pm 0.01c	8.47 \pm 0.00c	8.38 \pm 0.01b	8.37 \pm 0.01b	8.36 \pm 0.01b	8.21 \pm 0.01a	8.22 \pm 0.00a	8.22 \pm 0.01a
SOC (g kg ⁻¹)	49.61 \pm 0.58c	49.83 \pm 0.38c	50.27 \pm 0.22c	28.56 \pm 1.15b	27.46 \pm 0.45b	28.78 \pm 0.99b	19.22 \pm 0.49a	19.64 \pm 0.20a	19.08 \pm 0.39a
TP (g kg ⁻¹)	0.54 \pm 0.01c	0.54 \pm 0.01c	0.55 \pm 0.00c	0.44 \pm 0.00b	0.45 \pm 0.01b	0.43 \pm 0.00b	0.40 \pm 0.01a	0.41 \pm 0.00a	0.42 \pm 0.01a
AP (mg kg ⁻¹)	3.72 \pm 0.03a	3.67 \pm 0.03a	3.69 \pm 0.05a	5.12 \pm 0.05b	5.07 \pm 0.02b	5.13 \pm 0.05b	6.36 \pm 0.08c	6.24 \pm 0.17c	6.17 \pm 0.12c
TN (g kg ⁻¹)	0.73 \pm 0.02c	0.75 \pm 0.01c	0.73 \pm 0.01c	0.38 \pm 0.00a	0.35 \pm 0.01a	0.37 \pm 0.03a	0.52 \pm 0.01b	0.50 \pm 0.01b	0.51 \pm 0.02b
AN (mg kg ⁻¹)	35.54 \pm 1.48b	36.08 \pm 1.08b	34.38 \pm 0.66b	21.80 \pm 0.51a	21.86 \pm 0.47a	21.27 \pm 0.19a	66.80 \pm 1.44c	68.91 \pm 0.76c	67.33 \pm 1.83c
Sucrase (mg g ⁻¹ h ⁻¹)	0.16 \pm 0.00b	0.15 \pm 0.00b	0.16 \pm 0.01b	0.12 \pm 0.00a	0.12 \pm 0.01a	0.11 \pm 0.00a	0.28 \pm 0.00c	0.29 \pm 0.01c	0.28 \pm 0.01c
Urease (mg g ⁻¹ h ⁻¹)	0.08 \pm 0.00b	0.09 \pm 0.01b	0.08 \pm 0.01b	0.07 \pm 0.01a	0.07 \pm 0.00a	0.07 \pm 0.00a	0.15 \pm 0.00c	0.15 \pm 0.00c	0.15 \pm 0.01c
Catalase (mg g ⁻¹ h ⁻¹)	3.83 \pm 0.06b	3.80 \pm 0.04b	3.88 \pm 0.03b	4.11 \pm 0.02b	4.10 \pm 0.02b	4.12 \pm 0.01b	2.66 \pm 0.54a	2.97 \pm 0.31a	2.34 \pm 0.31a
POP (mg g ⁻¹ h ⁻¹)	0.003 \pm 0.01b	0.003 \pm 0.00b	0.002 \pm 0.01b	0.001 \pm 0.02a	0.001 \pm 0.01a	0.001 \pm 0.00a	0.003 \pm 0.01c	0.003 \pm 0.00c	0.003 \pm 0.02c
ALP (mg g ⁻¹ h ⁻¹)	0.03 \pm 0.02a	0.03 \pm 0.00a	0.04 \pm 0.01a	0.06 \pm 0.01bc	0.06 \pm 0.00c	0.06 \pm 0.02c	0.05 \pm 0.02b	0.05 \pm 0.00b	0.05 \pm 0.01b

Bacteria (10 ⁶ cfu g ⁻¹)	6.05±0.10bc	5.92±0.04b	6.03±0.12bc	4.01±0.06a	3.98±0.08a	3.91±0.03a	6.22±0.03c	6.19±0.01c	6.21±0.03c
Fungi (10 ³ cfu g ⁻¹)	13.41±0.19b	13.78±0.18b	13.59±0.32b	13.89±0.05b	13.90±0.04b	13.85±0.02b	7.49±0.19a	7.92±0.24a	7.74±0.37a
ACT (10 ⁴ cfu g ⁻¹)	18.19±0.14b	18.44±0.11bc	18.28±0.21bc	9.95±0.12a	9.91±0.09a	10.05±0.05a	19.51±0.81cd	19.71±0.66d	18.78±0.33bcd
NFB (10 ⁴ cfu g ⁻¹)	13.63±0.55a	14.05±0.25a	13.42±0.39a	18.86±0.56bc	18.23±0.21b	18.81±0.32bc	19.32±0.21bc	19.84±0.55c	19.94±0.47c
DEB (10 ⁴ cfu g ⁻¹)	5.74±0.04abc	5.80±0.02c	5.75±0.05bc	5.66±0.02a	5.69±0.01ab	5.68±0.03ab	6.18±0.01d	6.21±0.02d	6.20±0.02d

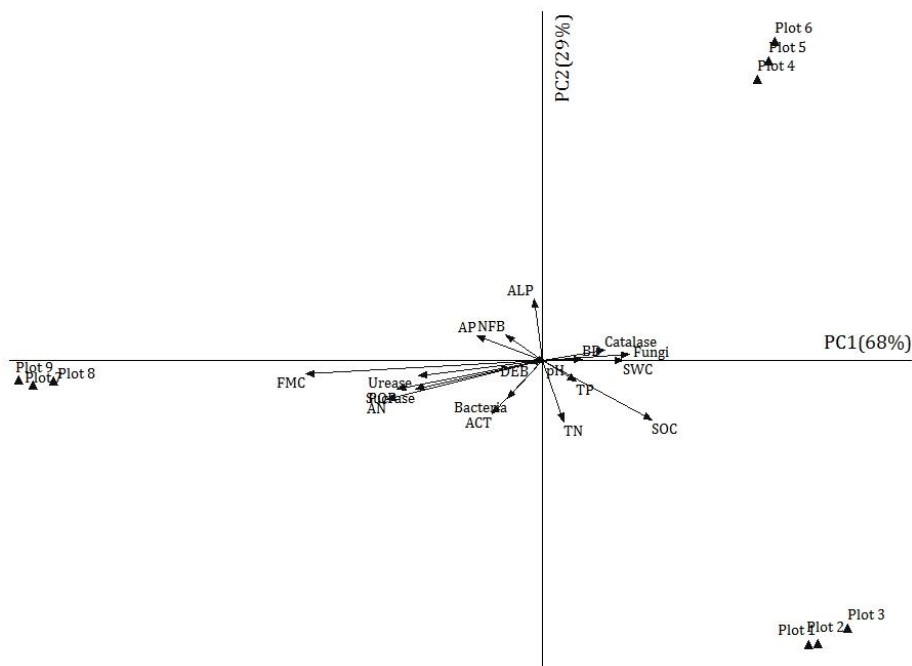


Figure 2. PCA of the physicochemical and biological properties of the soil in the three plots. Abbreviations: SWC soil water content, FMC field moisture capacity, BD bulk density, SOC soil organic carbon, TP total phosphorus, AP available phosphorus, TN total nitrogen, AN available nitrogen, POP polyphenol oxidase, ALP alkaline phosphatase, ACT actinomycetes, NFB nitrogen-fixing bacteria, DEB denitrifying bacteria

The majority of physicochemical properties (bulk density, soil water content, pH, soil organic carbon, and total phosphorus) pointed to the positive side of the axis, and most biological properties (urease, sucrase, polyphenol oxidase, denitrifying bacteria, actinomycetes, bacteria, nitrogen-fixing bacteria) pointed to the negative side, thus showing a clear division: plot 1, plot 2 and plot 3 with high values of physicochemical properties, and plot 7, plot 8, and plot 9 with high values of biological properties. Alkaline phosphatase activity and soil total nitrogen were located close to the second principal component axis, which accounted for 29% of the variance (Table 3). Plot 4, plot 5, and plot 6 were the nearest to alkaline phosphatase, which indicates the soil in these plots have high alkaline phosphatase activity; similarly, plot 1, 2 and 3 was the closest to soil total nitrogen, indicating high total nitrogen content of the soil in these plots.

Growth variables and leaf nutrient concentrations

With the exception of P, there were significant differences in leaf nutrient concentrations ($P < 0.05$) among the nine plots (Table 4). The concentrations of leaf C, N, Fe, Mn, and Zn were higher in plot 7 to 9, but lower in plot 1 to 3. The concentrations of leaf K ranged from 3.39 g kg^{-1} in plot 9 to 11.96 g kg^{-1} in plot 3. The leaf Ca and Mg contents were the highest in plot 6, with 55.92 and 2.97 mg kg^{-1} , respectively. The leaf Cu content ranged from 6.51 mg kg^{-1} in plot 9 to 7.29 mg kg^{-1} in plot 5. The growth variables of black locust were higher in plot 4 to 6, with the highest values of DBH (9.78 cm), CD (13.95 m^2), and H (7.21 m), and the lowest DR (19.11%). Furthermore, the DBH (5.32 cm) and H (4.16 m) were the lowest in plot 8, while the DR (38%) was the highest in plot 1, which showed the lowest value of CD (3.51 m^2).

Table 3. Contribution rate of principal components and scores of variables. Abbreviations: SWC soil water content, FMC field moisture capacity, BD bulk density, SOC soil organic carbon, TP total phosphorus, AP available phosphorus, TN total nitrogen, AN available nitrogen, POP polyphenol oxidase, ALP alkaline phosphatase, ACT actinomycetes, NFB nitrogen-fixing bacteria, DEB denitrifying bacteria

Axis	Eigenvalue	% of variance	Cum.% of variance	Variables	Eigenvector	
					Axis 1	Axis 2
1	12.887	67.828	67.828	FMC	-0.9944	-0.0833
2	5.564	29.287	97.114	SWC	0.9941	-0.0069
				Fungi	0.9936	0.1068
				Urease	-0.9828	-0.1809
				BD	0.9826	0.0548
				DEB	-0.9689	-0.2191
				Catalase	0.9485	0.2333
				Sucrase	-0.9441	-0.3246
				AN	-0.9342	-0.3500
				pH	0.9321	-0.3596
				AP	-0.8674	0.4942
				SOC	0.7690	-0.6381
				POP	-0.7580	-0.2281
				TP	0.7354	-0.6743
				NFB	-0.6791	0.7261
				ACT	-0.5271	-0.8451
				Bacteria	-0.5163	-0.8562
				TN	0.2192	-0.9733
				ALP	-0.0855	0.9853

Table 4. Leaf nutrient concentration and growth variables of black locust in the different plots. Data are shown as the mean \pm SE, $n=3$. a, b, c, and d indicate that there is a significant difference between the nine plots ($P<0.05$)

Plant performance	Plot								
	1	2	3	4	5	6	7	8	9
C (g kg ⁻¹)	448.50±0.02a	448.51±0.01a	448.49±0.01a	450.46±0.01b	450.44±0.02b	450.44±0.02b	460.93±0.02c	460.93±0.02c	460.91±0.01c
N (g kg ⁻¹)	15.56±0.02a	15.50±0.05a	15.51±0.06a	16.23±0.03b	16.15±0.06b	16.16±0.08b	18.63±0.07c	18.44±0.12c	18.49±0.16c
P (g kg ⁻¹)	2.29±0.05	2.26±0.07	2.21±0.03	2.25±0.06	2.19±0.10	2.13±0.06	2.21±0.07	2.22±0.06	2.14±0.03
K (g kg ⁻¹)	11.08±0.30b	11.81±0.77b	11.96±0.66b	4.43±0.02a	4.50±0.05a	4.49±0.06a	3.57±0.06a	3.42±0.16a	3.39±0.14a
Ca (g kg ⁻¹)	48.50±0.50b	48.19±0.72b	47.66±0.35b	55.07±0.63c	55.22±0.75c	55.92±0.29c	46.06±0.12a	45.83±0.28a	45.73±0.21a
Mg (g kg ⁻¹)	2.44±0.03a	2.44±0.02a	2.41±0.01a	2.94±0.03c	2.95±0.02c	2.97±0.01c	2.55±0.04b	2.59±0.01b	2.54±0.03b
Fe (mg kg ⁻¹)	243.33±3.33a	240.00±5.77a	236.67±3.33a	450.00±5.77b	453.33±3.33b	446.67±3.33b	583.33±3.33c	580.00±5.77c	576.67±3.33c
Mn (mg kg ⁻¹)	156.68±0.44a	156.70±0.42a	156.20±0.16a	380.93±0.44b	380.76±0.57b	380.28±0.24b	400.24±0.16c	400.19±0.19c	400.01±0.08c
Cu (mg kg ⁻¹)	6.94±0.03b	6.93±0.03b	6.90±0.01b	7.25±0.02c	7.29±0.01c	7.26±0.05c	6.52±0.02a	6.53±0.02a	6.51±0.01a
Zn (mg kg ⁻¹)	17.36±0.25a	17.37±0.24a	17.09±0.09a	20.02±0.08b	19.85±0.19b	19.79±0.15b	22.27±0.26c	22.19±0.33c	21.90±0.13c
DBH (cm)	6.99±0.10b	6.85±0.21b	6.76±0.14b	9.30±0.16c	9.70±0.42c	9.78±0.36c	5.63±0.15a	5.32±0.26a	5.48±0.15a
CD (m ²)	3.51±0.08a	3.74±0.20a	3.74±0.12a	13.95±1.12b	13.82±1.22b	12.55±0.46b	5.07±0.45a	4.61±0.79a	4.15±0.46a
H (m)	4.84±0.21c	4.92±0.15c	4.68±0.10bc	6.95±0.23d	7.21±0.09d	6.94±0.23d	4.33±0.15abc	4.16±0.27ab	4.18±0.17a
DR (%)	38.00±2.00c	36.00±3.46c	34.00±2.00bc	24.44±1.94ab	19.11±3.64a	20.44±4.64a	19.33±2.91a	25.33±6.96abc	27.33±5.46abc

MDS, which was used to analyze similarities between changes in soil properties, leaf nutrient concentration and growth variables, grouped the variables DBH and H with soil water content, bulk density, soil total phosphorus, total nitrogen, soil fungi and catalase (Fig. 3A,C). Moreover, DBH correlated positively with soil water content ($r=0.737$; $P<0.05$), bulk density ($r=0.714$; $P<0.05$), fungi ($r=0.703$; $P<0.05$) and catalase ($r=0.695$; $P<0.05$), while DBH and H correlated negatively with soil total nitrogen. CD was grouped with soil alkaline phosphatase, leaf Mn, and leaf Fe (Fig. 3B), in addition, CD correlated significantly positively with soil alkaline phosphatase ($r=0.703$; $P<0.05$). DR was grouped with leaf K, soil organic carbon and total nitrogen (Fig. 3D), which were positively related to DR.

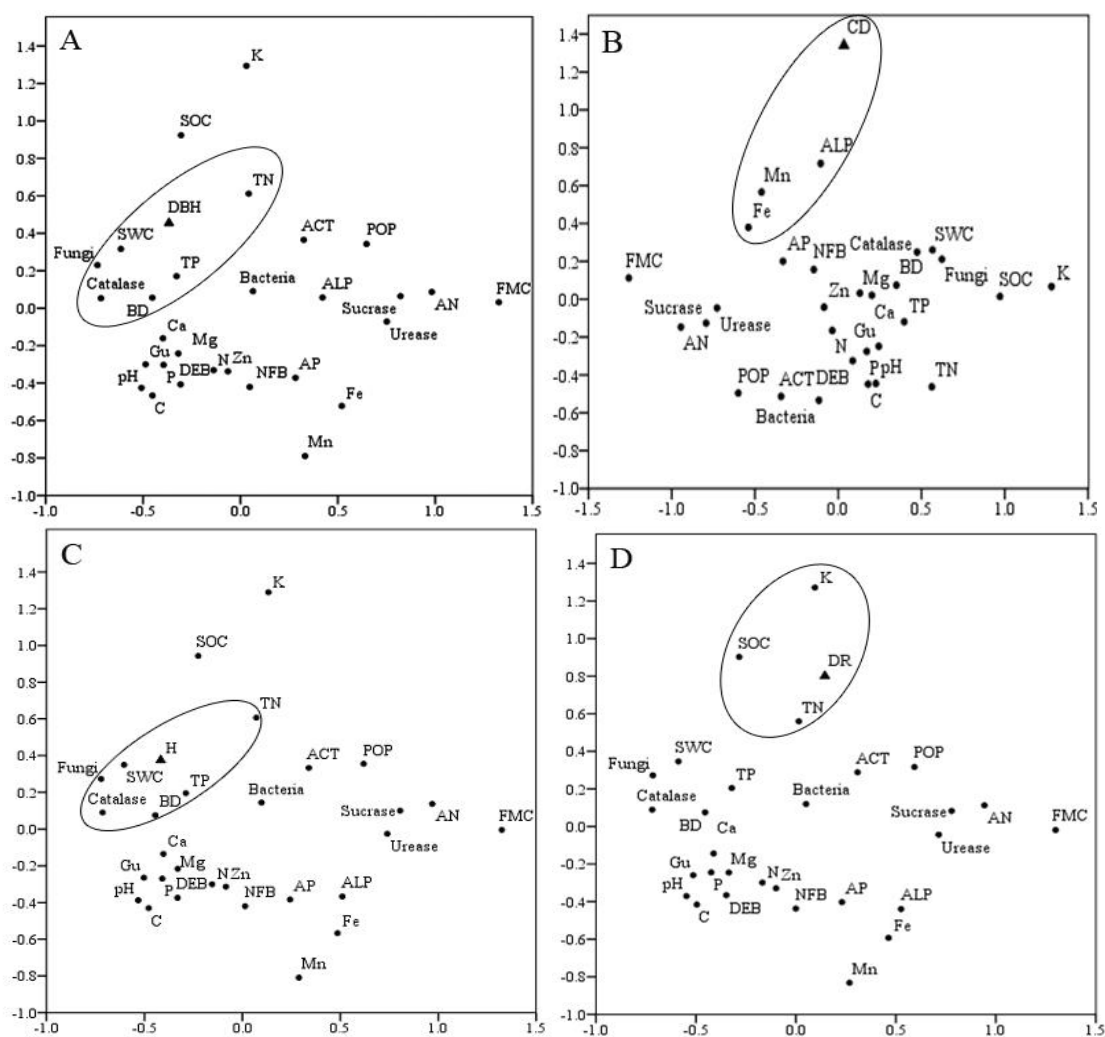


Figure 3. MDS analysis based on similarity matrices between soil physicochemical properties, biological properties, leaf nutrient content, and DBH (A), CD (B), H (C), and DR (D)

Discussion

There were significant differences in soil properties between different plots. In plot 1 to 3, soil water content was higher, which promoted the degradation of organic matter (Berger et al., 2015), and the soil contained higher organic carbon, total nitrogen and total phosphorus. This was related to their higher stand density and more litter. At the same time, the soil bulk density and pH were also higher, which limited the growth of soil microorganisms (Hu et al., 2010), and the soil enzymes involved in minerals decomposition, nutrient transformation and circulation were lower, resulting in lower nutrients that could be directly absorbed by black locust. In plot 7 to 9, higher field moisture capacity, lower soil bulk density and soil pH provided favorable conditions for the growth of soil microorganisms (Shao et al., 2020). Under the action of a large number of soil microorganisms and soil enzymes, soil minerals were well decomposed and transformed (Lanuza et al., 2019), and the soil available phosphorus and available nitrogen contents were higher. However, due to the higher altitude, the soil water content was lower (Sternberg and Shoshany, 2001; Liu and Wang, 2013), which limits the growth of black locust to a certain extent. In plot 4 to 6, the soil organic matter and mineral contents were lower, due to the lower stand density and less litter. Appropriate soil bulk density, water content and pH were beneficial to the growth of soil fungi (Wang et al., 2015), resulting in the higher content of soil catalase and alkaline phosphatase. The nutrient content of leaves also reflected that the soil promoted the growth of black locust.

Soil properties have a significant effect on the growth of black locust (Calvaruso et al., 2011; Vondráčková et al., 2014; Miatto and Batalha, 2016). Soil water content, bulk density, soil fungi and catalase affected DBH and H of black locust. Soil water content influences plants through affecting the transpiration and photosynthesis as well as root growth (Chen et al., 2021), while soil bulk density, indicative of soil tightness, influence on field moisture capacity and soil pores (Lü et al., 2006), thus affects the stretching of plant roots (Wang et al., 2011; Ma et al., 2012). Compared with bacteria or actinomycetes, fungi are more tolerant to adverse environments. Mycelia of fungi loosen the soil structure and improved soil aerobic conditions (Sinegani et al., 2005). Fungi help the root to absorb nutrients, but also improve the tolerance of black locust to non-environmental environmental factors (Jahromi et al., 2008). Catalase is an important enzyme that is activated under stress, which reduces the hazard of black locust from hydrogen peroxide (Keshavarz et al., 2022). The CD was significantly related to alkaline phosphatase activity: a high alkaline phosphatase activity is predominantly due to rich macro vegetation, which is mainly forest vegetation in alkaline soils (Dick et al., 2000; Fierer et al., 2003). There were many factors that caused the death of black locust, and the correlation between mortality and soil factors was not significant. Further research is still to be done.

Conclusion

Evaluation of black locust performance and soil properties in different plots showed that soil water content, soil bulk density and soil fungi had important effects on performance of black locust. Therefore, attention must be paid to soil water content of black locust plantation in the reclamation area and ensure that each individual plant can absorb necessary water. At the same time, suitable soil bulk density and fungal inoculation may promote black locust's growth.

Acknowledgements. The study was supported by the National Natural Science Foundation of China (No. U1810107) and the Natural Science Foundation of Shanxi, China (No. 201701D121123). We thank the members of the Plant Resource and Ecology Laboratory for help with data collection in the field. We thank two anonymous reviewers for valuable comments on the draft manuscript.

Author Contributions. Chunyan Guo planned the experiments, analyzed the data and wrote the manuscript. Jinhua Zhang revised the manuscript. Yuzhen Wu and Yingui Cao completed the soil microorganisms experiment. Hao Qin helped data analysis.

REFERENCES

- [1] Berger, T. W., Duboc, O., Djukic, I., Tatzber, M., Gerzabek, M. H., Zehetner, F. (2015): Decomposition of beech (*Fagus sylvatica*) and pine (*Pinus nigra*) litter along an Alpine elevation gradient: decay and nutrient release. – *Geoderma* 251-252: 92-104.
- [2] Calvaruso, C., N'Dira, V., Turpault, M. P. (2011): Impact of common European tree species and Douglas-fir (*Pseudotsuga menziesii* [Mirb.] Franco) on the physicochemical properties of the rhizosphere. – *Plant Soil* 342: 469-480.
- [3] Cao, Y. G., Wang, J. M., Bai, Z. K., Zhou, W., Zhao, Z. Q. (2015): Differentiation and mechanisms on physical properties of reconstructed soils on open-cast mine dump of loess area. – *Environ. Earth Sci.* 7: 6367-6380.
- [4] Chang-Seok, L., Hyun-Je, C., Hoonbok, Y. (2003): Stand dynamics of introduced black locust (*Robinia pseudoacacia* L.) plantation under different disturbance regimes in Korea. – *Forest Ecol. Manage.* 175: 223-228.
- [5] Chen, W. L., Wang, S. X., Qi, T. X., Jiao, L., Wang, C., Keyimu, M., Li, Z. S., Fu, B. J. (2021): Spatiotemporal dynamics and temporal stability of soil moisture at black locust plantations with different restoration years on hilly region of the loess plateau, China. – *Acta Ecologica Sinica* 41(14): 5643-5657. doi: 10.5846/stxb202008272223.
- [6] Converse, T. E., Betters, D. R. (1995): Biomass yield equations for short rotation black locust plantation in the Central Plains. – *Biomass Bioenerg.* 8: 251-254.
- [7] Dick, W. A., Cheng, L., Wang, P. (2000): Soil acid and alkaline phosphatase activity as pH adjustment indicators. – *Soil Biol. Biochem.* 32: 1915-1919.
- [8] Fierer, N., Schimel, J. P., Holden, P. (2003): Variations in microbial community composition through two soil depth profiles. – *Soil Biol. Biochem.* 35: 167-176.
- [9] Filcheva, E., Noustorova, M., Gentcheva-Kostadinova, S. (2000): Organic accumulation and microbial action in surface coal-mine spoils, Pernik Bulgaria. – *Ecol. Eng.* 15: 1-15.
- [10] Guan, S. Y. (1986): Soil enzyme and the research methods. – Chinese Agricultural Press, China, pp. 248-250.
- [11] Guo, C. Y., Zhang, F., Wang, X., Lu, N. (2020): Effects of meteorology and soil on the herb species diversity in plantations in a reclamation area of coal mine after 6 years. – *Environmental Science and Pollution Research* 27(19): 24231-24241.
- [12] Hu, C. J., Fu, B. J., Liu, G. H., Jin, T. T. (2010): Vegetation patterns influence on soil microbial biomass and functional diversity in a hilly area of the Loess Plateau, China. – *J. Soils Sedim.* 10: 1082-1091.
- [13] Hu, L., Zi, H. B., Wu, P. F., Wang, Y., Lerdau, M., Wu, X. W., Wang, C. T. (2019): Soil bacterial communities in grasslands revegetated using *Elymus nutans* are largely influenced by soil pH and total phosphorus across restoration time. – *Land Degrad Dev.* 30: 2243-2256.
- [14] Jahromi, F., Aroca, R., Porcel, R., Ruiz-Lozano, J. M. (2008): Influence of salinity on the in vitro development of *Glomus intraradices* and on the in vivo physiological and molecular responses of mycorrhizal lettuce plants. – *Microbial Eco.* 55: 45-53. <https://doi.org/10.1007/s00248-007-9249-7>.
- [15] Kandeler, E., Gerber, H. (1988): Short-term assay of soil urease activity using colorimetric determination of ammonium. – *Biol. Fert. Soils.* 6: 68-72.

- [16] Keshavarz, H., Hosseini, S. J., Sedibe, M. M., Achilonu, M. C. (2022): Arbuscular mycorrhizal fungi used to support Iranian barley cultivated on cadmium contaminated soils (*Hordeum vulgare* L.). – *Applied Ecology and Environmental Research* 20(1): 43-53. http://dx.doi.org/10.15666/aeer/2001_043053.
- [17] Lanuza, O., Casanoves, F., Delgado, D. F., Van den Meersche, K. (2019): Leaf litter stoichiometry affects decomposition rates and nutrient dynamics in tropical forests under restoration in Costa Rica. – *Restoration Ecology* 27: 549-558.
- [18] Liu, W. X., Wang, G. (2013): Responses of plant community diversity and soil factors to slope aspect in alpine meadow. – *Chin. J. Ecol.* 32: 259-265.
- [19] Liu, J. N., Neergaard, A. D., Jensen, L. S. (2019): Increased retention of available nitrogen during thermal drying of solids of digested sewage sludge and manure by acid and zeolite addition. – *Waste Management* 100: 306-317.
- [20] Lü, D. Q., Shao, M. A., Liu, C. P. (2006): Effect of bulk density on soil saturated water movement parameters. – *J. Soil Water Conserv.* 20: 154-157.
- [21] Ma, W. W., Wang, B., Wang, Y. S., Wang, H., Zhao, H. R. (2012): Soil properties of meadow wetlands for different altitudes in Gahai of Gannan. – *Acta Agric. Sin.* 20: 44-50.
- [22] Mallavarapu, M., Möhler, I., Krüger, M., Hosseini, M. M., Bartels, F., Timmis, K. N., Holtel, A. (1998): Genetic requirements for the expression of benzylamine dehydrogenase activity in *Pseudomonas putida*. – *FEMS. Microbiol. Lett.* 166: 109-114.
- [23] Melgar, J. C., Benlloch, M., Fernandez-Escobar, R. (2006): Calcium increases sodium exclusion in olive plants. – *Sci. Hort.* 109: 303-305.
- [24] Miatto, R. C., Batalha, M. A. (2016): Leaf chemistry of wood species in the Brazilian cerrado and seasonal forest: response to soil and taxonomy and effects on decomposition rates. – *Plant Ecol.* 217: 1467-1479.
- [25] Parkinson, J. A., Allen, S. E. (1975): A wet oxidation procedure suitable for the determination of nitrogen and mineral. – *Commun Soil Sci. Plant Anal.* 6: 1-11.
- [26] Rayment, G. E., Higgingson, F. R. (1992): *Australian Laboratory Handbook of Soil and Water Chemical Methods*. – Inkata Press, Australia.
- [27] Redei, K., Osváth-Bujtás, Z., Balla, I. (2001): Propagation methods for black locust (*Robinia pseudoacacia* L.) improvement in Hungary. – *J. For. Res.* 12: 215-219.
- [28] Schinner, F., Mersi, W. V. (1990): Xylanase-, CM-cellulase-, and invertase activity in soil: an improved method. – *Soil Biol. Biochem.* 22: 511-515.
- [29] Shao, T. Y., Zhao, J. J., Liu, A. H., Long, X. H., Rengel, Z. (2020): Effects of soil physicochemical properties on microbial communities in different ecological niches in coastal area. – *Appl. Soil. Ecol.* 150: 1-9. <https://doi.org/10.1016/j.apsoil.2019.103486>.
- [30] Sinegani, A. A. S., Emtiazi, G., Hajrasuliha, S., Shariatmadari, H. (2005): Biodegradation of some agricultural residues by fungi in agitated submerged cultures. – *Afr. J. Biotechnol.* 4: 1058-1061.
- [31] Sternberg, M., Shoshany, M. (2001): Influence of slope aspect on Mediterranean woody formations: comparison of a semiarid and an arid site in Israel. – *Ecol. Res.* 16: 335-345.
- [32] van der Putten, W. H., Bardgett, R. D., Bever, J. D., Bezemer, T. M., Casper, B. B., Fukami, T., Kardol, P., Klironomos, J. N., Kulmatiski, A., Schweitzer, J. A., Suding, K. N., Van de Vooorde, T. F. J., Wardle, D. A. (2013): Plant-soil feedbacks: The past, the present and future challenges. – *J. Ecol.* 101(2): 265-276.
- [33] Vondráčková, S., Hejčman, M., Száková, J., Müllerová, V., Tlustoš, P. (2014): Soil chemical properties affect the concentration of elements (N, P, K, Ca, Mg, As, Cd, Cr, Cu, Fe, Mn, Ni, Pb, and Zn) and their distribution between organs of *Rumex obtusifolius*. – *Plant Soil* 379: 231-245.
- [34] Wang, L., Lu, D. Q., Qin, Z. B., Wang, H., Hou, X. L., Liu, X. M. (2011): Review and analysis of soil physical and chemical characteristics on woodland slope in Yuelu Mountain. – *J. Nat. Sci. H. Norm. Univ.* 34: 84-88.

- [35] Wang, J. T., Zheng, Y. M., Hu, H. W., Zhang, L. M., Li, J., He, J. Z. (2015): Soil pH determines the alpha diversity but not beta diversity of soil fungal community along altitude in a typical Tibetan forest ecosystem. – *J. Soils Sediments* 15: 1224-1232.
doi: 10.1007/s11368-015-1070-1.
- [36] Xun, S. H., Qiao, Y. L., Mao, X. H., Kang, Z., Zhang, J. T., Zhang, L. J. (2014): Development on database for species of locust genus (*Robinia*). – *Shandong for Sci. Technol.* 210: 1-8.
- [37] Zhao, J., Nie, Y., Qiao, Z., Ren, Y., Liang, H., Huang, J., Chen, Z., Dong, Y., Qin, L., Xiao, R., Cao, Q. (2018): Preliminary investigation of the relationship between vegetation types and soil microbial flora and biomass in northern Shanxi Province. – *Intl. J. Agric. Biol.* 20: 1695-1700.

DROUGHT-HARDENING IMPROVES FLOODING TOLERANCE OF MAIZE AT SEEDLING STAGE UNDER DROUGHT-FLOOD ABRUPT ALTERNATIONS

LI, C. X.^{1,2*} – HAMANI, A. K. M.¹ – SUN, J. S.^{1,2} – WANG, G. S.^{1,2} – NING, H. F.^{1,2} – LIU, Z. D.^{1,2} – HAN, Q. S.^{1,2}

¹*Institute of Farmland Irrigation of Chinese Academy of Agricultural Sciences, Xinxiang 453002, China*

²*Key Laboratory of Crop Water Use and Regulation, Ministry of Agriculture and Rural Affairs, Xinxiang 453002, China*

**Corresponding author
e-mail: licaixia@caas.cn*

(Received 16th Jan 2022; accepted 10th Jun 2022)

Abstract. In recent years, the frequency and intensity of drought–flood abrupt alterations due to global climate change have drastically increased. In contrast, plant response to the drought-flood abrupt alternations remains unclear. In the current study to reveal maize’s physiological response to drought-flood abrupt alternations, these were carried out in two stages in this study, i.e., three levels of water deficit (WD, i.e., 75%, 65%, and 55% of the field capacity) in stage I, and then five durations of flooding (75%-WDi, 65%-WDi and 55%-WDi) in stage II. The results indicated that the 65%-WDi treatment significantly decreased the leaf area and biomass of maize seedlings in stage I, while maintaining plant growth and reaching the control level in stage II. Abscisic acid (ABA) concentration in maize leaves and roots of 0-5 cm depth was sensitive to drought stress. Under drought–flood abrupt alternations, the root system in 55%-WD₅ and 65%-WD₇ exhibited strong ABA signal, which was sensitive to drought-flood abrupt alternations. Therefore, at the maize seedling stage, proper control of soil moisture is beneficial for improving stress tolerance at later stages, but stress tolerance after drought–flood abrupt alternations is related to the degree of drought exposure at the early stage.

Keywords: leaf area, biomass, ABA concentration, stomatal conductance *e*, transpiration

Introduction

Climate change is an ongoing issue that affects global agricultural development. Drought, flooding, and their secondary hazards are the primary problems that limit agricultural development, and severely affect crop growth and yield formation (Ashraf et al., 2010; Kim et al., 2018; Kakanur et al., 2021; Kerddee et al., 2021; Mehar et al., 2021). It was demonstrated that drought stress in the early crop growth stages can promote the emergence of certain metabolites and structural functions which are beneficial for the improvement of crop resistance to stresses in the later growth stages (Reddy et al., 2004). Drought stress in crop seedling stage causes an extension of the root system to the deep layers of soil (Li et al., 2020) and alters crop’s biological performances (Wang et al., 2020), etc. An essential physiological response to drought stress in plants is the change in the abscisic acid (ABA) concentration (Hussain et al., 2012), which is produced in plant tissues after drought and transported to regulate the leaf stomatal conductance, thereby maintaining water balance in the plant (Gil et al., 2007; Ren et al., 2018). The degree of crop damage due to water stress depends on soil water content, crop species, growth stages, etc. Timely replenishment of water after drought helps to restore the crop growth, while the drought-flood abrupt alternations cause the crop to experience flooding

after drought, and flooding weakens the respiration of crop roots. It causes weakening or loss of leaf stomatal conductance of the crop, which is not conducive to healthy growth (Gil et al., 2007). Most drought-stricken fields can be irrigated in time to alleviate drought conditions. Still, it is challenging to control flooding in drought-flood abrupt alternations due to the uncertainty of farm infrastructure and rainfall intensity and duration. Furthermore, there is a lack of reliable prevention and control technology. In most areas of China, maize seedlings are susceptible to uncertain drought and flood stresses. For effective disaster prevention and mitigation, in this study, we aimed to answer two key questions: (1) Does drought in maize seedlings improve resilience to drought-flood abrupt alternations? (2) What are the limits to which maize can withstand the drought-flood abrupt alternations? The results of this study are intended to provide potential solutions for disaster mitigation and prevention in response to the drought-flood abrupt alternations.

Materials and Methods

Experimental design

The experiment was conducted in a temperature-controlled greenhouse with a photosynthetic photon flux density of 400~600 $\mu\text{mol m}^{-2}\cdot\text{s}^{-1}$, 14 h photoperiod, and day and night temperature of 19/24°C. Maize variety sweet corn F1 Early Sunglow, commercialized seeds acquired from the lab in the Environment Centre, Lancaster University, were planted in black cylinders made of polyvinyl chloride (PVC) plastic, with an outer diameter of 6.6 cm, a thickness of 2 mm, and a height of 24.5 cm. The bottom of each cylinder was sealed with a stainless-steel net to facilitate drainage and stabilize the cylinder. The cultivated organic loam John Innes No. 2 was used as experimental soil. This soil type is traditional British soil compost containing loam, sphagnum peat, grit, humus, and fertilizers that promote the healthy growth of plants. Owing to its good performance, John Innes No. 2 has been widely used in the UK for more than 60 years. Each cylinder was filled with 1050 g soil, which was divided into four equal parts and compressed in the cylinder orderly, the bulk density was determined as 1.55 g cm^{-3} . Two maize seeds were sown in each cylinder and watered with 50 mL of water. The water amount was determined with a measuring cup. As evaporation from topsoil cannot be measured precisely, in order to reduce soil evaporation and accurately determine the daily transpiration of maize plant in each pot, the pots were covered with tinfoil in stage I, and wrapped with plastic film to prevent water leaching and evaporation in stage II, respectively (Fig. 1a).

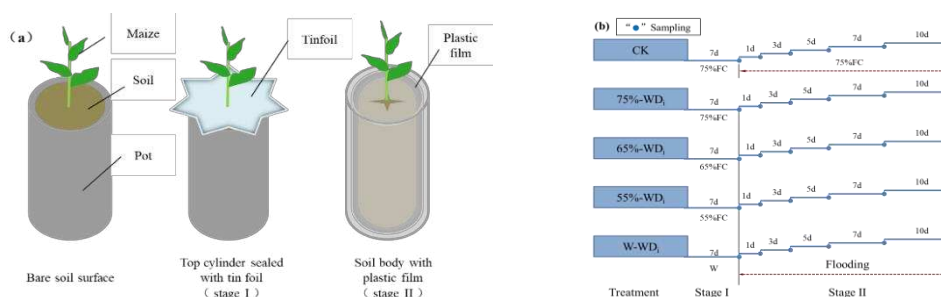


Figure 1. Schematic diagram of (a) covering pots and (b) experimental design. In stage I, 75%-WD, 65%-WD, and 55%-WD represents the three levels of water deficit (WD, i.e., 75%, 65%, and 55% of the field capacity), and W-WD means the waterlogging-alone treatment. In stage II, WD_i represents the five durations of flooding. CK means the treatment of water control at 75% of the field capacity

Based on the weight of dry soil in each pot and the field capacity, soil moisture was determined with daily changes in pot weight, which was weighed with an electronic balance at 8:00 a.m. Soil water was controlled from the three-leaf stage of maize, and the experiment was divided into two stages, i.e., Stage I (7 days) and Stage II (10 days). The soil water content was kept at 55%, 65%, and 75% of the field capacity in stage I. In the waterlogging-alone (W-WD) treatment, a water layer of 1 cm was maintained on the soil surface. In stage II, the treatments at stage I were subjected to waterlogging for 1, 3, 5, 7, and 10 days (55%-WD_i, 65%-WD_i, and 75%-WD_i, where *i* is the duration of the plant subjected to waterlogging, *Table 1* and *Fig. 1b*). The treatment of water control at 75% of the field capacity (sufficient soil moisture for maize growth) was used as CK. There were 17 treatments in total, each repeated five times.

Table 1. Experimental design for maize under drought-flood abrupt alternations

Treatment	Treatment count	Stage I (7 days)	Stage II (≤10 days)
CK	1	75% FC	75% FC (10 days)
75%-WD _i	5	75% FC	Waterlogging, <i>i</i> = 1, 3, 5, 7, 10
65%-WD _i	5	65% FC	Waterlogging, <i>i</i> = 1, 3, 5, 7, 10
55%-WD _i	5	55% FC	Waterlogging, <i>i</i> = 1, 3, 5, 7, 10
W-WD _i	1	Waterlogging	Waterlogging, <i>i</i> = 1, 3, 5, 7, 10

Note: FC is the field capacity

Measurement set-up

During the experiment, the top of each cylinder was sealed with tin foil to expose only the maize plants. The total mass of the cylinders was weighed every morning from 8:00 to 9:00 to calculate the daily water loss owing to plant transpiration. The lost water was then supplemented. Maize seedlings were harvested at the end of stage II. Aboveground parts of the seedlings were cut and separated into stem and leaf in each pot. The soil in each pot with the root system was divided into 0~5 cm, 5~10 cm, 10~15 cm, and 15~20 cm from the soil surface. The roots in each segment were then washed. The leaf area was measured by an automatic leaf area meter (Licor Model 3100 Area Meter, Cambridge, UK). Stem, leaf, and root samples were dried at 65°C for 72 h, and their dry matter was then determined.

ABA concentration in leaves and roots was measured by radioimmunoassay using the monoclonal antibody AFRC MAC 252 (Quarrie et al., 1988). The youngest and fully expanded leaflet was harvested for ABA measurement. The sampling was conducted simultaneously (10:00~10:30) on each harvesting day to avoid diurnal effects on foliar ABA concentration. Leaflets and roots (of the same plant) were sampled, frozen in liquid nitrogen, freeze-dried for 48 h, and then finely ground. Small amounts of samples (10~15 mg dry weight for leaflets, and 30~40 mg dry weight for roots) were used for ABA analysis. The powdered samples were diluted with deionized, distilled water (1:70 for leaflets and 1:25 for roots) and placed on a shaker in a cold room (4°C) overnight to extract ABA. A standard curve was determined with standards in a serial dilution of synthetic unlabeled (±)-cis, trans-ABA (Sigma Let., Dorset, UK). ABA concentration was calculated by reference to the standard curve after linearization using the ‘logit’ transformation.

Statistical analysis

All data were analyzed by one-way analysis of variance (ANOVA). A less significant difference (LSD) and Duncan test were carried out ($P < 0.05$) using Statistica 10.0 (StatSoft, Inc., Tulsa, OK, USA).

Results

Changes in leaf area and biomass

Leaf area is directly related to crop respiration, photosynthesis, and biomass formation, can markedly affect crop yield improvement. The changes in leaf area at the end of the two stages are presented in Fig. 2. At the end of stage I, there was no significant difference in maize leaf area between 65%-WD and 75%-WD, while 55%-WD and W-WD exhibited significantly lower leaf area, which was 24.66% and 75.68% lower than that of 75%-WD, respectively (Fig. 2). At the end of stage II, compared with CK, the leaf area of 65%-WD₁₀ was slightly lower, but the difference was not significant, while the leaf areas of 75%-WD₁₀, 55%-WD₁₀, and W-WD₁₀ were reduced by 14.23%, 32.34%, and 49.38%, respectively, which was significantly different.

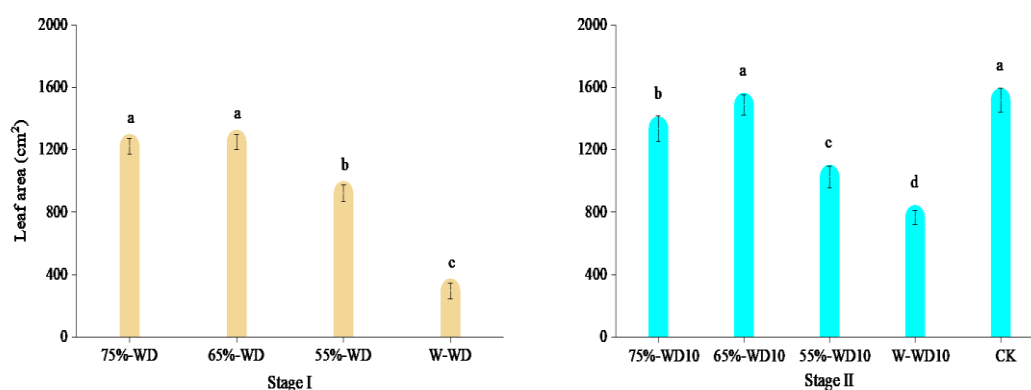


Figure 2. Effects of drought and flood stress on leaf area of maize seedlings. Different letters indicate significant difference between the treatments at $P < 0.05$. In stage I, 75%-WD, 65%-WD, and 55%-WD represents the three levels of water deficit (WD, i.e., 75%, 65%, and 55% of the field capacity), and W-WD means the waterlogging-alone treatment. In stage II, WD_i represents the five durations of flooding. CK means the treatment of water control at 75% of the field capacity

Fig. 3 depicts the changes in biomass of each part of maize seedlings at the end of stage I. The leaf biomass was significantly higher in the 75%-WD and 65%-WD treatments than that in the 55%-WD and W-WD treatments, and the leaf, stem, and root biomass was severely suppressed in W-WD. The different drought treatments insignificantly affected the stem biomass, and the 55%-WD treatment exhibited the most developed root system, with significantly higher biomass and lower shoot-root ratio than the other treatments. In contrast, the W-WD treatment exhibited a lower shoot to root ratio than the drought treatments (Fig. 3). The results in Fig. 3 indicated that different degrees of drought exposure at the maize seedling stage affected the biomass. The greater the drought intensity is, the more developed the root system and aboveground inhibition are. However, drought-affected maize seedlings to a weaker extent than flood stress.

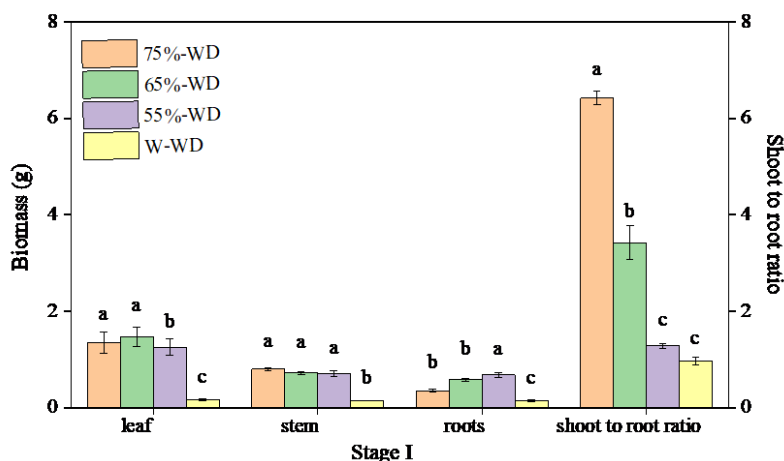


Figure 3. Biomass of leaf, stem, roots, and the shoot to root ratio of maize seedlings at the end of stage I. Different letters indicate significant difference between the treatments at $P < 0.05$. 75%-WD, 65%-WD, and 55%-WD represents the three levels of water deficit (WD, i.e., 75%, 65%, and 55% of the field capacity), and W-WD means the waterlogging-alone treatment

The most direct effect of stress on plants is the inhibition of crop growth. In the present study, the drought-flood abrupt alternations affected maize biomass at the seedling stage (Fig. 4a-d). Differences in the biomass of maize organs were already evident at 3 d of stage II, where the biomass of different parts of maize seedlings under 55%-WD₃ and 65%-WD₃ reached the control level. In contrast, the leaf biomass under 55%-WD₃ exceeded the control by 10.72% (Fig. 4a). Under the 75%-WD₃ and W-WD₃ treatments, the biomass of leaves and roots was significantly lower than that of CK (Fig. 4a and c). At 5 d of stage II, the biomass of leaves, stems, and roots under 65%-WD₅ maintained rapid growth and reached the control level, while the biomass under other treatments exhibited significant inhibition and the shoot to root ratio of the treatments did not differ significantly (Fig. 4a-c). At 7 d of stage II, the differences in maize organs biomass among treatments were similar with the results at 5 d of stage I. Compared with CK, the leaf biomass in 75%-WD₇, 55%-WD₇, and W-WD₇ decreased by 51.24%, 41.23%, and 82.44% (Fig. 4a), respectively; the stem biomass decreased by 42.27%, 25.80%, and 55.66% (Fig. 4b), respectively, which increased the degree of inhibition of biomass of each organ compared with CK at 3 to 5 d of stage II. With the increase in flood duration, the shoot-root ratio was continuously adjusted, and under the 65%-WD₁₀ treatment, it reached the control level (Fig. 4d). Furthermore, the degree of root inhibition was higher under other treatments than in aboveground organs (Fig. 4d). The results indicated that maize plants experienced varying degrees of drought in stage I. The aboveground parts of maize seedlings exhibited significant compensatory growth in stage II, thereby reflecting its biological adaptation to the drought-flood abrupt alternations. Therefore, when maize plants were subjected to drought-hardening with severe stress (55% of the field capacity), the subsequent waterlogging of no more than 3 days had insignificant influence on maize vegetative growth. Under the condition of drought-hardening with moderate stress (65% of the field capacity), the effects of subsequent waterlogging of no more than 7 days on maize vegetative growth were insignificant. However, the maize plants with sufficient water supply (75% of the field capacity) lost the resistance to water lodging, so the plant vegetative growth was limited significantly with water lodging at stage II.

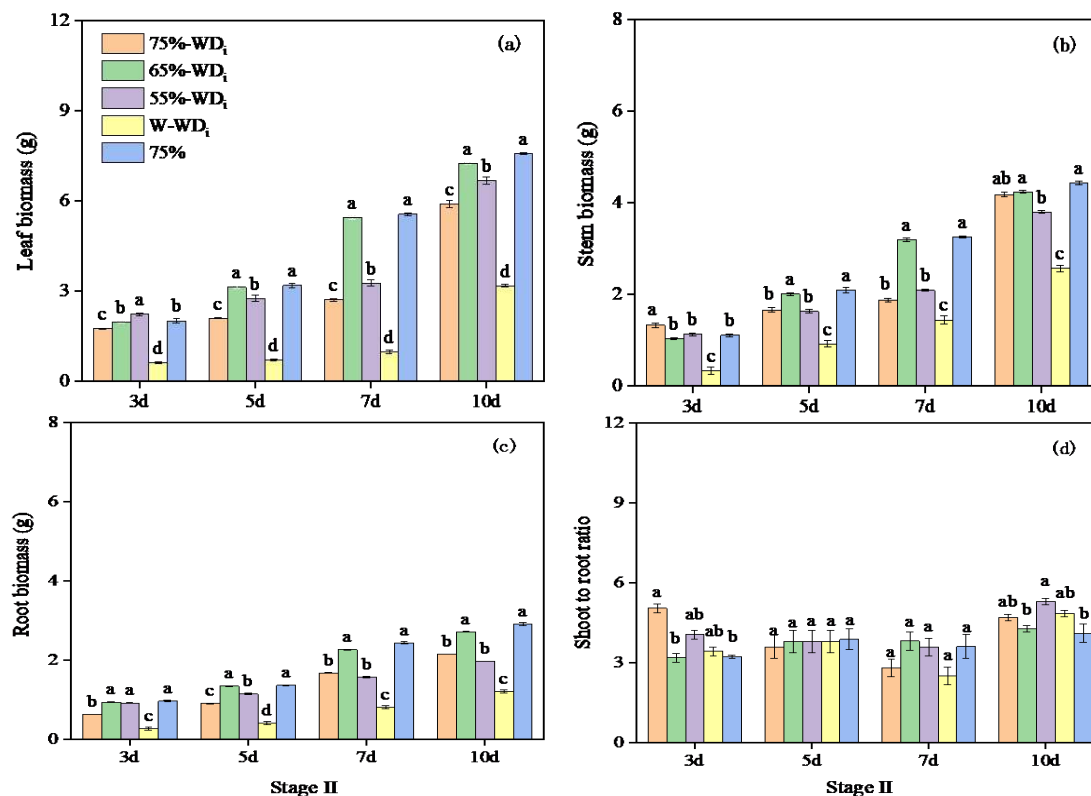


Figure 4. Biomass of (a) leaf, (b) stem, (c) roots, and (d) the shoot to root ratio of maize seedlings during stage II. Different letters indicate significant difference between the treatments at $P < 0.05$. 75%-WD, 65%-WD, and 55%-WD represents the three levels of water deficit (WD, i.e., 75%, 65%, and 55% of the field capacity), and W-WD means the waterlogging-alone treatment. CK means the treatment of water control at 75% of the field capacity

Changes in ABA concentration

The changes in ABA concentration in maize leaves and roots at the end of stage I are presented in Fig. 5. ABA concentration in leaves was significantly higher than in roots under all treatments. ABA concentration in each treatment changed gradually from maize leaves to roots, and gradually decreased from maize leaves to roots. In stage I, the greater the degree of water stress is, the greater the ABA concentration in the leaves is, with the maximum ABA concentration in maize leaves of the 55%-WD treatment being significantly higher than the 65%-WD and 75%-WD treatments, and significantly higher than the W-WD treatment ($P < 0.05$). Compared to 75%-WD, leaf ABA concentration increased by 21.10% and 33.81% for 65%-WD and 55%-WD, respectively, and decreased by 24.65% for W-WD (Fig. 5), indicating that the leaf ABA concentration is highly sensitive to drought stress. At the end of stage I, the greater the degree of water stress is, the greater the ABA concentration in maize roots in 0-5 cm depth is. The root ABA concentration was significantly higher in 55%-WD than in 75%-WD and W-WD. Compared with 75%-WD, ABA concentration of roots in 0-5 cm depth was 12.05% and 28.75% higher in 65%-WD and 55%-WD, respectively, and 3.59% lower in W-WD. ABA concentration in the 5-20 cm depth remained around $70 \text{ ng g}^{-1} \text{ DW}$, with gradually decreasing differences between different treatments (Fig. 5).

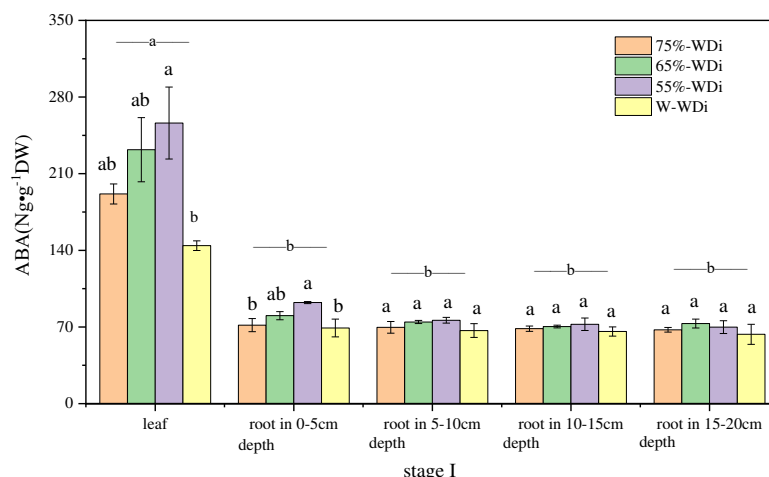


Figure 5. ABA (abscisic acid) concentration in leaf and root of maize seedlings at the end of stage I. Different letters indicate significant difference between the treatments at $P < 0.05$. 75%-WD, 65%-WD, and 55%-WD represents the three levels of water deficit (WD, i.e., 75%, 65%, and 55% of the field capacity), and W-WD means the waterlogging-alone treatment. — a—and—b— indicates the difference in ABA between maize leaf and roots in different layers at $P < 0.05$

At 1 d of stage II, leaves under the 75%-WD₁, 65%-WD₁, and 55%-WD₁ treatments exhibited significantly higher ABA concentrations than those under the corresponding treatments in stage I. Under the 55%-WD₁ and 65%-WD₁ treatments, the mean ABA concentration in leaves reached up to 465.32 and 427.18 ng g⁻¹ DW, respectively, which was significantly higher than that in the treatment of W-WD₁ and CK (Fig. 6). At 3-7 d of stage II, leaf ABA concentration in 75%-WD₁, 65%-WD₁, and 55%-WD₁ remained around 200 ng g⁻¹ DW, which was significantly higher than that in W-WD₁ (Fig. 6).

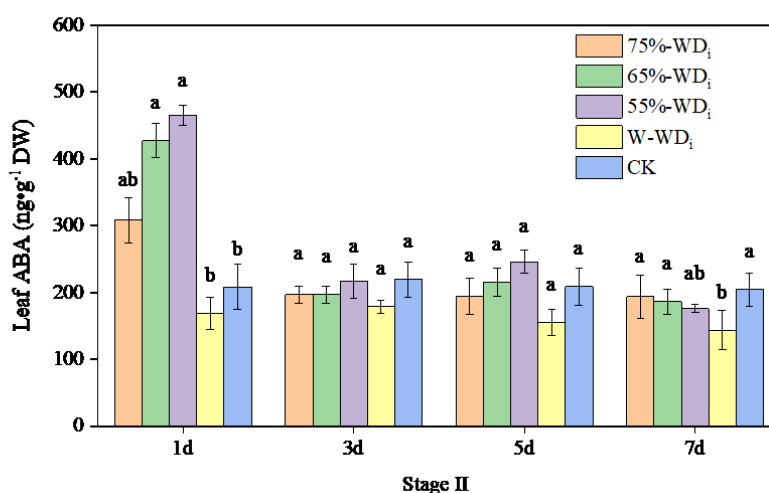


Figure 6. Variations of ABA concentration in maize leaves during stage II. Different letters indicate significant difference between the treatments at $P < 0.05$. 75%-WD, 65%-WD, and 55%-WD represents the three levels of water deficit (WD, i.e., 75%, 65%, and 55% of the field capacity) in stage I, and W-WD means the waterlogging-alone treatment. CK means the treatment of water control at 75% of the field capacity

Fig. 7 presents the variation of ABA concentration in the root system of maize seedlings at different depths in stage II. Under the 75%-WD₁ treatment, the ABA concentration of the root system gradually decreased from topsoil to deeper soil and was higher than that of CK, with significant differences at the depth of 0-5 cm. Compared with the 75%-WD₁ treatment, the ABA concentration in all root layers decreased by 21.39-35.39% under the 75%-WD₃ treatment, which was significantly higher than that at 5-7 d of stage II, indicating that the maize leaves and roots still had a strong ABA signal after 1 d of the drought-flood abrupt alternations, and the strong ABA signal was abolished after 3 d of the drought-flood abrupt alternations (*Fig. 7a*).

Under the 65%-WD₁ treatment, the root ABA concentration decreased gradually from topsoil to deeper soil and was higher than that of CK, with significant differences at the depth of 0-5 cm. Compared with the 65%-WD₁ treatment, the ABA concentration of each root layer under the 65%-WD₃ treatment decreased by 27.80% to 47.88%, and after 3 d of the drought-flood abrupt alterations, the ABA concentration of the root system increased as the flood duration increased, and it increased by 6.96% to 65.01% at 3-5 d and 92.06% to 151.15% at 5-7 d. The ABA concentration of each root layer in the 65%-WD₇ treatment was significantly higher than that in CK (*Fig. 7b*).

Compared with the 55%-WD₁ treatment, the root ABA concentration under the 55%-WD₃ treatment decreased by 22.15% to 44.84%, but the difference between the root layers was not significant. During 3-7 d in stage II, the root ABA concentration gradually increased. Compared with the 55%-WD₅ treatment, the root ABA concentration in all layers under the 55%-WD₇ treatment increased by 5.73% to 30.30%, which was significantly higher than that of CK (except the depth of 15-20 cm) (*Fig. 7c*). However, ABA concentration in the root system was significantly lower under the 55%-WD₇ treatment compared with the 65%-WD₇ treatment.

The root ABA concentration under persistently flooding treatment of W-WD_i was relatively stable, with root ABA concentration being around 70 ng g⁻¹ DW at each sampling date (*Fig. 7d*), which was comparable to stage I.

Leaf stomatal and transpiration changes

Stomata is an important water channel for photosynthesis and the transpiration of crops. Stomatal characteristics under different drought-flood abrupt alternations affect crop yield and water use efficiency. The changes in leaf stomata and plant transpiration of maize seedlings under different drought and flood stresses are presented in *Fig. 8*. In stage I, the leaf stomatal conductance of maize seedlings in the 65%-WD, 55%-WD, and W-WD treatments was lower than the CK values. The more severe the drought stress is, the worse the stomatal conductance is. At 1 d of stage II, the stomatal conductance of maize seedlings in drought treatments exhibited an increasing trend, then the stomatal conductance in the 55%-WD_i and 75%-WD_i treatments were decreased by a fluctuating trend with the increase of flooding duration. However, the leaf stomatal conductance in 65%-WD_i increased closer to the value in CK at 3-5 d of stage II, and then decreased gradually. At 3-5 d of stage II, the leaf stomatal conductance in 65%-WD_i were greater than these in 55%-WD_i and 75%-WD_i. During the whole experimental period (stage I and II), CK had greater stomatal conductance than the drought treatments, drought-flood treatments, and the flood treatments. The treatment of W-WD_i had lower stomatal conductance than the drought treatments and the drought-flood treatments (*Fig. 8a*).

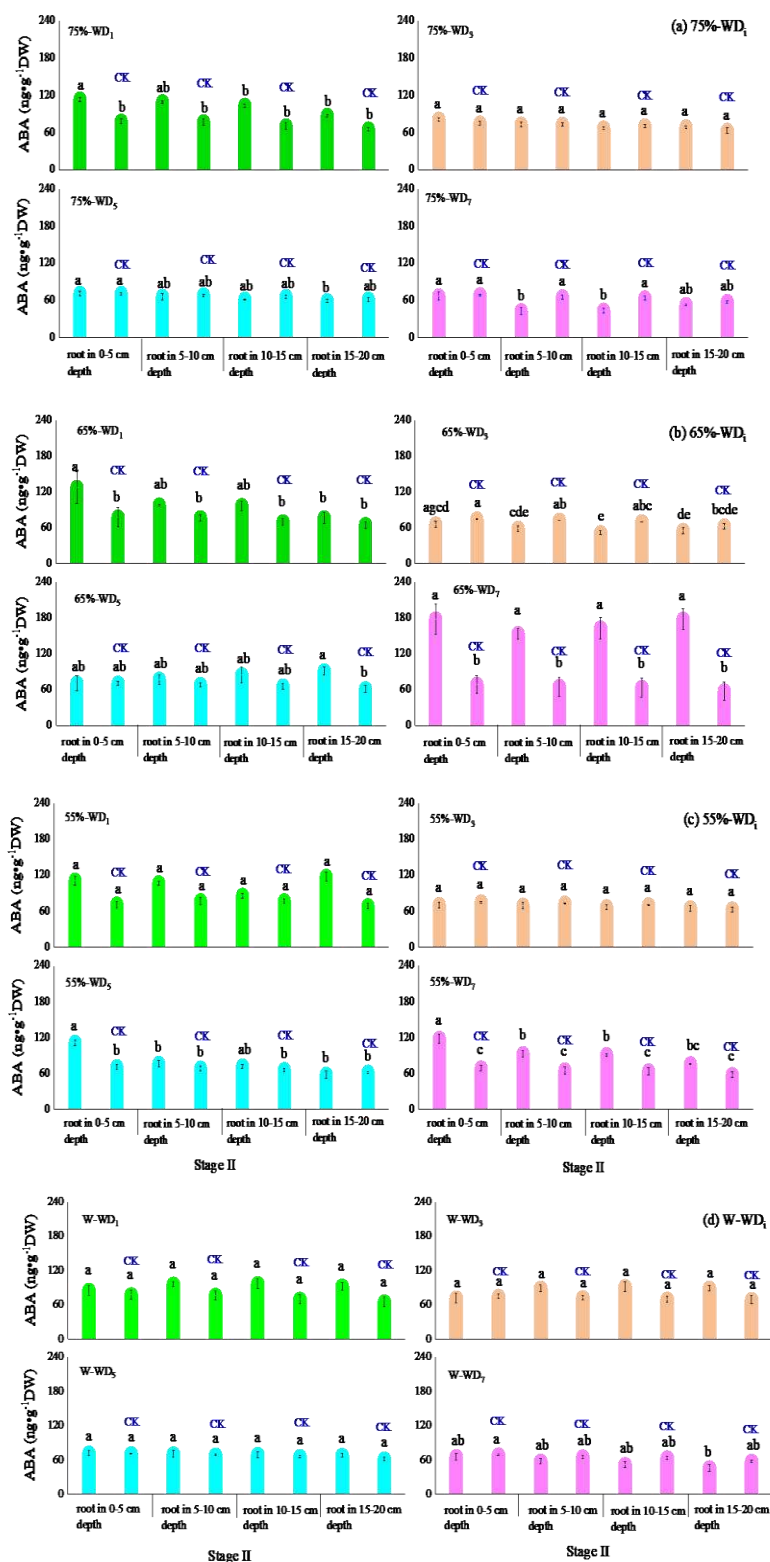


Figure 7. Variations of ABA concentration in maize roots of different treatments during stage II. Different letters indicate significant difference between the treatments at $P < 0.05$. 75%-WD, 65%-WD, and 55%-WD represents the three levels of water deficit (WD, i.e., 75%, 65%, and 55% of the field capacity) in stage I, and W-WD means the waterlogging-alone treatment. CK means the treatment of water control at 75% of the field capacity

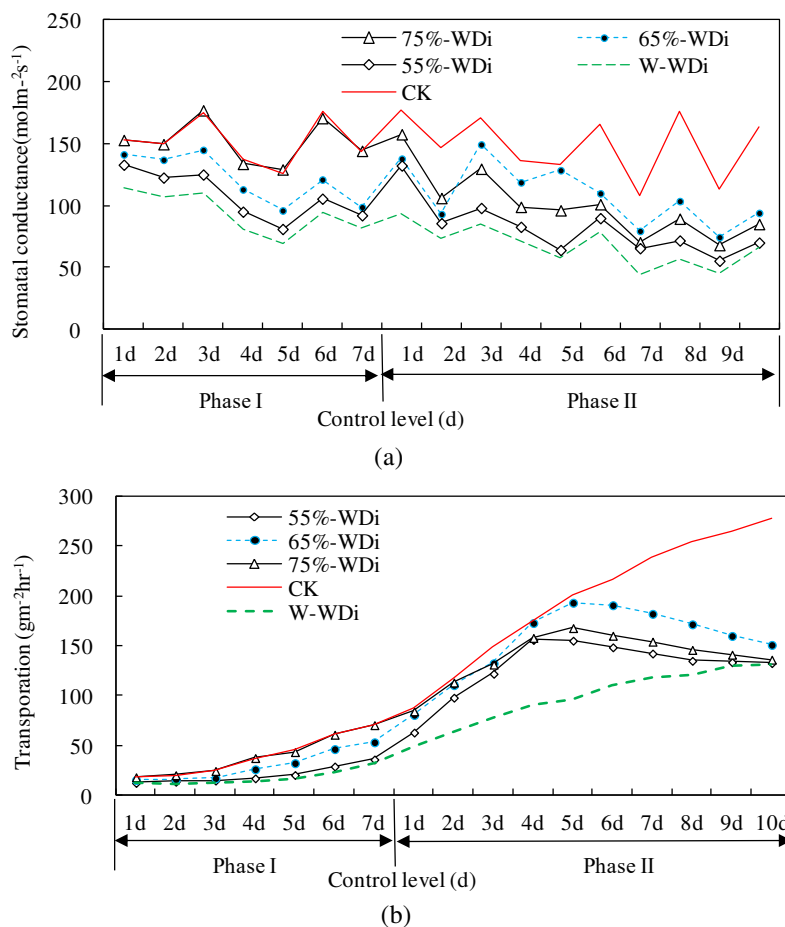


Figure 8. Changes in (a) stomatal conductance and (b) plant transpiration of maize seedlings during stage I and II. 75%-WD, 65%-WD, and 55%-WD represents the three levels of water deficit (WD, i.e., 75%, 65%, and 55% of the field capacity) in stage I, and W-WD means the waterlogging-alone treatment. CK means the treatment of water control at 75% of the field capacity

Daily transpiration in maize seedlings was related to soil moisture. In stage I, the higher the soil moisture, the higher is the daily transpiration, which in descending order was W-WD, 75%-WD, 65%-WD, and 55%-WD; the differences between different treatments gradually increased with crop growth and the duration of moisture control (Fig. 8b). The flood treatments restricted plant transpiration compared with the drought treatments (Fig. 8b). Plant transpiration in 75%-WD_i increased closer to the 65%-WD_i during 1-3 d of stage II, while lower than the 65%-WD_i at 3 d of stage II, and reached the maximum transpiration at 3 d of stage II. The maximum transpiration in 55%-WD_i and 65%-WD_i was measured at 3 d and 5 d of stage II, respectively. The daily transpiration in 55%-WD_i, 65%-WD_i, and 75%-WD_i decreased after the peak, and the difference between the two treatments and CK gradually increased. At 10 d of stage II, the daily transpiration was similar between 55%-WD_i, 75%-WD_i, and W-WD_i, and lower than the value in 65%-WD_i.

Discussion

Drought and flood stress are the leading natural disasters worldwide, and the most direct effect of stress on crops is the inhibition of crop growth and reduction of biomass (Wu et al., 2013; Zhen et al., 2018). Therefore, biomass is often essential for assessing crop resistance under abiotic stresses. In the present study, the leaf area of maize seedlings under 65%-WD₁₀ was not significantly reduced (Figs. 2-4), indicating that maize seedlings that experienced a suitable water stress exhibit better resistance to flood stress at the later stage. Under water stress, a series of metabolite changes will occur in crops, which can regulate the osmotic capacity of crop leaves, thus maintaining the extended growth of cells and their stomatal conduction and photosynthetic production capacity. Therefore, the maize seedlings in 65%-WD_i exhibited high stomatal conductance and transpiration after drought-flood abrupt alternations, and then maintained photosynthate accumulation, which plays an important role in the resistance to flood stress in the late stage. The response of crops to drought stress activates crop resilience function. At stage II, the 65%-WD_i measured high biomass, indicating the facilitating effects of drought hardening in the early stage on the flood resistance at the late stage. However, the strength of flood resistance at late stage was depended on the degree of drought stress at the early stage. Maize seedlings in 55%-WD_i suffered severe drought stress at stage I and had low water potential in the root zone, resulting in low stomatal conductance and limited photosynthate accumulation. At 1-4 d of stage II, the seedlings in 55%-WD_i exhibited a high rate of biomass accumulation and high stomatal conductance, showing the rapid growth of stress resistance. While this response only lasted for 4 days at stage II, indicating that the severe water stress at stage I was not conducive to the response of crops to waterlogging in the late stage. The less capacity of maize seedlings in response to waterlogging in 55%-WD_i than 65%-WD_i confirmed it. The seedlings in 75%-WD_i were supplied by sufficient water and exhibited a good base of biomass at stage I; after 3 d at stage II, however, leaf senescence was measured in 75%-WD_i, and the stomatal conductance and transpiration lower than the treatment of 65%-WD_i (Fig. 8), and the biomass accumulation rate decreased, lower than that in 65%-WD_i. The results indicated that the sufficient water supply at stage I was ineffective for improving crop resistance capacity after drought-flood abrupt alternations. At stage I, the biomass and leaf area of maize seedlings in W-WD_i were significantly restricted by stress. Under waterlogging stress, the stomatal conductance and photosynthetic capacity of crops decrease, and the transport of photosynthate also slows down. The root zone is hypoxic, and the stomatal resistance of CO₂ diffusion increases, which affects their photorespiration. The chlorophyll content decreases, and the leaves' premature senescence and abscission are obvious, limiting their ability to resist waterlogging adversity. Therefore, moderate drought exposure in the early stage is beneficial in alleviating or ameliorating the effects of flood on the biomass in the later stage, which promotes a good material basis for improving crop yield, thereby securing the economic returns (Zhen et al., 2017; Liang et al., 2019). The shoot-root ratio, a marker of the sensitivity of crops to stressful environments, is related to ABA synthesis and is considered as an adaptative mechanism to stress (Boursiac et al., 2013). In this study, the greater the degree of water stress in stage I, the greater the effects on the aboveground stem and leaf growth, and the more developed root system. After 10 d of stage II, the root inhibition resulted in differences in the shoot-root ratio among different treatments (Fig. 4d). Water stress at stage I promoted the root growth and expanded the root functional area, which laid a good physiological foundation for crop survival under late flood stress and exerted a buffering

and regulatory effect on the maintenance of the late root zone flooding damage. Therefore, the stress resistance of crops can be improved to some extent through soil moisture regulation.

As a phytohormone, ABA plays a significant role in regulating plant growth and development, especially in several physiological processes during abiotic stresses (high salt, low temperature, drought, etc.) (Dong et al., 2015; Li et al., 2017). It has been shown that a variety of abiotic stresses increase ABA concentrations in plants (Shinozaki et al., 2003; Boursiac et al., 2013). The root system is the first site to sense the soil moisture changes under water stress, and plant ABA concentrations are derived from the root system. Furthermore, soil water stress derives from the changes in this physiological characteristic (Puértolas et al., 2013). Therefore, changes in plant ABA concentrations are often adjusted or ameliorated through irrigation, leading to optimal production (Davies et al., 2011). In the present study, the sharp alternation to flooding from stage I to stage II caused a gradual change in ABA concentration in maize leaves and roots, which decreased from the leaves to roots, with the root system originating the drought stress signal, and this signal was heavily aggregated and transmitted upstream to the leaves along with the plant fluid flow, so that, the leaves are the end point of the heavily aggregated ABA signal and exhibit the highest ABA concentration. However, at 1 d of stage II, the leaf ABA concentrations of the 75%-WD₁, 65%-WD₁, and 55%-WD₁ treatments were significantly higher than those of the 75%-WD₁, 65%-WD₁, and 55%-WD₁ treatments at the end of stage I. The reason for this difference may be that the exposure of the crop to a new stress prompted the plant cells to actively regulate the osmotic substances in response to the stress (Wu et al., 2013). The increase in osmoregulatory capacity caused a significant increase in the leaf ABA signal at 1 d of stage 75%-WD₁, 65%-WD₁, and 55%-WD₁ treatments, which gradually attained a stable stage. Due to ABA degradation in the crop caused by the fold stress, the leaf ABA concentration in each treatment in this study dropped to a lower level at 7 d of stage II, but the leaf ABA concentration in each treatment subjected to drought stress in stage I at this time point was still significantly higher than that of the continuous flood stress treatment. It was suggested that the flood stress also leads to a significant increase in ABA concentration in the crop (Chen et al., 2006; Hiroaki et al., 2007). When the leaf stomatal conductance decreases, transpiration rate decreases, and ABA synthesis in roots increases. Furthermore, ABA accumulation increases in the roots under the influence of reduced transpiration pull. Therefore, the root ABA concentration in this study was significantly elevated at 7 d after the drought-flood abrupt alternations, indicating that the physiological resistance signal of maize is strongest at 7 d after the drought-flood abrupt alternations. Studies on other plants revealed that plant physiological functions were recovered to varying degrees at 15 d after rehydration (Song et al., 2012; Wang et al., 2015), and exhibited a compensatory effect on growth (Li et al., 2013; Wang et al., 2015). In this study, at stage I, the leaf ABA concentrations under 55%-WD and 65%-WD were significantly higher than that under 75%-WD, and it increased with an increase in water stress, and leaf stomatal conductance, and then, plant transpiration subsequently decreased. At the end of stage I, leaf area and biomass of the 65%-WD treatment group were not affected. During 1-5 d of stage II, the leaf-root ABA concentration difference increased with an increase in water stress. With regards to the leaf stomatal conductance, plant transpiration and biomass, the recovery ability of each marker under 55%-WD_i was weaker than that under 65%-WD_i. By 7 d of stage II, since the gradient of ABA concentration between leaves-roots became smaller, ABA concentration between leaves-

roots attained a more balanced state; the leaf stomatal conductance and plant transpiration slowly decreased under the 65%-WD₇ and 55%-WD₇ treatments. The rate of dry matter accumulation declined under 65%-WD₇ and was significantly decreased under 55%-WD₇. The results of this study revealed that in stage I, when the water was controlled at 55% of the field capacity, the rehydration effect on biomass occurred within 3 d after the drought-flood abrupt alternation. However, in stage I, when the water was controlled at 65% of the field capacity, the rehydration effect occurred 5 d after the drought-flood abrupt alternations, compensatory growth was observed in all markers, which was similar to the control level. Considering the restoration effect of the crop itself and the relief duration for disaster mitigation and prevention, 65% of the field capacity at the maize seedling stage can be considered as a more suitable water control measure, and the duration of flooding should not exceed 7 d after the drought-flood abrupt alternation.

Conclusions

Maize seedlings undergo a certain degree of water stress (55%-WD_i and 65%-WD_i) and compensatory crop biomass growth occurs after the drought-flood abrupt alternations. Under the condition of drought and flood, ABA concentration in maize leaves was significantly higher than that in roots. The most sensitive site in maize to drought stress was found to be the leaf. After the drought-flood abrupt alternations, there was a strong ABA signal in the roots under 55%-WD₅ and 65%-WD₇. At maize seedling stage, the water level is controlled at 65% of the field capacity, and the duration of flooding should not exceed 7 d after the drought-flood abrupt alternations. Analyses of metabolomics, proteomics, etc. should be carried out in future to further reveal effects of the drought-flood abrupt alternations on plant physiological-biochemical characteristics.

Funding. This research was funded by the China Agriculture Research System of MOF and MARA (CARS-02-14), the Basic Scientific Research Project of Chinese Academy of Agricultural Sciences (FIRI20210104), and the Agricultural Science and Technology Innovation Program (ASTIP).

Data Availability Statement. The datasets used and/or analyzed during the current study are available from the corresponding author on reasonable request.

Acknowledgments. We thank Dr. Ian Dodd in Lancaster University for his invaluable guidance and assistance.

Conflicts of Interests. The authors declare no conflict of interests.

REFERENCES

- [1] Ashraf, M. (2010): Inducing drought tolerance in plants: recent advances. – *Biotechnology Advances* 28: 169-183.
- [2] Boursiac, Y., L eran, S., Corratg e-Faillie, C., Gojon, A., Lacombe, B. (2013): ABA transport and transporters. – *Trends in Plant Science* 18(6): 325-333.
- [3] Chen, J., Pan, K. W. (2006): Physiological Function and Mechanism of Abscisic Acid in Plants under Stress. – *Plant Physiology Communications* 6: 1176-1182.
- [4] Davies, W. J., Zhang, J., Yang, J., Dodd, I. C. (2011): Novel crop science to improve yield and resource use efficiency in water-limited agriculture. – *Journal of Agricultural Science* 149: 123-131.

- [5] Dong, T., Park, Y., Hwang, I. (2015): Abscisic acid: biosynthesis, inactivation, homeostasis and signaling. – *Essays in Biochemistry* 58: 29-48.
- [6] Gil, P., Schaffer, B., Gutiérrez, S. M., Li, C. (2007): Effect of Waterlogging on Plant Water Status, Leaf Gas Exchange and Biomass of Avocado (*Persea Americana* Mill). – *Viña Del Mar, Chile* 12(16): 413-421.
- [7] Hiroaki, S., Masanori, O., Kentaro, M., Tetsuo, K., Shoko, S., Yusuke, J., Masaru, F., Taku, A., Hirokazu, T., Miho, A. (2007): Ethylene promotes submergence-induced expression of OsABA8ox1, a gene that encodes ABA 8'-hydroxylase in rice. – *Plant Cell Physiol* 48(2): 287-298.
- [8] Hussain, S., Ali, A., Ibrahim, M., Saleem, M. F., Bukhsh, M. A. A. (2012): Exogenous Application of Abscisic Acid for Drought Tolerance in Sunflower (*Helianthus annuus* L). – *Journal of Animal and Plant Sciences* 22(3): 806-826.
- [9] Kakanur, Y., Baviskar, V. S., Navathe, S., Patil, R. M., Singh, G. P. (2021): Impact of heat and drought stress on phenological development and yield in bread wheat. – *Plant Physiology Reports* 26(2): 357-367.
- [10] Kerdee, S., Kongsil, P., Nakasathien, S. (2021): Waterlogging Tolerance and Recovery in Canopy Development Stage of Cassava (*Manihot esculenta* Crantz). – *Agrivita* 43(2): 233-244.
- [11] Kim, Y., Seo, C. W., Khan, A. L., Mun, B. G., Shahzad, R., Ko, J. W., Yun, B. W., Park, S. K., Lee, I. J. (2018): Exo-ethylene application mitigates waterlogging stress in soybean (*Glycine max* L.). – *BMC Plant Biology* 18: 254.
- [12] Li, S. X., Guo, H., Li, M., Sun, Y. J., Ma, J. (2013): Young panicle formation stage after water stress on the production and transport of photosynthate in rice. – *Acta agriculturae boreali-sinica* 28(5): 133-137.
- [13] Li, W. R., Li, Y. J., Feng, S. Z. (2017): Regulation of root-sourced ABA to growth and water use efficiency of cotton seedlings and their response to different nitrogen levels and distribution ratios. – *Acta Ecologica Sinica* 37(20): 6712-6723.
- [14] Li, C. X., Sun, J. S., Wang, S. S. (2020): Simulation of farmland water and heat transfer under alternate ditch irrigation. – Yellow River Water Conservancy Press.
- [15] Liang, J. Y., Wang, C. Q., Li, B., Long, S. F., Chen, L. (2019): Effects of combined application of pig manure with urea on grain yield and nitrogen utilization efficiency in rice-wheat rotation system. – *Chinese Journal of Applied Ecology* 30(4): 1088-1096.
- [16] Mehar, F., Iqbal, N., Gautam, H., Sehar, Z., Khan, N. (2021): Ethylene and sulfur coordinately modulate antioxidant system and aba accumulation in mustard plants under salt stress. – *Plants* 10(1): 180.
- [17] Puértolas, J., Alcobendas, R., Alarcón, J. J., Dodd, I. C. (2013): Long-distance abscisic acid signalling under different vertical soil moisture gradients depends on bulk root water potential and average soil water content in the root zone. – *Plant, Cell and Environment* 36: 1465-1475.
- [18] Quarrie, S., Whitford, P., Appleford, N., Wang, T., Cook, S., Henson, I., Loveys, B. (1988): A monoclonal antibody to (S)-abscisic acid: its characterisation and use in a radioimmunoassay for measuring abscisic acid in crude extracts of cereal and lupin leaves. – *Planta* 173: 330-339.
- [19] Reddy, A. R., Chaitanyaa, K., Vivekanandan, M. (2004): Drought-induced responses of photosynthesis and antioxidant metabolism in higher plants. – *Journal of Plant Physiology* 161: 1189-1202.
- [20] Ren, C. G., Kong, C. C., Xie, Z. H. (2018): Role of abscisic acid in trigolactone-induced salt stress tolerance in arbuscular mycorrhizal *Sesbania cannabina* seedlings. – *BMC plant biology* 18(1): 74-74.
- [21] Shinozaki, K., Yamaguchi-Shinozaki, K., Seki, M. (2003): Regulatory network of gene expression in the drought and cold stress responses. – *Current Opinion in Plant Biology* 6(5): 410-417.

- [22] Song, J. Z., Li, P. P., Fu, W. G. (2012): Effect of water stress and rewatering on the physiological and biochemical characteristics of *Phalaris arundinacea*. – *Acta Prataculturae Sinica* 21(2): 62-69.
- [23] Wang, L. B., Zu, W., Dong, S. K., Liu, L. J., Xu, Y. H., Li, X. N. (2015): Effects of drought stresses and times on compensation effect after re-watering in soybean. – *Transactions of the Chinese Society of Agricultural Engineering (Transactions of the CSAE)* 31(11): 150-156.
- [24] Wang, H., Sun, H., Xia, H., Wu, T., Yang, Z. (2020): Natural variation and domestication selection of *zmckx5* with root morphological traits at the seedling stage in maize. – *Plants* 10(1): 1.
- [25] Wu, D., Zou, H. W. (2013): Effects of Waterlogging Stress on Plant Growth and Its Chemical Control Techniques. – *Hubei Agricultural Sciences* 52(1): 9-12.
- [26] Zhen, B., Guo, X. P., Lu, H. F., Zhou, X. G., Wang, Z. C., Li, X. P. (2017): Impact of Alternating Drought and Waterlogging during Tillering Stage on Physiological Traits of Rice. – *Journal of Irrigation and Drainage* 36(5): 36-41.
- [27] Zhen, B., Guo, X. P., Lu, H. F., Zhou, X. G. (2018): Response of Rice Growth and Soil Redox Potential to Alternate Drought and Waterlogging Stresses at the Jointing Stage. – *Journal of Irrigation and Drainage* 37(10): 42-48.

A REVIEW OF THE IMPACT OF EXTREME ENVIRONMENTAL FACTORS ON EARTHWORM ACTIVITIES AND THE FEEDBACK ON THE CLIMATE

OPUTE, P. A.^{1,2*} – MABOETA, M. S.¹

¹*Unit for Environmental Sciences and Management, North-West University, Private Bag X6001, Potchefstroom 2520, South Africa*

²*Department of Animal and Environmental Biology, Faculty of Life Sciences, University of Benin, Benin City, Nigeria
(ORCID: 0000-0003-3324-0206)*

**Corresponding author
e-mail: ashibudike.opute@uniben.edu*

(Received 17th Jan 2022; accepted 2nd May 2022)

Abstract. Soils support a diverse range of organic life and provide several ecosystem functions and services that allow terrestrial life to thrive. Earthworms influence greenhouse gas (GHG) emissions from the soil both biologically (via respiration and litter modification) and physically (via increased macroporosity and altered air and water movement pathways). They improve soil carbon sequestration but also actively contribute to the release of major greenhouse gases. Shifting geographical ranges of earthworms due to changes in climatic conditions might affect the composition, structure and function of the soil ecosystem. This review examines the possible effects of the projected change in climate on earthworm communities and resulting implications for soil GHGs due to changes in environmental endpoints such as temperature and moisture. Earthworm activity, abundance, and biomass increase as soil moisture content increases, but drought and flooding reduce earthworm productivity. Climate change is likely to exacerbate earthworm invasions at higher latitudes and altitudes. However, because higher temperatures inhibit earthworm activities during droughts, anticipated warmer and drier climates may impede earthworm invasions. Climate change may disrupt the delicate balance between carbon sequestration and greenhouse gas emissions from soil in the coming century, but there are currently insufficient field studies to back up these prognostications.

Keywords: *temperature, precipitation, soil moisture, drought, flooding, ecosystem engineers, carbon sequestration*

Introduction

Climate change is becoming a significant problem with potentially far-reaching global consequences. Emissions of greenhouse gases (GHG) have increased significantly in recent years and will continue to increase over time, owing to global industrialization. According to projection models, by 2100, air temperatures would have risen from 1.1 °C to 6.4 °C, possibly altering species' spatial distribution, phenotypic and phenological variations, extinction, and consequently, environmental degradation (Múgica et al., 2015). Most importantly, the projected possibilities for climate change (high atmospheric CO₂, temperature, precipitation, ultraviolet radiation, and frequency of extreme events) will have significant implications for the structure and function of the soil ecosystem (Grimm et al., 2013). The most plausible effects to occur in soils, as indicated by the Intergovernmental Panel on Climate Change (IPCC), are those associated with temperature increases, fluctuations in moisture content, hypoxia phenomena, and acidification, as well as soil feedback to the atmosphere via the release of more GHGs (IPCC, 2014).

One of the primary fields of ecology, sustainable agriculture, and global change studies, among others, is the influence of soil fauna on organic matter decomposition (van Groenigen et al., 2014). Earthworms act as ecosystem engineers, regulating microbiota activities in the soil and associated carbon cycling through multiple processes on different time scales and at different spatial scales. Earthworms contribute to the organic matter dynamics in agroecosystems by ingesting 2 to 15 Mg ha⁻¹ year⁻¹ of residual organic materials and processing up to 10% of the topsoil each year (Medina-Sauza et al., 2019). After consumption, soil and organic materials are mixed with intestinal mucus and digested with the aid of enzymes produced from earthworms, indigenous gut microbiota and ingested microbes. Several physical, chemical, and biological changes occur in the soil as it goes through the earthworm's gut until undigested elements are egested as casts (Abail et al., 2017). These processes describe the differences between the many niches available for earthworms in cycling ecosystem carbon. Earthworms are referred to as "predators" when they have a top-down effect on carbon C, cycling through controlling the microbiota population. When they modify C cycling via the bottom-up processes of supplying microbiota with simple inorganic substrates, they are called "primary decomposers." Anthropogenic greenhouse gas emissions tend to increase long-term radiative forcing, resulting in global warming with the levels of atmospheric carbon dioxide (CO₂), nitrous oxide (N₂O) and methane (CH₄) growing by approximately 41%, 20% and 160%, respectively in 2012, compared to 1850–1900 (IPCC, 2013). Earthworms play significant roles in the global greenhouse gas balance, affecting both the biotic and abiotic soil characteristics that affect the soil's GHG emissions, carbon sequestration, and plant growth. Climate change dramatically influences ecosystems' biodiversity (Bardgett and van der Putten, 2014) which include shifts in ecosystem dynamics, habitat selection, species abundance and distribution, phenology, and invasiveness (Eisenhauer et al., 2014). While some efforts have been made towards integrating data on soil organisms' possible response to climate change, there is still insufficient research on soil community responses and their most important drivers, especially for large soil invertebrates. Furthermore, despite the known significance of the role earthworms play in ecosystems and the evident threats posed by climatic change scenarios, there is scarcely any comprehensive research on climate change impact on earthworms and the possible implications for soil greenhouse balance. More recent reports (including Blume-Werry et al., 2020; Phillips et al., 2019; Singh and Singh, 2019; and Singh et al., 2019) have indicated that the impact of earthworms will increase in the coming years. These effects, they claim, will boost not only carbon sequestration in the soils but also greenhouse gas emissions such as CO₂, N₂O, and CH₄. Singh et al. (2019) established a baseline for predicting earthworm distribution in the coming decades, however, they identified a knowledge gap in the interacting effects of the various climate change drivers on earthworms. Therefore, this review seeks to assess how distal climate change drivers, such as temperature, moisture, drought, and floods, affect earthworms and how this might affect the delicate balance between earthworms' positive contribution to soil health and greenhouse gas emissions from the soil.

This paper systematically reviewed a range of scientific literature to analyze the possible impacts of climate change drivers on earthworm populations and their probable implications for soil greenhouse balance. The climate change drivers focused on include temperature and precipitation changes and extreme events such as drought and flood. A Web of Science (WoS) search was conducted (June 2021) focusing on literature published between 1991 and 2020, using the search syntax: ('climate change' OR

‘warming’ OR ‘flood’ OR ‘precipitation’ OR ‘moisture’ OR ‘temperature’) AND (‘lumbric*’ OR ‘earthworm*’) AND (‘GHGs*’ OR ‘emission’ OR ‘soil’). We streamlined the search to the WoS categories: Zoology and Ecology and WoS document type: Articles, returning 336 publications. The published articles from the restricted search were between 1991 and 2020, with the highest number of publications (7.14% of 336) occurring in 2015 (Fig. 1). The majority of the studies were from temperate countries like the United States (25.30%), England (12.20%), and Germany (10.42%) and very few studies from tropical areas such as Nigeria (0.89%), South Africa (2.98%) and Zimbabwe (0.30%) (Fig. 2).

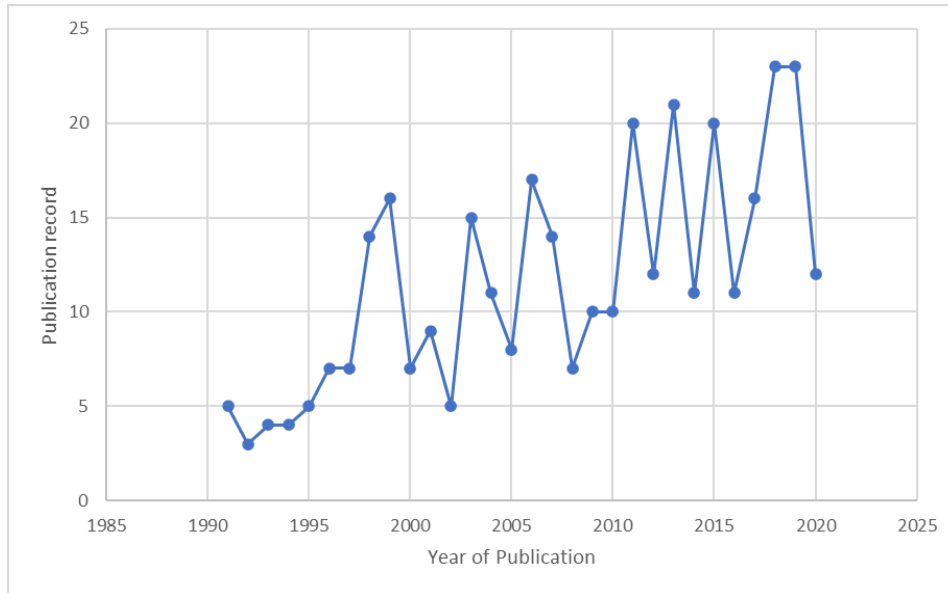


Figure 1. Publication output by year based on WoS search criteria

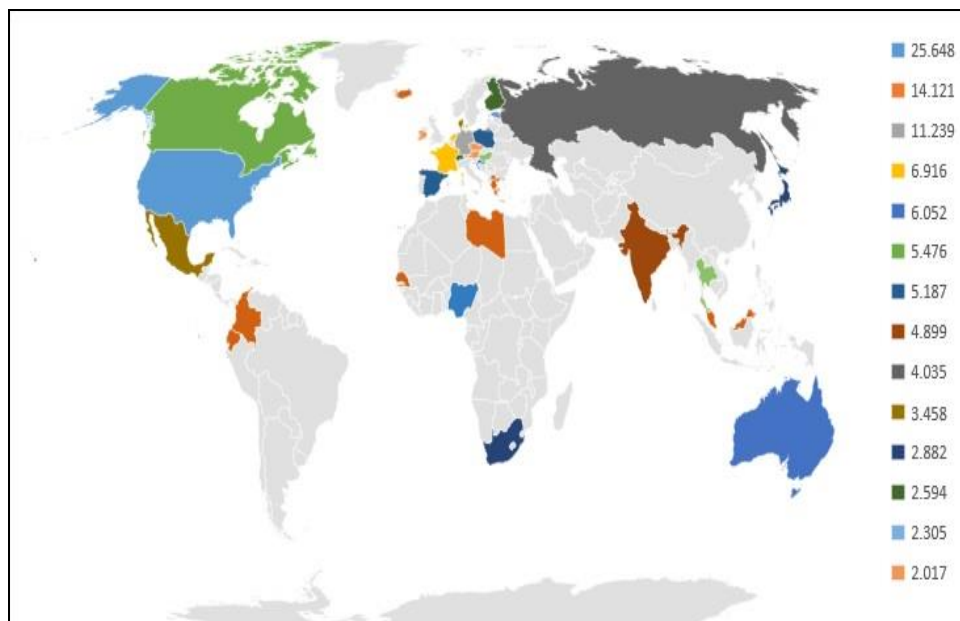


Figure 2. Percentage distribution of publications across countries/regions based on WoS search criteria

Climate change projections

Climate change will become one of the greatest threats to biodiversity in the coming years, with most ecosystem functions and services at risk (Siebert et al., 2019). As evidenced by changes in the unpredictability of its drivers, for instance, temperature, moisture or precipitation, and wind, climate change will persist for a prolonged period, and its effects will be difficult to reverse. It is likely to coincide with an increased probability of extreme climatic events, such as flooding and drought (IPCC, 2013). Many climate change models anticipate that extreme precipitation events will become more often (Singh et al., 2019), while average precipitation will remain steady but with a great deal of variability. Although changes in rainfall may appear to show considerable variability on a small scale, the projected rise in global mean air temperature remains undeniable. The overall global surface temperature increases for 2016–2035 will be similar across the four representative concentration pathways (RCP) with a range of 0.3 to 0.7 °C for the medium confidence (IPCC, 2014). This prediction rests on the assumption that no significant events such as volcanic eruptions, alterations in nitrogen and carbon dioxide concentrations will occur or sudden increases in energy balance following changes in anthropogenic climate forcing agents such as greenhouse gases. A global mean surface temperature increase of 0.3 °C to 1.7 °C is predicted under RCP2.6, 1.4 °C to 3.1 °C under RCP6.0, 1.1 °C to 2.6 °C under RCP4.5 and 2.6 °C to 4.8 °C under RCP8.5 (Fig. 3a).

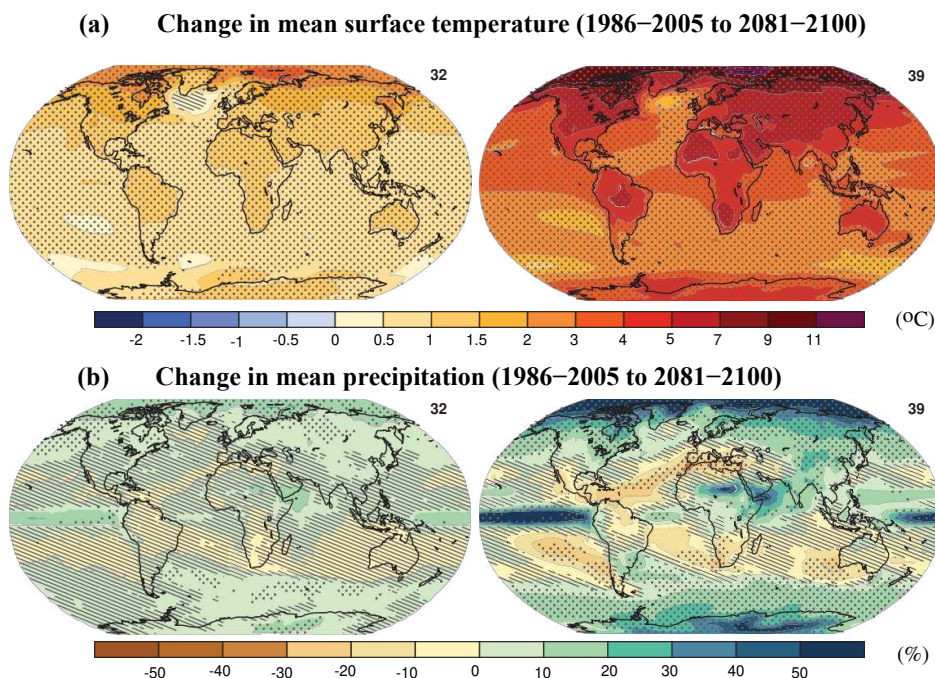


Figure 3. Change in mean surface temperature (a) and change in mean precipitation (b) based on multi-model mean projections under RCP2.6 (left) and RCP8.5 (right) scenarios for 2081–2100 relative to 1986–2005. In the upper right corner of each panel, the number of models used to determine the multi-model mean is indicated. Stippling (dots) illustrates regions where the projected alteration is significant compared to natural internal variability and where the sign of change is correlated by at least 90% of models. Hatching (diagonal lines) indicates regions where the expected change is less than one standard deviation from natural internal variability (Adapted from IPCC SPM, 2014)

Temperature extremes (hot/cold) will inevitably be more frequent as the global mean surface temperature increases, e.g. heatwaves become more frequent and intense. The occasional winter weather will continue to occur (IPCC, 2014). However, precipitation changes are not going to be homogenous. The high latitudes and equatorial Pacific are likely to increase the mean annual precipitation under the RCP8.5 scenarios. Also, under the RCP8.5 scenario, mean precipitation in arid environments will decline, while mean precipitation in wet areas will increase (*Fig. 3b*).

Europe's mean temperature has steadily increased over the years, with more significant warming occurring in its higher latitudes (IPCC, 2014). The warming in Scandinavia in the 1980s was the strongest, while warming in the Iberian Peninsula was most remarkable in summer (EEA, 2012). The decadal mean land surface temperature is 1.3 ± 0.11 °C for 2002–2011. This temperature is far above the projected average for 1850–1899 based on the analysis of the gridded surface temperature from Hadley Centre/Climatic Research Unit (data set 3), Merged Land-Ocean Surface Temperature and Goddard Space Studies Institute (GISS) (Brohan et al., 2006; Smith et al., 2008; Hansen et al., 2010). Different climate change models agree significantly with each other for all warming scenarios within Europe. The highest warming rate is predicted during summer in Southern Europe and Northern Europe during winter. Even if the current global warming is assumed to be limited to 2 °C in comparison to 1850-1899 (preindustrial times), European climates will differ from what they are today in the next few decades (Jacob and Podzun, 2010). During the summer, rainfall may likely decrease in the south of Sweden and increase in winter. Near the end of the 21st century, a reduction in the mean long-term winter snowfall in Northern Europe is expected (Räisänen and Eklund, 2012). Alterations in severe precipitation will be on the high confidence range for high rainfall in Northern and Continental Europe for all seasons besides summer.

Africa's temperatures will rise higher than the worldwide 21st-century average (James and Washington, 2013). Under the RCP4.5 and RCP8.5 frameworks, the global average surface air temperature will most likely rise above the range observed during the twentieth century by 2069. However, these unprecedented climates will come between 1-2 decades sooner than the average global events across the tropics. Insignificant climatic changes can push tropical West Africa's narrow climatic boundaries (Niang et al., 2014). Projections suggest that African regions will reach increases of 2 °C in the preceding two decades towards the end of this century compared to the annual mean temperature for the late 20th century and the whole of Africa under the high emissions scenario. Based on RCP prediction, the exceedance of the critical global average temperature rise of 2 °C would occur in much of Africa by mid-21st century. Southern Africa's mean land surface will experience higher-than-average mean global land warming across all seasons (James and Washington, 2013). Additionally, the projected warming of between 3.4 °C and 4.2 °C by the year 2100 would be at the high end of the natural variability of the climate (Moise and Hudson, 2008). The projected elevated warming of semi-arid regions of the southwestern subregions will encompass South Africa, Botswana and Namibia (Engelbrecht et al., 2009). Projections for precipitation have higher geographical and seasonal variability than projections in temperature, although rain tends to be more unpredictable than temperature. Still unclear are the projected changes in rainfall across sub-Saharan Africa in the middle part of the 21st century (James and Washington, 2013). In countries with high or complex topography, downscaled projections suggest that rainfall and rainfall extremes will intensify near the end of the 21st century.

Effects of climate change drivers on earthworms

Globally, ecosystems are under unprecedented stress due to climate change (Masson-Delmotte et al., 2018). The soil ecosystem provides critical services and sustains the high biological diversity on which terrestrial life depends. Earthworms, along with other organisms, are essential parts of terrestrial ecosystems. Phillips et al. (2019) compared earthworm communities sampled from a variety of regions around the world. They discovered that species richness and abundance were higher at high latitudes, thus, contradicting previous reports for organisms above ground. They found that climate variables also influenced earthworm communities despite the effects of habitat cover and soil parameters. Climate change also significantly reduces soil moisture (Poll et al., 2013). Earthworms are at a disadvantage because of the permeability of their integuments and the fact that they rely on moist habitats for survival (Siebert et al., 2019). The diversity, abundance and richness of many earthworm groups decline with increasing drought and rise in temperature due to the deleterious impacts on their physiology, development, and reproduction caused by global climate change (Geisen et al., 2014). Distal climate change drivers that affect earthworms with possible influence on soil GHG emissions on larger scales include temperature, moisture or precipitation, flooding and drought (*Table 1*).

Effects of temperature

Temperature is a significant climate change driver contributing to global warming and influencing soil species' activity and decomposition processes. Thus, many researchers have studied the effects of temperature on individual soil-dwelling micro- and macro-organisms. Earthworms are poikilothermic; therefore, temperature affects them, influencing their activity, growth, density, metabolism, respiration, and reproduction (Eisenhauer et al., 2014). When exposed to the ideal environment for their metabolic processes, high and low temperatures trigger the same set of behaviours. Lower extreme temperatures are less documented than upper-extreme temperatures, ranging from 25 °C to 35 °C and differ significantly between species. Tropical species become more adapted to higher temperatures in time than temperate species, while temperate species become more resistant to lower temperatures (Singh et al., 2019). Earthworms may have profound seasonal variation in their occurrence and activity patterns, especially in areas with dry or cold climates.

Earthworm abundance increases during summer and decreases during winter due to soil conditions and climate change (Singh et al., 2019). The activity of decomposer organisms will be affected by future increases in soil temperatures, potentially increasing the cycling of elements and emission of greenhouse gases. Marhan et al. (2015) studied the effects of incorporating *Phacelia tanacetifolia* Benth. (a nitrogen-rich green manure litter) in arable soil by introducing *Aporrectodea caliginosa* coupled with increasing soil temperatures (+3.5 °C) on carbon and nitrogen cycling for 42 days in a three-factorial microcosm experiment. They found that higher CO₂ emissions increased with increasing soil temperatures, although emission was stronger in litter-free treatments. This result implies that as temperature increases, resulting in drought and reduced litter, endogeic earthworms' CO₂ emissions will increase. Earthworm activity significantly increased N₂O emissions by 70–90%. They concluded that there is a higher risk of N losses in the form of leaching or N₂O emission in earthworm-populated arable soils with warmer climatic conditions. In a Hohenheim climate change experiment,

Siebert et al. (2019), suggested that reduced earthworm density and warming alter ecosystem functions and services in the soil simultaneously, owing to changes in soil biota diversity and density which would likely result in inefficient belowground food webs. Findings from this research emphasize the need to maintain a higher population of earthworms to mitigate the negative consequences of climate change in agriculture. Climate change, on the other hand, has been observed to lower earthworm density and biomass. In the context of a field experiment, earthworm density and biomass exhibited strong negative correlations with temperature, with densities across all sites lower than the global average, according to Mcinga et al. (2021). The study found that earthworm diversity and density were highest in sub-humid habitats and that temperature influenced earthworm distribution, diversity, and density.

According to González-Alcaraz and van Gestel (2016), *Eisenia andrei* loses weight at higher temperatures than at lower temperatures. Similarly, Lima et al. (2015), observed that *Eisenia andrei* lost more weight at a higher temperature of 26 °C than at 20 °C, thus, confirming the effects of warming on earthworms. Both studies, however, focused on earthworms' responses to contaminated environments. Therefore, global warming may be less severe in temperate and wet areas (Berman and Meshcheryakova, 2013). In contrast, a steady rise in temperature across tropical and arid regions can put earthworms in these soils under significant water and metabolic stress, especially during year-round intermittent rainfall (Hughes et al., 2019). Hughes et al. (2019) employed climatic niche modelling to estimate the distribution of *Rhinodrilus alatus*, a species that has been historically harvested and sold as fishing bait in Brazil. According to their findings, climate change will alter the breadth of earthworm distribution and cause severe dispersion outside of the already defined geographical boundaries of the worms. Climatic conditions are significant determinants in the diversity of earthworms and their geographical distribution. Thus, earthworm populations continue to decrease during the dry or cold season and reach their most incredible abundance in a favourable environment (Singh et al., 2019). Generally, for plants and other animal species, a warming climate will have a negative impact in equatorward and low elevation populations but a positive impact in poleward or high elevation populations of a given species range. Furthermore, even if the effects of rising climate are entirely negative for a given species, other species function better in the new, warmer climate, so it is a matter of mismatch of climate and species, as well as species' ability to migrate to stay in an optimum climate.

Effects of soil moisture

According to IPCC (2013), the likelihood of severe rainfall and flooding events is on the rise globally. The report further stated that more places experienced higher frequencies of heavy precipitation events than those experiencing lower frequencies; for instance, precipitation events have increased considerably over the last 50 years across North America and Europe. However, confidence in trends is at a low level in other countries. Under the SRES A1B and A2 scenarios, in the 21st-century, precipitation is likely to decrease in North Africa and South Africa (medium to high confidence). There is uncertainty surrounding rainfall predictions across sub-Saharan Africa from the middle to the later part of this century (Niang et al., 2014). Soil moisture content is a significant factor affecting water and heat energy exchange between the surface of the earth and atmosphere via plant transpiration and the process of evaporation, essential for the survival of earthworms, growth, and population increase. Bessolitsyna (2012)

evaluated the abundance and distribution of earthworms in southern-middle Siberia and found that soil moisture and soil types changed their richness and distribution. Andriuzzi et al. (2015) demonstrated that earthworms are affected by altered rainfall patterns; thus, they may alter their burrowing behaviour. Poorly drained soil can also be disadvantageous to earthworm survival, such as in the case of anaerobic conditions. However, when earthworms, such as *Lumbricus Terrestris* are present, soil moisture drops much faster after heavy rainfall (Eisenhauer et al., 2014; Andriuzzi et al., 2015). Earthworms' survival in arid environments is contingent upon having adequate moisture in the soil, which is unlikely to be an issue in more temperate climates. Many earthworm species can enter diapause, para-diapause, or aestivation to survive in dry soil. *Aporrectodea trapezoides*, for example, might be able to withstand reduced moisture conditions by aestivation and remaining dormant pending improvement in soil moisture (McDaniel et al., 2013). Soil moisture influences microbially mediated nitrogen (N) cycle reactions by regulating redox potential (Chen et al., 2014). The nitrifier denitrification pathway is a significant contributor of N₂O fluxes from soil and a function of moisture content (Kool et al., 2011). Previous drying-rewetting research found that the rate of the drying and recovery cycles could affect N₂O emissions (Chen et al., 2014).

Effects of flooding

Flood-prone areas have a complex topsoil composition, which provides a diverse range of habitats for earthworms (Bullinger-Weber et al., 2012). Flooding has a profound impact on the soil's physical and chemical qualities. Water diffuses oxygen at a far slower rate than air, roughly 104 times slower (Schlesinger, 2013). Thus, during flooding in soils, oxygen demand quickly exceeds the supply (Wilshire-Kiss, 2019). Microorganisms and plant roots absorb oxygen shortly after flooding, leaving a depleted level of oxygen near the air-water interface; as a result, the soil becomes anoxic within 24 h (Tanji et al., 2003) and remaining at a low ebb throughout the inundation period (Unger et al., 2009). Endogeic species is the most commonly found earthworms in agricultural soils, followed by anecic and epigeic earthworms (Pelosi et al., 2009). In aerated water, earthworms can live for extended periods and are capable of surviving flooding, but their survival and behavioural responses vary between species (Zorn et al., 2008). To avoid drying and maintain hydrostatic pressure, all soft-bodied organisms such as earthworms need moist conditions. Therefore, moisture is an essential element of earthworms' survival. Their high abundance and high frequency of occurrence in floodplains of temperate regions are therefore not surprising. On the other hand, flooding and torrential rain can make earthworms hard to find, and many earthworms die after being exposed to heavy rain (Zorn et al., 2005). *Lumbricus rubellus* (Epigeic species) are the first to colonize floodplains within the first five years of a severe flooding event, even with the poor soil quality of such habitats (Fournier et al., 2012). According to Zorn et al. (2005), the number and biomass of *L. rubellus* declined to near-zero in flooded areas but recovered quickly within six months to pre-flood levels. Furthermore, epigeic species in a frequently flooded habitat attain maturity faster than those in less frequently flooded habitats (Klok et al., 2006). However, the breakdown of soil structure is the most common devastating physical effect of flooding in soils. It dissolves soil cementing agents and biological films, causing soil particle cohesiveness to decrease. Soil organic matter content increases as a result of regular floods. Once the ecosystem is impacted by a flood, returning to the previous state takes several years (Gerisch et al., 2012).

Table 1. Effects of climate change drivers on earthworms and greenhouse gas emission from soil

Earthworm species	Climate change drivers				Experimental period (days)	Type of experiment	Earthworm diversity, abundance and ecosystem function	Effect on CO ₂ emission	Effect on N ₂ O emission	Effect on CH ₄ emission	C/N ratio of soil	References
	Temperature	Precipitation/soil moisture	Flooding	Drought								
<i>Dendrobaena octaedra</i> ; <i>Aporrectodea caliginosa</i> ; <i>Pontoscolex corethrurus</i> (Rhinodrilidae); <i>Allolobophora chlorotica</i> <i>Amyntas aspergillum</i> , <i>Lumbricus terrestris</i> and <i>Fimoscolex sporadochaetus</i>	Increased temperature	Increased rainfall	-	-	-	Field	7 exotic earthworm species present; Earthworm density and biomass decreased with temperature; Earthworm density and biomass increased with rainfall	-	-	-	-	Mcinga et al. 2021
<i>Eisenia fetida</i>	20 ± 0.5 °C	12, 25, 50 and 75% WHC	-	-	20 days	Laboratory	-	Increased CO ₂ flux at 75% WHC	-	Detectable CH ₄ emissions 50 and 75% WHC	-	Gorbunova et al. 2020
<i>Eisenia fetida</i>	20 °C	60 % WHC	-	-	35 days	Laboratory	-	Increased emission	Increased emission	-	-	Zhu et al. 2018
<i>Aporrectodea caliginosa</i>	Elevated	-	-	-	42 days	Field	Increased nitrification activity in warmed soils; increased NO ₃ ⁻ leaching	Warming significantly increased cumulative CO ₂ emission by 14.9%	Strongly increased by 70–90%	low	-	Marhan et al. 2015
<i>Lumbricus terrestris</i>	-	Increased soil moisture	-	-	105 days	Field and laboratory	-	Increased by 13%	Increased by 27%	-	-	Nieminen et al. 2015

<i>Lumbricus terrestris</i> , <i>Aporrectodea longa</i> , <i>Aporrectodea caliginosa</i> , <i>Aporrectodea icterica</i> and <i>Aporrectodea rosea</i>	Elevated temperature	-	-	-	-	Field	Lower species richness and modify ecosystem functions	-	-	-	-	Siebert et al. 2019
<i>Lumbricus terrestris</i>	Increased temperature	-	-	Dryer conditions	-	-	Exacerbate the effects of deep ploughing on <i>L. terrestris</i> population declines	-	-	-	-	Johnston et al. 2018
<i>Eisenia fetida</i>	Increased air temperature	Reduced soil moisture content	-	-	21 days	Laboratory	Increased weight loss	-	-	-	-	González-Alcaraz and van Gestel (2016)
<i>Amyntas agrestis</i>	Increased temperature	Reduced moisture	-	-	-	Laboratory	Increased weight loss and reduced survival and	-	-	-	-	Richardson et al. 2009
<i>Eisenia fetida</i>	-	-	-	-	139 days	Laboratory	-	Increased emission	Increased emission	-	-	Tejada et al. 2014
<i>Eisenia fetida</i>	Increased temperature	-	-	-	14 days	Laboratory	Increased weight	-	-	-	-	Lima et al. 2015
<i>Lumbricus rubellus</i>	-	-	-	-	83 days	Field	-	Increased CO ₂ emission by 33%	Increase N ₂ O emission 42%	-	-	Lubbers et al. 2013
<i>Eisenia foetida</i>	-	-	-	-	15 days	Laboratory	-	Increased emission	-	Increased emission	-	Majumdar et al. 2006
<i>Eisenia nordenskioldi nordenskioldi</i> and <i>Eisenia nordenskioldi pallida</i>	Reduced temperature (-3 to -25 °C)	50-60 % WHC	-	-	14 days	Laboratory	Worms & cocoons of <i>Eisenia n. nordenskioldi</i> withstand temperatures of -34 & -40°C, and those of <i>E. n. pallida</i> , -28 & -23°C, respectively.	-	-	-	-	Berman and Meshcheryakova (2013)

<i>Aporrectodea caliginosa</i>	-	-	-	Average soil water matric potentials of -0.061, -0.085, -0.13, and -0.19 MPa	21 days	Laboratory	Drought did not affect earthworm mass, but drought lasting 2 or 3 wk increased the number of <i>A. caliginosa</i> in estivation. Three weeks of drought resulted in a mortality rate of 14%	-	-	-	-	McDaniel et al. 2013
<i>Aporrectodea turgida</i> and <i>Lumbricus terrestris</i>	-	33% water-filled pore space (WFPS), constant 97% WFPS	-	-	69 days	-	-	-	Earthworms increased N ₂ O emissions by 50% in the 33% WFPS soil but decreased N ₂ O emissions by 34% in the 97% WFPS soil	-	-	Chen et al. 2014
<i>Allolobophora chlorotica</i> , <i>Aporrectodea caliginosa</i> and <i>Lumbricus rubellus</i>	-	-	35%, 45% (field capacity), 55%, 65% (saturated) to 65%+ (saturated and an extra water layer) (% , w/w)	-	42 days	Laboratory	<i>A. chlorotica</i> was tolerant to water; <i>A. caliginosa</i> showed little response to flooding; <i>L. rubellus</i> was sensitive towards flooding	-	-	-	-	Zorn et al. 2008

Effects of drought

Water availability and low levels of organic matter in the soil limit the distribution of earthworms in many regions; however, they adapt to reduced moisture by entering aestivation to survive the harsh conditions occasioned by the low level of soil moisture (McDaniel et al., 2013). During severely reduced soil moisture, the soil becomes harder, severely reducing soil animals' mobility. There is a likely loss of plant diversity due to drought-induced changes in the soil's functioning, altering ecosystem services. Earthworms sustain critical ecological services such as litter decomposition and nutrient cycling, both of which may be affected by climate change. Drought stress directly affects earthworms by reduced soil moisture and indirectly by the decline of the quality plant supply on which they feed (Mariotte et al., 2016). Endogeic earthworms, for example, *Aporrectodea caliginosa*, living in horizontal burrows, are often very susceptible to drought (Bayley et al., 2010). Their ability to survive short droughts is because they can burrow into the soils and from aestivation chambers. Anecic earthworms may enter into diapause in dry periods and maintain dormancy for a few months (Jiménez and Decaëns, 2004). Several physiological mechanisms help earthworms survive prolonged periods of drought. Holmstrup et al. (2016) recently discovered the adaptive significance of the amino acid, alanine, in three species of earthworms (*Aporrectodea tuberculata*, *Aporrectodea icterica*, and *Aporrectodea longa*). They suggested that alanine accumulation sufficiently protects against the adverse effects of desiccation in earthworms. The findings of the study prove that earthworms respond to dry conditions by changing their metabolism and physiology

Climate change: earthworms and soil greenhouse emission

Earthworms play a significant role in the greenhouse gas balance of soils globally, and their impact will increase in the coming next decades (Lubbers et al., 2013). Earthworms are soil ecosystem engineers, triggering and responding to soil structural changes by feeding, burrowing, and casting activities. In a review by Lubbers et al. (2013), their findings unequivocally indicate a positive contribution to the net soil GHG emissions from soils in the presence of earthworms, suggesting that earthworms increase net soil-GHG emissions of nitrous oxide by 42% and carbon dioxide by 33%. According to Singh and Singh (2019), earthworms increased CO₂, N₂O, and CH₄ levels; however, emission rates vary depending on the physicochemical properties of the soil, organic matter incorporation, and earthworm feeding strategy.

An average of 20% of global carbon dioxide emissions are from soils (Rastogi et al., 2002), and approximately 33% of CH₄ and 67% of nitrous oxide (N₂O) emissions originate from soils globally (Lubbers, 2013) as shown in *Figure 4*. The production of greenhouse gases in soil ecosystems is the outcome of several biological processes. Carbon dioxide originates naturally from respiratory activities in soil (faunal, microbial, root respiration). Methane is produced through methanogenesis, while N₂O is by a combination of microbial activities. These processes thrive with the availability of carbon, soil temperature, moisture, and diffusivity, all of which influence microbial processes (Lubbers et al., 2013).

Furthermore, with the presence of earthworms, several investigations have indicated enhanced CO₂ and N₂O fluxes from the soil (e.g., Charpuis-Lardy et al., 2010; Nieminen et al., 2015). Few studies, on the other hand, revealed that earthworms elevated soil C stock, reduced CO₂ emissions, and contributed to soil C stability

(Bossuyt et al., 2005; Pulleman et al., 2005; Lubbers et al., 2013); no soil CO₂ efflux (Fisk et al., 2004) and lower N₂O emissions from soils (Lubbers et al., 2013). However, earthworms' effect on CH₄ fluxes has received less attention. Lubbers et al. (2013) concluded that the increasing emission of CO₂ by earthworms was insignificant during short experiments but significant after 200 days. Earthworms most likely accelerate initial C decomposition, but they may not affect the total amount decomposed over time. The reverse was the case for N₂O as well as earthworm-induced fluxes increased over time. These can be attributed to the anaerobic conditions in the earthworms' gut and the labile carbon and nitrogen present there. Soil greenhouse gas balance is best defined in the context of agroecosystems as the rate of carbon influx into soil carbon pools compared to the rates of carbon outflow and other GHG emissions from the soil (Lubbers et al., 2013). If the outflow rates equal inflow rates, then the C stock will be said to be stable. However, soil carbon stocks have decreased in recent decades due to the lower rates in the return of crop residues in soils.

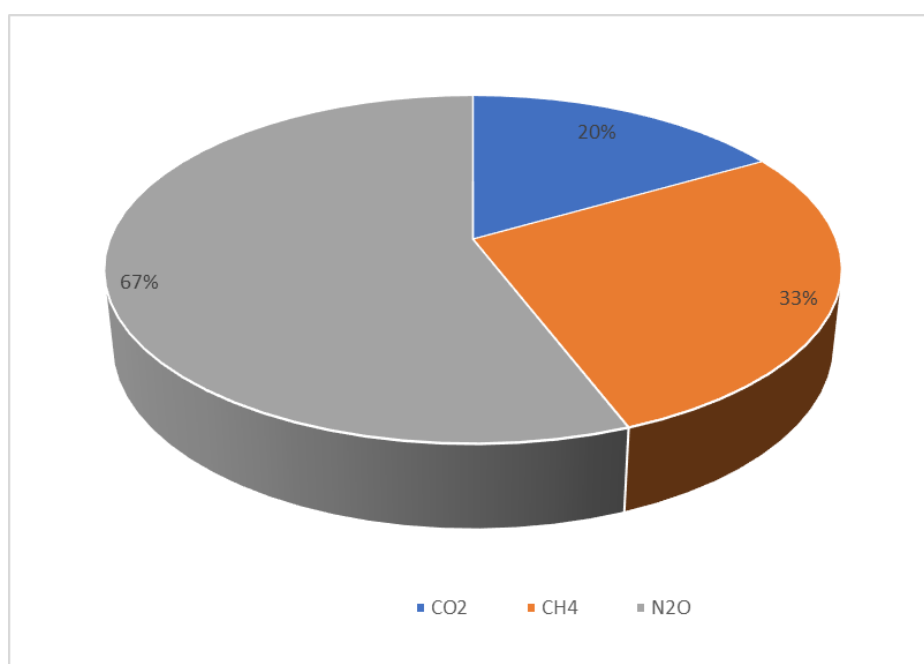


Figure 4. Percentage of global GHG (CO₂, N₂O and CH₄) emissions from the soils (Rastogi et al., 2002; Lubbers, 2013)

Earthworms increase soil carbon sequestration, which elevates greenhouse gas emissions. Soil activities that contribute to greenhouse gas emissions are dependent on the availability of substrates such as nitrogen (N) and carbon (C) for N₂O and physicochemical variables of the soil that ultimately determine microbial activity. The earthworm gut promotes anaerobic conditions by retaining moisture, carbon and mineral N during the denitrification process (Drake et al., 2006). When soil containing earthworms, their castings, mucus, and burrowing activities compared to soils without them, the outcome was a threefold emission of N₂O from the latter (Lemtiri et al., 2014). Earthworms ingest plant residues, and the microorganisms in their gut provide an ideal environment for mucus formation, thus, increasing the absorption of carbon and nitrogen in the foregut. Nitrogen fixation occurs in this region through clostridium, and

the ammonification process enhances N₂O production; at the same time, other microorganisms digested the organic substrate by enzyme action (Singh and Singh, 2019) (Fig. 5). The hindgut is an area where carbon is re-assimilated, increasing CO₂ percentage (Lubbers et al., 2013). Earthworms digest crop residues, thus, increasing the availability of organic nutrients in soils (Blouin et al., 2013). Thus, nitrous oxide comes from denitrification, nitrate, and nitrite processes which starts in the digestive system of earthworms. Earthworms are essential denitrifiers and significantly impact soil N₂O and N₂ emissions (Giannopoulos et al., 2010). Earthworms are responsible for over 50% of the soil-emitted nitrate (Drake et al., 2006). While earthworms hardly generate any GHGs, they can significantly impact the availability of substrates and physicochemical characteristics of the soil and indirectly affect emissions. The question of whether earthworms contribute to the soil sink or a source soil-GHGs emission has remained debatable. However, this review discusses how climate change drivers including, increased temperature, precipitation/moisture, flooding and drought, affect the distribution and biodiversity of earthworms and how that affects GHG emissions. Based on the findings from the reviewed literature, there is a strong indication that with the increasing impact of climate change, GHG emissions from the soil could increase (Fig. 5).

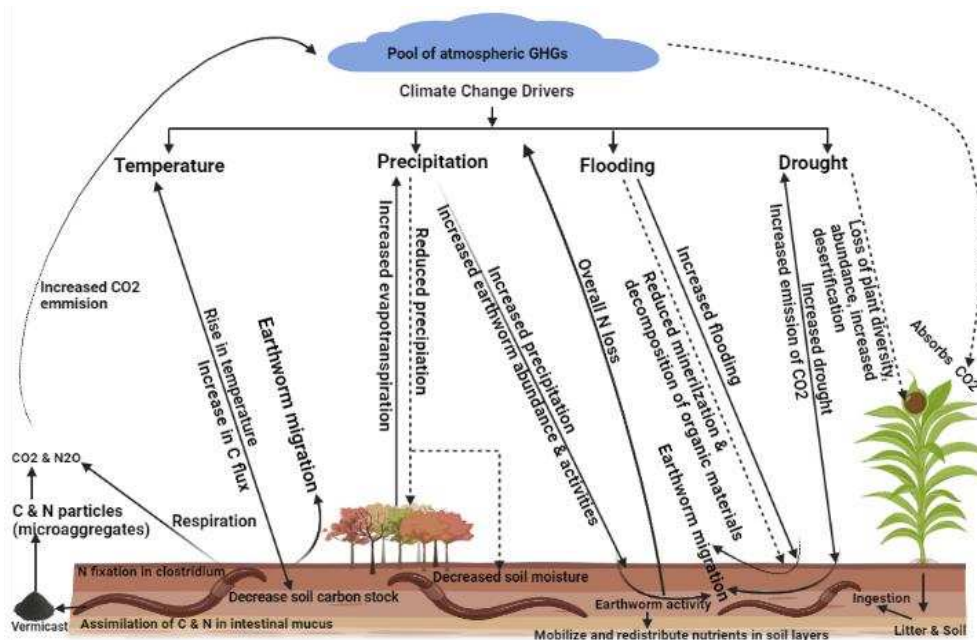


Figure 5. Simple representation of the impact of climate change on earthworms and the potential impacts of global warming on soil greenhouse gas balance (Solid lines indicate an increase while dotted lines signify a decrease in parameters)

In a bid to project the trends in the diversity, biomass and abundance of earthworms, Phillips et al. (2019) collected samples of earthworms from 6928 sampling locations across 57 countries, comprising temperate and tropical regions. They provided global, local, and regional abundance and biomass maps. They collected 180 published articles and several unpublished field study datasets from the 57 countries covering all continents except Antarctica. They studied the community patterns and determined the climatic factors that influence the abundance of earthworms. They added soil properties

into the earthworm model, which may play a role in earthworm population decision making (Rutgers et al., 2016). Their result demonstrated a strong association between climate variables and earthworm metrics. Although the link between the identified climatic factors and the evaluated community metrics is consistent with other studies, climate change will continue unabated because of increased anthropogenic activities. Their findings further highlighted the effects of temperature and precipitation on the diversity of earthworms, distribution and abundance, with consequences for their function and ecosystem services. When invasive earthworms impact ecosystems due to climate change, such as in parts of North America, distribution shifts may be problematic (Craven et al., 2017). Climate change may influence earthworm dispersal before it affects earthworm abundance and biomass since dispersal capabilities are relatively low in earthworms. Several terrestrial species ranges have recently moved to higher elevations and higher latitudes, and the rate of movements have tripled previously observed movement in the last few decades (Chen et al., 2020).

Earthworms will become more prevalent in ecosystems globally over the next few decades, as more organic fertilizers are applied to agricultural soils to feed the burgeoning population, which will provide more food for earthworms. Earthworm activity is likely to be stimulated as the world turns away from traditional land management techniques toward zero- or sustainable tillage. Both forms of tillage decrease the disturbance of the soil, which is beneficial to earthworms. Furthermore, several studies (Butterbach-Bahl et al., 2013; Lubbers et al., 2013) have improved our understanding of soil CO₂ and N₂O emission dynamics over the past decades. However, there are many considerable uncertainties and limitations in knowledge; for instance, soil biodiversity, physicochemical characteristics, and organism functions impact soil-GHG gas emissions. Among these gaps in knowledge, soil fauna's effects will be very significant in reducing, accelerating, or slowing down the emissions of CO₂ and N₂O from soils, most especially from agricultural soils subjected to different regimes of tillage. Over the next century, climate change will be one of the main drivers in altering the delicate balance between carbon sequestration in the soil by earthworms and soil greenhouse gas emission. In addition, invasive earthworms are spreading into new ecosystems due to global warming, causing soil disturbances and ecosystem transformation. This accelerated movement of earthworms into new territories has the potential to alter the climate and significantly release large chunks of stored carbon in these otherwise undisturbed soils. Thus, it has become expedient to understand the link between climate change, earthworms, and soil greenhouse gas balance.

Conclusions

This article puts the projected climate change data in context. We assessed how climate change drivers, such as temperature, moisture, drought, and floods, affect earthworms and the potential to affect the delicate balance between earthworms and greenhouse gas emissions. The structure, diversity, ecosystem function, the spread and success of invasive species of earthworms will be affected by climate change. The activity, abundance, and biomass of earthworms will increase when the soil is sufficiently moist. Additionally, climate extremes like drought and flooding are likely to impact earthworms negatively. Most of the data reviewed in this paper come from the world's temperate regions due to lack of data from other parts of the globe, such as Africa, the Mediterranean, and Antarctica. However, regardless of this gap in published

research data between regions, we expect all these climate change drivers to have nearly the same effects. Available scientific literature has shown that earthworms are likely to increase in environmentally diverse ecosystems in the future. Over the last few decades, we have gained a lot of knowledge about the dynamics of carbon dioxide (CO₂) and nitrous oxide (N₂O) emissions from agricultural soils. Conclusively, earthworms can influence CO₂ and N₂O release from arable soils, especially as the effects of climate change continues unabated. However, the number of earthworms that will significantly stimulate the overall emission of soil greenhouse gases is unclear. Therefore, we recommend that long-term studies of earthworms in natural systems or controlled climate chambers combined with field studies are required. This aspect of earthworm ecological studies will establish and improve our understanding of the significant fraction of the total soil GHG emissions (feedback) due to earthworms' activity influenced by climate change.

Acknowledgements. We thank the North-West University for providing the research fellowship.

Funding. This research did not receive any specific grants from public, commercial, or non-profit funding agencies.

Author contributions: PAO conceived the idea for the article and performed the literature search and data analysis, as well as drafted the article, while MSM critically revised the work (conceptual inputs) and the approved submission.

Conflict of interests. The authors declare that they have no competing interests.

REFERENCES

- [1] Abail, Z., Sampedro, L., Whalen, J. K. (2017): Short-term carbon mineralization from endogeic earthworm casts as influenced by properties of the ingested soil material. – *Appl. Soil Ecol.* 116: 79-86.
- [2] Andriuzzi, W. S., Pulleman, M. M., Schmidt, O., Faber, J. H., Brussaard, L. (2015): Anecic earthworms (*Lumbricus terrestris*) alleviate negative effects of extreme rainfall events on soil and plants in field mesocosms. – *Plant Soil* 397: 103-113.
- [3] Bardgett, R. D., van der Putten, W. H. (2014): Belowground biodiversity and ecosystem functioning. – *Nature* 515: 505-511.
- [4] Bayley, M., Overgaard, J., Høj, A. S., Malmendal, A., Nielsen, N. C., Holmstrup, M., Wang, T. (2010): Metabolic changes during estivation in the common earthworm *Aporrectodea caliginosa*. – *Physiological and Biochemical Zoology* 83: 541-550.
- [5] Berman, D. I., Meshcheryakova, E. (2013): Ranges and cold hardiness of two earthworm subspecies (*Eisenia nordenskiöldi*, Lumbricidae, Oligochaeta). – *Biology Bulletin* 40: 719-727.
- [6] Bessolitsyna, E. P. (2012): Ecological and geographic distribution patterns of earthworms (*Oligochaeta*, *Lumbricidae*) in landscapes of southern middle Siberia. – *Russian Journal of Ecology* 43: 82-85.
- [7] Blouin, M., Hodson, M. E., Delgado, E. A., Baker, G., Brussaard, L., Butt, K. R., Dai, J., Dendooven, L., Peres, G., Tondoh, J. E., Cluzeau, D., Brun, J. J. (2013): A review of earthworm impact on soil function and ecosystem services. – *Eur J Soil Sci* 64: 161-182.
- [8] Blume-Werry, G., Krab, E. J., Olofsson, J., Sundqvist, M. K., Väisänen, M., Klaminder, J. (2020): Invasive earthworms unlock arctic plant nitrogen limitation. – *Nature Communications* 11: 1766. <https://doi.org/10.1038/s41467-020-15568-3>.
- [9] Bossuyt, H., Six, J., Hendrix, P. F. (2005): Protection of soil carbon by microaggregates within earthworm casts. – *Soil Biol Biochem* 37: 251-258.

- [10] Brohan, P., Kennedy, J. J., Harris, I., Tett, S. F. F., Jones, P. D. (2006): Uncertainty estimates in regional and global observed temperature changes: a new data set from 1850. – *Journal of Geophysical Research* 111(D12): D12106. DOI: 10.1029/2005JD006548.
- [11] Bullinger-Weber, G., Guenat, C., Salomé, C., Gobat, J., Le Bayon, R. C. (2012): Impact of flood deposits on earthworm communities in alder forests from a subalpine floodplain (Kandersteg, Switzerland). – *European Journal of Soil Biology*. 49: 5-11.
- [12] Butterbach-Bahl, K., Baggs, E. M., Dannenmann, M., Kiese, R., Zechmeister-Boltenstern, S. (2013): Nitrous oxide emissions from soils: how well do we understand the processes and their controls? *Philos. – Trans. R. Soc. B: Biol Sci* 368: 0122.
- [13] Charpuis-Lardy, L., Brauman, A., Bernard, L., Pablo, A. L., Toucet, J., Mano, M. J., Weber, L., Brunet, D., Razafimbelo, T., Chotte, J. L., Blanchart, E. (2010): Effect of the endogeic earthworm *Pontoscolex corethrurus* on the microbial structure and activity related to CO₂ and N₂O fluxes from a tropical soil (Madagascar). – *Appl Soil Ecol* 45: 201-208.
- [14] Chen, C., Whalen, J. K., and Guo, X. (2014): Earthworms reduce soil nitrous oxide emissions during drying and rewetting cycles, *Soil Biol. – Biochem.* 68: 117-124.
- [15] Chen, X., Wang, L., Niu, Z., Zhang, M., Li, C., Li, J. (2020): The effects of projected climate change and extreme climate on maize and rice in the Yangtze River Basin, China. – *Agricultural and Forest Meteorology* 282-283: 107867.
- [16] Ciais, P., Sabine, C., Bala, G., Bopp, L., Brovkin, V., Canadell, J., Chhabra, A., DeFries, R., Galloway, J., Heimann, M., Jones, C., Le Quéré C., Myneni, R. B., Piao, S., Thornton, P. (2013): Carbon and Other Biogeochemical Cycles. – In: Stocker, T. F., Qin, D., Plattner, G. K., Tignor, M., Allen, S. K., Boschung, J., Nauels, A., Xia, Y., Bex, V., Midgley, P. M. (eds.) *Climate Change 2013: The Physical Science Basis. Contribution of Working Group I to the Fifth Assessment Report of the Intergovernmental Panel on Climate Change*. Cambridge University Press, Cambridge, UK and New York, pp. 465-570. <http://www.climatechange2013.org/report/full-report/>.
- [17] Craven, D., et al. (2017): The unseen invaders: introduced earthworms as drivers of change in plant communities in North American forests (a meta-analysis). – *Glob. Change Biol* 23: 1065-1074.
- [18] Drake, H. L., Schramm, A., Horn, M. A. (2006): Earthworm Gut Microbial Biomes: Their Importance to Soil Microorganisms, Denitrification, and the Terrestrial Production of the Greenhouse Gas N₂O. – In: König, H., Varma, A. (eds.) *Intestinal Microorganisms of Termites and Other Invertebrates*. Springer, Berlin, pp. 65-87.
- [19] EEA (2012): *Climate Change, Impacts and Vulnerability in Europe 2012, an Indicator-Based Report*. – EEA Report No. 12/2012, European Environment Agency (EEA), Copenhagen.
- [20] Eisenhauer, N., Stefanski, A., Fisichelli, N. A., Rice, K., Rich, R., Reich, P. B. (2014): Warming shifts ‘worming’: effects of experimental warming on invasive earthworms in northern North America. – *Scientific Reports* 4: 6890.
- [21] Engelbrecht, F. A., McGregor, J. L., Engelbrecht, C. J. (2009): Dynamics of the conforal-cubic atmospheric model projected climate-change signal over southern Africa. – *International Journal of Climatology* 29(7): 1013-1033.
- [22] Fahey, D. W., Doherty, S. J., Hibbard, K. A., Romanou, A., Taylor, P. C. (2017): *Physical Drivers of Climate Change*. – In: *Climate Science Special Report: Fourth National Climate Assessment, Volume I*.
- [23] Fisk, M. G., Fahey, T. J., Groffman, P. M., Bohlen, P. J. (2004): Earthworm invasion, fine-root distributions, and soil respiration in North temperate forests. – *Ecosystems* 7(1): 55-62.
- [24] Fournier, B., Samaritani, E., Shrestha, J., Mitchell, E. A. D., Le Bayon, R. C. (2012): Patterns of earthworm communities and species traits in relation to the perturbation gradient of a restored floodplain. – *Applied Soil Ecology* 59: 87-95.

- [25] Geisen, S., Bandow, C., Römbke, J., Bonkowski, M., (2014): Soil water availability strongly alters the community composition of soil protists. – *Pedobiologia* 57: 205-213.
- [26] Gerisch, M., Dziock, F., Schanowski, A., Ilg, C., Henle, K. (2012): Community resilience following extreme disturbances: the response of ground beetles to a severe summer flood in a central European lowland stream. – *River Research and Applications* 28: 81-92.
- [27] Giannopoulos, G., Pulleman, M. M., van Groenigen, J. W. (2010): Interactions between residue placement and earthworm ecological strategy affect aggregate turnover and N₂O dynamics in agricultural soil. – *Soil Biol. Biochem* 42: 618-625.
- [28] González-Alcaraz, M. N., van Gestel, C. A. A. (2016): Metal/metalloid (As, Cd and Zn) bioaccumulation in the earthworm *Eisenia andrei* under different scenarios of climate change. – *Environmental Pollution* 215: 178-186.
- [29] Gorbunova, A. Y., Korobushkin, D. I., Kostina, N. V., Maxim, I., Degtyarev, M. I., Gongalsky, K. B., Andrey Zaitsev, A. S. (2020): Level of soil moisture determines the ability of *Eisenia fetida* to reincorporate carbon from decomposed rice straw into the soil. – *European Journal of Soil Biology* 99(2020): 103209.
- [30] Grimm, N. B., Chapin III, F. S., Bierwagen, B., Gonzalez, P., Groffman, P. M., Luo, Y., Melton, F., Nadelhoffer, K., Pairis, A., Raymond, P. A., Schimel, J., Williamson, C.E (2013): The impacts of climate change on ecosystem structure and function. – *Front Ecol Environ* 11(9): 474-482. DOI: 10.1890/120282.
- [31] Hansen, J., Ruedy, R., Sato, M., Lo, K. (2010): Global surface temperature change. – *Review of Geophysics* 48(4): RG4004. DOI: 10.1029/2010RG000345.
- [32] Holmstrup, M., Slotsbo, S., Henriksen, P. G., Bayley, M. (2016): Earthworms accumulate alanine in response to drought. – *Comparative Biochemistry and Physiology Part A: Molecular & Integrative Physiology* 199: 8-13.
- [33] Hughes, F. M., Cortês-Figueira, J. E., Drumond, M. A. (2019): Anticipating the response of the Brazilian giant earthworm (*Rhinodrilus alatus*) to climate change: implications for its traditional use. – *Anais da Academia Brasileira de Ciências* 91(1): e20180308.
- [34] Intergovernmental Panel on Climate Change (IPCC) (2013): Confidence and Likelihood in the IPCC Fifth Assessment Report. – IPCC, Geneva.
- [35] IPCC (2014): Climate Change 2014: Synthesis Report. – In: Core Writing Team R, Pachauri, K., Meyer, L. A. (eds.) Contribution of Working Groups, I, II and III to the Fifth Assessment Report of the Intergovernmental Panel on Climate Change. IPCC, Geneva, Switzerland.
- [36] Jacob, D., Podzun, R. (2010): Global warming below 2°C relative to pre-industrial level: how might climate look like in Europe. – *Nova Acta Leopoldina* 384: 71-76.
- [37] James, R., Washington, R. (2013): Changes in African temperature and precipitation associated with degrees of global warming. – *Climatic Change* 117(4): 859-872.
- [38] Jiménez, J. J., Decaëns, T. (2004): The impact of soil organisms on soil functioning under neotropical pastures: a case study of a tropical anecic earthworm species. – *Agriculture, Ecosystems and Environment* 103: 329-342.
- [39] Johnston, A. S. S., Sibly, R. M., Thorbek, P. (2018): Forecasting tillage and soil warming effects on earthworm populations. – *Journal of Applied Ecology*. 55: 1498-1509.
- [40] Klok, C., Zorn, M., Koolhaas, J. E., Eijsackers, H. J. P., Van Gestel, C. A. M. (2006): Does reproductive plasticity in *Lumbricus rubellus* improve the recovery of populations in frequently inundated river floodplains? – *Soil Biology & Biochemistry* 38: 611-618.
- [41] Kool, D. M., Dolfing, J., Wrage, N., Van Groenigen, J. W. (2011): Nitrifier denitrification as a distinct and significant source of nitrous oxide from soil. – *Soil Biology & Biochemistry* 43: 174-178.
- [42] Lemtiri, A., Colinet, G., Alabi, T., Cluzeau, D., Zirbes, L., Haubruge, E., Francis, F. (2014): Impacts of earthworms on soil components and dynamics. A review. – *Biotechnol Agron Soc Environ* 18(1): 121-133.

- [43] Lima, M. P. P., Cardoso, D. N., Soares, A. M., M. M., Loureiro, S. (2015): Carbaryl toxicity prediction to soil organisms under high and low temperature regimes. – *Ecotoxicology and Environmental Safety* 114: 263-272.
- [44] Lubbers, I. M., van Groenigen, K. J., Steven, J. F., Six, J., Brussaard, L., van Groenigen, J. W. (2013): Greenhouse-gas emissions from soils increased by earthworms. – *Nature* 3: 187-194.
- [45] Majumdar, D., Patel, J., Bhatt, N., Desai, P. (2006): Emission of methane and carbon dioxide and earthworm survival during composting of pharmaceutical sludge and spent mycelia. – *Biores Technol* 97(4): 648-658.
- [46] Marhan, S., Auber, J., Poll, C. (2015): Additive effects of earthworms, nitrogen-rich litter and elevated soil temperature on N₂O emission and nitrate leaching from an arable soil. – *Applied Soil Ecology* 86: 55-61.
- [47] Mariotte, P., Le Bayon, R., Eisenhauer, N., Guenat, C., Buttler, A. (2016): Subordinate plant species moderate drought effects on earthworm communities in grasslands. – *Soil Biology and Biochemistry* 96: 119-127.
- [48] Masson-Delmotte, V., Zhai, P., Pörtner, H., Roberts, D., Skea, J., Shukla, P., Waterfield, T. (2018): Global warming of 1.5 C. An IPCC Special Report on the impacts of global warming of 1.5 C above pre-industrial levels and related global greenhouse gas emission pathways, in the context of strengthening the global response to the threat of climate change, sustainable development, and efforts to eradicate poverty. Summary for Policymakers Edited by Science Officer Science Assistant. – IPCC, Geneva.
- [49] McDaniel, J. P., Stromberger, M. E., Barbarick, K. A., Cranshaw, W. (2013): Survival of *Aporrectodea caliginosa* and its effects on nutrient availability in biosolids amended soil. – *Applied Soil Ecology* 71: 1-6.
- [50] Mcinga, S., Manyevere, A., Mkeni, P. (2021): Earthworm diversity and density as affected by soil and climatic factors in Raymond Mhlaba municipality, Eastern Cape province, South Africa. – *South African Journal of Plant and Soil* 38(1): 19-26. DOI: 10.1080/02571862.2020.1822453.
- [51] Medina-Sauza, R. M., Álvarez-Jiménez, M., Alix Delhal, A., Reverchon, F., Blouin, M., Guerrero-Analco, J. A., Cerdán, C. R., Guevara, R., Villain, L., Barois, I. (2019): Earthworms building up soil microbiota, a review. – *Front. Environ. Sci.* <https://doi.org/10.3389/fenvs.2019.00081>.
- [52] Moise, A. F., Hudson, D. A. (2008): Probabilistic predictions of climate change for Australia and southern Africa using the reliability ensemble average of IPCC CMIP3 model simulations. – *Journal of Geophysical Research D: Atmospheres* 113(15): D15113. DOI: 10.1029/2007JD009250.
- [53] Múgica, M., Sokolova, I., Izagirre, U., Marigómez, I. (2015): Season-dependent effects of elevated temperature on stress biomarkers, energy metabolism and gamete development in mussels. – *Mar. Environ. Res* 103: 1-10.
- [54] Niang, I., Ruppel, O. C., Abdrabo, M. A., Essel, A., Lennard, C., Padgham, J., Urquhart, P. (2014): Africa. – In: Barros, V. R., Field, C. B., Dokken, D. J., Mastrandrea, M. D., Mach, K. J., Bilir, T. E., Chatterjee, M., Ebi, K. L., Estrada, Y. O., Genova, R. C., Girma, B., Kissel, E. S., Levy, A. N., MacCracken, S., Mastrandrea, P. R., White, L. L. (eds.) *Climate Change 2014: Impacts, Adaptation, and Vulnerability. Part B: Regional Aspects. Contribution of Working Group II to the Fifth Assessment Report of the Intergovernmental Panel on Climate Change.* Cambridge University Press, Cambridge, UK and New York, pp. 1199-1265.
- [55] Nieminen, M., Hurme, T., Mikola, J., Regina, K., Nuutinen, V. (2015): Impact of earthworm *Lumbricus terrestris* living sites on the greenhouse gas balance of no-till arable soil. – *Biogeosciences* 12: 5481-5493.
- [56] Pelosi, C., Bertrand, M., Capowicz, Y., Boizard, H., Roger-Estrade, J. (2009): Earthworm collection from agricultural fields: comparisons of selected expellants in presence/absence of hand-sorting. – *European Journal of Soil Biology* 45(2): 176-183.

- [57] Phillips, H. R. R., Guerra, C. A., Bartz, M. L. L., Briones, M. J. J., Brown, G., et al. (2019): Global distribution of earthworm diversity. – *Science* 366: 480-485. DOI: 10.1126/science.aax4851.
- [58] Poll, C., Marhan, S., Back, F., Niklaus, P. A., Kandeler, E. (2013): Field-scale manipulation of soil temperature and precipitation change soil CO₂ flux in a temperate agricultural ecosystem. – *Agric. Ecosyst. Environ.* 165: 88-97.
- [59] Pulleman, M. M., Six, J., van Breemen, N., Jongmans, A. G. (2005): Soil organic matter distribution and microaggregate characteristics as affected by agricultural management and earthworm activity. – *Eur J Soil Sci* 56: 453-467.
- [60] Räisänen, J., Eklund, J. (2012): 21st century changes in snow climate in Northern Europe: a high-resolution view from ENSEMBLES regional climate models. – *Climate Dynamics* 38(11-12): 2575-2591.
- [61] Rastogi, M., Singh, S., Pathak, H. (2002): Emission of carbon dioxide from soil. – *Curr. Sci.* 82: 510-518.
- [62] Richardson, D. R., Snyder, B. A., Hendrix, P. F. (2009): Soil moisture and temperature: tolerances and optima for a non-native earthworm species, *Amyntas agrestis* (Oligochaeta: Opisthopora: Megascolecidae). – *Southeastern Naturalist* 8: 325-334.
- [63] Rutgers, M. et al. (2016): Mapping earthworm communities in Europe. – *Appl. Soil Ecol.* 97: 98-111.
- [64] Saunio, M., Jackson, R. B., Bousquet, P., Poulter, B., Canadell, J. G. (2016): The growing role of methane in anthropogenic climate change. – *Environmental Research Letters* 11: 120207. <http://dx.doi.org/10.1088/1748-9326/11/12/120207>.
- [65] Schlesinger, W. H. (2013): *Biogeochemistry: An Analysis of Global Change*. – Academic Press, Oxford.
- [66] Siebert, J., Eisenhauer, N., Poll, C., Marhan, S., Bonkowski, M., Hines, J., Koller, R., Ruess, L., Thakur, M. P. (2019): Earthworms modulate the effects of climate warming on the taxon richness of soil meso- and macrofauna in an agricultural system. – *Agriculture, Ecosystems & Environment*. 278: 72-80.
- [67] Singh, A., Singh, G. S. (2019): Is earthworm a protagonist or an antagonist in greenhouse gas (GHG) emissions from the soil? – *International Journal of Environmental Science and Technology* 16: 1145-1158.
- [68] Singh, J., Schädler, M., Demetrio, W., Brown, G. G., Eisenhauer, N. (2019): Climate change effects on earthworms - a review. – *Soil Org.* 91(3): 114-138. DOI: 10.25674/so91iss3pp114.
- [69] Smith, T. M., Reynolds, R. W., Peterson, T. C., Lawrimore, J. (2008): Improvements to NOAA's historical merged land-ocean surface temperature analysis (1880-2006). – *Journal of Climate* 21(10): 2283-2293.
- [70] Tanji, K. K., Gao, S., Scardaci, S. C., Chow, A. T. (2003): Characterizing redox status of paddy soils with incorporated rice straw. – *Geoderma* 114: 333-353.
- [71] Tejada, M., Sanchez-Monedero, M. A., Isidoro, G. (2014): Influence of particle size of municipal solid waste amendments and presence or absence of *Eisenia fetida* on soil greenhouse gases emission. – *Commun Soil Sci Plant Anal* 45(9): 1214-1226.
- [72] Unger, I. M., Motavalli, P. P., Muzika, R. M. (2009): Changes in soil chemical properties with flooding: a field laboratory approach. – *Agriculture Ecosystems & Environment* 131: 105-110.
- [73] van Groenigen, J. W., Lubbers, I. M., Vos, H. M. J., Brown, G. G., De Deyn, G. B., van Groenigen, K. J. (2014): Earthworms increase plant production: a meta-analysis. – *Scientific Reports* 4: 6365.
- [74] Wilshire-Kiss, T. B. (2019): *Earthworms, flooding, and sewage sludge*. – PhD Thesis, University of York.
- [75] Zhu, X., Chang, L., Lic, J., Liu, J., Feng, F., Wu., D. (2018): Interactions between earthworms and mesofauna affect CO₂ and N₂O emissions from soils under long-term conservation tillage. – *Geoderma* 332: 153-160.

- [76] Zorn, M. I., Van Gestel, C. A. M., Eijsackers, H. (2005): Species-specific earthworm population responses in relation to flooding dynamics in a Dutch floodplain soil. – *Pedobiologia* 49(3): 189-198.
- [77] Zorn, M. I., Van Gestel, C. A. M., Morrien, E., Wagenaar, M., Eijsackers, H. (2008): Flooding responses of three earthworm species, *Allolobophora chlorotica*, *Aporrectodea caliginosa*, and *Lumbricus rubellus*, in a laboratory-controlled environment. – *Soil Biology and Biochemistry* 40: 587-593.

RESEARCH ON THE CHANGE OF ECOSYSTEM SERVICES AND THEIR TRADE-OFF IN URBANIZATION AREA

FAN, Q. D.* – YANG, X. Y. – LI, H.

*School of Architecture, North China University of Water Resources and Electric Power,
Zhengzhou, Henan 450046, PR China*

**Corresponding author
e-mail: fanqindong@126.com*

(Received 17th Jan 2022; accepted 20th May 2022)

Abstract. Rapid urbanization causes changes in regional ecosystem services and has an impact on human well-being. Understanding the changes and trade-offs of ecosystem services in urbanized areas is very important to improve the overall benefits of ecosystem services and maintain regional ecological security. Taking the urbanized area between Zhengzhou City and Kaifeng City in Henan Province, China as an example, the changes in ecosystem services and their trade-offs during the “2005-2010-2015” years were analyzed. The results show that in the process of urbanization, the four selected ecosystem services are in a declining state; The relationship between ecosystem services shows obvious dynamic changes. The traditional method of using a single time period or a time node to study trade-offs is often misjudged, and the research on continuous multi-time series should be strengthened in the future.

Keywords: *landscape pattern, evaluation, carbon sequestration, habitat quality, landscape aesthetics, grain yield*

Introduction

Urbanization brings agglomeration effect, which can effectively promote the comprehensive development of economy, society and culture (Ouyang et al., 2021; Asgarian et al., 2015). At the same time, in the process of urbanization, a large number of natural and semi-natural land has been transformed into construction land, and the land use type has changed significantly (Vahmani et al., 2016). Substance-recycling and energy-flowing of the ecosystem on the surface are strongly disturbed, and the process of the ecosystem cannot be completed, resulting in a serious impact on the service supply of the ecosystem (Smiraglia et al., 2016).

Ecosystem services are all material products and services obtained by human beings from the ecosystem, which are divided into provision services, regulation services, cultural services and support services (Millennium Ecosystem Assessment, 2005; Redhead et al., 2018). Urbanization leads to landscape fragmentation, reduction of natural and semi-natural habitats, etc. A large number of originally synergistic and competitive relationships among ecosystem services are transformed into trade-off relationships, resulting in a continuous decline in the overall supply of ecosystem services in urbanized areas (Ramyar et al., 2020). Urbanization is the most important factor affecting the change of landscape surface pattern in recent decades, and it is also the human behavior that has the greatest impact on ecosystem services (Moein et al., 2018). Ecosystem is facing increasing urbanization pressure. Exploring the impact of urbanization on ecosystem services has become the focus of global change research (Taylor and Hochuli, 2015; Augustynczyk and Yousefpour, 2021).

The research on the impact of urbanization on ecosystem services mainly involves the quantitative evaluation (Yang, 2015), spatio-temporal change and simulation (Li et al.,

2020), driving force analysis (Ndong et al., 2020) of ecosystem services and its impact on human well-being (Yang et al., 2021; Xiao et al., 2021). Ecosystem service assessment is the most studied aspect. The initial research methods are equivalent factor method, market value method, shadow engineering method, opportunity cost method, willingness to pay method and so on. With the advancement of research, model evaluation combined with ecosystem service mechanism has gradually become the mainstream (Torres et al., 2021). Common evaluation models include ARIES (Artificial Intelligence for Ecosystem Services) (Villa et al., 2014; Bagstad, 2011), SoLVES (Social Values for Ecosystem Services) (Estoque and Murayama, 2016; Sherrouse et al., 2014) and InVEST (Integrated Valuation of Ecosystem Services and Tradeoffs) (Tallis and Polasky, 2009; Sharp et al., 2014).

The overall research moves from static ecosystem service assessment to dynamic spatio-temporal analysis and scenario simulation (Li et al., 2020). In terms of urbanization, relevant research has moved from the impact theory of urbanization on ecosystem services to the management and regulation of ecosystem services in the process of urbanization (Liang et al., 2021). Direct or indirect adoption of landscape measures (such as ecological process control, scale adjustment, spatial planning, policy intervention, etc.) has become the mainstream of ecosystem service management. However, due to the correlation between most ecosystem services, ecosystem service management without “trade-offs” often leads to another negative ecological result (Xu et al., 2018). In the process of urbanization, the trade-off of ecosystem services has become an important aspect of research (Zheng et al., 2019). However, in the current research, the trade-off determination is mostly concentrated in a single period or a time period, and there is a lack of long-term uninterrupted serial research. Moreover, there is a lack of specific mechanistic explanations between the assessment of ecosystem services and the determination of trade-offs.

Taking the urbanization area between Zhengzhou City and Kaifeng City in Henan Province, China as an example, the changes of four ecosystem services including carbon sequestration services, habitat quality, landscape aesthetics, and grain yield under the background of urbanization in 2005, 2010 and 2015 were analyzed. Then, the trade-off relationships between the four ecosystem services were determined.

Trying to explain the reasons for the trade-off relationship from the mechanism, and discussing the importance of multi-period trade-off research. It is of great significance to strengthen the accuracy of trade-off studies.

Materials and methods

Study area

The study area is the core area of the integrated development of Zhengzhou city and Kaifeng city in Henan Province, China. Since 2015, with the urban development strategy of Zhengzhou to the East and Kaifeng to the west, as well as the implementation of regional plans such as “Zheng Bian Integration” and “Zheng Bian Industrial Belt Planning”, the original agricultural landscape of the study area has been strongly disturbed and ecosystem services have changed greatly.

The study area is located in the east of Zhengzhou and the west of Kaifeng. It starts from Zhengzhou section of Beijing Hong Kong Macao Expressway in the west, Jinming Road in Kaifeng in the East, Lianhuo Expressway in the north and national highway 310 in the south. The geographical location is between 34°72'- 34°85'N and 113°81'- 114°30'E, with a total area of about 47314 hm². The details are shown in *Figure 1*.

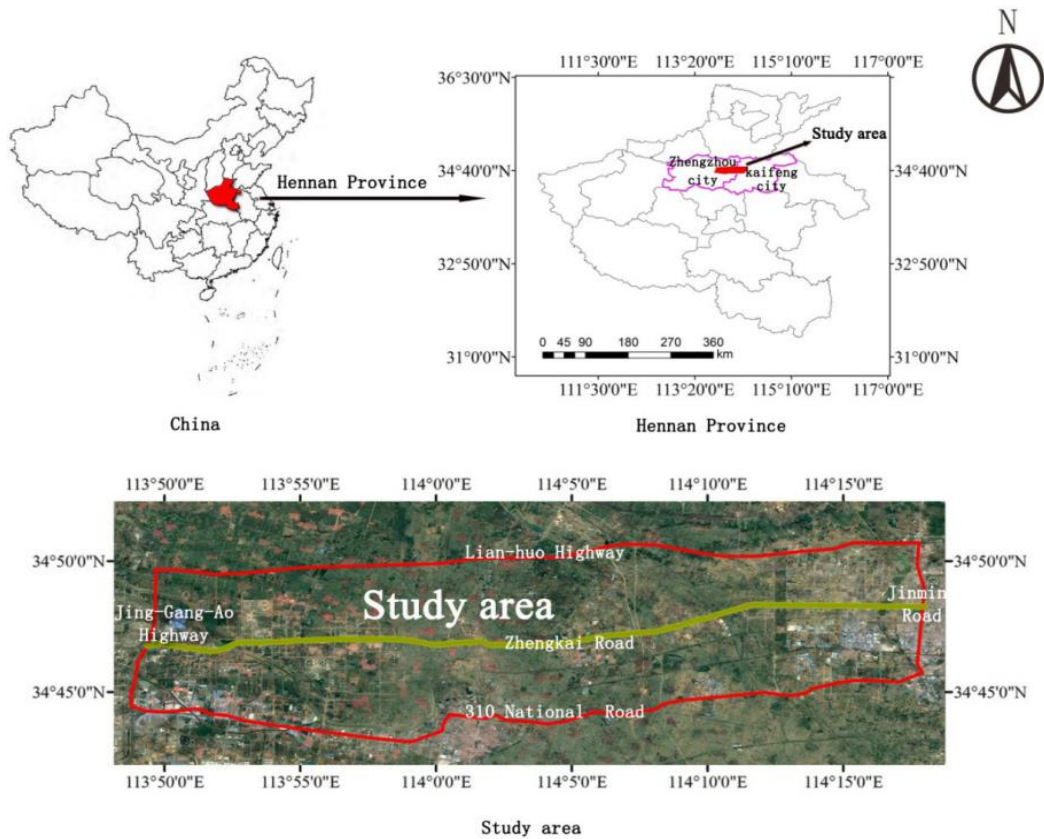


Figure 1. Location and the study area

Data sources

The image data are come from the geospatial cloud data platform. Three time periods of the study area in May 2005, 2010 and 2015 were obtained and processed. On the basis of the previous investigation, the landscape elements in the study area are divided into five types (farmland, forest land, water area, construction land, and unused land) by visual interpretation. The image data of the study area were processed by GIS 10.0 to obtain the landscape pattern data of the study area in three periods. According to the previous research results (Fan et al., 2018), it is determined that the best analysis grain size of landscape pattern in the study area is 20 m × 20 m.

The grain yield and area data in Henan Province mainly comes from the Henan Provincial Statistical Yearbook, National Agricultural Product Cost and Benefit Data Compilation, Zhongmu County Statistical Yearbook and other related materials.

Data related to carbon storage are mainly from local forestry departments. Part of the data comes from previous scholars' research in this region, and has been revised based on the climatic conditions of the study year (Huang et al., 2014, 2006; Guang, 2007; Chen et al., 2007; Peng et al., 2013).

Ecosystem services assessment methods

Carbon sequestration service

Carbon sequestration services are evaluated using the Carbon Model module in the InVEST model. The formula is shown in *Equation 1*:

$$C_{\text{stored}}=C_{\text{above}}+C_{\text{below}}+C_{\text{soil}}+C_{\text{dead}} \quad (\text{Eq.1})$$

where C_{stored} is the total carbon storage; C_{above} is the above-ground material carbon storage (t/hm²); C_{below} is the underground material carbon storage (t/hm²); C_{soil} is the soil carbon storage (t/hm²); C_{dead} is the litter carbon storage (t/hm²).

Habitat quality assessment

The Habitat Quality module in the InVEST model was used to evaluate the habitat quality of the study area. The formula is as follows (Eq. 2):

$$Q_{xj}=H_j-H_j \times \frac{D_{xj}^z}{D_{xj}^z+K^z} \quad (\text{Eq.2})$$

where Q_{xj} is the habitat quality of grid X in land use type J; D_{xj} is the stress level of grid X in land use type J; K is the semi-saturation constant, usually half of the maximum value of D_{xj} ; H_j is the habitat suitability of habitat J in land use type. When habitat is studied only from a macro perspective without involving species, the H_j value is often defined by dichotomy; Z is the normalization constant, generally 2.5. The dxj calculation is shown in Equation 3:

$$D_{xj}=\sum_{r=1}^R \sum_{y=1}^{Y_r} \left(\frac{W_r}{\sum_{r=1}^R W_r} \right) r_y i_{rxy} \beta_x S_{jr} \quad (\text{Eq.3})$$

In the formula, R is the habitat stress factor; y is the grid number of the habitat stress factor r grid layer; Y_r is the number of grids occupied by the habitat stress factor; W_r is the weight of the stress factor, indicating that a certain stress factor affects all habitats. The relative damage degree of r is 0-1; r_y is the stress factor value of grid y (0 or 1); i_{rxy} is the stress factor value of grid y and the stress level of r_y to habitat grid x; β_x is accessibility level of grid x, and the value 0-1, 1 means extremely easy to reach; S_{jr} is the sensitivity of the habitat type j to the stress factor r, and the value is 0-1, the closer the value is to 1, the more sensitive it is. i_{rxy} can be obtained by Equation 4:

$$i_{rxy}=1-\frac{d_{xy}}{d_{rmax}} \quad (\text{Eq.4})$$

In the formula, d_{xy} is the straight-line distance between grid x and grid y; d_{rmax} is the maximum influence distance of stress factor r.

Landscape aesthetics

Landscape aesthetics is evaluated by the expert knowledge-based ecosystem service value assessment method constructed by Xie et al. (2015). This is a dynamic equivalent factor method for the evaluation of ecosystem services in China, which has been verified and recognized in many regions of China (Fan, 2016). The equivalent factor method is a dynamic equivalent data accounting based on the sowing area and net profit of local main agricultural products in the current year. The calculation is shown in Equation 5:

$$D=S_r \times F_r+S_w \times F_w+S_c \times F_c \quad (\text{Eq.5})$$

where d represents the ecosystem service value of one standard equivalent (yuan/hm²); S_r , S_w and S_c respectively represent the percentage of the sown area of rice, wheat and corn in the total sown area of the three crops in the study year; FR , FW and FC respectively represent the national average net profit per unit area of rice, wheat and corn in the study year (yuan/hm²).

After the D value is obtained, combined with different land use types, the value equivalent of each land use type can be calculated. Then multiply the area of the land use type to get the landscape aesthetic value of the land use type.

Grain yield

It is calculated based on the unit area yield and planting area of grain crops in the study year.

Result

Carbon sequestration services

The four carbon pool values and landscape pattern data in the study area were input into the InVEST model to calculate the carbon sequestration service distribution map in three periods (Fig. 2).

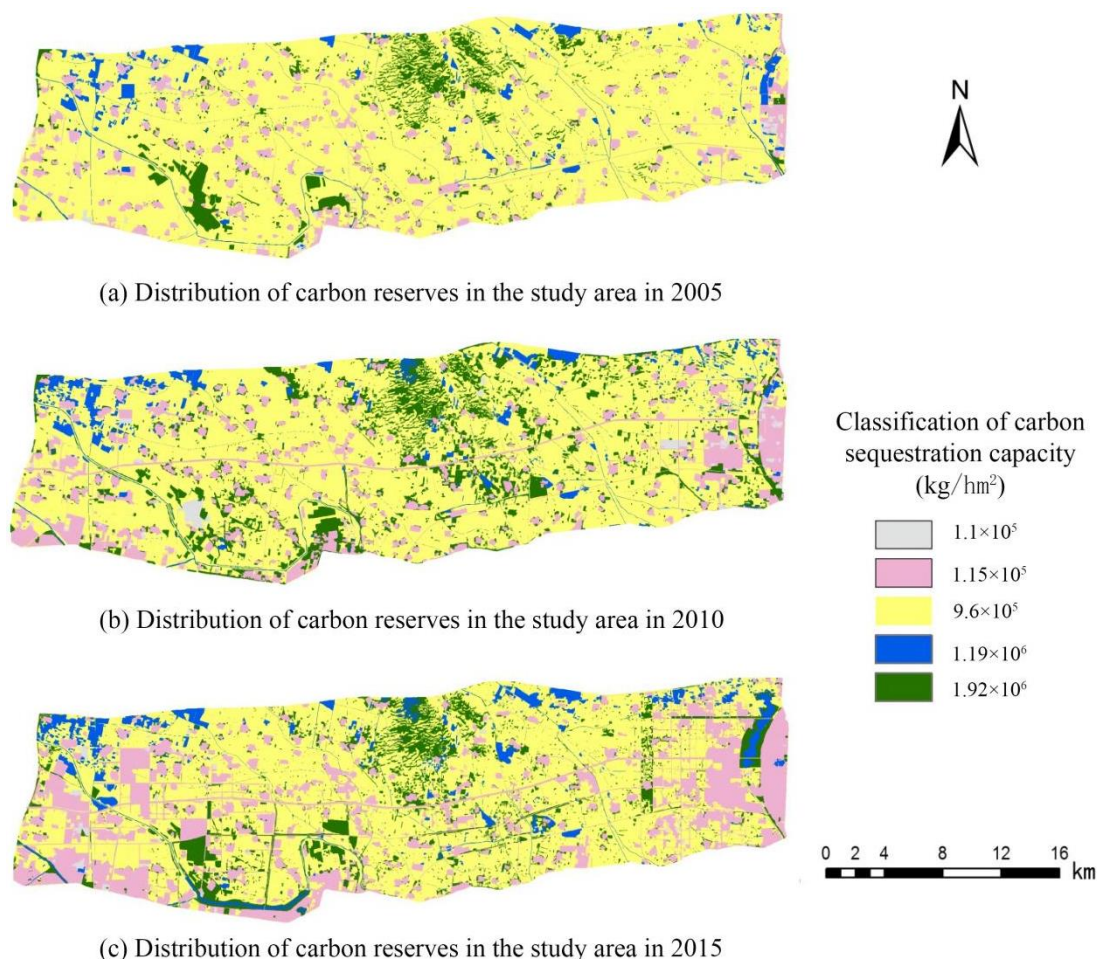


Figure 2. Distribution of carbon storage per unit area in the study area in 2005, 2010 and 2015

Subsequently, using the spatial statistical tool of ArcGIS 10.0, the carbon storage in the three periods of the study area was summarized and mapped in *Figure 3*.

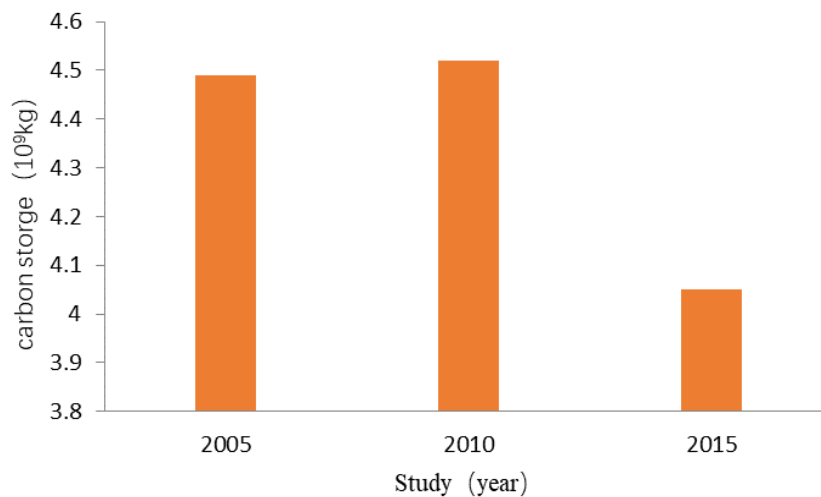


Figure 3. Changes in carbon storage in the study area from 2005 to 2015

The overall carbon storage in the study area is in a downward trend, from 2005 to 2015, it decreased by about 3.9×10^8 kg. In 2010, it fluctuated slightly, reaching 4.52×10^9 kg, which was 3×10^7 kg higher than that in 2005. The carbon storage in the study area is in a trend of rising first and then falling (\uparrow , \downarrow).

Habitat quality assessment

The 20 m \times 20 m landscape pattern data, threat factor layer data, threat factor attribute table and the sensitivity attribute table data of different landscape types to threat factors in the three periods of the study area are input into the Habitat Quality module in the InVEST model for calculation, and evaluation results of habitat quality is obtained. Then, the habitat quality of the three periods of 2005, 2010 and 2015 is divided into three intervals from low to high under the GIS platform: poor (0-0.2), medium (0.21-0.55), and good (0.56-0.9). The details are shown in *Figure 4*.

The closer the habitat value is to 1, the higher the habitat quality, and the closer the habitat value is to 0, the worse the habitat quality. It can be seen from the above three figures that the areas with poor habitats in the study area are generally dominated by construction land, while the areas with good habitats are dominated by forest land and water areas, and the habitat quality of farmland is between construction land and forest land. The area proportion comparisons of different habitat qualities in the study area in 2005, 2010 and 2015 are shown in *Figure 5*. According to *Figure 5*, it can be concluded that the overall habitat quality in 2005 > the overall habitat quality in 2010 > the overall habitat quality in 2015. Therefore, the change trend of habitat quality is (\downarrow , \downarrow).

Landscape aesthetic evaluation

According to the method described above and the relevant data of the study area, the aesthetic value of the study area in the three periods was obtained (*Table 1*). According to *Table 1*, the landscape aesthetic value of the study area increases first and then decreases (\uparrow , \downarrow).

Grain yield evaluation

According to the data of crop yield and area in the study area, the grain production value in the study area is obtained (Table 2). According to Table 2, it can be concluded that the grain yield in the study area is in a downward trend (↓, ↓).

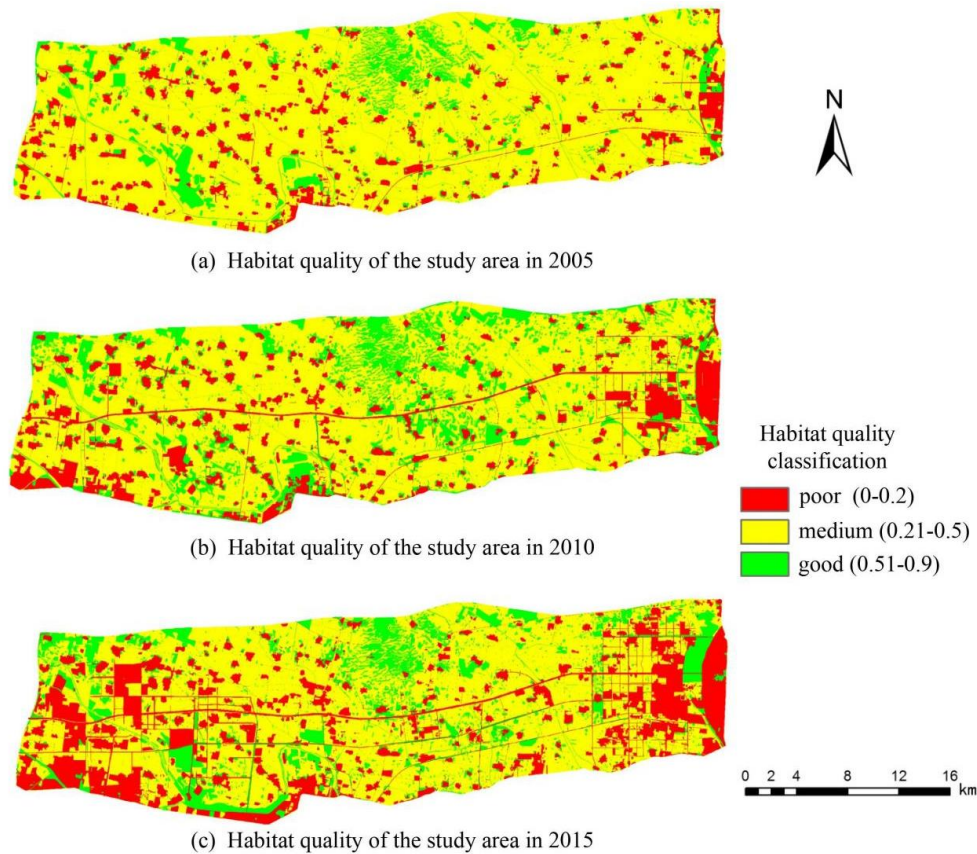


Figure 4. Distribution of habitat quality in the study area in 2005, 2010 and 2015

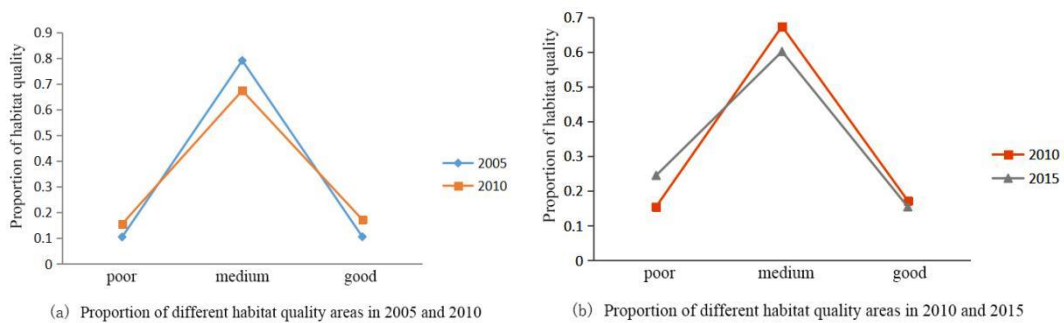


Figure 5. Comparison of different habitat quality areas in different periods

Table 1. Aesthetic value of the study area in different periods (RMB: yuan)

Year	2005	2010	2015
Total	3.79*10 ⁷	4.25*10 ⁷	2.42*10 ⁷

Table 2. The grain production value of the three periods in the study area

Year	2005	2010	2015
Total output (kg)	1.91×10 ⁸	1.88×10 ⁸	1.69×10 ⁸

Overall trade-off relationship of four ecosystem services

Combined with 3.1-3.4, the change trend of four types of ecosystem services is tabulated (Table 3).

Table 3. Change trend of four types of ecosystem services

Types of ecosystem services	Trend from 2005 to 2010	Trend from 2010 to 2015
Carbon sequestration services	↑	↓
Grain production	↓	↓
Habitat quality	↓	↓
Landscape aesthetics	↑	↓

As shown in Table 3, the relationship between any two ecosystem services in the same period can be obtained. But the relationship between them may be inconsistent at different periods. For example, carbon sequestration services and food production showed a trade-off relationship from 2005 to 2010, but a synergistic relationship from 2010 to 2015. Therefore, studying the relationship of ecosystem services in a short period is likely to lead to misjudgment results. Looking at the entire time period 2005-2020 and 2010-2015, carbon sequestration services (↑, ↓) and aesthetic landscape (↑, ↓) show a synergistic relationship, as well as the relationship between food production (↓, ↓) and habitat quality (↓, ↓).

Discussion

Research period of ecosystem service trade-offs

At present, the research on ecosystem service trade-off is mainly based on spatial distribution mapping and correlation analysis (Deng et al., 2020), and the research is mostly concentrated in a single period or between two periods. There are few studies on three or more consecutive periods (Yin et al., 2019; Wang et al., 2020). This study found that the trade-off study in a single period may misjudge the relationship between ecosystem services. Therefore, strengthening multi period research is helpful to improve the scientificity of research.

Determination of research methods on trade-offs

There are many previous studies on trade-offs. Almost all studies first evaluate ecosystem services, and then make trade-offs according to the changes of results (Li et al., 2021). There are many evaluation methods of ecosystem services. Different evaluation methods often get different evaluation results of ecosystem services, so the accuracy of trade-off judgment is also affected. In addition, the traditional research does not analyze the relationship between different ecosystem service assessment methods, which is also the limitation of the current research.

Take the carbon sequestration service and landscape aesthetics studied in this paper as an example. The carbon module in the InVEST model is used for valuing carbon sequestration service. The calculation method of carbon reserves in the study area can be simplified as: area of different landscape elements \times Carbon reserves per unit area, and then sum; The aesthetic landscape value is evaluated by dynamic equivalent method, which can also be simplified as: the area of different landscape elements \times The value equivalent per unit area is then summed.

These two ecosystem services have a relatively consistent calculation method: the area of different landscape elements \times the ecological value service per unit area, and then summed. In terms of calculation principle, these two ecosystem services have relatively consistent calculation methods. At the same time, in the process of urbanization, the change area of landscape elements they contain is also the same, so carbon sequestration services and landscape aesthetics show a synergistic relationship.

In fact, the ecosystem service assessment method is the determinant of the trade-off relationship and the basis for explaining the trade-off of ecosystem services. Therefore, a scientific method of ecosystem services assessment is a prerequisite for trade-off studies.

Conclusion

Through the research on the changes of ecosystem services in the process of urbanization in the study area in 2005-2010-2015, some obvious conclusions and suggestions for future research are as follows:

Main conclusions

Ecosystem services are greatly affected by urbanization

The four ecosystem services in this study are selected from supply service, support service, regulation service and cultural service. They have all undergone significant changes in the process of urbanization and are obviously representative. In addition, a large number of ecosystem services exist on the surface landscape as a carrier, and urbanization drives changes in landscape patterns, which will inevitably lead to a large number of changes in ecosystem services.

Ecosystem services research only in a single period may misjudge the trade-off relationship between them

For example, in this study, carbon sequestration services and food production showed a trade-off relationship in 2005-2010, and a synergistic relationship in 2010-2015. Analysis of a single time period will misjudge their relationship.

The scientificity of ecosystem services assessment directly affects the accuracy of trade-offs

From the trade-off study of four ecosystem services in this paper, it can be seen that the evaluation method of ecosystem services has obvious explanatory power for the trade-off judgment between them. Inconsistent ecosystem service assessment methods may lead to different trade-off results. Therefore, a scientific ecosystem service assessment method involving mechanism is very important for trade-off research.

Main recommendations

Ecosystem services research needs to choose research methods derived from ecosystem mechanisms

Evaluating ecosystem service trade-offs requires quantifying different ecosystem services. However, there are many evaluation methods for the same ecosystem service, and the evaluation methods for different ecosystem services are also different. Different methods will lead to different results. Therefore, scientific evaluation methods which were selected from the ecosystem mechanism, can ensure the accuracy of the research.

Accurate trade-off law research needs continuous and long-time data support

Due to the dynamicity of ecosystem services, the trade-offs between them will inevitably change. Short time trade-off performance cannot represent the accurate trade-off law. In future research, it is necessary to add long-time series data to ensure the accuracy of research results.

Acknowledgements. This study is financed by 2022 Key R&D and Promotion Projects in Henan Province (No. 222102320064), 2022 Henan Science and Technology Think Tank Research Project (Hnkjzk-2022-51B).

REFERENCES

- [1] Asgarian, A., Amiri, B. J., Sakieh, Y. (2015): Assessing the effect of green cover spatial patterns on urban land surface temperature using landscape metrics approach. – *Urban Ecosystems* 18(1): 209-222.
- [2] Augustynczyk, A., Yousefpour, R. (2021): Assessing the synergistic value of ecosystem services in European beech forests. – *Ecosystem Services* 49: 101264.
- [3] Bagstad, K. J., Villa, F., Johnson, G., Voigt, B. (2011): ARIES – Artificial Intelligence for Ecosystem Services: A Guide to Models and Data, Version 1.0 Beta. – The ARIES Consortium, Bilbao, Spain.
- [4] Chen, G. S., Yang, Y. S., Liu, L. Z., Li, X. B., Zhao, Y. C., Yuan, Y. D. (2007): Research review on total belowground carbon allocation in forest ecosystems. – *Journal of Subtropical Resources and Environment* 2(1): 34-42.
- [5] Deng, C. X., Zhu, D. M., Nie, X. D., Liu, C. C., Li, Z. W., Liu, J. Y., Zhang, G. Y., Xiao, L. H., Zhang, Y. T. (2020): Progress of research regarding the trade-offs of ecosystem services. – *Chinese Journal of Eco-Agriculture* 28(10): 1509-1522.
- [6] Estoque, R. C., Murayama, Y. (2016): Quantifying landscape pattern and ecosystem service value changes in four rapidly urbanizing hill stations of Southeast Asia. – *Landscape Ecology* 31(7): 1481-1507.
- [7] Fan, Q. D. (2016): Response of Ecosystem Service to the Core Area of Zhengzhou & Kaifeng Integration. – Henan University, Henan.
- [8] Fan, Q. D., Liang, Z. Z., Liang, L. K., Ding, S. Y., Zhang, X. P. (2018): Landscape pattern analysis based on optimal grain size in the core of the Zhengzhou and Kaifeng integration area. – *Polish Journal of Environmental Studies* 27(3).
- [9] Guang, Z. Y. (2007): Study on forest biomass carbon storage in Henan Province. – *Areal Research and Development* 1: 76-79.
- [10] Huang, M., Ji, J. J., Cao, M. K., Li, K. R. (2006): Modeling study of vegetation shoot and root biomass in China. – *Acta Ecologica Sinica* 12: 4156-4163.

- [11] Huang, C. H., Yang, J., Zhang, W. J. (2014): The application of forest inventory data in an ecosystem service evaluation model: InVEST. – *Forest Resources Management* 05: 126-131.
- [12] Li, L., Wu, D. F., Wang, F., Liu, Y. Y., Liu, Y. H., Qian, L. X. (2020): Prediction and trade off analysis of ecosystem service value in the rapidly urbanizing Foshan City of China: a case study. – *Acta Ecologica Sinica* 40(24): 9023-9036.
- [13] Li, D. H., Zhang, X. Y., Wang, Y., Zhang, X., Li, L., Lu, L. (2021): Evolution process of ecosystem services and the trade-off synergy in Xin'an River Basin. – *Acta Ecologica Sinica* 41(17).
- [14] Liang, C., Zeng, J., Shen, Z. J., Wang, Q. W. (2021): Spatial pattern analysis and management of urban ecosystem services under rapid urbanization: a case study of Xiamen. – *Acta Ecologica Sinica* 41(11): 4379-4392.
- [15] Millennium Ecosystem Assessment (2005): *Ecosystems and Human Well-Being: Biodiversity Synthesis*. – Island Press, Washington, DC.
- [16] Moein, M., Asgarian, A., Sakieh, Y., Soffianian, A. (2018): Scenario-based analysis of land-use conflict in central Iran: finding the trade-off between urban growth patterns and agricultural productivity. – *Sustainable Cities & Society*, S221067071731199X.
- [17] Ndong, G. O., Therond, O., Cousin, I. (2020): Analysis of relationships between ecosystem services: a generic classification and review of the literature. – *Ecosystem Services* 43: 101120.
- [18] Ouyang, X., Tang, L., Wei, X., Li, Y. (2021): Spatial interaction between urbanization and ecosystem services in Chinese urban agglomerations. – *Land Use Policy* 109(4): 105587.
- [19] Peng, Y., Wang, Y. K., Fu, B., Ma, F. (2013): Spatial distribution of carbon storage function and seismic damage in Wenchuan earthquake stricken areas. – *Acta Ecologica Sinica* 03: 798-808.
- [20] Ramyar, R., Saedi, S., Bryant, M., Davatgar, A., Hedjri, G. M. (2020): Ecosystem services mapping for green infrastructure planning – The case of Tehran. – *Science of the Total Environment* 703: 135466.
- [21] Redhead, J. W., May, L., Oliver, T. H., Hamel, P., Sharp, R., Bullock, J. M. (2018): National scale evaluation of the InVEST nutrient retention model in the United Kingdom. – *Science of the Total Environment* 610-611: 666-677.
- [22] Sharp, R., Tallis, H. T., Ricketts, T., Guerry, A. D., Wood, S. A., Chaplin-Kramer, R., ... Vogl, A. L. (2014): *InVEST user's guide*. – The Natural Capital Project: Stanford, CA.
- [23] Sherrouse, B. C., Semmens, D. J., Clement, J. M. (2014): An application of social values for ecosystem services (SOLVES) to three national forests in Colorado and Wyoming. – *Ecological Indicators* 36: 68-79.
- [24] Smiraglia, D., Ceccarelli, T., Bajocco, S., Salvati, L., Perini, L. (2016): Linking trajectories of land change, land degradation processes and ecosystem services. – *Environmental Research* 147: 590-600.
- [25] Tallis, H., Polasky, S. (2009): Mapping and valuing ecosystem services as an approach for conservation and natural-resource management. – *Annals of the New York Academy of Sciences* 1162(1): 265-283.
- [26] Taylor, L., Hochuli, D. F. (2015): Creating better cities: how biodiversity and ecosystem functioning enhance urban residents' wellbeing. – *Urban Ecosystems* 18(3): 747-762.
- [27] Torres, A. V., Tiwari, C., Atkinson, S. F. (2021): Progress in ecosystem services research: a guide for scholars and practitioners. – *Ecosystem Services* 49(2): 101267.
- [28] Vahmani, P., Sun, F., Hall, A., Ban-Weiss, G. (2016): InVEST igating the climate impacts of urbanization and the potential for cool roofs to counter future climate change in Southern California. – *Environmental Research Letters* 11(12): 124027.
- [29] Villa, F., Bagstad, K. J., Voigt, B., Johnson, G. W., Portela, R., Honzák, M., Batker, D. (2014): A methodology for adaptable and robust ecosystem services assessment. – *PLoS One* 9(3): e91001.

- [30] Wang, S. H., Huang, L., Xu, X. L., Xu, S. W. (2020): Spatial and temporal evolution of ecosystem services and its trade-offs and synergies in Guangdong- Hong Kong- Macao Greater Bay Area. – *Acta Ecologica Sinica* 40(23): 8403-8416.
- [31] Xiao, H. B., He, X. Y., Wang, Y., Wang, J. N., Jiang, Q. Z. (2021): Research progress on the correlation between urban green space and residents' physical and mental wellbeing from a perspective of matching ecosystem services supply and demand. – *Acta Ecologica Sinica* 41(12): 5045-5053.
- [32] Xie, G. D., Zhang, C. X., Zhang, L. M., Chen, W. H., Li, S. M. (2015): Improvement of the evaluation method for ecosystem service value based on per unit area. – *Journal of Natural Resources* 30(08): 1243-1254.
- [33] Xu, X. B., Yang, G. S., Tan, Y., Liu, J. P., Hu, H. Z. (2018): Ecosystem services trade-offs and determinants in China's Yangtze River Economic Belt from 2000 to 2015. – *Science of the Total Environment* 634: 1601-1614.
- [34] Yang, W. R. (2015): Spatiotemporal change and driving forces of urban landscape pattern in Beijing. – *Acta Ecologica Sinica* 35(13): 4357-4366.
- [35] Yang, X. T., Qiu, X. P., Xu, Y., Zhu, F. B., Liu, Y. W. (2021): Spatial heterogeneity and dynamic features of the ecosystem services influence on human wellbeing in the West Sichuan Mountain Areas. – *Acta Ecologica Sinica* 41(19): 7555-7567.
- [36] Yin, L. C., Wang, X. F., Zhang, K., Xiao, F. Y., Cheng, C. W., Zhang, X. R. (2019): Trade-offs and synergy between ecosystem services in National Barrier Zone. – *Geographical Research* 38(09): 2162-2172.
- [37] Zheng, H., Wang, L. J., Peng, W. J., Zhang, C. P., Li, C., Robinson, B. E., Wu, X. C., Kong, L. Q., Li, R. N., Xiao, Y., Xu, W. H., Ouyang, Z. Y., Daily, G. C. (2019): Realizing the values of natural capital for inclusive, sustainable development: informing China's new ecological development strategy. – *Proceedings of the National Academy of Sciences of the United States of America* 116(17): 8623-8628.

ANALYSIS OF THE CHANGE IN VEGETATION COVERAGE OF CHALK SOIL WASTELAND DURING THE GROWING SEASON BASED ON UAV SEQUENCE IMAGE

WANG, Y.¹ – QIAO, L. F.¹ – YAO, Z. Y.¹ – QI, A. G.¹ – ZHANG, Y. C.^{1,2*}

¹*School of Horticulture and Landscape Architecture, Henan Institute of Science and Technology, Xinxiang 453003, P. R. China*

²*Henan Province Engineering Center of Horticultural Plant Resource Utilization and Germplasm Enhancement, Xinxiang 453003, P. R. China*

**Corresponding author
e-mail: zhangyichuan@hist.edu.cn*

(Received 22nd Jan 2022; accepted 2nd May 2022)

Abstract. Normalized Difference Vegetation Index (NDVI), the most widely applied vegetation index, can accurately reflect the vegetation coverage and growth on chalk soil wasteland, and provide bases for the further optimization of vegetation. In this research, a chalk soil wasteland located in Fengquan District of Xinxiang city of China was taken as the study target, and photos of the vegetation coverage of the chalk soil wasteland during the growing season (March to October) were taken with a multispectral camera carried on Dajiang unmanned aerial vehicle (UAV). The results have shown that the mean NDVI of the wasteland during the growing season is 0.21. After almost two decades of treatment, the ecological environment improves, but it just reaches medium coverage. The monthly mean NDVI of the wasteland during the growing season ranges between 0.12 and 0.30, which is of medium coverage or level below. The monthly NDVI level distribution of the wasteland during the growing season indicates that the ratio of high vegetation coverage is relatively low, and the vegetation environment of the wasteland still needs further improvement. The monthly NDVI gap of the wasteland during the growing season shows that the ratio of NDVI increasing area of most months is far greater than the NDVI decreasing area. But the decreasing area caused by the management, high temperature and draught in May and June is far greater than the increasing area. In August and September, leaves begin to fall, and the chlorophyll content decreases, so the ratio of NDVI decreasing area increases rapidly to the second peak. The species and area coverage of evergreen plants, LAI value of plants and canopy structure would influence NDVI.

Keywords: *NDVI, wasteland, vegetation coverage, unmanned aerial vehicle, multispectral, ecological restoration*

Introduction

There are numerous wastelands generated by all forms of mineral mining in China, which has caused great damage to the ecological environment (Zhou, 2021). The wastelands include several types. For instance, the wasteland polluted by heavy metals is severely hazardous; mining wasteland like quarries are not toxic, but still suffer from damaged landform, sparse or disappeared vegetation, poor soil and pose a safety hazard (Li, 2019). Chalk soil wasteland is a relatively special ore wasteland, which is free from toxic pollution but characterized by complex terrain, poor soil, sparse vegetation and severe dust pollution. At present, the ecological restoration of mining wasteland usually aims at recovering the vegetation, to build a recreational land with such functions as recreation, tourism, production, and popular education on this basis. Nanning Garden Expo adopts various methods and approaches to reconstruct the quarry landscape, such as waste-scape creation, vegetation restoration and increase of recreational facilities (Wang and Lin, 2019). Through mountain, water, forest, soil and pit belt treatment and

restoration, an ore wasteland in Tongluo Mountain, Chongqing was reconstructed to a national mining park (Du et al., 2021). In the design of Zishan Park in Handan, in-depth research has been carried out from the landscape, network of rivers, vegetation and ecological environment (Wu et al., 2021). A mining wasteland in Tangshan was reconstructed to be an ecological park through the ecological restoration of vegetation, water body construction and other ecological measures (Huang and Guo, 2020).

Currently, vegetation restoration, soil improvement, construction of an artificial wetland with pit pond, and mining relic protection and utilization, etc. have been used for the ecological environmental treatment of the chalk soil wasteland (Zhang et al., 2006; Chang et al., 2020). Vegetation restoration is mainly measured by vegetation indexes, which includes NDVI, optimized soil adjusted vegetation index (OSAVI), green-red vegetation index (GRVI), ratio vegetation index (RVI), difference vegetation index (DVI), modified soil adjusted vegetation index (MSAVI) (Guo et al., 2020) etc., NDVI is the most widely-applied vegetation index (Fan et al., 2016). NDVI is highly correlated with leaf area index (LAI), biomass and net primary productivity, which can perfectly reflect the vegetation coverage and vegetation growth (Yuan, 2016). Luo (2019) studied the impact of NDVI time course on the vegetation restoration and climate change in the mining area with Landsat data and meteorological data. Shao (2017) analyzed the impact of mining on the vegetation coverage based on the NDVI analysis with Landsat data. Zhou et al. (2016) analyzed the loss of net primary productivity of vegetation caused by rare earth mining based on NDVI data. At present, the data source for the research on vegetation restoration of wasteland is mainly based on satellite remote sensing image, with such disadvantages as low resolution, poor timeliness, disturbance of cloud cover and high cost, which influences the accuracy of analysis to a certain extent. In recent years, UAV technology has developed rapidly, and become an important approach for obtaining the information about ecological environment safely and efficiently (Zhang et al., 2019), with a bright application prospect in the research on vegetation restoration for wastelands.

Growing season refers to the period in which plants begin to revive and turn green (beginning of the growing season) till they turn yellow and wither (end of the growing season), which is usually between March and October in Henan. Spatial information on wasteland could play an important role in urban land management (Grădinaru et al., 2019). This study attempts to use UAV carrying a multispectral camera to monitor and analyze the changes of vegetation coverage on the wasteland during the growing season in a monthly time sequence, so as to provide a basis for vegetation improvement and plant configuration of wastelands.

Materials and methods

General situation of the research area

The research area is located in Luwangfeng Village, Fengquan District, Xinxiang, Henan Province of China as shown in *Figure 1*, with a total coverage of 83.97 hectares. It is in the north of Henan Province, featuring a warm temperate continental monsoon climate, with four distinct seasons, cold winter, hot summer, cool autumn and early spring. The mean precipitation throughout the year is 573.4 mm. Fengquan District was the largest supply base of building materials in northern Henan in the last century. The chalk soil of this wasteland was used to produce cement. In 2000, it was shut down and abandoned, and treated with private capital under the guidance of the government, by

virtue of vegetation restoration, landform utilization, landscape reconstruction and other methods. Currently, it is operated in the form of recreational agricultural sightseeing park (Wang and Zhang, 2015). The vegetation species are complicated in the park, such as nursery garden, crop plantation, orchards, vegetable gardens, lotus ponds, wetlands, landscape plants, etc.

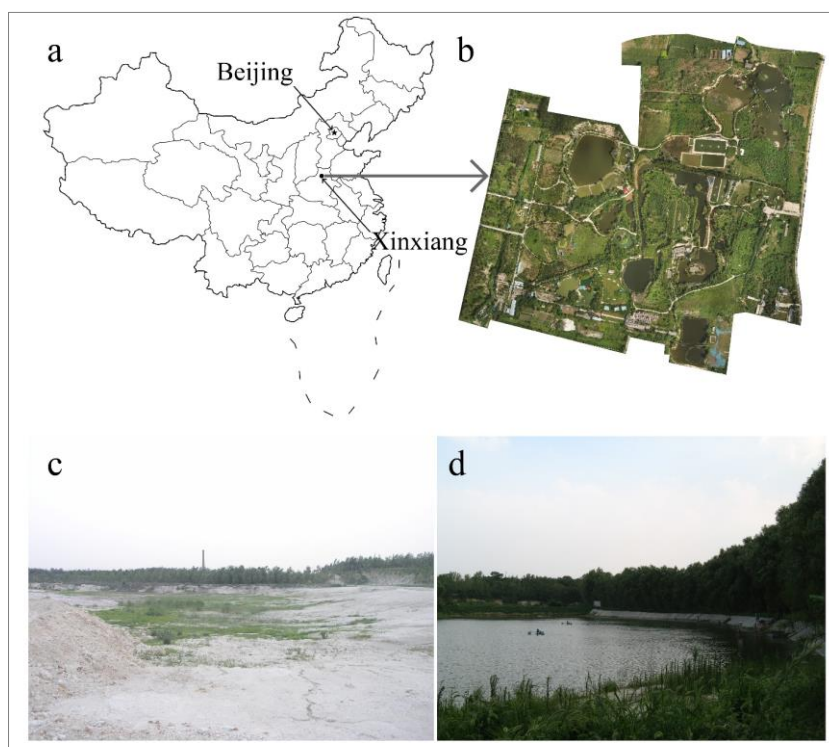


Figure 1. Location of the study area (a); Orthographic projection of the study area (b); Ecological restoration photo of chalk wasteland in 2003 (c); Ecological restoration photo of chalk wasteland in 2020 (d)

Data acquisition and processing

Data acquisition

Phantom 4 Multispectral was used, and its integrated multispectral imaging system combines a visible light camera and five multispectral cameras (blue light, green light, red light, red edge and near-infrared). This wasteland was photographed from March to September in 2021. To avoid the influence of the weather on UAV flight, photos were taken when there was no wind and cloud around the 25th day of each month. The same settings were used on every flight: UAV flight height was 200 m, the course overlap was 78%, the side overlap was 75%, the main route angle was 83°, the ground resolution was 10.72 cm, the flight area was 85.24 hectares, and the route length was 21028 meters. 669 photos were taken in each band.

Image pre-processing

Pix4D mapper pro was applied for single-band image stitching, to obtain the stitched images of red, blue, green, near-infrared and red edge bands. Phantom 4 multispectral

positioning system supports the connection to D-RTK 2 high-precision GNSS mobile station and network RTK. Therefore, the images obtained have precise geographic coordinates, and there is no need for geographic registration. The multispectral light intensity sensor integrated on the top of Phantom 4 multispectral could capture the solar irradiance and record it in the image file. Solar irradiance data could be applied for compensating the illumination of the image, to eliminate the disturbance of the ambient light to data acquisition. Consequently, there is no need for atmospheric correction. ENVI 5.3 software was applied for cutting the stitched images along the boundary of the research area.

NDVI extraction and classification

NDVI extraction

NDVI is the ratio of the difference between the reflectivity of near-infrared band and red band to the sum of the two, which usually ranges between -1 and 1. Negative means the ground is covered by cloud, water, snow, etc. which can highly reflect visible lights. 0 means there is rock or bare soil, etc. NIR is approximately equivalent to R. Positive means there is vegetation coverage, and it increases with the expansion of coverage (Xu and Wang, 2021). In this research, vegetation index was studied, and the value less than 0 was zeroed. The calculation formula is as follows:

$$NDVI = \frac{NIR - R}{NIR + R} \quad (\text{Eq.1})$$

where: NIR represents the reflectivity of the near-infrared wave band, and R represents the reflectivity of the red light wave band.

NDVI mean value and classification

According to *Equation 1*, the mean value and monthly mean value of NDVI within the research area during the growing season were worked out, since both the mean value and monthly mean value could reflect the general vegetation coverage and monthly vegetation coverage on the wasteland.

Currently, there is no unified standard for NDVI classification. In some research, it is insisted that green vegetation ranges between 0.2 and 1 (Wang et al., 2021). Due to the extremely high resolution of UAV remote sensing image, NDVI was classified into six levels. Specifically, I level, ranging between 0 and 0.1, bared land; II level, ranging between 0.1 and 0.2, low coverage; III level, ranging between 0.2 and 0.4, middle coverage; IV level, ranging between 0.4 and 0.6, relatively high coverage; V level, ranging between 0.6 and 0.8, high coverage; VI level, ranging between 0.8 and 1.0, extremely high coverage.

NDVI difference change

The difference between the current month's NDVI and last month's NDVI can reflect coverage change in different months. NDVI increase means an increase in vegetation coverage, while NDVI decrease means a decrease in vegetation coverage.

Result and analysis

Mean NDVI of chalk soil wasteland in the growing season

Total mean NDVI of chalk soil wasteland in the growing season

The total mean NDVI of the wasteland in the growing season is only 0.21, of middle coverage level. After almost two decades of treatment, the vegetation index is still low, because there is still a large area of bare chalk soil in the research area, which is free of plant growth or only has sparse grasses; trees and shrubs are mostly planted through local soil replacement for vegetation restoration on the wasteland, and the barren soil leads to slow growth; most planting areas have certain gentle slopes, which are not conducive to soil and water conservation and affect the water supply for plants; insufficient wasteland treatment also affects the post management.

Monthly mean NDVI of chalk soil wasteland in the growing season

According to *Table 1*, it is clear that mean NDVI is the lowest in March, and it is mainly contributed by *Cedrus deodara*, *Ligustrum lucidum*, *Sabina chinensis*, *Platycladus orientalis*, *Euonymus japonicus*, *Photinia serrulata*, *Pittosporum tobira*, *Sabina chinensis*, *Phyllostachys bambusoides* and other evergreen plants. Since April, LAI of deciduous plants increases rapidly, and mean NDVI reaches 0.3 in August, 2.5 times of that in March. The growth range of mean NDVI in April is the biggest, since plants enter the vigorous growth stage as the temperature rises gradually. The mean NDVI in June declines due to the sales of seedling, wheat crop harvesting, orchard weeding, and draught. Plant LAI still grows in July and August, so the mean value is still on the rise, but decreases rapidly after reaching the peak in August, lower than the NDVI by the end of April, since deciduous plants begin to enter the deciduous stage.

Table 1. Monthly mean NDVI of chalk soil wasteland in the growing season

Month	Mar.	Apr.	May	Jun.	Jul.	Aug.	Sep.	Oct.
Monthly mean	0.12	0.21	0.25	0.21	0.27	0.30	0.18	0.16
Coverage level	II	III	III	III	III	III	II	II

NDVI level and distribution of chalk soil wasteland in the growing season

Total mean NDVI level and distribution of chalk soil wasteland in the growing season

The total mean NDVI of wasteland was classified (*Figure 2*, *Table 2*), in which, I level accounted for 29.66%, II level 19.03%, III level 36.44%, IV level 14.82%, V level 0.04%, and VI level 0%, indicating that about 2/3 of the area was covered by vegetation in the growing season. After nearly 2 decades of ecological restoration, the ecological environment of the park has been greatly improved, but high-coverage area still takes up a small percentage, and plants still need to be adjusted to improve the ecological environment.

Monthly NDVI level distribution of chalk soil wasteland in the growing season

According to *Table 3* and *Figure 3*, I level coverage of the wasteland was the highest. It decreased gradually from March to May, rose slightly in June, continued to decrease in July and August, rose substantially in September, and reached the peak by the end of

October. In March, the ratio of II level to V level coverage decreased gradually, by then most plants were grasses, evergreen trees and shrubs accounted for a small percentage, and deciduous plants were in the early stage of growth. In April, the ratio of II level to IV level coverage increased gradually then dropped quickly, since trees and shrubs were in steady growth, but community coverage had not taken shape yet. In May, all kinds of plants entered prosperous stage, and the ratio of II level to IV level coverage increased gradually and then decreased, basically equal to that in April, but its V level coverage increased evidently when compared to that in April. In June, the ratio of II level to III level coverage increased slightly when compared to that in May, but its IV level and V level coverage decreased, mainly due to the high temperature and drought, and lack of rainfall in June, which resulted in the death or decay of plants. The rainfall was ample in July and August. In July, II level coverage decreased slightly when compared to that in June, but III level and IV level coverage increased evidently. In August, II level to IV level coverage was almost the same as that in July or increased slightly, but V level coverage was 2.18 times of that in July. In September, the ratio of II level and III level coverage increased when compared to that in August, but IV level and V level coverage decreased evidently. By the end of October, I level coverage exceeded 50%, while other levels were the same as that by the end of September or decreased slightly. At this moment, the chlorophyll content of some deciduous plants decreased, and a few plants began to enter the deciduous period.

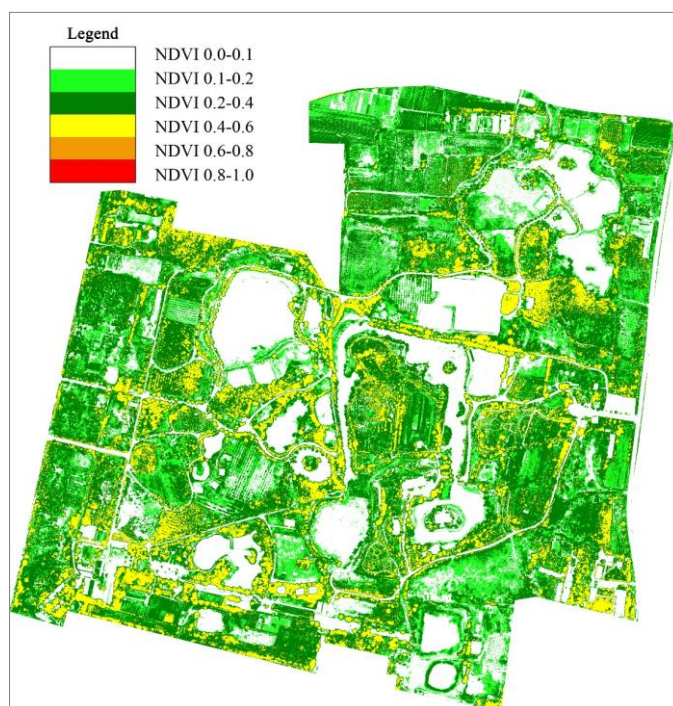


Figure 2. Levels of the total mean NDVI of the chalk soil wasteland in the growing season

Table 2. Total mean NDVI level distribution of the chalk soil wasteland in the growing season

Coverage level	I	II	III	IV	V	VI
Percentage (%)	29.66	19.03	36.44	14.82	0.04	0.00

Table 3. Monthly NDVI level distribution of chalk soil wasteland in the growing season

	Mar. (%)	Apr. (%)	May (%)	Jun. (%)	Jul. (%)	Aug. (%)	Sep. (%)	Oct. (%)
I	56.58	46.45	39.19	43.67	34.95	31.64	44.62	50.27
II	23.12	8.62	10.35	11.81	5.78	5.88	12.88	12.92
III	13.1	18.28	17.97	19.46	21.72	20.11	28.52	23.61
IV	5.76	23.15	23.78	21.13	34.12	35.01	13.66	12.63
V	1.43	3.50	8.69	3.92	3.37	7.33	0.27	0.58
VI	0.00	0.00	0.01	0.01	0.06	0.03	0.03	0.00

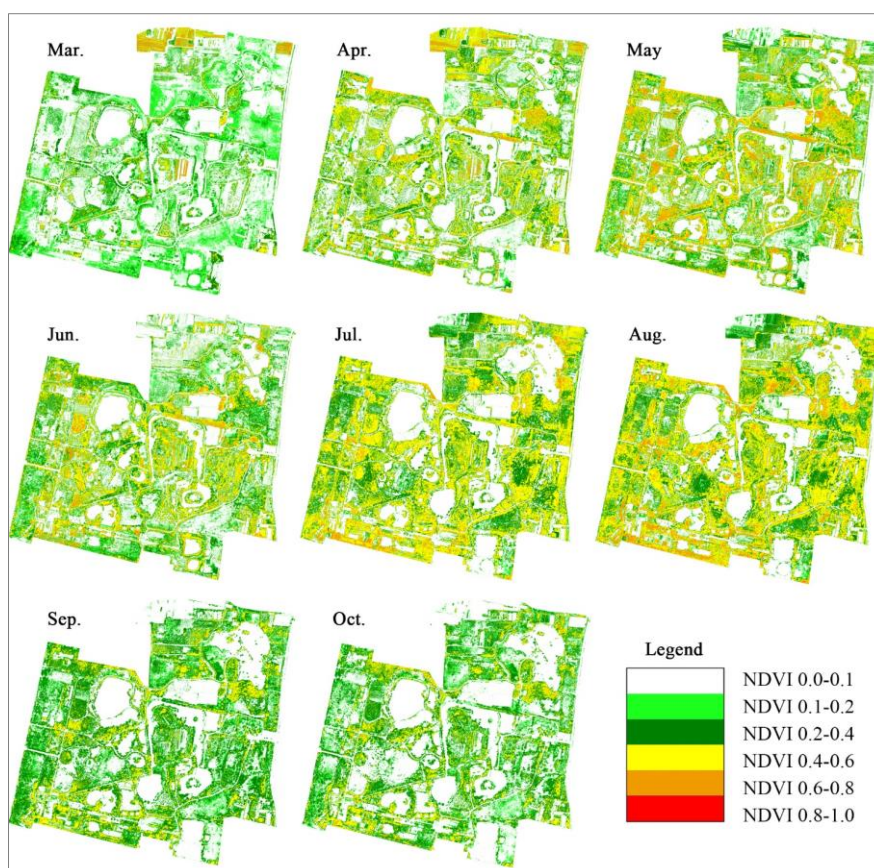


Figure 3. Diagram of monthly NDVI level distribution of chalk soil wasteland in the growing season

Monthly NDVI difference of chalk soil wasteland in the growing season

According to Table 4 and Figure 4, NDVI of the wasteland in the growing season was always in dynamic changes. Generally, NDVI increasing area between March and April and between April and May was far greater than the decreasing area. Especially in April and May, due to the fast growth of plants, the increasing area reached the maximum 55.3%, the first peak. The NDVI decreasing area in May and June was far greater than the increasing area, reached the first peak, mainly due to the sales and transplanting of seedlings. For instance, after the transplanting of privet nursery in the southwest of the park, NDVI dropped rapidly. In addition, the wheat harvesting, Orchard weeding and

other management activities also led to the decrease of NDVI. But the primary reason shall be drought and little rain. In June in Xinxiang, there were 16 days with the highest temperature above 35°C, and 6 days with the highest temperature above 37°C. In days of high temperature, the moisture of soil lost quickly, and the poor irrigation condition led to prominent draught. With the increase of rainfall, NDVI increasing area in June to July and July to August increased rapidly and reached the second peak by the end of August. By the end of August to September, plants entered deciduous period, the chlorophyll content decreased, NDVI decreasing area increased rapidly to the second peak, and only a few areas were growing. By the end of September to October, NDVI decreasing area was still greater than the increasing area, but there were still some areas in growing state. The area of unchanged NDVI was relatively stable, since it was mainly waste bare land, road and water.

Table 4. Monthly NDVI difference of the wasteland in the growing season

	Percentage of NDVI decreasing area (%)	Percentage of NDVI unchanging area (%)	Percentage of NDVI increasing area (%)
Mar. – Apr.	32.34	19.50	48.16
Apr. – May	22.23	22.47	55.30
May – Jun.	54.30	20.98	24.72
Jun. – Jul.	33.25	19.53	47.22
Jul. – Aug.	25.90	23.96	50.14
Aug. – Sep.	68.24	23.36	8.40
Sep. – Oct.	40.16	31.21	28.63

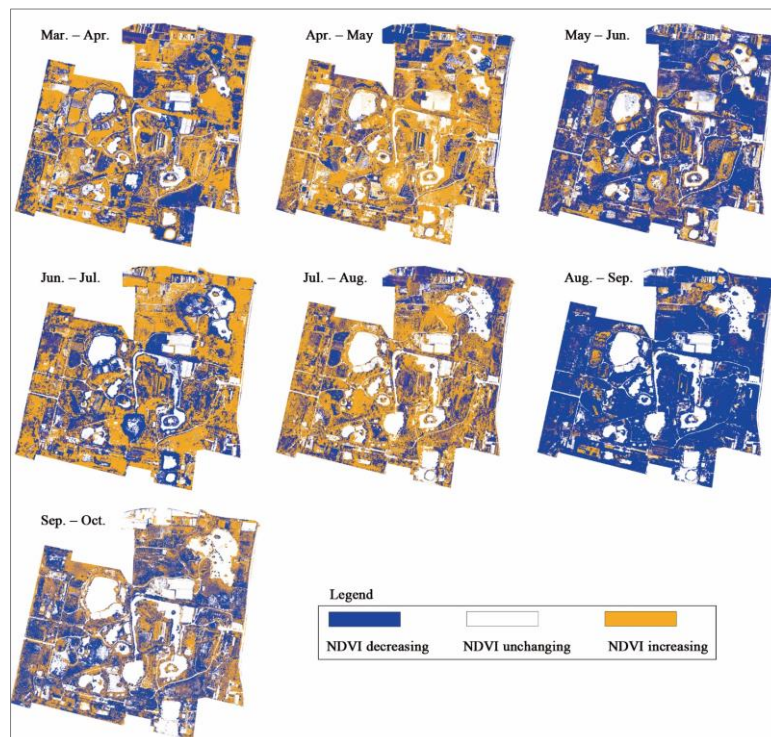


Figure 4. Distribution diagram of monthly NDVI difference of the wasteland in the growing season

Discussion

Impact of evergreen vegetation on NDVI

The vegetation of chalk soil wasteland entered the growth stage in March, and at this moment, NDVI basically reflected the coverage in winter. The dust pollution was relatively severe in winter, especially in windy days, the dust pollution had caused a great disturbance to surrounding residents. The low ratio of evergreen plants on the wasteland led to a poor dust retention effect in winter (Yin et al., 2020). The research showed that the dust retention capability of plants was impacted by the density, size, roughness and dip angle of leaves, but it generally had a good dust retention effect. The dust retention performance of different plants is ranked as follows: Coniferous tree > shrub > broadleaved tree > herbs and vines. In northern China, coniferous trees with rough leaves and secreting mucus is a reasonable choice (Liu et al., 2021). According to the research results of Li et al. (2021), *Cedrus deodara*, *Sabina chinensis*, *Photinia serrulata*, *Nerium oleander*, *Eriobotrya japonica* and other plants can be taken into account. Due to the impact of vegetation distribution zone, deciduous plants usually account for a large proportion in the landscape design in Northern Henan, but due to the particularity of wasteland transformation, so priority shall be given to ecological benefits. In order to make up for the shortcomings of low NDVI and poor ecological benefits in winter, the planting ratio of evergreen plants in the wasteland should be further increased, and evergreen plants could be planted on bare lands, and the ratio could even exceed 50%. In addition, the large area of bare land and the single species of evergreen plants usually lead to poor visual effect. In order to improve NDVI in winter, it is necessary to increase the species of evergreen plants and increase the planting ratio, so as to better play the ecological service function.

Impact of plant LAI on NDVI in the growing season

One of the reasons why the NDVI of wasteland is at a low level shall be the low LAI of some plants. LAI is an important structural parameter in the land surface process, as well as one of the most fundamental parameters to characterize the canopy structure of vegetation (Cai and Sha, 2019). Generally, the higher LAI the better the ecological benefits. It is of great significance to take LAI-based green volume ratio as the index to measure the greening ratio of the city (Li et al., 2004). Currently, the index has not been widely used, since it is difficult to be determined. Due to the different growth regions and environments, LAI of the same plant may vary greatly. In different studies, the relationship between LAI and NDVI may be linear or non-linear, but there is a positive correlation between LAI and NDVI, namely, the higher the leaf area index, the higher NDVI (Sun et al., 2021). The main reason is that when the plant LAI is high, the clearance of the leaves decreases and the covering effect on the ground is enhanced in the vertical projection.

According to the dynamic tracking of LAI of major green plants in Xinxiang by Zhang et al. (2017), there were certain rules for the leaf area index of adult plants growing in the same area, and LAI interval calibration could be conducted through mass sampling. The LAI of *Cedrus deodara*, *Juniperus chinensis*, *Ligustrum lucidum*, *Pyrus betulifolia*, *Aesculus chinensis*, *Eucommia ulmoides*, *Ailanthus altissima*, *Chaenomeles sinensis*, *Eugenia caryophyllata*, *Prunus cerasifera*, *Eriobotrya japonica*, *Photinia serrulata*, *Hibiscus syriacus*, *Prunus persica*, *Chimonanthus praecox*, *Lonicera maackii*, *Punica granatum*, *Sabina chinensis*, *Platycladus orientalis*, *Viburnum odoratissimum*,

Phyllostachys bambusoides and other plants is relatively high in Xinxiang, while that of *Albizia julibrissin*, *Salix babylonica*, *Ailanthus altissima*, *Acer pictum*, *Sapium sebiferum*, *Salix matsudana*, and *Melia azedarach* is relatively low. Therefore, plants with higher LAI should be selected as the main tree species for the plant configuration optimization of this wasteland, while plants with lower LAI can be used as matching tree species to increase the NDVI and enhance the species diversity and ornamental properties. Of course, it is necessary to test planting in advance to test the adaptability of plants to site conditions.

Impact of the canopy configuration on the NDVI in the growing season

Improving the canopy structure of vegetation is an important measure to increase NDVI. There are mainly four types vegetation canopy structure: single-layer loose type, single-layer closed type, multi-layer loose type and multi-layer closed type. Pure forests, trees, shrubs and grasses are mainly adopted for the vegetation restoration of this wasteland, which is dense in the plane but simple in the façade (Li et al., 2015). Although it is relatively dense in horizontal layout, but the main canopy structure is single-layer loose and multi-layer loose type. The single-layer closed type accounts for a small proportion, while the multi-layer closed type only appears in a few areas. Therefore, the plant restoration in this wasteland should be further optimized, and a community structure with compact horizontal distribution and rich vertical structure can be formed as much as possible, and high-density, multi-level complex communities can be formed where possible. In terms of specific methods, the density can be increased in horizontal distribution and layers can be added for the vertical distribution. But it is worth noting that during vegetation arrangement, higher LAI may not be better. The plants' needs for light, ventilation and nutrients shall be taken into account for the shaping of artificial plant layers, and further research is needed to establish a more stable plant community.

Conclusions

Through the research on chalk soil wasteland, the following conclusions can be drawn:

(1) After nearly two decades of treatment, the ecological environment of the wasteland has been remarkably improved, but it is still of middle coverage level. The monthly mean NDVI of wasteland in the growing season ranges between 0.12 and 0.3, of middle coverage level and levels below.

(2) The monthly NDVI level distribution of the wasteland in the growing season shows that the high vegetation coverage ratio is relatively low, and the vegetation environment of the wasteland still needs to be greatly improved and enhanced. The monthly NDVI difference of the wasteland indicates that operation and extreme weather have a significant impact on NDVI.

(3) UAV remote sensing can be effectively applied for the rapid image acquisition of ecological environment of the chalk soil wasteland, and it can provide high-quality vegetation index information and scientific basis for the optimization of ecological environment after data processing and analysis. UAV multispectral image features a fast speed, low cost and high precision when being applied for monitoring the changes of vegetation coverage of chalk soil wasteland, and it is suitable to be promoted and applied for the treatment of ecological environment for wastelands.

It is an important direction in future to conduct more in-depth research on the NDVI data obtained by UAV and the vegetation data obtained from ground surveys to provide a scientific basis for the ecological restoration of chalk soil wasteland.

Acknowledgements. This work was financially supported by the following projects: Key Science and Technology Research and Development Program of Henan Province, China (212102310841), Key Science and Technology Research and Development Program of Henan Province, China (212102310843) and Key Science and Technology Research and Development Program of Henan Province, China (222102320221).

REFERENCES

- [1] Cai, W. J., Sha, J. M. (2019): Inversion of leaf area index based on geographical environment factors. – *Journal of Subtropical Resources and Environment* 14(2): 55-64.
- [2] Chang, J., Li, C. K., Song, Y. C. (2020): Research progress on landscape reconstruction of mining wasteland in China. – *Chinese and Foreign Buildings* 9: 63-66.
- [3] Du, Y. C., Xiong, C., Duan, Y., Yu, M., Li, J. H. (2021): Landscape planning and design of Chongqing Causeway Mountain National Mine Park based on ecological restoration. – *Southern Agriculture* 15(16): 16-22.
- [4] Fan, D. Q., Zhao, X. S., Zhu, W. Q., Zheng, Z. T. (2016): Review of influencing factors of accuracy of plant phenology monitoring based on remote sensing data. – *Progress in Geography* 35(3): 304-319.
- [5] Grădinaru, S. R., Kienast, F., Psomas, A. (2019): Using multi-seasonal Landsat imagery for rapid identification of abandoned land in areas affected by urban sprawl. – *Ecological Indicators* 96(2): 79-86.
- [6] Guo, Y. K., Liu, J. Q., Guo, Y. Q., Cao, X., Xie, Q. (2020): GLIBERTY-DSAIL coupled model inversion of vegetation LAI in southern mixed forest LAI. – *Bulletin of Surveying and Mapping* 11: 39-42, 75.
- [7] Hu, Z H. (2020): Remote sensing monitoring of Lingling Manganese Mine Restoration Project based on timing NDVI. – *Chinese High and New Technology* 13: 117-118.
- [8] Huang, H., Guo, S. M. (2020): From "Ugly Chaos" to "Picture-pictured" landscape art improvement design of waste land in coal mine industry - A case study of Nanhu Park in Tangshan. – *Architecture and Culture* 1: 128-129.
- [9] Li, F., Wang, R. S., Juergen, P. (2004): Research on green space ecological concept planning in Beijing. – *Urban Planning Transactions* 4: 61-64, 96.
- [10] Li, L., Zhou, G., Yao, C. H. (2015): Study on the green volume of different types of urban green spaces. – *Chinese Landscape Architecture* 31(9): 17-21.
- [11] Li, X. J. (2019): Landscape regeneration design of abandoned mining land from the perspective of aesthetic value - A case study of Huairou Open-pit mine in Beijing. – Southwest Jiaotong University, Dissertation.
- [12] Li, C. M., Wang, J. M., Wang, T. F., Wang, Z. X., Lei, Y. K., He, D. (2021): Dust-retention capability and leaf traits of common park greening plant species in Zhengzhou City. – *Journal of Northwest Forestry University* 36(2): 123-129.
- [13] Liu, W. H., Li, W. W., Pei, S. X., Li, X. G. (2021): Analysis on the dust-retention ability of common garden plants in China. – *Forestry and Ecological Sciences* 36(3): 328-336.
- [14] Luo, J. W. (2019): The result analysis of the vegetation restoration effect of rare earth tailings based on NDVI and object spectral characteristic. – Nanchang Institute of Technology, Dissertation.
- [15] Shao, Y. P. (2017): Study on dynamic monitoring and vegetation coverage of rare earth mines. – China University of Geosciences (Beijing), Dissertation.

- [16] Sun, Y., Gu, Z. J., Li, D. L. (2021): Study on remote sensing retrieval of leaf area index based on unmanned aerial vehicle and satellite image. – *Science of Surveying and Mapping* 46(2): 106-112, 145.
- [17] Wang, J. P., Zhang, Y. C. (2015): From wasteland to the wonderful land: the ecological restoration and landscape reconstruction of chalk mine land in suburb. – *Chinese Landscape Architecture* 31(4): 20-24.
- [18] Wang, X. R., Lin, Q. (2019): The revealing and reconstitution of landscape - Quarry Gardens in Nanning Garden Expo Park. – *Chinese Landscape Architecture* 35(7): 24-33.
- [19] Wang, D., Zhao, P., Sun, J. B., Niu, L. Y., Liu, B. F. (2021): Inversion of chlorophyll content in summer maize based on UAV multi-spectrum. – *Shandong Agricultural Sciences* 53(6): 121-126, 132.
- [20] Wu, X. M., Kang, Y., Xiao, H. J., Yang, T. (2021): Elastic shaping of water ecology in abandoned mine - the design practice of Zishan Park in Handan City. – *Chinese Landscape Architecture* 37(6): 105-110.
- [21] Xu, J. H., Wang, S. D. (2021): Spatio temporal analysis of vegetation cover in mining city - A case study of Xuzhou city. – *GrassLand and Turf* 41(3): 91-98.
- [22] Yin, Z. J., Shen, X. X., Li, R. L., Gao, H. H., Yu, L. Y., Zhou, L., Wu, H. L., Cao, Y. (2020): Study on the dust retention effect of common garden plants in Shenzhen. – *Acta Scientiarum Naturalium Universitatis Pekinensis* 56(6): 1081-1090.
- [23] Yuan, M. X., Zou, L., Lin, A. W., Zhu, H. J. (2016): Analyzing dynamic vegetation change and response to climatic factors in Hubei Province, China. – *Acta Ecologica Sinica* 36(17): 5315-5323.
- [24] Zhang, Y. C., Qiao, L. F., Zhao, Y. P., Yao, L. F. (2006): The study of the potential values of abandoned land in suburb - Takes the Shili Agricultural Ecological Park as an example. – *Research of Soil and Water Conservation* 6: 94-96.
- [25] Zhang, Y. C. (2017): Rainwater characteristics and optimization of typical green space under sponge city-oriented - Take Xinxiang City as an example. – Wuhan University, Dissertation.
- [26] Zhang, M. X., Mei, D. Y., Gao, W. J., Bao, Q. X., Li, F. Z. (2019): Review on the applications of UAV remote sensing technology to urban green space monitoring. – *Journal of Chinese Urban Forestry* 7(5): 5-11.
- [27] Zhou, X. F., Zhu, W. Q., Ma, G. X., Zhang, D. H., Zheng, Z. T. (2016): Assessing the vegetation net productivity loss resulted from the mining of rare earth ore based on remote sensing technology - A case study in Ganzhou, Jiangxi Province. – *Remote Sensing Technology and Application* 31(2): 307-315.
- [28] Zhou, P. F., Zhang, S. W., Luo, M., Wei, H. B., Song, Q., Fang, B., Zhuang, H. J., Chen, H. Y. (2022): Characteristics of plant diversity and heavy metal enrichment and migration under different ecological restoration modes in abandoned mining areas. – *Environmental Science* 43(2): 985-994.

SEASONAL AND REGIONAL VARIATION IN CAROTENOIDS OF KOREAN FIR (*ABIES KOREANA*) ON MT. HALLA, SOUTH KOREA

LEE, C.^{1,2} – BAE, H.¹ – LIM, S.¹ – KIM, S.^{2*} – KIM, J.^{1*}

¹*Biomimicry Team, Division of Ecological Information, National Institute of Ecology, Seocheon 33657, Korea*

²*Department of Agricultural Chemistry, Chungnam National University, Daejeon 34134, Korea*

*Corresponding authors

e-mail: sckim@cnu.ac.kr (Kim, S.); jkim@nie.re.kr (Kim, J.)

(Received 25th Jan 2022; accepted 2nd May 2022)

Abstract. Climate change affects the decline of coniferous forests in the subalpine zone in Korea, and causes significantly changes in the composition and content of carotenoids. In the present study, we analyzed the effect of temperature variation on carotenoid content in *Abies koreana* native to Mt. Halla National Park to establish a scientific basis for the conservation of the species. To understand habitat variation, fir leaves of *A. koreana* were collected from three different regions (Yeongsil, Witseoreum, and Jindallaebat) of Mt. Halla during April, July, and October to quantify lutein, α -carotene, and β -carotene. The total carotenoid contents in the regions were significantly high in October when the temperature was low compared to July. The carotenoid contents in October were 8.5 times, 4.7 times, and 4 times higher at Yeongsil, Witseoreum, and Jindallaebat each. The lutein content was significantly higher at the Witseoreum region where *A. koreana* is more abundant than in Jindallaebat where *A. koreana* is in decline. The result showed that changes in carotenoid contents were affected by temperature which could influence the *A. koreana* abundancy and health status at Mt. Halla. This study could contribute to understanding physiological changes of *A. koreana* caused by environmental changes on Mt. Halla.

Keywords: *subalpine, carotene, lutein, quantification, climate change*

Introduction

Many studies were reported on the global forest decline caused by climate change (Wildi and Lütz, 1996; Lim et al., 2006; Allen et al., 2010; Körner, 2012; Tsuyama et al., 2015). In particular, the Intergovernmental Panel on Climate Change (IPCC, 2014) pointed out the possibility of the widespread death of plants due to temperature increases and drought resulting from global warming, and Antos et al. (2008) predicted extinction risks of the genus *Abies* in alpine regions. Subalpine plant species found at 1,300 to 1,800 m above sea level are greatly affected by limited opportunities for genetic exchange and various environmental factors, including temperature rise and water stress (Kim et al., 2017).

The Korean fir (*Abies koreana*) is a native Korean species that was introduced to the world by British botanist Wilson in 1920. The subalpine plant is a climate-sensitive bioindicator and is only found in subalpine zones such as Mt. Halla and Mt. Jiri in South Korea. Mt. Halla has the only large colony of Korean fir in the world (Kim et al., 2017). The distribution of the Korean fir, a species of the genus *Abies*, decreased in 15.2% from 738.3 ha to 626.0 ha at Mt. Halla for 9 years (2006-2015). Because of continuous decline of the Korean fir, *Abies koreana* was listed as an internationally endangered species by the International Union for Conservation of Nature (IUCN, 2011). Several studies claimed the causes of the decline of Korean fir in various ways. Continuous temperature

increase, heterogeneous invasion, weakening of the support base due to typhoons or droughts, and lack of water required for photosynthesis were found as factors hindering the growth of the Korean fir species (Koo et al., 2001, 2017; Song et al., 2014, 2020; Park et al., 2018). Of these, the temperature increase not only changes the moisture content in soil, affects plant growth and reproduction, and causes a decrease in nutrient intake capacity and yield, but is also a leading greenhouse gas contributor that triggers the release of carbon from the soil to the atmosphere (Körner and Paulsen, 2004; Lee et al., 2013; Hatfield and Prueger, 2015).

Variations in the habitat of trees induced physiological changes in genetic composition and chemical compounds (Hwang et al., 2018). Especially, plants in alpine regions produced large amounts of carotenoids for protection against antioxidants to survive in the harsh environment of low temperatures (Streb et al., 1997; Kim and Park, 2018). Some conifers produced a high level of carotenoids for survival during cold winters (García-Plazaola et al., 1999). The most common carotenoids include lutein, α -carotene, β -carotene, lycopene, zeaxanthin, and astaxanthin (Nisar et al., 2015). Study showed the carotenoid content in Korean fir seedlings and changes in photosynthetic apparatus caused by high luminous intensity and moisture stress (Je et al., 2018). Even though lutein and β -carotene contents were changed depending on the temperature changes with altitudes in the Jindallaebat region of Mt. Halla (Oh et al., 2013), the role of carotenoids for the Korean fir on Mt. Halla in a changing growth environment and the adaptation process are still largely unknown.

The object of this study was to compare the carotenoid content of Korean firs on Mt. Halla by area and season to identify the effect of temperature variation, and to analyze the correlation between carotenoid contents and temperatures. Considering the topographical and environmental differences of each slope on Mt. Halla, the carotenoid contents in Korean fir leaves collected from three colonies (Yeongsil, Witseoreum, and Jindallaebat) was quantified by season.

Materials and Methods

Study sites and sampling

The study was conducted in Mt. Halla National Park, Cheju Island, Korea. Study sites were selected in near hiking trails, 1,300 to 1,700 m above sea level, in three Korean fir colonies (YS: Yeongsil, WS: Witseoreum, JD: Jindallaebat) on each slope of Mt. Halla located in the southern part of the Korean Peninsula (*Fig. 1a*). The Korean fir leaves were harvested over three years from 2016-2018. Considering that the different seasons are based on temperature changes, Korean fir leaf samples were collected in three different seasons (April, July, and October). Based on the sample collection method of Oh et al. (2013), the samples were collected randomly from nine or more mature trees (≥ 2 m) with health conditions at a height of 1.5 to 2.5 m with sufficient sunlight. Weather data were collected from three or more portable thermo-hygrometers (HOBO®, Onset Corp., U23-001, Boston, MA, USA), and automatic weather systems were installed in each research area (*Fig. 1b*).

Standard materials and reagents

The study used lutein, zeaxanthin, α -carotene, and β -carotene produced by Sigma-Aldrich (Saint Louis, USA) as reference materials for carotenoids. For the extraction and

analysis of carotenoids, high-performance liquid chromatography (HPLC)-grade ethanol (EtOH), methanol (MeOH), ethyl acetate (EtOAc), potassium hydroxide (KOH), hexane, dichloromethane (DCM), acetonitrile (ACN), and water were used.

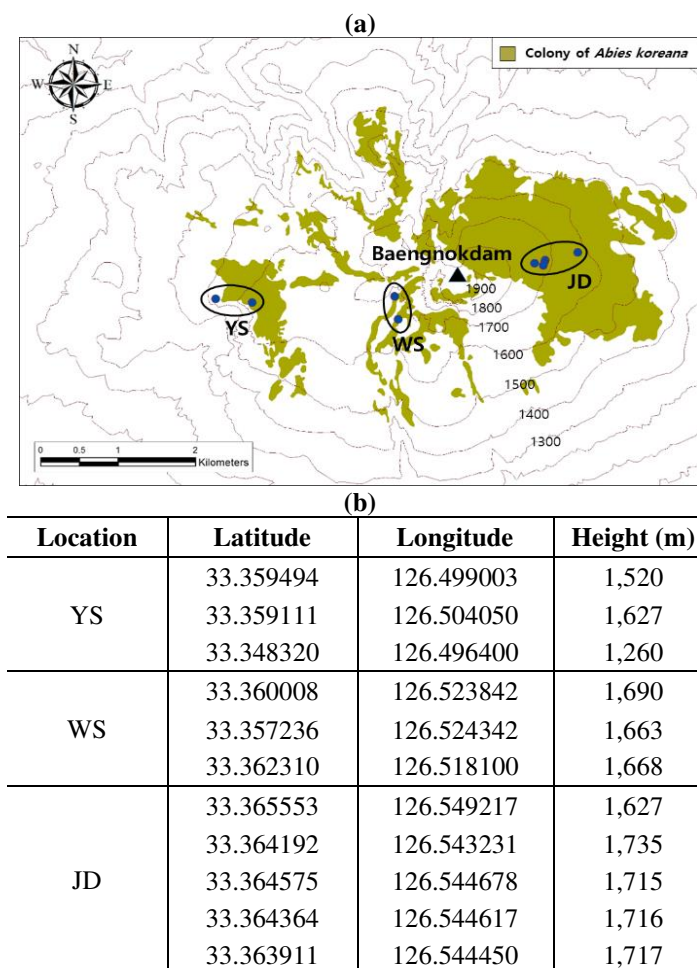


Figure 1. (a) Map of the study sites (▲: Top of Mt. Halla, ●: Area of sampling locations) and (b) sampling locations in Mt. Halla

Extraction of carotenoids in Korean fir

Carotenoids were extracted for 5 min in a constant-temperature water bath (75 °C) with a 50 mL tube containing 0.5 g of dried Korean fir leaf powder and 5 mL of EtOH. An amount of 1.5 mL of 80% KOH was added to the extract, which was reacted for 10 min in a constant-temperature water bath (75 °C) and then cooled in ice for 5 min. Then, 2.5 mL of water and hexane were added to the tube once the reaction stopped and were well mixed. The mixture was centrifuged for 3 min (3,000 rpm, 4 °C). Thereafter, the supernatant was collected, and this process was repeated three times for a proper mix. After removing the solvent through lyophilization, the extract was dissolved in 1 mL of a MeOH:DCM (1:1, v/v) solution to be used as a sample for high-performance liquid chromatography (HPLC) analysis (Lee et al., 2017).

Carotenoids were analyzed using an Ultimate 3000 HPLC system (Thermo Dionex, Waltham, USA). The column used was INNO C-18 (4.6 × 250 mm, 5 μm, Youngjin

Biochrom, Seongnam, Korea), and its temperature was maintained at 50 °C. Ten microliters of the sample was injected at a rate of 1 mL/min, and the wavelength of the detector was set to 440 nm. As regards the development conditions, water was used as mobile phase solvent A, ACN as solvent B, and MeOH:EtOAc (50:50, v/v) as solvent C. The slope conditions were as follows: 40% for solvent A, 10% for solvent B, and 50% for solvent C, maintained for 5 min. Solvent B was steadily raised to 50% up to 20 min. Solvents B and C were maintained at 50% to 30 min, followed by 40% for solvent A, 10% for solvent B, and 50% for solvent C up to 35 min. For quantitative analysis, an experiment was performed for five concentrations (10, 20, 50, 100, and 200 ppm) under the HPLC conditions established for the reference solution of each component, and a calibration curve was obtained. The correlation coefficient (R^2) of the calibration curve was > 0.99 . Carotenoid contents were expressed as $\mu\text{g/g}$ dry weight (DW).

Statistical analysis

This study conducted a multivariate analysis of the carotenoid content of Korean firs on Mt. Halla by region and season using R v3.6.1 (R Core Team, 2019), the stats and DescTools package version 0.99.28 (Signorell, 2019). A one-way ANOVA ($p < 0.05$) was performed using Scheffe's test to analyze the significance of carotenoids in Korean fir leaves by region and season, and a partial least squares-discriminant analysis (PLS-DA) and a variable importance in projection (VIP) score analysis were carried out to identify differences in the content of carotenoids based on the area, season, and health of trees.

As a method to determine which one of two or more populations a given sample was extracted from, the PLS-DA aimed to maximize the variance between groups using discriminant functions consisting of a combination of one or more discriminant variables. The VIP score has a higher value depending on the contribution to the variance between groups, and only those with a value of 1 or above were judged to have significance (Wilson, 2002). In addition, Pearson's correlation coefficient analysis ($p < 0.01$) was performed to analyze the correlation between the carotenoid content in Korean fir and temperature, and the correlation coefficient (r) was expressed as a value between -1 and +1.

Results and Discussion

Analysis of microclimate data in the Korean fir colony

After collecting data from the automatic weather systems in the research areas of Yeongsil, Witseoreum, and Jindallaebat on Mt. Halla, changes in the average temperature of the three Korean fir colonies were plotted on a graph (Fig. 2). During the research period (2016-2018), the average temperature ranged between 7.4 °C and 9.0 °C in Yeongsil, 6.38 °C and 7.4 °C in Witseoreum, and 6.4 °C and 7.6 °C in Jindallaebat. The average temperature in Yeongsil was at least 1 °C higher than that in Witseoreum and Jindallaebat. According to the average temperature data for 10 years (2010-2019) collected from the Korean Meteorological Administration, the average temperature in Yeongsil (8.9 °C) was higher than that in Witseoreum (6.2 °C) and Jindallaebat (7.5 °C). Carotenoids, essential photosynthetic pigments, prevent damage protect to photosynthetic machinery under abiotic stress conditions such as temperature (Hatfield and Prueger, 2015; Nisar et al., 2015). Therefore, carotenoid contents and monthly mean temperature

were displayed in *Figure 2*. Total carotenoid contents were between 1.17 and 28.15 $\mu\text{g/g}$. Interestingly; the level of total carotenoids was consistently higher in October from 2016 to 2018.

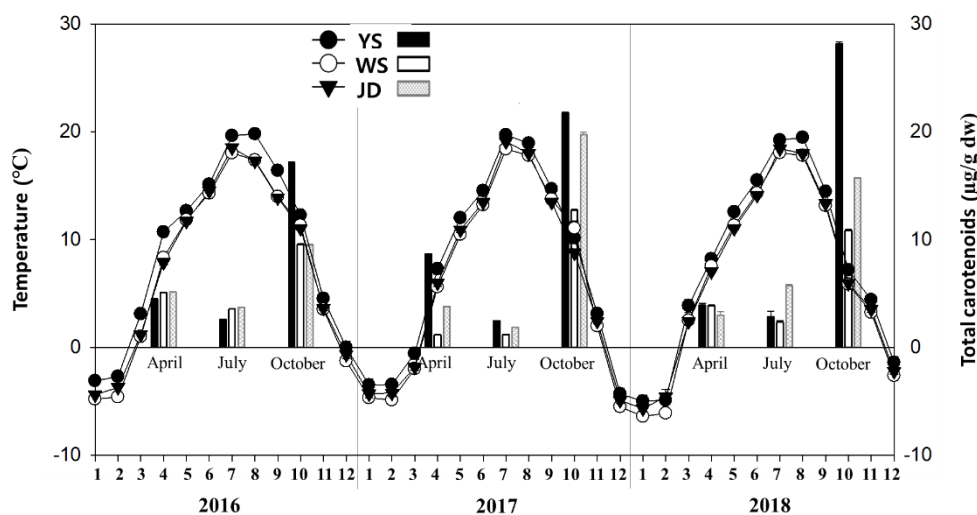


Figure 2. Temperature changes and carotenoid contents at Yeongsil (YS), Witseoreum (WS), and Jindallaebat (JD) on Mt. Halla during 2016-2018

Carotenoid compounds of Korean fir at different harvesting years

In this study, three types of carotenoids, namely lutein, α -carotene, and β -carotene were mainly found, and the Korean fir leaves contained relatively high levels of lutein compared to α -carotene and β -carotene in the years 2016-2018 (*Table 1*).

Zeaxanthin compound was expected in this study, but it was not found in the Korean fir. The content of lutein ranged from 0.82 to 23.30 $\mu\text{g/g}$, α -carotene between 0.02 and 2.01 $\mu\text{g/g}$, and β -carotene between 0.11 and 2.84 $\mu\text{g/g}$, and the total content of carotenoids was between 1.17 and 28.15 $\mu\text{g/g}$. Carotenoids are known as auxiliary pigments mainly present in the chloroplasts of plants and are involved in the photoprotection of plants by reducing excessive thermal energy generated during photosynthesis and keep reactive oxygen species from being produced by photooxidation (Howitt and Pogson, 2006). Therefore, it is expected that the health of the Korean fir trees could be predicted by the concentration of carotenoids, representatively, lutein, α -carotene, and β -carotene.

Carotenoids in Korean fir at different seasons and regions

A comparison of the carotenoids in Korean firs harvested in three different seasons and regions of April, July, and October, representing spring, summer and fall, respectively. The total carotenoids of lutein, α -carotene and β -carotene were significantly high in October and low in July in all research areas. Carotenoids in recorded 8.5, 4.7, and 4.0 times in October higher than that in July at Yeongsil, Witseoreum, and Jindallaebat, respectively (*Table 2*). The higher lutein concentrations could be attributed to the higher contents of carotenoids in Korean fir. Particularly, carotenoids increased in October when temperature is relatively low, compared to April and July.

Table 1. Carotenoid contents in *Abies koreana* collected from three regions on Mt. Halla

(µg/g DW)						
Month	Place	Year	Lutein	α-Carotene	β-Carotene	Total ^{a)}
Apr	YS ^{b)}	2016	3.54±0.08	0.17±0.00	0.70±0.02	4.42±0.10
		2017	7.41±0.08	0.21±0.01	1.02±0.01	8.65±0.07
		2018	3.22±0.13	0.15±0.01	0.54±0.03	3.91±0.17
	WS	2016	4.04±0.03	0.25±0.00	0.80±0.01	5.09±0.02
		2017	1.03±0.01	0.02±0.00	0.11±0.01	1.17±0.01
		2018	3.28±0.04	0.15±0.00	0.44±0.01	3.87±0.06
	JD	2016	3.87±0.01	0.48±0.00	0.78±0.01	5.14±0.02
		2017	3.24±0.01	0.11±0.01	0.44±0.01	3.80±0.01
		2018	2.58±0.31	0.10±0.01	0.29±0.03	2.97±0.35
Jul	YS	2016	1.59±0.03	0.49±0.01	0.51±0.01	2.59±0.05
		2017	1.67±0.03	0.41±0.01	0.38±0.01	2.47±0.02
		2018	1.94±0.36	0.46±0.09	0.44±0.08	2.84±0.54
	WS	2016	2.28±0.05	0.61±0.00	0.67±0.00	3.56±0.05
		2017	0.82±0.04	0.15±0.01	0.19±0.01	1.17±0.04
		2018	1.60±0.10	0.29±0.02	0.45±0.03	2.34±0.15
	JD	2016	2.16±0.02	0.70±0.01	0.88±0.01	3.74±0.03
		2017	1.27±0.02	0.26±0.01	0.32±0.01	1.85±0.03
		2018	3.76±0.09	0.98±0.02	1.01±0.02	5.74±0.14
Oct	YS	2016	13.42±0.12	1.45±0.01	2.27±0.04	17.13±0.09
		2017	18.12±0.11	1.37±0.03	2.25±0.02	21.74±0.08
		2018	23.30±0.05	2.01±0.06	2.84±0.08	28.15±0.19
	WS	2016	8.71±0.06	0.36±0.02	0.46±0.05	9.54±0.07
		2017	11.33±0.03	0.48±0.02	0.92±0.04	12.73±0.06
		2018	9.90±0.06	0.33±0.01	0.60±0.04	10.83±0.10
	JD	2016	8.12±0.01	0.65±0.04	0.77±0.03	9.53±0.06
		2017	15.97±0.12	1.75±0.03	2.03±0.08	19.75±0.21
		2018	12.83±0.01	1.18±0.04	1.71±0.02	15.72±0.05

^{a)} All data are shown as mean±SD (n=3)

^{b)} YS: Yeongsil, WS: Witseoreum, JD: Jindallaebat

Being structurally more stable than chlorophyll, carotenoids are sustained at a relatively high level during leaf senescence caused by temperature changes, which cause leaves to turn yellow (Biswal, 1995; Merzlyak and Solovchenko, 2002). The total content of carotenoids was the highest in Yeongsil (22.34 µg/g), followed by Jindallaebat (15.00 µg/g), and Witseoreum (11.03 µg/g). The major of lutein content was also high in the order of Yeongsil (18.24 µg/g), Jindallaebat (12.30 µg/g), and Witseoreum (9.98 µg/g) (Table 2). This is due to the topographical differences in the slopes, including periglacial landforms in the subalpine climate of Mt. Halla, which frequently cause weathering and erosion resulting from freezing, fragmentation, and turf destruction (Kim, 2008). Because of such topographic features, each slope of Mt. Halla presents a different environment (such as exposed rock, broad-leaf bamboo coverage, and vegetation), as well as

meteorological conditions, including temperature, precipitation, and wind. A study showed that variation in the lapse rate throughout the year was also different: West slope (Yeongsil), -0.62 °C/100 m, south slope (Witseoreum), -0.55 °C/100 m, east slope (Jindallaebat), -0.45 °C/100 m, and north slope, -0.48 °C/100 m (Choi, 2011). Therefore, it proved our result that carotenoids concentration was high in the order temperature for each slope of Mt. Halla.

Table 2. Carotenoid compounds ($\mu\text{g/g DW}$) of *Abies koreana* leaves harvested from different seasons and locations

Place	Month	Lutein	α -Carotene	β -Carotene	Carotene	Total ^{a)}
YS ^{b)}	Apr	4.73±2.02 ^a	0.18±0.03 ^a	0.75±0.22 ^a	0.93±0.24 ^a	5.66±2.25 ^a
	Jul	1.73±0.28 ^a	0.45±0.07 ^b	0.44±0.07 ^b	0.90±0.14 ^a	2.63±0.37 ^a
	Oct	18.28±4.28 ^b	1.61±0.30 ^c	2.45±0.30 ^c	4.06±0.60 ^b	22.34±4.79 ^b
WS	Apr	2.78±1.35 ^a	0.14±0.10 ^a	0.45±0.30 ^a	0.59±0.40 ^a	3.38±1.74 ^a
	Jul	1.57±0.64 ^a	0.35±0.20 ^b	0.43±0.21 ^a	0.78±0.41 ^{ab}	2.36±1.04 ^a
	Oct	9.98±1.14 ^b	0.39±0.07 ^b	0.66±0.21 ^a	1.05±0.27 ^b	11.03±1.39 ^b
JD	Apr	3.23±0.59 ^a	0.23±0.19 ^a	0.50±0.22 ^a	0.74±0.40 ^a	3.97±0.97 ^a
	Jul	2.40±1.09 ^a	0.64±0.31 ^a	0.74±0.32 ^a	1.38±0.63 ^a	3.78±1.69 ^a
	Oct	12.30±3.42 ^b	1.19±0.48 ^b	1.50±0.57 ^b	2.70±1.04 ^b	15.00±4.46 ^b

^{a)} Means with the different letter are significantly different from each other ($P < 0.05$)

^{b)} YS: Yeongsil, WS: Witseoreum, JD: Jindallaebat

Variable importance in projection (VIP) score analysis

Among the three research areas on Mt. Halla, Jindallaebat (east slope) is most severely affected by typhoons as it is directly affected by heavy rains caused by counter-clockwise water advection when a typhoon approaches (Choi, 2011). The decline in the Korean fir colony in Jindallaebat between 2006 and 2015 accounted for 71.8% of the total decline of Korean fir colonies on Mt. Halla (Kim et al., 2017). In this study, assuming the Witseoreum as a relatively vulnerable area and Jindallaebat as a relatively healthy area for Korean fir colonies, PLS-DA was performed. Witseoreum and Jindallaebat were significantly distinguished due to concentration of lutein and total carotenoids manifested in Korean firs in October, suggesting that lutein and total carotenoids are the most important discriminatory variables (Fig. 3, Table 3).

The VIP score analysis showed that lutein and total carotenoids are the distinguished indicators for the seasonal variations in the three areas (Yeongsil, Witseoreum, and Jindallaebat). Lutein as a major component of carotenoids showed a significant difference in Korean fir leaves according to seasonal changes, regardless of region (Table 3). This study demonstrated an increasing pattern of carotenoid components in October, and relatively healthy and declined regions for Korean firs were classified based on the carotenoid concentrations. Although it could be difficult to determine the degree of healthy regions of trees including Korean firs only measured by carotenoids analysis, it seems that changes in carotenoid contents caused by temperature variation are considered to be related to the health of Korean firs. The results provide knowledge on the physiological responses of declining Korean firs' habitats and could provide clues or basic materials for preparing future conservation measures.

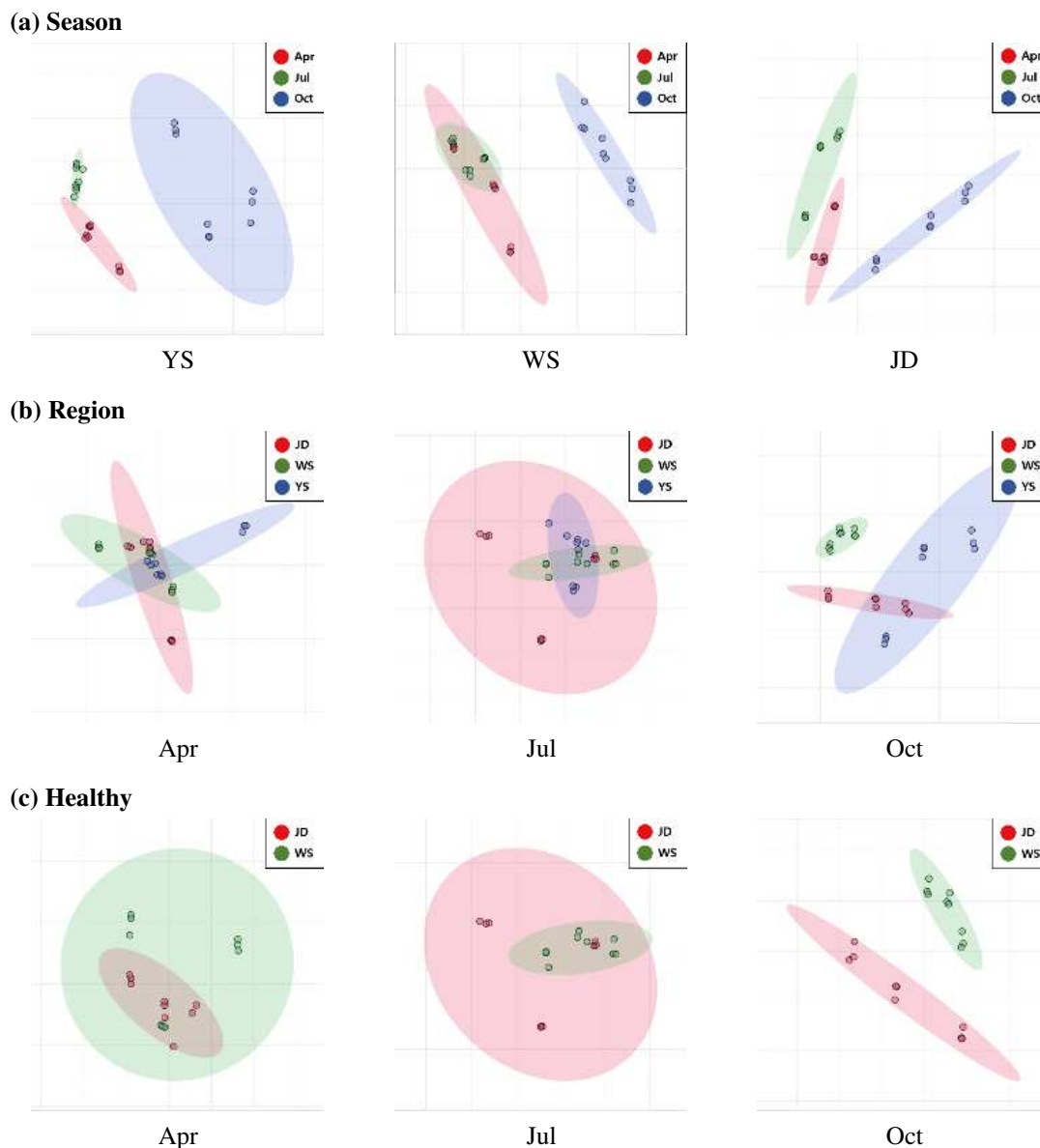


Figure 3. Partial least squares discriminant analysis (PLS-DA) score plot for carotenoid contents of *Abies koreana* on Mt. Halla. (YS: Yeongsil, WS: Witseoreum, JD: Jindallaebat)

Carotenoid content and temperature interactions for Korean firs

An analysis of the correlation coefficients between the carotenoid content of Korean fir leaves and the monthly average temperature of each area and season ($p < 0.01$) showed that the total content of lutein (-0.58), β -carotene (-0.54), and carotenoids (-0.56) were significantly negatively correlated with temperature in Yeongsil (Table 4).

The changes in carotenoid content caused by temperature variation differ according to plant species; as a result of this study, in general, the lower the temperature, the higher the carotenoid contents (Massacci et al., 1995; Ormrod et al., 1999; Lisiewska et al., 2004; Lefsrud et al., 2005; Rivera-Pastrana et al., 2010; Lee et al., 2014). According to Oh et al. (2013), the lutein content of Korean firs in Jindallaebat on Mt. Halla increased with increasing altitude and decreasing temperature. In this study, the carotenoid contents of

Korean firs on Mt. Halla was remarkably low in July when the temperature was high, and increased as the temperature decreased in October, showing a negative correlation with temperature. This is because carotenoids, including lutein, contribute to the removal of free radicals generated during the oxidation process by light in the photosynthetic process, and loss increases upon exposure to excessive light and heat (Ahmad et al., 2013). It also seems to be for the purpose of photoprotection and the maintenance of efficient photosynthetic function in conifers during winter, when photosynthesis is minimal due to low temperatures (Öquist and Huner, 2003; Oh et al., 2013).

Table 3. VIP scores by PLS-Discriminant Analysis

Division		Lutein	α -Carotene	β -Carotene	Total
Season	YS	1.3880	0.1466	0.1739	1.7085
	WS	1.5293	0.0529	0.0447	1.6269
	JD	1.4006	0.1483	0.1543	1.7032
Region	Apr	1.4653	0.0510	0.2449	1.6591
	Jul	1.0232	0.2914	0.4504	1.7650
	Oct	1.3887	0.0973	0.2205	1.7066
Healthy	Apr	1.3115	0.2599	0.1628	1.7342
	Jul	1.0272	0.3642	0.3759	1.7673
	Oct	1.0346	0.3568	0.3761	1.7674

Means are significant at score > 1.0000, YS: Yeongsil, WS: Witseoreum, JD: Jindallaebat

Table 4. Correlation analysis (*Abies koreana* carotenoids and temperature)

Division			Lutein	α -Carotene	β -Carotene	Carotene	Total ^{a)}
Temperature	Season	Apr	+0.2279	+0.3242	+0.4734*	+0.4588*	+0.2787
		Jul	- 0.2176	- 0.1401	- 0.2602	- 0.2037	-0.2155
		Oct	- 0.2590	- 0.1409	- 0.1111	- 0.1247	-0.2318
	Region	YS ^{b)}	- 0.5866**	- 0.2731	- 0.5420**	- 0.4367*	-0.5640**
		WS	- 0.3808	+ 0.3983*	- 0.0445	+0.1427	-0.3442
		JD	- 0.4485*	- 0.0086	- 0.2033	- 0.1119	-0.3947*

^{a)} Significant at *P<0.05, **P<0.01 (n=9)

^{b)} YS: Yeongsil, WS: Witseoreum, JD: Jindallaebat

Conclusions

Temperature greatly affects the survival of alpine plants. However, interactions in the ecosystem occur organically through various abiotic and biotic factors such as precipitation and soil characteristics. Thus, it is still difficult to predict the cause of the rapid decline and change in the distribution of the Korean fir. In this study, the carotenoid content of Korean firs on Mt. Halla was measured by area and season, and the results confirmed a significant increase in carotenoids in October. It was also found that Witseoreum and Jindallaebat regions had significantly different carotenoid contents because of temperature characteristics, suggesting possibilities to assess health. There are still insufficient studies on the various secondary metabolites involved in the growth of

trees, including carotenoids. Therefore, further studies are needed to elucidate physiological changes and environmental variables for a comprehensive approach to the preservation of Korean firs on Mt. Halla.

Acknowledgements. This study was supported by the National Institute of Ecology through grant number NIE-B-2022-18.

REFERENCES

- [1] Ahmad, F. T., Asenstorfer, R. E., Soriano, I. R., Mares, D. J. (2013): Effect of temperature on lutein esterification and lutein stability in wheat grain. – *Journal of Cereal Science* 58(3): 408-413.
- [2] Allen, C. D., Macalady, A. K., Chenchouni, H., Bachelet, D., McDowell, N., Vennetier, M., Cobb, N. (2010): A global overview of drought and heat-induced tree mortality reveals emerging climate change risks for forests. – *Forest ecology and management* 259(4): 660-684.
- [3] Antos, J. A., Parish, R., Nigh, G. D. (2008): Growth patterns prior to mortality of mature *Abies lasiocarpa* in old-growth subalpine forests of southern British Columbia. – *Forest ecology and management* 255(5-6): 1568-1574.
- [4] Biswal, B. (1995): Carotenoid catabolism during leaf senescence and its control by light. – *Journal of Photochemistry and Photobiology B: Biology* 30(1): 3-13.
- [5] Choi, G. (2011): Variability of temperature lapse rate with height and aspect over Halla mountain. – *Journal of Climate Research* 6(3): 171-186.
- [6] García-Plazaola, J. I., Artetxe, U., Becerril, J. M. (1999): Diurnal changes in antioxidant and carotenoid composition in the Mediterranean sclerophyll tree *Quercus ilex* (L) during winter. – *Plant Science* 143(2): 125-133.
- [7] Hatfield, J. L., Prueger, J. H. (2015): Temperature extremes: Effect on plant growth and development. – *Weather and climate extremes* 10: 4-10.
- [8] Howitt, C. A., Pogson, B. J. (2006): Carotenoid accumulation and function in seeds and non-green tissues. – *Plant, cell & environment* 29(3): 435-445.
- [9] Hwang, J. E., Kim, Y. J., Shin, M. H., Hyun, H. J., Bohnert, H. J., Park, H. C. (2018): A comprehensive analysis of the Korean fir (*Abies koreana*) genes expressed under heat stress using transcriptome analysis. – *Scientific reports* 8(1): 1-11.
- [10] IPCC. (2014): Contribution of working groups I, II and III to the fifth assessment report of the Intergovernmental Panel on Climate Change. – *Climate Change 2014: Synthesis Report*, 151p.
- [11] IUCN. (2011): The IUCN Red List of Threatened Species. – Available at: <https://www.iucnredlist.org/species/31244/9618913>.
- [12] Je, S. M., Kim, S. H., Woo, S. Y. (2018): Responses of the photosynthetic apparatus of *Abies koreana* to drought under different light conditions. – *Ecological research* 33(2): 413-423.
- [13] Kim, T. (2008): Thufur and turf exfoliation in a subalpine grassland on Mt Halla, Jeju Island, Korea. – *Mountain Research and Development* 28(3): 272-278.
- [14] Kim, J. K., Koh, J. G., Yim, H. T., Kim, D. S. (2017): Changes of spatial distribution of Korean fir forest in Mt. Hallasan for the Past 10 Years (2006, 2015). – *Korean Journal of Environment and Ecology* 31(6): 549-556.
- [15] Kim, J., Park, E. J. (2018): Chemical and Biological Properties of the Genus *Abies*. – In: *Advances in Plant Phenolics: From Chemistry to Human Health*, American Chemical Society, pp. 225-236.

- [16] Koo, K. A., Park, W. K., Kong, W. S. (2001): Dendrochronological analysis of *Abies koreana* W. at Mt. Halla, Korea: effects of climate change on the growths. – The Korean Journal of Ecology 24(5): 281-288.
- [17] Koo, K. A., Kong, W. S., Park, S. U., Lee, J. H., Kim, J., Jung, H. (2017): Sensitivity of Korean fir (*Abies koreana* Wils.), a threatened climate relict species, to increasing temperature at an island subalpine area. – Ecological Modelling 353: 5-16.
- [18] Körner, C., Paulsen, J. (2004): A world-wide study of high altitude treeline temperatures. – Journal of Biogeography 31(5): 713-732.
- [19] Körner, C. (2012): Alpine Treelines: Functional Ecology of the Global High Elevation Tree Limits. – Springer Science & Business Media, pp. 15-19.
- [20] Lee, J. H., Yi, J. S., Chun, Y. M., Chae, N. Y., Lee, J. S. (2013): Discussion of soil respiration for understanding ecosystem carbon cycle in Korea. – Korean Journal of Ecology and Environment 46(2): 310-318.
- [21] Lee, S., Oh, C. Y., Han, S. H., Kim, K. W., Kim, P. G. (2014): Photosynthetic Responses of *Populus alba* × *glandulosa* to Elevated CO₂ Concentration and Air Temperature. – Korean Journal of Agricultural and Forest Meteorology 16(1): 22-28.
- [22] Lee, H. J., Chun, J. H., Kim, S. J. (2017): Effects of water stress on carotenoid and proline contents in kale (*Brassica oleracea* var. *acephala*) leaves. – Korean Journal of Environmental Agriculture 36(2): 97-105.
- [23] Lefsrud, M. G., Kopsell, D. A., Kopsell, D. E., Curran-Celentano, J. (2005): Air temperature affects biomass and carotenoid pigment accumulation in kale and spinach grown in a controlled environment. – HortScience 40(7): 2026-2030.
- [24] Lim, J. H., Woo, S. Y., Kwon, M. J., Chun, J. H., Shin, J. H. (2006): Photosynthetic capacity and water use efficiency under different temperature regimes on healthy and declining Korean fir in Mt. Halla. – Journal of Korean Society of Forest Science 95(6): 705-710.
- [25] Lisiewska, Z., Kmiecik, W., Słupski, J. (2004): Contents of chlorophylls and carotenoids in frozen dill: effect of usable part and pre-treatment on the content of chlorophylls and carotenoids in frozen dill (*Anethum graveolens* L.), depending on the time and temperature of storage. – Food chemistry 84(4): 511-518.
- [26] Massacci, A., Lannelli, M. A., Pietrini, F., Loreto, F. (1995): The effect of growth at low temperature on photosynthetic characteristics and mechanisms of photoprotection of maize leaves. – Journal of Experimental Botany 46(1): 119-127.
- [27] Merzlyak, M. N., Solovchenko, A. E. (2002): Photostability of pigments in ripening apple fruit: a possible photoprotective role of carotenoids during plant senescence. – Plant Science 163(4): 881-888.
- [28] Nisar, N., Li, L., Lu, S., Khin, N. C., Pogson, B. J. (2015): Carotenoid metabolism in plants. – Molecular plant 8(1): 68-82.
- [29] Oh, S., Adams III, W. W., Demmig-Adams, B., Koh, S. C. (2013): Seasonal photoprotective responses in needles of Korean fir (*Abies koreana*) over an altitudinal gradient on Mount Halla, Jeju Island, Korea. – Arctic, Antarctic, and Alpine Research 45(2): 238-248.
- [30] Öquist, G., Huner, N. P. (2003): Photosynthesis of overwintering evergreen plants. – Annual review of plant biology 54(1): 329-355.
- [31] Ormrod, D. P., Lesser, V. M., Olszyk, D. M., Tingey, D. T. (1999): Elevated temperature and carbon dioxide affect chlorophylls and carotenoids in Douglas-fir seedlings. – International journal of plant sciences 160(3): 529-534.
- [32] Park, J. S., Shin, H. S., Choi, C. H., Lee, J., Kim, J. (2018): Hierarchical environmental factors affecting the distribution of *Abies koreana* on the Korean Peninsula. – Forests 9(12): 777.
- [33] Rivera-Pastrana, D. M., Yahia, E. M., González-Aguilar, G. A. (2010): Phenolic and carotenoid profiles of papaya fruit (*Carica papaya* L.) and their contents under low temperature storage. – Journal of the Science of Food and Agriculture 90(14): 2358-2365.

- [34] Signorell, A. (2019): Package DescTools. version 0.99.28. – Available at: <https://cran.r-project.org/web/packages/DescTools/index.html>.
- [35] Song, K. M., Kang, Y. J., Hyeon, H. J. (2014): Vegetation structure at the slope direction and characteristic of seedlings of *Abies koreana* in Hallasan Mountain. – Journal of Environmental Science International 23(1): 39-46.
- [36] Song, K. M., Kim, J. H., Choi, H. S. (2020): Growth Changes in *Abies koreana* Seedlings of the Hallasan Mountain Over a 10-year Period. – Journal of Environmental Science International 29(3): 209-218.
- [37] Streb, P., Feierabend, J., Bigny, R. (1997): Resistance to photoinhibition of photosystem II and catalase and antioxidative protection in high mountain plants. – Plant, Cell & Environment 20(8): 1030-1040.
- [38] Tsuyama, I., Higa, M., Nakao, K., Matsui, T., Horikawa, M., Tanaka, N. (2015): How will subalpine conifer distributions be affected by climate change Impact assessment for spatial conservation planning. – Regional Environmental Change 15(2): 393-404.
- [39] Wildi, B., Lütz, C. (1996): Antioxidant composition of selected high alpine plant species from different altitudes. – Plant, Cell & Environment 19(2): 138-146.
- [40] Wilson, E. H. (1920): Four new conifers from Korea. – Journal of the Arnold Arboretum 1(3): 186-190.
- [41] Wilson, D. I. (2002): Derivation of the chalk superficial deposits of the North Downs, England: an application of discriminant analysis. – Geomorphology 42(3-4): 343-364.

EFFECT OF HARVEST AT DIFFERENT MATURATION STAGES ON FRESH EAR YIELD AND EAR CHARACTERISTICS OF SWEET CORN (*Zea mays* L. *saccharata*) GENOTYPES

AGACKESEN, M. N.¹ – OKTEM, A. G.² – OKTEM, A.^{2*}

¹*Harran University, Birecik Vocational School, Sanliurfa, Turkey*

²*Harran University, Faculty of Agriculture, Department of Field Crops, Sanliurfa, Turkey*

**Corresponding author*

e-mail: aoktem@harran.edu.tr; phone: +90-414-318-3686; fax: +90-414-318-3682

(Received 29th Jan 2022; accepted 20th May 2022)

Abstract. This research was conducted in order to determine the effect of harvesting at different maturation stages in some sweet corn genotypes on fresh ear yield and ear components. The experiment was carried out in 2016 and 2017 under Sanliurfa conditions, Turkey. Experiment was established according to the split plots experimental design with three replications. Five sweet corn varieties, Baron, Vega, Jubile, GSS-5649 and Merit were used as plant material in the research. As the harvest maturation stages; according to the Zadoks scale, the periods of early milk maturation (Z73), middle milk maturation (Z75), late milk maturation (Z77), early yellow maturation (Z83), middle yellow maturation (Z85) and late yellow maturation (Z87) were used. The varieties used in the study were placed in the main parcels and the harvest times in the sub plots. During the research, ear features and fresh ear yield were determined. The research results indicated that tested characteristics showed statistically significant difference according to cultivars and harvest time in both years ($p \leq 0.01$). It was determined that fresh ear yield, fresh kernel weight of single ear, fresh single ear weight and ear diameter increased at the harvests made in late maturation stages. Fresh ear yield was lower in harvests made in early maturation periods. The highest fresh ear yield was determined in the middle yellow maturation period. GSS-5649 sweet corn variety was found the best among other tested varieties.

Keywords: *Zadoks scale, growing stage, cob yield, variety, ear properties*

Introduction

Sweet corn is one of the most popular vegetables and it is gaining importance day by day throughout the countries of the globe including Turkey. It is a variety of corn with high sugar content and has a high nutritional value (Santos, 2014). Sweet corn, which is a grain, is used in human nutrition and can be used fresh as well as consumed as processed food. It is a product used in canning, corn flour, starch and oil industries. In addition, by using sweet corn, snacks, chips, confectionery, baby foods and salad dressings are made (Oktem and Oktem, 2005).

Fresh sweet corn products like sweet corn milk and soups are gaining popularity in many countries, while sweet corn ears are eaten green as highly prized fresh product. In addition, frozen sweet corn ears and kernels are preferred in many countries (Oktem et al., 2010). Processing of corn is used to increase its shelf life but as a consequence, a significant loss of nutrients may occur via heat degradation or leaching (Scott and Eldridge, 2005). Sweet corn is harvested at immature stages of endosperm development and used as both fresh and processed vegetable, besides serving as an important source of fibre, minerals, and vitamins (Khanduri et al., 2011).

In recent years, it has also been used in the field such as the fuel industry. Due to early harvest of sweet corn cobs, the remaining green parts can be used in the animal feeding

directly or as silage (Oktem et al., 2003). Further, after the harvest of sweet corn cobs, green plants serve as a source of large quantities of fodder to the cattle, and therefore provide extra sources of income to farmers (Bian et al., 2015). The demand of sweet corn has increased tremendously in the last few years primarily due to urbanization, increased consumption and availability of organized food processing industries (Lertrat and Pulam, 2007).

Subaedah et al. (2021) reported that effect of the harvest time on ear length and ear diameter were statistically significant. Master sweet corn variety had the longest ear (28.08 cm), whereas the Talenta variety had the shortest (25.33 cm) in ear length. Longest ear diameter was found in the Bonanza variety (6.18 cm), whereas the shortest was found in the Talenta variety (5.96 cm). Harvest of 75 day after planting produced the largest ear diameters. Fresh ear weight of sweet corn was influenced by harvest time. The highest ear weight was seen at harvesting of 75 day after planting (372.22 g ear⁻¹). Bonanza variety produced the heaviest ear (374.17 g ear⁻¹), whereas the Talenta variety produced the lightest (310.83 g ear⁻¹). Fresh ear yield ranged from 16.98 to 22.33 tons ha⁻¹ and delaying harvest time resulted higher yield.

Soon et al. (2004) researched harvest times at sweet corn. Ears were harvested at 21, 28, 35, 42, 49 and 56 days after silking. In parallel with the development of the seeds, the seed weight and yield of sweet corn increased with the delay of the harvest time. The optimum harvest time was reported as 42 days after silking. In addition, it was reported that the ear yield was influenced by harvest time and late harvest was the most favourable for high yield (12.2 t ha⁻¹), whereas early harvest gave the least (13.9 t ha⁻¹) ear yield (Mehta et al., 2017).

Szymanek (2009) stated that ear length was between 20 and 23 cm and ear diameter 41 and 49 mm, the number of kernels per row between 27 and 28 pcs. Also Szymanek (2009) emphasized that the fresh ear yield increased from 15.88 to 18.64 t ha⁻¹ with delaying harvest time. When the moisture content decreased from 77.41% to 69.83% with delayed harvest date, a decline was observed in the sweet corn quality but yield increased.

Since sweet corn is mostly used fresh in human nutrition, it is very important to harvest it when its nutritional values, ear and kernel yield are highest (Oktem and Oktem, 1999). Yield of sweet corn is influenced by varieties and by harvest time (Saruhan and Oktem, 2021). In this study, it was aimed to determine the effect of different harvest times on the fresh corn yield and some ear characteristics and to determine the most appropriate harvest time for different sweet corn varieties.

Material and Methods

This research was conducted in 2016 and 2017 under Sanliurfa, Turkey conditions in order to determine the effect of harvesting at different maturation stages in some sweet corn genotypes on fresh grain yield and ear characteristics.

Looking at the climate data of the research area from *Table 1*, it is seen that the experimental area has a semi-arid climate, a significant part of the annual precipitation occurs in winter and spring, and the weather is dry and hot in summer and autumn months. During the trial years, rainfall and relative humidity was seen very low in June, July and August (*Table 1*). There was no climatic factor limiting corn cultivation, and the plants were grown without any problems with the irrigation.

Table 1. Some climatic data of 2016 and 2017 years of the research area

Months	Av. Temp. (°C)			Precipitation (kg m ²)			Relative humidity (%)		
	2016	2017	Long years	2016	2017	Long years	2016	2017	Long years
January	4.7	5.4	5.7	95.6	9.0	85.7	70.3	61.9	70.3
February	11.6	7.7	7.0	17.1	1.8	71.4	61.8	45.3	66.9
March	13.6	12.7	11.0	13.0	55.2	64.1	50.3	57.1	60.4
April	20.6	16.6	16.2	27.1	79.2	46.8	36.1	50.2	56.2
May	23.2	22.9	22.3	12.3	7.2	28.1	38.3	39.0	44.9
June	29.8	29.7	28.2	0.6	0.0	3.6	28.0	27.0	32.8
July	33.0	34.2	31.9	0.2	0.0	0.6	25.4	22.9	30.0
August	33.2	32.2	31.2	0.0	0.0	0.8	30.6	35.7	33.1
September	26.4	29.6	26.8	0.0	0.0	3.3	32.1	28.8	35.8
October	22.1	20.5	20.2	22.0	17.1	27.4	35.9	36.9	46.4
November	12.6	13.4	12.7	23.3	17.4	46.0	42.9	56.0	59.9
December	5.4	10.3	7.5	101.1	9.5	77.4	70.1	60.2	69.9
Mean	19.7	19.6	18.4	26.0	16.4	37.9	43.5	43.4	50.6

The soil properties of the research area have a clay structure, low organic matter, alluvial, flat and deep soils. In addition, the soils of this area are calcareous and rich in potassium. Cation Exchange Capacity (CEC) was high and increasing towards the lower layers depending on the clay content. Field capacity of the soil was 33.8% on dry basis, permanent wilting point was 22.6% and bulk density was 1.41 g cm⁻³ (Dinc et al., 1988). The soil properties are given in Table 2.

Table 2. Some physical and chemical properties of the trial area soil

Deep (cm)	Organic matter (%)	EC (ds m ⁻¹)	pH	Lime (%)	P ₂ O ₅ (kg da ⁻¹)	K ₂ O (kg da ⁻¹)
0-20	1.04	1.0	8.06	25.8	5.76	144.8

Baron, Vega, Jubile, GSS-5649 and Merit single cross hybrid sweet corn genotypes were used as plant material due to they were high yielding, the most grown cultivars and the preferred by consumer.

The experiment was set up in a split-plot design with 3 replications. Genotypes were placed in the main plots, and the harvest times were placed in sub plots. As the harvest times; according to the Zadoks scale (Zadoks et al., 1974), the periods of early milk maturation (Z73), middle milk maturation (Z75), late milk maturation (Z77), early yellow maturation (Z83), middle yellow maturation (Z85) and late yellow maturation (Z87) were used. Harvest was done at the times indicated for each variety.

At sowing, 80 kg ha⁻¹ of pure N, P and K, as a 15-15-15 composed fertilizer, was applied to each plot; this was followed by 170 kg ha⁻¹ of pure N as urea when the plants reached 30-40 cm in height.

Research area first ploughed with a mouldboard plough, then processed with a goble disc and made ready for planting by pulling the float. In the experiment, each plot consisted of 4 rows with 5 m long. Row spacing was 70 cm, intra row spacing was 20 cm and sowing depth was 3-4 cm. Sowing was done on 20 June 2016 and 22 June 2017 with a pneumatic seed drill.

After sowing, parcels were irrigated by sprinkler irrigation method and germination of seeds was provided. After the emergence of plants, plots were irrigated equally by the furrow irrigation system towards to harvest time. Plants were irrigated with 10-day intervals and 830 mm of total irrigation water was given throughout the vegetation period. In order to prevent the passage of water between the parcels, a two-meter gap was left between the parcels and the parcels were surrounded by a bank.

Fresh ear length value was measured as cm by measuring the distance from the point where the ear stalk meets the grain to the ear tip in 10 samples taken randomly from each plot. Fresh ear diameter was found by measuring in mm with the help of a caliper from the mid-point of the ear in 10 samples taken randomly from each plot.

In 10 ear samples taken randomly from each plot, kernel number of ear value was determined by counting the kernels present on the ear. Fresh kernel weight of ear value was calculated by averaging the grain weight of 10 samples taken randomly from each parcel.

Fresh single ear weight was determined by weighing and averaging 10 ear samples taken randomly from each plot. Fresh ear yield was obtained by taking the fresh ear weight in each trial plot and converting it to decare. When the plants reached 15-20 cm, the hoe was made with the tractor. Weed control was done mechanically.

An analysis-of-variance (ANOVA) was performed using Jump 5.0.1. statistical package program to evaluate statistically differences between results. Means of the data obtained from research were compared using DUNCAN test at $P \leq 0.05$.

Results and Discussion

Fresh ear length (cm)

The results of variance analysis of fresh ear length (cm) values of sweet corn genotypes harvested at different maturation stages are given in *Table 3*.

Table 3. Results of variance analysis of fresh ear length (cm) values of sweet corn genotypes harvested at different maturation stages

Variation sources	Sum of Squares	Degrees of freedom	Mean Squares	F
Replicates	0.608	2	0.304	1.747ns
Genotype (G)	125.291	4	31.323	87.746**
Error1	5.712	16	0.357	
Harvest maturation stage (H)	31.516	5	6.303	8.694**
G*H	43.029	20	2.151	2.968**
Error2	72.499	100	0.725	
General	395.366	179		

*: $P \leq 0.05$, **: $P \leq 0.01$, ns: no significant

According to the results of analysis of variance, it was determined that variety, harvest maturation stage and variety*harvest maturation stage interaction were statistically significant ($P \leq 0.01$) (*Table 3*).

The highest fresh ear length was determined in Jubile (20.4 cm) variety, and the lowest fresh ear length was determined in Baron (18.5 cm). However, Vega, Jubile and

GSS-5649 genotypes take placed in the same statistical group. The fresh ear length is a feature originating from the genetic characteristics of the plants (Oktem and Oktem, 2020a).

The fresh ear lengths of the cultivars were different from each other, and the increase in the fresh ear length continued with the increase in the harvest time (Table 4). The lowest fresh ear length value was reached in the early milk maturation (18.9 cm), and the highest fresh ear length was reached in the middle yellow maturation (20.2 cm).

Table 4. Fresh ear length (cm) values and multiple comparisons of sweet corn genotypes harvested at different maturation stages

Genotypes						
Maturation stages	Baron	Vega	Jubile	GSS-5649	Merit	Mean
Z73*	17.9 lm [†]	19.6 e-i	20.2 a-e	19.6 e-j	17.3 m	18.9 D [†]
Z75	17.8 lm	20.3 a-e	20.6 a-d	19.7 d-h	19.3 f-k	19.5 BC
Z77	18.7 jkl	20.5 a-e	20.4 a-e	20.9 ab	19.8 c-g	20.1 A
Z83	18.5 kl	20.7 abc	20.7 abc	21.0 a	18.7 l-l	19.9 AB
Z85	19.1 g-k	20.8 ab	20.1 a-f	20.0 b-f	20.2 a-e	20.2 A
Z87	18.8 h-k	19.7 d-h	20.1 a-f	20.7abc	17.4 m	19.3 CD
Mean	18.5 B	20.3 A	20.4 A	20.3 A	18.8 B	19.6

[†]: There is no significant difference at the 5% level between the averages shown in the same letter group in the same column according to Duncan test.

*: Z73: early milk maturation, Z75: middle milk maturation, Z77: late milk maturation, Z83: early yellow maturation, Z85: middle yellow maturation, and Z87: late yellow maturation

At the variety*harvest maturation stage interaction, the highest fresh ear length was obtained from GSS-5649 sweet corn variety at the early yellow maturation stage as 21 cm while the lowest value was seen at Merit variety at the early milk maturation stage as 17.3 cm (Fig. 1).

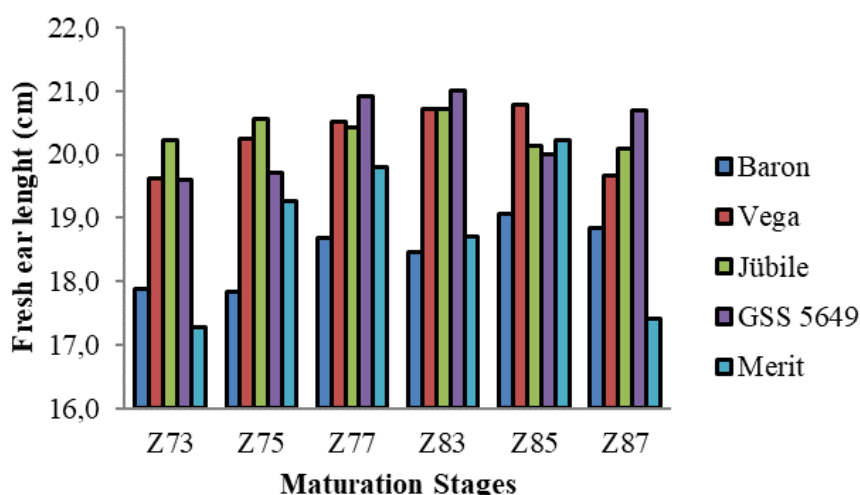


Figure 1. Fresh ear length of sweet corn genotypes harvested at different maturation stages. Z73: early milk maturation, Z75: middle milk maturation, Z77: late milk maturation. Z83: early yellow maturation, Z85: middle yellow maturation, Z87: late yellow maturation

Findings were supported by some researchers. Szymanek (2009) stated that fresh ear length was between 20 and 23 cm. Budak and Kinaci (2012) found that the fresh ear length was between 18.7 and 21.2 cm. Sonmez et al. (2013) emphasized that fresh ear length changed between 21.6-22.3 cm, while Kula and Karadogan (2017) stated that it ranged between 10.2 and 14.0 cm. Subaedah et al. (2021) reported that the fresh ear length in sweet corn varies between 25.33 and 28.08 cm, which is higher than our findings.

Fresh ear diameter (mm)

According to the results of the analysis of variance of fresh ear diameter, it was determined that there were a statistically significant ($P \leq 0.01$) differences at variety, harvest maturation stage and variety*harvest maturation stage interaction (*Table 5*).

Table 5. Analysis of variance results of fresh ear diameter (mm) values of sweet corn genotypes harvested at different maturation stages

Variation sources	Sum of Squares	Degrees of freedom	Mean Squares	F
Replicates	12.085	2	6.043	7.616ns
Genotype (G)	635.459	4	158.865	69.283**
Error1	36.688	16	2.293	
Harvest maturation stage (H)	1395.722	5	279.144	152.727**
G*H	108.055	20	5.403	2.956**
Error2	182.773	100	1.828	
General	3223.186	179		

* : $P \leq 0.05$, ** : $P \leq 0.01$, ns: no significant

The highest fresh ear diameter was found in GSS-5649 (43.3 mm) variety, and the lowest fresh ear diameter was found in Jubile (37.6 mm) variety. It was observed that the fresh ear diameter increased with the delay of the harvest time.

The lowest fresh ear diameter data was found in the early milk maturation period (35.5 mm), and the highest fresh ear diameter data was determined in the middle yellow maturity period.

It has been reported that stem thickness increases depending on the presence of nutrients and its use by plants (Oktem and Oktem, 2020b). Stem diameter values were lower in harvests made in early maturation periods, since dry matter accumulation in the grain was less. Since the amount of dry matter accumulated in the grain increased during the late ripening periods, the ear thickness increased.

According to variety*harvest maturation stage interaction, GSS-5649 sweet corn variety gave the highest fresh ear diameter (45.7 mm) at the early yellow maturation stage the whereas the lowest value was found at Jubile variety (31.5 mm) at the early milk maturation stage (*Fig. 2, Table 6*).

Similar to the research findings, Oktem and Oktem (2006) reported that the ear diameter ranged from 37.87 to 47.45 mm, Idikut et al. (2016) stated that it varies between 38.65 – 45.56 mm. Lower than our findings, Panahi et al. (2010) reported ear diameter values between 30.1 and 40.1 mm, while Alan et al. (2011) reported higher ear diameter values with 49.37-54.54 mm and Can and Akman (2014) with 43.0-46.9 mm. Szymanek (2009) stated that ear diameter was between 41 and 49 mm.

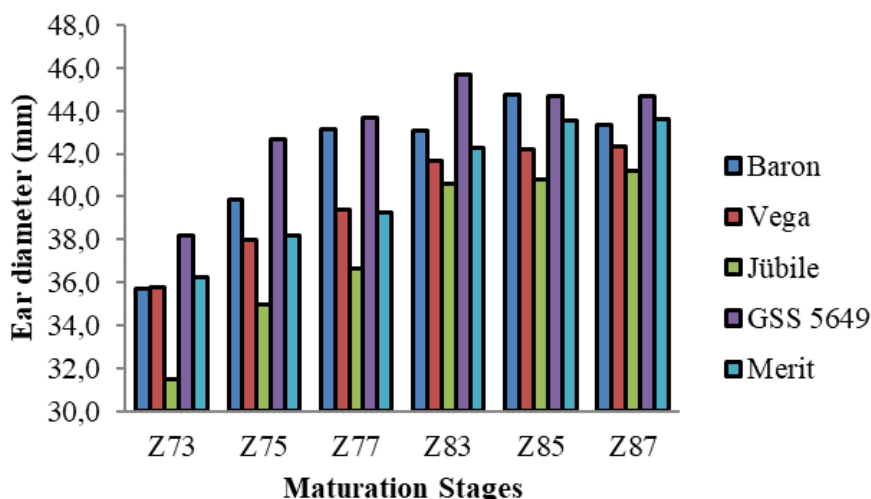


Figure 2. Ear diameter values of sweet corn genotypes harvested at different maturation stages. Z73: early milk maturation, Z75: middle milk maturation, Z77: late milk maturation, Z83: early yellow maturation, Z85: middle yellow maturation, Z87: late yellow maturation

Table 6. Fresh ear diameter (mm) values and multiple comparisons of sweet corn genotypes harvested at different maturation stages

Maturation stages	Genotypes					Mean
	Baron	Vega	Jubile	GSS-5649	Merit	
Z73*	35.7 mn	35.8 mn	31.5 o	38.2 k	36.3 mn	35.5 D [†]
Z75	39.8 ij	38.0 kl	35.0 n	42.7 def	38.2 k	38.7 C
Z77	43.2 cde	39.4 jk	36.6 lm	43.7 bcd	39.3 jk	40.4 B
Z83	43.1 de	41.7 e-h	40.6 hij	45.7 a	42.3 d-g	42.7 A
Z85	44.8 ab	42.2 d-g	40.8 g-j	44.7 abc	43.5 bcd	43.2 A
Z87	43.4 bcd	42.3 d-g	41.2 f-i	44.7 abc	43.6 bcd	43.0 A
Mean	41.7 B	39.9 C	37.6 D	43.3 A	40.5 C	40.6

†: There is no significant difference at the 5% level between the averages shown in the same letter group in the same column according to Duncan test.

*: Z73: early milk maturation, Z75: middle milk maturation, Z77: late milk maturation, Z83: early yellow maturation, Z85: middle yellow maturation, and Z87: late yellow maturation

Kernel number of ear (number ear⁻¹)

Analysis of variance results showed that the differences between variety, harvest maturation stage and variety*harvest maturation stage interaction were determined to be statistically significant ($P \leq 0.01$) (Table 7).

The highest kernel number of ear value was observed in GSS-5649 (596.3 number), and the lowest kernel number of ear value was observed in Baron (415.0 number). Generally, the number of grains on the cob varies depending on the cob length. As the cob length increases, the number of grains in the cob also increases. The long cob has more grains than the short cob.

Table 7. Analysis of variance results of kernel number of ear values of sweet corn genotypes harvested at different maturation stages

Variation sources	Sum of Squares	Degrees of freedom	Mean Squares	F
Replicates	3423.926	2	1711.963	45.583ns
Genotype (G)	620546.412	4	155136.603	421.590**
Error1	5887.670	16	367.979	
Harvest maturation stage (H)	72969.852	5	14593.970	54.120**
G*H	111671.051	20	5583.553	20.706**
Error2	26965.817	100	269.658	
General	1196643.97	179		

* : $P \leq 0.05$, **: $P \leq 0.01$, ns: no significant

When the harvest time delayed, the kernel number of ear first increased and then remained stable (Table 8). The lowest kernel number of ear value was reached in the early milk maturation period (475.9 number), and the highest kernel number of ear value was found in the late milk maturation period (540.2 number).

Table 8. Kernel number of ear (number) values and multiple comparisons of sweet corn genotypes harvested at different maturation stages

Maturation stages	Genotypes					Mean
	Baron	Vega	Jubile	GSS-5649	Merit	
Z73*	384.1 s	494.2 m-o	497.9 mn	539.5 gh	463.9 pq	475.9 D [†]
Z75	393.3 s	490.3 no	524.3 h-l	580.9 d	575.6 de	512.9 C
Z77	413.6 r	534.0 g-j	501.7 l-n	645.2 a	606.6 c	540.2 A
Z83	419.6 r	537.0 ghi	517.6 jkl	628.8 ab	547.7 fg	530.1 B
Z85	457.0 q	486.3 no	519.5 i-l	562.4 d-f	561.4 ef	517.3 C
Z87	422.2 r	511.7 k-m	512.1 k-m	621.1 bc	478.6 op	509.1 C
Mean	415.0 D	508.9 C	512.2 C	596.3 A	539.0 B	514.3

†: There is no significant difference at the 5% level between the averages shown in the same letter group in the same column according to Duncan test.

*: Z73: early milk maturation, Z75: middle milk maturation, Z77: late milk maturation, Z83: early yellow maturation, Z85: middle yellow maturation, and Z87: late yellow maturation

At the variety*harvest maturation stage interaction, the highest kernel number of ear value obtained from GSS-5649 sweet corn variety as 645.2 numbers at the late milk maturation stage while the lowest kernel number of ear value was found at Baron variety as 384.1 number at early milk maturation stage (Fig. 3). Environmental conditions and genetic factors affect the number of grains on the ear (Ozel and Oktem, 2021).

Parallel to the results of the research, some researchers stated that the number of grains per ear varied between 531.3 and 749.9 number (Oktem and Oktem, 2006), 410.3 and 536.9 (Atakul, 2011), 510.9 and 573.9 (Can and Akman, 2014).

While some researchers stated lower grain count values with 263.3-441.6 pieces (Bozkurt and Karadogan, 2017), 249.1- 420.0 pieces (Kula and Karadogan, 2017), some

others indicate higher grain count values on the ear with 685-930 pieces (Alan et al., 2011), 498.31-518.88 pieces (Inan, 2019).

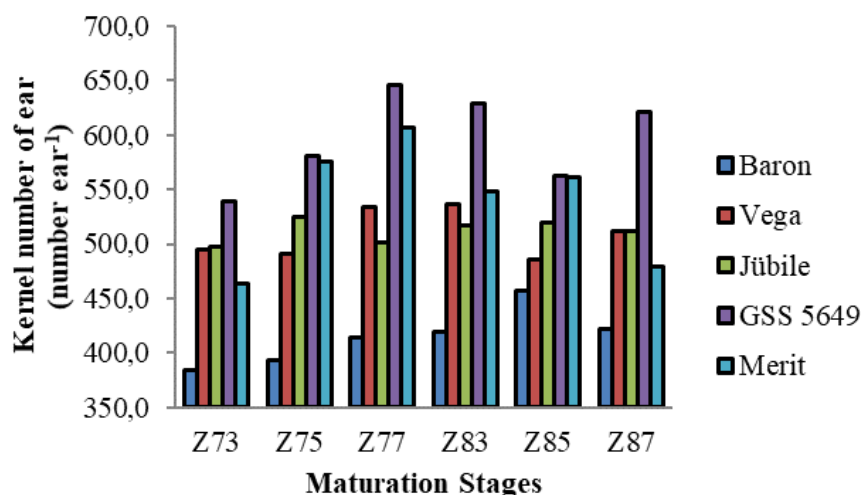


Figure 3. Kernel number of ear (number) values of sweet corn genotypes harvested at different maturation stages. Z73: early milk maturation, Z75: middle milk maturation, Z77: late milk maturation, Z83: early yellow maturation, Z85: middle yellow maturation, Z87: late yellow maturation

Fresh kernel weight of ear (g ear⁻¹)

At the performed variance analysis, differences between cultivars, harvest maturation stage and cultivar*harvest maturation stage interaction were statistically significant ($P \leq 0.01$) (Table 9).

Table 9. Analysis of variance results of fresh kernel weight of ear values of sweet corn genotypes harvested at different maturation stages

Variation sources	Sum of Squares	Degrees of freedom	Mean Squares	F
Replicates	13.329	2	6.665	0.060ns
Genotype (G)	90766.528	4	22691.632	1390.722**
Error1	261.063	16	16.316	
Harvest maturation stage (H)	229357.557	5	45871.511	1507.785**
G*H	17174.040	20	858.702	28.225**
Error2	3042.311	100	30.423	
General	396730.112	179		

* : $P \leq 0.05$, ** : $P \leq 0.01$, ns: no significant

The highest fresh kernel weight of ear was determined in GSS-5649 (187.4 g ear⁻¹) variety, and the lowest fresh kernel weight of ear was determined in Jubile (124.6 g ear⁻¹) variety (Table 10). This result is consistent with the previous studies that reported differences kernel weight of ear values in corn plant from various genotypes (Oktem et al., 2004; Subaedah et al., 2016; Khan et al., 2017).

Table 10. Fresh kernel weight of ear (g) values and multiple comparisons of sweet corn genotypes harvested at different maturation stages

Harvest time	Genotypes					
	Baron	Vega	Jubile	GSS-5649	Merit	Mean
Z73*	73.03 r	74.03 r	60.76 s	114.9 n	69.36 r	78.4 E†
Z75	103.2 p	106.3 op	83.93 q	159.3 hij	109.9 no	112.5 D
Z77	178.8 e	165.7 fg	149.8 k	230.6 a	164.5 gh	177.9 A
Z83	161.2 g-j	170.8 f	129.5 m	224.0 b	151.2 k	167.3 B
Z85	140.6 l	158.0 ij	159.0 hij	188.0 d	161.8 ghi	161.5 C
Z87	131.7 m	155.7 ijk	164.5 gh	207.5 e	155.3 jk	162.9 C
Mean	131.4 D	138.4 B	124.6 E	187.4 A	135.3 C	143.4

†: There is no significant difference at the 5% level between the averages shown in the same letter group in the same column according to Duncan test.

*: Z73: early milk maturation, Z75: middle milk maturation, Z77: late milk maturation, Z83: early yellow maturation, Z85: middle yellow maturation, and Z87: late yellow maturation

With the delay of the harvest time, the fresh kernel weight of ear increased first, but decreased in the later harvest periods. The lowest fresh ear kernel weight was determined in the early milk maturation period (78.4 g ear⁻¹), and the highest fresh ear kernel weight value was found in the late milk maturation period (177.9 g ear⁻¹).

Since the dry matter accumulation in the grain was lower in the early ripening periods, the grain weight was lower on the ear.

In terms of variety*harvest maturation stage interaction, GSS-5649 sweet corn variety gave the highest kernel weight of ear value (230.6 g) at the late milk maturation stage while the lowest kernel weight of ear value was determined from Jubile sweet corn variety (60.76 g) at early milk maturation stage (Fig. 4). Budak and Kinaci (2012) stated that the grain weight on the ear varied between 188.8 - 277.7 g ear⁻¹, Ozerkisi (2016) changed between 113.9 - 153.5 g ear⁻¹ and Albayrak (2013) 106.1 g ear⁻¹.

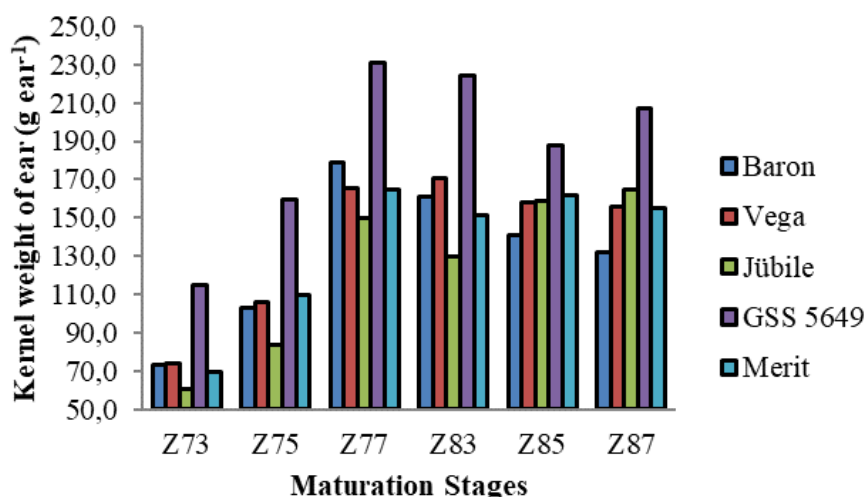


Figure 4. Kernel weight of ear (g) values of sweet corn genotypes harvested at different maturation stages. Z73: early milk maturation, Z75: middle milk maturation, Z77: late milk maturation, Z83: early yellow maturation, Z85: middle yellow maturation, Z87: late yellow maturation

Fresh single ear weight (g)

In terms of fresh single ear weight, it was determined that the difference between cultivar, harvest maturation stage and cultivar*harvest maturation stage interactions was statistically significant ($P \leq 0.01$) (Table 11).

Table 11. Analysis of variance results of fresh single ear weight values of sweet corn genotypes harvested at different maturation stages

Variation sources	Sum of Squares	Degrees of freedom	Mean Squares	F
Replicates	89.315	2	44.658	0.303ns
Genotype (G)	113907.762	4	28476.941	322.941**
Error1	1410.881	16	88.180	
Harvest maturation stage (H)	147600.012	5	29520.002	571.705**
G*H	23837.626	20	1191.881	23.083**
Error2	5163.499	100	51.635	
General	385540.562	179		

* : $P \leq 0.05$, **: $P \leq 0.01$, ns: no significant

The highest fresh single ear weight was found in GSS-5649 variety with 247.7 g, and the lowest fresh single ear weight was found in Jubile variety with 173.9 g (Table 12). Fresh single ear weight also showed wide genetic variation and indicated the diverse nature of the genotypes. Several researchers have reported the existence of genetic variation for ear weight among various sweet corn hybrids (Oktem and Oktem, 2006; Khanduri et al., 2011; Solomon et al., 2012; Rosa, 2014).

Table 12. Fresh single ear weight (g) values and multiple comparisons of sweet corn genotypes harvested at different maturation stages

Maturation stages	Genotypes					
	Baron	Vega	Jubile	GSS-5649	Merit	Mean
Z73*	150.4 lm	154.8 kl	130.2 n	202.4 g	133.1 n	154.2 E [†]
Z75	192.6 h	161.0 jk	153.1 kl	237.9 cd	186.3 h	186.2 C
Z77	172.6 i	185.5 h	143.2 m	233.5 d	165.4 ij	180.0 D
Z83	202.2 g	245.8 c	193.3 h	285.5 a	218.2 e	229.0 A
Z85	209.3 fg	219.2 e	211.7 ef	260.7 b	240.8 cd	228.3 A
Z87	190.7 h	219.4 e	212.1 ef	266.4 b	232.5 d	224.2 B
Mean	186.3 C	197.6 B	173.9 D	247.7 A	196.0 B	200.3

†: There is no significant difference at the 5% level between the averages shown in the same letter group in the same column according to Duncan test.

*: Z73: early milk maturation, Z75: middle milk maturation, Z77: late milk maturation, Z83: early yellow maturation, Z85: middle yellow maturation, and Z87: late yellow maturation

While the lowest fresh single ear weight values were determined in the early milk-setting period (154.2 g), the highest fresh single ear weight values were obtained in the early yellow maturity period (229.0 g). Fresh single ear weight values are found higher

because the amount of dry matter accumulated in the grain increases in late ripening periods. Subaedah et al. (2021) reported that the highest ear weight was seen at late harvesting of 75 day after planting (372.22 g ear⁻¹).

At the variety*harvest time interaction, the highest fresh single ear weight was obtained from GSS-5649 variety at the early yellow maturation stage as 285.8 g while the lowest value was seen at Jubile variety at the early milk maturation stage as 130.2 g (Fig. 5).

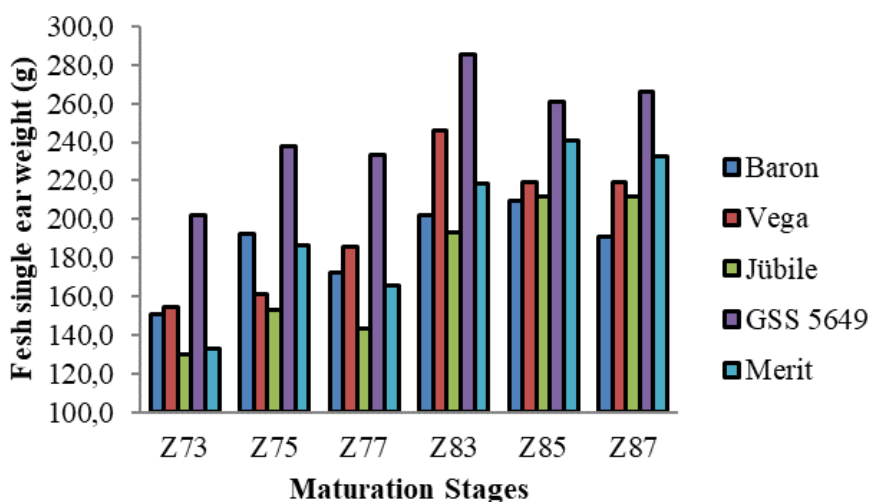


Figure 5. Fresh single ear weight (g) values of sweet corn genotypes harvested at different maturation stages. Z73: early milk maturation, Z75: middle milk maturation, Z77: late milk maturation, Z83: early yellow maturation, Z85: middle yellow maturation, Z87: late yellow maturation

Some researchers stated higher fresh single ear weight than our findings. Sonmez et al. (2013) reported that fresh ear weight values ranged between 358 and 384 g, Budak and Kınacı (2012) between 252.0 and 355.6 g, while Atar and Kara (2017) stated lower values with 143.0 and 169.5 g. Similar to our findings, Idikut et al. (2016) reported fresh ear weight values varying between 184.5 and 208.99 g. Subaedah et al. (2021) emphasized that Bonanza variety produced the heaviest ear (374.17 g ear⁻¹), whereas the Talenta variety produced the lightest (310.83 g ear⁻¹).

Fresh ear yield (kg da⁻¹)

In terms of fresh ear yield, variety, harvest maturation stage and variety*harvest maturation stage interactions were found to be statistically significant ($P \leq 0.01$) (Table 13). The highest fresh ear yield was determined as 1994 kg da⁻¹ in GSS-5649 variety and the lowest value was found in Jubile variety with 1381 kg da⁻¹ (Table 14).

Our findings were similar with previous studies. According to some researchers, the fresh ear yield was reported between 845 and 1651 kg da⁻¹ (Aprilianti et al., 2016), between 1121 and 1912 kg da⁻¹ (Bozkurt and Karadogan, 2017), between 860 and 1459 kg da⁻¹ (Kula and Karadogan, 2017). Akgun et al. (2017) reported a lower fresh ear yield values as 464-490 kg da⁻¹, while Alan et al. (2011) reported higher fresh ear yield values (1756-2108 kg da⁻¹).

Table 13. Analysis of variance results of fresh ear yield values of sweet corn genotypes harvested at different maturation stages

Variation sources	Sum of Squares	Degrees of freedom	Mean Squares	F
Replicates	4357.924	2	2178.962	1.807ns
Genotype (G)	8277455.442	4	2069363.860	2962.084**
Error1	11177.880	16	698.617	
Harvest maturation stage (H)	6988853.314	5	1397770.663	1214.895**
G* H	1089964.088	20	54498.204	47.368**
Error2	115052.766	100	1150.528	
General	18403368.026	179		

* : P<0.05, **: P<0.01, ns: no significant

Table 14. Fresh ear yield values (kg da⁻¹) and multiple comparisons of sweet corn genotypes harvested at different maturation stages

Maturation stages	Genotypes					Mean
	Baron	Vega	Jubile	GSS-5649	Merit	
Z73*	1129 op	1164 o	981 q	1622 h	1103 p	1200 F [†]
Z75	1462 ij	1420 kl	1216 n	1989 c	1390 l	1495 E
Z77	1627 h	1671 g	1430 jk	2120 a	1601 h	1690 C
Z83	1444 ijk	1665 g	1344 m	2078 b	1476 i	1601 D
Z85	1595 h	1794 e	1592 h	2019 c	1890 d	1778 A
Z87	1458 ijk	1730 f	1724 f	2138 a	1714 f	1753 B
Mean	1452 D	1574 B	1381 E	1994 A	1529 C	1586

†: There is no significant difference at the 5% level between the averages shown in the same letter group in the same column according to Duncan test.

*: Z73: early milk maturation, Z75: middle milk maturation, Z77: late milk maturation, Z83: early yellow maturation, Z85: middle yellow maturation, and Z87: late yellow maturation

The lowest fresh ear yield was observed in the early milk maturation period (1200 kg da⁻¹), and the highest fresh ear yield was observed in the middle yellow maturation period (1778 kg da⁻¹). Similar to the findings, it has been reported that genotypes behave differently at different harvest dates (Khanduri et al., 2011; Oktem, 2019).

With delaying of harvest time, fresh ear yield increased. It was determined that fresh ear yield increased at the harvests made in late maturation stages. Similar to our results, it was stated by some researchers that the yield increased in advanced maturation periods (Soon et al., 2004; Szymanek, 2009; Subaedah et al., 2021; Saruhan and Oktem, 2021).

Subaedah et al. (2021) also stated that fresh ear yield was ranged from 16.98 to 22.33 t ha⁻¹ and delaying harvest time resulted higher yield. Szymanek (2009) emphasized that the yield increased from 15.88 to 18.64 t ha⁻¹ with delaying harvest time. In addition, it was reported that the ear yield was influenced by harvest time and late harvest was the most favourable for high yield (Mehta et al., 2017).

Fresh ear yield was lower in harvests made in early maturation periods. While the fresh ear yield is lower due to the low dry matter accumulation in the grain in the first ripening periods, it increases in the later maturation periods and reaches the highest level in the middle yellow maturation period. However, after this level, the fresh ear yield decreases due to moisture loss in the grain. However, the decrease in grain moisture causes the grains to harden and the market value of sweet corn cobs to decrease. Szymanek (2009) stated that the moisture content decreased from 77.41% to 69.83% with delayed harvest date, a decline was observed in the sweet corn quality.

According to variety*harvest maturation stage interaction, GSS-5649 sweet corn variety gave the highest fresh ear yield (2138 kg da⁻¹) at the late yellow maturation stage whereas the lowest value was found at Jubile variety (981 kg da⁻¹) at the early milk maturation stage (Fig. 6). Growing conditions and genotype characteristics affect the fresh ear yield (Oktem and Oktem, 2009).

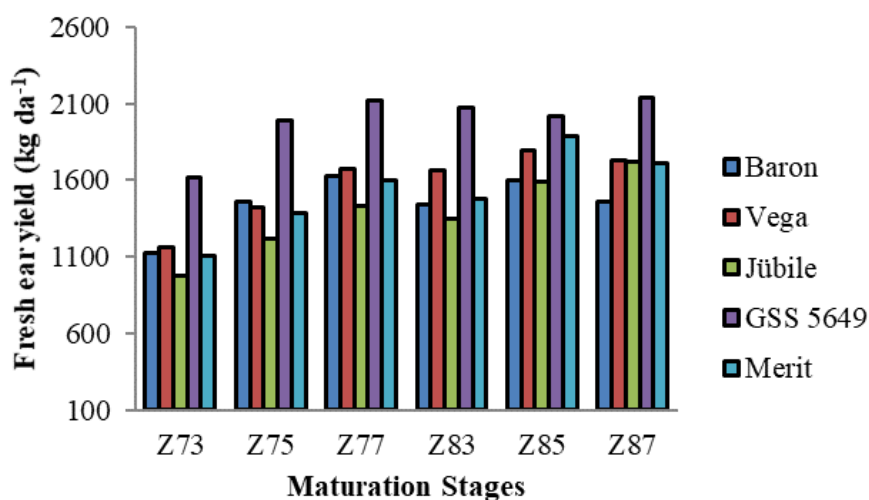


Figure 6. Fresh ear yield (kg da⁻¹) values of sweet corn genotypes harvested at different maturation stages. Z73: early milk maturation, Z75: middle milk maturation, Z77: late milk maturation, Z83: early yellow maturation, Z85: middle yellow maturation, Z87: late yellow maturation

Conclusion

It was determined that fresh ear yield, fresh kernel weight of single ear, fresh single ear weight and ear diameter increased at the harvests made in late maturation stages. Fresh ear yield was lower in harvests made in early maturation periods. The highest fresh ear yield was found in the middle yellow maturation period. GSS-5649 sweet corn variety gave the highest fresh ear yield (2138 kg da⁻¹) at the late yellow maturation stage whereas the lowest value was determined at Jubile variety (981 kg da⁻¹) at the early milk maturation stage.

REFERENCES

- [1] Akgun, I., Burcu, Y., Karaman, R., Kaya, M. (2017): The effects of plant density and different sowing dates on fresh ear weight and some agricultural characters of sweet corn (*Zea mays saccharata* Sturt.) grown under Isparta conditions. – Journal of Field Crops Central Research Institute 26: 23-30.
- [2] Alan, O., Sonmez, K., Budak, Z., Kutlu, I., Ayter, N. G. (2011): The effect of sowing dates on yield and agricultural characteristics of sweet corn (*Zea mays saccharata* Sturt.) in Eskisehir ecological conditions. – Selcuk J. of Agricultural and Food Sci. 25(4): 34-41.
- [3] Albayrak, O. (2013): Determination of sweet corn (*Zea mays* L. *saccharata* Sturt.) varieties for Diyarbakir conditions. – Dicle University, Institute of Science and Technology, Department of Field Crops, M.Sc. 57p.
- [4] Aprilianti, D. K., Syukur, M., Suwarno, W. B. (2016): Evaluation of yield components of new sweet corn hybrids in Bogor. – Indonesia J. of Tropical Crop Science 3(1): 13-18.
- [5] Atakul, S. (2011): The effect of different sowing times on fresh cob and grain yield and some agricultural characteristics of five sugar corn varieties in Diyarbakir conditions. – Cukurova University, Institute of Science and Technology, M.Sc. 90p.
- [6] Atar, B., Kara, B. (2017): The effect of different planting depths on fresh cob yield and some cob properties of sweet corn. – Derim 34(2): 182-185.
- [7] Bian, Y., Gu, X., Sun, D., Wang, Y., Yin, Z., Deng, D., Wang, Y., Li, G. (2015): Mapping dynamic QTL of stalk sugar content at different growth stages in maize. – Euphytica 205: 85-94.
- [8] Bozkurt, M., Karadogan, T. (2017): Determination of appropriate sowing frequency in sugar corn (*Zea mays saccharata* Sturt.) varieties cultivated under greenhouse conditions. – Journal of Suleyman Demirel University Faculty of Agriculture 12(2): 19-29.
- [9] Budak, Z., Kinaci, E. (2012): The effects of different sowing arrangements on yield and yield components of intercropping dwarf beans and sugar corn in Eskisehir. – Journal of Suleyman Demirel University Faculty of Agriculture 7(2): 93-102.
- [10] Can, M., Akman, Z. (2014): The effect of different nitrogen doses on yield and quality traits of sugar corn (*Zea mays Saccharata* Sturt.) in Usak ecological conditions. – Journal of Suleyman Demirel University Faculty of Agriculture 9(2): 93-101.
- [11] Dinc, U., Senol, S., Satin, M., Kapur, S., Guzel, N., Derici, R. (1988): Southeastern Anatolia soils of Turkey, I. Harran Plain. – TUBITAK, TOAG-534, Final Result Report, Ankara, Turkey.
- [12] Idikut, L., Zulkadir, G., Colkesen, M., Yururdurmaz, C. (2016): Comparison of composite sugar corn population and hybrid sugar corn varieties in terms of some agronomic characteristics. – Nevsehir Journal of Science and Technology, Special Issue, pp. 41-50.
- [13] Inan, Y. (2019): The Effect of different potassium and sulfur doses on agronomic and technological properties of sugar corn (*Zea mays saccharata* Sturt.). – Ordu Univ. Science Inst. M.Sc. 75p.
- [14] Khan, M., Khan, K., Afzal, S. U. (2017): Seed yield performance of different maize (*Zea mays* L.) genotypes under agro climate conditions of Haripur. – International Journal of Environmental Sciences and Natural Resources 5: 1-6.
- [15] Khanduri, A., Hossain, F., Lakhera, P. C., Prasanna, B. M. (2011): Effect of harvest time on kernel sugar concentration in sweet corn. – Indian J. Genet. 71: 231-234.
- [16] Kula, N., Karadogan, T. (2017): Determination of appropriate planting times in sugar corn (*Zea mays saccharata* Sturt.) varieties cultivated under greenhouse conditions. – Journal of Suleyman Demirel University Faculty of Agriculture 12(1): 39-48.
- [17] Lertrat, K., Pulam, T. (2007): Breeding for increased sweetness in sweet corn. – Int. J. of pland Breeding 1(1): 27-30.
- [18] Mehta, B. K., Hossain, F., Muthusamy, V., Zunjare, R. U., Sekhar, J. C., Gupta, H. S. (2017): Analyzing the role of sowing and harvest time as factors for selecting super sweet (sh2) corn hybrids. – Indian J. Genet. 77(3): 348-356.

- [19] Oktem, A., Oktem, A. G. (1999): Determination of fresh and grain yields and important agricultural characteristics of some sweet corn varieties (*Zea mays saccharata* Sturt). – GAP 1st Agriculture Congress, May 26-28, Volume II, pp. 893-900, Sanliurfa.
- [20] Oktem, A., Simsek, M., Oktem, A. G. (2003): Deficit irrigation effects on sweet corn (*Zea mays saccharata* Sturt) with drip irrigation system in a semi-arid region. I. Water-yield relationship. – *Agricultural Water Management* 61(1): 63-74.
- [21] Oktem, A., Oktem, A. G., Coskun, Y. (2004): Determination of sowing dates of sweet corn. (*Zea mays* L. *saccharata* Sturt.) under Sanliurfa Conditions. – *Turkish J Agric. Forestry* 28: 83-91.
- [22] Oktem, A. G., Oktem, A. (2005): Effect of nitrogen and intra row spaces on sweet corn (*Zea mays saccharata* Sturt) ear characteristics. – *Asian Journal of Plant Science* 4(4): 361-364.
- [23] Oktem, A., Oktem, A. G. (2006): Determination of yield characteristics of some sweet corn (*Zea mays saccharata* Sturt) genotypes in Harran Plain conditions. – *Uludag. Univ. Faculty of Agriculture Journal* 20(1): 33-46.
- [24] Oktem, A., Oktem, A. G. (2009): Yield characteristics of sweet corn under deficit irrigation in Southeastern Turkey. – *The Philippine Agricultural Scientist* 92(3): 39-44.
- [25] Oktem, A., Oktem, A. G., Emeklier, H. Y. (2010): Effect of nitrogen to yield and some quality parameters of sweet corn. – *Communications in Soil Science and Plant Analysis* 41(7): 832-847.
- [26] Oktem, A. G. (2019): Effects of different zinc levels on grain yield and some phenological characteristics of red lentil (*Lens culinaris* Medic.) under arid conditions. – *Turkish Journal of Agriculture and Forestry* 43(3): 360-367.
- [27] Oktem, A. G., Oktem, A. (2020a): Effect of farmyard manure application on yield and some quality characteristics of popcorn (*Zea mays* L. *evarta* Sturt) at the organic farming. – *Journal of Agriculture and Ecology Research International* 21(9): 35-42.
- [28] Oktem, A. G., Oktem, A. (2020b): Impact of vermicompost to dent corn (*Zea mays* L. *indentata*). – *Int. Journal of Innovative Approaches in Agricultural Research* 4(1): 48-55.
- [29] Ozel, M., Oktem, A. G. (2021): The Effect of vermicompost application at different levels on yield and yield characteristics in dent corn (*Zea mays* L. *indendata*). – *BEU Journal of Science* 10(4): 1324-1333.
- [30] Ozerkisi, E. (2016): The effect of different row spacing on fresh ear yield and quality traits of some sugar corn (*Zea mays* L. *Saccharata* Sturt.) varieties in Tekirdag conditions. – *Namik Kemal Univ. Institute of Science and Technology, Department of Horticulture, M.Sc.* 60p.
- [31] Panahi, M., Naseri, R., Soleimani, R. (2010): Efficiency of some sweet corn hybrids at two sowing dates in central Iran. – *Middle - East Journal of Scientific Research* 6(1): 51-55.
- [32] Rosa, R. (2014): Response of sweet corn cultivated in eastern Poland to different sowing dates and covering with non-woven pp. Part I: Corn yield. – *Acta Scientiarum Polonorumseria Agricultura* 13: 93-112.
- [33] Santos, P. H. A. D., Pereira, M. G., dos Santos Trindade, R., da Cunha, K. S., Entringer, G. C., Vettorazzi, J. C. F. (2014): Agronomic performance of super-sweet corn genotypes in the north of Rio de Janeiro. – *Crop Breeding and Applied Biotechnology* 14(1): 8-14.
- [34] Saruhan, M. A., Oktem, A. G. (2021): The effect of different sowing times on morphological and technological characteristics and grain yield of some corn (*Zea mays* L.) cultivars under Diyarbakır conditions. – *Journal of Bahri Dagdas Crop Research* 10(2): 145-154.
- [35] Scott, C. E., Eldridge, A. L. (2005): Comparison of carotenoid content in fresh, frozen and canned corn. – *Journal of Food Composition and Analysis* 18: 551-559.
- [36] Solomon, K. F., Zeppa, A., Mulugeta, S. D. (2012): Combining ability, genetic diversity and heterosis in relation to F1 performance of tropically adapted shrunken (*sh2*) sweet corn lines. – *Plant Breed* 131: 430-436.

- [37] Sonmez, K., Alan, O., Kinaci, E., Kinaci, G., Kutlu, I., Basciftci, Z. K., Evrenesoglu, Y. (2013): Plant, cob and yield characteristics of some sugar corn varieties (*Zea mays saccharata* Sturt). – Journal of Suleyman Demirel University Faculty of Agriculture 8(1): 28-40.
- [38] Soon, L. S., Hee, Y. S., Moon, S. J. (2004): Optimum harvest time for high quality seed production of sweet and super sweet corn hybrids. – Korean Journal of Crop Science 49(5): 373-380.
- [39] Subaedah, S., Takdir, A., Netty, H. (2016): Evaluation of potential production of maize genotypes of cobly maturity in rainfed lowland. – International Journal of Biological, Biomolecular, Agricultural, Food and Biotechnological Engineering 10: 584-587.
- [40] Subaedah, St., Edy, E., Mariana, K. (2021): Growth, Yield, and sugar content of different varieties of sweet corn and harvest time. – International Journal of Agronomy 2021: 8882140.
- [41] Szymanek, M. (2009): Influence of sweet corn harvest date on kernels quality. – Res. Agr. Eng. 55(1): 10-17.
- [42] Zadoks, J. C., Chang, T. T., Konzak, C. F. (1974): A decimal code for the growth stages of cereals. – Weed Research 14: 415-421.

MONITORING SPATIO-TEMPORAL DYNAMICS OF LAND USE/LAND COVER CHANGES USING REMOTE SENSING AND GIS – A CASE STUDY OF ERNAKULAM DISTRICT, INDIA

VILASAN, R. T.* – KAPSE, V. S.

*Department of Architecture and Planning, Visvesvaraya National Institute of Technology,
Nagpur, Maharashtra 440010, India
(phone: +91-712-222-2828)*

**Corresponding author
e-mail: reshmavilasan@gmail.com; phone: +91-960-570-5798*

(Received 30th Jan 2022; accepted 20th May 2022)

Abstract. Urbanisation is presently one of the most serious environmental challenges, spreading at unprecedented rates and intensifying across all countries, with far-reaching implications for ecosystems, biodiversity, and human well-being. Rapid increases in activities such as urbanisation, socioeconomic activity, and environmental change create changes in land use and land cover. Therefore, it is essential to comprehend LULC change to assess its effects on hydrology. The study reveals that the agricultural land area reduced from 56.53% in the year 2006 to 50.41% in the year 2016, which shows the urbanisation and the conversion of the vacant lands to the built-up lands. It is clear from the data that there was an increase in the built-up area from 8.27% in the year 2006 to 14.80% in the year 2016. In 2006, the area under the water body class was 189.19 km². Also, the wasteland area reduced from 1.77% in the year 2006 to 0.87% in the year 2016, which shows the effect of the vacant land being converted into built-up areas. The purpose of this study was to evaluate land use/land cover changes in Kerala's Ernakulam district using remote sensing and geospatial information system (GIS) techniques. This research includes LULC classification and accuracy assessment. The LULC classification had overall accuracy (OA) of 81.49%, 81.87%, and 82.79% respectively. The overall kappa coefficient was 0.75, 0.75, and 0.77 respectively for the year 2006-06, 2011-11, and 2016-16.

Keywords: *land use/land cover, remote sensing, geospatial information system (GIS), overall accuracy, kappa coefficient*

Introduction

Land cover refers to the surface cover of lands such as vegetation, water, urban infrastructure, and bare land, and land use refers to the purpose for which the land serves like recreation, wildlife habitat, or agriculture (Coffey, 2013). For worldwide monitoring studies, resource management, and planning operations, identifying, defining, and mapping land cover is critical (Treitz, 2004). Land cover identification gives a baseline against which monitoring operations (Change detection) can be carried out and also, gives information on the ground cover for baseline thematic maps (Mishra et al., 2020). It is crucial to understand the distinction between land cover and land use, as well as the information that each may provide. Land cover is one of the properties assessed using remote sensing methods, from which land use can be inferred, particularly with ancillary data (Roy and Roy, 2010; Pal and Ziaul, 2017; Siddhartha and Mukherjee, 2019)

Urbanization is a spatial phenomenon involving population increase, structural transformation, and the continued expansion of built-up regions that has a direct influence on the land use land cover (LULC) of urban landscapes (Fan et al., 2017). It is important to realise that urbanisation is not a disaster, but rather a need (Siddhartha and

Mukherjee, 2019; World Economic Forum, 2018). The positive impacts of urbanisation can only be accomplished if cities are economically viable and capable of providing long-term economic growth (Hammer et al., 2011). When it comes to Kerala, the state's urbanisation and settlement pattern are distinct. Kerala has an urban-rural continuum with a reasonably uniform distribution of housing units, as well as an urban-rural settlement pattern (Firoz et al., 2014). Rapid urbanisation has had a significant impact on the local and regional socio-ecological system, resulting in diminishing biodiversity, elevated city temperature, loss of productive agriculture, and fragmented wildlife habitat (Aithal and Ramachandra, 2016).

Changes in land use characteristics such as wetlands, forests, and cultivated land in urban areas increase the impermeable regions of the Earth's surface which result in the disruption in the hydrologic cycle (El Garouani et al., 2017). Satellite data on the Earth's resources are now available, and it is important and useful for studies of LULC transformation (Selçuk et al., 2003; Kadhim et al., 2016; Lo et al., 2004).

Remote sensing imageries and techniques are frequently utilised to analyse urban development and sprawl all over the world (Congalton, 1991; Campbell and Wynne, 2011). Researchers and decision-makers can use remote sensing data to track changes in a field of long-term interest without much on-site field monitoring. With the emergence of Geographical information systems (GIS) and remote sensing, land use/cover mapping has provided a helpful and comprehensive method for improving area selection of agricultural, urban, and/or industrial areas of a region (Jensen, 2005; Muzein, 2006). With the introduction of high spatial resolution satellite images and more advanced image processing and GIS technologies, land use/land cover trends are now being monitored and modelled on a more regular and consistent basis. Land use/cover mapping has become one of the most significant uses of remote sensing, with remote sensing being frequently utilised to update land use/cover maps (Bakker et al., 2004).

Validation of accuracy assessment is an important phase in the processing of remote sensing data (Gautam and Chennaiah, 1985). It determines the user's information value of the generated data (Borak et al., 2000). The overall accuracy of the classified image is determined by comparing how each pixel is categorised to the specified land cover conditions generated from the ground truth data (Chen and Wang, 2010; Cohen et al., 2017). Producer's accuracy measures errors of omission, which is a measure of how well real-world land cover types can be classified. User's accuracy measures errors of commission, which represents the likelihood of a classified pixel matching the land cover type of its corresponding real-world location (Mironga, 2004; Mohajane et al., 2018; Manandhar et al., 2009).

This study attempts to map out the status of land use/cover of Ernakulam district in view to determine the land consumption rate and the change that has occurred over the last few years using geospatial techniques. This research is anticipated to provide useful information for the decision-makers and planners to develop strategies for sustainable LULC management and environmental planning policies.

The methods

Geo-environmental setting of the study area

The study focuses on the Ernakulam district located almost in the middle of Kerala State and on the coast of the Arabian Sea. The district lies between the longitude of 76° 16' 48.00" and latitude of 9° 58' 48.00" N and spans an area of about 3068 km². The

district is bounded on the North by Thrissur district, on the south by Kottayam and Alappuzha districts, and on the east by Idukki district and the Arabian Sea lies all along the western boundary of the district. The district is split into three distinct sections: highland, midland, and lowland, which are comprised of hills and forests, plains, and the coastline, respectively. A part of the Western Ghats forms the hilly or eastern portion. The midland is primarily flat land with natural drainage systems such as backwaters and canals. The low land region makes up 20% of the overall area.

There is a tropical humid climate in the area, with a long hot season and plenty of seasonal rain. The hot season from March to May is followed by the South-West Monsoon season from June to September and the North-East Monsoon season from October to November/mid-December. From the end of December until the beginning of February, the weather is usually dry. The district receives on an average 3450 mm of annual rainfall. About 67% of the rainfall is due to the south-west monsoon. This district's seacoast is fully within Cochin taluk, and Cochin port, a large natural harbour, is also inside this taluk.

About 30% of the area is urban where about 49% of the district's population lives (Census, 2011). In all development initiatives, the population parameter acts as the foundation. One of the goals of all types of planning is to provide the highest level of benefit to the maximum number of people. The land use pattern reflects the district's characteristics in terms of growth, development, and activity pattern. It also indicates the amount of land suitable for future development in an informal way. *Figure 1* shows the location of the study area.

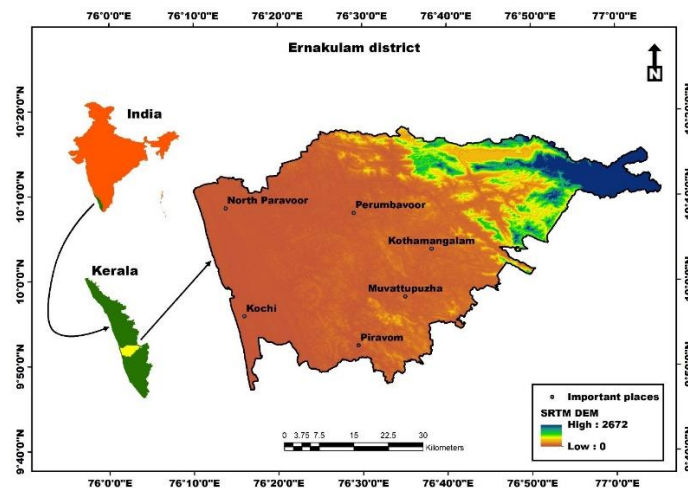


Figure 1. Location of the study area

Data acquisition and processing

The current study used geo-informatics and Remote Sensing to analyse differences in LULC classes in the Ernakulam District. Remote sensing (RS) is the science of acquiring and analysing information about objects or phenomena from a distance (Lu and Weng, 2007; Hogland et al., 2013; Rwanga and Ndambuki, 2017). To avoid cloud cover, the images were taken during the dry season (Durieux et al., 2003). Satellite images are subjected to image pre-processing to minimize distortions caused by the

sensor, the sun, the atmosphere, and the topography. This is to improve the image component's quality and interpretability for remote sensing analysis (Kar et al., 2018).

Cloud-free and haze-free satellite images were georeferenced and corrected during the pre-processing stage concerning the UTM zone 43 N (Universal Transverse Mercator) based on the WGS84 (World Geodetic System) datum (Ganaie et al., 2021). The data were resampled using the methodology of a nearby pixel to keep the same brightness values of the unaffected pixels. This approach allocates the present value of the adjacent pixel to the value of the output pixel, relocating the original pixel values without averaging and preserving the subtleties and extremes of the pixel values. A representative ground truth data set is required in remote sensing research to correlate this reflectance attribute with the object, train classifiers, and allow accurate automated categorization.

Image classification

Image classification is one of the most effective methods of processing satellite image data. An image is classified based on the actual classes it represents on the ground or earth's surface as it helps detect, identify, and classify its different features (Srivastava et al., 2012; Kalra et al., 2013). In remote sensing, image classification can be categorized into supervised and unsupervised techniques. Here in this study, we adopted the supervised classification using a maximum likelihood classifier (MLC) which is one of the most widely used supervised classification algorithms due to its availability and simple training process. This method classifies satellite image pixels based on their probability of occurrence. It assumes equal probabilities for all classes and normal distributions for all input bands.

The image classification procedure involved the generation of 150 training samples for each satellite image using the region of interest (ROI) tool in ENVI 5.3 image processing software. To successfully classify land use/land cover spectral classes, this method was done. In addition, we validate the prepared map with the existing maps obtained from the authorised agencies in the study area and Google Earth maps.

Landsat imageries for the years 2006, 2011, and 2016 for the study area were obtained from the online portals, Global Land Cover Facility (GLCF), and Earth Explorer with a spatial resolution of 30 m. The images were enhanced, registered, georeferenced, and classified into various land use types using supervised classification (Lillesand et al., 2015; Onur et al., 2009). Later, using supplementary data from topographic maps and Google Earth photos, geometric improvement, and data validation was performed.

Aggregated the classes of LULC shapefile into 5 broad classes named Agricultural Land, Built-Up, Forest, Wastelands, and Waterbodies. Then, assigned 5 classes a unique integer/number value. Converted shapefile to raster of pixel 5 m spatial resolution *Figure 2a, b, and c*. The pictures were improved, registered, geo-referenced, and categorised into different land use categories using supervised classification. The supervised classification procedure makes a preliminary assessment of areas on the image that delineate land parcels to be mapped (Prasad and Ramesh, 2019). Supervised Maximum Likelihood Classification Technique (MLCT) is adopted to generate different categories of LULC maps of the study area.

Additionally, to improve the accuracy level and to reduce errors in maximum likelihood classification, the Landsat images of the study area were categorised and the points were chosen from various parts of the study area and were verified using Google

Earth's latitude and longitude. The Validation/accuracy was performed into QGIS using the GRASS tool kappa. The per-class area was calculated in QGIS using the tool 'Raster layer unique values report' for the years 2006, 2011, and 2016.

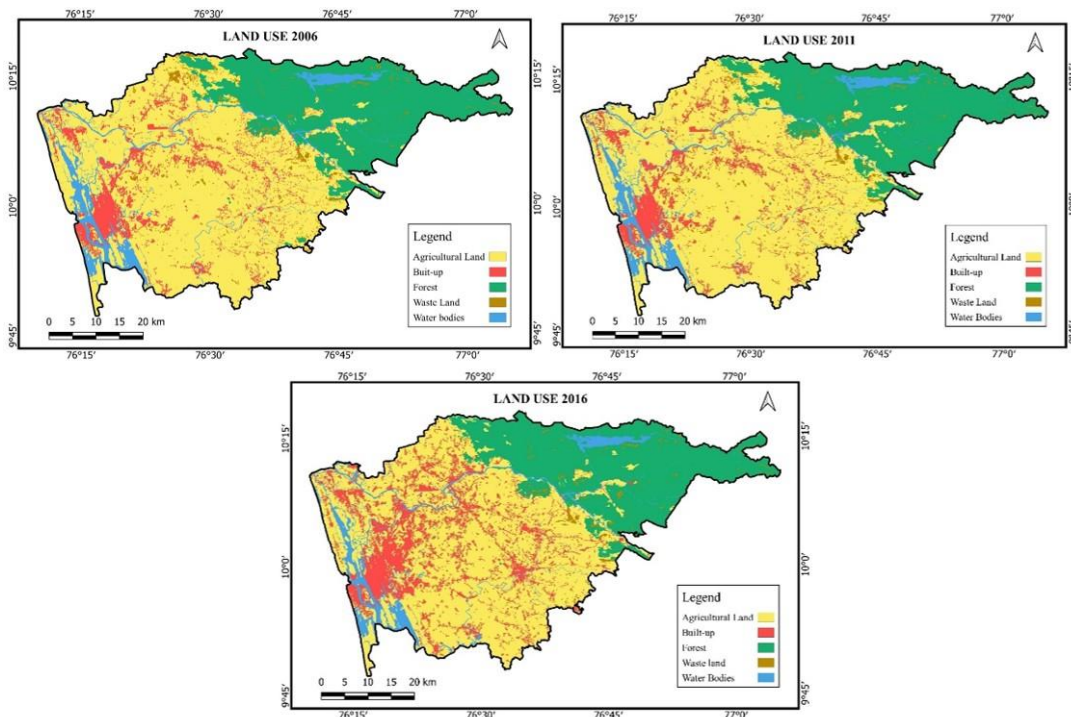


Figure 2. Land use land cover – (a) 2006, (b) 2011, (c) 2016

Accuracy assessment

The accuracy assessment is a necessary step in the feature abstraction process from classified images (Maxwell et al., 2021). The accuracy assessment involved the determination of thematic or classification accuracy (Maxwell and Warner, 2020; Borana and Yadav, 2017). For the thematic accuracy, 100 points are chosen on the map and the same is displayed in the image using the “Accuracy Assessment Tool” in ERDAS Imagine software. The field verification of randomly selected points is also done. The value is derived by overlaying these ground truth locations on the land use land cover map.

Accuracy assessment was done through ERDAS imagine with a ground control point of Google Earth Pro software and GPS ground data sets (Ragheb and Ragab, 2015; Aguilar et al., 2020). A classified image or change detection map needs to be compared against reference data, assumed to be true, to assess its performance and quantify its accuracy (Mengistu and Salami, 2007; Guler et al., 2007). The process had used to estimate the accuracy of image classification by comparing the classified map with a reference map. Therefore, a full accuracy assessment needs to include the report on Overall accuracy, User Accuracy, and Producer Accuracy had investigated using the Kappa coefficient. User Accuracy quantifies the error of commission while Producer Accuracy quantifies the error of omission. The user and producer accuracies, on the other hand, differed amongst LULC classes and study areas (Morales-Barquero et al., 2019; Nutini et al., 2013).

$$\text{User Accuracy} = \frac{\text{Number of correctly classified pixels in a class}}{\text{Total number of pixels in a class}} \quad (\text{Eq.1})$$

$$\text{Producers Accuracy} = \frac{\text{Number of correctly classified pixels in a class}}{\text{Total number of pixels in all classes}} \quad (\text{Eq.2})$$

$$\text{Overall Accuracy} = \frac{\text{Total number of all correctly classified pixels}}{\text{Total number of pixels in all classes}} \quad (\text{Eq.3})$$

Another method that quantifies classification accuracy is Kappa statistics; it measures the chance agreement (Kadhim et al., 2016; Vitousek, 1992). It is more efficient than the overall accuracy of satellite images. To achieve high overlay accuracy for better results, the satellite imageries were geo-referenced and rectified. Kappa coefficient (k), a discrete multivariate technique (Rawat and Kumar, 2015), was used to assess the accuracy of the results found through analysis of Landsat 5, 7, and 8 data (Rawat and Kumar, 2015; Msofe et al., 2019). Kappa (k) is a statistical tool used widely to assess the accuracy of derived maps (Dame et al., 2019). Kappa statistics, which measures chance agreement, is another approach for quantifying categorization accuracy. It is more efficient than the overall accuracy of satellite images.

$$\text{Cohen's Kappa (k)} = \frac{(P_0 - P_e)}{(1 - P_e)} \quad (\text{Eq.4})$$

where P_0 is observed accuracy and P_e is change agreement.

The kappa coefficient varies from 0 to 1, where 0 means agreement equivalent to chance; 0.1 to 0.20 means slight agreement; 0.21 to 0.40 means fair agreement; 0.41 to 0.60 means moderate agreement; 0.61 to 0.81 means substantial agreement; 0.81 to 0.99 means near-perfect agreement or good performance; and 1 means perfect agreement (Ferreira et al., 2019).

LULC change detection

The significance of change detection is determining which land-use class is transitioning from one to the other. Change detection was conducted utilising the most common and accurate change detection method, post-classification comparison (PCC) (Du et al., 2017). While reducing the difficulty of radiometric calibration between images of various dates, post-classification comparison explains the nature of changes between study periods (Mallupattu and Sreenivasula Reddy, 2013; Bhat et al., 2017).

The most commonly used land change detection methods include change vector analysis, image overlay, principal component analysis, classification comparisons of land cover statistics, image rationing, and the differencing of normalized difference vegetation index (NDVI) (Han et al., 2009; Muttitanon and Tripathi, 2005).

$$\text{Change percentage (\%)} = \frac{\text{Present LULC area} - \text{Previous LULC area}}{\text{Previous LULC area}} \times 100 \quad (\text{Eq.5})$$

The final and initial LULC areal coverage were compared using the above procedure to get the LULC change in percentage (%). The capacity to measure temporal impacts using multi-temporal data sets is essentially what it is all about (Singh, 1989). Several researchers have attempted to solve the challenge of change detection by using digits.

Approaches for digital change detection can be generally classified by *Equation 1* analysis techniques used to delineate areas of significant alterations and *Equation 2* the data transformation procedure (if any). In this study, the land use statistics of the Ernakulam district for the years 2006-06, 2011-11, and 2016-16 were detected by applying the post-classification comparison method. This approach was used in this study because of its simplicity and ability to compare two images from two distinct sensors and time (Alphan et al., 2009). It is important to note that most change detection algorithms need good spatial alignment of the two pictures (Dewidar, 2004; Mengistu and Salami, 2007; Guler et al., 2007). A well-designed methodology was adopted for the current study.

Results

The land use maps were prepared using Landsat images for the years 2006, 2011, and 2016. Changes in land use/cover are a major driver of global change, with significant implications for many international policy issues. The Ernakulam district encompasses a wide range of land uses: agricultural land, built-up, forest, wastelands, and water bodies. For the analysis, the total area and percentage for each land-use class for the years 2006, 2011, and 2016 were computed. From 2006 to 2016, the percentage changes in land use classifications were calculated. It is apparent from this that the built-up land has increased in value from 2006 to 2016 (*Tables 1* and *2*).

Table 1. Land use statistics of the Ernakulam district for the year 2006, 2011, and 2016

LULC class	2006		2011		2016	
	Area (km ²)	% Cover	Area (km ²)	% Cover	Area (km ²)	% Cover
Agricultural land	1728.33	56.53	1746.57	57.11	1541.00	50.41
built up	252.93	8.27	246.09	8.05	452.28	14.80
Forest	832.65	27.24	830.15	27.14	850.73	27.83
Wastelands	54.11	1.77	46.60	1.52	26.64	0.87
Waterbodies	189.19	6.19	189.00	6.18	186.07	6.09
Total area (km ²)	3057.20		3058.40		3056.71	

Table 2. Dynamics of LULC change between 2006 and 2016 (km²)

LULC class	LULC change 2006-2011		LULC change 2011-2016		LULC change 2006-2016	
Agricultural land	18.24	0.58	-205.57	-6.7	-187.33	-6.12
Built up	-6.84	-14.80	206.19	6.75	199.35	6.53
Forest	-25.00	-0.10	20.58	0.69	18.08	0.59
Wastelands	-7.51	-0.25	-19.96	-0.65	-27.47	-0.9
Waterbodies	-0.19	-0.01	-2.93	-0.09	-3.12	-0.1

The study area's land use and land cover categories exhibited both positive and negative growth in the area of total geographical area. The agricultural area occupies an area of 56.33% in 2006, it could be shown a slightly positive trend in 2011 around 57.11%. Whereas the rest of the classes showed a negative trend. A negative value denotes the decline of the area. During the study period, all the categories showed both

positive and negative growth in the total geographical area. The agricultural land occupies an area of 57.11% in 2011, got reduced to 50.41% in 2016. The agricultural land area reduced from 56.53% in the year 2006 to 50.41% in the year 2016, which shows the urbanisation and the conversion of the vacant lands being converted to the build-up lands (*Fig. 3a*).

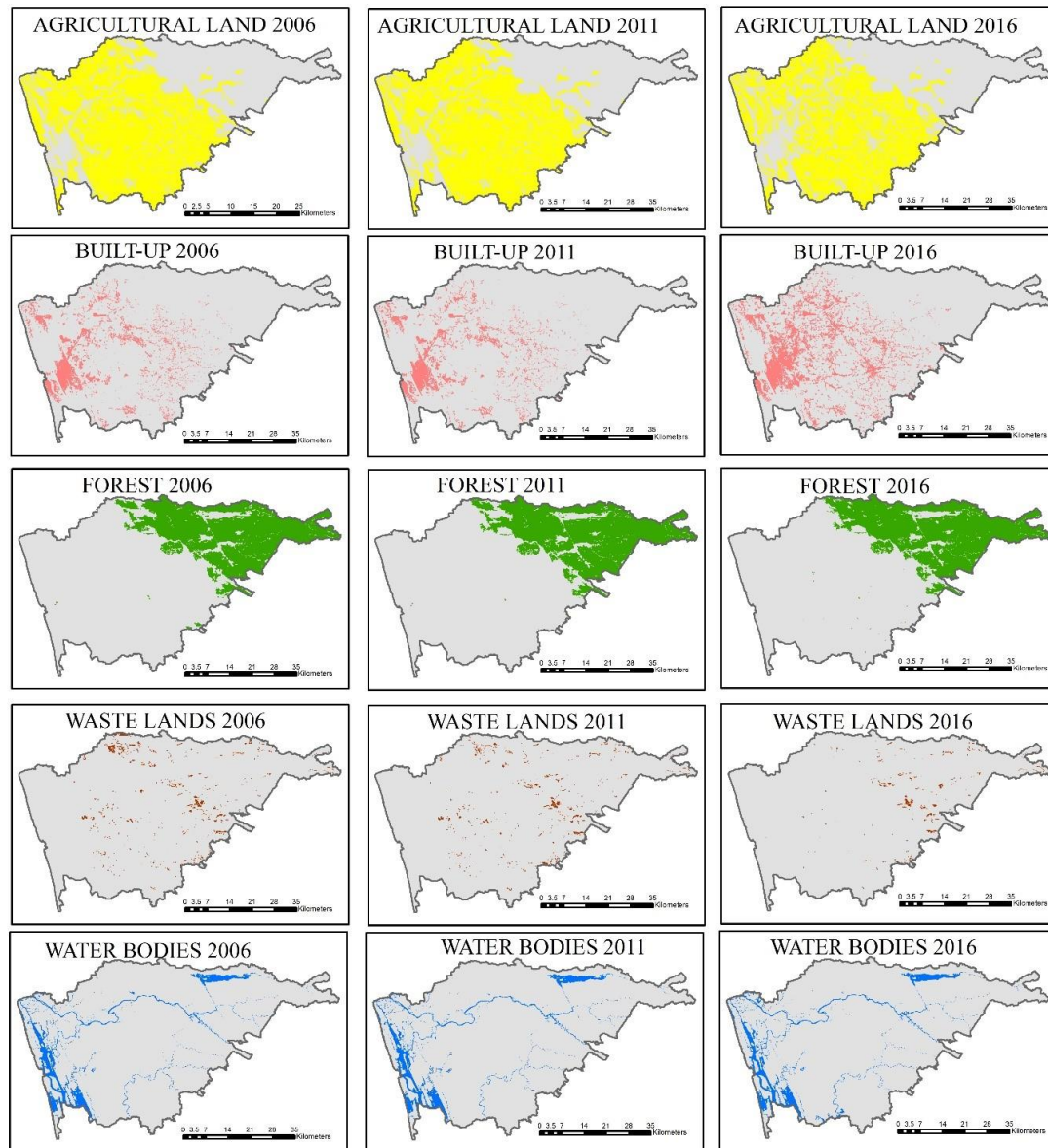


Figure 3. Synoptic view of different land use and land cover pattern. (a) Agricultural land (b) built-up (c) forest (d) waste lands (e) water bodies

The spatio-temporal changes of the built-up area have a significant impact on the reclamation of wetlands. In this study, the built-up area represents both rural and urban built-up along with the mining/industrial area. It is clear from the data that there was an increase in the built-up area from 8.27% in the year 2006 to 14.80% in the year 2016 (*Fig. 3b*). The census data show that the population of the study area in 2001 was 3,105,798, whereas in 2011 it was 3,282,388 which portrays demographic growth.

Forests are thick canopies of trees. Forest in the study area represents the deciduous (Dry/Moist/Thorn), evergreen/semi-evergreen, a forest plantation, littoral/swamp forest (Mangrove/Forest Water Swamp), and scrub forest. In the study area, it was clear that there was an increase in the forest area from 27.24% in the year 2006 to 27.83% in the year 2016 (Fig. 3c). During the research period, there was no encroachment due to human activity, deforestation, agriculture, or plantation. The wasteland area reduced from 1.77% in the year 2006 to 0.87% in the year 2016, which shows the effect of the vacant land being converted into built-up areas. In the waterbody and waterlogged regions, there was little change (Fig. 3d). Water bodies include lakes/ponds, Reservoir/tanks, and rivers/streams. The area under the water body class was reduced from 189.19 km² which is 6.19% in 2006 to 6.09% in 2016 (Fig. 3e).

The results from the accuracy assessment showed an overall accuracy of 81.49%, 81.87%, and 82.79% respectively in the years 2006, 2011, and 2016. In the year 2016, Users' accuracy ranged from 74.26% to 95.83% while producer's accuracy ranged from 74.19% to 95.83%. The producer's accuracy reflects the accuracy of prediction of the particular category and the user's accuracy reflects the reliability of the classification to the user. The wasteland was found to be more reliable with 95.83% of the user's accuracy (Table 3).

The overall kappa coefficient was 0.75, 0.75, and 0.77 respectively for the year 2006-06, 2011-11, and 2016-16 (Table 4).

Table 3. The producer's accuracy and user's accuracy matrix for the years 2006, 2011, 2016

LULC class	Producer's accuracy (%)			User's accuracy (%)		
	2006	2011	2016	2006	2011	2016
Agricultural land	89.30	89.74	81.59	74.22	74.47	81.19
Built up	64.81	66.96	81.45	79.55	81.05	74.26
Forest	93.90	93.98	95.83	92.77	91.76	92.00
Wastelands	80.00	80.77	74.19	94.12	95.45	95.83
Waterbodies	75.00	74.29	77.00	89.29	89.66	85.56

Table 4. The kappa coefficient per class matrix for the years 2006, 2011, and 2016

LULC class name	Kappa coefficient		
	2006	2011	2016
Agricultural land	0.59	0.59	0.70
Built up	0.74	0.76	0.67
Forest	0.91	0.90	0.90
Wastelands	0.94	0.95	0.96
Waterbodies	0.87	0.87	0.82

Discussion and conclusion

The rate of urbanisation and land being converted is astounding. Urbanization exacerbates the conflict between land and water development. The study demonstrated the value of remote sensing and geographic information systems (GIS) in mapping and identifying urban LULC dynamics on both spatial and temporal scales. Multi-temporal

Landsat data has also been shown to accurately detect urban LULC changes despite their moderate. The current urbanisation trend has the most visible environmental effects on the surrounding ecosystems, land resources, urban form and pattern, and therefore quality of life. It has also been observed that some sort of urbanisation is taking place in the region's protected zones. Rapid urban/built-up expansions resulted in substantial changes in land use and cover, as seen by steep reductions in the agricultural, wasteland, and water bodies.

Increased built-up land stemmed from a significant rise in rural-to-urban people's migration toward district centres. In addition, the expansion of the tourism industry, as well as the noticeable improvements in socio-economic development, has contributed to this rise in the built-up area. Between 2006 and 2016, the built-up area expanded dramatically. It was 8% in 2006 and increased to 14% in 2016. The increase in the built-up area is directly proportional to population growth. As a result of the overuse of natural resources, the delicate environmental balance is disrupted, and waste management difficulties are exacerbated. Because human systems are not closed-loop, they frequently have detrimental consequences for ecosystems.

In 2006 the percentage of agricultural land was 57% and in 2016 it was 50%. A large agricultural land was converted to non-agricultural land in the year 2016. As per the 2011 census, Ernakulam became Kerala's most urbanised district with a 68.07% urban populace. Various human activities had resulted in significant changes in the studied area's land use/land cover. Information on the LULC pattern dynamics over a period is vital to the effective management of an area. The effectiveness of the use of remote sensing and GIS integration for mapping and detecting LULC changes in the Ernakulam district was demonstrated in this study.

For a harmonic ecological balance and long-term development, a well-thought-out land-use strategy is required. A judicious land use plan should be put in place, with a focus on controlling developed land that encroaches on paddy fields, waterlogged areas, and water bodies. To sustain eco-friendly biodiversity, ecological preservation tenets should be woven into LULC management. The findings and analysis of the study imply significant policy implications for various urban planning activities for sustainable land-use/cover practices in the Ernakulam district. However, in future research, the use of high-resolution temporal data, as well as the integration of the study's zoning rules and development plans, might assist to increase the accuracy of the findings, planning for urban utilities, assessing the environmental consequences of urban sprawl, and preserving socio-environmentally significant regions are all essential tasks. Land cover changes and population growth need to be examined in greater depth in future research. By utilizing demographic data, we can gain an understanding of the long-term dynamics of LULC change and how it holistically impacts sustainable development.

Acknowledgements. This research did not receive any specific grant from funding agencies in the public, commercial, or not-for-profit sectors. The authors declare that they have no known competing financial interests or personal relationships that could have appeared to influence the work reported in this paper.

REFERENCES

- [1] Aguilar, M. A., Jiménez-Lao, R., Nemmaoui, A., Aguilar, F. J. (2020): Geometric accuracy assessment of deimos-2 panchromatic stereo pairs: sensor orientation and digital surface model production. – *Sensors* 20(24): 1-17.

- [2] Aithal, B. H., Ramachandra, T. V. (2016): Visualization of urban growth pattern in Chennai using geoinformatics and spatial metrics. – *Journal of the Indian Society of Remote Sensing* 44(4): 617-633.
- [3] Alphan, H., Doygun, H., Unlukaplan, Y. I. (2009): Post-classification comparison of land cover using multitemporal Landsat and ASTER imagery: the case of Kahramanmaras, Turkey. – *Environmental Monitoring and Assessment* 151(1-4): 327-336.
- [4] Bakker, W. H., Grabmaier, K. A., Huurneman, G. C., Meer, F. D. van der, Prakash, A., Tempfli, K., Gieske, A. S. M., Hecker, C. A., Janssen, L. L. F., Parodi, G. N., Reeves, C. V., C. Weir, M. J., Gorte, B. G. H., Horn, J. A., Kerle, N., Pohl, C., Ruitenbeek, F. J. van, Woldai, T. (2004): *Principles of Remote Sensing*. – The International Institute for Geo-Information Science and Earth Observation (ITC), Enschede.
- [5] Bhat, P. A., Shafiq, M. ul, Mir, A. A., Ahmed, P. (2017): Urban sprawl and its impact on landuse/land cover dynamics of Dehradun City, India. – *International Journal of Sustainable Built Environment* 6(2): 513-521.
- [6] Borak, J. S., Lambin, E. F., Strahler, A. H. (2000): The use of temporal metrics for land cover change detection at coarse spatial scales. – *International Journal of Remote Sensing* 21(6-7): 1415-1432.
- [7] Borana, S. L., Yadav, S. K. (2017): Accuracy assessment of land cover classification in Jodhpur City using remote sensing and GIS. – *International Journal of Advanced Research in Computer and Communication Engineering* 6(10): 220-224.
- [8] Campbell, J. B., Wynne, R. H. (2011): *Introduction to Remote Sensing*. 5th Ed. – Guilford, New York.
- [9] Chen, Z., Wang, J. (2010): Land use and land cover change detection using satellite remote sensing techniques in the mountainous Three Gorges Area, China. – *International Journal of Remote Sensing* 31(6): 1519-1542.
- [10] Coffey, R. (2013): The Difference Between “Land Use” and “Land Cover”. – Michigan State University Extension, East Lansing, MI.
- [11] Cohen, W. B., Kauffman, J. B., Guild, L. S. (2017): Detection of deforestation and land conversion in Rondônia, Brazil using change detection techniques. – *International Journal of Remote Sensing*: 731-750.
- [12] Congalton, R. G. (1991): A review of assessing the accuracy of classifications of remotely sensed data. – *Remote Sensing of Environment* 37(1): 35-46.
- [13] Dame, J., Schmidt, S., Müller, J., Nüsser, M. (2019): Urbanisation and socio-ecological challenges in high mountain towns: insights from Leh (Ladakh), India. – *Landscape and Urban Planning*: 189-199.
- [14] Dewidar, K. M. (2004): Detection of land use/land cover changes for the northern part of the Nile delta (Burullus region), Egypt. – *International Journal of Remote Sensing* 25(20): 4079-4089.
- [15] Du, C. W. B., Cui, X., Zhang, L. (2017): A post-classification change detection method based on iterative slow feature analysis and Bayesian soft fusion. – *Remote Sensing of Environment*: 241-255.
- [16] Durieux, L., Machado, L. A. T., Laurent, H. (2003): The impact of deforestation on cloud cover over the Amazon arc of deforestation. – *Remote Sensing of Environment* 86(1): 132-140.
- [17] El Garouani, A., Mulla, D. J., El Garouani, S., Knight, J. (2017): Analysis of urban growth and sprawl from remote sensing data: case of Fez, Morocco. – *International Journal of Sustainable Built Environment* 6(1): 160-169.
- [18] Fan, C., Myint, S. W., Rey, S. J., Li, W. (2017): Time series evaluation of landscape dynamics using annual Landsat imagery and spatial statistical modeling: evidence from the Phoenix metropolitan region. – *International Journal of Applied Earth Observation and Geoinformation* 58: 12-25.

- [19] Ferreira, L. M. R., Esteves, L. S., de Souza, E. P., dos Santos, C. A. C. (2019): Impact of the Urbanisation process in the availability of ecosystem services in a tropical ecotone area. – *Ecosystems* 22(2): 266-282.
- [20] Firoz, M., Banerji, H., Sen, J. (2014): A methodology to define the typology of rural urban continuum settlements in Kerala. – *Journal of Regional development and Planning* 3(1): 49-60.
- [21] Ganaie, T. A., Jamal, S., Ahmad, W. S. (2021): Changing land use/land cover patterns and growing human population in Wular catchment of Kashmir Valley, India. – *GeoJournal* 86(4): 1589-1606.
- [22] Gautam, N. C., Chennaiah, G. C. (1985): Land-use and land-cover mapping and change detection in Tripura using satellite Landsat Data. – *International Journal of Remote Sensing* 6(3-4): 517-528.
- [23] Guler, M., Yomralioglu, T., Reis, S. (2007): Using Landsat data to determine land use/land cover changes in Samsun, Turkey. – *Environmental Monitoring and Assessment*: 155-167.
- [24] Hammer, S., Kamal-chaoui, L., Robert, A., Plouin, M. (2011): *Cities and Green Growth: A Conceptual Framework*. – OECD Regional Development Working Papers 2011/08. OECD Publishing, Paris. <http://dx.doi.org/10.1787/5kg0tflmzx34-en>.
- [25] Han, J., Hayashi, Y., Cao, X., Imura, H. (2009): evaluating land-use change in rapidly urbanizing china: case study of Shanghai. – *Journal of Urban Planning and Development* 135(4): 166-171.
- [26] Hogland, J., Billor, N., Anderson, N. (2013): Comparison of standard maximum likelihood classification and polytomous logistic regression used in remote sensing. – *European Journal of Remote Sensing* 46(1): 623-640.
- [27] Jensen, J. R. (2005): *Introductory Digital Image Processing. A Remote Sensing Perspective*. 3rd Ed. – Prentice Hall, Upper Saddle River.
- [28] Kadhim, N., Mourshed, M., Bray, M. (2016): Advances in remote sensing applications for urban sustainability. – *Euro-Mediterranean Journal for Environmental Integration* 1(1): 1-22.
- [29] Kalra, K., Kumar Goswami, A., Gupta, R. (2013): A comparative study of supervised image classification algorithms for satellite images. – *International Journal of Electrical* 1(10): 2320-2084.
- [30] Kar, R., Obi Reddy, G. P., Kumar, N., Singh, S. K. (2018): Monitoring spatio-temporal dynamics of urban and peri-urban landscape using remote sensing and GIS. A case study from Central India. – *Egyptian Journal of Remote Sensing and Space Science* 21(3): 401-411.
- [31] Lillesand, T., Kiefer, R. W., Chipman, J. (2015): *Remote Sensing and Image Interpretation*. – Wiley, Hoboken.
- [32] Lo, C. P., Jinmu Choi (2004): A hybrid approach to urban land use/cover mapping using Landsat 7 Enhanced Thematic Mapper Plus (ETM+) images. – *International Journal of Remote Sensing* 25(14): 2687-2700.
- [33] Lu, D., Weng, Q. (2007): A survey of image classification methods and techniques for improving classification performance. – *International Journal of Remote Sensing* 28(5): 823-870.
- [34] Mallupattu, P. K., Sreenivasula Reddy, J. R. (2013): Analysis of land use/land cover changes using remote sensing data and GIS at an urban area, Tirupati, India. – *The Scientific World Journal*: 1-7.
- [35] Manandhar, R., Odehi, I. O. A., Anevt, T. (2009): Improving the accuracy of land use and land cover classification of Landsat data using post-classification enhancement. – *Remote Sensing* 1(3): 330-344.
- [36] Maxwell, A. E., Warner, T. A. (2020): Thematic classification accuracy assessment with inherently uncertain boundaries: an argument for center-weighted accuracy assessment metrics. – *Remote Sensing* 12: 1905.

- [37] Maxwell, A. E., Warner, T. A., Guillén, L. A. (2021): Accuracy assessment in convolutional neural network-based deep learning remote sensing studies—part 2: Recommendations and best practices. – *Remote Sensing* 13: 2591.
- [38] Mengistu, D. A., Salami, A. T. (2007): Application of remote sensing and GIS inland use/land cover mapping and change detection in a part of south western Nigeria. – *African Journal of Environmental Science and Technology* 1(5): 99-109.
- [39] Mironga, J. M. (2004): Geographic information systems (GIS) and remote sensing in the management. – *Applied Ecology and Environmental Research* 2(1): 83-103.
- [40] Mishra, P. K., Rai, A., Rai, S. C. (2020): Land use and land cover change detection using geospatial techniques in the Sikkim Himalaya, India. – *Egyptian Journal of Remote Sensing and Space Science* 23(2): 133-143.
- [41] Mohajane, M., Essahlaoui, A., Oudija, F., Hafyani, M. El, Hmaid, A. El, Ouali, A. El, Randazzo, G., Teodoro, A. C. (2018): Land use/land cover (LULC) using Landsat data series (MSS, TM, ETM+ and OLI) in Azrou forest, in the central middle atlas of Morocco. – *Environments MDPI* 5(12): 1-16.
- [42] Morales-Barquero, L., Lyons, M. B., Phinn, S. R., Roelfsema, C. M. (2019): Trends in remote sensing accuracy assessment approaches in the context of natural resources. – *Remote Sensing* 11(19): 1-16.
- [43] Msofe, N. K., Sheng, L., Lyimo, J. (2019): Land use change trends and their driving forces in the Kilombero Valley Floodplain, Southeastern Tanzania. – *Sustainability* 11(2): 505.
- [44] Muttitanon, W., Tripathi, N. K. (2005): Land use/land cover changes in the coastal zone of Ban Don Bay, Thailand using Landsat 5 TM data. – *International Journal of Remote Sensing* 26(11): 2311-2323.
- [45] Muzein, B. S. (2006): Remote Sensing a GIS for Land Cover/Land Use Change Detection and Analysis in the Semi-Natural Ecosystems and Agriculture Landscapes of the Central Ethiopian Rift Valley. Thesis Report. – Technische Universität Dresden, Fakultät Forst-, Geo- und Hydrowissenschaften: Institut für Photogrammetrie und Fernerkundung, Dresden.
- [46] Nutini, F., Boschetti, M., Brivio, P. A., Bocchi, S., Antoninetti, M. (2013): Land-use and land-cover change detection in a semi-arid area of Niger using multi-temporal analysis of Landsat images. – *International Journal of Remote Sensing* 34(13): 4769-4790.
- [47] Onur, I., Maktav, D., Sari, M., Kemal Sönmez, N. (2009): Change detection of land cover and land use using remote sensing and GIS: a case study in Kemer, Turkey. – *International Journal of Remote Sensing* 30(7): 1749-1757.
- [48] Pal, S., Ziaul, S. (2017): Detection of land use and land cover change and land surface temperature in English Bazar urban centre. – *Egyptian Journal of Remote Sensing and Space Science* 20(1): 125-145.
- [49] Prasad, G., Ramesh, M. V. (2019): Spatio-temporal analysis of land use/land cover changes in an ecologically fragile area—Alappuzha District, Southern Kerala, India. – *Natural Resources Research* 28: 31-42.
- [50] Ragheb, A. E., Ragab, A. F. (2015): Enhancement of google earth positional accuracy. – *International Journal of Engineering Research and Technology* 4(1): 627-630.
- [51] Rawat, J. S., Kumar, M. (2015): Monitoring land use/cover change using remote sensing and GIS techniques: a case study of Hawalbagh block, district Almora, Uttarakhand, India. – *Egyptian Journal of Remote Sensing and Space Science* 18(1): 77-84.
- [52] Roy, P. S., Roy, A. (2010): Land use and land cover change in India: a remote sensing & GIS perspective. – *Journal of the Indian Institute of Science* 90(4): 489-502.
- [53] Rwanga, S. S., Ndambuki, J. M. (2017): Accuracy Assessment of land use/land cover classification using remote sensing and GIS. – *International Journal of Geosciences* 8(4): 611-622.

- [54] Selçuk, R., Nisnci, R., Uzun, B., Yalçın, A. (2003): Monitoring land use changes by gis and remote sensing technique: case study of Trabzon. – 2nd FIG Regional Conference, Morocco.
- [55] Siddhartha, K., Mukherjee, S. (2019): Cities Urbanisation and Urban Systems (Settlement Geography). – Kitab Mahal Publication, New Delhi.
- [56] Singh, A. (1989): Review article: Digital change detection techniques using remotely-sensed data. – International Journal of Remote Sensing 10(6): 989-1003.
- [57] Srivastava, P. K., Han, D., Rico-Ramirez, M. A., Bray, M., Islam, T. (2012): Selection of classification techniques for land use/land cover change investigation. – Advances in Space Research 50(9): 1250-1265.
- [58] Treitz, P. (2004): Remote sensing for mapping and monitoring land-cover and land-use change. – Progress in Planning 61(4): 267.
- [59] Vitousek, P. M. (1992): Global environmental change: an introduction. – Annual Review of Ecology and Systematics 23: 1-14.
- [60] World Economic Forum (2018): The Global Risks Report 2018. 13th Ed. – World Economic Forum, Geneva.

DIVERSITY OF INSECT PESTS AND THEIR NATURAL ENEMIES IN HOT PEPPER (*CAPSICUM ANNUM* L.) ECOSYSTEM OF INDONESIA

PRABANINGRUM, L.¹ – MOEKASAN, T. K.¹ – HASYIM, A.¹ – SETIAWATI, W.¹ – MURTININGSIH, R.¹
– UDIARTO, B. K.¹ – SULASTRINI, I.¹ – KORLINA, E.¹ – GUNAENI, N.¹ – WULANDARI, A. W.¹ –
GUNADI, N.¹ – PRIANI, R. A.² – LUKMAN, L.³ – MEJAYA, M. J.^{4*}

¹*Indonesian Vegetable Research Institute (IVEGRI), Jl. Tangkuban Parahu No. 517, Lembang, Bandung Barat 40391, West Java, Indonesia*

²*West Java-Assessment Institute for Agricultural Technology (AIAT), Jl. Kayu Ambon No. 80, Lembang, Bandung Barat 40391, West Java, Indonesia*

³*Directorate General of Horticulture, Ministry of Agriculture, Republic of Indonesia, Jl. AUP No.3, Pasar Minggu, Jakarta Selatan, Indonesia*

⁴*Indonesian Legumes and Tuber Crops Research Institute (ILETRI), Jl. Raya Kendal Payak Km 8, PO BOX 66, Malang 65101, East Java, Indonesia*

*Corresponding author

e-mail: mmejaya@yahoo.com; phone +62-341-801-468

(Received 3rd Feb 2022; accepted 20th May 2022)

Abstract. The objective of this study was to determine the diversity and structure of insect communities in hot pepper ecosystem of Indonesia. The study was carried out in Lembang, in 2020 using yellow sticky and fruit fly traps. The study showed 18 insect families belonging to the following orders: Coleoptera, Diptera, Hemiptera, Hymenoptera, Thysanoptera and Lepidoptera. These families consisted of 23 species and 45,489 individuals. The Shannon-Wiener (H') diversity index showed that the ecosystem had low to moderate diversity, which increased from planting to harvesting stages. The species evenness index (E) was low during the vegetative growth and increased during reproductive and harvesting stages. Simpson's dominance index (D) decreased with increasing diversity, from medium to low dominance category.

Keywords: abundance, beneficial insect, dominance, hot pepper, phytophagous

Introduction

Hot pepper (*Capsicum annum* L.) is an important vegetable crop with high economic value grown in tropical and subtropical regions throughout the world (Hundall and Dhall, 2004; Cakrabarty et al., 2019). Hot pepper is used as a source of nutrients that are beneficial for health (Shetty et al., 2013; Padilha and Barbieri, 2016; Saleh et al., 2018), as a source of vitamins and minerals (Kerketta et al., 2018), and as a cooking spice and coloring (Pugliese et al., 2013; Materska, 2014; Loizzo et al., 2015). Hot pepper is widely cultivated in developing countries, including Indonesia (Lin et al., 2015; Ganefianti et al., 2017) and it is a special commodity because it can cause inflation (Mariyono, 2016).

Hot pepper consumption per capita in Indonesia was 2.9 kg per year (Farid and Subekti, 2012). However, national hot pepper production is still relatively low, at around 8.82 tons/ha (Ministry of Agriculture, Republic of Indonesia, 2019), even though the potential yield can reach 20 tons/ha (Soetiarso and Setiawati, 2010). One of the causes of low hot pepper productivity is pests that could result in yield losses

between 50% and 90%, so farmers rely heavily on pesticides to control them (Setiawati et al., 2011).

In Indonesia, vegetative stages of hot pepper were injured by several insect pest such as cotton jassid (*Empoasca lybica* [*Jacobiasca lybica*]), thrips (*Thrips parvispinus*), oriental fruit fly (*Bactrocera dorsalis*), tropical armyworm (*Spodoptera litura* [*S. littoralis*]), and yellow tea mite (*Polyphagotarsonemus latus*). During fruiting and harvesting stages, the hot pepper were injured by cotton boll worm (*Helicoverpa armigera*) and oriental fruit fly (*Bactrocera dorsalis*) (Vos and Frinking, 1998). About 80% of farmers in Bangladesh use pesticides (Alam et al., 2016). However, the yield losses were still quite high, around 26% to 40% (Islam et al., 2020). Therefore, the chemical control methods need are evaluated.

Initial steps are necessary to develop appropriate control strategies is an information about the diversity of insect pests and their natural enemies in the hot pepper ecosystem. Such information can be used as a baseline to determine the next steps of sustainable pest control. Moekasan et al. (2004) reported that insecticide residue in hot pepper fruits in routinely sprayed conventional system have surpassed the maximum residue level.

The objective of this study was to determine the diversity and structure of insect communities in hot pepper ecosystem of Indonesia.

Methodology

Place and time of study

The study was conducted at the Margahayu Research Field Station, Lembang, West Java, Indonesia from March to October 2020.

Research design

The experiment was carried out on an unsprayed hot pepper crop sizing of size of 900 m² (30 m x 30 m). The 9 light traps (set at an interval of 15 m) and 5 yellow sticky traps (set at an interval of 15 m) were installed inside planting area and 4 fruit fly traps (set at an interval of 30 m) were installed outside planting area. All traps were installed on the planting day to trap the insect pests and natural enemies.

Pancanaka Agrihorti variety of hot pepper was grown using basic fertilizers that were applied at seven days before planting: chicken manure 20 t ha⁻¹, N 220 kg ha⁻¹, P₂O₅ 110 kg ha⁻¹ and K₂O 180 kg ha⁻¹ (Moekasan et al., 2014).

Weekly observations were made on 50 randomly selected sample plants and tagged, starting at 14 days after planting. On each sample plant, sucking insects such as aphids, thrips, whiteflies and leafhoppers found on the two shoots were recorded. While numbers of caterpillars or Lepidopteran larvae found on entire sample plant were counted. Numbers of insects caught in light traps was recorded twice a week, started from seven days after planting. The number and type of insects trapped on the yellow sticky traps and fruit fly traps were determined every week.

Insects identification

Insects sampled by each method were counted and separated according to species. Identification was carried out using insect identification keys by Borror et al. (1976) and Kashoven (1981).

Data analysis

The pest population recorded during the observation then subjected into the following formulas to obtain the value of insect abundance, diversity, evenness and dominance. There was no statistical analysis conducted following the calculation.

1. Relative abundance was calculated using the following formula (Krebs, 1978):

$$RA = \frac{n}{N} \times 100\% \quad (\text{Eq.1})$$

where RA = relative abundance; n = number of individuals of the focal insect species; N = total number of individual insect.

2. The Shannon-Wiener diversity index was calculated using the formula (Krebs, 1978):

$$H' = \sum_{i=1}^S Pi \ln Pi \quad (\text{Eq.2})$$

where H' = Shannon-Wiener diversity index; Pi = relative abundance of species i ; S = number of species found.

Classification of Shannon-Wiener diversity index values:

< 1 = low species diversity, low distribution of individuals per species and usually interpreted as low community stability

1–3 = medium species diversity, distribution of the number of individuals of each species is moderate and interpreted as the stability of the community is moderate

> 3 = high species diversity, distribution of the number of individuals of each species is high and community stability is interpreted as high

3. The evenness index or E was calculated using the following formula (Odum, 1971):

$$E = \frac{H'}{H_{max}} \quad (\text{Eq.3})$$

where E = evenness index; H' = Shannon-Wiener diversity index; $H_{max} = \ln S$ (S = number of species found).

Classification of evenness index values (Odum, 1971):

$0 < E \leq 0.5$ = depressed community

$0.5 < E \leq 0.75$ = unstable community

$0.75 < E \leq 1$ = stable community

4. Simpson's dominance index was calculated using the following formula (Odum, 1971):

$$C = \sum_{i=1}^S (Pi)^2 \quad (\text{Eq.4})$$

where C = dominance index; Pi = relative abundance of species i ; S = number of insect species found.

Classification of dominance index values (Simpson, 1946 cited in Odum (1971):

$0 < C \leq 0.5$ = low dominance

$0.5 < C \leq 0.75$ = medium dominance

$0.75 < C \leq 1$ = high dominance

Results and discussion

Insects abundance

Insects found during planting period of hot pepper belong to the order Coleoptera, Diptera, Hemiptera, Hymenoptera, Thysanoptera and Lepidoptera. Insects of the orders as a whole consisting of 18 families. All orders were found in vegetative, reproductive and harvest (Fig. 1).

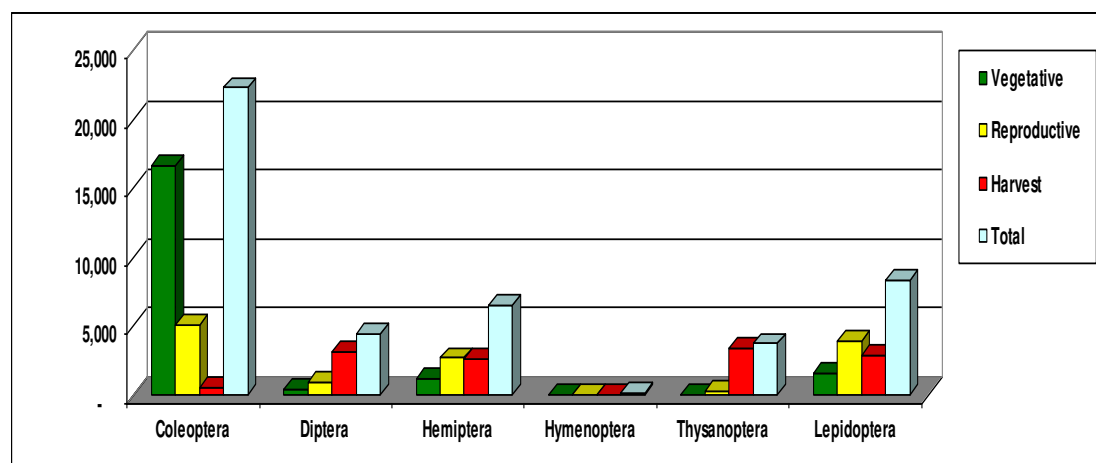


Figure 1. Population density within insect orders found in hot pepper ecosystem

The relative abundance of insects associated with hot pepper plants is shown in Table 1. The highest populations of insects were from the order Coleoptera during the vegetative and reproductive growth stages. For the order Diptera (fruit fly, the highest populations occurred during the harvesting phase when the hot pepper fruits as its' target were abundance. The populations of insects from the order Hemiptera which consists of leafhoppers, whiteflies and aphids increased in the reproductive and harvest growth stages, when the hot pepper leaves, which were their target, were dense. Compared to other orders, Hymenoptera populations was the lowest. Population densities of parasitoids was very low, even though the hot pepper field was not sprayed with insecticides. The intensively insecticides sprayed vegetable crops surrounding the hot pepper experiment field could be the cause of the low density of parasitoids in that area.

The populations of Thysanoptera which is the main pest of hot pepper in the vegetative and reproductive growth stages was low but increased when crop reached harvesting time. This might be because Thysanoptera competed with Hemiptera, which both have a same niche i.e. the shoots of hot pepper plants. The highest Lepidoptera populations occurred during the plants' reproductive growth stage, followed by harvest stage, that could be due to the abundance leaves and fruits in these stages.

Table 1. Relative abundance of insects in hot pepper ecosystem

Plant growth stages (weeks after transplanting [WAT])	Orders	Relative abundance (%)
Vegetative (0 – 8 WAT)	Coleoptera	83.5
	Diptera	2.0
	Hemiptera	6.2
	Hymenoptera	0.1
	Thysanoptera	0.4
	Lepidoptera	7.7
Reproductive (9 – 16 WAT)	Coleoptera	39.4
	Diptera	7.0
	Hemiptera	21.0
	Hymenoptera	0.4
	Thysanoptera	1.9
	Lepidoptera	30.4
Harvest (17 – 22 WAT)	Coleoptera	4.2
	Diptera	24.7
	Hemiptera	20.8
	Hymenoptera	0.5
	Thysanoptera	27.0
	Lepidoptera	22.9

During the vegetative stage, the insect population of the order Coleoptera which consisted of predatory and pest beetles was the largest with an abundance value of 83.5%. However, during this time, the populations of insect pests that feed on leaves were still low because the plants were still small. During the reproductive stage, insect populations within the order Coleoptera were the largest (39.4%) followed by Lepidoptera (30.4%) and Hemiptera (21%). Species of pests such as *Spodoptera litura* and *Aphis gossypii* increased as the plants grew. In addition, during the harvest stage, Thysanoptera had the highest populations (27.0%), followed by Diptera (24.7%), Lepidoptera (22.9%) and Hemiptera (20.8%). Populations of Hymenopteran parasitoids were the lowest, throughout the growing season.

Insects associated with hot pepper plants are shown in Table 2. The Coccinellidae family caught in sticky traps only contained one species i.e. *Menochilus sexmaculatus*, which is a predator of thrips, aphids and whiteflies. Nelly et al. (2012) and Efendi et al. (2016) stated *M. sexmaculatus* as a biological agent because its predatory activity increased with the increasing prey density.

The families Staphylinidae (*P. fuscipes*) and Cicindellidae (*Cicindella* sp.) caught by light traps, are important ground-dwelling predators with a wide host range, including eggs and larvae of Lepidoptera (Vijayahavendra et al., 2019; Zuharah and Maryam, 2020; Rewics and Jaskula, 2018). There were Scarabaeidae imago caught in the light traps, while its larvae commonly attacking crops root (Alfatah et al., 2020).

There were four families of Diptera caught in sticky traps, included (1) Tachinidae, the parasitoids of Lepidopteran larvae, (2) Cecidomyiidae species that known as rice plants pest, (3) Tephritidae (*Bactrocera* spp.), the hot pepper fruits pest, and (4)

Ceratopogonidae which were predators of small insects larvae of (Kalshoven, 1981; Kurniawati, 2015).

Table 2. Insects encountered in hot pepper ecosystem

No.	Family	Species	Number of individual insect	Nature of insect	Plant part harboured/prey
I. Coleoptera					
1.	Coccinellidae	<i>Menochilus sexmaculatus</i>	56	Predator	Thrips, aphids, whiteflies
2.	Staphylinidae	<i>Paederus fuscipes</i>	21,815	Predator	Eggs and larvae of Lepidoptera
3.	Cicindellidae	<i>Cicindella</i> sp.	17	Predator	Larvae of Lepidoptera
4.	Scarabaeidae	<i>Aphodius</i> sp.	408	Pest	Roots
II. Diptera					
5.	Tachinidae	<i>Tritaxis braueri</i>	2,533	Parasitoid	Larvae of Lepidoptera
6.	Cecidomyiidae	<i>Orseolia</i> sp.	93	Pest, visitor	Leaves
7.	Tephritidae	<i>Bactrocera</i> spp.	127	Pest	Fruits
8.	Ceratopogonidae	<i>Forcipomyia</i> spp.	1,667	Predator	Small larvae of insects
III. Hemiptera					
9.	Cicadellidae	<i>Empoasca</i> sp.	2,603	Pest	Leaves
10.	Aleyrodidae	<i>Bemisia tabaci</i>	873	Pest	Leaves
11.	Aphididae	<i>Aphis gossypii</i>	3,095	Pest	Leaves
IV. Hymenoptera					
12.	Ichneumonidae	<i>Diadegma semiclausum</i>	111	Parasitoid	Larvae of <i>P. xylostella</i>
13.	Braconidae	<i>Cotesia</i> sp.	27	Parasitoid	Larvae of <i>P. xylostella</i>
V. Thysanoptera					
14.	Thripidae	<i>Thrips parvispinus</i>	3,721	Pest	Leaves
VI. Lepidoptera					
15.	Noctuidae	<i>Spodoptera litura</i>	508	Pest	Leaves, fruits
		<i>Spodoptera exigua</i>	482	Pest	Leaves
		<i>Spodoptera frugiperda</i>	255	Pest, visitor	Corn
		<i>Plusia chalcites</i>	62	Pest	Leaves
		<i>Helicoverpa armigera</i>	384	Pest	Fruits
		<i>Agrotis ipsilon</i>	258	Pest	Young plants
16.	Gelechiidae	<i>Phthorimaea operculella</i>	612	Pest, visitor	Potato
17.	Plutellidae	<i>Plutella xylostella</i>	5,096	Pest, visitor	Cabbage
18.	Crambidae	<i>Crocidolomia binotalis</i>	688	Pest	Cabbage
Total			45,489		

The order Hemiptera was represented by three families, i.e.: Cicadellidae (*Empoasca* sp.), Aleyrodidae (*Bemisia tabaci*) and Aphididae (*Aphis gossypii*). *Empoasca* sp., the secondary pest of hot pepper plants, that could become a major pest if the population of the competitors are low and the temperature is extremely high (Vos and Frinking, 1998). *Bemisia tabaci* (Aleyrodidae), which known as the Gemini Yellow Virus vector, commonly found in low population as temporary visitor in hot pepper crops (Sudiono and Yasin, 2006). *Aphis gossypii* (Aphididae) is a pest of hot pepper plants as well as a vector for several types of viruses, including the mosaic virus in hot pepper (Suwandi, 2020).

The Hymenopteran found consisted of two families, namely Ichneumonidae (*Diadegma semiclausum*) and Braconidae (*Cotesia* sp.) which are larvae parasitoids of the cabbage pest, *Plutella xylostella* (Kahuthia-Gathu and Othim, 2019). The hot pepper fields were surrounded by brassica crops which explains why cabbage pest parasitoids were caught by the yellow sticky traps.

The Thysanopteran caught in yellow sticky traps consisted of one species, namely *Thrips. parvispinus*, which is the main pest of hot pepper plants (Murtiningsih et al., 2021).

The captured Lepidopteran insects consisted of four families i.e.: (1) Noctuidae family which included *Spodoptera litura*, *Spodoptera exigua*, *Plusia chalcites*, *Helicoverpa armigera*, and *Agrotis ipsilon* were hot pepper pests (Murtiningsih et al., 2021), but *Spodoptera frugiperda* is a pest of corn planted around hot pepper fields. Gelechiidae (*Phthorimaea operculella*) is a potato pest, while Plutellidae (*P. xylostella*) and Crambidae (*Crociodolomia binotalis*) are cabbage pests. Potatoes and cabbage were planted around the hot pepper fields. All Lepidopteran insects were found in light traps.

Species diversity

The species diversity index states the stability of an ecosystem. The higher the value of the species diversity index, the more stable the ecosystem. The diversity of species in the hot pepper ecosystem from the vegetative growth stage to harvest has increased, from low to medium diversity ($H' = 0.87$ to 2.32). The uniformity index in the vegetative growth stage showed that the number of species was low, then became unstable during the reproductive and harvest stages ($E = 0.28$ to 0.75). Meanwhile, the dominance index (C) decreased from 0.68 to 0.14 (Table 3).

Table 3. Diversity index, evenness index, and dominance index of insect species in hot pepper ecosystem

Plant growth stages	Diversity index	Evenness index	Dominance index
Vegetative (0 – 8 WAT)	0.87	0.28	0.68
Reproductive (9 – 16 WAT)	1.98	0.64	0.21
Harvest (17 – 22 WAT)	2.32	0.75	0.14

The three parameters of diversity indicated that at first the hot pepper ecosystem was unstable, depressed and medium dominated, because it was dominated by only one species from order Coleoptera. Furthermore, along with the growth of hot pepper plants, the number of leaves increased so that colonization of insect species increased. This condition caused the dominance of the species decreasing. Thus, the ecosystem stability increased, it was still moderately unstable. In the harvest stage, the fruit pest populations increased, which made the dominance of the species decreased. Although the stability of the hot pepper ecosystem slightly increased it was still at a moderate level.

Without insecticide applications, the high stability yield of the hot pepper ecosystem could not be maintained. That could be caused by the high correlation of pest population and yield reduction. Based on 17 years' observation, Furlan et al. 2020 found the significant correlation between seasonal *Agriotes* spp. (maize pest) adult catches in-field, subsequent wireworm populations, and plant damage/yield reduction in which plant damage increase with the increase of pest population. Paudel et al. 2021 additionally mentioned that in the context of climate change, the increasing temperatures at higher latitudes or temperate regions could resulting the higher insect abundance and consequently increasing the crop losses.

There was limited natural enemies species of chili pepper pest found in the field, and only a low number of *M. sexmaculatus* was found in the field. Therefore, the population of natural enemies should be increased to be able to suppress pest population, reduce the dominance of pest species and increase the ecosystem stability. Habitat manipulation, for instance the implementation of intercropping of hot pepper and refugee flowering plants such as maize, basil and marigold, could conserve the natural enemies since this system provide nectar, pollen and shelter (Kumar et al., 2013; Aldini et al., 2019; Anggraini et al., 2020; Habibi and Fuadah, 2021). Intercropping planting system could also reduce pests populations and crop damage (Ellahi et al., 2017). Letourneau et al. (2011) reported that presence of refugee plants could increase the number of natural enemies by 72% and reduce the number of pest population by 74%.

Implementation of control threshold is the other tactic for reducing insecticide application. Setiawati et al. (2013) reported that it could reduce insecticide application up to 73.33%. Moekasan et al. (2004) mentioned that it could reduce the pesticide residue in fruits under the maximum residue level. Additionally, it is important to develop genetically resistance hot pepper varieties against various detected pests. Until recently, the work on developing chili pepper resistance against pests that have been done included against *T. parvispinus* and *T. occidentalis* (Maharijaya et al., 2011) and against fruit fly (Kirana et al., 2021).

Conclusions

The insects found in the hot pepper ecosystem belong to the Order of Coleoptera (four families), Diptera (four families), Hemiptera (three families), Hymenoptera (two families), Thysanoptera (one family) and Lepidoptera (four families). Altogether there were 23 species and 45,489 individuals. The Shannon-Wiener (H') diversity index showed that the hot pepper ecosystem had low to moderate diversity, which had increased from initial planting to harvest. The species evenness index (E) was depressed in the vegetative growth stage and increased became unstable in reproductive and harvest stages. Simpson's dominance index (D) decreased along with increasing diversity, from the medium to the low. The role of natural enemies, especially the parasitoid *M. sexmaculatus* needed to be increased to suppress the key pest population.

Funding statement. We would like to declare that the research of this manuscript was funded by the DIPA 2020 of the Indonesian Vegetable Research Institute (IVEGRI), Indonesian Agency for Agricultural Research and Development, Ministry of Agricultural of the Republic of Indonesia (Grant number: 1804.409.001.051.B).

Acknowledgements. We thank to Prof. Dr. B. M. Shepard (Professor Emeritus in Clemson University, South Carolina, United States) and Prof. Kazuki Tsuji (Laboratory of Subtropical Zoology, Department of Environmental Sciences and Technology, Faculty of Agriculture, University of the Ryukyus, Japan) for valuable comments and corrected English grammar of the manuscript.

REFERENCES

- [1] Alam, M. Z., Haque, M. M., Islam, M. S., Hossain, E., Hassan, S. B., Hossain, M. S. (2016): Comparative study of integrated pest management and farmers practices on sustainable environment in the rice ecosystem. – International Journal of Zoology 7286040. <http://dx.doi.org/10.1155/2016/7286040>.

- [2] Aldini, G. M., Martono, E., Trisyono, Y. A. (2019): Diversity of natural enemies associated with refugee flowering plants of *Zinnia elegans*, *Cosmos sulphureus*, and *Tagetes erecta* in rice ecosystem. – *Jurnal Perlindungan Tanaman Indonesia* 23(2): 285-291. DOI: 10.22146/jpti.33947.
- [3] Alfatah, R. F., Witjaksono, Harjaka, T. (2020): Effect of soil moisture on *Lepidiota stigma*: number of flying beetles and the vertical movement of larvae in the soil. – *Journal of Science, Technology and Entrepreneurship* 2(1): 17-24. <http://www.ejournal.umbandung.ac.id/index.php/jste>.
- [4] Anggraini, E., Pardingotan, R., Herlinda, S., Irsan, C., Harun, M. U. (2020): Diversity of predatory arthropods in soybean (*Glycine max* L.) refugia. – *Journal of Applied Agricultural Sciences and Technology* 4(2): 101-117. <https://doi.org/10.32530/jaast.v4i2.165>.
- [5] Borror, D. J., DeLong, D. M., Triplehorn, C. A. (1976): *An Introduction to the Study of Insects*. 4th Ed. – Holt, Rinehart and Winston, New York.
- [6] Chakrabarty, S., Islam, A. K. M. A., Mian, M. A. K., Ahamed, T. (2019): Combining ability and heterosis for yield and related traits in hot pepper (*Capsicum annuum* L.). – *The Open Agricultural Journal* 13(1): 34-43. DOI: 10.2174/1874331501913010034.
- [7] Efendi, S., Yaherwandi Nelly, N. (2016): Study of preference and functional response of *Menochilus sexmaculatus* and *Coccinella transversalis* in several preys. – *Proceeding of National Seminar of Indonesian Biodiversity Community* 2(2): 125-131. DOI: 10.13057/psnmbi/m020201.
- [8] Ellahi, F., Lanjar, A. G., Chang, B. H., Magsi, F. H., Khushk, G. M., Raza, A., Chang, A. H., Miano, F. N. (2017): Insect biodiversity on mix cropping of chilli and onion crops. – *International Journal of Fauna and Biological Studies* 4(3): 14-19.
- [9] Farid, M., Subekti, N. A. (2012): Review of production, consumption, distribution and price dynamics of hot pepper in Indonesia. – *Bulletin of Scientific Research and Development* 6(2): 211-234.
- [10] Furlan, L., Contiero, B., Chiarini, F., Benvegnù, I., Tóth, M. (2020): The use of click beetle pheromone traps to optimize the risk assessment of wireworm (Coleoptera: Elateridae) maize damage. – *Scientific Reports* (2020) 10: 8780. <https://doi.org/10.1038/s41598-020-64347-z>.
- [11] Ganefianti, D. W., Fahrurrozi, F., Armadi, Y. (2017): Hybrid performance testing of hot pepper (*Capsicum annuum* L.) for resistance to yellow leaf curl Begomovirus grown in lowland environments. – *Sabrao Journal of Breeding and Genetics* 49(2): 179-191.
- [12] Habibi, I., Fuadah, A. S. (2021): Effect of refugee plants on the population of natural enemy of *Nilaparvata lugens* in rice (*Oriza sativa* L.). – *F. Saintek* 4(2): 319-325.
- [13] Hundall, J. S., Dhall, R. K. (2004): Breeding for hybrid hot pepper. – *Journal of New Seeds* 6(2-3): 31-50.
- [14] Islam, A. H. M. S., Schreinemachers, P., Kumar, S. (2020): Farmers' knowledge, perception and management of hot pepper anthracnose disease in Bangladesh. – *Crop Protection* 133: 105139. <https://doi.org/10.1016/j.cropro.2020.105139>.
- [15] Kahuthia-Gathu, R., Othim, S. T. O. (2019): Effects of two cultivated *Brassica* spp. on the development and performance of *Diadegma semiclausum* (Hymenoptera: Ichneumonidae) and *Cotesia vestalis* (Hymenoptera: Braconidae) parasitizing *Plutella xylostella* (Lepidoptera: Plutellidae) in Kenya. – *Journal of Economic Entomology* 112(5): 2094-2102. <https://doi.org/10.1093/jee/toz144>.
- [16] Kalshoven, L. G. E. (1981): *Pests of Crops in Indonesia*. – PT Ichtiar Baru - van Hoeve, Jakarta.
- [17] Kerketta, A., Collis, J. P., Tiekey, M., Lal, R., Singh, N. V. (2018): Evaluation of hot pepper (*Capsicum annuum* L.) genotypes for growth, yield and quality characters under Allahabad agro climatic condition. – *International Journal of Pure and Applied Bioscience* 6(4): 451-455. DOI: <http://dx.doi.org/10.18782/2320-7051.5367>.

- [18] Kirana, R., Karjadi, A. K., Faizal, Syamsudin, T. S. (2021): The expression of chili defense gene due to oviposition of fruit fly (*Bactrocera dorsalis*). – IOP Conf. Series: Earth and Environmental Science 752(2021): 012044. DOI: 10.1088/1755-1315/752/1/012044.
- [19] Krebs, C. J. (1978): Ecology: The Analysis of Distribution and Abundance. – 3rd Ed. Harper and Row Publishers, New York.
- [20] Kumar, L., Yogi, M. K., Jagdish, J. (2013): Habitat manipulation for biological control of insect pests: A review. – Research Journal of Agriculture and Forestry Sciences 1(1): 27-31.
- [21] Kurniawati, N. (2015): Diversity and abundance of natural enemy of pest at manipulated rice habitat using flowering plant. – Agricultural Science 18(1): 31-36.
- [22] Letourneau, D. K., Ambrecht, I., Rivera, B. S., Lerna, J. M., Carmona, E. J. (2011): Does plant diversity benefit agroecosystems? A synthetic review. – Ecological Application 21: 9-21.
- [23] Lin, S. W., Chou, Y. Y., Shieh, H. C., Ebert, A. W., Kumar, S., Mavlyanova, R., Rouamba, A., Tenkouano, A., Afari-Sefa, V., Gniffke, P. A. (2013): Pepper (*Capsicum* spp.) germplasm dissemination by AVRDC-The World Vegetable Center: an overview and introspection. – Chronica Horticulture 53(3): 21-27.
- [24] Loizzo, M. R., Pugliese, A., Bones, M., Menichini, F., Tundis, R. (2015): Evaluation of chemical profile and antioxidant activity of twenty cultivars from *Capsicum annuum*, *Capsicum baccatum*, *Capsicum chacoense* and *Capsicum chinense*: A comparison between fresh and processed peppers. – Food Science and Technology 64: 623-631.
- [25] Maharijaya, A., Vosman, B., Steenhuis-Broers, G., Harpenas, A., Purwito, A., Visser, R. G. F., Voorrips, R. E. 2011. Screening of pepper accessions for resistance against two thrips species (*Frankliniella occidentalis* and *Thrips parvispinus*). – Euphytica 177: 401410. DOI: 10.1007/s10681010-0227-x.
- [26] Mariyono, J. (2016): Integrated disease management for chili farming in Brebes and Magelang-Central Java: Social economic impacts. – Agriekonomika 5(2): 114-124. <http://journal.trunojoyo.ac.id/agriekonomika>.
- [27] Materska, M. (2014): Bioactive phenols of fresh and freeze-dried sweet and semi-spicy pepper fruits (*Capsicum annuum* L.). – Journal of Function Foods 7: 269-277.
- [28] Ministry of Agriculture, Republic of Indonesia (2019): National productivity of hot pepper according to the provinces in 2015-2019. – <http://www.pertanian.go.id/home/?show=page&act=view&id=61> (accessed July 1, 2021).
- [29] Moekasan, T. K., Suryaningsih, E., Sulastrini, I., Gunadi, N., Adiyoga, W., Hendra, A., Martono, M. A., Karsum (2004): Technical and economical feasibility of integrated pest management technology in intercropping system of shallot and hot pepper. – Journal of Horticulture 14(3): 188-203.
- [30] Moekasan, T. K., Prabaningrum, L., Adiyoga, W., dePutter, H. (2014): Practical Guide to Red Hot Pepper Cultivation Based on IPM Conception. – PT Penebar Swadaya, Jakarta.
- [31] Murtiningsih, R., Kirana, R., Hermanto, C. (2021): Evaluation of hot pepper accessions for resistance against *Thrips* sp. (Thysanoptera: Thripidae). – IOP Conference Series: Earth and Environmental Science 653(2021)012077. DOI: 10.1088/1755-1315/653/1/012077.
- [32] Nelly, N., Trizelia, Shuhadah, Q. (2012): Functional response of *Menochilus sexmaculatus* Fabricius (Coleoptera: Coccinellidae) on *Aphis gossypii* (Glover) (Homoptera: Aphididae) at different ages of hot pepper plants. – Indonesian Journal of Entomology 9(1): 23-31. DOI: 10.5994/jei.9.1.23.
- [33] Odum, E. P. (1971): Fundamentals of Ecology. – WB Saunders Publisher, London.
- [34] Padilha, H. K. M., Barbieri, R. L. (2016): Plant breeding of hot pepper (*Capsicum*, Solanaceae). A review. – Australian Journal of Basic and Applied Sciences 10(15): 148-154.

- [35] Paudel, S., Kandel, P., Bhatta, D., Pandit, V., Felton, G. W., Rajotte, E. G. (2021): insect herbivore populations and plant damage increase at higher elevations. – *Insects* 12: 1129. <https://doi.org/10.3390/insects12121129>.
- [36] Pugliese, A., Loizzo, M. R., Tundis, R., O’Callaghan, Y., Menichini, F., O’Brien, N., Galvin, K. (2013): The effect of domestic processing in the content and bioaccessibility of carotenoids from hot pepper (*Capsicum* species). – *Food Chemistry* 141: 2606-2613.
- [37] Rewicz, T., Jaskula, R. (2018): Catch fast and kill quickly: do tiger beetles use the same strategies when hunting different types of prey? – *Peer J.* 6: e5971. DOI: 10.7717/peerj.5971.
- [38] Saleh, B. K., Omer, A., Teweldemedhin, B. (2018): Medicinal uses and health benefits of hot pepper (*Capsicum* spp.): a review. – *MOJ Food Processing and Technology* 6(4): 325-328.
- [39] Setiawati, W., Murtiningsih, R., Hasyim, A. (2011): Laboratory and field evaluation of essential oils from *Cymbopogon nardus* as oviposition deterrent and ovicidal activities against *Helicoverpa armigera* on chili pepper. – *Indonesian Journal of Agricultural Science* 12(1): 9-16.
- [40] Setiawati, W., Sumarni, N., Koesandriani, Y., Hasyim, A., Uhan, T. S., Sutarya, R. (2013): Implementation of integrated pest management for mitigation of climate change on chili pepper. – *Journal of Horticulture* 23(2): 174-183.
- [41] Shetty, A. A., Maganum, S., Managanvi, K. (2013): Vegetables as sources of antioxidants. – *Journal of Food and Nutritional Disorders* 2(1): 1-5.
- [42] Soetiarso, A. T., Setiawati, W. (2010): Kajian teknis dan ekonomis sistem tanam dua varietas cabai merah di dataran tinggi. – *Journal Hortikultura* 20(3): 284-298.
- [43] Sudiono, N., Yasin (2006): Characterization of whitefly (*Bemisia tabaci*) as gemini virus vector based on RAPD-PCR. – *Journal of Tropical Plant Pests and Diseases* 6(2): 113-119.
- [44] Suwandi, S., Irsan, C., Muslim, A., Herlinda, S. (2020): Protection of hot pepper from mosaic virus disease and *Aphis gossypii* by a fermented water extract of compost. – *IOP Conference Series: Earth and Environmental Science* 468 012043.
- [45] Vijayarahavendra, R., Lakshmi, K. V., Shanker, C., Seetalam, M., Jagadeeshwar, R., Raju, C. H. D. (2019): Olfactory response of rove beetle *Paederus fuscipes* (Curtis) to flower volatiles?. – *Journal of Pharmacognosy and Phytochemistry* 8(1): 2258-2260.
- [46] Vos, J. G. M., Frinking, H. D. (1998): Pests and diseases of hot pepper (*Capsicum* spp.) in tropical lowlands of Java, Indonesia. – *Journal of Plant Protection in the Tropics* 11(1): 53-71.
- [47] Zuharah, W. F., Maryam, S. (2020): Multifarious roles of feeding behaviors in rove beetle, *Paederus fuscipes*. – *Sains Malaysiana* 49(1): 1-10. <http://dx.doi.org/10.17576/jsm-2020-4901-01>.

BENTHIC MACROINVERTEBRATE DIVERSITY AND WATER QUALITY BIOASSESSMENT OF THE CENTRAL LAKE IN QINGTONGXIA RESERVOIR WETLAND NATURE RESERVE, CHINA

EKOKO, W. A.^{1,2} – QU, G. J.³ – LIU, M. H.^{1*} – SHABANI, I. E.^{1,4}

¹*Department of Ecology, College of Wildlife and Protected Area, Northeast Forestry University, Harbin P.O. Box 150040, China*

²*Department of Water and Forest, University of Kisangani, PO Box 2012 – Kisangani, Democratic Republic of the Congo*

³*Key Laboratory of Animal Production, Product Quality and Security, Ministry of Education, Jilin Agriculture University, Changchun P.O. Box 130118, China*

⁴*Official University of Bukavu, P.O. Box 570-Bukavu, Democratic Republic of the Congo*

*Corresponding author
e-mail: manhong@nefu.edu.cn

(Received 5th Feb 2022; accepted 20th May 2022)

Abstract. The lake is a dynamic lentic ecosystem subject to different pressures that influence and compromise its ecological structure. The main aim of this study was to evaluate the potential of using the benthic macroinvertebrate to assess the water quality. Ten sites were sampled in spring, summer and autumn in 2021. We collected 969 individuals of benthic macroinvertebrates belonging to 42 species and 22 families. *Leander modestus* (Palaemonidae) with 48.71%, followed by *Radix ovata* (Lymnaeidae) with 18.27% were the most abundant species and collected at all study sites in all seasons. We used biological indices, including Shannon index (H'), Pielou's evenness index (J) and biological monitoring working party (BMWP). This study showed H' scores ranged from 0.65 to 2.18, Pielou's evenness index (J) scores fluctuated from 0.21 to 0.68 and BMWP values assessed ranging from 19 to 40. Our findings showed that the water quality of the Central Lake ranged from polluted to slightly impacted or "poor to good". Further water resource management and the pollution control should be a high priority to prevent benthic organisms in this lake.

Keywords: water pollution, Shannon-Wiener diversity index (H'), Pielou's evenness index (J), biological monitoring working party (BMWP)

Introduction

Freshwater systems provide unique biotopes that enhance ecological services and the survival of different life forms (Turner et al., 2000; Johnson and Pflugh, 2008; Zhang et al., 2010). Systematically, monitoring of a freshwater resource (such as the lake) is necessary to understand its socioeconomic function (Turner et al., 2000). The Central Lake, one of the largest water bodies in the Qingtongxia Reservoir Wetland Nature Reserve is mainly covered on the bottom channels by submerged plants, especially reeds. Currently, factors such as human activities and climate change are obstructing the stability of most freshwater environments, thereby causing a loss in diversity of benthic macroinvertebrates (Hilsenhoff, 1988). While, macroinvertebrates are an important biological component of freshwater systems and their population changes and community structure affect the function of the ecosystem directly (Krisanti et al., 2017). Benthic

macroinvertebrates have become increasingly important in biological monitoring projects because of their rapid response to water environmental changes (Mlambo et al., 2011; Liu, 2012; Bird et al., 2013). Thus, the assessment of the benthic macroinvertebrate community structure, their abundance and functional groups, and the factors that affect its distribution in the Central Lake is necessary, because macroinvertebrates are widely accepted and irreplaceable biological indicators in the monitoring of water quality, ecological conservation and management of freshwater environments (Krisanti et al., 2017; Shabani, 2021). Despite their ecological importance, the richness and diversity of benthic macroinvertebrates are unknown in the Central Lake. So, understanding the behavior of the benthic macroinvertebrate composition under seasonal environment conditions is necessary to support a healthy and productive freshwater environment (Liu, 2012; Shabani, 2021).

Diversity indices are used to measure the species richness and evenness of diversity (Magurran, 2004; Hosokawa et al., 2021). Because these indices aid in the interpretation of changes in benthic communities, they can be used as ecological indicators of water quality status (Chariton et al., 2016), and have advantages over several other freshwater assessment approaches, such as physical and chemical evaluations, because of their more realistic application under field conditions (Chapman, 2002). For benthic macroinvertebrate communities, diversity indices are usually estimated from counts of individuals obtained by using a real unit sampler such as bottom sampler (Wong and Dowd, 2015; Hosokawa et al., 2021; Momota and Hosokawa, 2021). The species richness, Shannon-Wiener index and Pielou's evenness are diversity indices that are commonly estimated from these variables, and they all tend to decrease with increasing water environmental contamination (Johnston and Roberts, 2009).

Besides, as for physicochemical indexes of water quality; the species composition, diversity of benthic macroinvertebrates and biological monitoring working party (BMWP) can reflect water condition better as been widely used globally that evaluating water quality pollution (Hong and Chen, 2002; Ren et al., 2011; Shabani, 2021). In this paper, the benthic macroinvertebrate diversity, water quality condition, and relationships between functional feeding groups and environmental variables were investigated and studied, aiming at providing reference for the water resources management and the pollution control of the Central Lake.

Materials and methods

Study area

The Central Lake is located in the Qingtongxia Reservoir Wetland Nature Reserve, between Zhongning county and Qingtongxia city in the middle part of upper reaches of the Yellow River, with a total area of 197.376 ha from 105°47'30" to 106°00' 11"E, and from 37°33'14" to 37° 53' 22"N. The vegetation that grows naturally in the wetland, including *Suaeda glauca*, *Kalidium cuspidatum*, *Nitraria tangutorum*, *Nitraria sibirica*, *Tripolium vulgare*, *Sophora alopecuroides*, *Phragmites australis*, *Setaria viridis*, *Karelinia caspia*, *Halerpestes*, *Xanthium sibiricum*, *Plantago asiatica*, *Artemisia argyi*, *Artemisia annua*, *Heteropappus altaicus*, *Saussurea japonica*, *Achnatherum splendens*, *Taraxacum mongolicum*, *Lepidium apetalum*, etc.; aquatic plants are widely distributed. The main aquatic plants are *Phragmites australis*, *Typha angustifolia*, and *Typha angustata*. The main species of protected birds in the reserve, including *Ciconia nigra*, *Mergus squamatus*, *Gypaetus barbatus*, *Haliaeetus leucoryphus*, *Haliaeetus albicilla*,

Otis tarda, *Tetrax tetrax*, and *Larus relictus*. In the Central Lake, the culture of Cyprinidae fish has been carried out until 2017. Since 2017, fish culture has been stopped for ecological restoration reasons in this lake. For this research, ten sampling sites were selected based on prospected the Central Lake and accessibility. The latitude and longitude of these ten sampling sites were determined using a portable global positioning system (Table 1).

Table 1. Ten sampling site coordinates

Site	Latitude	Longitude
S1	N37°45'33.00"	E105°55'9.10"
S2	N37°45'31.85"	E105°55'10.89"
S3	N37°45'28.79"	E105°55'11.58"
S4	N37°45'9.96"	E105°55'17.80"
S5	N37°45'9.36"	E105°55'14.07"
S6	N37°45'6.48"	E105°55'12.11"
S7	N37°45'4.08"	E105°55'12.35"
S8	N37°45'15.45"	E105°54'29.88"
S9	N37°45'16.55"	E105°54'33.47"
S10	N37°45'10.61"	E105°54'26.90"

Collection methods and analyses

Data were collected at ten sampling sites in spring, summer and autumn in 2021. In each sampling site, environmental parameters were measured, including water temperature (°C), electrical conductivity (mS/m), pH, water depth (cm), and transparency (cm) using a multiparameter probe YSI Professional (YSI 06E2512AG). Additionally, water samples (500 ml) were collected and transported to the laboratory for further analyses. In the laboratory, we analyzed water samples to determine the concentrations of ammonium (mg/L), total nitrogen (mg/L), total phosphorus (mg/L), dissolved oxygen (mg/L), and chemical oxygen demand with chrome index (mg/L) following the standard protocol for the examination of water and wastewater described by EPBC (Environmental Protection Bureau of the People's Republic of China, 2002).

Benthic macroinvertebrate samples were collected using D-net of 500-µm mesh following the standard procedures (Pinto et al., 2021). In each study site, three replicate samples were done along one meter of the substrate and aquatic plants, resulting in a composite sample. The samples were preserved in labelled bottles containing 75% ethanol for identification and counting in the laboratory. Benthic macroinvertebrate populations were identified to species or genus level under a binocular and a microscope "Motic" at magnification (10 to 40 times) using identification keys of Tong (1996); Qi (1998); Tsuda (1998); Epler (2001); Duan et al. (2010); Wang and Wang (2011); Ding et al. (2014); Zhou et al. (2015); Lu et al. (2017). Benthic macroinvertebrate taxa were classified into five functional feeding groups (FFG), including gathering collectors (GC), omnivores (OM), predators (PR), scrapers (SC), and shredders (SH) (Cummins, 1973; Cummins and Klug, 1979).

Statistical analysis and water quality assessment

Benthic macroinvertebrates were characterized regarding abundances and species richness. Shannon-Wiener diversity index “ H' ” (Shannon, 1949) and Pielou’s evenness index “ J ” (Pielou, 1966) were integrated to analyze the diversity of benthic macroinvertebrates in the study sites. As well as the biological monitoring working party (BMWP) was calculated for each sampling site. The BMWP score is the sum of the values for all families present in the sample (Walley and Hawkes, 1996; Zeybek et al., 2014). Pollution-sensitive families have high scores and pollution-tolerant one low-scores (Walley and Hawkes, 1996, 1997). Biological indices can reflect the comprehensive effects of pollutants on the benthic macroinvertebrate community and long-term accumulation of pollutants objectively. This study used the ecological approaches to evaluate the water quality of the Central Lake. The status of water quality was assessed by H' , J and BMWP (Table 2).

Table 2. Classes of water quality based on H' , J and BMWP (China Environmental Monitoring Station, 2021)

	Very poor	Poor	Moderate	Good	Very Good
Shannon-Weiner index (H')	$H = 0$	$0 < H \leq 1$	$1 < H \leq 2$	$2 < H \leq 3$	$3 < H$
Pielou’s evenness index (J)	$J = 0$	$0 < J \leq 0.3$	$0.3 < J \leq 0.5$	$0.5 < J \leq 0.8$	$0.8 < J \leq 1$
BMWP	$BMWP \leq 10$	$11 \leq BMWP < 22$	$22 \leq BMWP < 32$	$32 \leq BMWP < 43$	$43 \leq BMWP$

To perceive relationships between the physicochemical parameters and benthic macroinvertebrate FFGs, a canonical correspondence analysis (CCA) was conducted using vegan package in R software (version 4.1.2; R Core Team, 2017). Previously, before the latter analysis, physicochemical variables were standardized, and redundant variable was removed for the analysis. As data did not fit to the normal distribution, we employed the non-parametric Kruskal-Wallis test using the Rcmdr package for comparing means, and test was considered significant at the $p < 0.05$ level.

Results and discussion

Physicochemical parameters

Table 3 presented mean values of physicochemical parameters measured in each site over the sampling period. Overall, comparing the mean values of water parameters in the three seasons, the electrical conductivity, dissolved oxygen, transparency, total phosphorus and chemical oxygen demand with chrome index increased in spring. Kruskal–Wallis test showed that electrical conductivity, dissolved oxygen and chemical oxygen demand with chrome index varied significantly in spring ($p = 0.000$). Unlike transparency and total phosphorus did not change significantly with seasons ($p = 0.6653$, $p = 0.1103$, respectively). Water temperature and pH increased significantly in summer ($p = 0.0000$). Moreover, it was recorded that water depth, concentrations of ammonium and total nitrogen varied significantly in autumn ($p = 0.000$).

The highest water temperature value in summer could be a natural phenomenon in the study area. Shabani (2021) reported that the highest water temperature during summer was affected by the temporary warming of water due to high radiation in Sanjiang National Nature Reserve, China. Manjare et al. (2010) highlighted that the increase of

water temperature in summer is due to low water level, high air temperature and a clear atmosphere. Water temperature is an important factor that influences the chemical and biological characteristics of waterbodies (Shabani, 2021). We recorded high mean value of pH in summer. pH is one of the most significant among the operational water quality characteristics (Dede et al., 2013). It is an important parameter that can influence chemical and biological processes in the freshwater systems (Rosenberg and Resh, 1993; Resh, 1995; Dow and Zampella, 2000; Teferi et al., 2013). Besides, it is highlighted that variations in pH within 24h time can be caused by photosynthesis and respiration cycles of algae in eutrophic waters (Hawkins, 1978; Teferi et al., 2013). pH control is important for adequate water disinfection during the water treatment process (WHO, 2011). Moreover, pH level of the surface water may affect the respiratory cycle of aquatic organisms (Dede et al., 2013). Riley and Chester (1971); and Manjare et al. (2010) found that pH values in the aquatic ecosystems were influenced by carbon dioxide during photosynthesis activities, respiration and decomposition (Suratman et al., 2014). The highest mean value of dissolved oxygen was recorded in spring. Pinto et al. (2021) reported that the low dissolved oxygen levels recorded in some sites can be associated with the eutrophic conditions. Conductivity is a measure of salinity in the water and it is related to the type and concentration of dissolved ions in water (Dede et al., 2013). Our results showed that the mean value of electrical conductivity was high in spring. The increases in surface water salinity pose the greatest threat to the biodiversity of freshwater ecosystems (Nielsen and Brock, 2009), given that increasing salinity in freshwater systems often leads to reductions in biodiversity (Mabidi et al., 2017).

Table 3. Means and standard deviations of environmental parameters. WT = water temperature (°C), EC = electrical conductivity (ms/m), DO = dissolved oxygen (mg/L), NH₄⁺ = ammonium (mg/L), WD = water depth (cm), Trans = transparency (cm), TN = total nitrogen (mg/L), TP = total phosphorus (mg/L), COD_{Cr} = chemical oxygen demand with chrome index (mg/L)

Physicochemical variables	Spring	Summer	Autumn	p-value
WT °C	25.85±1.12	27.21±0.50	3.12±0.52	0.0000***
EC (mS/m)	1.82±0.82	1.78±0.14	0.91±0.08	0.0006***
DO (mg/L)	15.00±4.28	5.94±0.69	8.83±1.88	0.0000***
pH	8.32±0.37	8.80±0.39	7.29±0.50	0.0000***
NH ₄ ⁺ (mg/L)	2.01±5.73	1.51±2.73	5.73±27.12	0.0000***
WD (cm)	86.50±16.17	123.35±27.29	137.50±10.87	0.0004***
Trans (cm)	62.00± 14.57	57.12±10.53	60.50±6.35	0.6653
TN (mg/L)	1.44±0.92	2.18±1.99	6.40±0.36	0.0002***
TP (mg/L)	0.25±0.06	0.21±0.17	0.21±0.06	0.1103
COD _{Cr} (mg/L)	31.09±7.09	19.06± 9.37	7.27±1.11	0.0000***

Benthic macroinvertebrate composition and water quality assessment

A total of 969 individuals of benthic macroinvertebrates were collected from ten sampling sites of the Central Lake belonging to 42 species, 24 genera, 22 families and 9 orders. Among all species, *Leander modestus* (Palaemonidae) with 48.71%, followed by *Radix ovata* (Lymnaeidae) with 18.27% were the most abundant species and collected at all study sites in all seasons (Table 4).

Table 4. Benthic macroinvertebrate species, functional feeding groups (FFG) and abundances at ten sites of the Central Lake

Species	FFG	S1	S2	S3	S4	S5	S6	S7	S8	S9	S10
<i>Branchiura sowerbyi</i>	GC	2	0	0	0	0	0	0	0	0	0
<i>Chironomus flaviplumus</i>	GC	0	0	23	0	0	0	0	0	0	1
<i>C. pallidivittatus</i>	GC	0	0	0	0	0	0	1	0	0	0
<i>C. riparius</i>	GC	2	3	3	0	0	0	0	0	0	0
<i>C. sinicus</i>	GC	0	0	0	8	0	0	0	0	0	0
<i>Chironomus</i> sp.	GC	0	2	2	3	0	0	0	0	0	5
<i>Dicrotendipes pelochloris</i>	GC	0	0	0	0	2	1	0	0	0	0
<i>Dicrotendipes lobifer</i>	GC	0	0	0	0	1	0	0	0	0	0
<i>Dicrotendipes</i> sp.	GC	0	0	0	0	0	1	0	0	0	0
<i>D. tritonus</i>	GC	0	0	2	0	0	0	0	0	0	0
<i>Paracricotopus</i> sp.	GC	0	0	0	1	0	0	0	4	12	11
<i>Leander modestus</i>	OM	116	15	19	168	22	57	45	11	5	14
<i>Macrobrachium nipponense</i>	OM	0	0	1	0	0	0	0	0	0	0
<i>Agriocnemis lacteola</i>	PR	2	1	1	2	1	1	8	11	2	15
<i>Agriocnemis</i> sp.	PR	0	0	0	0	0	4	0	0	0	0
<i>Belostoma bakeri</i>	PR	0	0	0	0	0	0	1	0	0	0
<i>Bezzia</i> sp.	PR	0	0	0	0	0	1	0	0	0	0
<i>Buenoa scimitra</i>	PR	0	0	0	0	0	1	0	0	0	0
<i>Callicorixa culnerata</i>	PR	0	0	3	0	0	0	0	0	0	0
<i>Cercion</i> sp.	PR	0	0	6	0	0	0	0	0	0	0
<i>Corisella decolor</i>	PR	8	1	0	0	4	1	0	3	4	4
<i>Corixa substriata</i>	PR	0	0	23	0	1	0	0	0	0	0
<i>Cybister</i> sp.	PR	0	1	0	1	0	1	0	1	0	2
<i>Davidius</i> sp.	PR	0	0	0	0	0	0	0	0	0	1
<i>Dicranota</i> sp.	PR	0	0	0	0	0	0	0	0	1	0
<i>Dineutus</i> sp.	PR	0	0	1	0	0	0	0	1	1	0
<i>Diplonychus rusticus</i>	PR	0	0	1	0	0	0	0	16	1	10
<i>Dytiscus</i> sp.	PR	1	3	0	0	0	1	0	0	0	0
<i>Hebrus sobrinus</i>	PR	0	0	1	0	0	0	0	0	0	0
<i>Hydrochara</i> sp.	PR	0	1	0	0	0	0	0	0	0	0
<i>Lestes</i> sp.	PR	0	1	0	3	0	0	0	0	0	0
<i>Micrommata</i> sp.	PR	0	1	0	0	0	0	0	0	1	1
<i>Micronecta</i> sp.	PR	0	1	0	0	1	1	0	0	0	0
<i>Pelocoris</i> sp.	PR	0	0	0	0	0	0	0	0	0	1
<i>Sinictino gomphus</i>	PR	0	0	0	0	0	0	1	0	0	0
<i>Gyraulus convexiusculus</i>	SC	1	2	1	0	7	0	1	3	0	19
<i>Radix ovata</i>	SC	28	19	28	8	6	13	3	62	5	5
<i>Bagous</i> sp.	SH	0	0	1	1	0	0	1	1	0	0
<i>Galerucella</i> sp.	SH	0	0	2	0	0	1	1	0	0	0
<i>Polypedilum nubifer</i>	SH	0	0	2	0	3	6	4	0	0	0
<i>P. paraviceps</i>	SH	0	1	0	0	0	0	0	0	0	0
<i>P. scalaenum</i>	SH	4	0	0	0	0	0	0	0	0	0
Total		164	52	120	195	48	90	66	113	32	89

Benthic macroinvertebrate species richness and Shannon-Wiener diversity index were high at site S3 (Table 4, Figure 1a,b), while the highest abundance was recorded at site S4 (Table 4) and the maximum Pielou's evenness index was recorded at sites S9 and S10 (Figure 1c). The results showed that the species abundance, richness, Shannon-Wiener index and Pielou's evenness index did not vary significantly with seasons among study sites (Kruskal–Wallis test, $p = 0.572$, $p = 0.864$, $p = 0.866$, $p = 0.536$, respectively). The BMWP values assessed ranging from 19 to 40 with the highest value at site S3 (Figure 1d). Kruskal–Wallis test results ($p > 0.05$) indicated that the BMWP did not show statistical differences between sampling sites and seasons.

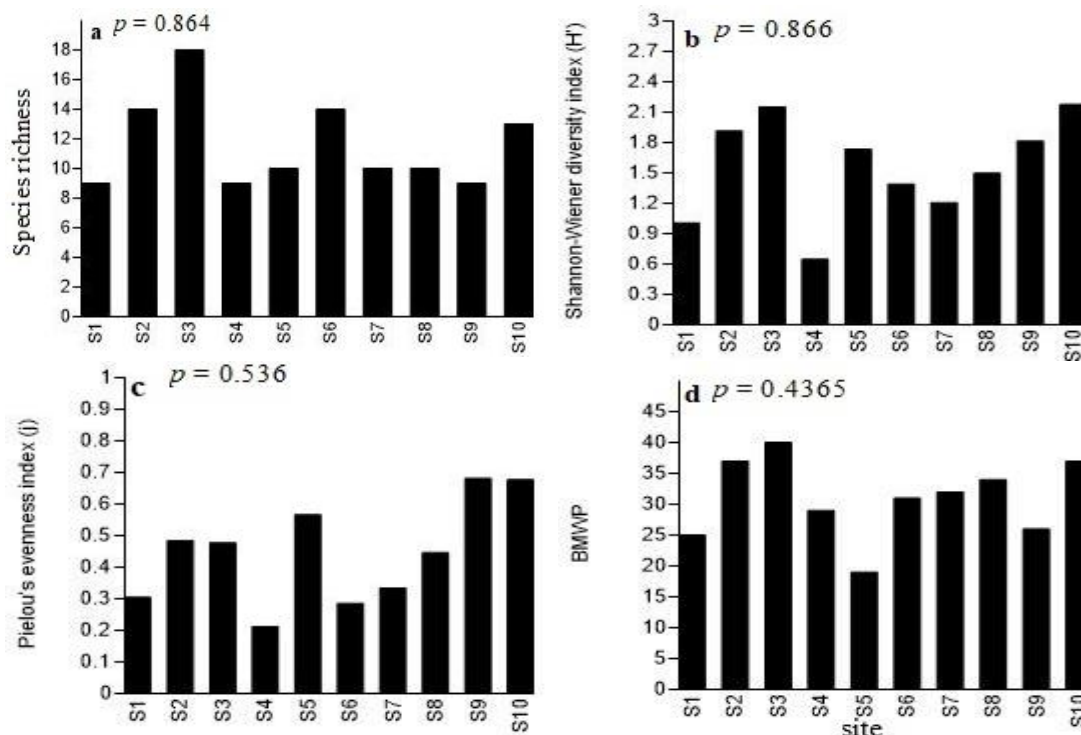


Figure 1. Trends in number of species (a), Shannon-Wiener's index "H" (b), Pielou's evenness index "J" (c) and BMWP: Biological Monitoring Working Party (d) for each sampling site in autumn, spring and summer

Benthic macroinvertebrates are excellent candidates as indicators of the environmental impacts that may be associated with fracturing activities (Mabidi et al., 2017), given their use as biological indicators of other human impacts in various freshwater environments (Hodkinson and Jackson, 2005; Feld and Hering, 2007). Biological indices as numerical estimators of ecological health status, based on the tolerance or sensitivity of macroinvertebrates to an environmental gradient, are now widely established in monitoring regimes around the world (BMWP, 1978; Hilsenhoff, 1988; Chessman, 1995, 2003; Simpson and Norris, 2000; Mustow, 2002; Davy-Bowker et al., 2005; Hued and de los Angeles Bistoni, 2005). Moreover, the importance of using a biological index that is based on local or indigenous benthic macroinvertebrates is well understood (Blakely et al., 2014).

Table 5 showed the water quality analysis based on Shannon index, Pielou's evenness index and BMWP values. The scores of Shannon index indicated that Sites S3 and S10

were “good”; while sites S2, S5-S9 were moderately polluted; unlike sites S1 and S4 were “poor” or polluted. The values of Pielou’s evenness index demonstrated that sites S5, S9 and S10 were “good”; while sites S2, S3, S7 and S8 were moderately impacted; unlike sites S1, S4 and S6 were polluted. The BMWP scores showed that sites S2, S3, S6, S8 and S10 were “good”, while sites S1, S4, S7 and S9 were moderately polluted; moreover, site S5 was polluted.

Table 5. Classes of water quality based on Shannon-Wiener’s index (H'), Pielou’s evenness index (J) and Biological Monitoring Working Party (BMWP)

Site	H'	Interpretation	J	Interpretation	BMWP	Interpretation
S1	1.00	Poor	0.30	Poor	25	Moderate
S2	1.91	Moderate	0.48	Moderate	37	Good
S3	2.15	Good	0.48	Moderate	40	Good
S4	0.65	Poor	0.21	Poor	29	Moderate
S5	1.73	Moderate	0.56	Good	19	Poor
S6	1.39	Moderate	0.28	Poor	31	Good
S7	1.21	Moderate	0.33	Moderate	32	Moderate
S8	1.49	Moderate	0.45	Moderate	34	Good
S9	1.81	Moderate	0.68	Good	26	Moderate
S10	2.18	Good	0.68	Good	37	Good

Overall, H' , J and BMWP values characterized the water quality of the Central Lake which ranged from polluted to slightly impacted water (Table 5). This observation can be due to the presence of human activities, which can be sufficient to heavily impact the water environments at some study sites.

Benthic macroinvertebrate functional feeding groups associated with environmental factors

The 42 benthic macroinvertebrate species were categorized into 5 functional feeding groups as follows: predators with 22 species, gathering-collectors (11 species), shredders (5 species), omnivores (2 species), and scrapers (2 species) (Table 4). In general, the omnivores were the most abundant benthic macroinvertebrate FFGs at all of the study sites and seasons, with scores up to 48.81%, followed by scrapers (21.78%), predators (17.24%), gathering-collectors (9.29%), and shredders (2.88%). However, our Kruskal-Wallis results showed that the FFG abundance data did not change significantly between sampling sites and seasons ($p = 0.7428$).

Figure 2 showed the canonical correspondence analysis ordinations performed for benthic macroinvertebrate FFGs and environmental variables at ten sampling sites. The first two axes explained 92.36% of benthic community variances, with eigenvalues of 0.3664 and 0.1010, respectively. The results displayed that the gathering-collectors (*Branchiura sowerbyi*, *Chironomus* sp., *C. flaviplumus*, *C. pallidivittatus*, *C. riparius*, *C. sinicus*, *Dicrotendipes pelochloris*, *Dicrotendipes* sp., *D. lobifer*, *D. tritonus*, and *Paracricotopus* sp.) and predators (*Agriocnemis* sp., *A. lacteola*, *Belostoma bakeri*, *Bezzia* sp., *Buenoa scimitra*, *Callicorixa culnerata*, *Cercion* sp., *Corisella decolor*, *Corixa substriata*, *Cybister* sp., *Davidius* sp., *Dicranota* sp., *Dineutus* sp., *Diplonychus rusticus*, *Dytiscus* sp., *Hebrus sobrinus*, *Hydrochara* sp., *Lestes* sp., *Micrommata* sp.,

Micronecta sp., *Pelocoris* sp., and *Sinictino gomphus*) were strongly correlated to dissolved oxygen ($r = 0.62$) and total phosphorus ($r = 0.66$) at sites S3, S9 and S10 on the first axis. While the second axis indicated that the scrapers, including *Gyraulus convexiusculus* and *Radix ovata* were positively associated with electrical conductivity ($r = 0.44$) and total nitrogen ($r = 0.18$) at sites S2 and S8.

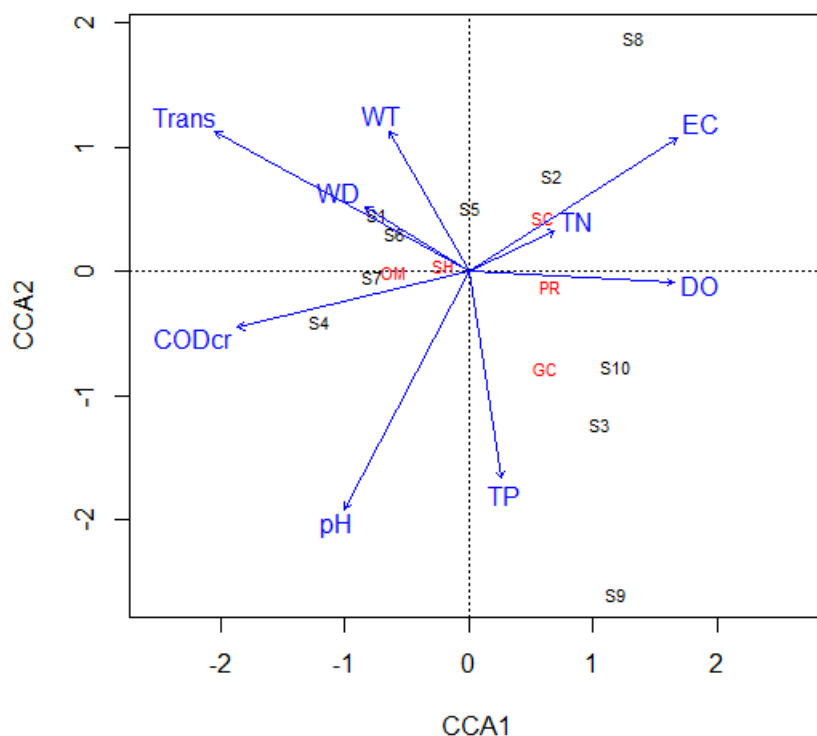


Figure 4. Canonical Correspondence Analysis (CCA) plots relating the benthic macroinvertebrate FFGs associated with environmental parameters at ten study sites. WT = Water temperature, EC = electrical conductivity, DO = dissolved oxygen, WD = water depth, Trans = transparency, TN = total nitrogen, TP = total phosphorus, CODcr = chemical oxygen demand with chrome index. GC = gathering-collectors, OM = omnivores, PR = predators, SC = scrapers, SH = shredders

The Central Lake is characterized by high diversity of benthic macroinvertebrate FFGs (five) recorded in this study. Overall, the omnivores predominated the study area. They play a vital role in clarifying water, and therefore considered ecosystem engineers. This can be due to the omnivores, which regularly consumes all or everything including plants, animals, algae, and fungi (Shabani, 2021). *Leander modestus*, which was collected in large proportion (48.71%) in this study, is efficient omnivore.

The scrapers were the second most abundant FFG feed off and consume the organic matter attached to stones and other substrate surfaces, primarily periphyton (Cummins, 1973; Cummins and Klug, 1979). The scrapers sampled in this study include snails (Mollusca eg. *Radix ovata* and *Gyraulus convexiusculus*). *Radix ovata*, which was the second most collected (21.78%) in sampling sites. This proportion of *Radix ovata* can be attributed to more abundant periphyton, especially diatoms and biofilms owing to more light that reaches the water surface (Vannote et al., 1980; Makaka et al., 2018).

Predators were the third most abundant overall. The abundance of predators is largely determined by the availability of their prey (Vannote et al., 1980; Makaka et al., 2018). We found that *Agriocnemis lacteola* (Odonata) was the most abundant predator in this study. The odonata are known to prey on larvae of Hydroptilidae caddis, Megaloptera, Mollusca, Diptera, and Coleoptera (Cummins, 1973; Cummins and Klug, 1979).

Gathering-collectors were the fourth most abundant feeding guild. Gathering-collectors such as Chironomidae and Oligochaeta are often the most abundant macroscopic organisms in many shallow-water habitats (Wallace and Webster, 1996), and thus their conversion of detritus and microbial biomass to invertebrate biomass is significant for larger consumers such as fishes and waterfowl (Shabani, 2021), which heavily rely on these groups for food (Thorpe and Covich, 2001).

The shredders, including *Bagous* sp., *Galerucella* sp., *Polypedilum nubifer*, *P. paraviceps* and *P. scalaenum* were the least FFG and constituted the least proportion (2.88%). They consume detritus, either in the form of leaves and wood or as finer benthic organic material (Cummins and Klug, 1979). Shredders are intimately related with the riparian vegetation (Makaka et al., 2018), because of their reliance on allochthonous feeding resources and hence contribute much in the degradation of leaf materials dropping into aquatic environments from overhanging vegetation (Allan and Castillo, 2007; Brasil et al., 2014). However, this degradation function is very important, especially in temperate regions where temperatures tend to limit the role of other decomposers like aquatic bacteria and fungi (Makaka et al., 2018).

Conclusion

The current work demonstrated that the benthic macroinvertebrate communities can be a sensitive tool for assessing the ecological status of lentic ecosystems. Our results displayed that Shannon index, Pielou's evenness index and Biological Monitoring Working Party are ecological methods, which respond potentially to the assessment of water quality. The findings showed that water environments of the Central Lake ranged from poor to good water conditions. The benthic macroinvertebrate FFG compositions obtained in this study offered some insights into the overall functioning of the Central Lake system and reflected a food availability, which can be affected by the change of water quality and aquatic plants. From the findings, we recommend further water resources management and the pollution control in this lake.

Acknowledgements. This research was supported by the Protection of Rare and Endangered Wildlife, 2021 Central Financial Forestry Subsidy Fund for Qingtongxia Reservoir Area Nature Reserve (Fund No. 2021-135), which the authors gratefully acknowledge. Our thankful feelings are also addressed to Xu Lei, Liu Jiamin and Ming Xiaoyang (postgraduate students from Northeast Forestry University) and Zhou Yutong, Yang Dongni, Zhang Feiran, Guo Xuefei and Buliduerxin Dulikenbieke (undergraduate students) for their help during sampling period.

REFERENCES

- [1] Allan, J. D., Castillo, M. M. (2007): Stream ecology: structure and function of running waters. – Springer, Dordrecht, the Netherlands.
- [2] Bird, M. S., Mlambo, M. C., Day, J. A. (2013): Macroinvertebrates as unreliable indicators of human disturbance in temporary depression wetlands of the south-western Cape, South Africa. – *Hydrobiologia* 720: 19-37.

- [3] Blakely, T. J., Eikaas, H. S., Harding, J. S. (2014): The Singscore: a macroinvertebrate biotic index for assessing the health of Singapore's streams and canals. – *Raffles Bulletin of Zoology* 62: 540-548.
- [4] BMWP (Biological Monitoring Working Party) (1978): Final Report: Assessment and Presentation of the Biological Quality of Rivers in Great Britain. – BMWP, Department of the Environment, London.
- [5] Brasil, S., Juen, L., Batista, J. D., Pavan, M. G., Cabette, H. S. R. (2014): Longitudinal Distribution of the Functional Feeding Groups of Aquatic Insects in Streams of the Brazilian Cerrado Savanna. – *Neotropical Entomology* 43: 421-428.
- [6] Chapman, P. M. (2002): Integrating toxicology and ecology: Putting the 'eco' into ecotoxicology. – *Marine Pollution Bulletin* 44: 7-15.
- [7] Chariton, A. A., Pettigrove, V., Baird, D. J. (2016): Ecological assessment. – In: Simpson, S. L., Batley, G. E. (eds.) *Sediment Quality Assessment: A Practical Guide* Vol. 346. CSIRO Publishing, Clayton.
- [8] Chessman, B. C. (1995): Rapid assessment of rivers using macroinvertebrates: a procedure based on habitat-specific sampling, family-level identification and a biotic index. – *Australian Journal of Ecology* 20: 122-129.
- [9] Chessman, B. C. (2003): New sensitivity grades for Australian river macroinvertebrates. – *Marine and Freshwater Research* 54: 95-103.
- [10] China Environmental Monitoring Station (2021): Technical guidelines for monitoring and evaluation of water ecological environment quality of lakes and reservoirs. (In Chinese).
- [11] Cummins, K. (1973): Trophic relations of aquatic insects. – *Annual Review of Entomology* 18: 183-206.
- [12] Cummins, K. W., Klug, M. J. (1979): Feeding ecology of stream invertebrates. – *Annual Review of Ecology and Systematics* 10: 147-172.
- [13] Davy-Bowker, J., Murphy, J. F., Rutt, G. P., Steel, J. E. C., Furse, M. T. (2005): The development and testing of a macroinvertebrate biotic index for detecting the impact of acidity on streams. – *Archiv für Hydrobiologie* 163: 383-403.
- [14] Dede, T. O., Telci, I. T., Aral, M. M. (2013): The Use of Water Quality Index Models for the Evaluation of Surface Water Quality: A Case Study for Kirmir Basin, Ankara, Turkey. – *Water Quality, Exposure and Health* 5(1): 41-56.
- [15] Ding, Y., Weihai, L., Fang, Z. (2014): *Fauna Sinica: Insecta* vol. 58 "Plecoptera: Nemouroidea". – Science Press, Beijing China.
- [16] Dow, C. L., Zampella, R. A. (2000): Specific conductance and pH as indicators of watershed disturbance in streams of the New Jersey Pinelands, USA. – *Environmental Management* 26(4): 437-446.
- [17] Duan, X., Wang, Z., Xu, M. (2010): *Benthic Macroinvertebrate and Application in the Assessment of Stream Ecology*. – Tsinghua University Press.
- [18] EPBC (Environmental Protection Bureau of the People's Republic of China) (2002): Standard methods for the monitoring and analysis on water and wastewater, 4th edition. – Beijing: Chinese Environmental Science Press.
- [19] Epler, H. J. (2001): Identification manual for the larval Chironomidae (Diptera) of North and South Carolina. – EPA Region 4 and Human Health and Ecological Criteria Division.
- [20] Feld, C. K., Hering, D. (2007): Community structure or function: effects of environmental stress on benthic macroinvertebrates at different spatial scales. – *Freshwater Biology* 52(7): 1380-1399.
- [21] Hawkins, H. A. (1978): Invertebrate indicators of river water quality. – *Proceeding of Symposium on Biological Indicators of Water Quality*, University of Newcastle upon Tyne 1(2): 1: 2-45.
- [22] Hilsenhoff, W. L. (1988): Rapid field assessment of organic pollution with a family-level biotic index. – *Journal of the North American Benthological Society* 7: 65-68.

- [23] Hodkinson, I. D., Jackson, J. K. (2005): Terrestrial and aquatic invertebrates as bioindicators for environmental monitoring, with particular reference to mountain ecosystems. – *Environmental Management* 35(5): 649-666.
- [24] Hong, S., Chen, J. S. (2002): Structure characteristics of aquatic community from the main rivers in China. – *Acta Hydrobiologica Sinica* 26(3): 295-305.
- [25] Hosokawa, S., Momota, K., Chariton, A. A., Naito, R., Nakamura, Y. (2021): The use of diversity indices for local assessment of marine sediment quality. – *Scientific Reports* 11: 14991.
- [26] Hued, A. C., de los Ángeles Bistoni, M. (2005): Development and validation of a Biotic Index for evaluation of environmental quality in the central region of Argentina. – *Hydrobiologia* 543: 279-298.
- [27] Johnson, B. B., Pflugh, K. K. (2008): Local officials' and citizens' views on freshwater wetlands. – *Society and Natural Resources* 21: 387-403.
- [28] Johnston, E. L., Roberts, D. A. (2009): Contaminants reduce the richness and evenness of marine communities: A review and meta-analysis. – *Environmental Pollution* 157: 1745-1752.
- [29] Krisanti, M., Wardiatno, Y., Anzani, Y. M. (2017): Assessing the ecological status of the Cisadane River's headwaters using benthic macroinvertebrates. – *IOP Conference Series: Earth and Environmental Science* 54: 012023.
- [30] Liu, M. H. (2012): The Ecological Monitoring and Health Assessment of Aquatic Animals Community in Hulan Estuary Natural Reserves. – Northeast Forestry University.
- [31] Lu, J., Huo, T., Wang, H. (2017): Ecology of Benthic Macroinvertebrates in Songliao Basin. – Jilin University Press. (In Chinese).
- [32] Mabidi, A., Bird, M. S., Perissinotto, R. (2017): Distribution and diversity of aquatic macroinvertebrate assemblages in a semi-arid region earmarked for shale gas exploration (Eastern Cape Karoo, South Africa). – *PLoS ONE* 12(6): e0178559.
- [33] Magurran, A. E. (2004): *Measuring Biological Diversity*. – Blackwell Publishing, New York.
- [34] Makaka, C., Muteveri, T., Makoni, P., Phiri, C., Dube, T. (2018): Longitudinal distribution of the functional feeding groups (FFGs) of aquatic macroinvertebrates and ecosystem integrity of Tokwe River, Zimbabwe. – *Journal of Biodiversity and Environmental Sciences (JBES)* 13(1): 16-33.
- [35] Manjare, S. A., Vhanalakar, S. A., Muley, D. V. (2010): Analysis of water quality using physico-chemical parameters Tamdalge tank in Kolhapur district, Maharashtra. – *International Journal of Advanced Biotechnology and Research* 1(2): 115-119.
- [36] Mlambo, M. C., Bird, M. S., Reed, C. C., Day, J. A. (2011): Diversity patterns of temporary wetland macroinvertebrate assemblage in the south-western Cape, South Africa. – *African Journal of Aquatic Science* 36: 299-308.
- [37] Momota, K., Hosokawa, S. (2021): Potential impacts of marine urbanization on benthic macrofaunal diversity. – *Scientific Reports* 11: 4027.
- [38] Mustow, S. E. (2002): Biological monitoring of rivers in Thailand: use and adaptation of the BMWP score. – *Hydrobiologia* 479: 191-229.
- [39] Nielsen, D. L., Brock, M. A. (2009): Modified water regime and salinity as a consequence of climate change: prospects for wetlands of Southern Australia. – *Climatic Change* 95(3): 523-533.
- [40] Pielou, E. C. (1966): The measurement of diversity in different types of biological collections. – *Journal of Theoretical Biology* 13: 131-144.
- [41] Pinto, I., Rodrigues, S., Antunes, S. C. (2021): Assessment of the Benthic Macroinvertebrate Communities in the Evaluation of the Water Quality of Portuguese Reservoirs: An Experimental Approach. – *Water* 13: 3391.
- [42] Qi, Z-Y. (1998): *Economic Mollusca of China*. – China Agriculture Press. (In Chinese).
- [43] R Core Team (2017): *R: A language and environment for statistical computing*. – R Foundation for Statistical Computing, Vienna, Austria. <https://www.R-project.org/>.

- [44] Ren, L., Zhang, Z., Zeng, X., Ma, Y., Zeng, Y., Zhou, C. (2011): Community Structure of Zooplankton and Water Quality Assessment of Jialing River in Nan Chong. *Procedia. – Environmental Sciences* 10: 1321-1326.
- [45] Resh, V. H. (1995): Freshwater benthic macroinvertebrates and rapid assessment procedures for water quality monitoring in developing and newly industrialized countries. – In: Davis, W. S., Simon, T. P. (eds.) *Biological Assessment and Criteria - Tools for Water Resource Planning and Decision Making*. Lewis Publishers, Boca Raton, U.S.A.
- [46] Riley, J. P., Chester, R. (1971): *Introduction to Marine Chemistry*. – United States: Academic Press.
- [47] Rosenberg, D. M., Resh, V. H. (1993): *Freshwater Biomonitoring and Benthic Macroinvertebrates*. – Chapman & Hall, New York.
- [48] Shabani, E. I. (2021): The Diversity and Ecology of Benthic Macroinvertebrates in the Wetlands of Sanjiang National Nature Reserve, Northeast China. – *Northeast Forestry University*.
- [49] Shannon, C. E. (1949): *The mathematical theory of communication*. – Urbana: Univ. of Illinois Press.
- [50] Simpson, J., Norris, R. H. (2000): Biological assessment of water quality: development of AUSRIVAS models and outputs. – In: Wright, J. F., Sutcliffe, D. W., Furse, M. T. (eds.) *RIVPACS and Similar Techniques for Assessing the Biological Quality of Freshwaters*. Freshwater Biological Association and Environment Agency, Ambleside, Cumbria, U.K.
- [51] Suratman, S., Hussein, A. N. A. R., Latif, M. T., Weston, K. (2014): Reassessment of Physico-Chemical Water Quality in Setiu Wetland, Malaysia. – *Sains Malaysiana* 43(8): 1127-1131.
- [52] Teferi, M., Haileselassie, T. H., Asmelash, T., Selassie, H. G., Alem, G., Amare, S., Weldegerima, K., Tesfay, S., Kiros, S., Equar, G., Bitew, H. L. (2013): Influence of water quality on the diversity and distribution of macro-invertebrates in highland stream, Northern Ethiopia. – *Scholarly Journal of Agricultural Science* 2(2): 18-26.
- [53] Thorp, J. H., Covich, A. P. (2001): *Ecology and classification of North American freshwater invertebrates*, 2nd edition. – San Diego, CA: Academic Press.
- [54] Tong, Y. (1996): *Fauna Sinica: Annelida “Hirudinea”*. – Science Press, Beijing China.
- [55] Tsuda, M. (1998): *Aquatic Entomology*. – Entomological Society of Liaoning. (In Chinese).
- [56] Turner, R. K., van den Bergh, K. C. J. M., Söderqvist, T., Barendregt, A., van der Straaten, J., Maltby, E., van Ierland, E. C. (2000): Ecological economic analysis of wetlands: scientific integration for management and policy. – *Ecological Economics* 35: 7-23.
- [57] Vannote, R. L., Minshall, G. W., Cummins, K. W., Sedell, J. R., Cushing, C. E. (1980): The River Continuum concept. – *Canadian Journal of Fish and Aquatic Sciences* 37: 130-137.
- [58] Wallace, J. B., Webster, J. R. (1996): The role of macroinvertebrates in stream ecosystem function. – *Annual Review of Entomology* 41: 115-139.
- [59] Walley, W. J., Hawkes, H. A. (1996): A computer-based reappraisal of the Biological Monitoring Working Party scores using data from the 1990 river quality survey of England and Wales. – *Water Research* 30(9): 2086-2094.
- [60] Walley, W. J., Hawkes, H. A. (1997): A computer-based development of the biological monitoring working party score system incorporating abundance rating, site type and indicator value. – *Water Research* 31(2): 201-210.
- [61] Wang, J., Wang, X. (2011): Larva of Chironomidae of Northern China. – China Yanhi publishing House. (In Chinese).
- [62] WHO (2011): *Hardness in drinking-water, background document for development of WHO guidelines for drinking-water quality*. WHO/HSE/WSH/10.01/10/Rev/1. – World Health Organization, Geneva.
- [63] Wong, M. C., Dowd, M. (2015): Patterns in taxonomic and functional diversity of macrobenthic invertebrates across seagrass habitats: A case study in Atlantic Canada. – *Estuaries Coasts* 38: 2323-2336.

- [64] Zeybek, M., Kalyoncu, H., Karakaş, B., Özgül, S. (2014): The use of BMWP and ASPT indices for evaluation of water quality according to macroinvertebrates in Değirmendere Stream (Isparta, Turkey). – *Turkish Journal of Zoology* 38: 603-613.
- [65] Zhang, C., Robinson, D., Wang, J., Liu, J., Liu, X., Tong, L. (2010): Factors Influencing Farmers' Willingness to Participate in the Conversion of Cultivated Land to Wetland Program in Sanjiang National Nature Reserve, China. – *Environmental Management* 47(1): 107-120.
- [66] Zhou, C., Su, C., Gui, H. (2015): *Outline of Chinese mayflies*. – Science Press. (In Chinese).

ASSESSMENT OF CLIMATE-INDUCED SEA-LEVEL RISE SCENARIOS AND ITS INUNDATION IN COASTAL ODISHA, INDIA

KHRISTODAS, P. M.¹ – PALANIVELU, K.¹ – RAMACHANDRAN, A.^{1*} – ANUSHIYA, J.¹ – PRUSTY, B. A. K.² – GUGANESH, S.¹

¹*Centre for Climate Change and Disaster Management, Anna University, Chennai, India
(e-mail: punya.khristodas@gmail.com)*

²*Department of Environment Studies, Berhampur University, Berhampur-760007, Odisha, India
(e-mail: anjaneia@gmail.com)*

**Corresponding author
e-mail: andimuthu.ramachandran@gmail.com*

(Received 8th Feb 2022; accepted 20th Jun 2022)

Abstract. Climate-induced Sea levels rise (SLR) has been one of the major concerns of the world community in recent decades. The present work attempts to find the current and future SLR and its inundation magnitude in the coastal districts of Odisha, India. Long-term monthly sea level data were used to assess the recent sea-level rise. The SLR projections were generated under different IPCC's Representative Concentration Pathway (RCP2.6, RCP4.5, RCP6.0, and RCP8.5) scenarios using the site-specific SLR scenario generator tool 'SimCLIM'. At last, the coastal area, which would be inundated for 0.5 m and 1 m SLR, was estimated and geospatially mapped using the ArcGIS tool. The observed SLR trend along the coast is 0.19 cm/yr from 1966 to 2015, equivalent to a change of 19.50 cm/100 years. The future SLR would be in the range of 4.15 to 9.09 cm for 2040, 13.71 to 37.73 cm for 2070, and 20.20 to 76.74 cm for 2100. Approximately 992.7 km² area would be inundated due to 0.5 m SLR and 1720.1 km² for 1 m SLR. This visible stress will pose a severe threat to the coastal natural resource base of Odisha.

Keywords: *coastal resilience, digital elevation model, representative concentration pathways, sea level rise projections, SimCLIM climate software*

Introduction

Sea level rise (SLR) is one of the most noticeable distresses of climate change and its extremities. Recent Intergovernmental Panel on Climate Change (IPCC) 2021 report alarms that there is a 0.20 m rise in global mean sea level from 1901 to 2018. The average rate of SLR was 0.13 cm/yr (1901-1971) and rose by 0.37 cm/yr (2006-2018), and it would continue to rise to 2 m by the end of the Century under a very high emissions scenario (SSP5-85 low confidence) (IPCC, 2021). The significant threats of SLR include inundation of low-lying areas, increasing coastal flooding, increasing salinity, loss of wetlands, loss of biodiversity and shoreline change, etc. (IPCC, 2007; Carrasco et al., 2015). Eventually, these will have huge imprints on river deltas, coastal areas with high population density, and infrastructure (Nicholls et al., 2007; McGranahan et al., 2007). People are becoming more vulnerable to SLR and climatic extremities with increasing developmental activities in coastal areas. As almost 600 million people live at mean sea level or below 10 m it leads to the generation of around US\$1 trillion in global wealth, while the environmental and socio-economic consequences of recurrent coastal flooding can be devastating (Kirezci et al., 2020). If civilization does not adapt to sea-level rise; in that case, coastal areas will experience more regular and severe floods, costing trillions of dollars, harming hundreds of

millions of people throughout the world and putting their lives and livelihoods in danger (Hinkel et al., 2014; Neumann et al., 2015; Kulp and Strauss, 2019). Coastal populations are in jeopardy due to the effects of SLR on their socio-economic conditions. These factors influence physical habitats, fish stocks, coastal ecosystems, infrastructures, and marine and inland fishing practices (Allison et al., 2008; Shah et al., 2013). Nicholls et al. (1999) estimated that a 38 cm rise in global sea level would lead to an approximate loss of 22% of coastal wetlands and that a 1 m SLR would yield a loss of 46% of the coastal wetlands.

Predictions of changes in coastal habitat boundaries due to expected relative SLR allow for advanced preparation for particular parts of the coastline to mitigate and offset anticipated losses and reduce risks to coastal growth and human safety (Gilman et al., 2007). Thus, a better understanding of SLR and its impacts is needed to anticipate risks associated with SLR. The first move in such direction will be to project SLR at the local level at various time scales and scenarios formulated by the IPCC (Ramachandran et al., 2017). These projections will facilitate more efficient coastal planning and management of natural resources and develop adaptation strategies for the coastal communities. Long-term datasets on climate change variables are a prerequisite for projection studies, and in recent times, computer-based climate models/tools have supported the research community by providing scenarios. Various models for coastal studies are available for climate change projection, such as Bathtub, BTELSS, DIVA, SimCLIM, etc. The SimCLIM model has been hailed as a helpful tool for determining the risk-based influences of climate change at the local level (Warrick, 2009).

Study area

The current work aims to provide sea-level rise projections for the Odisha state of India at the local scale. Odisha state is situated along the eastern coast of India with a 480 km long coastline stretching from Baleshwar on the north to Ganjam on the south (17°48' to 22°34' N and 81°24' to 87°29'E). The state has six coastal districts: Baleshwar, Bhadrak, Kendrapara, Jagatsingpur, Puri, and Ganjam (*Fig. 1*). These coastal districts have predominant agricultural landscapes. Farming and related practices are the mainstays of the locals' livelihoods. The coastal stretch of the state is bestowed with unique landforms such as lagoons, sandy (nesting) beaches, dunes, wetlands and estuaries. Asia's largest brackish water lagoon, Chilika Lake, is located along the Odisha coast. Bhitarkanika national park, India's second-largest mangrove forest after Sundarbans of West Bengal and Gahirmatha- the world's largest nesting beach for the Olive Ridley sea turtle Odisha (Mohanty et al., 2008; Kumar et al., 2010; Hauer, 2016). In contrast, the coast of Odisha is subject to extreme tidal variations, strong littoral drift, frequent cyclones, and flooding. Tropical storms that originate in the Bay of Bengal regularly inflict deaths and significant damage in the coastal districts (Das et al., 1983; Murty et al., 1986; Dube et al., 1994, 1997, 2000; Chittibabu et al., 2002; Kumar et al., 2010). In addition to cyclones, Odisha has a history of rigorous flood hazards due to storm surges produced in the Bay of Bengal, floods from the rivers, and substantial rainfall related to tropical hurricanes and monsoon depressions (Chittibabu et al., 2002). Severe flooding caused by storm surges devastated the lives and property of thousands of people living along the coast. Tourism hotels and resorts, fishing communities, and townships have already been vulnerable to frequent storm surge disasters (Kumar et al., 2010).

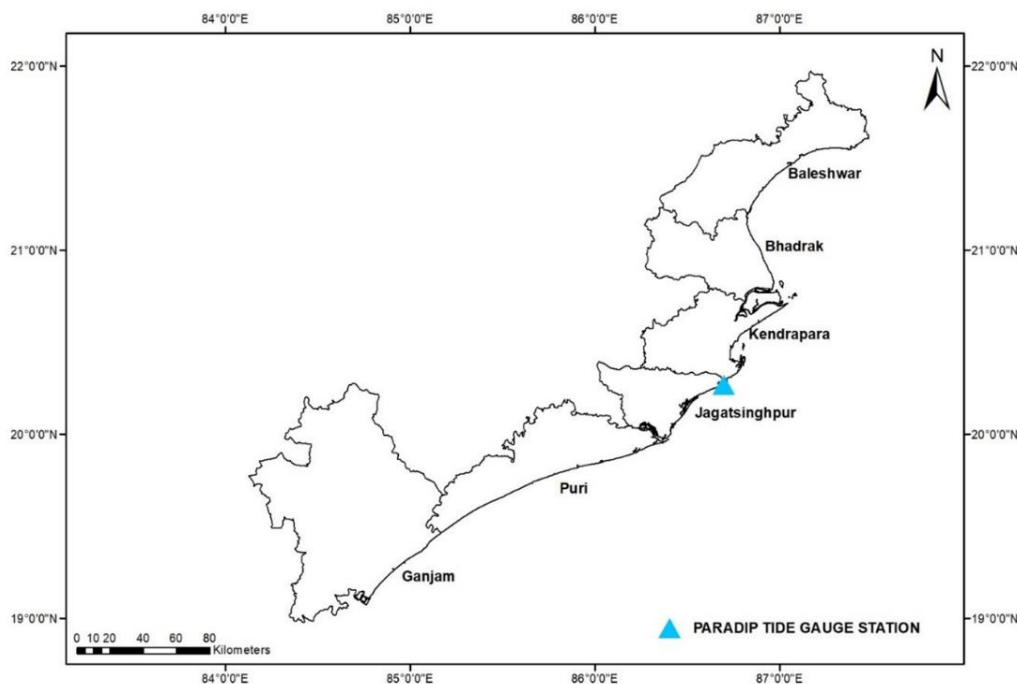


Figure 1. Study area: coastal districts of Odisha

Additionally, coastal areas of Odisha are at risk of rapid erosion (Ramesh et al., 2011). In recent decades, the native population has begun to migrate to other cities, searching for better livelihood support systems and income opportunities (Velan and Mohanty, 2015). Furthermore, the increase in sea level will also pose a significant threat to Odisha's coastal stretch. Thus, it is necessary to assess the sea-level rise and its effects along the coastline stretch of Odisha.

The current research has three objectives: (i) to analyze the observed sea-level rise in Odisha's coast and (ii) to provide future SLR projections for Odisha under IPCC AR5 based for Representative Concentration Pathways (RCP) RCP2.6, RCP4.5, RCP6.0, and RCP8.5 scenarios and (iii) to assess the magnitude of inundation and portray the area of inundation for the two SLR scenarios, i.e., of 0.5 m and 1 m. This study is the first attempt to project SLR for the coast of Odisha, India.

Methods

In this work, IPCC criteria for assessing the SLR were followed. The detailed methods of determining past sea-level changes along the coast using historical data projection of sea-level rise were generated under different IPCC's Representative Concentration Pathway (RCP2.6, RCP4.5, RCP6.0, and RCP8.5) scenarios and estimation of inundation area under future SLR are as follows:

Assessing past sea-level changes

Many studies use monthly mean sea-level values to estimate past sea-level rise (Unnikrishnan et al., 2006, 2015; Ramachandran et al., 2017). The monthly mean sea level data are available in Permanent Service for Mean Sea Level (PSMSL) archives at

<http://www.psmsl.org>. PSMSL is a global data bank for long-term sea-level change information from tide gauges and bottom pressure records, which contains monthly and annual mean values of sea level from over 1800 tide gauge stations across the globe. Paradip tide gauge station is the only tide gauge station of Odisha available in the PSMSL archive (Station ID: 1161). This station lay in 20.26 N and 86.7 E and owned tide gauge data from 1966 till 2015 with 77% completeness. The monthly mean sea level data of Paradip tide gauge station were downloaded and analyzed to observe the changes in sea level and its trend along the coast of Odisha.

Developing SLR projections using IPCC scenario

Future SLR projections were developed as per IPCC's RCP scenarios using the SimCLIM tool. SimCLIM, a user-friendly tool, includes a scenario generator that uses pattern-scaling approaches at essential scales (Warrick, 2009). It deals with different patterns of climate change from complex global climate models (GCM) that display time-variant global climate change predictions (Amin et al., 2018). In recent years, the majority of the studies have neglected the calculation of regional assessments of fluctuations in sea level, owing to the lack of technological knowledge (Mary et al., 2021). SimCLIM software is developed to provide solutions to this problem by re-gridding the pattern scaling system to a 720×360 grid (i.e., $0.5^\circ \times 0.5^\circ$) using a bilinear interpolation method (Yin et al., 2013). SimCLIM version 4.0, a site-specific scenario generator tool, was used to calculate the SLR projection for the six coastal districts of Odisha. The observed MSL trend of the Paradip tide gauge station was given as a reference datum in the scenario generator to project future SLR. The model has 28 global climate models (GCMs) (Table 1). GCMs were organized hierarchically based on normalized GCM values (pattern scaling) by SimCLIM to perform the sensitivity analysis. The measure of the central tendency was calculated based on the median value of the constructed ensemble (SimCLIM, 2011). All the 28 GCMs were selected to construct an ensemble, and the central tendency was calculated as follows:

$$\text{Median value} = (n-1) \times 50\% + 1 \quad (\text{Eq.1})$$

where 'n' denotes the number of GCMs chosen, which, in this case, is 28.

$$\text{Median Value} = (28-1) \times 50\% + 1 = 14.5$$

with the value in the 14th and 15th places in terms of magnitude selected as the median value (SimCLIM, 2011).

The contributions from the components at the global, regional, and local scales were considered when computing the SLR projection for a specific location, and it is expressed as follows (Nicholls et al., 2011):

$$\Delta\text{RSL} = \Delta\text{SL}_G + \Delta\text{SL}_{RM} + \Delta\text{SL}_{RG} + \Delta\text{SL}_{VLM} \quad (\text{Eq.2})$$

where ΔRSL stands for relative sea-level change, ΔSL_G stands for global mean sea-level change, ΔSL_{RM} stands for regional variation in sea level from the global mean due to metro-oceanographic factors, ΔSL_{RG} stands for regional variation in sea level due to changes in the earth's gravitational field, and ΔSL_{VLM} stands for change in sea level due to vertical land movement.

The tool has a unique facility of considering climate sensitivity range to project sea-level change. The SLR changes of low, medium and high range for all RCP scenarios were considered (SimCLIM, 2011). Then, future SLR projections were generated under different IPCC's Representative Concentration Pathway RCP2.6, RCP4.5, RCP6.0, and RCP8.5 scenarios for three time slices 2040, 2070, and 2100.

Table 1. Available GCMs with sea-level rise variables in CMIP5

S. No.	GCM	S. No.	GCM
1	ACCESS1-0	15	GISS-E2-R-CC
2	ACCESS1-3	16	HadGEM2-CC
3	bcc-csm1-1	17	HadGEM2-ES
4	bcc-csm1-1-m	18	inmcm4
5	CanESM2	19	IPSL-CM5A-LR
6	CCSM4	20	IPSL-CM5A-MR
7	CMCC-CM	21	MIROC5
8	CMCC-CMS	22	MIROC-ESM
9	CNRM-CM5	23	MIROC-ESM-CHEM
10	CSIRO-Mk3-6-0	24	MPI-ESM-LR
11	GFDL-CM3	25	MPI-ESM-MR
12	GFDL-ESM2G	26	MRI-CGCM3
13	GFDL-ESM2M	27	NorESM1-M
14	GISS-E2-R	28	NorESM1-ME

Estimating inundation area and mapping

Due to future SLR along the coast, the inundation area was estimated using inundation mapping in the ArcGIS 10.5 tool (Malik and Abdalla, 2016). The Cartosat-1 (30 m resolution) digital elevation model (DEM) from National Remote Sensing Centre (NRSC), Hyderabad, India, was used in this study. Eight CartoDEM tiles, which cover coastal districts of Odisha, were downloaded from the Bhuvan portal on 22/04/2021 (Table 2). These eight tiles are combined into a single DEM file. The CartoDEM was post-processed for geoid correction, and the null values were removed. The processed DEM was clipped with Odisha's coastal district shapefile. Then the inundation area for 0.5 m and 1 m SLR scenarios were calculated and mapped using the Raster Calculator tool in ArcGIS. Finally, the raster output was transformed into a polygon, and the inundation area was measured for each district.

Table 2. Details of CartoDEM tiles representing the coastal Odisha

Sl. No.	Tile number	Bounding box
1	F45P	87E21N – 88E22N
2	F45O	86E21N – 87E22N
3	F45U	86E20N – 87E21N
4	F45T	85E20N – 86E21N
5	E45C	86E19N – 87E20N
6	E45B	85E19N – 86E20N
7	E45A	84E19N – 85E20N
8	E45G	84E18N – 85E19N

Results

The observed sea-level change from 1966 to 2015, the SLR projections for the six coastal districts for four different scenarios at three-time scales, and district-wise inundation areas due to future SLR are presented here.

Observed sea-level changes from 1966 to 2015

The monthly mean sea-level data from 1966 to 2015 were analyzed to see the changes along the coast. This 50-year-long monthly data from the Paradip tide gauge station shows that the sea level along Odisha's coast has increased steadily (*Fig. 2*). The observed relative sea level trend is 0.19 cm per year with a 95% confidence interval of +/- 0.09 cm per year, comparable to a change of 19.50 cm in 100 years.

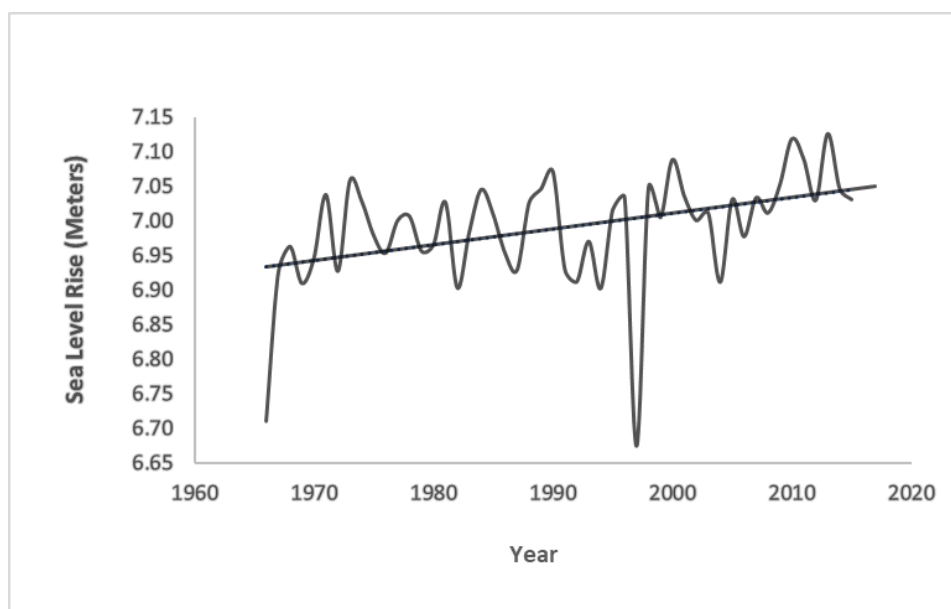


Figure 2. The observed SLR projection for Paradip (Odisha) tide gauge station

Future IPCC scenarios of SLR for Odisha

SLR projections (low, medium, and high) of IPCC RCPs 2.6, 4.5, 6.0, and 8.5 were made for three different timescales with an interval of 30 years, i.e., for 2040, 2070, and 2100. The detailed projections for each timescale are described below:

SLR scenarios for the year 2040

The estimated SLR projections would be between 4.28 to 9.25 cm for the RCP2.6 scenario; 4.35 to 9.18 cm for the RCP4.5 scenario; 4.15 to 9.09 cm under the RCP6.0, and 4.65 to 9.51 cm for the RCP8.5 scenario. The SLR would be 4.15 to 4.94 cm (low), 6.35 to 7.18 cm (medium) and 8.50 to 9.51 cm (high) sensitivity. The district-wise SLR projections for RCP2.6, RCP4.5, RCP6.0, and RCP8.5 are listed in *Table 3*. The SLR projections of the Baleshwar district are 4.29 to 4.81 cm (low), 6.54 to 6.99 cm (medium) and 8.63 to 9.26 cm (high) range. For the Bhadrak district, the projected SLR levels are 4.39 to 4.94 cm, 6.69 to 7.18 cm and 8.84 to 9.51 cm, respectively, for low, medium and high ranges, respectively. For the Kendrapara district, the projected SLR

levels are 4.25 to 4.76 cm (low), 6.49 to 6.94 cm (medium) and 8.57 to 9.19 cm (high) range. For Jatatsinghpur district, SLR would be 4.48 to 4.89 cm (low), 6.89 to 7.11 cm (medium) and 9.17 to 9.42 cm (high). For Puri and Ganjam districts, the projected SLR levels would be 4.15 to 4.65 cm and 4.17 to 4.68 cm, 6.35 to 6.79 cm and 6.37 to 6.82 cm, 8.40 to 9.00 cm and 8.43 to 9.04 cm under low, medium and high sensitivity, respectively.

Table 3. District wise SLR projections for the year 2040

Scenario Range Districts	RCP2.6			RCP4.5			RCP6.0			RCP8.5		
	Low	Medium	High	Low	Medium	High	Low	Medium	High	Low	Medium	High
Baleshwar	4.43	6.80	9.05	4.49	6.96	8.96	4.29	6.54	8.63	4.81	6.99	9.26
Bhadrak	4.62	6.95	9.25	4.61	6.93	9.18	4.39	6.69	8.84	4.94	7.18	9.51
Kendrapara	4.38	6.75	8.98	4.45	6.71	8.89	4.25	6.49	8.57	4.76	6.94	9.19
Jagatsinghpur	4.48	6.89	9.17	4.56	6.86	9.09	4.56	6.86	9.09	4.89	7.11	9.42
Puri	4.28	6.60	8.80	4.35	6.57	8.71	4.15	6.35	8.40	4.65	6.79	9.00
Ganjam	4.31	6.63	8.83	4.37	6.60	9.00	4.17	6.37	8.43	4.68	6.82	9.04

SLR scenarios for the year 2070

The SLR projections of Odisha for 2070 have been estimated as 13.71 to 30.30 cm for the RCP2.6; 15.76 to 32.45 cm for RCP4.5; 15.01 to 31.16 cm under the RCP6.0, and 19.52 to 37.73 cm for the RCP8.5 scenario. While the SLR would be between 13.71 to 20.09 cm, 21.84 to 28.63 cm and 29.49 to 37.73 cm under the low, medium and high range, respectively. The SLR projections under IPCC RCP2.6, RCP4.5, RCP6.0, and RCP8.5 scenarios for all the districts are given in Table 4.

Table 4. Sea Level Rise projection for the year 2070

Scenario Range Districts	RCP2.6			RCP4.5			RCP6.0			RCP8.5		
	Low	Medium	High	Low	Medium	High	Low	Medium	High	Low	Medium	High
Baleshwar	14.15	22.46	30.30	16.25	24.25	32.45	15.48	23.31	31.16	20.09	28.63	37.73
Bhadrak	14.08	22.37	30.17	16.17	24.15	32.32	15.41	23.21	31.04	20.00	28.51	37.58
Kendrapara	14.03	22.29	30.08	16.11	24.07	32.22	15.35	23.13	30.94	19.93	28.42	37.46
Jagatsinghpur	13.93	22.16	29.90	16.01	23.92	32.03	16.01	23.92	32.03	19.81	28.25	37.25
Puri	13.71	21.84	29.49	15.76	23.58	31.59	15.01	22.67	30.34	19.52	27.86	36.75
Ganjam	13.77	21.93	29.60	15.83	23.68	31.71	15.08	22.76	30.45	19.60	27.78	36.66

SLR scenarios for the year 2100

The SLR projections for 2100 have been estimated as 20.20 to 49.64 cm for the RCP2.6; 25.92 to 57.36 cm for RCP4.5; 26.32 to 57.62 cm under the RCP6.0 and 38.69 to 76.74 cm for the RCP8.5. While the SLR would be between 20.20 to 39.77 cm (low), 33.92 to 57.04 cm (medium), and 48.33 to 76.74 cm (high) range, respectively. The SLR projections under RCP2.6, RCP4.5, RCP6.0, and RCP8.5 scenarios for all the districts such as Baleshwar, Bhadrak, Kendrapara, Jagatsinghpur, Puri, and Ganjam are listed in Table 5.

Overall, the projected SLR is high in the Baleshwar district, followed by Bhadrak, Kendrapara, Jagatsinghpur, Ganjam and Puri districts. Puri district would have a low

SLR compared to other districts. The SLR projection for the Baleshwar district would be 20.84 to 39.77 cm under low sensitivity; 34.89 to 57.04 cm under medium sensitivity; 49.64 to 76.74 cm under high sensitivity for the period 2100. Puri district would have a low SLR compared to other districts. The SLR projection for the Puri district would be 20.20 to 38.69 cm under low sensitivity; 33.92 to 55.56 cm under medium sensitivity; 48.51 to 75.08 cm under high sensitivity for 2100.

Table 5. Sea level rise projection for the year 2100

Scenario Range Districts	RCP2.6			RCP4.5			RCP6.0			RCP8.5		
	Low	Medium	High	Low	Medium	High	Low	Medium	High	Low	Medium	High
Baleshwar	20.84	34.89	49.64	26.70	41.60	57.36	27.36	42.11	57.62	39.77	57.04	76.74
Bhadrak	20.75	34.74	49.44	26.58	41.43	57.13	27.24	41.94	57.39	39.60	56.82	76.45
Kendrapara	20.67	34.62	49.28	26.49	41.29	56.95	27.15	41.80	57.21	39.47	56.64	76.21
Jagatsinghpur	20.53	34.41	48.99	26.32	41.05	56.63	26.32	41.05	56.63	39.23	56.31	75.79
Puri	20.20	33.92	48.33	25.92	40.48	55.87	26.57	40.98	56.12	38.69	55.56	74.81
Ganjam	20.29	34.06	48.51	26.03	40.64	56.08	26.68	41.14	56.33	38.84	55.77	75.08

Coastal inundation due to future SLR

The inundation model using ArcGIS indicates that nearly 992.7 km² (4.48%) area would be under the threat of inundation for 0.5 m SLR (Fig. 3). An approximate area of 1720.1 km² (7.77%) would be under the threat of inundation for 1 m SLR (Fig. 3). The district-wise inundated area for 0.5 m and 1 m SLR is listed in Table 6. The results reveal that the Kendrapara district is highly vulnerable to SLR risks, followed by Puri, Bhadrak, Jagatsinghpur, Baleshwar and Ganjam district. Nearly 492.9 km² area would be inundated for 0.5 m SLR and 770.69 km² for 1 m SLR in Kendrapara district. In Puri district, around 314.12 km² area would be inundated for 0.5 m SLR and 557.9 km² for 1 m SLR. There would be about 98.63 km² inundated area for 0.5 m SLR and 327.79 km² for 1 m SLR in Bhadrak district. In the Jagatsinghpur district, around 65.97 km² area would be inundated for 0.5 m SLR and 107.75 km² area would be inundated for 1 m SLR followed by Baleshwar (14.33 and 42.95 km²) and Ganjam (5.7 and 11.29 km²) for 0.5 m and 1 m SLR, respectively.

Discussion

The observed and projected SLR of the State and its pact with national and international studies, the significance of district wise SLR projections and its inundation through the lens of its ecological importance are elaborately discussed below.

The monthly mean sea level data of Paradip tide gauge station shows that the sea level along the coast of Odisha is increasing steadily from 1966 to 2015 with a 0.19 cm/yr rise. Globally, Sea levels are rising because of the continental ice melt and thermal expansion of ocean water due to global warming. The global mean sea level rose to 20 cm from 1901 to 2018, and the average rate of SLR was 0.13 cm/yr (1901-1971) and rose by 0.37 cm/yr (2006-2018) (IPCC, 2021). While SLR in the Indian Ocean is non-uniform, the rate of north Indian Ocean rise was 0.10-0.17 cm/yr from 1874 to 2004 and 0.33 cm/yr from 1993 to 2015 (Swapna et al., 2020). The estimated relative sea-level trend of Odisha's coast agrees well with the Indian scenario of SLR.

Table 6. District-wise area of inundation in Odisha

S. No.	Districts	Total area of the district (km ²)	Inundation area (km ²)		% Inundation area (%)	
			0.5 m SLR	1 m SLR	0.5 m SLR	1 m SLR
1	Baleshwar	3,634	14.33	42.95	0.39	1.18
2	Bhadrak	2,505	98.63	327.79	3.93	13.08
3	Ganjam	8,071	5.7	11.29	0.07	0.13
4	Puri	3,479	314.12	457.9	9.02	13.16
5	Kendrapara	2,644	492.82	770.69	18.63	29.14
6	Jagatsinghpur	1,759	65.97	107.75	3.75	6.12

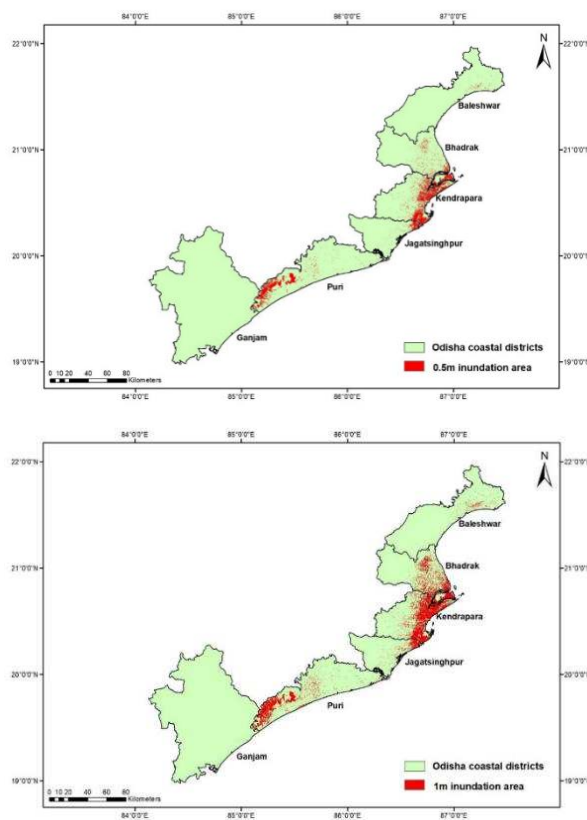


Figure 3. Map showing area of inundation due to 0.5 m SLR (left) and map showing area of inundation due to 1 m SLR (right)

The projected SLR of Odisha's coast indicated a 20.20 to 39.77 cm increase under low emission scenarios, 33.92 to 57.04 cm under medium emission scenarios and 48.33 to 76.74 cm under high emission scenarios for the year 2100. The global mean sea level rise is expected to be 19 cm in 2050 and 44 cm by 2100 under a low emission scenario. The very high emission scenario is expected to be 23 cm in 2050 and 77 cm in 2100 (IPCC, 2021). At the same time, the steric sea level in the north Indian Ocean is projected to rise by approximately 30 cm relative to the average over 1986–2005 under the RCP4.5 scenario at the end of the twenty-first Century, with the corresponding projection for the global mean rise being approximately 18 cm (Krishnan et al., 2020).

Earlier, Unnikrishnan et al. (2015) also estimated the increasing trend of SLR reaching the values close to the global mean SLR trends (0.32 cm/yr) from 1993-2012. The present study findings agree with the other regional SLR studies in India (Unnikrishnan et al., 2006; Khan, 2013; Ramachandran et al., 2017). The results of the present research slightly deviate from the global mean SLR. For RCP8.5, the global mean SLR for 2081–2100 compared to 1986–2005 would likely be in the range of 45–82 cm, whereas the SLR forecast for the Odisha coast range from 48.33 to 76.74 cm. These ranges were calculated using CMIP5 climate forecasts, process-based models, and a literature review of glacier and ice sheet contributions (IPCC, 2013). Under ocean circulation, regional differences in ocean density, and atmospheric pressure, local sea levels generally differ from the global mean (Khan, 2013). Climate model forecasts for the twenty-first Century indicate that, in addition to global mean sea level rises, the large-scale spatial pattern may also alter, potentially affecting local SLR (Pardaens et al., 2010). To validate the total trend SLR projections based on GCM performances; this research compared the observed tide gauge data from 1966 to 2015. However, the future predictions of the estimates of total trend SLR by SimCLIM are depends on the performance of the multi-model ensemble, which is made up of 28 GCMs, arranged hierarchically based on the normalized GCMs values by the pattern scaling method.

Regardless of the exact extent of the rise, a rise in sea level is unavoidable in the next decades. Nuisance floods will become more common and more substantial as sea levels rise, converting a once-in-a-lifetime event into a common and potentially damaging problem due to road closures, inundated storm drains, and infrastructural compromises (Chisholm et al., 2021). The estimated projected SLR in this study will pose a series of threats to the sensitive coastal Odisha. Even though the cumulative areas of inundation in all the six coastal districts are 4.48% and 7.77% of the total area to 0.5 m and 1 m SLR, the towns, human settlements, infrastructures, and habitats are located along the coast will be under severe threat. According to IPCC (2001), a 1 m rise in sea-level rise in India could render nearly 7 million people homeless. In the next three decades, Odisha will be one of the worst affected states due to sea-level rise, with the entire stretch from Baleswar to Ganjam at risk of flooding and inundation by 2050 (Climate Central, 2019). The coast of Odisha is gifted with rich wetlands and ecosystems, which support a diverse range of habitats and provide various ecological goods and services. Nearly 114,238 marine fisherfolk families depend on the Odisha coast for their livelihood (Kumar and Pattnaik, 2014). Major Biodiversity in wetlands includes Subarnarekha, Baitarina, Gahirmatha, Bhitarkanika, Mahanadi, Devi, Chilika Lake, and Rusikulya River, hotspots with high ecological importance are lying in these coastal districts. The environmental significance of the study area and probable SLR impacts in each district are elaborately discussed below:

Kendrapara, the high prone district to SLR, has 35.82 km of coastal length. Approximately 18.63% area of Kendrapara district would be inundated to 0.5 m SLR and 29.14% area for 1 m SLR in Kendrapara district. This district has India's 2nd largest existing mangrove ecosystem, the 'Bhitarkanika Mangroves'. This mangrove ecosystem has ecological, geomorphological, and biological significance, including mangrove forests, rivers, creeks, estuaries, backwaters, accreted lands, and mudflats. Further, the ecosystem has high faunal importance, including the occurrence of a sizeable population of estuarine crocodiles (*Crocodylus porosus*). Besides this, the sanctuary is rich in other reptiles, birds and mammals, and people. Apart from this, these mangrove forests are moral habitat for king cobra, Indian python and water monitor lizards (Gopi

and Pandav, 2007). The district also has a forest cover of 305 km² (ISFR, 2017) and a 1350 km² agriculture area (Government of Odisha, 2015). Increasing SLR poses a significant threat to this district's mangrove ecosystems, forest and agriculture areas. Inundation stress, salinity increase, and sediment erosion at landward zones would be significant risks in this region.

Puri is identified as the second most vulnerable district to SLR risks. Even though the estimated SLR projection is low among other districts, the inundation vulnerability is high due to its topography. Nearly 9.02% area of Puri district would be inundated for 0.5 m SLR, and around 13.16% area would be inundated for 1 m SLR. The district covers 214 km² of forest land (ISFR, 2017) and 1340 km² of agricultural land (Government of Odisha, 2015). The famous Chilika Lake hosts a diverse environment that includes marine, brackish, and freshwater ecosystems. This lake is home to the Irrawaddy dolphin (Sutaria, 2007), critically endangered. It is one of the main wintering areas for migratory birds on the Indian subcontinent, with over 225 species at various phases of their life cycles. More than 0.2 million fishermen rely on the rich fish fauna (Mohanty et al., 2018), including roughly 317 species (Mohanty et al., 2015). Sea level rise also pushes native species from the area, searching for healthier habitats and allowing invasive species to dominate (Varela et al., 2018). Olive Ridley turtles use the vast sandy beaches of Odisha as nesting habitat (Chattopadhyay et al., 2018).

The third vulnerable district to SLR is Bhadrak district, with nearly 1700 km² of agriculture area and 75 km² of forest cover. Out of this, almost 3.93% of the district area would be inundated for 0.5 m SLR, and around 13.08% area would be inundated for 1 m SLR, followed by the Jagatsinghpur district. Nearly 3.75% of the district area would be inundated for 0.5 m SLR, and 6.12% area would be inundated for 1 m SLR. Jagatsinghpur district has the Gahirmatha rookery, home to huge sea turtles, casuarina trees and mangrove patches along the mainland shore. Natural disasters, such as cyclones and oceanic pressures and shifting riverine discharge have caused noticeable alterations in the study region, particularly in the segments used most for nestings, such as the sand spit and the islets (Prusty et al., 2007). The rising sea levels resulting from climate change threaten these nesting sites (National Research Council, 1990; Leatherman et al., 2000; Garcia et al., 2015; Grases et al., 2020). This district covers 136 km² (ISFR, 2017) of forestland and 900 km² of agricultural land (Government of Odisha, 2015). Already the Jagatsinghpur district has experienced major floods during the last two decades, causing extensive damage through loss of livestock, human life, and property and the inundation of agricultural lands, waterlogging, salt-water intrusion, and tidal inundation (Jena, 2018).

The fifth vulnerable district to SLR is the Baleshwar district. An approximately 0.39% area would be inundated for 0.5 m SLR, and around 1.18% area would be inundated for 1 m SLR in the Baleshwar district. Agriculture is a principal activity of the district. Nearly 1910 km² are net sown area (Government of Odisha, 2015). The forest covers 380 km² (ISFR, 2017) of Ganjam, the least vulnerable district to SLR, which has Rushikulya rookery - the third-largest rookeries in the world. Thousands of turtles congregate in the nearshore water of the study area every winter for reproduction. Marine turtle species are vulnerable to climate change-induced SLR (Fuentes et al., 2013). Ganjam has a coastal length of 62.90 km with 3890 km² of agriculture area (Government of Odisha, 2015) and 2103 km² of forest cover (ISFR, 2017). Low-lying coastal areas are more vulnerable to rising sea levels because they face submergence or salt-water intrusion (Kakani et al., 2011). Seawater intrusion will

stress plants and animals and may even cause the disappearance of certain species when the salinity level reaches above their tolerance. Consequently, SLR would affect farmlands due to land flooding and seawater intrusion. Thereby, agriculture in low-lying coastal areas or adjacent to deltas could be severely impacted by SLR (Rosenzweig and Hillel, 1995; Nicholls et al., 2007; Kibria et al., 2010).

Furthermore, the Ministry of Environment, Forest & Climate of India (2015) has declared the Bhitarkanika Wildlife Sanctuary, Bhitarkanika National Park and Gahirmatha (Marine) Wildlife Sanctuary in Odisha as an example Eco-Sensitive Zone (ESZ). Nearly 45 villages in the Bhadrak district and 157 villages in Kendrapara come under the ESZ. Thus, rising sea levels will severely affect coastal Odisha and its rich Biodiversity.

Climate uncertainty can affect habitats such as mangroves and coral reefs, fisheries, and tourism (IPCC, 2007). The coastline of Odisha, endowed with natural ecosystems, lagoons, olive ridley rookeries, and beaches, attracts more tourism activities in this region and has generated better employment opportunities, thereby sustaining livelihood. Carrasco et al. (2015) indicated that these coastal landforms are also not an exemption from the impacts of SLR. Odisha is particularly vulnerable to cyclones, floods, and droughts, causing widespread damage to the fishing community (DoF, 2014). The findings indicate that sea-level rise is a major concern on the coast of Odisha, along with already evidenced cyclones, storm surges, coastal erosion, and tsunamis, among other disasters. The coastal areas of Odisha, which provide numerous ecological socio-economic benefits to the citizens, will be under threat due to SLR. Even with adopting strategies to stabilize climate forcing by 2050, SLR is predicted to accelerate during the next Century. Therefore, an integrated strategic adaptation plan is needed urgently for this coastal area to reduce SLR vulnerability. The projected SLR and inundation area map of the coastal stretch of Odisha would be a valuable resource for policymakers and planners in developing adaptation strategies. The vulnerable coastal areas, natural resources, and dependent societies at risk demand immediate action to increase their resilience.

Conclusions

This work analyzes sea-level changes during past decades and projects future SLR at the local level at various time scales (2040, 2070, and 2100) under all four IPCC AR5 emission scenarios. The inundation area due to future SLR is also estimated and geospatially mapped. The specifics of this study are:

- An increasing trend of 0.19 cm/yr SLR was observed along the coast of Odisha from 1966 to 2015.
- SLR will continue to rise till the end of the Century under all emission scenarios. The projected SLR of Odisha's coast indicated a 48.33 to 76.74 cm under high emission scenarios for the year 2100.
- Ganjam district, which has 3890 km² of agriculture area and 2103 km² of forest cover, is alarming to note that these two considerable areas will be inundated shortly.
- The biological and ecological hotspots of Odisha, such as Bhitarkanika wildlife sanctuary, Chilika Lagoon, and Gahirmatha Olive Ridley rookery, which lies along the coast, would be at risk of rising sea level.

- Even though the highest SLR projection is observed for the Bhadrak district, the Kendrapara district is highly vulnerable to SLR scenarios. Nearly 18.63% (492.82 km²) area would be inundated for 0.5 m SLR and 29.69% (770.69 km²) area for 1 m SLR in Kendrapara district, followed by Puri and Bhadrak.
- The current study uses CARTOSAT-1 (30 m) DEM data and climate scenarios from GCM data. The significant difference would be observed with higher resolutions DEM data and future climate scenarios.
- The outputs will help decision-makers to develop synergetic adaptation strategies to reduce the risks in the coastal districts of Odisha.
- The study urges to frame SLR inclusive planning in coastal zone management in the state.

Acknowledgements. The author Mr. Punya Murthy Khristodas is thankful to the University Grants Commission (UGC), Government of India, for funding this project under (Maulana Azad National Fellowship)-scheme- 2016-2021 (ref. no.: F1-17.1/2014-2015-CHR-ORI-42755, February 2017). All authors of this research work are indeed grateful to all the colleagues of the Center for Climate Change and Disaster Management (CCCDM), Anna University, Chennai, for their technical support.

REFERENCES

- [1] Allison, E. H., Perry, L. A., Badjeck, M. C., Adger, W. N., Brown, K., Conway, D., Halls, A. S., Pilling, G. M., Reynolds, J. D., Andrew, N. L. (2008): Vulnerability of National Economies to the Impacts of Climate Change on Fisheries. – *Fish* 10(2): 173-196.
- [2] Amin, A., Nasim, W., Mubeen, M., Sarwar, S., Urich, P., Ahmad, A., Wajid, A., Khaliq, T., Rasul, F., Hammad, H. M., et al. (2018): Regional climate assessment of precipitation and temperature in Southern Punjab (Pakistan) using SimCLIM climate model for different temporal scales. – *Theoretical and Applied Climatology* 131(1-2): 121-131.
- [3] Carrasco, A. R., Ferreira, Ó., Roelvink, D. J. A. (2015): Coastal lagoons and rising sea level: A review. – *Earth Science Reviews* 154: 356-368.
- [4] Chattopadhyay, N. R., Chetia, A., Machahary, K. Q., Dupak, O. (2018): Assessment of Conservation Measures for Olive Ridley Sea Turtle (*Lepidochelys Olivacea*) Along Rushikulya Rookery, Ganjam District, Odisha, India. – *International Journal of Marine Biology Research* 3(1): 1-9.
- [5] Chisholm, L., Talbot, T., Appleby, W., Tam, B., Rong, R. (2021): Projected changes to air temperature, sea-level rise, and storms for the Gulf of Maine region in 2050. – *Elementa: Science of the Anthropocene* 9(1): 1-14.
- [6] Chittibabu, P., Dube, S. K., Sinha, P. C., Rao, A. D., Murty, T. S. (2002): Numerical Simulation of Extreme Sea Levels for the Tamil Nadu (India) and Sri Lankan Coasts. – *Marine Geodesy* 25(3): 235-244.
- [7] Climate Central (2019): Flooded Future: Global Vulnerability to Sea Level Rise Worse than Previously Understood. – Climate Central, Princeton, NJ, pp 1-12.
- [8] Das, P. K., Dube, S. K., Mohanty, U. C., Sinha, P. C., Rao, A. D. (1983): Numerical simulation of the surge generated by the June 1982 Orissa cyclone. – *Mausam* 34(4): 359-366.
- [9] DoF (2014): Disaster Management Plan of Fisheries Department. – Directorate of Fisheries, Cuttack, Odisha.

- [10] Dube, S. K., Rao, A. D., Sinha, P. C., Chittibabu, P. (1994): A real time storm surge prediction system: An application to east coast of India. – Proceedings of the Indian National Science Academy 60: 157-170.
- [11] Dube, S. K., Rao, A. D., Sinha, P. C., Murty, T. S., Bahulayan, N. (1997): Storm surge in the Bay of Bengal and Arabian Sea: The problem and its prediction. – Mausam 48(2): 283-304.
- [12] Dube, S. K., Chittibabu, P., Rao, A. D., Sinha, P. C., Murty, T. S. (2000): Extreme sea levels associated with severe tropical cyclones hitting Orissa coast of India. – Marine Geodesy 23(2): 75-90.
- [13] Fuentes, M. M. P. B., Pike, D. A., Dimatteo, A., Wallace, B. P. (2013): Resilience of marine turtle regional management units to climate change. – Global Change Biology 19(5): 1399-1406.
- [14] Garcia, Y. C., Ramírez-Herrerac, M. T., Delgado-Trejod, C., Legorreta-Pauline, G., Coronaf, N. (2015): Modeling sea-level change, inundation scenarios, and their effect on the Colola Beach Reserve - a nesting-habitat of the black sea turtle, Michoacán, Mexico. – Geofísica Internacional 54(2): 179-190.
- [15] Gilman, E., Ellison, J., Coleman, R. (2007): Assessment of mangrove response to projected relative sea-level rise and recent historical reconstruction of shoreline position. – Environmental Monitoring and Assessment 124: 105-130.
- [16] Gopi, G. V., Pandav, B. (2007): Conservation of Avifauna of Bhitarkanika Mangroves, India. – Zoosprint 22: 2839-2847.
- [17] Government of Odisha (2015): Odisha Agricultural Statistics 2013-14. – Directorate of Agriculture and Food Production, Bhubaneswar.
- [18] Grases, A., Vicente, G., Manuel, G., Jue, L., Joan, P. S. (2020): Coastal flooding and erosion under a changing climate: implications at a low-lying coast (Ebro Delta). – Water 12(2): 1-26.
- [19] Hauer, M. E., Evans, J. M., Mishra, D. R. (2016): Millions projected to be at risk from sea-level rise in the continental United States. – Nature Climate Change 6(7): 691-695.
- [20] Hinkel, J., Lincke, D., Vafeidis, A., Perrette, M., Nicholls, R., Tol, R., Marzeion, B., Fettweis, X., Ionescu, C., and Levermann, A. (2014): Coastal flood damage and adaptation costs under 21st Century sea-level rise. – Proceedings of the National Academy of Science USA 111(9): 3292-3297.
- [21] IPCC (2001): Climate Change 2001. The Scientific Basis. Contribution of Working Group I to the Third Assessment Report of the Intergovernmental Panel on Climate Change (TAR-IPCC). – Cambridge University Press, Cambridge.
- [22] IPCC (2007): Climate Change 2007: The Physical Science Basis. Contribution of Working Group I to the Fourth Assessment Report of the Intergovernmental Panel on Climate. – Cambridge University Press, Cambridge, pp. 385-432.
- [23] IPCC (2013): Summary for Policymakers. – In: Stocker, T. F., Qin, D., Plattner, G. K., Tignor, M., Allen, S. K., Boschung, J., Nauels, A., Xia, Y., Bex, V., Midgley, P. M. Climate change 2013: The physical science basis. Contribution of Working Group I to the Fifth Assessment Report of the Intergovernmental Panel on Climate Change. Cambridge University Press, Cambridge.
- [24] IPCC (2021): Summary for Policymakers. – In: Masson-Delmotte, V., Zhai, P., Pirani, A., Connors, S. L., Péan, C., Berger, S., Caud, N., Chen, Y., Goldfarb, L., Gomis, M. I., Huang, M., Leitzell, K., Lonnoy, E., Matthews, J. B. R., Maycock, T. K., Waterfield, T., Yelekçi, O., Yu, R., Zhou, B. (eds.) Climate Change 2021: The Physical Science Basis. Contribution of Working Group I to the Sixth Assessment Report of the Intergovernmental Panel on Climate Change. Cambridge University Press, Cambridge.
- [25] ISFR (2017): India State of Forest Report. – Forest Survey of India, Dehradun, Ministry of Environment, Forests and Climate Change. Government of India. <https://www.fsi.nic.in/forest-report-2017>.

- [26] Jena, P. P. (2018): Climate change and its worst effect on coastal Odisha-an overview of its impact in Jagatsinghpur District. – *Journal of Humanities and Social Science* 23(1): 1-15.
- [27] Kakani, N. R., Subraelu, P., Kommireddi, V. N. K., Malini, B. H., Ramakrishnan, R., Rajawat, A. S., Ajai (2011): Climate change and sea-level rise: impact on agriculture along Andhra Pradesh coast—a geomatics analysis. – *Journal of the Indian Society of Remote Sensing* 39: 415-422.
- [28] Khan, A. S. (2013): Climate change induced sea level rise projection and its predicted impact on the Tamil Nadu coast, India: Framing ecosystem and community based adaptation strategies. – Ph. D. Thesis, Anna University, Chennai, India.
- [29] Kibria, G., Haroon, A. K. Y., Nuggeoda, D., Rose, G. (2010): *Climate Change and Chemicals: Environmental and Biological Aspects*. – New India Publishing Agency, New Delhi, India.
- [30] Kirezci, E., Young, I., Ranasinghe, R., Muis, S., Nicholls, R., Lincke, D., Hinkel, J. (2020): Projections of global-scale extreme sea levels and resulting episodic coastal flooding over the 21st century. – *Scientific Reports* 10(1): 11629.
- [31] Krishnan, R., Sanjay, J., Gnanaseelan, C., Mujumdar, M., Kulkarni, A., Chakraborty, S. (2020): *Assessment of Climate Change over the Indian Region*. – A Report of the Ministry of Earth Sciences (MoES), Government of India, New Delhi.
- [32] Kulp, S. A., Strauss, B. H. (2019): New elevation data triple estimates of global vulnerability to sea-level rise and coastal flooding. – *Nature Communications* 10(1): 1-12.
- [33] Kumar, S. T., Patnaik, S. (2014): Marine fisheries; its current status, sustainable management and socio economic status of the marine fishers of Odisha, through Indian marine policy: a case study. – *Research Journal of Animal, Veterinary and Fishery Sciences* 2(7): 10-19.
- [34] Kumar, T., Mahendra, R. S., Nayak, S., Radhakrishnan, K., Sahu, K. (2010): Coastal vulnerability assessment for Orissa State, East Coast of India. – *Journal of Coastal Research* 26: 523-534.
- [35] Leatherman, S., Zhang, K., Douglas, B. (2000): Sea level rise shown to drive coastal erosion. EOS. – *Transactions American Geophysics Union* 81(6): 55-57.
- [36] Malik, A., Abdalla, R. (2016): Geospatial modeling of the impact of sea level rise on coastal communities: application of Richmond, British Columbia, Canada. – *Modelling Earth System and Environment* 2(3): 146.
- [37] Mary, O. O., Williams, A. B., Benson, N. U. (2021): Simulated sea-level rise under future climate scenarios for the Atlantic Barrier lagoon coast of Nigeria using SimCLIM. – *IOP Conference Series: Earth and Environmental Science* 665: 012068.
- [38] McGranahan, G., Balk D., Anderson, B. (2007): The rising tide: assessing the risks of climate change and human settlements in low elevation coastal zones. – *Environment & Urbanization* 19(1): 17-37.
- [39] Mohanty, P., Pal, S. R., Mishra, P. (2008): Monitoring and management of environmental changes along the Orissa coast. – *Journal of Coastal Research* 24(2B): 13-27.
- [40] Mohanty, S., Mishra, S., Mohanty, R., Mohapatra, A., Pattanaik, A. (2015): Ichthyofaunal diversity of Chilika Lake, Odisha, India: an inventory, assessment of biodiversity status and comprehensive systematic checklist (1916-2014). – *Check List* 11(6): 1-19.
- [41] Mohanty, S. K., Bhatta, K., Nanda, S. (2018): *Bibliography of Publications: Research and Investigations in Chilika Lake (1872-2017)*. – Chilika Development Authority, Bhubaneswar.
- [42] Murty, T. S., Flather, R. A., Henry, R. F. (1986): The storm surge problem in the Bay of Bengal. – *Progress in Oceanography* 16(4): 195-233.
- [43] National Research Council. (1990): *Decline of the Sea Turtles: Causes and Prevention*. – National Academy Press, Washington.

- [44] Neumann, A. T., Vafeidis, J., Zimmermann, R., Nicholls, J. (2015): Future coastal population growth and exposure to sea-level rise and coastal flooding—A global assessment. – *PloS One* 10(3): e0118571.
- [45] Nicholls, R. J., Hoozemans, F., Marchand, M. (1999): Increasing flood risk and wetland losses due to global sea-level rise: regional and global analyses. – *Global Environmental Change - Human and Policy Dimensions* 9(1): 69-87.
- [46] Nicholls, R. J., Wong, P. P., Burkett, V. R., Codignotto, J. O., Hay, J. E., McLean, R. F., Ragoonaden, S., Woodroffe, C. D. (2007): Coastal Systems and Low-Lying Areas. – In: Parry, M. L., Canziani, O. F., Palutikof, J. P., van der Linden, P. J., Hanson, C. E. (eds.) *Climate Change 2007: Impacts, Adaptation and Vulnerability. Contribution of Working Group II to the Fourth Assessment Report of the Intergovernmental Panel on Climate Change* Parry. Cambridge University Press, Cambridge, pp. 315-356.
- [47] Nicholls, R. J., Hanson, S. E., Lowe, J. A., Warrick, R. A., Lu, X., Long, A. J., Carter, T. R. (2011): Constructing sea level scenarios for impact and adaptation assessment of coastal areas: a guidance document. – *Technical Guidelines of the Task Group on Data and Scenario Support for Impact and Climate Analysis (TGICA) of the Intergovernmental Panel on Climate Change*. IPCC, Geneva.
- [48] Pardaens, A. K., Gregory, J. M., Lowe, J. A. (2010): A model study of factors influencing projected changes in regional sea level over the twenty-first Century. – *Clim Dyn* 36(9-10): 2015-2033.
- [49] Prusty, G., Dash, S., Singh, M. P. (2007): Spatio-temporal analysis of multi-date IRS imageries for turtle habitat dynamics characterization at Gahirmatha coast, India. – *International Journal of Remote Sensing* 28: 871-883.
- [50] Ramachandran, A., Khan, A. S., Palanivelu, K., Prasannavenkatesh, R., Jayanthi, N. (2017): Projection of climate change-induced sea-level rise for the coasts of Tamil Nadu and Puducherry, India using SimCLIM: a first step towards planning adaptation policies. – *Journal of Coastal Conservation* 21(23): 1-12.
- [51] Ramesh, R., Purvaja, R., Senthilvel, A. (2011): National assessment of shoreline change: Odisha coast. – *NCSCM/MoEF Report*, 2011-01.
- [52] Rosenzweig, C., Hillel, D. (1995): Potential impacts of climate change on agriculture and food supply. – *Consequence* 1(2): 23-32.
- [53] Shah, K. U., Dulal, H. B., Johnson, C., Baptiste, A. (2013): Understanding livelihood vulnerability to climate change: applying the livelihood vulnerability index in Trinidad and Tobago. – *Geoforum* 47: 125-137.
- [54] SimCLIM (2011): *SimCLIM Essentials: Training Book 1, Version 2.0*. – Climsystems, Hamilton.
- [55] Sutaria, D. (2007): *Irrawaddy Dolphin – India*. – Whale and Dolphin Conservation Society. <http://www.wdcs.org/submissionsbin/consprojectirr.pdf>. Accessed: 25 Dec 2008.
- [56] Swapna, P., Ravichandran, M., Nidheesh, G., Jyoti, J., Sandeep, N., Deepa, J. S., Unnikrishnan, A. S. (2020): *Sea-Level Rise. Assessment of Climate Change over the Indian Region*. – Springer, Singapore, pp. 175-189.
- [57] Unnikrishnan, A. S., Shankar, D. (2006): Are sea-level-rise trends along the coasts of the north Indian Ocean consistent with global estimates? – *Global and Planetary Change* 57(3): 301-307.
- [58] Unnikrishnan, A., Gangan, N., Lengaigne, M. (2015): Sea-level-rise trends off the Indian coasts during the last two decades. – *Current Science* 108(5): 966-971.
- [59] Varela, M. R., Patricio, A. R., Anderson, K., Godley, B. J. (2018): Assessing climate change associated sea level rise impacts on sea turtle nesting beaches using drones, photogrammetry and a novel GPS system. – *Global Change Biology* 25(2): 753-762.
- [60] Velan, N., Mohanty, R. K. (2015): *Gender Wise Rural-to-Urban Migration in Orissa, India: An Adaptation Strategy to Climate Change*. – In: Delgado-Ramos, G. C. (ed.) *Inequality and Climate Change: Perspectives from the South*. CODESRIA, Dakar, pp. 137-170.

- [61] Warrick, R. A. (2009): Using SimCLIM for modeling the impacts of climate extremes in a changing climate: a preliminary case study of household water harvesting in Southeast Queensland. – 18th World IMACS/MODSIM Congress, Cairns, Australia, pp. 2583-2589.
- [62] Yin, C., Li, Y., Urich, P. (2013): SimCLIM 2013 Data Manual. —CLIM Systems Ltd., Hamilton.

WATER ECOLOGICAL HEALTH ASSESSMENT OF THE MULING RIVER BASIN BASED ON ANALYTIC HIERARCHY PROCESS IN NORTHEAST CHINA

SUN, X.^{1,2,3#} – CHAI, Y. H.^{4#} – CHAI, Q. Y.⁵ – SONG, S. D.⁶ – JU, Y. F.⁷ – YU, T.⁸ – LI, X. Y.^{2,3}
– YU, H. X.^{2,3*} – CHAI, F. Y.^{2,3,9*} – WANG, W.^{1*}

¹*Key Laboratory of Applied Biology and Aquaculture of Northern Fishes in Liaoning Province, College of Fisheries and Life Science, Dalian Ocean University, Dalian 116023, China*

²*Wetland Biodiversity Conservation and Research Center, Northeast Forestry University, Harbin 150040, China*

³*College of Wildlife and Protected Area, Northeast Forestry University, Harbin 150040, China*

⁴*Aulin College, Northeast Forestry University, Harbin 150040, China*

⁵*College of Economics and Management, Northeast Forestry University, Harbin 150040, China*

⁶*Sports Business School, Beijing Sport University, Beijing 100084, China*

⁷*School of Geography and Tourism, Harbin University, Harbin 150086, China*

⁸*Rural Water Conservancy and Hydropower Guarantee Center of Heilongjiang Province, Heilongjiang Provincial Water Resources Department, Harbin 150001, China*

⁹*School of Management, Heilongjiang University of Science and Technology, Harbin 150020, China*

#Co-first authors

These authors contributed to the work equally.

**Corresponding authors*

e-mail: china.yhx@163.com (Yu, H. X.); chaifangying@126.com (Chai, F. Y.); wangwei@dlou.edu.cn (Wang, W.)

(Received 8th Feb 2022; accepted 10th Jun 2022)

Abstract. In order to explore the water ecological health of the Muling River, the largest tributary of Wusuli River in northeast China. The environmental factors and aquatic organisms of the Muling River were investigated in different seasons. During the investigation, 83 species and 17 functional groups of phytoplankton, and 36 species and seven functional groups of zooplankton, and 158 genera/species and six functional feeding groups of macroinvertebrates, and 46 species and seven fish functional groups were found. The evaluation system of water ecological health in the Muling River Basin, including 27 indexes, was established by analytic hierarchy process by calculating, which values in each season were 0.4177, 0.4428, 0.5071, 0.4699, 0.4799 and 0.6434, respectively. The seasonal changes of water ecological health classification rise from level III to level II, and the health status rises from the general level to the sub-health level. The overall trend is rising, the average value is 0.4935, the health classification is level III, and the health status is general. Generally speaking, the water ecological health level of the Muling River Basin is the highest in autumn.

Keywords: *freshwater, wetland, aquatic life, functional groups, hydroecology*

Introduction

Globally, most aquatic ecosystems including lakes, rivers, reservoirs, freshwater and marine wetlands have changed due to human disturbance caused by land use activities centered on human settlements, agriculture and industrial activities (Tockner et al., 2010). Phytoplankton are one of the most important primary producers, forming an important source of energy in the first trophic layer (Shen, 2014). They are also food for many aquatic animals, they also play an important role in the material cycle of aquatic ecosystems by controlling growth, reproductive capacity and population characteristics of aquatic organisms (Michele and Mark, 2006). Changes in physical and chemical factors of aquatic systems can directly affect the structure of aquatic communities (Ptacnik et al., 2008). Therefore, scientists use the composition of aquatic communities to study and understand aquatic ecosystems (Becker et al., 2009). Monitoring the composition of aquatic organisms to comprehensively evaluate the local water environment, the community structure of organisms in different water quality has obvious characteristics (Sukatar et al., 2020), and preliminary evaluation of the nutritional status of water bodies can be carried out in actual water quality monitoring (Li et al., 2021). The community structure and composition of aquatic organisms will directly affect the structure and function of aquatic ecology (Lu et al., 2019). At the same time, when the nutritional status of water changes, first it will be reflected in the changes in individual aquatic organisms, populations, communities, and productivity. The growth of aquatic organisms is affected by a variety of factors, such as predation, competition, and parasitism among organisms, and environmental factors such as water velocity, nutrients, temperature, and light (Nash et al., 2021). The changes of each of the above factors will cause certain changes in the structural state of individuals, populations and communities (Ren et al., 2021).

River ecosystems are one of the basic types of freshwater ecosystems, and can serve as a bridge connecting the two major ecosystems of the ocean and the land. Especially in the energy flow and substance cycles of the biosphere, which is vividly called the blood circulation of the Earth, has the characteristics of fluidity (Allan and Castillo, 2007). The river is vital to human development. It provides water and a range of services such as transportation, entertainment, and commerce. The river ecosystem is also an important channel for the material circulation of the global biosphere, which can transform and digest various nutrients and pollutants (Jungwirth et al., 2000). Therefore, it is necessary to monitor the phytoplankton functional group in the river. Most of the researches on the functions of river ecosystems are carried out on the basis of traditional species classification. However, recent studies have shown that ecosystem functions mainly depend on the diversity of functional traits, that is, the spatial and temporal patterns of the distribution and abundance of functional traits (Elliott and Quintino, 2010; Li et al., 2015). Functional traits are sensitive to environmental changes and play a key role in the study of the relationship between biodiversity and ecosystem functions. Functional diversity based on biological characteristics is closely related to ecosystem processes and is the key to understanding ecosystem and community functions (Han, 2021). Macroinvertebrates are widely used to monitor the destruction of aquatic ecosystems (Lu et al., 2020). They are also an important part of the aquatic food web and are the basis for the nutrient cycle and ecological balance of the ecosystem (Mangadze et al., 2016). The species characteristics of functional groups are more closely related to the environment, can directly reflect the ecological process of the ecological environment on the aquatic community, and better understand the aquatic

ecosystem and its biodiversity (Lu et al., 2021). Fish provide a powerful tool for assessing the aquatic environment (Chowdhury et al., 2011). The sensitivity of fish to most forms of human disturbance, their utility at all levels of biological tissue, and the favorable cost-benefit ratio of fish evaluation schemes (Wetzel, 2011). Fish can be used as indicators in a wide range of time and space, because they cover all nutritional levels of consumer ecology, and fish can effectively integrate all ecological processes in waterways. Fish play many different roles in assessing river health and monitoring the response to remedial management (Beaugrand et al., 2000). Plankton exists in almost all kinds of water bodies. Compared with other aquatic animals, they are numerous and have strong metabolic activity. Zooplankton feed on phytoplankton, bacteria, debris and other organisms. Zooplankton also participates in the decomposition and circulation of organic matter in the aquatic ecosystem through excretion and secretion, energy transfer from primary producers to advanced consumers (David et al., 2005). Changes in zooplankton can affect the structure of other nutrient levels in aquatic ecosystems (Lobry et al., 2008). The structure, abundance and biomass of zooplankton communities are affected by the upward and downward effects, and are one of the determinants of water quality, which is due to the interaction between biological organisms and environmental factors (Ejsmont-Karabin and Karabin, 2013).

Muling River Basin is located in the agricultural wetland ecological zone of the Sanjiang Plain in Heilongjiang Province, surrounded by cultivated land. Muling River has experienced long-term sand dredging activities, and the river bed has been seriously damaged. In addition, due to the continuous increase in agricultural non-point source pollution, industrial discharge pollution and urban life pollution in recent years, the water quality of Muling River has deteriorating, which has adversely affected the production and life of local people. This study objective is by investigating the aquatic organisms and environmental factors of the Muling River, it is very important to find out the environmental factors that affect the water quality of the Muling River Basin, which has important practical significance for the evaluation of the water ecological health of the Muling River Basin.

Materials and methods

Study area

Muling River (44°01'~45°58' N, 130°11'~133°40' E) is the largest tributary on the left bank of the Ussuri River, the border river between China and Russia. The length of the river is 834 km and the drainage area is 18427 km². The upper reaches have a temperate continental climate, with hot and rainy summers and long and cold winters. The upstream average annual precipitation is 530 mm, mainly in July to September. The midstream has a temperate semi-humid monsoon climate with an average annual temperature of 3.1°C (-18°C~21°C). The annual water flow is 2.35 billion m³, the annual precipitation is 522 mm, and the frost-free period is 149 days. The lower reaches have a temperate continental monsoon climate. Precipitation in the valley plains of the middle and lower reaches of the Muling River Basin is the main source of supplementary water, followed by surface water and paddy field infiltration. The flood lasts about 3~7 days, generally 15~30 days on the main stream, the sunshine duration is 2400~2800 h, and the annual evaporation is about 1100~1300 mm.

Field sampling

According to the local climate characteristics and ecological environment characteristics of the Muling River Basin, six sampling surveys were carried out in May (spring), July (summer) and September (autumn) in 2015 and 2017, and a total of 28 water plants were set up in the whole basin. Sampling points for biological and environmental factors, with 3 replicates for each sampling site (Fig. 1, Table 1).

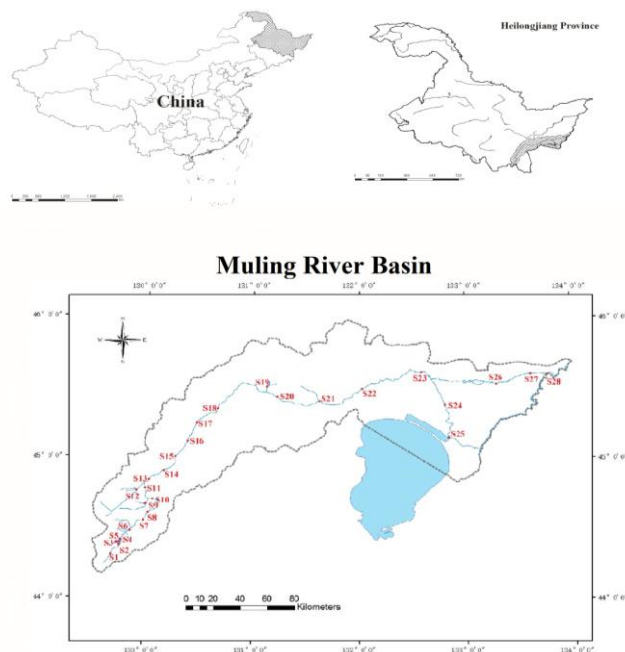


Figure 1. Location of sampling sites in Muling River basin

Table 1. The sampling stations and coordinates in Muling River basin

Sampling sites	Coordination	Altitude(m)	Sampling sites	Coordination	Altitude(m)
S1	44°01'48"N, 130°11'24"E	508	S15	44°40'12"N, 130°26'24"E	292
S2	44°03'36"N, 130°10'48"E	495	S16	44°53'24"N, 130°30'36"E	273
S3	44°03'00"N, 130°09'36"E	504	S17	45°00'00"N, 130°32'24"E	232
S4	44°04'12"N, 130°10'48"E	506	S18	45°04'48"N, 130°40'12"E	229
S5	44°04'48"N, 130°10'48"E	499	S19	45°18'00"N, 131°00'36"E	191
S6	44°11'24"N, 130°15'36"E	454	S20	45°18'00"N, 131°03'36"E	181
S7	44°13'12"N, 130°15'00"E	435	S21	45°20'24"N, 131°31'48"E	150
S8	44°13'48"N, 130°15'36"E	419	S22	45°27'00"N, 131°52'12"E	115
S9	44°21'36"N, 130°16'48"E	386	S23	45°42'00"N, 132°25'12"E	75
S10	44°24'36"N, 130°19'12"E	358	S24	45°35'24"N, 132°36'36"E	76
S11	44°28'12"N, 130°14'24"E	338	S25	45°19'48"N, 132°48'36"E	76
S12	44°28'12"N, 130°12'36"E	324	S26	45°44'24"N, 132°57'00"E	78
S13	44°29'24"N, 130°13'48"E	312	S27	45°45'36"N, 133°06'00"E	49
S14	44°34'48"N, 130°19'48"E	298	S28	45°58'12"N, 133°40'12"E	67

Phytoplankton was collected with a 5 L plexiglass water harvester and 25# plankton net (mesh 0.064 mm), 1 L water sample was collected at each sampling point, 10~15 ml Luger reagent was added and shaken, and brought back to the laboratory for static Set aside for 1~2 d, draw the supernatant and concentrate to 30 ml. Zooplankton was collected with a 5 L plexiglass water collector to collect 20 L water samples, filter them through 25# plankton net (mesh 0.064 mm), and add 75% alcohol and 5% formaldehyde solution for storage. Macroinvertebrates were collected with a Peterson mud harvester (open area 1/16 m²) and a D-net. The collected mud samples are filtered through a sample sieve and placed in a white porcelain dish. The specimens are selected and placed with a straw and tweezers. 75% alcohol solution preservation. Fish were collected with 40 m gill net (mesh 3~7 cm) and electric fish device (2000W, 650V), and relevant fish biological indicators were measured (eg. species classification and identification, abundance, and biomass, etc). Unidentified specimens were stored in 75% alcohol and brought back to the laboratory for further identification.

Environmental factors analysis

The environmental factors are measured in situ: transparency (SD, m), water depth (WD, m), electrical conductivity (EC, mS/cm), dissolved oxygen (DO, mg/L), pH value (pH), water temperature (T, °C), turbidity (NTU), oxidation-reduction potential (ORP, mv), and flow velocity (FV, m/s).

In the lab, total nitrogen (TN, mg/L), total phosphorus (TP, mg/L), ammonia nitrogen (NH₄⁺-N, mg/L), nitrate nitrogen (NO₃⁻-N, mg/L), chemical oxygen demand (COD_{Mn}, mg/L), five day biochemical oxygen demand (BOD₅, mg/L) were measured by HACH laboratory/portable water quality analyzer, which according to the requirements of monitoring methods for water and wastewater (Fourth Edition) (Wei, 2002).

Aquatic organisms and functional groups classification

Phytoplankton species and functional groups (FGs) identifications refer to Hu and Wei (2006), and *Table 2*.

Table 2. Phytoplankton functional groups of Muling River Basin

FGs	Habitat characteristics
C	Eutrophic medium and small water bodies
D	Shallow and turbid water
F	Meso eutrophic lake, clean and mixed water body
H1	Eutrophic stratified water body, shallow water and low nitrogen content
J	High nutrient mixed shallow water body
L0	Deep water or shallow water, poor eutrophic, medium large water body
M	Diurnal mixed layer of small eutrophic lakes
MP	Disturbed turbid shallow water body
N	Continuous or semi continuous mesotrophic mixed water body
P	Continuous or semi continuous medium eutrophic mixed water body
S1	Turbid mixed water with low transparency
W1	Shallow water body polluted by organic pollutants
W2	Mesotrophic shallow water body
X1	Super eutrophic shallow water body with high mixing degree
X2	Medium eutrophic shallow water body with high mixing degree
X3	The mixing layer is a shallow water body with high degree of mixing and poor nutrition
Y	Still water body (wide adaptability)

Zooplankton species and functional groups identifications refer to Shen (1999), Wang (1961), Chiang and Du (1979), Shen et al. (1979) and *Table 3*.

Table 3. Zooplankton functional groups of Muling River Basin

FGs	Body size	Feeding habits
Protozoas filter feeders (PF)	<300µm	Filter feeders feed on bacteria, algae and organic matter
Rotifers filter feeders (RF)	<300µm	Filter feeders feed on bacteria, algae and organic matter
Small copepods and claoocera filter feeders (SCF)	<0.7mm	Filter feeders feed on bacteria, algae, organic matter and protozoa
Middle copepods and claoocera filter feeders (MCF)	0.7~1.5mm	Filter feeders feed on bacteria, algae, organic matter and protozoa
Middle copepods and claoocera carnivora (MCC)	0.7~1.5mm	Predators feed on rotifers, cladocerans, Diptera insects (chironomid larvae) and oligochaetes
Large copepods filter feeders (LCF)	>1.5mm	Filter feeders feed on bacteria, algae, organic matter and protozoa
Large copepods carnivora (LCC)	>1.5mm	Predators feed on rotifers, cladocerans, Diptera insects (chironomid larvae) and oligochaetes

Macroinvertebrates species and functional groups identifications refer to Cummins (1973), Morse et al. (1984) and *Table 4*.

Table 4. Macroinvertebrates functional groups of Muling River Basin

FGs	Feeding habits
Predators (PR)	Direct swallowing or stabbing of prey
Omnivorous (OM)	Relying on the skin or gills to directly absorb the organic matter dissolved in water, it can also eat plant rotten leaves, small bivalves and crustaceans
Gather collectors (GC)	It mainly feeds on various organic particles at the bottom of the river
Filter collectors (FC)	Feed on fine organic particles (0.45mm < particle size < 1mm) in the water flow
Scrapers (SC)	It mainly feeds on various fixed living biological groups
Shredders (SH)	It mainly feeds on all kinds of falling objects and coarse organic particles (1mm ≤ particle size)

Fish species and functional groups identifications refer to Zhang and He (1993), Zhang (1995), Chen (1998), Zhu (1995) and *Table 5*.

Table 5. Fish functional groups of Muling River Basin

FGs	Catchments
Aquatic plant feeding habits (herbivores, HE)	<i>Ctenopharyngodon idellus</i> , <i>Phoxinus phoxinus</i> , <i>Phoxinus lagowskii</i>
Aquatic insect feeding habits (insectivores, IN)	<i>Phoxinus percnurus</i> , <i>Lefua costata</i> , <i>Misgurnus bipartitus</i>
Phytoplankton feeding habits (phytoplanktivores, PH)	<i>Phoxinus czekanowskii</i> , <i>Rostrigobio amurensisi</i> , <i>Hypophthalmichthys molitrix</i>
Zooplankton feeding habits (zooplanktivores, ZO)	<i>Aristichthys nobilis</i>
Benthic feeding habits (benthivores, BE)	<i>Hemiculter leucisclus</i> , <i>Pseudorasbora parva</i> , <i>Abbottina rivularis</i> , <i>Saurogobio dabryi</i> , <i>Cobitis lutheri</i> , <i>Cobitis granoci</i> , <i>Misgurnus mohoity</i>
Omnivorous (omnivores, OM)	<i>Cyprinus carpio</i> , <i>Carassius auratus gibelio</i>
Carnivorous (piscivores, PI)	<i>Silurus asotus</i> , <i>Perccottus glehni</i> , <i>Lampetra reissneri</i>

Data analysis

Normalization of evaluation system indicators: in order to unify the indicators of different orders of magnitude, dimensionless standardization is carried out on the original data:

$$X_{ij}' = \frac{X_{ij} - X_{min}}{X_{max} - X_{min}} \quad (\text{Eq.1})$$

$$X_{ij} = 1/X' \quad (\text{Eq.2})$$

where, X_{ij}' is the standard data after normalization, X_{ij} is the actual value of the forward indicator, X' is the actual value of the reverse indicator, X_{max} is the actual maximum value, and X_{min} is the actual minimum value.

Analytic Hierarchy Process (AHP) is a systematic and hierarchical multi-objective decision ranking method combining qualitative and quantitative methods proposed by A. L. Saaty, Professor of operations research at the University of Pittsburgh in the 1970s (Cao, 2012). Its basic principle is to form a hierarchical structure of multiple objectives of a system according to the dominant relationship, group each level according to the dominant relationship, and determine the relative importance and quantitative ranking through the pairwise comparison of various factors. The model judgment matrix quantifies the importance by using the 1 ~ 9 proportional scale method proposed by Professor A. L. Saaty (Wang et al., 2005) (Table 6).

Table 6. Judgment matrix scale and its meaning

No.	Comparison of importance of indicators <i>i</i> and <i>j</i>	C_{ij} quantitative values
1	<i>i</i> and <i>j</i> are equally important	1
2	<i>i</i> index is slightly more important than the <i>j</i> index	3
3	<i>i</i> index is significantly more important than <i>j</i> index	5
4	<i>i</i> index is more important than <i>j</i> index	7
5	<i>i</i> index is extremely important than the <i>j</i> index	9
6	<i>i</i> index is slightly less important than the <i>j</i> index	1/3
7	<i>i</i> index is significantly less important than the <i>j</i> index	1/5
8	<i>i</i> index is not strongly less important <i>j</i> index	1/7
9	<i>i</i> index is less important than the <i>j</i> index	1/9

Note: $C_{ij} = \{2,4,6,8,1/2,1/4,1/6,1/8\}$ indicates the importance comparison of indicators *I* and *j*, between $C_{ij} = \{1,3,5,7,9,1/3,1/5,1/7, \text{ and } 1/9\}$

Water ecological health composite index (WEHCI) (Zuo et al., 2015):

$$WEHCI = \sum_{i=1}^n (W_i \times I_i) \quad (\text{Eq.3})$$

where, W_i is the weight of the evaluation index, I_i is the normalized value of the evaluation index, and the water ecological health classification and health status are shown in Table 7.

Table 7. Classification of water ecological health

WEHCI	0~0.2	0.2~0.4	0.4~0.6	0.6~0.8	0.8~1.0
Health classification	V	IV	III	II	I
Health status	Sick	Sub-sick	General	Sub-health	Health

Results

Characteristics of aquatic life community structure

During the investigation, 83 species and variants of 43 genera and 7 phyla of phytoplankton were identified, with biomass ranging from 0.03 to 23.21 mg/L. According to the research of Padisák et al. (2009), 17 functional groups (C, D, F, H1, J, L0, M, MP, N, P, S1, W1, W2, X1, X2, X3, Y) were found, and seasonal succession is $M+P \rightarrow F+MP+P \rightarrow MP+P \rightarrow M \rightarrow M+Y \rightarrow M+MP+P$ (Fig. 2a).

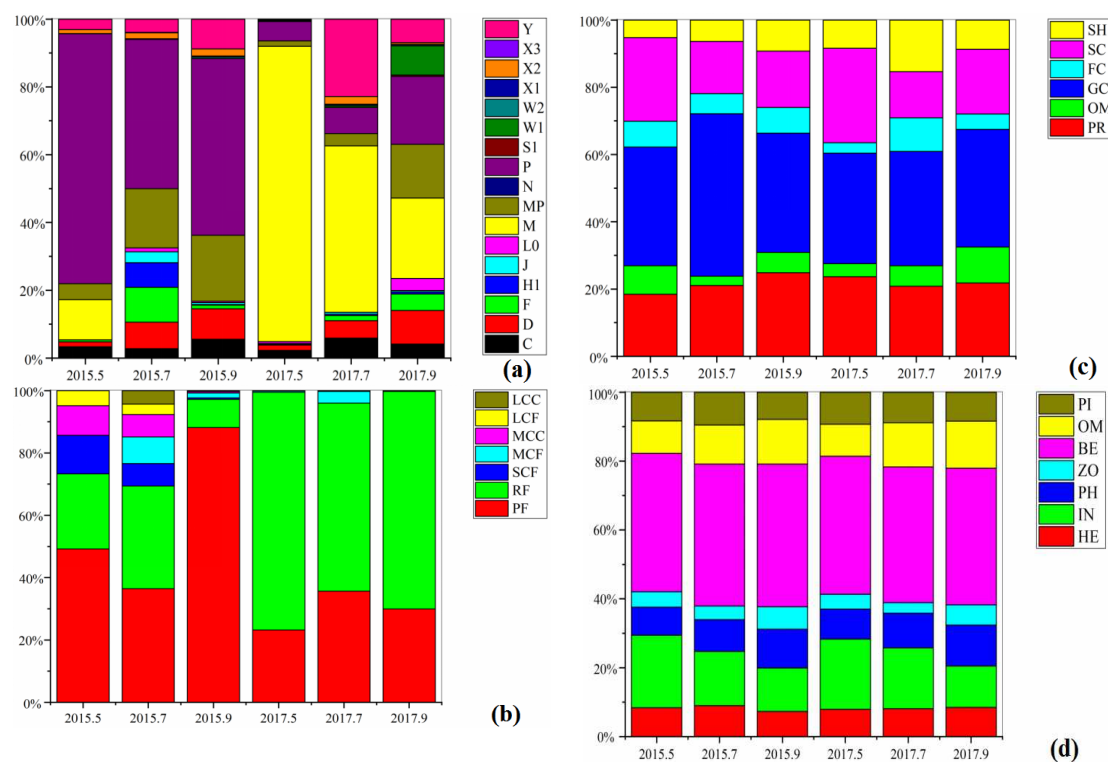


Figure 2. Relative biomass or relative abundance of aquatic functional groups in different seasons in Muling River Basin

There are 4 types of zooplankton, 27 genera and 36 species, with biomass ranging from 0.01 to 16.68 mg/L. According to the research of An et al. (2017), 7 functional groups (PF, RF, SCF, MCF, MCC, LCF, LCC) are divided into 7 functional groups (PF, RF, SCF, MCF, MCC, LCF, LCC, of which copepod nauplii is not divided into functional groups), and the seasonal succession is $PF+RF+SCF \rightarrow PF+RF \rightarrow P \rightarrow PF+RF \rightarrow PF+RF \rightarrow PF+RF$ (Fig. 2b).

Macroinvertebrates fauna, 4 phyla, 13 orders, 46 families, 158 genera/species, with abundance ranging from 9.23 to 353.3 ind./m². According to the research of Cummins

et al. (1973), 6 functional groups (PR, OM, GC, FC, SC, SH) are divided, and the seasonal succession is GC+SC→PR+GC→PR+GC→PR+GC+SC →PR+GC→PR+GC (Fig. 2c).

There are 46 species of fishes in 5 orders, 12 families, and their biomass ranges from 8.22 to 770.36 g/m³. According to the research of Ding and Liu (2011), 7 functional groups (HE, IN, PH, ZO, BE, OM, PI) are divided, and the seasonal succession is IN+BE→IN+BE+OM→IN+PH+BE+OM→IN+PH+BE+OM (Fig. 2d).

Characteristics of environmental factors

The time distribution characteristics of environmental factors in the Muling River Basin are shown in Table 8.

Table 8. Environmental factors values of Muling River Basin (Mean±SE)

	2015.5	2015.7	2015.9	2017.5	2017.7	2017.9
SD	0.35±0.05	0.32±0.07	0.48±0.04	0.44±0.04	0.24±0.03	0.34±0.04
WD	2.72±0.76	3.13±1.04	3.02±0.95	3.23±0.89	4.12±1.18	3.18±0.96
EC	0.15±0.01	0.15±0.01	0.21±0.02	0.1±0.01	0.12±0.01	0.16±0.02
DO	7.45±0.29	8.73±0.29	7.5±0.56	7.95±0.39	3.74±0.44	9.91±0.4
pH	7.42±0.12	7.03±0.26	7.99±0.06	7.78±0.14	7.92±0.04	8.31±0.05
T	14.81±0.47	22.26±0.55	6.89±0.43	14.2±0.51	22±0.57	13.24±0.47
TN	1.73±0.14	1.99±0.21	1.62±0.16	1.54±0.2	4.73±0.16	3.66±0.25
TP	0.6±0.05	0.69±0.04	0.36±0.03	0.44±0.06	0.29±0.02	0.27±0.03
NH ₄ ⁺ -N	0.22±0.02	0.35±0.04	0.13±0.01	0.51±0.26	0.16±0.01	0.54±0.09
NO ₃ ⁻ -N	0.58±0.07	1.52±0.5	0.28±0.03	1.05±0.09	2.46±0.19	5.01±0.68
COD _{Mn}	3.8±0.13	3.98±0.1	4.06±0.12	3.9±0.11	5.01±0.07	3.58±0.23
ORP	51.81±3.7	64.3±4.47	57.09±2.98	43.09±3.42	47.84±3.06	55.01±2.79
BOD ₅	1.71±0.13	1.43±0.12	1.93±0.21	1.74±0.14	1.55±0.12	2.6±0.26
NTU	37.65±4.04	91.38±18.43	82.85±17.54	40.17±5.29	191.98±53.41	77.74±18.63
FV	0.17±0.02	0.2±0.04	0.08±0.01	0.14±0.02	0.15±0.04	0.08±0.01

Water transparency (SD), water depth (WD), electroconductibility (EC), dissolved oxygen (DO), pH value (pH), temperature (T), total nitrogen (TN), total phosphorus (TP), ammonium nitrogen (NH₄⁺-N), nitrate (NO₃⁻-N), chemical oxygen demand (COD_{Mn}), oxidation-reduction potential (ORP), five-day biochemical oxygen demand (BOD₅), turbidity (NTU) and flow velocity (FV)

In May 2015 (spring), WD were significantly lower than other sampling seasons.

In July 2015 (summer), T, ORP and FV were significantly higher than other sampling seasons, while pH and BOD₅ were significantly lower than other sampling seasons.

In September 2015 (autumn), SD and EC were significantly lower than other sampling seasons, while T, NH₄⁺-N and FV were significantly lower than other sampling seasons.

In May 2017 (spring), EC, TN, NO₃⁻-N and ORP were significantly lower than other sampling seasons.

In July 2017 (summer), WD, TN, NO₃⁻-N and NTU were significantly higher than other sampling seasons, while SD and DO were significantly lower than other sampling seasons.

In September 2017 (autumn), DO, pH, NH₄⁺-N, NO₃⁻-N and BOD₅ were significantly higher than other sampling seasons. TP and COD_{Mn} were significantly lower than other sampling seasons.

Water ecological health evaluation

Water ecological health evaluation system of the Muling River Basin is set as follows, with 3 indicators at the target level, 6 indicators at the criterion level, and 27 indicators at the index level, and finally get the index weights of each level (Table 9). The climatological and hydrological data from Heilongjiang Provincial Department of water resources and Jixi Water Affairs Bureau

Table 9. Weight table of ecosystem health assessment system in Muling River Basin

Target layer	Criterion layer	Index layer	Weight
River water environmental factors(A1) 0.328508	Physical factor(B1) 0.333333	pH(C11)	0.059089
		ORP(C12)	0.017895
		EC(C13)	0.032518
	Chemical factor(B2) 0.666667	DO(C21)	0.084635
		COD _{Mn} (C22)	0.005513
		BOD ₅ (C23)	0.005513
		TN(C24)	0.042511
		TP(C25)	0.042511
		NH ₄ ⁺ -N(C26)	0.019161
		NO ₃ ⁻ -N(C27)	0.019161
River hydrological quality(A2) 0.266407	River hydrology(B3) 0.633975	SD(C31)	0.027547
		NTU(C32)	0.008236
		WD(C33)	0.042967
		T(C34)	0.017541
		FV(C35)	0.007898
		Ecological runoff(C36)	0.064707
	River structure(B4) 0.366025	River bottom(C41)	0.054978
		River bending coefficient(C42)	0.005365
		Riparian vegetation coverage(C43)	0.025682
		Riparian habitat(C44)	0.011486
River ecosystem services(A3) 0.405085	Bio-functional group diversity(B5) 0.636364	Phytoplankton functional group diversity(C51)	0.120345
		Zooplankton functional group diversity(C52)	0.071558
		Macroinvertebrates functional feeding group diversity(C53)	0.041314
		Fish functional group diversity(C54)	0.024565
	Social service function(B6) 0.363636	Public satisfaction(C61)	0.058669
		Water resources development and utilization rate(C62)	0.055647
		Flood control indicators(C63)	0.032988

Water transparency (SD), water depth (WD), electroconductibility (EC), dissolved oxygen (DO), pH value (pH), temperature (T), total nitrogen (TN), total phosphorus (TP), ammonium nitrogen (NH₄⁺-N), nitrate (NO₃⁻-N), chemical oxygen demand (COD_{Mn}), oxidation-reduction potential (ORP), five day biochemical oxygen demand (BOD₅), turbidity (NTU) and flow velocity (FV)

Comprehensive water ecological health index of the target layer: The comprehensive water ecological health index of the 3 target layers of the Muling River Basin Water Ecological Health Evaluation System is between 0.2743 and 0.7526. The health classification and health status were at level IV sub-sick, III general, II sub-health status respectively (*Table 10*).

Table 10. WEHCI of target layer

Target layer	2015.5	2015.7	2015.9	2017.5	2017.7	2017.9	Average
River water environmental factors	0.3894	0.5509	0.4645	0.3717	0.331	0.7526	0.4767
Classification, status	IV, Sub-sick	III, General	III, General	IV, Sub-sick	IV, Sub-sick	II, Sub-health	III, General
River hydrological quality	0.4325	0.5657	0.4423	0.5006	0.6832	0.4233	0.5079
Classification, status	III, General	III, General	III, General	III, General	II, Sub-health	III, General	III, General
River ecosystem services	0.4309	0.2743	0.5842	0.5293	0.4671	0.6995	0.4975
Classification, status	III, General	IV, Sub-sick	III, General	III, General	III, General	II, Sub-health	III, General

Comprehensive index of water ecological health of the criterion level: The comprehensive index of water ecological health of the 6 criterion level of the Muling River Basin Water Ecological Health Evaluation System is between 0.256 and 0.8205. The health classification and health status were at IV sub-sick, III general, II sub-health, I health status, respectively (*Table 11*).

Table 11. WEHCI of criterion layer

Criterion layer	2015.5	2015.7	2015.9	2017.5	2017.7	2017.9	Average
Physical factor	0.3578	0.4049	0.7663	0.3349	0.4328	0.8205	0.5195
Classification, status	IV, Sub-sick	III, General	II, Sub-health	IV, Sub-sick	III, General	I, Health	III, General
Chemical factor	0.4052	0.6239	0.3136	0.3902	0.2801	0.7187	0.4553
Classification, status	III, General	II, Sub-health	IV, Sub-sick	IV, Sub-sick	IV, Sub-sick	II, Sub-health	III, General
River hydrology	0.3801	0.5360	0.3830	0.4424	0.6380	0.3057	0.4476
Classification, status	IV, Sub-sick	III, General	IV, Sub-sick	III, General	II, Sub-health	IV, Sub-sick	III, General
River structure	0.5233	0.6172	0.5449	0.6013	0.7616	0.6269	0.6125
Classification, status	III, General	II, Sub-health	III, General	II, Sub-health	II, Sub-health	II, Sub-health	II, Sub-health
Bio-functional group diversity	0.2936	0.2560	0.5567	0.4481	0.5591	0.7378	0.4752
Classification, status	IV, Sub-sick	IV, Sub-sick	III, General	III, General	III, General	II, Sub-health	III, General
Social service function	0.6713	0.3062	0.6324	0.6713	0.3062	0.6324	0.5366
Classification, status	II, Sub-health	IV, Sub-sick	II, Sub-health	II, Sub-health	IV, Sub-sick	II, Sub-health	III, General

Index layer water ecological health comprehensive index: The comprehensive target layer and criterion layer finally get the comprehensive water ecological health index of the Muling River Basin (Table 12). The ecological health classification rose from level III to level II, and the health status rose from general to sub-health level, with an overall upward trend. The average value was 0.4935, the health classification was level III, and the health status was average. In September 2017 (autumn), the Muling River Basin had the highest comprehensive water ecological health index, and the health status of the Muling River Basin improved.

Table 12. WEHCI table of ecosystem health assessment system in Muling River Basin

	2015.5	2015.7	2015.9	2017.5	2017.7	2017.9
pH(C11)	0.018839	0.0126149	0.0439227	0.0310095	0.0381506	0.0590892
ORP(C12)	0.0068347	0.0168284	0.0113673	0.0009107	0.0040845	0.0093535
EC(C13)	0.0135114	0.0148941	0.0286193	0.0047487	0.0051586	0.0214055
DO(C21)	0.0422883	0.0607683	0.041912	0.0519836	0.0012149	0.0841406
COD _{Mn} (C22)	0.0021349	0.0026173	0.0026368	0.002181	0.0055132	0.0008138
BOD ₅ (C23)	0.0012552	0.0011883	0.0026969	0.0018005	0.001629	0.0048939
TN(C24)	0.0095786	0.0182735	0.005607	0.0046809	0.0399681	0.0286367
TP(C25)	0.0258162	0.0379393	0.0157343	0.0144458	0.0023835	0.0024275
NH ₄ ⁺ -N(C26)	0.0064664	0.0112471	9.284E-05	0.0074593	0.0019045	0.0173238
NO ₃ ⁻ -N(C27)	0.0011912	0.0045999	5.083E-20	0.0029019	0.0087295	0.0191609
SD(C31)	0.0121862	0.0076306	0.0222439	0.0207826	0.0044329	0.0125422
NTU(C32)	0.0003642	0.0030525	0.0033236	0.0005071	0.0075098	0.0030742
WD(C33)	0.0189015	0.0094863	0.013539	0.0218909	0.0281763	0.0044069
T(C34)	0.0087378	0.0172628	0.0002943	0.008506	0.0163435	0.0057532
FV(C35)	0.0053248	0.0067476	0.0003703	0.0043531	0.0049459	0.0006445
Ecological runoff(C36)	0.018688	0.0463469	0.0252158	0.018688	0.0463469	0.0252158
River bottom(C41)	0.0386493	0.0386493	0.0386493	0.0386493	0.0386493	0.0386493
River bending coefficient(C42)	0.0049532	0.0049532	0.0049532	0.0049532	0.0049532	0.0049532
Riparian vegetation coverage(C43)	0.0024462	0.0116039	0.0045479	0.0100525	0.0256825	0.0125531
Riparian habitat(C44)	0.0049789	0.0049789	0.0049789	0.0049789	0.0049789	0.0049789
Phytoplankton functional group diversity(C51)	0.0484634	0.0236319	0.1144441	0.0258784	0.0305872	0.0804393
Zooplankton functional group diversity(C52)	0.0051496	0.0140533	0.0091625	0.0540971	0.0699923	0.0642071
Macroinvertebrates functional feeding group diversity(C53)	0.006511	0.0069479	0.0047469	0.0248902	0.0271283	0.04058
Fish functional group diversity(C54)	0.0155561	0.0213589	0.0151496	0.0106452	0.0164109	0.0049635
Public satisfaction(C61)	0.0537792	0.0003649	0.048052	0.0537792	0.0016434	0.048052
Water resources development and utilization rate(C62)	0.0305368	0.0305368	0.0305368	0.0305368	0.0305368	0.0305368
Flood control indicators(C63)	0.0145699	0.0145699	0.0145699	0.0145699	0.0145699	0.0145699
WEHCI	0.4177	0.4428	0.5071	0.4699	0.4799	0.6434
Classification, status	III, General	III, General	III, General	III, General	III, General	II, Sub-health
WEHCI average: 0.4935; Health classification: III; Health status: General						

Discussion

Usage of pesticides does not result in an accumulation of nutrients in the water (Reed et al., 2000). The survey found that the trend of TN concentration in 2015 and 2017 was similar, and it was higher in summer than in spring and autumn. The higher concentration in summer is due to the increase of surface runoff by rainfall, which indirectly increases the concentration of nutrients in the river. The average concentration of TN (3.31 mg/L) in 2017 was twice that in 2015. A more obvious high concentration of TP was observed in July (summer) of the same year, which may be caused by villagers reclaiming farmland and using pesticides and fertilizers. The $\text{NH}_4^+\text{-N}$ concentration in May 2017 (0.51 mg/L) was higher than that in May 2015 (0.22 mg/L); On the contrary, in July, the maximum concentration of $\text{NH}_4^+\text{-N}$ was 2.731 mg / L > 1.5 mg / L (higher than class IV water), which was not suitable for human drinking. In September 2015, the concentration of $\text{NO}_3^-\text{-N}$ was as low as 0.28 mg / L. In 2017, the concentration continued to rise to 5.01 mg / L, 18 times higher than before. At the same time, nitrogen limitation and phosphorus limitation were also observed. The change trend of TN: TP ratio shows that it is nitrogen limited in 2015 (TN: TP < 16) (Redfield, 1934), reaching the lowest value in May 2017 (spring), but it is still nitrogen limited (TN: TP = 5.21). In July (summer) of the same year, it increased rapidly, reached the peak (TN: TP = 17.97 > 16) and turned to phosphorus limit, which was still close to the critical value in autumn, up to 15.76. In addition, the change range of COD_{Mn} in 2015 was small, from 3.80 mg/L to 4.06 mg/L. In May 2017, it decreased to 3.90 mg/L in July 2017 (summer), the highest value was 5.01 mg/L, and rapidly decreased to 3.58 mg/L in September.

As Muling River Basin is located in the agricultural wetland ecological area of Sanjiang Plain, large-scale cultivation is carried out in spring, and the total biomass of phytoplankton reaches the maximum in spring and the minimum in summer. This survey result is consistent with that of Daning River (Zhu et al., 2013). The studies of Fasham et al. (1990) show that the increase of nutrient concentration will lead to the increase of plankton quantity, which is the main driving factor for the dynamic change of plankton community structure. Plankton is sensitive to environmental changes and is considered a good indicator (Jeppesen et al., 2011). In addition, the plankton community structure is affected by hydrological conditions (Rennie and Jackson, 2005). Summer rainfall raises the water level of Muling River, and the river continuously scours the exposed riparian zone, resulting in a significant increase in the concentration of suspended particulate matter, a decrease in the effective utilization rate of light, and an impact on the growth of plankton (Shi et al., 2020). At the same time, water and soil loss in the riparian zone leads to a large amount of sediment entering the river. The surface of river sediment is covered with muddy soil. These sediments will also adhere to the body surface, trachea and gills of macroinvertebrates, resulting in the inability of macroinvertebrates to breathe and finally die. Substrate types and aquatic vascular plants are factors affecting the growth and functional group distribution of macroinvertebrates. The community structure of macroinvertebrates is usually determined by the physical structure and complexity of habitat (Leason et al., 2018). Aquatic vascular plants play an important role in constructing benthic species and selecting species related to functional group dynamics and feeding habits (Li et al., 2022). The distribution of benthos also depends on vegetation types, especially the structure and growth form of aquatic vascular plants, which affect underwater climate

and chemical properties by absorbing and releasing chemicals (such as nutrients and antagonists) (Valinti et al., 2011).

Ecosystem function essentially depends on the functional groups of species, which has become a powerful and reliable method to study the dynamic changes of community functional characteristics (Diaz et al., 2004). Functional groups are species with similar morphological and physiological characteristics. The great difference in their spatial pattern is the response to environmental changes and the trade-off between different functions, which can greatly simplify the food web (Morgan, 1985). According to Padišák et al. (2009), 17 phytoplankton functional groups were investigated in this study, which exceeded Mudanjiang (11) located in the same province (Yu et al., 2012). The density of zooplankton functional groups is affected by phytoplankton biomass of primary producers (Trevisan and Forsberg, 2007). Globally, land use change, especially the loss of riparian vegetation, may lead to the reduction or change of benthic community structure, function and diversity. Vegetation litter is the main food source of macroinvertebrates functional feeding group SH. the reduction of food will hinder their growth and development and imbalance the aquatic ecosystem (Liu et al., 2019).

The pollution and damage around Muling River Basin are serious, and the habitat is also investigated during the sampling period. As an integral part of the basin, the characteristics of Muling River are determined by the characteristics of the basin in the final analysis (Liang et al., 2021). River ecosystem is a complex, open, dynamic, non-equilibrium and nonlinear system. The core of understanding the essential characteristics of rivers is to understand the composition, structure and function of river ecosystem. Repairing damaged river ecosystem is river ecological restoration (Rakhit, 2021). To understand a river, we must first understand its physical geography, climate, geology and land use. The external influencing factors of the river ecosystem determine the physical and hydrochemical characteristics of the river, such as runoff, channel, matrix type, water and sediment characteristics (Boulion, 2020). At the same time, the river water ecosystem is easily affected by the areas around the shore. There is a correlation between the impact of local human activities on the water ecosystem in Muling River Basin and the changes of other ecosystems (Ajagbe, 2021). In addition, river is always an important and active ecological factor in terrestrial ecosystem, and the study of terrestrial ecosystem can never be carried out alone without the study of river (Haidri and Sabri, 2020). Therefore, it is very necessary to regard the watershed as a composite ecosystem and combine the research of river ecosystem and terrestrial ecosystem in theory and practice.

Conclusion

During the survey, 83 species of phytoplankton belonging to 43 genera and 7 phyla were found in Muling River Basin, which were divided into 17 functional groups. The seasonal succession was $M+P \rightarrow F+MP+P \rightarrow MP+P \rightarrow M \rightarrow M+Y \rightarrow M+MP+P$. There are 4 classes, 27 genera and 36 species of zooplankton, which are divided into 7 functional groups. The seasonal succession is $PF+RF+SCF \rightarrow PF+RF \rightarrow P \rightarrow PF+RF \rightarrow PF+RF \rightarrow PF+RF$. Macroinvertebrates belong to 4 phyla, 13 orders, 46 families and 158 genera/species, which are divided into 6 functional groups. The seasonal succession is $GC+SC \rightarrow PR+GC \rightarrow PR+GC \rightarrow PR+GC+SC \rightarrow PR+GC \rightarrow PR+GC \rightarrow PR+GC$. There are 46 species, 12 families and 5 orders of fish, are divided into 7 functional groups. The

excellent seasonal succession is
IN+BE→IN+BE+OM→IN+PH+BE+OM→IN+BE→IN+PH+BE+OM→IN+PH+BE+OM→IN+PH+BE+OM.

By calculating the comprehensive index of water ecological health in Muling River Basin, the index in the target layer is between 0.2743 and 0.7526, which is in the state of grade IV Sub-sick to grade II Sub-health. In the criterion layer, the index is between 0.256 and 0.8205, which is in grade IV Sub-sick to grade I Healthy state. The comprehensive index of water ecological health in Muling River Basin in each season is 0.4177, 0.4428, 0.5071, 0.4699, 0.4799 and 0.6434 respectively. The water ecological health rating rises from grade III to grade II, and the health status rises from the general level to the Sub-health level. The overall trend is upward, with an average value of 0.4935. The health rating is grade III, and the health status is General.

Acknowledgements. This study was supported by Dalian Ocean University Talent Introduction Project “Investigation of Liaohe Fishery Resources and Environment” (HDYJ202128), the Research on Protection and Sustainable Utilization Technology of Sturgeon Resources in Heilongjiang Province (HLJSCXH2019003), the central government supports the reform and development fund projects of local colleges and universities “Research on integrated technology innovation of sustainable utilization of cold water fish resources industrialization” (2020GSP14), the Key research topics of economic and social development in Heilongjiang Province (20309), the major special projects of science and technology in Liaoning Province (2020JH1/10200002), the Dalian Science and Technology Innovation Fund Project (2019J12SN64), and special project on agricultural financial fund from the Ministry of Agriculture and Rural Affairs of China entitled “Survey of fishery resources and environment in key waters of Northeast China”. The authors are grateful to the people that helped with all aspects of the fieldwork.

REFERENCES

- [1] Ajagbe, S. O. (2021): Impacts of loss of vegetation cover on biodiversity of Ikere-gorge, Oyo State Nigeria. – *Nigerian Journal of Animal Production* 48(4): 14-23.
- [2] Allan, J. D., Castillo, M. M. (2007): *Stream ecology: structure and function of running waters*. – Springer Science & Business Media.
- [3] An, R., Wang, F. Y., Yu, H. X., Ma, C. X. (2017): Seasonal dynamics of zooplankton functional groups and their relationships with environmental factors in the Sanhuanpao wetland reserve. – *Acta Ecologica Sinica* 37(6): 1851-1860. (in Chinese with English abstract).
- [4] Beaugrand, G., Ibañez, F., Reid, P. C. (2000): Spatial, seasonal and long-term fluctuations of plankton in relation to hydroclimatic features in the English Channel, Celtic Sea and Bay of Biscay. – *Marine Ecology Progress Series*.
- [5] Becker, V., Huszar, V. L. M., Crossetti, L. O. (2009): Responses of phytoplankton functional groups to the mixing regime in a deep subtropical reservoir. – *Hydrobiologia* 628(1): 137-151.
- [6] Boulion, V. V. (2020): The Ratio between Primary Production Values of Lake and Terrestrial Ecosystems. – *Doklady Biological Sciences* 493(1): 107-109.
- [7] Cao, M. L. (2012): Determination of evaluation index weight by analytic hierarchy process and excel calculation. – *Jiangsu Science & Technology Information* 2: 39-40. (in Chinese with English abstract).
- [8] Chen, Y. Y. (1998): *Chinese zoology, Osteichthyes*. – Beijing: Science and Technology Press. (in Chinese).
- [9] Chiang, S. C., Du, N. S. (1979): *Freshwater Cladocera*. – Beijing: Science Press. (in Chinese).

- [10] Chowdhury, M., Hossain, M. S., Das, N. G., Barua, P. (2011): Environmental variables and fisheries diversity of the Naaf River Estuary, Bangladesh. – *Journal of Coastal Conservation* 15(1): 163-180.
- [11] Cummins, K. W. (1973): Trophic Relations of Aquatic Insects. – *Annual Review of Entomology* 18(1): 183-206.
- [12] David, V., Sautour, B., Chardy, P., Leconte, M. (2005): Long-term changes of the zooplankton variability in a turbid environment: The Gironde estuary (France). – *Estuarine, Coastal and Shelf Science* 64(2-3): 171-184.
- [13] Diaz, S., Hodgson, J. G., Thompson, K., Cabido, M., Zak, M. R. (2004): The plant traits that drive ecosystems: evidence from three continents. – *Journal of Vegetation Science* 15(3): 295-304.
- [14] Ding, B. Q., Liu, H. Z. (2011): Analysis of the Fish Feeding Guild Composition in the Yangtze River. – *Sichuan Journal of Zoology* 30(1): 31-35. (in Chinese with English abstract).
- [15] Ejsmont-Karabin, J., Karabin, A. (2013): The suitability of zooplankton as lakes ecosystem indicators: crustacean trophic state index. – *Polish Journal of Ecology* 61(3): 561-573.
- [16] Elliott, M., Quintino, V. (2010): *Benthic Macroinvertebrate and Application in the Assessment of Stream Ecology*. – Tsinghua University Press, Beijing.
- [17] Fasham, M. J. R., Ducklow, H. W., Mckelvie, S. M. (1990): A nitrogen-based model of plankton dynamics in the oceanic mixed layer. – *Journal of Marine Research* 48(3): 591-639.
- [18] Haidri, H., Sabri, A. (2020): Boratha Intersection Signal Design and Assess the Impact of Its Noise on The Surrounding Areas. – *Solid State Technology* 63(3): 5427-5442.
- [19] Han, X. M., Gong, Z. L., Yang, X. M., Li, Y. Y., Chen, Z. J., Zhu, H. H., Wang, F. M. (2021): Diversity and Function Prediction of Bacterioplankton Under Human Disturbance in the Main Stream of the Laoguan River Before and After the Flood Season. – *Environmental Science* 42(2): 831-841. (in Chinese with English abstract).
- [20] Hu, H. J., Wei, Y. X. (2006): *The Freshwater Algae of China: Systematics, Taxonomy and Ecology*. – Science press, Beijing China. (in Chinese).
- [21] Jeppesen, E., Nøges, P., Davidson, T. A., Haberman, J., Nøges, T., Blank, K., Lauridsen, T. L., Sondergaard, M., Sayer, C., Laugaste, R., Johansson, L. S., Bjerring, R., Amsinck, S. L. (2011): Zooplankton as indicators in lakes: a scientific-based plea for including zooplankton in the ecological quality assessment of lakes according to the European Water Framework Directive (WFD). – *Hydrobiologia* 676(1): 279-297.
- [22] Jungwirth, M., Muhar, S., Schmutz, S. (2000): Assessing the ecological integrity of running waters. – *Hydrobiologia* 422-423(2): 85-97.
- [23] Leason, G. J. E., Bortolotti, Y. J., Rooney, C. R. (2018): Wetland microhabitats support distinct communities of aquatic macroinvertebrates. – *Journal of Freshwater Ecology* 33(1): 73-82.
- [24] Li, D. D., Xu, X. M., Hu, X. Q., Liu, Q. G., Wang, Z. C., Zhang, H. Z., Wang, H., Wei, M., Wang, H. Z., Liu, H. M., Li, C. H. (2015): Genome-wide analysis and heavy metal-induced expression profiling of the HMA gene family in *Populus trichocarpa*. – *Frontiers in Plant Science* 6: 1149.
- [25] Li, L., Gou, M. M., Wang, N., Ma, W., Xiao, W. F., Liu, C. F., La, L. M. (2021): Landscape configuration mediates hydrology and nonpoint source pollution under climate change and agricultural expansion. – *Ecological Indicators* 129: 107959.
- [26] Li, D. D., Yang, J. L., Pa, S., Zeng, M. Z., Sun, J. L., Yu, S., He, Y. T., Li, C. H. (2022): PuC3H35 confers drought tolerance by enhancing lignin and proanthocyanidin biosynthesis in the roots of *Populus ussuriensis*. – *New phytologist* 233(1): 390-408.
- [27] Liang, X., Xie, Q., He, M., Liu, Q., Morozov, V. (2021): Reservoir Characteristics and Its Comprehensive Evaluation of Gray Relational Analysis on the Western Sulige Gas Field, Ordos Basin, China. – *Geofluids* 2: 1-12.

- [28] Liu, M. H., Meng, Y., Cao, J. J., Cui, X. B., Al, M. N. (2019): Functional Traits of Macroinvertebrates in Naolihe Wetland. – *Journal of Northeast Forestry University* 47(1): 76-82. (in Chinese with English abstract).
- [29] Lobry, J., David, V., Pasquaud, S., Lepage, M., Éric, R. (2008): Diversity and stability of an estuarine trophic network. – *Marine Ecology Progress Series* 358(1): 13-25.
- [30] Lu, K., Wu, H., Xue, Z., Lu, X., Batzer, D. P. (2019): Development of a multi-metric index based on aquatic invertebrates to assess floodplain wetland condition. – *Hydrobiologia* 827(1): 141-153.
- [31] Lu, K., Wu, H., Guan, Q., Lu, X. (2020): Aquatic invertebrate assemblages as potential indicators of restoration conditions in wetlands of northeastern china. – *Restoration Ecology* 29(1): e13283.
- [32] Lu, K., Batzer, D. P., Wu, H. (2021): Aquatic invertebrate assemblages during the spring-thaw season in wetlands of northeastern china. – *Hydrobiologia* 848(1): 1-11.
- [33] Mangadze, T., Bere, T., Mwedzi, T. (2016): Choice of biota in stream assessment and monitoring programs in tropical streams: a comparison of diatoms, macroinvertebrates and fish. – *Ecological Indicators* 63(4): 128-143.
- [34] Michele, A. B., Mark, J. O. (2006): A comparison of phytoplankton community assemblages in artificially and naturally mixed subtropical water reservoirs. – *Freshwater Biology* 51(5): 973-982.
- [35] Morgan, M. D. (1985): The Effect of Altered pH on Zooplankton Community Structure in a Disturbed New Jersey Pine Barrens Pond. – *Journal of Freshwater Ecology* 3(4): 467-476.
- [36] Morse, J. C., Yang, L. F., Tian, L. X. (1984): *Aquatic Insects of China useful for monitoring water quality*. – Nanjing: Hohai University Press.
- [37] Nash, J. A., Miesel, J. R., Bonito, G. M., Sakalidis, M. L., Ren, H., Warnock, D., Tiemann, L. K. (2021): Biochar restructures plant-soil-microbe relationships in a woody cropping system. – *Soil Science Society of America Journal* 85(6): 2019-2039.
- [38] Padisák, J., Crossetti, L. O., Naselli-Flores, L. (2009): Use and misuse in the application of the phytoplankton functional classification: a critical review with updates. – *Hydrobiologia* 621(1): 1-19.
- [39] Ptacnik, R., Lepistö, L., Willén, E., Brettum, P., Andersen, T., Rekolainen, S., Lyche Solheim, A., Carvalho, L. (2008): Quantitative responses of lake phytoplankton to eutrophication in Northern Europe. – *Aquatic Ecology* 42(2): 227-236.
- [40] Rakshit, R. (2021): Macro-mechanical characteristics and their control on the strength of sandstones of western Indo-Burmese Ranges, NE India. – *Acta Geodynamica et Geomaterialia* 18(2): 241-252.
- [41] Redfield, A. C. (1934): *On the Proportions of Organic Derivatives in Sea Water and Their Relation to the Composition of Plankton*. – University Press of Liverpool, Liverpool, UK.
- [42] Reed, S. D., Grisso, R. D., Woldt, W. E., Niemeyer, S. M. (2000): Waste Assessment of Agricultural Chemicals, Petroleum Products and Maintenance Residuals on Farmsteads. – *Applied Engineering in Agriculture* 16(2): 175-190.
- [43] Ren, H., Warnock, D. D., Tiemann, L. K., Quigley, K., Miesel, J. R. (2021): Evaluating foliar characteristics as early indicators of plant response to biochar amendments. – *Forest Ecology and Management* 489(42): 119047.
- [44] Rennie, M. D., Jackson, L. J. (2005): The influence of habitat complexity on littoral invertebrate distributions: patterns differ in shallow prairie lakes with and without fish. – *Canadian Journal of Fisheries and Aquatic Sciences* 62(9): 2088-2099.
- [45] Shen, J. R., Dai, A. Y., Song, R. X. (1979): *Freshwater Copepods*. – Beijing: Science Press. (in Chinese).
- [46] Shen, Y. F. (1999): *Protozoology*. – Beijing: Science Press. (in Chinese).
- [47] Shen, H. L. (2014): Phytoplankton functional groups in a high spatial heterogeneity subtropical reservoir in China. – *Journal of Great Lakes Research* 40(4): 859-869.

- [48] Shi, P. C., Zhu, G. W., Yang, W. B., Xu, H., Zhu, M. Y., Liu, M. L., Yu, Z. M., Wu, Z. X., Zheng, W. T., Wang, Y. C., Da, W. Y., Hu, L. N. (2020): Spatial-temporal Distribution of Suspended Solids and Its Sedimentation Flux and Nutrients Effects in Xin'anjiang Reservoir, China. – *Environmental Science* 41(5): 2137-2148. (in Chinese with English abstract).
- [49] Sukatar, A., Ertas, A., Gülle, S., Kizilkaya, N. T. (2020): Trophic State Assessment of Brackish Bafa Lake (Turkey) Based on Community Structure of Zooplankton. – *LimnoFish - Journal of Limnology and Freshwater Fisheries Research* 6(2): 88-99.
- [50] Tockner, K. M., Pusch, D., Borchardt, M. S. L. (2010): Multiple stressors in coupled river-floodplain ecosystems. – *Freshwater Biology* 55(1): 135-151.
- [51] Trevisan, G. V., Forsberg, B. R. (2007): Relationships among nitrogen and total phosphorus, algal biomass and zooplankton density in the central Amazonia lakes. – *Hydrobiologia* 586(1): 357-365.
- [52] Valinoti, C. E., Ho, C. K., Armitage, A. R. (2011): Native and exotic submerged aquatic vegetation provide different nutritional and refuge values for macroinvertebrates. – *Journal of Experimental Marine Biology and Ecology* 409(1-2): 42-47.
- [53] Wang, J. Y. (1961): *Freshwater rotifers of China*. – Beijing: Science Press. (in Chinese).
- [54] Wang, B. X., Yang, L. F., Hu, B. J., Shan, L. N. (2005): A preliminary study on the assessment of stream ecosystem health in south of Anhui Province using Benthic-Index of Biotic Integrity. – *Acta Ecologica Sinica* 25(6): 1481-1490. (in Chinese with English abstract).
- [55] Wei, F. S. (2002): *Water and wastewater monitoring method (Fourth Edition)*. – Beijing: China Environmental Science Press. (in Chinese).
- [56] Wetzel, R. G. (2001): *Limnology*. – Academic Press, San Diego, California, USA.
- [57] Yu, H. X., Wu, J. H., Ma, C. X., Qin, X. B. (2012): Seasonal dynamics of phytoplankton functional groups and its relationship with the environment in river: a case study in northeast China. – *Journal of freshwater ecology* 27(3): 429-441.
- [58] Zhang, J. M., He, Z. H. (1993): *Inland waters fisheries natural resources survey manual*. – Beijing: Science Press. (in Chinese).
- [59] Zhang, J. M. (1995): *Fishes of Heilongjiang Province*. – Harbin: Heilongjiang Science & Technology Press. (in Chinese).
- [60] Zhu, S. Q. (1995): *The synopsis of freshwater fishes of China*. – Nanjing: Jiangsu Science and Technology Press. (in Chinese).
- [61] Zhu, K. X., Bi, Y. H., Hu, Z. Y. (2013): Responses of phytoplankton functional groups to the hydrologic regime in the Daning River, a tributary of Three Gorges Reservoir, China. – *Science of the Total Environment* 450-451(1): 169-177.
- [62] Zuo, Q. T., Chen, H., Zhang, Y. Y. (2015): Impact factors and health assessment of aquatic ecosystem in Upper and Middle Huai River Basin. – *Shuili Xuebao* 46(9): 1019-1027. (in Chinese with English abstract).

ANTIMICROBIAL AND ANTIOXIDANT ACTIVITY AND CHARACTERIZATION OF SILVER NANOPARTICLES GREEN-SYNTHESIZED USING SOME MEDICINAL PLANT EXTRACTS

AL-FAWWAZ, A. T.^{1*} – ALMUHUR, R. A.¹ – AL-BARRI, S. N. – AL-SHIRA’H, H. H.²

¹Department of Biological Sciences, Faculty of Science, Al al-Bayt University, P.O.BOX 130040, Mafraq 25113; Jordan
(phone: +96-2629-7000 ext. 2168; mobile: +96-2777-626-144)

²Al Meshrif School, Ministry of Education, Mafraq, Jordan
(phone: +96-2779-519-898)

*Corresponding author

e-mail: al_fawwaz@aabu.edu.jo; phone: +96-2777-626-144

(Received 9th Feb 2022; accepted 20th Jun 2022)

Abstract. Research on nanoparticles is very important because of their widespread applications in human life, such as in cancer research, food industry, and wastewater treatment. The aims of the current study were to synthesize silver nanoparticles (AgNPs) using different plant extracts and to evaluate their antimicrobial and antioxidant activities. The biosynthesis of silver nanoparticles was confirmed by color changes and characterization techniques such as Fourier transform infrared spectroscopy (FTIR) and ultraviolet–visible (UV–vis.) spectroscopy. The antioxidant properties were evaluated by 2,2-diphenyl-1-picrylhydrazyl (DPPH) radical scavenging methods, and the antimicrobial activities were determined using the well diffusion method. The results confirmed the highest inhibition zone was found in *Syzygium aromaticum*-AgNPs against *Escherichia coli*, *Staphylococcus aureus*, and *Bacillus subtilis*, with 19.0±2.64, 19±2.17, and 19±1.5mm, respectively, followed by *Thymus vulgaris*-AgNPs with 18.0±2.7, 15.0±2.64, and 15.0±2.17mm, respectively. *Artemisia judaica* and *Thymus vulgaris*-AgNPs presented antifungal activity against *Candida albicans* (28.0±2.5 and 25±1.5mm, respectively, compared to 20±2.5 and 13±1.2mm. The AgNPs of *Cinnamomum verum* exhibited the greatest antioxidant activity (92.0%), while the antioxidant activity was only 43.7% for *C. verum* extracts. The green synthesis of silver nanoparticles using plant extracts exhibited antimicrobial and antioxidant activities due to the different functional groups, which will lead to the use of AgNPs in different medical applications in the near future.

Keywords: nanomedicine, bioactivity, plant extracts, antimicrobial activity, radical scavenging, FTIR

Introduction

Recently, nanoscience is attracting increasing attention, and nanostructures have been developed for use in microelectronics as well as medical, and biological studies (Bhagat et al., 2015). Modern research focuses on the designation, synthesis, and development of nanoparticles to be used in pharmaceutical therapy. Nanoparticles can be derived from biological or chemical origins. Microorganisms, enzymes, and plants are considered the foundations of biological nanoparticles. Furthermore, medicinal plants’ therapeutic characteristics are adding more value to their derived nanoparticles since many medicinal plants that possess compounds with antioxidant and antimicrobial activities, such as phyto-compounds, show additive potential with these nanoparticles (Pasupuleti et al., 2008; Keshari et al., 2020). Moreover, the use of biological nanoparticles that do not require toxic chemicals during their synthesis is considered advantageous compared to the use of other types of nanoparticles (Forough and Farhadi, 2010; Khali et al., 2014). The distinct properties of metal nanoparticles were, moreover, found to vary depending

on the method of synthesis (Samat and Nor, 2013). A wide range of metal nanoparticles have been developed and synthesized depending on their intended applications. Au, Ag, Cu, Zn, and many others have been used in metallic nanoparticle synthesis based on the biological method (Samat and Nor, 2013; Bhagat et al., 2015). Silver nanoparticles (AgNPs) are considered a valuable choice due to their toxic potential against causes of disease, such as bacteria, viruses, and fungi, in addition to their unrivaled physical, chemical, electrical, and magnetic characteristics (Bhagat et al., 2015) making them suitable for use in nanomedicine applications such as drug delivery (Praveen et al., 2012), treating cancer (Nayak et al., 2016; Castro-Aceituno et al., 2016), and wound healing (Satyavani et al., 2011; Rigo et al., 2013). The low production yields of AgNPs and the toxicity of their chemical reagents present challenges during the physical or chemical production of nanoparticles. Researchers are also focusing on plant-extract use for AgNP synthesis, thereby avoiding exposure to microorganism pathogenicity. Several extracts derived from plants that are used widely in folk medicine or feature bioactive compounds were employed to synthesize silver nanoparticles such as *Origanum vulgare*, *Brassica nigra*, *Berberis vulgaris* (Salayová et al., 2021), *Azadirachta indica* (Sitaramanjaneya et al., 2018), and *Cestrum nocturnum*. The silver nanoparticles synthesized using *C. nocturnum* extract showed greater potential antioxidant and antibacterial activities against several bacterial strains compared to non-plant-extracted AgNPs (Keshari et al., 2020).

Metabolites found in different plant extracts are responsible for decreasing the particle sizes of nanoparticles because metabolites act as reducing agents (Sitaramanjaneya et al., 2018). Synthesizing nanoparticles from plant extracts can enhance the biological properties of the nanoparticles. Therefore, biological methods for synthesizing nanoparticles using various plant extracts have gained considerable importance in different biological and medical applications (Lalitha et al., 2013; Sitaramanjaneya et al., 2018; Salayová et al., 2021). Recently, silver nanoparticles have been widely used as antioxidant and antimicrobial agents (Asirvatham et al., 2013; Chandra et al., 2014; Bhumi et al., 2015; Sitaramanjaneya et al., 2018). In the present study, *Artemisia judaica*, *Thymus vulgaris*, *Salvia rosmarinus*, *Cinnamomum verum*, *Allium sativum*, and *Syzygium aromaticum* were selected because they used in Jordan as medicinal plants or as food additives and they had not been synthesized previously in Jordan as nanoparticles and test their antimicrobial and antioxidant activity. The main objective of this research was to synthesize silver nanoparticles using different plant extracts and evaluate their antimicrobial and antioxidant activities. The synthesized nanoparticles were characterized via different techniques such as Fourier transform infrared spectroscopy (FTIR) and UV-visible (UV-vis) spectroscopy.

Materials and Methods

Plant Material Collection and Preparation

Aerial parts of *Artemisia judaica*, *Thymus vulgaris*, and *Salvia rosmarinus* were collected from Al-Mafraq in northern Jordan during March 2021, while *Cinnamomum verum*, *Allium sativum*, and *Syzygium aromaticum* were purchased as commercial products from Al-Mafraq, Jordan. All plant samples were washed with distilled water, dried in an oven at 60 °C, and ground in a blender to achieve a fine powder. Ethanol and distilled water were used for the extraction. Based on the preliminary results, ethanol was used as the extraction solvent in all following experiments.

Extract Preparation

The extract was prepared using a 500 ml Erlenmeyer flask containing 25 g plant powder and 200 ml ethanol at room temperature for 48 h in the dark. The extract was obtained by centrifuging the mixture at 3500 rpm for 15 min. The obtained extracts were concentrated using a rotary evaporator until completely dried and resuspended in 100 ml ethanol. The extracts were then stored in a refrigerator for further studies (Ashour et al., 2015).

Biosynthesis of Silver Nanoparticles (AgNPs)

To synthesize AgNPs, 0.169 g of silver nitrate was dissolved in 100 ml sterile deionized distilled water (ddw) to form 10 mM AgNO₃ solution. Exactly 20 ml of the prepared extract was added dropwise to 80 ml of aqueous AgNO₃ (at a ratio of 1:4 (v/v)) at 60 °C and stirred continuously with a magnetic stirrer for 2 h. The change in color of the solution indicated the reduction of silver nitrate into AgNPs (Fig.1). The solution containing AgNPs was centrifuged at 4500 rpm for 25 min two times, and the resulting pellets were dried in an oven at 90 °C for 48 h. The dried AgNPs were then resuspended in methanol solvent for antioxidant-activity testing and further characterizations (Abdel-Aziz et al., 2014; Sitaramanjaneya et al., 2018; Otunola and Afolayan, 2018; Aritonang et al., 2019; Keshari et al., 2020; Kailas et al., 2020; Deegendra et al., 2020). A visual observation of color changes of the solutions using a laser beam and spectral analysis confirmed the formation of silver nanoparticles. The laser scattered when passing through the nanoparticle solution. However, scattering was not observed when the laser passed through the methanol solvent or extract solutions (Fig.1).

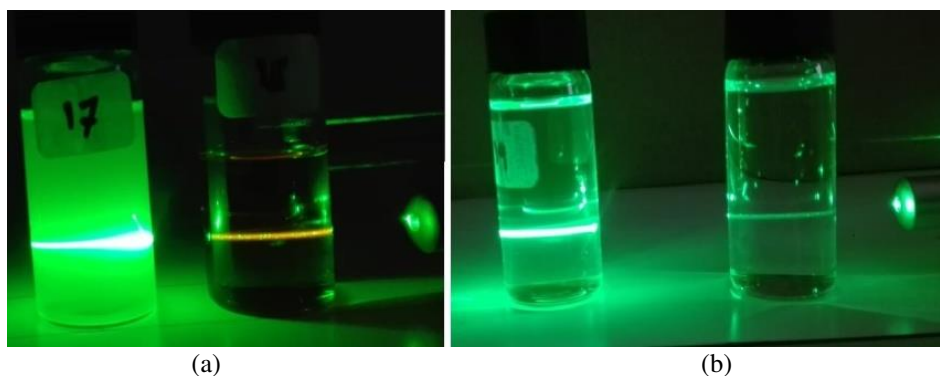


Figure 1. Image of different solutions facing a laser pointer: (a) AgNPs from the plant extract solution (left) and plant extract (right); (b) AgNP control (left) and methanol solution (right)

Evaluation of Antimicrobial Properties of Silver Nanoparticles (AgNPs)

Antimicrobial assays of the AgNPs obtained from the plant extracts were carried out according to the agar-well-diffusion method (Alsohaili and Al-Fawwaz, 2014). The antimicrobial activities of AgNPs and plant extracts were tested against two Gram-positive bacterial strains (*Bacillus subtilis* and *Staphylococcus aureus*), Gram-negative bacteria strain (*Escherichia coli*), and three fungal species (*Aspergillus niger*, *Penicillium fimum*, and *Candida albicans*). The bacteria were incubated at 37 °C in a nutrient broth before experimental use. The microbial suspensions (overnight bacterial culture) were streaked over the surface of the media using a sterile cotton swab to ensure confluent

growth of the organism. Wells were then punched in the agar and filled with 75 μ l of AgNPs and plant-extract samples. The plates were incubated at 37 °C for 24 h, and the fungi were incubated at 28 °C for 72 h. Next, the zones of inhibition were observed, and the diameters of the inhibition zones were measured. Then, the plates were photographed. Each test was carried out in three replicates, all values are expressed as the mean \pm standard deviation (Alsohaili and Al-Fawwaz, 2014; Salayová et al., 2021).

Evaluation of Antioxidant activity of Silver Nanoparticles (AgNPs)

Antioxidant activity was determined by a 2,2-diphenyl-1-picrylhydrazyl (DPPH)-free radical scavenging assay according to Bhakya et al. (2016) with slight modifications (Bhakya et al., 2016; Al-Barri et al., 2021). Briefly, 3.94 mg of DPPH was dissolved in 100 ml methanol to acquire a stock solution. The free radical scavenging activities of the AgNPs, plant extracts, and standard Ascorbic acid were determined using stable radical DPPH by mixing 0.5 ml of the samples (AgNPs or plant extracts) with 2.5 ml of DPPH and allowing the mixture to first stand for 30 min, followed by 60 min at room temperature in the dark. During these times, the absorbance was measured at 517 nm using a spectrophotometer (Jenway 635001-6305 UV/Visible Spectrophotometer). Methanol was used as a blank solution, while ascorbic acid was used as a reference whose efficiency was compared with that of the AgNPs and plant extracts (Al-Barri et al., 2021). The free radical scavenging activity was calculated according to *Equation (1)*:

$$\text{The free radical scavenging activity percentage (\%)} = \frac{\text{Abs DPPH} - \text{Abs Sample}}{\text{Abs DPPH}} \times 100\% \quad (\text{Eq.1})$$

where Abs_{DPPH} is the absorbance of the control sample (DPPH solution without the test sample), and Abs_{Sample} is the absorbance of the test sample (DPPH solution with AgNPs or plant extracts).

Characterization of Silver Nanoparticles (AgNPs)

The synthesized Silver Nanoparticles AgNPs were characterized using the following methods. (a) UV–vis spectroscopy (Specord S 600-Molecular Spectroscopy-UV Vis Diode-array Spectrophotometers, Germany). In this method, the reduction of silver nitrate was monitored at different time intervals (30, 60, 90, 120, 150, 180, and 210 min) by measuring the UV–visible spectrum of the reaction mixture at a scanning speed of 280–680 nm with a quartz cuvette and methanol as a reference. (b) Fourier transform infrared spectroscopy (FTIR) (Bruker Vertex 70 FTIR, wavelength range of 4000–400 cm^{-1} , Germany). FTIR of the biosynthesized AgNPs was used to determine the presence of different functional groups in the sample. The silver nanoparticle (AgNP) solution was evaporated in an oven at 65 °C for 48h to obtain the AgNPs in a powdered form and then loaded into a sample holder using the KBr method. Next, background screening of potassium bromide (KBr) was performed, and a potassium bromide pellet was produced with silver nanoparticles and scanned again. The spectra showed different frequencies, which were analyzed using infrared and Raman spectroscopy. All measurements were carried out in the range of 400–4000 cm^{-1} at a resolution of 4 cm^{-1} to identify the presence of functional groups on the synthesized silver nanoparticles (Deegendra et al., 2020).

Results

Biosynthesis of Silver Nanoparticles (AgNPs)

In the present study, silver nanoparticles (AgNPs) were synthesized from medicinal plants that are well-known in Jordan and used in folk medicine. The antimicrobial and antioxidant activities were investigated, and then the AgNPs were characterized using UV–vis spectroscopy and FTIR. The formation of AgNPs started after mixing the plant extracts with the silver nitrate solution (Fig.1).

Antimicrobial Activity of AgNPs

Tables 1 and 2 outline the antimicrobial results obtained using the well-diffusion method. The ethanolic extract of *S. aromaticum* was active against all tested microorganisms, and *Candida albicans* was the most sensitive. The highest inhibitory activity was seen against *Candida albicans* (30±2.5mm) using the *S. rosmarinus* extract, while the weakest activity was demonstrated against *E. coli* using the *Allium sativum* extract. On the other hand, the aqueous extracts of most plants used in this research presented no inhibitory activities against the tested microorganisms. *Candida albicans* was the most susceptible tested organism to the aqueous extract (22±1.75mm) when using the *S. aromaticum* extract, which also showed inhibitory activity against all tested microorganisms except for *Penicillium fimorum*. The ethanol extracts exhibited better antimicrobial results than the aqueous extracts, so the ethanolic extracts was used in the biosynthesis of silver nanoparticles in the following experiments.

Table 1. Antimicrobial activities of different ethanol plant extracts using the well-diffusion method

	<i>Escherichia coli</i>	<i>Staphylococcus aureus</i>	<i>Bacillus subtilis</i>	<i>Aspergillus niger</i>	<i>Penicillium fimorum</i>	<i>Candida albicans</i>
<i>Artemisia judaica</i>	13±2.17 mm	12±0.25 mm	12±1.5 mm	13±1.73 mm	0	24±2.64 mm
<i>Thymus vulgaris</i>	13±2.64 mm	12±0.5 mm	12±0.75 mm	0	11±0.75 mm	15±2.0 mm
<i>Salvia rosmarinus</i>	12±0.5 mm	14±1.5 mm	14±2.5 mm	16±2.5 mm	0	30±2.5 mm
<i>Cinnamomum verum</i>	11±0.75 mm	12±0.75 mm	0	0	0	10±1.5 mm
<i>Allium sativum</i>	10±1.73 mm	11±1.5 mm	11±0.75 mm	0	12±1.5 mm	26±2.17 mm
<i>Syzygium aromaticum</i>	16±2.0 mm	15±2.64 mm	14±0.25 mm	11±1.5 mm	13±0.5 mm	25±1.73 mm

Table 2. Antimicrobial activity of different aqueous plant extracts using the well-diffusion method

	<i>Escherichia coli</i>	<i>Staphylococcus aureus</i>	<i>Bacillus subtilis</i>	<i>Aspergillus niger</i>	<i>Penicillium fimorum</i>	<i>Candida albicans</i>
<i>Artemisia judaica</i>	0	0	0	0	0	11±1.5 mm
<i>Thymus vulgaris</i>	0	0	0	0	0	16±2.0 mm
<i>Salvia rosmarinus</i>	0	0	0	0	0	0
<i>Cinnamomum verum</i>	0	0	0	0	0	0
<i>Allium sativum</i>	0	0	0	0	0	0
<i>Syzygium aromaticum</i>	17±0.75 mm	11±0.5 mm	11±1.5 mm	12±0.75 mm	0	22±1.75 mm

Antibacterial Activity of AgNPs

The antibacterial activities of the plant extracts and AgNP solutions were evaluated against one Gram-positive (*Escherichia coli*) and two Gram-negative (*Staphylococcus aureus* and *Bacillus subtilis*) bacterial species. As shown in Fig. 2, the results revealed that the antibacterial activities of AgNPs against *E. coli* were higher than the activities of all plant extracts. Moreover, the antibacterial activities of AgNPs against *B. subtilis* and *S. aureus* were higher than the antibacterial activities of all plant extracts, except for *Cinnamomum verum* and *Artemisia judaica*. The zone of inhibition confirmed that the AgNPs offered greater antibacterial activities than the plant extracts.

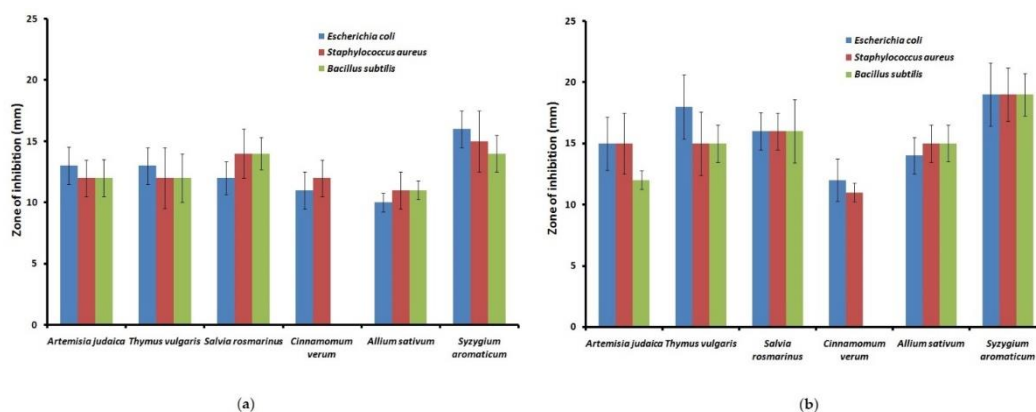


Figure 2. Antibacterial activities of (a) plant extracts and (b) AgNP–plant against the tested bacterial species for 24 hours. The results represent the means of three replicates, and the error bars represent the standard deviation

Figure 2 shows that the antibacterial activities of the AgNPs using *T. vulgaris* and *C. verum* against *E. coli* were higher than those against *S. aureus*, whereas the activities of *S. rosmarinus* extracts against *E. coli* were less significant than those against *B. subtilis* and *S. aureus*. When AgNPs of *Allium sativum* and its extracts were tested for antibacterial activity, *B. subtilis* and *S. aureus* showed higher activity than *E. coli*. In both tested *C. verum* solutions, no antimicrobial effect was observed against *B. subtilis*. The results indicated that the plant extract alone exerted less significant antimicrobial effects than those of the plant-based AgNPs, which exhibited a broad spectrum of antibacterial action on the tested Gram-negative and Gram-positive bacteria.

Antifungal Activity of AgNPs

The antifungal activities of the AgNPs and plant extracts were tested against 3 fungi (*Aspergillus niger*, *Penicillium fimorum*, and *Candida albican*), and the results are presented in Fig. 3. The results show that the antifungal activity of the AgNP–plant solution was higher than that of plant extracts against *A. niger*, whereas *C. verum* and *A. sativum* showed no activity in either solution (AgNP–plant and plant extracts) against *A. niger*. The maximum zone of inhibition against *A. niger* was 17 ± 2.17 mm, exhibited by the AgNPs of *S. rosmarinus* compared to 16 ± 2.64 mm exhibited by *S. rosmarinus* extracts. The antifungal activities of AgNPs using *Artemisia judaica*, *Thymus vulgaris*, *Allium sativum*, and *Syzygium aromaticum* against *Penicillium fimorum* were higher than the activities of the related plant extracts. However, there was no antifungal activity

observed for *S. rosmarinus* and *C. verum* extracts or AgNP solutions against *Penicillium fimorum*. *Candida albican* was susceptible to all plant AgNPs and extracts, the antifungal activities of AgNPs using *Artemisia judaica*, *Thymus vulgaris*, and *C. verum* against *C. albicans* were higher than those of the plant extracts, whereas the antifungal activities of the *S. rosmarinus*, *Allium sativum*, and *Syzygium aromaticum* extracts were higher than those of the plant AgNP solutions.

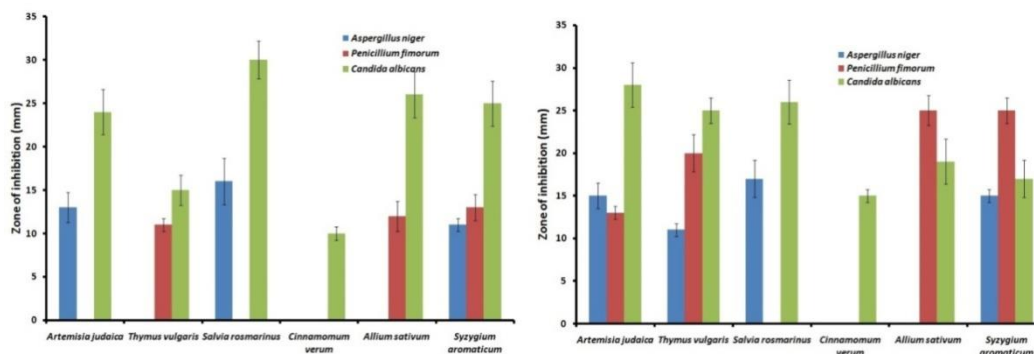


Figure 3. Antifungal activities of (a) plant extracts and (b) AgNP-plant solutions against the tested fungal species for 24 hours. The results represent the means of three replicates, and the error bars represent the standard deviation

Antioxidant Activity of AgNPs

The antioxidant properties of plant extracts and AgNPs were evaluated using DPPH scavenging and compared to standard ascorbic acid. As shown in Fig. 4, differences were observed between the values obtained. The results confirmed that the plant extracts and AgNPs have antioxidant activities. However, ascorbic acid presented greater antioxidant activity than that of the AgNPs or plant extracts. The recorded value for the lowest antioxidant activity was 18.0% for AgNPs of *Allium sativum*, while the highest antioxidant values were found for AgNPs using *Cinnamomum verum* (92.0%) and plant extract of *Salvia rosmarinus* (92.0%), which is close to the value of standard ascorbic acid (97.0%).

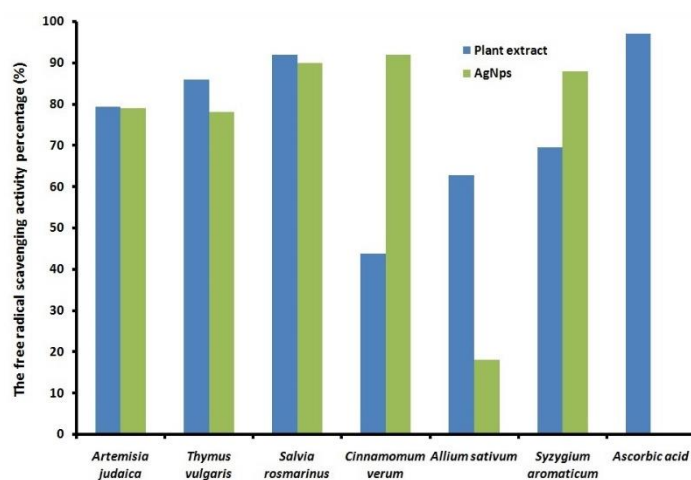


Figure 4. The percentage of Antioxidant (DPPH) scavenging activity of silver nanoparticles and ascorbic acid

The values were 92.0% and 88.0% for *Cinnamomum verum* and *Syzygium aromaticum*–AgNPs, respectively, indicating that silver nanoparticles of these plants exerted higher scavenging activity than did the plant extract alone (43.7% and 69.5%, respectively). However, the antioxidant activity of *Thymus vulgaris* and *Allium sativum* extracts (85.9 and 62.7%, respectively) represented higher scavenging activity than the 78.0% and 18.0% values for AgNPs when using *Thymus vulgaris* and *Allium sativum*.

UV–vis Spectra Analysis of AgNPs

Preliminary characterization of the biosynthesized silver nanoparticles (AgNPs) was carried out using the ultraviolet–visible (UV–vis) spectrum, which is the simplest and most indirect technique able to indicate the formation of metal nanoparticles, provided that SPR (surface plasmon resonance) exists for the metal nanoparticles. Color changes of the extracts confirmed the synthesis of AgNPs. Spectrophotometric analysis of the produced colored solution through a spectra range of 280–680 nm using a Shimadzu UV–vis spectrophotometer showed an SPR hike between 410 and 460 nm, which confirmed the formation of AgNPs (Fig.5). The UV–vis spectrum of plant–silver nanoparticles was recorded as a function of time at different time intervals (30, 60, 90, 120, 150, 180, and 210 min). The AgNPs of the plant *Cinnamomum verum* exhibited a peak at 429 nm after 210 min under UV–vis spectroscopy. The formation of AgNPs was monitored by observing the increase in intensity overtime, which also indicated an increase in the amount of nanoparticles formed.

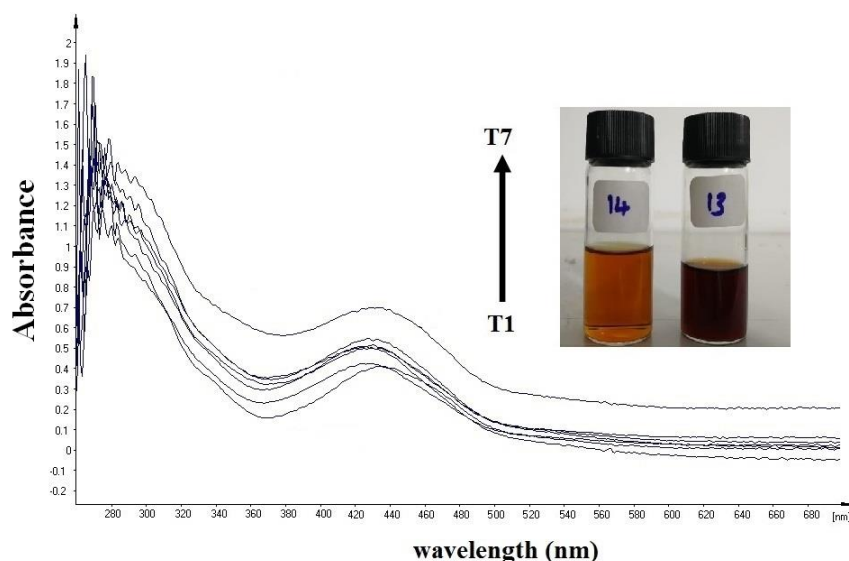


Figure 5. Ultraviolet–visible (UV–vis) spectra of silver nanoparticles using *Cinnamomum verum* extract as a function of time at intervals of 30, 60, 90, 120, 150, 180, and 210 min, with transformation the reaction mixture's color

Fourier Transform Infra-Red (FTIR) Spectra Analysis of AgNPs

Fourier Transform Infrared FTIR spectroscopic analysis was applied to identify the functional groups present on the surfaces of the bioactive compounds and responsible for the reduction of AgNPs from the plant samples. FTIR data for the AgNPs revealed different peaks assigned to different functional groups of bioactive compounds. FTIR

analysis of the AgNPs was performed in the range of 4000-400 cm^{-1} , as shown in *Figs. 6* and *7*. The FTIR analysis revealed different stretches of bonds at different absorption peaks for each of the bioactive compounds.

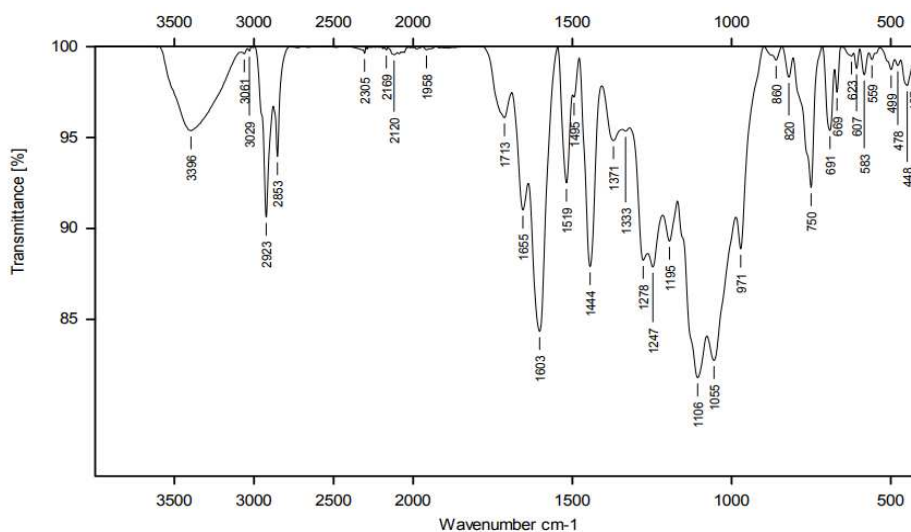


Figure 6. The IR spectra of *Thymus vulgaris* plant extract (4)

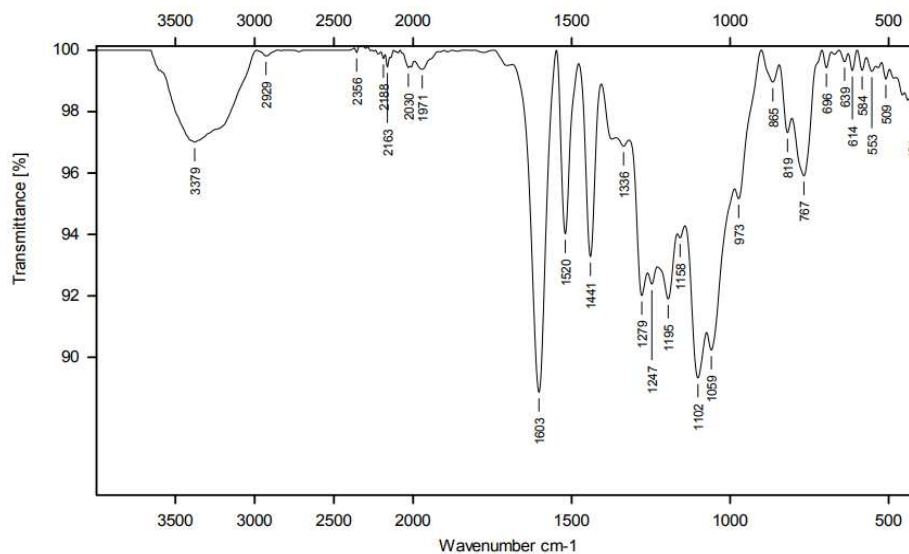


Figure 7. The IR spectra of AgNPs mediated by *Thymus vulgaris* plant extract (10)

Discussion

In the present study, silver nanoparticles were synthesized from the medicinal plants *Artemisia judaica*, *Thymus vulgaris*, *Syzygium aromaticum*, *Cinnamomum verum*, *Allium sativum*, and *Salvia rosmarinus*, which are used locally as medicine for different types of illness. The biosynthesis of silver nanoparticles has emerged as an alternative to other methods because the biological synthesis of nanoparticles is considered eco-friendly, cost-efficient, and suitable for biomedical and pharmaceutical applications (Sharma et al., 2009; Kumar et al., 2012; Rajan et al., 2015; Ahmed et al., 2016; Mussin et al., 2021).

Silver nanoparticles using plant extracts were investigated for their antimicrobial and antioxidant activities and were characterized using FTIR and UV–vis spectroscopy. Several previous reports in the literature reported that silver nanoparticles can be synthesized by different plants such as *Chenopodium murale*, *Eucalyptus hybrid*, *Gliricidia sepium*, *Carica papaya*, *Azadirachta indica*, and *Capsicum annum* (Shankar et al., 2004; He et al., 2007; Bar et al., 2009; Dubey et al., 2009; Jha and Prasad, 2010; Raut et al., 2010; Abdel-Aziz et al., 2014; Anand et al., 2020).

Silver ions in the plant extract were reduced to silver NPs after mixing with the plant extract for 3 hours. The plant extracts transformed into a wide range of different colors (dark amber, light amber, reddish brown, and pale yellow). This change of color confirmed the reduction of silver nitrates into silver nanoparticles (Anand et al., 2020). Color change was also observed in several previous reports. These reports suggested that the color changed due to the surface plasmon resonance (SPR) of deposited silver nanoparticles (Vigneshwaran et al., 2006; Saxena et al., 2010; Khandelwal et al., 2010; Abdel-Aziz et al., 2014). The intense peak of the SPR absorption of silver nanoparticles in the region of 250-300 nm was caused by scattering laser due to the Tyndall effect and the AgNPs present in the solution. According to the Tyndall effect, when a laser beam is allowed to pass through the solution, the path of the beam becomes illuminated. This illumination occurs because the laser beam is scattered when it hits the nanoparticles in the solution. When the particles in the solution are less than 1nm, the light passes through without scattering (Goncharova et al., 2019).

Medicinal plant extracts are usually prepared by water or organic solvents to determine their activities and efficacy. In ancient times, people could not use organic solvents, so they instead used water to extract plants. Usually, this process does not extract all the active compounds. Consequently, the produced extracts may not contain all the pharmacologically active compounds (Hussain et al., 2015). In this study, the ethanol extracts of all plants, except for those of *Syzygium aromaticum*, showed greater antimicrobial activity than those of water extracts. All bacterial and fungal species used in this study, except for *Candida albican*, were found to be more resistant against aqueous extracts than ethanolic extracts. Similar results have been reported by Hussain et al. (2015), Nair et al. (2005), Nisha et al. (2013), and Shetty et al. (2016). Antimicrobial activity differs according to the type of solvent used, which may be due to differences in the active ingredients of the plant extracts. Most antimicrobial compounds already identified in plants are reportedly aromatic or saturated organic molecules that can be easily extracted with organic solvents (Cowan, 1999; Nair et al., 2005; Shetty et al., 2016). Thus, in our experiments, ethanolic extracts were used for the biosynthesis of silver nanoparticles.

In recent years, the research and development of new antimicrobial drugs have increased due to an increase in resistant strains (Tacconelli et al., 2018; Mussin et al., 2021). In response, nanoparticles and medicinal plants have been used as promising alternatives for the treatment of various infections (Ahmed et al., 2016; Tacconelli et al., 2018; Amparo et al., 2019; Mussin and Giusiano, 2020; Mussin et al., 2021). The traditional Indian medicine Ayurveda was perhaps the first to use metallic herbal extracts. These extracts are used to treat many diseases. The medicinal properties of silver-extract preparations have been known since the 17th century BC. These preparations were created by using a series of physico-chemical processes to obtain metal extracts after exposure to metallic silver in the presence of medicinal plants (Mukkavalli et al., 2017; Mussin et al., 2021).

The enhanced antimicrobial activity of biosynthesized nanoparticles is due to the synergistic effect between the natural compounds present in plant extracts and nanoparticles (Duran et al., 2016; Kailas et al., 2020). Plants and their parts contain various compounds that act as reducing agents to produce nanoparticles from metal salts. These compounds include proteins, nucleic acids, fats, carbohydrates, pigments, and several types of secondary metabolites (Khwaja et al., 2018). Various studies reported that AgNPs have shown excellent antimicrobial effects against a wide range of microorganisms (Siddiqi and Husen, 2016a,b; Khwaja et al., 2018).

In the present results, the AgNPs exhibited promising antimicrobial activities against both bacteria (Gram-positive and Gram-negative bacteria) and fungi. The extent of the inhibitory effects on bacterial growth was observed on selected bacterial strains, among which *E. coli* was found to be more sensitive when *Syzygium aromaticum*-AgNP solution was used followed by *Staphylococcus aureus* and *Bacillus subtilis* strains. Moreover, the bacterial membranes of Gram-positive and Gram-negative bacteria show differences in their structures. The most distinctive difference is the double lipopolysaccharide layer in Gram-negative bacteria and the thick peptidoglycan layer in Gram-positive bacteria. According to a series of reports, Gram-negative bacteria are more susceptible to silver nanoparticles because the positive charges of silver ions interact with the negatively charged lipopolysaccharide of the cell membrane with greater affinity when compared to Gram-positive bacteria; these activities disable cell membrane functions due to holes in the cell membrane (Sondi and Salopek-Sondi, 2004; Gogoi et al., 2006; Otunola and Afolayan, 2018). However, even in Gram-positive bacteria, which have relatively thick and continuous peptidoglycan, cell walls could restrict the entry of bare silver nanoparticles, while interactions of teichoic acid with bioreductive capping agents such as phenol, proteins, esters, etc. of the silver nanoparticles may facilitate their possible entry into Gram-positive bacteria species (Jain et al., 2015; Otunola and Afolayan, 2018).

The antimicrobial activity of silver nanoparticles was previously reported by (Rai et al., 2009; Jha and Prasad, 2010; Khandelwal et al., 2010; Govindaraju et al., 2010; Abdel-Aziz et al., 2014). In the present study, silver nanoparticles produced by different plant extracts were found to be effective against *Candida albican* followed by *Penicillium fimorum* and *Aspergillus niger*, similar to previous reports that showed a zone of inhibition when the synthesized NPs were tested against *Aspergillus niger* and *Aspergillus flavus* (Govindaraju et al., 2010; Abdel-Aziz et al., 2014). Different theories were proposed to explain the antimicrobial actions of colloidal silver solutions, such as membrane damage due to free-radical generation Kim et al. (2007), cell membrane permeability alterations Sondi and Salopek-Sondi(2004) and the release of membrane proteins and lipopolysaccharides (Amro et al., 2000; Abdel-Aziz et al., 2014).

The results of the present study demonstrated the antioxidant activities of plant extracts and AgNPs, compared to those of standard ascorbic acid, using a DPPH scavenging assay. A difference was observed between the plant extracts and AgNPs, while ascorbic acid presented greater antioxidant activity than both solutions (AgNPs and plant extracts). The values recorded for both *C. verum* and *S. aromaticum* nanoparticles (92.0% and 88.0%, respectively) indicated that the silver nanoparticles of these plants possessed higher scavenging activity than that of the plant extract alone (43.7% and 69.5%, respectively). If the plant extract presents some antioxidant activity, the whole solution may exhibit antioxidant activity, but the nanoparticles alone are incapable of having this property (Khwaja et al., 2018). Previous research demonstrated that the antioxidant activities of biosynthesized AgNPs can be attributed to the integration of existing functional groups

on the surfaces of silver nanoparticles originating from the plant extract (He et al., 2017; Kailas et al., 2020). Similarly, proteins, enzymes, and biosurfactants may act as reducing agents and could be used as stabilizing agents (Khwaja et al., 2018).

However, the antioxidant values of *T. vulgaris* with plant extract alone was higher in scavenging activity than silver nanoparticles. Similar results were also found in *A. sativum* extract, the same results were obtained by other researchers using grapefruit pomace extract/AgNPs and *Thymus vulgaris* and *Thymus citriodorus* (Maliar et al., 2017; Habashy et al., 2018; Kumar et al., 2019; Saratale et al., 2020) these results may indicate the effect of the synthesis of nanoparticles in different plant extract have different trend.

Previous research demonstrated that the antioxidant activities of biosynthesized AgNPs can be attributed to the integration of existing functional groups on the surfaces of silver nanoparticles originating from the plant extract (He et al., 2017; Kailas et al., 2020). Similarly, proteins, enzymes, and biosurfactants may act as reducing agents and could be used as stabilizing agents (Khwaja et al., 2018).

Earlier studies on the antioxidant activities of biosynthesized AgNPs from *P. pinnata* showed considerable free radical scavenging potential (Priya et al., 2016). Moreover, phyto synthesized silver nanoparticles using *Elephantopus scaber* exhibited strong antioxidant activity in terms of DPPH radical scavenging (Kharat and Mendhulkar, 2016). Similarly AgNPs synthesized using plant extracts showed significant antioxidant potential (Nagaich et al., 2016; Roy et al., 2019; Kailas et al., 2020).

Phenolic compounds in plants are strong antioxidants with high reduction capacity. Higher total phenolic content in plants facilitates the reduction of silver ions to nanoscale-sized silver particles due to the electron donating ability of these phenolic compounds. It is well documented that phenolic compounds may contribute to antioxidant activities. However, antioxidant activities are likely attributable to the phenolic contents in plants due to their redox properties, which allow these nanoparticles to act as reducing agents, hydrogen donors, and singlet oxygen quenchers (Pietta, 2000; Chang et al., 2001; Awika et al., 2003; Nsimba et al., 2008). Moreover, the increase in the antioxidant activity of AgNP extracts, compared to that of some plant extracts, suggests that the plant extract itself is responsible for the majority of antioxidant activity, whereas silver nanoparticles contribute little to antioxidant activity (Abdel-Aziz et al., 2014). The FTIR results confirmed the various functional groups present on the surfaces of the bioactive compounds. The DPPH assay confirmed that the AgNPs have antioxidant scavenging activities. These properties of silver nanoparticles emerge due to the presence of functional groups on the surfaces of silver nanoparticles (Anand et al., 2020).

The primary method for detecting AgNPs produced through the bioreduction of Ag^+ was by a visual color change and confirmed by UV–vis spectral analysis (Salayová et al., 2021). In the present study, a single peak between 410 and 460 nm in the UV–visible region, with an absorption peak at 429 nm, was recorded via surface plasmon resonance (SPR), which confirmed the formation of silver nanoparticles (Kailas et al., 2020). The intensity of the color increased as incubation time increased. Previous studies reported that silver nanoparticles give an absorption peak at 420–450 nm as a result of the SPR characteristics of the nanoparticles (Mohanta et al., 2016; Nayak et al., 2016; Mohanta et al., 2017). Other reports have shown that AgNPs exhibit an absorption peak in the range of 410–450 nm based on SPR (Yazdi et al., 2019; Mohammad et al., 2020; Heikal et al., 2020). The SPR band in the UV–vis spectrum is due to electron oscillation around the surfaces of the nanoparticles. Moreover, SPR is dependent on the size, shape, and

agglomeration of silver nanoparticles, which are reflected by the UV–vis spectra (Mohammad et al., 2020). However, the lack of LSPR suggests the formation of ultra small silver nanoparticles or silver clusters containing a small number of atoms (Santos et al., 2015; Anand et al., 2020).

The IR spectra of AgNPs derived from *Artemisia judaica* 1, *Cinnamomum verum* 2, *Allium sativum* 3, *Thymus vulgaris* 4, *Syzygium aromaticum* 5, and *Salvia rosmarinus* 6 extracts were determined to identify the functional groups responsible for the stabilization of silver nanoparticles. The IR data of the AgNPs mediated by plant extracts were analyzed and compared to the IR data observed for the extract control before reacting with AgNO₃.

The IR spectra of extracts 1-6 showed very strong absorption peaks in the region of 3300-3428 cm⁻¹, whereas the IR spectra of the AgNPs mediated by the plant extracts (7-12) showed that the absorption of the OH peaks shifted to a lower wave number and was only observable in the range of 3284-3415cm⁻¹. For example, the absorption peak of the hydroxyl group of *Thymus* plant extract 4 appeared at 3396 cm⁻¹ (Figure 6), while the peak at 3408 cm⁻¹ revealed O–H stretching vibrations, which were induced by the presence of alcohol and phenol (Raut et al., 2010; Deegendra et al., 2020). The absorption for the same group shifted to a lower frequency and appeared at 3379 cm⁻¹ for the AgNPs mediated by *Thymus* plant extract 10 (Figure 7).

Moreover, the IR spectral data showed that the absorption peaks of carbonyl groups were lower for the AgNPs mediated by the plant extracts compared to the absorption peaks of the plant extracts, indicating the interaction of the silver cation (Ag⁺) with the carbonyl group. For example, the absorption peak of the carbonyl group of *Thymus* plant extract 4 appeared at 1713 cm⁻¹ (Figure 6), where absorption of the carbonyl group disappeared for AgNPs mediated by *Thymus* plant extract 10 (Figure 7). The IR spectra revealed the absorption of many groups responsible for the stabilization of nanoparticles acting as capping or stabilizing agents. Therefore, these bioextracts may have been involved in the reduction, capping, and stabilization of the produced AgNPs (Otunola and Afolayan, 2018; Sitaramanjaneya et al., 2018).

Conclusions

Compared to other metallic nanoparticles, silver nanoparticles (AgNPs) are considered among the most vital and attractive nanomaterials and are used in different applications of human life. In the present work, green synthesis of silver nanoparticles was performed by using organic solvent extracts of some medicinal plants traditionally used in Jordan. Plant extracts have bioactive compounds that are responsible for the reduction and capping of AgNO₃ into AgNPs. The synthesized silver nanoparticles exhibited antimicrobial activities against both Gram-positive and Gram-negative bacteria, as well as some fungi. The AgNPs also displayed high antioxidant activities against free radicals. Silver nanoparticles were further characterized by UV–vis. spectroscopy and FTIR analysis. These AgNPs could be used as antimicrobial agents in medicine, health care, and biotechnology in the future because they are non-toxic, cost effective, and eco-friendly. The long-term effects of silver nanoparticles and other metalNPs on human health and crops, however, remains unclear. Therefore, further studies are needed to fully characterize the cytotoxic activities of silver nanoparticles and other metal NPs against anticancer cells and the effects of these particles on the environment.

Acknowledgments. The authors would like to thank the department of biological sciences, Al al-Bayt University, for providing administrative and research support. Also, the authors would like to express their gratitude to Prof. Mohammad M. Ibrahim for the FTIR analysis and Prof. Raed A. Ghanem and Mr. Omar Mashaqba for the UV–vis Spectroscopy analysis.

REFERENCES

- [1] Abdel-Aziz, M. S., Shaheen, M. S., El-Nekeety, A. A., Abdel-Wahhab, M. A. (2014): Antioxidant and antibacterial activity of silver nanoparticles biosynthesized using *Chenopodium murale* leaf extract. – Journal of Saudi Chemical Society 18: 356-363.
- [2] Ahmed, S., Ahmad, M., Swami, B. L., Ikram, S. (2016): A review on plants extract mediated synthesis of silver nanoparticles for antimicrobial applications: a green expertise. – J. Adv. Res. 7: 17-28.
- [3] Al-Barri, S. N., Al-Deeb, T. M., Al-Fawwaz, A. T., Al-Omari, M. M., Al-Qaoud, K. M. (2021): Antimicrobial, Antioxidant and Cytotoxic Activities of *Ephedra aphylla* and *Bassia muricata* Plants Collected From Northern Jordan. – Plant Cell Biotechnology and Molecular Biology 22: 47-64.
- [4] Alshahili, S., Al-Fawwaz, A. T. (2014): Composition And Antimicrobial Activity of *Achillea Fragrantissima* Essential Oil Using Food Model Media. – European Scientific Journal 10: 156-165.
- [5] Amparo, T. R., Janaína, B. S., Paula, M. V., Luiz, F. T., Orlando, D. D., Gustavo, H. S. (2019): Herbal medicines to the treatment of skin and soft tissue infections: advantages of the multi-targets action. – Phyther. Res. 34: 94-103.
- [6] Amro, L.P., Kotra, K., Wadu-Mesthrige, A., Bulchevy, S., Mobashery, G.Y., Liu, Y. (2000): High resolution atomic force microscopy studies of the *E. coli* outer membrane: the structural basis for permeability. – Langmuir 16: 2789-2796.
- [7] Anand, K. K., Ragini, S., Payal, S., Virendra, B. Y., Gopal, N. (2020): Antioxidant and antibacterial active ty of silver nanoparticles synthesized by *Cestrum nocturnum*. – Journal of Ayurveda and Integrative Medicine 11: 37-44.
- [8] Aritonang, H.F., Koleangan, H., Wuntu, A.D. (2019): Synthesis of Silver Nanoparticles Using Aqueous Extract of Medicinal Plants' (*Impatiens balsamina* and *Lantana camara*) Fresh Leaves and Analysis of Antimicrobial Activity. – Int J Microbiol. doi: 10.1155/2019/8642303.
- [9] Ashour, A.A., Raafat, D., El-Gowell, H. M., El-Kamel, A.H. (2015): Green synthesis of silver nanoparticles using cranberry powder aqueous extract: characterization and antimicrobial properties. – Int J Nanomed. 10: 7207-7221.
- [10] Asirvatham, R., Christina, A.J., Murali, A. (2013): In vitro antioxidant and anticancer activity studies on *Drosera Indica* L (*Droseraceae*). – Adv Pharm Bull. 3(1): 115-120.
- [11] Awika, J.M., Rooney, L.W., Wu, X., Prior, R.L., Zevallos, L.C. (2003): Screening methods to measure antioxidant activity of sorghum (*Sorghum bicolor*) and sorghum products. – J. Agric. Food Chem. 51: 6657-6662.
- [12] Bar, H., Bhui, D.K., Sahoo, G.P., Sarkar, P., DeAjay Misra, S. P. (2009): Green synthesis of silver nanoparticles using latex of *Jatropha curcas*. – Colloids Surf. A. 339: 134-139.
- [13] Bhagat, M., Rajput, S., Arya, S., Khan, S., Lehana, P. (2015): Biological and electrical properties of biosynthesized silver nanoparticles. – Bull. Mater. Sci. 38: 1253-1258.
- [14] Bhakya, S., Muthukrishnan, S., Sukumaran, M., Muthukumar, M. (2016): Biogenic synthesis of silver nanoparticles and their antioxidant and antibacterial activity. – Appl Nanosci. 6: 755-766.
- [15] Bhumi, G., LingaRao, M., Savithamma, N. (2015): Green synthesis of silver nanoparticles from the leaf extract of *Adhtoda vasicanees* and assessment of its antibacterial activity. – Asian J Pharm Clin Res. 8: 62-67.

- [16] Castro-Aceituno, V., Ahn, S., Simu, S.Y., Singh, P., Mathiyalagan, R., Lee, H.A. (2016): Anticancer activity of silver nanoparticles from *Panax ginseng* fresh leaves in human cancer cells. – Biomed Pharmacother 84:158-165.
- [17] Chandra, M.S., Sasikala, K., Anand, T., Vengaiah, P.C., Krishnaraj, S. (2014): Green synthesis, antimicrobial and antioxidant effects of silver nanoparticles using *Canthium coromandelicum* leaves extract. – J Microbiol. 9: 142-150.
- [18] Chang, S.T., Wu, J.H., Wang, S.Y., Kang, P.L., Yang, N.S., Shyur, L.F. (2001): Antioxidant activity of extracts from *Acacia confusabark* and heartwood. – J. Agric. Food Chem. 49: 3420-3424.
- [19] Cowan, M. (1999): Plant products as antimicrobial agents. – Clin Microbiol Rev. 12: 564-582.
- [20] Deegendra, Kh., Rachana, R., Mitesh, Sh., Megha, R. B. (2020): Green Synthesis of Silver Nanoparticles using Medicinal Plants *Berberis asiatica* and *Cassia fistula* and Evaluation of Antioxidant and Anti-bacterial Activities. – Nepal Journal of Science and Technology 19: 25-32.
- [21] Dubey, M. N., Seema, B., Kushwah, B.S. (2009): Green synthesis of nanosilver particles from the extract of *Eucalyptus hybrid* (Safeda leaves). – Digest J. Nanomater. Biostruct. 5: 537-543.
- [22] Duran, N., Duran, M., de Jesus, M. B., Seabra, A. B., Favaro, W. J., Nakazato, G. (2016): Silver nanoparticles: a new view on mechanistic aspects on antimicrobial activity. – Nanomed: Nanotech Biol Med. 12: 789-799.
- [23] Forough, M., Farhadi, K. (2010): Biological and green synthesis of silver nanoparticles. – Turkish J. Eng. Environ.Sci. 34: 281-287.
- [24] Gogoi, S.K., Gopinath, P., Paul, A. (2006): Green fluorescent protein-expressing *Escherichia coli* as a model system for investigating the antimicrobial activities of silver nanoparticles. – Langmuir 22: 9322-9328.
- [25] Goncharova, D. A., Kharlamova, T. S., Lapin, I. N., Svetlichny, V. A. (2019): Chemical and Morphological Evolution of Copper Nanoparticles Obtained by Pulsed Laser Ablation in Liquid. – The Journal of Physical Chemistry C. 123: 21731-21742.
- [26] Govindaraju, K., Tamilselvan, S., Kiruthogs, V., Simgaravelu, G. (2010): Biogenic silver nanoparticles by *Solanum torvum* and their promising antimicrobial activity. – J. Biopest. 3: 394-399.
- [27] Habashy, N., Serie, M., Attia, W., Abdelgaleil, S. (2018): Chemical Characterization, Antioxidant and Anti-Inflammatory Properties of Greek *Thymus Vulgaris* Extracts and Their Possible Synergism with Egyptian *Chlorella Vulgaris*. – J. Funct. Foods. 40: 317-328.
- [28] He, Z., Guo, Y., Zhang, S., Zhang, J., Wang, N., Gu, N. (2007): Biosynthesis of gold nanoparticles using the bacteria *Rhodospseudomonas capsulate*. – Mater. Lett. 61: 3984-3987.
- [29] He, Y., Wei, F., Ma, Z., Zhang, H., Yang, Q., Yao, B. (2017): Green synthesis of silver nanoparticles using seed extract of *Alpinia katsumadai*, and their antioxidant, cytotoxicity, and antibacterial activities. – RSC Advances. 7: 39842-39851.
- [30] Heikal, Y.M., Şutañ, N.A., Rizwan, M. (2020): Green synthesized silver nanoparticles induced cytogenotoxic and genotoxic changes in *Allium cepa* L. Varies with nanoparticles doses and duration of exposure. – Chemosphere 243:125430.
- [31] Hussain, K. A., Tarakji, B., Binu Purushothaman, P. K., John, J., Mathews, J., Ramphul, V., Divakar, D. D. (2015): Antimicrobial Effects of *Citrus Sinensis* Peel Extracts against *Periodontopathic* Bacteria: An In Vitro Study. – Rocznik Panstw Zakl Hig. 66:173-178.
- [32] Jain, N., Bhargava, A., Rathi, M. (2015): Removal of protein capping enhances the antibacterial efficiency of biosynthesized silver nanoparticles. – PLoS ONE 10: 0134337.
- [33] Jha, A.K., Prasad, K. (2010): Green synthesis of silver nanoparticles using *Cycas* leaf. – Int. J. Green Nanotech. Phy. Chem. 1(2): 110-117.

- [34] Kailas, D. D., Patil, S. R., Pratik, P. D., Madhavi, N. P., Nilam, J. J., Vinit, N. D. (2020): Studies on Antioxidant and Antimicrobial Potential of Biogenic Silver Nanoparticles Synthesized Using *Nothapodytes foetida* Leaf Extract (Wight) Sleumer. – Biomed. and Pharmacol. J. 13: 441-448.
- [35] Keshari, A.K., Srivastava, R., Singh, P., Yadav, V.B., Nath, G. (2020): Antioxidant and antibacterial activity of silver nanoparticles synthesized by *Cestrum nocturnum*. – Journal of Ayurveda and Integrative Medicine 11: 37-44.
- [36] Khali, M. M., Ismail, E. H., El-Baghdady, K. Z., Mohamed, D. (2014): Green synthesis of silver nanoparticles using olive leaf extract and its antibacterial activity. – Arabian J. Chem. 7: 1131-1139.
- [37] Khandelwal, N., Singh, A., Jain, D., Upadhyay, M.K., Verma, H.N. (2010): Green synthesis of silver nanoparticles using *Argimone maxicana* leaf extract and evaluation of their activity. – Digest. J. Nanomater. Biostruct. 5: 483-489.
- [38] Kharat, S. N., Mendhulkar, V. D. (2016): Synthesis, characterization and studies on antioxidant activity of silver nanoparticles using *Elephantopus scaber* leaf extract. – Mater Sci Eng (C). 62: 719-724.
- [39] Khwaja, S., Siddiqi, K.S., Azamal, H., Rifaqat, A. K. (2018): A review on biosynthesis of silver nanoparticles and their biocidal properties. – J. Nanobiotechnol. 16:14.
- [40] Kim, E., Kuk, K.N., Yu, J.H., Kim, S.J., Park, H.J., Lee, S.H., Kim, Y.K., Park, Y.H., Park, C.Y., Hwang, Y.K., Kim, Y.S., Lee, D.H., Jeong, M.H., Cho, H. (2007): Antimicrobial effects of silver nanoparticles. – Nanomed. Nanotechnol. Biol. Med. 3: 95-101.
- [41] Kumar, K.M., Sinha, M., Mandal, B.K., Ghosh, A.R., Kumar, K.S., Reddy, P.S. (2012): Green synthesis of silver nanoparticles using *Terminalia chebula* extract at room temperature and their antimicrobial studies. – Spectrochim Acta A Mol Biomol Spectrosc. 91: 228-233.
- [42] Kumar, V., Singh, S., Srivastava, B., Bhadouria, R., Singh, R. (2019): Green Synthesis of Silver Nanoparticles Using Leaf Extract of *Holoptelea integrifolia* and Preliminary Investigation of Its Antioxidant, Anti-Inflammatory, Antidiabetic and Antibacterial Activities. – J. Environ. Chem. Eng. 7:103094.
- [43] Lalitha, A., Subbaiya, R., Ponmurugan, P. (2013): Green synthesis of silver nanoparticles from leaf extract *Azadirachta indica* and to study its antibacterial and antioxidant property. – Int J Curr Microbiol Appl Sci. 2: 228-235.
- [44] Maliar, T., Nemecek, P., Ūrgeová, E., Maliarová, M., Nesvadba, V., Krofta, K., Vulganová, K., Krošlák, E., Kraic, J. (2017): Secondary Metabolites, Antioxidant and Anti-Proteinase Activities of Methanolic Extracts from Cones of Hop (*Humulus lupulus* L.) Cultivars. – Chem. Pap. 71: 41-48.
- [45] Mohammad, E. T., Majid, D., Mohammad, S. A., Hasan, A. H., Fahimeh, N., Mohammad, M., Malihe, F., Seyed, M., Seyed, H. (2020): Anticancer, antimicrobial, and dye degradation activity of biosynthesized silver nanoparticle using *Artemisia kopetdaghensis*. – Micro and Nano Letters 15(14): 1046-1050.
- [46] Mohanta, Y. K., Panda, S. K., Biswas, K., Tamang, A., Bandyopadhyay, J., De, D. (2016): Biogenic synthesis of silver nanoparticles from *Cassia fistula* (Linn.): in vitro assessment of their antioxidant, antimicrobial and cytotoxic activities. – IET Nanobiotechnol. 10: 438-444.
- [47] Mohanta, Y.K., Panda, S.K., Jayabalan, R., Sharma, N., Bastia, A.K., Mohanta, T.K. (2017): Antimicrobial, Antioxidant and Cytotoxic Activity of Silver Nanoparticles Synthesized by Leaf Extract of *Erythrina suberosa* (Roxb.). – Front. Mol. Biosci. 4: 14.
- [48] Mukkavalli, S., Chalivendra, V., Singh, B. R. (2017): Physico-chemical analysis of herbally prepared silver nanoparticles and its potential as a drug bioenhancer. – Open Nano. 2: 19-27.
- [49] Mussin, J., Giusiano, G. (2020): Ethno-Phytopharmacology: Product Validation Process Based on Traditional Knowledge of Medicinal Plants. – In: Chong, P. A., Newman, D.J.,

- Steinmacher, D. A. (eds.) Agricultural, Forestry and Bioindustry Biotechnology and Biodiscovery. Springer, Cham. pp. 331-353.
- [50] Mussin, J., Robles-Botero, V., Casañas-Pimentel, R., Rojas, F., Angiolella, L., San Martín-Martínez, E., Giusiano, G. (2021): Antimicrobial and cytotoxic activity of green synthesis silver nanoparticles targeting skin and soft tissue infectious agents. – Scientific Reports 11:14566.
- [51] Nagaich, U., Gulati, N., Chauhan, S. (2016): Antioxidant and Antibacterial Potential of Silver Nanoparticles: Biogenic Synthesis Utilizing Apple Extract. – J Pharm. 2016: 7141523.
- [52] Nair, R., Kalariya, T., Sumitra, C. (2005): Antibacterial activity of some selected Indian medicinal flora. – Turk J Biol. 29:41-47.
- [53] Nayak, D., Ashe, S., Rauta, P. R., Kumari, M., Nayak, B. (2016): Bark extract mediated green synthesis of silver nanoparticles: evaluation of antimicrobial activity and antiproliferative response against osteosarcoma. – Mater. Sci. Eng. C. 58: 44-52.
- [54] Nisha, S.N., Swedha, A.A., Rahaman, J.S. (2013): Antibacterial activity of citrus sinensis peel against enteric pathogens. – IJPRBS2(5): 1-13.
- [55] Nsimba, R.Y., Kikuzaki, H., Konishi, Y. (2008): Antioxidant activity of various extracts and fractions of *Chenopodium quinoa* and *Amaranthus* spp. – Seeds.Food Chem. 106: 760-766.
- [56] Otunola, G. A., Afolayan, A. J. (2018): In vitro antibacterial, antioxidant and toxicity profile of silver nanoparticles green-synthesized and characterized from aqueous extract of a spice blend formulation. – Biotechnology and Biotechnological Equipment 32: 724-733.
- [57] Pasupuleti, V.R., Prasad, T.V., Sheikh, R.A., Balam, S.K., Narasimhulu, G., Reddy, C.S. (2008): Biogenic silver nanoparticles using *Rhinacanthus nasutus* leaf extract: synthesis, spectral analysis, and antimicrobial studies. – Int J Nanomed. 8:3355-3364.
- [58] Pietta, P.G. (2000): Flavonoids as antioxidants. – J. Nat. Prod. 63: 1035-1042.
- [59] Praveen, S., Misra, R., Sahoo, S. (2012): Nanoparticles: a boon to drug delivery, therapeutics, diagnostics and imaging. – Nanomed: Nanotechnol Biol Med. 8:147-166.
- [60] Priya, R. S., Geetha, D., Ramesh, P. S. (2016): Antioxidant activity of chemically synthesized AgNPs and biosynthesized *Pongamia pinnata* leaf extract mediated AgNPs– A comparative study. – Ecotoxicol Environ Saf. 134:308-318.
- [61] Rai, M., Yadav, A., Gade, A. (2009): Silver nanoparticles as a new generation of antimicrobials. – Biotechnol. Adv. 27: 76-83.
- [62] Rajan, R., Chandran, K., Harper, S. L., Yun, S.-I., Kalaichelvan, P. T. (2015): Plant extract synthesized silver nanoparticles: an ongoing source of novel biocompatible materials. – Ind. Crop. Prod. 70: 356-373.
- [63] Raut, N.S., Kolekar, J.R., Lakkakula, V.D., Mendhulkar, S.B., Kashid, B. (2010): Extracellular synthesis of silver nanoparticles using dried leaves of *Pongamia pinnata*(L) Pierre. – Nano-Micro Lett. 2: 106-113.
- [64] Rigo, C., Ferroni, L., Tocco, I., Roman, M., Munivrana, I., Gardin, C. (2013): Active silver nanoparticles for wound healing. – Int J Mol Sci 14: 4817-4840.
- [65] Roy, A., Bulut, O., Some, S., Mandal, A. K., Yilmaz, M. D. (2019): Green synthesis of silver nanoparticles: Biomolecule nanoparticle organizations targeting antimicrobial activity. – RSC Advanc. 9:2673-2702.
- [66] Salayová, A., Bedlovicová, Z., Daneu, N., Baláž, M., Lukáčová Bujnáková, Z., Balážová, L., Tkáčiková, L. (2021): Green Synthesis of Silver Nanoparticles with Antibacterial Activity Using Various Medicinal Plant Extracts: Morphology and Antibacterial Efficacy. – Nanomaterials 11: 1005-1025.
- [67] Samat, N.A., Nor, R.M. (2013): Sol-gel synthesis of zinc oxide nanoparticles using *Citrus aurantifolia* extracts. – Ceramics International 39: 545-548.
- [68] Santos, E.D., Madalossi, N.V., Sigoli, F.A., Mazali, I.O. (2015): Silver nanoparticles: green synthesis, self-assembled nanostructures and their application as SERS substrates. – New J Chem. 39: 2839-2846.

- [69] Saratale, G., Saratale, R., Kim, D., Kim, D., Shin, H. (2020): Exploiting Fruit Waste Grape Pomace for Silver Nanoparticles Synthesis, Assessing Their Antioxidant, Antidiabetic Potential and Antibacterial Activity Against Human Pathogens: A Novel Approach. – *Nanomaterials* 10: 1457.
- [70] Satyavani, K., Ramanathan, T., Gurudeebam, S. (2011): Plant mediated synthesis of biomedical silver nanoparticles by using leaf extracts of *Citrullus colosynthis*. – *Res. J. Nanosci. Nanotechnol.* 1: 95-101.
- [71] Saxena, A., Tripathi, R.M., Singh, R.P. (2010): Biological synthesis of silver nanoparticles by using onion (*Allium cepa*) extract and their antibacterial activity. – *Digest J. Nanomater. Biostruct.* 5: 427-432.
- [72] Shankar, S.S., Rai, A., Ankamwar, B., Singh, A., Ahmed, A., Sastry, M.(2004): Biological synthesis of triangular gold nanoprisms. – *Nat. Mater.* 3: 482-488.
- [73] Sharma, V. K., Yngard, R. A., Lin, Y. (2009): Silver nanoparticles: green synthesis and their antimicrobial activities. – *Adv. Colloid Interface Sci.* 145: 83-96.
- [74] Shetty, S.B., Mahin-Syed-Ismail, P., Varghese, S., Thomas-George, B., Kandathil-Thajuraj, P., Baby, D., Haleem, S., Sreedhar, S., Devang-Divakar, D. (2016): Antimicrobial effects of *Citrus sinensis* peel extracts against dental caries bacteria: An in vitro study. – *J Clin Exp Dent.* 8: 71-77.
- [75] Siddiqi, K.S., Husen, A. (2016a): Fabrication of metal and metal oxide nanoparticles by algae and their toxic effects. – *Nano Res Lett.* 11: 363-374.
- [76] Siddiqi, K.S., Husen, A. (2016b): Fabrication of metal nanoparticles from fungi and metal salts: scope and application. – *Nano Res Lett.* 11:98-113.
- [77] Sitaramanjaneya, R. G., Sampath Kumar, N.S., Manasa, M., Vijaya, R. (2018): In Vitro Studies of the Antimicrobial and Free-Radical Scavenging Potentials of Silver Nanoparticles Biosynthesized from the Extract of *Desmostachya bipinnata*. – *Analytical Chemistry Insights* 13: 1177390118782877.
- [78] Sondi, I., Salopek-Sondi, B. (2004): Silver nanoparticles as antimicrobial agent: a case study on *E. coli* as a model for Gram-negative bacteria. – *J Colloid Interface Sci.* 275: 177-182.
- [79] Tacconelli, E., Carrara, E., Savoldi, A., Harbarth, S., Mendelson, M., Monnet, D. L., Pulcini, C., Kahlmeter, G., Kluytmans, J., Carmeli, Y., Ouellette, M., Outtersson, K., Patel, J., Cavaleri, M., Cox, E. M., Houchens, C. R., Grayson, M. L., Hansen, P., Singh, N., Theuretzbacher, U., Magrini, N. (2018): Discovery, research, and development of new antibiotics: the WHO priority list of antibiotic-resistant bacteria and tuberculosis. – *Lancet Infect. Dis.* 18: 318-327.
- [80] Vigneshwaran, A., Kathe, P.V., Varadrajana, R.P., Nachane, R.H., Balasubramanya, H. (2006): Biomimetics of silver nanoparticles by white rot fungi *Phaenerochaete chrysosporium*. – *Colloids Surf.* 53: 55-59.
- [81] Yazdi, M.E., Amiri, M.S., Hosseini, H. (2019): Plant-based synthesis of silver nanoparticles in *Handelia trichophylla* and their biological activities. – *Bull. Mater. Sci.* 42: 155-163.

SPATIOTEMPORAL EVOLUTION AND LAG EFFECT OF DROUGHT AND VEGETATION DYNAMICS IN SOUTHWEST CHINA

YANG, C. P. – WANG, Y. Q. – WU, J. J. – SHEN, H. Z. – MA, X. Y.*

*Key Laboratory of Agricultural Soil and Water Engineering in Arid Area of Ministry of Education, Northwest A&F University, Yangling 712100, China
(e-mail: yang_cuiping@nwfau.edu.cn)*

**Corresponding author
e-mail: xma@nwfau.edu.cn*

(Received 10th Feb 2022; accepted 20th May 2022)

Abstract. In this study, the temporal and spatial characteristics of drought and vegetation dynamics as well as the lag time of vegetation's response to drought in Southwest China were determined. The normalized difference vegetation index (NDVI) and standardized precipitation and evapotranspiration index (SPEI) were used to evaluate the effects of drought on vegetation and determine the response of vegetation to hydrological and climatic changes in different seasons and time scales. The results indicated that from 1970 to 2020, the climate in Southwest China showed a aridity trend with a decreasing rate of 0.024/10a. In autumn, the drought trend intensified, and 90.62% of the study area exhibited a trend toward drought; the most significant drought trend was in Yunnan Province ($P < 0.05$). On a seasonal level, the NDVI had a downward trend in summer, with a decrease rate of 0.033/10a and an increasing trend in spring, autumn, and winter, with increase rates of 0.016/10a, 0.009/10a, and 0.15/10a, respectively. The areas with the most obvious improvement in vegetation cover were southern Guangxi Province and eastern Sichuan Province, which had the fastest improvement rate, 0.24/10a. The NDVI was most sensitive to the 6-month SPEI (SPEI₆). The lag time of the NDVI for SPEI at different time scales was 1 month, whereas the lag time for SPEI₆ was up to 2 years. The time delay effect of the NDVI on drought in northwest Sichuan, west Yunnan, southeast Guizhou, and north Guangxi was significantly correlated ($P < 0.05$). The region with the weakest correlation between the NDVI and SPEI was the agricultural area in eastern Sichuan ($P > 0.05$). This study provides a crucial theoretical basis for water balance, ecosystem protection, and efficient water resource management in Southwest China.

Keywords: *drought, vegetation, lag effect, multi-time scale, Southwest China*

Introduction

A drought is usually a natural phenomenon in which the available water is significantly below normal levels for a given period of time and the water supply does not meet current needs (Vicente-Serrano et al., 2015). In the context of global climate change, which is mainly characterized by warming, drought has become a change trend that cannot be ignored, and the frequency and intensity of extreme droughts are increasing, as well as their destructiveness (Sahoo et al., 2015; Vicente-Serrano et al., 2012). For example, a drought in Southwest China in 2010 led to a great negative impact on the ecosystem and agricultural economy of the southwest (Li et al., 2019). Drought affects the vegetation growth status of ecosystems. Studying the sensitivity of vegetation to drought at different time scales and its response characteristics is crucial to understand the response mechanism of dynamic vegetation changes (Piao et al., 2011a, b).

Vegetation is the most sensitive component to climate change (Jiang et al., 2017; Qi et al., 2019). Using the SPEI to scale drought conditions and quantifying

vegetation growth based on the NDVI and radial growth of vegetation, Vicente-Serrano et al. (2015) studied the response of vegetation to drought on a global scale. In vegetation studies, a large number of studies have shown that vegetation growth is susceptible to drought, and studies have found varying degrees of positive correlation between vegetation growth trends and SPEI in most regions (Zhang et al., 2019; Lawal et al., 2019). Liu et al. (2015) demonstrated that the annual maximum NDVI was positively correlated with the SPEI in Yunnan Province, China. Wang et al. (2016) found a strong and positive correlation between the NDVI and SPEI in arid and semiarid areas, China. Vegetation growth was not only affected by drought at the same time, but also by the cumulative and lagged effects of drought (Nils et al., 2018). The lagged effect of vegetation response to drought refers to the fact that vegetation growth conditions are affected not only by the current climatic conditions but also by the climate change in the previous period (Rippin et al., 2011; Hoover et al., 2018). Krishna et al. (2019) analyzed the effect of drought on vegetation based on SPEI index. They found that the effect of SPEI on monthly mean NDVI values at different time scales has a lag effect. Yao et al. (2020) found that meteorological drought has a lagged effect on crop growth at different seasonal scales. Zhao et al. (2020) pointed out that drought has an extensive cumulative effect on the growth of grassland on the Loess Plateau, and the drought and vegetation The time lag effect of drought affects 50% of the grasslands on the Loess Plateau. In addition, vegetation growth is also affected by a combination of many factors such as soil texture, hours of light, flooding, pests and diseases, grazing, and human activities (Wu et al., 2010; Liu et al., 2013).

A large number of studies have been done on vegetation growth conditions based on NDVI indices. And the research areas mainly include the interrelationship between spatial and temporal changes of vegetation and climate factors at regional scale, among which climate factors are mainly temperature and precipitation, and the single factor changes cannot give a comprehensive response to climate change (Li et al., 2015; Che et al., 2014; Sun et al., 2015; Wang et al., 2015). In this paper, the multi-temporal scale SPEI drought index can combine multiple climate factors to more accurately respond to the evolution of dryness and wetness in southwest China, and explore the response mechanism of vegetation to multi-temporal scale drought. However, research on the time-lag characteristics of vegetation growth and drought at different spatial scales in Southwest China remains limited. Therefore, this study investigated (1) the spatiotemporal evolution of drought at annual and seasonal scales based on an Mann–Kendall (MK) trend analysis, (2) the spatiotemporal characteristics of vegetation dynamics at annual and seasonal scales, and (3) the time-delay effect of the NDVI and SPEI at different time scales and spatial distribution patterns. We elucidated the response mechanism of vegetation dynamic changes to drought over multiple time scales and analyzed the time-lag effect of drought in Southwest China, providing a scientific basis for ecosystem protection and drought monitoring.

Materials and methods

Study area

The study area was in Southwest China (20°54'–34°19'N, 97°21'–112°04'E). The administrative region comprises Yunnan, Guizhou, Sichuan, Guangxi, and Chongqing (Fig. 1a). This area covers approximately 1.37×10^6 km², accounting for 14.34% of the

country. The region is bounded by the Qinghai–Tibet Plateau in the west, and it is influenced by southwest and southeast monsoons in the south. The region’s topography is complex; it features both plateaus and basins. Thus, it is a typical area with a variable climate. The climate type is mainly a subtropical monsoon climate. The average annual temperature in most areas is 14–24 °C, and the annual average precipitation is more than 900 mm; precipitation generally decreases from southeast to northwest, and the seasonal distribution of precipitation is extremely uneven (Zhu et al., 2017). Precipitation from May to October accounts for 80%–90% of that of the entire year. However, precipitation from November to April of the next year only accounts for 10%–20% of precipitation, and the annual precipitation variability in the entire region is generally between 10% and 20% (Zhao et al., 1997).

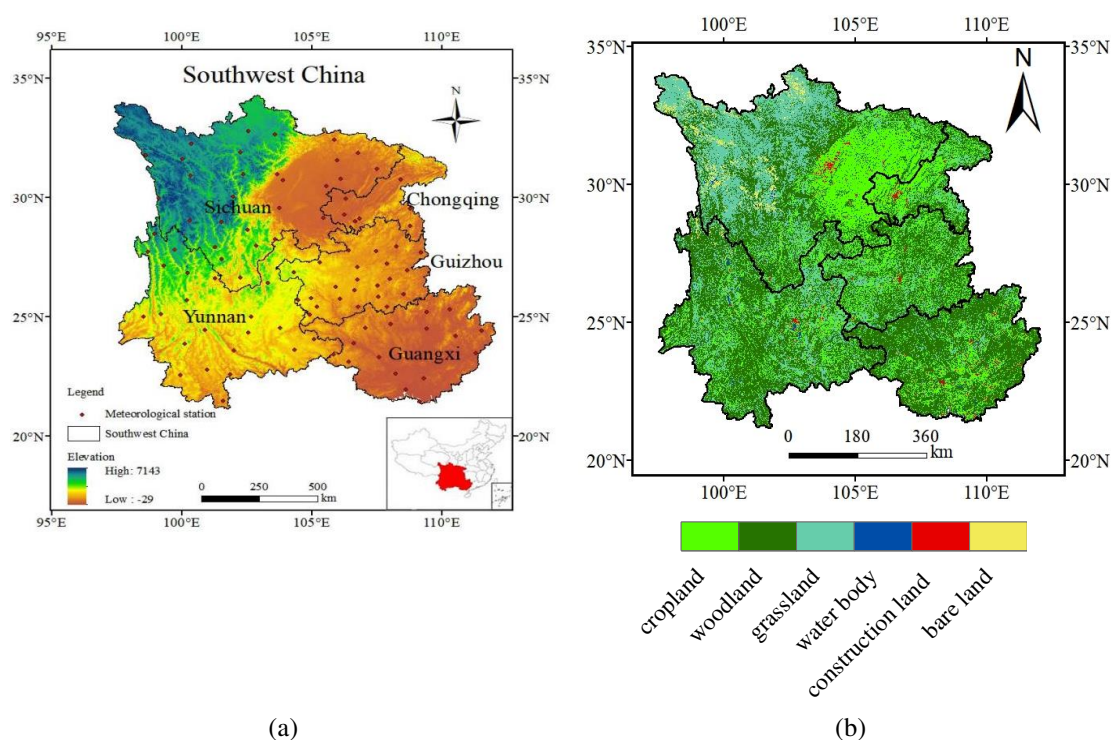


Figure 1. (a) Study area, comprising four provinces (Yunnan, Guizhou, Sichuan, and Guangxi) and a municipality (Chongqing) and (b) land use map in Southwest China

Data sources and processing

In this study, daily average atmospheric pressure, average temperature, relative humidity, average wind speed, sunshine duration, and wind speed from 96 basic meteorological stations in Southwest China from 1970 to 2020 provided by China Meteorological Data Sharing Network (<http://cdc.cma.gov.cn>) were used, and the data with missing measurement values were interpolated using linear regression. Moderate-Resolution Imaging Spectroradiometer (MODIS) NDVI data were obtained from MODIS Terra satellite sensor data available in the MOD13Q1 data set (<https://lpdaac.usgs.gov/products/mod13q1v006/>); the year range for data is 2000 to 2020. The spatial resolution was 500 m × 500 m, and the temporal resolution was 16 d. In this study, the maximum value composite procedure was used to synthesize NDVI

data into monthly values such that they corresponded to monthly SPEI values (Cong et al., 2012; Zhao et al., 2017). The SPEI data was resampled to match the MODIS NDVI data at 500 m spatial resolution by using a majority function in the Resample Tool of ArcGIS. Land use data are obtained from data Center for Resources and Environmental Sciences, Chinese Academy of Sciences. Scale 1:100,000; According to the national standard of Classification of Land Use Status (GB/T21010-2007), the land use in the study area was divided into six land use modes: cultivated land, forest land, grassland, water area, construction land and bare land.

Methods

Standardized precipitation and evapotranspiration index (SPEI)

The SPEI reflects the water balance between precipitation and evapotranspiration. It was devised by Vicente-Serrano et al. (2010), who introduced the concept of potential evapotranspiration based on the SPI. Beguería et al. (2014) improved the SPEI and used the Food and Agriculture Organization of the United Nations (FAO) Penman–Monteith (PM) equation to calculate evapotranspiration instead of using Thornthwaite’s value. The PM equation has a clearer physical meaning and higher accuracy compared with Thornthwaite’s value. The calculation formula is as follows:

(1) The PM equation was used to calculate potential evapotranspiration (ET_0)

$$ET_0 = \frac{0.408\Delta(R_n - G) + \gamma \frac{900}{T + 273} u_2 (e_s - e_a)}{\Delta + \gamma(1 + 0.34u_2)} \quad (\text{Eq.1})$$

where ET_0 is the potential evapotranspiration (mm d^{-1}); Δ is the slope of temperature changes with saturated vapor pressure ($\text{kPa } ^\circ\text{C}^{-1}$); R_n is the net radiation [$\text{MJ (m}^2 \text{d}^{-1})$]; and G is soil heat flux density [$\text{MJ (m}^2 \text{d}^{-1})$], which is small relative to R_n , especially when vegetation cover and calculation step size are equal to or close to 1 d; this value is ignored as 0. The hygrometer constant is represented by γ ($\text{kPa } ^\circ\text{C}^{-1}$); T is the average daily temperature ($^\circ\text{C}$); u_2 is the wind speed at a height of 2 m (m s^{-1}), which can be converted from wind speed at 10 m; e_s is the saturated vapor pressure (kPa); and e_a is the actual vapor pressure (kPa).

(2) The difference between monthly precipitation and potential evapotranspiration is calculated as follows:

$$D_m = P_m - ET_0 \quad (\text{Eq.2})$$

where m is the number of months, P_m is monthly precipitation, and ET_0 is the potential evapotranspiration.

(3) Pairs are clustered and normalized for different time scales as follows:

$$\begin{cases} D_{m,n}^i = \sum_{j=13-i+n}^{12} D_{m-1,j} + \sum_{j=1}^n D_{m,j}, n < i \\ D_{m,n}^i = \sum_{j=n-i+1}^n D_{m,j}, n \geq i \end{cases} \quad (\text{Eq.3})$$

where $D_{m,n}^i$ is the cumulative value of differences between precipitation and evapotranspiration in month i starting from the n th month of m year.

(4) The log-logistic probability distribution function was used to fit the D_m sequence and obtain the cumulative probability density function as follows:

$$F(D) = \left[1 + \left(\frac{\alpha}{D - \gamma} \right)^\beta \right]^{-1} \quad (\text{Eq.4})$$

where parameters α , β , and γ represent the size, shape, and position parameters, respectively, estimated using the linear moment method.

The cumulative probability density is normalized using the following equations:

$$SPEI = W - \frac{c_1 + c_2W + c_3W^2}{1 + t_1W + t_2W^2 + t_3W^3} \quad (\text{Eq.5})$$

$$W = \sqrt{-2\ln(P)} \quad (\text{Eq.6})$$

where P is the probability of a value being greater than a certain D_m value, $P \leq 0.5$, $P = 1 - F(D)$; $P = 1 - P$; $c_0 = 2.515517$, $c_1 = 0.802853$, $c_2 = 0.010328$, $t_1 = 1.432788$, $t_2 = 0.189269$, and $t_3 = 0.001308$.

The SPEI reveals degrees of dryness and wetness. The higher the SPEI value, the wetter an area, and the smaller the SPEI value, the drier an area. *Table 1* presents the corresponding classification of drought grades.

Table 1. Standardized precipitation and evapotranspiration index (SPEI) drought classification

Level	Type	SPEI
1	None	(-0.5,0.5)
2	Light drought	(-1,-0.5]
3	Moderate drought	(-1.5,-1]
4	Severe drought	(-2,-1.5]
5	Extreme drought	($-\infty$,-2]

Normalized difference vegetation index (NDVI)

The NDVI is a crucial remote-sensing parameter that provides information on plant growth and nutrition. The calculation formula is as follows:

$$NDVI = \frac{NIR - RED}{NIR + RED} \quad (\text{Eq.7})$$

where NIR is near-infrared reflectance and RED is visible light reflectance. Areas with vegetation $NDVI > 0.1$ are usually considered to have vegetation cover, and an increase in NDVI indicates an increase in green vegetation; areas with $NDVI < 0.1$ indicate no

vegetation cover, such as construction land, bare soil, desert, Gobi, water bodies, snow and ice, and clouds.

Trend analysis method

(1) Mann-Kendall (MK) trend test

The MK trend test is nonparametric, and it can distinguish whether the sequence variability trend is deterministic or stochastic without following a specific distribution and is widely used in meteorological and hydrological studies (Mann et al., 1945; Kendall et al., 1975).

With n time series exist of sample size (x_1, \dots, x_n) , for all $k, j \leq n$ and $k \neq j$ and different distributions for x_k and x_j , test statistic S can be calculated as follows:

$$S = \sum_{i=1}^{n-1} \sum_{j=i+1}^n \text{sgn}(x_j - x_i) \quad (\text{Eq.8})$$

$$\text{sgn}(x_j - x_i) = \begin{cases} 1, & x_j - x_i > 0 \\ 0, & x_j - x_i = 0 \\ -1, & x_j - x_i < 0 \end{cases} \quad (\text{Eq.9})$$

$$\text{Var}(S) = \frac{n(n-1)(2n+5) - \sum_{i=1}^m t_i(t_i-1)(2t_i+5)}{18} \quad (\text{Eq.10})$$

When $n > 10$, the standard normal statistical variable can be derived as follows:

$$Z = \begin{cases} \frac{S-1}{\sqrt{\text{Var}(S)}}, & S > 0 \\ 0, & S = 0 \\ \frac{S+1}{\sqrt{\text{Var}(S)}}, & S < 0 \end{cases} \quad (\text{Eq.11})$$

If the Z value is regular, an upward trend is exhibited; if the Z value is negative, a downward trend is exhibited.

Trends were detected at specific significance levels (α). When $|Z| > Z_{1-\alpha/2}$, the null hypothesis that a significant trend would exist in the time series was rejected. $Z_{1-\alpha/2}$ was obtained from the standard normal distribution table. Significance levels (α) of 0.01 and 0.05 were used in this study. At the 5% significance level, for $|Z| > 1.96$, the null hypothesis was rejected. At the 1% significance level, for $|Z| > 2.576$, the null hypothesis was rejected.

(2) Linear regression analysis

The least square method was applied to the slope (gradient) of the trend line to dynamically analyze vegetation changes in Southwest China. The calculation formula is as follows:

$$\lambda_{slope} = \frac{n \sum_{i=1}^n i \times C_i - \sum_{i=2}^n i \sum_{i=1}^n C}{n \sum_{i=1}^n i^2 - \left(\sum_{i=1}^n i \right)^2} \quad (\text{Eq.12})$$

where λ_{slope} is the slope of the trend line, n is the study time, and C_i is the NDVI of year i .

Correlation analysis

Correlation coefficient R between the NDVI and SPEI at different time scales is calculated as follows:

$$R = \frac{\sum_{i=1}^n (x_i - \bar{x})(y_i - \bar{y})}{\sqrt{\sum_{i=1}^n (x_i - \bar{x})^2 \sum_{i=1}^n (y_i - \bar{y})^2}} \quad (\text{Eq.13})$$

where x_i and y_i represent SPEI and NDVI values in the i th year, respectively, and \bar{x} and \bar{y} are the average SPEI and NDVI values over the study years, respectively.

Results and analysis

Temporal and spatial variations in drought characteristics in Southwest China

Figure 2 illustrates the annual and seasonal variations in the SPEI for Southwest China. The 3-month SPEI value (SPEI_3) was selected to analyze the characteristics for seasonal SPEI variations, and the 12-month SPEI (SPEI_12) was used to analyze the characteristics for annual SPEI variations. Figure 2 reveals that the SPEI for Southwest China had a downward trend during 1970–2020, an upward trend during 1970–2000 with a slope of 0.0107, and a sharp decline after 2000. A large-scale severe drought event occurred in Southwest China in 2010 (Cheng et al., 2019) (Fig. 2). However, at a seasonal level, the autumn SPEI in Southwest China exhibited a downward trend from 1970 to 2000 with a slope of -0.0171 , indicating that the autumn drought was exacerbated, whereas the autumn SPEI indicated wetter conditions from 2001 to 2020. From 1970 to 2020, the SPEI of Southwest China has exhibited a trend of drought.

The Z statistic of the MK trend analysis of 96 meteorological stations was calculated to analyze variations in SPEI at annual and seasonal levels in Southwest China (Fig. 3). Annually, SPEI values exhibited a downward trend ($Z < 0$) in 55.21% of Southwest China, mainly concentrated in Yunnan Province, Chongqing City, and southeast Sichuan Province. The SPEI in 8.33% of the area exhibited a significant downward trend ($Z \leq -1.96$, $P < 0.05$), mainly distributed in Yunnan Province, which indicates a significant trend of drought in Yunnan Province from 1970 to 2020. The regions with increased SPEI ($Z > 0$) values were mainly distributed in northern Sichuan, Guizhou, and Guangxi. The SPEI increased significantly ($Z \geq 1.96$, $P < 0.05$) in the northwest of Sichuan Province, indicating that the climate in this region was humid. At the seasonal

level, the SPEI increased significantly in 7.29% of the study area ($Z \geq 1.96$, $P < 0.05$) in spring; this increase was mainly in southern Yunnan Province, eastern Sichuan Province, and northern Guangxi Province. In summer, the SPEI values in Sichuan, Guizhou, and Guangxi Provinces exhibited an increasing trend, whereas in Yunnan Province, the SPEI values indicated a trend toward drought. In autumn, the SPEI of 90.62% of the study area exhibited a downward trend ($Z < 0$) of drought, and 11.46% of the area had a significant downward trend of drought ($Z \leq -1.96$, $P < 0.05$). The main distribution areas were the east and south of Yunnan Province, which indicated that the autumn drought trend in Southwest China has increased in the past 51 years, with the autumn drought in Yunnan Province having the most significant upward trend.

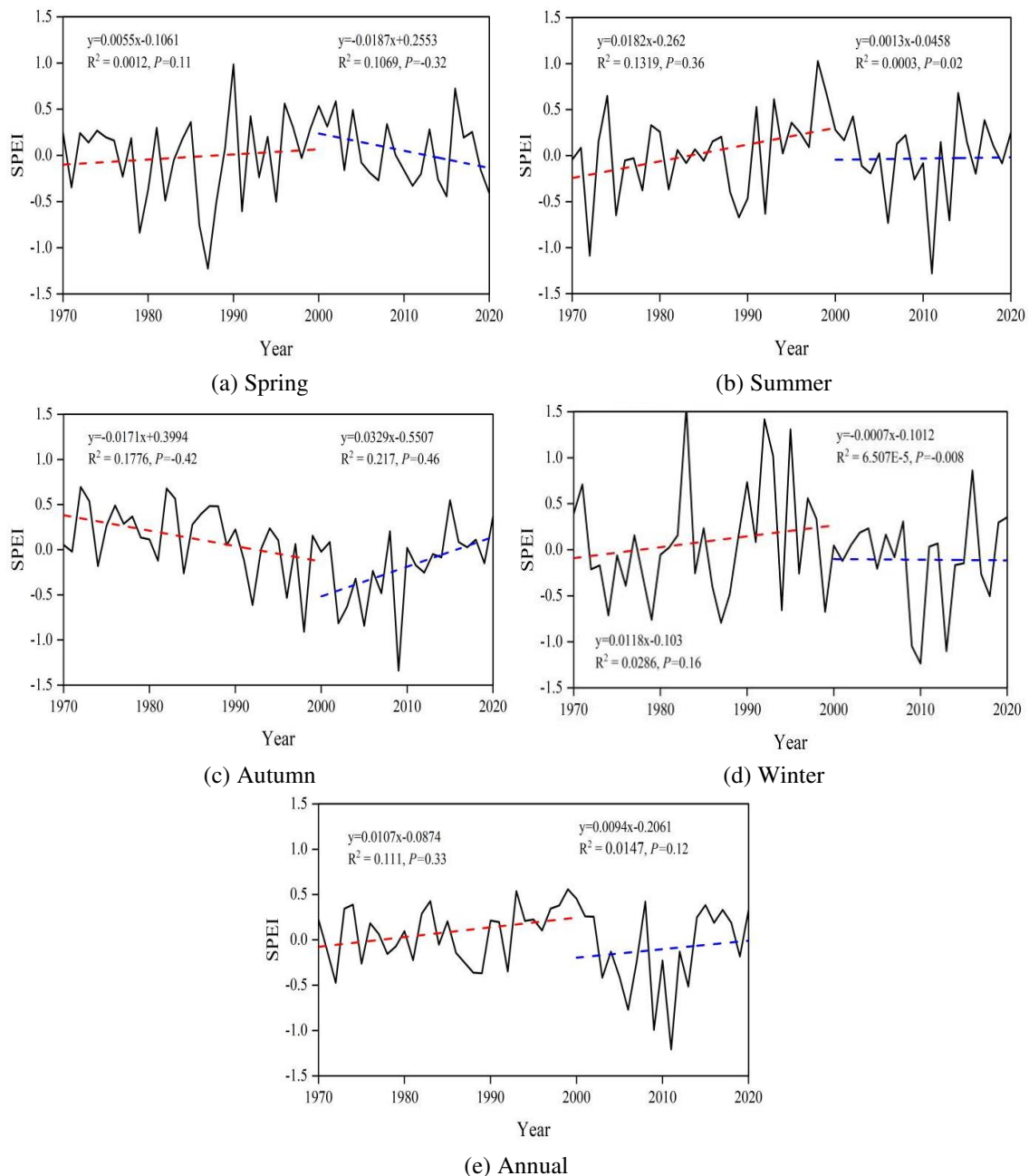


Figure 2. Annual and seasonal variations in the SPEI in Southwest China from 1970 to 2020

In winter, the SPEI in 52.08% of the study area exhibited a downward trend ($Z < 0$), and in 9.38% of the area, it had a significant downward trend ($Z \leq -1.96$, $P < 0.05$), which was mainly distributed in eastern Sichuan (the Sichuan Basin). Generally, most of Southwest China had a trend of drought during 1970–2020. This trend was most pronounced in autumn. The spatial distributions of drought in Southwest China were diverse, while the trend of aridification was most serious in Yunnan Province.

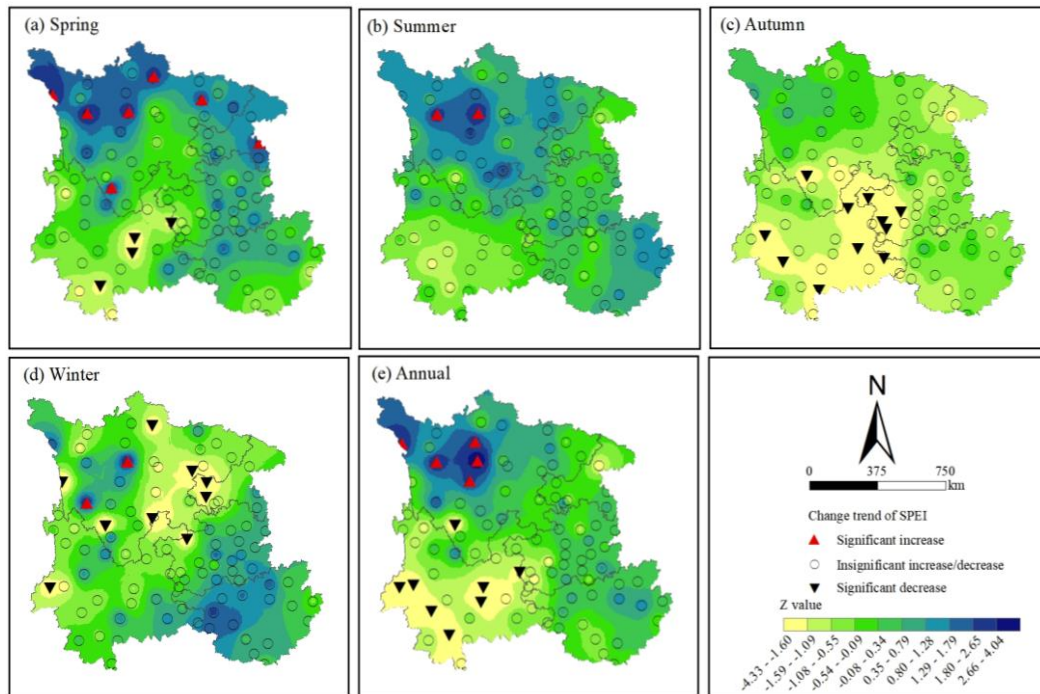


Figure 3. Spatial distribution and variations in the SPEI yearly from 1970 to 2020 in Southwest China as well as in spring, summer, autumn, and winter

Dynamic spatiotemporal changes in vegetation cover in Southwest China

The results of a linear trend analysis (Fig. 4) revealed that the annual average NDVI in Southwest China decreased slightly from 2000 to 2020, but the change was relatively stable. In summer, the NDVI decreased at a rate of 0.033/10a, whereas in spring, autumn, and winter, the NDVI increased slowly at a rate of 0.016/10a, 0.009/10a, and 0.015/10a, respectively.

Figure 5 displays the significant spatial heterogeneity of NDVI trends in Southwest China. Figure 5a presents the spatial distribution of annual mean NDVI in Southwest China, and Figure 5b depicts the regional changes in average NDVI slope from 2000 to 2020. Because of the complex topographic and geomorphological conditions in Southwest China, the annual average NDVI exhibited an obvious upward trend, ranging from -0.09 to 0.82 . The NDVI value in the southwest region of the study area is larger, whereas that in the northwest is smaller. This is because the northwest region is located on the Zoige Plateau, and the high altitude affects climate conditions, resulting in sparse vegetation coverage, such as forest and grassland. Therefore, the NDVI is generally below 0.43, whereas in most other areas, it is above 0.43. In terms of NDVI trend variations, 55.21% of the study area

exhibited a decreasing trend during 2000–2020, with 29.16% of the area exhibiting a significant decreasing trend ($P < 0.05$). The average annual NDVI exhibited an increasing trend in the remaining 44.79% of the area, of which 28.12% had a significant increasing trend ($P < 0.05$). In summary, the NDVI trend distribution in Southwest China indicated a zonal change from east to west; the trend decreased at first, increased, and then decreased.

The areas with the most obvious improvement in vegetation cover were southern Guangxi Province and eastern Sichuan Province, which had the fastest improvement rate of 0.24/10a (Fig. 5b). However, the NDVI in southern Guangxi Province, northeastern Guizhou Province, northeastern Sichuan Province, and some areas of Yunnan Province exhibited negative trends; these areas had a trend of vegetation degradation, and the fastest degradation rate was 0.36/10a, which is higher than the maximum vegetation improvement rate (0.24/10a). This trend was observed because vegetation coverage was affected by high altitude and human activities.

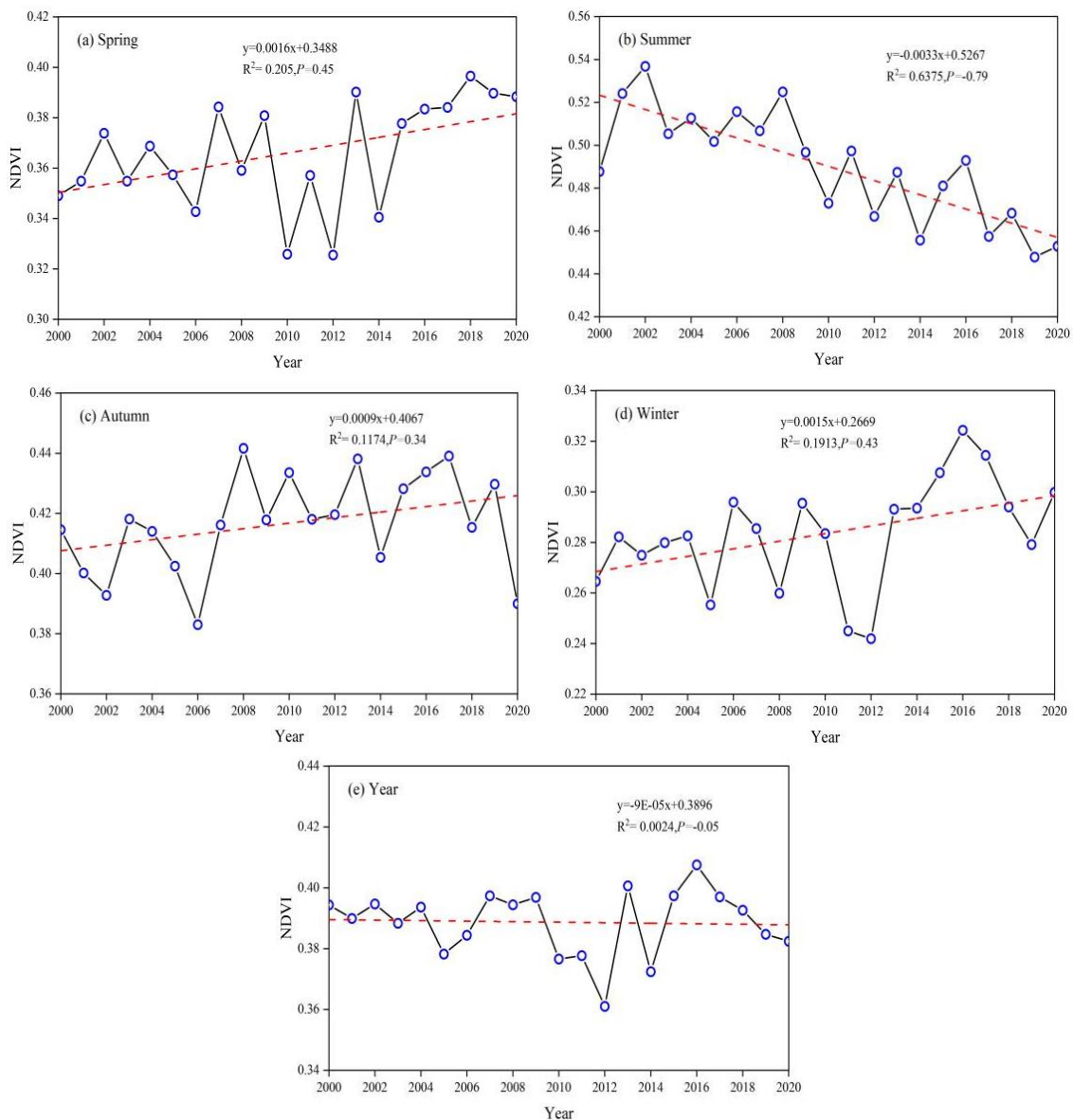


Figure 4. Annual and seasonal NDVI trends in Southwest China from 2000 to 2020

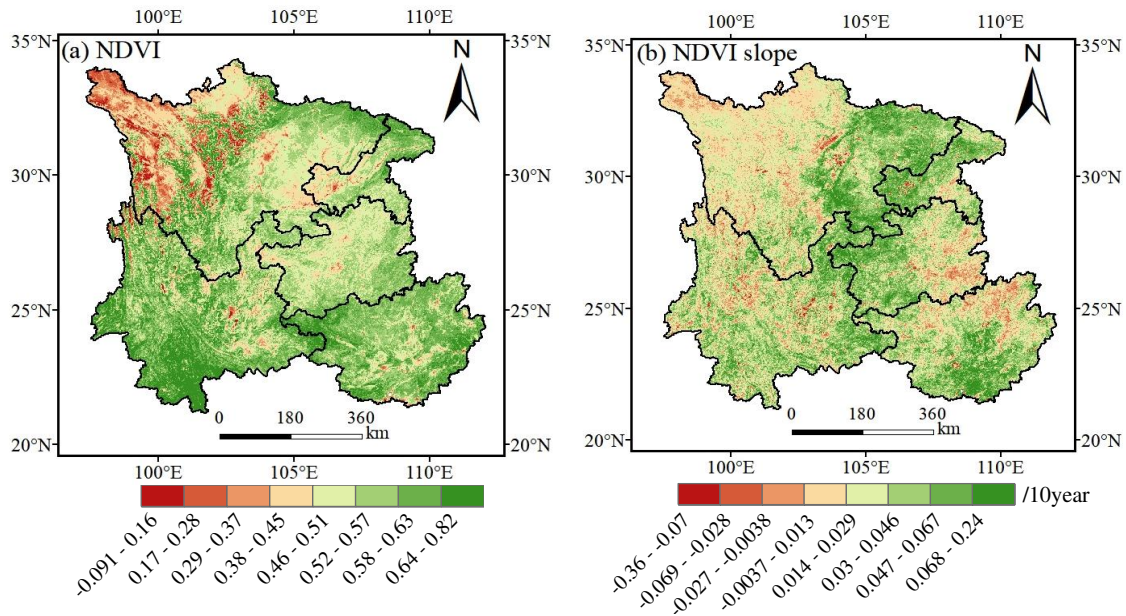


Figure 5. (a) Annual average normalized difference vegetation index (NDVI) values and (b) slopes of annual normalized difference vegetation index (NDVI) variation in Southwest China from 2000 to 2020

Analysis of the lag effect between the NDVI and SPEI at different time scales in Southwest China

The spatial distribution of correlation coefficients between the NDVI and SPEI at different time scales in Southwest China were analyzed. With consideration of the lag effect of the NDVI on drought, the lag correlation between the NDVI and SPEI was further analyzed. The correlation between the NDVI (NDVI for the year, 1-month lagged NDVI series, 3-month lagged NDVI series, 6-month lagged NDVI series, 1-year lagged NDVI series, and 2-year lagged NDVI series) and 1-month SPEI (SPEI_1), 3-months SPEI (SPEI_3), 6-month SPEI (SPEI_6), and 12-months SPEI (SPEI_12) was investigated. The proportions of areas for which the correlation coefficient between the NDVI and SPEI passed the significance test ($P < 0.05$) are also presented (Fig. 6; Tables 2 and 3).

The results indicated that over time, the correlation between the NDVI and SPEI increased, and the correlation between the NDVI and SPEI_6 was the most significant. The correlation between 1 month lagged NDVI and SPEI_6 was the highest ($R = 0.227$, $P < 0.01$), followed by the correlation between 2-year lagged NDVI and SPEI_6 ($R = 0.171$, $P < 0.01$; Table 2). The regions with significant correlations ($P < 0.05$) between the NDVI at different lag times (NDVI for the year, 1-month lagged NDVI series, 3-month lagged NDVI series, 6-month lagged NDVI series, 1-year lagged NDVI series, and 2-year lagged NDVI series) and the SPEI_6 accounted for 22.92%, 35.42%, 17.71%, 13.54%, 20.83% and 15.63% (Table 3) in Southwest China, respectively. Therefore, responses of the NDVI to the SPEI at different time scales in Southwest China had a lag effect of 1 month, and the lag effect of the NDVI and SPEI_6 could reach up to 2 years. The correlations of different time scales indicated that droughts are among the most important factors affecting vegetation growth in the study area. The results verified the hypothesis that vegetation growth has a delayed response to drought.

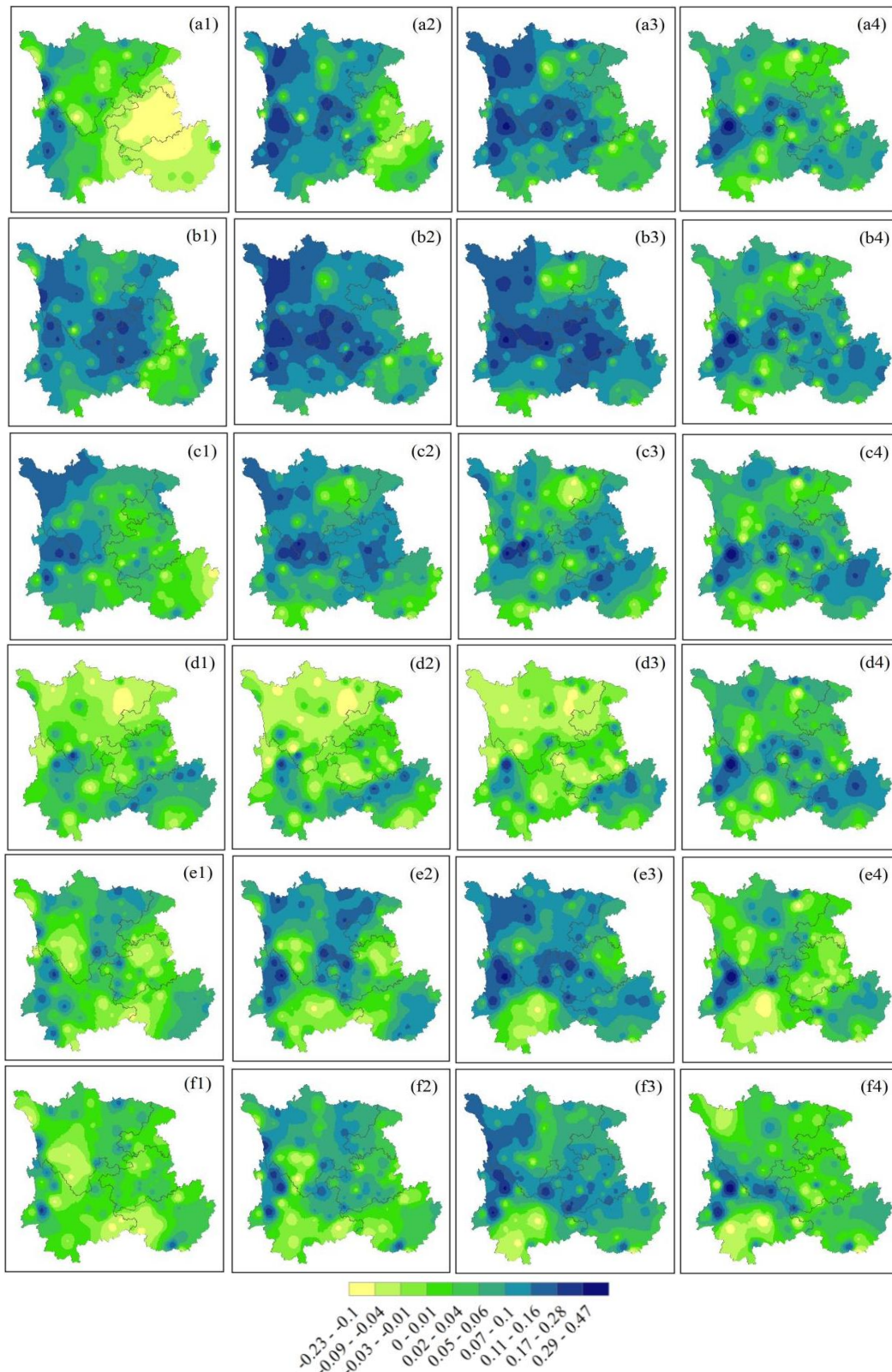


Figure 6. Spatial distribution of correlation coefficients between annual mean NDVI and SPEI at different time scales in Southwest China (a, b, c, d, e, and f denote NDVI for the year, 1-month lagged NDVI series, 3-month lagged NDVI series, 6-month lagged NDVI series, 1-year lagged NDVI series, and 2-year lagged NDVI series, respectively; 1, 2, 3, 4 denote 1-month, 3-month, 6-month, and 12-month SPEI, respectively)

According to the spatial distribution patterns related to the correlation coefficient, the regions with significant correlations between the NDVI and SPEI ($P < 0.05$) in Southwest China were mainly distributed in northwest Sichuan (the Zoige Plateau), west Yunnan (the Hengduan Mountains), southeast Guizhou (the Yunnan–Guizhou Plateau), and northern Guangxi. In east Sichuan (the Sichuan Basin), the correlation between the NDVI and SPEI was small compared with that in other regions, indicating that the regional vegetation changes induced by drought were small. This was because this region is mainly agricultural (*Fig. 1b*); crop growth requires irrigation, and thus, the correlation between vegetation and climate change was weak.

Table 2. Correlation coefficients between annual mean NDVI and SPEI at different time scales in Southwest China from 2000 to 2020

NDVI	SPEI_1	SPEI_3	SPEI_6	SPEI_12
NDVI for the year	-0.059	0.107	0.162	0.053
1-month lagged NDVI series	0.128*	0.203**	0.227**	0.085
3-months lagged NDVI series	0.094	0.185**	0.132**	0.094
6-months lagged NDVI series	0.026	-0.031	-0.069	0.078
1-year lagged NDVI series	0.004	0.105	0.169**	0.007
2-year lagged NDVI series	0.022	0.116	0.171**	0.037

*Statistically significant at the 5% level. **Statistically significant at the 1% level

Table 3. Proportion of areas in which the correlation coefficient between the NDVI and SPEI was significant

	Area ratio (%)			
	SPEI_1	SPEI_3	SPEI_6	SPEI_12
NDVI for the year	22.92	16.67	22.92	10.42
1-month lagged NDVI series	22.92	29.17	35.42	19.79
3-months lagged NDVI series	11.46	16.67	17.71	14.58
6-months lagged NDVI series	7.29	12.50	13.54	15.63
1-year lagged NDVI series	5.21	15.63	20.83	9.38
2-year lagged NDVI series	5.21	9.38	15.63	10.42

Discussion

Vegetation growth is influenced by climatic factors such as precipitation and temperature. Koutsodendris et al. (2018) found that with increasing temperatures, the return of vegetation to green at high latitudes in the Northern Hemisphere was advanced. The effect of precipitation on vegetation growth varies in different regions, where NDVI is significantly and positively correlated with precipitation in arid and semi-arid regions as well as in monsoon climate zones. Especially, the most important constraint for the germination and growth period of vegetation in arid zones is precipitation (Jha et al., 2018). Vegetation growth in harsh environments, such as those with drought, generates corresponding drought resistance through self-regulatory mechanisms. Studies have demonstrated that different vegetation types have different drought resistance, with the lag effect of extreme drought on forest vegetation being up to 4 years, while the response period for grassland is only 1 year (Dash et al., 2019; Xu

et al., 2018), which is explained by the soil water is distributed in different proportions at different soil depths in different types of vegetation areas (Wu et al., 2018; Girardin et al., 2016). With increasing soil thickness, the soil water content in forested areas gradually increases, thus resisting drought at longer time scales. Therefore, the response of vegetation to drought displays a lag effect.

Li et al. (2020) analyzed the lag effect of the NDVI on precipitation in each climatic region of China, and they found that the lag time differed significantly among different climatic zones. The vegetation growth in the arid regions of northwest China is governed by precipitation, which can promote the early growth of vegetation in the growing season and therefore has a relatively short lag time. However, in southwest China, where precipitation is abundant and vegetation is mainly forested, the lag time in response to drought is relatively long. This study revealed that by contrast with changes in the summer and annual SPEI, the NDVI exhibited a decreasing trend, and the minimum annual NDVI (0.36) was in 2012 (*Fig. 4e*), whereas the corresponding minimum SPEI (-1.21) appeared in 2011 (*Fig. 2e*), confirming the lag effect between the NDVI and climate change. In a study on Southwest China, the correlation between NDVI and drought indices, with a lag of approximately 1 month, was high, and the lag time was significant (Li et al., 2019). Our study concluded that the response of vegetation in Southwest China to drought at different times lagged by 1 month, whereas the lag effect of SPEI₆, which is the most sensitive to drought response by NDVI, can reach up to 2 years' time, and the above studies are basically consistent with the conclusion of this study.

The response of the NDVI to drought varies with topographic features, elevation, vegetation type, and human activities (Ghebrezgabher et al., 2020; Guan et al., 2020). In terms of spatial distribution, the correlations between the NDVI and SPEI were high and significant in northwest Sichuan Province (the Ruoerge Plateau), west Yunnan Province (the Hengdian Mountains), southeast Guizhou Province (the Yunnan–Guizhou Plateau), and northern Guangxi Province, whereas the correlations between the NDVI and SPEI were weak and mostly nonsignificant in eastern Sichuan Province (the Sichuan Basin). These findings were related to the complex geomorphological conditions of the study area. Northwest Sichuan Province, west Yunnan Province, and southeast Guizhou Province are high-altitude areas, and precipitation and temperature conditions in the region are the most influential factors governing vegetation dynamics; thus, the NDVI and SPEI in this region have a strong correlation. In the eastern part of Sichuan, where crop growth is dominant, anthropogenic disturbances such as irrigation and fertilization create favorable conditions for crop growth, and thus, the correlation between the NDVI and SPEI in this region is low (Li et al., 2018). The NDVI and SPEI exhibited a mainly weak positive correlation and a partially negative correlation; the main reason for these results is that vegetation growth is less influenced by moisture, and temperature becomes the main factor affecting vegetation growth due to terrain conditions (Thavorntam et al., 2013).

This study mainly explored the influence of climatic factors on vegetation dynamics in Southwest China. Subsequent studies should explore other factors that may affect vegetation growth, such as topographic and geomorphological features, soil physical and chemical properties, and human economic activities (Gouveia et al., 2017; Lai et al., 2018). Some studies have confirmed that the NDVI is generally increasing in Southwest China, but marshes and grasslands have exhibited a decreasing trend. Zhou et al. (2018) found a significant increase in annual mean NDVI in high-altitude

subalpine scrub in southwest China. Liu et al. (2015) found that vegetation growth was closely related to groundwater level, and the groundwater level in the best vegetation growth area in the Qaidam River basin was 1.70 m, for example. In economically and socially developed areas such as the Yangtze River Delta, a trend of NDVI reduction is exhibited at all time scales, which indicating that urbanization development has adversely affected vegetation cover, and that the physical characteristics of vegetation are influenced by factors such as the expansion of traffic roads, high population density, and the heat island effect (Xu et al., 2017; Rmg et al., 2019). Therefore, multiple influencing factors should be integrated to analyze vegetation dynamic changes in subsequent studies.

Conclusions

The dynamic evolution of drought and vegetation cover in Southwest China was analyzed using the SPEI and NDVI to identify the seasons and regions with the most severe aridification trends and to reveal the time lag effect of vegetation dynamics on drought. The main conclusions are as follows:

(1) The whole area of Southwest China presented a trend of aridity. The most significant trend of drought was in autumn, with 90.62% of the regions exhibiting a decrease in SPEI. The regions exhibiting a significant decrease in SPEI were mainly in Yunnan Province, and those with a significant increase were mainly in northwestern Sichuan.

(2) In spatially, the NDVI changes in strips from east to west, with the most obvious the greatest vegetation growth in southern Guangxi Province and eastern Sichuan Province.

(3) The NDVI response to different SPEI time scales in Southwest China had a 1-month lag effect, and the longest lag effect for the NDVI was for SPEI₆ (up to 2 years).

This research had crucial implications for drought monitoring and vegetation conservation in Southwest China. However, the response of vegetation evolution to various influencing factors, such as land use, soil texture, and human activities would be further explored.

Acknowledgements. This study was financially supported by The National Natural Science Foundation of China, grant number 51279167; Distributed Monitoring and Forecasting Technology of Soil Moisture in Irrigation District (No.2017YFC0403202).

REFERENCES

- [1] Beguería, S., Vicente-Serrano, S. M., Reig, F., Latorre, B. (2014): Standardized precipitation evapotranspiration index (SPEI) revisited: parameter fitting, evapotranspiration models, tools, datasets and drought monitoring. – *International Journal of Climatology* 34(10): 3001-3023.
- [2] Che, M., Chen, B., Innes, J. L. et al. (2014): Spatial and temporal variations in the end date of the vegetation growing season throughout the Qinghai-Tibetan Plateau from 1982 to 2011. – *Agricultural and Forest Meteorology* 189: 81-90.
- [3] Cheng, Q., Gao, L., Zuo, X., Zhong, F. (2019): Statistical analyses of spatial and temporal variabilities in total, daytime, and nighttime precipitation indices and of extreme

- dry/wet association with large-scale circulations of Southwest China, 1961-2016. – *Atmospheric Research* 219: 166-182.
- [4] Cong, N., Piao, S., Chen, A., Wang, X., Lin, X., Chen, S., Han, S., Zhou, G., Zhang, X. (2012): Spring vegetation green-up date in China inferred from SPOT NDVI data: a multiple model analysis. – *Agric For Meteorol* 165: 104-113.
- [5] Dash, S., Sahoo, B., Raghuvanshi, N. (2019): A SWAT-Copula based approach for monitoring and assessment of drought propagation in an irrigation command. – *Ecological Engineering* 127: 417-430.
- [6] Ghebregabher, M., Yang, T., Yang, X. (2020): Assessment of NDVI variations in responses to climate change in the Horn of Africa. – *Egyptian Journal of Remote Sensing and Space Science* 23(03): 249-261.
- [7] Girardin, M., Hogg, E., Bernie, P. (2016): Negative impacts of high temperatures on growth of black spruce forests intensify with the anticipated climate warming. – *Global Change Biology* 22: 627-643.
- [8] Gouveia, C., Trigo, R., Begueria, S., Vicente-Serrano, S. M. (2017): Drought impacts on vegetation activity in the Mediterranean region: an assessment using remote sensing data and multi-scale drought indicators. – *Glob Planet Chang* 151: 15-27.
- [9] Guan, Y., Lu, H., Yin, C. (2020): Vegetation response to climate zone dynamics and its impacts on surface soil water content and albedo in China. – *Science of the Total Environment* 747: 141-153.
- [10] Hoover, R., Gayloro, D., Cooper, C. (2018): Dune mobility in the St. Anthony Dune Field, Idaho, USA: effects of meteorological variables and lag time. – *Geomorphology* 309: 29-37.
- [11] Jha, S., Srivastava, R. (2018): Impact of drought on vegetation carbon storage in arid and semi-arid regions. – *Remote Sensing Applications: Society and Environment* 11: 22-29.
- [12] Jiang, L., Jiapaer, G., Bao, A., Guo, H., Ndayisaba, F. (2017): Vegetation dynamics and responses to climate change and human activities in Central Asia. – *Science of the Total Environment* 599: 967-980.
- [13] Kendall, M. (1975): *Rank Correlation Methods*. – Griffin, London.
- [14] Koutsodendris, A., Allstädt, F., Kern, O., Kousis, I. (2019): Late Pliocene vegetation turnover on the NE Tibetan Plateau (Central Asia) triggered by early Northern Hemisphere glaciation. – *Elsevier* 180: 117-125.
- [15] Krishna, R., William, R. (2019): Satellite-based vegetation optical depth as an indicator of drought-driven tree mortality. – *Remote Sensing of Environment* 227: 471-482.
- [16] Lai, C., Li, J., Wang, Z., Wu, X., Zeng, Z., Chen, X., Lian, Y., Yu, H., Wang, P., Bai, X. (2018): Drought induced reduction in net primary productivity across mainland China from 1982 to 2015. – *Remote Sens* 10: 1-27.
- [17] Lawal, S., Lennard, C., Jack, C. (2019): The observed and model-simulated response of southern African vegetation to drought. – *Agricultural and Forest Meteorology* 279: 534-542.
- [18] Li, S., Yang, S., Liu, X. (2015): NDVI based analysis on the influence of climate change and human activities on vegetation restoration in the Shaanxi-Gansu-Ningxia region, Central China. – *Remote Sensing* 7(9): 11163-11182.
- [19] Li, K., Tong, Z., Liu, X. (2018): Quantitative assessment and driving force analysis of vegetation drought risk to climate change: methodology and application in Northeast China. – *Agricultural and Forest Meteorology* 8: 282-283.
- [20] Li, X., Li, Y., Chen, A. (2019): The impact of the 2009/2010 drought on vegetation growth and terrestrial carbon balance in Southwest China. – *Agricultural and Forest Meteorology* 269: 239-248.
- [21] Li, Q., Shi, X., Wu, Q. (2020): Exploring suitable topographical factor conditions for vegetation growth in Wanhuigou catchment on the Loess Plateau, China: a new perspective for ecological protection and restoration. – *Ecological Engineering* 158: 106-114.

- [22] Liu, Y., Lei, H. (2015): Responses of natural vegetation dynamics to climate drivers in China from 1982 to 2011. – *Remote Sensing* 7(8): 10243-10268.
- [23] Liu, M., Qin, P., Liu, K. (2013): Response of lake water level of Honghu Lake to SPEI/SPI drought indices at different time scales. – *Meteorological Monthly* 39(9): 1163-1170.
- [24] Liu, S., Tian, Y., Yin, Y., An, N., Dong, S. (2015): Effects of climate change on normalized difference vegetation index based on the multiple analysis of standardized precipitation evapotranspiration index methods in the Lancang River basin. – *Climatic and Environmental Research* 20: 705-714.
- [25] Mann, H. (1945): Nonparametric tests against trend. – *Econometrica* 13: 245-259.
- [26] Nils, H., Peter, S., Christian, A. (2018): Drought sensitivity and stem growth variation of nine alien and native tree species on a productive forest site in Germany. – *Agricultural and Forest Meteorology* 256/257: 431-444.
- [27] Piao, S., Wang, X., Ciais, P., Zhu, B., Wang, T., Liu, J. (2011a): Changes in satellite-derived vegetation growth trend in temperate and boreal Eurasia from 1982 to 2006. – *Glob. Change Biol* 17: 3228-3239.
- [28] Piao, S., Cui, M., Chen, A., Wang, X., Ciais, P., Liu, J., Tang, Y. (2011b): Altitude and temperature dependence of change in the spring vegetation green-up date from 1982 to 2006 in the Qinghai-Xizang Plateau. – *Agricultural and Forest Meteorology* 151: 1599-1608.
- [29] Qi, X., Jia, J., Liu, H., Lin, Z. (2019): Relative importance of climate change and human activities for vegetation changes on China's silk road economic belt over multiple timescales. – *Catena* 180: 224-237.
- [30] Rippin, D., Carrivick, J., Williams, C. (2011): Evidence towards a thermal lag in the response of Karsaglaciaren, northern Sweden, to climate change. – *Journal of Glaciology* 57(205): 895-903.
- [31] Rmg, A., As, B., Haaq, A. (2019): A fuzzy model integrating shoreline changes, NDVI and settlement influences for coastal zone human impact classification. – *Applied Geography* 113: 267-277.
- [32] Sahoo, A., Sheffield, J., Pan, M. (2015): Evaluation of the tropical rainfall measuring mission multi-satellite precipitation analysis (TMPA) for assessment of large-scale meteorological drought. – *Remote Sens. Environ* 159: 181-193.
- [33] Shiru, M., Shahid, S., Chung, E. (2019): Changing characteristics of meteorological droughts in Nigeria during 1901-2010. – *Atmospheric Research* 223: 60-73.
- [34] Sun, W., Song, X., Mu, X. (2015): Spatiotemporal vegetation cover variations associated with climate change and ecological restoration in the Loess Plateau. – *Agricultural and Forest Meteorology* 209: 87-99.
- [35] Thavorntam, W., Tantemsapya, N. (2013): Vegetation greenness modeling in response to climate change for Northeast Thailand. – *Journal of Geographical Sciences* 23: 1052-1068.
- [36] Vicente-Serrano, S. M., Beguería, S., Lorenzo-Lacruz, J. I. (2010): A multiscale drought index sensitive to global warming: the standardized precipitation evapotranspiration index. – *Journal of Climate* 23(7): 1696-1718.
- [37] Vicente-Serrano, S. M., Beguería, S., Lorenzo-Lacruz, J. I. (2012): Performance of drought indices for ecological, agricultural, and hydrological applications. – *Earth Interact* 16: 1-27.
- [38] Vicente-Serrano, S. M., Gouveia, C., Camarero, J. (2013): Response of vegetation to drought time-scales across global land biomes. – *Proceedings of the National Academy of Sciences* 110(1): 52-57.
- [39] Vicente-Serrano, S., Cabello, D., Tomásburguera, M. (2015): Drought variability and land degradation in semiarid regions: assessment using remote sensing data and drought indices (1982-2011). – *Remote Sensing* 7: 4391-4423.

- [40] Wang, H., Chen, Y., Pan, Y. (2015): Spatial and temporal variability of drought in the arid region of China and its relationships to teleconnection indices. – *Journal of Hydrology* 523: 283-296.
- [41] Wang, Z., Huang, Z., Li, J. (2016): Assessing impacts of meteorological drought on vegetation at catchment scale in China based on SPEI and NDVI. – *Transactions of the Chinese Society of Agricultural Engineering* 32(14): 177-186.
- [42] Wu, P., Zhao, X. (2010): Impact of climate change on agricultural water use and grain production in China. – *Transactions of the Chinese Society of Agricultural Engineering* 26(2): 1-6.
- [43] Wu, X., Liu, H., Li, X. (2018): Differentiating drought legacy effects on vegetation growth over the temperate Northern Hemisphere. – *Global Change Biology* 24: 504-516.
- [44] Xu, Y., Xu, Y., Wang, Y. (2017): Spatial and temporal trends of reference crop evapotranspiration and its influential variables in Yangtze River Delta, eastern China. – *Theoretical and Applied Climatology* 130(3/4): 945-958.
- [45] Xu, H., Wang, X., Zhao, C. (2018): Diverse responses of vegetation growth to meteorological drought across climate zones and land biomes in northern China from 1981 to 2014. – *Agricultural and Forest Meteorology* 262: 1-13.
- [46] Yao, N., Zhao, H., Li, Y., Biswas, A. (2020): National-scale variation and propagation characteristics of meteorological, agricultural, and hydrological droughts in China. – *Remote Sensing* 12(20): 256-264.
- [47] Zhang, X., Zhang, B. (2019): The responses of natural vegetation dynamics to drought during the growing season across China. – *Journal of Hydrology* 574: 706-714.
- [48] Zhao, J. (1997): *Physical Geography of China*. 4th Ed. – Higher Education Press, Beijing.
- [49] Zhao, A., Yu, Q., Feng, L. (2020): Evaluating the cumulative and time-lag effects of drought on grassland vegetation: a case study in the Chinese Loess Plateau. – *Journal of Environmental Management* 261: 110214.
- [50] Zhou, Q., Luo, Y., Zhou, X., Cai, M., Zhao, C. (2018): Response of vegetation to water balance conditions at different time scales across the karst area of southwestern China-A remote sensing approach. – *Science of the Total Environment* 645: 460-470.
- [51] Zhu, G., Qin, D., Liu, Y., et al. (2017): Accuracy of TRMM precipitation data in the southwest monsoon region of China. – *Theoretical and Applied Climatology* 129(1/2): 353-362.

APPENDIX

Table A1. *The list of the 96 meteorological stations in Southwest China*

Station number	Province	Station name	Latitude (°)	Longitude (°)	Elevation (m)
56144	Sichuan	Dege	31.80	98.58	3201.2
56146	Sichuan	Ganzi	31.62	100.00	3393.5
56152	Sichuan	Seda	32.28	100.33	3893.9
56172	Sichuan	Maerkang	31.90	102.23	2669.8
56173	Sichuan	Hongyuan	32.80	102.55	3462.9
56178	Sichuan	Xiaojin	31.00	102.35	2367
56182	Sichuan	Songpan	32.65	103.57	2827.7
56187	Sichuan	Wenjiang	30.75	103.87	539.1
56188	Sichuan	Dujiangyan	31.00	103.67	706.7
56247	Sichuan	Batang	30.00	99.10	2589.2
56251	Sichuan	Xinlong	30.93	100.32	3000
56357	Sichuan	Daocheng	29.05	100.30	3727.7

56374	Sichuan	Kangding	30.05	101.97	2615.7
56386	Sichuan	Leshan	29.57	103.75	424.2
56444	Yunnan	Deqin	28.48	98.92	3588.6
56459	Sichuan	Muli	27.93	101.27	2666.6
56462	Sichuan	Jiulong	29.00	101.50	2987.3
56475	Sichuan	Yuexi	28.65	102.52	1661.6
56479	Sichuan	Zhaojue	28.00	102.85	2132.4
56485	Sichuan	Leibo	28.27	103.58	1474.9
56533	Yunnan	Gongshan	27.75	98.67	1591.3
56543	Yunnan	Zhongdian	27.83	99.70	3276.1
56548	Yunnan	Weixi	27.17	99.28	2325.6
56565	Sichuan	Yanyuan	27.43	101.52	2439.4
56651	Yunnan	Lijiang	26.85	100.22	2393.2
56664	Yunnan	Huaping	26.63	101.27	1244.8
56671	Sichuan	Huili	26.65	102.25	1788.4
56684	Yunnan	Huize	26.42	103.28	2109.5
56691	Guizhou	Weining	26.87	104.28	2234.5
56739	Yunnan	Tengchong	25.02	98.50	1647.8
56748	Yunnan	Baoshan	25.12	99.18	1653.5
56751	Yunnan	Dali	25.70	100.18	1990.5
56778	Yunnan	Kunming	25.00	102.65	1891.4
56792	Guizhou	Puan	25.78	104.97	1620
56793	Guizhou	Panxian	25.72	104.47	1527.1
56856	Yunnan	Jingdong	24.47	100.87	1162.3
56875	Yunnan	Yuxi	24.33	102.55	1636.5
56886	Yunnan	Lixi	24.53	103.77	1704.3
56951	Yunnan	Lincang	23.88	100.08	1463.5
56954	Yunnan	Lancang	22.57	99.93	1054.8
56964	Yunnan	Simao	22.78	100.97	1302.1
56966	Yunnan	Yuanjiang	23.60	101.98	396.6
56969	Yunnan	Mengla	21.48	101.57	639.1
56977	Yunnan	Jiangcheng	22.58	101.85	1119.5
56991	Yunnan	Yanshan	23.62	104.33	1554
57206	Sichuan	Guangyuan	32.43	105.85	487
57306	Sichuan	Langzhong	31.58	105.97	382.2
57313	Sichuan	Bazhong	31.87	106.77	358.7
57328	Sichuan	Daxian	31.20	107.50	310.4
57405	Sichuan	Suining	30.50	105.55	278.2
57411	Sichuan	Nanchong	30.78	106.10	297.7
57432	Chongqing	Wanxian	30.77	108.40	186.7
57512	Chongqing	Hechuan	29.97	106.28	230.6
57517	Chongqing	Jiangjin	29.28	106.25	208.6
57536	Chongqing	Qianjiang	29.53	108.78	635.7
57606	Guizhou	Tongzi	29.13	106.83	972
57608	Sichuan	Xuyong	29.17	105.43	377.5
57612	Chongqing	Qijiang	29.02	106.65	252.7

57633	Chongqing	Youyang	28.83	108.77	663.7
57707	Guizhou	Jijie	27.30	105.28	1510.6
57710	Guizhou	Renhuai	27.80	106.40	850
57718	Guizhou	Xifeng	27.10	106.73	1038.1
57722	Guizhou	Meitan	27.77	107.47	791.8
57729	Guizhou	Yuqing	27.23	107.88	600
57731	Guizhou	Sinan	27.95	108.25	416.3
57741	Guizhou	Tongren	27.72	109.18	283.5
57806	Guizhou	Anshun	26.25	105.90	1392.9
57816	Guizhou	Guiyang	26.58	106.73	1071.2
57825	Guizhou	Kaili	26.60	107.98	720.3
57827	Guizhou	Duyun	26.32	107.53	760
57832	Guizhou	Sansui	26.97	108.67	610.5
57902	Guizhou	Xingyi	25.43	105.18	1378.5
57907	Guizhou	Xingyi	25.08	104.90	1305
57910	Guizhou	Ziyun	25.77	106.08	1161
57912	Guizhou	Huishui	26.13	106.63	949.7
57916	Guizhou	Luodian	25.43	106.77	440.3
57922	Guizhou	Dushan	25.83	107.55	972.2
57926	Guizhou	Libo	25.42	107.88	432.9
57932	Guizhou	Rongjiang	25.97	108.53	325.1
57947	Guangxi	Rongan	25.22	109.40	119.7
57957	Guangxi	Guilin	25.32	110.30	166.7
59007	Yunnan	Guangnan	24.07	105.07	1250.5
59021	Guangxi	Fengshan	24.55	107.03	485.1
59023	Guangxi	Hechi	24.70	108.03	214.4
59046	Guangxi	Liuzhou	24.52	109.40	96.9
59058	Guangxi	Mengshan	24.20	110.52	144
59065	Guangxi	Hexian	24.42	111.53	108
59209	Guangxi	Napo	23.42	105.83	794.7
59211	Guangxi	Baise	23.90	106.60	173.1
59218	Guangxi	Jingxi	23.13	106.42	739.1
59228	Guangxi	Pingguo	23.32	107.58	107.8
59265	Guangxi	Wuzhou	23.48	111.30	119.2
59431	Guangxi	Nanning	22.63	108.22	72.2
59446	Guangxi	Lingshan	22.42	109.30	65.6
59632	Guangxi	Qinzhou	21.95	108.62	4
59644	Guangxi	Beihai	21.45	109.13	14.6

ENERGY-RELATED CARBON EMISSIONS AND ITS INFLUENCING FACTORS DECOMPOSITION IN THE YANGTZE RIVER DELTA REGION, CHINA

TANG, Z. X. – DONG, S. S. – XIONG, H. M.*

School of Economics, Zhejiang University of Finance and Economics, Hangzhou 310018, China

**Corresponding author
e-mail: hmxiong2000@126.com*

(Received 11th Feb 2022; accepted 10th Jun 2022)

Abstract. With rapid economic growth, energy consumption and emission reduction have become one of the most urgent issues in the Yangtze River Delta region (YRD), China's first important economic circle. In this paper, we estimate the energy-related CO₂ emissions in the YRD during 2005-2016 using the emission measurement method provided by the IPCC (2006). In addition, the effects of various driving factors, such as population size, economic scale, industrial structure, energy intensity and energy structure, on CO₂ emissions in this region are quantitatively analyzed by applying the LMDI factor decomposition model. The results show that the primary influencing factors of CO₂ emissions in the YRD are economic growth and energy intensity. Population size and economic growth promoted CO₂ emissions during 2005-2016, and economic growth is the decisive driving factor. On the contrary, the industrial structure, energy intensity, and energy structure of the YRD have inhibitory effects, and energy intensity is the dominant factor among them to restrain the growth of CO₂ emissions. Besides, we discuss these results in detail and find that industrial structure and energy structure have great potential for CO₂ emission reduction in the YRD. Finally, we put forward corresponding sustainable policy suggestions for optimizing industrial structure and energy structure to promote low-carbon economic development.

Keywords: *energy, carbon emissions, factors decomposition, LMDI, Yangtze River Delta region, China*

Introduction

Global warming has become an environmental issue that many countries and regions have attached great importance to in recent years. The main reason for global warming is that with the growth of the world economy, human beings have used a large number of fossil fuels (such as coal, oil, etc.) for nearly a century, and the major component of greenhouse gas emissions is carbon dioxide (CO₂). According to the Kyoto Protocol, China does not have to undertake binding emission reduction tasks as a developing country. Still, China's rapid economic growth has brought increasing pressure to reduce CO₂ emissions as well. On September 3, 2016, China signed the Paris Agreement, pledging to reduce carbon emissions intensity by 40% to 50% by 2020 (Musa et al., 2018; Pan et al., 2018).

According to the International Energy Agency (IEA) report, China's CO₂ emissions accounted for about 27% of the total global CO₂ emissions in 2017, ranking first in the world, which will make China even more difficult to achieve emission reduction goals. As one of the three major economic circles in China, the Yangtze River Delta region (YRD) contributes 207.96 million tons of standard coal in 2016 to China's total energy consumption (Ding et al., 2018; Xiao et al., 2018). Therefore, it is of practical significance to analyze the CO₂ emission of energy consumption in the YRD. Given this, this paper calculated the overall energy-related CO₂ emissions in the YRD (Shanghai, Jiangsu, and Zhejiang) from 2005 to 2016 and used the factor decomposition model of the Logarithmic Mean Divisia Index (LMDI) to analyze the effects of population size,

economic growth, industrial structure, energy intensity, and energy structure on CO₂ emissions of the YRD.

At present, in the methods for quantitatively studying CO₂ emissions, the commonly used decomposition methods mainly include Data Envelopment Analysis (DEA) (Wang et al., 2018a,b; Zhou et al., 2018), Index Decomposition Analysis (IDA) and Structural Decomposition Analysis (SDA) (Wang et al., 2018, 2018a; Meng et al., 2018b; Zou et al., 2018; Li et al., 2018a; Gu et al., 2018b), and the econometric model (Meng et al., 2018a; Zhao and Zhang, 2018b; Song, 2018). The Logarithmic Mean Divisia Index (LMDI) has been considered as an improvement in the exponential decomposition method. Compared with other decomposition methods, the LMDI model is more effective in studying the factor decomposition analysis, and its results are also more applicable. Furthermore, one crucial difference between the LMDI and other models lies in the form of weighted decomposition of residuals. The LMDI method can continue to calculate when the data appears zero and has no residual items in the decomposition process (Ang, 2004; Ang, 2007), which becomes a significant advantage. Therefore, it has been widely applied in recent decomposition studies.

There have been many studies on energy consumption or CO₂ emissions in the context of China by the LMDI decomposition method in recent years. These researches applying the LMDI decomposition model could be divided into two areas: one is the overall level, that is, the study of China's carbon emissions on a national scale; the other is the local level, that is, regional research on China's provinces or cities or parts of some regions. On a national scale, Liu et al. analyzed the changes in industrial carbon emissions from 36 industrial sectors in China based on a time series decomposition of the LMDI method (Liu et al., 2007). Zhang et al. presented a decomposition analysis of energy-related CO₂ emissions in China from 1991–2006 divided into three equal time intervals (Zhang et al., 2009). Wang et al. used the LMDI method to analyze the driving factors of carbon emission growth in China and found that the main positive driving factor is per capita GDP. In contrast, the main negative factor is the improvement of energy efficiency (Wang et al., 2010). Tan et al. (2011) examined the driving forces for reducing China's CO₂ emission intensity during 1998–2008, utilizing the LMDI technique. Jiao et al. (2013) used the LMDI model to forecast China's energy demand and CO₂ emissions in 2020 under five scenarios. They analyzed the contributions of five factors to CO₂ emissions in China's nine industries. Yang et al. (2020) analyzed the change in carbon emissions from China's fossil energy consumption by using a Kaya identity model and the LMDI method from 2006 to 2018. Some studies also concentrate on different specific industries in China, such as the cement industry (Xu et al., 2012), chemical industry (Lin et al., 2016), and petroleum refining and coking industry (Xie et al., 2016).

There are also plenty of studies on China's regions, provinces, and city level using the LMDI method. Liu et al. (2012) studied the regional and sectoral disparity and driving factors on greenhouse gas emissions in 30 Chinese provinces. Ren et al. (2012) assessed the drivers of industrial carbon emissions in China's nine economic regions. Zhou et al. (2017) conducted a comparative study on industrial carbon emissions in eight major regions of China. Similar LMDI-based literature also included studies in other specific regions in China, such as the Beijing-Tianjin-Hebei region (Zong et al., 2016), Yangtze River Economic Zone (Ye et al., 2020), Northwestern China (Li et al., 2020), Liaoning province (Yan et al., 2019), Shandong province (Dong et al., 2018), Inner Mongolia region (Tseng et al., 2019), Zhejiang province (Xia et al., 2017), Beijing

(Cui et al., 2020), Tianjin (Wang et al., 2017), Shanghai (Zhao et al., 2009), and Guangzhou (Wang et al., 2019). Some existing studies are related to the YRD. For example, Zhu et al. (2017) analyzed the industrial energy-related CO₂ emissions of cities in the YRD and predicted the CO₂ reduction potential routes of these cities. Song et al. measured the carbon emissions related to energy consumption in the YRD from 1995 to 2010 and set up an incremental factor decomposition model of carbon emissions with the LMDI (Song et al., 2015). The two studies mentioned above have made relatively adequate research about the YRD. However, they preferred to focus on some cities in this region and only used a few types of fuels, such as coal, oil, and natural gas, to calculate. As we can see in the previous literature, studies on CO₂ emission factor decomposition of regions in China have not focused much on the YRD, especially applying multiple energy types, concentrating on a variety of industries, and focusing intensively on CO₂ emission driving factors of the YRD as a whole. Given this, this paper adopts six industries and ten types of fuels to calculate energy-related CO₂ emissions. Based on the LMDI factor decomposition model, quantitative analyses are made on the driving factors of CO₂ emissions, such as population size, economic growth, industrial structure, energy intensity, and energy structure, and the corresponding policy suggestions are finally proposed. The objective of this study is to analyze the impacts of these economic, social, energy and environmental factors on regional carbon emissions in the YRD by estimating the carbon emissions and decomposing their driving factors, then to identify trends in carbon emissions in the YRD by analyzing their path growth. This article is arranged as follows. Section 2 introduces CO₂ emission measurement method and data sources, Section 3 illustrates the factor decomposition model, Section 4 is an empirical analysis and discussion in detail, Section 5 concludes and puts forward corresponding policy suggestions.

Methodology and data

CO₂ emission measurement methods

Energy-related CO₂ emissions of the YRD are calculated according to the measurement methods recommended by the Emissions Technical Guidelines of the Intergovernmental Panel on Climate Change (IPCC, 2006). The calculation formula is as follows:

$$C = \sum_{i=1}^m \sum_{j=1}^n C_{ij} = \sum_{i=1}^m \sum_{j=1}^n E_{ij} \times R_j \quad (\text{Eq.1})$$

where C is the total CO₂ emissions (unit: 10,000 tons); E_{ij} is the jth energy consumption in the ith industry (unit: 10,000 tons of standard coal); R_j is the CO₂ emission coefficient of the jth energy (unit: tce/t for fuels; tce/10⁴m³ for gas); and where m = 3, n = 10. Since the units of consumption of raw coal, clean coal, coke, crude oil, gasoline, kerosene, diesel, fuel oil, and liquefied petroleum gas are 10,000 tons, while the unit of consumption of natural gas is 10000 cubic meters, we unified the units to 10,000 tons of standard coal. Carbon emission factors and standard coal coefficients of ten kinds of fuels are as follows (see *Table 1*.)

Table 1. Carbon emission factor and standard coal coefficient

Fuels	Carbon Emission Factor (t/tce)	Standard Coal Coefficient (tce/t; tce/10 ⁴ m ³)
Raw Coal	0.7559	0.7143
Washed Coal	0.7559	0.9000
Coke	0.8550	0.9714
Crude Oil	0.5857	1.4286
Gasoline	0.5538	1.4714
Kerosene	0.5714	1.4714
Diesel	0.5921	1.4571
Fuel Oil	0.6185	1.4286
Liquefied Petroleum Gas	0.5042	1.7143
Natural Gas	0.4483	12.2900

Source: Converted from the IPCC Guidelines for National Greenhouse Gas Emission Inventory

Data sources

This paper selects six industrial sectors and classifies them into the primary industry, secondary industry, and tertiary industry, respectively. The primary industry includes "Agriculture, forestry, animal husbandry, fishery, and water conservancy", the secondary industry includes "industry" and "construction", and the tertiary industry includes "transport, storage and post", "wholesale and retail trades and hotels and catering services" and "other sectors". The data on the terminal energy consumption of the six industrial sectors in the YRD is derived from the "Regional Energy Balance Sheet (physical quantity)" of Jiangsu, Shanghai, and Zhejiang in China Energy Statistical Yearbook, 2006-2017.

The demographic and economic data are derived from the China Statistical Yearbook and the Statistical Yearbook of provinces (Shanghai, Jiangsu, and Zhejiang), 2006-2017. The population of each region is the resident population counted in the China Statistical Yearbook. Due to the impact of price changes, it is not suitable to directly use the nominal GDP of the current year for comparative analysis. Therefore, the economic data of this paper have been converted into prices based on 2005 to eliminate the price change impacts. CO₂ emissions data are calculated based on the consumption of various terminal energies and their carbon emission factors.

Decomposition model

For the factor decomposition of CO₂ emissions, Yoichi Kaya proposed the Kaya identity at a seminar organized by the UN's IPCC in 1989. Kaya identity combines carbon emissions on energy, population level, and economic scale to quantify the relative roles of key drivers of CO₂ emissions (Kaya, 1990):

$$C = P \times \frac{G}{P} \times \frac{E}{G} \times \frac{C}{E} \quad (\text{Eq.2})$$

where C is the CO₂ emissions; E is the total energy consumption; G is the gross product (GDP); P is the population size. In order to facilitate the analysis by industry and energy

types, the endogenous factors of energy CO₂ emissions are decomposed according to the Kaya identity and rewritten into the following formula (Ang, 2005):

$$\begin{aligned}
 C &= \sum_{i=1}^3 \sum_{j=1}^{10} C_{ij} = \sum_{i=1}^3 \sum_{j=1}^{10} P \times \frac{G}{P} \times \frac{G_i}{G} \times \frac{E_i}{G_i} \times \frac{E_{ij}}{E_i} \times \frac{C_{ij}}{E_{ij}} \\
 &= \sum_{i=1}^3 \sum_{j=1}^{10} P \times A \times S_i \times E_i \times N_{ij} \times R_{ij}
 \end{aligned}
 \tag{Eq.3}$$

where C represents the total CO₂ emissions; C_{ij} the CO₂ emissions generated by the jth type energy consumption in the ith industry; E_{ij} the consumption of the jth energy in the ith industry; E_i the total energy consumption in the ith industry; G_i the industrial added value of the ith industry; G the gross domestic product (GDP) of the YRD; P the population size. Therefore, in the formula (3), A is the GDP per capita (economic growth factor); S_i the ratio of the industrial added value of the ith industry (industrial structure factor); E_i the energy consumption intensity of the ith industry (energy intensity factor); N_{ij} the proportion of the jth energy consumption of the ith industry (energy structure factor); R_{ij} the CO₂ emission coefficient of the jth energy of the ith industry (carbon emission factor).

The total CO₂ emission in the base period is set as C⁰. In this paper, the year 2005 is taken as the base period, the total amount of CO₂ emissions in the t period is C^t, and the change of CO₂ emissions amount from the base period to the t period is ΔC, which means the comprehensive effect of CO₂ emissions. Thus, the influencing factors of energy-related CO₂ emission can be divided into population size effect ΔC_p, economic growth effect ΔC_a, industrial structure effect ΔC_s, energy intensity effect ΔC_e, energy structure effect ΔC_n, and carbon emission factor effect ΔC_r.

LMDI decomposition methods can be divided into "multiplicative" and "additive" decomposition methods. However, the final decomposition results of both methods are consistent. Based on Equation 3, this paper adopts the additive decomposition method as follows:

$$\begin{aligned}
 \Delta C &= C^t - C^0 = \sum_i \sum_j (P^t A^t S_i^t E_i^t N_{ij}^t R_{ij}^t) - \sum_i \sum_j (P^0 A^0 S_i^0 E_i^0 N_{ij}^0 R_{ij}^0) \\
 &= \Delta C_p + \Delta C_a + \Delta C_s + \Delta C_e + \Delta C_n + \Delta C_r
 \end{aligned}
 \tag{Eq.4}$$

According to the actual situation in the YRD in recent years, the carbon emission coefficient of various energy sources in the YRD has not changed much. That is, the carbon emission factor effect ΔC_r can be considered zero, then formula 4 can be rewritten as:

$$\begin{aligned}
 \Delta C &= C^t - C^0 \\
 &= \Delta C_p + \Delta C_a + \Delta C_s + \Delta C_e + \Delta C_n
 \end{aligned}
 \tag{Eq.5}$$

The formula for the yearly effect of each factor is as follows (Ang and Liu, 2007; Zhu et al., 2017):

Population size effect:

$$\Delta C_p = \sum_{i=1}^3 \sum_{j=1}^{10} L(C_{ij}^{t-1}, C_{ij}^t) \ln \left[\frac{P^t}{P^{(t-1)}} \right] \quad (\text{Eq.6})$$

Economic growth effects:

$$\Delta C_a = \sum_{i=1}^3 \sum_{j=1}^{10} L(C_{ij}^{t-1}, C_{ij}^t) \ln \left[\frac{A^t}{A^{(t-1)}} \right] \quad (\text{Eq.7})$$

Industrial structure effect:

$$\Delta C_s = \sum_{i=1}^3 \sum_{j=1}^{10} L(C_{ij}^{t-1}, C_{ij}^t) \ln \left[\frac{S_i^t}{S_i^{(t-1)}} \right] \quad (\text{Eq.8})$$

Energy intensity effect:

$$\Delta C_e = \sum_{i=1}^3 \sum_{j=1}^{10} L(C_{ij}^{t-1}, C_{ij}^t) \ln \left[\frac{E_i^t}{E_i^{(t-1)}} \right] \quad (\text{Eq.9})$$

Energy structure effect:

$$\Delta C_n = \sum_{i=1}^3 \sum_{j=1}^{10} L(C_{ij}^{t-1}, C_{ij}^t) \ln \left[\frac{N_{ij}^t}{N_{ij}^{(t-1)}} \right] \quad (\text{Eq.10})$$

where $L(C_{ij}^{t-1}, C_{ij}^t)$ in equations (6)-(10) is defined as

$$L(C_{ij}^{t-1}, C_{ij}^t) = \begin{cases} C_{ij}^t - C_{ij}^{t-1} / (\ln C_{ij}^t - \ln C_{ij}^{t-1}), & C_{ij}^t \neq C_{ij}^{t-1} \\ C_{ij}^t, & C_{ij}^t = C_{ij}^{t-1} \\ 0, & C_{ij}^t = C_{ij}^{t-1} = 0 \end{cases} \quad (\text{Eq.11})$$

The formula for the cumulative effect of each influencing factor can be changed by replacing (t-1) in *Equations 6-11* with (t=0), which means the base period. To more intuitively and clearly reflect the contribution of each influencing factor on the comprehensive impacts, the formula for calculating the contribution of each factor effect can be rewritten as follows:

$$\delta_\mu = \text{sgn}(\Delta C) \frac{\Delta C_\mu}{\Delta C} \quad (\text{Eq.12})$$

$$\text{sgn}(\Delta C) = \begin{cases} 1, & \Delta C > 0 \\ -1, & \Delta C < 0 \end{cases} \quad (\text{Eq.13})$$

where $\delta\mu$ represents the contribution degree of each factor effect. When $\delta\mu > 0$, it indicates that the factor μ promotes the increase of CO₂ emission, and when $\delta\mu < 0$, it indicates that the factor μ inhibits the growth of CO₂ emission. $\text{sgn}(\Delta C)$ denotes the direction of the change of energy consumption CO₂ emissions. If CO₂ emissions increase, $\text{sgn}(\Delta C)$ is positive; otherwise, it is negative.

Results of factor decomposition

Results of LMDI decomposition

According to *formulas 5-10*, the driving factors of energy-related CO₂ emissions in the YRD can be decomposed into the effects of population size, economic growth, industrial structure, energy intensity, and energy intensity. As for the results of LMDI decomposition, the contribution values and the ratios of various factors to CO₂ emissions in the YRD are shown in *Table 2* and *Table 3*.

As can be seen in *Table 2*, in general, the annual contributions of population size factor and economic development fact to the energy-related CO₂ emissions in the YRD were positive from 2005 to 2016, indicating that economic development scale and population size were the main factors contributing to the increase of CO₂ emissions. *Table 3* shows that the effect of population size on CO₂ emissions was relatively small, while the impact of economic size was very significant, indicating that the effect of economic development was much higher than that of population size. The annual contribution of energy intensity effect to CO₂ emissions was negative during 2006-2015, and the absolute value of its cumulative effect and the ratio of cumulative contribution both placed the second rank among the five factors, indicating that the energy intensity effect was the essential factor to restrain the growth of CO₂ emissions in the YRD. The contribution values of industrial structure effect and energy structure effect to energy CO₂ emission varied during this period. However, on the whole, the cumulative effects of both factors were negative, which indicated that some changes in the YRD, such as the adjustment of industrial structure, the improvement of energy structure, the use of clean energy, or the awareness of carbon emission reduction, could effectively reduce the energy-related CO₂ emission during this period.

There are also some similar trends and high correlations among the total influencing effects, energy consumption, and energy-related carbon emissions in the YRD during this period (*Table 2, Figures 1,2*). From the perspective of total effects, according to *Table 2*, the cumulative impacts of all combined effects in the YRD were positive during 2005-2016. However, from the year-to-year effect, the yearly effects in 2011-2012, 2012-2013, and 2015-2016 are negative, indicating that the energy-related CO₂ emissions have declined in these three periods. It was just in line with the changes in the annual overall CO₂ emissions in these three periods, which can be seen in *Figure 1*. It can also be seen from *Figure 1* that the CO₂ emissions per capita in the YRD tended to be consistent with the overall CO₂ emissions. From 2005 to 2010, CO₂ emissions per capita maintained a slight upward trend. The CO₂ emissions per capita in 2011 also peaked at 0.85 tons per capita, and the total CO₂ emissions reached a peak of 144.12 million tons this year as well.

Table 2. Influencing factors of energy-related CO₂ emissions in the Yangtze River Delta, 2005-2016 (unit: 10,000 tons)

Year	Population size		Economic growth		Industrial structure		Energy intensity		Energy structure		Total effects	
	ΔC_p	Accumulative effects	ΔC_a	Accumulative effects	ΔC_s	Accumulative effects	ΔC_e	Accumulative effects	ΔC_n	Accumulative effects	ΔC	Accumulative effects
2005-2006	160.29	160.29	1202.11	1202.11	51.04	51.04	-929.13	-929.13	-371.43	-371.43	112.89	112.89
2006-2007	190.26	350.56	1375.69	2577.80	-136.85	-85.81	-1081.30	-2010.43	40.59	-330.84	388.40	501.29
2007-2008	139.45	490.00	1139.29	3717.09	-123.60	-209.41	-859.82	-2870.24	33.65	-297.19	328.96	830.25
2008-2009	149.80	639.81	1094.16	4811.25	-80.95	-290.36	-667.75	-3538.00	-188.52	-485.71	306.74	1136.99
2009-2010	270.79	910.60	1192.51	6003.75	-25.55	-315.91	-824.06	-4362.06	-90.96	-576.68	522.72	1659.71
2010-2011	79.86	990.46	1205.97	7209.73	-97.02	-412.93	-719.52	-5081.58	211.67	-365.00	680.96	2340.67
2011-2012	61.40	1051.86	1147.93	8357.65	-185.86	-598.79	-1370.72	-6452.30	-478.20	-843.20	-825.45	1515.22
2012-2013	65.96	1117.82	1100.25	9457.91	-262.34	-861.13	-1136.37	-7588.67	-131.16	-974.36	-363.66	1151.56
2013-2014	36.22	1154.03	1042.04	10499.95	-145.52	-1006.65	-493.35	-8082.02	47.54	-926.82	486.93	1638.49
2014-2015	33.19	1187.23	1073.68	11573.63	-299.69	-1306.34	-349.74	-8431.76	-294.93	-1221.75	162.53	1801.01
2015-2016	70.11	1257.34	970.17	12543.80	-207.09	-1513.43	-1657.04	-10088.80	48.24	-1173.51	-775.62	1025.40

Table 3. Contributions of various factors of energy-related CO₂ emissions in the YRD, 2005-2016 (unit: %)

Year	Population size	Economic growth	Industrial structure	Energy intensity	Energy structure
2005-2006	21.55	161.61	6.86	-124.91	-49.93
2006-2007	24.88	179.92	-17.90	-141.41	5.31
2007-2008	17.66	144.25	-15.65	-108.87	4.26
2008-2009	44.51	325.12	-24.05	-198.42	-56.02
2009-2010	69.73	307.08	-6.58	-212.20	-23.42
2010-2011	6.46	97.48	-7.84	-58.16	17.11
2011-2012	13.51	252.55	-40.89	-301.56	-105.21
2012-2013	36.20	603.79	-143.97	-623.62	-71.98
2013-2014	8.52	245.04	-34.22	-116.01	11.18
2014-2015	11.78	380.88	-106.31	-124.07	-104.62
2015-2016	17.03	235.64	-50.30	-402.47	11.72
Cumulative contribution	271.81	2933.35	-440.85	-2411.70	-361.60

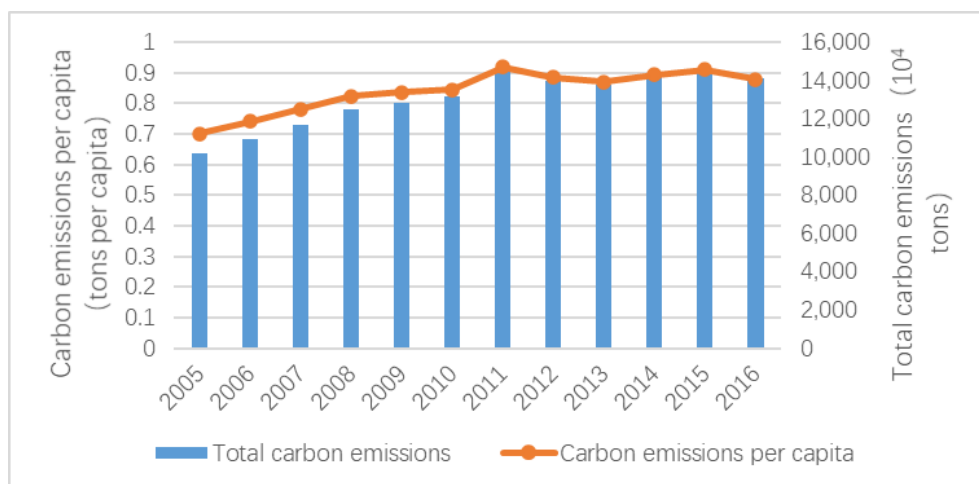


Figure 1. Total and per capita CO₂ emissions in the YRD, 2005-2016

After that time, both the per capita and total emissions began to decline. From 2000 to 2016, the resident population of the YRD was 144.69-160.10 million, with an annual growth rate of 1.00-1.02%, indicating that the resident population in the YRD increased slightly but was relatively stable. Therefore, the change of emissions per capita in this area was mainly due to the difference in the total CO₂ emissions. Compared with the Beijing-Tianjin-Hebei region, another important economic region in China, the Per capita carbon emissions in the YRD have a different trend. From 2005 to 2016, the per capita GDP of The Beijing-Tianjin-Hebei region has been on the rise, and the per capita carbon emissions basically showed an "inverted U-shaped" trend of first rising and then declining, reaching a peak of 1.47 tons per person in 2012. It shows that the low carbon economic development route of the YRD and the BTH is in different stages.

By comparing with *Figure 2*, it can be found that the trend of the total energy-related CO₂ emissions was almost the same as that of energy consumption in the YRD, which means that the energy intensity was closely related to the CO₂ emission intensity during this period. The energy consumption per capita was also consistent with the overall energy consumption trend during this period. Since 2010, the total energy consumption in the YRD has reached more than 200 million tons of standard coal and peaked at 213.13 million tons in 2015. In the same year, the energy consumption per capita peaked, reaching 1.34 tons of standard coal per capita. The energy consumption per capita increased steadily from 2005 to 2011, indicating that with the rapid urbanization and economic growth, the demand for energy became higher and higher in the YRD.

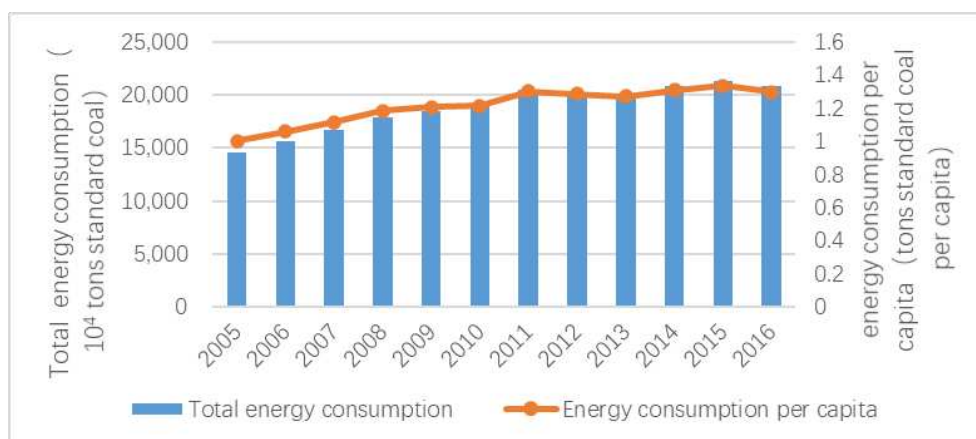


Figure 2. Total and per capita energy consumption in the YRD, 2005-2016

Analysis and Discussion

Population size effect

As can be seen from *Table 2* and *Table 3*, the annual effect and the contribution ratio of population size effect of CO₂ emissions in the YRD were always positive from 2005 to 2016, which promotes the increase of CO₂ emissions to some extent. First of all, the YRD has attracted a large number of non-native immigrants due to its economic development, environment, welfare, education, and other reasons, making it one of the leading destinations for population inflow in China. The resident population has been increasing from 144.69 million in 2005 to 160.09 million in 2016, an increase of about 10.6%. Secondly, to build the YRD into an international metropolitan region, its urbanization level has been increasing rapidly, which may also be the result of the increase of population size in the YRD. Increasing population size in the YRD leads to increasing demand, which leads to increasing energy consumption and CO₂ emissions. Although the population size was a promoting effect on the increase of the overall CO₂ emissions in the YRD, the positive effect is not so significant when compared with the economic effect, as shown in *Table 2* and *Table 3*.

Economic growth effect

GDP per capita can measure the average production capacity of a region by its market value of products and services produced in a certain period, and it can reflect not only the economic growth of this region, but also the material prosperity of the residents.

This paper chooses GDP per capita as the index to measure economic scale and development. As shown in *Figure 3*, the GDP and GDP per capita in the YRD maintained the same steady growth trend from 2005 to 2016. The regional economy has been in a state of rapid and steady growth, the actual GDP per capita increasing from 28,500 yuan in 2005 to 75,600 yuan in 2016, and the average annual growth of the actual income per capita as high as 8.47%. Therefore, the rapid economic growth directly led to the increase of CO₂ emissions in the YRD.

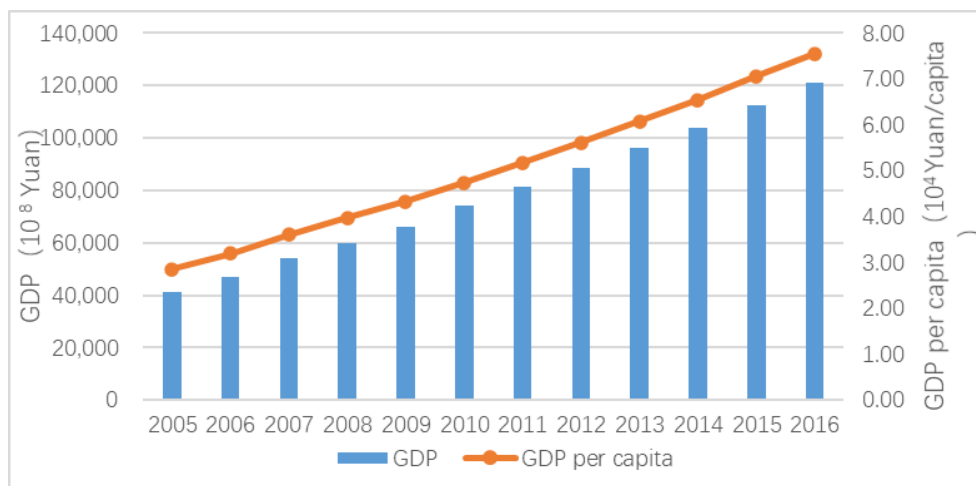


Figure 3. GDP and GDP per capita of the YRD, 2005-2016

As can be seen from the decomposition results of the model in *Table 2*, the continuous expansion of the economic scale in the YRD was the decisive factor causing the growth of energy CO₂ emissions. The yearly effect of the economic growth of the YRD has been positive in 2005-2016, indicating that the factor of economic growth directly leads to an increase in CO₂ emissions year by year. During 2011-2015, the year-to-year economic growth effect was almost declining. This may be because, during the 12th Five-Year Plan period, the economic growth of the YRD was facing unprecedentedly complex international and domestic environments. Affected by the 2008 financial crisis, there were still unstable and uncertain factors in the economic recovery. The economic operation modes of high foreign trade dependence, high investment, and high growth in the YRD were facing major adjustments, and the economic growth rate in this region was correspondingly slowing down. According to the contribution ratio of economic growth (see *Table 3*), the economic growth effect on energy-related CO₂ emissions in the YRD is all positive, reaching the highest in 2012-2013 (603.79%) and the lowest in 2010-2011 (97.48%). The contribution degrees in almost years were all over 100%. Energy consumption supported the regional economic development, and the economic development characterized by industrialization and urbanization of this region, in turn, promoted the increase of energy consumption and CO₂ emissions. Therefore, the growth of CO₂ emissions in the YRD was an inevitable consequence of its economic development.

Industrial structure effect

According to *Table 2*, the yearly effect of industrial structure in the YRD was negative from 2005 to 2016, except for the positive impact from 2005 to 2006, which indicated that the industrial structure in the YRD had a specific inhibiting effect on energy-related CO₂ emission reduction.

Figures 4,5 show that the total energy consumption in the YRD is more consistent with the total energy consumption in the secondary industry from 2005 to 2016, and the trend remained relatively stable. From the perspective of industrial structure development, the industrial structure in the YRD presented a tendency of evolution from the primary industry to the secondary one, then to the tertiary one. The ratio of the tertiary industry in the YRD has been rising steadily, indicating that the industrial structure was developing in a more reasonable direction. It could be noted from *Table 3* that the industrial structure had a significant negative effect on CO₂ emissions during 2010-2015. The contribution value of the industrial structure effect rose sharply from -97.02 in 2011 to -185.86 in 2012, with most other years of this period exceeding -100, reaching the highest value of -299.69 in 2015. From *Table 3*, the contribution ratio of industrial structure suddenly rose from about -8% in 2011 to -41% in 2012, and the contribution ratio in 2013 was as high as -144%. It showed that during the period of the 12th Five-Year Plan, the industrial structure of the YRD has entered the stage of "reshuffle" and encountered the bottleneck of the transformation from capital-labor-intensive industry to technology-capital-intensive industry. The proportion of the secondary industry remained relatively flat, while the ratio of the tertiary industry continued to rise, in line with the optimization and up-gradation of the regional industrial structure. The YRD gradually entered the post-industrial society and began to shift the industrial structure upward to the tertiary industry, which is dominated by high value-added products and high-tech products, thus inhibiting the increase of CO₂ emissions to a certain extent.

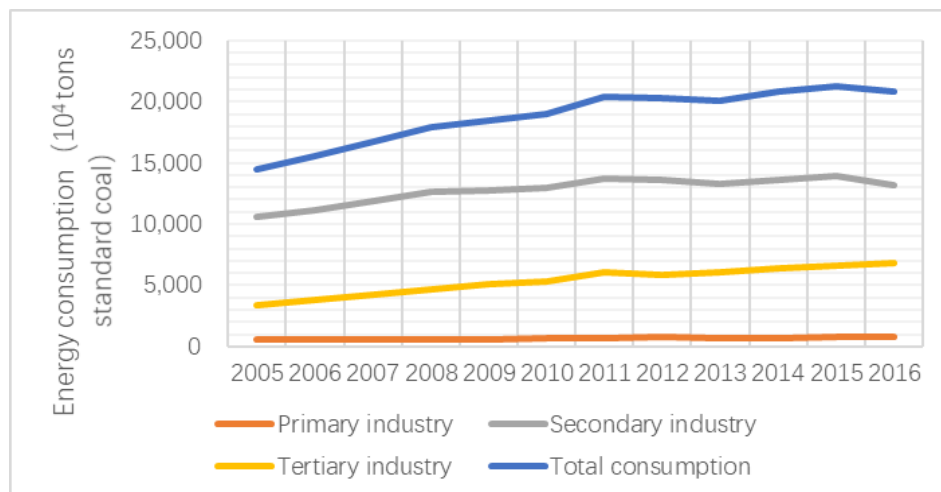


Figure 4. Energy consumption of the three industries in the YRD, 2005-2016

As shown in *Figure 6*, the trend of "industry" or the secondary industry's CO₂ emissions in the YRD was utterly consistent with that of total CO₂ emissions during this period. It is well known that the major CO₂ emission industry in the YRD was the secondary industry. As the YRD was in an important stage of urbanization and

industrialization during this period, with the manufacturing industry and especially the construction industry having sustained rapid development. If the CO₂ emissions of the secondary industry were controlled, the total CO₂ emissions could be reduced a lot. Therefore, to reduce the increment of CO₂ emissions in the YRD, the proportion of the secondary industry in the economy should be gradually reduced to a certain extent, and the tertiary industry should be vigorously developed. In addition, it could be a good policy choice to appropriately improve industrial technology to realize the transformation of industrial structure.



Figure 5. The industrial added value of the three industries in the YRD, 2005-2016

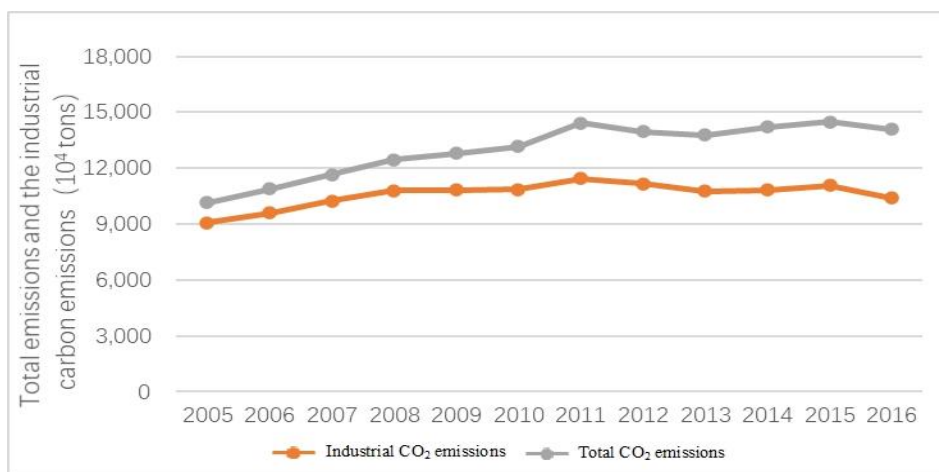


Figure 6. Total CO₂ emissions and industrial CO₂ emissions in the YRD, 2005-2016

Energy intensity effect

Energy intensity refers to the total energy quantity consumed per unit of GDP, and the reduction of energy intensity directly reflects the improvement of regional energy utilization efficiency and the level of energy conservation and emission reduction technologies. It can be seen from *Table 2* that the annual energy intensity of the YRD in 2005-2016 was all negative, indicating that the improvement of energy efficiency played

a significant role in restraining CO₂ emissions from energy consumption. According to the change of energy consumption intensity of the YRD in 2005-2016 (see *Figure 7*), the absolute value of energy intensity contribution ratio in the YRD varied from 58.16% to 623.65%. The cumulative contribution of the energy intensity effect was as high as 2411.70%, ranking second among the five driving factors. It could be seen that energy intensity plays a significant role in inhibiting CO₂ emissions. The energy intensity effects in 2011-2012, 2012-2013, and 2015-2016 fluctuated greatly, which was mainly influenced by the dual factors of total energy consumption and economic growth. Although CO₂ emissions in the YRD are increasing year by year, the effect of energy intensity always played a role in restraining emissions to a large extent. Thus, improving energy utilization equipment and enhancing energy utilization efficiency are effective measures to control CO₂ emissions.

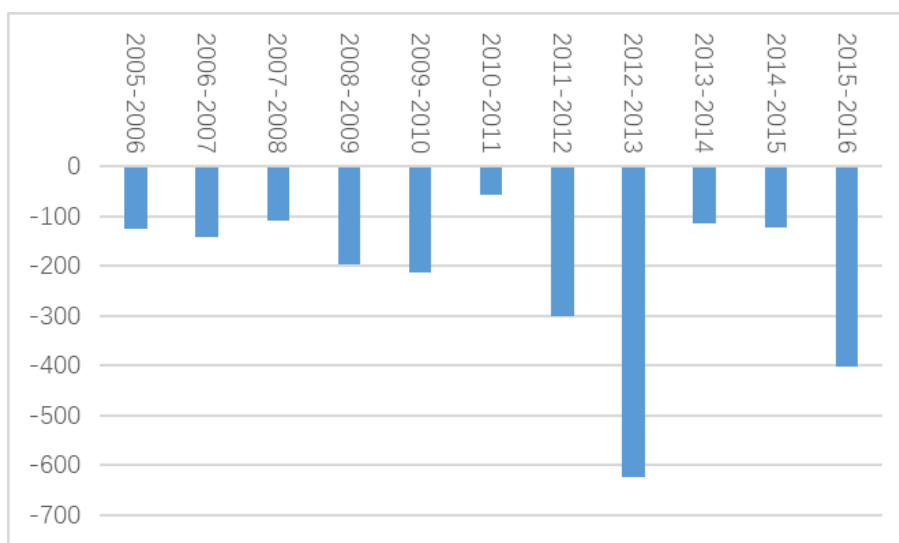


Figure 7. Energy intensity effect contributions in the YRD, 2005-2016 (unit: %)

Energy structure effect

According to *Table 2* and *Table 3*, during 2005-2016, the annual energy structure effect of the CO₂ emission in the YRD changed year by year, the negative effect of the energy structure leading to the reduction of CO₂ emissions while the positive effect leading to an increase. Since the impact of the negative effect was more apparent, the cumulative effect was correspondingly negative, indicating that the energy structure had an inhibitory effect on the growth of CO₂ emissions in the YRD. According to the carbon emission factors of fuels in *Table 1*, the carbon emission factor of coal is the highest, followed by oil, and the carbon emission factor of natural gas is the lowest. That is to say, given the other factors remaining unchanged, if the proportion of coal-based energy in the energy consumption structure declines substantially, the CO₂ emissions may decrease accordingly, even if the ratio of consumption of petroleum and natural gas increases.

As shown in *Figure 8*, during 2005-2016, the energy consumption structure of the YRD was characterized by the facts of coal as the main energy and oil as the auxiliary. The proportion of natural gas consumption increased year by year during this period, and the proportion of coal and oil consumption both decreased, indicating that the adjustment

of energy structure in the YRD is starting to work in reducing emissions. Overall, the energy structure in the YRD has improved, and the proportion of coal consumption has decreased from 58.86% in 2005 to 49.85% in 2016. However, the coal-based energy consumption structure adjustment has not been entirely successful due to the energy endowment, so the YRD, as the most significant economic circle in China, having high technology level and many high-tech industries, still has a lot of room for improving its energy structure.

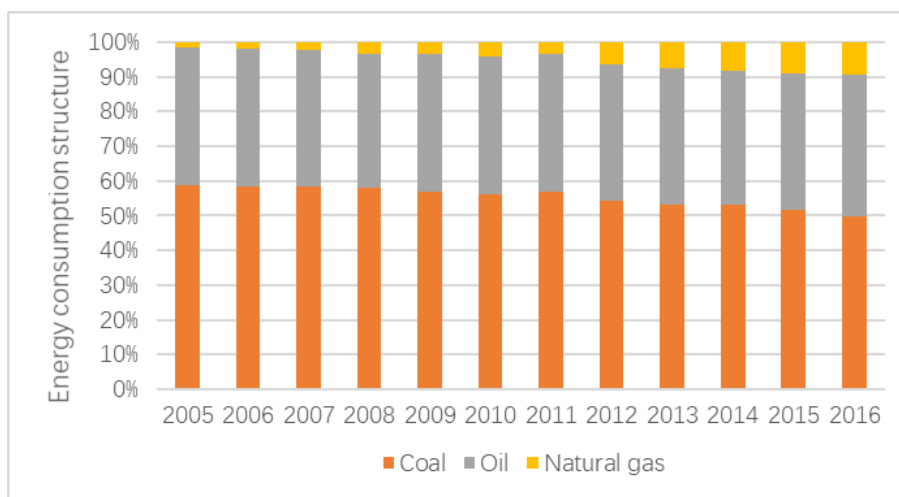


Figure 8. Consumption structure of coal, oil, and natural gas in the YRD, 2005-2016

Conclusions and policy implications

In this paper, we calculated the energy-related CO₂ emissions in the YRD during 2005-2016 and analyzed its driving factors from the population size, economic scale, industrial structure, energy intensity, and energy structure by applying the LMDI model. We showed that the main promoting factor of energy-related CO₂ emission in the YRD is the economic scale, followed by population size. On the contrary, energy intensity had the most important inhibitory effect on CO₂ emissions, and industrial structure and energy structure also inhibited CO₂ emissions as a whole. However, the inhibitory effects of the two latter are far less than that of energy intensity, and the negative impact from the industrial structure is more evident than that from the energy structure.

To be specific, the cumulative effect of economic scale on the energy-related CO₂ emissions was a positive effect of 2933.35% in the YRD, with its absolute value ranking one among the five factors, and the cumulative effect of population size is 271.81%, with its absolute value ranking 5. While the cumulative effect of energy intensity showed a negative effect of -2411.50%, ranking 2 among the five factors, the cumulative effect of industrial structure is a negative effect of -440.85%, ranking 3, and the cumulative effect of energy structure is a negative effect of -361.6%, ranking 4.

At the same time, we found that the industrial sector was the main source of energy-related CO₂ emissions in the YRD, which could closely relate to the industrial structure of the "secondary, tertiary, primary" of the YRD nowadays. The total CO₂ emissions in the YRD showed an evident trend of increasing year by year, which may be related to the bottleneck of industrial transformation and upgrading and to the acceleration of urbanization and industrialization during this period. Some of the

volatility may be related to domestic and international economic conditions, such as the fallout from the 2008 financial crisis. In general, energy consumption and CO₂ emissions in the YRD will continue to increase year by year for a long time in the future. Now we propose several relevant policy suggestions for improving industrial structure and energy structure in the YRD.

(1) For industrial structure, the industrial structure should be optimized to promote the development of green industries. The feasible policy is, on the one hand, to vigorously develop the high-tech industry and service industry, such as the IT industry ecological tourism, and to constantly increase the proportion of the tertiary industry. On the other hand, we can establish a reasonable industrial echelon, accelerate industrial innovation, and optimize the layout and strategy of regional pillar industries as well.

(2) For energy intensity, technological progress should be combined to improve energy utilization efficiency. The YRD has many well-known universities and research institutions in China, full of superior human resources. A large number of 985 and 211 universities and major research institutions there have strong research capabilities, and the YRD also has a relatively better transfer system for technology and a more mature market environment. It should actively explore the development paths of industry-education-research and strengthen the research and development in the field of CO₂ emission reduction technology. The local government can also increase the investment in energy-saving technology as much as possible and carry out technological innovation in promoting energy exploitation, conversion, and utilization, to improve the technical support capacity of CO₂ emission reduction. Moreover, it is well known that the production of renewable energy contributes to the reduction of CO₂ emissions more effectively than the use of natural gas. Renewable energy use and green energy production have become a long-term trend, so some economic incentive policies for renewable and green energy will greatly improve the energy intensity in the YRD.

(3) For energy structure, reasonable and coordinated ways should be chosen to improve the current energy consumption ratios. The proportion of coal consumption in the period from 2005 to 2016 showed a trend of substantial and stable decline. This trend is highly favorable to the improvement of the energy structure in the YRD. However, the sustainable rate of coal consumption still needs to be further studied and determined that could guarantee to complete the goals of the Paris Agreement. We need to proceed with the "coal to gas" plan in the YRD, reduce the raw coal consumption of direct burning, and use more clean energy such as wind, nuclear, solar, and biomass energy to reduce CO₂ emissions and environmental pressure. The energy efficiency can also be improved by increasing the consumption proportion of relatively cleaner energy such as electricity or natural gas.

Acknowledgment. This research was funded by financial support from the Zhejiang Province Natural Science Foundation (No. LY20G030017).

REFERENCES

- [1] Ang, B. W. (2004): Decomposition analysis of policymaking in energy: Which is preferred method? – *Energy Policy* 32: 1131-1139.
- [2] Ang, B. W. (2005): The LMDI approach to decomposition analysis: a practical guide. – *Energy Policy* 33: 867-871.

- [3] Ang, B. W., Liu, N. (2007): Handling zero values in the logarithmic mean Divisia index decomposition approach. – *Energy Policy* 35: 238-246.
- [4] China National Bureau of Statistics (2006-2017): *China Energy Statistical Yearbook 2006-2017*. – China Statistics Press: Beijing, China.
- [5] China National Bureau of Statistics (2006-2017): *China Statistical Yearbook*. – China Statistics Press: Beijing.
- [6] Cui, G., Yu, D., Zhou, Z., Zhang, H. (2020): Driving forces for carbon emissions changes in Beijing and the role of green power. – *Sci. Tot. Environ.* 728: 138688.
- [7] Ding, X., Cai, Z., Xiao, Q., Gao, S. (2019): A Study on The Driving Factors and Spatial Spillover of Carbon Emission Intensity in The Yangtze River Economic Belt under Double Control Action. – *Int. J. Environ. Res. Public Health* 16: 4452.
- [8] Dong, F., Li, J., Zhang, Y.-J., Wang, Y. (2018): Drivers Analysis of CO₂ Emissions from the Perspective of Carbon Density: The Case of Shandong Province, China. – *Int. J. Environ. Res. Public Health* 15: 1762.
- [9] Gu, A., Lv, Z. (2016): The impact of economic structure changes on carbon emissions in China: An IO-SDA approach. – *China Popul. Res. Environ.* 26: 37-45. (In Chinese).
- [10] IPCC. (2006): *Guidelines for National Greenhouse Gas Inventories*. – Cambridge University Press: Cambridge, UK.
- [11] Jiao, J., Qi, Y., Cao, Q., Liu, L., Liang, Q. (2013): China's targets for reducing the intensity of CO₂ emissions by 2020. – *Energy Strat. Rev.* 2: 176-181.
- [12] Kaya, Y. (1990): Impact of Carbon Dioxide Emission Control on GNP Growth: Interpretation of Proposed Scenarios. – Paper Presented to the IPCC Energy and Industry Subgroup, Response Strategies Working Group; IPCC Energy and Industry Subgroup, Response Strategies Working Group: Paris, France.
- [13] Li, A., Zhang, A., Zhou, Y. (2017): Decomposition analysis of factors affecting carbon dioxide emission across provinces in China. – *J. Clean. Prod.* 141: 1428-1444.
- [14] Li, A., Zhou, D., Chen, G., Liu, Y., Long, Y. (2020): Multi-region comparisons of energy-related CO₂ emissions and production water use during energy development in northwestern China. – *Renew. Energy* 153: 940-961.
- [15] Lin, B., Long, H. (2016): Emissions reduction in China's chemical industry-based on LMDI. – *Renew. Sustain. Energy Rev.* 53: 1348-1355.
- [16] Liu, L., Fan, Y., Wu, G., Wei, Y. (2007): Using LMDI method to analyze the change of China's industrial CO₂ emissions from final fuel use: An empirical analysis. – *Energy Policy* 35: 5892-5900.
- [17] Liu, Z., Geng, Y., Lindner, S., Guan, D. (2012): Uncovering China's greenhouse gas emission from regional and sectoral perspectives. – *Energy* 45: 1059-1068.
- [18] Meng, L., Huang, B. (2018): Shaping the Relationship Between Economic Development and Carbon Dioxide Emissions at the Local Level: Evidence from Spatial Econometric Models. – *Environ. Resour. Econ.* 71: 127-156.
- [19] Meng, L., Crijns-Graus, W., Worrell, E., Huang, B. (2018): Impacts of booming economic growth and urbanization on carbon dioxide emissions in Chinese megalopolises over 1985–2010: an index decomposition analysis. – *Energy Effic.* 11: 203-223.
- [20] Musa, S. D., Tang, Z., Ibrahim, A. O., Habib, M. (2018): China's energy status: A critical look at fossils and renewable options. – *Renew. Sustain. Energy Rev.* 81: 2281-2290.
- [21] Pan, X., Wang, H., Wang, L., Chen, W. (2018): Decarbonization of China's transportation sector: In light of national mitigation toward the Paris Agreement goals. – *Energy* 155: 853-864.
- [22] Ren, S., Fu, X., Chen, X. (2012): Regional variation of energy-related industrial CO₂ emissions mitigation in China. – *China Econ. Rev.* 4: 1134-1145.
- [23] Song, M., Guo, X., Wu, K., Wang, G. (2015): Driving effect analysis of energy-consumption carbon emissions in the Yangtze River Delta region. – *J. Clean. Prod.* 103: 620-628.

- [24] Song, Z. G. (2020): Spatial Effect of Carbon Emissions: A Perspective of China's External Economy by Spatial Econometric Model. – *Int. J. Environ. Sci. Dev.* 11: 305-310.
- [25] Statistic Bureau of Jiangsu (2006-2017): *Jiangsu Statistical Yearbook*. – China Statistics Press: Beijing, China.
- [26] Statistic Bureau of Shanghai (2006-2017): *Shanghai Statistical Yearbook*. – China Statistics Press: Beijing, China.
- [27] Statistic Bureau of Zhejiang (2006-2017): *Jiangsu Statistical Yearbook*. – China Statistics Press: Beijing, China.
- [28] Tan, Z., Li, L., Wang, J., Wang, J. (2011): Examining the driving forces for improving China's CO₂ emission intensity using the decomposing method. – *Appl. Energy* 88: 4496-4504.
- [29] Tseng, S.-W. (2019): Analysis of Energy-Related Carbon Emissions in Inner Mongolia, China. – *Sustainability* 11: 7008.
- [30] Wang, F., Wu, L., Yang, C. (2010): Research on the driving factors of carbon emission growth in China's economic development. – *Econ. Res. J.*, pp. 123-136. (In Chinese).
- [31] Wang, Y., Zhao, H., Li, L. (2013): Carbon dioxide emission drivers for a typical metropolis using input–output structural decomposition analysis. – *Energy Policy* 58: 312-318.
- [32] Wang, Y., Ge, X., Liu, J., Ding, Z. (2016): Study and analysis of energy consumption and energy-related carbon emission of industrial in Tianjin, China. – *Energy Strat. Rev.* 10: 18-28.
- [33] Wang, Q., Chiu, Y., Chiu, C. (2016): Non-radial meta frontier approach to identify carbon emission performance and intensity. – *Renew. Sustain. Energy Rev.* 69: 664-672.
- [34] Wang, Y., Jia, W., Bi, Y. (2017): Analysis of China's 2030 carbon dioxide emission peak target from the perspective of efficiency: A study based on zero-sum return DEA model. – *Act. Scient. Circum.* 37: 4399-4408. (In Chinese).
- [35] Wang, B., Wang, Q., Wei, Y., Li, Z. (2018): Role of renewable energy in China's energy security and climate change mitigation: An index decomposition analysis. – *Renew. Sustain. Energy Rev.* 90: 187-194.
- [36] Wang, C., Wu, K., Zhang, X., Wang, F., Zhang, H., Ye, Y., Wu, Q., Huang, G., Wang, Y., Wen, B. (2019): Features and drivers for energy-related carbon emissions in mega-city: The case of Guangzhou, China: based on an extended LMDI model. – *PLoS One* 14(2): e0210430.
- [37] Xia, C., Li, Y., Ye, Y., Shi, Z., Liu, J. (2017): Decomposed Driving Factors of Carbon Emissions and Scenario Analyses of Low-Carbon Transformation in 2020 and 2030 for Zhejiang Province. – *Energies* 10: 1747.
- [38] Xiao, H., Shan, Y., Zhang, N., Zhou, Y., Wang, D., Duan, Z. (2019): Comparisons of CO₂ emission performance between secondary and service industries in Yangtze River Delta cities. – *J. Environ. Manag.* 252: 109667.
- [39] Xie, X., Shao, S., Lin, B. (2016): Exploring the driving forces and mitigation pathways of CO₂ emissions in China's petroleum refining and coking industry: 1995-2031. – *Appl. Energy* 184: 1004-1015.
- [40] Xu, J. H., Fleiter, T., Eichhammer, W., Fan, Y. (2012): Energy consumption and CO₂ emissions in China's cement industry: a perspective from LMDI decomposition analysis. – *Energy Policy* 50: 821-832.
- [41] Yan, Y., Pan, A., Wu, C., Gui, S. (2019): Factors Influencing Indirect Carbon Emission of Residential Consumption in China, A Case of Liaoning Province. – *Sustainability* 11: 4414.
- [42] Yang, P., Liang, X., Drohan, J. P. (2020): Using Kaya and LMDI models to analyze carbon emissions from the energy consumption in China. – *Environ. Sci. Poll. Res.* 27: 26495-26501.
- [43] Ye, L., Wu, X., Huang, D. (2020): Industrial Energy-Related CO₂ Emissions and Their Driving Factors in the Yangtze River Economic Zone (China): An Extended LMDI Analysis from 2008 to 2016. – *Int. J. Environ. Res. Public Health* 17: 5880.

- [44] Zhang, M., Mu, H., Ning, Y., Song, Y. (2009): Decomposition of energy-related CO₂ emission over 1991-2006 in China. – *Ecol. Econ.* 68: 2122-2128.
- [45] Zhang, J., Li, D., Hao, Y., Tan, Z. (2018): A hybrid model using signal processing technology, econometric models and neural network for carbon spot price forecasting. – *J. Clean. Prod.* 204: 958-964.
- [46] Zhao, M., Zhang, W., Yu, L. (2009): Analysis of carbon emissions from energy consumption in Shanghai. – *Environ. Sci. Res.* 22: 984-989. (In Chinese).
- [47] Zhou, X., Zhang, M., Zhou, M., Zhou, M. (2017): A comparative study on decoupling relationship and influence factors between China's regional economic development and industrial energy-related carbon emissions. – *J. Clean. Prod.* 142: 783-800.
- [48] Zhou, Y., Liu, W., Lv, X., Chen, X., Shen, M. (2019): Investigating interior driving factors and cross-industrial linkages of carbon emission efficiency in China's construction industry: Based on Super-SBM DEA and GVAR model. – *J. Clean. Prod.* 241: 118322.
- [49] Zhu, X.-H., Zou, J.-W., Feng, C. (2017): Analysis of industrial energy-related CO₂ emissions and the reduction potential of cities in the Yangtze River Delta region. – *J. Clean. Prod.* 168: 791-802.
- [50] Zong, G., Niu, Q., Chi, Y. (2016): Decomposition analysis of carbon emission factors for energy consumption in Beijing-Tianjin-Hebei region. – *Ecological Science* 35: 111-117.
- [51] Zou, J., Tang, Z., Wu, S. (2019): Divergent leading factors in energy-related CO₂ emissions change among subregions of the Beijing-Tianjin-Hebei area from 2006 to 2016: An extended LMDI analysis. – *Sustainability* 11: 4929.

RECOVERY RESPONSES OF SIMULATED HAIL-DAMAGED *Pelargonium graveolens* L'Hér. (cv. 'Bourbon') TO DIFFERENT MIXTURES OF BIOSTIMULANTS

KHETSHA, Z. P.^{1*} – SEDIBE, M. M.¹ – PRETORIUS, R. J.¹ – BILA, L.²

¹Central University of Technology, Free State, Department of Agriculture, Private Bag X20539, Bloemfontein 9301, South Africa

²Potchefstroom College of Agriculture, Department of Animal Production, Private Bag X1292, Potchefstroom 2520, South Africa

*Corresponding author

e-mail: zkhetsha@cut.ac.za; phone: +27-51-507-3130

(Received 3rd Feb 2022; accepted 20th May 2022)

Abstract. The aim of this study was to determine the potential ability of biostimulant-mixtures to recover the herbage and essential oil yield, as well improve the essential oil quality, of simulated hail-damaged rose geranium (*Pelargonium graveolens* L'Her.). The experiment was carried out in a 3 × 4 factorial treatment design and laid out in a randomised complete block design in a temperature-controlled greenhouse during 2019 season. Treatments consisted of three hail damage simulation levels and three biostimulant-mixtures and a control. Plants grew taller when biostimulant-mixtures were applied from levels 2 up to 3. Level 3 treatment increased the essential oil yield of plants which sustained up to 50% foliage loss, and intact plants. Citronellol and geraniol content, as well the citronellol to geraniol ratio improved with the level 2 treatment in plants that sustained 100% foliage loss. It can be concluded that the application of biostimulants-mixture should be applied from level 3 concentration to improve the herbage yield and the essential oil quality of rose geranium plants with more than 50% foliage loss. Plants with less than 50% foliage loss can be treated with a biostimulant-mixture from level 2 to improve essential oil yield and the densities of brevicollate trichomes.

Keywords: 'Bourbon-type', brassinosteroids, cytokinin, essential oil, gibberellic acid, hail damage simulation, trichome density

Introduction

Prolonged droughts, increased floods, and frequent extreme weather events are evidence of climate change, as a consequence of global warming (Tack et al., 2015). Agriculture is adapting to the variability in global climatic conditions, with farmers continually developing strategies to respond to changing weather patterns (Burke et al., 2015). Aromatic and medicinal plants are among those plants which are negatively affected by climate change (Cavaliere, 2009). In addition, there is a concern over climate change affecting the secondary metabolites of many medicinal and aromatic plants (Das et al., 2016; Kundu and Gantait, 2017). This has been demonstrated with muña (*Minthostachys mollis* [Kunth] Griseb.), where leaf puncturing resulted in reduced menthone levels, while the pulegone concentration increased during the first 48 hours of the experiment (Banchio et al., 2007).

Loss of plant yield, associated with hail damage, is often variable and dependent on the plant species, the timing of injury, relative growth rate, and the prevailing conditions following the damage (Conley et al., 2008; Atkinson et al., 2014). Hailstones >H2 (15.2 to 20.3 mm) can cause extensive damage to growing crops through defoliation, leaf shredding, and stand losses (Changnon, 1999; Conley et al., 2008). Hailstones may cause

significant damage to aromatic and medicinal plants, such as rose geranium (*Pelargonium graveolens* L'Hér.): post-hail damage strategies are therefore required to recover the lost herbage material. Studies have shown that some species recover slowly from hail damage due to delayed growth patterns, i.e. canola (*Brassica napus* L.), Alaska pea (*Pisum sativum* L.), guar (*Cyamopsis tetragonoloba* [L.] Taub.), and lentil (*Lens culinaris* L.) (Miller and Muehlbauer, 1984; McGregor, 1987; Sij et al., 2005; Bueckert, 2011).

Following hail damage, the tissue around the damaged site initiates a cascade of biochemical or physiological processes to repair the damaged tissue: this further depletes energy stores to rebuild photosynthetic material and regenerate lost plant tissue (Suttle et al., 2013; Atkinson et al., 2014). These physiological activities are primarily driven by the upregulation of endogenous plant growth regulators (Ikeuchi et al., 2017; Nanda and Melnyk, 2018). Extensive studies have demonstrated that exogenous applications of agricultural biostimulants on plants may effectively stimulate vegetative growth, improve nutrient acquisition, and increase the antioxidant capacity of the plant tissue (Torres et al., 2018; Parađiković et al., 2019).

The effects of biostimulant are based on the synergism to improve the growth and development, as well as the recovery, resistance and survival of stressed plants (Prins et al., 2010; Parađiković et al., 2019). Therefore, the objective of this study was to determine the ability of biostimulants-mixtures to recover the herbage and essential oil yield attributes, and as well improve the essential oil quality of simulated hail-damaged rose geranium plants. It is hypothesized that high concentrations of biostimulants-mixtures will improve the essential oil yield and quality of simulated hail-damaged rose geranium plants.

Materials and methods

Experimental site description, plant material and agronomic practices

This experiment was conducted in a 72 m² temperature-controlled, plastic-covered greenhouse for 122 days using a drain-to-waste hydroponic system, on the campus of the Central University of Technology, Free State (29°07'S 26°12'E) in Republic of South Africa (RSA). The temperature in the greenhouse was maintained by a fan, which was triggered at ca. 26° C. Rooted rose geranium cuttings 'Bourbon-type' (ca. 10 cm tall) were sourced and obtained from a reputable commercial grower (Siyakholwa Development Foundation, RSA). These rooted cuttings were transplanted into 5 L potting bags filled with a sterile silica-sand root-medium, with a standard average grain size diameter of 2 mm. A single rooted cutting was transplanted into each potting container.

Water analysis was conducted during the growing season and taken into account during the formulation of the nutrient solution. Plants were fertigated three times per day (8:00 am, 12:00 pm, and 4:00 pm) using a 'drain to waste' drip irrigation system, where each dripper supplied 2 L/h of water and nutrient solution (Khetsha et al., 2020). The electric conductivity (EC) and pH of the nutrient solutions were maintained at 1.6 mS/cm and 5.5, respectively. Using a pH and EC meter (Hanna HI 98129 Digital meter), the desired pH and EC levels were achieved by using nitric acid and adjusting the nutrient solution concentration to reach the desired EC (Combrink, 2019). No phytophagous pests were documented during the experiment, however, Malasol (an organophosphate) was preventatively sprayed at 1.75 ml/L throughout the cropping seasons. These applications were repeated for three to six days, at four-week intervals.

Treatments

A 3 x 4 factorial design, arranged in a randomized complete block design was used, and had three replications. Treatments consisted of three hail damage simulation levels (0% [non damaged plants], 50%, and 100% leaf defoliation). The levels of biostimulants evaluated for are illustrated in *Table 1*.

Table 1. Treatment levels used as biostimulants-mixtures in this study

Component	Biostimulants-mixtures treatments (mg/kg)			
	Level 1	Level 2	Level 3	Level 4
Gibberellic acid	Zero	1.26	2.55	3.83
Brassinosteroids	Zero	0.51	1.02	1.53
Cytokinin (traces)	Zero	0.025	0.05	0.075

Hail damage was simulated 61 days after transplanting days using manually-operated garden secateurs, following the procedures described by Khetsha et al. (2021) at ca. 14:00. The 50% hail damage simulation level was achieved by defoliating the top half (average plant height per experimental unit) of each experimental plant (Obeso, 2002). The 100% hail damage simulation treatment was achieved by the total removal of all leaves (Changnon, 1999; Obeso, 2002). This was followed by the removal of stem terminal buds and random bruising of the main stem and lateral branches (using a pair of hand secateurs) on the same day. Plants were subsequently sprayed with a fine water mist, using a nozzle calibrated precision sprayer (0.3 MPa pressure), to simulate humid summer afternoon conditions (Irigoyen et al., 2010; Bal et al., 2014). Subsequently, biostimulants application treatments followed same on the day, an hour after simulated hail damage. A full cover spray of approximately 50 mL of biostimulants treatment solution was applied to each plant. Treatments were subsequently repeated every 14 days between 13:00 and 14:00, and this continued until harvesting that occurred on 31 December 2019.

Parameters

Plant height was determined for six plants in each treatment unit, a day before harvesting using the procedures described by Wood and Roger (2000). The number of branches for each plant was determined during harvesting by counting the number of shoots developing from the main stem, continuing to the last top node (both old and new shoots), following the procedure of Pérez-Harguindeguy et al. (2013). The B:H ratio was used as an indication of bushiness, by dividing the number of branches by plant height (Sedibe, 2012). The plant stand loss, which is the difference between the initial plant stand and the stand after recovery, was also determined (Sij et al., 2005).

Two plants were randomly selected from each treatment to determine the leaf area: all leaves were removed, and the leaf area for each plant was measured using a LI3000 leaf area meter (LI-COR Inc., USA). LI3000 leaf area meter follows a destructive methods to analyse the leaf area, therefore, only two plants were used from six plants to compensate for other destructive sampling for other parameters. Before harvesting, the chlorophyll content was determined using a portable non-destructive chlorophyll meter (Optisciences CCM 200, USA), according to the procedure described by Chen and Black (1992). Readings were taken randomly from the upper-six fully-developed leaves of the crop.

Data for the external leaf morphology was collected from the new fourth leaf from the apical bud, seventy-five days following the recovery of simulated hail-damaged rose geranium plants. Data was collected on a cloudless day, between 10:00 am and 11:00 am. Because the younger leaves have a denser indumentum than the older ones, only the uppermost young fully expanded leaves were selected (Oosthuizen and Coetzee, 1983; Tozin et al., 2015). A sample (ca. 1 cm²) was cut from the middle part of the leaf blade with a surgical blade and prepared for scanning electron microscopy (SEM - Shimadzu SSX-550; Kyoto, Japan) following the procedures by Aly et al. (2021). The morphology and density of trichome groups were determined from digital photos obtained from a computer connected to the SEM. Photos were analysed with Photoshop 7 Savvy (Sybex San Francisco, USA), then two-dimensional selections were made using the SEM scales printed on the photos.

Plant foliar fresh mass (FFM) was determined following the procedures of Wood and Roger (2000) by weighing foliar fresh plant material with a PGL 2002 Adam scale (USA). Rose geranium essential oil was extracted from three plants using a custom-built steam distillation unit (Sedibe, 2012). Approximately 2 kg - 5 kg fresh plant material was distilled at ca. 98°C for one hour. Oil mass (yield) was determined by weighing the oil volume using a PGL 2002 Adam scale (USA) immediately following extraction, as described by Swamy and Rao (2009).

The extracted essential oil was analysed using gas chromatography (GC) (Agilent 7890B), equipped with a 30 mm x 0.25 mm x 0.25 µm column (Agilent 19091S 433 UI, HP5-MS UI) and a mass selective detector (Agilent 5977A) as described by Sedibe (2012). The compounds were identified using the NIST11 mass spectral library (<https://www.nist.gov/system/files/documents/srd/Ver20Man.pdf>). The ISO standard (ISO 4731 2012) was used to characterise rose geranium ('Bourbon-type' cv.) essential oil quality parameters for the perfumery industry.

The relative growth rate (RGR) of the main stem and the free proline parameters are described in detail. The RGR was measured every week, measurement only commenced after the first application of biostimulants (Pérez-Harguindeguy et al., 2013). Weekly plant height data were used to determine the RGR (cm cm⁻¹/day) by means the following formula:

$$RGR = \ln(\text{height}2) - \ln(\text{height}1) / (\text{time}2 - \text{time}1) \quad (\text{Eq.1})$$

where: *in (height1)* = height at the start of the interval; *in (height2)* = height at the end of the interval; *time1* = time at the start of the interval (in days); *time2* = time end of the interval (Meyer, 1998).

Free proline was extracted and analysed using a ninhydrin-based method (Gibon et al., 2000; Carillo and Gibon, 2011):

$$\text{Proline} = (\text{Abs extract} - \text{blank}) / \text{slope} \\ * \text{Vol extract} / \text{Vol aliquot} * 1 / \text{FW} \quad (\text{Eq.2})$$

where: *Abs extract* is the absorbance of the extract, the absorbance of the *blank*, and the *slope* (expressed as absorbance/nmol) is determined by linear regression, *Vol extract* is the total volume of the extract, *Vol aliquot* is the volume used in the assay and *FW* (expressed in mg) is the amount of plant material extracted.

Statistical analysis

All parameters were statistically analysed and compared using PROC GLIMMIX, SAS version 9.4 (PROC GLIMMIX, SAS Institute 2013). Significantly different means among the treatments were separated using Tukey's least significant difference *ad hoc* mean comparison tests, at the 0.05 level of significance (Steel and Tourie, 1980). The data was then subjected to an appropriate analysis of variance (ANOVA) to determine the effects of the tested factors and their interactions. The Shapiro-Wilks test was performed on standardised residuals to test for any deviations from normality (Shapiro and Wilk, 1965).

Results

Plant parameters, leaf trichomes and essential oil yield attributes

The number of branches, branches to height ratio (B:H ratio), leaf area, and chlorophyll content were not affected by interactions between simulated hail damage and the subsequent application of biostimulants-mixture (*Table 2*). Only the plant height was affected by interactions between simulated hail damage and the subsequent application of biostimulants ($P < 0.001$) (*Table 2*). Intact plants tended to grow taller when biostimulant-mixtures (all levels) were applied, compared to the control: only level 2 was not statistically different from the control. In the 50% defoliated plants, plant height was similar with all biostimulant treatments, including the control. In 100% defoliated plants, the results were inconsistent between the levels: a marginal increase in growth was recorded when the biostimulant-mixture was applied at level 3 compared to the control; however, this application was not statistically different to levels 2 and 4.

The number of branches per plant declined by 37.9% when the simulated hail damage was intensified up to 100% defoliation compared to 0% defoliation (intact plants) (*Table 2*). The significant decline in number of branches per plant significantly affected the FFM, which declined by 56.1% when the simulated hail damage was intensified up to 100% defoliation compared to 0% defoliation (*Table 2*). Intact plants continued with normal straight elongation of the terminal shoots (*Figure 1*); however, this was not the case in 50% and 100% simulated hail-damaged plants, in which the number of branches were affected. Branches of the 50% and 100% defoliated plants tended to be plagiotropic, with the terminal bud tips drying and not showing any signs of recovery (*Figure 1*). Plants that suffered 100% simulated hail damage were less bushy, with significantly smaller leaves compared to the intact plants and those that suffered 50% simulated hail damage. This is shown by the lower B:H ratio and smaller leaf area in *Table 2*.

The application of biostimulant-mixtures at levels 3 and 4 increased the FFM for all hail damage levels (*Table 2*): this could also be ascribed to the proline content (*Figure 2*). A significantly lower proline content was recorded when levels 3 and 4 were applied, compared to the control and the level 2 treatment ($P < 0.02$).

The stem RGR was affected by the interaction between hail damage simulation and time (week factor) (*Table 3, Figure 3*). During the first week, the rate of stem development did not differ between the simulated hail damage intensities. The RGR tended to vary significantly from the second week until the sixth week for all hail damage levels; however, this trend remained the same throughout the recovery period. A consistent RGR was recorded on intact plants; however, a relatively constant slow RGR was recorded on plants that endured simulated hail damage.

Table 2. The effects of hail-simulated damage and the application of biostimulants-mixtures on selected plant growth parameters of rose geranium

Treatments	Plant height	№ of branches	B:H ratio	Leaf area	Chlor. (%)	FFM
Simulated hail damage						
0% defoliation	59.10 ^a	32.51 ^a	55.003 ^a	44.61 ^a	14.65 ^a	692.60 ^a
50% defoliation	47.37 ^b	27.53 ^b	58.11 ^a	42.33 ^a	14.66 ^a	556.04 ^b
100% defoliation	46.45 ^b	20.18 ^c	44.44 ^b	27.82 ^b	13.33 ^a	304.08 ^c
<i>P</i> -value	*0.001	*0.002	*0.03	*0.001	0.18 ^{ns}	*0.01
Biostimulant (Bio.)						
Level 1	44.93 ^b	23.37 ^a	52.00 ^a	35.51 ^a	13.63 ^a	401.80 ^b
Level 2	51.83 ^a	25.21 ^a	48.64 ^a	38.15 ^a	14.63 ^a	505.55 ^{a,b}
Level 3	55.16 ^a	27.82 ^a	50.54 ^a	39.92 ^a	14.57 ^a	554.58 ^a
Level 4	51.80 ^a	30.50 ^a	60.88 ^a	39.44 ^a	14.03 ^a	608.35 ^a
<i>P</i> -value	*0.001	0.08 ^{ns}	0.22 ^{ns}	0.29 ^{ns}	0.66 ^{ns}	*0.001
HD x Bio. levels						
0% x Level 1	51.75 ^{b,c}	29.36 ^a	56.72 ^a	42.74 ^a	11.86 ^a	565.41 ^a
0% x Level 2	57.41 ^{a,b}	32.25 ^a	56.17 ^a	43.75 ^a	17.15 ^a	717.50 ^a
0% x Level 3	64.08 ^a	35.75 ^a	55.78 ^a	46.61 ^a	14.58 ^a	759.16 ^a
0% x Level 4	63.16 ^a	32.69 ^a	51.73 ^a	45.36 ^a	15.21 ^a	728.33 ^a
50% x Level 1	43.58 ^{c,d}	24.50 ^a	56.21 ^a	38.63 ^a	14.16 ^a	446.25 ^a
50% x Level 2	51.50 ^{b,c}	25.64 ^a	49.78 ^a	42.13 ^a	14.88 ^a	546.66 ^a
50% x Level 3	50.08 ^{b,c,d}	26.77 ^a	53.45 ^a	43.51 ^a	17.06 ^a	582.91 ^a
50% x Level 4	44.33 ^{c,d}	33.22 ^a	74.93 ^a	45.04 ^a	12.54 ^a	648.33 ^a
100% x Level 1	39.83 ^d	16.25 ^a	40.79 ^a	25.17 ^a	12.08 ^a	193.75 ^a
100% x Level 2	46.58 ^{c,d}	17.75 ^a	38.10 ^a	28.56 ^a	11.86 ^a	252.50 ^a
100% x Level 3	51.33 ^{b,c}	21.14 ^a	41.18 ^a	29.63 ^a	14.35 ^a	321.66 ^a
100% x Level 4	47.91 ^{b,c,d}	25.61 ±	53.45 ^a	27.94 ^a	15.05 ^a	448.41 ^a
<i>P</i> -value	*0.001	0.46 ^{ns}	0.54 ^{ns}	0.99 ^{ns}	0.22 ^{ns}	0.39 ^{ns}

Means followed by the same letter in the same column are statistically non-significant ($P < 0.05$); ns = not significant; * = *F*-ratio probability of $P < 0.05$. Plant height (cm/plant); Leaf area (cm²/plant); Chlor. = Chlorophyl; FFM = Foliar fresh mass (g/plant)

Two groups of trichomes were identified: glandular (peltate and capitate) and non-glandular trichomes (attenuate) (Table 4). The attenuate trichome type is insignificant to essential oil biosynthesis; therefore, they are also not discussed any further. The peltate type: this type is characterised by a short neck with bigger, rounded tips, and is regarded as a brevicollate trichome, while the capitate type: is characterised by a short, segmented capitate, with a columnar hatchet-shaped tip that has a slightly bent apical cell pointing towards at the leaf apex (Sedibe et al., 2013; Khetsha et al., 2021).

An interaction was observed between simulated hail damage and the subsequent application of biostimulant-mixtures for the asciiform trichome densities on both leaf surfaces of the rose geranium plant (Table 4). On intact plants, the densities of the asciiform trichome were significantly ($P < 0.01$) high when biostimulant-mixtures were applied at level 2 on the adaxial leaf surface compared with the control; however, this treatment was not significantly different to level 3. The density of the asciiform trichome started to decline when the biostimulant-mixture was applied from level 3 to level 4.

When plants sustained 50% simulated hail damage, biostimulant-mixture application produced inconsistent results: a marginally higher density of the asciiform trichomes were recorded when biostimulants-mixture were applied at levels 3 and 4, however, these applications were not significantly different to the control. On the 100% defoliated plants, the asciiform trichome densities declined by 60.6% when biostimulants were applied at level 2 compared with the control.

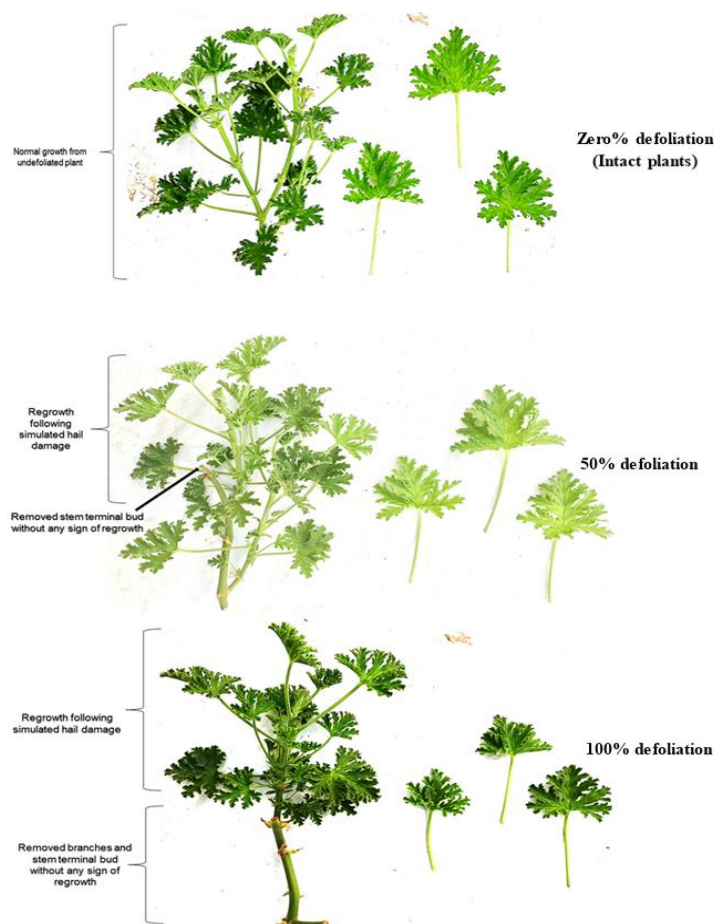


Figure 1. Terminal buds from simulated hail-damaged rose geranium plant

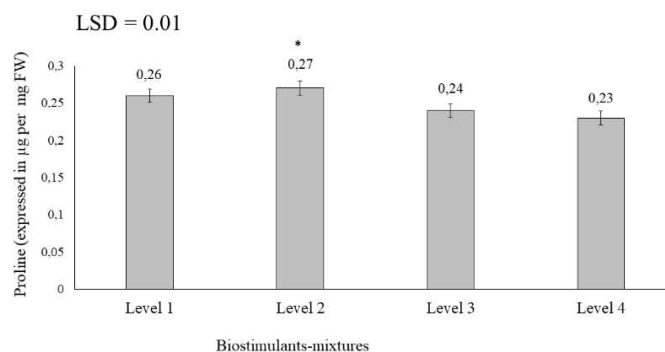


Figure 2. The effects of biostimulants-mixtures on free proline of rose geranium. Means followed by the same letter in the same column are statistically non-significant ($P < 0.05$); ns = not significant; * = F-ratio probability of $P < 0.05$

Table 3. Summary of ANOVA for the relative growth of the stem (RGR) as affected by hail-simulated damage and the application of biostimulants-mixtures in six weeks on rose geranium plants

Treatments	Df	F-value	P-value
Week	5	0.48	0.78
Simulated hail damage	2	5.83	*0.001
Biostimulants	3	5.01	*0.002
Week x Simulated hail damage	10	1.96	*0.04
Week x Biostimulants	15	0.59	0.88
Simulated hail damage x Biostimulant	6	2.06	0.06
Week x Simulated hail damage x Biostimulant	30	0.64	0.92

Means followed by the same letter in the same column are statistically non-significant ($P < 0.05$); ns = not significant; * = F-ratio probability of $P < 0.05$

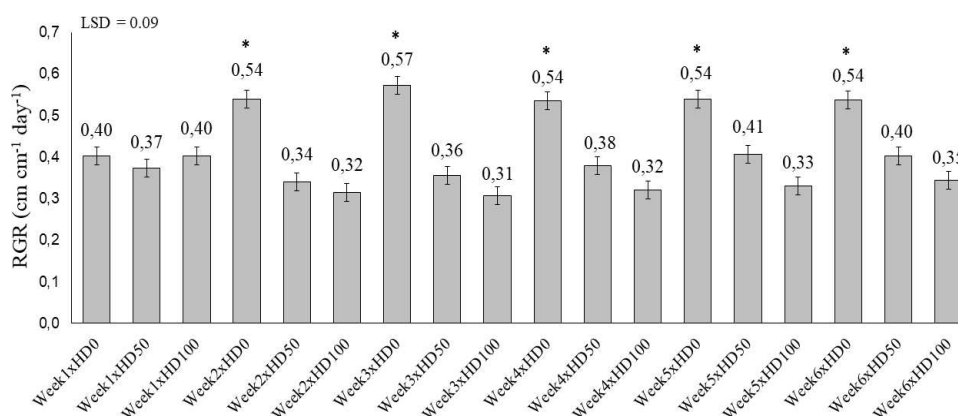


Figure 3. The effects of simulated hail damage between six weeks on the relative growth rate of rose geranium stems. Abbreviations: HD0 = zero% defoliation; HD50 = 50% defoliation; HD100 = 100% defoliation. Means followed by the same letter in the same column are statistically non-significant ($P < 0.05$); ns = not significant; * = F-ratio probability of $P < 0.05$

On the abaxial leaf surface, the opposite effect was recorded on refoliating plants that had lost up to 50% defoliation (Table 4), with the asciiform trichome densities increasing by 39% when the biostimulants-mixture was applied at level 2. Asciiform trichome densities gradually declined when the biostimulants-mixture was increased from level 2 up to level 4 ($P < 0.001$). The intact plants, and those that sustained 100% simulated hail damage, had similar asciiform trichome densities following all biostimulants treatments, including the control. The asciiform trichome densities were increased by 32.1% on the 50% simulated hail-damaged plants compared to 100% defoliated plants when biostimulants-mixture was applied at level 2.

Brevicollate trichome densities were significantly ($P < 0.001$) higher when biostimulants were applied at level 3 on the adaxial leaf surface (Table 4). However, this was not significantly different from level 4. On the abaxial leaf surface, the densities of the brevicollate trichome were affected by the interaction between simulated hail damage and the subsequent application of biostimulants-mixtures (Table 4). On the intact plants, the densities of brevicollate trichome were higher when the biostimulant-mixtures were applied compared with the control, from level 3 to level 4 ($P < 0.005$). On the 50%

defoliated plants, the biostimulants-mixture applied at level 4 resulted in marginally higher densities of brevicollate trichomes, compared to the control ($P < 0.005$). With the 100% defoliated plants, all biostimulants treatments were similar to the control.

Table 4. The effects of hail-simulated damage and the application of biostimulants-mixtures on the leaf surfaces of rose geranium leaves

Treatments	Adaxial leaf surface		Abaxial leaf surface	
	Asciiform	Brevicollate	Asciiform	Brevicollate
Simulated hail damage				
0% defoliation	27.55 ^a	21.11 ^a	41.33 ^a	47.33 ^a
50% defoliation	24.66 ^a	29.66 ^a	33.77 ^b	44.99 ^a
100% defoliation	15.99 ^b	27.77 ^a	37.55 ^{a,b}	47.22 ^a
<i>P</i> -value	*0.001	0.69 ^{ns}	*0.001	0.69 ^{ns}
Biostimulant (Bio.)				
Level 1	22.44 ^a	21.55 ^c	39.55 ^a	30.88 ^b
Level 2	20.33 ^a	25.33 ^{b,c}	39.00 ^a	47.88 ^a
Level 3	25.11 ^a	30.11 ^a	37.66 ^a	55.00 ^a
Level 4	23.00 ^a	27.55 ^{a,b}	33.00 ^a	52.22 ^a
<i>P</i> -value	0.14 ^{ns}	*0.001	0.80 ^{ns}	*0.001
HD x Bio. levels				
0% x Level 1	22.00 ^{b,c}	18.33 ^a	48.66 ^a	27.33 ^{c,d}
0% x Level 2	37.66 ^a	21.33 ^a	35.66 ^{a,b,c}	46.66 ^{a,b,c,d}
0% x Level 3	27.33 ^{a,b,c}	24.66 ^a	41.66 ^{a,b}	63.66 ^a
0% x Level 4	23.33 ^{b,c}	20.33 ^a	38.50 ^{a,b,c}	51.66 ^{a,b}
50% x Level 1	25.00 ^{b,c}	24.33 ^a	29.33 ^{b,c}	25.66 ^d
50% x Level 2	15.33 ^{c,d}	30.66 ^a	48.33 ^a	48.00 ^{a,b,c,d}
50% x Level 3	32.00 ^{a,b}	37.00 ^a	35.00 ^{a,b,c}	47.00 ^{a,b,c,d}
50% x Level 4	26.33 ^{a,b,c}	25.00 ^a	22.33 ^c	68.33 ^a
100% x Level 1	20.33 ^{c,d,e}	22.00 ^a	40.66 ^{a,b}	39.66 ^{b,c,d}
100% x Level 2	8.00 ^f	24.00 ^a	33.00 ^{b,c}	49.00 ^{a,b,c}
100% x Level 3	16.00 ^{c,d}	28.66 ^a	36.33 ^{a,b,c}	54.33 ^{a,b}
100% x Level 4	19.33 ^{c,d}	36.33 ^a	40.00 ^{a,b}	36.66 ^{b,c,d}
<i>P</i> -value	*0.001	0.08 ^{ns}	*0.001	*0.005

Means followed by the same letter in the same column are statistically non-significant ($P < 0.05$); ns = not significant; * = *F*-ratio probability of $P < 0.05$

Essential oil mass and essential oil content were significantly affected by the interaction between reduced simulated hail damage levels and the subsequent application of biostimulants (Table 5). In the intact plants, the highest essential oil mass was recorded when biostimulants-mixtures were applied at level 3 ($P < 0.006$); however, the essential oil content was similar in all biostimulants-mixtures levels. In 50% defoliated plants, the essential oil mass was marginally increased ($P < 0.01$) when the biostimulants-mixtures were applied at level 3 compared with the control; however, this was not statistically different from levels 2 and 4. A similar trend was recorded for the essential oil content on the 50% defoliated plants: there were no statistical differences between all biostimulants treatments for both essential oil yield attributes when plants sustained 100% simulated hail damage.

Table 5. The effects of hail-simulated damage and the application of biostimulants-mixtures on essential oil mass yield of rose geranium

Treatments	Oil mass (g/plant)	Oil content (%)
Simulated hail damage		
0% defoliation	3.06 ^a	0.44 ^a
50% defoliation	2.24 ^b	0.39 ^a
100% defoliation	0.55 ^c	0.17 ^b
<i>P-value</i>	*0.001	*0.001
Biostimulant (Bio.)		
Level 1	1.29 ^c	0.27 ^b
Level 2	1.78 ^{b,c}	0.32 ^{a,b}
Level 3	2.45 ^a	0.38 ^a
Level 4	2.29 ^{a,b}	0.36 ^{a,b}
<i>P-value</i>	*0.01	*0.02
HD x Bio. levels		
0% x Level 1	2.44 ^b	0.43 ^{a,b,c}
0% x Level 2	2.51 ^b	0.35 ^{a,b,c,d}
0% x Level 3	3.98 ^a	0.53 ^a
0% x Level 4	3.31 ^{a,b}	0.45 ^{a,b}
50% x Level 1	1.18 ^{c,d}	0.25 ^{b,c,d,e}
50% x Level 2	2.39 ^{b,c}	0.43 ^{a,b}
50% x Level 3	3.02 ^{a,b}	0.52 ^a
50% x Level 4	2.38 ^{b,c}	0.37 ^{a,b,c}
100% x Level 1	0.25 ^d	0.12 ^{d,e}
100% x Level 2	0.44 ^d	0.19 ^{c,d,e}
100% x Level 3	0.35 ^d	0.10 ^e
100% x Level 4	1.17 ^{c,d}	0.26 ^{b,c,d,e}
<i>P-value</i>	*0.01	*0.01

Means followed by the same letter in the same column are statistically non-significant ($P < 0.05$); ns = not significant; * = *F*-ratio probability of $P < 0.05$

Essential oil quality

The levels of *cis*-Rose oxide and *trans*-Rose oxide declined by 75% and 80%, respectively, with increasing defoliation intensity, while the linalool content increased in plants that had lost 100% foliage (Table 6). In this study, the geraniol esters and the citronellyl formate content were significantly higher in plants that sustained 100% simulated hail damage. The citronellyl formate content accumulated ($P < 0.007$) up to 20.2% when biostimulants were applied at level 4; however, this was not significantly different compared to the control. Interactions were observed between simulated hail damage and the subsequent application of different levels of biostimulants for citronellol, geraniol, and the citronellol to geraniol (C:G) ratio (Table 6). The highest ($P < 0.006$) citronellol content was recorded when biostimulants were applied at level 4 on the intact plants compared with the control; however, this biostimulant level was not significantly different from level 3. On 50% and 100% defoliated plants, the citronellol content was similar in all biostimulant treatments. Although citronellol and geraniol share a similar biosynthetic pathway, the geraniol results were not the same: the geraniol content of the

intact plants, and those that suffered 50% simulated hail damage were not significantly affected by the subsequent application biostimulants, at any treatment level (Table 6). In the 100% defoliated plants, a higher ($P < 0.02$) geraniol content was recorded when the level 2 treatment was applied compared with the control: however, this treatment level was not significantly different to level 4.

Table 6. The effects of hail-simulated damage and the application of biostimulants-mixtures on essential oil compounds and quality of rose geranium

Treatments	cis-RO	trans-RO	Isom.	Lin.	Geranyl formate	Geranyl butyrate	Geranyl tiglate	Citronellyl formate	Guaia-6,9-diene	Citronellol	Geraniol	C:G ratio
Simulated hail damage												
0% defoliation	0.20 ^a	0.10 ^a	1.75 ^a	0.41 ^b	5.40 ^b	1.01 ^b	1.93 ^b	18.71 ^b	11.35 ^a	23.23 ^a	8.37 ^a	2.77 ^a
50% defoliation	0.13 ^b	0.06 ^b	1.83 ^a	0.63 ^a	5.85 ^b	0.93 ^b	1.98 ^b	18.65 ^b	11.92 ^a	24.26 ^a	8.98 ^a	2.70 ^a
100% defoliation	0.05 ^c	0.02 ^c	1.07 ^a	0.76 ^a	8.37 ^a	1.30 ^a	2.74 ^a	19.87 ^a	12.23 ^a	19.97 ^b	9.11 ^a	2.19 ^b
<i>P</i> -value	*0.001	*0.01	0.10 ^{ns}	*0.009	*0.001	*0.002	*0.001	*0.001	0.20 ^{ns}	*0.003	0.13 ^{ns}	*0.001
Biostimulant (Bio.)												
Level 1	0.11 ^a	0.05 ^a	1.36 ^a	0.61 ^a	6.46 ^a	1.16 ^a	2.32 ^a	19.39 ^a	11.86 ^a	20.26 ^b	8.14 ^c	2.48 ^a
Level 2	0.15 ^a	0.08 ^a	1.91 ^a	0.67 ^a	6.40 ^a	0.99 ^a	1.97 ^a	18.23 ^b	11.59 ^a	23.50 ^a	9.76 ^a	2.40 ^a
Level 3	0.13 ^a	0.06 ^a	1.32 ^a	0.54 ^a	6.61 ^a	1.15 ^a	2.42 ^a	18.52 ^b	12.16 ^a	23.31 ^a	8.30 ^{a,c}	2.81 ^a
Level 4	0.12 ^a	0.05 ^a	1.71 ^a	0.61 ^a	6.72 ^a	0.99 ^a	2.04 ^a	20.15 ^a	11.67 ^a	23.28 ^a	9.24 ^{a,b}	2.51 ^a
<i>P</i> -value	0.60 ^{ns}	0.34 ^{ns}	0.58 ^{ns}	0.56 ^{ns}	0.95 ^{ns}	0.18 ^{ns}	0.14 ^{ns}	*0.007	0.12 ^{ns}	*0.02	*0.03	0.09 ^{ns}
HD x Bio. levels												
0% x Level 1	0.17 ^a	0.08 ^a	2.00 ^a	0.80 ^a	5.84 ^a	1.23 ^a	2.33 ^a	18.32 ^a	11.29 ^a	17.36 ^d	9.15 ^{a,b}	1.89 ^f
0% x Level 2	0.22 ^a	0.11 ^a	2.23 ^a	0.73 ^a	5.62 ^a	0.97 ^a	1.79 ^a	18.33 ^a	11.26 ^a	24.24 ^b	8.83 ^b	2.75 ^{b,c,d}
0% x Level 3	0.20 ^a	0.10 ^a	0.99 ^a	0.69 ^a	5.31 ^a	1.01 ^a	1.91 ^a	18.72 ^a	11.47 ^a	24.99 ^{a,b}	7.84 ^b	3.18 ^{a,b}
0% x Level 4	0.22 ^a	0.10 ^a	1.78 ^a	0.88 ^a	4.56 ^a	0.78 ^a	1.57 ^a	19.87 ^a	11.38 ^a	27.87 ^a	7.30 ^b	3.81 ^a
50% x Level 1	0.13 ^a	0.06 ^a	1.34 ^a	0.68 ^a	5.60 ^a	1.02 ^a	2.03 ^a	19.44 ^a	11.89 ^a	24.26 ^b	7.65 ^b	3.17 ^{b,c}
50% x Level 2	0.13 ^a	0.06 ^a	1.65 ^a	0.71 ^a	6.48 ^a	0.94 ^a	1.96 ^a	17.93 ^a	11.90 ^a	23.85 ^b	9.37 ^{a,b}	2.54 ^{c,d,e}
50% x Level 3	0.15 ^a	0.07 ^a	2.11 ^a	0.56 ^a	5.53 ^a	0.89 ^a	1.92 ^a	17.81 ^a	12.09 ^a	25.09 ^{a,b}	8.78 ^b	2.85 ^{b,c,d}
50% x Level 4	0.11 ^a	0.05 ^a	2.24 ^a	0.60 ^a	5.77 ^a	0.89 ^a	2.03 ^a	19.41 ^a	11.88 ^a	23.86 ^b	10.11 ^{a,b}	2.36 ^{d,e,f}
100% x Level 1	0.04 ^a	0.01 ^a	0.73 ^a	0.35 ^a	7.93 ^a	1.27 ^a	2.74 ^a	20.43 ^a	12.65 ^a	19.17 ^{d,c}	7.61 ^b	2.51 ^{b,c,d,e}
100% x Level 2	0.08 ^a	0.05 ^a	1.83 ^a	0.53 ^a	7.46 ^a	1.10 ^a	2.27 ^a	18.53 ^a	11.61 ^a	21.86 ^{b,c}	11.74 ^a	1.86 ^f
100% x Level 3	0.03 ^a	0.01 ^a	0.85 ^a	0.36 ^a	8.99 ^a	1.55 ^a	3.42 ^a	19.02 ^a	12.92 ^a	19.85 ^{d,c}	8.29 ^b	2.39 ^{d,e,f}
100% x Level 4	0.06 ^a	0.03 ^a	1.14 ^a	0.46 ^a	8.79 ^a	1.27 ^a	2.37 ^a	21.07 ^a	11.66 ^a	19.65 ^{d,c}	9.68 ^{a,b}	2.02 ^{e,f}
<i>P</i> -value	0.71 ^{ns}	0.53 ^{ns}	0.55 ^{ns}	0.76 ^{ns}	0.07 ^{ns}	0.18 ^{ns}	0.14 ^{ns}	0.25 ^{ns}	0.30 ^{ns}	*0.006	*0.02	*0.01

Means followed by the same letter in the same column are statistically non-significant ($P < 0.05$); ns = not significant; RO = Rose oxide; Iso. = Isomenthone; Lin. = Linalool; * = *F*-ratio probability of $P < 0.05$

As expected, changes in citronellol and geraniol content affected the C:G ratio (Table 6). The perfumery industry prefers a C:G ratio of <3:1 (Saxena et al., 2008). In the intact plants, the C:G ratio was higher than 3:1 when biostimulants-mixtures were applied at levels 3 and 4 ($P < 0.01$). In the 50% defoliated plants, the lowest C:G ratio was recorded when biostimulants were applied at level 4, compared to the control. On plants that suffered 100% simulated hail damage, the C:G ratio was lower when the level 2 treatment was applied, compared to the control ($P < 0.01$). A significantly lower C:G ratio (<3:1) was recorded on all defoliated plants (50 & 100%) compared to the intact plants ($P < 0.01$).

Discussion

Taller plants in this study after addition of biostimulants could be ascribed to increased plasticity of the cell wall, regulated by the action of GA and BRs (Yamaguchi et al., 2010): Matusmoto et al. (2016) indicated that GA and BRs also regulate stem elongation. Therefore, the accumulation of BRs following the biostimulant application could have facilitated GA to promote stem elongation. According to Sun (2010), an increase in cell elongation and cell division occurs during stem growth because GA induces the transcription of genes involved in growth processes. Dayan et al. (2012) found that endogenous concentrations of bioactive GA in young internodes of defoliated tobacco plants (*Nicotiana tabacum* L.) were reduced by 60% compared to those of intact plants, however, 0.8 mg/L GA restored the cambium and xylem fibre differentiation. In the 100% defoliated plants, taller plants could be attributed to the action of BRs, since this also regulates abiotic stress (Yamaguchi et al., 2010). The stem terminal buds were removed following defoliation to simulate hail bruising in this study, therefore, the accumulation of BRs could have been slower in the stem as the plant recovered from defoliation.

Defoliation and the removal of the shoot apex through hail damage simulations may affect the apical dominance, and stimulate the growth of branches from auxiliary buds (Prins and Verkaar, 1992). Therefore, the alteration of branching patterns following apex removal is not uncommon, as was the case with the simulated hail-damaged plants (50% and 100%) in this study. This could be due to delayed plant growth, as auxiliary branches must first form new leaves before the photosynthetic rate can reach the same levels as pre-defoliation (Prins and Verkaar, 1992).

As expected, the B:H ratio decreased in plants that sustained 100% defoliation. The removed stem terminal buds showed no signs of regrowth (*Figure 1*). This could be attributed to the nutrients and carbohydrates requirements between the auxiliary buds and the shoot apex, since plants need to recuperate following defoliation (Prins and Verkaar, 1992). In this study, the bushiness of rose geranium plants did not recover following the application of biostimulants.

Plant leaf development follows a standard basic sequence that is flexible and adjusted according to species, developmental stage, and environmental conditions (Bar and Ori, 2014). Meyer (1998) also reported that the plant response to extreme defoliation is affected by its capacity to draw upon sufficient resources to maintain growth recovery, which directly affects the leaf maturation process. In a study with perennial ryegrass (*Lolium perenne* L.), decreased leaf area could be ascribed to decreased cell production and expansion. In this study, the intact and 50% simulated hail-damaged plants had a significantly higher number of mature leaves at harvest, compared to plants that endured 100% simulated hail damage (*Figure 1*). Therefore, the reduction in the leaf area in the 100% simulated hail-damaged plants could be because of reduced photosynthetic capacity following complete defoliation (Bar and Ori, 2014). Contrary results were reported for goldenrod (*Solidago altissima* L.), where refoliating plants had bigger leaves compared to the control plants (Meyer, 1998).

According to Pérez-Harguindeguy et al. (2013), agronomic parameters such as plant height, the number of branches, leaf area, and FFM are essential parameters in determining the morphological characteristics and yield components of indeterminate crops, such as rose geranium. Reduced FFM following simulated hail is due to fewer branches per plant, a reduced number of branches per meter, and a smaller leaf area. This confirms the hypothesis of resultant decrease in biomass and related attributes where rose geranium plants endure extreme simulated hail damage intensity (Swamy et al., 1960;

Dermane and van der Walt, 1989; Weiss, 1997). Similar findings were recorded in a study by Bueckert (2011) on lentils (*Lens culinaris* L.), which is also an indeterminate crop species.

Plants accumulate proline as an adaptive mechanism for stress, but it is also beneficial under normal plant growth conditions (Zhang and Becker, 2015). Besides its proteogenic function, proline also plays a role in energy utilization (Hare and Cress, 1997), protein unfolding (Liang et al., 2013), as well as cell reprogramming and development (D'Aniello et al., 2015). Moreover, recent studies have also shown that proline plays a vital role in plant growth and differentiation at different growth stages (Kishor et al., 2015). In this study, the application of biostimulants could have increased energy utilization, and improved cell development, subsequently increasing the FFM (Hare and Cress, 1997). Therefore, results on the increased FFM and declined proline content could be ascribed to the biostimulants and proline in the chloroplast and cytoplasm. In addition, Li et al. (2012) reported that a BRs and GA interact at the signalling level to promote plant growth and development. This occurs through the regulation of BRs, which directly affects plant growth by modulating GA levels. Amiri et al. (2014) reported that FFM was significantly increased by the application of GA (100 ppm) on German chamomile (*Matricaria recutita* L.).

Growth rate, as an indicator of life history and ecological strategy, may be crucial to post-defoliation recovery strategies. According to Atkinson et al. (2014), plants deploy stored resources to rebuild photosynthetic material following defoliation. Meyer (1998) reported similar results on goldenrod, where less damaged plants recovered more rapidly than completely defoliated plants. In this study, fortnightly applications of biostimulants did not affect the rate of relative stem growth (Table 3).

In this study, the densities of asciiform trichomes on both leaf surfaces differed between the simulated hail damage levels. Generally, the intact plants, and those that suffered 50% foliage loss on both leaf surfaces recorded higher asciiform trichome densities than those that suffered 100% simulated hail damage. Prins et al. (2010) also demonstrated that the development of trichomes, and the biosynthesis of essential oil could be influenced by exogenous applications of biostimulants. GA positively contributes to the regulation of trichome development (Zhou et al., 2013). According to Traw and Bergelson (2003), GA modifies the epidermal cell surface area, and also the cell number per unit area. However, in this study, the activities associated with asciiform trichome development on refoliated plants could be ascribed to TEMs (Jiao, 2016). TEMs regulate the signalling of CK at the later developmental stage compared to GA, signalling in earlier developmental stage. CK is a plant growth regulator that also promotes trichome formation under normal growth conditions. Moreover, since BRs and jasmonic acid are directly involved in the formation and variation of trichome density (Campos et al., 2009): the *dpy* mutant (BR-deficient) is the one which enhances pubescence, while the jasmonic acid *jail-1* mutant produces the opposite phenotypic effect (Campos et al., 2009; Fambrini and Pugliesi, 2019). The Arabidopsis *bls1* mutant, which is impaired in the BR response, developed fewer trichomes on both the abaxial and adaxial leaf surfaces, indicating the possible involvement of BR in trichome development (Pattanaik et al., 2014). There are no studies on refoliating plants treated with biostimulant. Therefore, the changes in asciiform trichome densities is attributed to the traces of CKs.

The increased density of brevicolate trichomes on the intact plants and those suffering 50% simulated hail damage could also be ascribed to the GA and CK in the biostimulants-mixture. Zhou et al. (2011, 2013) reported similar findings in Arabidopsis (*Arabidopsis thaliana* [L.] Heynh.), where GA and CK, at concentrations as low as 100 μ M, increased

the density of glandular trichomes. According to the author, this was ascribed to GA and CK molecules, which regulated the development of glandular trichome through the combined action of *ZFP5* and *ZFP6* transcription factors (Zhou et al., 2013). As for the 50% defoliated rose geranium, plants deploy stored resources to rebuild photosynthetic material and regenerate new organs or tissues following defoliation and wounding (Stobbe et al., 2002; Nanda and Melnyk, 2018). During the refoliation, it is possible that the endogenous CK content in 50% defoliated plants was already too high; then GA accumulation occurred at the later stage to regulate growth. GA and CK could have combined during these periods via antagonistic crosstalk effects following the fortnightly applications of biostimulants. According to Barnes (2013), the amalgamation of CK and GA following hail damage may cause alterations in morphological features, such as increased trichome density. Other than GA and CK, BRs and jasmonic acid directly affect trichome formation through the accumulation of *zgb* and *PI-I* transcripts, indicating the importance of BRs in leaf recovery following defoliation or wounding (Campos et al., 2009). This was not the case for the 100% defoliated plants, as most energy was focused on recovering plant leaf material.

Asciiform trichome type is characterised by a short segmented capitate with a columnar hatchet-shaped tip, that has a slightly bent apical cell pointing at the leaf apex (Payne, 1978). On the other hand, brevicollate trichomes are characterised by a short neck with bigger round tips (Payne, 1978). Eiasu et al. (2009) reported that the capitate group (asciiform trichome) lack stored essential oil in their sub-cuticular areas compared to the brevicollate trichome. Thus, in this study, biostimulants-mixture should be applied at a rate of level 3 on rose geranium plants that have lost up to 50% foliage to increase the densities of the brevicollate trichomes, with the aim of improving the essential oil yield.

Biostimulants stimulate plant growth and terpene biosynthesis in a large number of aromatic plant species, which result in beneficial changes in terpene accumulation (Farooqi and Shukla, 1990). There are no reports in the literature where a combination of GA, BRs, and CK affected essential oil yield attributes of refoliating plants, however, Poyh and Ono (2006) recorded higher essential oil content for sage (*Salvia officinalis* L.) treated with 100 mg/L GA. Fraternali et al. (2003) reported a higher essential oil yield of Spanish marjoram (*Thimus mastichina* L.) using a medium culture with CK as low as 0.1 mg/L. In the leaves of Spanish marjoram treated with CK, there were a greater number of glandular trichomes recorded at the later leaf developmental stage, which could be ascribed to increased essential oil yield. Foliar application of a plant growth regulator-28-homobrassinolide (10^{-6} M) also enhanced the essential oil yield of mint (*Mentha arvensis* L.) (Naeem et al., 2014). In this study, it is evident that only the 50% hail-damaged plants yield higher essential oil, following treatment with biostimulants at level 3.

Croteau et al. (2000) reported that molecules could change before undergoing enzymatic oxidation, with a vast array of compounds, of remarkably different structures formed under various environmental conditions. *cis*-Rose oxide and *trans*-Rose oxide can be synthesised from the conversion of citronellol, through citronellyl diphosphate (phosphorylated citronellol) in rose geranium (Wüst et al., 1999). This may also occur because of a photo-oxygenation mechanism, including singlet oxygen as the oxidising agent (Yamaguchi, 1981). In this study, the enzymatic oxidation of citronellol could have gradually declined as a result of defoliation, directly affecting the cyclization of the diol to *cis*-Rose oxide and *trans*-Rose oxide (Wüst et al., 1999). Takana et al. (2010) reported

that when plant tissues undergo physio-morphological changes, such as wounding or defoliation, some chemical compounds are converted to secondary polyphenols by enzymatic and non-enzymatic reactions. This could have been the case in this study; however, there are no similar cases in the literature to support this hypothesis.

Linalool content tends to increase with an increase in the intensity levels of defoliation and wounding, and this could be due to the ontogeny of the leaf factor (Maia et al., 2007). Severely simulated hail-damaged plants could contain younger leaves at the time of recovery, compared to intact and those plants with at least 50% leaf loss. With the ontogeny of the leaf factor, this metabolic process affect the primary and secondary metabolic processes during refoliation. This was demonstrated on balsam fir (*Abies balsamea* L.), where linalool content was higher in defoliated plants compared to intact plants (Deslauriers et al., 2015). In sweet basil (*Ocimum basilicum* L.), younger leaves had higher linalool content compared to mature leaves (Fischer and Hammerschmidt, 2011).

Citronellol shares a similar biosynthesis pathway with geraniol and its esters (Bergman et al., 2019). Chacón et al. (2019) reported that the biotransformation of geraniol occurs through endogenous enzymatic changes. On the intact plants in this study, increased citronellol content could be ascribed to the exogenous application of agricultural biostimulants (Suga and Shishibori, 1973). The results on increased geraniol in this study could be ascribed to leaf ontogeny as well as the effects of GA in the biostimulants-mixture. According to Prins et al. (2010), plants produce essential oils in response to physiological stress, pathogen attack, and other ecological factors. Therefore, simulated hail damage in this study could be responsible for increased geraniol content. Geraniol content fluctuates significantly during leaf development, which subsequently affects its esters and citronellol biosynthesis (Chacón et al., 2019). In this study, 100% simulated hail-damaged plants had younger leaves compared to intact plants at the time of harvest. It is also possible that as plants refoliated, the fortnightly-applied biostimulants could have also affected the biosynthesis of the geraniol. According to Burlat et al. (2004), geraniol and GA share a similar biosynthetic route: the mevalonic acid pathway. This pathway could have been affected at a lower concentration of biostimulants treatment (level 2), and improved the accumulation of geraniol and citronellol as plants refoliated. However, an increase in the biostimulants-mixture up to level 3 & 4 could have led to the toxicity of the GA, causing the decline of the geraniol content.

The C:G ratio is used to classify rose geranium essential oil quality, and is a requirement of the perfumery industry and ISO standards (Saxena et al., 2008). Biosynthesis of citronellol and geraniol affected the C:G ratio in this study. The higher citronellol and low geraniol contents observed in this study after the application of biostimulants could be related to the metabolic pathway of geraniol biosynthesis, GA concentration, and the leaf ontogeny (Suga and Shishibori, 1973; Burlat et al., 2004; Motsa et al., 2006). In this study, it may be beneficial to apply mixtures of biostimulants at level 2 only when plants have suffered complete defoliation, resulting in a lower and favourable C:G ratio <3. This may improve the essential oil quality.

Geranyl formate, geranyl butyrate, and geranyl tiglate are geraniol esters (Liu et al., 2016). The equal accumulation of these esters could be attributed to the biosynthesis of geraniol, and leaf development (Motsa et al., 2006). Plant defoliation affects leaf ontogeny and biosynthesis of secondary metabolites (Burlat et al., 2004; Motsa et al., 2006). Therefore, the conversion rate of geraniol into geraniol esters could have differed between leaf developmental stages in this study. Ganjewala and Luthra (2009) reported

similar findings, with geraniol esters declining from 59% to 3% during the leaf growth period from day 10 to day 50 after transplanting. In addition, Motsa et al. (2006) also demonstrated that geraniol content declines as rose geranium plants age. Therefore, it may be concluded that the variations between the geraniol esters changed with leaf age factor, especially following the defoliation treatment.

Citronellyl formate is an ester to citronellol. Both constituents, along with geraniol and its esters, share the same chemical structure (citronellyl moiety) and biosynthetic pathway (Lis-Balchin, 2002; Sedibe, 2012; Bergman et al., 2019). In this study, citronellol, as well as geraniol and its esters, were improved by leaf ontogeny factor. Interestingly, this was also the case with citronellyl formate: Malatova et al. (2011) reported a similar situation for rose geranium, where a change in citronellol content affected the citronellyl formate content. Therefore, refoliating plants could have accumulated high content of these compounds (citronellol and geraniol esters), including citronellyl formate.

Conclusion

In this study, simulated hail damage affected the recovery and growth of the measured rose geranium foliage parameters. However, it can be concluded that the application of a mixture of biostimulants should be applied at 2.55 mg/kg (GA), 1.02 mg/kg (BRs), and 0.05 mg/kg (CKs) (level 3 in this study) in order to improve the foliage yield and essential oil quality (to <3, as per industry standards) for plants suffering more than 50% foliage loss. Plants with less than 50% foliage loss can be treated with a lower level of biostimulants: level 2 to level 3 in this study, to improve the essential oil yield and brevicollate trichome density.

Acknowledgements. Authors would like to thank Agraforum (Germany) and Dr Elmarie Van Der Watt (University of the Free State) for providing the biostimulants (registered as *Lucky Plant*[®]: EP1051075B1 & EP1933626), and the National Research Foundation (Thuthuka Funding Instrument: PhD Track, and Black Academics Advancement Programme) for financial assistance.

REFERENCES

- [1] Aly, K., Lubna, M., Bradford, P. D. (2021): Low density, three-dimensionally interconnected carbon nanotube/silicon carbide nanocomposites for thermal protection applications. – *Journal of the European Ceramic Society* 41: 233-243.
- [2] Amiri, S., Sharafzadeh, S., Ordoorkhani, K. (2014): The effect of gibberellic acid and benzyladenine on growth and essential oils of German chamomile. – *Indian Journal of Fundamental and Applied Life Science* 4: 186-188.
- [3] Atkinson, R. R. L., Burrell, M. M., Rose, K. E., Osborne, C. P., Rees, M. (2014): The dynamics of recovery and growth: How defoliation affects stored resources. – *Proceedings of the Royal Society B: Biological Sciences* 281: 20133355.
- [4] Bal, S. K., Saha, S., Fand, B. B., Singh, N. P., Rane, J., Minhas, P. S. (2014): Hailstorms: Causes, damage and post-hail management in agriculture. – *National Institute of Abiotic Stress Management Technical Bulletin-5: India*.
- [5] Banchio, E., Valladares, G., Zygadlo, J., Bogino, P. C., Rinaudi, L. V., Giordano, W. (2007): Changes in composition of essential oils and volatile emissions of *Minthostachys mollis*, induced by leaf punctures of *Liriomyza huidobrensis*. – *Biochemical Systematics and Ecology* 35: 68-74.

- [6] Bar, M., Ori, N. (2014): Leaf development and morphogenesis. – *Development* 141: 4219-4230.
- [7] Barnes, H. W. (2013): Gibberellins and cytokinins: a review. – *Acta Horticulturae* 1055: 323-336.
- [8] Bergman, M. E., Chávez, Á., Ferrer, A., Phillips, M. A. (2019): Distinct metabolic pathways drive monoterpene biosynthesis in a natural population of *Pelargonium graveolens*. – *Journal of Experimental Botany* 91: 258-271.
- [9] Bueckert, R. A. (2011): Simulated hail damage and yield reduction in Lentil. – *Canadian Journal of Plant Science* 91: 117-124.
- [10] Burke, M., Hsiang, S. M., Miguel, E. (2015): Climate and conflict. – *Annual Review of Economics* 7: 577-617.
- [11] Burlat, V., Oudin, A., Courtois, M., Rideau, M., St-Pierre, B. (2004): Co-expression of three MEP pathway genes and geraniol 10-hydroxylase in internal phloem parenchyma of *Catharanthus roseus* implicates multicellular translocation of intermediates during the biosynthesis of monoterpene indole alkaloids and isoprenoid-derived primary metabolites. – *Plant Journal* 38: 131-141.
- [12] Campos, M. L., de Almeida, M., Rossi, M. L., Martinelli, A. P., Junior, C. G. L., Figueira, A., Rampelotti-Ferreira, F. T., Vendramim, J. D., Benedito, V. A., Peres, L. E. P. (2009): Brassinosteroids interact negatively with jasmonates in the formation of anti-herbivory traits in tomato. – *Journal of Experimental Botany* 60: 4347-4361.
- [13] Carillo, P., Gibon, Y. (2011): Protocol: extraction and determination of proline. – PrometheusWiki. Available at: <http://prometheuswiki.publish.csiro.au/tiki-index.php?page=PROTOCOL%3A+Extraction+and+determination+of+proline> (Retrieved on 22 March 2020).
- [14] Cavaliere, C. (2009): The effects of climate change on medicinal and aromatic plants. – *Herbal Gram* 81: 44-57.
- [15] Chacón, M. G., Marriott, A., Kendrick, E. G., Styles, M. Q., Leak, D. J. (2019): Esterification of geraniol as a strategy for increasing product titre and specificity in engineered *Escherichia coli*. – *Microbial Cell Factories* 18: 105.
- [16] Changnon, S. A. (1999): Data and approaches for determining hail risk in the contiguous United States. – *Journal of Applied Meteorology* 38: 1730-1739.
- [17] Chen, J. M., Black, T. A. (1992): Defining leaf area index for non-flat leaves. – *Agricultural and Forest Meteorology* 57: 1-12.
- [18] Combrink, N. J. J., Kempen, E. (2019): Nutrient solution management. – Department of Agronomy Stellenbosch University.
- [19] Conley, S. P., Abendroth, L., Elmore, R., Christmas, E. P., Zarnstorff, M. (2008): Soybean seed yield and composition response to stand reduction at vegetative and reproductive stages. – *American Society of Agronomy* 100: 1666-1669.
- [20] Croteau, R., Kutchan, T. M., Lewis, N. G. (2000): Natural products (Secondary metabolites). – *Biochemistry and Molecular Biology of Plants* 24: 1250-1319.
- [21] D'aniello, C., Fico, A., Casalino, L., Guardiola, O., Di Napoli, G., Cermola, F., De Cesare, D., Tate, R., Cobellis, G., Patriarca, E. J., Minchiotti, G. (2015): A novel autoregulatory loop between the Gcn2-Atf4 pathway and L-Proline metabolism controls stem cell identity. – *Cell Death & Differentiation* 22: 1094-1105.
- [22] Das, M., Jain, V., Malhotra, S. (2016): Impact of climate change on medicinal and aromatic plants. – *Indian Journal of Agricultural Science* 86: 1375-1382.
- [23] Dayan, J., Voronin, N., Gong, F., Sun, T. P., Hedden, P., Fromm, H., Aloni, R. (2012): Leaf-induced gibberellin signaling is essential for internode elongation, cambial activity, and fiber differentiation in tobacco stems. – *The Plant Cell* 24: 66-79.
- [24] Demarne, F. E., van de Walt, J. J. A. (1989): Origin of rose-scented *Pelargonium* cultivar grown on Reunion Island. – *South African Journal of Botany* 55: 184-191.

- [25] Deslauriers, A., Caron, L., Rossi, S. (2015): Carbon allocation during defoliation: testing a defense-growth trade-off in balsam fir. – *Frontiers in Plant Science* 6: 338.
- [26] Eiasu, B. K., Steyn, J. M., Soundy, P. (2009): Rose-scented geranium (*Pelargonium capitatum* x *P. radens*) growth and essential oil yield response to different soil water depletion regimes. – *Agricultural Water Management* 96: 991-1000.
- [27] Fambrini, M., Pugliesi, C. (2019): The dynamic genetic-hormonal regulatory network controlling the trichome development in leaves. – *Plants* 8: 253.
- [28] Farooqi, A. H. A., Shukla, A. (1990): Utilization of plant growth regulators in aromatic plant production. – *Chromatography* 12: 152-157.
- [29] Fischer, J., Hammerschmidt, K. (2011): Ultrasonic vocalizations in mouse models for speech and socio-cognitive disorders: insights into the evolution of vocal communication. – *Genes, Brain and Behavior* 10: 17-27.
- [30] Fraternali, D., Giamperi, L., Ricci, D., Rocchi, M. B. L., Guidi, L., Epifano, F., Marcotullio, M. C. (2003): The effect of triacntanol on micropropagation and on secretory system of *Thymus mastichina*. – *Plant Cell Tissue and Organ Culture* 74: 87-97.
- [31] Ganjewala, D., Luthra, R. (2009): Geranyl acetate esterase controls and regulates the level of geraniol in lemongrass (*Cymbopogon flexuosus* Nees ex Steud.) mutant cv. GRL-1 leaves. – *Zeitschrift für Naturforschung C* 64: 251-259.
- [32] Gibon, Y., Sulpice, R., Larher, F. (2000): Proline accumulation in canola leaf discs subjected to osmotic stress is related to the loss of chlorophylls and to the decrease of mitochondrial activity. – *Physiologia Plantarum* 110: 469-76.
- [33] Hare, P. D., Cress, W. A. (1997): Metabolic implications of stress- homoinduced proline accumulation in plants. – *Plant Growth Regulation* 21: 79-102.
- [34] Ikeuchi, M., Iwase, A., Rymen, B., Lambalez, A., Kojima, M., Takebayashi, Y., Heyman, J., Watanabe, S., Seo, M., De Veylder, L., Sakakibara, H., Sugimoto, K. (2017): Wounding triggers callus formation via dynamic hormonal and transcriptional changes. – *Plant Physiology* 175: 1158-1174.
- [35] Irigoyen, I., Domeno, I., Muro, J. (2010): Effect of defoliation by simulated hail damage on yield of potato cultivars with different maturity performed in Spain. – *American Journal of Potato Research* 88: 82-90.
- [36] Jiao, Y. (2016): Trichome formation: Gibberellins on the move. – *Plant Physiology* 170: 1174-1175.
- [37] Khetsha, Z. P., Sedibe, M. M., Pretorius, R. J. (2020): Effects of abscisic acid and methyl jasmonate on the recovery of hail damaged rose geranium (*Pelargonium graveolens*) plants. – *Acta Horticulturae* 1287: 31-40.
- [38] Khetsha, Z. P., Sedibe, M. M., Pretorius, R. J., van der Watt, E. (2021): Cytokinin, gibberellic acid and defoliation on density and morphology of trichome of *Pelargonium graveolens* (L'Hér.) for essential oil biosynthesis. – *Agrociencia* 55: 331-346.
- [39] Khetsha, Z. P., Sedibe, M. M., Pretorius, R. J., Van Der Watt, E. (2021): Plant growth regulators and simulated hail-damage improve rose-geranium (*Pelargonium graveolens* L'Hér.) leaf mineral status and phenolic composition. – *Applied Ecology and Environmental Research* 19: 3083-3095.
- [40] Kishor, P. B. K., Kumari, P. H., Sunita, M. S. L., Sreenivasulu, N. (2015): Role of proline in cell wall synthesis and plant development and its implications in plant ontogeny. – *Frontiers of Plant Science* 6: 544.
- [41] Kundu, S., Gantait, S. (2017): Abscisic acid signal crosstalk during abiotic stress response. – *Plant Gene* 11: 61-69.
- [42] Li, Q. F., Wang, C., Jiang, L., Li, S., Sun, S. S., He, J. X. (2012): An interaction between BZR1 and DELLAs mediates direct signaling crosstalk between brassinosteroids and gibberellins in *Arabidopsis*. – *Science Signaling* 5: ra72.
- [43] Liang, X., Zhang, L., Natarajan, S. K., Becker, D. F. (2013): Proline mechanisms of stress survival. – *Antioxidants & Redox Signalling* 19: 998-1011.

- [44] Lis-Balchin, M. (2002): Essential oils from different *Pelargonium* species and cultivars: their chemical composition (using GC, GC/MS) and appearance of trichomes (under EM). *Geranium and Pelargonium: history of nomenclature, usage and cultivation*. – Taylor and Francis: London.
- [45] Liu, W., Xu, X., Zhang, R., Cheng, T., Cao, Y., Li, X., Guo, J., Liu, H., Xian, M. (2016): Engineering *Escherichia coli* for high-yield geraniol production with biotransformation of geranyl acetate to geraniol under fed-batch culture. – *Biotechnology for Biofuels* 9: 1-8.
- [46] Maia, J. G. S., Andrade, E. H. A., Couto, H. A., da Silva, A. C. M., Marx, F., Henke, C. (2007): Plant sources of Amazon rosewood oil. – *Quimica Nova Chemistry in Brazil* 30: 1906-1910.
- [47] Malatova, K., Hitimana, N., Niyibizi, T., Simon, J. E., Julianui, H. R. (2011): Optimization of harvest regime and post-harvest handling in geranium production to maximize essential oil yield in Rwanda. – *Industrial Crops and Products* 34: 1348-1352.
- [48] Matusmoto, T., Yamada, K., Yoshizawa, Y., Oh, K. (2016): Comparison of effect of brassinosteroid and gibberellin biosynthesis inhibitors on growth of rice seedlings. – *Rice Science* 23: 51-55.
- [49] McGregor, D. I. (1987): Effect of plant density on development and yield of rape seed and its significance to recovery from hail damage injury. – *Canadian Journal of Plant Science* 67: 43-51.
- [50] Meyer, G. A. (1998): Pattern of defoliation and its effect on photosynthesis and growth of goldenrod. – *Functional Ecology* 12: 270-279.
- [51] Miller, D. G., Muehlbauer, F. J. (1984): Stem excision as a means of simulating hail injury on 'Alaska' Peas 1. – *Agronomy Journal* 76: 1003-1005.
- [52] Motsa, N. M., Soundy, P., Steyn, J. M., Learmonth, R. A., Mojela, N., Teubes, C. (2006): Plant shoot age and temperature effects on essential oil yield and oil composition of rose-scented geranium (*Pelargonium* spp.) grown in South Africa. – *Journal Essential Oil Research* 1: 106-110.
- [53] Naeem, M., Idrees, M., Aftab, T., Alam, M. M., Khan, M. M., Uddin, M., Varshney, L. (2014): Employing depolymerised sodium alginate, triacontanol and 28-homobrassinolide in enhancing physiological activities, production of essential oil and active components in *Mentha arvensis* L. – *Industrial Crops and Products* 55: 272-279.
- [54] Nanda, A. K., Melnyk, C. W. (2018): The role of plant hormone during grafting. – *Semi-in-vivo Developmental Biology* 131: 49-58.
- [55] Obeso, J. R. (2002): The costs of reproduction in plants. – *New Phytologist* 155: 321-348.
- [56] Oosthuizen, L., Coetzee, J. (1983): Morphogenesis of trichomes of *Pelargonium scabrum*. – *South African Journal of Botany* 2: 305-310.
- [57] Paradiković, N., Teklić, T., Zeljković, S., Lisjak, M., Špoljarević, M. (2019): Biostimulants research in some horticultural plant species-A review. – *Food and Energy Security* 8: e00162.
- [58] Pattanaik, S., Patra, B., Singh, S. K., Yuan, L. (2014): An overview of the gene regulatory network controlling trichome development in the model plants, *Arabidopsis*. – *Frontier in Plant Science* 5: 259.
- [59] Payne, W. (1978): A glossary of plant hair terminology. – *Brittonia* 30: 239-255.
- [60] Pérez-Harguindeguy, N., Díaz, S., Garnier, E., Lavorel, S., Poorter, H., Jaureguiberry, P. (2013): New handbook for standardised measurement of plant functional traits worldwide. – Collingwood: CSIRO Publishing.
- [61] Poyh, J. A., Ono, E. O. (2006): Performance of the essential oil of *Salvia officinalis* L. under the action of plant regulators. – *Acta Scientiarum Biological Sciences* 28: 189-193.
- [62] Prins, A. H., Verkaar, H. J. (1992): Defoliation: do physiological and morphological responses lead to (over) compensation? *Pests and pathogens: Plant responses to foliar attack*. – *BIOS* 1992: 13-31.
- [63] Prins, C. L., Viera, I. J. C., Freitas, S. P. (2010): Growth regulators and essential oil production. – *Brazilian Society of Plant Physiology* 22: 91-102.

- [64] Saxena, G., Verma, P. C., Banerjee, S., Kumar, S. (2008): Field performance of somaclones of rose scented geranium (*Pelargonium graveolens* L'Her Ex Ait.) for evaluation of their essential oil yield and composition. – *Industrial Crops and Products* 27: 86-90.
- [65] Sedibe, M. M. (2012): Yield and quality response of hydroponically grown rose geranium (*Pelargonium* spp.) to changes in the nutrient solution and shading. – PhD thesis, University of the Free State, South Africa.
- [66] Sedibe, M. M., Khetsha, Z. P., Malebo, N. (2013): Salinity effects on external and internal morphology of rose geranium (*Pelargonium graveolens* L.) leaf. – *Life Science Journal* 10: 99-103.
- [67] Shapiro, S. S., Wilk, M. B. (1965): An analysis of variance test for normality (complete samples). – *Biometrika* 52: 591-611.
- [68] Sij, J. W., Ott, J. P., Olson, B. L. S., Baughman, T. A. (2005): Growth and yield response to simulated hail damage in Guar. – *American Society of Agronomy* 97: 1636-1639.
- [69] Steel, R. G. D., Tourie, J. H. (1980): Principles and procedures of statistics: biometrical approach, 2nd ed. – McGraw-Hill, Kogakusha, Tokyo: Japan.
- [70] Stobbe, H., Schmitt, U., Eckstein, D., Dujesiefken, D. (2002): Developmental stages and fine structure of surface callus formed after debarking of living lime trees (*Tilia* sp.). – *Annals of Botany* 89: 773-782.
- [71] Suga, T., Shishibori, T. (1973): The biosynthesis of geraniol and citronellol in *Pelargonium roseum* Bourbon. – *Bulletin of the Chemical Society of Japan* 46: 3545-3548.
- [72] Sun, T. P. (2010): Gibberellin-GID1-DELLA: a pivotal regulatory module for plant growth and development. – *Plant Physiology* 154: 567-570.
- [73] Suttle, J. C., Lulai, E., Huckle, L. L., Neubauer, J. D. (2013): Wounding of potato tubers induces increases in ABA biosynthesis and catabolism and alters expression of ABA metabolic genes. – *Journal of Plant Physiology* 170: 560-566.
- [74] Swamy, S. A. Y., Sreshta, N. J., Kalyanasundaram, S. (1960): Cultivation of scented geranium (*Pelargonium graveolens*) in Nigris. – *Indian Perfumer* 4: 3-9.
- [75] Swamy, K. N., Rao, S. S. R. (2009): Effect of 24-Epibrassinolide on growth, photosynthesis, and essential oil content of *Pelargonium graveolens* (L.) Herit. – *Russian Journal of Plant Physiology* 56: 616-620.
- [76] Tack, J., Barkley, A., Nalley, L. L. (2015): Effect of warming temperatures on US wheat yields. – *Proceedings of the National Academy of Sciences* 112: 6931-6936.
- [77] Takana, T., Matsuo, Y., Kouno, I. (2010): Chemistry of secondary polyphenols produced during processing of tea and selected foods. – *International Journal of Molecular Sciences* 11: 14-40.
- [78] Torres, N., Goicoechea, N., Antolín, M. C. (2018): Influence of irrigation strategy and mycorrhizal inoculation on fruit quality in different clones of Tempranillo grown under elevated temperatures. – *Agricultural Water Management* 202: 285-298.
- [79] Tozin, L. R., Marques, M. O., Rodrigues, T. M. (2015): Glandular trichome density and essential oil composition in leaves and inflorescences of *Lippia origanoides* Kunth (Verbenaceae) in the Brazilian Cerrado. – *Anais da Academia Brasileira de Ciências* 87: 943-53.
- [80] Traw, M. B., Bergelson, J. (2003): Interactive effects of jasmonic acid, salicylic acid, and gibberellin on induction of trichomes in *Arabidopsis*. – *Plant Physiology* 133: 1367-1375.
- [81] Weiss, E. A. (1997): Essential oil crops. – CAB International: United Kingdom.
- [82] Wood, A. J., Roger, J. (2000): A simple and non-destructive technique for measuring plant growth and development. – *American Biology Teacher* 62: 215-217.
- [83] Wüst, M., Beck, T., Mosandl, A. (1999): Conversion of citronellyl diphosphate and citronellyl β -D-glucoside into rose oxide by *Pelargonium graveolens*. – *Journal of Agricultural and Food Chemistry* 47: 1668-1672.
- [84] Yamaguchi, K. (1981): Theoretical studies of photo-oxidative cleavage reactions of nitrogen-activated C=C double bonds of enamines, indoles, and tryptamines. – *International Journal of Quantum Chemistry* 20: 393-406.

- [85] Yamaguchi, M., Ohtani, M., Mitsuda, N., Kubo, M., Ohme-Takagi, M., Fukuda, H., Demura, T. (2010): VND-INTERACTING2, a NAC domain transcription factor, negatively regulates xylem vessel formation in Arabidopsis. – *The Plant Cell* 22: 1249-1263.
- [86] Zhang, L., Becker, D. F. (2015): Connecting proline metabolism and signaling pathways in plant senescence. – *Frontiers of Plant Science* 6: 552.
- [87] Zhou, Z., An, L., Sun, L., Zhu, S., Xi, W., Broun, P., Yu, H., Gan, Y. (2011): Zinc Finger Protein5 Is required for the control of trichome initiation by acting upstream of Zinc Finger Protein8 in Arabidopsis. – *Plant Physiology* 157: 673-682.
- [88] Zhou, Z., Sun, L., Zhao, Y., An, L., Yan, A., Meng, X., Gan, Y. (2013): Zinc Finger Protein 6 (ZFP6) regulates trichome initiation by integrating gibberellin and cytokinin signaling in Arabidopsis thaliana. – *New Phytologist* 198: 699-708.

THE EFFECT OF COCONUT WATER AND MORINGA LEAF EXTRACT ON THE GROWTH AND YIELD OF SHALLOTS

ANSAR, M.^{1*} – PAIMAN²

¹*Department of Agrotechnology, Faculty of Agriculture, Tadulako University, Palu 94118, Indonesia*

(e-mail: ansharpassigai@gmail.com; phone: +62-813-9212-2864)

²*Department of Agrotechnology, Faculty of Agriculture, Universitas PGRI Yogyakarta, Yogyakarta 55182, Indonesia*

(e-mail: paiman@upy.ac.id; phone: +62-813-2862-9000)

**Corresponding author*

e-mail: ansharpassigai@gmail.com; phone: +62-813-9212-2864; fax: +62-451-429-738

(Received 12th Feb 2022; accepted 20th Jun 2022)

Abstract. In Central Sulawesi Province, Indonesia, there are shallots as raw materials for the fried onion industry with the best quality. However, the main problem of productivity is still low (< 4 tons ha⁻¹) as a result of the use of small bulbs (seeds) with low plant growth regulator (PGR) content to support their growth. Therefore, it is necessary to provide effective PGR in increasing the growth and yield of shallots, especially the Lembah Palu shallot variety (LPSV). One of the PGRs is natural PGR, including coconut water (CW) and moringa leaf extract (MLE). Both of these materials are pretty much available around the research site. This study aimed to know the effect of CW and MLE at various concentrations on the growth and yield of LPSV. This research was experimental and arranged in a randomized complete block design (RCBD) and three replications. The treatment was that the natural PGR types consisted of two kinds, i.e., CW and MLE. Each natural PGR type consisted of five concentration levels, i.e., 20, 40, 60, 80, and 100%. The results showed a significant interaction between PGR types and concentration affecting the growth and yield of shallots, including tillers number, tubers number clump⁻¹, the tuber fresh weight clump⁻¹, and tubers dried weight ha⁻¹. The CW application at a concentration of 40% as a natural PGR showed the best effect to increase the growth and yield of shallots, while MLE up to a concentration of 100% was still a trend towards increasing. The research findings show that the PGR type of CW at a concentration of 40% provides the highest growth and yield of shallots. Besides, it is necessary to conduct further research on various sources of other natural PGR.

Keywords: *natural PGR, Lembah Palu, concentration, fried onion*

Introduction

Central Sulawesi, as one of the provinces in Indonesia, has the potential as a development area for shallots cultivation. One of the varieties that have enormous potential to be developed is the LPSV, one of the local types. It results from a natural cross between local onions, widely cultivated in the Lembah Palu area. This shallot has a high adaptation, suitable for planting in lowlands < 400 m above sea level (ASL) with dry climates and low rainfall. The tubers are slightly white, oval, and relatively small (Rabinowitch and Currah, 2002).

The productivity of LPSV was generally lower than that of other types of shallots, while the Bima, Brebes, and Philippine varieties can reach 20 tons ha⁻¹. In comparison, the LPSV only had a productivity potential of 9.7 tons ha⁻¹, but at this farmer's level, it only ranges from 4-5 tons ha⁻¹ so that it can increase. The low productivity of LPSV caused the need for raw materials in the fried onion industry in Palu city, and its surroundings could not be fulfilled continuously. The low shallots productivity of LPSV

was due to the application of cultivation techniques that are not according to the recommended technical standards (Pasigai et al., 2016).

Applying natural PGR is one way of improving cultivation techniques to get a good yield because it can affect plant growth. The provision of appropriate growth regulators in composition and concentration can lead to better plant growth and development. Some PGRs are synthetic, but some are natural. The PGRs can be mixed to stimulate plant growth and development (Manurung et al., 2020). The CW and MLE were alternative natural PGR sources that can be utilized. The CW contained auxins, various cytokinins such as trans-zeatin and kinetin, gibberellin, and ABA. In addition, CW contains indole-3-acetic acid (IAA) and is the main auxin in plants (Yong et al., 2009).

Higher concentrations contained more inorganic elements and growth hormones than low concentrations. MLE effectively improves cereal forages' growth and productivity under stressful environments of salinity and aridity (Abusuwar and Abohassan, 2017). The CW produced higher protocorm multiplication than those without CW. Application of 15% CW + 0.5 mg L⁻¹ Thidiazuron had higher plantlet numbers and a greater percentage of normal putative polyploidy of *Phalaenopsis amabilis* (Aziz et al., 2019). The MLE at a concentration of 3% provided maximum growth potential at low temperatures for moringa seeds. The content of mineral nutrients, antioxidants, and growth hormones can increase the number of branches (92%), leaves (141%), leaf blades (61%), leaf chlorophyll (51%), and b (71%) and the total chlorophyll content (54%), membrane stability index (60%) and phenolic leaf content (78%) in moringa seedlings (Batool et al., 2019).

Application of MLE 10% at two weeks after emergence and every two weeks after that significantly increased growth of plant height, shoot length, fresh weight and dry weight of shoot, and yield components like the number of grains cob⁻¹, 100-grain weight, and grain weight plant⁻¹ in maize plant (Biswas et al., 2016). Leaf of *Moringa oleifera* Lam. and other plant parts may contain potential novel properties, namely secondary metabolites (Carbungco et al., 2017). The MLE performance of sprayed at tillering, jointing, and booting stages was the best as it produced the growth and yield of wheat (Jhulik et al., 2017). Applying MLE increased cumulative yield and nutrient uptake by Sudan grass compared with the untreated (Merwad, 2017).

The highest values of straw and grain yield, quality yield, and nutrient uptake by plants were obtained with 4% of MLE, while the lowest values were obtained with untreated plants. Also, the highest percentage increase in grain yield of 71 and 88% was recorded from the treatment of 4% MLE in the first and second seasons, respectively (Merwad and Abdel-Fattah, 2016). Therefore, foliar applications of 6% MLE aqueous extract can be used effectively to improve fruit set, yield, fruit weight, firmness, color, soluble solids content, vitamin C, anthocyanin content, and antioxidant activity of "Hollywood" plum (Thanaa et al., 2017).

Ethanol extract of drumstick leaf contained flavonoids total 71.9 mg quercetin equivalent g⁻¹, alkaloids total of 3 mg quinine equivalent g⁻¹, tannin as 24.7 mg tannic acid equivalent g⁻¹, and saponin as 44.4 mg g⁻¹. Therefore, drumstick leaf extract's minimum inhibition concentration (MIC) is 3.125%, while the minimum bactericidal concentration (MBC) was 6.25%. Therefore, the drumstick leaf can be used as an alternative natural antibacterial agent, which can be applied especially in aquaculture (Kenconojati and Rukmana, 2019).

The CW has many applications. For example, coconut water is traditionally used as a plant tissue culture/micropropagation growth supplement. The wide applications of CW

can be justified by its unique chemical composition of sugars, vitamins, minerals, amino acids, and phytohormones (Yong et al., 2009). For example, morphogenesis of watermelon can be obtained from explants in vitro germinated seedlings on a culture media supplemented with CW (Krug et al., 2005).

CW has identified various beneficial biochemicals such as vitamins, minerals, proteins, sugars, and enzymes. Phytohormones, particularly cytokinins, were one of the most interesting components reported in CW. Different maturation levels of CW were found to affect the cytokinin concentration, higher at coconut's immature and mature stages (Lazim et al., 2015). The IAA content decreased while the T-ZR content increased with fruit maturity. Treatments with CW from fully matured dried fruits produced the largest and the most vigorously growing plantlets (Mintah et al., 2018).

The concentration of plant growth hormones (auxin, cytokinin, gibberellins) in CW changes with fruit maturation. It has affected the in-vitro growth of potato plantlets significantly. Therefore, it can be used instead of synthetic PGR in media for potato micropropagation (Muhammad et al., 2015). The CW significantly promoted hypocotyl elongation. Germination of seeds in liquid MS medium supplemented with 0.1 mg L⁻¹ kinetin before callus initiation slightly delayed callus induction but did not significantly affect callus size. At two weeks of culture, kinetin significantly decreased the length of hypocotyls (Tantasawat et al., 2010).

Based on previous literature studies, it turns out that no one has applied natural PGR and its concentration on shallots cultivation, especially LPSV. However, applying PGR with an optimal concentration was crucial to accelerate plant growth, especially in LPSV. Therefore, testing types and concentrations of natural PGR in the study can contribute to an increase in the growth and yield of LPSV.

Based on the literature review above, this study aimed to know the effect of CW and MLE at various concentrations on the growth and yield of LPSV.

Materials and methods

Study area

This research was conducted in Oloboju Village, Sigi-Biromaru District, Sigi Regency, Central Sulawesi, Indonesia. The research was carried out from May to August 2019. The location of the study is at coordinates S 1°01'14.6532" and E 119°59'29.0256"; a place altitude of 120 m above sea level (ASL), with a daily average temperature of 30.8°C and air humidity of 62.3%.

Experimental design

This research was arranged in an RCBD with three replications. The treatment was the natural PGRs types, which consisted of two kinds, i.e., CW and MLE. Each natural PGR type consisted of five concentration levels, i.e., 20, 40, 60, 80, and 100%. Therefore, this study needed 30 experimental plots.

Research procedures

Procedure to make the natural PGR solution from CW. The CW was used from young green coconuts. The fruit's skin was smooth and slippery, free from pests and diseases, and had an endosperm that was still soft and thin. Furthermore, the water from this coconut was used as a stock solution with a concentration of 100%. Furthermore,

making MLE was done by taking young moringa leaves that were a maximum of 35 days old since they appear as leaf buds. Cleaned moringa leaves were added to water in a ratio of 1:1 (100 g of moringa leaves were added to 100 ml of water), then blended until smooth. Furthermore, MLE was filtered into a container as a stock solution with a concentration of 100%. Dilution was carried out for each concentration of young CW and MLE according to each treatment.

The population was all shallot plants in the experimental plot. The sample was part of the number and characteristics possessed by the population observed as a representative of the population of 119 plants in each experimental plot. The sample plants were determined systematically by selecting the observed plants, as many as five clumps of plants per experimental plot.

Soil cultivation was preceded by clearing the land from the remains of previous plants. Apart from that, the first plowing of the land was carried out using a tractor. The second hijack that took place was done one week later. The beds were made according to the experimental plot with a size of 255 cm (length) × 105 cm (width) × 25 cm (height). Shallot seedlings should be free of pests and diseases with relatively the same weight (uniform), then the outermost skin that has dried and the remaining roots are cleaned.

The young coconut that was used is a green color with the characteristics of smooth skin color, free from pests and diseases, and a soft and thin endosperm. Meanwhile, MLE was made by refining the material and giving it water in a ratio according to the treatment. Young moringa leaves were used for the maximum age of 35 days since appearing as leaf buds. The cleaned moringa leaves were added with water in a ratio of 1:1 (100 g of moringa leaves were added with 100 ml of water), then blended until smooth. Furthermore, the MLE was filtered into a container to obtain a stock solution of MLE with a concentration of 100%. To get each concentration of MLE in the treatment was necessary to do dilution. After completing the preparation of the planting media, prepared RGR for the treatment of planting material. Shallot seeds ready for planting were soaked according to the treatment set for 90 minutes. After that, the seeds were dried.

The bed experiment was covered with black silver plastic mulch. The plant spacing in the bed used 15 cm × 15 cm. The seeds were immersed in the planting hole and planted upright, like turning a screw, until the tuber's end appeared flat with the soil surface. Watering was done by sprinkles. The beds were watered until wet evenly every three days or as needed. Embroidering was done at the beginning of growth until the age of 7 days after planting by replacing dead or rotten seeds with spare seeds that have been prepared. Weeding was done with the aim of clearing weeds so that there was no competition with onion plants. Weeding was done manually by removing the growing grass according to conditions in the field. Weeding activities were carried out in conjunction with soil tilling. Tilling aimed to weaken the soil, supporting early plant growth and making it easier for tubers to develop optimally. Fertilizers were used, namely bokashi goat manure and inorganic fertilizers of NPK (15:15:15). Bokashi was given before planting by mixing the fertilizer with the soil.

Meanwhile, NPK was given when the plants were two weeks after planting at a dose of 2 g.plant⁻¹. Pest and disease control depends on fielding conditions. Therefore, manual control (picked) and discarded was done when an egg and leeks show signs of attack. Pest control was also carried out by spraying insecticides of the ingredient

Karbosulfan 200, with a concentration of 10 g L⁻¹ of water, and fungicides with ingredient Propineb 70%, with a concentration of 5 g L⁻¹ of water.

Harvesting was done when the plant's age of ≥ 70 DAP. The plants had shown signs of being ready to harvest. The tubers have been lifted above the soil surface. 80–90% of the leaves had turned yellow, and the stems had fallen. Harvesting was done by pulling the shallot plants and their tubers, then cleaning them from the remaining soil that sticks.

Measurement

Observations of plant growth and yield of LPSV included tillers number, tubers number clump⁻¹, tuber fresh weight clump⁻¹, and tubers dried ha⁻¹.

Statistical analysis

The data observations were analyzed with analysis of variance (ANOVA) at 5% significant level using IBM SPSS Statistics 23 software. In addition, differences between treatments were compared using Duncan's new multiple range test (DMRT) at 5% significant level.

Results

The results of ANOVA on tillers number, tubers number clump⁻¹, tubers fresh weight clump⁻¹, and the tuber dried weight ha⁻¹ showed no significant between the PGR types of CW and MLE. The CW concentration significantly affected all of the parameters observed, but the MLE concentration had no significant effect. The results of ANOVA can be represented in *Table 1*.

Table 1. The results of ANOVA on tillers number, tubers number clump⁻¹, tubers fresh weight clump⁻¹, and the tubers dried weight ha⁻¹

Source of variation	Degree of freedom	Mean square				F table 5%
		Tillers number	Tubers number clump ⁻¹	Tubers fresh weight clump ⁻¹	Tubers dried weight ha ⁻¹	
Block	2	13.617 *	3.7476 *	113.724 *	22.690 *	3.55
Treatment	9	1.829 ns	1.4555 ns	22.297 ns	4.404 ns	2.46
Type PGRs	1	0.432 ns	1.5687 ns	21.505 ns	4.256 ns	4.41
CW	4	3.424 *	2.0558 *	26.203 *	5.175 *	2.93
MLE	4	0.583 ns	0.8269 ns	18.589 ns	3.670 ns	2.93
Error	18	0.963	0.6469	8.668	1.661	

Remarks: * = Significant at the 5% significance levels, and ns = Not significant at 5% significance level.

The results of DMRT at the 5% on tillers number, tubers number clump⁻¹, tubers fresh weight clump⁻¹, and the tuber dried weight ha⁻¹ can be seen in *Table 2*.

Table 2 shows that CW at 40% concentration is the best treatment combination and yielded the maximal tiller number, tubers number clump⁻¹, tubers fresh weight clump⁻¹, and the tuber dried weight ha⁻¹.

Table 2. Tillers number, tubers number clump⁻¹, tubers fresh weight clump⁻¹, and the tuber dried weight ha⁻¹

PGR types	PGR concentration (%)	Tillers number clump ⁻¹	Tubers number clump ⁻¹	Tubers fresh weight (g clump ⁻¹)	Tubers dried weight (tons ha ⁻¹)
CW	20	7.93 ab	4.49 a	17.87 ab	7.94 ab
	40	9.00 b	5.99 b	22.40 b	9.96 b
	60	7.40 a	4.47 a	17.07 ab	7.59 ab
	80	6.13 a	3.76 a	15.33 a	6.81 a
	100	7.00 a	4.32 a	15.07 a	6.70 a
MLE	20	7.20 p	4.06 p	14.93 p	6.64 p
	40	6.93 p	3.30 p	12.27 p	5.45 p
	60	6.73 p	4.47 p	17.40 p	7.73 p
	80	7.73 p	4.65 p	15.87 p	7.05 p
	100	7.67 p	4.27 p	18.80 p	8.36 p
CW		7.49 x	4.62 x	17.55 x	7.79 x
MLE		7.45 x	4.15 x	15.85 x	7.05 x

Remarks: the average number of treatment combinations in the column followed by the same letter is not significantly different based on DMRT at 5% significance level.

The effect of PGR type and concentration on tillers number, tubers number clump⁻¹, tubers fresh weight clump⁻¹, and the tubers dried weight ha⁻¹ are presented in *Figure 1*.

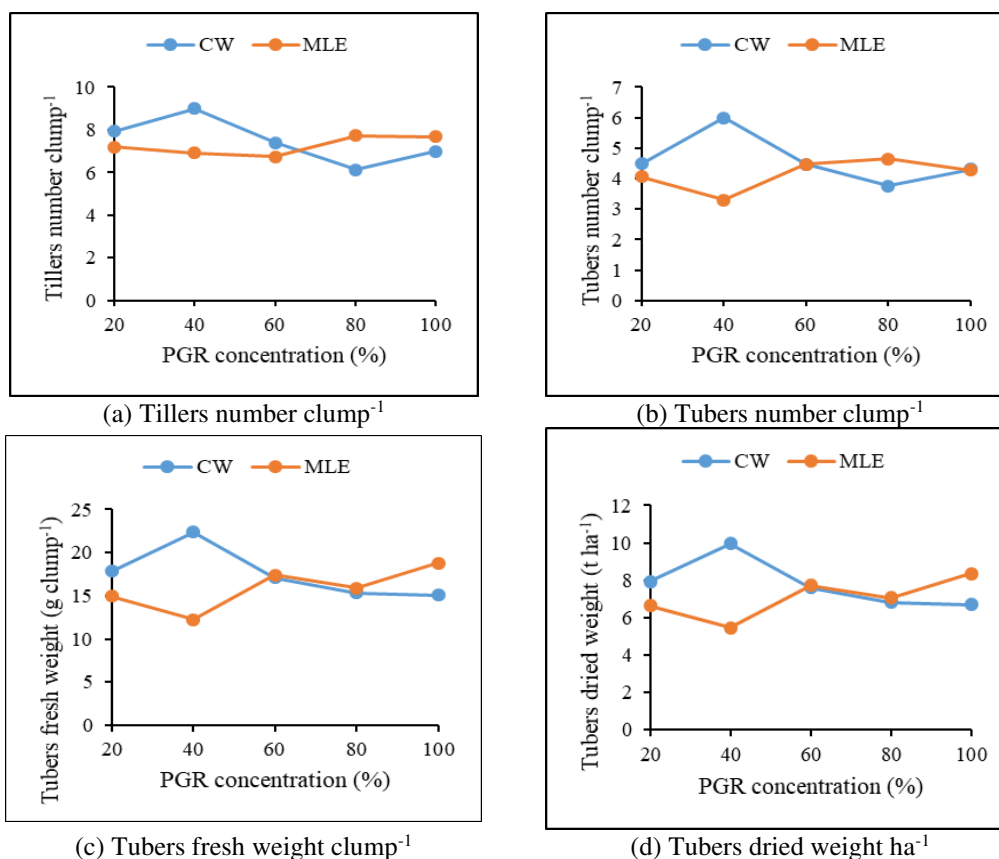


Figure 1. The effect of PGR type and concentration on (a) tillers number, (b) tubers number clump⁻¹, (c) tubers fresh weight clump⁻¹, and (d) tubers dried weight ha⁻¹

Figure 1 shows a difference in the trend between the two PGR types. The CW showed an increase of the tillers number, tubers number clump⁻¹, tubers fresh weight clump⁻¹, and the tubers dried weight ha⁻¹ from concentrations of 20-40%, but after a 40% continues to decrease to 100% concentration. It was different in MLE. There was a decrease in tillers number from a concentration of 20-60%, but after 60% continued to increase until 100%. Therefore, tubers of number clump⁻¹, fresh weight clump⁻¹, and dried weight ha⁻¹ decreased from 20-40%, but after a concentration of 40% increased to 100%. Low concentrations of 20-40% for CW increased the growth and yield. In contrast, MLE was better at 60-100% higher concentrations.

Discussion

This experiment found that CW at a concentration of 40% resulted in the highest tillers number. CW is a natural ingredient that contains various hormones, such as auxins and cytokinins, which can stimulate plant growth, thus increasing the growth parameters of the shallots. The CW is a natural PGR that can provide the most optimal results for the growth of the LPSV. Auxins can promote plant growth and development and work by stimulating the apical meristem cells of the stems and shoots (Tarigan et al., 2017). The combination of auxins and cytokines stimulates cell division and influences the differentiation pathway (Widiastoety, 2014). Supported by Sukamta (2015), CW concentration significantly affected the number of roots, shoot length, number of leaves, and leaf area. The concentration of 40% was the best treatment for pepper cutting compared to 20, 60, 80, and 100%. The CW contains PGR and other compounds that can stimulate and accelerate roots, shoots, and leaves. The content of cytokinins in CW can stimulate cell division in leaf primordia. Cytokinins can accelerate the formation of leaves and promote cell division and enlargement (Wulandari and Mukalina, 2013). Auxins can stimulate the work of cytokinins in cell division and enlargement.

The CW at a concentration of 40% produced the highest number of tubers clump⁻¹. The CW contains several hormones that play an important role in plant growth. Following the general nature of the relatively low concentrations hormone, it can stimulate cell division and elongation, thereby affecting plant growth and development. Young et al. (2009) stated that CW contains auxins, trans-zeatin, kinetin, gibberellin, and ABA. The CW also contains indole-3-acetic acid (IAA), the main auxin in plants. IAA is a weak acid that is synthesized in the meristematic region located in the shoot shoots and then transported to the root tips in the plant. Cytokinins are also found in coconut water cell division and thus promote rapid growth. One of the advantages of CW was that it produced sufficient plant cell proliferation without increasing the number of unwanted mutations.

The tubers of fresh weight clump⁻¹ and dried weight ha⁻¹ can be influenced by the leaf area number as the source of the photosynthesis process, producing dry plant matter. In addition, it was also affected by the tillers number, which directly forms the tubers number as a sink for stored photosynthetic products. Therefore, increasing the tillers number will increase the tubers number clump⁻¹, and a high rate of photosynthesis will increase the tubers yields plant⁻¹ and ha⁻¹. The CW is a natural hormone that contains auxins, cytokinins, and gibberellin. The CW can provide the most optimal results for the shallot's yield because it contains many hormones needed for plant

growth. Natural PGR types contain different growth hormones and minerals so they will have different effects on the growth and yield of LPSV plants.

For this reason, natural PGR was needed to obtain maximum results, which contained a complete type of hormone with a concentration that needs plant growth and development, including the shallots. The main cause, the highest parameter, was found in the application of young CW because the content of growth regulators in coconut water was more complex. As indicated by Indriani et al. (2014), the complexity of hormone and mineral content in CW resulted in a significant multiplication effect compared to the addition of BA synthetic hormone.

Conclusion

Based on the results and discussion, there was a significant interaction between PGR types and concentration on the growth and yield of shallots, including tillers number, tubers number clump⁻¹, the tuber fresh weight clump⁻¹, and tubers dried weight ha⁻¹. The CW application at a concentration of 40% as a natural PGR showed the best effect to increase the growth and yield of shallots, while MLE up to a concentration of 100% was still a trend towards increasing. The research findings show that the PGR type of CW at a concentration of 40% provides the highest growth and yield of shallots. We suggest that it is necessary to conduct further research with various sources of other types of natural PGR.

Acknowledgements. Thanks to Mr. Wahdi, who has provided the research area and supporting facilities. Thanks are also conveyed to Mr. Waiz and Mrs. Sifa, who have helped conduct research in the field.

REFERENCES

- [1] Abusuwar, A. O., Abohassan, R. A. (2017): Effect of *Moringa oleifera* leaf extract on growth and productivity of three cereal forages. – Journal of Agricultural Science 9(7): 236-243. <https://doi.org/10.5539/jas.v9n7p236>.
- [2] Aziz, S. A., Putri, A. A., Sukma, D., Syukur, M. (2019): Enhanced growth of in vitro plantlets by cytokinin and pre-colchicine application in *Phalaenopsis amabilis* Blume protocorms. – In Proc. III International Orchid Symposium, pp. 205-212. <https://doi.org/10.17660/ActaHortic.2019.1262.27>.
- [3] Batool, S., Khan, S., Basra, S. M. A. (2019): Foliar application of moringa leaf extract improves the growth of moringa seedlings in winter. – South African Journal of Botany 129: 347-353. <https://doi.org/10.1016/j.sajb.2019.08.040>.
- [4] Biswas, A., Hoque, T., Abedin, M. (2016): Effects of moringa leaf extract on growth and yield of maize. – Progressive Agriculture 27(2): 136-143. <https://doi.org/10.3329/pa.v27i2.29322>.
- [5] Carbungco, E. S., Pedroche, N. B., Panes, V. A., De la Cruz, T. E. (2017): Identification and characterization of endophytic fungi associated with the leaves of *Moringa oleifera* Lam. – In Proc. I International Symposium on Moringa, pp. 373-380. <https://doi.org/10.17660/ActaHortic.2017.1158.42>.
- [6] Indriani, B. S., Suwarsi, E., Pukan, K. K. (2014): Efektivitas substitusi sitokinin dengan air kelapa pada multiplikasi tunas krisan secara in vitro. – Unnes J. Life Sci. 3(2): 148-155.

- [7] Jhilik, N. Z., Hoque, T. S., Moslehuddin, A. Z. M., Abedin, A. M. A. (2017): Effect of foliar application of moringa leaf extract on growth and yield of late sown wheat. – Asian Journal of Medical and Biological Research 3(3): 323-329. <https://doi.org/10.3329/ajmbr.v3i3.34520>.
- [8] Kenconoajati, H., Rukmana, N. R. (2019): Inhibition potency of drumstick leaf extract (*Moringa oleifera*) towards *Aeromonas hydrophila*: Preliminary Study for Aeromoniasis Treatment. – Journal of Aquaculture Science 4(1): 12-20.
- [9] Krug, M. G. Z., Stipp, L. C. L., Rodriguez, A. P. M., Mendes, B. M. J. (2005): In vitro organogenesis in watermelon cotyledons. – Pesq. Agropec. Bras 40(9): 861-865.
- [10] Lazim, M. I. M., Badruzaman, N. A., Peng, K. S., Long, K. (2015): Quantification of cytokinins in coconut water from different maturation stages of Malaysia's coconut (*Cocos nucifera* L.) varieties. – J. Food Process Technol 6(11): 1-8. <https://doi.org/10.4172/2157-7110.1000515>.
- [11] Manurung, G. C. T., Hasanah, Y., Hanum, C., Mawarni, L. (2020): The role of bamboo shoot and shallot extracts combination as natural plant growth regulator on the growth of Binahong (*Anredera cordifolia* (Ten.) Steenis.) in Medan. – In IOP Conference Series: Earth and Environmental Science. <https://doi.org/10.1088/1755-1315/454/1/012169>.
- [12] Merwad, A. M. A. (2017): Effect of humic and fulvic substances and Moringa leaf extract on Sudan grass plants grown under saline conditions. – Can. J. Soil Sci 97: 703-716.
- [13] Merwad, A. M. A., Abdel-Fattah, M. K. (2016): Improving productivity and nutrients uptake of wheat plants using *Moringa oleifera* leaf extract in sandy soil. – Journal of Plant Nutrition 40(10). <https://doi.org/10.1080/01904167.2016.1263318>.
- [14] Mintah, L. O., Arhin, L., Ofosu-Anim, J., Nkansah, G. O. (2018): Effect of coconut (*Cocos nucifera* L.) water of different fruit maturity stages on axillary bud initiation, growth, and development of plantain (*Musa AAB.*). – Journal of Applied Horticulture 20(1): 42-47.
- [15] Muhammad, K., Gul, Z., Jamal, Z., Ahmed, M., Rehman, A., Khan, Z. U. (2015): Effect of coconut water from different fruit maturity stages, as natural substitute for synthetic PGR in vitro potato micropropagation. – Int. J. Biosci 6(2): 84-92.
- [16] Pasigai, M. A., Thaha, A. R., Nasir, B., Lasmini, S. A., Bahrudin, M. (2016): Teknologi budidaya bawang merah varietas lembah palu. – UNTAD Press 190.
- [17] Rabinowitch, H. D., Currah, L. (2002): Allium crop science: recent advances. – CABI Publishing. <https://doi.org/10.1079/9780851995106.0000>.
- [18] Sukamta (2015): Pengaruh konsentrasi air kelapa terhadap pertumbuhan stek lada bertapak berdaun tunggal (*Piper nigrum* L.). – Jurnal Online Mahasiswa (JOM) Faperta 4(1): 1-10. (in Indonesian).
- [19] Tantasawat, P., Chaowiset, W., Sorntip, A., Kativat, C., Wannajindaporn, A. (2010): The effects of proline and coconut water on callus Induction of cucumber (*Cucumis sativus* L.). – In Proc. 4th IS on Cucurbits, pp. 589-598.
- [20] Tarigan, P. L., Nurbaiti, Yoseva, S. (2017): Application of onion extract as a natural growth regulator on pepper (*Piper nigrum* L.) cuttings. – Jom Faperta 4(1): 1-11.
- [21] Thanaa, S. M., Kasim, N. E., Abourayya, M. S., Abdalla, A. M. (2017): Influence of foliar application with moringa (*Moringa oleifera* L.) leaf extract on yield and fruit quality of Hollywood plum cultivar. – Journal of Horticulture 4(1): 1-7. <https://doi.org/10.4172/2376-0354.1000193>.
- [22] Widiastoety, D. (2014): Effect of auxin and cytokinin on the growth of Mokara orchid plantlets. – J. Hort 24(3): 230-238.
- [23] Wulandari, R. C., Mukalina, R. L. (2013): Pertumbuhan stek melati putih (*Jasminum sambac* (L.) W. Ait.) dengan pemberian air kelapa dan IBA (indole butyric acid). – Protobiont 2(2): 39-43. (in Indonesian).
- [24] Yong, J. W. H., Ge, L., Ng, Y. F., Tan, S. N. (2009): The chemical composition and biological properties of coconut (*Cocos nucifera* L.) water. – Molecules 14: 5144-5164. <https://doi.org/10.3390/molecules14125144>.

GROWTH AND PRODUCTION RESPONSES OF BOSCHVELD CHICKENS TO BAKERS' YEAST SUPPLEMENTATION

MAOBA, S.¹ – OGBUEWU, I. P.^{1,2*} – OGUTTU, J. W.¹ – MBAJORGU, C. A.¹

¹*Department of Animal Agriculture and Animal Health, University of South Africa, Florida 1710, Republic of South Africa*

²*Department of Animal Science and Technology, Federal University of Technology, P.M.B. 1526 Owerri, Nigeria*

**Corresponding author*

e-mail: dr.ogbuewu@gmail.com; ifeanyi.ogbuewu@futo.edu.ng

ORCID No: <https://orcid.org/0000-0003-4895-7867>

(Received 14th Feb 2022; accepted 20th May 2022)

Abstract. The purpose of this study was to determine the impact of probiotic-yeast supplementation on growth and productivity of Boschveld chickens reared intensively from 1 - 91 days of age. Birds were raised on commercial starter mash (1 - 49 days) and grower mash (50 to 91 days). Six hundred unsexed Boschveld chicks with a mean live weight of 27.8 ± 1.07 g were allotted into six treatment groups. Each group was divided into five replicates of 20 chickens. Birds in each group were assigned to a diet containing 18 -20% crude protein and 3001.38 - 3009.98 Kcal/kg energy, but with increasing levels of bakers' yeast (TS) at 0 (TS0), 2.5 (TS2.5), 5.0 (TS5), 7.5 (TS7.5), 10.0 (TS10) and 12.5 g/kg feed (TS12.5). Experimental chickens were raised in a deep litter house; feed and water were given ad libitum. Data on growth performance indices, apparent metabolizable energy (AME) and nitrogen retention were collected and analysed statistically at $p < 0.05$. Treatment means where significant were separated using Duncan's test for multiple comparisons. Results revealed that dietary probiotic-yeast supplementation had no significant influence on feed intake and AME in Boschveld chickens. Chickens fed treatment diets had better final live weight (FLW), feed conversion efficiency (FCE), average daily gain (ADG) and nitrogen retention in comparison with chickens fed control diet. Our results demonstrated that probiotic-yeast supplementation at 5.0, 7.5 and 10.0 g/kg feed had a positive effect on performance indices of indigenous Boschveld chickens reared in a closed confinement from 1 up to 91 days of age.

Keywords: *indigenous chickens, probiotics, feed intake, feed conversion efficiency, live weight, nutrient digestibility*

Introduction

Indigenous chickens play an important socio-economic role in developing countries where they are reared for meat and eggs. They are an integral part of the poultry industry and are reared under a free-range system where they occasionally receive kitchen leftovers, damaged grains and insects among others. To the majority of resource-poor households, indigenous chickens serve as a quick source of income when money is needed for urgent family needs (FAO, 2010), and hence indigenous chickens are reared in most rural households because of their low requirements on labour, maintenance and production cost when compared with exotic chicken breeds. Furthermore, as suggested by Dessie and Ogle (2001) indigenous chickens have a slow growth rate and lay few eggs per clutch. Despite their low productivity and slow growth rates, indigenous chickens have good features such as hardiness, excellent meat quality, high disease-resistant ability, hardy eggshells and thermo-tolerance (Dessie and Ogle, 2001; Adesola et al., 2012). For many years, researchers have been investigating the possibility of increasing the productivity of indigenous chickens under an intensive production system through

dietary manipulation without compromising their desirable features. Thus, it has become imperative to use some readily available probiotics to enhance the productivity of indigenous chickens.

Probiotics are live microorganisms which when administered in adequate amounts confer a beneficial health effects on the host (FAO/WHO, 2002). The mechanisms of action of probiotics include modulation of the gut microbial ecosystem in favor of the growth of beneficial microbes, stabilization of the gut barrier function, stimulation of immune response, enhanced enzymatic activity resulting in higher digestibility and nutrient utilization (Timmerman et al., 2005), culminating in improved chicken performance (Junaid et al., 2018; Ogbuewu et al., 2019). There is ample evidence that yeast (*Saccharomyces cerevisiae*), one of such probiotics, enhances digestibility and nutrient uptake in poultry (Ezema and Ugwu, 2014; Nath et al., 2016; Ogbuewu et al., 2019; Ogbuewu et al., 2020). Yeast is rich in crude protein (45%), phosphorus and potassium (Reed and Naodawithana, 1999). It also contains mannan and 1.3/1.6 β -glucans which stimulate the immune response (Abaza et al., 2008). Current feeding studies in our research station have shown that dietary yeast improves blood characteristics, carcass yield, cut-out part and organ weights in Boschveld chickens (Maoba et al., 2021a,b). The positive influence of dietary yeast on the production and health indices of exotic chicken breeds has been demonstrated (Ahmed et al., 2015; Ogbuewu et al., 2019; Ogbuewu and Mbajjorgu, 2020). However, little or no information exists on the growth and productivity of indigenous chicken breeds such as the Boschveld chickens fed diets supplemented with different yeast supplementation levels.

Historically, Boschveld chicken is a cross of three South African indigenous chicken breeds. The strain was developed by a white farmer (Mike Bosch) in the mid-1970s to assist in pests (ticks) control in his beef cattle farm. It is made up of 50, 25 and 25% of Venda, Ovambo and Matabele breed traits (Bosch, 2018). Boschveld chickens are reared both for meat and egg production, and according to Okoro et al. (2017), they weigh between 1.7 and 2.6 kg at 20 weeks of age. Boschveld chicken attains sexual maturity at 20 weeks of age (Okoro et al., 2017). It also has a pea-shaped comb and plumage colour ranging from red to light brown with white patches. The hens lay brown eggs and are broody with good mothering ability.

Currently, there is little or no information on dietary yeast supplementation as a nutritional approach for increasing the productivity of indigenous chicken. At the same time, it is assumed that such approach will help in ensuring optimal productivity in terms of body weight gain, feed efficiency, live weight, egg production and product quality. Also, as far as indigenous chicken production is concerned, it is very imperative to note that one important factor in intensive indigenous chicken farming is efficient nutrient utilization as feed solely contributes about 60-70% of the total cost of chicken production. Therefore, increasing feed efficiency and minimizing feed wastages could be the leading factor in profit maximization. Such information could be very helpful to rural farmers in South Africa and elsewhere. The purpose of this study, therefore, was to determine the effect of probiotic-yeast supplementation on growth and productivity of Boschveld chickens reared in a tropical environment from day-old up to 91 days of age.

Materials and methods

Ethics statement and study location

The study adhered strictly to the guidelines of the University of South Africa's Animal Ethics Committee (2018/CAES/101). This experiment was done at Portion 22 of the farm Elandsfontein 334 IQ (26.3898 S 27.9235 E) in Gauteng Province, South Africa. The farm is situated about 30 km south of Johannesburg in the Midvaal Local Municipality within Sedibeng District Municipality. The study lasted from January to April 2019.

Preparation of poultry house and source of yeast

The poultry house had 30-floor pens with equal surface area (2 m²/pen) and was divided into three rows of 10-floor pens. The floor of each pen was covered with a layer of wood shavings (7 cm deep). Baker's yeast (*S. cerevisiae*) used for the study was obtained from Anchor Yeast 22 Bunsen Street, Johannesburg, South Africa. Boschveld chicks were purchased at Boschveld Ranching (PTY) Limited, Limpopo, South Africa.

Experimental chickens, diets and design

600 day old unsexed Boschveld chicks with an average live weight of 27.8 ± 1.07 g were used for the study that lasted 91 days. Birds were raised on a commercial starter mash (1 to 49 d) and grower mash (50 to 91 d). Boschveld chicks were assigned to six dietary groups with five replications, each having 20 chicks in a completely randomized design. Experimental birds were fed mash diets (*Table 1*) mixed with different levels of baker's yeast designated: TS0 (0), TS2.5 (2.5), TS5 (5.0), TS7.5 (7.5), TS10 (10.0) and TS12.5 (12.5 g/kg feed). Diets and water were offered *ad libitum* throughout the feeding trial. Light was provided to the experimental chickens 24 hours daily. The vaccination program was implemented following the Boschveld chicken management guide (Bosch, 2018).

Table 1. Proximate composition of the experimental diets

Nutrients (g/kg)	Starter feed (1 – 49 days)	Grower feed (50 - 91 days)
Crude protein*	200.00	180.00
Lysine*	13.30	10.50
Methionine*	4.70	4.40
Moisture*	120.00	120.00
Crude fat*	25.00	25.00
Crude fibre*	50.00	60.00
Calcium*	10.50	9.50
Phosphorus*	6.00	4.52
Determined analysis		
Dry matter	914.63	912.53
Moisture	85.37	87.47
Crude protein	229.96	193.19
Ash	58.96	47.79
Nitrogen free extract	55.06	58.65
GE (MJ/kg)	17.74	17.17
ME (Kcal/kg)	3009.98	3001.38

* As illustrated in the feed label, Kcal – kilocalorie, GE –gross energy, ME - metabolisable energy

Data collection

The initial live weights of chicks were weighed and recorded at the beginning of the feeding trial. Thereafter it was weighed at the end of each week of experiment to determine the weekly live weight and weight differences. FI was determined daily as the difference between the quantity of feed given and the leftover the following morning on the replicate basis. At the end of the feeding trial, the difference between the FLW and initial live weight (ILW) was determined and recorded as weight gain. The mean weight gained per replicate was further divided by the duration of study to determine ADG. FCE was calculated by dividing the feed intake (FI) by ADG.

Laboratory analysis

The feed samples were oven-dried at 105°C for 48 hours and finely ground (1-mm, Polymix PX-MFC 90 D) to pass through a 1-mm mesh sieve and thereafter analysed for ash, nitrogen, crude fibre (CF), ether extracts (EE) and nitrogen-free extract (NFE) content following the procedures outlined by AOAC (2008). The crude protein (CP) was calculated as $N \times 6.25$. The GE of the diets and the fecal samples were determined by measuring the heat of combustion in the samples using a bomb calorimeter (Parr 6100, Moline, IL, USA). ME was calculated using the prediction equation of Ponzenga (1985) as follows: $ME = 37 \times CP \% + 81.8 \times EE \% + 35.5 \times NFE \%$.

A digestibility trial was conducted when chickens were aged between 42 and 49 days (starter phase) and between days 84 and 91 (grower phase). On days 42 and 84, two birds per replicate were transferred to a metabolic cage equipped with a drinker and feeder. The birds were stabilized for three days before droppings were collected from each chicken daily at 9:00 am following a standard procedure. AME and nitrogen retention were calculated using the methods of AOAC (2008).

Statistical analysis

Data were analysed for statistical differences between treatments using one-way analysis of variance and Pearson's product moment correlation following the General Linear Model procedure of the Statistical Analysis System (SAS 2010). The statistical model used was as described in *equation (1)*.

$$Y_{ijk} = \mu + T_1 + \Sigma_{ijk} \quad (\text{Eq.1})$$

where: Y_{ijk} = the overall observation (FI, LW, FCE, ADG, AME and nitrogen retention), μ = the population means, T_1 = the effect of probiotic-yeast supplementation levels and Σ_{ijk} = the residual effect. Where significant ($p < 0.05$), means were separated using Duncan's test for multiple comparisons to determine the significant differences among the treatment means due to dietary effect (SAS, 2010).

Results

The proximate biochemical composition of experimental diets is shown in *Table 1*. The analysis revealed that starter and grower diets contained a crude protein content of 229.96 and 193.19 g/kg, respectively. *Tables 2, 3 and 4* summarized the impact of probiotic-yeast supplementation on production variables of Boschveld chickens aged 1 - 49, 51 - 91 and 1 - 91 d. Probiotic-yeast had no effect ($p > 0.05$) on FI and AME.

However, chickens offered TS5, TS7.5 and TS10 had higher ($p < 0.05$) than those diets TS0, TS2.5 and TS12.5, with the exception of chickens aged 1 - 49 d fed TS12.5, who had similar FLW to chickens fed TS5.0 and TS10.0. Boschveld chickens (51 - 91 and 1 - 91 d) fed diets TS5, TS7.5 and TS10.0 had significantly better ($p < 0.05$) FCE and ADG compared with those fed TS0, TS2.5 and TS12.5. However, no significant differences ($p > 0.05$) were found amongst the birds (51 - 91 and 1 - 91 d) fed TS5, TS7.5 and TS10.0 in terms of FCE and ADG. Similarly, chickens (51 - 91 and 1 - 91 d) fed TS0, TS2.5 and TS12.5 had comparable ($p > 0.05$) FCE and ADG values, whereas chickens (1- 49 d) fed TS5, TS7.5, TS10.0 and TS12.5 had better ($p < 0.05$) FCE and ADG than those fed TS0 and TS2.5. Boschveld chickens (50 - 91 d and 1 - 91 d) offered TS5, TS7.5, TS10.0 and TS12.5 retained more nitrogen than those fed TS0. A similar pattern was observed in Boschveld chickens aged 1 - 49 d, with the exception of birds fed TS2.5 that have the same nitrogen retention value as birds fed TS0.

Table 2. Effect of probiotic-yeast on production indices of Boschveld chickens aged 1 to 49 days

Diet (g/kg)	Production variables						
	ILW (g/b/d)	FLW (g/b)	FI (g/b/d)	ADG (g/b/d)	FCE	AME (MJ ME/kg)	N-retention (g/b/d)
TS0	28.4	540.5 ^c	38.1	10.5 ^c	3.7 ^a	11.3	1.84 ^c
TS2.5	26.4	548.3 ^c	36.8	10.7 ^c	3.5 ^a	10.7	1.90 ^c
TS5.0	27.7	633.3 ^{ab}	34.8	12.4 ^{ab}	2.8 ^c	11.9	2.26 ^b
TS7.5	27.0	646.9 ^a	37.2	12.7 ^a	2.9 ^c	11.7	2.54 ^a
TS10.0	29.4	634.6 ^{ab}	36.4	12.4 ^{ab}	3.0 ^{bc}	11.6	2.42 ^{ab}
TS12.5	27.5	583.7 ^b	37.3	11.4 ^{bc}	3.3 ^{ab}	10.8	2.26 ^b
Mean	27.8	597.9	36.8	11.7	3.2	11.3	2.20
SD	1.07	46.8	1.11	0.97	0.35	0.49	0.28
CV (%)	3.85	7.83	3.02	8.29	10.9	4.34	12.73
SEM	0.44	19.1	0.45	0.40	0.14	0.20	0.11
p-value	0.050	0.001	0.130	0.001	0.001	0.200	0.001

Means in the same column not sharing a common superscript are significant at $p < 0.05$. g – grams, b - bird, kg – kilograms, MJ – megajoules, ME – metabolisable energy, d - day, p - probability, ILW - initial live weight, FLW - final live weight, FI – feed intake, ADG – average daily gain, FCE – feed conversion efficiency, AME- - apparent metabolizable energy, N – nitrogen, SD - standard deviation, CV - coefficient of variation, SEM - standard error of the mean

The results of correlation coefficients among the production variables of Boschveld chickens aged 1 to 49 d and 51-91 d are shown in *Tables 5 and 6*. Positive and significant correlations existed between nitrogen retention and growth performance (ADG and FLW) in Boschveld chickens. In addition, significant ($p < 0.05$) and positive correlations were found between nitrogen retention and growth performance variables (ADG and FLW) in Boschveld chickens. However, negative and significant correlations existed between nitrogen retention and FCE ($p < 0.05$) in chickens aged 50 - 91 d. Nitrogen retention was not correlated ($p > 0.05$) to FI and AME in Boschveld chickens. On the other hand, significant and negative correlations were found between FCE, ADG and FLW. Similarly, AME was positively correlated with ADG ($p < 0.05$) in Boschveld chickens aged 51-91d.

Table 3. Effect of probiotic-yeast on production indices of Boschveld chickens aged 50 to 91 days

Diet (g/kg)	Production variables					
	FLW (g/b)	FI (g/d)	ADG (g/b/d)	FCE	AME (MJ ME/kg)	N-retention (g/b/d)
TS0	1313.8 ^d	76.0	18.4 ^b	4.1 ^a	10.7	1.8 ^c
TS2.5	1388.6 ^c	75.7	20.0 ^b	3.9 ^a	11.0	2.2 ^b
TS5.0	1587.8 ^b	74.4	22.7 ^a	3.3 ^b	10.8	2.4 ^a
TS7.5	1634.6 ^{ab}	75.3	23.5 ^a	3.2 ^b	11.4	2.4 ^a
TS10.0	1685.6 ^a	74.4	25.0 ^a	3.0 ^b	11.9	2.5 ^a
TS12.5	1380.4 ^c	72.6	19.0 ^b	3.9 ^a	10.8	2.1 ^b
Mean	1498.5	74.7	21.4	3.56	11.1	2.2
SD	156.0	1.23	2.69	0.46	0.47	0.25
CV (%)	10.4	1.65	12.6	12.9	4.23	11.3
SEM	63.67	0.50	1.10	0.19	0.19	0.10
p-value	<.001	0.574	0.001	0.005	0.421	0.001

Means in the same column not sharing a common superscript are significant at $p < 0.05$. g - gram, b - bird, d - day, p - probability, FLW - final live weight, FI - feed intake, ADG - average daily gain, FCE - feed conversion efficiency, AME - apparent metabolizable energy, kg - kilograms, MJ - megajoules, ME - metabolizable energy, SD - standard deviation, CV - coefficient of variation, SEM - standard error of the mean

Table 4. Effect of probiotic-yeast on production indices of Boschveld chickens at 91 days of age

Diet (g/kg)	Production variable					
	FLW (g/b)	FI (g/b/d)	FCE	ADG (g/b/d)	AME (MJ ME/kg)	N-retention (g/b/d)
TS0	1313.8 ^d	57.1	4.0 ^a	14.4 ^c	10.96	1.84 ^d
TS2.5	1388.6 ^c	56.2	3.7 ^{ab}	15.3 ^c	10.84	2.03 ^c
TS5	1587.8 ^b	54.6	3.1 ^c	17.6 ^b	11.35	2.34 ^{ab}
TS7.5	1634.6 ^{ab}	56.2	3.1 ^c	18.1 ^{ab}	11.56	2.48 ^a
TS10	1685.6 ^a	55.4	3.0 ^c	18.7 ^a	11.71	2.46 ^a
TS12.5	1380.4 ^c	54.9	3.6 ^{ab}	15.2 ^c	10.80	2.20 ^{bc}
Mean	1498.5	55.7	3.4	16.7	11.20	2.23
SD	156.0	0.92	0.4	1.79	0.397	0.25
CV (%)	10.4	1.65	0.11	10.7	3.54	11.2
SEM	63.67	0.376	0.16	0.73	0.162	0.10
P-value	0.001	0.455	0.001	0.001	0.230	0.001

^{a,b,c,d}: Means in the same column not sharing a common superscript are significant at $p < 0.05$. g - gram, b - bird, d - day, p - probability, FLW - final live weight, FI - feed intake, FCE - feed conversion efficiency, ADG - average daily gain, AME - apparent metabolizable energy, kg - kilograms, MJ - megajoules, ME - metabolizable energy, SD - standard deviation, CV - coefficient of variation, SEM - standard error of the mean

Table 5. Correlation among the production variables of Boschveld chickens aged 1-49 days

Variables	N-retention	Feed intake	ADG	FLW	FCE	AME
N-retention	1					
Feed intake	-0.3258	1				
ADG	0.9421**	-0.5638	1			
FLW	0.9407**	-0.5639	0.9998**	1		
FCE	-0.8029	0.7813	-0.9202**	-0.9155*	1	
AME	0.5625	-0.5095	0.7625	0.7694	-0.6387	1

*Correlation is significant at $p < 0.05$. N - Nitrogen, ADG - average daily gain, FLW - final live weight, FCE - feed conversion efficiency, AME - apparent metabolisable energy

Table 6. Correlation among productive variables of Boschveld chickens aged 50 to 91 days

Variables	N-retention	Feed intake	ADG	FLW	FCE	AME
N-retention	1					
Feed intake	-0.2173	1				
ADG	0.9246*	-0.0289	1			
FLW	0.9282*	-0.1072	0.9908*	1		
FCE	-0.9258*	0.1270	-0.9907*	-0.9992*	1	
AME	0.7167	0.0139	0.8334*	0.7836	0.7857	1

*Correlation is significant at $p < 0.05$. N – Nitrogen, ADG - average daily gain, FLW - final live weight, FCE - feed conversion efficiency, AME - apparent metabolizable energy

Discussion

This experiment assessed the impact of probiotic-yeast on growth and productivity of unsexed Boschveld chickens. The proximate composition indicated that yeast supplemented diets were rich in essential nutrients and met the nutrient requirements of Boschveld chickens (Bosch, 2018). ADG and FCE are important performance indicators in poultry production. Although, several variables should be considered for the ideal performance of the chickens such as its genetic potential, the composition of the diet, ecological condition and health of the chicken amongst others (Selvaggi et al., 2015; Sugiharto, 2016). Probiotic-yeast did not influence FI and AME in the present study. In agreement, Wulandari and Syahnar (2018) reported no effect of dietary yeast supplementation on feed intake in broiler chickens. However, contrary to the present findings, Ahmed et al. (2015) found that inclusion of yeast at 3% in the diet of broiler chickens aged 1-21 days increased feed intake. These differences could be attributed to genetic variation and growth potential of broiler chickens, since they are selected to reach market weight fast than the indigenous Boschveld chickens. The lack of significant changes in AME in the present investigation ruled out the likelihood of weight loss or muscle tissue alteration that occurs when animals use non-carbohydrate sources (amino acids and glycerol part of fat) to meet their body energy needs. Additionally, the comparable AME values in all the dietary groups is an indication that diets were similar in terms of digestibility and energy utilization. However, no similar studies in Boschveld chickens were found in the literature to compare with the findings of the present study.

The FLW recorded in chickens fed treatment diets with the exception of chickens (1 - 49 d) fed TS2.5 diet were higher than those fed control diet, which is similar to the

live weights recorded by Aluwong et al. (2012) in broiler chickens offered yeast at 5, 15 and 20 g/kg and Ding et al. (2019) in Chinese native chickens fed yeast beta-1, 3-1, 6-glucan at 0.5, 1.0 and 2.0 g/kg for 6 weeks. The improved FLW of chickens fed treatment diets when compared with control could be attributed to yeast's ability to improve digestibility and nutrient uptake in chickens (Ezema and Ugwu, 2014; Ogbuewu et al., 2019; Ogbuewu and Mbajjorgu, 2020). Another possible explanation for the increased live weights of chickens in treatment groups could be ascribed the capability of yeast to maintain a healthy gut through the production of lactic acid which makes the gastrointestinal tract acidic, thus reducing the population of pathogenic microbes (Ding et al., 2019; Ogbuewu et al., 2019). The FLW of chickens age 51- 91d and 1- 91 d fed probiotic-yeast at 5.0, 7.5 and 10.0 g/kg were higher than the value of 1555 g/bird/day as reported by Nherera (2018) in Boschveld chickens reared under improved management conditions for 17 weeks.

The significantly better FCE and ADG recorded in chickens fed probiotic-yeast at 5.0, 7.5 and 10.0 g/kg feed in the present study, when compared with those fed a diet without yeast supplementation, suggests the superiority of the diets in terms of digestibility and nutrient utilization. On the same hand, Shankar et al. (2017) found an improvement in ADG and FCE of broiler chickens offered yeast at a level (2 g/kg feed) below the values supplemented in the present study. Similar results were reported by Rafique et al. (2017) in broiler chickens fed diet incorporated with yeast at 1.5 g/kg feed, thus supporting Mabelebele et al. (2014), who found that broiler chickens have higher rate of small intestine development which is positively correlated with digestion and assimilation. The increased performance in terms of ADG and FCE in chickens offered 5.0, 7.5 and 10.0 g yeast/kg feed could be attributed to the yeast's ability to modulate intestinal microbial ecosystem in favor of the growth of lactic acid bacteria such as *Lactobacillus* species, stabilization of the gut epithelial function, improvement in gut immune system and digestive enzyme activity (Timmerman et al., 2005). However, the poor FCE and ADG recorded in chickens fed yeast at 2.5 g/kg feed in the present study could be attributed to the inability of yeast at this level to improve Boschveld chicken productivity. Contrary to the results of the improved performance of Boschveld chickens fed yeast at 5, 7.5 and 10 g/kg feed current study, Junaid et al. (2018) found that the addition of probiotics in the diets of broiler chickens did not affect ADG and FCE in broiler chickens aged 0 to 42 days. Similarly, Ahmed et al. (2015) reported poor ADG and FCE in chickens (0 - 3 weeks) fed yeast at 20 g/kg feed. The observed disparity could be ascribed to supplementation level reported to affect chicken performance (Ogbuewu et al., 2020). The ADG value of 21.4 g/bird/day recorded in chickens aged 51-91 days in the current study was higher than the value of 12.73 g/bird/day reported by Nherera (2018) in Boschveld chickens reared under improved feeding and health management for 17 weeks. This variation could be linked to differences in diet composition and health care. This result indicates that yeast has a growth-promoting effect in Boschveld chickens. The observed significant increase on ADG at a comparable feed intake in the present study is an indication that the chickens on treatment diets is gaining weight at a similar feed intake with the control.

The difference in quantity and nitrogen excretion routes has a strong influence in its retention, which is considered an index of protein status in animals, and has a direct consequence on animal performance (Chanjula et al., 2016). The significantly higher nitrogen retention in Boschveld chickens offered yeast at 5.0, 10.0 and 12.5 compared with the control, could in part be attributed to the quality of protein contained in the diets.

Similar results were found in Indonesia's native chickens (Ma'rifah et al., 2013). The present findings show that nitrogen retention value increased progressively as the amount of yeast in the diet was increased, and thereafter declined, which is similar to the finding of Mbajorgu et al. (2011) in South African unsexed Venda chickens. The significantly higher nitrogen retention recorded in birds fed treatment diets indicates the ability of the diets to support muscle development leading to better growth. This also suggests greater efficiency of the use of nitrogen in birds fed treatment diets over the control diet. Oyedeji et al. (2008) found a similar pattern in Ross 355 broiler chickens offered yeast culture at 0.2, 0.25 and 0.3 g/kg feed. Furthermore, the significant decline in nitrogen retention value of birds offered yeast at 12.5 g/kg feed in comparison with birds fed yeast at 7.5 g/kg indicates that 12.5 g yeast/kg feed could be higher than the level the Boschveld chickens could utilize.

Positive and significant correlations existed between nitrogen retention and ADG and FLW in Boschveld chickens aged 1 to 49 d and 51-91 d. This is expected because; at these stages there is greater nitrogen retention for protein tissue deposition in the muscles (Nery et al., 2007). The high and positive correlation found between nitrogen retention and ADG in chickens implies that as the nitrogen retention value increases, ADG and FLW also increase. The negative and strong correlations found between ADG and FCE suggest that a decrease in FCE increases ADG. These results are in harmony with Iji et al. (2001), who found that inclusion of yeast metabolites in chicken diets has a beneficial influence on digestive enzyme activity which leads to better digestion and nutrient utilization efficiency.

Conclusion

In conclusion, it can be inferred from the results of this study, that the range of yeast supplemented in the diet of chickens in the present study did not influence feed intake and apparent metabolizable energy intake of Boschveld chickens reared intensively from day old up 91 days. In fact, this implies that the type as well as the range of the yeast supplement used in the present study is acceptable by the birds. Also, given the fact that Boschveld chickens fed diets supplemented with yeast at 5.0, 7.5 and 10.0 g/kg feed had significantly higher final live weight, average daily gain, better nitrogen retention and feed conversion efficiency when compared to those offered a diet without yeast supplementation is a good indication that there is ample evidence that probiotic-yeast used in the present study has the ability to enhance digestibility and nutrient uptake in poultry as similarly observed by researchers (Ezema and Ugwu, 2014; Nath et al., 2016; Ogbuwu et al., 2019, 2020). Identifying the exact mechanism of action of probiotic-yeast that will allow the prediction of its ability to enhance digestibility and nutrient uptake in poultry remains a challenge.

Acknowledgement. Appreciation is expressed to University of Africa (UNISA) for sponsoring this study under UNISA Postgraduate Bursary (UNISA/CAES/ 64035247).

REFERENCES

- [1] Abaza, I., Shehata, M., Shoieb, M., Hassan, I. (2008): Evaluation of some natural feed additive in growing chicks' diet. – *International Journal of Poultry Science* 7: 872-879.

- [2] Adesola, A. A., Ng'ambi, J. W., Norris, D. (2012): Effect of ascorbic acid supplementation level to diets of indigenous Venda hens on egg production, hatchability and subsequent productivity of chicks. – *African Journal of Biotechnology* 11: 12606-12611.
- [3] Ahmed, M. E., Abbas, T. E., Abdlhag, M. A., Mukhtar, D. E. (2015): Effect of dietary yeast (*Saccharomyces cerevisiae*) supplementation on performance, carcass characteristics and some metabolic responses of broilers. – *Animal and Veterinary Sciences, Special Issue: Poultry Welfare: Housing Systems and Feeding* 3: 5-10.
- [4] Aluwong, T., Raji, M. A., Hassan, B. F., Kawu, M. U., Kobo, P. I., Ayo, J. O. (2012): Effect of different levels of supplemental yeast on performance indices and serum biochemistry of broiler chickens. – *The Open Conference Proceedings Journal* 3: 41-45.
- [5] AOAC (2008): Association of Analytical Chemists, Official Methods of Analysis. – 17th ed., Washington, D.C., USA.
- [6] Bosch, M. (2018): Boschveld village chicken management guide. – Edition #1.
- [7] Chanjula, P., Pongprayoon, S., Kongpan, S., Cherdthong, A. (2016): Effects of crude glycerin from waste vegetable oil supplementation on feed intake, ruminal fermentation characteristics, and nitrogen utilization of goats. – *Tropical Animal Health and Production* 48: 995-1004.
- [8] Dessie, T., Ogle, B. (2001): Village poultry production systems in the Central Highland of Ethiopia. – *Tropical Animal Health and Production* 33: 521-537.
- [9] Ding, B., Zheng, J., Wang, X., Zhang, L., Sun, D., Xing, Q., Pirone, A., Fronte, B. (2019): Effects of dietary yeast beta-1,3-1, 6-glucan on growth performance, intestinal morphology and chosen immunity parameters changes in Haidong chicks. – *Asian-Australasian Journal of Animal Science* 32: 1558-1564.
- [10] Ezema, C., Ugwu, C. C. (2014): Probiotic effects of *Saccharomyces cerevisiae* on nutrient digestibility and pH of the gastrointestinal tract of broilers. – In: Proceedings of the international conference on beneficial microbes ICOBM 2014: microbes for the benefits of mankind, May 27–29, Parkroyal Penang Resort, Penang, Malaysia,- A-3, pp. 10-13.
- [11] FAO (2010): Organic Agriculture and Genetic Resources for Food and Agriculture: Rearing native chickens through organic Agriculture. South Africa. – Food and Agriculture Organisation of the United Nations. www.fao.org/docrep/FAO/010/a1120e/a1120e04.pdf.
- [12] FAO/WHO (2002): Guidelines for the evaluation of probiotics in food. – Joint FAO/WHO (Food and Agriculture Organization/World Health Organization) working group report on drafting guidelines for the evaluation of probiotics in food, London, Ontario, Canada, pp. 1-11.
- [13] Iji, P. A., Saki, A. A., Tivey, D. R. (2001): Intestinal structure and function of broiler chickens on diets supplemented with a mannanoligosaccharide. – *Journal of the Science of Food and Agriculture* 81: 1186-1192.
- [14] Junaid, N., Biswas, A., Kumawat, M., Mandal, A. B. (2018): Production performance, immune response and carcass traits of broiler chickens fed diet incorporated with probiotics. – *Indian Journal of Animal Research* 8: 1-6.
- [15] Mabelebele, M., Alabi, S. J., Ng'ambi, J. W., Norris, D., Ginindza, M. M. (2014): Comparison of gastrointestinal tracts of Ross 308 broiler chickens and indigenous Venda chickens fed the same diet. – *Asian Journal of Animal and Veterinary Advances* 9: 71-76.
- [16] Maoba, S., Ogbuewu, I. P., Oguttu, J. W., Mbajiorgu, C. A. (2021a): Prediction of responses of indigenous Boschveld chickens to probiotic-yeast additive levels using a quadratic optimization model. – *Tropical Animal Health and Production* 53(148): 1-11.
- [17] Maoba, S., Ogbuewu, I. P., Oguttu, J. W., Mbajiorgu, C. A. (2021b): Haematological profiles of indigenous Boschveld chickens on probiotic-yeast (*Saccharomyces cerevisiae*) supplementation. – *Comparative Clinical Pathology* 30: 293-299.
- [18] Ma'rifah, B., Atmomarsono, B., Suthama, N. (2013): Nitrogen retention and productive performance of crossbred native chicken due to feeding effect of Kayambang (*Salvinia molesta*). – *International Journal of Science and Engineering* 5: 19-24.

- [19] Mbajiorgu, C. A., Ng'ambi, J. W., Norris, D., Alabi, O. J. (2011): Effect of dietary lysine and energy ratio on performance of unsexed indigenous Venda chickens. – *Asian Journal of Animal and Veterinary Advances* 6: 517-524.
- [20] Nath, B. K., Hossain, M. A., Bari, M. S., Barua, M., Islam, K., Chanda, G. C. (2016): Growth performance and serum biochemical responses of commercial broilers fed diets containing rubber seed and yeast. – *Asian Journal of Poultry Science* 10: 96-103.
- [21] Nery, L. R., Albino, L. F. T., Rostagno, H. S., Campos, A. M. A., Silva, C. R. (2007): Valores de energia metabolizável de alimentos determinados com frangos de corte. – *Revista Brasileira de Zootecnia* 36: 1354-1358.
- [22] Nherera, V. (2018): The performance of selected village chicken strains reared under improved feed and health management. – Bachelor of Agricultural Science Dissertation, Department of Animal Science, Bindura University of Science Education, 40p.
- [23] Ogbuewu, I. P., Okoro, V. M., Mbajiorgu, E. F., Mbajiorgu, C. A. (2019): Yeast (*Saccharomyces cerevisiae*) and its effect on production indices of livestock and poultry - a review. – *Comparative Clinical Pathology* 51: 669-677.
- [24] Ogbuewu, I. P., Mbajiorgu, C. A. (2020): Meta-analysis of probiotic-yeast (*Saccharomyces cerevisiae*) intervention on feed intake, feed efficiency and egg production indices in laying hens. – *Animal Production Science*. <https://doi.org/10.1071/AN20192>.
- [25] Ogbuewu, I. P., Okoro, V. M., Mbajiorgu, C. A. (2020): Probiotic-yeast improves performance indicators in broiler chickens: Evidence from meta-analysis. – *Applied Ecology and Environmental Research* 18: 2823-2843.
- [26] Okoro, V. M. O., Ravhuhali, K. E., Mapholi, T. H., Mbajiorgu, E. F., Mbajiorgu, C. A. (2017): Effect of age on production characteristics of Boschveld indigenous chickens of South Africa reared intensively. – *South African Journal of Animal Science* 47: 157-167.
- [27] Oyedeji, J. O., Ajayi, H. I., Egere, T. (2008): The effects of increasing levels of yeast culture (Levucel SB) in a high fibre diet on the performance and nutrient retention of broiler chicks. – *Asian Journal of Poultry Science* 2: 53-57.
- [28] Pauzenga, U. (1985): Feeding Parent Stock. – *Zootech International*, pp. 22-25.
- [29] Rafique, K., Rahman, A., Mahmood, M. (2017): Effect of dietary supplementation of different levels of *Saccharomyces cerevisiae* on growth performance and haematology in broiler. – *Indian Journal of Animal Research*, pp. 1-6.
- [30] Reed, G., Naodawithana, T. W. (1999): *Yeast Technology*. – 2nd edition, Van Nostrand Reinhold, New York.
- [31] SAS (2010): *SAS User Guide: Release 9.2*. – Statistical Analysis System. SAS Institute Inc, Cary N.C., USA.
- [32] Selvaggi, M., Laudadio, V., Dario, C., Tufarelli, V. (2015): Modelling growth curves in a nondescript Italian chicken breed: An opportunity to improve genetic and feeding strategies. – *Journal of Poultry Science* 52: 288-294.
- [33] Shankar, P. A., Premavalli, K., Omprakash, A. V., Kirubakaran, J. J., Hudson, G. H. (2017): Effect of dietary yeast supplementation on the production performance of broilers. – *International Journal of Advanced Biological Research* 7: 222-228.
- [34] Sugiharto, S. (2016): Role of nutraceuticals in gut health and growth performance of poultry. – *Journal of the Saudi Society of Agricultural Sciences* 15: 99-111.
- [35] Timmerman, H. M., Mulder, L., Everts, H., van Espen, D. C., van der Wal, E., Klaassen, G., Rouwers, S. M., Hartemink, R., Rombouts, F. M., Beynen, A. C. (2005): Health and growth of veal calves fed milk replacers with or without probiotics. – *Journal of Dairy Science* 88: 2154-2165.
- [36] Wulandari, S., Syahniar, T. M. (2018): The effect of adding probiotic *Saccharomyces cerevisiae* on dietary antibiotic- free on production performance and intestinal lactic acid bacteria growth of broiler chicken. – *Earth and Environmental Science* 207: 1-5.

EFFECT OF ORGANIC AND INORGANIC FERTILIZERS ON SOYBEAN (*Glycine max* L.) GRAIN YIELD IN DRY LAND OF INDONESIA

KUNTYASTUTI, H.¹ – LESTARI, S. A. D.¹ – PURWANINGRAHAYU, R. D.¹ – SUTRISNO¹ – MEJAYA, M. J.^{1*} – DARIAH, A.² – TRISILAWATI, O.³ – SUDARYONO, T.⁴

¹*Indonesian Legumes and Tuber Crop Research Institute, Jl. Raya Kendalpayak km 8. PO. Box 66 Malang 65101, East Java, Indonesia*

²*Indonesian Soil Research Institute, Jl. Tentara Pelajar No. 12 Bogor 16114, West Java, Indonesia*

³*Indonesian Spice and Medicinal Crops Research Institute, Jl. Tentara Pelajar No. 3 Bogor 16111, West Java, Indonesia*

⁴*Assessment Institute for Agricultural Technology East Java, Indonesian Agency for Agriculture Research and Development, Ministry of Agriculture, Malang, Indonesia*

*Corresponding author

e-mail: mmejaya@yahoo.com; madjmejaya@gmail.com.

(Received 16th Feb 2022; accepted 20th May 2022)

Abstract. Increasing soybean (*Glycine max* L.) production in dry land can be done through intensification using organic and inorganic fertilizer. The aim of the study was to evaluate the optimization use of organic and inorganic NPK fertilizers on soil and soybean productivity on dry land. The experiment was arranged in a randomized complete block design with three replications on dry land in Gresik, East Java, Indonesia. The treatments evaluated were 12 dosage combinations of ZA (ammonium sulphate), SP-18 (super phosphate-18), KCl (potassium chloride), and chicken manure. The study was conducted on dry land without and with 5,000 kg cow manure/ha. The soybean seed used in this research was Argomulyo. The results showed that (1) application of 5,000 kg cow manure/ha increased the yield of Argomulyo soybean variety by 0.21 t/ha (9%), (2) application of 100 kg KCl/ha + 50 kg ZA/ha + 100 kg SP-18/ha + 5,000 kg cow manure/ha, and 50 kg ZA/ha + 2,500 kg chicken manure/ha + 5,000 kg cow manure/ha increased soybean yield by 0.95-1.38 t/ha (50-74%), (3) application of 100 kg KCl/ha increased P uptake by 68%, Ca uptake by 60%, and Mg uptake by 54% compared to without fertilizer, (4) application of 50 kg KCl/ha + 2,500 kg chicken manure/ha increased N uptake by 48%, application of 50 kg ZA/ha + 100 kg SP-18/ha increased K uptake by 117%, and application of 50 kg ZA/ha increased Ca uptake by 60% compared without fertilizer, and (5) application of 5,000 kg cow manure/ha improved the physical properties of the soil by reducing soil bulk density by 7% and soil penetration by 37% and increasing soil permeability of 2.20 cm/hour from 1.78 cm/hour to 3.98 cm/hour. Soybean cultivation of the Argomulyo variety on dry land in Gresik requires the addition of organic cow manure 5000 kg/ha plus ZA fertilizer 50 kg/ha + chicken manure 2500 kg/ha or ZA fertilizer 50 kg/ha + SP-18 100 kg/ha + KCl 100 kg/ha to increase yield 0.95–1.38 t/ha and improve soil physical fertility. This study gives the information that the use of organic and inorganic fertilizer is an alternative technology that is required to maintain and increase the productivity of soybean and soils in dry land to support sustainable soybean cultivation.

Keywords: *Argomulyo* variety, application, chicken manure, optimization, productivity

Introduction

Dry land is defined as land that has never been waterlogged most of the year. The productivity of dry land is generally low, thus limiting the productivity of cultivated plants. Physical characteristics of dry land soils in Indonesia especially in East Java and

Central Java that are planted with maize (*Zea mays* L.), soybean (*Glycine max* L.), and peanuts (*Arachis hypogea* L.) is dominated by clay and silt fractions. The soil organic-C content ranges from 0.47-3.09%, the N-total content ranges from 0.11-0.22%, with pH (H₂O) 4.65-7.60, level of P₂O₅ Bray-1 ranged from 3 to 87 ppm, and level of P₂O₅ Olsen is between 5 and 64 ppm. K content is between 0.08 and 1.20 me/100 g. Fe-P and Al-P levels > 50 ppm are more than 50% of the survey locations; the highest Ca-P levels (25 ppm) is only in one location. On average, Fe-P > Al-P >> Ca-P. The diversity of soil fertility causes diversity in soybean yields (Iletri, 1998; Harsono, 1999; Kuntyastuti and Radjit, 2000). According to Nurjaya et al. (1998) soils rich in P and K elements are found in intensification areas, while those with low P and K status are found in non-intensified or rainfed areas. Taufiq (2001) reported that Alfisol soil in East Java and Central Java is potentially deficient in P. Dry land needs improvement to increase productivity by providing ameliorant materials such as agricultural lime, dolomite, organic matter or biochar. Balanced fertilization is very effective and efficient to increase soil productivity, and is carried out based on soil nutrient status and nutrient needs by plants (Kasno, 2019).

Apart from paddy fields, soybeans are also grown on dry land with lower productivity compared to rice fields. The role of dry land soybean is in supporting efforts to increase production through intensification using organic and inorganic fertilizers. Increasing soybean yield on suboptimal land requires the addition of organic fertilizers, biological fertilizers, lime, and inorganic fertilizers. In addition, the use of varieties suitable for specific agroecology is also highly recommended (Barus, 2013).

Nutrients that limit soybean growth in dry land are elements of P and K (Kuntyastuti and Radjit, 2000) and organic matter (Kuntyastuti and Taufiq, 2008). The addition of organic fertilizers and inorganic fertilizers is reported to improve and increase growth, soybean yield, and soil fertility (Vende et al., 2013; Hanifa and Lutojo, 2014; Naini, 2015; Juarsah, 2016; Widiastuti and Latifah, 2016; Wijanarko, 2016; Sari et al., 2017; Setiawati et al., 2017; Yuniarti et al., 2019; Kristiono et al., 2020). On dry land, the use of SP36 (super phosphate-36) fertilizer and chicken manure increases soybean yield (Kuntyastuti, 2000), and the addition of 100 kg S fertilizer/ha increases the efficiency of KCl fertilizer on soybeans (Kuntyastuti and Santoso, 2001). Sulfur fertilization and *Rhizobium* sp inoculation can also increase soybean yields (Getachew, 2017). The use of organic fertilizers can reduce the need for NPK inorganic fertilizers (Sitawati, 2020). The yield of soybean fertilized by 50 kg Urea/ha + 75 kg SP36/ha + 100 kg KCl/ha is not different from that fertilized by 25 kg Urea/ha + 37.5 kg SP36/ha + 50 kg KCl/ha + 500 kg guano manure/ha (Wahyudin et al., 2017). Meanwhile, the addition of biological fertilizers of *Rhizobium*, *Azotobacter* sp., *Azospirillum* sp., or endomycorrhizae also improves soybean growth in dry land (Permanasari et al., 2014; Kartina et al., 2015; Kiuk et al., 2019). The addition of biofertilizer Agrimeth + NPK inorganic fertilizer 50% recommendation increases soybean yield 1.26 t/ha (100%) compared to recommended 100% NPK fertilizer (Purba, 2016). Application of 50% NPK + 50% poultry manure and 100% poultry manure improved soil chemical properties and nutrient uptake of soybean (Almaz, 2017).

The use of P inorganic fertilizer and manure is one of the alternatives to improve soil P fertility status, increase yields, and sustain better productivity of soy-wheat cropping patterns on dry land Vertisols (Reddy et al., 1999). Phosphorus deficiency significantly decreased nutrient uptake by all plant parts especially in drought conditions (Rotaru et al., 2014). Continuous application of P fertilizer enhanced available P (Bray-P), but

application of lime reduced the accumulation of P in soil. Balanced fertilizer management with suitable amendment (organic manure/lime) compulsorily required for optimum nutrient supply without affecting soil health for sustainable production (Vishwanath, 2020). On dry land with a pH of 6.9, 1.21% organic C, low levels of P, K, and S elements, the use of 150 kg rock phosphate/ha increases soybean yields 35-50% and increases the efficiency of using chicken manure and cow manure by 50% (Kuntyastuti et al., 2003). According to Ghosh et al. (2003) 100% recommended dose of NP fertilization can increase the sustainable yield index. The agronomic efficiency was higher at the 50% recommended dose of NP fertilization compared to 100% recommended dose of NP fertilization. Soil organic C content decreased after four years of planting and availability of P elements increased with continuous NP fertilization for four years. In Latosol and Podsolik soils, the use of cow dung is better than that of straw compost. The addition of cow dung and straw is better given after the application of P-inorganic fertilizer (Sari et al., 2017).

The use of 4,000 kg manure + 30 kg N + 26 kg P + 25 kg K/ha in each growing season is an alternative fertilizer to improve soil physical properties and soybean productivity because it increases the efficiency of water and nutrient use (Bandyopadhyay et al., 2010). Improvement of soil fertility due to the use of manure caused by the activity of dehydrogenase enzymes; acid and alkaline phosphatase; cellulose; and protease activity, which ultimately improves nutrient transformation (Saha et al., 2008). The best soybean growth and yield was obtained in the treatment of 20 t/ha manure + *Trichoderma* sp. 20 g/polybag (Sarawa, 2014).

Intensive cultivation, the use of inorganic fertilizers and erosion can reduce the carbon content of microorganisms (Susilawati, 2013) and cause a decrease in yield. Ding et al. (2016) reported that inorganic fertilizer plus manure increased microbial size and diversity and changed microbial composition.

Cultivation of plants without organic fertilizers reduced soil organic C content by 39-43% compared to soil treated with organic fertilizers. The increase in soil organic C was 26, 18, and 6% of the total C-organic in added manure, rice straw, and green manure (Ghosh et al., 2012). The use of manure for 15 years increased the C-organic and N-total soil as well as the enzyme activity of invertase, b-glucosidase, urease, acid and alkaline phosphatase, and dehydrogenase in the soil. Long term use of manure is the best alternative to improve soil quality and microbial activity (Liang et al., 2014). The activity of the plasma membrane H⁺-ATPase enzyme can be increased by the addition of Ca, thereby increasing nutrient uptake (Liang and Zhang, 2018). Ca nutrient promotes a more positive partial N-balance in soybean, contributing N to the rotation, reducing the dependency on synthetic N fertilizers and the mining of soil N reservoir from soil organic matter, and increasing the long-term sustainability (Alves et al., 2021). In connection with the foregoing research that has been carried out, this study aimed was to evaluate the optimization use of organic and inorganic NPK fertilizers on soil and soybean productivity on dry land.

Materials and Methods

Place and time of study

The study was conducted on dry land in Bolo Village, Ujungpangkah District, Gresik Regency, East Java Province, Indonesia at the coordinates of 6.957881 and 112.531537 East Longitude.

Research design

The experiment was arranged in a randomized complete block design with three replications. The treatments evaluated were 12 dosage combinations of ZA (ammonium sulphate), SP-18 (super phosphate-18), KCl (potassium chloride), and chicken manure (Table 1). The study was conducted on dry land without and with application of 5,000 kg cow manure/ha. ZA inorganic fertilizer contains 20.8% N and 23.8% S, SP-18 contains 18% P₂O₅, and KCl contains 60% K₂O. Chemical properties of cow manure and chicken manure presented in Table 2.

Table 1. Combination treatments of organic and NPK inorganic fertilizer

No.	ENVIRONMENT A (without cow manure)				ENVIRONMENT B (5,000 kg cow manure/ha)			
	ZA	SP-18	KCl	Chicken manure	ZA	SP-18	KCl	Chicken manure
	(kg/ha)				(kg/ha)			
1	0	0	0	0	0	0	0	0
2	50	0	0	0	50	0	0	0
3	0	100	0	0	0	100	0	0
4	0	0	100	0	0	0	100	0
5	50	100	0	0	50	100	0	0
6	50	0	100	0	50	0	100	0
7	0	100	100	0	0	100	100	0
8	50	100	100	0	50	100	100	0
9	50	0	0	2,500	50	0	0	2,500
10	0	50	0	2,500	0	50	0	2,500
11	0	0	50	2,500	0	0	50	2,500
12	0	0	0	2,500	0	0	0	2,500

Table 2. Chemical properties of cow manure and chicken manure

Chemical properties	Cow manure	Chicken manure	Methods
Organic-C (%)	3.86	26.9	Curmic
P ₂ O ₅ (%)	0.13	4.21	Wet destruction HNO ₃ + HClO ₄
SO ₄ (%)	3.07	7.45	Wet destruction HNO ₃ + HClO ₄
K (%)	0.44	2.62	Wet destruction HNO ₃ + HClO ₄
Ca (%)	5.35	2.67	Wet destruction HNO ₃ + HClO ₄
Mg (%)	0.28	0.34	Wet destruction HNO ₃ + HClO ₄
CEC (%)	25.1	32.0	NH ₄ OAc pH 7
Fe (%)	0.39	0.18	Wet destruction HNO ₃ + HClO ₄
Mn (%)	0.170	0.08	Wet destruction HNO ₃ + HClO ₄
Cu (%)	0.011	0.08	Wet destruction HNO ₃ + HClO ₄

Remarks: Analysis were carried out in Soil and Plant Chemical Laboratory, Iletri

Seeds of Argomulyo variety (mixed with carbosulfan insecticide) were planted at a 3.2 m x 3.2 m plot with a planting space of 40 cm x 10 cm, without basic fertilizer. Between plots were made a drainage channel of 30 cm wide with a depth of 25 cm. Cultivated land, the fertilizers were supplied at planting time by making a hole in the soil of 10 cm apart next to the seedling hole. Weeding was carried out at the age of 21 and 35 days after planting (DAP). Thinning and replanting were carried out at the age of 10 DAP and leaving two plants/clumps. Pests and disease controls were carried out

intensively according to the field conditions using deltametrin 25 g/l, fipronil 50 g/l, diafentiuron, mankozeb, and propinop 70%. At the research locations, water pump facility is available, so that soybean plants can be irrigated once every 20 days using underground water.

Observation

Soil samples were taken at a depth of 0-20 cm and 20-40 cm. Nutrient uptake analysis was carried out at the pod formation phase at 51 DAP. Parameters observed were (1) leaves chlorophyll indexes using chlorofilmeter digital SPAD brand Minolta (*Figure 1*); nutrient uptake of N, P, K, Ca, and Mg in the pod formation phase at 51 DAP, (2) plant height, number of filled pods, and weight of 100 seeds from 10 sample plants at harvest time, and (3) soybean yields in the 3.2 m x 2.5 m plots. Data obtained were subjected to analysis of variance followed by LSD test at a significant level of 5%. The condition of soybean crop in the study site is shown in *Figures 2 and 3*.



Figure 1. Measurement of leaf chlorophyll index using a SPAD digital chlorophyllmeter



Figure 2. Leaf growth of Argomulyo variety during pod filling phase, Alfisol Gresik.



Figure 3. Crop of Argomulyo variety during pod harvesting phase, Alfisol Gresik.

Data analysis

Analysis of the physical and chemical properties of the soil was carried out before planting and after harvesting. Soil texture of dry land in the research location at Gresik is clay loam with a soil water holding capacity in the top soil of a depth of 0-20 cm by 16%. Soil is dominated by the silt fraction so that is loose and has the potential to support the achievement of high productivity. Farmers rarely cultivate the soil to a depth of more than 20 cm. This can be seen from the saturated hydraulic conductivity of the soil with a depth of 0-20 cm of 2.01 cm/hour, which is 65% higher than the soil depth of 20-40 cm, which is 1.22 cm/hour (*Table 3*). Saturated hydraulic conductivity (soil permeability) is the velocity of movement of water in the saturated soil (vertical flow). Water can flow easily in soil which has large pores and has good inter-pore relationships. Small pores with uniform inter-pore relationships have lower permeability because the movement of water in the soil is slower. Low soil permeability can also be caused by the soil that has never been cultivated, so that the soil pores are very small and the soil becomes compact.

Table 3. Physical properties of Gresik dry land

Physical properties	Depth of 0-20 cm	Depth of 20-40 cm	Methods
Saturated hydraulic conductivity (cm/hour)	2.01	1.22	Constan heat
Bulk density (g/cm ³)	1.28	1.30	Cylinder
Particle density (g/cm ³)	2.51	2.48	Picnometer
Porosity (%)	49	47	Equation BI, BJ
Penetration (N/cm ²)	259	271	Penetrometer
COLE	0.027	0.074	
Water content pF 2,5 (%)	35	38	Gravimetry
Water content pF 4,2 (%)	19	19	Gravimetry
Water holding capacity (%)	16	19	
Sand fraction (%)	22	23	Pipette
Silt fraction (%)	43	39	Pipette
Clay fraction (%)	35	38	Pipette
Texture class	Clay loam	Clay loam	Triangle texture

Remarks: Analysis was carried out in Physical Soil Laboratory, Brawijaya University

Soil compaction with a depth of 20-40 cm was also observed based on the soil penetration value, namely 271 N/cm² in soil depth of 20-40 cm, higher than the soil depth of 0-20 cm, namely 259 N/cm². Soil penetration is the power needed for an object to enter the ground. The high value of soil penetration can inhibit plant root development.

Gresik dry land soil has a neutral pH, poor in organic matter, nutrients N, S, Na, Ca, and Mg, but rich in P and K nutrients (Table 4). If water needs are fulfilled and fertilized, the physical and chemical fertility of the Gresik dry land soil can support the achievement of high productivity. In soil with a neutral pH, the level of macro nutrient availability is at its maximum, so that it can meet the needs of soybean plants. Chicken manure as research material is richer in organic-C, P, S, K, and Mg elements compared to cow manure, and vice versa for elements of Ca (Table 2).

Table 4. Chemical properties of Gresik dry land

Chemical properties	Depth of 0-20 cm	Depth of 20-40 cm	Methods
pH H ₂ O	6.75	7.45	pH meter
Organic-C (%)	1.77	1.34	Curmic
Total-N (%)	0.11	0.11	Kjeldhal
P ₂ O ₅ Bray I (ppm)	55.0	40.5	Bray-1
SO ₄ (ppm)	19.8	15.9	NH ₄ OAc pH 4,8
K (cmol(+) kg ⁻¹)	0.65	0.23	NH ₄ OAc pH 7
Na (cmol(+) kg ⁻¹)	0.05	0.03	NH ₄ OAc pH 7
Ca (cmol(+) kg ⁻¹)	0.82	1.55	NH ₄ OAc pH 7
Mg (cmol(+) kg ⁻¹)	0.10	0.52	NH ₄ OAc pH 7
Al (cmol(+) kg ⁻¹)	0.0	0.0	KCl 1 N
H (cmol(+) kg ⁻¹)	0.0	0.0	KCl 1 N
CEC (cmol(+) kg ⁻¹)	25.1	32.0	NH ₄ OAc pH 7
Fe (ppm)	20.2	16.0	DTPA extract
Mn (ppm)	44.1	45.0	DTPA extract
Cu (ppm)	8.25	7.59	DTPA extract
Zn (ppm)	4.06	3.46	DTPA extract

Remarks: Analysis were carried out in Soil and Plant Chemical Laboratory, Iletri

Results and Discussion

On dry land in Gresik, optimal growth of Argomulyo soybean varieties can be obtained with good management. The application of organic fertilizer in the form of cow and chicken manure, NPK inorganic fertilizer in the form of ZA, SP-18, and KCl did not affect the chlorophyll index of soybean leaves at the age of 51 DAP on pod development stage, plant height at harvest, weight of 100 seeds, and number of filled pods/plants (Table 5). The chlorophyll index of soybean leaves averaged 42.3. At harvest time, the soybean plant reaches a height of 59 cm with 26 filled pods/plant and a weight of 100 seeds 19.6 g. Argomulyo weight of 100 seeds based on the description of superior varieties is 16 g, including the large seed soybean category (Iletri, 2018).

Application of 5,000 kg cow manure/ha increase Anjasmoro soybean leaves chlorophyll index at 60 DAP from 39.7 to 46.6. The soybean plant grows on dry land with pH 6.74, 1.35% organic-C, 9.5 ppm P₂O₅, 0.29 me/100 g K, 52.5 me/100 g Ca, and 7.22 me/100 g Mg. Soil is poor in P and K nutrient, but rich in Ca and Mg nutrient (Muzaiyanah et al., 2015). The availability and P nutrient uptake can be inhibited by

high levels of Ca and Mg nutrient. In this study, soybean was grown on dry land with a pH of 6.75, 1.77% organic-C, 55 ppm P₂O₅, 0.65 me/100 g K, 0.82 me/100 g Ca, and 0.10 me/100 g Mg (Table 4). Soil rich in P and K nutrients, but poor in Ca and Mg nutrient.

Table 5. Effect of organic and inorganic fertilizer on growth and yield component Argomulyo soybean varieties in Gresik dry land

Treatment	Leaf chlorophyll index at 51 DAP	Plant height at harvest (cm)	Number of filled pods/plant	Weight of 100 seeds (g)
Environment				
Without cow manure	41.8	59.9	24.3	19.15
5,000 kg cow manure/ha	42.7	57.9	27.1	20.03
Organic and NPK inorganic fertilizer				
1. Control (without fertilizer)	40.6	56.1	23.9	18.86
2. ZA 50 kg/ha	42.9	58.5	26.4	18.85
3. SP-18 100 kg/ha	43.1	56.0	24.5	19.85
4. KCl 100 kg/ha	41.8	59.4	29.6	20.10
5. ZA 50 kg + SP-18 100 kg/ha	41.6	60.1	25.0	19.03
6. ZA 50 kg + KCl 100 kg/ha	41.7	62.9	25.2	19.63
7. SP-18 100 kg + KCl 100 kg/ha	42.5	57.4	26.7	20.14
8. ZA 50 kg+ SP-18 100 kg + KCl 100 kg/ha	43.5	59.7	25.9	19.10
9. ZA 50 kg + chicken manure 2500 kg/ha	41.7	58.5	26.9	19.77
10. SP-18 50 kg + chicken manure 2500 kg/ha	42.6	59.6	26.3	19.82
11. KCl 50 kg + chicken manure 2500 kg/ha	41.9	59.6	25.5	19.94
12. Chicken manure 2500 kg/ha	43.2	59.5	22.8	20.00
Average	42.3	58.9	25.7	19.59
LSD 5%	ns	ns	ns	ns

Remarks: ns = not significant, DAP = days after planting

Application of cow manure and interaction with chicken manure and inorganic fertilizer (ZA, SP-18, and KCl) not affected growth and yield component, but affected the seeds yield of Argomulyo varieties in Gresik dry land. Application 5,000 kg cow manure/ha as an environmental differentiator can increase soybean yield by 0.27 t/ha (15%) from 1.76 t/ha to 2.03 t/ha.

At environment without cow manure, Argomulyo soybean yield reach 1.43 t/ha on without fertilizer treatment. Addition of 50 kg ZA/ha (10.4 kg N + 11.9 kg S/ha) increase soybean yield 0.61 t/ha (43%) from 1.43 t/ha to 2.04 t/ha (Table 6). Addition of 100 kg KCl/ha (60 kg K₂O/ha) increase soybean yield 0.71 t/ha (50%) from 1.43 t/ha to 2.14 t/ha and not different with application of 50 kg ZA/ha. Addition 100 kg SP-18/ha + 100 kg KCl/ha (18 kg P₂O₅ + 60 kg K₂O/ha) and 50 kg ZA + 100 kg SP-18 + 100 kg KCl/ha (10.4 kg N + 11.9 kg S + 18 kg P₂O₅ + 60 kg K₂O/ha) increase 0.56 t/ha (40%) the average of soybean yield. Conversely, application of 100 kg SP-18/ha; 50 kg ZA + 100 kg SP-18/ha; 50 kg ZA + 100 kg KCl/ha, 2,500 chicken manure/ha without or with 50 kg ZA/ha or 50 kg SP-18/ha or 50 kg KCl/ha did not increase soybean yield.

Table 6. Effects of organic and inorganic fertilizer on Argomulyo varieties soybean yield in Gresik dry land

Treatment	Yield with moisture content 12% (t/ha)	
	Without cow manure	5,000 kg cow manure/ha
1. Control (without fertilizer)	1.43 ef	2.00 bcd
2. ZA 50 kg/ha	2.04 bcd	1.96 bcd
3. SP-18 100 kg/ha	1.78 bcde	1.56 def
4. KCl 100 kg/ha	2.14 b	1.79 bcde
5. ZA 50 kg + SP-18 100 kg/ha	1.18 f	2.72 a
6. ZA 50 kg + KCl 100 kg/ha	1.83 bcde	2.20 b
7. SP-18 100 kg + KCl 100 kg/ha	2.01 bcd	2.05 bcd
8. ZA 50 kg + SP-18 100 kg + KCl 100 kg/ha	1.99 bcd	2.12 bc
9. ZA 50 kg + chicken manure 2500 kg/ha	1.56 def	2.23 ab
10. SP-18 50 kg + chicken manure 2500 kg/ha	1.63 cdef	1.87 bcde
11. KCl 50 kg + chicken manure 2500 kg/ha	1.83 bcde	1.97 bcd
12. Chicken manure 2500 kg/ha	1.74 bcde	1.85 bcde
Average	1.76 P	2.03 Q
LSD 5% (interaction)	0.5048	

In the environment with 5,000 kg cow manure/ha, Argomulyo soybean yield reached 2 t/ha without application of NPK inorganic fertilizers or chicken manure. These results were not different if 5,000 kg cow manure/ha was combined with N, P, K, NK, PK, NPK inorganic fertilizer, and 2,500 kg chicken manure/ha with or without N, P, or K inorganic fertilizer. The highest yield of 2.72 t/ha was obtained when soybean plants were given 5,000 kg cow manure/ha plus 50 kg ZA + 100 kg SP-18/ha (10.4 kg N + 11.9 kg S + 18 kg P₂O₅/ha). This yield was 1.29 t/ha (90%) higher than the control treatment without cow manure, chicken manure, and inorganic fertilizer (ZA, SP-18, and KCl) or increased 0.72 t/ha (36%) compared to 5,000 kg cow manure/ha without chicken manure and NPK inorganic fertilizer (Table 6). The addition of 5,000 kg cow manure + 50 kg ZA + 100 kg SP-18/ha also causes different and higher soybean yields compared to soybean yields on other fertilization treatment. In contrast, giving 2,500 kg chicken manure/ha with or without NPK inorganic fertilizer did not increase soybean yields. The dosage of chicken manure given might still be insufficient, so it does not increase soybean yield. On dry land in Lamongan and Blitar, increasing soybean yield requires 10-20 t chicken manure/ha (Kuntyastuti, 2000).

Increasing Argomulyo soybean yield $\geq 50\%$ (>0.7 t/ha) becomes 2.14-2.72 t/ha can reach with application of 100 kg KCl/ha; 5,000 kg cow manure + 50 kg ZA + 100 kg SP-18/ha; 5,000 kg cow manure + 50 kg ZA + 100 kg KCl/ha or 5,000 kg cow manure + 2,500 kg chicken manure + 50 kg ZA/ha. The yield of Argomulyo soybean based on the variety description is 1.5-2.0 t/ha (Iletri, 2018). In the dry land of Penukal Abab Lematang Ilir, South Sumatra, fertilizing 25 kg Urea + 150 kg SP36 + 100 kg KCl + 2.000 kg manure + 1.000 kg dolomite/ha produces seeds 2.49 t/ha on Anjasmoro soybean varieties and 1.37 t/ha Burangrang soybean varieties (Somantri et al., 2019). On the dry land of Bima, West Nusa Tenggara, giving 100 kg NPK fertilizer (15:15:15) + 1 liter of liquid fertilizer/ha can produce seeds of 2.41 t/ha in Anjasmoro variety and 2.35 t/ha in Burangrang variety (Hipi et al., 2015). Anjasmoro soybean variety can produce seeds of 1.8 t/ha in dry land Sampang, Madura (Iletri, 2021). In contrast, in drought condition, 75 kg Urea + 100 kg SP36 + 100 kg KCl + 1,000 kg organic manure

+ 500 kg dolomite/ha can produce only 0.74 t/ha Grobogan seeds soybean variety (Mustikawati et al., 2018).

Han (2006) reported that the addition of NPK inorganic fertilizer could increase soybean yields on Lampineung, Banda Aceh dry land. The use of combination organic fertilizer and inorganic fertilizer to increase soybean yield was also obtained on dry land in Blitar and Blora (Kuntyastuti et al., 2003), in Konawe Selatan, Southeast Sulawesi (Wahab et al., 2019), in South Kalimantan (Adie et al., 2019), and in West Sumatra (Nofriani, 2019). According to Bandyopadhyay et al. (2010), the application of manure and NPK inorganic fertilizer can improve the allocation of dry matter to pods compared to only NPK inorganic fertilizer, thus increasing soybean yields.

Application of 5,000 kg cow manure/ha did not increase N, P, K, Ca, and Mg nutrient uptake, but application of NPK inorganic fertilizer with chicken manure giving reverse information. Application of NPK inorganic fertilizer and chicken manure can increase 10-48% N nutrient uptake; the highest was 50 kg KCl + 2,500 kg chicken manure/ha, namely 115 mg N/plant. P nutrient uptake increased 10-69%, highest on 100 kg/ha KCl treatment that was 30 mg P/plant. K nutrient uptake increased 71-130%, highest on 50 kg ZA + 100 kg SP-18/ha treatment that was 186 mg K/plant. Ca nutrient uptake increased 33-63%, highest on 50 kg ZA/ha and 100 kg KCl/ha that was 90 mg Ca/plant. Mg nutrient uptake increased 25-53%, highest on 100 kg KCl/ha that was 24 mg Mg/plant (Table 7). Application of 2-4 t organic manure/ha can increase NPK nutrient on soybean stem (Sabilu et al., 2015). Application of 20-40 t banana stalk bokashi/ha can increase NPK nutrient uptake on soybean plant, otherwise on application 10^3 - 10^5 CFU *Azotobacter* sp./mL + 23-35 g *Mycorrhizae* bio-fertilizer did not affect NPK nutrient on soybean stem (Faozi et al., 2019).

Table 7. Effect of organic and inorganic fertilizer on Argomulyo soybean variety macro nutrient uptake at 51 DAP in Gresik dry land

Treatment	Macro nutrient uptake (mg/plant)				
	N	P	K	Ca	Mg
Environment					
Without cow manure	100.3	22.6	156.0	79.4	21.0
5,000 kg cow manure/ha	101.4	21.2	157.3	81.5	20.9
Organic and NPK inorganic fertilizer					
1. Control (without fertilizer)	77.9	17.7	86.0	55.9	15.5
2. ZA 50 kg/ha	112.0	28.3	175.8	89.6	22.9
3. SP-18 100 kg/ha	85.8	23.3	140.2	75.1	19.3
4. KCl 100 kg/ha	108.7	29.7	182.5	89.5	23.8
5. ZA 50 kg + SP-18 100 kg/ha	102.5	29.0	186.2	85.0	22.4
6. ZA 50 kg + KCl 100 kg/ha	101.8	23.8	150.6	74.3	20.4
7. SP-18 100 kg + KCl 100 kg/ha	107.8	21.2	157.6	85.9	21.0
8. ZA 50 kg+ SP-18 100 kg + KCl 100 kg/ha	100.7	21.2	175.6	83.0	21.6
9. ZA 50 kg + chicken manure 2500 kg/ha	96.1	19.1	151.6	78.1	20.5
10. SP-18 50 kg + chicken manure 2500 kg/ha	99.4	18.8	145.6	76.6	21.2
11. KCl 50 kg + chicken manure 2500 kg/ha	114.9	21.8	161.0	82.6	23.2
12. Chicken manure 2500 kg/ha	96.0	17.3	158.9	77.1	20.1
Average	100.3	22.6	156.0	79.4	21.0

In this study, the average soybean yield of Argomulyo varieties reached 1.90 t/ha and absorbed 100 mg N/plant, 23 mg P/plant, 156 mg K/plant, 79 mg Ca/plant, and 21 mg

Mg/plant. In Vertisol soil Ngawi, soybean plants absorbed 430 mg N/plant, 790 mg P/plant, 450 mg K/plant, 490 mg Ca/plant, and 910 mg Mg/plant to produce 1.74 t/ha (Kuntyastuti et al., 2012). In Entisol soil Malang, soybean yield of 1.72 t/ha was obtained in soybean plant which absorbed 450 mg N/plant, 47 mg P/plant, 203 mg Ca/plant, and 55 mg Mg/plant (Kuntyastuti and Sutrisno, 2014).

Application of 5,000 kg cow manure/ha can improve physical soil fertility in Gresik dry land. Bulk density decreased from 1.25 g/cm³ to 1.16 g/cm³. Soil penetration measured in the field using a penetrometer at a depth of 5 cm reduced 63% and at a depth of 15 cm declined 44% (Table 8). Soil structure can improve with application of 5,000 kg cow manure/ha. Application cow, goat, and chicken manure can decrease bulk density or increase soil porosity, permeability rate, and soybean yield in degraded Ultisol soil Jambi. Conversely, at a depth of 25 cm, the use of cow manure does not affect soil penetration (Abdurachman et al., 2000). A soil layer of 22.5-30 cm depth, the use of 10 t manure/ha + NPK fertilizer recommended dosage (25 kg N + 25.8 kg P + 16.6 kg K/ha) does not affect saturated hydraulic conductivity and soil bulk density (Hati et al., 2006).

Table 8. Effect of organic and inorganic fertilizer on bulk density and soil penetration after Argomulyo soybean varieties harvesting in Gresik dry land

Treatment	Bulk density (g/cm ³)	Penetration 5 cm (t/feet ²)	Penetration 15 cm (t/feet ²)	Penetration 25 cm (t/feet ²)
Environment				
Without cow manure	1.25 a	3.5 a	4.5 a	4.9 a
5,000 kg cow manure/ha	1.16 b	1.3 b	2.5 b	4.8 a
Organic and NPK inorganic fertilizer				
1. Control (without fertilizer)	1.26	2.8	3.4	5.0
2. ZA 50 ZA kg/ha	1.22	2.7	3.7	4.8
3. SP-18 100 kg/ha	1.19	2.5	4.0	5.0
4. KCl 100 kg/ha	1.18	2.6	3.5	4.7
5. ZA 50 kg + SP-18 100 kg/ha	1.21	2.3	3.3	4.8
6. ZA 50 kg + KCl 100 kg/ha	1.23	2.2	3.1	5.0
7. SP-18 100 kg + KCl 100 kg/ha	1.23	2.2	4.1	5.0
8. ZA 50 kg+ SP-18 100 kg + KCl 100 kg/ha	1.22	2.5	3.6	5.0
9. ZA 50 kg + chicken manure 2500 kg/ha	1.17	2.3	3.3	4.8
10. SP-18 50 kg + chicken manure 2500 kg/ha	1.24	1.9	3.2	4.5
11. KCl 50 kg + chicken manure 2500 kg/ha	1.15	2.3	3.5	4.8
12. Chicken manure 2500 kg/ha	1.20	2.3	3.5	4.6
Average	1.21	2.4	3.5	4.8
LSD 5%	ns	ns	ns	ns

ns = not significant based on 5% probability level

The results of measurements in the laboratory showed that application of 5,000 kg cow manure/ha improves the soil physical properties. The saturated hydraulic conductivity increased from 1.78 cm/hour to 3.98 cm/hour, while particle density and soil penetration decreased by 7.8% and 36% (Table 9). Available water is no different. Similar results were presented by Bandyopadhyay et al. (2010), that the application of 4,000 kg manure + 30 kg N + 26 kg P + 25 kg K/ha reduced soil bulk density by 9.3% and soil penetration 42.6%, increased hydraulic conductivity 95.8%, aggregate diameter stable 13.8%, and 45.2% organic-C content compared to the treatment without fertilizer.

Table 9. Effect of organic and inorganic fertilizer on saturated hydraulic conductivity (SHC), particle density (PD), penetration depth of 0-10 cm and available soil water after harvesting Argomulyo soybean varieties in Gresik dry land

Treatment	SHC (cm/hour)	PD (g/cm ³)	Soil penetration (N/cm ²)	Available soil water (%)
Environment				
Without cow manure	1.78	2.58	360.8	12.7
5,000 kg cow manure/ha	3.98	2.38	228.7	12.3
Organic and NPK inorganic fertilizer				
1. Control (without fertilizer)	2.55	2.50	260.0	12.5
2. ZA 50 kg/ha	3.45	2.50	227.0	11.5
3. SP-18 100 kg/ha	2.00	2.45	235.0	14.0
4. KCl 100 kg/ha	2.05	2.55	215.5	12.0
5. ZA 50 kg + SP-18 100 kg/ha	3.00	2.55	240.0	12.5
6. ZA 50 kg + KCl 100 kg/ha	2.60	2.55	330.0	11.0
7. SP-18 100 kg + KCl 100 kg/ha	2.75	2.40	351.0	12.5
8. ZA 50 kg + SP-18 100 kg + KCl 100 kg/ha	2.95	2.50	340.5	14.0
9. ZA 50 kg + chicken manure 2500 kg/ha	3.55	2.45	352.0	12.5
10. SP-18 50 kg + chicken manure 2500 kg/ha	4.05	2.40	317.0	13.5
11. KCl 50 kg + chicken manure 2500 kg/ha	2.55	2.45	353.5	11.5
12. Chicken manure 2500 kg/ha	3.05	2.40	315.5	12.0
Average	2.88	2.48	294.8	12.5

The diversity of combination between NPK inorganic fertilizer and chicken manure caused variations in soil physical properties. Application of 50 kg SP-18 + 2,500 kg chicken manure/ha makes the highest saturated hydraulic conductivity (4.05 cm/hour). The lowest soil particle density (2.4 g/cm³) was found at application 100 kg SP-18 + 100 kg KCl/ha and 2,500 kg chicken manure/ha with or without 100 kg SP-18/ha. The lowest soil penetration at the depth 0-10 cm (215.5 N/cm²) was found at application 100 kg KCl/ha. The highest water availability (14%) was found at application 100 kg SP-18/ha or 50 kg ZA + 100 kg SP-18 + 100 kg KCl/ha.

Application of NPK inorganic fertilizers and crop residues play an important role in improving fertility and maintaining soil quality (Jiang et al., 2008). Application of 10 t manure/ha + recommended dosage of NPK fertilizer (25 kg N + 25.8 kg P + 16.6 kg K/ha) increase soybean yield from 0.90 t/ha to 1.83 t/ha (Hati et al., 2006). The increase in yield is supported by improvements in soil physical properties. The highest RLD (root length density) to a depth of 30 cm was obtained in the manure + NPK fertilizer treatment, 31.9% and 70.5% higher than NPK fertilizer and without fertilizer, and negatively correlated ($r = -0.88^{**}$) with soil penetration.

Application of manure for 8 years decreases soil bulk density, increases aggregate diameter, and soil organic-C content (Bhattacharyya et al., 2007). The infiltration rate at steady state conditions in the NPK + manure treatment was 1.98 cm/hour, without fertilizer 0.72 cm/hour, and 1.20 cm/hour on NPK fertilization. Soil water sorptivity with NPK + manure was 1.06 cm/min^{0.5} higher than NPK (0.61 cm/min^{0.5}). Application of manure and inorganic fertilizer for long term can increase organic-C and improve soil physical properties. Bhattacharyya et al. (2008) reported the results for 30 years, that NPK + manure increased soil water holding capacity, infiltration rate, organic-C, total-N, P-Olsen, K-dd, C-microbial biomass, and dehydrogenase activity compared to NPK treatment or without fertilizer. Recommendations for inorganic fertilization are

incomplete, on the other hand, the provision of manure + NPK fertilizer every year is necessary for sustainable soil and plant productivity.

Cultivation of crops on dry land without P fertilizer will not be sustainable in the long term (unsustainable). Fertilization of 15-20 kg P/ha/year is needed to maintain soil fertility in order to provide available P which is sufficient for plant to produce (Ryan et al., 2008). Soybean cultivation without the addition of manure and inorganic P-fertilizer suppressed soil organic-P. The addition of manure and inorganic P-fertilizers stimulated soil organic-P. Therefore, application of manure and inorganic P-fertilizers is an effective strategy to improve soil organic-P and provide P-soil in the long term for sustainable crop production (Reddy et al., 2000).

The dry land used as the research location is intensive agricultural land and the highest Argomulyo soybean yield, 2.72 t/ha was obtained by adding 5,000 kg cow manure + 50 kg ZA + 100 kg SP-18/ha (10.4 kg N + 11.9 kg S + 18 kg P₂O₅/ha). Fan et al. (2005) recommend a balance of fertilizers to ensure continued productivity in intensive cropping patterns. The highest increase in soil organic C, namely 160 mg/ha/year was obtained by adding rice straw + N fertilizer every year + P fertilizer every two years or by adding manure + N + P fertilizer every year. The addition of organic matter to the soil in the long term can increase the soil water holding capacity, which in turn improves water availability for crops and restrains yield losses, reduces CO₂ emissions from agricultural land and sustains land productivity. Research by Manna et al. (2007) on dry land for 30 years showed that soybean yields decreased by 21 kg/ha/year in the NP fertilizer treatment and 30 kg/ha/year in the treatment without fertilizer. However, the continuous use of NPK + manure or NPK + lime can maintain soybean yields without worsening soil quality.

Soil quality index indicators are available levels of N, K, S, microbial biomass carbon and hydraulic conductivity. Conventional tillage + legume residue + 90 kg N fertilizer/ha produced the highest soil quality index (Sharma et al., 2005). Therefore, the management of yield and quality of dry land for sustainable agriculture requires soil cultivation with the addition of organic fertilizer residues and N fertilizers. The use of manure + NPK increases total biomass (Mandal et al., 2009), leaf area index, growth rate, fuel, contribution renewable energy, net energy output, non-renewable energy productivity, and higher efficiency in the use of non-renewable energy, resulting in higher yields, so that soybean yield higher than the use of NPK and control. The combination of NPK + manure can be a viable nutrient management alternative for soybean production.

According to Evanylo et al. (2008) the negative effect of use manure on the environment and ground water can be prevented by estimating the rate of N mineralization accurately. The increased risk of transporting nutrients by run off due to increased concentrations of organic-C, N, and P in the run off from compost as a soil amendment is offset by increased infiltration, porosity, and soil water holding capacity which can reduce run off volume. Jacobsen et al. (2012) explained that improving plant productivity on dry land can be done in several ways, namely initial planting with minimum soil cultivation, increasing the use of organic matter and efficient weed control, and crop rotation.

Soybean cultivation on dry land with land characteristics such as dry land in Gresik requires inorganic fertilizers to increase yield by 50% (0.7 t/ha) and a combination of inorganic fertilizers with organic fertilizers to increase yields by 90% (1.29 t/ha). According to Anshori et al. (2019) soybean productivity has a positive correlation with

land quality. Technological improvements from farmers manual such as the use of new superior varieties, quality seed, drainage channels, regular planting, IPM principles and 2.000 kg organic fertilizer + 100 kg NPK fertilizer/ha and foliar fertilizers can increase soybean yields 0.4-0.7 t/ha (33-43%). Residues of applying organic fertilizers, P-inorganic and inoculation also have a positive impact on subsequent crop productivity (Rurangwa, 2018).

Information on increasing soybean yields and improving physical, chemical, and biological soil fertility due to intensification dry land shows that input of organic and inorganic fertilizers is still needed to increase and maintain soil and soybean productivity on dry land. However, the low soybean price factor causes farmers not to be interested in adopting the recommended technology package as a whole. Farmers are interested in applying some technology components, such as new superior varieties or regular spacing (Elizabeth and Suhartina, 2019). Input of dry land cultivation technology through amelioration measures to improve soil quality by utilizing local resources that are in-situ and prioritized diversification of superior dry land commodities must be in accordance with the regional agro-ecosystem conditions, that is acceptable to the local community and provide added value to farm income (Matheus et al., 2017).

Conclusion

Application of 5,000 kg cow manure/ha increased 0.21 t/ha (9%) Argomulyo varieties soybean yield. Application of 100 kg KCl/ha, 50 kg ZA + 100 kg SP-18 + 5,000 kg cow manure/ha, and 50 kg ZA + 2,500 kg chicken manure + 5,000 kg cow manure/ha increase 0.95-1.38 t soybean yield/ha (50-74%). Application of 5,000 kg cow manure/ha improve soil physical properties by reducing 7% soil bulk density and 37% soil penetration, and increasing soil permeability 2.20 cm/hour from 1.78 cm/hour to 3.98 cm/hour. Soybean cultivation of the Argomulyo variety on dry land in Gresik requires the addition of organic cow manure 5000 kg/ha plus ZA fertilizer 50 kg/ha + chicken manure 2500 kg/ha or ZA fertilizer 50 kg/ha + SP-18 100 kg/ha + KCl 100 kg/ha to increase yield 0.95 – 1.38 t/ha and improve soil physical fertility. The results of this study gives the information that the use of organic and inorganic fertilizer is an alternative technology that needed to maintain and increase the productivity of soybean and soils in dry land to support sustainable soybean cultivation.

Acknowledgements. The authors thank Salam Agus Rianto and Rofi'i (field technicians); Angesti P, Mayar, and Ekmi L.Y. (lab technicians) for their efforts and assistance in conducting field research and analyzing soil, plants, and fertilizers in the ILETRI soil and plant chemistry laboratory.

REFERENCES

- [1] Abdurachman, A., Juarsah, I., Kurnia, U. (2000): Effects of the use of various types and dosage of manure on productivity of degraded Ultisol in Batin Village, Jambi. – Proceedings of the National Seminar on Soil Resources, Climate, and Fertilizer, 6-8 December 1999. Lido-Bogor, Indonesia, pp. 303-319. (in Indonesian).
- [2] Adie, M. M., Krisnawati, A., Suryati, D. (2019): Characterization of adaptive and productive soybean (*Glycine max* L.) genotypes in dry land of Kalimantan, Indonesia. –

- The 2nd International Conference on Natural Resources and Life Sciences (NRLS), IOP Conf. Series: Earth and Environmental Science 293: 012027.
- [3] Almaz, M. G., Halim, R. A., Martini, M. Y., Samsuri, A. W. (2017): Integrated application of poultry manure and chemical fertiliser on soil chemical properties and nutrient uptake of maize and soybean. – Malaysian Journal of Soil Science 21: 13-28. ISSN 1394-7990.
- [4] Alves, L. A., Ambrosini, V. G., de Oliveira Denardin, L. G., Flores, J. P. M., Martins, A. P., Filippi, D., Bremm, C., César de Faccio Carvalho, P., Farias, G. D., Ciampitti, I. A., Tiecher, T. (2021): Biological N₂ fixation by soybeans grown with or without liming on acid soils in a no-till integrated crop-livestock system. – Soil and Tillage Research 209: 1-9.
- [5] Anshori, A., Srihartanto, E., Riyanto, D. (2019): Productivity of several soybean varieties on dry land in Kab. Gunung Kidul, DI Yogyakarta. – Research Fair Unisri 3(1): 463-467. (in Indonesian).
- [6] Bandyopadhyay, K. K., Misra, A. K., Ghosh, P. K., Hati, K. M. (2010): Effect of integrated use of farmyard manure and chemical fertilizers on soil physical properties and productivity of soybean. – Soil and Tillage Research 110: 115-125.
- [7] Barus, J. (2013): Potensi pengembangan dan budidaya kedelai pada lahan suboptimal di Lampung. – Prosiding Seminar Nasional Lahan Suboptimal, Palembang, 20-21 September 2013. Hlm 1-12.
- [8] Bhattacharyya, R., Chandra, S., Singh, R. D., Kundu, S., Srivastva, A. K., Gupta, H. S. (2007): Long-term farmyard manure application effects on properties of a silty clay loam soil under irrigated wheat–soybean rotation. – Soil and Tillage Research 94: 386-396.
- [9] Bhattacharyya, R., Kundu, S., Prakash, V., Gupta, H. S. (2008): Sustainability under combined application of mineral and organic fertilizers in a rainfed soybean–wheat system of the Indian Himalayas. – European Journal of Agronomy 28: 33-46.
- [10] Ding, J., Jiang, X., Ma, M., Zhou, B., Guan, D., Zhao, B., Zhou, J., Cao, F., Li, L., Li, J. (2016): Effect of 35 years inorganic fertilizer and manure amendment on structure of bacterial and archaeal communities in black soil of northeast China. – Applied Soil Ecology 105: 187-195.
- [11] Elisabeth, D. A. A., Suhartina (2019): Farmers response on introduction of soybean cultivation technology under teak shade. – International Conference on Biology and Applied Science (ICOBAS) AIP Conf. Proc. 2120, 040013-1–040013-9.
- [12] Evanylo, G., Sherony, C., Spargo, J., Starner, D., Brosius, M., Haering, K. (2008): Soil and water environmental effects of fertilizer, manure, and compost based fertility practices in an organic vegetable cropping system. – Agriculture, Ecosystems, and Environment 127: 50-58.
- [13] Fan, T., Stewart, B. A., Yong, W., Junjie, L., Guangye, Z. (2005): Long-term fertilization effects on grain yield, water-use efficiency and soil fertility in the dryland of Loess Plateau in China. – Agriculture, Ecosystems, and Environment 106: 313-329.
- [14] Faozi, K., Yudono, P., Indradewa, D., Maás, A. (2019): Nutrient uptake of N, P, K, and soybean seed yields (*Glycine max* L. Merrill) in application bokashi banana stalk to sand beach soil. – Vegetalika 8(3): 177-191. (in Indonesian).
- [15] Getachew, Z., Abera, G., Beyene, S. (2017): Rhizobium inoculation and sulphur fertilizer improved yield, nutrients uptake and protein quality of soybean (*Glycine max* L.) varieties on Nitisols of Assosa area, Western Ethiopia. – African Journal of Plant Science 11(5): 123-132. DOI 10.5897/AJPS2017.1519. <http://www.academicjournals.org/AJPS>.
- [16] Ghosh, P. K., Dayal, D., Mandal, K. G., Wanjari, R. H., Hati, K. M. (2003): Optimization of fertilizer schedules in fallow and groundnut-based cropping systems and an assessment of system sustainability. – Field Crops Research 80: 83-98.
- [17] Ghosh, S., Wilson, B., Ghoshal, S., Senapati, N., Mandal, B. (2012): Organic amendments influence soil quality and carbon sequestration in the Indo-Gangetic plains of India. – Agriculture, Ecosystems, and Environment 156: 134-141.

- [18] Han, B. (2006): Adaptation test of several soybean varieties (*Glycine max* (L) Merrill) on site specific dry land agro ecosystems during the June planting season at the Lampineung Experimental Farm in Nanggroe Aceh Darussalam. – *Jurnal Floratek* 2: 78-85. (in Indonesian).
- [19] Hanifa, A., Lutojo, L. (2014): Penggunaan pupuk organik berbahan urine sapi terhadap kualitas kimia tanah di lereng Merapi. – *Buana Sains* 14(2): 157-163.
- [20] Harsono, A. (1999): Location Specific Peanut Cultivation Technology in Tegal and Rice Fields. – Iletri, Malang, Indonesia, 65p. (in Indonesian).
- [21] Hati, K. M., Mandal, K. G., Misra, A. K., Ghosh, P. K., Bandyopadhyay, K. K. (2006): Effect of inorganic fertilizer and farmyard manure on soil physical properties, root distribution, and water-use efficiency of soybean in Vertisols of central India. – *Bioresource Technology* 97: 2182-2188.
- [22] Hipi, A., Herawati, N., Sulistyawati, Y., Sudarto (2015): Agronomic characteristic and productivity seven superior varieties of soybean at dry land. – *Proceedings of the National Seminar on the Results of Research on Tuber and Crops in 2014*. 5 June 2014. Iletri, Malang, Indonesia, pp. 149-155. (in Indonesian).
- [23] Iletri. (1998): Iletri Annual Report on 1997/1998. – Malang, Indonesia, 124p.
- [24] Iletri. (2018): Deskripsi Varietas Terbaru. – Retrieved from <http://balitkabi.litbang.pertanian.go.id/informasi/deskripsi-varietas-terbaru>.
- [25] Iletri. (2021): Gelar Teknologi Budidaya Kedelai di Lahan Kering Beriklim Kering. – Retrieved from <http://balitkabi.litbang.pertanian.go.id/berita/gelar-teknologi-budidaya-kedelai-di-lahan-kering-beriklim-kering/>.
- [26] Jacobsen, S. E., Jensen, C. R., Liu, F. (2012): Improving crop production in the arid Mediterranean climate. – *Field Crops Research* 128: 34-47.
- [27] Jiang, D., Zeng, X., Gao, J., Li, L. (2008): Changes of Organic Matter, N, P and K Content of Soils in Red Soil Areas Under Long-Term Experiment. – *Agricultural Sciences in China* 7(7): 853-859.
- [28] Juarsah, I. (2016): Konservasi tanah mendukung pertanian organik untuk peningkatan produktivitas lahan. – Hlm. 60-67. *Prosiding Seminar Nasional Pengembangan Teknologi Pertanian*. Politeknik Negeri Lampung, 8 September 2016. ISBN 978-602-70530-4-5.
- [29] Kartina, A. M., Nurmawalis, Fatmawaty, A. A., Firnia, D. (2015): Exploration of the potential of soil microbes in increasing soybean yield (*Glycine max*) on dry land. – *Journal Agroekotek* 7(2): 121-128. (in Indonesian).
- [30] Kasno, A. (2019): Perbaikan tanah untuk meningkatkan efektivitas dan efisiensi pemupukan berimbang dan produktivitas lahan kering masam. – *Jurnal Sumberdaya Lahan* 13(1): 27-40.
- [31] Kiuk, Y., Rai, I. N., Kesumadewi, A. A. I. (2019): The effectiveness of indigenous endomycorrhiza and rhizobium inoculum in increasing nutrient uptake and yield of soybean in dry land. – *International Journal of Biosciences and Biotechnology* 7(1): 18-30.
- [32] Kristiono, A., Purwaningrahayu, R. D., Elisabeth, D. A. A., Wijanarko, A., Taufiq, A. (2020): Kesesuaian varietas, jenis pupuk organik dan pupuk hayati untuk peningkatan produktivitas kedelai di lahan pasang surut. – *Buletin Palawija* 18(2): 94-104.
- [33] Kuntyastuti, H. (2000): Application of SP-36 and chicken manure in Ultisol and Alfisol dry land. – *Penelitian Pertanian Tanaman Pangan* 19(3): 59-65. (in Indonesian).
- [34] Kuntyastuti, H., Radjit, B. S. (2000): Efficiency of P, K Fertilizer, and Soil Enhancer in Dry Land. – *Technical Report 1999/2000*, Iletri, Malang, Indonesia, 15p. (in Indonesian).
- [35] Kuntyastuti, H., Santoso, G. W. A. (2001): Potassium and sulfur fertilization of soybeans in paddy fields and dry land. – *Tropika* 9(1): 32-44. (in Indonesian).
- [36] Kuntyastuti, H., Taufiq, A., Heryanto (2003): Application of P, K, S, and manure on soybean in Alfisol dry land. – *Penelitian Pertanian Tanaman Pangan* 22(1): 14-22. (in Indonesian).

- [37] Kuntyastuti, H., Taufiq, A. (2008): Technology component of soybean cultivation in dry land. – Buletin Palawija 16: 1-31. (in Indonesian).
- [38] Kuntyastuti, H., Wijanarko, A., Purwaningrahyu, R. D., Taufiq, A. (2012): Effect of organic fertilizer residues and NPK on changes and soil conditions in Ngawi Vertisols in soybean plants. – Proceedings of the National Seminar on the Results of Research on Tuber and Crops in 2011. 15 November 2011. Puslitbang Tanaman Pangan, Bogor, Indonesia, pp. 177-188. (in Indonesian).
- [39] Kuntyastuti, H., Sutrisno (2014): Effect of chicken, bagasse, and zeolite manure residues after six growing seasons on mungbean and soybean in Entisol soil. – Proceedings of the National Seminar on Organic Agriculture. 28-29 August 2013. Soil Department, Agricultural Faculty, Gadjah Mada University, Yogyakarta, Indonesia, pp. 156-164. (in Indonesian).
- [40] Liang, Q., Chen, H., Gong, Y., Yang, H., Fan, M., Kuzyakov, Y. (2014): Effects of 15 years of manure and mineral fertilizers on enzyme activities in particle-size fractions in a North China Plain soil. – European Journal of Soil Biology 60: 112-119.
- [41] Liang, C., Zhang, B. (2018): Effect of exogenous calcium on growth, nutrients uptake and plasma membrane H⁺-ATPase and Ca²⁺-ATPase activities in soybean (*Glycine max*) seedlings under simulated acid rain stress. – Ecotoxicology and Environmental Safety 165: 261-269. <https://doi.org/10.1016/j.ecoenv.2018.09.019>.
- [42] Mandal, K. G., Hati, K. M., Misra, A. K. (2009): Biomass yield and energy analysis of soybean production in relation to fertilizer-NPK and organic manure. – Biomass and Bioenergy 33: 1670-1679.
- [43] Manna, M. C., Swarup, A., Wanjari, R. H., Mishra, B., Shahi, D. K. (2007): Long-term fertilization, manure and liming effects on soil organic matter and crop yields. – Soil and Tillage Research 94: 397-409.
- [44] Matheus, R., Basri, M., Rompon, M. S., Neonufa, N. (2017): Dry land agricultural management strategies to improve food security in East Nusa Tenggara. – Partner 22(2): 529-541. (in Indonesian).
- [45] Mustikawati, D. R., Mulyanti, N., Arief, R. W. (2018): Productivity of soybean on different agroecosystems. – International Journal of Environment, Agriculture and Biotechnology 3(4): 1154-1159.
- [46] Muzaiyanah, S., Kristiono, A., Subandi (2015): The effect of nutrient-rich organic fertilizers from Santap NM1 and Santap NM2 on the growth and yield of soybean in Vertisols. – Buletin Palawija 13(1): 74-82. (in Indonesian).
- [47] Naini, I., Minwal, M., Syafrullah, S. (2015): Pengaruh takaran pupuk organik plus terhadap pertumbuhan dan produksi tanaman kedelai (*Glycine max* L. Merrill) di lahan lebak. – KLOORFIL 10(2): 63-67. ISSN 2085-9600.
- [48] Nofrianil (2019): Response of Anjasmoro soybean variety to the application of compost made from mol bamboo clumps on suboptimal land. – Journal of Applied Agricultural Science and Technology 3(1): 29-40. (in Indonesian).
- [49] Nurjaya, Kasno, A., Moersidi, S., Santoso, D., Adiningsih, J. S. (1998): Nutrient status of phosphorus and potassium in Pantura rice fields. – Proceedings No. 14: Meeting for Discussion and Communication of Soil and Agro-climate Research Results. 10-12 February 1998. Puslittanak. Bogor, Indonesia, pp. 231-250. (In Indonesian).
- [50] Permanasasi, I., Irfan, M., Abizar (2014): Soybean growth and yield (*Glycine max* (L.) Merrill) on application of rhizobium and Urea fertilizer in peat media. – Journal Agroteknologi 5(1): 29-34. (in Indonesian).
- [51] Purba, R. (2016): Response of soybean growth and yield on biological fertilizer in dry land Pandeglang, Banten. – Jurnal Pengkajian and Pengembangan Teknologi Pertanian 19(3): 253-261. (in Indonesian).
- [52] Reddy, D. D., Rao, A. S., Reddy, K. S., Takkar, P. N. (1999): Yield sustainability and phosphorus utilization in soybean-wheat system on Vertisols in response to integrated use of manure and fertilizer phosphorus. – Field Crops Research 62: 181-190.

- [53] Reddy, D. D., Rao, A. S., Rupa, T. R. (2000): Effect of continuous use of cattle manure and fertilizer phosphorus on crop yields and soil organic phosphorus in a Vertisol. – *Bioresource Technology* 75: 113-118.
- [54] Rotaru, V., Toma, S., Bursan, A. (2014): The effects of phosphorus deficiency and rhizobacteria on phosphorus contents of two soybean (*Glycine max* L.) cultivars grown at low water supply. – *Scientific Papers. Series A. Agronomy*. LVII:316-321. ISSN 2285-5785. ISSN CD-ROM 2285-5793. ISSN Online 2285-5807. ISSN-L 2285-5785.
- [55] Rurangwa, E., Vanlauwe, B., Giller, K. E. (2018): Benefits of inoculation, P fertilizer and manure on yields of common bean and soybean also increase yield of subsequent maize. – *Agriculture, Ecosystems and Environment* 261: 219-229.
- [56] Ryan, J., Ibrikci, H., Singh, M., Matar, A., Masri, S., Rashid, A., Pala, P. (2008): Response to residual and currently applied phosphorus in dry land cereal/legume rotations in three Syrian Mediterranean agroecosystems. – *European Journal of Agronomy* 28: 126-137.
- [57] Sabilu, Y., Damhuri, Imran (2015): N, P, and K levels of soybean (*Glycine max* (L.) Merrill) applied by *Azotobacter* sp., Mycorrhizae, and organic fertilizer. – *Biowallacea* 2(1): 153-161. (In Indonesian).
- [58] Saha, S., Prakash, V., Kundu, S., Kumar, N., Mina, B. L. (2008): Soil enzymatic activity as affected by long term application of farm yard manure and mineral fertilizer under a rainfed soybean–wheat system in N-W Himalaya. – *European Journal of Soil Biology* 44: 309-315.
- [59] Sarawa, O., Gusnawaty, H. S., Sartika (2014): Efek residu pupuk kandang dan trichoderma terhadap pertumbuhan dan produksi tanaman kedelai (*Glycine max* L.). – *AGRIPLUS* 24(02): 169-176. ISSN 0854-0128.
- [60] Sari, M. N., Sudarsono, Darmawan (2017): Pengaruh bahan organik terhadap ketersediaan fosfor pada tanah-tanah kaya Al dan Fe. – *Buletin Tanah dan Lahan* 1(1): 65-71.
- [61] Setiawati, M. R., Sofyan, E. T., Nurbaity, A., Suryatmana, P., Marihot, G. P. (2017): Pengaruh aplikasi pupuk hayati, vermikompos dan pupuk anorganik terhadap kandungan N, populasi *Azotobacter* sp. dan hasil kedelai edamame (*Glycine max* (L.) Merrill) pada Inceptisols Jatinangor. – *Agrologia* 6(1): 1-10.
- [62] Sharma, K. L., Mandal, U. K., Srinivas, K., Vittal, K. P. R., Mandal, B., Grace, J. K., Ramesh, V. (2005): Long-term soil management effects on crop yields and soil quality in a dryland Alfisol. – *Soil and Tillage Research* 83: 246-259.
- [63] Sitawati, R., Turmuktini, T., Kurniawan, A. (2020): Paket inovasi bahan organik untuk efisiensi pupuk anorganik (NPK) peningkatan pertumbuhan dan hasil beberapa genotipe kedelai hitam (*Glycine max* L. Merrill). – *Agroscience* 10(2): 160-168. ISSN Cetak: 1979-4681. e-ISSN: 2579-7891.
- [64] Somantri, R. U., Syahri, Thamrin, T. (2019): Potential yields of several new high yielding varieties (VUB) of soybeans in dry land South Sumatera. – *Proceedings of the Suboptimal Land National Seminar 2018: Challenges and Solutions for the Development of Pajale and Second Generation Palm Oil (Replanting) on Suboptimal Lands*. 18-19 October 2018. Unsri, Palembang, Indonesia, pp. 473-481. (in Indonesian).
- [65] Susilawati, M., Budhisurya, E., Anggono, R. C. W., Simanjuntak, B. H. (2013): Analisis kesuburan tanah dengan indikator mikroorganisme tanah pada berbagai sistem penggunaan lahan di plateau Dieng. – *AGRIC*. 25(1): 64-72.
- [66] Taufiq, A. (2001): Evaluation of Alfisol viability and increase in productivity for peanuts. – *Ilmu Pertanian* 8(1): 16-25. (in Indonesian).
- [67] Verde, B. S., Danga, B. O., Mugwe, J. N. (2013): Effects of manure, lime and mineral P fertilizer on soybean yields and soil fertility in a humic nitisol in the Central Highlands of Kenya. – *International Journal of Agricultural Science Research* 2(9): 283-291. ISSN 2327-3321. Available online at <http://academeresearchjournals.org/journal/ijar>. *Academe Research Journals*.

- [68] Vishwanath, Kumar, S., Purakayastha, T. J., Datta, S. P., Rosin, K. G., Mahapatra, P., Sinha, S. K., Yadav, S. P. (2020): Impact of forty-seven years of long-term fertilization and liming on soil health, yield of soybean and wheat in an acidic Alfisol. – Archives of Agronomy and Soil Science. DOI 10.1080/03650340.2020.1843023.
- [69] Wahab, A., Adnan, A. M., Sarjoni, Karimuna, S. R. (2019): Soybean fertilizer package for dry land in South Konawe, Southeast Sulawesi. – Penelitian Pertanian Tanaman Pangan 3(1): 32-34. (In Indonesian).
- [70] Wahyudin, A., Wicaksono, F. Y., Irwan, A. W., Ruminta, Fitriani, R. (2017): Response of Wilis soybean (*Glycine max*) due to the application of various doses of N, P, K, and guano fertilizer to the Inceptisol Jatiningor soil. – Jurnal Kultivasi 16(2): 333-339. (In Indonesian).
- [71] Widiastuti, E., Latifah, E. (2016): Keragaan Pertumbuhan dan Biomassa Varietas Kedelai (*Glycine max* (L)) di Lahan Sawah dengan Aplikasi Pupuk Organik Cair. – Jurnal Ilmu Pertanian Indonesia (JIPI) 21(2): 90-97. ISSN 0853-4217. <http://journal.ipb.ac.id/index.php/JIPI>. EISSN 2443-3462. DOI: 10.18343/jipi.21.2.90.
- [72] Wijanarko, A., Taufiq, A., Harnowo, D. (2016): Effect of liming, manure, and NPK fertilizer application on growth and yield performance of soybean in swamp land. – Journal of degraded and mining lands management 3(2): 527-533. ISSN:2339-076X. DOI:10.15243/jdmlm.2016.032.527.
- [73] Yuniarti, A., Damayan, M., Mustika Nur, D. (2019): Efek pupuk organik dan pupuk NKP terhadap C-organik, N-total, C/N, serta hasil padi hitam pada Inceptisols. – Jurnal Pertanian Presisi 3(2): 90-105. <https://doi.org/10.35760/jpp.2019.v3i2.2205>.

STUDY ON DEGRADATION MECHANISM OF CORN STRAW BY DIFFERENT FUNGI IN NON-SOIL ENVIRONMENT

ZHANG, Y. F. – DOU, S.* – ZHANG, D. D. – NDZELU, B. S. – MA, R. – YE, S. F.

*College of Resource and Environmental Science, Jilin Agricultural University
Changchun 130118, Jilin Province, China*

**Corresponding author
e-mail: dousen1959@126.com*

(Received 18th Feb 2022; accepted 20th May 2022)

Abstract. Studies on optimizing the best composting conditions using microorganisms producing enzymes have a long history, yet few studies have emphasized the similarities and differences in the decomposition mechanisms of different fungi during the same conditions in non-soil environments. The degradation and transformation of corn straw treated with three different fungi (*Trichoderma reesei*, *Phanerochaete chrysosporium* and *Trichoderma harzianum*) under 25-day solid-state aerobic composting was investigated, including total organic carbon (TOC) and C/N ratios, lignocellulose, enzyme activities and scanning electron microscope (SEM) observation. The present study illustrated that under the same non-soil environment, *T. reesei* had the best general degradation and utilization ability among the three fungi, with a cumulative TOC consumption of 58.5 g·kg⁻¹ in 25 days and a cumulative decrease of 5.8 in C/N. *T. reesei* and *P. chrysosporium* were more suitable for further exploration of the mechanism of corn straw degradation and transformation in soil environment than *T. harzianum*.

Keywords: total organic carbon, *Trichoderma reesei*, *Phanerochaete chrysosporium*, *Trichoderma harzianum*, C/N ratio

Introduction

Corn straw is composed of 25-35% cellulose, 20-40% hemicellulose, and 10-25% lignin (Martinez et al., 2004), which are chemically bonded and entangled to form a plant cell wall harsh to degrade (Heck et al., 2002; Sánchez, 2009). With vigorous agricultural activity, a large amount of corn straws is produced annually as relatively redundant agricultural waste. The Food and Agriculture Organization of the United Nations (FAO) estimates that one-third of all food produced is lost or wasted (Hebrok and Boks, 2017; Salihoglu et al., 2017). Hence reasonable organic waste management has become a global environmental challenge, especially in developing countries (Guo et al., 2016; Onwosi et al., 2017). Methods for better use of corn straw have become a research hotspot. Straw returning has been shown to be an effective means to improve soil fertility and manage crop residues. However, the decomposition process of straw residues when directly returned to the field is slow and is affected by soil microorganisms, enzymes, soil texture, and pH. As a result, several physical, chemical, and biological technologies to treat corn straw have been developed to achieve a beneficial use of this ubiquitous waste product (Guo et al., 2013; Wang et al., 2015; Zou et al., 2016). Solid-state aerobic composting is regarded as an efficient utilization method under non-soil environment, which involves the process of degrading and transforming the straw organic matter through microbial intervention under optimized physical and chemical conditions. The process consists of both organic matter mineralization and humification (formation of Humic substances). The final product of

composting can be used as an organic fertilizer and soil improver (Maeda et al., 2010; Jurado et al., 2015).

Fungi are the predominant micro-organisms that degrade lignocellulose, and the efficiency and rate of fungal degradation of corn straw is generally much higher than that of bacteria. In the common ecological concept, the selection of organisms that increases the intrinsic growth rate is called r-selection; the selection of organisms that is conducive to the increase of competitiveness is called K-selection (Pianka, 1970; Blagodatskaya et al., 2007). K-strategists can degrade complex insoluble organic substances due to the diversity of metabolic pathways, providing the minimal substrate flux necessary for slow growth. In the soil environment, fungi that are K-strategic microorganisms mainly decompose refractory organic matter, while bacteria that are r-strategic microorganisms prefer to use active organic matter (Dorodnikov et al., 2009; Grover et al., 2015). Fungi are also more susceptible to decomposition and therefore contribute more to soil organic matter. The mechanism of fungal degradation of lignocellulose is mainly due to two mechanisms: (i) production of extracellular enzymes by the fungi, and (ii) mechanical perforation of the straw by the fungal hyphae which facilitate the decomposition. Studying the use of fungi in corn straw can achieve maximum utilization benefits and value. *Trichoderma* is a genus that secretes and forms cellulase systems that researchers know best so far (Vijai et al., 2014). *Trichoderma reesei* (*T. reesei*) has been investigated in the degradation of cellulose from renewable substrates such as spruce, bagasse, waste paper, cow dung, and willow (Shin et al., 2000; Sørensen et al., 2014; Sukumarana et al., 2009; Wen et al., 2005). Tangnu et al. (1981) did not find changes of cellulase yield and final yield of *T. reesei* in the pH range of 4-6. Xia and Cen (1999), Latifian et al. (2007) also reported similar phenomena about *T. reesei* MCG77. But for filamentous fungi, the optimal pH of exoglucanase and β - glucosidase is 5-6 (Prasetyo et al., 2009). Li et al. (2013) found that 5.0 was the best pH of *T. reesei* for hyphal branching and cellulase production. Nazanin et al. (2018) found that the enzyme activity of *T. reesei* was the highest at 30 °C. *Trichoderma harzianum* (*T. harzianum*) is also the most widely used fungus of the genus *Trichoderma*. The optimal growth temperature of *T. harzianum* proposed by Zhang and Yang (2015) is 30 °C. Compared with *T. reesei*, some *T. harzianum* strains produced a cellulolytic complex with higher β -glucosidase and endoglucanases activities, and the xylanase activity of some *T. harzianum* strains was higher than *T. reesei*. However, the efficiency of simultaneous cellulose and hemicellulose hydrolysis by the secretome of *T. harzianum* was still low (Hu et al., 2014; Zhao et al., 2016). Castro et al. (2010) reported endoglucanase and cellulase activities and demonstrated that cellulose degradation occurred within 72 h under 30 °C when bagasse was pre-treated with *T. harzianum* IOC-3844. Paz et al. (2018) observed that *T. harzianum* EM0925 growing on corn stalk had high content of lignocellulosic enzymes and high capacity of producing enzymes without any additives. Zhang et al. (2020b) found that the cellulase activity and xylanase activity of *T. harzianum* had the highest relative activities at pH = 5. *Phanerochaete chrysosporium* (*P. chrysosporium*) is a fungal species capable of degrading lignin by excreting extracellular oxidases such as lignin peroxidase (LiP), manganese peroxidase (MnP), and lactase (Lac) (Law et al., 2003; Tamagawa et al., 2005; Bak et al., 2009; Lin et al., 2015). Rodríguez et al. (2012) used outside and inside corn cob to study ligninolytic enzymes produced by *P. chrysosporium* ATCC 24725 during solid state fermentation conditions (pH 4.5-5) and achieved a maximum MnP activity of 96

U·L⁻¹. It was the optimum value for the growth of oxidin peroxidase by *P. chrysosporium* when the pH was 4.5-5 (Aksu and Donmez, 2003; Cetin and Donmez, 2006; Liu et al., 2015). Zhang et al. (2019a) showed that the metabolism of *P. chrysosporium* was more effectively promoted at 30 °C.

Studies on optimizing the best composting conditions using pure microbial producing enzymes have a long history, but few studies have emphasized the similarities and differences in the decomposition mechanisms of different fungi during the same condition in non-soil environments. This work reports choosing *T. reesei*, *P. chrysosporium*, and *T. harzianum* to determine the similarities and differences in the decomposition mechanism of corn straw in non-soil environments. Through the background investigation of three kinds of fungi, we found and chose the common best condition (pH = 5, temp = 30 °C) to compare the degradation differences of three kinds of fungi on corn straw. It promotes the further screening of strains that can effectively transform corn straw and provides a theoretical basis for future applications in the soil environment.

Materials and methods

Site description and corn straw sampling

The sampling site of corn straw (N43°48'43.5", E125°23'38.50") presented by maize cropland located in Jilin Agricultural University, Nangan District, Changchun City, Jilin Province, China. The area is in a temperate continental semi-humid region and receives a mean annual rainfall of 618 mm, a mean annual relative air humidity of 68%, and an average annual temperature of 5.1 °C. The highest average temperature of 23.1 °C occurs in July and August, while the lowest average temperature of -10.6 °C occurs in November and December. Black soils (Chinese Soil taxonomy) is the main soil in the region and is classified as Argiudolls by the United States Department of Agricultural Soil Taxonomy (Soil Survey Staff, 2014).

The corn cultivar Zhongjin 368 type (Beijing Golden Grain Seed Co., Ltd.), was planted at the end of April 2016 and harvested in early October. The basic properties of the corn straw are shown in *Table 1*. After the harvest, the whole corn straw was naturally dried and cut into 0.5 cm segments.

Table 1. Basic properties of corn straw

Organic material	Total organic carbon (g.kg ⁻¹)	Total nitrogen (g.kg ⁻¹)	Total phosphorus (g.kg ⁻¹)	Total potassium (g.kg ⁻¹)	C/N ratio (mol)
Corn straw	376.4	7.22	7.7	4.5	60.8

Preparation of microorganisms and microbiological liquid

Three fungal strains used in this study: *T. reesei* MCG77, *P. chrysosporium* ATCC 24725 were purchased from the American Type Culture Collection (ATCC). The *T. harzianum* was isolated and purified from fresh soil at the Jilin Agricultural University experimental field after one year of straw returning (Provided by The Microbial laboratory of Environment and Resource Department, Jilin Agricultural University).

The three strains of fungi were placed in a solid bevel tube containing 30 ml of potato dextrose agar (PDA). The solid bevel tube was incubated at 28 °C for 72 h to obtain mature microbial spores (mycelium). The method for preparing a spore solution was given the same as Zhang et al. (2020a). The concentration was calculated through a haemocytometer and diluted to a final concentration of 1×10^7 CFU mL⁻¹. The spore suspension was transferred to a liquid medium considering a ratio of 1:10. The culture was incubated at 30 °C and 100 rpm for six days. PDA medium: potato (peeled, 200 g·L⁻¹) boiled for 30 min and filtered; glucose: 20 g·L⁻¹; agar: 20 g·L⁻¹. Liquid medium: potato (peeled, 200 g·L⁻¹) boiled for 30 min and filtered; glucose: 20 g·L⁻¹.

Solid-state fermentation

This fermentation was conducted in a BIOTECH-30SS solid fermentation tank (Shanghai Baoxing Biological Engineering Equipment Co., Ltd). This tank has a volume of 30 L, a sterilizing function, automatic stirring, controlled humidity and temperature, and air intake. A KQ-C type automatic steam generator (Shanghai Fengxian Xiexinji Power Plant) was used to generate steam for sterilization.

Prior to the fermentation, 1.5 kg of corn straw powder (segments size = 0.5 cm) was sterilized in the solid fermenter. The sterilization was conditioned at 121 °C for 25 min. After the sterilization, the microbial liquid containing the spore mycelia (0.6 L) and the mineral salt solution (3.75 L) were mixed. The fermentation was set at 30 °C, 60% humidity and 6.0 rpm.

Corn straw was inoculated with: (i) *Phanerochaete chrysosporium* (*P. chrysosporium*), (ii) *Trichoderma harzianum* (*T. harzianum*), (iii) *Trichoderma reesei* (*T. reesei*), and (iv) un-inoculated corn straw (CK). The CK treatment was prepared without microbial inoculation on corn straw and designated as a control.

The mineral salt solution contained at a final pH of 5 was prepared by adding: urea 4.2 g·L⁻¹, ammonium sulfate 19.6 g·L⁻¹, calcium chloride 0.028 g·L⁻¹, potassium dihydrogen phosphate 28 g·L⁻¹, magnesium sulfate 4.2 g·L⁻¹, ferrous sulfate 0.07 g·L⁻¹, manganese sulfate 0.021 g·L⁻¹, zinc sulfate 0.019 g·L⁻¹, cobalt chloride 4.2 g·L⁻¹, and yeast extract 7 g·L⁻¹.

Sample collection

The samples were homogenously mixed before the fermentation process. The experiment was performed in triplicates: 3 samples per treatment were collected from the fermenter from three random positions every day. At each sampling, the straw and the liquid were uniformly mixed. The monitoring lasted for 25 days with the samples analysed separately. The fermentation process was performed under the same experimental condition for each treatment.

Analytical methods

Scanning electron microscope observation

A small amount of straw residues sample was taken and fixed on the sample stage with conductive double-sided tape, and gold plating was performed under vacuumed conditions. After forming a conductive film on the surface of the material, the samples of corn straw residues were observed by scanning electron microscope (SEM, SHIMADZU S-550, operating voltage: 15 kV).

Measuring residual rates of corn straw

To determine the water content of straw fermentation products, an empty aluminium box was placed in Oven at 105 °C for 30 min. After cooling, the mass of the empty box was recorded. Three parallel samples were then weighed from the mixture up to 5 g each (~0.01 g). The sample was added to the aluminium box and the combined weight was recorded. The aluminium box with the sample was then placed in an oven at 85 °C. The mixture was placed in a desiccator, cooled for 20 min, and weighed again. The straw residual rate (*n*%) was calculated as follows:

$m_{n(\text{dry})}$: mass of the sample and the aluminium box after drying (g) during the *n*th day.

$m_{n(\text{box})}$: mass of aluminium box (g) during the *n*th day.

The dry weight of the *n*th day was measured and recorded as R_n :

$$R_n = m_{n(\text{dry})} - m_{n(\text{box})} \quad (\text{Eq.1})$$

The straw residual rate of the *n*th day was measured and recorded as *n*%:

$$n\% = R_n / R_0 \times 100\% \quad (\text{Eq.2})$$

TOC (total organic carbon) content and C/N ratios of corn straw residues

Weighed 0.25 g of dried (55 °C for 6 h) and fine ground corn straw sieved at 0.25 mm. The TOC content was determined using the potassium dichromate volumetric method (Lu, 2000).

The elemental composition of the residue of the straw after solid-state fermentation was analysed using an Elemental Vario EL III elemental analyser from Germany in the C/H/N mode. The contents of C, and N elements were measured. The C/N ratio was calculated based on the result of element composition as follows:

$$C/N = C(\text{g} \cdot \text{kg}^{-1}) / N(\text{g} \cdot \text{kg}^{-1}) \quad (\text{Eq.3})$$

Determination of lignin and cellulose in corn straw

The determination of straw cellulose and lignin content was based on Sluiter's work (Sluiter et al., 2008). Exactly, 0.3 g sample was digested with 3 mL of 72% H₂SO₄ and heated at 30 °C for 1 h. The mixture was then transferred to a 500 mL reagent bottle, and 84 mL of deionized water was added. The mixture was then sterilized in an autoclave at 121 °C for 1 h. The solution was filtered using vacuum filtration and the residue weight and glucose content were measured. The cellulose and lignin contents were calculated using the formula described by Anuradha and Valli (2011).

Determination of enzyme activity

Determination of cellulase activity: a Whatman filter paper (6 × 1 cm) was folded and put into the bottom of a sterile test tube, added into which 1 mL of citrate buffer (pH = 4.8). 0.5 mL diluted spore suspension was then added following five different concentrations: 0.04, 0.05, 0.057, 0.1, 0.2 g·mL⁻¹. After 60 min at 50 °C, added 3 mL of 3,5-dinitrosalicylic acid (DNS), added, thereafter, the mixture was heated in a boiling

water bath for 5 min, then cooled immediately. 200 μL of the above solutions were diluted afterwards with 2.5 mL deionized (DI) water. Absorbance was measured on a visible spectrophotometer (SP-722E) at OD540, and the glucose content was calculated according to the NREL method (Sluiter et al., 2008). The ratio of 0.37 corresponding to the enzyme concentration, releasing 2 mg glucose, is defined as the cellulase activity (Ghose et al., 1987).

Determination of xylanase activity: 1.0 g of xylan (Production company is Sigma, level is AR) was dissolved into 80 mL of 50 mM citrate buffer (pH = 4.8), balanced at 60 °C water bath for 1 h, then transferred to another water bath at 100 °C until boiling. The mixture was homogenized using magnetic stirrer during the cooling process. The solution was left overnight and then refilled with citrate buffer (pH = 4.8) to 100 mL to prepare xylan stock with concentration 10 $\text{mg}\cdot\text{mL}^{-1}$. Stored it at 4 °C up to one week. After a week, 1.8 mL of the stocked xylan and 200 μL of fermented sample solution was diluted to 1:10 with deionized water, where pipettes into 15 mL test tube, and then placed in a water bath at 50 °C for 5 min. Exactly, 3.0 mL of DNS reagent was added into the test tube, boiled for another 5 min, and then cooled immediately. Absorbance was measured at OD540. The amount of enzyme to produce 1.0 μmol xylose per minute was defined as a unit of xylanase activity (Bailey et al., 1992).

The β -glucosidase activity was measured by cellobiose method. 200 μL fermented sample solution was diluted to 1:200 with citrate buffer (pH = 4.8). 1.0 mL of the above solution and 1.0 mL of 15 $\text{mmol}\cdot\text{L}^{-1}$ cellobiose were pipette into a sterile centrifuge tube, then placed in a water bath at 50 °C for 30 min, and then transferred to 100 °C water bath for 5 min. The tube was then removed and cooled. The mixed solution was used to measure glucose content with a glucose kit (Huili Biotech, China). Another 1.0 mL of the diluted sample solution and added 1.0 mL of citrate buffer into a sterile centrifuge tube as an enzyme blank. The ratio of the corresponding enzyme concentration to 0.0926 when the glucose content in the sample is 1 $\text{mg}\cdot\text{mL}^{-1}$ was defined as the glucosidase activity. For details, see the previous report (Anuradha and Valli, 2011).

Determination of the total fungal content

The fungal quantity was measured on the samples at 0 d, 5 d, 10 d, 15 d, 20 d, and 25 d after the start of the culture in each group. Weigh 10 g of each sample to be tested and put it in 90 mL of sterile water. After shaking and culturing for 20 min, shake thoroughly for 15-20 min, leave it for 30 min, and separate the suspension into layers. The dilution coating plate counting method was based on Pitt and Hocking (2009). Total fungal counts were expressed as colony forming units per gram (CFU g^{-1}).

Data processing

Microsoft Office Excel 2017 was used for data analysis and processing. Mean values and standard deviations of triplicate measurements were reported in this study. Significant differences among treatment means were evaluated using the least significant difference test with TUKEYs adjustment at $P < 0.05$. The SPSS 19 for Windows® software (IBM Corp., Armonk, NY, USA) was used for all statistical analysis. The figures were drawn using the Origin 2019b software.

Results

Scanning electron microscope (SEM) observation of the corn straw after different treatments

Figure 1 shows the Scanning Electron Microscopy results of corn straw residues of different treatments in solid-state aerobic composting for 25 days (O: Original corn straw; A: CK; B: *T. reesei*; C: *T. harzianum*; D: *P. chrysosporium*). The surface of untreated corn straw was smooth and free of fungi (Fig. 1O). In SEM observation of the treated corn straw residue, due to the invasion of fungi, the original structure on the surface of the corn straw was destroyed in a large area, and many cracks appeared. These filamentous fungi mechanically attacked and swelled corn straw, invaded the interior through narrow cracks, and eventually decomposed the straw. Fungi can be distributed in communities to participate in decomposition. CK (Fig. 1A) treatment still maintained the original shape of the straw, and no obvious mechanical damage was observed. The corn straw treated by *T. reesei* (Fig. 1B) was severely damaged both in internal and external; *T. harzianum* (Fig. 1C) damaged the surface of the corn straw to a certain extent, but the erosion of the internal structure is not apparent; *P. chrysosporium* (Fig. 1D) penetrated the external pores of corn straw and destroyed its internal structure.

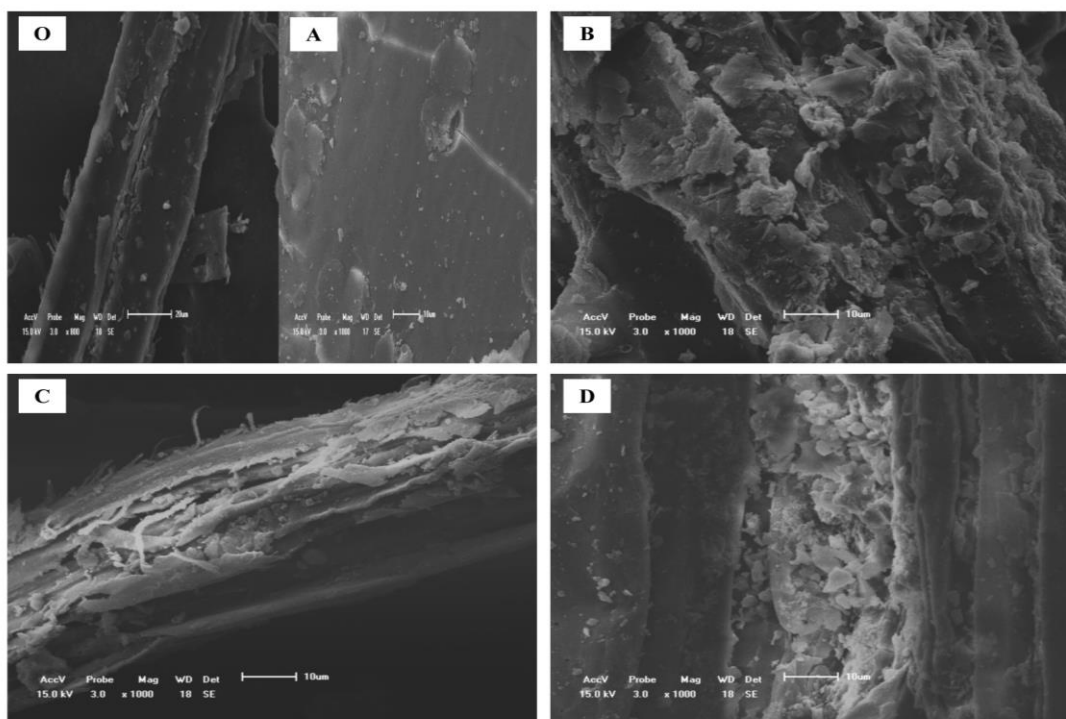


Figure 1. Electron microscopy results of corn straw residues under different treatments in a solid-state aerobic composting for 25 days. The treatments represented by the capital letters in the figure are as follows: O: Original corn straw; A: CK, B: *T. reesei*; C: *T. harzianum*; D: *P. chrysosporium*

Dynamic changes of residual rates

The residual rate of the straw residues gradually decreased with fermentation time regardless of treatments (Fig. 2). The most significant reduction in water was noted for

the *T. reesei* treatment on 16-20 d, with an average reduction of 1.66% per day and residual rate of $78.6 \pm 0.77\%$ at 25 d (Fig. 2). The *P. chrysosporium* and *T. harzianum* were completely fermented by 13-16 d in which a significant decrease was observed by respectively 1.31% and 1.16% per day. CK treatment decreased slowly throughout the entire culture process, with an average reduction of 0.31% per day. At the end of the fermentation, the total weight loss of straw under the four treatments can be ordered as the following: *T. reesei* > *P. chrysosporium* > *T. harzianum* > CK (Fig. 2). The straw residue rates were respectively $78.6 \pm 0.8\%$, $84.6 \pm 0.8\%$, $86.1 \pm 1.7\%$, and $92.2 \pm 1.2\%$. (Notes: Number of technical replications is three.)

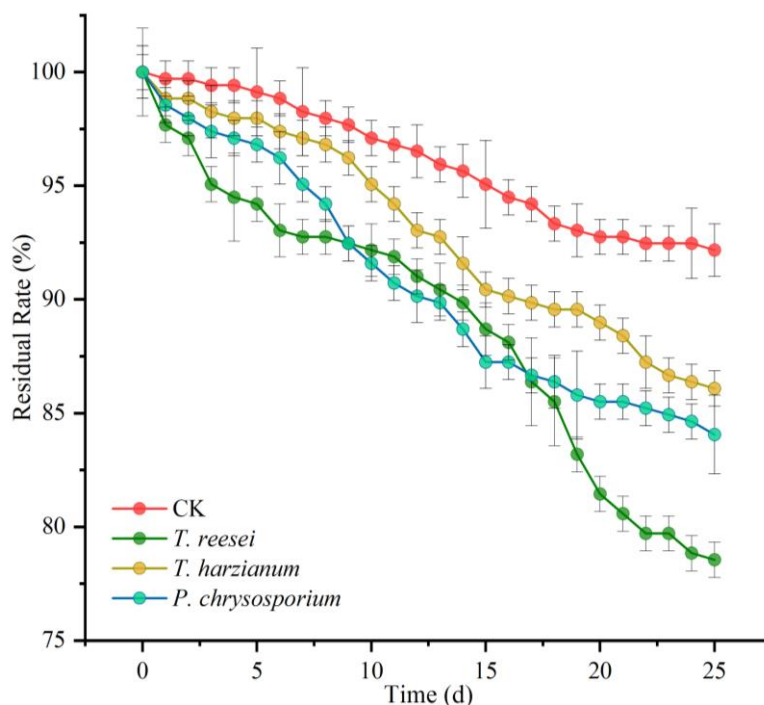


Figure 2. The corn straw residual rates of different treatments over time under solid-state aerobic composting. Results are means \pm SD ($n = 3$) on every single time-point

Changes of total organic carbon and C/N ratios in corn straw residues

TOC and C/N ratio are essential indicators to characterize the degradation and transformation of corn straw (Bernal et al., 1998; Bertoldi et al., 1983). Through Figure 3 we can observe the degradation and transformation of corn straw by different treatments during the 0-25 days. According to the statistics of the TOC distribution of different treatments, it showed that TOC of CK treatment was almost unchanged, always concentrated at $370 \text{ g}\cdot\text{kg}^{-1}$; TOC of *T. reesei* treatment in 5-25 days were all lower than $350 \text{ g}\cdot\text{kg}^{-1}$; *T. harzianum* and *P. chrysosporium* treatments had similar distributions, with TOC concentrated between $340 \text{ g}\cdot\text{kg}^{-1}$ and $370 \text{ g}\cdot\text{kg}^{-1}$, respectively. According to the statistics of the distribution of C/N ratios of different treatments, it showed that the distribution of CK treatment was concentrated at 24-26, with a little change. The C/N ratios of *T. reesei* after 10 d were all lower than 22; and the C/N ratio of *P. chrysosporium* treatment had a more significant decline than *T. harzianum*. The TOC and C/N ratios of the corn straw under the three fungal treatments gradually

decreased with the duration in fermentation time. The *T. reesei* had the best ability to reduce TOC and C/N in the four treatments. While, *P. chrysosporium* showed a stronger ability to degrade corn straw TOC than *T. harzianum*.

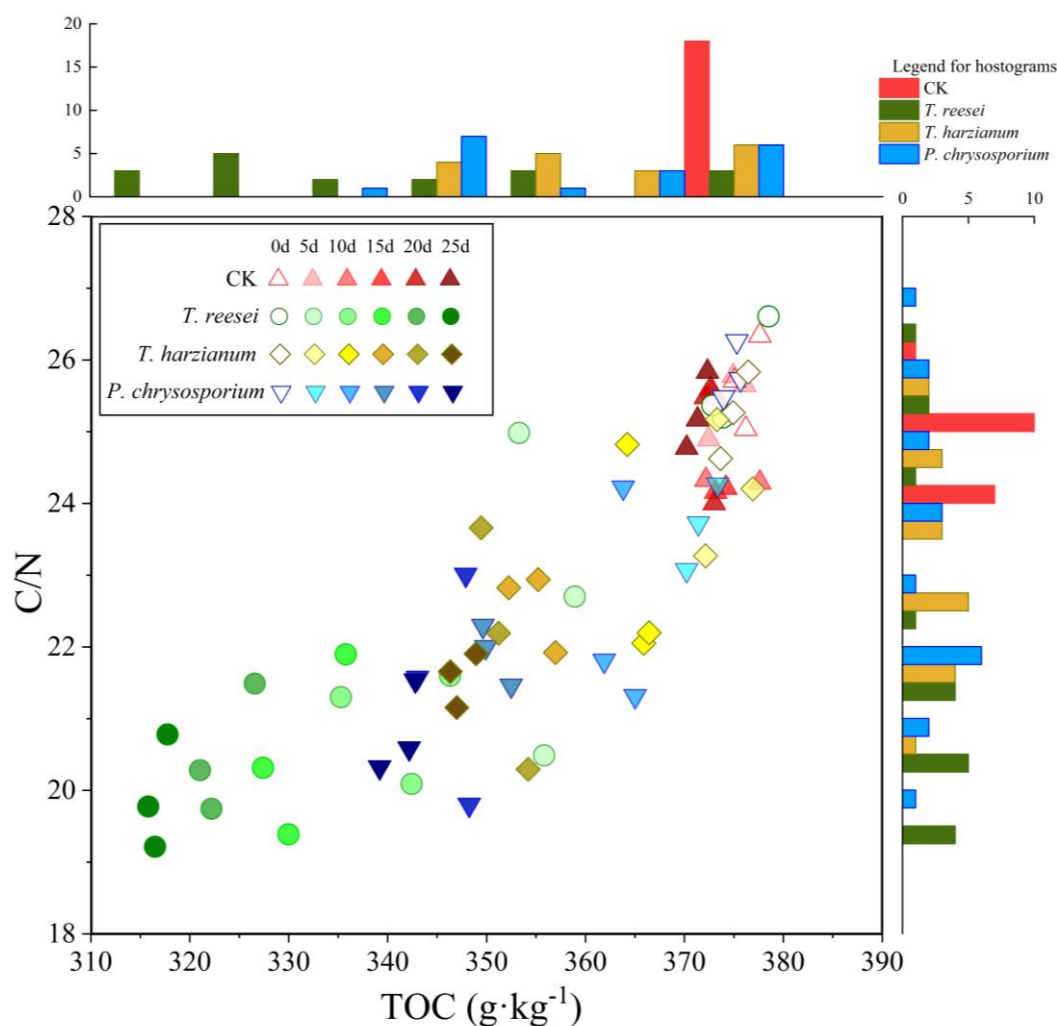


Figure 3. The TOC contents and C/N ratios of corn straw treated by different treatments over the course of the solid-state aerobic composting. The upper histogram shows the data amounts of different treatments in different TOC content ranges. The histogram on the right shows the data amounts of different treatments in different C/N ratios ranges

Cumulative degradation rates of cellulose and lignin

The cumulative degradation rates of cellulose and lignin of corn straw treated by different fungi are shown in Figure 4. The degradation of CK treatment was far poorer than that of the other three fungal treatments in 25 days, and its cellulose degradation was less than 5% with nearly no lignin degradation. In the treatments inoculated with fungi: The *T. reesei*'s cellulose showed the best degradation ability, and the cumulative degradation reached 70.28%; *T. harzianum*'s ability to degrade cellulose and lignin was at a medium level among the three fungi treatments; Lastly, the *P. chrysosporium* had the best lignin degradation ability, which can total 66.75%.

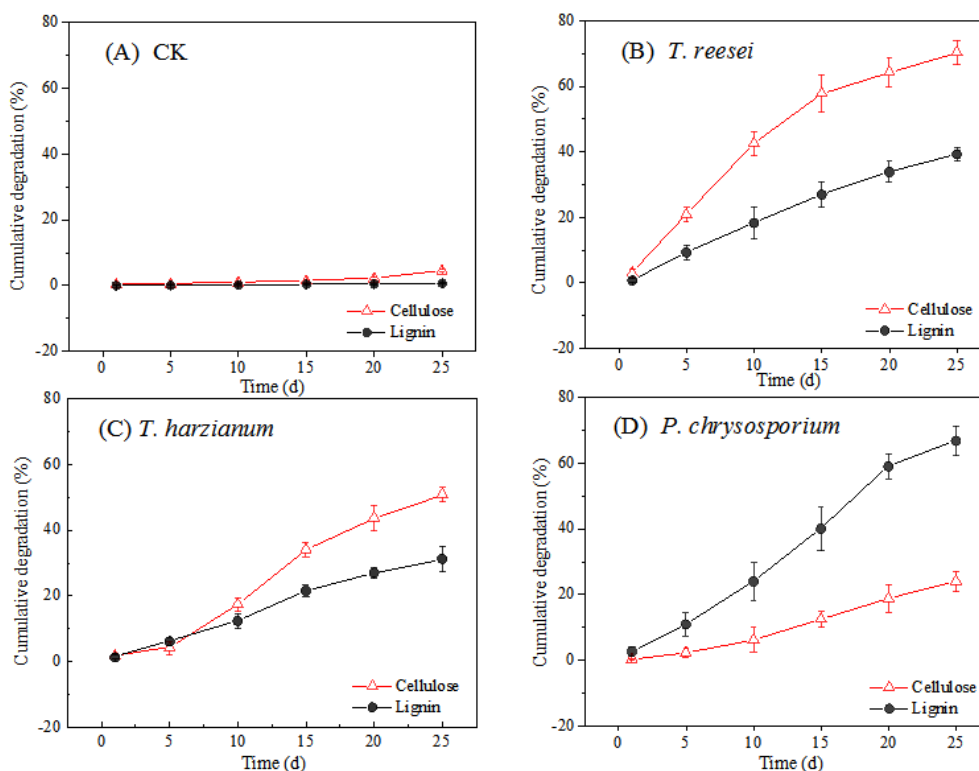


Figure 4. The changes in the cumulative degradation rates of cellulose and lignin under different treatments. Results are means \pm SD ($n = 3$) on every single time-point of each treatment. A: CK; B: *T. reesei*; C: *T. harzianum*; D: *P. chrysosporium*

Enzyme activity

Cellulase, xylanase, and β -glucosidase, which were produced by *T. reesei*, *P. chrysosporium* and *T. harzianum* during fermentation of corn straw are shown in Figure 5. Throughout the composting process the cellulase and β -glucosidase activities of *T. reesei* were much higher than those of *P. chrysosporium* and *T. harzianum*. However, the xylanase activity of *T. reesei* was just slightly higher than *P. chrysosporium* and *T. harzianum*.

The peak values under *T. reesei* of cellulase, xylanase, and β -glucosidase activities were respectively, $8.45 \text{ FPU}\cdot\text{mL}^{-1}$, $0.61 \text{ IU}\cdot\text{mL}^{-1}$, and $80.3 \text{ IU}\cdot\text{mL}^{-1}$. The peak values under of cellulase, xylanase, and β -glucosidase activities were $6.12 \text{ FPU}\cdot\text{mL}^{-1}$, $0.68 \text{ IU}\cdot\text{mL}^{-1}$, and $71.3 \text{ IU}\cdot\text{mL}^{-1}$, respectively. The peak values under *T. harzianum* of cellulase, xylanase, and β -glucosidase activities were $5.15 \text{ FPU}\cdot\text{mL}^{-1}$, $0.54 \text{ IU}\cdot\text{mL}^{-1}$, and $68.5 \text{ IU}\cdot\text{mL}^{-1}$, respectively.

Total fungal content

Figure 6 records the changes in the total fungal contents under different treatments during the 25-day solid-state aerobic composting. The fungal contents of *T. reesei* and *T. harzianum* before the 15th day was higher than that of *P. chrysosporium*. Among the treatments, *T. reesei* treatment peaked at $32.4 \pm 2.1 \text{ CFU}\cdot\text{g}^{-1}$ on the 5th day, and *T. harzianum* treatment peaked on the 10th day $27.2 \pm 2.1 \text{ CFU}\cdot\text{g}^{-1}$. At the 15th day, the *P. chrysosporium* reached a peak of $24.3 \pm 1.3 \text{ CFU}\cdot\text{g}^{-1}$, and exceeded the other two

treatments at the same time. In the whole process, the total fungal contents of *T. harzianum* were always lower than that of *T. reesei* (Fig. 6).

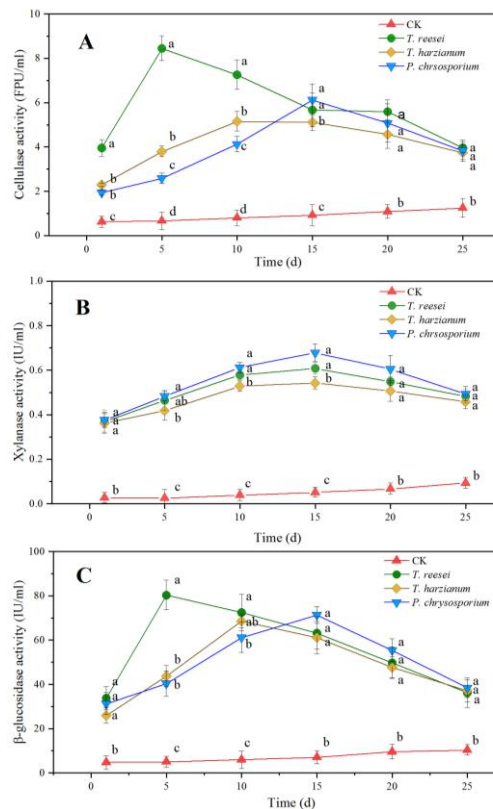


Figure 5. The activity changes of enzymes at different fermentation time. (a: cellulase; b: xylanase; c: β -glucosidase). Error bars represent the standard deviations of the mean ($n = 3$). Different lowercase letters mean significant differences ($P < 0.05$) among different treatments at the same time

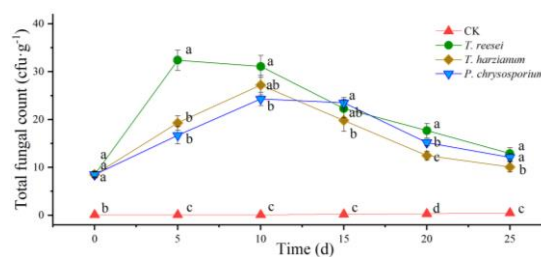


Figure 6. Total fungal counts of different time during 25-day solid-state aerobic composting. Error bars represent the standard deviations of the mean ($n = 3$). Different lowercase letters mean significant differences ($P < 0.05$) among different treatments at the same time

Discussion

In the early stages of cultivation, corn straw degradation rate was fast which is due to the expansion and growth of fungi's population (Fig. 6), and the subsequent increase of enzyme-producing content (Fig. 5), and the area of the matrix. As the substrates accumulate, the gap between the straws becomes smaller, the carbon source and

ventilation gradually decrease, which inhibits the growth (*Fig. 6*) of the strain to some extent. The decomposition rate of *T. reesei* increased quickly in the first 16 days, which may be due to the ability of *T. reesei* to destroy the substrate and multiply more effectively than the other two fungi, and the total fungal contents at 20-25 d were also the highest among the three treatments (*Fig. 6*). The results of the damage degree of corn straw by the four treatments observed by SEM (*Fig. 1*) were consistent with the results of residual rate (*Fig. 2*).

Generally, an initial carbon-to-nitrogen ratio of 25 to 30 is considered to be the best ratio for aerobic composting (Kumar et al., 2010; Silva et al., 2014). In this study, we adjusted the initial matrix C/N ratio to 25.8 by adding an exogenous N-containing mineral culture solution. Wu et al. (2017b) reported that an initial C/N ratio of 25 is favorable for the formation of high-quality and low-toxic compost. The C/N ratio of the three fungal treatments decreased significantly compared to the CK treatment (*Fig. 3*). This indicates that fungi utilized carbon as a source of energy, and it further proved that adding $\text{NH}_4^+ - \text{N}$ and $\text{NO}_3^- - \text{N}$ to the compost can supplement the depleted N source, stimulate the activity of microorganisms in time, and promote decomposition and transformation to form HS (Humic substances) precursor process (Wu et al., 2017a). The *T. reesei* treatment had the most obvious significant decrease in the C/N ratio during the whole composting process (*Fig. 3*), which is due to its nitrogen mineralization rate being lower than the carbon mineralization rate. The decomposition and utilization of TOC by *T. reesei* were much higher than the other two fungi. The degradation rate of organic carbon in corn straw during the fermentation process showed a tendency to first increase and then decrease. This may be related to the growth status of fungi (*Fig. 6*). Fungal microorganisms can to grow rapidly with straw as a carbon source in the early stages. During the late stages of fermentation, with the carbon source availability decreasing, the microbial enzyme activities gradually decrease, and the decomposition is slowed (Jiang et al., 2015). Notably, carbon sources play a crucial role in the production of enzymes since carbohydrates and their derivatives generate most cellulolytic enzymes (Adav et al., 2012). Among all treatments, the *T. reesei* was more effective in utilizing the carbon source in the straw, indicating that *T. reesei* can produce a large amount of degradable corn straw enzyme in the aerobic composting process (*Fig. 5*).

Lignin is the most challenging component to degrade and transform in corn straw. Under the same culture conditions in the present study, the degree of utilization of lignin components in corn straw by *P. chrysosporium* was much higher than that of the other two fungi (*Fig. 4*). This indicated that *P. chrysosporium* was more conducive in degrading lignin in corn straw residues. Several other studies have shown that inoculation of *P. chrysosporium* in mixed compost of sludge, straw and bran effectively promoted biodegradation of lignocellulose and encouraged the formation of HA (humic acid) (Zhang et al., 2018). Even so, the TOC content of *P. chrysosporium* treatment remained higher than that of *T. reesei* treatment at the end of the culture process. This indicated that during mineralization and decomposition of lignin components by *P. chrysosporium* corn straw derived-C was not entirely converted into CO_2 and moisture. Rather, other C sources (non-lignin) were synthesized or left undecomposed. These C sources may be lignin monomers, or other pure compounds (HS precursors) may have been synthesized by *P. chrysosporium*. Relevant studies have shown that *P. chrysosporium* can first crack the lignin and the C—O bond connected to the aromatic ring, split it into lignin monomer or small molecules of lignin (Wang et al., 2015). In the

theory of lignin (Stevenson, 1994), it has been described that HS is synthesized from compounds derived from lignin, which is the raw material and skeleton of HS precursors (Campitelli and Ceppi, 2008; Kulikowska, 2016). This may be the reason why TOC content of *P. chrysosporium* was still high at the end of composting, even though xylanase activity was high and the lignin content was low.

Among the three enzyme activities measured in this study (Fig. 5), the cellulase activity and β -glucosidase enzyme activity of *T. reesei* were the highest among all the treatments. When Lee et al. (2011) fermented 1:1 mixed bagasse and palm mash with *T. reesei*, they observed that the cellulase activity reached its highest level in 5 days. Similarly, Mekala et al. (2008) used bagasse as a substrate for *T. reesei* in the solid-state fermentation, and found that the cellulase activity peaked at 72 h. Furthermore, Zhao et al. (2011) used water hyacinth as a substrate for fermentation, and reported that the cellulase activity increased four-fold after 7 days of fermentation by *T. reesei*. From previous published research, it appears that cellulase activity reached the highest between 3 to 5 days. Our work also supports these results, and implies that *T. reesei* may adapt quickly into a new environment at the early stages. Although the cumulative degradation rates of lignin by *T. harzianum* was lower than the other two fungi in the early stages of fermentation (Fig. 4C), *T. harzianum* still had strong degradation ability of cellulose (Fig. 4C). In other studies, it was found that *T. harzianum* can use domestic sewage as a substrate to produce cellulase (Libardi et al., 2017). Similarly, Rocha et al. (2013) found that under optimal conditions, the cellulase and β -glucosidase activities of *T. harzianum* IOC-3844 reached the highest after 42 h. While both *Trichoderma* were more inclined to degrade cellulose, the xylanase activity of *T. reesei* was higher than that of *T. harzianum* (Fig. 5). Hu et al. (2014) and Zhao et al. (2016) had the similar results.

Even though the results of our study showed that the general degradation and utilization of *T. reesei* was the best among the three fungi. But, did *T. reesei* mineralize corn straw into simple compounds during the composting process? Does it synthesize substances such as HS? Although not tested in the present, previous related studies have shown that *T. reesei* can produce more HA in 8 days (Yang et al., 2019) and increase the relative HAL (humic acid -like) content in solid-state fermentation (Yang et al., 2019; Zhang et al., 2019b). It can be found from the results of this study that the decrease in TOC content under *T. reesei* at the first 0-10 d was much higher than that in the 10-25 d, and the C/N in 10-25 d also had a slower decline (Fig. 3). The reasons for this phenomenon are: on one hand, due to the slower growth and degradation of the C source itself, and the other important reason is that during the cultivation process, some fungal metabolites and fungal residues remain as N sources. In the culture substrate, the circulating input of the N source was maintained for the living fungi to use (Bernal et al., 2009; Jiang et al., 2015), thereby decreasing C/N ratio. Therefore, the residues produced by the fungi using corn straw have a potential for improving soil fertility and could be used as a soil conditioner.

Conclusion

Under the same non-soil environment and culture conditions, *T. reesei* and *T. harzianum* still maintained their preference for cellulose degradation and utilization, and the ability of *P. chrysosporium* to degrade lignin was more substantial. *T. reesei* had the best general degradation and utilization ability among the three fungi, with a cumulative

TOC consumption of 58.5 g·kg⁻¹ in 25 days and a cumulative decrease of 5.8 in C/N. In summary, we can infer that the comprehensive treatment capacity of fungi in corn straw is: *T. reesei* > *P. chrysosporium* > *T. harzianum* > CK. Indeed, *T. reesei* and *P. chrysosporium* were more conducive to the decomposition of corn straw than *T. harzianum*. The *T. reesei* and *P. chrysosporium* are more suitable for further exploration of the mechanism of corn straw degradation and transformation in soil environment.

Acknowledgements. The study was supported by the National Natural Science Foundation of China (42077022) and the Key Research and Development Program of Jilin Province (20200402098NC). We are very grateful to Jianying Zhou for her contribution to Data curation and Validation.

REFERENCES

- [1] Adav, S. S., Chao, L. T., Sze, S. K. (2012): Quantitative secretomic analysis of *Trichoderma reesei* strains reveals enzymatic composition for lignocellulosic biomass degradation. – *Molecular & Cellular Proteomics* 11: M111.012419.
- [2] Aksu, Z. and Donmez, G. (2003): A comparative study on the biosorption characteristics of some yeasts for Remazol blue reactive dye. – *Chemosphere* 50: 1070-1075.
- [3] Anuradha, J. S., Valli, N. C. (2011): Utilization of pretreated bagasse for the sustainable bioproduction of cellulase by *Aspergillus nidulans* MTCC344 using response surface methodology. – *Industrial Crops and Products* 34: 1564-1571.
- [4] Bailey, M. J., Biely, P., Poutanen, K. (1992): Interlaboratory testing of methods for assay of xylanase activity. – *Journal of Biotechnology* 23: 257-270.
- [5] Bak, J. S., Ko, J. K., Choi, I. G., Park, Y. C., Seo, J. H., Kim, K. H. (2009): Fungal pretreatment of lignocellulose by *Phanerochaete chrysosporium* to produce ethanol from rice straw. – *Biotechnology Bioengineering* 104(3): 471-482.
- [6] Bernal, M. P., Paredes, C., Sánchez-Monedero, M. A., Cegarra, J. (1998): Maturity and stability parameters of composts prepared with a wide range of organic wastes. – *Bioresource Technology* 63: 91-99.
- [7] Bernal, M. P., Alburquerque, J. A., Moral, R. (2009): Composting of animal manures and chemical criteria for compost maturity assessment. A review. – *Bioresource Technology* 100: 5444-5453.
- [8] Bertoldi, M. D., Vallini, G., Pera, A. (1983): The biology of composting: a review. – *Waste Management and Research* 1: 157-176.
- [9] Blagodatskaya, E. V., Blagodatsky, S. A., Anderson, T. H., Kuzyakov, Y. (2007): Priming effects in Chernozem induced by glucose and N in relation to microbial growth strategies. – *Applied Soil Ecology* 37: 95-105.
- [10] Campitelli, P., Ceppi, S. (2008): Effects of composting technologies on the chemical and physicochemical properties of humic acids. – *Geoderma* 144: 325-333.
- [11] Cetin, D., Donmez, G. (2006): Decolorization of reactive dyes by mixed cultures isolated from textile effluent under anaerobic conditions. – *Enzyme and Microbial Technology* 38: 926-930.
- [12] De Castro, A. M., Ferreira, M. C., Da Cruz, J. C., Pedro, K. C. N. R., Carvalho, D. F., Leite, S. G. F., Pereira, N. (2010): High-yield endoglucanase production by *Trichoderma harzianum* IOC-3844 cultivated in pretreated sugarcane mill by product. – *Enzyme Research* 2010(854526): 1-8.
- [13] Dorodnikov, M., Blagodatskaya, E., Blagodatsky, S., Fangmeier, A., Kuzyakov, Y. (2009): Stimulation of r- vs. K-selected microorganisms by elevated atmospheric CO₂ depends on soil aggregate size. – *FEMS Microbiology Ecology* 69: 43-52.
- [14] Ghose, T. K. (1987): Measurement of cellulase activities. – *Pure Applied Chemistry* 59: 257-268.

- [15] Grover, M., Maheswari, M., Desai, S., Gopinath, K. A., Venkateswarlu, B. (2015): Elevated CO₂: Plant associated microorganisms and carbon sequestration. – *Applied Soil Ecology* 95: 73-85.
- [16] Guo, H., Chang, J., Yin, Q., Wang, P., Lu, M., Wang, X., Dang, X. (2013): Effect of the combined physical and chemical treatments with microbial fermentation on corn straw degradation. – *Bioresource Technology* 48: 361-365.
- [17] Guo, X., Huang, J., Lu, Y., Shan, G., Li, Q. (2016): The influence of flue gas desulphurization gypsum additive on characteristics and evolution of humic substance during co-composting of dairy manure and sugarcane pressmud. – *Bioresource Technology* 219: 169-174.
- [18] Hebrok, M., Boks., C. (2017): Household food waste: drivers and potential intervention points for design - an extensive review. – *Journal of Cleaner Production* 151: 380-392.
- [19] Heck, J. X., Hertz, P. F., Ayub., M. A. Z. (2002): Cellulase and xylanase productions by isolated Amazon *Bacillus* strains using soybean industrial residue based solid-state cultivation. – *Brazilian Journal of Microbiology* 33: 213-218.
- [20] Hu, J., Arantes, V., Pribowo, A., Gourlay, K., Saddler., J. N. (2014): Substrate factors that influence the synergistic interaction of AA9 and cellulases during the enzymatic hydrolysis of biomass. – *Energy Environment Science* 7: 2308-2315.
- [21] Jiang, J., Liu, X., Huang, Y., Huang., H. (2015): Inoculation with nitrogen turnover bacterial agent appropriately increasing nitrogen and promoting maturity in pig manure composting. – *Waste Management* 39: 78-85.
- [22] Jurado, M. M., Suárez-Estrella, F., López, M. J., Vargas-García, M. C., López-González, J. A., Moreno, J. (2015): Enhanced turnover of organic matter fractions by microbial stimulation during lignocellulosic waste composting – *Bioresource Technology* 186: 15-24.
- [23] Kulikowska, D. (2016): Kinetics of organic matter removal and humification progress during sewage sludge composting. – *Waste Management* 49: 196-203.
- [24] Kumar, M., Ou, Y. L., Lin, J. G. (2010): Co-composting of green waste and food waste at low C/N ratio. – *Waste Management* 30: 602-609.
- [25] Latifian, M., Hamidiesfahani, Z., Barzegar, M. (2007): Evaluation of culture conditions for cellulase production by two *Trichoderma reesei* mutants under solid-state fermentation conditions. – *Bioresource Technology* 98: 3634-3637.
- [26] Law, W. M., Lau, W. N., Lo, K. L., Wai, L. M., Chiu., S. W. (2003): Removal of biocide pentachlorophenol in water system by the spent mushroom compost of *Pleurotus pulmonarius*. – *Chemosphere* 52: 1531-1537.
- [27] Lee, C. K., Darah, I., Ibrahim, C. O. (2011): Production and optimization of cellulase enzyme using *Aspergillus niger* USM AI 1 and comparison with *Trichoderma reesei* via solid state fermentation system. – *Biotechnology Research International*. <https://doi.org/10.4061/2011/658493>.
- [28] Li, C., Yang, Z., He, R., Zhang, C., Zhang, D., Chen, S., Ma., L. (2013): Effect of pH on cellulase production and morphology of *Trichoderma reesei* and the application in cellulosic material hydrolysis. – *Journal of Biotechnology* 168: 470-477.
- [29] Libardi, N., Soccol, C. R., Góes-Neto, A., De Oliveira, J., Vandenberghe, L. P. de S. (2017): Domestic wastewater as substrate for cellulase production by *Trichoderma harzianum*. – *Process Biochemistry* 57: 190-199.
- [30] Lin, B., Lyu, J., Lyu, X., Yu, H., Hu, Z., Lam, J. C. W., Lam, P. K. S. Characterization of cefalexin degradation capabilities of two *Pseudomonas* strains isolated from activated sludge. – *Journal of Hazardous Materials* 282: 158-164.
- [31] Liu, J., Song, Y., Liu, Y., Ruan, R. (2015): Fungal Pretreatment of Effluent from Piggery Anaerobic Digestion by *Phanerochaete chrysosporium*. – *CLEAN-Soil Air Water* 43: 1190-1196.
- [32] Lu, R. K. (2020): Analytical Methods for Soil and Agro-chemistry. – China Agricultural Science and Technology Press, Beijing (in Chinese).

- [33] Maeda, K., Hanajima, D., Morioka, R., Osada, T. (2010): Characterization and spatial distribution of bacterial communities within passively aerated cattle manure composting piles. – *Bioresource Technology* 101: 9631-9637.
- [34] Martinez, D., Larrondo, L. F., Putnam, N., Gelpke, M. D. S., Huang, K., Chapman, J., Helfenbein, K. G., Ramaiya, P., Detter, J. C., Larimer, F., Coutinho, P. M., Henrissat, B., Berka, R., Cullen, D., Rokhsar, D. (2004): Genome sequence of the lignocellulose degrading fungus *Phanerochaete chrysosporium* strain RP78. – *Nature Biotechnology* 22: 695-700.
- [35] Mekala, N. K., Singhania, R. R., Sukumaran, R. K., Pandey, A. (2008): Cellulase production under solid-state fermentation by *Trichoderma reesei* RUT C30: statistical optimization of process parameters. – *Applied Biochemistry and Biotechnology* 151: 122-131.
- [36] Nazanin, D., Zohreh, H. E., Parisa, H. (2018): Optimization of cellulase production under solid-state fermentation by a new mutant strain of *Trichoderma reesei*. – *Food Science and Nutrition* 7: 572-578.
- [37] Onwosi, C. O., Igbokwe, V. C., Odimba, J. N., Eke, I. E., Nwankwoala, M. O., Iroh, I. N., Ezeogu, L. I. (2017): Composting technology in waste stabilization: on the methods, challenges and future prospects. – *Journal of Environmental Management* 190: 140-157.
- [38] Paz, A., Outeirino, D., Perez, G. N., Domínguez, J. M. (2018): Enzymatic hydrolysis of brewer's spent grain to obtain fermentable sugars. – *Bioresource Technology* 275: 402-409.
- [39] Pianka, E. R. (1970): On r-and K-selection. – *American Naturalist* 104: 592-597.
- [40] Pitt, J. I., Hocking, A. D. (2009): *Fungi and Food Spoilage*. 3rd Ed. – Blackie Academic and Professional, London.
- [41] Prasetyo, J., Sumita, S., Okuda, N., Park, E. Y. (2009): Response of Cellulase Activity in pH-Controlled Cultures of the Filamentous Fungus *Acremonium cellulolyticus*. – *Applied Biochemistry Biotechnology* 16: 52-61.
- [42] Rocha, V. A. L., Maeda, R. N., Santa Anna, L. M. N., Pereira Jr, N. (2013): Sugarcane bagasse as feedstock for cellulase production by *Trichoderma harzianum* in optimized culture medium. – *Electronic Journal of Biotechnology* 16(5).
- [43] Rodríguez-Rodríguez, C. E., Jesús García-Galán, M., Blánquez, P., Díaz-Cruz, M. S., Barceló, D., Caminal, G., Vicent, T. (2012): Continuous degradation of a mixture of sulfonamides by *Trametes versicolor* and identification of metabolites from sulfapyridine and sulfathiazole. – *Journal of Hazardous Materials* 213-214: 347-354.
- [44] Salihoglu, G., Salihoglu, N. K., Ucaroglu, S., Banar, M. (2017): Food loss and waste management in Turkey. – *Bioresource Technology* 248: 88-99.
- [45] Sánchez, C. (2009): Lignocellulosic residues: biodegradation and bioconversion by fungi. – *Biotechnology Advances* 27: 185-194.
- [46] Shin, C. S., Lee, J. P., Lee, J. S., Park, S. C. (2000): Enzyme production of *Trichoderma reesei* rut C-30 on various lignocellulosic substrates. – *Applied Biochemistry Biotechnology* 84-86: 237-245.
- [47] Silva, M. E. F., de Lemos, L. T., Nunes, O. C., Cunha-Queda, A. C. (2014): Influence of the composition of the initial mixtures on the chemical composition, physicochemical properties and humic-like substances content of composts. – *Waste Management* 34: 21-27.
- [48] Sluiter, A., Hames, B., Ruiz, R., Scarlata, C., Sluiter, J., Templeton, D., Crocker, D. (2008): Determination of structural carbohydrates and lignin in biomass. Laboratory Analytical Procedure (LAP). – National Renewable Energy Laboratory (NREL), Denver.
- [49] Soil Survey Staff.: *Keys to Soil Taxonomy*. 12th Ed. – Natural Resources Conservation Service, USDA-Natural Resources Conservation Service, Washington, DC.
- [50] Sørensen, A., Andersen, J. J., Ahring, B. K., Teller, P. J., Lübeck, M. (2014): Screening of carbon sources for beta-glucosidase production by *Aspergillus saccharolyticus*. – *International Biodeterioration & Biodegradation* 93: 78-83.

- [51] Stevenson, F. J. (1994): Humus Chemistry: Genesis, Composition, Reactions. Second Ed. – John Wiley and Sons, New York.
- [52] Sukumarana, R. K., Singhania, R. R., Mathewa, G. M., Pandey, A. (2009): Cellulase production using biomass feed stock and its application in lignocellulose saccharification for bio-ethanol production. – Renewable Energy 34: 421-424.
- [53] Tamagawa, Y., Hirai, H., Kawai, S., Nishida, T. (2005): Removal of estrogenic activity of endocrine-disrupting genistein by ligninolytic enzymes from white rot fungi. – FEMS Microbiology Letters 244: 93-98.
- [54] Tangnu, S. K., Blanch, H. W., Wilke, C. R. (1981): Enhanced production of cellulase, hemicellulase, and β -glucosidase by *Trichoderma reesei* (Rut C-30). – Biotechnology and Bioengineering 23: 1837-1849.
- [55] Vijai, K. G., Monika, S., Alfredo, H. E., Upadhyay, R. S., Irina, D., Maria, G. T. (2014): Biotechnology and Biology of *Trichoderma*. – Elsevier's Science & Technology Rights Department, Oxford, UK.
- [56] Wang, W., Ling, H., Zhao, H. (2015): Steam explosion pretreatment of corn straw on xylose recovery and xylitol production using hydrolysate without detoxification. – Process Biochemistry 50: 1623-1628.
- [57] Wen, Z., Liao, W., Chen, S. (2005): Production of cellulase by *Trichoderma reesei* from dairy manure. – Bioresource Technology 96: 491-499.
- [58] Wu, J., Zhao, Y., Qi, H., Zhao, X., Yang, T., Du, Y., Zhang, H., Wei, Z. (2017a): Identifying the key factors that affect the formation of humic substance during different materials composting. – Bioresource Technology 244: 1193-1196.
- [59] Wu, S., Shen, Z., Yang, C., Zhou, Y., Li, X., Zeng, G., Ai, S., He, H. (2017b): Effects of C/N ratio and bulking agent on speciation of Zn and Cu and enzymatic activity during pig manure composting. – International Biodeterioration and Biodegradation 119: 429-436.
- [60] Xia, L., Cen, P. (1999): Cellulase production by solid state fermentation on lignocellulosic waste from the xylose industry. – Process Biochemistry. 34: 909-912.
- [61] Yang, Y., Wang, L., Zhang, Y., Li, L., Shi, X., Liu, X., Ren, X., Dou, S. (2019): Transformation of corn stalk residue to humus-like substances during solid-state fermentation. – Sustainability 11: 6771.
- [62] Zhang, J. D., Yang, Q. (2015): Optimization of solid-state fermentation conditions for *Trichoderma harzianum* using an orthogonal test. – Genetics and Molecular Research 14: 1771-1781.
- [63] Zhang, C., Xu, Y., Zhao, M., Rong, H., Zhang, K. (2018): Influence of inoculating white-rot fungi on organic matter transformations and mobility of heavy metals in sewage sludge based composting. – Journal of Hazardous Materials 344: 163-168.
- [64] Zhang, T., Cai, L., Xu, B., Li, X., Qiu, W., Fu, C., Zheng, C. (2019a): Sulfadiazine biodegradation by *Phanerochaete chrysosporium*: mechanism and degradation product identification. – Chemosphere 124418.
- [65] Zhang, Y., Dou, S., Ye, S., Zhang, D. (2019b): Specificity of humic acid-like (HAL) substance from *Trichoderma reesei* inoculated corn straw. – Journal of Agro-Environment Science 38: 2184-2192.
- [66] Zhang, Y., Dou, S., Hamza, B., Ye, S., Zhang, D. (2020a): Mechanisms of three fungal types on humic-like substances formation during solid-state fermentation of corn straw. – International Journal of Agriculture and Biology 24: 970-976.
- [67] Zhang, Y., Yang, J., Luo, L., Wang, E., Wang, R., Liu, L., Liu, J., Yuan, H. (2020b): Low-Cost Cellulase-Hemicellulase Mixture Secreted by *Trichoderma harzianum* EM0925 with Complete Saccharification Efficacy of Lignocellulose. – International Journal of Molecular Sciences 2020(21): 371.
- [68] Zhao, S. H., Liang, X. H., Hua, D. L., Ma, T. S., Zhang, H. B. (2011): High-yield cellulase production in solid-state fermentation by *Trichoderma reesei* SEMCC-3.217 using water hyacinth (*Eichhornia crassipes*). – African Journal of Biotechnology 10: 10178-10187.

- [69] Zhao, X., Xiong, L., Zhang, M., Bai, F. (2016): Towards efficient bioethanol production from agricultural and forestry residues: exploration of unique natural microorganisms in combination with advanced strain engineering. – *Bioresource Technology* 215: 84-91.
- [70] Zou, H., Ye, X., Li, J., Lu, J., Fan, Q., Yu, N., Zhang, Y., Dang, X., Zhang, Y. (2016): Effects of straw return in deep soils with urea addition on the soil organic carbon fractions in a semi-arid temperate cornfield – *PLoS One* 11: e0153214.

THE EFFECT OF DROUGHT STRESS ON THE GROWTH AND YIELD OF SOYBEAN (*GLYCINE MAX L.*)

AZIEZ, A. F.^{1*} – PRASETYO, A.¹ – PAIMAN²

¹*Department of Agrotechnology, Faculty of Agriculture, Universitas Tunas Pembangunan, Surakarta 57139, Indonesia*
(e-mail: agungpras17@gmail.com; phone: +62-858-6728-5000, +62-821-5705-0834)

²*Department of Agrotechnology, Faculty of Agriculture, Universitas PGRI Yogyakarta, Yogyakarta 55182, Indonesia*
(e-mail: paiman@upy.ac.id; phone: +62-813-2862-9000)

*Corresponding author

e-mail: achmad.aziez@lecture.utp.ac.id; phone: +62-858-6728-5000; fax: +62-271-739-048

(Received 19th Feb 2022; accepted 20th May 2022)

Abstract. Drought stress affects the growth and yield of soybean. Stunted growth will have an impact on yield. This study aims to determine the effect of drought stress on the growth characteristics and grain yield of soybean. This research uses a randomized complete block design (RCBD) and three replications. The first factor was soil moisture content consisting of four levels, i.e., 100%, 75%, 50%, and 25% field capacity. The second factor was the growth stage consisting of three kinds, i.e., the vegetative active, flowering, and seed filling stages. The results showed that soil moisture content below 75% field capacity reduced the leaf area index (LAI), leaf area duration (LAD), specific leaf area (SLA), net assimilation rate (NAR), crop growth rate (CGR), the seed weight per 100 seeds, and the weight of the seeds per plant. In seed filling stage is more sensitive to water shortages than the vegetative or flowering stages. At all stages of growth, a higher drought level equals a higher decrease in the soybean growth and yield. For future research, we suggest that soybean planting utilize 100% field capacity.

Keywords: field capacity, grain, growth analysis, growth phase, soil moisture

Introduction

Drought stress has significantly reduced agricultural productivity worldwide, including in soybean (*Glycine max* L.) seeds (Buezo et al., 2019). In Indonesia, soybeans are often grown as an intercropping plant after rice and are widely cultivated in times of drought. Soybean production during the dry season is constrained by limited water availability. Therefore, some or all stages of plant development are affected by drought.

Along with the increase in air temperature caused by global warming, drought also harms soybean production, decreasing seed yields (Daryanto et al., 2015). Ahmed et al. (2010) stated that the lack of water increased the canopy's root ratio to increase water utilization. Thu et al. (2014) found that roots were distributed to the topsoil zone if sufficient water was available. If not, roots would grow and develop in deeper soil.

In general, drought stress affected the vegetative and generative phases of plants and resulted in a yield decrease. The reproduction phase is sensitive to drought stress as it directly affects the flowering and pod filling stages (Hatfield et al., 2011). Ghassemi-Golezani et al. (2010) found that drought stress decreased the number of flowers and filled pods in the reproductive phase. The plant can not effectively distribute carbohydrates from leaves to pods, reducing the amount and size of produced seeds.

Alqudah et al. (2011) and Ozalkan et al. (2010) stated that the LAI, NAR, and CGR continued to increase until the pod filling stage. Over its entire vegetation period, chickpeas had a reduced LAD, specifically in their initial pod arrangement while their biomass increases. LAD positively correlated with the biomass and yield of chickpeas in Southern Spain (López-Bellido et al., 2008). In several varieties, Ozalkan et al. (2010) found that CGR was greater at the pod filling stage compared to earlier stages. Furthermore, Ozalkan et al. (2010) stated that the growth process, namely CGR, RGR, and NAR, directly affected economic gains, as seen in greater grain yields. In plants, researchers had identified development parameters such as optimum LAI and CGR during the flowering stage as the main determinants of yield (Baloch et al., 2006). The vegetative and generative growth stages of soybean consisted of emergence, first trifoliolate, second trifoliolate, third to fifth trifoliolate, sixth trifoliolate, beginning bloom, full bloom, beginning pod, full pod, beginning seed, full seed, beginning maturity, and full maturity (Nleya and Sexton, 2019).

Maleki et al. (2013) examined soybean plants undergoing drought stress treatment at various stages of growth in several varieties. The results showed that drought stress and variant significantly affected plant height, fertile pods, harvest index, oil, and protein percentages. Under drought stress, the seed filling and flowering stages showed the lowest production with a yield of 2,682 kg.ha⁻¹ and 2,918 kg.ha⁻¹, respectively. Luo et al. (2016) examined cotton plants in four growth phases given light and moderate water stress. The results showed that the water deficit significantly reduced leaf water potential, net photosynthetic rate, and stomatal conductance in cotton. In this study, there was no clear mention of moisture levels for mild or moderate stress.

Marchese et al. (2010) examined *Artemisia annua* L. plants with five water deficit treatments, namely irrigated, 14, 38, 62, 86 hours, and without irrigation. The results showed that water deficit limits plant growth but can trigger the accumulation of secondary metabolites. Water deficits of 38 and 62 hours increased leaf artemisinin content. However, only the 38-hour treatment caused a significant increase in leaf and plant artemisinin without negatively affecting plant biomass production. In a greenhouse study, Samarah et al. (2009) compared four wheat varieties with a soil moisture content of 75%, 50%, and 25% field capacity. This research did not attempt to determine the optimal moisture content for growth; it compared variants and their relation with drought and yield. Zulfiqar et al. (2020) studied two varieties of marigolds under the stress of 60% and 40% field capacity. The results showed that leaf thickness decreased at 40% field capacity and the Inca variety was more resistant than the Bonanza variety to water stress.

Sacita et al. (2018) researched two varieties in their vegetative and generative phases, with irrigation intervals of 2.5 and 10 days. The results showed that water stress in the vegetative stage had no significant effect on soybean production. Soybean plants adapt to water stress by reducing the leaf number, leaf area, and stomata openings and responding to a motion by folding the leaves.

Many previous studies examined the effect of drought stress on plant morphological characteristics and only a few examined the effect of drought stress on plant physiological characteristics, especially soybeans, and this physiological observation was only observed at harvest time. Research that has not been carried out is to examine drought stress on physiological characters and soybean yields at various growth stages. There has been no attempt to examine the effects of drought stress at various stages of growth on the growth characteristics and yield of soybean. This research will attempt to

determine the stage of soybean growth most affected by water stress which can impact soybean yield. Based on the description above, this research aims to determine the effect of drought stress on the growth characteristics and yield of soybean.

Materials and methods

Study area

The team conducted the research in a plastic house in Demangan, Sambu, Boyolali, Central Java, Indonesia, from August to November 2020 with alfisol soil. The Department of Food Crops Agriculture, Grobogan, Central Java, Indonesia provides soybean seeds with a drought-resistant variant of Grobogan. A geographical position was between 110° 22'-110° 50' east longitude and between 7°7'-7°36' south latitude with a height of 184 m above sea level (ASL). The average rainfall and temperature were 139 mm month⁻¹ and 26-32°C, respectively.

Experimental design

This research was arranged in a randomized completely block design (RCBD) with two factors and three replications. The first factor was soil moisture content consisting of four levels, i.e., 100%, 75%, 50%, and 25% field capacity. The second factor was the growth stage, which consisting of three kinds, i.e., the active vegetative, flowering, and pod filling stages. In this study, there were 12 treatment combinations. Each treatment combination was three times replications, and each replication consisting of four plant samples. Overall, the study required 144 polybags.

Research procedures

Before the research, the team conducted a chemical analysis of the soil used for the research substrate. The results showed an H₂O pH of 6.38 (slightly sour), C concentration of 3.60% (very high), organic matter concentration of 6.22% (very high), total N concentration of 0.15% (low), available P of 8.10 ppm (very high), available K of 0.79 me/100 g (high) and CEC value of 26.12 me/100 g (high).

The media used was 10 kg of alfisol soil and manure at a ratio of 1:1. After being prepared and mixed, the media filled a 35 × 35 cm polybag as a medium for soybean seeds. NPK Phonska and SP-36 fertilizers at a dose of 100 and 75 kg ha⁻¹, respectively, were applied at planting time and five weeks after planting.

The planting utilized a depth of 3 cm, with each polybag containing three soybean seeds. The selection process took 14 days selected one plant. Thinning was conducted 1 week after planting (WAP), leaving one plant per polybag. During the research, no weeds, pests, or diseases caused significant problems. Therefore, the team did not carry out control measures. According to the treatment, water application must reach a soil moisture content of 100%, 75%, 50%, and 25% field capacity by accounting for the growth stages, namely the active vegetative, flowering, and pod filling stages. Harvesting was conducted 90 days after planting (DAP).

Measurement

The parameters observed were the leaf area index (LAI), leaf area duration (LAD), specific leaf area (SLA), net assimilation rate (NAR), crop growth rate (CGR), and the weight of the seeds per plant. The data observation was conducted in 4, 6, 8, and 10

WAP. LAI was calculated from the ratio between the total leaf surface area per unit ground area. LAI was determined by the intensity of radiation intercepted divided planting spacing. LAD is the time a leaf could last on the plant. LAD was calculated from leaf area (cm²) divided by time (week).

NAR is the ability of plants to produce dry materials that assimilate each unit of leaf area at each unit of time, which is stated in *Eq. 1*.

$$\text{NAR} = \frac{W_2 - W_1}{t_2 - t_1} \times \frac{\ln LA_2 - \ln LA_1}{LA_2 - LA_1}, \text{ (in g.cm}^{-2}\text{.weeks}^{-1}\text{)} \quad (\text{Eq.1})$$

CGR is the ability of plants to produce dry materials that assimilate each unit of land area at each unit of time, which is stated in *Eq. 2*.

$$\text{CGR} = \frac{1}{G} \times \frac{W_2 - W_1}{t_2 - t_1}, \text{ (in g.m}^{-2}\text{.weeks}^{-1}\text{)} \quad (\text{Eq.2})$$

Description: W_1 = total dry weight per plant at the time of t_1 . W_2 = Total dry weight per plant at the time of t_2 . LA_1 = Total leaf area per plant at the beginning. LA_2 = Total leaf area per plant at the time of t_2 . G = the area of land overgrown with plants. t_1 = harvest time in the beginning. t_2 = harvest time in the end.

Statistical analysis

Observational data were analyzed using analysis of variance (ANOVA) with the SAS 9.1 program. If the treatment had a significant effect, then to know the difference between treatments was done using Duncan's new multiple range tests (DMRT) at 5% significance level (Gomez and Gomez, 1984).

Results

Analysis of variance

Based on the analysis of variance, there is an interaction between the level of drought and the growth rate on the parameters of LAI, LAD, NAR, SLA, CGR, at 4-6, 6-8, 8-10, and 10-12 WAP, the weight of 100 seeds and seeds per plant at harvest (*Table 1*).

Leaf area index

The ANOVA showed a significant interaction between soil moisture and growth rate on LAI at the ages of 4-6, 6-8, 8-10, and 10-12 WAP. The result of DMRT at 5% significant levels on the average LAI in ages of 4-6, 6-8, 8-10, and 10-12 WAP are shown in *Table 2*.

Leaf area duration

The ANOVA on LAD showed a significant interaction between soil moisture and growth rate at the ages of 4-6, 6-8, 8-10, and 10-12 WAP. The result of DMRT at 5% significant levels on the average LAD in ages of 4-6, 6-8, 8-10, and 10-12 WAP are shown in *Table 3*.

Table 1. Analysis of variance of all parameters

Parameter	Time observation (WAP)	Drought stress level (S)	Growth stage (G)	S x G
Leaf area index (LAI)	4-6	4.94**	0.67 ns	3.31 **
	6-8	9.86**	0.04 ns	3.18 **
	8-10	3.74*	0.30 ns	2.81 *
	10-12	9.33**	0.73 ns	4.89 **
Leaf area duration (LAD)	4-6	6.42 **	1.47 ns	3.90 **
	6-8	9.19 **	0.04 ns	2.46 *
	8-10	3.99 *	0.06 ns	3.05 *
	10-12	13.68 **	5.77 **	13.15 **
Specific Leaf Area (SLA)	4-6	3.83 *	0.19 ns	3.28 **
	6-8	3.34 *	0.19 ns	2.62 *
	8-10	2.58 ns	0.43 ns	3.08 *
	10-12	8.67 **	1.57 ns	5.48 **
Net assimilation rate (NAR)	4-6	3.02 *	0.14 ns	2.42 *
	6-8	4.27 *	0.13 ns	2.73 *
	8-10	2.77 *	0.08 ns	2.41 *
	10-12	5.46 **	0.22 ns	3.76 **
Crop Growth Rate (CGR)	4-6	5.15 **	0.73 ns	2.80 *
	6-8	4.81 **	0.29 ns	2.25 *
	8-10	5.05 **	0.29 ns	3.40 **
	10-12	2.39 ns	0.20 ns	2.24 *
Weight of 100 seeds	12	15.42 **	33.73 **	49.36 **
Seeds per plant	12	25.09 **	5.71 **	8.95 **

Note: ** = Significance at 1% significant levels, * = Significance at 5% significant levels, and ns = Non significant at 5%. WAP = week after planting

Table 2. LAI at various levels of drought and growth stages at 4-6, 6-8, 8-10, and 10-12 WAP

Soil moisture (% field capacity)	Growth stage	LAI			
		4-6 WAP	6-8 WAP	8-10 WAP	10-12 WAP
100	Active vegetative	0.75 ab	1.05 ac	1.20. b	0.88 ab
	Flowering	0.85 a	1.21 ab	1.24 ab	0.90 ab
	Seed filling	0.69 ab	1.34 a	1.34. a	0.95 a
75	Active vegetative	0.73 ab	1.04 a-c	1.26 ab	0.87 ab
	Flowering	0.70 ab	0.99 b-d	1.22 ab	0.86 ab
	Seed filling	0.70 ab	1.02 a-c	1.26 ab	0.90 ab
50	Active vegetative	0.59 b	0.87 b-d	1.22 ab	0.86 ab
	Flowering	0.61 b	0.86 b-d	1.20 b	0.83 bc
	Seed filling	0.72 ab	0.83 cd	1.15 bc	0.72 d
25	Active vegetative	0.63 ab	0.84 cd	1.23 ab	0.81 b-d
	Flowering	0.34 c	0.82 cd	1.15 bc	0.74 cd
	Seed filling	0.63 ab	0.67 d	1.06 c	0.71 d
Interaction treatments		(+)	(+)	(+)	(+)

Note: The numbers followed by the same characters in the same column indicate no significant difference based on DMRT at 5% significant levels. LAI = leaf area index WAP = week after planting

Table 3. LAD at various levels of drought and growth stages at 4-6, 6-8, 8-10, and 10-12 WAP

Soil moisture (% field capacity)	Growth stage	LAD ($cm^2 week^{-1}$)			
		4-6 WAP	6-8 WAP	8-10 WAP	10-12 WAP
100	Active vegetative	959 ab	1318 a-c	1258 b-d	1220 ab
	Flowering	1021 a	1505 ab	1271 a-d	1140 bc
	Seed filling	926 ab	1596 a	1362 a	1268 a
75	Active vegetative	944 ab	1303 a-c	1317 ab	1118 b-d
	Flowering	895 ab	1249 a-c	1260 b-d	1239 ab
	Seed filling	913 ab	1281 a-c	1305 ab	934 ef
50	Active vegetative	833 ab	1079 bc	1256 b-d	1129 b-d
	Flowering	794 b	1013 c	1286 a-c	1037 c-e
	Seed filling	824 ab	1032 c	1190 cd	915 ef
25	Active vegetative	814 ab	1005 c	1221 b-d	1008 de
	Flowering	533 c	1007 c	1244 b-d	929 ef
	Seed filling	865 ab	898 c	1171 d	845 f
Interaction treatments		(+)	(+)	(+)	(+)

Note: The numbers followed by the same characters in the same column indicate no significant difference based on DMRT at 5% significant levels. LAD = leaf area duration, and WAP = week after planting

Table 3 shows that LAD had the same pattern as LAI. The highest value occurred at a soil moisture content of 100% field capacity during the seed filling stage, while the lowest occurred at a soil moisture content of 25% field capacity during the seed filling stage at 6-8, 8-10, and 10-12 WAP.

Specific leaf area

The ANOVA on SLA showed a significant interaction between soil moisture and growth rate at the ages of 4-6, 6-8, 8-10, and 10-12 WAP. The result of DMRT at 5% significant levels on the average SLA in ages of 4-6, 6-8, 8-10, and 10-12 WAP are shown in Table 4.

Table 4 shows that the highest specific leaf area during 4-6, 6-8, 8-10, and 10-12 WAP were at a soil moisture content of 100% field capacity during the seed filling stage. Meanwhile, the lowest SLA occurred at a soil moisture content of 25% field capacity during the seed filling the stage at 6-8, 8-10, and 10-12 WAP. Drought stress is most detrimental to soybean plants during generative growth, especially during the seed filling stage.

Net assimilation rate

The ANOVA on NAR showed a significant interaction between soil moisture and growth rate at the ages of 4-6, 6-8, 8-10, and 10-12 WAP. The result of DMRT at 5% significant levels on the average NAR in ages of 4-6, 6-8, 8-10, and 10-12 WAP are shown in Table 5.

Table 5 shows that during 4-6 WAP, the NAR value was highest at a soil moisture content of 100% field capacity during the flowering stage, while the lowest was at a soil moisture content of 25% field capacity during the flowering stage. Conditions during 6-8 and 8-10 WAP had the same pattern as previous observations. Conditions during

10-12 WAP contradict previous results, as the NAR value was highest at a soil moisture content of 25% field capacity during the seed filling stage, while the lowest was at a soil moisture content of 100% field capacity during the seed filling stage.

Table 4. SLA at various levels of drought and growth stages at 4-6, 6-8, 8-10, and 10 -12 WAP

Soil moisture (% field capacity)	Growth stage	SLA (cm ² .g ⁻¹)			
		4-6 WAP	6-8 WAP	8-10 WAP	10-12 WAP
100	Active vegetative	287.33 ab	230.00 ab	246.67 ab	225 a-d
	Flowering	321.67 a	237.00 ab	241.67 b	254 ab
	Seed filling	298.33 ab	270.00 a	313.67 a	278 a
75	Active vegetative	275.00 ab	232.33 ab	272.00 ab	245 a-c
	Flowering	291.67 ab	225.67 ab	241.33 b	169 d
	Seed filling	283.33 ab	230.67 ab	272.33 ab	220 a-d
50	Active vegetative	282.33 ab	236.00 ab	268.00 ab	224 a-d
	Flowering	288.67 ab	219.67 b	231.33 b	192 b-d
	Seed filling	280.33 ab	225.67 ab	249.67 ab	162 de
25	Active vegetative	287.67 ab	224.33 ab	241.00 b	184 cd
	Flowering	199.00 c	221.67 b	246.67 ab	167 d
	Seed filling	264.33 b	169.00 c	156.33 c	102 e
Interaction treatments		(+)	(+)	(+)	(+)

Note: The numbers followed by the same characters in the same column indicate no significant difference based on DMRT at 5% significant levels. SLA = specific leaf area, WAP = week after planting

Table 5. NAR at various levels of drought and growth stages at 4-6, 6-8, 8-10, and 10-12 WAP

Soil moisture (% field capacity)	Growth stage	NAR (x 10 ⁻⁵ g.cm ⁻² .week ⁻¹)			
		4-6 WAP	6-8 WAP	8-10 WAP	10-12 WAP
100	Active vegetative	332.33 bc	306.67 ab	168.33 ab	24.47 c-e
	Flowering	560.99 a	243.67 a-d	151.00 a-c	317.26 a-d
	Seed filling	502.00 ab	372.00 a	208.33 a	219.47 e
75	Active vegetative	451.43 ab	277.00 a-c	144.67 bc	277.15 b-e
	Flowering	464.67 ab	283.67 a-c	192.33 ab	228.48 de
	Seed filling	480.43 ab	304.00 ab	160.33 a-c	229.36 de
50	Active vegetative	402.33 ab	254.67 a-d	164.33 ab	286.29 b-e
	Flowering	445.67 ab	261.33 a-d	135.00 bc	298.46 b-e
	Seed filling	384.67 a-c	373.33 cd	141.33 bc	351.27 ab
25	Active vegetative	417.67 ab	189.00 b-d	139.67 bc	320.32 a-c
	Flowering	194.33 c	259.67 a-d	155.00 a-c	301.68 b-e
	Seed filling	340.00 bc	137.67 d	101.00 c	387.76 a
Interaction treatments		(+)	(+)	(+)	(+)

Note: The numbers followed by the same characters in the same column indicate no significant difference based on DMRT at 5% significant levels. NAR = net assimilation rate, WAP = week after planting

Crop growth rate

The ANOVA on CGR showed a significant interaction between soil moisture and growth rate at the ages of 4-6, 6-8, 8-10, and 10-12 WAP. The result of DMRT at 5% significant levels on the average CGR in ages of 4-6, 6-8, 8-10, and 10-12 WAP are shown in *Table 6*.

Table 6. CGR at various levels of drought and growth stages at 4-6, 6-8, 8-10, and 10-12 WAP

Soil moisture (% field capacity)	Growth stage	CGR (x 10 ⁻⁵ mg.cm ⁻² .week ⁻¹)			
		4-6 WAP	6-8 WAP	8-10 WAP	10-12 WAP
100	Active vegetative	272.33 ab	271.00 bc	193.67 a-c	330.85 bc
	Flowering	318.00 a	300.00 a-c	185.67 a-d	252.36bc
	Seed filling	267.67 ab	418.00 a	234.67 a	188.62 c
75	Active vegetative	274.33 ab	321.67 ab	186.00 a-d	233.82 bc
	Flowering	246.33 a-c	303.67 a-c	227.33 ab	251.48 bc
	Seed filling	252.33 a-c	311.67 a-c	186.33 a-d	232.69 bc
50	Active vegetative	240.33 bc	239.67 bc	200.00 a-c	270.26 ab
	Flowering	189.33 c	238.67 bc	182.67 b-d	246.47 bc
	Seed filling	276.33 ab	242.00 bc	154.00 cd	272.62 ab
25	Active vegetative	220.67 bc	255.00 bc	168.00 cd	256.38 bc
	Flowering	187.67 c	224.33 bc	154.67 cd	236.78 bc
	Seed filling	223.00 bc	182.00 c	141.00 d	334.32 a
Interaction treatments		(+)	(+)	(+)	(+)

Note: The numbers followed by the same characters in the same column indicate no significant difference based on DMRT at 5% significant levels. CGR = Crop Growth Rate and WAP = week after planting

Table 6 shows that 4-6, 6-8, and 8-10 WAP showed the same pattern, namely having the highest Crop Growth Rate (CGR) at 100% soil moisture content during the seed filling stage while having the lowest at a soil moisture content of 25% during the seed filling stage. However, conditions during 10-12 WAP had the opposite pattern to previous observations. The CGR value was highest at a soil moisture content of 25% field capacity during the seed filling stage, while the lowest was at a soil moisture content of 100% field capacity during the seed filling stage. NAR showed the same pattern, meaning that CGR related to NAR.

Seeds weight

The ANOVA on seed weight per 100 seeds and per plant showed a significant interaction between soil moisture and growth rate at the ages of 4-6, 6-8, 8-10, and 10-12 WAP. The result of DMRT at 5% significant levels on the average seed weight per 100 seeds and plants is shown in *Table 7*.

Table 7 shows that the highest seed weight per plant occurred at a soil moisture content of 100% field capacity in the active vegetative stage, while the lowest was at a soil moisture content of 25% field capacity in the seed filling stage. This pattern was identical to the pattern of the weight of 100 seeds.

Table 7. Weight of 100 seeds (g) and weight of seeds per plant (g) at various levels of drought and growth stages

Soil moisture (% field capacity)	Growth stage	Seed weight	
		g 100 seeds ⁻¹	g plant ⁻¹
100	Active vegetative	14.013 a	4.285 a
	Flowering	13.580 a	3.594 ab
	Seed filling	13.187 a	3.837 ab
75	Active vegetative	13.183 a	3.315 b
	Flowering	13.793 a	3.565 ab
	Seed filling	10.353 c	2.994 bc
50	Active vegetative	11.787 b	3.303 b
	Flowering	13.607 a	2.941 bc
	Seed filling	7.293 d	2.231 cd
25	Active vegetative	11.477 bc	2.174 cd
	Flowering	11.890 b	2.332 c
	Seed filling	5.307 c	1.441 d
Interaction treatments		(+)	(+)

Note: The numbers followed by the same characters in the same column indicate no significant difference based on DMRT at 5% significant levels

Discussion

Regardless of drought stress, the LAI value increased from 4-6 to 6-8 and from 6-8 to 8-10 WAP. However, from 8-10 to 10-12 WAP, the LAI value decreased. This decrease was due to the harvest age, in which the leaves begin to experience senescence. In this research, 8-10 WAP showed the highest LAI value. However, Özalkan et al. (2010) found the highest LAI and LAD values during the linear vegetative growth stage.

The four observation periods showed that rather than the growth stage, drought stress determines the value of LAI. Drought stress was inversely proportional to the LAI value. One of the functions of water was to support the photosynthetic process. With decreased photosynthesis, the size of the leaves will also decrease. The disruption in cell division and enlargement in drought stress conditions was due to loss of turgor and decreased photosynthesis and energy supply caused a decrease in leaf area (Talbi et al., 2020).

Hatfield et al. (2011), stated that drought stress affected the growth of the vegetative and generative stages of plants, decreasing crop yields. However, the reproductive stage was highly sensitive to drought stress as it directly affected the flowering and pod filling stages. The linear vegetative growth stage showed the highest LAI and LAD values (Özalkan et al., 2010). The NAR represents the ability of plants to produce dry matter (Li et al., 2012). The NAR value showed a positive correlation with RGR (Li et al., 2016). Therefore, NAR can act as the main determinant of the RGR value. In general, SLA increases from initial growth to 10 WAP, after which it decreased as leaves begin to experience senescence. Plants with severe drought did not experience an increase in SLA, especially in the vegetative or seed filling stages. One of the functions of water is to accommodate photosynthesis. With low photosynthesis activity, leaf size will not increase at its usual rate.

Regardless of drought stress, the CGR value increased from 4-6 WAP to 6-8 WAP and decreased from 6-8 to 8-10 WAP. The plants have entered the seed filling stage from 6-8 to 8-10 WAP, decreasing dry weight. According to Anjum et al. (2014), CGR will be continued to increase until the middle growth stage and decrease towards maturity.

During rice plant growth, NAR and RGR generally show an increase (height) at the beginning of the growth phase, then decrease rapidly with plant age (Sridevi and Chellamuthu, 2015). At 40-50 days after planting, NAR had a weak positive correlation with grain yield. The flowering stage showed the highest NAR and CGR scores (Ozalkan et al., 2010). Ozalkan et al. (2010) stated that there was a significant correlation among most of the growth parameters during all growth stages.

One of the functions of water is to translocate the assimilation from the leaf (source organ) to the seed (sink organ). A lack of water will hamper the seed filling process. Drought stress affects seed production and quality (Alqudah et al., 2011). Ghassemi-Golezani et al. (2010) stated that drought stress experienced during the reproductive phase decreases flowers and filled pods. This stress inhibited the distribution of carbohydrates from the leaf to the pod, resulting in a decrease in the number and size of seeds (Alqudah et al., 2011).

A considerable lack of water will reduce the quality and quantity of soybean production. Hatfield et al. (2011) stated that drought stress affected the growth of plants during the vegetative and generative stages, which ultimately resulted in a decrease in crop yields. The occurrence of water shortages and high temperatures at the beginning of the flowering to the ripening stage accelerated the pod filling period and reduced yield weight (Kobraei et al., 2011).

Plant morpho-physiological characteristics, such as leaf thickness and plant growth rates affected productivity, considering that these characteristics affected photosynthesis speed. For long periods, a high seed filling rate will produce a high seed weight as long as the seed as a sink can accommodate a high assimilation rate. Conversely, a large enough sink with a low assimilation rate can result in a seed void. Source limitations often occur during the seed filling stage but sink limitations can occur even in non-stress conditions (Egli, 1999). Production had a significant positive correlation with the net photosynthetic rate (NAR) (Li et al., 2012). Drought stress reduced the yield of soybean. A soil moisture content of 80 and 60% field capacity reduced the yield of soybean genotypes by 15.7% and 23.4%, respectively (Patriyawaty and Anggara, 2020). Daryanto et al. (2015) stated that yield reduction was generally higher in legumes experiencing drought during their reproductive stage than during their vegetative stage. Sridevi and Chellamuthu (2015) found that higher grain yields reflected satisfactory dry matter production, LAI, LAD, CGR, NAR, and RGR values.

Conclusion

In conclusion, our study found that soil moisture content at below 75% field capacity reduced the LAI, LAD, SLA, NAR, CGR, the seed weight per 100 seeds, and seed weight per plant. In seed filling stage is more sensitive to water shortages than the vegetative or flowering stages. At all stages of growth, a higher drought level equals a higher decrease in soybean growth and yield. For future research, we suggest that soybean planting utilize 100% field capacity.

Acknowledgements. We would like to thank the Directorate of Research and Community Service for Publication, Universitas Tunas Pembangunan Surakarta, Indonesia, for approving this research. We would also like to show our highest gratitude to Mr. Sugiman, who has assisted in field activities.

REFERENCES

- [1] Ahmed, S. U., Senge, M., Ito, K., Adomako, J. T. (2010): The effect of deficit irrigation on root/shoot ratio, water use efficiency and yield efficiency of soybean. – *Journal of Rainwater Catchment Systems* 15(2): 39-45.
- [2] Alqudah, A. M., Samarah, N. H., Mullen, R. E. (2011): Drought stress effect on crop pollination, seed set, yield, and quality. – In *Alternative Farming Systems, Biotechnology, Drought Stress, and Ecological Fertilisation, Sustainable Agriculture Reviews* 6: 193-213.
- [3] Anjum, S. A., Ashraf, U., Tanveer, M. (2014): Morphological and phenological attributes of maize affected by different tillage practices and varied sowing methods. – *American Journal of Plant Sciences* 5: 1657-1664.
- [4] Baloch, M. S., Awan, I. U., Hassan, G. (2006): Growth and yield of rice as affected by transplanting dates and seedlings per hill under high temperature of Dera Ismail Khan, Pakistan. – *Journal of Zhejiang University* 7(7): 572-579.
- [5] Buezo, J., Sanz-Saez, Á., Moran, J. F., Soba, D., Aranjuelo, I., Esteban, R. (2019): Drought tolerance response of high-yielding soybean varieties to mild drought: physiological and photochemical adjustments. – *Physiologia Plantarum* 166(1): 88-104.
- [6] Daryanto, S., Wang, L., Jacinthe, P. A. (2015): Global synthesis of drought effects on food legume production. – *PLoS ONE* 10(6): e0127401.
- [7] Egli, D. B. (1999): Variation in leaf starch and sink limitations during seed filling in soybean. – *Crop Science* 39(5): 743-745.
- [8] Ghassemi-Golezani, K., Zafarani-Moattar, P., Raey, Y., Mohammadi, A. (2010): Response of pinto bean cultivars to water deficit at reproductive stages. – *Journal of Food, Agriculture and Environment* 8(2): 801-804.
- [9] Gomez, A. G., Gomez, K. A. (1984): *Statistical procedures for agricultural research*. – (Second ed.) New York, Chichester, Brisbane, Toronto, Singapore: John Wiley & Sons, Inc.
- [10] Hatfield, J. L., Boote, K. J., Kimball, B. A., Ziska, L. H., Izaurralde, R. C., Ort, D., Thomson, A. M., Wolfe, D. (2011): Climate impacts on agriculture: implications for crop production. – *Agronomy Journal* 103(2): 351-370.
- [11] Kobraei, S., Etminan, A., Mohammadi, R., Kobraee, S. (2011): Effects of drought stress on yield and yield components of soybean. – *Annal of Biological Research* 2(5): 504-509.
- [12] Li, Zhang, Z., Zheng, D., Jiang, L., Wang, Y. (2012): Comparison of net photosynthetic rate in leaves of soybean with different yield levels. – *Journal of Northeast Agricultural University* 19(3): 14-19.
- [13] Li, X., Schmid, B., Wang, F., Paine, C. E. T. (2016): Net assimilation rate determines the growth rates of 14 species of subtropical forest trees. – *PLoS ONE* 11(3): e0150644.
- [14] López-Bellido, F. J., López-Bellido, R. J., Khalil, S. K., López-Bellido, L. (2008): Effect of planting date on winter Kabuli chickpea growth and yield under rainfed Mediterranean conditions. – *Agronomy Journal* 100(4): 957-964.
- [15] Luo, H. H., Zhang, Y. L., Zhang, W. F. (2016): Effects of water stress and rewatering on photosynthesis, root activity, and yield of cotton with drip irrigation under mulch. – *Photosynthetica* 54(1): 65-73.
- [16] Maleki, A., Naderi, A., Naseri, R., Fathi, A., Bahamin, S., Maleki, R. (2013): Physiological performance of soybean cultivars under drought stress. – *Bulletin of Environment, Pharmacology and Life Sciences* 2: 38-44.

- [17] Marchese, J. A., Ferreira, J. F. S., Rehder, V. L. G., Rodrigues, O. (2010): Water deficit effect on the accumulation of biomass and artemisinin in annual wormwood (*Artemisia annua* L., Asteraceae). – Brazilian Journal of Plant Physiology 22(1): 1-9.
- [18] Nleya, T., Sexton, P. (2019): Soybean Growth Stages. – In Soybean Extension and Research Program, available at:
https://crops.extension.iastate.edu/soybean/production_growthstages.html.
- [19] Ozalkan, C., Sepetoglu, H. T., Daur, I., Sen, O. F. (2010): Relationship between some plant growth parameters and grain yield of chickpea (*Cinger arietinum* L.) during different growth stages. – Turkish Journal of Field Crops 15(1): 79-83.
- [20] Patriyawaty, N. R., Anggara, G. W. (2020): Pertumbuhan dan hasil genotipe kedelai (*Glycine max* (L.) Merrill) pada tiga tingkat cekaman kekeringan. – Agromix 11(2): 151-165. (In Indonesian).
- [21] Sacita, A. S., June, T., Impron. (2018): Soybean adaptation to water stress on vegetative and generative phases. – Agrotech Journal ATJ 3(2): 42-52.
- [22] Samarah, N. H., Alqudah, A. M., Amayreh, J. A., Mcandrews, G. M. (2009): The effect of late-terminal drought stress on yield components of four barley cultivars. – J. Agronomy & Crop Science 195: 427-441.
- [23] Sridevi, V., Chellamuthu, V. (2015): Growth analysis and yield of rice as affected by different systems of rice intensification (SRI) practices. – International Journal of Research in Applied, Natural and Social Sciences 3(4): 29-36.
- [24] Talbi, S., Rojas, J. A., Sahrawy, M., Rodríguez-Serrano, M., Cárdenas, K. E., Debouba, M., Sandalio, L. M. (2020): Effect of drought on growth, photosynthesis and total antioxidant capacity of the Saharan plant *Oudeneya africana*. – Environmental and Experimental Botany 176: 104099.
- [25] Thu, N. B. A., Nguyen, Q. T., Hoang, X. L. T., Thao, N. P., Tran, L. S. P. (2014): Evaluation of drought tolerance of the Vietnamese soybean cultivars provides potential resources for soybean production and genetic engineering. – BioMed Research International 2014: 809736.
- [26] Zulfiqar, F., Younis, A., Riaz, A., Mansoor, F., Hameed, M., Akram, N. A., Abideen, Z. (2020): Morpho-anatomical adaptations of two *Tagetes erecta* L. cultivars with contrasting response to drought stress. – Pakistan Journal of Botany 52(3): 801-810.

BROWN BEAR (*URSUS ARCTOS*) POPULATION DENSITY IN THE EASTERN BLACK SEA MOUNTAINS IN TÜRKİYE

BAŞKAYA, E.^{1*} – GÜNDOĞDU, E.² – BAŞKAYA, Ş.³

¹Anatolian Wildlife Association, Trabzon, Türkiye
(e-mail: ebrubaskaya1@gmail.com; phone: +90-533-543-7061)

²Department of Forest Engineering, Bursa Teknik University, Türkiye
(e-mail: ebubekirgundogdu@gmail.com; phone: +90-505-934-3200)

³Department of Wildlife Ecology and Management, Faculty of Forestry,
Karadeniz Technical University, Trabzon, Türkiye
(e-mail: sagdanbaskaya@gmail.com; phone: +90-532-686-7809)

*Corresponding author
e-mail: ebrubaskaya1@gmail.com; phone: +90-533-543-7061

(Received 21st Feb 2022; accepted 10th Jun 2022)

Abstract. Brown bear (*Ursus arctos*) population density has not been determined so far in the Eastern Black Sea Mountains, Türkiye, where the most fatal attacks are experienced in the country. Therefore, in order to determine the bear population density, studies were carried out from 2008 to 2017 in 12 sampling sites with a total area of 900 km². Field studies were carried out in all sampling sites, in groups of 2-4 people, generally by establishing tented camps. In addition, 5 comprehensive inventory studies were conducted with groups of 10-30 people in 3 of these sampling sites. Direct and indirect counting methods were used together in all inventories in the sampling sites. Direct counts were performed using line counting, point counting, camera traps and thermal camera. Indirect counts are the recording of tracks and signs. As a result of the study, while the population density of bears in the sampling sites varied between 40-466 bears/1000 km², the average density was determined as 194 bears/1000 km². The population size of bears in the study area, which is approximately 28,000 km², was calculated as 5432 individuals, of which 3259 are adults and 2173 are cubs and yearlings.

Keywords: bear inventory, point count, camera trap, thermal camera, footprint

Introduction

The human-bear conflict is most intense in the Eastern Black Sea Region in Türkiye. As a result of these conflicts, many people are seriously injured, some of them experience permanent trauma, and some of them lose their lives. In addition, people also suffer significant economic losses. After the bear attacks in Türkiye between 2009-2021, it was determined that 31 people were killed and about 120 people were injured. Of these, 7 deaths and 30 serious injuries occurred in the Eastern Black Sea Region. The number of injuries here is very likely to be higher than detected.

Bears come into conflict with humans more or less in parallel with their population density wherever they live in the world. In total, 44 subpopulations of brown bear have been identified globally; most occur in the southern portions of their circumpolar distribution across the northern hemisphere (McLellan et al., 2008; Calvignac et al., 2009; Proctor et al., 2012). The total number of brown bears on earth is estimated to exceed 200000 (Lynch, 2021). It is stated that 123,869 bears live in Russia, where the most bears live (Swenson et al., 2000). Today the total number of brown bears in Europe is about 50000 bears (ca. 14000 outside Russia) within an area of more than

2.5 million km² (800000 km² outside Russia) (Zedrosser et al., 2001). Bear populations in Europe are very scattered and their densities are very low. The Carpathians are home to the largest number of bears in Europe, with 8100 individuals (4455 adults) in an area of 122600 km². The population density of 6000 individuals living on 69000 km² in the Carpathian Mountains in Romania is 100-200 bears in 1000 km² (Servheen et al., 1999; Swenson et al., 2000; Ministry of Agriculture, Forestry and Rural Development - Ministry of Environment and Water Management -MAFRD-MEWM-, 2005). The local bear population has been reported to exceed 400 bears/1000 km² in the Dinaric mountains of Slovenia (Jerina et al., 2013).

In North America, there are 58000 bears (Lynch, 2021). In Kodiak Island, where they are most abundant in North America, a total of 3500 individuals (2400 adults older than 3 years of age) with an increasing trend live in an area of 9311 km² (Van Daele et al., 2012). They have high reproductive rates (Smith and Van Daele, 1991; Van Daele et al., 2012) and are found in high densities (Miller et al., 1997; Van Daele, 2007; Van Daele and Cyre, 2007). Coastal bear populations in Alaska range from 191–551 per 1000 km² (Morton, 2013). Bear densities in Alaska vary from region to region; 551 bears/1000 km² of all ages on the coast of Katmai National Park; 439.5 bears/1000 km² on Admiralty Island; 342 bears/1000 km² at Terror Lake (Kodiak Island); 323 bears/1000 km² at Karluk Lake (Kodiak Island); 191 bears/1000 km² in Black Lake, 27 bears/1000 km² in the Middle Susitna River Basin, 10.7 bears/1000 km² in the Upper Susitna River (Miller et al., 1997). In British Columbia, the most densely bear populations in 2015 were at 40-50 bears/1000 km² (Committee on the Status of Endangered Wildlife in Canada -COSEWIC-, 2012).

It is stated that a total of 6300 individuals, 3465 of which are adults, live in an area of 2400000 km² in Central Asia, East Turkestan and Western China (Gong and Harris, 2006). In Japan, a total of 2200-6500 bears lives in an area of 78000 km². The Shiretoko Peninsula, located in eastern Hokkaido, has one of the highest bear densities in Japan. The minimum population size was estimated at 200 in 1135 km² including the towns of Shari and Rausu (Shimozuru et al., 2017). In the Northern and Central Taiga Section of the European part of Russia and the North Caucasus Mountain Forest Zone in 1990, an average of 0.18 bears per 1000 km² was detected, while in the Southern Taiga and Northern Temperate Forests of the European part of Russia 0.26 bears per 1000 km²; 0.19 bears per 1000 km² in the Ural Mountains; 0.40 bears per 1000 km² in the Altai Mountains; 0.05-0.06 bears per 1000 km² have been detected in Siberia (Servheen et al., 1999).

It is estimated that 2000–2500 bears remain in the South Caucasus, where they are protected in Georgia and Armenia but hunted in Azerbaijan (Lortkipanidze, 2010). The minimum density in Central Georgia is given as 13 bears/1000 km² (Lortkipanidze, 2010). Similarly, it is reported that the total number of brown bears in the Caucasus Ecoregion does not exceed 3000 individuals (Caucasus Biodiversity Council -CBC-, 2012). Bear density in Iran's Arasbaran Biosphere reserve was determined as 48.8 bears/1000 km² (Murtskhvaladze and Tarkhnishvili, 2006; Moqanaki et al., 2018). In Armenia, a total population density estimates of 59.4 bears/1,000 km² (Burton, 2018).

Brown bear lives in all regions of Türkiye except the European part (Başkaya et al., 2012). It is stated that a maximum of approximately 4300 bears live in Türkiye (International Union for Conservation of Nature -IUCN-, 2016). The population size of the brown bear in Türkiye is estimated to be less than 3000 (Can, 2004). It is stated that

the total potential in Türkiye is 17500 individuals (Gündoğdu and Başkaya, 2013). It is stated that the largest number of bears in Türkiye live in Eastern Anotolia-Lesser Caucasus with an area of 161,880 km² with 2000-2400 individuals (IUCN, 2016). Other populations living in Türkiye are 750-800 individuals in Küre Mountains-Western Black Sea, 300-400 individuals in Western Anatolia, ~<250 in Eastern Toros Mountains, ~<250 in Western Toros Mountains, 100-150 in Aegean and Datça <50 (Ambarlı et al., 2016; IUCN, 2016). Similarly, it is emphasized that brown bear is abundant in Eastern Black Sea and Eastern Anatolia, but rare in other regions (Turan, 1990; Demirsoy, 1996). According to a study conducted in Bolu, in the Western Black Sea region, it is stated that there are 10 bears in every 1000 km², and the population status in other regions is not clear (Can and Togan, 2004). It is stated that the density of 230-260 bears per 1000 km² detected in the upper parts of Yusufeli, Barhal valley is the highest density in Türkiye (Ambarlı, 2012).

Brown bear, Türkiye's largest predatory mammal species, is a protected species (Central Hunting Commission Decision -CHCD-, 2021). However, in the recent past, it has been allowed to hunt in certain numbers in the provinces where the damage has been detected. Finally, in 2015, a total of 15 bears were allowed to be hunted throughout the country, 7 of which were in the Eastern Black Sea Region (CHCD, 2015). It is known that it is poaching in the country, especially in many regions where human-bear conflict is intense.

Bears are indicator taxa to monitor ecosystem health. Protecting bears and maintaining their habitat also helps protect the habitat of many other species. In addition, as a result of the protection of bears, resources needed by local people such as water, wildlife and local culture are also protected. However, it is reported that most of the populations of bear species, whose distribution has narrowed, will be in a constant trend of extinction in the next 20 years (Servheen et al., 1999).

In the Eastern Black Sea Region, the Bears use it from the seaside to the 3700 m altitude of Kaçkar Mountain, the highest mountain of the region. After the human-bear conflict in the region, since there is no regional population study, administrative decisions regarding bears cannot be made or are taken incorrectly. Bear populations are increasing in the country, where the rulers only try to protect the bears with stricter measures. As a result of increasing populations, human-bear conflict increases, citizens lose faith in authorities, reactions increase and citizens resort to illegal solutions. Therefore, in this study, it is aimed to determine the population density of the Bear in the Eastern Black Sea Region, where the human-bear conflict is most intense in the country.

Material and methods

Study area

The Eastern Black Sea Mountains, with a total of 32000 km², are the second highest mountainous region in Türkiye. Kaçkar Mountain (3932 m), which has the highest peak of the mountain ranges in the region, is the fourth highest peak in the country. Populated areas are mostly at lower altitudes, and above 1000 m the density of people is <50 per km². The Eastern Black Sea Mountains are located on the territory of six provinces. The most populous of these provinces is Trabzon with 811901 people, and Bayburt has the least population with 81910 people. The average population density in the region is 66 people per km² (Türkiye Statistical Institute -TUIK-, 2020). In the

Eastern Black Sea Mountains, the most intense human destruction was experienced on the slopes facing the sea. There are extreme human settlements and agricultural areas on these slopes, which are up to about 800 m above sea level. The forests in this belt have been transformed into tea gardens in the east of the region and hazelnut orchards in the west.

About 10% of the study area is protected area. It is the region with the highest rainfall in the country. The maximum precipitation occurs in Rize (altitude 30 m), with an average total of 2500 mm, and where the mean daily temperature is 8–14°C. The alpine zone above 2000 m is usually covered with snow for at least 6 months of the year. Forests covering 63% of the region are the main vegetation type. Other vegetation types in the region are dune, stream, pseudo-maquis, subalpine and alpine vegetation. The brown bear is the region's largest predatory mammal species. Other major predator species; Leopard (*Panthera pardus*) (Başkaya and Bilgili, 2004), Lynx (*Lynx lynx*), Wolf (*Canis lupus*), Golden jackal (*Canis aureus*) and Striped Hyena (*Hyaena hyaena*) (Sarı et al., 2020).

Sampling sites

This study was carried out in 12 sample areas with a total area of 900 km² (Figures 1 and 2; Table 1). Sampling sites include all habitat types except densely populated and agricultural areas below 800 meters. Eleven sampling sites were selected in the Eastern Black Sea Mountains, and one in the neighboring region of Posof, Sesödile Mountain (2438 m). Sesödile Mountain is a sample area that is very similar to the region in many ways such as climate, vegetation and geographical features.

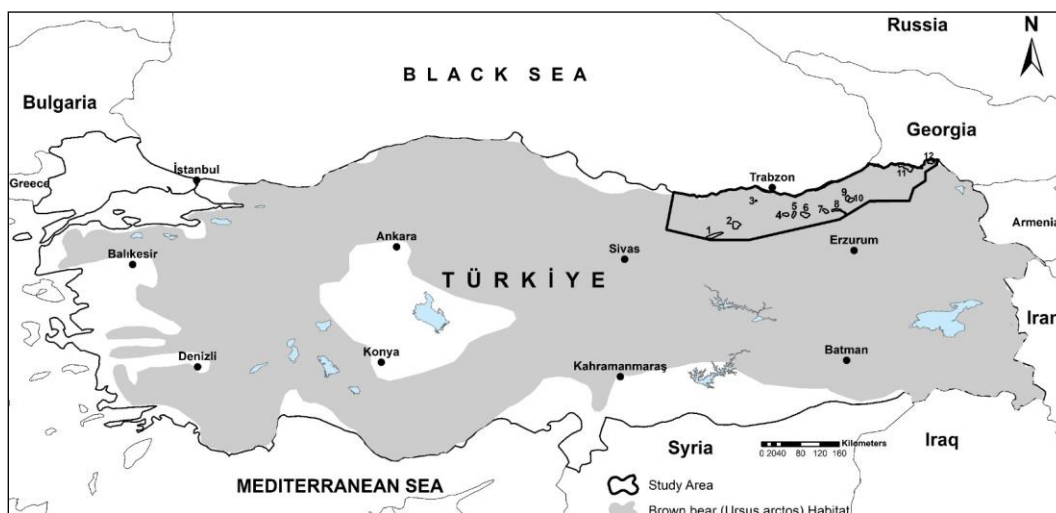


Figure 1. Distribution of the brown bear in Türkiye (Başkaya et al., 2008) and 12 sampling sites in Eastern Black Sea Mountains

The areas from the Black Sea coast to an altitude of about 800 meters contain the most densely residential and agricultural areas. In this belt below 800 meters, bears come down to the beach only in some seasons and in some parts. In the sampling and density calculations, altitudes lower than 800 m were excluded and the remaining 28,000 km² area was studied.



Figure 2. Sampling sites in the Eastern Black Sea Mountains

Table 1. Area of sampling sites, elevation zones, important settlements and protected areas at some sites

No.	Sampling sites (Province / County)	Area (km ²)	Elevation zone (m)	Important settlements and protected areas at some sites
1	Sarıçiçek Mt. (Giresun / Alucra, Çamoluk, Şebinkarahisar)	140	950-2335	Sarpkaya, Doludere ve Çamlıyayla Plateau, Arda, Yeniköy, Eğnir
2	Gavur Mt. (Gümüşhane / Şiran - Torul; Giresun / Alucra)	100	1600-3331	Yukarı Kulaca, Yeniköy, Akbulak, Kopuz, Gülaçar, Gümüştug, Yukarı Kulaca Wildlife Reserve Area, Artabel Nature Park
3	Haçka Plateau (Trabzon / Düzköy, Akçaabat, Maçka)	50	1000-1970	Haçka Plateau, Yerlice Plateau, Kayabaşı Plateau
4	Tilkibeli (Trabzon / Araklı)	50	1400-2450	Tilkibeli, Bahçecik, Erikli, Boğalı, Güngören, Yağmurdere, Aslanca
5	Uzuntarla (Trabzon / Çaykara; Bayburt / Aydıntepe)	50	1200-2400	Uzuntarla, Sultan Murat Plateau, Limonsuyu Plateau, Günbuldu
6	Uzungöl (Trabzon / Çaykara)	80	1100-3376	Demirli Köyü, Yaylaönü, Arpaözü, Demirkapı, Demirkapı Mts., Uzungöl Special Environmental Protection Area
7	Ovit Mt. (Rize / İkizdere; Erzurum / İspir)	50	1500-3300	Çamlıköy, Sivrikaya, Ovit Pass
8	Yedigöl (Erzurum / İspir; Rize / İkizdere)	70	980-3375	Aksu-Yedigöl Valley
9	North Kaçkar (Rize / Çamlıhemşin)	50	1650-3932	Galer düzü, Yukarı Kavron Plateau, Yukarı Ceymakçur Plateau, North of Kaçkar National Park
10	South Kaçkar (Artvin / Yusufeli; Erzurum / İspir)	60	1900-3932	Yaylalar, Olgunlar, Dübe Plateau ve Hastaf Plateau, South of Kaçkar National Park
11	Meydancık (Artvin / Şavşat, Borçka)	150	800-2800	Meydancık, Papart Plateau, Akdamla, Dutlu, Demirci
12	Sesödile Mt. (Ardahan / Posof)	50	1600-2400	Sarıçiçek, Yaylaltı, Kurşunçavuş, Binbaşı Eminbey, Posof Wildlife Reserve Area

The main features taken into account in the selection of sampling sites are as follows; Sample areas were selected from all kinds of places such as Alucra, Şavşat, Çamlıhemşin and Çaykara, where the human-Bear conflict is most intense, and Trabzon / Düzköy, where there is less conflict in general. The data on the Human-Bear conflicts were obtained from many studies on different wildlife issues in the Eastern Black Sea Mountains for about 30 years, news in the media and the last 10 years of complaint records of the General Directorate of Nature Conservation and National Parks. The sample areas were chosen to represent the entire Eastern Black Sea Mountain range and to have at least one from each province. The sampling sites were chosen to represent all the elevation, aspect and habitat types between 800 m and the Kaçkar peak, which is the highest elevation of the region with 3932 m.

Counting methods

Studies were carried out on 12 sampling sites from 2008 to 2017 (*Table 2, Figure 2*). For the population density of each sampling site, only the census results from the highest bear numbers in 2016 and 2017 were used. Because, in these censuses, more attention was paid to making inventory in the same period at sampling sites that are close to each other. Although it is difficult to count all sites in the same period in the same year, counting was made in 10 sites in 2016 and 7 sites in 2017. As an exception, only the 2013 census results in Meydancık were taken into account. Because, in this census made with large teams of 15-20 people, observations could be made in much larger areas on sampling sites. All other census results after 2008 are presented here in order to compare the census results used for population density and to give more information about the sites (*Table 2*).

Direct and indirect counting techniques were used in the inventories. Direct counting is seeing bears with eye, binoculars, telescope and thermal camera or photographing them with any device. Direct counts were performed using line counting, point counting, camera traps and thermal camera. During all direct counts, observed tracks and signs were also recorded. Footprints and fresh feces were mainly used for indirect counts. The width and length of the detected front and hind footprints were measured. Fresh tracks with differences in measurements >4 cm was assumed to belong to different individuals. During field observations, everyone used a 10x42 binocular, and each team of two used an 80 mm (20-60x) spotting scope. In addition, digital (12-24x) and SLR (300 mm x2) cameras with different magnifications were used by each team.

Point count method

This method was carried out at 1-3 points every day with a small team of 4 people in all sampling sites. At one point, two people usually observed. Three people made observations at points in the forest, where there is a high probability of encountering a bear. In addition, counts were made twice in Meydancık and Gavur Mountain, and once in Uzungöl, with a team of 15-20 people, at 6-10 points a day, for 2-3 days, with a large team. In the counts made with large teams, each point count team included a guide, usually a hunter, and a technical staff member.

Point counts were made during the first 2-3 hours after sunrise in the morning and 2-3 hours before sunset in the evening. Sometimes, point counts are made at noon or afternoon in weather and places where bears are likely to roam during the day. In the counts made with large teams of 15-20 people, the teams generally stayed in highland houses, village houses and bungalows, and partially in tents.

Table 2. Inventory dates, bear numbers and population densities in the sampling sites

No.	Sampling sites	Inventory dates	Adults	Cub and Yearlings	Directly observed highest number of bears	Indirectly observed highest number of bears	Directly and indirectly observed highest number of bears	Area (km ²)	Density (1000 km ²)
1	Sarıççek Mt.	Every month after May in 2013*	6	4	8	2	10	140	114,3
		every month from Apr. to Dec. in 2014*	7	4	9	2	11		
		every month from Apr. to Dec. in 2015*	5	4	7	2	9		
		May.16	8	7	11	4	15		
		Sep. 2016	5	6	10	1	11		
		Nov. 2016	7	3	4	6	10		
		May.17	8	8	11	5	16***		
		June 2017	7	5	11	1	12		
Nov. 2017	8	6	10	4	14				
2	Gavur Mt.	21-22 Nov. 2012**	5	0	5	0	5	100	100
		27-29 Nov. 2013**	6	4	7	3	10		
		Sep. 2014	4	2	3	3	6		
		Nov. 2015	5	4	7	2	9		
		Sep. 2016	6	4	7	3	10***		
3	Haçka Plateau	July 2009	1	0	1	0	1	50	40
		Aug. 2010	1	0	1	0	1		
		Aug. 2011	1	1	0	2	2		
		Nov. 2015	1	0	1	0	1		
		Sep. 2016	1	1	1	1	2		
		May.17	2	0	1	1	2***		
		Nov. 2017	1	0	1	0	1		
4	Tilkibeli	July 2010	2	2	1	3	4	50	140
		Nov. 2011	4	2	5	1	6		
		Aug. 2013	3	2	4	1	5		
		Sep. 2015	4	1	4	1	5		
		Nov. 2016	4	3	5	2	7		
		May.17	4	3	5	2	7***		
		July 2017	3	3	5	1	6		
5	Uzuntarla	Sep. 2010	3	1	2	2	4	50	160
		July 2011	3	2	4	1	5		
		Aug. 2013	3	3	5	1	6		
		July 2014	4	4	5	3	8		
		May.15	5	3	5	2	7		
		Sep. 2016	4	4	5	3	8***		
6	Uzungöl	July 2010	5	4	7	2	9	80	187,5
		June 2011	5	3	7	1	8		
		July 2012	4	3	6	1	7		
		26-27 Oct. 2013**	7	8	7	8	15		
		July 2013	4	3	3	4	7		
		Aug. 2014	4	4	7	1	8		
		Oct. 2015	6	4	7	3	10		
		Nov. 2015	4	4	7	1	8		
July 2015	4	3	6	1	7				

No.	Sampling sites	Inventory dates	Adults	Cub and Yearlings	Directly observed highest number of bears	Indirectly observed highest number of bears	Directly and indirectly observed highest number of bears	Area (km ²)	Density (1000 km ²)
		June 2017	8	5	7	6	13		
		Oct. 2017	10	5	7	8	15***		
7	Ovit Mt.	July 2014	2	2	2	2	4	50	140
		Nov. 2015	2	2	3	1	4		
		Sep. 2016	5	2	4	3	7		
		May.17	3	4	4	3	7***		
		Nov. 2017	3	1	3	1	4		
8	Yedigöl	Nov. 2013	3	1	3	1	4	70	114,2
		Nov. 2014	5	3	5	3	8		
		July 2015	3	2	5	0	5		
		Aug. 2017	4	4	5	3	8***		
9	North Kaçkar	Aug. 2009	9	3	8	4	12	50	240
		Aug. 2015	4	2	4	2	6		
		July 2016	7	5	8	4	12***		
10	South Kaçkar	Aug. 2009	2	2	1	3	4	60	166,6
		July 2015	6	4	6	4	10		
		June 2016	5	2	6	1	7		
		Aug. 2017	6	4	6	4	10***		
11	Meydancık	10-12 Oct. 2012**	14	6	12	8	20	150	466,6
		22-24 May 2013**	43	22	65	5	70***		
		July 2015	14	8	21	1	22		
		Aug. 2016	17	7	23	1	24		
12	Sesödile Mt.	Aug. 2008	6	2	7	1	8	50	200
		July 2009	6	2	8	0	8		
		June 2010	3	2	2	3	5		
		July 2011	4	2	5	1	6		
		Aug. 2012	5	5	8	2	10		
		Oct. 2014	5	2	7	0	7		
		Nov. 2014	5	3	6	2	8		
		July 2015	5	5	7	3	10		
		June 2016	6	4	8	2	10***		

*Average result of all months of the year, ** Large team counts, ***Counts used for density

In the counts made with a small team of 4 people, the teams generally stayed in tents. In some point counts made with a small team, when it was concluded that the area around the point was scanned in the morning, it was moved to another point in the evening in order to scan much more area. Maximum effort has been made to ensure that the areas observed by the teams at the points do not overlap with each other. First, the observed bears were photographed and documented, sometimes very clearly, sometimes in a way that was at least identifiable.

Each team at the points recorded the information they obtained during the observations on their observation cards. The observation cards include the name of the team members, date, time, coordinate, number of adult bears, number of cubs-yearlings, gender, color, behavior, weather and habitat information. In addition, the places where the bear was seen are marked with their coordinates on the maps found in each team.

Line count method

This method was carried out by 2 teams, each consisting of 1 or 2 people. Line counts were also made when traveling to places where point counts were to be made, returning from points, or changing points. In the selection of lines, routes with a high probability of using bears or routes that see places that bears can use were preferred.

This method was generally performed in foggy, cloudy and rainy weather where visibility is low. Sometimes counts were made by walking along two parallel lines. In these cases, the distance between the lines varied between 20-100 m depending on the factors affecting the vision such as vegetation density and rocks. Line lengths varying between 2-10 km were realized as 6 km on average.

During the walks, fields were scanned with binoculars and a telescope, stopping as the field of view changed or in case of doubt. The teams photographed traces and signs they saw walking along the line counts, such as footprints, excrement, stone turning, scraping, and fragmented logs. All census results were marked on observation cards and maps by each team.

Camera trap counts

The camera trap was used for the first time on Sarıçiçek Mountain in 2013. Later, camera traps were also used in Uzuntarla and Uzungöl. Camera traps were placed in the field considering the water and food resources, paths and roads that are important for the bears. Bushnell and Cuddeback camera traps that can shoot at night, record 720p HD video up to one minute, 12 MP resolution, 8 or 12 AA batteries, and operate between -15 °C and 60 °C were used. An average of 15-30 camera traps was installed on Sarıçiçek Mountain, and 5-10 on average in Uzuntarla and Uzungöl. The camera traps on Sarıçiçek Mountain generally shot in the field throughout the year between 2013 and 2017. The camera traps in Uzuntarla and Uzungöl were used twice in the field, with periods of approximately one month each.

Thermal camera counts

The thermal camera was only used in Uzungöl, Uzuntarla and Güney Kaçkar throughout 2017. Very successful observations were made during the day with the thermal camera, which is generally better observed at night when the objects in the field get cold. TİCAM 750 thermal camera with a range of 2 km (x2), a resolution of 640x480 and powered by 4 AA batteries was used. With the thermal camera, it was easily scanned between 500 meters and 2 km by standing at the dominant points of the area. Because the scanned area was narrowed, observations were generally made without using magnification. Double magnification was used only when a suspicious object was detected or when it was desired to see the detected animal more clearly.

Results

As a result of the censuses carried out at 12 sampling sites with a total area of 900 km² in the Eastern Black Sea Mountains, a maximum of 175 adults, cub and yearling bears were identified. It has been determined that 40% of 175 bears consist of cubs and yearlings. In other words, it has been determined that 175 bears are composed of 105 adults and 70 cubs and yearlings. Of these 175 bears, 132 bears were observed directly and 43 bears indirectly. While the average bear densities at 1000 km² at

sampling sites varied between 40-466 bears, the average density for all sampling sites was 194.4 bears/1000 km² (Table 2).

It has been calculated that a total of 5432 individuals, consisting of 3259 adults, 2173 cubs and yearlings, live in the Eastern Black Sea Mountains, which has a suitable area of 28000 km² for bears. In the Eastern Black Sea Mountains, with a total area of approximately 32000 km², areas up to 800 m above sea level, where human use is very intense, and where bears generally do not live, are not included in the potential bear habitats. Litter size varied from 1 to 4 and averaged 2.

The lowest bear density was found in Haçka Plateau with 40 bears per 1000 km², and the highest density was found in Meydancık with 466 bears per 1000 km². The highest number of bears directly observed in a narrow area were detected in North Kaçkar. Here, 12 bears were observed between 2200-2700 m altitudes in an area of approximately 15 km². The reason why bears are concentrated in this area is *Petasites* sp., *Heracleum* sp. or *Angelica* sp. plants that are abundant in this region. It has been observed that bears are abundantly fed with the stems of these plants at the beginning of summer.

The highest number of bears hibernating in a narrow area were found in Demirdöven, at 1900 m altitude, on inaccessible forested steep slopes away from human influence. It was determined that 7 active dens here were excavated in an area of approximately 200 m² with 3-5 meters' intervals. Similarly, it was observed that 5 bears hibernate side by side in a narrow area of 50 m² in Uzungöl at an altitude of 1700 m. It has been determined that the dens here are located on the steep slopes of the old growth forest, at the bottom of overturned large logs or under large rocks.

Discussion

It has been determined that the bear population density in the Eastern Black Sea Mountains is 194.4 bear/1000 km², one of the highest bear density areas in the world. Regions with the highest bear density in the world; Katmai (551 bears), Admiralty (439.5 bears) in Alaska (Miller et al., 1997; LeFranc et al., 1987; Sellers et al., 1999), Romanian Carpathians (100-200 bears /1000 km²) (Swenson et al., 2000; MAFRD-MEWM, 2005), Dinaric Mountains of Slovenia (exceeding 400 bears/1000 km²) (Jerina et al., 2013) and the Shiretoko Peninsula (200 bears/1135 km²) in Hokkaido, Japan (Shimozuru et al., 2017).

The 194.4 bears/1000 km² detected in the Eastern Black Sea Mountains is much higher than most areas in the world. The bear population density in most parts of the world is below 50 bears/1000 km². The highest population density in British Columbia in 2015 was 40-50 bears/1000 km² (COSEWIC, 2012). In another study, the bear density in North America was 122 bears/1000 km² (Miller et al., 1997), while the bear density in Alaska was 31.4-54.5 bears/1000 km², with an average of 40.4 bears (Walsh et al., 2010). Bear densities detected in Europe are 0.096-0.105 bears/1000 km² in the Cantabrian Mountains (López-Bao et al., 2021), 0.5 bears /1000 km² in the south of Norway, 20-25 bears /1000 km² in central Sweden (Swenson et al., 2000; MAFRD-MEWM, 2005), 11.1±8.9 bears/1000 km² in Norway and 29.3±18.9 bears/1000 km² in Sweden (Støen et al., 2006) and 100 bears/1000 km² in Slovenia (Petram et al., 2004). While only 8-9 bears remain in France, populations in many regions have also disappeared (Swenson et al., 2000).

The density of bears detected in the Eastern Black Sea Mountains is higher than in all regions of Russia, where the most bears live in the world. In Russia, where 123869 bears live (Swenson et al., 2000), in 1990, the average density in the Northern and Central Taiga Part of the European part and the North Caucasus Mountain Forest Region was 0.18 bear/1000 km², the average density in the Southern Taiga and Northern Temperate Forests of the European part was 0.26 bear/1000 km², in the Ural Mountains the average density is 0.19 bear/1000 km², in the Altai Mountains the average density is 0.40 bear/1000 km², and in Siberia the average density is 0.05-0.06 bear/1000 km² was detected (Servheen et al., 1999). It is stated that a total of 6300 individuals, of which 3465 are adults, live in an area of 2400000 km² in East Turkestan and Western China in Central Asia (Gong and Harris, 2006). In the Southern Caucasus adjacent to the Eastern Black Sea Mountains, the bear population size is 2000-2500 and the minimum bear density is about 13 bears/1000 km² (Lortkipanidze, 2010). The highest density in the Caucasus was estimated at 59.4 bears/1000 km² in Armenia (Burton et al., 2018).

Bear densities in Alaska, which has the highest bear densities in the world, vary from region to region. Density distributions in the Eastern Black Sea Mountains also differ from region to region, as in Alaska. Bear densities in different regions in Alaska; Katmai National Park coastal (Bears of all ages, 551 bears/1000 km²), Admiralty Island (439.5 bears/1000 km² per bear), Kodiak Island (342 at Terror Lake and 323 at Karluk Lake), Black Lake /Alaska (191 bears/1000 km² per bear), The middle Susitna River Basin/Alaska (27 bears/1000 km²) and Portion of upper Susitna River/Alaska (10.7 bears/1000 km²) (Miller et al., 1997). In the Eastern Black Sea Mountains, the highest population density was determined in Meydancık with 466 individuals per 1000 km², followed by North Kaçkar with 240 individuals and Uzungöl with 187.5 individuals. The lowest population densities were determined in the western part of the area with 40 individuals in the Haçka Plateau and in the Gavur Mountains with 100 individuals.

The main reasons for these high differences in bear densities between the east and west of the area are due to habitat qualities and human population densities. Ahmadiparia et al. (2021) determined that bears, which they define as a species dependent on water and vegetation, generally prefer high elevations and areas away from humans in Iran. While habitat quality increases towards the east of the study area, human population density decreases. The population in the eastern part of the region with difficult living conditions migrated more to big cities and abroad. Bears benefit from fruits such as pears, apples, walnuts, cherries, rosehips, wild pear and figs in the villages whose population has decreased as a result of migration, more than in the past. Also, people in areas with high bear density are much more tolerant towards bears. There is less poaching and illegal killing here. It is stated that the main reason for the high bear density in the research area is that human pressure has decreased or disappeared in most places in the last 30-40 years (Başkaya et al., 2012). This decrease in human pressure is due to the decreasing population as a result of increasing immigration in the last 30-40 years, the increasing awareness of the people, the decrease in animal husbandry, and the abandonment of rural life and traditional life. So much so that the number of young people who can shoot a bear with a rifle or set a trap has decreased in the villages, and young people with these skills are not growing. For this reason, it is not possible to deal with bears as intensely as before. In addition to all these, teams, hunters and villagers counting in Meydancık, which has the highest bear density, state that there are actually many more bears than observed in the field. In

Meydancık inventories, only 1/4 of the area could be observed. In addition to the individuals that observers may not be able to see, it is thought that there are a large number of bears that do not come out of the forest into open areas and therefore cannot be observed.

All of the census results obtained at 12 sampling sites support each other for each site. It is seen that the results used for the population density at each site were obtained consecutively from the same sites in successive years. For example, 7 bears were observed consecutively on Mount Ovit and Tilkibeli in 2016 and 2017, and 10 bears were observed on South Kaçkar and Sesödile Mt. in 2015 and 2016 (Table 2). As an exception, censuses were carried out in 2015 and 2016 in Meydancık, where 2013 census results were used instead of 2016 and 2017 census results. In these censuses made with the small team of 4 people, less area of the sampling site could be observed. However, the 2015 and 2016 results obtained in Meydancık show that the census results obtained with the large teams in 2013 are still valid for the site.

Cubs and yearlings constituted 40% of the observed bears. Litter size varied from 1 to 4. The average litter size, which was determined as 2 by Nezami and Farhadina (2011) in Iran, was the same in this study. However, the average litter size was relatively lower in sampling areas with high bear density. The main reasons for this situation can be infanticide by males, high competition between females, or other predators such as wolves.

In order to minimize the duplication of counts, censuses in adjacent areas such as North Kaçkar and South Kaçkar and in areas close to each other such as Tilkibeli and Uzuntarla were carried out consecutively, with a maximum interval of one week. Only the censuses in Ovit and Yedigöl, which are close to each other, were made with an interval of two months. In cases where a clear distinction cannot be made, the records of the team that saw the most bears in that region were taken into account. The counts of other teams were not taken into account, thus avoiding duplicate counts.

Results of direct observation were combined with results of indirect observation, where very fresh footprints and feces were taken into account. For example, in an area where only male bears were observed in direct observations, fresh tracks determined to belong to a female with cubs were added to the results. Similarly, a bear footprint that is directly observed and wanders alone is considered as a separate individual since it does not belong to a mother bear walking with her cub. The footprints of a mother with a cub, a mother with two cubs, or an individual wandering alone, detected in two neighboring areas, are in different places and no matter how many, only one of the determinations has been added to the results. In addition, if there is a difference of more than 4 cm in the dimensions of the footprints, it is accepted that they belong to different individuals. A very fresh bear feces detected in an area where no bears were seen directly was also accepted as information that there was a bear in the field. Here, in doubtful cases, data obtained from indirect observations are not added to the results.

Conclusion

The proportion of habitats with similar characteristics to Meydancık, where the highest bear density is determined, is at least 10% of the total study area. Major similar areas are the Yağlıdere Valley and the north of Karagöl in Giresun; north of Çat Valley and Verçenik Mountain in Rize; Sırakonak and Çamlıkaya Valleys in Erzurum; Dokumacılar, Çevreli, Tekkale, Balcı and Berta Valleys in Artvin. In other words, the

high-density value obtained in Meydancık is not a factor that increases the average result. Even if Meydancık is excluded, the bear population density in the Eastern Black Sea Mountains is 161 individuals/1000 km², which is higher than many places mentioned in the literature.

Inventory teams, local people and hunters estimate that there are more bears than detected in all sampling areas. Because, in reality, most of the sampling areas could not be observed due to forests, vegetation and rocks. Only individuals who went out into the open field and were definitely identified were taken into account. In addition, all suspicious observations and situations with the possibility of duplicate counting were avoided. For this reason, it is estimated that much higher density values will be obtained than those obtained in this study, if counting with DNA analysis is performed.

Acknowledgments. This manuscript is a part of a PhD thesis written by Ebru BAŞKAYA. We would like to thank Dr. Alptuğ SARI and Dr. Ahmet ARPACIK from Karadeniz Technical University, Department of Wildlife Ecology and Management, Edva Tuna PİRSELİMOĞLU, President of the Eastern Black Sea Hunting Federation, and Forest Engineer Yakup KÖSE for their valuable assistance in some inventories. We also thank the General Directorate of Nature Conservation and National Parks for their contributions to the large teams' inventories in Meydancık, Gavur Mountain and Uzungöl.

REFERENCES

- [1] Ahmadiparia, M., Yavaria, A., Ghobadib, M. (2021): Ecological monitoring and assessment of habitat suitability for brown bear species in the Oshtorankoooh protected area, Iran. – *Ecological Indicators* 126: 107606.
- [2] Ambarlı, H. (2012): Spatio-temporal ecology, habitat use and population size of brown bears (*Ursus arctos*) in Yusufeli, Turkey. – PhD, Middle East Technical University, Ankara, Turkey.
- [3] Ambarlı, H., Ertürk, A., Soyumert, A. (2016): Current status, distribution, and conservation of brown bear (Ursidae) and wild canids (gray wolf, golden jackal, and red fox; Canidae) in Turkey. – *Turkish Journal of Zoology* 40: 944-956.
- [4] Başkaya, Ş., Bilgili, E. (2004): Does the leopard *Panthera pardus* still exist in the Eastern Karadeniz Mountains of Turkey? – *Oryx* 38: 228-232.
- [5] Başkaya, Ş., Başkaya, E., Bilgili, E., Gülci, S. (2008): Population status and principal threats for big carnivores in alpine areas of Turkey. – *Mammalian Biology* 73, 82nd Annual Meeting of the German Soc. of Mammalogy, ISSN 1616–5047, 4-45, Vienna.
- [6] Başkaya, Ş., Başkaya, E., Arpacık, A. (2012): Relationship between forest protection and hunting tourism in Turkey. – *African Journal of Agric. Res.* 7(42): 5620-5628.
- [7] Burton, A. C., Fisher, J. T., Adriaens, P., Treweek, J., Paetkau, D., Wikstrom, M., Callender, A., Vardanyan, R., Stepanyan, A. (2018): Density and distribution of a brown bear (*Ursus arctos*) population within the Caucasus biodiversity hotspot. – *Journal of Mammalogy* 99(5): 1249-1260.
- [8] Calvignac, S., Hughes, S., Hänni, C. (2009): Genetic diversity of endangered brown bear (*Ursus arctos*) populations at the crossroads of Europe, Asia and Africa. – *Biodiversity Research, Diversity and Distributions*, Blackwell Publishing Ltd.
- [9] Can, Ö. E. (2004): Status, conservation and management of large carnivores in Turkey. – *Convention on the Conservation of European Wildlife and Nature Habitats, Standing Committee, 24th meeting, T-PVS/Inf, Strasbourg.*
- [10] Can, Ö. E., Togan, İ. (2004): Status and management of brown bears in Turkey. – *Ursus* 15(1): 48-53.

- [11] Caucasus Biodiversity Council (CBC). (2012): Ecoregion conservation plan for the Caucasus. – World Wildlife Fund for Nature, KFW Entwicklungsbank and Federal Ministry for Economic Cooperation and Development. 64 pages.
- [12] Central Hunting Commission Decision (CHCD). (2015): Central Hunting Commission Decision for 2015-2016. – Official Gazette of the Republic of Türkiye, Ankara.
- [13] Central Hunting Commission Decision (CHCD). (2021): Central Hunting Commission Decision for 2021-2022. – Official Gazette of the Republic of Türkiye, Ankara.
- [14] Committee on the Status of Endangered Wildlife in Canada (COSEWIC). (2012): Cosewic assessment and status report on the Grizzly Bear *Ursus arctos* in Canada. – Ottawa. Xiv, 84.
- [15] Demirsoy, A. (1996): Türkiye omurgalıları (Turkey vertebrates), Memeliler (Mammals). – Çevre Bakanlığı, Proje No: 90, Yayın No: 03-06-Y-0057-06, Ankara.
- [16] Gong, J., Harris, R. (2006): The status of bears in China. – Understanding Asian bears to secure their future, pp. 96-101. Japan Bear Network, Ibaraki, Japan.
- [17] Gündoğdu, E., Başkaya, Ş. (2013): Sustainable hunting management sub-working group report. – 1st Forestry and Water Council, Ankara, Türkiye, 21-23, 1-3.
- [18] International Union for Conservation of Nature (IUCN). (2016): Brown bear (*Ursus arctos*). – Red list, Supplementary Information, 26 pages.
- [19] Jerina, K., Jonozovič, M., Krofel, M., Skrbinšek, T. (2013): Range and local population densities of brown bear *Ursus arctos* in Slovenia. – Eur. J. Wildl. Res. 59: 1-9.
- [20] LeFranc, M. N., Moss, M. B., Patnode, K. A., Sugg, W. C. (1987): Grizzly bear compendium. – The National Wildlife Federation Washington D.C.
- [21] López-Bao, J. V., Godinho, R., Palomero, G., Ballesteros, F., Blanco, J., Jimenez, J. (2021): Monitoring of the expanding Cantabrian brown bear population (Chapter 2). – Cantabrian bears. Demographics, Coexistence and Conservation Challenges, pp. 23-37.
- [22] Lortkipanidze, B. (2010): Brown bear distribution and status in the South Caucasus. – Ursus 21: 97-103.
- [23] Lynch, W. (2021): Bears of the north: A year inside their worlds. – JHU Press, Nature, 352p.
- [24] McLellan, B. N., Servheen, C., Huber, D. (2008): *Ursus arctos*. – The IUCN Red List of Threatened Species 2008, e.T41688A10513490.
- [25] Miller, S. D., White, G. C., Sellers, R. A., Reynolds, H. V., Schoen, J. W., Titus, K., Barnes, V. G., Smith, R. B., Nelson, R. R., Ballard, W. B., Schwartz, C. C. (1997): Brown and black bear density estimation in Alaska using radiotelemetry and replicated mark-resight techniques. – Wildlife Monographs 133: 3-55.
- [26] Ministry of Agriculture, Forestry and Rural Development - Ministry of Environment and Water Management (MAFRD-MEWM) (2005): Management and action plan for the bear population in Romania. – 79 pages.
- [27] Moqanaki, E. M., Jiménez, J., Bensch, S., López-Bao, J. V. (2018): Counting bears in the Iranian Caucasus: Remarkable mismatch between scientifically-sound population estimates and perceptions. – Biological Conservation 220: 182-191.
- [28] Morton, J. M., Bray, M., Hayward, G. D., White, G. C., Paetkau, D. (2013): The Kenai brown bear population on Kenai National Wildlife Refuge and Chugach National Forest. – US Fish and Wildlife Service - US Forest Service. 39p.
- [29] Murtskhvaladze, M., Tarkhnishvili, D. (2006): Estimation of brown bear abundance and population structure in Borjom-Kharagauli National Park with molecular-genetic methods. – In Proceedings of the Georgian Academy of Sciences, Biological Series B, Tbilisi, Georgia, pp. 43-50.
- [30] Nezami, B., Farhadina, M. S. (2011): Litter sizes of brown bears in the Central Alborz Protected Area, Iran. – Ursus 22(2): 167-171.
- [31] Petram, W., Knauer, F., Kaczensky, P. (2004): Human influence on the choice of winter dens by European brown bears in Slovenia. – Biol. Conservation 119: 129-136.

- [32] Proctor, M. F., Paetkau, D., McLellan, B. N., Stenhouse, G. B., Kendall, K. C., Mace, R. D., Kasworm, W. F., Servheen, C., Lausen, C. L., Gibeau, M. L., Wakkinen, W. L. (2012): Population fragmentation and inter-ecosystem movements of grizzly bears in western Canada and the northern United States. – *Wildlife Monographs* 180(1): 1-46.
- [33] Sarı, A., Gündoğdu, E., Başkaya, Ş., Arpacık, A. (2020): Habitat preference by the Anatolian leopard (*Panthera pardus tulliana* Valenciennes, 1856) in North-eastern Anatolia, Turkey. – *Belgian Journal of Zoology* 150: 153-168.
- [34] Sellers, R. A., Miller, S., Smith, T., Potts, R. (1999): Population dynamics of a naturally regulated brown bear population on the coast of Katmai national park and preserve. – Final Resource Report NPS/AR/NRTR-99/36, National Park Service, Alaska Region and Alaska Department of Fish and Game, 49p.
- [35] Servheen, C., Herrero, S., Peyton, B. (1999): Status survey and conservation action plan, Bears. – International Union for Conservation of Nature - IUCN/SSC Bear Specialist Group, IUCN/SSC Polar Bear Spec. Group, 320.
- [36] Shimozuru, M., Yamanaka, M., Nakanishi, M., Moriwaki, J., Mori, F., Tsujino, M., Shirane, Y., Ishinazaka, T., Kasai, S., Nose, T., Masuda, Y., Tsubota, T. (2017): Reproductive parameters and cub survival of brown bears in the Rurua area of the Shiretoko Peninsula, Hokkaido, Japan. – *PLoS One* 12(4): e0176251.
- [37] Smith, R. B., Van Daele, L. J. (1991): Terror Lake hydroelectric project, Kodiak Island, Alaska. – Final Report 1. Brown bear studies (1982-86). Alaska Department of Fish and Game and Alaska Power Authority.
- [38] Støen, O. G., Zedrosser, A., Sæbø, S., Swenson, J. E. (2006): Inversely density-dependent natal dispersal in brown bears *Ursus arctos*. – *Oecologia* 148: 356-364.
- [39] Swenson, J. E., Gerstl, N., Dahle, B., Zedrosser, A. (2000): Action plan for the conservation of the brown bear in Europe (*Ursus arctos*). – Nature and Environment, Council of Europe Publishing, Strasbourg 114: 1-70.
- [40] Turan, N. (1990): Türkiye'nin Av ve Yaban Hayvanları (Türkiye's Game and Wild Animals), Kuşlar (Birds). – OGM Eğitim Dairesi Başkanlığı Yayın ve Tanıtma Şube Müdürlüğü Matbaası, Ankara, 267.
- [41] Türkiye Statistical Institute (TUIK). (2020): Address based population registration system results. – Türkiye Statistical Institute Bulletin, Ankara, Türkiye.
- [42] Van Daele, L. J. (2007): Population dynamics and management of brown bears on Kodiak Island, Alaska. – Doctoral dissertation, University of Idaho.
- [43] Van Daele, L. J., Crye, J. R. (2007): Brown bear management report of survey and inventory activities, 1 July 2004-30 June 2006. – Alaska Department of Fish and Game, Juneau, Alaska, Unit 8, pp. 75-108.
- [44] Van Daele, L. J., Barnes, V. G., Jerrold, L., Belant, J. L. (2012): Ecological flexibility of brown bears on Kodiak Island, Alaska. – *Ursus* 23(1): 21-29.
- [45] Walsh, P., Reynolds, J., Collins, G., Russell, B., Winfree, M., Denton, J. (2010): Application of a double-observer aerial line-transect method to estimate brown bear population density in southwestern Alaska. – *J. of Fish and Wildlife Management* 1: 47-58.
- [46] Zedrosser, A., Dahle, B., Swenson, J. E., Gerstl, N. (2001): Status and management of the brown bear in Europe. – *Ursus* 12: 9-20.

DIFFERENCES IN THE STRUCTURAL AND FUNCTIONAL TRAITS OF *POPULUS EUPHRATICA* AND *POPULUS PRUINOSA* WITH TREE HEIGHT

ZHAI, J. T.^{1,2,3} – LI, Z. J.^{1,2,3*} – ZHANG, S. H.^{1,2,3} – HAN, X. L.^{1,2,3} – LI, X.^{1,2,3}

¹Key Laboratory of Protection and Utilization of Biological Resources in Tarim Basin Xinjiang Production and Construction Corps, Alar, Xinjiang 843300, China

²Desert Poplar Research Center of Tarim University, Alar, Xinjiang 843300, China

³College of Life Science, Tarim University, Alar, Xinjiang 843300, China

*Corresponding author

e-mail: lizhijun0202@126.com; phone: +86-997-468-1202

(Received 24th Feb 2022; accepted 20th May 2022)

Abstract. *Populus euphratica* Oliv. and *Populus pruinosa* Schrenk are distributed on the banks of desert rivers in arid and semi-arid regions. By studying the variation of the structural and functional traits of *P. euphratica* and *P. pruinosa* with tree height, the differences in the structural and functional traits of the heteromorphic leaves were compared. The study determined the changes of the morphological structure, photosynthetic water physiology, osmotic adjustment substances and endogenous hormone content of the two species with the height of the tree. The results showed that with the increase of tree height, the leaf area (LA), leaf thickness (LT), palisade tissue thickness (PT), main vein xylem area (MXA), vessel area (VA), vessel number (VN) and net photosynthetic rate (Pn) of *P. euphratica* and *P. pruinosa*, $\delta^{13}\text{C}$, proline content, malondialdehyde (MDA) and endogenous hormone GA₃, IAA, ZR content showed an increasing trend, and there was a significant positive correlation with tree height. The Pn at 10 m, the Tr at 6 m, 8 m, and 10 m, the $\delta^{13}\text{C}$ and the content of MDA, soluble protein, ABA, and IAA at each height for *P. euphratica* is significantly larger than *P. pruinosa*. These results suggested that *P. euphratica* have the more stronger ability to resistance to drought than *P. pruinosa* for its more invests in leaves, more xerophytic leaf morphology and anatomical structure, higher photosynthetic water use efficiency, stronger ability of osmotic adjustment.

Keywords: desert poplars, heteromorphic leaves, morphological structure, osmotic adjustment, endogenous hormones, photosynthetic water physiology

Abbreviations: LI = leaf index; LA = leaf area; LT = leaf thickness; SLA = Specific Leaf Area; PT = Palisade tissue thickness; PSR = Ratio of palisade tissue to spongy tissue; MVBA = Main vein vascular bundle area; MXA = Main vein xylem area; XVBR = Main vein xylem/main vascular bundle area; VA = Vessel area; Pn = Photosynthetic rate; Tr = Transpiration rate; Gs = Stomatal conductance; Ci = Intercellular CO₂ concentration; WUEi = Instantaneous water use efficiency; $\delta^{13}\text{C}$ = Stable carbon isotope value; Pro = Proline; MDA = Malondialdehyde; SS = Soluble sugar; SP = Soluble protein; BA = Abscisic acid; GA₃ = Gibberellin; IAA = Indoleacetic acid; ZR = Zeatin Riboside

Introduction

Populus euphratica Oliv. and *Populus pruinosa* Schrenk. have different distribution areas. The total area of *P. euphratica* forests in the world is about $6.48 \times 10^5 \text{ hm}^2$, and its distribution spans across the three continents of Europe, Asia and Africa. Among them, 60% of *P. euphratica* in the world is distributed in China, and 91.1% of *P. euphratica* in China is concentrated in the Tarim River Basin in Xinjiang (Wang, 1996), while *P. pruinosa* is only distributed in the Tarim Basin in China, and both are the dominant riparian tree species of the Tarim River (Li et al., 2021). The phenomenon of plant leaf morphology changes along the longitudinal axis is called heterophylly, which is the

result of leaf phenotypic plasticity and helps plants adapt to environmental changes (Nakayama et al., 2017; Zeng et al., 2019), while *Populus euphratica* and *P. pruinosa* are heteromorphic leaf plants, but their leaves have morphological differences. For example, from the base to the top of the crown, the leaves of mature *Populus euphratica* will appear in four leaf shapes: strip, lanceolate, ovate and broad-ovate. In contrast, *P. pruinosa* is found on seedlings, saplings and adult trees, and oval, round and broad-ovate-shaped leaves appear in sequence (Liu et al., 2016; Yu et al., 2020).

Leaves are the most sensitive organs to environmental factors and show different adaptation strategies in different environments (Bao et al., 2009; Zirbel et al., 2017). The different canopies of trees often produce vertical gradients due to the projection of sunlight, which causes differences in the anatomical structure and physiological metabolism of the leaves on the upper and lower layers of the canopy (Aranda et al., 2004; Niinemets et al., 2015). At the same time, as the water potential of the xylem of the tree decreases as the height of the tree increases, the difference in water pressure in the height gradient will affect the morphological structure of the leaves of the corresponding tree height. The upper leaves of the tree can only hinder the water loss through a more obvious xeromorphic structure in order to cope with water stress caused by tree height (He et al., 2008; Ryan et al., 1997). Previous studies have shown that the heteromorphic leaves of *P. euphratica* are isofaceted, with thick stratum corneum, subcutaneous layer and subporous chambers, containing more mucous cells, and showing obvious xerophytic structural characteristics. However, from stomata density, stomata size, compared with the degree of stomata subsidence and the degree of mesophyll development, the broad-ovate xerophyte structure is more developed than other leaf shapes and has a stronger ability to resist adversity (Bai et al., 2011; Wang, 1996; Yang et al., 2004; Zhao et al., 2016; Zheng et al., 2007). Leaf area, leaf thickness and petiole length of *P. euphratica* and *P. pruinosa*, showed the positive correlation with the diameter at breast height and tree height (Liu et al., 2016; Zhao et al., 2016). At the same time, the ABA and ZR content of *P. euphratica* showed an increasing trend with the increase of tree age and tree height (Huang et al., 2010a, b). In coniferous trees, the net photosynthetic rate usually decreases with the increase in tree height (Ishii et al., 2008), while in broad-leaved trees, the net photosynthetic rate varies with the height of the tree (Miyata et al., 2016; Sendall et al., 2013; Zhang et al., 2009). At different canopy heights of the same tree, the broad-ovate leaves at the top of the *P. euphratica* canopy have stronger photosynthetic capacity, osmotic adjustment capacity and water use efficiency than the rest of the leaf shape (Bai et al., 2011; Zhai et al., 2020; Zheng et al., 2007), with more effective energy distribution and utilization strategies. In addition, the salt and drought stress studies on *P. euphratica* and *P. pruinosa* seedlings have shown that *P. euphratica* and *P. pruinosa* have species-specific variations. Under the influence of drought stress, salt stress and interactions, *P. euphratica* suffers a greater negative impact than *P. pruinosa* (Yu et al., 2020).

For woody plants, growth is not only affected by environmental soil drought, but also by changes in water potential caused by changes in their height (Ryan and Yoder, 1997). Previous studies on the heteromorphic leaves of *P. euphratica* under suitable water conditions found that the morphology, anatomical structure and physiological characteristics of the leaves are related to the coronal position, and they change synergistically along the tree height gradient (Li et al., 2021; Zhai et al., 2020). However, there is currently no research under soil drought conditions. In addition, the changes in the morphological structure and photosynthetic water physiology of *P. pruinosa* with tree

height are still unclear. We hypothesized that under soil drought stress, *P. euphratica* and *P. pruinosa* have different adaptation strategies for leaf traits as the height of the tree increases, and *P. euphratica* shows stronger adaptability than *P. pruinosa*.

Materials and methods

Study area

The study area, located in the north-western margin of the Tarim Basin in Xinjiang Province of China, has a typical temperate desert climate. The annual average annual rainfall is approximately 50 mm, the potential evaporation reaches up to 1,900 mm, the yearly annual average temperature is 10.8 °C, and the average annual average sunshine hours duration is 2,900 h (Zhai et al., 2020). As sampling points for comparison located in Shaya County (82°00'22.69" E, 40°41'10.91" N, 977 m a.s.l.), with a groundwater level of 5 m (Fig. A1).

Plant samples and sampling method

In the sampling area, 5 *Populus euphratica* and 5 *Populus pruinosa* with diameter at breast height of 15 cm, tree age of 12 years and height of 10 m were selected, respectively. Samples were obtained at heights of 2, 4, 6, 8, and 10 m starting from the base of the trunk of each tree. We collected 30 branches from each sampling layer, selected the fourth node leaf from each branch, and took 30 leaves in total. A portion of the leaves was quickly frozen with liquid nitrogen and stored at -80 °C to determine the content of proline, malondialdehyde, soluble sugar, and hormones; another sample of the leaves was fixed with formalin-alcohol-glacial acetic acid mixed fixative (FAA). The fixed samples were used to prepare tissue sections; a part of the leaves was used to determine the morphological indicators of abnormal leaves. Sampling was done during the vigorous growth period of *P. euphratica* in mid-July. The leaf photosynthetic index was measured from 11:00 to 13:00 on clear and cloudless days.

Determination of the morphological and anatomical structural indexes of heteromorphic leaves

We used a scanner (MRS-9600TFU2, China) and the LA-S plant image analysis software to measure the leaf length, leaf width, and leaf area of *P. euphratica* and *P. pruinosa*. The leaf shape index (LI) was calculated on the basis of the leaf length/width ratio. The collected leaves were processed for deactivation (10 min) at 105 °C and heated at 65 °C to a constant weight. After the sample reached a constant weight, the material was cooled to room temperature (25 °C) in a desiccator and weighed with an electronic balance with an accuracy of 0.001 g; the specific leaf area (SLA) was then calculated.

The leaf blade was cut transversely at its widest section. The material that retained the primary vein and leaf margin was selected and fixed in a formalin–acetic acid–alcohol (FAA) solution. Paraffin-embedded tissue sections (8 µm thick) were prepared, double-stained with safranin–fast green, and mounted in a neutral resin. Observation and determination of the palisade tissue (PT), main vein vascular bundle area (MVBA), main vein xylem area (MXA), main vein xylem area (VA) were performed using a Leica microscope (Leica DM4 B, Wetzlar, Germany). The gate-to-sea ratio (PSR), main vein xylem, vascular bundle area ratio (XVBR), five fields of view per leaf, 20 values

per field of view, and average value of leaf anatomical structure parameters of five fields of view were taken as the parameter values of anatomical structural index of each leaf.

Determination of gas exchange indices of heteromorphic leaves

Branch shears were used to cut branches of the current year. The branches were wrapped immediately with fresh-keeping film to cover the cut ends. The fourth node leaves from the base of the branches were used to measure the gas exchange parameters with a LI-COR 6400 portable photosynthesis measuring system (LI-COR, Lincoln, NE). The net photosynthetic rate (P_n), transpiration rate (T_r), stomatal conductance (G_s), and intercellular CO_2 concentration (C_i) values were obtained.

The photosynthetic physiological indices of the leaves were measured with the Li-6400 photosynthesis instrument, and the instantaneous water use efficiency ($WUE_i = P_n/T_r$) of the irregular leaves was calculated. The leaf samples were washed and air-dried, then dried at 65 °C for 36 h, pulverised with a grinder, and passed through a 90-mesh sieve to prepare test samples. The carbon isotope analysis of the plant samples was prepared using a glass vacuum system. The furnace temperature of the burner was controlled at 1,000 °C. The system was evacuated and O_2 was passed through. The porcelain spoon containing the sample of *P. euphratica* leaves was placed in the combustion tube in the high-temperature zone. After burning for 2 min, the CO_2 gas was collected and purified by freezing. A stable gas isotope mass spectrometer (Thermo Fisher Scientific, Inc., Waltham, MA) was used to analyse the carbon isotope composition ($\delta^{13}C$ value) of the purified CO_2 gas.

Determination of physiological and biochemical indices of heteromorphic leaves

The acid ninhydrin method was used to determine the leaf proline content. The MDA content was determined with the thiobarbituric acid colour method, and the SS content was determined with the anthrone colourimetry method. The Coomassie brilliant blue G-250 dyeing method was used to determine the SP content of leaves (Zhai et al., 2020).

Determination of endogenous hormone content in heteromorphic leaves

We took the leaves (without petioles) at the fourth node of the branches, quickly froze them with liquid nitrogen, and stored them at -80 °C. The enzyme-linked immunoassay method was used to determine the content of abscisic acid (ABA), gibberellin (GA_3), indoleacetic acid (IAA), and zeatin riboside (ZR).

Statistical analysis

Statistical analyses were performed using the Statistical Package for the Social Sciences (SPSS, Chicago, IL, USA) version 18.0. Tukey's HSD test was conducted to detect significant differences between different heights and different tree species. All statistical effects were considered significant at $P < 0.05$. All data were normally distributed and single-peaked. In addition, pearson correlation analysis was used to analyze the correlation between the indicators, comprehensive evaluation of drought resistance of *P. pruinosa* and *P. euphratica* by membership function method. We used linear regression analysis to evaluate the impact of endogenous hormone on structural traits.

Results

Changes in the morphological characters of heteromorphic leaves with the increase of tree height

P. euphratica and *P. pruinosa* heteromorphic leaf morphology changes significantly with the increase of tree height (Fig. 1a-c). For example, the leaf shape index (LI) at a height of 2 m is significantly larger than the other heights. LA and LT show an increasing trend with the increase of tree height, and have a significant positive correlation with tree height (Tables A1 and A2). From the height of the tree from 2 m to 10 m, the LA of *P. euphratica* increased by 73.79%, which was greater than the 22.54% increase of *P. pruinosa*, and the SLA of *P. euphratica* decreased by 18.32%, which was less than the decrease of 38.47% of *P. pruinosa*, and the height of the top (10 m) of the LA and SLA of *P. euphratica* were significantly larger than *P. pruinosa*, and the LT at 8 m and 10 m of *P. euphratica* was significantly larger than that of *P. pruinosa*.

Correlation analysis showed that the LA of *P. euphratica* and *P. pruinosa* showed a significant positive correlation with LT and a significant negative correlation with the LI. The SLA of *P. pruinosa* showed a significant negative correlation with LT, while *P. euphratica* had no significant correlation (Tables A1 and A2), indicating that the relationship between *P. euphratica* and *P. pruinosa* with the increase of the height of the leaf morphology is different.

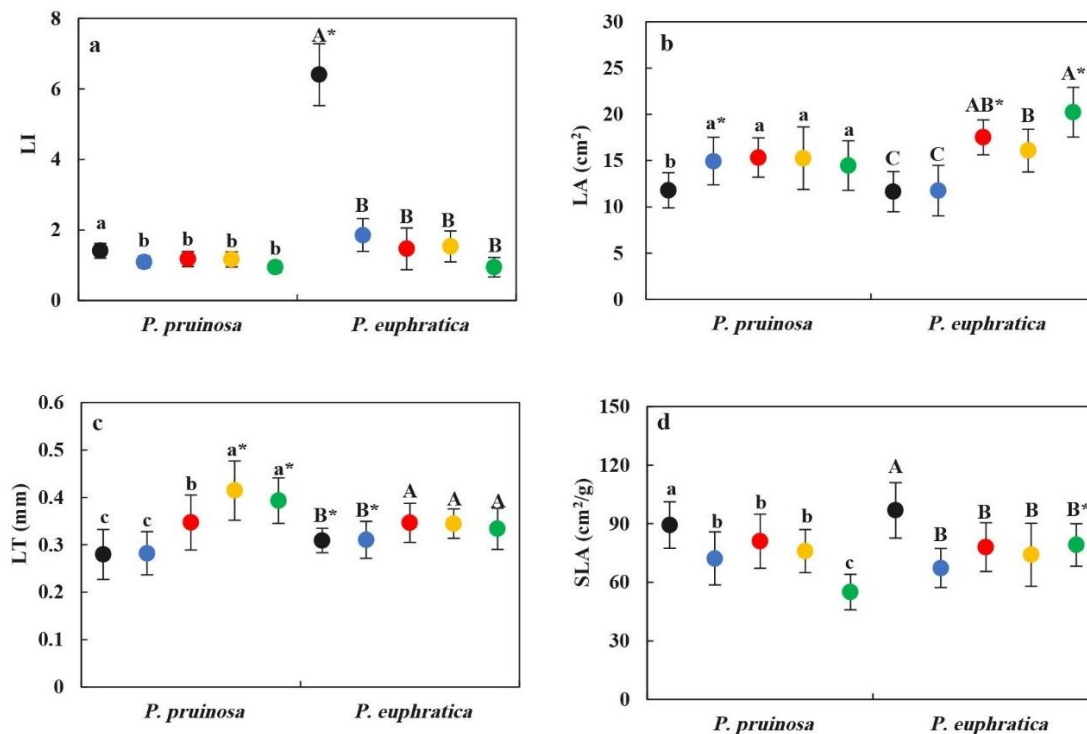


Figure 1. Changes in morphological characteristics of heteromorphic leaves with tree height of *P. pruinosa* and *P. euphratica*. Each value is the mean \pm SE. Note: The black dot indicates the height of the 2 m tree, the blue dot indicates the height of the 4 m tree, the red dot indicates the height of the 6 m tree, the yellow dot indicates the height of the tree 8 m, and the green dot indicates the height of the 10 m tree. According to Tukey's HSD test, lowercase and uppercase letters represent the significance of the difference between different sampling heights of *P. pruinosa* and *P. euphratica*. * The representing the comparison of the same height among species was significantly higher value ($P < 0.05$)

Changes of anatomical structure characters of heteromorphic leaves with increase tree height

P. euphratica and *P. pruinosa* heteromorphic leaf PT, MXA, VA, and VN showed an increasing trend with the increase of tree height (Fig. 2a-f), and there was a significant positive correlation with tree height (Tables A1 and A2). *P. euphratica* PSR, XVBR increased with the increase of tree height, and showed a significant positive correlation with tree height, while *P. pruinosa* had no significant correlation, indicating that the characteristics of the xerophytic structure of *P. euphratica* the increase in tree height is reflected in more aspects than *P. pruinosa*. At the same time, it was also found that the PT, MXA, XVBR, and VA at 8 m and 10 m were significantly larger than that of *P. pruinosa*. From the height of the tree from 2 m with 10 m, *P. euphratica* of PSR increased by 26.03%, which is obviously greater than the 0.37% increase of *P. pruinosa*, indicating that the xerophytic structural characteristics of the top leaves of the tree height are more obvious than that of *P. pruinosa*.

Changes in gas exchange capability of heteromorphic leaves with increase of tree height

The photosynthetic capacity of *P. euphratica* and *P. pruinosa* showed an increasing trend with the increase of tree height (Fig. 3a-d). The Pn, Tr with tree height are significantly positively correlated (Tables A1 and A2). From the height of 2 m to 10 m, the Pn of *P. euphratica* and *P. pruinosa* were increased by 49.36% and 33.95%, and the Tr increased by 86.76% and 20.28% respectively. At the same time, the Ci of *P. euphratica* at a height of 10 m was significantly lower than that of other heights, while the Ci of *P. euphratica* had no significant difference at different tree heights. In addition, the Pn, Tr and Gs of *P. euphratica* heteromorphic leaves are significantly positively correlated with LA, while only the Pn of *P. pruinosa* is significantly positively correlated with LA, indicating that with the increase of tree height under drought stress conditions, The photosynthetic capacity of *P. euphratica* and *P. pruinosa* have different changes.

The $\delta^{13}\text{C}$ of the heteromorphic leaves of *P. euphratica* and *P. pruinosa* showed an increasing trend with the increase of tree height (Fig. 4b). Although there is no significant change in WUE_i, the $\delta^{13}\text{C}$ value is positively correlated with tree height (Tables A1 and A2). The $\delta^{13}\text{C}$ value of *P. euphratica* is significantly positively correlated with the Pn and LA, indicating that the water use efficiency increases with the height of the tree and is closely related to the height and LA of the tree where the heteromorphic leaves are located. Compared with different species, *P. euphratica* had significantly higher $\delta^{13}\text{C}$ values than those of *P. pruinosa* in different heights, and the long-term water use efficiency of *P. euphratica* was higher than that of *P. pruinosa*.

Changes in physiological characteristics of heteromorphic leaves with increase of tree height

The Pro content of the heteromorphic leaves of *P. euphratica* at a height of 2 m was significantly smaller than the other heights, and the proline content of *P. pruinosa* at 2 m was significantly less than that of 8 m. From 2 m to 10 m, the increase in Pro content of *P. euphratica* is twice that of *P. pruinosa* (Fig. 5a-d). The Pro content of 8 m and 10 m and the content of MDA and SP in each height of *P. euphratica* were

significantly higher than those of *P. pruinosa*, indicating that the osmotic adjustment ability of the heteromorphic leaves at the top of the crown of *P. euphratica* was stronger than that of *P. pruinosa*.

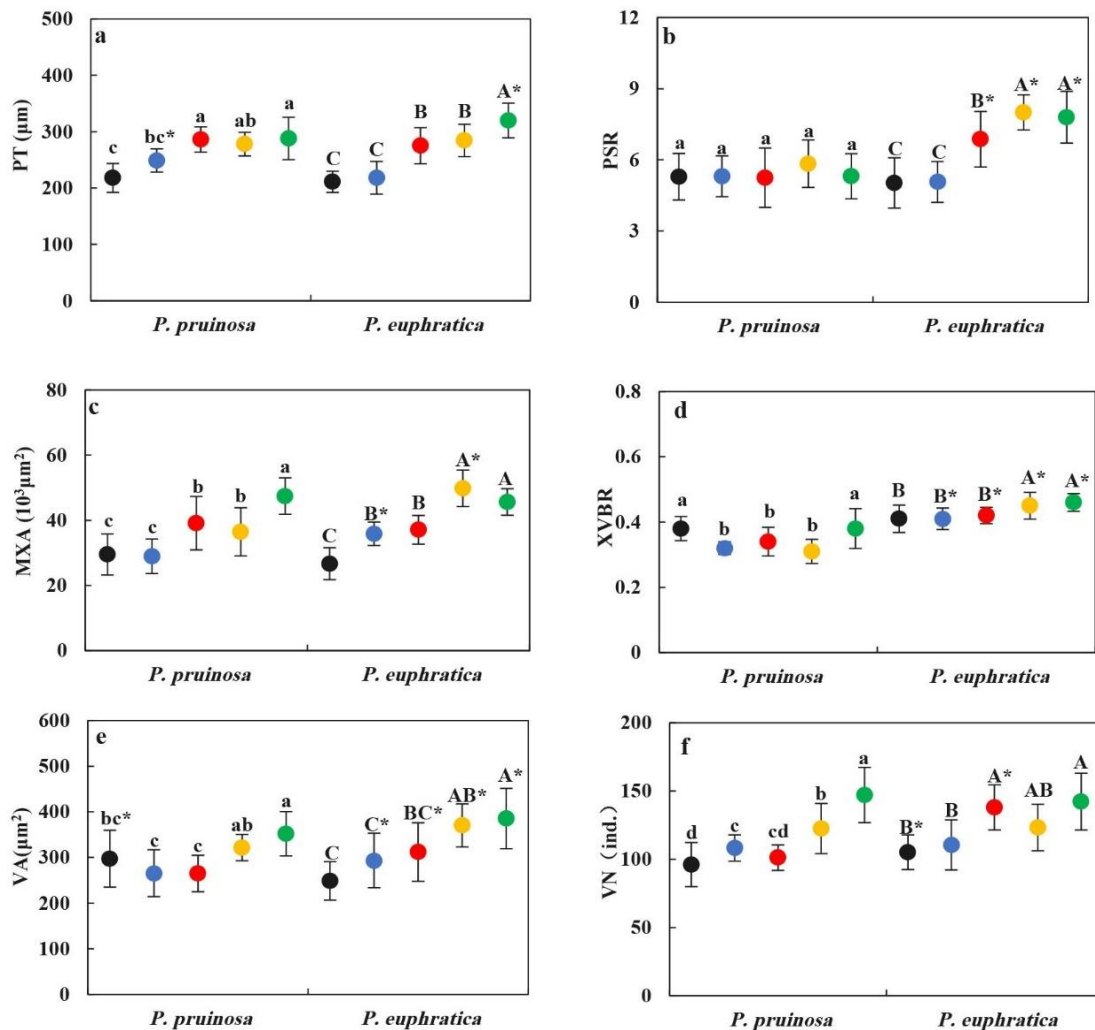


Figure 2. Changes in anatomical structure characters of heteromorphic leaves with tree height of *P. pruinosa* and *P. euphratica*. Each value is the mean \pm SE. Note: The black dot indicates the height of the 2 m tree, the blue dot indicates the height of the 4 m tree, the red dot indicates the height of the 6 m tree, the yellow dot indicates the height of the tree 8 m, and the green dot indicates the height of the 10 m tree. According to Tukey's HSD test, lowercase and uppercase letters represent the significance of the difference between different sampling heights of *P. pruinosa* and *P. euphratica*. * The representing the comparison of the same height among species was significantly higher value ($P < 0.05$)

Correlation analysis showed that the Pro content of *P. euphratica* was significantly positively correlated with tree height, LA, RT, PSR, VA, and Pn, while the Pro content of *P. pruinosa* was only relate LA and Pn significantly positive correlation (Tables A1 and A2), It shows that the increase of Pro content with the height of the tree is closely related to the increase of the height and LA of the tree where the heteromorphic leaves are located.

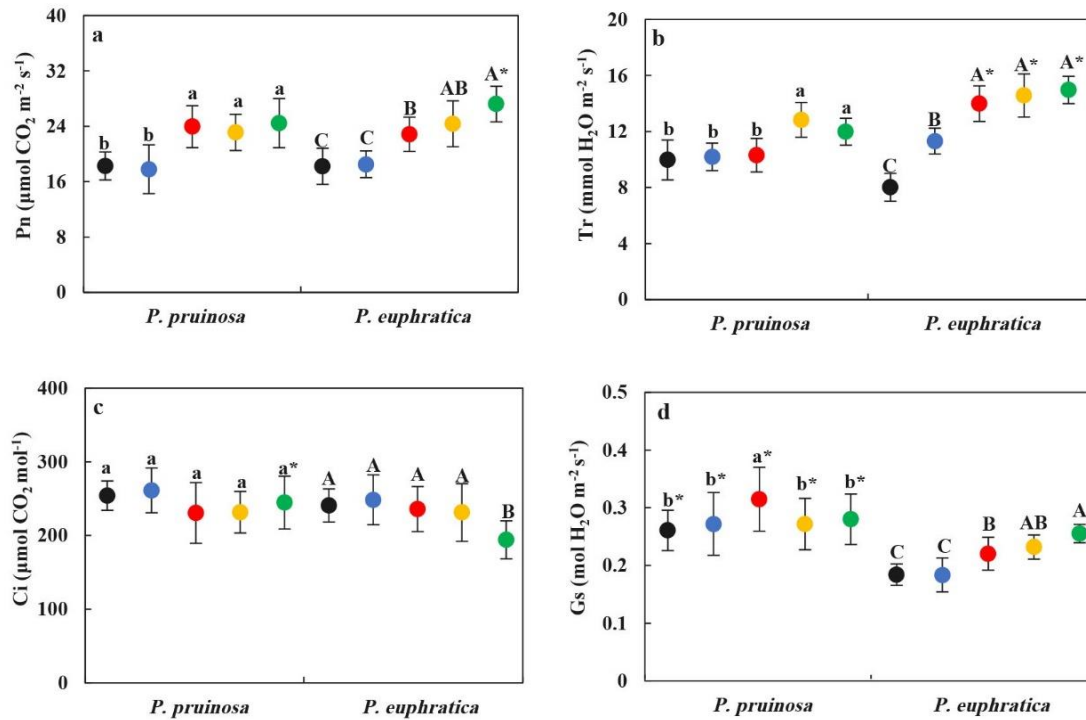


Figure 3. Changes in photosynthetic physiological parameters of heteromorphic leaves with tree height of *P. pruinosa* and *P. euphratica*. Each value is the mean \pm SE. Note: The black dot indicates the height of the 2 m tree, the blue dot indicates the height of the 4 m tree, the red dot indicates the height of the 6 m tree, the yellow dot indicates the height of the tree 8 m, and the green dot indicates the height of the 10 m tree. According to Tukey's HSD test, lowercase and uppercase letters represent the significance of the difference between different sampling heights of *P. pruinosa* and *P. euphratica*. * The representing the comparison of the same height among species was significantly higher value ($P < 0.05$)

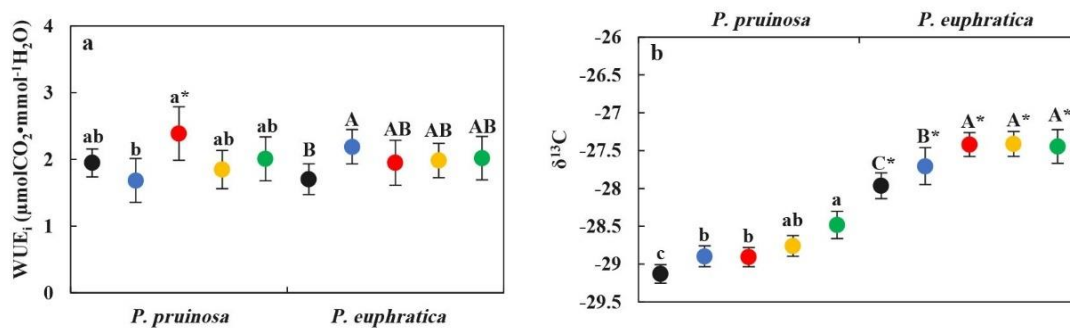


Figure 4. Changes in water use efficiency of heteromorphic leaves with tree height of *P. pruinosa* and *P. euphratica*. Each value is the mean \pm SE. Note: The black dot indicates the height of the 2 m tree, the blue dot indicates the height of the 4 m tree, the red dot indicates the height of the 6 m tree, the yellow dot indicates the height of the tree 8 m, and the green dot indicates the height of the 10 m tree. According to Tukey's HSD test, lowercase and uppercase letters represent the significance of the difference between different sampling heights of *P. pruinosa* and *P. euphratica*. * The representing the comparison of the same height among species was significantly higher value ($P < 0.05$)

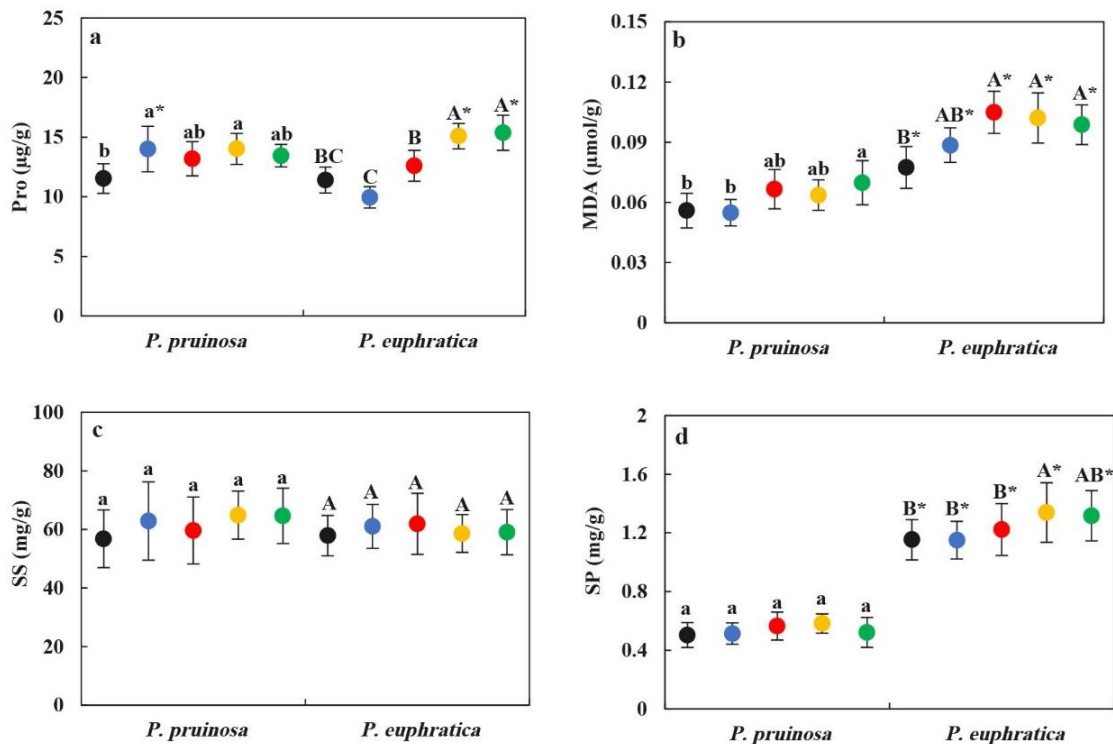


Figure 5. Changes in physiological characteristics of heteromorphic leaves with tree height of *P. pruinosa* and *P. euphratica*. Each value is the mean \pm SE. Note: The black dot indicates the height of the 2 m tree, the blue dot indicates the height of the 4 m tree, the red dot indicates the height of the 6 m tree, the yellow dot indicates the height of the tree 8 m, and the green dot indicates the height of the 10 m tree. According to Tukey's HSD test, lowercase and uppercase letters represent the significance of the difference between different sampling heights of *P. pruinosa* and *P. euphratica*. * The representing the comparison of the same height among species was significantly higher value ($P < 0.05$)

Changes in endogenous hormones of heteromorphic leaves with increase of tree height

The content of GA₃, IAA, and ZR in the heteromorphic leaves of *P. euphratica* and *P. pruinosa* all showed an increasing trend with the increase of tree height (Fig. 6a-d), and the contents of GA₃, IAA and ZR in the heteromorphic leaves were significantly positively correlated with the height of the tree (Tables A1 and A2). The ABA content of *P. euphratica* showed a decreasing trend with the increase of tree height, while *P. pruinosa* showed an increasing trend. From the height of 2 m to 10 m, the increase of GA₃, IAA and ZR content of *P. euphratica* is about 2 times, 4 times and 2 times of that of *P. pruinosa* respectively.

Correlation analysis showed that the content of IAA and ZR in the heteromorphic leaves of *P. euphratica* and *P. pruinosa* were significantly positively correlated with the Pn. The content of GA₃ and IAA was significantly positively correlated with tree height and LA, PT, MXA, and VN. At the same time, GA₃ content was significantly positively correlated with Pro content, indicating that under drought stress, the endogenous hormone changes of *P. euphratica* and *P. pruinosa* with the increase of tree height are closely related to leaf morphology and physiological functions.

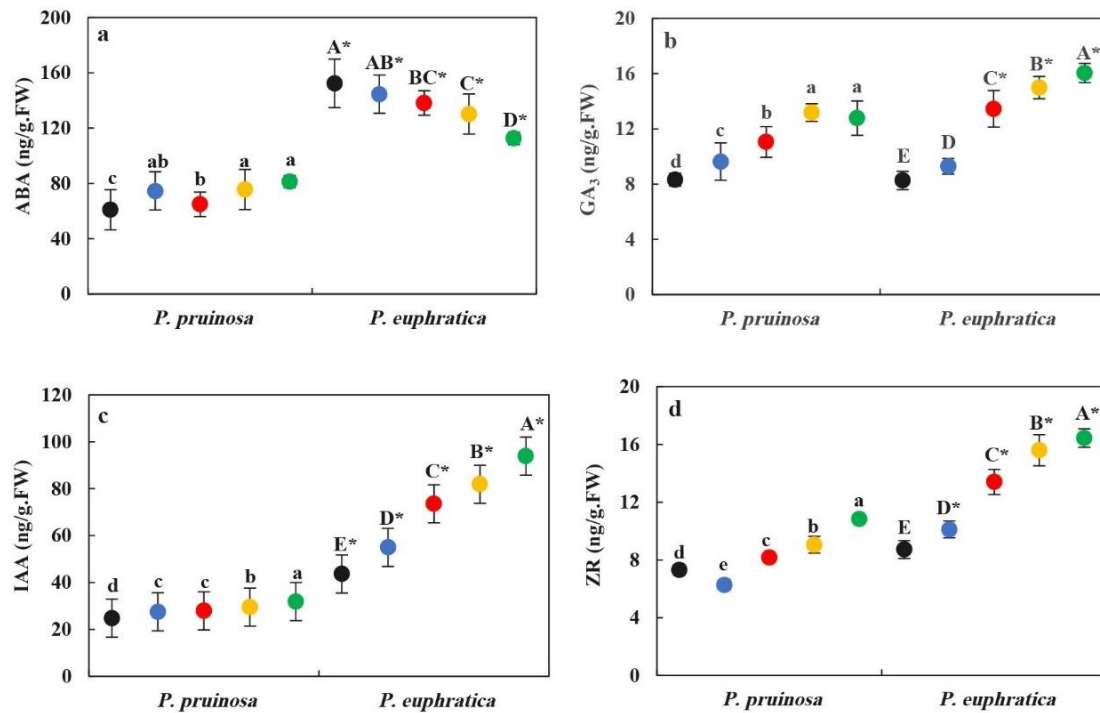


Figure 6. Changes in endogenous hormones of heteromorphic leaves with tree height of *P. pruinosa* and *P. euphratica*. Each value is the mean \pm SE. Note: The black dot indicates the height of the 2 m tree, the blue dot indicates the height of the 4 m tree, the red dot indicates the height of the 6 m tree, the yellow dot indicates the height of the tree 8 m, and the green dot indicates the height of the 10 m tree. According to Tukey's HSD test, lowercase and uppercase letters represent the significance of the difference between different sampling heights of *P. pruinosa* and *P. euphratica*. * The representing the comparison of the same height among species was significantly higher value ($P < 0.05$)

Effects of endogenous hormones on the structural traits of heteromorphic leaves

The endogenous hormone content was used as the independent variable, and the leaf morphology and anatomical structure traits were respectively used as the dependent variable for stepwise regression analysis. The results showed that there is a very significant linear relationship between the dependent variable Y and the independent variable X (Tables 1 and 2). It is found that the content of IAA affects the change of *P. euphratica* LI, and also affects the change of LT and the anatomical structure characteristics of the main vein of the leaf, such as the MXA and the VN; In addition, GA₃ content also affects the changes in PT, XVBR, and VA. With the increase of tree height, *P. euphratica* heteromorphic leaf LA, PT, and MXA are mainly affected by the content of GA₃, ZR, and IAA respectively, and the PSR is mainly affected by the content of ABA.

Similarly, the content of endogenous hormone IAA in *P. pruinosa* heteromorphic leaves affects the change of LI. Unlike *P. euphratica*, the IAA content of heteromorphic leaves of *P. pruinosa* also mainly affects LA, SLA and PT, while GA₃ content is mainly affects the change of LT. With the increase of tree height, the LA and PT of *P. pruinosa* are mainly affected by the content of IAA, and the MXA of the main vein is mainly affected by the content of ZR.

Table 1. Stepwise regression model of *P. euphratica* heteromorphic leaf structure traits and endogenous hormones

Model	Dependent variable (Y)	Regression equation	R	R ²	F	Sig.
LI	Y ₁	Y ₁ = 7.373 - 0.07X ₃	0.73	0.53	25.99	0.00
LA	Y ₂	Y ₂ = 1.65 + 0.62X ₂ + 0.48X ₄	0.84	0.71	26.47	0.00
LT	Y ₃	Y ₃ = 0.27 + 0.001X ₃	0.56	0.31	10.29	0.00
PT	Y ₄	Y ₄ = 115.01 + 3.85X ₂ + 7.71X ₄	0.85	0.73	29.41	0.00
PSR	Y ₅	Y ₅ = 12.22 - 0.04X ₁	0.43	0.19	5.24	0.03
MXA	Y ₆	Y ₆ = 15477.67 + 344.85X ₃	0.73	0.53	25.81	0.00
XVBR	Y ₇	Y ₇ = 0.31 + 0.01X ₂	0.65	0.42	16.45	0.00
VA	Y ₈	Y ₈ = 134.92 + 5.85X ₂ + 9.10X ₄	0.85	0.72	28.72	0.00
VN	Y ₉	Y ₉ = 93.08 + 0.49X ₃	0.57	0.33	11.26	0.00

Y₁: LI; Y₂: LA; Y₃: LT; Y₄: PT; Y₅: PSR; Y₆: MXA; Y₇: XVBR; Y₈: VA; Y₉: VN; X₁: ABA; X₂: GA₃; X₃: IAA; X₄: ZR

Table 2. Stepwise regression model of *P. pruinosa* heteromorphic leaf structure traits and endogenous hormones

Model	Dependent variable (Y)	Regression equation	R	R ²	F	Sig.
LI	Y ₁	Y ₁ = 1.90 - 0.03X ₃	0.52	0.27	8.59	0.00
LA	Y ₂	Y ₂ = 6.48 + 0.28X ₃	0.41	0.17	4.75	0.04
LT	Y ₃	Y ₃ = 83.83 + 23.78X ₂	0.80	0.64	40.99	0.00
SLA	Y ₄	Y ₄ = 182.10 - 3.78X ₃	0.76	0.57	30.95	0.00
PT	Y ₅	Y ₅ = 3.23 + 9.24X ₃	0.71	0.51	23.74	0.00
MXA	Y ₆	Y ₆ = 3594.08 + 3923.81X ₄	0.81	0.66	44.57	0.00
VA	Y ₇	Y ₇ = 146.61 + 18.20X ₄	0.64	0.42	16.44	0.00
VN	Y ₈	Y ₈ = 24.82 + 11.19X ₄	0.68	0.46	19.92	0.00

Y₁: LI; Y₂: LA; Y₃: LT; Y₄: SLA; Y₅: PT; Y₆: MXA; Y₇: VA; Y₈: VN; X₁: ABA; X₂: GA₃; X₃: IAA; X₄: ZR

Comparison of drought resistance of *P. euphratica* and *P. pruinosa*

The membership function method was used to comprehensively analyze the drought resistance of *P. euphratica* and *P. pruinosa* with different heights and heteromorphic leaves. The results show (Table A3) that the average membership function value of *P. euphratica* at 6 m, 8 m, and 10 m is 0.52, which is greater than the average function value at 2 m and 4 m. The average membership function value of *P. pruinosa* at 8 m and 10 m is greater than 2 m and 4 m. It shows that the broad oval leaves of *P. euphratica* and *P. pruinosa* with large crowns are larger than the heteromorphic leaves at the bottom under drought resistance. Comparing the two species, the average membership function value of each height is that *P. euphratica* is greater than that of *P. pruinosa*.

Discussion

Adaptation strategies of heteromorphic leaf structure traits with increasing tree height

As the water potential of the xylem of the tree decreases as the height of the tree increases, the difference in water pressure in the height gradient will affect the morphology and structure of the leaves at the corresponding tree height. The upper leaves

of the tree can only hinder water loss through a more obvious xeromorphic structure to cope with water stress (He et al., 2008; Ryan and Yoder, 1997). For example, the leaf size of *Eucalyptu srobusta* decreases with the increase of tree age and tree height, reducing the area of transpiration and photosynthesis (England et al., 2005). The LA of *Parashorea chinensis* also decreases along the height of the tree, while the anatomical structure of the leaf shows a stronger xerophytic structure as the height of the tree increases, such as PT, PSR increases with the increase of tree height (He et al., 2008). *P. euphratica* exhibits LA, PT and PSR at different developmental stages, which increase with the increase in diameter at breast height and the height of the heteromorphic leaves, the heteromorphic leaves show a stronger xerophytic structure as the height of the tree increases features (Zhai et al., 2020). In the results of this study, *P. euphratica* under soil drought stress conditions increased the LA, LT, PT, MXA with the increase of tree height, the xeromorphic structural characteristics increased with the increase of tree height. The change rule is consistent with the above results. Similarly, under soil drought conditions, with the increase of tree height, *P. pruinosa* also has obvious xerophytic characteristics as the leaf area increases, and the change pattern is similar to that of *P. euphratica*.

The size of the leaf strongly affects its anatomical characteristics, and the anatomical characteristics are reflected in the mechanical support and physiological capabilities of the leaf. The increase in leaf area will inevitably require an increase in supporting tissue and transpiration rate. *P. euphratica* and *P. pruinosa* have the largest LA at the top of the crown, the LA has a significant positive correlation with the PT, MXA and Tr. The LT of the heteromorphic leaves at the top of the canopy is also the largest, which is good for water storage and reduces transpiration. The PT and MXA increase with the increase of tree height, reflecting the enhancement of leaf water transport efficiency, mechanical support and physiological ability, at the same time, the investment of leaves in the mesophyll fence organization and vascular organization is also the main reason why the specific leaf area decreases with the height of the tree. Leaf anatomical characteristics are related to CO₂ diffusion resistance (Crous et al., 2021; Terashima et al., 2011), The thicker leaves at the top of *P. euphratica* and *P. pruinosa* have more palisade layers and dense mesophyll, leaving less intercellular air space in the upper leaves of the canopy, reducing the internal limitation of CO₂ transfer during photosynthesis, which is conducive to the enhancement of photosynthetic capacity. Comparing the two at the same height, it is found that the anatomical structures such as the LA at the top (10 m) of the tree height, PT, and MXA were *P. euphratica* was significantly larger than *P. pruinosa*. In addition, *P. euphratica* PSR, VBXR with tree height were significantly positively correlated. In response to soil drought stress, *P. euphratica* and *P. pruinosa* showed different adaptation strategies in leaf morphology. *P. pruinosa* mainly enhances the xerophytic structure characteristics through the increase of LT, PT, MXA, VA increase and SLA decrease. *P. euphratica* mainly enhances the characteristics of xerophytic structure through coordinated changes in the PSR and XVBR in addition to the LA, PT, MXA, and VA. In addition, with the increase of tree height, *P. euphratica* reduced the percentage of SLA less than that of *P. pruinosa*, which shows that *P. euphratica* has the ability to utilize resources while increasing drought resistance.

Adaptation strategies of heteromorphic leaf functional traits with increasing tree height

The leaves at the top of the canopy must maintain photosynthetic and hydraulic functions under high light and high evaporation requirements (Shiraki et al., 2017). The

photosynthetic efficiency of an adult *P. euphratica* leaf broad-ovate leaf is significantly greater than that of striped leaf (Bai et al., 2011; Su et al., 2003; Zhai et al., 2020), broad oval leaves have a relatively large photosynthetic area, better light resources, a relatively large net photosynthetic rate, and higher photosynthetic efficiency can accumulate more photosynthetic products (Wang et al., 2014). In addition, the osmotic adjustment of many species allows them to maintain normal functions during droughts (Martorell et al., 2015; Merchant et al., 2007). Plants can cope with stress by absorbing water to the maximum, minimizing water loss or accumulating some osmotic regulators, thereby avoiding drought (Ma et al., 2014). The osmotic adjustment ability of *P. euphratica* broad-ovate leaves is stronger than that of other leaves (Wang et al., 2011; Yang, 2004). Under suitable water conditions, the net photosynthetic rate, transpiration rate, stomatal conductance, instantaneous water use efficiency, $\delta^{13}\text{C}$, proline, and malondialdehyde content of *P. euphratica* heteromorphic leaves all increase with the increase of diameter step and sampling height, the photosynthetic capacity and osmotic adjustment capacity of broad oval leaves are stronger than other leaves (Wang et al., 2011, 2014; Zhai et al., 2020). This study shows that under soil drought stress, the photosynthetic capacity, water use efficiency and osmotic adjustment ability of *P. euphratica* and *P. pruinosa* with the increase of tree height increase with the increase of tree height, which is similar to the change law of *P. euphratica* under suitable water conditions.

Leaf anatomy has a great influence on photosynthetic capacity, for example, thicker fence tissue can maximize light absorption (Coble et al., 2016), The MXA provides support for the high photosynthetic rate (Johnson et al., 2012), and the transportation of water in the leaves is the key to maintaining the high photosynthetic rate. Investment in water transportation systems is also an important part of reducing the limitation of photosynthesis. The Pn of *P. euphratica* and *P. pruinosa* canopy top leaves was higher than the other heights, and was significantly correlated with the PT, VN, and the $\delta^{13}\text{C}$ value. At the same time, the Pn of *P. euphratica* was also significantly positively correlated with the MXA. Because the heteromorphic leaves of *P. euphratica* and *P. pruinosa* have thicker PT, larger MXA and $\delta^{13}\text{C}$ value in the high canopy layer, it shows that the efficiency of water transportation is improved while the efficiency of long-term water use is also enhanced, this is conducive to the enhancement of photosynthetic capacity. Compared with the two species, the photosynthetic capacity, long-term water use efficiency and osmotic adjustment ability of the top leaves of the tree height showed that *P. euphratica* was stronger than *P. pruinosa*. As we mentioned earlier, the LA at the top of the canopy, PT, and MXA of *P. euphratica* are significantly larger than that of *P. pruinosa*, which provides the basis for strong stomata exchange capacity, the Pn of *P. euphratica* is significantly positively correlated with Gs, while *P. pruinosa* has no significant correlation with Gs, but it is significantly negatively correlated with the C_i , this may be related to the dense accumulation of palisade tissue to reduce the internal limitation of CO_2 transfer in photosynthesis. In addition, the content of proline and soluble protein in the broad ovoid leaves of *P. euphratica* canopy is significantly greater than that of *P. pruinosa*, and the net photosynthetic rate is significantly positively correlated with proline, the increase in the content of these osmotic adjustment substances can maintain a certain osmotic potential, provide a certain water absorption capacity, and ensure a normal physiological response.

Hormones not only coordinate internal developmental procedures, but also drive adaptability with external assistance (Ali et al., 2020). They can induce the accumulation of soluble osmotic substances through regulation of intracellular

metabolism and enhance the chances of survival of plants in adversity (Yao et al., 2011). Li (2017) research shows that the hormone content of *P. euphratica* leaves changes with the change of the morphology of the abnormal leaves, which reflects the physiological adjustment of *P. euphratica* to adapt to arid desert environment (Li et al., 2017). This study showed that the content of endogenous hormones GA₃, IAA, and ZR in *P. euphratica* and *P. pruinosa* leaves increased with the increase of tree height, similar to the change trend of proline and soluble protein content, and GA₃ and proline showed a significant positive correlation. Under soil drought conditions, *P. euphratica* responds to drought endogenous hormone ABA content stronger than *P. pruinosa*, and its ABA content at each height is significantly greater than *P. pruinosa*, at the same time, the endogenous hormone ABA content of *P. euphratica* heteromorphic leaves showed a decreasing trend with the increase of tree height, while that of *P. pruinosa* was the opposite. When plants are subjected to drought stress, ABA accumulates rapidly in the body, which promotes the closure of stomata and reduces transpiration. The ABA content at the top of the *P. pruinosa* canopy is the highest compared to the rest of the canopy, however broad ovoid leaves of *P. euphratica* have the lowest ABA content, and the net photosynthetic rate and stomatal conductance are significantly negatively correlated with ABA content. lower ABA content can reduce the negative impact on the photosynthetic capacity of heteromorphic leaves and provide support for the enhancement of photosynthetic capacity. To cope with the water stress caused by soil drought and tree height increase, as far as the endogenous hormone ABA in the heteromorphic leaves is concerned, compared with *P. euphratica*, *P. pruinosa* chose a more conservative adaptation strategy.

Phytohormones especially GA₃, IAA, ABA, ZR affect the formation and development of many plant heteromorphic leaves (Li et al., 2019; Nakayama et al., 2017). Auxin affects the structure of leaf cells, increases the morphology and development of cell volume (Barkoulas et al., 2008), affects the formation of leaf vascular tissue and the morphology and development of leaves (Avsian-Kretchmer et al., 2002; Donner et al., 2009). Although the endogenous hormone IAA of *P. euphratica* and *P. pruinosa* affects the change of LI, the main influence points on the anatomical structure are different, the leaf hormone IAA of *P. euphratica* and *P. pruinosa* mainly affects MXA and PT, respectively. In addition, the leaf IAA of *P. euphratica* and *P. pruinosa* showed a significant positive correlation with MXA, PT, and Pn, *P. euphratica* IAA affects the water transport efficiency of the main vein to ensure normal photosynthetic physiology, while *P. pruinosa* IAA affects the thickness of the fence tissue to ensure photosynthetic capacity. In addition, the ABA content of *P. euphratica* hormone is significantly negatively correlated with PT, PSR, Pn, Tr, and Gs, which can support the enhancement of gas exchange capacity by influencing the change of PSR.

Conclusions

Adaptation strategies of heteromorphic leaf structure traits with increasing tree height *P. euphratica* and *P. pruinosa* have different response strategies to water stress caused by tree height. With the increase of tree height, the abnormal leaves of the two species strengthen the xerophytic structure through the increase of leaf area, palisade tissue, main vein xylem area, duct area and reduction of specific leaf area. In addition, *P. euphratica* also enhances the xerophytic structure characteristics through the changes in the PSR and the XVBR. The functional traits of *P. euphratica*, such as photosynthetic

capacity and osmotic adjustment ability, are stronger than those of *P. pruinosa*. It is because the LA at the top of the canopy, the PT, PSR, MXA, the $\delta^{13}\text{C}$ value, the proline, and the soluble protein content show that *P. euphratica* is significantly larger than that of *P. pruinosa*. At the same time, endogenous hormones also participate in the enhancement of osmotic regulation. The different influencing factors of the endogenous hormone IAA is also one of the reasons for the different adaptation strategies of the two. IAA mainly affects the water transport efficiency of the main veins of *P. euphratica*, and mainly affects the leaf morphology of *P. pruinosa*. In addition, the comprehensive comparison of membership function method shows that the drought resistance of *P. euphratica* heteromorphic leaves is greater than that of *P. pruinosa*.

Acknowledgements. This work was financially supported by the National Natural Sciences Foundation of China (31860198, 31060026), Innovative team Building Plan for key areas of Xinjiang Production and Construction Corps (2018BC003).

REFERENCES

- [1] Ali, S., Baloch, A. M. (2020): Overview of sustainable plant growth and differentiation and the role of hormones in controlling growth and development of plants under various stresses. – *Recent patents on Food, Nutrition & Agriculture* 11: 105-114.
- [2] Aranda, I., Pardo, F., Gil, L., Pardos, J. A. (2004): Anatomical basis of the change in leaf mass per area and nitrogen investment with relative irradiance within the canopy of eight temperate tree species. – *Acta Oecologica* 25: 187-195.
- [3] Avsian-Kretchmer, O., Cheng, J., Chen, L., Moctezuma, E., Sung, Z. (2002): Indole acetic acid distribution coincides with vascular differentiation pattern during arabidopsis leaf ontogeny. – *Plant Physiology* 130: 199-209.
- [4] Bai, X., Zhang, S. J., Zheng, C. X., Hao, J. Q., Yang, Y. (2011): Comparative study on photosynthesis and water physiology of polymorphic leaves of *Populus euphratica*. – *Journal of Beijing Forestry University* 33: 47-52.
- [5] Bao, L., Liu, Y. H. (2009): Comparison of leaf functional traits in different forest communities in mt. Dongling of Beijing. – *Acta Ecologica Sinica* 29: 3692-3703.
- [6] Barkoulas, M., Hay, A., Kougioumoutzi, E., Tsiantis, M. (2008): A developmental framework for dissected leaf formation in the arabidopsis relative *Cardamine hirsuta*. – *Nature genetics* 40: 1136-1141.
- [7] Coble, A. P., VanderWall, B., Mau, A., Cavaleri, M. A. (2016): How vertical patterns in leaf traits shift seasonally and the implications for modeling canopy photosynthesis in a temperate deciduous forest. – *Tree Physiology* 36(9): 1077-1091.
- [8] Crous, K., Company, C., Lopez, R., Cano, F., Ellsworth, D. (2021): Canopy position affects photosynthesis and anatomy in mature eucalyptus trees in elevated CO_2 . – *Tree Physiology* 41: 206-222.
- [9] Donner, T., Sherr, I., Scarpella, E. (2009): Regulation of preprocambial cell state acquisition by auxin signaling in Arabidopsis leaves. – *Development (Cambridge, England)* 136: 3235-3246.
- [10] England, J. R., Attiwill, P. M. (2005): Changes in leaf morphology and anatomy with tree age and height in the broadleaved evergreen species, *Eucalyptus regnans* f. Muell. – *Trees* 20: 79-90.
- [11] He, C., Li, J., Zhou, P., Guo, M., Zheng, Q. (2008): Changes of leaf morphological, anatomical structure and carbon isotope ratio with the height of the *Parashorea chinensis* in Xishuangbanna, China. – *Journal of Integrative Plant Biology* 50: 168-173.

- [12] Huang, W., Li, Z., Yang, Z., Bai, G. (2010a): The structural traits of *Populus euphratica* heteromorphic leaves and their correlations. – *Acta Ecologica Sinica* 30: 4636-4642.
- [13] Huang, W., Li, Z., Yang, Z., Liang, J., Bai, G. (2010b): Heteromorphic leaf structural characteristics and their correlations with diameter at breast height of *Populus euphratica*. – *Chinese Journal of Ecology* 29: 2347-2352.
- [14] Ishii, H., Jennings, G., Sillett, S., Koch, G. (2008): Hydrostatic constraints on morphological exploitation of light in tall sequoia sempervirens trees. – *Oecologia* 156: 751-763.
- [15] Johnson, D. M., McCulloh, K. A., Woodruff, D. R., Meinzer, F. C. (2012): Hydraulic safety margins and embolism reversal in stems and leaves: why are conifers and angiosperms so different? – *Plant Science* 195: 48-53.
- [16] Li, Y., Zhang, X., Feng, M., Han, Z., Li, Z. (2017): Characteristics of endohormones in leaf blade of *Populus euphratica* heteromorphic leaves. – *Journal of Tarim University* 29: 7-13.
- [17] Li, G., Hu, S., Hou, H., Kimura, S. (2019): Heterophylly: phenotypic plasticity of leaf shape in aquatic and amphibious plants. – *Plants (Basel, Switzerland)* 8: 420.
- [18] Li, Z., Jiao, P., Wu, Z., Zhai, J., Zhang, X., Zhang, S., Gai, Z., Guo, X. (2021): Heterophylly and Growth Adaptation Strategies of *Populus Euphratica* and *Populus Pruinosa*. – Science Press, Beijing.
- [19] Liu, S., Jiao, P., Li, Z. (2016): Diversifolious types and spatiotemporal characteristics of *Populus pruinosa* schrenk. – *Arid Zone Research* 33: 1098-1103.
- [20] Ma, T., Christie, P., Luo, Y. M., Teng, Y. (2014): Physiological and antioxidant responses of germinating mung bean seedlings to phthalate esters in soil. – *Pedosphere* 24: 9.
- [21] Miyata, R., Kohyama, T. (2016): Light-exposed shoots of seven coexisting deciduous species show common photosynthetic responses to tree height. – *Oecologia* 182: 373-383.
- [22] Nakayama, H., Sinha, N., Kimura, S. (2017): How do plants and phytohormones accomplish heterophylly, leaf phenotypic plasticity, in response to environmental cues. – *Frontiers in Plant Science* 8: 1717.
- [23] Niinemets, U., Keenan, T. F., Hallik, L. (2015): A worldwide analysis of within-canopy variations in leaf structural, chemical and physiological traits across plant functional types. – *New Phytol* 205: 973-993.
- [24] Ryan, M. G., Yoder, B. J. (1997): Hydraulic limits to tree height and tree growth. – *Bioscience* 47: 235-242.
- [25] Sendall, K., Reich, P. (2013): Variation in leaf and twig CO₂ flux as a function of plant size: a comparison of seedlings, saplings and trees. – *Tree Physiology* 33: 713-729.
- [26] Shiraki, A., Azuma, W., Kuroda, K., Ishii, H. (2017): Physiological and morphological acclimation to height in cupressoid leaves of 100-year-old *Chamaecyparis obtusa*. – *Tree Physiology* 37: 1327-1336.
- [27] Su, P-X., Zhang, L-X., Du, M-W., Bi, Y-R., Zhao, A-F., Liu, X-M. (2003): Photosynthetic character and water use efficiency of different leaf shapes of *Populus euphratica* and their response to CO₂ enrichment. – *Chinese Journal of Plant Ecology* 27: 34-40.
- [28] Terashima, I., Hanba, Y., Tholen, D., Niinemets, Ü. (2011): Leaf functional anatomy in relation to photosynthesis. – *Plant Physiology* 155: 108-116.
- [29] Wang, S. (1996): The status, conservation and recovery of global resources of *Populus euphratica*. – *World Forestry Research* 6: 37-44.
- [30] Wang, H., Han, L., Xu, Y., Wang, L., Jia, W. (2011): Response of chlorophyll fluorescence characteristics of *Populus euphratica* heteromorphic leaves to high temperature. – *Acta Ecologica Sinica* 31: 2444-2453.
- [31] Wang, H., Niu, J., Lu, H., Yali, X. (2014): Photosynthetic responses of the heteromorphic leaves in *Populus euphratica* to light intensity and CO₂ concentration. – *Chinese Journal of Plant Ecology* 38: 1099-1109.

- [32] Yang, S. D. (2004): Some difference of capacity of osmotic regulation between lanceolate and broad-ovate leaves in *Populus euphratica*. – *Acta Botanica Boreali-Occidentalia Sinica* 24: 6.
- [33] Yao, M., Liu, L., Zeng, Y. (2011): Several kinds of phytohormone in plants responses to salt-stress. – *Biotechnology Bulletin* 11: 1-5.
- [34] Yu, L., Dong, H., Li, Z., Han, Z., Korpelainen, H., Li, C. (2020): Species-specific responses to drought, salinity and their interactions in *Populus euphratica* and *P. pruinosa* seedlings. – *Journal of Plant Ecology* 13: 563-573.
- [35] Zeng, M., He, S., Hao, L., Li, Y., Zheng, C., Zhao, Y. (2019): Conjoint analysis of genome-wide lncRNA and mRNA expression of heteromorphic leaves in response to environmental heterogeneity in *Populus euphratica*. – *International Journal of Molecular Sciences* 20: 5148.
- [36] Zhai, J., Li, Y., Han, Z., Li, Z. (2020): Morphological, structural and physiological differences in heteromorphic leaves of Euphrates poplar during development stages and at crown scales. – *Plant Biology* 22: 366-375.
- [37] Zhang, Y. J., Meinzer, F. C., Hao, G. Y., Scholz, F. G., Bucci, S. J., Takahashi, F. S., Villalobos-Vega, R., Giraldo, J. P., Cao, K. F., Hoffmann, W. A., Goldstein, G. (2009): Size-dependent mortality in a neotropical savanna tree: the role of height-related adjustments in hydraulic architecture and carbon allocation. – *Plant Cell Environ* 32: 1456-1466.
- [38] Zhao, P., Feng, M., Jiao, P., Li, Z. (2016): Relationship between morphological or anatomical features of leaves and trunk diameter at breast height at different growing stages of *Populus euphratica*. – *Arid Zone Research* 33: 1071-1080.
- [39] Zheng, C., Qiu, J., Jiang, C., Yue, N., Wang, X., Wang, W. (2007): Comparison of stomatal characteristics and photosynthesis of polymorphic *Populus euphratica* leaves. – *Frontiers of Forestry in China* 2: 87-93.
- [40] Zirbel, C. R., Bassett, T., Grman, E., Brudvig, L. A., Cadotte, M. (2017): Plant functional traits and environmental conditions shape community assembly and ecosystem functioning during restoration. – *Journal of Applied Ecology* 54: 1070-1079.

APPENDIX

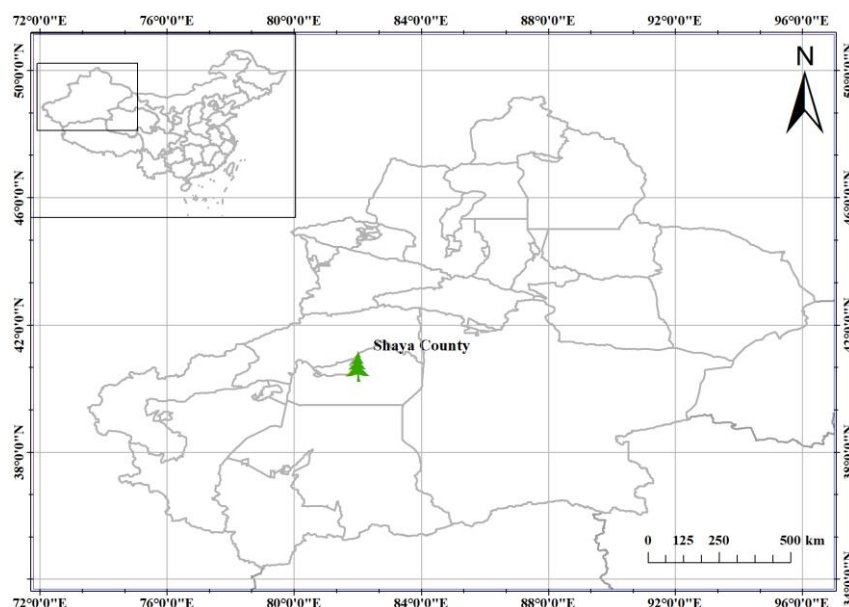


Figure A1. Overview of the study area

Table A1. Correlation analysis of structural and functional traits of *P. euphratica*

R	H	LI	LA	LT	SLA	PT	PSR	MXA	XA/VBA	VA	VN	Pn	Tr	Ci	Gs	WUEi	$\delta^{13}C$	Pro	MDA	SS	SP	ABA	GA3	IAA	ZR
LI	-0.73**	1																							
LA	0.67**	-0.65**	1																						
LT	0.65*	-0.57**	0.49*	1																					
SLA	0.34	0.55**	-0.09	-0.31	1																				
PT	0.87**	-0.66**	0.63**	0.27	0.24	1																			
PSR	0.82**	-0.57**	0.54**	0.07	0.24	0.71**	1																		
MXA	0.90**	-0.74**	0.50**	0.20	0.03	0.73**	0.81**	1																	
XVBR	0.71*	-0.23	0.55*	0.31	0.23	0.24	0.12	0.52**	1																
VA	0.95**	-0.69**	0.60**	0.19	0.28	0.73**	0.77**	0.66**	0.46*	1															
VN	0.67**	-0.62**	0.65**	0.26	-0.18	0.60**	0.32	0.55**	0.23	0.53**	1														
Pn	0.73**	-0.38	0.58**	0.25	0.29	0.46*	0.63**	0.41*	0.22	0.62**	0.54**	1													
Tr	0.65**	-0.42*	0.56**	0.28	0.04	0.47*	0.41*	0.51**	0.05	0.67**	0.49*	0.50*	1												
Ci	-0.70**	0.45*	-0.34	0.21	-0.59**	-0.60**	-0.59**	-0.17	-0.41*	-0.20	-0.33	-0.27	-0.065	1											
Gs	0.45*	-0.15	0.63**	0.27	0.35	0.32	0.16	0.17	0.27	0.48*	0.46*	0.54**	0.44*	-0.23	1										
WUEi	0.07	-0.08	-0.01	-0.11	0.17	-0.09	-0.05	0.02	-0.02	0.08	0.31	-0.14	-0.13	-0.08	0.07	1									
$\delta^{13}C$	-0.73*	0.63**	0.71*	0.18	0.23	-0.31	-0.18	0.34	0.33	0.28	0.23	0.63*	0.30	-0.15	0.30	-0.13	1								
Pro	0.71**	-0.32	0.60**	0.11	0.45*	0.51**	0.64**	0.39	0.29	0.47*	0.29	0.55**	0.22	-0.35	0.29	0.02	-0.01	1							
MDA	0.43*	-0.23	0.41*	-0.22	-0.20	0.14	-0.14	0.49*	0.46*	0.29	0.39	0.07	-0.03	-0.05	-0.01	0.39*	-0.07	0.31	1						
SS	0.01	-0.14	0.23	0.15	-0.13	0.07	-0.25	0.17	-0.09	0.04	0.08	0.15	0.29	-0.18	-0.25	-0.33	0.14	0.11	-0.16	1					
SP	0.41*	-0.25	0.17	-0.06	0.25	0.17	0.18	0.21	0.19	0.10	0.07	0.36	0.04	-0.01	0.25	0.03	0.13	0.24	0.05	-0.24	1				
ABA	-0.86**	0.61**	-0.47*	0.04	-0.36	-0.69**	-0.73**	-0.72**	-0.06	-0.76**	-0.45*	-0.51**	-0.53**	0.80**	-0.13	-0.02	0.23	-0.49*	-0.17	0.23	-0.33	1			
GA3	0.81**	-0.55**	0.82**	0.45*	0.27	0.76**	0.65**	0.75**	0.53**	0.79**	0.40*	0.63**	0.53**	-0.39	0.68**	0.03	-0.21	0.74**	-0.07	0.28	0.28	-0.45*	1		
IAA	0.95**	-0.67**	0.72**	0.25	0.38	0.77**	0.72**	0.85**	0.41*	0.93**	0.57**	0.70**	0.70**	-0.61**	0.59**	0.14	-0.19	0.78**	0.09	0.17	0.54**	-0.78**	0.84**	1	
ZR	0.80**	-0.55**	0.76**	0.43*	0.23	0.74**	0.62**	0.77**	0.53**	0.80**	0.52**	0.62**	0.53**	-0.35	0.66**	0.04	-0.18	0.72**	-0.05	0.29	0.28	-0.44*	0.98**	0.84**	1

Table A2. Correlation analysis of structural and functional traits of *P. pruinosa*

R	H	LI	LA	LT	SLA	PT	PSR	MXA	XA/VBA	VA	VN	Pn	Tr	Ci	Gs	WUEi	$\delta^{13}C$	Pro	MDA	SS	SP	ABA	GA3	IAA	ZR
LI	-0.53**	1.00																							
LA	0.43*	-0.77**	1.00																						
LT	0.82**	-0.33	0.43*	1.00																					
SLA	-0.68**	0.49*	-0.27	-0.43*	1.00																				
PT	0.71**	-0.50*	0.51**	0.50**	-0.46*	1.00																			
PSR	0.08	0.02	0.11	0.05	-0.02	0.36	1.00																		
MXA	0.78**	-0.37	0.29	0.53**	-0.54**	0.51**	-0.13	1.00																	
XVBR	0.02	0.30	-0.32	0.12	-0.13	-0.11	0.27	0.18	1.00																
VA	0.49*	-0.09	-0.02	0.50**	-0.17	0.21	0.02	0.28	0.15	1.00															
VN	0.76**	-0.47*	0.30	0.64**	-0.63**	0.48*	0.32	0.54**	0.35	0.50*	1.00														
Pn	0.53**	-0.30	0.52**	0.67**	-0.18	0.44*	0.45*	0.37	0.13	0.32	0.51**	1.00													
Tr	0.30	-0.10	0.03	0.39	-0.29	-0.03	0.11	0.21	0.33	0.02	0.29	0.40*	1.00												
Ci	-0.22	-0.12	-0.10	-0.32	0.04	-0.21	-0.52**	-0.09	-0.23	0.12	-0.22	-0.56**	-0.46*	1.00											
Gs	0.04	-0.12	0.07	0.04	0.00	0.00	0.27	0.14	0.19	-0.32	0.25	0.34	0.34	-0.45*	1.00										
WUEi	0.07	-0.14	0.39	0.16	0.05	0.28	0.34	0.15	0.13	0.16	0.19	0.52**	-0.26	-0.32	0.14	1.00									
$\delta^{13}C$	0.52**	-0.38	0.30	0.55**	-0.44*	0.41*	0.21	0.36	0.34	0.41*	0.55**	0.46*	0.30	-0.06	0.03	0.24	1.00								
Pro	0.35	-0.62**	0.51**	0.27	-0.46*	0.37	0.20	0.18	-0.25	-0.23	0.30	0.41*	0.22	-0.19	0.23	-0.09	0.27	1.00							
MDA	0.62**	-0.35	0.38	0.61**	-0.44*	0.41*	-0.07	0.67**	0.05	0.29	0.46*	0.51**	0.31	-0.15	0.24	0.33	0.57**	0.33	1.00						
SS	0.40*	-0.47*	0.19	0.32	-0.44*	0.22	-0.05	0.16	-0.05	0.22	0.46*	0.11	0.08	0.26	-0.05	-0.17	0.30	0.40*	0.16	1.00					
SP	0.20	0.19	0.03	0.15	0.05	0.26	0.23	0.22	0.05	-0.13	0.00	0.22	0.25	-0.26	0.05	-0.10	0.01	-0.07	0.15	-0.11	1.00				
ABA	0.49*	-0.48*	0.24	0.24	-0.41*	0.49*	-0.16	0.37	-0.38	0.46*	0.31	0.02	-0.02	0.32	-0.31	-0.17	0.21	0.30	0.22	0.39	0.00	1.00			
GA ₃	0.85**	-0.39*	0.36	0.80**	-0.49*	0.51**	0.19	0.60**	0.10	0.31	0.66**	0.58**	0.47*	-0.50*	0.19	0.09	0.50*	0.40*	0.51**	0.33	0.30	0.19	1.00		
IAA	0.86**	-0.52**	0.41*	0.58**	-0.75**	0.71**	0.02	0.65**	-0.16	0.42*	0.64**	0.41*	0.15	-0.14	-0.13	0.11	0.34	0.26	0.47*	0.36	0.09	0.60**	0.63**	1.00	
ZR	0.88**	-0.22	0.18	0.77**	-0.58**	0.56**	-0.03	0.81**	0.21	0.66**	0.68**	0.45*	0.24	-0.17	-0.06	0.09	0.42*	0.08	0.60**	0.29	0.12	0.44*	0.68**	0.78**	1.00

Table A3. Evaluation and analysis on drought resistance of *P. pruinosa* and *P. euphratica* by membership function method

Index	<i>P. pruinosa</i>					<i>P. euphratica</i>				
	2m	4m	6m	8m	10m	2m	4m	6m	8m	10m
H										
LI	0.51	0.47	0.46	0.36	0.77	0.48	0.36	0.53	0.63	0.55
LA	0.40	0.49	0.59	0.44	0.50	0.59	0.42	0.51	0.39	0.26
LT	0.40	0.51	0.49	0.51	0.41	0.67	0.67	0.56	0.40	0.53
SLA	0.46	0.62	0.50	0.52	0.61	0.52	0.62	0.63	0.51	0.64
PT	0.39	0.60	0.39	0.57	0.36	0.56	0.44	0.53	0.49	0.39
PSR	0.36	0.32	0.45	0.44	0.58	0.40	0.66	0.43	0.51	0.57
MXA	0.33	0.64	0.49	0.47	0.44	0.51	0.57	0.63	0.46	0.57
XVBR	0.36	0.45	0.63	0.38	0.50	0.54	0.43	0.45	0.64	0.50
VA	0.46	0.53	0.66	0.47	0.57	0.46	0.66	0.51	0.61	0.35
VN	0.63	0.63	0.36	0.54	0.40	0.53	0.39	0.43	0.47	0.58
Pn	0.41	0.40	0.43	0.43	0.54	0.57	0.38	0.70	0.58	0.33
Tr	0.52	0.27	0.57	0.56	0.54	0.45	0.58	0.62	0.54	0.53
Ci	0.27	0.38	0.44	0.42	0.41	0.44	0.47	0.47	0.67	0.59
Gs	0.44	0.54	0.58	0.66	0.40	0.33	0.54	0.57	0.40	0.67
WUE _i	0.43	0.46	0.29	0.65	0.60	0.52	0.27	0.35	0.52	0.57
δ ¹³ C	0.39	0.57	0.34	0.46	0.46	0.49	0.36	0.62	0.48	0.39
Pro	0.52	0.43	0.53	0.49	0.52	0.31	0.38	0.44	0.58	0.53
MDA	0.51	0.41	0.47	0.49	0.44	0.49	0.57	0.56	0.42	0.53
SS	0.58	0.54	0.53	0.57	0.37	0.49	0.50	0.47	0.66	0.55
SP	0.56	0.42	0.39	0.39	0.45	0.34	0.57	0.28	0.40	0.29
ABA	0.59	0.54	0.61	0.47	0.52	0.43	0.57	0.65	0.59	0.66
GA ₃	0.38	0.47	0.60	0.38	0.50	0.48	0.56	0.63	0.45	0.51
IAA	0.52	0.42	0.55	0.44	0.42	0.40	0.41	0.36	0.34	0.53
ZR	0.54	0.40	0.48	0.60	0.39	0.52	0.40	0.38	0.58	0.75
Average	0.45	0.48	0.49	0.49	0.49	0.48	0.49	0.51	0.51	0.52

N = 450. LI: leaf index; LA: leaf area; LT: leaf thickness; SLA: Specific Leaf Area; PT: Palisade tissue thickness; PSR: Ratio of palisade tissue to spongy tissue; MXA: The main vein xylem area; XVBR: Main vein xylem/main vascular bundle area; VA: Vessel area; VN: Vessel number; Pn: Photosynthetic rate; Tr: Transpiration rate; Gs: Stomatal conductance; C_i: Intercellular CO₂ concentration; WUE_i: Instantaneous water use efficiency; δ¹³C: Stable carbon isotope values; Pro: Proline; MDA: Malondialdehyde; SS: Soluble sugar; SP: Soluble protein; ABA: Abscisic acid; GA₃: Gibberellin; IAA: Indoleacetic acid; ZR: Zeatin Riboside

SELF-ORGANIZING FEATURE MAP CLASSIFICATION AND ORDINATION OF ENDANGERED MEDICINAL PLANT (*GLYCYRRHIZA URALENSIS*) COMMUNITIES IN NORTH CHINA

SONG, N. Q.¹ – XU, B.² – ZHANG, J. T.^{2*}

¹*School of Chinese Materia Medica, Beijing University of Chinese Medicine, Beijing 102488, China*

²*Key Laboratory of Biodiversity Sciences and Ecological Engineering, Ministry of Education; College of Life Sciences, Beijing Normal University, Xiwaidajie 19, Beijing 100875, China*

**Corresponding author*

e-mail: Zhangjt@bnu.edu.cn; phone: +86-10-5880-3093; fax: +86-10-5880-7721

(Received 24th Feb 2022; accepted 20th May 2022)

Abstract. *Glycyrrhiza uralensis* is an endangered medicinal plant and is mainly distributed in semiarid and arid areas in Northern China. The conservation of this species and its communities is important and urgent. In the present work, we examined, by artificial neural network theory and methods, the ecological relationships of *G. uralensis* communities in Northern China, which is the basis for conservation. Data from 100 samples of 2 × 2 m were collected along a precipitation gradient from east to west in Northern China. Species composition data and environmental data were measured and recorded for each sample. Self-organizing feature map (SOFM) is an important and superior network in neural network theory, and SOFM clustering and SOFM ordination was used to analyze ecological relations of these community data. The results showed that there were twelve communities dominated by *G. uralensis* in Northern China. These communities represent almost all community types and distribution of *G. uralensis* in China. They had different characteristics in composition, structure and environment. Precipitation was the key environmental factor affecting *G. uralensis* populations and communities. Water condition was a limited factor for plant community distribution in semiarid and arid areas in Northern China. Topographical variables, such as elevation, slope and slope direction, were also important to the studied communities. Conservation for *G. uralensis* populations and communities must consider these relations. SOFM clustering and ordination were effective and useful techniques in the study of endangered medicinal plant community and should be applied more frequently.

Keywords: *neural network, quantitative analysis, medicinal plant conservation, G. uralensis communities, semi-arid and arid area*

Introduction

Medicinal plants are important natural resources and significant to people's health in many countries and regions, such as China, Pakistan, India, and so on (Nautiyal et al., 2009). Multivariate analysis is important in studies of ecological relations between medicinal plant community and environmental variables (Kathe, 2006). The objective of multivariate analysis is normally to generate hypotheses about the relationships between the composition of the plant community and the environmental factors which determine it (Zhang, 2011; Moniruzzaman et al., 2021). There are many multivariate analysis methods available in plant ecology, such as Two-way indicator species analysis (TWINSPAN) classification, Principal components analysis (PCA) and Detrended correspondence analysis (DCA) ordination etc. (ter Braak, 1986). With the development of mathematics and statistics, some new multivariate techniques were applied to ecology, such as Fuzzy Set Ordination (FSO) (Roberts, 2008) and Self-Organizing

Feature Map classification and Ordination (SOFM) (Giraudel and Lek, 2001; Song et al., 2020).

Self-organizing feature map is a type of artificial neural network (ANN) that is trained using unsupervised learning to produce a two-dimensional, discretized representation of the input space of the training samples, called a topology-preserving projection map, and it is therefore a method to do dimensionality reduction (Kohonen, 1982; Murugesan and Murugesan, 2021). Giraudel and Lek (2001) introduced SOFM into ecology, and successfully analyzed the distribution data of eight plant species in Southern Wisconsin by using this method. After that, SOFM clustering was compared with TWINSpan and fuzzy C-means clustering in woodland study which confirmed its effectiveness (Zhang et al., 2010). SOFM ordination was applied and compared with PCA and DCA in the study of plant communities in the Taihang Mountains, which proved that they provided consistent results (Zhang et al., 2008). SOFM clustering and ordination have not been applied to studies of endangered medicinal plant communities and their conservation.

Glycyrrhiza uralensis is one of the most useful Chinese herbal medicines and widely used in medicine, food, tobacco, chemical industries in China (Zhou, 2006). Annual production of root medicine of this species is over 60000 tons in China. *Glycyrrhiza uralensis* is widely distributed from east to west in Northern China (Fig. 1). The wild resources of this medicinal species are reduced quickly since 1970s and it has been listed in the national endangered and protected plants and in IUCN red list as EN class. The conservation and restoration of this species and its community become urgent (Zhang et al., 2011). The objectives of this study are: 1) to apply SOFM clustering and ordination to the analysis of endangered medicinal plant (*G. uralensis*) community study and to test the effectiveness of these methods; 2) to analyze the relationships between *G. uralensis* communities and environmental variables and test the hypothesis that precipitation is the key factor to its populations and communities.

Materials and methods

Self-organizing feature map (SOFM)

Artificial neural networks (ANN) are comparatively new mathematical theory and have already been successfully used in ecology (Giraudel and Lek, 2001). Based on the mechanism of the human brain, the Artificial Neural Network is a convenient alternative tool to traditional statistical methods. The Kohonen Self-Organizing Feature Map (SOFM) is one of the most well-known neural networks with unsupervised learning rules (Kohonen, 1982).

SOFM uses unsupervised learning and produces a topologically ordered output that displays the similarity between the samples presented to it (Foody, 1999). The network consists of two layers, input layer and output layer (Schalkoff, 1992; Suding et al., 2008). The input layer contains a unit (neuron) for each variable (species) in the plant community data set. The output layer is a two-dimensional array of units and each of these units is connected to the input layer unit by the associated weight. The learning is a competitive process in which the network adapts to respond in different locations for input that differs. Consequently, samples that are similar should be associated with units that are close together in the output layer while a dissimilar sample would be associated with a distant unit elsewhere in the output layer (Chon et al., 1996).

SOFM clustering

Suppose the input data vector:

$$P_k = (P_1^k, P_2^k, \dots, P_N^k), (k = 1, 2, \dots, q) \quad (\text{Eq.1})$$

The associated weight vector,

$$W_{ji} = (W_{j1}, W_{j2}, \dots, W_{ji}, \dots, W_{jN}) \quad i = 1, 2, \dots, N; j = 1, 2, \dots, M \quad (\text{Eq.2})$$

Then, the SOFM clustering procedure:

1. Initializing. Giving initial values of W_{ij} within $[0, 1]$ randomly ($i = 1, 2, \dots, N$; $j = 1, 2, \dots, M$), initial values of learning rate $\eta(0)$ and neighborhood $Ng(0)$, and determining total learning times T .

2. Inputting a random sample unit drawn from the input dataset P_k into the network and calculating \bar{P}_k :

$$\bar{P}_k = \frac{P_k}{\|P_k\|} = \frac{(P_1^k, P_2^k, \dots, P_N^k)}{\left[(P_1^k)^2 + (P_2^k)^2 + \dots + (P_N^k)^2 \right]^{1/2}} \quad (\text{Eq.3})$$

3. Calculating \bar{W}_j :

$$\bar{W}_j = \frac{W_j}{\|W_j\|} = \frac{(W_{j1}, W_{j2}, \dots, W_{jN})}{\left[(W_{j1})^2 + (W_{j2})^2 + \dots + (W_{jN})^2 \right]^{1/2}} \quad (\text{Eq.4})$$

4) Calculating distance between \bar{W}_j and \bar{P}_k by Euclidean distance:

$$d_j = \left[\sum_{i=1}^N (\bar{P}_i^k - \bar{W}_{ji})^2 \right]^{1/2} \quad (j = 1, 2, \dots, M) \quad (\text{Eq.5})$$

5. Determining the minimum distance d_g , g is chosen as the winning neuron, called the Best Matching Unit (BMU).

$$d_g = \min [d_j] \quad j = 1, 2, \dots, M \quad (\text{Eq.6})$$

6. Adjusting the weights W_{ji} :

$$\overline{W_{ji}}(t+1) = \overline{W_{ji}}(t) + \eta(t) \cdot \left[\bar{P}_i^k - \overline{W_{ji}}(t) \right] \quad (j = 1, 2, \dots, M) \quad (\text{Eq.7})$$

where $\eta(t)$ is the learning rate at t time, here we define it as follows:

$$\eta(t) = \eta(0)(1 - t/T) \quad (0 < \eta(0) < 1) \quad (\text{Eq.8})$$

The neighborhood $N_g(t)$ is defined:

$$N_g(t) = \text{INT}[N_g(0)(1 - t/T)] \quad (\text{Eq.9})$$

$N_g(0)$ is the initial value of $N_g(t)$.

7. Increasing time t to $t + 1$. If $t < T$ then go to step 2), else stop the training.

The final topology map of small squares containing sample units can be used to classify samples into groups (Zhang et al., 2010). The number of small squares is usually determined according to the number of samples. We use 9×9 small squares for 100 samples (Chon et al., 1996).

SOFM ordination

Based on the topology map of small squares containing sample units above, a general ordination diagram can be obtained by rescaling the axes: considering the map of small squares of 9×9 is a diagram with coordinate scores of $[0.0 - 9.0]$, and each sample has its two-dimensional scores. Rescaling is the transformation of these scores into coordinate values between 0.0 and 1.0 (Zhang et al., 2008).

G. uralensis community data

In order to clarify the wild resources of *Glycyrrhiza uralensis*, a general survey was carried out in 2015. According to its community distribution, five study regions, Chifeng and Hengjinqi (Inner Mongolia), Minqin (Ganshu), Aletai and Kashi (Xinjing) along a precipitation gradient from east to west in Northern China, were selected as sampling sites (Zhang et al., 2011) (*Fig. 1*). Twenty samples (quadrats) of $5 \text{ m} \times 5 \text{ m}$ were set up randomly at each site. The species names, cover, mean height, and individual number was investigated in each sample. The cover was estimated by eyes, and the height was measured by use of a tape ruler. Totally 191 plant species were recorded in 100 samples. Elevation, slope and aspect for each sample were also measured and recorded. The elevation was measured by a GPS, slope and aspect measured by a compass meter.

The Importance Value (IV) of species was calculated and used as data in SOFM clustering and ordination analysis. The importance value was calculated by the following formulas (Zhang, 2011):

$$IV_{\text{Shrubs}} = (\text{Relative abundance} + \text{Relative cover} + \text{Relative height})/3 \quad (\text{Eq.10})$$

$$IV_{\text{Herbs}} = (\text{Relative cover} + \text{Relative height})/2 \quad (\text{Eq.11})$$

The relative abundance refers to the percentage of one species abundance over the sum of all species abundance in a sample, relative cover to the percentage of one species cover over the sum of all species cover in a sample, and relative height to the percentage of one species mean height over the sum of all species mean height in a sample. The species data matrix is consisted of importance values of 191 species in 100 samples.

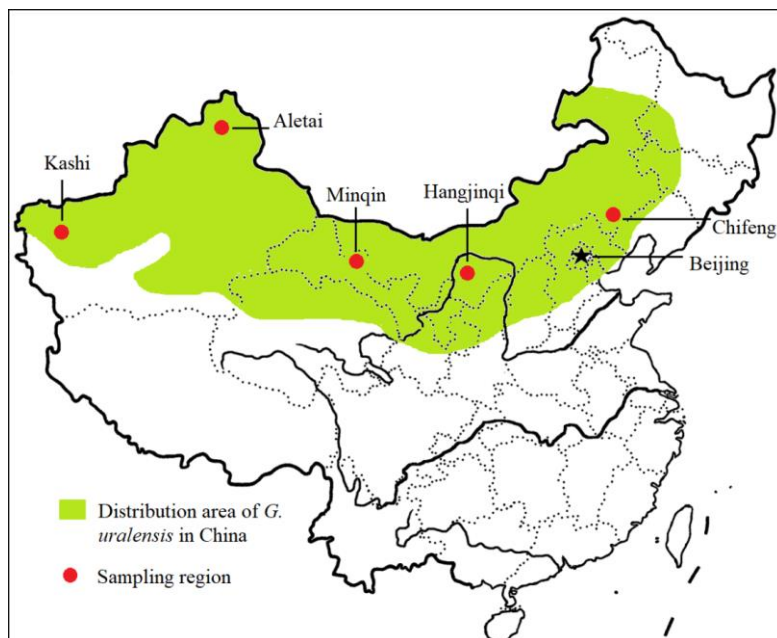


Figure 1. The distribution area of *Glycyrrhiza uralensis* in China and the five sampling regions

Results

In this study, SOFM was carried out with the learning rate of 0.1 for the ordinating phase and 0.02 for adjusting phase, 5000 steps for the ordinating phase and 50 000 steps for the tuning phase. A map of 9×9 small squares was chosen for 100 samples. When the learning process is finished, a topology map of 9×9 small squares is obtained and samples units can be mapped into the corresponding squares (*Fig. 2*).

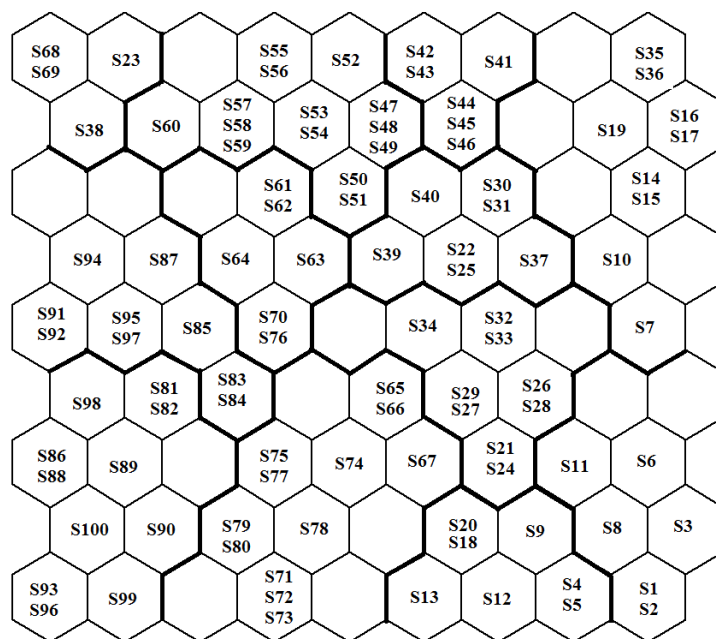


Figure 2. The topology map of 100 samples of *Glycyrrhiza uralensis* communities in 9×9 small squares from self-organizing feature map (SOFM) clustering. S with number refers to sample and its ordinal number

According to the similarity of neurons (units), small squares were clustered into 12 groups (Fig. 3). Samples in each neuron group constituted a community, and therefore 100 samples were classified into 12 *Glycyrrhiza uralensis* communities (Table 1). These communities represent the general vegetation types of *Glycyrrhiza uralensis* in Northern China (Zhang et al., 2011). The main characteristics of community composition, structure and environment were listed in Table 2.

Table 1. Twelve *Glycyrrhiza uralensis* communities and their composition of samples recognized by SOFM clustering along a precipitation gradient in Northern China

Community number	Sample composition
I	1, 2, 3, 6, 8, 11
II	4, 5, 9, 12, 13, 18, 20
III	7, 10, 14, 15, 16, 17, 19, 35, 36
IV	21, 24, 26, 27, 28, 29, 32, 33, 34
V	22, 25, 30, 31, 37, 39, 40
VI	41, 42, 43, 44, 45, 46, 54
VII	47, 48, 49, 50, 51, 52, 53, 55, 56, 57, 58, 59, 60
VIII	23, 38, 68, 69
IX	61, 62, 63, 64, 70, 76
X	65, 66, 67, 71, 72, 73, 74, 75, 77, 78, 79, 80
XI	83, 84, 85, 87, 91, 92, 94, 95, 97
XII	81, 82, 86, 88, 89, 90, 93, 96, 98, 100

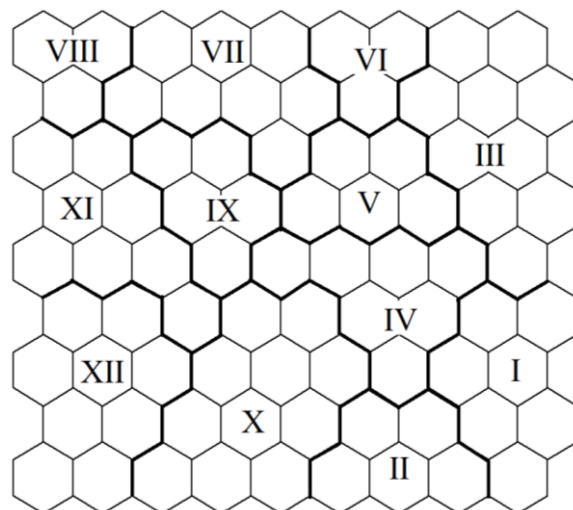


Figure 3. The groups of neurons on the SOFM topology map from self-organizing feature map (SOFM) clustering. I-XII refer to the twelve groups and *Glycyrrhiza uralensis* communities in Northern China

Variations of abundance (importance value) of dominant species among these communities were clearly shown by Figure 4. Each dominant species has its own distribution area and center.

By rescaling, a general SOFM ordination diagram was obtained (Fig. 5). The first SOFM axis was a precipitation gradient, i.e. the precipitation was increased from left to right. The second SOFM axis represented a comprehensive gradient of elevation, slope and aspect.

Table 2. The characteristics of the twelve *Glycyrrhiza uralensis* communities recognized by SOFM clustering along a precipitation gradient in Northern China

Community number and name	Community cover (%)	<i>G. uralensis</i> cover (%)	<i>G. uralensis</i> density (n/ha ⁻¹)	Elevation (m)	Slope (°)	Aspect	Common species
I. Comm. <i>Glycyrrhiza uralensis</i> + <i>Stipa bungeana</i>	75	25	3600	380 - 605	10-20	S, WS, ES	<i>Ziziphus jujuba</i> var. <i>spinosa</i> , <i>Lespedeza darurica</i> , <i>Pedicularis resupinata</i> , <i>Potentilla anserine</i> , <i>Saussurea epilobioides</i> , <i>Artemisia sacrorum</i> , <i>Artemisia mongolica</i> , and <i>Cynanchum hancockianum</i>
II. Comm. <i>Glycyrrhiza uralensis</i> + <i>Aneurolepidium chinense</i>	80	28	3950	350 - 650	10-20	S, WS	<i>Haloxylon Ammodendron</i> , <i>Caragana pygmaea</i> , <i>Lespedeza darurica</i> , <i>Berberis sibirica</i> , <i>Stipa glareosa</i> , <i>Artemisia mongolica</i> , <i>Cynanchum hancockianum</i> , <i>Carex duriuscul</i> , and <i>Carex stenophylloides</i>
III. Comm. <i>Glycyrrhiza uralensis</i> + <i>Potentilla anserine</i>	80	26	4120	350 - 580	10- 25	S, WS, ES	<i>Lespedeza darurica</i> , <i>Artemisia mongolica</i> , <i>Stipa bungeana</i> , <i>Vicia amoena</i> , <i>Carex duriuscul</i> , and <i>Saussurea amara</i>
IV. Comm. <i>Glycyrrhiza uralensis</i> + <i>Artemisia ordosica</i>	85	27	3680	300 - 650	15- 30	S, WS, ES, W, E	<i>Caryopteris mongolica</i> , <i>Lespedeza darurica</i> , <i>Artemisia mongolica</i> , <i>Stipa bungeana</i> , <i>Trigonella ruthenica</i> , <i>Trigonella ruthenica</i> , <i>Astragalus melilotoides</i> , and <i>Ephedra przewalskii</i>
V. Comm. <i>Glycyrrhiza uralensis</i> + <i>Carex duriuscul</i> + <i>Aneurolepidium chinense</i>	75	25	4500	300 - 600	20-30	S, WS, ES, W	<i>Lespedeza darurica</i> , <i>Haloxylon Ammodendron</i> , <i>Berberis sibirica</i> , <i>Cynanchum hancockianum</i> , <i>Stipa glareosa</i> , <i>Caragana pygmaea</i> , <i>Artemisia scoparia</i> , <i>Carex stenophylloides</i> , and <i>Astragalus melilotoides</i>
VI. Comm. <i>Glycyrrhiza uralensis</i> + <i>Polygonum bistorta</i>	70	35	5700	300 - 500	20- 30	S, WS, ES, W	<i>Oxytropis myriophylla</i> , <i>Polygonum divaricatum</i> , <i>Adenophora gmeliniia</i> , <i>Potentilla acaulis</i> , <i>Suaeda prostrate</i> , <i>Astragalus melilotoides</i> , <i>Allium condensatum</i> , <i>Artemisia ordosica</i> , and <i>Oxytropis grandiflora</i>
VII. Comm. <i>Glycyrrhiza uralensis</i> + <i>Ephedra przewalskii</i> + <i>Cancrinia discoidea</i>	70	40	59500	300 - 500	20-30	S, WS, ES, W, E	<i>Caragana korshinskii</i> , <i>Elaeagnus mooceroftii</i> , <i>Suaeda prostrate</i> , <i>Artemisia phaeocephala</i> , <i>Saussurea laciniata</i> , <i>Saposhnikovia divaricata</i> , <i>Oxytropis glabra</i> , and <i>Artemisia ordosica</i>
VIII. Comm. <i>Glycyrrhiza uralensis</i> + <i>Astragalinae triloa</i> + <i>Stipa sareptana</i>	75	40	6000	400 - 700	10-30	S, WS, ES	<i>Artemisia scoparia</i> , <i>Kochia prostrate</i> , <i>Potentilla acaulis</i> , <i>Artemisia frigida</i> , <i>Ceratoides lates</i> and <i>Atraphaxis frutescus</i>
IX. Comm. <i>Glycyrrhiza uralensis</i> + <i>Carex pediformis</i> + <i>Stipa sareptana</i>	60	33	5500	350 - 650	15-35	S, WS	<i>Cleistogenes squarrosa</i> , <i>Caragana pygmaea</i> , <i>Hordeum brevisublatum</i> , <i>Ephedra sinica</i> , <i>Achnatherum sibiricum</i> , <i>Artemisia frigida</i> , <i>Viola tianschanica</i> , <i>Carex duriuscula</i> , and <i>Alopecurus pratensis</i>
X. Comm. <i>Glycyrrhiza uralensis</i> + <i>Artemisia frigida</i>	65	37	4900	280 - 500	15-25	S, WS, ES	<i>Salicornia Bigelivii</i> , <i>Carex duriuscula</i> , <i>Stipa sareptana</i> , <i>Artemisia phaeocephala</i> , <i>Alopecurus pratensis</i> , <i>Saposhnikovia divaricata</i> , and <i>Carex pediformis</i>
XI. Comm. <i>Glycyrrhiza uralensis</i> + <i>Aneurolepidium chinense</i> + <i>Stipa sareptana</i>	70	29	4100	400 - 750	15-35	S, WS, ES	<i>Caragana pygmaea</i> , <i>Astragalinae triloa</i> , <i>Stipa purpurea</i> , <i>Festuca logae</i> , <i>Artemisia kaschgarica</i> , <i>Polygonum viiiiparum</i> , <i>Ephedra equisetina</i> , <i>Glycyrrhiza inflata</i> , and <i>Alyssum desertorum</i>
XII. Comm. <i>Glycyrrhiza uralensis</i> + <i>Festuca logae</i> + <i>Stipa sareptana</i>	80	30	4000	400 - 800	20-35	S, WS, ES	<i>Artemisia parvula</i> , <i>Scorzonera divaricata</i> , <i>Roegneria kamoji</i> , <i>Potentilla bifurca</i> , <i>Carex duriuscula</i> , and <i>Ranunculus japonicas</i>

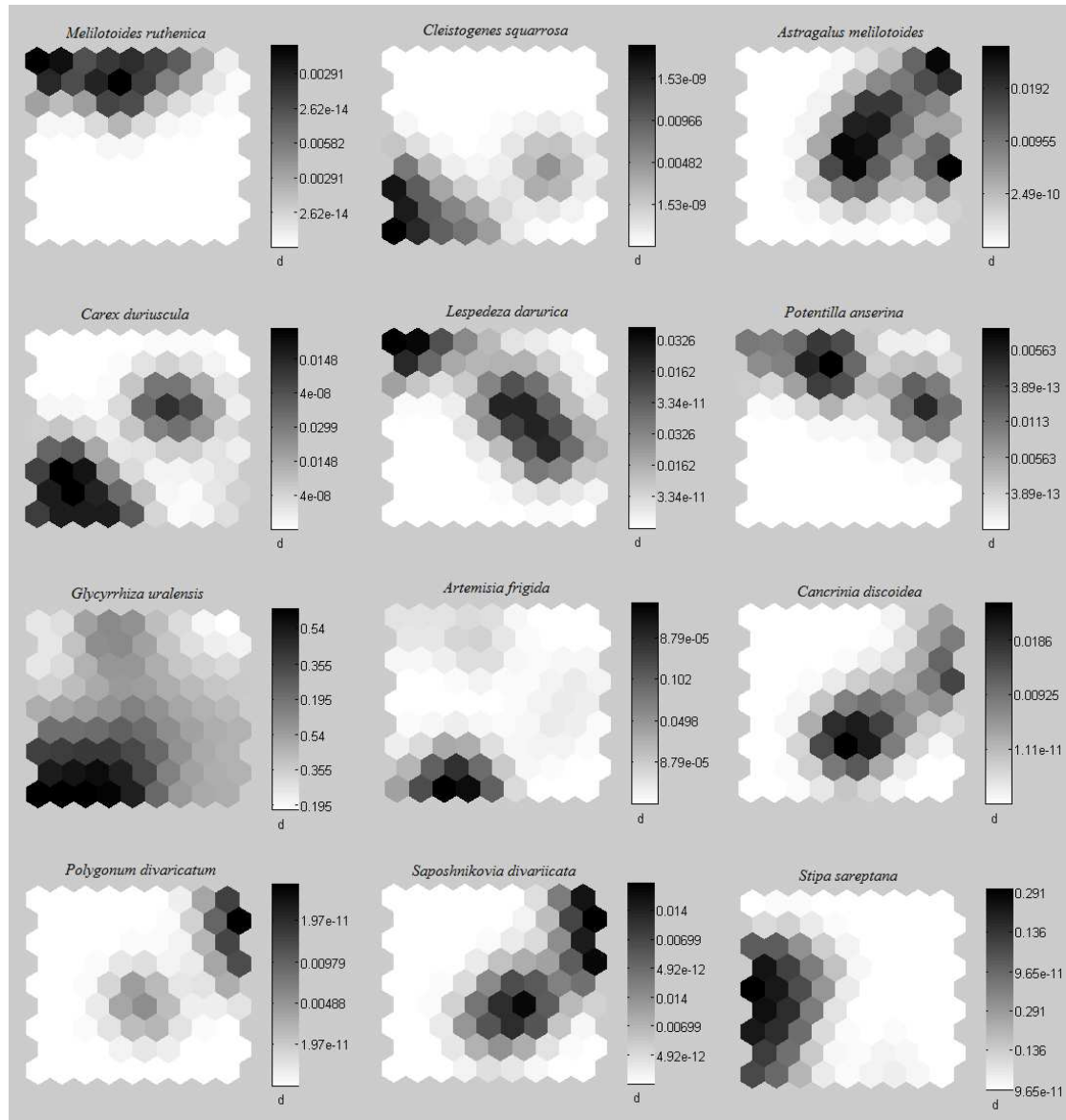


Figure 4. The variation of abundance of the dominant species on the topology map from Self-organizing feature map (SOFM) clustering of *Glycyrrhiza uralensis* communities in North China

Discussion

SOFM clustering classified 100 samples into 12 communities dominated by *Glycyrrhiza uralensis* in Northern China. These communities varied in composition, structure, distribution and environmental conditions. They distribute from temperate moisture grassland in eastern area, through dry steppe and desert grassland in middle area, and to temperate desert regions in western area and represent the general vegetation communities of *G. uralensis* from east to west in Northern China. To conserve wild medicinal plant resources of *G. uralensis*, the conservation of these communities is important because these communities provide suitable survival environment for the studied populations (Pan and Zhang, 2002). These vegetation types are also significant for protecting and improving the ecological environment in semi-

arid and arid regions in northern and western China (Wu, 1980; Zhang et al., 2010). The SOFM classification results were reasonable according to the Chinese vegetation classification system. These results were consistent with that of TWINSpan classification and fuzzy C-means clustering (Zhang et al., 2010; Song and Zhang, 2017), which suggests that SOFM clustering was useful and significant in analysis of endangered medicinal plant communities.

The variation of dominant species on the SOFM topology map showed their importance roles in clustering and in community structure and composition. These species living in *Glycyrrhiza uralensis* communities and have close relationships with it. To conserve these species will be helpful to the conservation of *Glycyrrhiza uralensis* populations and communities (Pan and Zhang, 2002; Zhang et al., 2011; SuriGuga et al., 2011; Moniruzzaman et al., 2021).

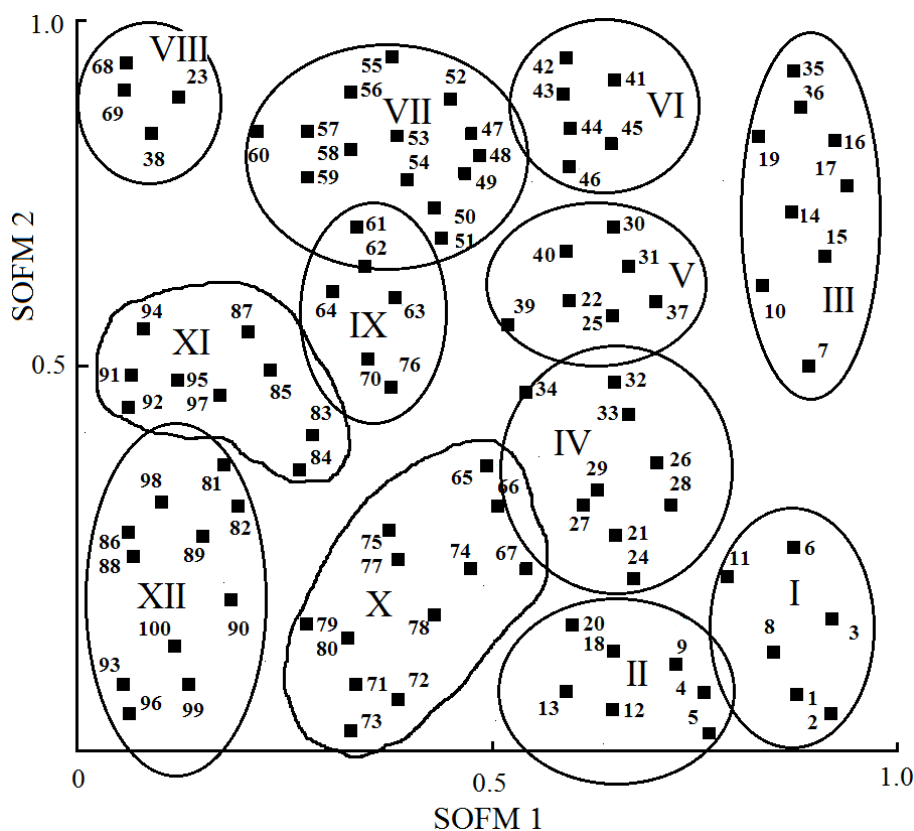


Figure 5. The Self-organizing feature map (SOFM) ordination diagram of 100 samples of *Glycyrrhiza uralensis* communities in Northern China. Numbers refer to samples, and I-XII refer to the twelve *Glycyrrhiza uralensis* communities

SOFM ordination displayed samples more clearly in topological space, which is identical to the result of SOFM clustering. Each community recognized by SOFM clustering had its own distribution area and center with clear boundary, which confirmed that SOFM clustering results were reasonable and reflected their differences of composition, structure and natural conditions. The first SOFM ordination axis was a precipitation gradient, which means that annual precipitation was the most important and key factor influencing *Glycyrrhiza uralensis* populations and communities. This is because water conditions are limitation variable in semi-arid and arid area for

vegetation maintaining and development in Northern China (Zhang et al., 2011; Cullotta et al., 2015; Song et al., 2020). This result is consistent with other studies in this area (Zhang et al., 2010). The second SOFM ordination axis was a comprehensive gradient of elevation, slope and aspect, which suggested that topographical variables were also significant for *Glycyrrhiza uralensis* populations and communities. Similar as SOFM clustering, SOFM ordination was useful and significant in analysis of endangered medicinal plant communities.

To conserve *Glycyrrhiza uralensis* populations and communities, the management of wild *G. uralensis* and its communities must be legally and effectively, e.g. digging must be strictly controlled and grazing in these communities should be limited to keep its ecosystem composition, structure and function. Soil fertilization and irrigation, if possible, should be used for improving their habitat conditions. To meet the demands for medicinal market, more large-scale cultivation bases of *G. uralensis* should be set up and developed in different area in northern China. Studies on biology, ecology, economy, utilization etc. for *G. uralensis* species, populations and communities must be strengthened (Zhou, 2006; Larsen and Olsen, 2007; Zhang et al., 2011).

Theoretically, Self-Organizing Feature Map neural network has advantages in solving non-linear problems and in studying complicated systems (Schalkoff, 1992; Park, 2003; Zhang et al., 2008; Murugesan and Murugesan, 2021). Medicinal plant community system is a complexity ecosystem with various non-linear and fuzzy relationships of species, communities and environmental variables (Sproull et al., 2015). Therefore, SOFM techniques should be perfect methods and applied more frequently in endangered medicinal plant community studies, and it may be suggestible to combine SOFM clustering and SOFM ordination in a same study (SuriGuga et al., 2011).

Acknowledgments. This study was financially supported by the Young Teachers Found of Beijing University of Chinese Medicine (Grant No. 2018-JYB-JS), National Natural Science Foundation of China (Grant No. 31170494).

REFERENCES

- [1] Chon, T.-S., Young, S. P., Yong, M. K., Cha, E. Y. (1996): Patternizing communities by using an artificial neural network. – *Ecological Modelling* 90: 69-78.
- [2] Cullotta, S., Puzzolo, V., Fresta, A. (2015): The southernmost beech (*Fagus sylvatica*) forests of Europe (Mount Etna, Italy): ecology, structural stand-type diversity and management implications. – *Plant Biosystems* 149: 88-89. DOI: 10.1080/11263504.2013.814603.
- [3] Foody, G. M. (1999): Applications of the self-organizing feature map neural network in community data analysis. – *Ecological Modelling* 120: 97-107.
- [4] Giraudel, J. L., Lek, S. (2001): A comparison of self-organizing map algorithm and some conventional statistical methods for ecological community ordination. – *Ecological Modelling* 146: 329-339.
- [5] Kathe, W. (2006): Conservation of Eastern-European medicinal plants - *Arnica montana* in Romania. – *Wageningen UR Frontis Series* 17: 203-211.
- [6] Kohonen, T. (1982): Self-organized formation of topologically correct feature maps. – *Biological Cybernetics* 43(1): 59-69.
- [7] Larsen, H. O., Olsen, C. S. (2007): Unsustainable collection and unfair trade? Uncovering and assessing assumptions regarding Central Himalayan medicinal plant conservation. – *Biodiversity and Conservation* 16: 1679-1697. DOI: 10.1007/s10531-006-9039-4.

- [8] Moniruzzaman, M., Bhowmick, A. R., Karan, S., Mukherjee, J. (2021): Spatial heterogeneity within habitat indicates the community assemblage pattern and life strategies. – *Ecological Indicators* 123: 107365.
- [9] Murugesan, V. P., Murugesan, P. (2021): Some measures to impact on the performance of Kohonen self-organizing map. – *Multimedia Tools and Application* 80: 26381-26409.
- [10] Nautiyal, B. P., Nautiyal, M. C., Khanduri, V. P., Rawat, N. (2009): Floral biology of *Aconitum heterophyllum* Wall: a critically endangered alpine medicinal plant of Himalaya, India. – *Turkish Journal of Botany* 33: 13-20. DOI 10.1007/s10531-011-0082-4.
- [11] Pan, B. R., Zhang, Y. M. (2002): Characteristics and conservation of biodiversity in Xinjiang. – *Science in China Series D - Earth Sciences* 45(Suppl.): 174-179.
- [12] Park, Y. S. (2003): Applications of artificial neural networks for patterning and predicting aquatic insect species richness in running waters. – *Ecological Modelling* 160: 265-273. DOI: 10.1016/S0304-3800(02)00258-2.
- [13] Roberts, D. W. (2008): Statistical analysis of multidimensional fuzzy set ordinations. – *Ecology* 89: 1246-1260.
- [14] Schalkoff, R. (1992): *Pattern Recognition: Statistical Structural and Neural Approaches*. – Wiley, New York, p. 364.
- [15] Song, N. Q., Zhang, J.-T. (2017): Fuzzy set ordination analysis of survival communities for an endangered medicinal plant species, *Phellodendron amurense*. – *Proceedings of the 13th International Conference on Natural Computation, Fuzzy Systems and Knowledge Discovery (ICNC-FSKD 2017)*, IEEE & CAS, PP: 1474-1478.
- [16] Song, N. Q., Yan, Y. M., Li, J. L. (2020): Bi-plot to show correlations of environmental variables in Self-Organizing Feature Map ordination. – *JP Journal of Biostatistics* 17: 359-370.
- [17] Sproull, G. J., Quigley, M. F., Sher, A., Gonzalez, E. (2015): Long-term changes in composition, diversity and distribution patterns in four herbaceous plant communities along an elevational gradient. – *Journal of Vegetation Science* 26: 552-563. DOI: 10.1007/s00213-011-2176-9.
- [18] Suding, K., Lavorel, S., CHAPIN III, F. (2008): Scaling environmental change through the community-level: a trait-based response-and-effect framework for plants. – *Global Change of Biology* 14(5): 1125-1140.
- [19] SuriGuga, Zhang, J.-T, Zhang, B., Cheng, J. J., Zhang, Q. D., Tian, S. G., Liu, S. J. (2011): Forest community analysis in the Songshan National Nature Reserve of China using self-organizing map. – *Russian Journal of Ecology* 42(3): 216-222. DOI: 10.1134/S1067413611030179.
- [20] Ter Braak, C. J. F. (1986): Canonical correspondence analysis: a new eigenvector method for multivariate direct gradient analysis. – *Ecology* 67: 1167-1179.
- [21] Wu, Z. Y. (ed). (1980): *Vegetation of China*. – Science Press, Beijing.
- [22] Zhang, J.-T. (2011): *Quantitative Ecology*. 2nd Ed. Science Press, Beijing (in Chinese).
- [23] Zhang, J.-T., Dong, Y. R., Xi, Y. X. (2008): A comparison of SOFM ordination with DCA and PCA in gradient analysis of plant communities in the midst of Taihang Mountains, China. – *Ecological Informatics* 3: 367-374.
- [24] Zhang, J.-T., Li, S., Li, M. (2010): A comparison of self-organizing feature map clustering with TWINSpan and fuzzy C-means clustering in the analysis of woodland communities in the Guancen Mts, China. – *Community Ecology* 11: 120-126. DOI: 10.1556/ComEc/11.2010.1.17.
- [25] Zhang, J.-T., Xu, B., Li, M. (2011): Diversity of communities dominated by *Glycyrrhiza uralensis*, an endangered medicinal plant species, along a precipitation gradient in China. – *Botanical Studies* 52: 493-501.
- [26] Zhou, C. M. (2006): Cultivation techniques for *Glycyrrhiza uralensis*. – *Xinjiang Farmland Reclamation Science and Technology* 15(1): 14-15.

IN-SITU MONITORING OF WATER INFILTRATION RECHARGE IN LARGE DEPTH IRRIGATION AREA UNDER PLANTING CONDITIONS

WANG, Y. Y.^{1,2} – LI, Z. P.¹ – ZHAO, J.¹ – HE, Y. J.^{2,3*}

¹*College of Geosciences and Engineering, North China University of Water Resources and Electric Power, 450045, Zhengzhou, China*

²*The Institute of Hydrogeology and Environmental Geology, Chinese Academy of Geological Science, 050061, Shijiazhuang, China*

³*Geothermal and Hot Dry Rock Exploration and Development Technology Innovation Center, Ministry of Natural Resource, 050061, Shijiazhuang, China*

**Corresponding author*

e-mail: heyujiang86@163.com; phone: +86-132-9831-2790

(Received 3rd Mar 2022; accepted 20th Jun 2022)

Abstract. To explore the recharge characteristics of soil water infiltration in the large buried irrigation system, in-situ monitoring tests were performed at the Comprehensive Agricultural Experiment Station in the pre-mountain area of the North China Plain. The agro-meteorological monitoring system was used to monitor meteorological elements such as precipitation and evaporation in the irrigation area, and the water content and water potential of typical soil profiles were measured in-situ using the neutron probe and negative pressure meter. The groundwater level was monitored using a groundwater level recorder. The study analyzed the water infiltration process in different growth stages of crops and elucidated water dynamics under heavy precipitation conditions. Therefore, the multi-year water balance of the study area was determined by defining the potential infiltration recharge boundary. The results showed that the types of soil water movement at different growth stages differed significantly, while the water potential profile showed the same trend on the time scale. The effect of Rainfall on soil water transport has a lagging effect, with precipitation greater than 10 mm recharging soil water to a certain extent. The main sources of water recharge for the large buried soil layer under planting conditions were rainfall (55.68%) and irrigation (44.32%) and the main source of discharge was evapotranspiration (97.89%), with very little recharge (2.11%) to groundwater. These findings identified the characteristics of water circulation in irrigation areas with large burial depths.

Keywords: *North China Plain, soil water, time scale, potential groundwater recharge, water balance*

Introduction

The groundwater level has been declining due to the severe overdraft in the North China Plain, resulting in a serious imbalance in groundwater recharge and discharge and triggering geological problems such as the formation of a large cone of groundwater depression and the downward shift of the salt and freshwater interface (Lu et al., 2021). These significant changes in groundwater recharge and discharge, especially in the North China irrigation area, result in substantial inconsistencies in agricultural water supply and demand. Scholars have observed that understanding the soil water supply, water dynamic evolution mechanisms, soil nutrient and pollution transport processes, and regional water resource potential characteristics are essential to address water shortage issues in the agricultural areas of the North China Plain (Adhikari and Wang, 2020; Kassaye et al., 2019). However, the dynamic evolutionary pattern of soil water infiltration recharge, which is the core of the above-mentioned problem, remains unclear (Jia et al., 2019), particularly under human cropping conditions when the process is more complex.

The soil water infiltration process is affected by various factors such as rainfall conditions, soil properties, crop coverage, and soil depth (Huang et al., 2021; Kamal et al., 2021). Soil water movement can be classified into four basic types: evaporation, infiltration, evaporation-infiltration, and infiltration-evaporation (Han et al., 2005). The analysis of soil water transport patterns is an important guide for water resource management in the North China Plains (Pereira et al., 2020). Pei et al. (2020) used a water cycle simulation of field experiments in large groundwater depth areas to quantify groundwater recharge and phreatic water supply. Zhang et al. (2020) and Pullens et al. (2021) studied the characteristics of soil water migration during the crop growth period by establishing a coupling model between hydrology and crop growth. Understanding the process of farmland water infiltration is essential for developing scientifically sound irrigation systems, planning and management of agricultural water resources, water-saving practices, and environmental assessment in major agricultural producing areas. Precipitation and irrigation are the primary sources of agricultural water recharge. The water content of the soil layer changes in a certain pattern because of external factors such as precipitation and irrigation, which affects the water absorption pattern, growth condition, distribution pattern of crops, and groundwater level (Zhang et al., 2007). The evolutionary mechanism of soil water movement after rainfall provides some guidance for crop irrigation mechanisms (Joly et al., 2019; Ayantobo et al., 2019). Researchers have experimentally verified that soil water transport has a certain lag after heavy precipitation (Kristo et al., 2019; Dias et al., 2021). Vermeire and Rinella (2020) studied the effects of seasonal rainfall on soil moisture and annual net primary production in a variety of plant combinations and observed that rainfall had no significant effect on soil moisture at 15–30 cm depth. Previous studies have scientifically evaluated soil water infiltration and soil-water environment dynamics in agricultural soils, which provide a foundation for this study (Xiao et al., 2021; Muhammad et al., 2021; Xu et al., 2021). However, the recharge characteristics of potential soil water infiltration under deep groundwater burial conditions and the influence of long-term precipitation were not considered, it is difficult to study the water regulation in the agricultural irrigation area of the deep vadose zone in North China that exhibits a large funnel area.

In this study, the Luancheng Agro-Ecosystem Experimental Station of the Chinese Academy of Sciences (32–48 m groundwater depth) was selected to conduct in-situ monitoring experiments for three consecutive years under summer maize and winter wheat. By observing the recharge characteristics of soil water under crop growth conditions, multiple growth stages and time scales, exploring the characteristics of precipitation impact in irrigation areas, defining the potential groundwater infiltration boundary to calculate the potential groundwater infiltration recharge in irrigation areas, and exploring the water balance characteristics of irrigation areas. It can provide reference indicators for the development of irrigation systems for farmland in the groundwater overdraft area of the North China Plain.

Materials and methods

Overview of the study area

The research site is located in Luancheng County, Shijiazhuang City (114°40'58"N, 37°53'16"E) in the middle of the piedmont Taihang Mountains in the North China plain. With a total area of 345 km² and 214 km² of arable land, this region is one of the main grain-producing regions in China (*Fig. 1*). The main crops of Winter Wheat and Summer Maize

are rotated (Hu et al., 2021, 2006; Shen et al., 2021) and planted every year in an area of 164 km² and 127 km², respectively, and the annual output is sufficient to supply the local area and export. The tillage method in this study is tillage cultivation. It has a sub-humid climate in the warm temperate zone, with an annual mean temperature of 12.8 °C and annual precipitation of 474.0 mm. The thickness of the vadose zone goes up to 30 m, and the infiltration of rainfall and irrigation water recharges the groundwater all year round (Wei et al., 2017; Ju et al., 2016). The dynamics of shallow soil water are less affected by the dynamics of the groundwater level. The main focus of the study was the soil water dynamics in the unsaturated zone above 3.4 m. The soil was mainly composed of clay, silt, fine sand, and medium sand. The study area is located on an alluvial fan in front of the Taihang Mountains. The groundwater recharge, runoff, and drainage conditions were good. The general runoff direction is from northwest to southeast and from shallow to deep runoff.

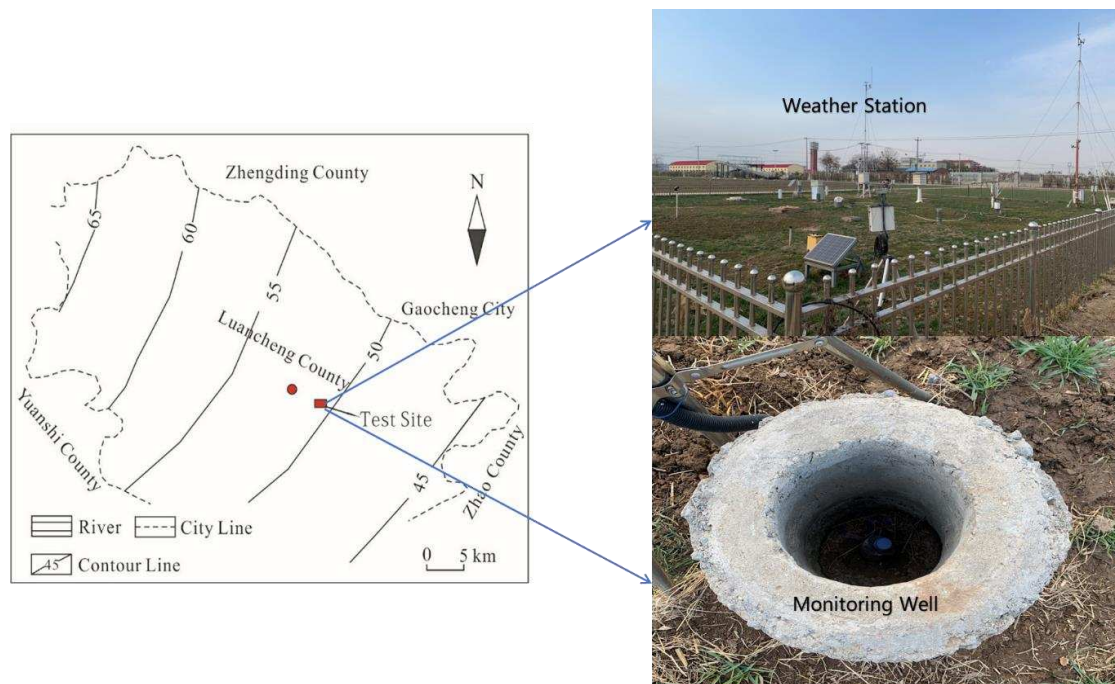


Figure 1. Contour and regional location map of the study area (the experimental site is located in the Taihang Mountain Front Plain, within the Agricultural Experimental Station of the Chinese Academy of Sciences, Luancheng County, Shijiazhuang City, Hebei Province, China)

Data

In-situ monitoring

The research site was equipped with monitoring systems that included negative pressure meters and neutron probes for monitoring soil water potential, groundwater level, and meteorological factors at the site. The neutron probes were calibrated in layers before the start of the test. Each monitoring system had 20 negative pressure meters and 20 neutron probes buried at depths of up to 340 cm. One negative pressure meter and one neutron probe were installed every 10 cm within the first 100 cm of depth, every 20 cm between 100–260 cm of depth, and every 40 cm between 260–340 cm of depth. The installation method was a buried oblique plug type. The Diver groundwater level recorder was used to monitor the changes in the groundwater level at the test site. In addition, there was a standard weather

station approximately 50 m away from the test field, which monitors rainfall, evaporation, and other parameters. The irrigation amount was determined according to the actual irrigation amount recorded by the field water meter. The irrigation method was broad irrigation. Some meteorological monitoring data in continuous monitoring years are shown in *Figure 2*, in which the E20 evaporator measures the water surface evaporation. Other meteorological data needed in the study are provided by the National Tibetan Plateau Data Center (<http://data.tpc.ac.cn>), mainly for daily maximum temperature, daily minimum temperature, daily average temperature, wind speed and sunshine hours.

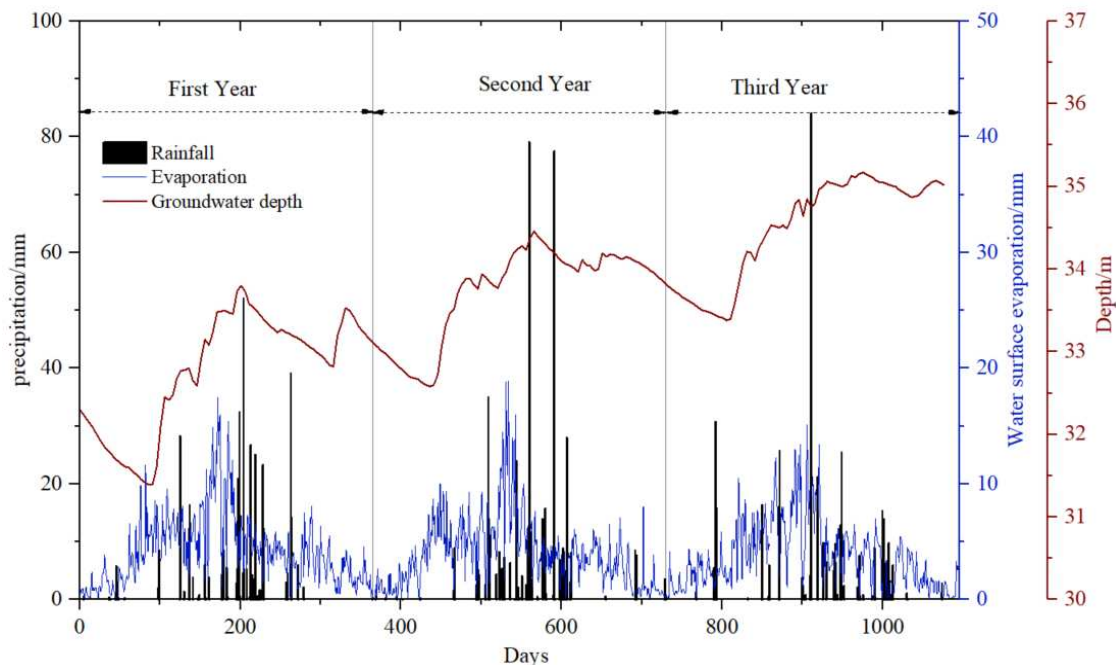


Figure 2. Meteorological conditions during the monitoring period in the Luancheng area (including groundwater levels, daily evaporation, and daily rainfall)

Field monitoring was carried out in three stages, with each stage lasting one year, from 2005-2007. The data on soil suction and moisture content were collected during the growth period of wheat and maize for three consecutive years. Monitoring frequencies are shown in *Table 1*. Precipitation or irrigation during the monitoring intensified the observations. Generally, the data were collected once in the first hour and then every 2–4 h, and the time interval was gradually extended until the regular observation time was restored.

Table 1. Monitoring items, instrumentation and frequency

Monitoring program	Instrument	Monitoring frequency
Groundwater level	Groundwater level automatic monitor Diver	Every 5 days
Moisture content	CNC503DR Neutron Probe	Every 3 days
Soil water potential	WM-1 mercury type negative pressure gauge system	Every 3 days
Meteorological data (rainfall, evaporation, etc.)	Rain gauge, E20 evaporator, etc.	Everyday

Methods

(1) Soil water potential measurements

A negative pressure meter is suitable for measuring soil moisture in irrigated farmlands and soils with high moisture content when used with a soil moisture meter. However, studying the soil water movement mechanism is essential for the development of an instrument. In this study, the soil water potential measurement was based on the reading of the mercury manometer, which can be derived from the negative soil pressure. As shown in *Equation 1* (Li et al., 2014):

$$\Psi_m = -12.6H_1 + 13.6H_0 - H_a + Z \quad (\text{Eq.1})$$

where Ψ_m is the negative soil pressure; H_1 is the height of the mercury level in the negative pressure meter; H_0 is the height of the mercury level in the mercury meter; H_a is the distance between the zero scales of the observation plate and the ground surface; and Z is the vertical distance between the center position of the clay head and the ground surface. The negative pressure meter H_a of the test point in this study is 133.5 cm.

The soil water potential was calculated using the observation data of the negative pressure meter to obtain the distribution curve of the soil water potential and subsequently determine the zero-flux surface. The zero-flux surface was used to analyze the soil water characteristics under different conditions and explore the effects of precipitation, irrigation infiltration, evaporation, and plant root water absorption on soil water movement.

(2) Potential infiltration recharge of groundwater

The maximum depth associated with zero flux downward development in the North China Plain can be evaluated in areas with substantial water level burial depth. Calculating the water flux of a specific boundary in the slowly changing gradient zone of soil water potential below the deepest zero flux surface, together with the soil water flux of that boundary, is equivalent to determining the vertical infiltration recharge of precipitation or irrigation water. The calculation of soil water flux Q at the location boundary Z must match with the water potential data near the location boundary Z and measure the unsaturated hydraulic conductivity $K(\theta)$ or $K(\psi_m)$. First, according to the soil water potential data, the calculated period was divided into n hours, and the soil water flux at the positioning boundary in each hour was calculated using Darcy's law. Then, the soil water flux for each hour was aggregated to obtain the soil water quantity passing through the positioning boundary in the calculation period (Jing et al., 1994). As shown in *Equation 2*.

$$Q_{(Z)} = -\sum_{i=1}^n K(\theta_i) \cdot \left(\frac{\Delta\psi}{\Delta z} \right) \cdot (\Delta t)_i, \quad i = 1, 2, \dots, n \quad (\text{Eq.2})$$

where $Q_{(Z)}$ is the amount of soil water passing from the localized boundary Z ; θ_i and $\frac{\Delta\psi}{\Delta z}$ are the average soil water content and average soil water potential gradient at the

positioning boundary Z in the i th period, respectively; $K(\theta_i)$ is the unsaturated hydraulic conductivity when the average value of soil water content is in the i th time period; and $(\Delta t)_i$ is the i th hourly period.

The key to calculating the infiltration recharge using this method is the determination of the unsaturated hydraulic conductivity $K(\theta_i)$. The zero flux plane method was used to determine the unsaturated hydraulic conductivity $K(\theta)$ of the soil using Darcy's law, as shown in Equation 3.

$$q(z) = -K(\theta) \frac{\partial \psi}{\partial z} \text{ or } q(z) = -K(\psi_m) \frac{\partial \psi}{\partial z} \quad (\text{Eq.3})$$

This equation can be rearranged as:

$$K(\theta) = -q(z) / \frac{\partial \psi}{\partial z} \text{ or } K(\psi_m) = -q(z) / \frac{\partial \psi}{\partial z} \quad (\text{Eq.4})$$

where θ , ψ , and $\frac{\partial \psi}{\partial z}$ are the average values of soil water content, matric potential, and soil water potential gradient at the positioning boundary Z from time period t_1 to t_2 , respectively. During the effective period of the zero-flux surface, the position $z_0(t_1)$ and $z_0(t_2)$ of the ZFP can be determined by the water content and water potential distribution at t_1 and t_2 . The ZFP method was used to calculate the water quantity D at Z from t_1 to t_2 . $D = \int_{z_0}^z \theta(z, t_1) dz - \int_{z_0}^z \theta(z, t_2) dz$. The soil water flux was obtained from the equation $q(z) = D / \Delta t (\Delta t = t_1 - t_2)$. The value of unsaturated hydraulic conductivity was derived based on Equation 4.

(3) Evapotranspiration

Rooting depths range from 0 to 200 cm for maize and 0 to 60 cm for wheat (Ordóñez et al., 2018; Li et al., 2022). Considering the different cropping patterns in the monitoring year, the evapotranspiration ET for the different cropping patterns is divided into evapotranspiration from the crop and evaporation from the soil in the no-crop period. Crop transpiration under standard conditions is calculated using Equation 5.

$$ET_c = ET_0 \times K_c \quad (\text{Eq.5})$$

where: ET_c is the crop transpiration (mm/d); ET_0 is the reference crop transpiration (mm/d); K_{cend} is the crop coefficient, determined according to the FAO56 recommended crop coefficient (Allen et al., 1998). The crop coefficients were divided into initial growth period K_{cini} , middle growth period K_{cmid} and maturity period K_{cend} , where the growth coefficients were 0.3, 1.2 and 0.4 for maize and 0.4, 1.15 and 0.3 for wheat.

The daily evapotranspiration of the reference crop was calculated using the Penman-Monteith Equation 6.

$$ET_0 = \frac{0.408\Delta(R_n - G) + r \frac{900}{T + 273} u_2 (e_s - e_a)}{\Delta + r(1 + 0.34u_2)} \quad (\text{Eq.6})$$

where R_n is the net radiation of canopy surface ($\text{MJ}/(\text{m}^2 \cdot \text{d})$); G is soil heat flux ($\text{MJ}/(\text{m}^2 \cdot \text{d})$); Δ is the slope of the relationship curve between saturated water vapor pressure and air temperature ($\text{kPa}/^\circ\text{C}$); T is the mean daily temperature ($^\circ\text{C}$) at 2 m; r is a constant of the hygrometer ($\text{kPa}/^\circ\text{C}$); u_2 is a hygrometer constant ($\text{kPa}/^\circ\text{C}$); e_s is saturated water pressure (kPa); e_a is the actual water pressure (kPa).

The E20 evaporator dish in the study measured the evaporation from the water surface, and the ET_s of evaporation from the soil surface can be found by converting Equation 7.

$$ET_s = \alpha \times E_{20} \quad (\text{Eq.7})$$

where ET_s is the Soil surface evaporation ($\text{mm} \cdot \text{a}^{-1}$); α is an empirical coefficient, here taken as 0.54 (Wang et al., 2005); E_{20} is the E20 evaporator reading ($\text{mm} \cdot \text{a}^{-1}$).

(4) Water balance

The water balance method involves the systematic use of meteorological, plant growth, and farmland irrigation data. The infiltration recharge (Q) of soil water from the surface to the soil, without considering lateral runoff, can be estimated with the help of Equation 8 (Li et al., 2017).

$$Q = P + I - E_T - \Delta W \quad (\text{Eq.8})$$

where E_T is the evapotranspiration ($\text{mm} \cdot \text{a}^{-1}$); E_{20} is the E20 evaporator reading ($\text{mm} \cdot \text{a}^{-1}$); Q is the soil moisture flux at the locus boundary (mm ; positive upward and negative downward); P is the rainfall (mm); I is the irrigation (mm); E_T is the evapotranspiration (mm), including soil surface evaporation and crop transpiration; and ΔW is the soil water storage variable (negative for the increase and positive for decrease), which can be determined by measuring the water content distribution in the soil profile.

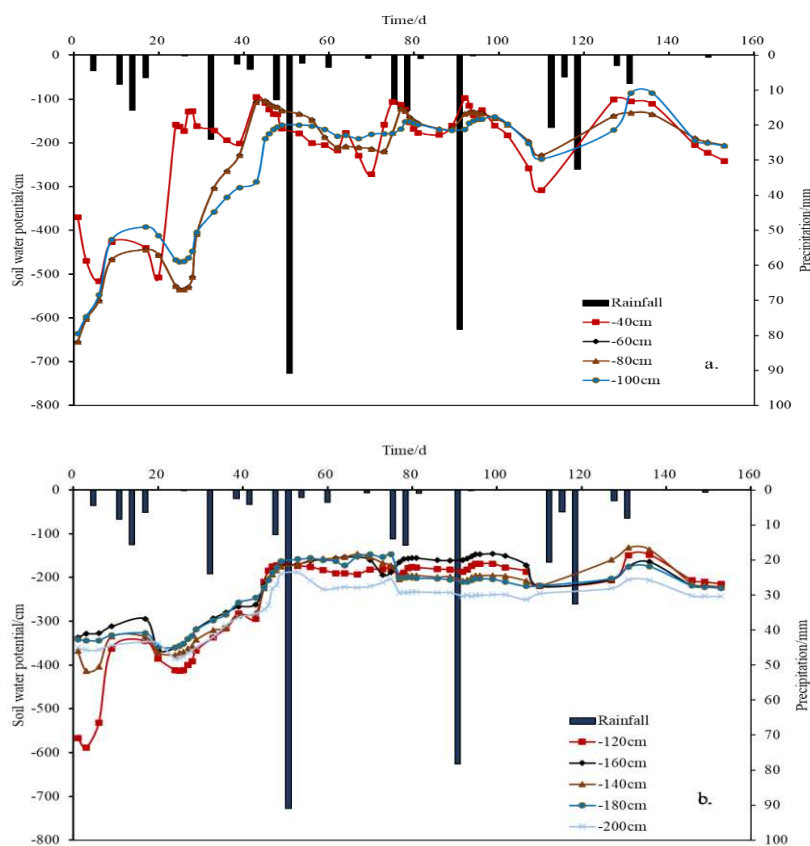
Results

Soil moisture movement under planting conditions

Water infiltration pattern during the complete crop growth period

The soil water potential at different depths during the crop growth period was analyzed and its variation with time was plotted (Fig. 3). By comparing the soil

moisture movement curves and rainfall at different depths during the complete growth period of maize (Fig. 3 a, b, and c) and wheat (Fig. 3 e, f, and g), it was observed that the distribution of water potential in the soil has noticeable zoning characteristics. The shallow soil (0–100 cm), which is a zone that exhibits a significant change in soil water potential, is susceptible to rainfall infiltration recharge, evaporation, and transpiration. The downward movement of soil water to the lower layers of soil is caused by precipitation and irrigation. Moreover, the upward movement of water, which has been generally used for crop growth or to recharge the atmosphere, is caused by evaporation, transpiration, root water uptake, and other functions. The soil layer between 100–200 cm depth, which represents the lag zone of soil water potential change, is affected by external influences and causes a change in the soil water movement state. Based on the change in soil water movement during the growth period of maize, it was observed that the changing trend of soil water potential gradually slowed over time, and the overall trend of water movement was stable. However, the water potential during the wheat growth period was stable up to 175 days and changed significantly after 175 days, indicating that the change in soil moisture movement was lagging by external factors during this period. The soil layer between 200–300 cm depth, which represents the zone that exhibits a stable soil water potential change, was less affected by external precipitation and evaporation; the soil water potential and water movement were relatively stable. The soil layer below the depth of 300 cm, which is a zone exhibiting deep soil water movement, was not affected by external factors such as precipitation and irrigation; however, the soil water potential changed significantly with time. The reason for this phenomenon may be the groundwater level or the effect of the dominant flow of large channels.



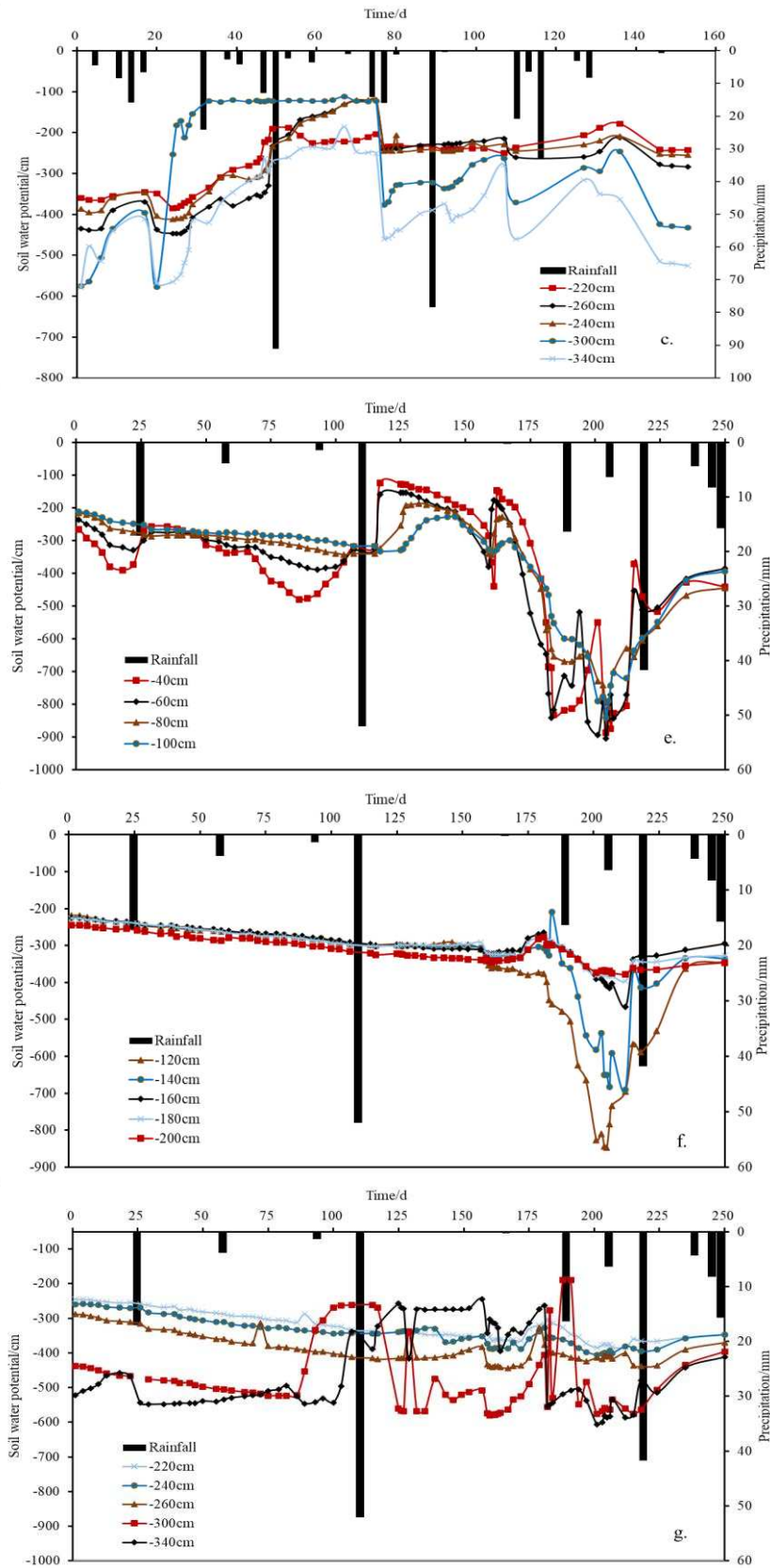


Figure 3. Soil water movement at different depths during the complete growth period of maize and wheat. a, b, and c are the changes of soil water movement at different depths of maize; e, f, g are the changes of soil water movement at different depths of wheat

Variation characteristics of soil water infiltration changes at different crop growth stages

In this study, we selected water potential change curves of two crops during their growth period (summer maize and winter wheat) to explore the soil water transport patterns in the study area. Subsequently, the second stage of the growth period of maize and wheat was selected for the study. Furthermore, the growth period of summer maize was divided into emergence, jointing, flaring, booting, and maturation stages. It was observed that the soil water potential of summer maize varies significantly at different growth stages (*Fig. 4a*). The soil water movement at the emergence and jointing stages was the evaporation-infiltration type, which may be affected by rainfall or irrigation. There is a polymeric zero-flux surface at 80–100 cm depths. The variation trend of the soil water potential was stable. The peak of the emergence stage was noted at a burial depth of 80 cm when the soil water potential reached -527.48 cm. The peak water potential at the same depth of the jointing stage was -107.96 cm, and the overall upward movement of soil moisture may be accounted for by the strong evaporation and high water demand at the early growth stage; thus, soil moisture was more affected.

The water potential difference at different depth ranges in the middle and later stages of maize growth narrowed under the influence of precipitation, evaporation, and other external conditions, and the trend of soil water potential change showed a relative flatness. There were several small zero-flux surfaces in the flaring stage, the soil water movement type was mainly evaporation-infiltration type, and soil water moved downward to supply the soil layer. The soil water potential was minimal at a depth of 140 cm during the emergence and jointing stages, and the water showed a trend of downward infiltration. The variation in soil water potential during the booting and maturation stages was relatively lower, and the soil water movement type was mainly of the infiltration type, with the zero-flux surface being positioned between 100–120 cm depth. The overall water potential gradually increased with an increase in the burial depth of the profile, and the overall soil water was in a downward movement state; however, at shallow depths, the soil water exhibited an upward movement.

The growth period of winter wheat was divided into emergence, overwintering, returning green, jointing, filling, and maturation stages. It can be seen from *Figure 4b* that the characteristics of the total water potential curves in the soil profile at each growth stage of wheat. The evaporation intensity was low during the emergence, overwintering, and returning green stages because of lower temperatures and rainfall in winter and early spring, and the soil water movement type of the three curves is the evaporation-infiltration type. The water potential was clearly inflected at a burial depth of 260 cm when soil moisture was recharged downward to groundwater. At the emergence and overwintering stages, the location of the zero-flux surface was at a burial depth of 80–100 cm. Small polymeric zero-flux surfaces existed near the ground during the returning green period. This phenomenon is observed due to the snow cover on the surface in winter, which melts in the warm weather and reduces the evapotranspiration; therefore, the soil moisture infiltrates downward near the surface. The soil water potential changes significantly during the jointing, filling, and maturation stages, and the soil water movement type is mainly infiltration. In the jointing period, there is a very large value at a burial depth of 50 cm, which is the location of the dispersion-type zero-flux surface where the upper part evaporates and

the lower part infiltrates; there is a high soil water potential point in the middle. At the filling and maturation stages, there is a very small value of soil water potential near the surface, and there is a polymeric type zero flux surface, which may be influenced by irrigation.

By analyzing the changes in the type of water movement during the crop growing period, it was shown that precipitation, irrigation, evaporation, and plant root uptake had significant effects on the type of soil water movement. During the growing period of summer corn, precipitation and irrigation were greater, evaporation was more intense, crop water demand was large, root uptake was stronger, and soil water movement was more complex. During the growth period of winter wheat, owing to the low temperature and low precipitation, soil water evaporation and root water absorption capability are weak. The soil moisture in the middle and late growth periods of wheat moves downward with the warming of temperature, which is affected by precipitation and irrigation.

Soil profile water transport variation rules on time scale

To demonstrate the trend of soil water potential overtime during the crop growth period, we selected three years of comparative soil water potential movement before and after the same growth stage of maize, with three growth stages: emergence, flaring, and maturation. From the soil water potential profile (*Fig. 5*), it was observed that the soil water potential of maize in the emergence stage (*Fig. 5a*) changed more significantly, and the type of soil water movement was complex for three consecutive years. The water potential of maize at the emergence stage showed multiple changes within the burial depth of 80–160 cm, which was significantly influenced by external factors such as precipitation, irrigation, and root water uptake. At the flaring stage (*Fig. 5b*), the soil water potential changes more gently. The soil water movement type is simple and stable for three consecutive years, showing an evaporation-based movement state. At the maturation stage (*Fig. 5c*), the soil water potential showed an inflection point, and the soil water potential was similar in the second and third years, and was significantly lower in the first year. This shows that the soil water content was significantly lower in the first year of maize maturity when the soil was subject to strong evaporation or less rainfall and other factors, as compared to that in the remaining two years. However, the trend of soil water potential change was stable, and the water movement basically showed an upward movement of soil water in the upper soil layer and a downward movement of soil water in the lower soil layer.

This research mainly studied the second year of the complete maize growth period, and conducted a correlation analysis of the soil water potential in the same growth period before and after two years of the study year. Pearson, Spearman, and Kendall correlation tests were used to verify the correlation. It was found that the soil water potential of maize in the study year at the emergence stage was not correlated with the two years before and after. This may verify the fact that the soil water potential is influenced by external factors such as irrigation and root water uptake during the emergence stage, and that the water movement is more complex and has no regularity. The study year of soil water potential at the flaring and maturation stages showed a significant correlation ($P > 0.01$) with the two years before and after the study year, which indicated that the trend of soil water potential change state in three consecutive years was similar. The analysis shows that at the early stage of crop growth, the soil

water movement state is susceptible to external factors and the soil water movement type is complex. The soil water potential is gradually stabilized as the crop growth period progresses, or due to the stability of crop water demand or other factors; the trend of water potential changes in each growth period is primarily the same. The water potential level is easily affected by external factors such as rainfall and irrigation.

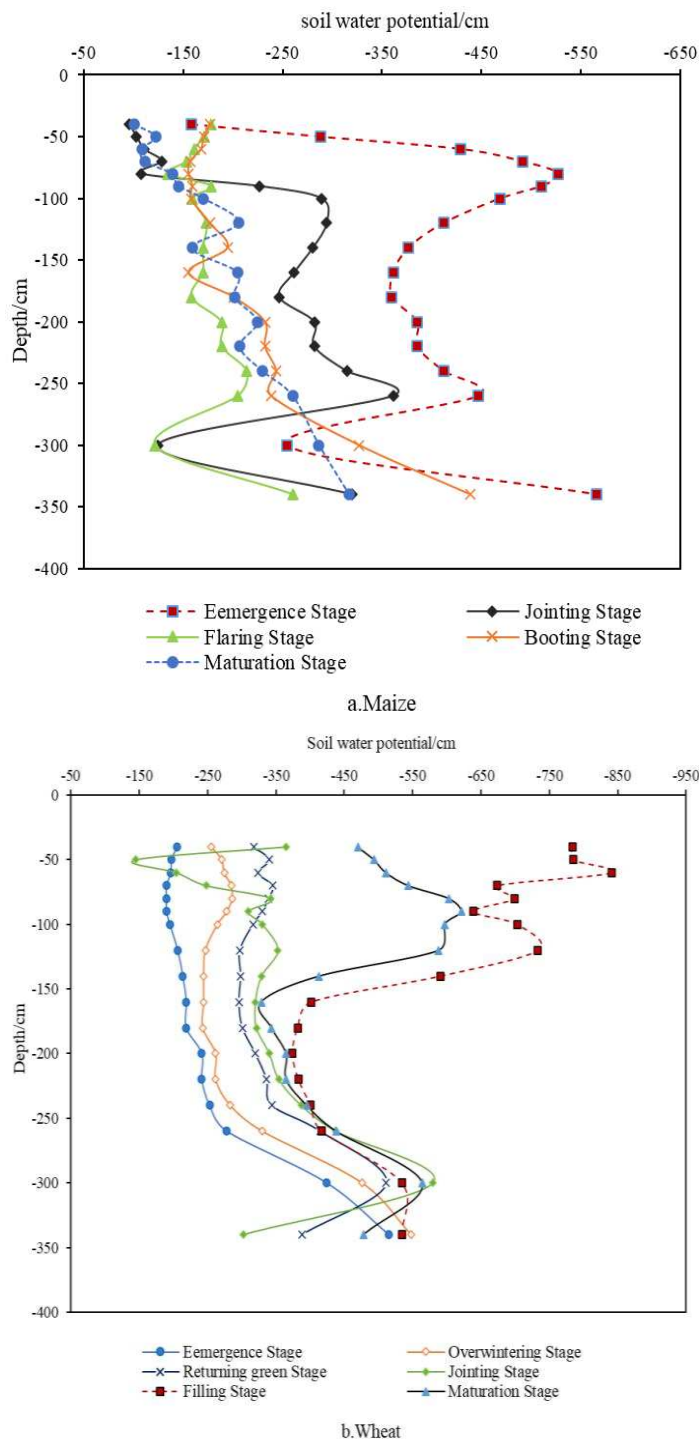


Figure 4. Water potential migration trends of summer maize and winter wheat in different growth stages

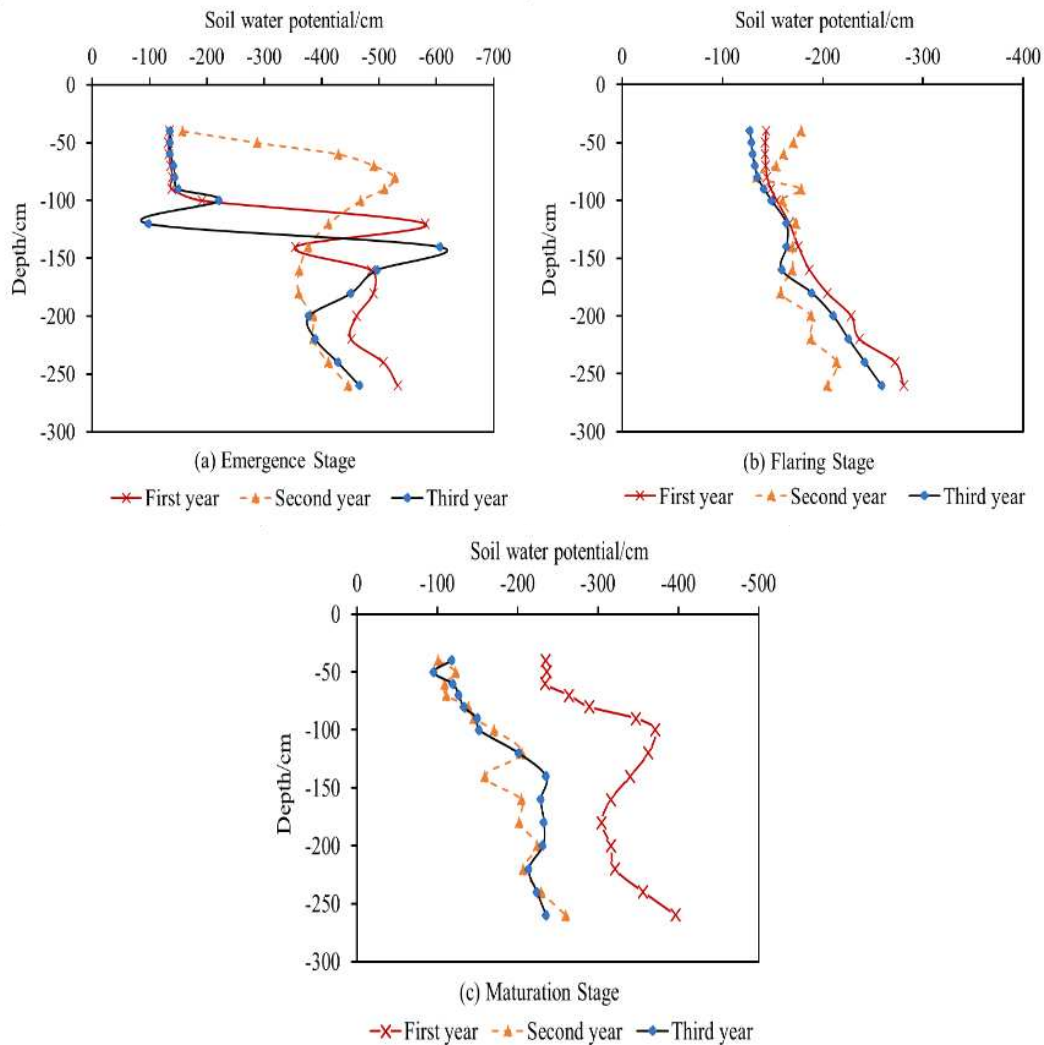


Figure 5. Comparison of soil water potential dynamics during the same growth period of maize for three consecutive years

Response of soil moisture movement to precipitation

The above section avoided the time points of precipitation and irrigation when discussing the types of soil moisture movement during the growth period of two crops. This section focuses on the effect of precipitation on soil water movement. A precipitation amount of 52.1 mm was selected to evaluate the effect of precipitation on soil moisture movement by analyzing the change in soil moisture movement type before and after precipitation in the study area.

Figure 6 shows a comparison of the total water potential curves of the soil profile before and after precipitation in the study area. The tendency of soil water movement was the same on day 5 and day 10, and it was considered that the effective impact depth of this precipitation reached 140 cm and the active impact time was 10 days. Therefore, only the movement state changes in soil moisture above 140 cm were discussed. It can be seen from the analysis that the soil water movement above 80 cm is complex and variable in the 5 days before precipitation, which is affected by evaporation and root water uptake, and the soil water movement type is mainly evaporation-infiltration type.

From the day of precipitation to 7 h after precipitation to 1 day after precipitation, a polymeric zero flux surface is formed at 60–100 cm near the surface, and the soil water movement type is infiltration-evaporation-infiltration. After 5 days of precipitation, the aggregated zero flux surface disappeared and the soil moisture movement type gradually turned into an infiltration type. The soil moisture movement type gradually returned to the evaporation-infiltration type after 20 days of precipitation.

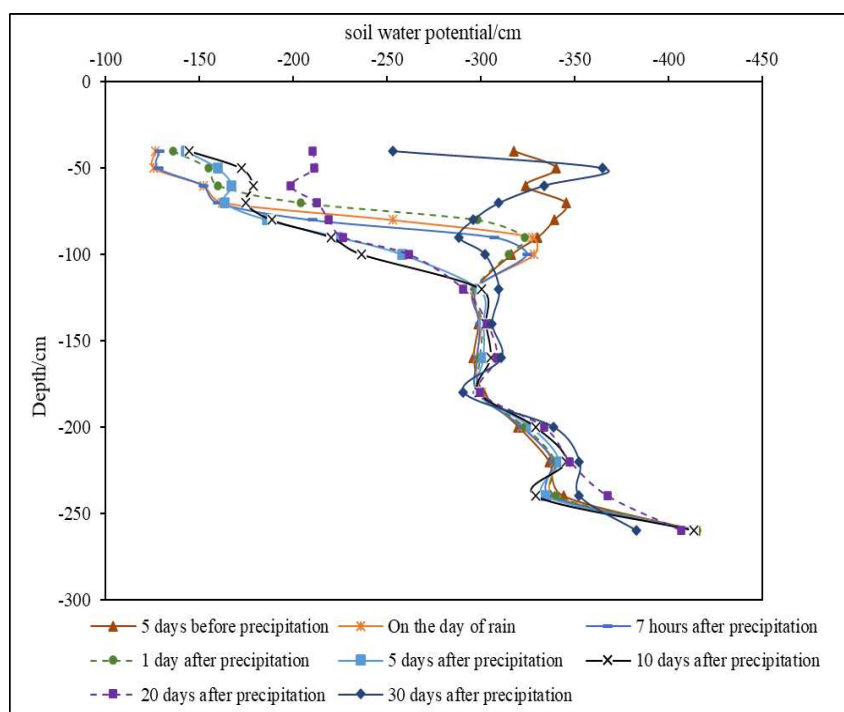


Figure 6. Characteristics of soil moisture movement before and after a single precipitation

The statistical analysis of precipitation intensity in the study area from the beginning of April to the end of October was carried out according to the classification criteria of precipitation intensity issued by the National Meteorological Administration. Among the 35 precipitation days, the frequency of light rainfall of 0.1–9.9 mm (27 times) accounted for 77.1%, medium rainfall of 10.0–24.9 mm (five times) accounted for 14.3%, heavy rainfall of more than 25.0–49.9 mm (one time) accounted for 3%, and the frequency of heavy rainfall of more than 50 mm (two times) accounted for 6% of the total rainfall. Therefore, the precipitation in the test area was primarily light rainfall. To reduce the influence of early precipitation on the soil water potential, only the first day of precipitation was considered in this study for precipitation events on consecutive days, and the influence of eight precipitation events on the soil water potential was analyzed.

The variation in soil water potential values (averaged across soil layers) on the 2nd day after precipitation relative to the previous precipitation is shown in Figure 7. The impact of soil water potential during a single strong rainfall event reached a depth of 140 cm; there were three precipitation events of less than 10 mm, and the soil water potential varied between 0 and 10 cm. It can be seen that precipitation of less than 10 mm had no significant effect on the soil water potential, which is consumed by the evapotranspiration of the surface soil, while precipitation greater than 10 mm increased the soil water potential. The water potential increased further with greater precipitation.

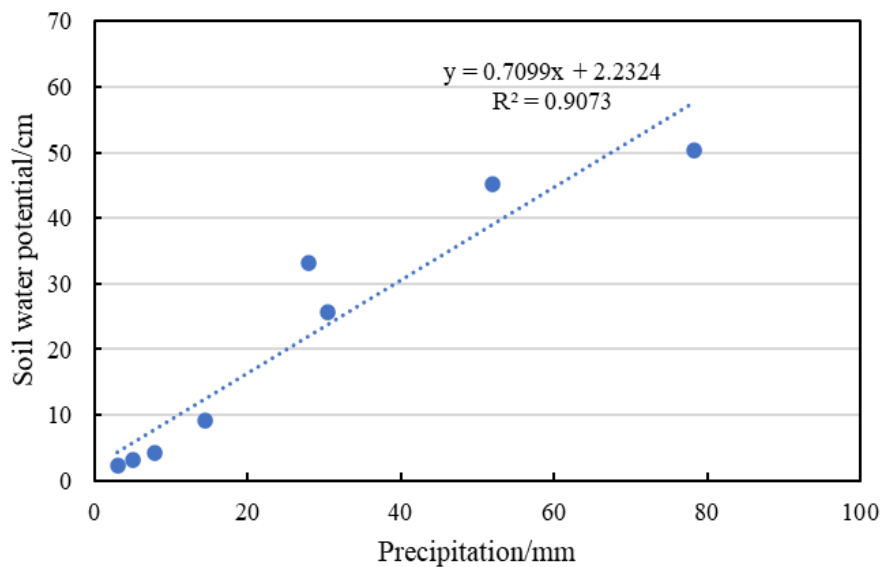


Figure 7. Response of soil water potential to precipitation

Potential groundwater recharge

The distribution of the soil profile water potential in the test plots during the study period is shown in *Figure 4*. The soil water potential near the surface is affected by precipitation, irrigation, and evaporation; therefore, it changes significantly. The soil water potential gradient difference is large and the direction of water flow also changes frequently, owing to the zone where the soil water potential gradient changed significantly. In this study, the upper boundary of this zone is the surface and the lower boundary can reach the maximum depth (180 cm) at which the dispersive zero-flux surface develops a downward trend for many years or at least for the entire study period. The soil water potential below the profile is less affected by precipitation, irrigation, and evaporation; therefore, it changes slowly. The difference in the soil water potential gradient is small and the direction of water flow is always downward, owing to the zone where the soil water potential gradient changed slightly. Based on the above principles, the location of the boundary was chosen at a depth of 200 cm from the surface below the deepest zero flux surface, where the direction of soil water movement is always downward; thus, the water flow through this boundary is equivalent to the potential infiltration recharge of precipitation or irrigation water (Wu et al., 2012).

Figure 8 shows the soil water fluxes at 200 cm from the location boundary calculated using *Equations 3, 4, and 5*, and demonstrates that the infiltration recharge has a certain relationship with precipitation and irrigation. The infiltration recharge was also large at the time of large precipitation and irrigation volume, but with a certain lag effect, indicating that root leakage still existed under the irrigation quota at that time. It is necessary to alleviate the irrigation quota to reduce deep leakage and improve the utilization efficiency of irrigation water. The infiltration recharge in the absence of rainfall or irrigation is small and it shows irregular fluctuations, which is related to the redistribution of soil moisture after precipitation or irrigation and has some influence on the length of the calculation period.

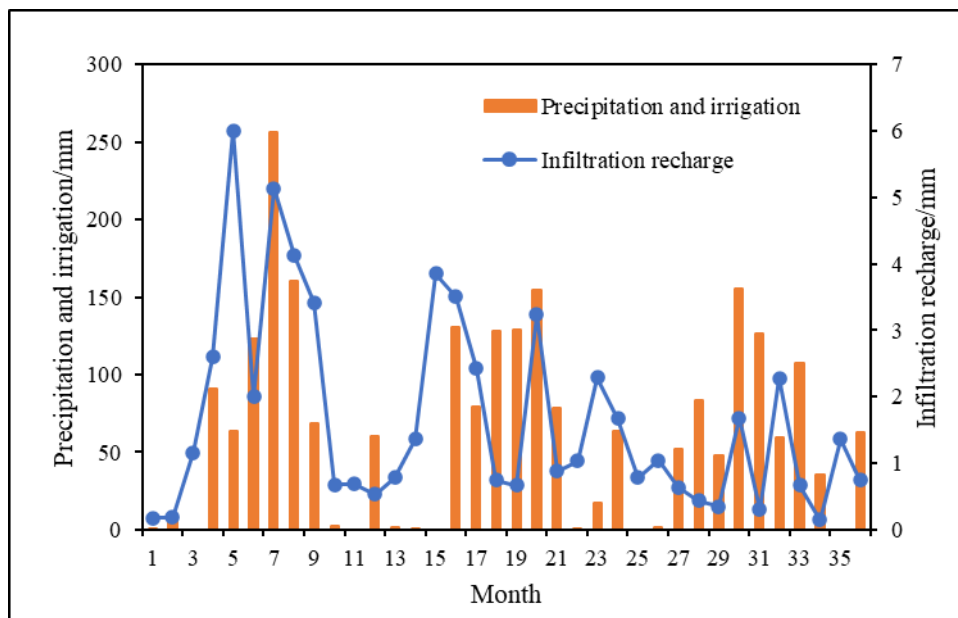


Figure 8. Cumulative infiltration recharge curve of soil water over time for three consecutive years

Water balance analysis in the study area

The main infiltration recharge in the study area comes from atmospheric precipitation and irrigation infiltration, and the main water consumption is sourced from surface evaporation and transpiration of crops (without considering the influence of runoff conditions). The North China Plain is an arid and semi-arid area with strong evaporation. The annual evapotranspiration for successive monitoring years can be seen in *Figure 9*, with evapotranspiration being highest in the no-crop period before maize planting, up to 9 mm, due to rainfall and cropping patterns. Transpiration is more intense in the middle and late stages of development in wheat and in the rapid growth stage in maize. The results of the water balance calculations show that the main sources of water recharge to the soil layer in the study area were precipitation (55.68%) and irrigation (44.32%), and the main source of discharge was evapotranspiration (97.89%) (*Table 2*). A few sources (2.11%) are used for groundwater recharge, and some are stored in the soil layer. *Table 2* shows that total evapotranspiration during the reproductive period is wheat > maize > fallow, with wheat requiring more irrigation water. The infiltration recharge is positive in all three years, indicating that the downward infiltration acts as a recharge to groundwater. The soil water in the basin showed a negative equilibrium in the full equilibrium period, indicating that irrigation infiltration recharge does not compensate for evapotranspiration during the continuous monitoring years, and that irrigation practices in the study area are causing some waste.

Discussion

The type of soil moisture movement varies significantly at different growth stages of the crop. In this study, soil moisture dynamics were found to show some regular changes in the profile, which is consistent with the research findings of Tian (2017). The state of change of the water potential is similar to continuous annual monitoring

and can be accurately analyzed by identifying the location of the zero flux surface and the type of soil moisture movement in the study area (Lin et al., 2014; Zhang et al., 2017). Many external factors affect soil moisture dynamics, such as meteorological factors (Sahaar et al., 2020), precipitation (Zhang et al., 2019a), crop type (Yetbarek et al., 2020), and depth of the buried water table (Zhang et al., 2019b). Jiang et al. (2021) analyzed the response of soil water potential to atmospheric precipitation in grasslands from April to October; they observed that precipitation affected soil water potential and increased continuously with rainfall, which is by the conclusion of the present study. After studying the effects of single heavy rainfall and multiple precipitation events on soil water potential, this paper finds that precipitation greater than 10 mm recharges soil water to some extent, The effect of rainfall on soil water transport has a lagging effect, its soil water movement type basically shows a cyclic change characteristic. However, the process of water redistribution in soil and its influence on deep soil water after rainfall is more complicated, and long-term monitoring is needed to elucidate the influence of different rainfall patterns and vegetation root distribution on soil layers at different depths.

Table 2. Calculation of water balance in the study area ($\text{mm}\cdot\text{a}^{-1}$)

Year	Crop types	Replenishment		Discharge		Storage variables
		Precipitation P($\text{mm}\cdot\text{a}^{-1}$)	Irrigation I($\text{mm}\cdot\text{a}^{-1}$)	Evapotranspiration E _T ($\text{mm}\cdot\text{a}^{-1}$)	Infiltration recharge Q($\text{mm}\cdot\text{a}^{-1}$)	ΔW ($\text{mm}\cdot\text{a}^{-1}$)
First year	Summer maize	305.6	180	291.8	26.7	-141.4
	Winter wheat	92.7	240	519.1		
	No crops	15.1		137.2		
Second year	Summer maize	294.5	134	284.5	22.5	-167.3
	Winter wheat	131.2	180	503.3		
	No crops	43		139.7		
Third year	Summer maize	172.9	120	289	10.5	-164.2
	Winter wheat	122.5	187	515.4		
	No crops	130.3		82		
Total/mm		1307.8	1041	2762	59.6	-472.9
Percentage		55.68%	44.32%	97.89%	2.11%	

Evapotranspiration is an important element in the soil-plant-atmosphere system and plays a vital role in crop growth and development (Bakhshoodeh et al., 2022; Nyawade et al., 2021). Many factors affect the evapotranspiration of crops, including meteorological factors (radiation, sunshine duration, temperature, saturation water-air pressure difference, wind speed, etc.), crop factors (plant height, leaf area, etc.) and soil factors (soil temperature, soil moisture, etc.). The transpiration in this study ranged from 284.5 to 291.8 mm for maize, 503.3 to 519.1 mm for wheat, and 82 to 139.7 mm for soil surface evaporation during the no-crop period. The evapotranspiration of summer maize under different water supply conditions was found to be 285.51-334.18 mm by Yu (2016), which is similar to the conclusions of the study. Irrigation and precipitation were the main sources of water consumed for evapotranspiration in the study area. However, due to the arid climate of the North China Plain, irrigation and rainfall were not sufficient to meet the evapotranspiration demand in a continuous monitoring year. Therefore, the farm management practices and irrigation patterns in the irrigation area were not reasonable.

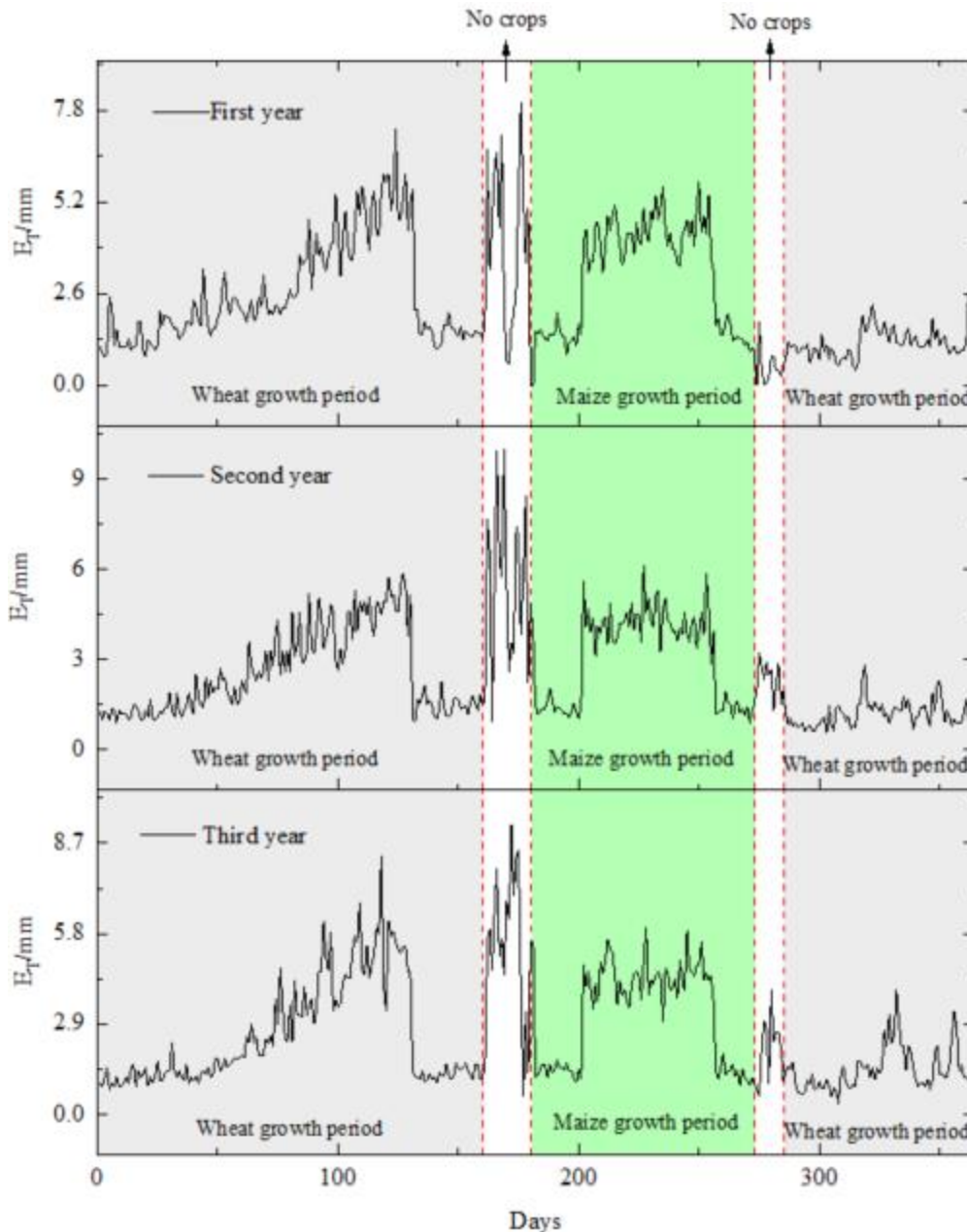


Figure 9. Annual evapotranspiration for consecutive monitoring years

The irrigation method used in the irrigation area is heavy irrigation, which can reach 240 mm in the winter wheat crop. The crude irrigation methods had resulted in a significant waste of water, thus affecting the water balance in large buried irrigation areas. The amount of infiltration recharge from precipitation and irrigation in the irrigation area did not compensate for the evapotranspiration discharge. The soil had a negative water storage capacity, but there was a certain amount of vertical infiltration recharge. This indicates that under current irrigation practices, soil water is not being used efficiently and is being wasted, which is one of the reasons for the constant decline in groundwater levels (Cheng et al., 2021). It is still difficult to determine potential infiltration recharge in large buried areas with severe groundwater overdrafts. Kendy et

al. (2004) and Wang et al. (2010) confirmed the existence of vertical recharge in irrigated farmland areas using experiments and numerical simulations to address the question of whether there is vertical recharge on the surface of farmland areas with a large burial depth of groundwater in the North China Plain. According to the above-mentioned research, the upper boundary of the stable zone of soil water potential change at a depth of 200 cm is used as the infiltration boundary of potential infiltration recharge, and finds that there is a certain amount of vertical infiltration recharge of precipitation or irrigation water in the typical irrigation areas of the North China Plain with large depth of burial, but due to the influence of the monitoring depth, this conclusion needs to be verified at a deeper level. However, the conclusion needs to be verified at a deeper level due to the limitation of the monitoring depth.

Conclusion

(1) The distribution of water potential in the soil has obvious zoning characteristics. Shallow soil (0–100 cm) is a strong change in the soil water potential zone, which is vulnerable to rainfall infiltration recharge, evaporation, plant transpiration, and other effects. The soil between 100–200 cm depth was the lagging zone of soil water potential change, and the soil layer was affected by external factors causing changes in the soil water movement state. The soil at the depth of 200–300 cm was the stable zone of soil water potential change, and the soil layer was less affected by precipitation and evaporation. The soil water potential and the soil water movement were relatively stable. The soil layer below 300 cm is called the deep soil water movement zone, which is not affected by external factors such as precipitation and irrigation. However, the soil water potential changes with time and the reason for this phenomenon may be the groundwater level or the effect of the dominant flow of large channels.

There were significant differences in the soil water infiltration status of crops at different growth stages. During the growing period of summer maize, soil water potential trends change significantly and soil water movement becomes more complex and is greatly affected by precipitation; there are generally multiple zero flux surfaces, and the zero-flux surface also decreases as the growing period progresses. The variation trend of soil water potential within the growth period of winter wheat becomes increasingly significant with the warming of weather. The zero-flux surface is easily formed near the ground under the influence of precipitation and irrigation, and the soil movement is mainly dominated by infiltration at the jointing, filling, and maturation stages.

(2) Precipitation greater than 10 mm recharges soil water to some extent. The soil moisture type gradually changes from evaporation-infiltration type before precipitation to infiltration-evaporation-infiltration type at the initial stage of precipitation; it then changes to infiltration type after precipitation, and finally reverts to evaporation-infiltration type after a longer period after precipitation, thus forming a complete cycle. Moreover, during the response of the soil water movement state to precipitation, the position of the zero-flux surface gradually moves down and returns to the position of the zero-flux surface before precipitation, and finally forms the infiltrated soil water state.

(3) In the study on the potential recharge of soil water in the area with a large burial depth of groundwater, the upper boundary of 200 cm of the zone exhibiting a stable soil water potential change was used to study the infiltration recharge of soil water in

Luancheng area. It was found that the infiltration recharge was related to rainfall and irrigation; that is, it increases with a rise in rainfall and irrigation, but it has a certain lag effect.

(4) The main recharge sources of soil moisture in the irrigation area were precipitation (55.68%) and irrigation (44.32%), and the main discharge source was evapotranspiration (98.89%). A few sources (2.11%) were used for groundwater recharge, and the soil water in the basin showed a negative equilibrium in the full equilibrium period.

Acknowledgments. Two anonymous reviewers and my editor are thanked for helpful suggestions on an earlier version of the manuscript. This study was funded by the National Natural Science Foundation of China (41877201) and the Geological Survey Project of China Geological Survey (DD20221676).

Conflict of interests. The authors declare that they have no known competing financial interests or personal relationships that could have appeared to influence the work reported in this paper.

REFERENCES

- [1] Adhikari, B., Wang, L. (2020): The potential contribution of soil moisture to fog formation in the Namib Desert. – *J Hydrol* 591: 125326. <https://doi.org/10.1016/j.jhydrol.2020.125326>.
- [2] Allen, R. G., Pereira, L. S., Raes, D., Smith, M. (1998): *Crop Evapo-Transpiration: Guidelines for Computing Crop Water Requirements*. – United Nations Food and Agriculture Organization, Irrigation and Drainage Paper No. 56. FAO, Rome.
- [3] Ayantobo, O. O., Wei, J. (2019): Appraising regional multi-category and multi-scalar drought monitoring using standardized moisture anomaly index (SZI): A water-energy balance approach. – *J Hydraul* 579: 124139. <https://doi.org/10.1016/j.jhydrol.2019.124139>.
- [4] Bakhshoodeh, R., Ocampo, C., Oldham, C. (2022): Evapotranspiration rates and evapotranspirative cooling of green façades under different irrigation scenarios. – *Energy and Buildings* 112223. <https://doi.org/10.1016/j.enbuild.2022.112223>.
- [5] Cheng, Z. S., Su, C., Zheng, Z. X., Chen, Z. Y., Wei, W. (2021): Characterize groundwater vulnerability to intensive groundwater exploitation using tritium time-series and hydrochemical data in Shijiazhuang, North China Plain. – *Journal of Hydrology*. 603: 126953. DOI: 10.1016/j.jhydrol.2021.126953.
- [6] Dias, A. S., Pirone, M., Nicotera, M. V., Urciuoli, G. (2021): Hydraulic characterization of an unsaturated vegetated soil: the role of plant roots and hydraulic hysteresis. – *Geomech Energy Envir* 100235. <https://doi.org/10.1016/j.gete.2021.100235>.
- [7] Han, S. P., Jing, J. H., Sun, J. C., Shi, Y. C., Wang, S. (2005): Analyses of moisture movement Types and movement mechanism of moisture and salinity at soil section. – *J Agro-Environ Sci* (S1): 148-152. <https://kns.cnki.net/kcms/detail/detail.aspx?FileName=NHBH2005S1034&DbName=CJFQ2005>.
- [8] Hu, X. Y., Lei, H. M. (2021): Fifteen-year variations of water use efficiency over a wheat-maize rotation cropland in the North China Plain. – *Agr Forest Meteorol* 306: 108430. <https://doi.org/10.1016/j.agrformet.2021.108430>.
- [9] Hu, C., Saseendran, S. A., Green, T. R., Ma, L., Li, X., Ahuja, L. R. (2006): Evaluating nitrogen and water management in a double-cropping system using RZWQM. – *Vadose Zone Journal* 5(1): 493-505. <https://doi.org/10.2136/vzj2005.0004>.

- [10] Huang, X. J., Wang, H. F., Zhang, M., Horn, R., Ren, T. (2021): Soil water retention dynamics in a Mollisol during a maize growing season under contrasting tillage systems. – *Soil Till Res* 209: 104953. <https://doi.org/10.1016/j.still.2021.104953>.
- [11] Jia, X. Y., O'Connor, D., Hou, D. Y., Jin, Y. L., Li, G. H., Zheng, C. M., Ok, Y. S., Tsang, D. C., Luo, J. (2019): Groundwater depletion and contamination: spatial distribution of groundwater resources sustainability in China. – *Sci Total Environ* 672: 551-562. <https://doi.org/10.1016/j.scitotenv.2019.03.457>.
- [12] Jiang, Z. C., Jiang, Z. R., Zhao, W. J., Liao, K. T., Luo, Y. M., Feng, J. Y. (2021): Study on the variation characteristics of grassland vegetation soil water potential in Xishui Forest Area of Qilian Mountains, Gansu. – *J Southwest Forestry Univ (Nat Sci)* 41(2): 177-181. <https://kns.cnki.net/kcms/detail/53.1218.S.20200829.1234.002.html>.
- [13] Jing, E. C., Fei, J., Zhang, X. H. (1994): *Experimental Study on Soil Water Flux Method*. – Earthquake Publishing, Beijing.
- [14] Joly, F., Weibel, A. K., Coulis, M., Throop, H. L. (2019): Rainfall frequency, not quantity, controls isopod effect on litter decomposition. – *Soil Biol Biochem* 135: 154-62. <https://doi.org/10.1016/j.soilbio.2019.05.003>.
- [15] Ju, Z. Q., Li, X. X., Hu, C. S. (2015): Water dynamics and groundwater recharge in a deep vadose zone. – *Water Science and Technology: Water Supply* 16(3): 579-586. <https://doi.org/10.2166/ws.2015.165>.
- [16] Kamal, E. G. M., Abdelaty, D., Moubark, K., Abdelkareem, M. (2021): Assessment of the groundwater possibility and its efficiency for irrigation purposes in the area east of Qena, Egypt. – *Arab J Geosci* 14(10): 839. <https://doi.org/10.1007/s12517-021-07041-2>.
- [17] Kassaye, K. T., Boulange, J., Lam, V. T., Saito, H., Watanabe, H. (2020): Monitoring soil water content for decision supporting in agricultural water management based on critical threshold values adopted for Andosol in the temperate monsoon climate. – *Agr Water Manage* 229: 105930. <https://doi.org/10.1016/j.agwat.2019.105930>.
- [18] Kendy, E., Zhang, Y., Liu, C., Wang, J., Steenhuis, T. (2004): Groundwater recharge from irrigated cropland in the North China Plain: case study of Luancheng County, Hebei Province, 1949-2000. – *Hydrol Process* 18(12): 2289-302. <https://doi.org/10.1002/hyp.5529>.
- [19] Kristo, C., Rahardjo, H., Satyanaga, A. (2019): Effect of hysteresis on the stability of residual soil slope. – *Int Soil Water Conse* 7(3): 226-38. <https://doi.org/10.1016/j.iswcr.2019.05.003>.
- [20] Li, M., He, Y. J., Lin, W. J., Wang, G. L. (2014): Research on soil moisture transport mechanism in the piedmont of the Taihang Mountain. – *J Arid Land Resour Environ* 28(3): 101-106. <http://dx.chinadot.cn/10.13448/j.cnki.jalre.2014.03.016>.
- [21] Li, P., Xu, H. L., Pan, Y., Sun, Y., Wang, X. J. (2017): A comparative study on precipitation infiltration recharge calculation methods for Beijing Plain. – *J China Hydrol* 37(2): 31-35. <https://kns.cnki.net/kcms/detail/detail.aspx?FileName=SWZZ201702006&DbName=CJFQ2017>.
- [22] Li, H. T., Li, L., Liu, N., Chen, S. Y., Shao, L. W., Sekiya, N., Zhang, X. Y. (2022): Root efficiency and water use regulation relating to rooting depth of winter wheat. – *Agricultural Water Management* 269: 107710. <https://doi.org/10.1016/j.agwat.2022.107710>.
- [23] Lin, D., Jin, M. G., Ma, B., Wang, B. G. (2014): Characteristics of infiltration recharge at thickening vadose zone using soil hydraulic parameters. – *Earth Sci* 39(6): 760-768. <https://kns.cnki.net/kcms/detail/detail.aspx?FileName=DQKX201406011&DbName=CJFQ2014>.
- [24] Lu, C. P., Song, Z. Y., Wang, W. J., Zhang, Y., Si, H. Y., Liu, B., Shu, L. C. (2021): Spatiotemporal variation and long-range correlation of groundwater depth in the Northeast China Plain and North China Plain from 2000~2019. – *J Hydrol-Reg Stud* 37: 100888. <https://doi.org/10.1016/j.ejrh.2021.100888>.

- [25] Muhammad, E. S., Ibrahim, M. M., El-Sayed, A. (2021): Effects of drain depth on crop yields and salinity in subsurface drainage in Nile Delta of Egypt. – *Ain Shams Eng J.* <https://doi.org/10.1016/j.asej.2021.01.008>.
- [26] Nyawade, S. O., Gitari, H. I., Karanja, N. N., Gachene, C. K. K., Schulte-Geldermann, E., Parker, M. L. (2021): Yield and evapotranspiration characteristics of potato-legume intercropping simulated using a dual coefficient approach in a tropical highland. – *Field Crops Research* 274: 108327. <https://doi.org/10.1016/j.fcr.2021.108327>.
- [27] Ordóñez, R. A., Castellano, M. J., Hatfield, J. L., Helmers, M. J., Licht, M. A., Liebman, M., Dietzel, R., Martinez-Feria, R., Iqbal, J., Puntel, L. A., Córdova, S. C., Togliatti, K., Wright, E. E., Archontoulis, S. V. (2018): Maize and soybean root front velocity and maximum depth in Iowa, USA. – *Field Crops Research* 215: 122-131. <https://doi.org/10.1016/j.fcr.2017.09.003>.
- [28] Pei, Y. S., Li, X. D., Zhao, Y., Zhai, J. Q. (2020): Research on vertical recharge and specific yield of the unconfined aquifer in a typical deep groundwater areas of North China Plain. – *South-to-North Water Tran Sci Technol* 18(1): 176-193. <http://dx.chinadoi.cn/10.13476/j.cnki.nsbdqk.2020.0019>.
- [29] Pereira, L. S., Paredes, P., Jovanovic, N. (2020): Soil water balance models for determining crop water and irrigation requirements and irrigation scheduling focusing on the FAO56 method and the dual Kc approach. – *Agr Water Manage* 241: 106357. <https://doi.org/10.1016/j.agwat.2020.106357>.
- [30] Pullens, J. W. M., Sørensen, C. A. G., Olesen, J. E. (2021): Temperature-based prediction of harvest date in winter and spring cereals as a basis for assessing viability for growing cover crops. – *Field Crop Res* 264: 108085. <https://doi.org/10.1016/j.fcr.2021.108085>.
- [31] Sahaar, S. A., Niemann, J. D. (2020): Impact of regional characteristics on the estimation of root-zone soil moisture from the evaporative index or evaporative fraction. – *Agr Water Manage* 238: 106225. <https://doi.org/10.1016/j.agwat.2020.106225>.
- [32] Shen, Y. J., Min, L. L., Wu, L., Shen, Y. J., Li, H. J., Zhang, G. L. (2021): Functions and applications of critical zone observatory of Luancheng agro-ecosystem experimental station, Chinese Academy of Sciences (Luancheng Critical Zone Observatory). – *Bulletin of Chinese Academy of Sciences* 36(4): 502-511. <https://doi.org/10.16418/j.issn.1000-3045.20210407001>.
- [33] Tian, Y. (2017): Dynamic Characteristics of Soil Water Potential in Larch Forest in Growing Season. – Inner Mongolia Agricultural University, Hohhot.
- [34] Vermeire, L. T., Rinella, M. J. (2020): Fall water effects on growing season soil water content and plant productivity. – *Rangeland Ecol Manag* 73(2): 252-8. <https://doi.org/10.1016/j.rama.2019.11.006>.
- [35] Wang, S. X., Zhou, J. L., Yu, F., Dong, X. G. (2005): Application of HYDRUS-1D model to evaluating soil water resource. – *Research of Soil and Water Conservation* 2: 36-38.
- [36] Wang, B. G., Jin, M. G., Wang, G. L. (2010): Effects of straw mulch on soil water in cropland. – *China Rural Water Hydropower* 6: 76-80+84. <https://kns.cnki.net/kcms/detail/detail.aspx?FileName=ZNSD201006024&DbName=CJFQ2010>.
- [37] Wei, W., Chen, Z. Y. (2017): The effects of climate change on potential groundwater recharge - a case study of Luancheng experimental station 15(5): 29-35. – <https://doi.org/10.13476/j.cnki.nsbdqk.2017.05.005>.
- [38] Wu, Q. H., Wang, G. L., Lin, W. J., Zhang, F. W. (2012): Estimating Groundwater Recharge of Taihang Mountain Piedmont in Luancheng County, Hebei Province, China. – *Bulletin of Geological Science and Technology* 31(2): 99-105. <http://10.3969/j.issn.1000-7849.2012.02.016>.
- [39] Xiao, D. P., Liu, D. L., Feng, P. Y., Wang, B., Waters, C., Shen, Y. J., Qi, Y. Q., Bai, H. Z., Tang, J. Z. (2021): Future climate change impacts on grain yield and groundwater use

- under different cropping systems in the North China Plain. – *Agr Water Manage* 246: 106685. <https://doi.org/10.1016/j.agwat.2020.106685>.
- [40] Xu, F., Liu, Y. L., Du, W. C., Li, C. L., Xu, M. L., Xie, T. C., Yin, Ying, Guo, H. Y. (2021): Response of soil bacterial communities, antibiotic residuals, and crop yields to organic fertilizer substitution in North China under wheat–maize rotation. – *Sci Total Environ* 785: 147248. <https://doi.org/10.1016/j.scitotenv.2021.147248>.
- [41] Yetbarek, E., Kumar, S., Ojha, R. (2020): Effects of soil heterogeneity on subsurface water movement in agricultural fields: a numerical study. – *J Hydrol* 590: 125420. <https://doi.org/10.1016/j.jhydrol.2020.125420>.
- [42] Yu, L. Y. (2016): Simulation of Water and Heat Transfer in SPAC System for Summer Maize Under Conditions of Different Water Supply. – Northwest A&F University, Yangling.
- [43] Zhang, G. H., Fei, Y. H., Shen, J. M., Yang, L. Z. (2007): Influence of unsaturated zone thickness on precipitation infiltration for recharge of groundwater. – *J Hydraul Eng* 5: 611-617. <https://kns.cnki.net/kcms/detail/detail.aspx?FileName=SLXB200705015&DbName=CJFQ2007>.
- [44] Zhang, S. Y., Shu, L. C., Min, X., Hu, H. J., Zou, Z. K. (2017): Calculation of precipitation infiltration recharge based on land-use type. – *J Jilin Univ (Earth Sci Edit)* 47(3): 860-867. <http://dx.chinadoi.cn/10.13278/j.cnki.jjuese.201703206>.
- [45] Zhang, H., Li, Y., Meng, Y. L., Cao, N., Li, D. S., Zhou, Z. G., Chen, B. L., Dou, F. G. (2019a): The effects of soil moisture and salinity as functions of groundwater depth on wheat growth and yield in coastal saline soils. – *J Integr Agr* 18(11): 2472-2482. [https://doi.org/10.1016/S2095-3119\(19\)62713-9](https://doi.org/10.1016/S2095-3119(19)62713-9).
- [46] Zhang, J., Little, D. N., Hariharan, N., Kim, Y. R. (2019b): Prediction of climate specific vertical movement of pavements with expansive soils based on long-term 2D numerical simulation of rainwater infiltration. – *Comput Geotech* 115: 103172. <https://doi.org/10.1016/j.compgeo.2019.103172>.
- [47] Zhang, Y. L., Wu, Z. Y., Singh, V. P., He, H., He, J., Yin, H., Zhang, Y. X. (2021): Coupled hydrology-crop growth model incorporating an improved evapotranspiration module. – *Agr Water Manage* 246: 106691. <https://doi.org/10.1016/j.agwat.2020.106691>.

NUTRITIONAL COMPOSITION OF THE EDIBLE WILD PLANT *OPUNTIA LITTORALIS* (ENGELM.) IN RELATION TO DIFFERENT SEASONS AND EDAPHIC FACTORS

ABD EL-MOATY, H. I.^{1,2*} – GOUDA, H. M.² – SOROUR, W. A.^{3,4} – METWALLY, A.^{1,5} – HASSAN, L. M.⁶ –
YOUSSEF, A. K.² – ALSHEDDI, T. H. S.⁷ – GALAL, T. M.⁶

¹*Biological Sciences Department, College of Science, King Faisal University, P.O. Box 380, Al-Ahsa 31982, Saudi Arabia*

²*Medicinal and Aromatic Plants Department, Desert Research Center El-Mataria, Cairo 11753, Egypt*

³*Department of Basic Sciences, Preparatory Year Deanship, King Faisal University, Al-Ahsa 31982, Saudi Arabia*

⁴*Department of Botany, Faculty of Science, Aswan University, Aswan 81528, Egypt*

⁵*Botany and Microbiology Department, Faculty of Science, Assiut University, Assiut 71516, Egypt*

⁶*Botany and Microbiology Department, Faculty of Science, Helwan University, Cairo 11790, Egypt*

⁷*Physics Department, College of Science, King Faisal University, P.O. Box 380, Al-Ahsa 31982, Saudi Arabia*

**Corresponding author*

e-mail: hitorkey@kfu.edu.sa; phone: +966-54-504-1183

(Received 3rd Mar 2022; accepted 20th Jun 2022)

Abstract. *Opuntia spp.* (Cactaceae) were used as food resources, folk medicine for centuries for its valuable nutritional properties and health benefits in some diseases, specifically diabetes, obesity and cardiovascular diseases. This study aimed to investigate the impact of environmental factors on the qualitative and quantitative nutritional composition of the plant. Physical and chemical soil analyses were performed using Particle Size Analysis, Inductively Coupled Argon Plasma, Flame Photometer and titration methods. The quantitative nutritional assessments for each cladode and fruit were performed using standard Association of Official Analytical Chemists methods. While determinations of amino acids, lipids, sugars have been studied using Amino Acid Analyzer, GC\MS and TLC; respectively. Seasonal variations in ash, crude fiber, carbohydrate, nitrogen, protein and lipid were observed to adapt the changes in climate. Cladodes and fruits contained 17 and 16 protein amino acids, respectively; the major was glutamic acid in both. The GC-MS chromatogram of the petroleum ether extract of the cladode showed the existence of 26 compounds dominated by Undecan and 34 compounds in fruit dominated by linoleic acid. Meanwhile, the TLC sugar profile revealed the presence of 8 free and 6 combined sugars in cladode, 9 free and 5 combined sugars in fruit.

Keywords: *Cactaceae, nutritional value, seasonal variations, primary metabolites, soil, energy value*

Introduction

The western Mediterranean desert of Egypt, as extensively as the whole Egyptian deserts, is characterized by high diversity and abundance of numerous wild plant species and varying climatic and edaphic conditions, which leads to accumulation of high concentrations of useful plant metabolites (Hendawy, et al., 2020; Abdel-Rahman and

Migahid, 2019). The impact of climatic and other environmental stimuli on the nutrient contents and plant growth have been studied in many previous studies. Crosby, et al. (2008) claimed that the nutritional content of plants is related to many variables, including soil conditions, environment and plant physiological status. Climate change has an impact on the accumulation of metabolites and proteins in plants; plants that suffer from certain types of stress when developing tend to accumulate more nutrients that are valuable to humans relative to those growing under less severe conditions (Ebifa-Othieno, et al., 2020). The Mediterranean coastal basin of Egypt has a warm coastal desert climate (Meigs, 1973) with the warmest summer month having an average temperature of less than 30 °C, and the coldest winter month with an average temperature of above 10 °C, even though occasional short rainstorms occur in winter and autumn (Galal, et al., 2019; UNESCO, 1977). *Opuntia* are xerophyte plants widely named as cactus pear or prickly pear and produce edible fruits and stems or cladodes (Galal, et al., 2019). *Opuntia* is a genus that includes 188 wild species and numerous cultivars; belonging to subfamily Opuntioideae among the Cactaceae family (Palacios and Valdivia, 2020). *Opuntia ficus-indica* were clarified for their proximate composition of fatty acid, inorganic elements, sugars, and polyphenol (Albergamo et al., 2022). The geographical distribution of the genus covers different ecosystems from sea level to 3400 a. l. m. Moreover, the most widespread habitat for *Opuntia* is in arid, semi-arid and deciduous forests and has been further introduced in the Mediterranean basin, Africa, Asia and Oceania. (Arakaki, et al., 2011). *Opuntia* has a significant degree of ecological adaptation owing to genetic variation and is distributed in nearly all climatic conditions (Bakar, et al., 2020). As nutrition is the most basic human need for development, productivity and mental health, *Opuntia* plants are used as human food and as folk medicines for their health benefits in chronic diseases such as cardiovascular disease, diabetes, obesity and cancer (Chougui, et al., 2013). *Opuntia littoralis* is predominantly grown as irregular clusters on sandy or rocky soils and usually observed as dense clusters spanning several meters (Galal, et al., 2017). Abd El-Moaty, et al., 2020 stated that *Opuntia littoralis*' fruit had strong antidiabetic and antimicrobial activity, as cladodes, against certain bacteria and fungi strains due to the existence of several active components in both. Consequently, no previous studies have been reported on its nutritional content, hence why this study aimed to investigate the proximate nutritional composition of *Opuntia littoralis* growing on the western Mediterranean coast of Egypt and the effect of seasonal environmental variations on it.

Material and methods

Climate of the study area

The study was conducted at Wadi Maged region -25 km to the west of Mersa-Matrouh city and south of Zawyat Umm El-Rakham area- (N 31° 16' 55", E 027° 05' 11", Elevation 2M) on the Northwestern Mediterranean coast of Egypt. The climate of Matrouh is classified as Arid Mediterranean, which is characterized by a long, warm, dry summer and short, cool, rainy winter. Monthly temperatures typically ranged from 14.4 °C to 26.8 °C; August is the warmest month with the maximum average temperature of 29.5 °C, while January is the coolest with a minimum average temperature of 8.7 °C (DRC Staff, 2015). The lowest and the highest relative humidity varies between 66 to 75% in April and July, respectively. The average annual rainfall ranged from 100 to 190 mm (DRC Staff, 2015). Notably in winter, Matrouh receives significant amounts of rainfall; the rainiest are December and January, in summer no or

few drops of rain are recorded, while occasionally heavy rains can occur in autumn and only about 10% falls during spring (El-Midany, et al., 2019). The main source of irrigation water in the Northwestern Mediterranean coastal zone is rainfall.

Determination of soil properties

Two depths of soils (0-20 and 20-40 cm) supporting plant samples were air-dried and grounded to pass a 2-mm sieve. Soil samples were used for further physical and chemical analysis.

Soil texture and water content

Analysis of soil texture was measured using Particle Size Analysis (PSA) (Gee and Bauder, 1986). The soil water content was determined for the two depths in summer and winter (Sparks, et al., 2020).

Chemical analysis

For chemical analysis, soil:water extract (1:5 w/v) was prepared (Harris, 1998) for the following analysis. Soil pH was determined using pH meter (3510, Jenway, UK), while EC was measured using an electrical conductivity meter (Orion 150A+, Thermo Electron Corporation, USA). Potassium and sodium content were determined using flame photometer [7, Jenway, UK] (Jankowski and Freiser, 1961), while calcium and magnesium were evaluated by versine titration method (Estefan et al., 2013). Carbonates and bicarbonates were determined by titration against 0.1 N HCl using phenolphthalein and methyl orange as an indicator. Sulphates were determined by precipitation as barium sulphate using barium chloride in slightly acidic media. Due to fine particles of barium sulphate turbidity formed is proportional to the amount of sulphate in the sample, a photometric reading [Unicam UV 300, Thermo Spectronic, USA] enables the sulphate concentration to be accurately determined (Tandon, 1991). Chloride was determined by titration according to the method described by Estefan et al. (2013).

Heavy metals and trace elements analysis

Soil samples were extracted according to the method described by Soltanpour and Schwab (1977) using NH_4HCO_3 /DTPA solution to determine the available heavy metals (Al, Co, Cr, Mo and V), trace elements (Fe, Mn, Cu, Ni and Zn) and phosphorus (P^+) using Inductively Coupled Argon Plasma (iCAP 6500 Duo), Thermo Scientific, England, 1000 mg L^{-1} multi-element. A Certified standard solution, Merck, Germany, was used as a stock solution for instrument standardization (Allen, 1989).

Plant sampling, proximate nutritional composition analysis

Opuntia littoralis was scientifically identified at the herbarium of the Agricultural Museum, Giza (CAIM). The fresh fruits and cladodes were collected seasonally (fruits were not found in spring), then transferred to the laboratory, air-dried at oven 45 °C till constant weight, ground to fine powder, and kept to be used for different plant analysis. Moisture content, ash, organic matter, lipid content and crude fiber analysis were carried out according to the standard procedures of the Association of Official Analytical Chemists (AOAC, 2000). The Kjeldahl method was used to determine crude protein by method number 978.04 (AOAC, 2000). Carbohydrate content was determined by dissolving one

gram of plant powder in 2-5 ml of 2 M HCl in a sealed tube, then heating it at 100 °C for a period of 5-6 h (Chaplin and Kennedy, 1994). Then the total carbohydrates were estimated using the general phenol-sulfuric acid assay using the method described by Chaplin and Kennedy (1994). All the values were calculated as percentage of the analyzed sample.

Determination of energy value

The energy value of fruits and cladodes of the plant was calculated using the following formula (Crisan and Sands, 1978; Ramchoun et al., 2017)

$$\text{Energy value (kcal/100 g)} = (2.62 \times \% \text{protein}) + (8.37 \times \% \text{fat}) + (4.2 \times \% \text{carbohydrate})$$

The results were expressed in kilocalories.

Qualitative analysis

Investigation of protein-amino acids was achieved according to Pellet and Young (1980) and Cohen et al. (1989) by using amino acid analyzer SYKAM system High-Performance Analyzer with the following parameters: Column: Na High-Performance column (150*4.6) LC AKO6 Na -24050313, Injected volume: 0.1 ml, Flow Rate: 0.45, Detection: 440 + 570 nm, Temperature: 57-74, Retention time and separated area were obtained using Hewlett Packard 3390 recording integrator. However, qualitative determination of free and combined sugars was carried out using TLC by silica gel plates following the method of Ribeiro et al. (2010), using high-purity reference sugars from Sigma-Aldrich: galactose, xylose, arabinose, glucose, fructose, dextrose, sorbitol, glucuronic acid, mannose and sucrose. The GC/MS analysis to determine the lipid content was performed using a Thermo Scientific, Trace GC Ultra/ISQ Single Quadrupole MS, TG-5MS fused silica capillary column (30 m, 250 mm, 0.25 mm film thickness), an electron ionization system with ionization energy of 70 eV, helium gas as the carrier gas at a constant flow rate of 1 ml/min. The identification of the compounds was performed based on the comparison of their relative retention time and mass spectra with those of the NIST and WILLY library data of the GC/MS system.

Statistical analysis

All chemical analysis was performed in triplicate with blank samples for quality control. One-way analysis of variance (ANOVA) was used to assess the significance of seasonal variations of nutritional composition using SPSS, 2006 software (SPSS Inc., Chicago, Ill., USA).

Results and discussion

Soil properties

Soil texture and moisture content are fundamental features for the natural ecosystems and relate to various hydrological and ecological functions in different soil layers (Zhang et al., 2019).

The results in *Table 1* showed climate changes the availability of soil moisture; it reached its maximum during winter coinciding with winter rains and its minimum in summer due to high temperature, drought, relative humidity and high rate of evaporation.

There was a gradual increase in soil moisture content with such an increase in soil depth attributed to the exposure of the upper layers of desert soil to extreme evaporation, other than that, lower layers have been protected. The desert soil beyond a certain depth has a continuously moist layer to provide deep roots with the water needed (Gao et al., 2014). The data in *Table 1* showed that the texture of the soil supporting *O. littoralis* at Wadi Maged is sandy loam; the soil is alkaline composed of calcium bicarbonate as a major component (*Table 2*), this result is consistent with the result of El-Nady and Shoman (2017) that Wadi Maged soils are moderate to strongly calcareous. Which is confirmed by the previous study by Galal et al. (2017) which reported that; *Opuntia littoralis* cladodes grown in Wadi Maged contain significant quantities of calcium oxalate crystals as druses that are often correlated with an increase in soil calcium accumulation. The analysis of available heavy metals and phosphorus in the soil samples at the two depths (0-20 and 20-40) are shown in *Table 3*. It was found that Fe had the highest concentration (3.41 and 3.35 mg kg⁻¹) followed by Mn (3.09 and 3.092 mg kg⁻¹) in the surface and bottom layers, respectively. Heavy metals exhibit a range of soil characteristics, though plant uptake was comparatively low compared to overall soil intake from different disperse and agricultural sources (Nicholson and Chambers, 2008). Fe and Mn compounds in soil play an important role in restricting the transport of inorganic pollutants in groundwater systems (Stipp et al., 2002) as well as for the purification of soil particles from heavy metals (Gasparatos, 2013). Since Fe and Mn oxides are capable of binding metals, they may be appropriate for the treatment of soils contaminated with toxic metals (Puschenreiter, et al., 2005; Gasparatos, 2013).

Table 1. Particle size distribution analysis and mean values of moisture content of soil supporting *O. littoralis* in Wadi Maged, Matrouh

Soil depth (cm)	Soil texture	Particle size distribution analysis of soil (%)				Soil moisture content (%)	
		Coarse sand	Fine sand	Silt	Clay	Winter	Summer
0 – 20	Sandy loam	46.75	19.2	20.18	13.88	22.12 ± 0.63	1.83 ± 0.15
20 – 40	Sandy loam	55.07	18.73	13.83	12.38	23.66 ± 0.18	2.13 ± 0.65

Values are expressed as mean of three replicates ± standard error

Table 2. Chemical analysis of soil supporting *O. littoralis*

Soil depth (cm)	pH	E.C (dS m ⁻¹)	Analysis of soil saturation extract							
			Soluble cations (meq 100 g ⁻¹)				Soluble anions (meq 100 g ⁻¹)			
			Na ⁺	K ⁺	Ca ⁺⁺	Mg ⁺⁺	CO ₃ [–]	HCO ₃ [–]	SO ₄ [–]	Cl [–]
0-20	8 ± 0.08	0.16 ± 0.85	0.15 ± 0.03	0.05 ± 0.0	0.94 ± 0.06	0.52 ± 0.02	N.D	0.67 ± 0.04	0.55 ± 0.01	0.36 ± 0.02
20-40	8.7 ± 0.14	0.15 ± 0.78	0.13 ± 0.0	0.04 ± 0.002	1.12 ± 0.06	0.40 ± 0.02	N.D	0.92 ± 0.04	0.45 ± 0.001	0.24 ± 0.03

Values are expressed as mean of three replicates ± standard error

Nutritional composition

Opuntia spp. has a high nutritional value owing to its mineral, protein, dietary fiber, and phytochemical contents (Del Socorro et al., 2017). Physiological responses of plants have been significantly threatened by climate change as the probability of suffering from different plant stress has increased owing to environmental extremities

and climate variability, the seasonal variations in the proximate composition of *Opuntia littoralis* cladodes and fruits are summarized in Table 4. The main constituents of cladodes and fruits are carbohydrates (in summer 24.1- 28.4%, respectively %), followed by ash (in spring and summer 12.0- 7.6%, respectively), fibers (in spring and summer 9.4- 6.8%, respectively), proteins (8.9- 5.1%, respectively) and lipids (in autumn 1.8- 4.0%, respectively).

Ash, organic matter and crude fiber content

Ash content is the index of mineral contents in plants such as calcium, sodium, potassium, nickel and zinc. The total ash content of *Opuntia littoralis* reached its maximum value (12.09%) for cladodes during spring, and (7.60%) for fruits in summer which showed that the cladodes were rich in minerals, while the organic matter reached its maximum value (88.72%) and (93.72%) for cladodes and fruits, respectively during autumn (Table 4). According to Michael and David (2002), ash content is vital in determining the nutritive value of foods by evaluating the quality of plant grading and providing an idea of the amount of minerals found in the plant. It is well known that *Opuntia* cladodes are a good source of dietary fibers (Uebelhack, et al., 2014) which may help in reducing body weight by binding to dietary fat and increasing its excretion which may explain why cladodes are considered as hypolipidemic and are also found to promote digestion and absorption processes in the small intestine (Díaz, et al., 2017). The percentage of pharmacopeial constants increased as a consequent increase in overall ion accumulation due to an increase in soil moisture stress (Agboola and Adejumo, 2013).

Table 3. Heavy metals nitrogen and phosphorus analysis of the soil supporting *O. littoralis* grown in Wadi Maged, Matrouh

Metal (mg kg ⁻¹)	Soil depth (cm)	
	0-20	20-40
Al (Aluminum)	0.42 ± 0.01	0.32 ± 0.02
Ba (Barium)	0.003 ± 0.00	0.28 ± 0.09
Cd (Cadmium)	0.01 ± 0.00	0.01 ± 0.00
Co (Cobalt)	0.03 ± 0.00	0.08 ± 0.04
Cr (Chromium)	0.04 ± 0.00	0.03 ± 0.00
Cu (copper)	0.56 ± 0.01	0.44 ± 0.04
Fe (Iron)	3.41 ± 0.34	3.35 ± 0.13
Mn (Manganese)	3.09 ± 0.09	3.09 ± 0.05
Mo (Molybdenum)	< 0.002	< 0.002
Ni (Nickel)	0.07 ± 0.01	0.08 ± 0.00
Pb (Lead)	0.28 ± 0.00	0.27 ± 0.01
Sr (Strontium)	0.73 ± 0.03	0.78 ± 0.00
V (Vanadium)	0.16 ± 0.03	0.17 ± 0.03
Zn (Zinc)	0.85 ± 0.05	0.86 ± 0.00
P (Phosphorus)	0.01 ± 0.00	0.02 ± 0.00
N (Nitrogen)	23.95 ± 0.15	35.30 ± 0.40

Values are expressed as mean of three replicates ± standard error

Table 4. The average seasonal variations of proximate composition of *Opuntia littoralis*

Variable	Season	Cladode	Fruit	Variable	Season	Cladode	Fruit
Total ash (%)	Autumn	11.28 ^c ± 0.21	6.28 ^c ± 0.03	Total nitrogen (%)	Autumn	0.76 ^c ± 0.02	0.75 ^b ± 0.01
	Winter	11.64 ^b ± 0.29	6.99 ^b ± 0.08		Winter	1.42 ^a ± 0.11	0.82 ^a ± 0.03
	Spring	12.09 ^a ± 0.07	--		Spring	1.24 ^b ± 0.04	--
	Summer	11.55 ^c ± 0.23	7.60 ^a ± 0.30		Summer	0.4 ^d ± 0.003	0.44 ^c ± 0.004
Organic matter (%)	Autumn	88.72 ^c ± 0.21	93.72 ^a ± 0.03	Protein content (%)	Autumn	4.77 ^c ± 0.15	4.69 ^b ± 0.07
	Winter	88.36 ^b ± 0.29	93.00 ^b ± 0.08		Winter	8.90 ^a ± 0.70	5.15 ^a ± 0.23
	Spring	87.91 ^a ± 0.07	--		Spring	7.73 ^b ± 0.23	--
	Summer	88.45 ^c ± 0.23	92.40 ^b ± 0.30		Summer	2.6 ^d ± 0.02	2.77 ^c ± 0.03
Crude fiber (%)	Autumn	6.83 ^b ± 0.189	5.78 ^b ± 0.206	Total lipids (%)	Autumn	1.86 ^a ± 0.03	4.09 ^a ± 0.20
	Winter	7.23 ^b ± 0.403	4.90 ^b ± 0.216		Winter	1.69 ^b ± 0.05	3.2 ^c ± 0.03
	Spring	9.48 ^a ± 0.403	--		Spring	1.59 ^c ± 0.07	--
	Summer	6.91 ^b ± 0.294	6.90 ^a ± 0.374		Summer	1.46 ^d ± 0.02	3.6 ^b ± 0.01
Total carbohydrates (%)	Autumn	23.23 ^c ± 0.369	21.55 ^b ± 0.526	Energy value (kcal/100 g)	Autumn	123.93 ^a ± 2.016	135.38 ^b ± 1.115
	Winter	15.45 ^a ± 0.493	9.63 ^c ± 0.419		Winter	99.10 ^c ± 0.982	78.95 ^c ± 0.982
	Spring	12.23 ^b ± 0.240	--		Spring	82.13 ^d ± 0.726	--
	Summer	24.18 ^c ± 0.793	28.40 ^a ± 0.963		Summer	119.58 ^b ± 1.127	155.80 ^a ± 0.245

Carbohydrate content

The total carbohydrate content of *Opuntia littoralis* reached its maximum values (24.15 and 28.41%) for cladodes and fruits, respectively during summer, while the minimum was 12.22% for cladodes and 9.63% for fruits in spring and winter. Carbohydrates provide energy to cells in the body, the brain depends only on carbohydrates as a source of energy (Ebifa-Othieno, et al., 2020). Excess water in the soil in winter can also result in a reduction of photosynthesis (Mielke and Schaffer, 2010). These results are also consistent with Xu and Zhou (2011) who stated that excessive moisture levels, photosynthesis and stomatal conductance, as well as carbohydrate content decreased.

Total carbohydrate represents the highest constituent among determined nutritional composition of *Opuntia littoralis* plant as shown in Table 4. Large amount of

carbohydrates is correlated with the high concentration of iron (Fe) and manganese (Mn) in the soil (*Table 3*). Iron is involved in the synthesis of chlorophyll and is essential for maintenance of chloroplast structure and function (Rout and Sa hoo, 2015). Manganese (Mn) also, plays a role in chlorophyll production which is essential in photosystem II (Mousavi et al., 2011).

TLC profile of free and combined sugars

Carbohydrates and their derivatives in living cells provide flexibility and structure, supply energy, and act as regulators and substrates for several specific biochemical processes (Bokov et al., 2017). Analysis of free and combined sugars of the cladodes and fruits using TLC (*Table 5*). Data revealed the presence of eight free sugars (glucose, fructose, xylose, arabinose, galactose, sorbitol, glucuronic acid and mannose) and six combined sugars (glucose, arabinose, galactose, sorbitol, mannose and dextrose) at the cladodes. Meanwhile, the fruits contain nine free sugars (glucose, fructose, xylose, arabinose, galactose, sorbitol, gluconic acid, mannose and dextrose) and five combined sugars (glucose, arabinose, galactose, sorbitol and mannose).

Table 5. Free and combined sugars of Opuntia littoralis cladodes and fruits using TLC

Sugar	Free sugars		Combined sugars	
	Cladodes	Fruits	Cladodes	Fruits
Glucose	+ ve	+ ve	+ ve	+ ve
Fructose	+ ve	+ ve	-ve	-ve
Sucrose	-ve	-ve	-ve	-ve
Xylose	+ ve	+ ve	-ve	-ve
Arabinose	+ ve	+ ve	+ ve	+ ve
Galactose	+ ve	+ ve	+ ve	+ ve
Sorbitol	+ ve	+ ve	+ ve	+ ve
Gluconic acid	+ ve	+ ve	-ve	-ve
Mannose	+ ve	+ ve	+ ve	+ ve
Dextrose	-ve	+ ve	+ ve	-ve

Nitrogen and protein content

The total nitrogen content reached its maximum values (1.42 and 0.82%) for cladodes and fruits, respectively during winter, while the minimum (0.41 and 0.44%) for cladodes and fruits in summer (*Table 4*). So, the percentage of total protein reached its maximum values 8.90% and 5.15% for cladodes and fruits, respectively in winter, while reached its minimum values 2.61% and 2.77% during summer for cladodes and fruits, respectively. The decrease of total nitrogen and protein content in summer may be attributed to the decrease of water resources of the soil, which was related to the accumulation of some amino acids (e.g. proline) that may participate in adjusting cell osmoregulation. Our results are in accordance with a previous study by Silva et al. (2020) which stated that water stress in summer led to large decreases in protein percentage of Wheat grains. The obtained results also agree with those of Cauquil et al. (2017); who reported a decrease in the level of protein with a progressive increase in the accumulation of amino acids in the tissue, which was

recorded in many plants during water stress. The protein promotes the formation of hormones that control many body functions such as growth, repair and maintenance of body protein (Mau et al., 1999).

Investigation of protein amino acids

Data on protein amino acid analysis of the cladodes and fruits are represented in *Figures 1* and *2*, respectively. The obtained data of protein amino acid analysis showed that 17 and 16 protein amino acids with different concentration ranges were detected in the cladodes and fruits of *Opuntia littoralis* respectively (*Figs. 1* and *2*). It can be concluded that the major protein amino acids were glutamic and aspartic acids in cladodes and fruits. On the other hand, methionine (0.09 and 0.08 mg g⁻¹) was the minor protein amino acid in cladodes and fruits, respectively. Aspartic acid is a non-essential amino acid, but it has an important role in purine, pyrimidine, and asparagine and inositol synthesis. Aspartic acid has been used as mineral salts such as magnesium aspartate or potassium aspartate to improve energy production in exercising muscles (Akram et al., 2011). Quantitative and qualitative changes in the synthesis of plant proteins may be due to a response to water deficiency (Pessarakali, 1995). Different amino acids are used in the human body as precursors for the synthesis of proteins and other nitrogen-containing compounds. Of the 20 amino acids commonly required by the body for protein synthesis and other compounds, 9 amino acids are essential in the diet of an adult man (Murray et al., 2006). It is also reported that, if one of the essential amino acids, which cannot be synthesized in the body, is lacking or inadequate, it will not be possible to maintain nitrogen balance since there will not be enough of that amino acid for protein synthesis regardless of the total intake of protein (Murray et al., 2006). Moreover, one of the important amino acids is proline with a concentration of 3.59 and 4.08 mg g⁻¹ in the cladodes and fruits, respectively. The accumulation of proline due to increased synthesis and decreased degradation under a variety of stress conditions such as salt and drought has been documented in many plant species (Kishor et al., 2005); it is thought to protect plants during drought condition (Chorkaew et al., 2017). Proline seems to have diverse roles under osmotic stress conditions, such as stabilization of proteins, membranes and sub-cellular structures and protecting cellular functions by scavenging reactive oxygen species (Szabados and Savouré, 2010). In addition, the increase in proline and glutamic content may be due to the increase in soil salinity according to Ali and Sawaf (1992) who reported that salinity inhibits the transmission reaction. Moreover, glutamic acid can be accumulated and transformed into other nitrogenous compounds such as proline. In general, drought causes an increase in amino acids in plants (Chorkaew et al., 2017).

Lipid content

The data presented in *Table 4* showed that the percentages of total Lipid content of *Opuntia littoralis* reached its maximum values (1.86 and 4.09%) for cladodes and fruits, respectively during autumn, while its minimum was 1.46% for cladodes in summer and 3.21% for fruits in winter. Water deficit in summer results in metabolic changes in plants. Among them are the stimulation of lipolytic, peroxidative activities and the inhibition of lipid biosynthesis which lowers the content of membrane lipids (Labusch et al., 2013). Drought affects the accumulation of oil in the seeds (Martínez Ballesta et al., 2013). Drought also reduces the accumulation of lipids in peas, sunflower, maize,

lupine, and wheat (Silva, et al., 2020). The highest percentage of total lipids in autumn and winter may be attributed to the enhancement in the metabolic rate of the plant, which leads to an increase in carbohydrate content, which converts to lipid by oxidation reaction (Stocker, 1960).

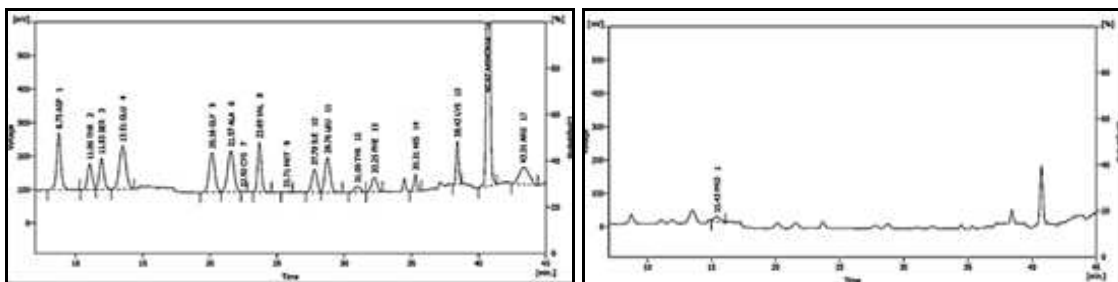


Figure 1. The separated hydrolyzed protein amino acids and proline of *O. littoralis* cladodes

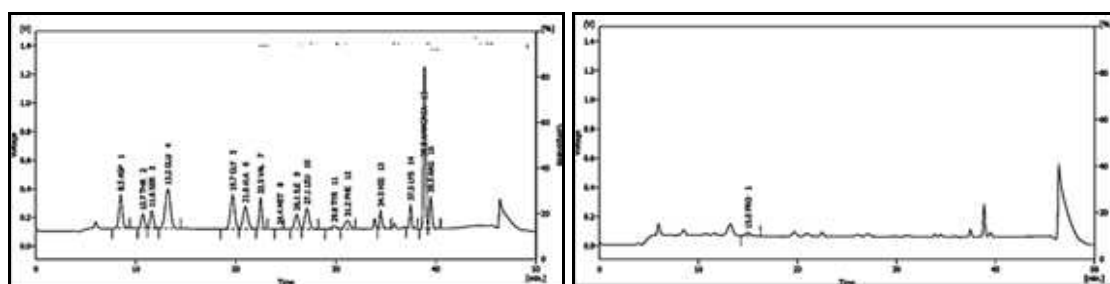


Figure 2. The separated hydrolyzed protein amino acids and proline of *Opuntia littoralis* fruits

GC-MS chromatogram of the petroleum ether extract of the cladodes of *Opuntia littoralis* showed the presence of 26 compounds {series of (C7-C44)}, predominated by Undecane followed by Dodecane (Fig. 3). Meanwhile, the chromatogram of the petroleum ether extract of the fruits revealed the presence of 34 compounds predominated by Linoleic acid followed by Palmitic acid with a significant percentage (Fig. 4). Several studies have indicated that cactus particularly; fruits, pulp, seed and prickly pear peel were rich in linolenic, oleic and palmitic acids (Soel, et al., 2007). The most important essential fatty acid in human nutrition is linolenic acid. A High amount of omega-6 linoleic acid was reported in cactus pulp and peel; as a precursor of arachidonic acid, linoleic acid has long been accepted as having a hypocholesterolemic effect and inhibitory properties against colon cancer metastatic cells (El-Beltagi, et al., 2019). Linoleic acid also found to prevent cardiovascular diseases (Afifi, et al., 2018). Fatty acids play a natural preventative role in cardiovascular diseases and the improvement of some other health problems (Faremi and Ekanem, 2011). Poly-unsaturated fats promote the reduction of both total and LDL cholesterol and a significant small decrease in HDL cholesterol (Chougui, et al., 2013). The fatty acid composition of the cactus pear fruits is similar to grape and rapeseed (Özcan and Al-Juhaimi, 2011). *Opuntia ficus indica* seed exhibits a higher proportion of polyunsaturated fats (linoleic acid), compared to certain conventional edible vegetable oils (Kolniak-Ostek et al., 2020). This characteristic demonstrates that *Opuntia* fruits may be a remarkable natural source of edible oil with high amounts of healthy fatty acids.

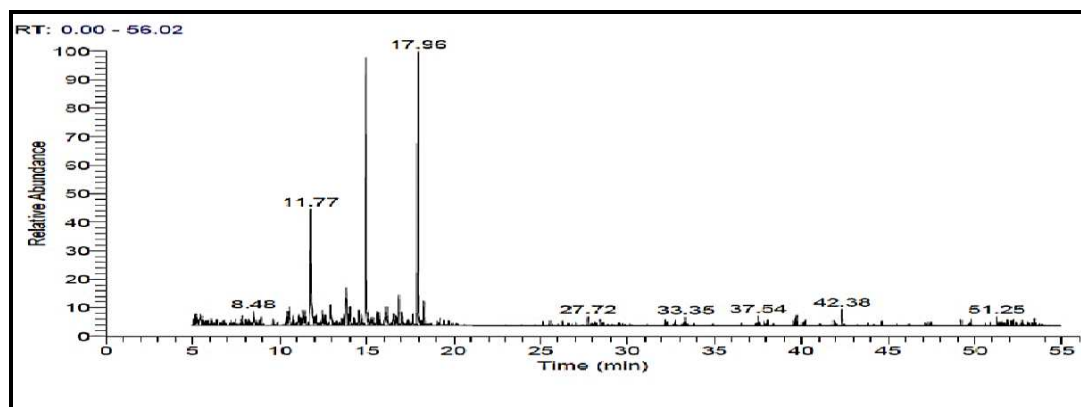


Figure 3. GC -MS chromatogram of the petroleum ether extract of cladodes

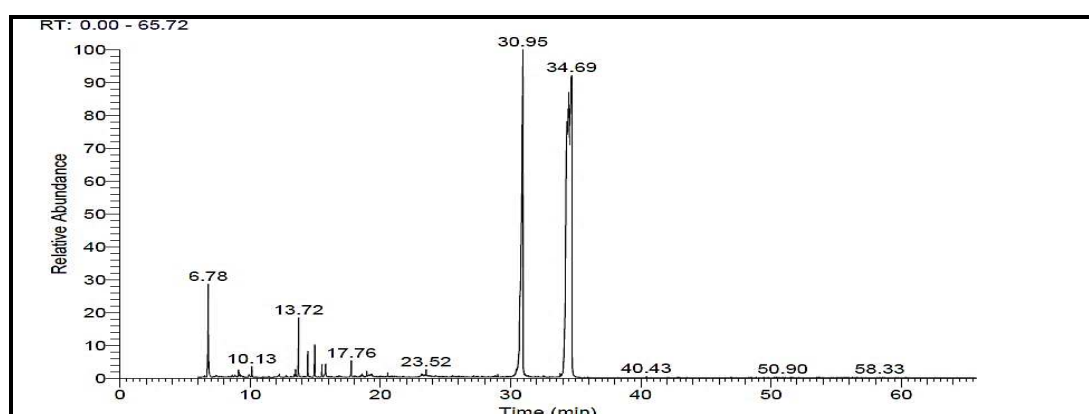


Figure 4. GC -MS chromatogram of the petroleum ether extract of the fruit

Energy value

Opuntia fruits ripening during the dry season are promising sources of nutrients during the dry season when food supply is inadequate. Energy is an essential demand to maintain the body's various functions, such as respiration, circulation, physical work, and protein synthesis (Ebifa-Othieno et al., 2020). The data in *Table 4* showed that the ranges for the estimated calorific value of cladodes are 82.1- 123.9 kcal/100 g in spring and autumn, respectively. While in fruits it is 135.3- 155.8 kcal/100 g in autumn and summer, respectively. These results indicate that *Opuntia littoralis* has the potential to contribute significantly to energy needs particularly during the drought period when food is limited.

Conclusion

Opuntia littoralis has a high nutritional value. The main constituent of cladodes and fruits is water followed by carbohydrates, ash, proteins then lipids. The plant adapted to climatic changes at Wadi Maged region by changing its chemical composition to overcome different types of stress. The plant tends to accumulate amino acids especially glutamic, aspartic and proline in summer to overcome the water deficiency. The lipid profile of *Opuntia* fruits may be an interesting natural source of edible oil containing high amounts of healthy fatty acids.

Acknowledgments. This work was supported by the Deanship of Scientific Research, Vice Presidency for Graduate Studies and Scientific Research, King Faisal University, Saudi Arabia [Project No. GRANT 22].

REFERENCES

- [1] Abd El-Moaty, H. I., Sorour, W. A., Youssef, A. K., Gouda, H. M. (2020): Structural elucidation of phenolic compounds isolated from *Opuntia littoralis* and their antidiabetic, antimicrobial and cytotoxic activity. – *South African Journal of Botany* 131: 320-327.
- [2] Abdel-Rahman, A. M., Migahid, A. M. (2019): The autecological characteristics of endangered medicinal plant *Thymus capitatus*, in the western Mediterranean region of Egypt. – *Egypt. Journal of Botany* 59(2): 387-398.
- [3] Afify, A. E., El-Beltagi, H. S., Fayed, S. A., El-Ansary, A. E. (2018): Enhancing effect of olive leaves extract on lipid profile and enzymes activity in streptozotocin induced diabetic rats. – *Fresenius Environmental Bulletin* 27(3): 1875-1883.
- [4] Agboola, O. S., Adejumo, A. L. (2013): Nutritional composition of the fruit of the Nigerian wild date palm, *Phoenix dactylifera*. – *World Journal of Dairy and Food Sciences* 8(2): 196-200.
- [5] Akram, M., Asif, H., Uzair, M., Akhtar, N., Madni, A., Shah, S. M. A., Hasan, Z., Ullah, A. (2011): Amino acids: a review article. – *Journal of Medicinal Plants Research* 5: 3997-4000.
- [6] Alberghamo, A., Potortí, A. G., Di Bella, G., Amor, N. B., Lo Vecchio, G., Nava, V., Lo Turco, V. (2022): Chemical characterization of different products from the Tunisian *Opuntia ficus-indica* (L.) Mill. – *Foods* 11(2): 155.
- [7] Ali, R., Sawaf, N. (1992): Effect of salinity alone and in combination with adipic acid or methylamine on free amino acid and alkaloids content of *Datura innoxia*. – *Journal of Faculty of Education, Ain Shams University* 17: 345-353.
- [8] Allen, S. E. (1989): *Chemical Analysis of Ecological Materials*. 2nd Ed. – Blackwell Scientific Publications, Oxford and London.
- [9] Aninbon, C., Jogloy, S., Vorasoot, N., Nuchadomrong, S., Holbrook, C., Kvien, C., Patanothai, A. (2017): Change of arginine content and some physiological traits under midseason drought in peanut genotypes with different levels of drought resistance. – *Turkish Journal of Agriculture and Forestry* 41(4): 285-293.
- [10] AOAC (2000): *Official Methods of Analysis of AOAC International*. 17th Ed. – Association of Official Analytical Chemists, Washington, DC.
- [11] Arakaki, M., Christin, P. A., Nyffeler, R., Lendel, A., Eggli, U., Ogburn, R. M., ... Edwards, E. J. (2011): Contemporaneous and recent radiations of the world's major succulent plant lineages. – *Proceedings of the National Academy of Sciences* 108(20): 8379-8384.
- [12] Bakar, B., Çakmak, M., Ibrahim, M. S., Özer, D., Saydam, S., Karatas, F. (2020): Investigation of amounts of vitamins, lycopene, and elements in the fruits of *Opuntia ficus-indica* subjected to different pretreatments. – *Biological Trace Element Research* 198(1): 315-323.
- [13] Bokov, D. O., Samylina, I. A., Nikolov, S. D. (2017): HPLC/RI and HPLC/PDA Phytochemical Analysis of Free and Bound Carbohydrates in *Galanthus woronowii* Losinsk. and *G. nivalis* L. Homeopathic Matrix Tinctures. – *Pharmaceutical Chemistry Journal* 50(12): 810-813.
- [14] Cauquil, A. S., Ory-Magne, F., Jardiné, V., Galitzky, M., Rosito, M., Brefel-Courbon, C., Celebrini, S. (2017): Parkinson's patients can rely on perspective cues to perceive 3D space. – *Brain Research* 1663: 161-165.
- [15] Chaplin, M. F., Kennedy, J. F. (1994): *Carbohydrate Analysis - A Practical Approach*. 2nd Ed. – Oxford University Press, Oxford.

- [16] Chorkaew, A., Sanun, J., Nimitr, V., Suporn, N., Corley, H., Craig, K., Aran, P. (2017): Change of arginine content and some physiological traits under midseason drought in peanut genotypes with different levels of drought resistance. – Turkish Journal of Agriculture and Forestry 41: 285-293.
- [17] Chougui, N., Tamendjari, A., Hamidj, W., Hallal, S., Barras, A., Richard, T., Larbat, R. (2013): Oil composition and characterisation of phenolic compounds of *Opuntia ficus-indica* seeds. – Food Chemistry 139(1-4): 796-803.
- [18] Cohen, S. A., Meys, M., Tarvin, T. L. (1988) The PicoTag Method. A Manual of Advanced Techniques for Amino Acid Analysis. – Waters Chromatography Division, Millipore Corp., Milford, MA.
- [19] Crisan, E. V., Sands, A. (1978): Nutritional Value. – In: Chang, S. T., Hayes, W. A. (eds.) The Biology and Cultivation of Edible Mushrooms. Academic Press, New York, pp. 137-168.
- [20] Crosby, K., Jifon, J., Leskovar, D. (2008): Agronomy and the Nutritional Quality of Vegetables. – In: Tomás-Barberán, F. A., Gil, M. I. (eds.) Improving the Health-Promoting Properties of Fruit and Vegetable Products. – CRC Press, Boca Raton, pp. 392-411.
- [21] del Carmen Martínez-Ballesta, M., Moreno, D. A., Carvajal, M. (2013): The physiological importance of glucosinolates on plant response to abiotic stress in Brassica. – International Journal of Molecular Sciences 14(6): 11607-11625.
- [22] Díaz, M. D. S. S., de la Rosa, A. P. B., Héliès-Toussaint, C., Guéraud, F., Nègre-Salvayre, A. (2017): *Opuntia* spp.: Characterization and benefits in chronic diseases. – Oxidative Medicine and Cellular Longevity. DOI: 10.1155/2017/8634249.
- [23] Do Nascimento Silva, A., Ramos, M. L. G., Júnior, W. Q. R., de Alencar, E. R., da Silva, P. C., de Lima, C. A., ... Silva, M. A. V. (2020): Water stress alters physical and chemical quality in grains of common bean, triticale and wheat. – Agricultural Water Management 231: 106023.
- [24] DRC Staff (2007-2015): Integrated Agriculture Development of Northwestern Coastal Wadies. Annual Report. – Desert Research Center Publications, Cairo.
- [25] Ebifa-Othieno, E., Kabasa, J. D., Nyeko, P., Nakimbugwe, D., Mugisha, A. (2020): Nutritional potential of tamarind (*Tamarindus indica* L.) from semi-arid and subhumid zones of Uganda. – Journal of Food Measurement and Characterization 14(2): 1125-1134.
- [26] El-Beltagi, H. S., Mohamed, H. I., Elmelegy, A. A., Eldesoky, S. E., Safwat, G. (2019): Phytochemical screening, antimicrobial, antioxidant, anticancer activities and nutritional values of cactus (*Opuntia ficus indica*) pulp and peel. – Fresenius Environmental Bulletin 28(2A): 1534-1551
- [27] El-Nady, M. A., Shoman, M. M. (2017): Assessment of soil erosion risk in the basin of wadi maged in northern west coast of Egypt using CORINE model and GIS techniques. – Assessment 32: 33.
- [28] Estefan, G., Sommer, R., Ryan, J. (2013): Methods of Soil, Plant, and Water Analysis: A Manual for the West Asia and North Africa Region. Third Ed. – International Center for Agricultural Research in the Dry Areas (ICARDA), Beirut.
- [29] Faremi, A. Y., Ekanem, J. T. (2011): Haematological parameters and enzyme studies in *Trypanosoma brucei*-infected rats reared on *Nigella sativa* oil-based diet. – Asian Journal of Biochemistry 6: 90-97.
- [30] Galal, T. M., Hassan, L. M., Youssef, A., El-Moaty, A., Gouda, H. (2017): Micromorphology and Phytochemical Screening of *Opuntia littoralis* engelm. – Cladodes. Egyptian Journal of Desert Research 67(1): 155-170.
- [31] Galal, T., Farahat, E., Mohsen, L. (2019): Phytosociology of rainfed barely along the western Mediterranean Coast, Egypt. – Taekholmia 39(1): 18-33.

- [32] Gao, X., Wu, P., Zhao, X., Wang, J., Shi, Y. (2014): Effects of land use on soil moisture variations in a semi-arid catchment: implications for land and agricultural water management. – *Land Degradation & Development* 25(2): 163-172.
- [33] Gasparatos, D. (2013): Sequestration of heavy metals from soil with Fe–Mn concretions and nodules. – *Environmental Chemistry Letters* 11(1): 1-9.
- [34] Gee, G. W. and Bauder, J. W. (1986): Particle-Size Analysis. – In: Klute, A. (ed.) *Methods of Soil Analysis. Part 1. 2nd Ed. Agron. Mongr. 9. ASA and SSSA, Madison, WI*, pp. 383-409.
- [35] Harris, D. C. (1998): *Análise Química Quantitativa. 6. Ed. – LTC, Rio de Janeiro.*
- [36] Hendawy, S., F., Abouziena, H. F., Abd El-Razik, T. M., Amer, H. M., Hussein, M. S. (2020): Winter weeds and its control in the medicinal plants in Egypt: a survey study. – *Egyptian Pharmaceutical Journal* 18(1): 16-26.
- [37] Jankowski, S. J., Freiser, H. (1961): Flame photometric methods of determining the potassium tetraphenylborate. – *Analytical Chemistry* 33(6): 773-775.
- [38] Kishor, P. K., Sangam, S., Amrutha, R. N., Laxmi, P. S., Naidu, K. R., Rao, K. S., ... Sreenivasulu, N. (2005): Regulation of proline biosynthesis, degradation, uptake and transport in higher plants: its implications in plant growth and abiotic stress tolerance. – *Current Science* 424-438.
- [39] Kolniak-Ostek, J., Kita, A., Miedzianka, J., Andreu-Coll, L., Legua, P., Hernandez, F. (2020): Characterization of bioactive compounds of *Opuntia ficus-indica* (L.) Mill. seeds from Spanish cultivars. – *Molecules* 25(23): 5734.
- [40] Labusch, C., Shishova, M., Effendi, Y., Li, M., Wang, X., Scherer, G. F. (2013): Patterns and timing in expression of early auxin- induced genes imply involvement of phospholipases mA (pPLAs) in the regulation of auxin responses. – *Molecular Plant* 6(5): 1473-1486.
- [41] López-Palacios, C., Peña-Valdivia, C. B. (2020): Screening of secondary metabolites in cladodes to further decode the domestication process in the genus *Opuntia* (Cactaceae). – *Planta* 251(4): 1-14.
- [42] Martínez-Ballesta, M. D., Moreno, D. A., Carvajal, M. (2013): The physiological importance of glucosinolates on plant response to abiotic stress in Brassica. – *International Journal of Molecular Sciences* 14(6): 11607-11625.
- [43] Mau, J. L., Miklus, M. B., Beelman, R. B. (1999): Shelf life studies of foods and beverages charalambous E. d. – *Chem. Biol. Phys. Nutr. Aspect* 57: 475-477.
- [44] Meigs, P. (1973): World Distribution of Coastal Deserts. – David, H. K., Amiran, Andrew, W. W. (eds.) *Coastal Deserts: Their Natural and Human Environments. University of Arizona Press, Tucson*, pp. 3-13.
- [45] Michael, K., David, M. (2002): The useful plants of West Tropical Africa. – *Nigerian Journal of Biochemistry and Molecular Biology* 12: 53-60.
- [46] Mielke, M. S., Schaffer, B. (2010): Leaf gas exchange, chlorophyll fluorescence and pigment indexes of *Eugenia uniflora* L. in response to changes in light intensity and soil flooding. – *Tree Physiology* 30(1): 45-55.
- [47] Mousavi, S. R., Shahsavari, M., Razaeei, M. (2011): A general overview on Manganese (Mn) importance for crop production. – *Australian Journal of Basic and Applied Sciences* 5(9): 1799-1803.
- [48] Murray, R. K., Granner, D. K., Rodwell, V. W. (2006): *Harper's Illustrated Biochemistry* (No. 577.1 HAR). – Lange Medical Books/McGraw-Hill, New York.
- [49] Nicholson, F. A., Chambers, B. J. (2008): Sources and Impacts of Past, Current and Future Contamination of Soil. Appendix 1: Heavy Metals SP0547. – Defra Science Directorate, Department for Environment Food and Rural Affairs, London.
- [50] Özcan, M. M., Al-Juhaimi, F. (2011): Nutritive value and chemical composition of prickly pear seeds (*Opuntia ficus indica* L.) growing in Turkey. – *International Journal of Food Sciences and Nutrition* 62: 533-536.

- [51] Pellet, P. L., Young, V. R. (1980): Nutritional Evaluation of Protein Foods. –United Nations University, Tokyo.
- [52] Pessarakali, M. (1995): Handbook of Plant Physiology. – Marc E-Dekker. Inc., New York.
- [53] Puschenreiter, M., Horak, O., Friesl, W., Hartl, W. (2005): Low-cost agricultural measures to reduce heavy metal transfer into the food chain—a review. – Plant Soil Environ 51(1): 1-11.
- [54] Ramchoun, M., Alem, C., Ghafoor, K., Ennassir, J., Zegzouti, Y. F. (2017): Functional composition and antioxidant activities of eight Moroccan date fruit varieties (*Phoenix dactylifera* L.). – Journal of the Saudi Society of Agricultural Sciences 16(3): 257-264.
- [55] Ribeiro, E. M. D. O., Silva, N. H. D., Lima Filho, J. L. D., Brito, J. Z. D., Silva, M. D. P. C. D. (2010): Study of carbohydrates present in the cladodes of *Opuntia ficus-indica* (fodder palm): according to age and season. – Food Science and Technology 30: 933-939.
- [56] Rout, G. R., and Sahoo, S. (2015): Role of iron in plant growth and metabolism. – Reviews in Agricultural Science 3: 1-24.
- [57] Soel, S. M., Choi, O. S., Bang, M. H., Park, J. H. Y., Kim, W. K. (2007): Influence of conjugated linoleic acid isomers on the metastasis of colon cancer cells in vitro and in vivo. – The Journal of Nutritional Biochemistry 18(10): 650-657.
- [58] Soltanpour, P. N., Schwab, A. P. (1977): A new soil test for simultaneous extraction of macro-and micro-nutrients in alkaline soils. – Communications in Soil Science and Plant Analysis 8(3): 195-207.
- [59] Sparks, D. L., Page, A. L., Helmke, P. A., Loeppert, R. H. (eds.): (2020): Methods of Soil Analysis. Part 3: Chemical Methods (Vol. 14). – John Wiley & Sons, Hoboken, NJ.
- [60] Stipp, S. L. S., Hansen, M., Kristensen, R., Hochella Jr, M. F., Bennedsen, L., Dideriksen, K. ... Mathieu, H. J. (2002): Behaviour of Fe-oxides relevant to contaminant uptake in the environment. – Chemical Geology 190(1-4): 321-337.
- [61] Stocker, O. (1960): Physiological and morphological changes in plants due to water deficiency. – Arid Zone Research 15: 63-104.
- [62] Szabados, L., Savouré, A. (2010): Proline: a multifunctional amino acid. – Trends in Plant Science 15(2): 89-97.
- [63] Tandon, H. L. S. (1991): Sulphur Research and Agricultural Production in India. 3rd Ed. – The Sulphur Institute, Washington, DC.
- [64] Uebelhack, R., Busch, R., Alt, F., Beah, Z. M., Chong, P. W. (2014): Effects of cactus fiber on the excretion of dietary fat in healthy subjects: a double blind, randomized, placebo-controlled, crossover clinical investigation. – Current Therapeutic Research 76: 39-44.
- [65] UNESCO (1977): Map of the World Distribution of Arid Regions. – MAB Technical Notes. 7. UNESCO, Paris.
- [66] Xu, Z., Zhou, G. (2011): Responses of photosynthetic capacity to soil moisture gradient in perennial rhizome grass and perennial bunchgrass. – BMC Plant Biology 11(1): 1-11.
- [67] Zhang, Q., Shao, M., Jia, X., Wei, X. (2019): Changes in soil physical and chemical properties after short drought stress in semi-humid forests. – Geoderma 338: 170-177.

RICE GROWTH AND YIELD RESPONSE ON BIOFERTILIZER APPLICATION ON LATOSOL PADDY FIELD OF INDONESIA

IKHWANI^{1*} – ARSANA, I. G. K. D.¹ – ARIEF, R. W.¹ – ASNAWI, R.¹ – SUDARYONO, T.¹ – MEJAYA, M. J.¹

¹*Research Organization for Agriculture and Food (ORPP)
National Research and Innovation Agency (BRIN), Indonesia*

**Corresponding author
e-mail: isunihardi21@gmail.com*

(Received 3rd Mar 2022; accepted 20th Jun 2022)

Abstract. Rice is a main staple food in Indonesia. There is a major focus on how to increase production to meet the need of the 250 million Indonesian population without deteriorating environmental conditions. This study aimed to evaluate the biofertilizer dosing method on rice growth and yield trait of lowland rice in West Java latosol soil. The experiment was conducted at the greenhouse of the Indonesian Center for Agricultural Land Resources Research and Development (ICALRRD), Bogor, West Java, Indonesia from March to June 2018. Rice variety Inpari 32 as a new plant type, was used in this study. The treatments were arranged in a factorial randomized block design with two factors and three replications. The first factor was the method of biofertilizer application (seed treatment, root dipping prior to transplanting and sown at planting). The second factor the dosage of biofertilizer consisted of 1) 0 g/pot, 2) 100 g/pot, 3) 200 g/pot, 4) 300 g/pot, and 5) 400 g/pot. Latosol soil samples were obtained from Muara experimental station, Bogor, West Java. The results showed that root dipping method prior to transplanting with the biofertilizer as much as 300 g and 400 g/ha showed the best results in terms of filled grain number, filled grain weight, total grain number and total grain weight as compared to other combination treatments. The dosage of biofertilizer and its integrated application can become alternative recommendation to increase yield on lowland rice at latosol soil. The highest correlation value ($r = 0.983$) was observed between total grain weight and percent of filled grain number while the lowest correlation value ($r = 0.008$) was observed between 1000 grain weight and percent of filled grain number.

Keywords: *Latosol soil, root dipping, filled grain number, grain weight, seed treatment*

Introduction

Rice is the main staple food for most people in the world, especially in Asia where 90% of the global rice consumption and production is focused (Arnold, 1999). As an Asian country, rice has become the most popular and the most important cereal crop consumed by the almost 250 million of Indonesian population while conserving environmental condition without destroying the forest for rice land extension (Nikmatul et al., 2020; Rahmah et al., 2017). The need of this commodity is going to increase year by year due to the population growth (Somchit et al., 2017). The increase of rice demand cannot be supplied if there is no improvement in rice production.

There are several strategies to improve rice production. High yielding varieties have given significant rice production increase (Long-ping, 2014). Rice breeding programs to obtain a new variety with a high grain yield have been reported by previous studies (Hasan et al., 2013; Akhtar et al., 2011; Khamwicht et al., 2006). Other strategy tended to use the combination of organic and chemical fertilizers to obtain not only a high yield but also to overcome environmental problems at the same time (Zaki et al., 2018). Organic matter combined with NPK chemical fertilizer positively affected soil and plant characteristics (Himmelstein, 2014). Organic matters are various i.e., animal, and green manure (Tejada et al., 2009; Nguyen, 2013), biochar (Jones et al., 2012; Bastida et al.,

2015) and composts (Noble and Convery, 2005). Another improvement can be made through application of biofertilizer (Vessey, 2003). The high productivity of agriculture is mostly achieved by using chemical fertilizers (Yang et al., 2019). Another strategy is the use of the combination of organic and chemical fertilizers. The manure could be used to increase rice productivity in order to reduce chemical fertilizers damage on the environment (Tahovska et al., 2013).

Different organic fertilizers, biofertilizers contain active or latent microorganism (bacteria and fungi) in order to increase nutrient availability for supporting plant growth and production (Wijebandara et al., 2009). Additionally, the application of biofertilizers also proved to maintain long term soil fertility (Punjee et al., 2020). Biofertilizers could be composed of single beneficial microorganisms like *Trichoderma* enriched biofertilizers or even the mix of several beneficial fertilizers such as Bio-N with active microorganisms. The success of a biofertilizer to boost plant growth is determined by the dosage and application method. The addition of biofertilizer Agrimeth + 50% of recommendation of NPK inorganic fertilizer increased soybean yield by 1.26 t/ha (100%) compared to the solely 100% NPK inorganic fertilizer (Purba, 2016). In the soil treated with organic fertilizers, the total C-organic increased by 26, 18, and 6% in the soil added with farm yard manure, paddy straw, and green manure, respectively (Ghosh et al., 2012).

The low biofertilizer adoption rate by farmers was due to relatively high biofertilizer price beside the low land area owned by farmers, rice planting pattern, farmer's educational level, biofertilizer quality, and response from the field officers (extension services). Therefore, it is necessary to improve field facilities, field extension service quality, decrease product price, and appreciate the farmers applying the bio fertilizer (Gama et al., 2016).

There is still limited study on applying biofertilizers on rice in Indonesia, therefore, this study aimed to evaluate the method of application and dosage of biofertilizers on rice growth and yield trait of lowland rice in West Java latosol soil of Indonesia.

Materials and methods

Place and time of study

The experiment was conducted at the green house of Indonesian Center for Agricultural Land Resources Research and Development (ICALRRD), Bogor Regency, West Java Province, Indonesia) during wet season from March to June 2018. It was located at 214.3 m above sea level (-6°34'47"S, 106°45'15.7"E. The mean minimum and maximum temperature inside the greenhouse in the morning were 22.3 °C and 38.8 °C, respectively. Meanwhile, the mean minimum and maximum temperature in the afternoon were 23.1 °C and 40.4 °C, respectively.

Research design

The experimental design used pots as rice plant containers that were arranged inside the greenhouse. The synthetic pots with a 50 cm diameter and 60 cm depth were filled with 10 kg of Latosol soil from Muara Garden, of Indonesian Center for Rice Research. All pots were irrigated with tap water and left for 20 days for organic material decomposition.

Pots were arranged in factorial randomized block design with two factors and three replications. The first factor was three biofertilizer application methods i.e. seed treatment, root dipping prior to transplanting, and sown at transplanting. The second factor was consisted of five levels of biofertilizer dosage: 0 g/pot as a control, 100 g/pot, 200 g/pot, 300 g/pot, and 400 g/pot. Total of 45 pots were observed in the present experiment.

Planting material was Inpari 32 that was categorized as new plant type rice variety from the Indonesian Center for Rice Research (ICRR) in Subang, West Java, Indonesia. The seed was continuously grown into seedling, and it was transplanted to the pot at 17 days after seedling (DAS). For dipping treatment, the seedling was removed from the soil and the root was dipped in biofertilizer prior to transplanting to the pot. For the sown treatment, the biofertilizer was sowed into the growing medium after the transplanting. The biofertilizer used in present experiment was obtained from the ICALRRD that composed of *Bradyrhizobium japonicum* and *Rhizobium japonicum*, *Azotobacter* sp, *Bacillus* sp and *Methylobacterium* sp in powder-shaped carrier material.

The Latosol soil that was collected from Muara experimental garden located at 287 m asl (S:6°36'54 S:106°47'29E"). Soil samplings were collected at the soil depth up to 20 cm below soil surface, in five spots for every location. The observed soil characteristics prior to the experiment were texture, pH, organic C, N total, available P, cation exchange capacity (CEC), K-dd, Ca-dd, Mg-dd, Na-dd, Al-dd, reduced Fe and fractionated P (Al, Ca and Fe). Soil sample was mixed to be a composite sample, and all mentioned analysis was carried out in the Soil Biology Laboratory, ICALRRD, following previous study methods (Kesaulya et al., 2015).

Data collection and analysis

The plants sampled for biomass and its partition to the root and crown part (both in fresh and dry forms) were observed from one plant in each treatment and three replications.

The observed variables were plant height, tiller number, panicle length, panicle number per hill, grains per panicle, percentage of filled grains and the weight of 1000 filled grains. The plant height and tiller number per hill were observed weekly starting from the 1st day after transplanting. The plant biomass and its partition to the root and crown part were observed both in fresh and dried form. The drying process was done in an oven at 60 °C for 2 days.

Data analysis

Data of various root and shoot growth, as well as yield parameters were subjected to analysis of variance (ANOVA). The mean comparison followed Duncan's Multiple Range Test with the Statistical Analysis System (SAS) 9.1.3 software version to delineate mean difference (Steel and Torrie, 1980).

Results and discussion

The analysis results of soil chemical properties conducted before experiment are shown in *Table 1*.

Table 1. Latosol soil chemical properties, Bogor, 2018

Soil characteristics	Value	Soil characteristics	Value
Sand (%)	13	K ₂ O HCl 25% (mg/100g)	20
Dust (%)	42	P ₂ O ₅ Olsen (ppm)	45
Clay (%)	45	K ₂ O Morgan (ppm)	183
pH H ₂ O	6.0	Ca-dd (cmol(+)/kg)*	8.92
pH KCl	4.7	Mg-dd (cmol(+)/kg)*	1.90
Al-dd (cmol(+)/kg)*	0	K-dd (cmol(+)/kg)*	0.26
H-dd (cmol(+)/kg)*	0.11	Na-dd dd (cmol(+)/kg)*	0.82
C-organic (%)	2.35	Total	11.9
N total (%)	0.31	Cation exchange capacity (cmol (+)/kg)	12.74
C/N ratio	8.0	Base saturation (%)	93
P ₂ O ₅ HCl25% (mg/100g)	191		

Note: *:The Al-dd, H-dd, Ca-dd, Mg-dd, K-dd and Na-dd are exchangeable values of Al, H, Ca, Mg, K and Na, respectively.

The Soil texture was dominated by fractions of clay (45%), dust (42%), and sand (13%). Total nutrient content of N (0.31%) and organic C (2.35%) levels were medium. The soil cation exchange capacity (CEC) of 12.74 cmol (+)/kg was low. The Ca-dd and Mg-dd values of values of 8.92 cmol (+)/kg and 1.90 cmol (+)/kg was categorized as medium. The available P₂O₅ (191 mg/100 g) was very high and K₂O (20 mg/100g) was low-medium. The available C/N ratio value of 8.0 (<15), which value is an indicator the soil fertility determining conditions. The higher the C/N ratio value, the slower the rate of soil organic matter decomposition by microorganisms. The N total in latosol soil was 0.31%. The P was extracted with 2 solvents i.e., HCl 25% (total P) and Olsen (available P). The total and available P solvent were 191 mg/100 g and 45 ppm, respectively. The K was extracted with 2 solvents i.e., HCl 25% (total K) and Morgan (available K). The dissolved total and Available K were 20 mg/100 g and 183 ppm, respectively. Both results showed that latosol soil had lower available P and total K. Meanwhile, cation exchange capacity (CEC) showed 12.74 cmol (+) kg.

Analysis of variance plant trait showed that the interaction between the application method and the difference in dose showed significant results for all characters except stem dry weight, panicle number/plant, panicle length, filled grains number/plant, unfilled grains number/plant and 1000 grain weight (Table 2). The diversity due to the biofertilizer application method was significant for all characters except plant height, panicle length, unfilled grains per plant, and 1000 grain weight. The difference in dose showed significant for all characters except plant height, tiller number, leaf fresh weight, panicle length, unfilled grains per plant and 1000 grain weight. The significant interaction illustrates that the application method treatment has a different effect on the difference in treatment dose. The plant height, number of tillers, number of panicles per plant, panicle length, 1000 grain weight, number of filled grains per panicle, filled grain weight, and total grain weight had the lowest coefficient of variability in various dosage treatments and biofertilizer application methods. Response at four biofertilizer dose in different application methods on plant height and tiller number at vegetative and generative stage is shown in Table 3.

Table 2. Variance analysis of observed rice traits, Bogor, 2018

Traits	Means square of			Coefficient of variation (%)
	Applied method (A)	Biofertilizer dosage (D)	A × D interaction	
Plant height (cm)	106.90*	13.89ns	59.93**	5.82
Tiller number	81.62**	81.62*	7.59**	15.07
Root fresh weight (g)	886.49**	126.33*	118.60*	24.30
Stem fresh weight (g)	2704.62**	300.70**	141.23*	19.42
Leaf fresh weight (g)	1141.42**	82133.30ns	142.87**	18.85
Root dry weight (g)	62.32**	18.65**	14.17*	35.24
Stem dry weight (g)	73.41**	26.82*	13.23ns	51.94
Leaf dry weight (g)	104.30**	9.27**	55.98*	15.42
Panicle number/plant	64.62**	6.28*	2.33ns	11.28
Panicle length (cm)	10.32ns	7.60ns	9.95ns	14.82
Filled grain number/plant	1858694.87**	439812.97*	212911.62ns	18.03
Unfilled grain number/plant	991766.69ns	1321759.48ns	989066.41ns	92.08
1000 grain weight (g)	7.63ns	2.19ns	3.50ns	10.78
Filled grain weight (g)	762.99**	184.55**	180.62**	13.09
Total grain weight (g)	775.80**	170.11**	153.64**	12.18

ns, * and **: non-significant, and significant at $P < 0.05$ and $P < 0.01$, respectively

Table 3. Mean performance of biofertilizer dose on plant height and tiller number at vegetative and generative stages in different application method, Bogor, 2018

Biofertilizer application	Traits					
	Plant height (cm)			Tiller Number		
	45 DAS	66 DAS	87 DAS	45 DAS	66 DAS	87 DAS
Seed treatment:						
0 g/plot (Control)	74.6abcd	110.5abc	113.1ab	19.3ab	20.0a	19.0a
100 g/plot	71.5d	106.2bc	110.8ab	17.0 abc	20.7a	18.3a
200 g/plot	80.6a	112.4ab	113.6ab	18.7ab	20.7a	17.7ab
300 g/plot	80.9a	111.3abc	112.8ab	18.3 ab	20.7a	16.7ab
400 g/plot	78.2abc	116.5a	119.3a	17.3 abc	17.7ab	17.0ab
Root dipping prior to planting:						
0 g/plot (Control)	73.5bcd	108.9abc	112.2ab	20.7a	22.7a	21.0a
100 g/plot	76.1abcd	107.8abc	111.6ab	18.0ab	19.7a	18.3a
200 g/plot	76.6abcd	110.6abc	117.1ab	16.0bc	21.3a	19.3a
300 g/plot	78.6abc	112.9ab	115.0ab	16.3bc	18.7ab	17.7a
400 g/plot	80.4a	113.9ab	117.5ab	17.3 abc	18.7ab	17.7ab
Application at planting time:						
0 g/plot (Control)	79.2ab	107.3abc	110.0ab	16.0bc	18.3ab	17.0ab
100 g/plot	78.3abc	116.1a	118.5a	10.7c	13.7bc	13.0bc
200 g/plot	70.7d	102.1c	105.b	7.3d	11.3c	13.0bc
300 g/plot	72.5cd	105.5bc	108.ab	6.3d	10.3c	11.0c
400 g/plot	60.3d	102.4c	106.8b	5.3d	15.2ab	17.7ab

Values with different letters in a column are significantly different according to Duncan's Multiple Range Test ($P \leq 0.05$)

The rice plant height was significantly affected by combination treatment of method and dosage of biofertilizer at all time observation series, except 87 days after sowing (DAS). The effect of biofertilizer dose of 200 g/pot, 300 g/pot at application at seed treatment and 400 g/pot at application at planting time had the highest plant height (at 80.6 cm, 80.9 cm and 80.4 cm) at the 45 DAS. The biofertilizer dose of 400 g/pot at application at seed treatment and 100 g/pot application at planting time showed the highest plant height of 116.5 cm and 116.1 cm, respectively at the 66 DAS. At the 87 DAS the biofertilizer dose of 400 g/pot at application at seed treatment and 100 g/pot at application at planting time showed the highest plant height of 119.3 cm and 118.5 cm, respectively. Treatment of biofertilizer dose on plant height was significant at 0.05 p-value in all three application methods at the 45, 66, and 87 DAS. Biofertilizer application effect was significant at 0.05 p-value on plant height response on vegetative and generative stages in all three application methods.

The tiller number correlated with grain yield and impacted rice growth development to total grain weight. The early development plant reached maximum of tiller number. In *Table 3*, the effect of biofertilizer on tiller number at vegetative and generative stage is presented. The treatment of biofertilizer dose of control had the largest tiller number and was significantly different with all dosages of biofertilizer and at all application methods at 45 days after sowing (DAS). The tiller number at 66 DAS was not significant at seed treatment and root dipping prior to planting but significantly different with application planting time method. At vegetative and generative stage all dose observation series of planting time application showed the lowest tiller number. The biofertilizer applied at planting time and at all dosages (100, 200, and 300 g/pot) gave lower tiller number compared to those applied at seed treatment as well as root dipping prior to planting application method. These results occurred at all vegetative and generative stages (45, 66, and 87 DAS).

Aside of growth variables, morphology traits variables i.e., root fresh weight, stem fresh weight, leaf fresh weight, root dry weight, stem dry weight, and leaf dry weight were also observed. There was significant variance in response to applied method and dosage of biofertilizer on rice plant fresh weight partitioned into root, stem and leaves (*Table 4*).

Biofertilizers are live microbes from the soil that provide certain nutrients for plants. The soil used was a silty clay textured soil with a low sand content. The bacteria from plant roots could increase the solubility of P in the soil as a *Pseudomonas fluorescens* (Yulistiana et al., 2020) and *Bacillus cereus* 11UJ for antifungal activity on rice plants (Suryadi et al., 2015). Through this study, we tried to show the response of method and dosage on morphology and yield component and correlation between treatment and rice plant characters. Regarding morphological aspects measured at vegetative and generative stage, the biofertilizers significantly improved rice plants height and growth by increasing soil nutrients such as nitrogen and phosphorus which influence rice seedlings growth (Isahak et al., 2012).

The effect of four treatment dose on root fresh weight response was significant in the dose 300 and 400 g/pot at application at planting time and not significantly different from control and all dose in three application methods. The highest root fresh weight was measured when 300 g of biofertilizer was applied by using root dipping method (38.7 g), while the lowest result was observed in 400 g of biofertilizer sown at planting (10.7 g).

The combination treatment of 400 g of biofertilizer sown at planting was determined as the lowest stem fresh weight (15.0 g), while the highest one was observed in no biofertilizer in seed treatment (63.0 g). The effect of the dose 300 and 400 g/pot application at planting time was significant in with control and all dose in three application methods. For the leaves part, the highest result was noticed at 300 g biofertilizer and no biofertilizer in seed treatment, while the lowest result was observed in 400 g of biofertilizer sown at planting (*Table 4*).

Table 4. Mean performance of biofertilizer dose on morphology traits at vegetative stage in different application method, Bogor, 2018

Biofertilizer application	Traits					
	RFW	SFW	LFW	RDW	SDW	LDW
Seed treatment:						
0 g/plot (Control)	34.3a	63.0a	42.3a	9.1a	10.6a	11.5a
100 g/plot	34.3a	54.0ab	40.3a	8.3a	10.5a	10.3ab
200 g/plot	29.7ab	50.7abc	36.3a	6.4ab	8.2ab	9.7ab
300 g/plot	35.0a	47.7bcd	42.3a	8.5a	7.3abc	9.9ab
400 g/plot	26.7ab	45.0bcd	41.7a	6.3ab	6.7abc	9.1bc
Root dipping prior planting:						
0 g/plot (Control)	34.3a	40.0bcd	34.0a	7.9a	5.2abc	8.3bcd
100 g/plot	32.0a	46.7bcd	36.0a	6.7ab	7.2abc	8.3bcd
200 g/plot	29.3ab	38.3cd	32.3ab	5.5abc	4.3abc	7.3cd
300 g/plot	38.7a	45.0bcd	40.0a	8.6a	6.5abc	8.8bc
400 g/plot	38.3a	45.7bcd	41.3a	9.6a	7.2abc	9.1bc
Application at planting time:						
0 g/plot (Control)	33.7a	41.3bcd	37.7a	9.1a	9.7a	8.3bcd
100 g/plot	26.0ab	33.7de	30.3ab	6.0ab	5.9abc	6.2de
200 g/plot	17.3bc	22.3ef	22.3bc	3.1bcd	2.6bc	4.5ef
300 g/plot	13.0c	16.0f	15.7c	1.5cd	1.8bc	3.2f
400 g/plot	10.7c	15.0f	13.7c	1.2d	1.2c	2.5f

Values with different letters in a column are significantly different according to Duncan's Multiple Range Test ($P \leq 0.05$). RFW: root fresh weight (g), SFW: stem fresh weight (g), LFW: leaf fresh weight (g), RDW: root dry weight (g), SDW: stem dry weight (g), LDW: leaf dry weight (g)

Similarly to fresh weight, the rice plant dry weight was also significantly affected by the interaction of method and dosage of biofertilizer. Rice plant was partitioned into three parts, i.e. root, stem and leaves. For root part, the heaviest dry weight was recorded in 400 g of biofertilizer by using root dipping prior to transplanting (9.6 g), while the lowest result was noted in 400 g of biofertilizer sown at planting (1.2 g).

In term of stem and leaves part, the lowest dry weight was noted in 400 g of biofertilizer sown at planting (1.2 g and 2.5 g), while the heaviest dry weight was found in no biofertilizer in seed treatment. The effect of biofertilizer dose of 300 g/pot had the highest root dry weight in the transplanting application method, while the lowest root dry weight was indicated by control in the dipping application method. Biofertilizer treatment dose of 300 g/pot had the highest root dry weight and was not significantly different from control dose in three application methods. Meanwhile, biofertilizer

treatment dose of 100 g/pot had the highest stem dry weight in application at planting time. The effect of biofertilizer dose of 400 g/pot had the highest leaf dry weight in planting time application method and was not significant from control dose.

There was significant result regarding the effect of interaction between method and dosage of biofertilizer on the yield variables, as indicated by the panicle number per hill, panicle length, filled grain number per hill, empty grain number per hill, filled grain weight and total grain weight (Table 5).

Table 5. Mean performance of yield component traits in response to different method and dosage of biofertilizer, Bogor, 2018

Biofertilizer application method	Dosage	Panicle number per hill	Panicle length (cm)	Filled grain number per hill	Empty grain number per hill	Filled grain weight	Total grain weight (g)
Seed treatment	Control	16.7a	21.8a	2198.7ab	1133.7b	48.8ab	54.1ab
	100 g	17.0a	21.3a	1811.7bcd	1000.3b	45.6ab	50.3ab
	200 g	15.7abc	21.5a	1890.7abcd	934.7b	41.8bc	46.1bc
	300 g	16.0ab	21.5a	1268.0d	1546.7ab	29.5d	36.8c
	400 g	15.3abc	22.7a	1827.7bcd	1112.7b	46.0ab	50.6ab
Root dipping prior to transplanting	Control	17.3a	21.4a	2286.3ab	972.3b	49.7ab	54.4ab
	100 g	16.3a	26.1a	2191.7ab	820.7b	49.7ab	54.0ab
	200 g	16.0ab	22.0a	2522.3ab	994.7b	52.3ab	57.7a
	300 g	16.3a	21.9a	2214.7a	3130.3a	55.7a	60.9a
	400 g	16.3a	22.5a	2471.0a	853.7b	54.2a	58.6a
Sown at planting	Control	15.3abc	27.3a	2195.3a	836.7b	54.1a	58.2a
	100 g	12.7cd	23.2a	1993.7ab	819.3b	45.1ab	49.3ab
	200 g	12.0d	21.7a	1394.3cd	659.0b	33.3cd	36.4c
	300 g	10.7d	21.6a	1346.3cd	676.0b	32.2cd	35.2c
	400 g	13.0bcd	23.4a	1444.7d	1223.7b	27.8d	36.0c

Means in the same column followed by the same letter were not significantly different at P = 0.05 using Duncan multiple range test (DMRT)

The highest number of panicles per hill was found in the combination treatment of root dipping prior to transplanting without any biofertilizer i.e., 17.3 panicle per hill that was significantly different to combination treatment of sown at planting with various biofertilizer dosage such as 100 g (12.7 panicle per hill), 200 g (12.0 panicle per hill), 300 g (10.7 panicle per hill) and 400 g (13 panicle per hill). In term of panicle length, all the combination treatments did not significantly differ from one to another. The highest number of filled grain per hill was observed in 400 g of biofertilizer that applied by using root dipping method prior to transplanting i.e., 2471 grain, while the lowest result was found in the 300 g biofertilizer applied in seed treatment i.e., 1268 grain. The biofertilizer application can increase grain yield (Simarmata et al., 2016; Marlina et al., 2014; Naher et al., 2016).

The highest number of empty grains per hill was noticed in the 200 g of biofertilizer applied by sown at planting method i.e., 659 grain, while the highest result was found in 300 g of biofertilizer applied by root dipping method prior to transplanting i.e., 3130.3 grain. The highest filled grain weight was observed in 300 g of biofertilizer

applied by root dipping technique while the lowest one was noted in the combination treatment of 400 g of biofertilizer sown at planting. In term of total grain weight, the highest result was found in 300 g of biofertilizer by using root dipping prior to transplanting while the lowest results were found in 400 g of biofertilizer sown at planting.

The rice growth and yields are significantly improved as the effect of bacterial inoculation of strain KKV2500-3 as biofertilizer (Banayo et al., 2012). Previous study reported that all tested biofertilizers have significant and positive effect for rice plant growth and yield (Simarmata et al., 2016). The biofertilizers addition that contained *Azospirillum sp*, *Rhizobium*, *Azotobacter sp.*, as active ingredients improved plant growth (Permanasari et al., 2014; Kartina et al., 2015; Kiuk et al., 2019).

Correlation coefficients between treat of rice plant characters are shown in *Table 6*.

Table 6. Yield and yield component correlation coefficients of studied traits, Bogor, 2018

	RFW	SFW	LFW	PH	TN	1000 GW	EGN	PN	PL	GNP	FGN	FGW	TGW
RFW	1	.814**	.818**	.324*	.225	-.086	.166	.470**	-.087	.505**	.286	.408**	.517**
SFW		1	.894**	.249	.327*	.093	.066	.556**	-.110	.464**	.217	.394**	.459**
LFW			1	.307*	.277	.153	.146	.572**	-.130	.537**	.263	.429**	.535**
PH				1	.060	.092	.041	.099	.137	.459**	.103	.473**	.432**
TN					1	.085	.127	.779**	-.038	.459**	-.244	.390**	.365*
1000 GW						1	.166	.079	-.209	.008	-.082	-.137	-.014
EGN							1	.252	.006	.200	-.112	.048	.148
PN								1	-.064	.584**	-.025	.484**	.518**
PL									1	.164	-.024	.080	.152
GNP										1	.450**	.849**	.983**
FGN											1	.401**	.596**
FGW												1	.845**
TGW													1

RFW: root fresh weight (g), SFW: stem fresh weight (g), LFW: leaf fresh weight (g), RDW: root dry weight (g), SDW: stem dry weight (g), LDW: leaf dry weight (g), PH: plant height, TN: tiller number, GW: Grain weight, EGN: Empty grain number per hill, PN: Panicle number per hill, PL: Panicle length, GNP: percent of filled grain number, FGN: Filled grain number, FGW: Filled grain weight, TGW: Total grain weight (g)

At the vegetative stage, the agronomic characters that had positive and significant relationship with total grain weight were root fresh weight ($r = 0.517$), stem fresh weight ($r = 0.459$), leaf fresh weight ($r = 0.535$), plant height ($r = 0.432$) and tiller number ($r = 0.365$). At the generative stage, the yield component that had positive and significant relationship with total grain weight were panicle number per hill ($r = 0.518$), percent of filled grain number ($r = 0.983$), filled grain number ($r = 0.596$) and filled grain weight ($r = 0.845$). The other characters, number of 1000 grain weight was inversely correlated with total grain weight, ($r = -0.148$) but not significantly. The number of empty grains per hill ($r = 0.152$), showed very weak correlation with grain yield. The results indicated positive correlations among traits tested in most of the cases. The highest correlation value ($r = 0.983$) was observed between total grain weight and percent of filled grain number while the lowest correlation value ($r = 0.008$) was observed between 1000 grain weight and percent of filled grain number.

The number of panicles per plant and the number of filled grains per panicle showed high significant value which could be used as selection criteria for rice yield improvement (Somchit et al., 2017).

Conclusion

The present study concluded that the method and dosage of biofertilizer application affected growth and yield of rice plant at Latosol soil. The root dipping method prior to transplanting with the biofertilizer showed the best results in terms of weigh and filled grain of rice. The dosage of biofertilizer and its integrated application could become alternative recommendation to increase rice grain yield on lowland or wetland at latosol soil. The total grain weight had positive and significant relationship with root fresh weight, stem fresh weight, leaf fresh weight, plant height, tiller number, panicle number per hill, percent of filled grain number, filled grain number, and filled grain weight. The highest value was found between total grain weight and percent of filled grain number.

Acknowledgements. The authors are very grateful for the Indonesian Center for Food Crops Research and Development (ICFORD), the Indonesian Agency for Agricultural Research and Development (IAARD) and Indonesian Soil Research Institute Laboratory which supported this research activity.

REFERENCES

- [1] Akhtar, N., Nazir, M. F., Rabnawaz, A., Mahmood, T., Safdar, M. E., Asif, M., Rehman, A. (2011): Estimation of heritability correlation and path coefficient analysis in fine grain rice (*Oryza sativa* L.). – J. Anim. Plant Sci. 21: 660-664.
- [2] Arnold, M. (1999): Feeding the Ten Billion: Plants and Population Growth. – In: Evans, L. T. (ed.). Experimental Agriculture. Cambridge University Press, Cambridge, pp. 507-516.
- [3] Banayo, N. P. M., Cruz, P. C. S., Aguilar, E. A., Badayos, R. B., Haefele, S. M. (2012): Evaluation of biofertilizers in irrigated rice: effects on grain yield at different fertilizer rates. – Agriculture 2: 73-86.
- [4] Bastida, F., Selevsek, I. F., Torres, T., Hernández, T., García, C. (2015): Soil restoration with organic amendments: linking cellular functionality and ecosystem processes. – Sci. Rep. 5: 1-12.
- [5] Gama, I. G. M., Oktaviani, Rifin, A. (2016): Analisis kepuasan petani terhadap penggunaan pupuk organik pada tanaman padi [Analysis of farmers' satisfaction on organic fertilizer application for rice farming]. – Jurnal Agro Ekonomi 34(2): 105-122.
- [6] Ghosh, S., Wilson, B., Ghoshal, S., Senapati, N., Mandal, B. (2012): Organic amendments influence soil quality and carbon sequestration in the Indo-Gangetic plains of India. – Agriculture, Ecosystems, and Environment 156: 134-141.
- [7] Hasan, M. J., Kulsum, A., Akter, A., Masuduzzaman, S. M., Ramesha, S. (2013): Genetic variability and character association for agronomic traits in hybrid rice (*Oryza sativa* L.). – Bangladesh J. Plant Breed. Genet. 24: 45-51.
- [8] Himmelstein, J. C., Maul, J. E., Everts, K. L. (2014): Impact of five cover crop green manures and actinovate on fusarium wilt of watermelon. – Plant Dis. 98: 965-72.
- [9] Isahak, A., Ahmad, A., Rosenani, A. B., Jamil, H. (2012): SRI rice crop establishment. – Trans. Malaysian Soc. Plant Physiol. 20: 20-20.

- [10] Jones, D. L., Rousk, J., Edwards-Jones, G., Luca, T. H. D., Murphy, D. V. (2012): Biochar-mediated changes in soil quality and plant growth in a three year field trial. – *Soil Biol. Biochem.* 45: 13-24.
- [11] Kartina, A. M., Nurmawalis, Fatmawaty, A. A., Firnia, D. (2015): Exploration of the potential of soil microbes in increasing soybean yield (*Glycine max*) on dry land. – *Jurnal Agroekotek* 7(2): 121-128 (in Indonesian).
- [12] Kesaulya, H., Baharuddin, Zakaria, B., Syaiful, S. A. (2015): Isolation and physiological characterization of PGPR from potato plant rhizosphere in medium land of Buru Island. – *Proc Food Sci* 3: 190-199. 10.1016/j.profoo.2015.01.021.
- [13] Khamwicheit, W., Sanongraj, W., Sanongraj, S. (2006): Study of environmental impacts before and after using the organic-chemical fertilizer in rice paddy fields. – *Walailak J. Sci. & Tech.* 3(1): 51-68.
- [14] Kiuk, Y., Rai, I. N., Kesumadewi, A. A. I. (2019): The effectiveness of indigenous endomycorrhiza and rhizobium inoculum in increasing nutrient uptake and yield of soybean in dry land. – *International Journal of Biosciences and Biotechnology* 7(1): 18-30.
- [15] Long-ping, Y. (2014): Development of hybrid rice to ensure food security. – *Rice Sci.* 21(1): 1-2.
- [16] Marlina, N., Meidelima, D., Asmawati, Aminah, I. S. (2018): Utilization of different fertilizer on the yield of two varieties of *Oryza sativa* in tidal lowland area. – *Biosaintifika* 10(3): 581-587.
- [17] Naher, U. A., Panhwar, O. A., Othman, R., Ismail, M. R., Berahim, J. (2016): Biofertilizer as a supplement of chemical fertilizer for yield maximization of rice. – *Journal of Agriculture Food and Development* 2: 16-22.
- [18] Nguyen, T. T., Fuentes, S., Marschner, P. (2013): Effect of incorporated or mulched compost on leaf nutrient concentrations and performance of *Vitis vinifera* cv. Merlot. – *J. Soil Sci. Plant Nutr.* 13: 485-97.
- [19] Nikmatul, K., Ratya, A., Nuhfil, H., Wahib, M. A. (2020): The analysis demand for animal source food in Indonesia: using quadratic almost ideal demand system. – *Business: Theory and Practice* 21(1): 427-43.
- [20] Noble, R., Coventry, E. (2005): Suppression of soil-borne plant diseases with composts: a review. – *Biocontrol Sci. Technol.* 15: 3-20.
- [21] Permanasasi, I., Irfan, M., Abizar. (2014): Soybean growth and yield (*Glycine max* (L.) Merrill) on application of rhizobium and Urea fertilizer in peat media. – *Jurnal Agroteknologi* 5(1): 29-34 (in Indonesian).
- [22] Punjee, P., Siripornadulsil, W., Siripornadulsil, S. (2020): Colonization by *Cupriavidus taiwanensis* KKKU2500-3 enhances the growth and yield of KDML105 jasmine rice. – *Walailak J. Sci. & Tech.* 17(1): 23-36.
- [23] Purba, R. (2016): Respons of soybean growth and yield on biological fertilizer in dry land Pandeglang, Banten. – *Jurnal Pengkajian and Pengembangan Teknologi Pertanian* 19(3): 253-261 (in Indonesian).
- [24] Rahmah, D. M., Rizal, F., Bunyamin, A. (2017): Dynamic model of corn production in Indonesia. – *J. Teknotan* 11: 30-40.
- [25] Simarmata, T., Turmuktini, T., Fitriatin, B. N., Setiawati, M. R. (2016): Application of bioameliorant and biofertilizers to increase the soil health and rice productivity. – *Hayati Journal of Biosciences* 23(4): 181-184.
- [26] Somchit, P., Sreewongchai, T., Sripichitt, P., Matthayathaworn, W., Uckarach, S., Keawsaard, Y., Worede, F. (2017): Genetic relationships of rice yield and yield components in RILs population derived from a cross between KDML105 and CH1 rice varieties. – *Walailak Journal of Science and Technology (WJST)* 14(12): 997-1004.
- [27] Steel, R. G. D., Torrie, J. H. (1980): *Principles and Procedures of Statistic*. – McGraw Hill, New York.

- [28] Suryadi, Y., Samudra, I. M., Priyatno, T. P., Susilowati, D. W., Lestari, P., Sutoro. (2015): Antifungal activity of *Bacillus cereus* 11UJ against *Rhizoctonia solani* and *Pyricularia oryzae*. – *Phytopathology Journal* 11(2): 35-42. DOI: 10.14692/jfi.11.2.35.
- [29] Tahovska, K., Kana, J., Barta, J., Oulehle, F., Richter, A., Santruckova, H. (2013): Microbial N immobilization is of great importance in acidified mountain spruce forest soils. – *Soil Biol Biochem* 59: 58-71. DOI: 10.1016/j.soilbio.2012.12.015.
- [30] Tejada, M., Hernandez, M. T., Garcia, C. (2009): Soil restoration using composted plant residues: effects on soil properties. – *Soil Tillage Res.* 102: 109-17.
- [31] Vessey, J. K. (2003): Plant growth promoting rhizobacteria as biofertilizers. – *Plant and Soil* 255: 571-586.
- [32] Wijebandara, D. M. D. I., Dasog, G. S., Patil, P. L., Hebbar, M. (2011): Effect of nutrient levels on Rice (*Oryza sativa* L.) under system of rice intensification (SRI) and traditional methods of cultivation. – *Journal of the Indian Society of Soil Science* 59(1): 67-73.
- [33] Yang, F., Tian, J., Fang, H., Gao, Y., Xu, M., Lou, Y., et al. (2019): Functional soil organic matter fractions, microbial community, and enzyme activities in a mollisol under 35 years manure and mineral fertilization. – *J. Plant Nutr. Soil Sc.* 19: 430-439. doi: 10.1007/s42729-019-00047-6.
- [34] Yulistiana, E., Widowati, H., Sutanto, A. (2020): Plant growth promoting rhizobacteria (PGPR) dari akar bambu apus (*Gigantochola apus*) meningkatkan pertumbuhan tanaman. – *Biolova* 1(1): 1-7.
- [35] Zaki, M. K., Komariah, K., Rahmat, A., Pujiasmanto, B. (2018): Organic amendment and fertilizer effect on soil chemical properties and yield of maize (*Zea mays* L.) in rainfed condition. – *Walailak Journal of Science and Technology* 17(1): 11-17. <https://doi.org/10.48048/wjst.2020.4590>.

THE PRINCIPLE OF SPACE-FOR-TIME SUBSTITUTION IN PREDICTING *BETULA* SPP. BIOMASS CHANGE RELATED TO CLIMATE SHIFTS

USOLTSEV, V. A.^{2,3} – LIN, H.^{1,4,5,6*} – SHOBAIRI, S. O. R.^{1*} – TSEPORDEY, I. S.³ – YE, Z.^{1,4,5,6} –
ANEES, S. A.⁷

¹*Research Center of Forestry Remote Sensing & Information Engineering, Central South
University of Forestry and Technology, Changsha 410004, China
(e-mail: Omidshobeyri214@gmail.com)*

²*Ural State Forest Engineering University, 620100 Yekaterinburg, Siberian tract, 37, Russia*

³*Botanical Garden of the Ural Branch of the Russian Academy of Sciences, 620144
Yekaterinburg, ul. 8 Marta, 202a, Russia*

⁴*Key Laboratory of Forestry Remote Sensing Based Big Data & Ecological Security for Hunan
Province, Changsha 410004, China
(e-mail: 1053460198@qq.com)*

⁵*Key Laboratory of State Forestry Administration on Forest Resources Management and
Monitoring in Southern Area, Changsha 410004, China*

⁶*Changsha Changchang Forestry Technology Consulting Co., Ltd., Changsha 410004, China
(e-mail: loyzer@163.com)*

⁷*Beijing Key Laboratory of Precision Forestry, Forestry College, Beijing Forestry University,
Beijing 100083, P. R. China
(e-mail: anees.shoaib@gmail.com)*

**Corresponding authors
e-mail: linhui@csuft.edu.cn; Omidshobeyri214@gmail.com*

(Received 19th Feb 2022; accepted 20th May 2022)

Abstract. Human society faces problems of a global scale today, as a result of which the priorities of environmental research are shifting to the macro level, and ecology has entered the era of "big data". The authors have created a database of 1,717 model trees of *Betula* spp. with measured indicators of diameter at breast height (DBH), tree height, age, and aboveground biomass growing in the territory of Eurasia. Regression models for aboveground biomass components are calculated, including the dendrological indices mentioned, and two climate indicators as independent variables. Based on the theory of space-for-time substitution, the obtained patterns of changes in aboveground biomass in the territorial climatic gradients of Eurasia are used to predict changes in biomass due to climate shifts. In accordance with the law of the limiting factor by Liebig, it is established that in sufficiently moisture-rich climatic zones, an increase in temperature by 1°C with a constant amount of precipitation causes an increase in biomass, and in water-deficient zones — its decrease. In warm climatic zones, a decrease in precipitation by 100 mm at a constant average January temperature causes a decrease in biomass, and in cold climatic zones — its increase.

Keywords: *hydrothermal gradients, biomass components, allometric models, mean January temperature, annual precipitation*

Introduction

Most of the environmental problems that human society faces today can only be solved on a global scale, and the priorities of environmental research are shifting to the macro level. Ecology has entered the era of "big data", "big science", and "big theories" (Niu et al., 2020). In the context of global climate shifts, understanding the development of forest ecosystems in terms of their ability to absorb atmospheric carbon is of increasing interest. In localized gradients of natural zones formed as a result of long-term vegetation evolution, changes in the biological productivity of vegetation cover occur (Kosanic et al., 2018; DeLeo et al., 2020).

These climatically determined spatial gradients of the productivity of trees and stands can be used to predict its changes in time under the influence of expected climate shifts based on the theory of space-for-time substitution. This term means using current patterns observed in spatial gradients to understand and model the same patterns in prospective time gradients that are currently unobservable (Blois et al., 2013). Methods based on space-for-time substitution are used in different fields; in particular, for the study of long-term nutrient cycling and plant succession (Johnson and Miyanishi, 2008) or for the prediction of biodiversity (Fitzpatrick et al., 2011), and there are encouraging results in this regard (Pickett, 1989; Blois et al., 2013).

A comparative analysis of the accuracy of various methods for determining the biological productivity of tree species has shown that models performed at a tree level give a lower error in estimating biomass per unit area compared to models performed at a stand level (Zeng et al., 2018). Allometric models of tree biomass are particularly relevant when assessing biomass in stands of mixed species composition (Shuman et al., 2011).

In Australian conditions ranging from dry ecotopes to tropical rainforests, simple allometric models of aboveground biomass for a combination of *Eucalyptus* and closely related species explained 84-95% of the total biomass variation. However, the effectiveness of the model improved only very slightly when such indicators as tree height, basic wood density, and climate variables were included in the model as independent variables. The loss of forecasting efficiency was <1% if generalized models were used instead of species-specific models. The use of generic multi-species models did not significantly distort the biomass forecast in 92% of the 53 tested species. In addition, the overall efficiency of predicting biomass at the stand level was 99%, and the average absolute prediction error was only 13% (Paul et al., 2016). In Tanzania's dry-to-wet conditions, the generic allometric model of aboveground biomass explained 95% of its variation. However, for a more accurate assessment of the biomass, it is recommended to calculate models taking into account the growing conditions (Mugasha et al., 2012).

The inclusion of territorial values of temperature and precipitation as additional independent variables in allometric models of tree biomass improved the accuracy of estimates and made it possible to predict changes in biomass in Chinese forests during climate shifts (Zeng et al., 2017; Fu et al., 2017). Warming by 1°C has been shown to increase the aboveground biomass of a tree by 0.9 % and to decrease the root biomass by 2.3%; an increase in precipitation by 100 mm causes the decrease in aboveground and underground biomass by 1.5 and 1.1%, respectively (Zeng et al., 2017). In these studies, the territorial differences in climate are extrapolated to the predicted climate shifts over time in accordance with the principle of space-for-time substitution (Zeng et al., 2017; Fu et al., 2017). However, such models are presented as single studies on regional levels (Lei et al., 2016; Forrester et al., 2017; Zeng et al., 2017; Fu et al., 2017).

It is known that the production of plant biomass is limited by a factor that is in minimum or excess in relation to its needs according to the principle of limiting factor (Liebig, 1840). At the polar limit of birch distribution in Siberia, the limiting factor is temperature, but as we move south, the heat deficit decreases and the role of moisture deficiency increases. At the same time, the change of the limiting factor occurs in the subzone of the middle taiga (Fonti, 2020).

In this study, we intend to: (a) identify the most efficient structure of the allometric model of biomass on the example of *Betula* spp. in Eurasia, (b) identify how the aboveground biomass of trees is related not only to the dendrometric indicators of trees, but also to the territorial average values of temperatures and precipitation at a transcontinental level, (c) to establish whether the effect of the law of the limiting factor is manifested when modeling changes in the biomass of trees of forest-forming species on the territory of Eurasia in relation to geographically determined changes in temperatures and precipitation; and (d) to show to what extent the constructed climate-conditioned models of biomass, sensitive to temperature and precipitation in territorial gradients, can be used to predict its changes in temporal gradients based on the principle of space-time substitution.

The genus *Betula* spp. is included in *Betulaceae* family. This family has 120-150 species (Grimm and Renner, 2013). Majority of species are present in northern climatic zones and have a wide natural distribution area on the Eurasian continent, ranging from the Atlantic to Pacific coasts. Birch is among ten common species in Russia. There are several species in the common birch category from the section *Albae* Rgl.: silver birch (*B. pendula* Roth.), downy birch (*B. pubescens* Ehrh.), mountain birch (*B. tortuosa* Ldb.), Japanese white birch or Siberian silver birch (*B. platyphylla* Suk.) (Hynynen et al., 2009).

Materials and Methods

To solve these problems, the database on the biomass of forest-forming species of Eurasia in the amount of 15,200 trees (Usoltsev, 2020) is used. From it, 1,717 sample trees of *Betula* spp. were selected with measured values of the DBH, tree age and height and components of aboveground biomass (Table 1). The genus *Betula* spp. is represented by some vicarage species, mainly *B. pubescens* Ehrh., *B. pendula* Roth, and in smaller numbers by *B. maximowicziana* Regel, *B. ermanii* Cham., *B. platyphylla* Suk., *B. costata* Trautv., and *B. dahurica* Pall.).

Table 1. Statistics of sample trees of *Betula* spp.

Designation of statistics ^(a)	Indices analyzed ^(b)						
	<i>A</i>	<i>D</i>	<i>H</i>	<i>Pf</i>	<i>Pb</i>	<i>Ps</i>	<i>Pa</i>
Mean	40	13.4	14.6	2.56	15.6	87.9	106.2
Min	3	0.2	0.7	0.003	0.003	0.02	0.03
Max	195	48.0	34.5	29.5	230.2	739.5	950.2
SD	21.8	8.1	6.2	3.3	27.7	113.9	141.3
CV, %	54.5	60.0	42.5	129.6	177.7	129.6	133.1
n	1716.0	1716.0	1715.0	1713.0	1715.0	1717.0	1712.0

^(a) Mean, Min and Max are the average, minimum, and maximum values, respectively; SD is standard deviation; CV is coefficient of variation; n is the number of observations.

^(b) *A* is tree age, yrs; *D* is stem diameter at breast height (DBH), cm; *H* is tree height, m; *Pf*, *Pb*, *Ps* and *Pa* are the biomass of foliage, branches, stem with bark and aboveground biomass in dry condition, kg

The joint analysis of different species is caused by the impossibility of growing the same tree species throughout Eurasia, as a result of which their areas within the genus are confined to certain ecoregions. When entering the transcontinental level of research, we are faced with the obvious fact that no species grows throughout the continent, precisely because of regional differences in climate. Moving from refugia under the influence of geological processes and climate changes, a particular species adapted to changing environmental conditions, forming a series of vicariant species within a genus (Tolmachev, 1962). In other words, differences in traits between species evolved as adaptations to different climates (Laughlin et al., 2021). This gives grounds for analyzing the response of birch trees to changes in climatic characteristics to create one climate-dependent unity within the entire genus *Betula* spp., since the differences in the ecophysiological traits of different species, for example, *B. pendula* vs. *B. platyphylla* vs. *B. costata* are derived from regional climatic features.

The available data of the geographical coordinates of the sample trees are plotted on the maps of the average January temperature (https://store.mapsofworld.com/image/cache/data/map_2014/currents-and-temperature-jan-enlarge-900x700.jpg) and the average annual precipitation (<http://www.mapmost.com/world-precipitation-map/free-world-precipitation-map/>) (World Weather Maps, 2007) (Fig. 1) and are combined with dendrometric indicators of sample trees. In our case, the schematic map of the isolines of mean January temperature, rather than that of the mean annual temperature, was used. With an inter-annual time step, the predominant influence of summer temperature is quite normal (Zubairov et al., 2018). However, against the background of long-term climatic shifts for decades, the prevailing influence is acquired by winter temperatures (Bijak, 2010; Toromani and Bojaxhi, 2010; Morley et al., 2016). In terms of regression analysis, a weak temporal trend of summer temperatures compared to a steep trend of winter ones, means a smaller regression slope and a worse ratio of residual variance to the total variance explained by this regression. Obviously, taking the mean winter temperature as one of the independent variables, we get a more reliable dependence having the higher predictive ability.

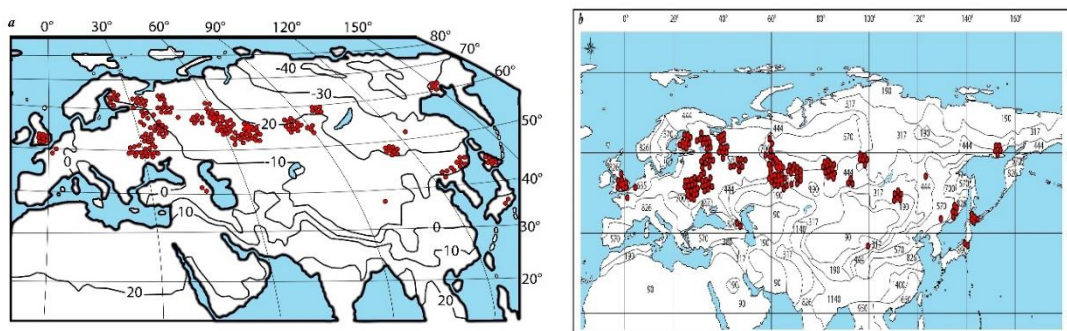


Figure 1. Allocation of the empirical data of 1,717 sample trees on the maps of the average January temperature, °C (a) and average annual precipitation, mm (b) (World Weather Maps, 2007)

The choice of winter temperature also has a bioecological background. It is known that each environmental factor has an optimal range of its effects in which it is most effective and beyond which this effect decreases or even has an overwhelming result (Tranquillini, 1955; Burian, 1970; Liepa, 1980; Cárdenas-Pérez et al., 2022). In our case, the winter

temperature, in particular, the long-term temperature of January, has the most effective effect on the tree biomass of forests.

The above-mentioned, previously published models of tree and stand biomass sensitive to climate change were performed at the regional levels and were adapted to regional climatic features (Lei et al., 2016; Forrester et al., 2017; Fu et al., 2017; Zeng et al., 2017). Due to regional allocation, none of them can be extrapolated to the transcontinental level. They give the visions of the local trends of biomass in connection with the local climate and may even be opposite in sign. Therefore, their totality cannot give the performance of what awaits biota and forest cover in particular at the global level.

Our database, which provides initial information on the biomass of trees of forest-forming species of Eurasia (Usoltsev, 2020), makes it possible to show, if not global, then at least trans-continental expectations of upcoming changes in tree biomass under the influence of possible climatic shifts at the continental level. Today we have databases on tree biomass for Eurasia (Falster et al., 2015; Schepaschenko et al., 2017; Usoltsev, 2020), which have many disadvantages, which limits the possibilities of developing empirical predictive models based on them. In particular, due to the lack of data for some regions, these gaps have to be covered by an interpolation technique in the modeling of biomass.

We also mean the limited explanatory possibilities of multiple regression analysis, as a result of which we consistently extract from the total variance of biomass, first of all, the variance that is most explained by the main dendrometric and climatic variables. The residual variance includes both unaccounted factors as well as methodological uncertainties and trivial calculation errors of the harvest data. Naturally, it is impossible to extract and explain the variability of biomass from such a residual dispersion, due, for example, to the unevenness of precipitation by month during the year. As a consequence, we cannot use such models to predict the impact of extreme events (droughts, floods, etc.) on the biomass of trees. Process-based models seem to be more suitable for this purpose (Sato et al., 2010).

Usually, when analyzing the productivity of trees or stands, the influence of a single factor is estimated: either temperature or precipitation (Lieth, 1975; Reich et al., 2014; Russell et al., 2015; Fonti, 2020; Frauendorf et al., 2020; Devi et al., 2020). Estimating biomass by a single climatic factor can lead to contradictory results, since the combined effect of temperatures and precipitation is not taken into account. The presence of the Eurasian database in the maximum ranges of temperatures and precipitation allowed us to assess the combined impact of temperatures and precipitation on the biomass of trees.

The ecologists who are engaged in extracting a climatic signal from the chronologies of tree rings may ask how the temperature of January affects the biomass of a tree when the tree is in winter "hibernation" and why the temperature of June or July, characteristic of the period of active growth, is not accepted? In the context of our research, there is no answer to such the question, since it indicates a substitution of the concept, in this case, the concept of temperature. We install the position of the sample plots with geographically distributed biomass data on the map of geographically distributed winter temperatures (*Fig. 1*) having the aim their conjugate analysis. The current territorial (geographical) distribution of temperatures and precipitation has been formed over millennia, and at the same time, the territorial biodiversity of vegetation cover has been formed in accordance with it (Mohan et al., 2009), including the division of a particular genus into species (Tolmachev, 1962), and this biodiversity determines the structural and functional traits of plant biomass. Since the average January and average annual temperatures are correlated to some extent, the named conjugation of the biomass could

be performed both with the average annual and with the average January temperature. We chose the latter for the above reasons.

The change of the limiting factor for birch growth as it moves from north to south was mentioned above (Fonti, 2020). In this phenomenon we did not mean climatic indicators in the form of geographically distributed temperatures and precipitation, as in our study, but meteorological data of temperatures and precipitation of specific years and months. Accordingly, our analysis of the factors limiting biomass does not include January temperature meteorological data or average annual precipitation meteorological data, but long-term geographically distributed temperatures and precipitation, the impact of which on biomass is extrapolated to the assumed temporal gradients of temperatures and precipitation through space-for-time substitution. However, there is the other opinion that is an alternative to the principle of a single limiting factor. Drawing an analogy with the distribution of resources in the economy, A. Bloom and co-authors (1985) believe that plants distribute the resources available for growth in such a way that the limiting effect is approximately the same from all resources, and not from the only one of them.

Optimization of the allometric model structure

Based on the analysis of literature sources, the following variants of the allometric model are subjected to comparative analysis:

$$\ln Pi = a_0 + a_1 \ln D \quad (\text{Eq.1})$$

$$\ln Pi = a_0 + a_1 \ln D + a_2 \ln H \quad (\text{Eq.2})$$

$$\ln Pi = a_0 + a_1 \ln(D^2 H) \quad (\text{Eq.3})$$

$$\ln Pi = a_0 + a_1 \ln A + a_2 \ln D + a_3 \ln H \quad (\text{Eq.4})$$

$$\ln Pi = a_0 + a_1 \ln D + a_2 \ln H + a_3 (\ln D)(\ln H) \quad (\text{Eq.5})$$

$$\ln Pi = a_0 + a_1 \ln A + a_2 \ln D + a_3 \ln H + a_4 (\ln D)(\ln H) \quad (\text{Eq.6})$$

where P_i is biomass of i -th component of a tree, kg.

Results and Discussion

The initial data on the biomass of trees, the characteristics of which are given in *Table 1*, are processed by the method of multiple regression analysis according to the structure of *models (1)-(6)*. The results of the regression analysis are summarized in *Table 2*. The biomass models shown in *Table 2* are valid within the actual ranges of age, stem diameter, and tree height shown in *Table 1*.

Based on the results of comparative regression analysis, the explanatory power of models (5) and (6) for all components of biomass is higher than that of models (1), (2), (3) and (4). The age of a tree, although as an important independent variable in explaining the variability of tree biomass (Qiu et al., 2018), was not statistically significant in this case at $p < 0.05$. In addition, this dendrometric indicator is difficult to measure in tree inventory on large areas compared to the stem diameter and tree height. Therefore, we have involved the model (5) in the procedure of further analysis.

Table 2. Results of calculation of equations (1)-(6)

	Dependent variables				Model number
	lnPf	lnPb	lnPs	lnPa	
a ₀ ^(a)	-4.0299	-4.2627	-2.3081	-2.0307	(1)
lnD	1.8216	2.4603	2.4248	2.3929	
adjR ^{2(b)}	0.822	0.902	0.962	0.964	
SE	0.627	0.597	0.358	0.343	
a ₀ ^(a)	-4.0957	-4.4841	-3.5953	-3.1239	
lnD	1.7809	2.3215	1.6368	1.7314	
lnH	0.0629 ^(d)	0.2146	1.2170	1.0217	
adjR ^{2(b)}	0.822	0.903	0.988	0.983	
SE	0.626	0.594	0.202	0.236	
a ₀ ^(a)	-4.6581	-5.1000	-3.3270	-3.0184	(3)
ln(D ² H)	0.6795	0.9171	0.9216	0.9061	
adjR ^{2(b)}	0.806	0.889	0.985	0.981	
SE	0.661	0.639	0.221	0.246	
a ₀ ^(a)	-3.8661	-4.6041	-3.7678	-3.2592	(4)
lnA	-0.1366	0.0684 ^(d)	0.0996	0.0780	
lnD	1.8318	2.2901	1.5956	1.6981	
lnH	0.1133 ^(d)	0.1963	1.1851	0.9978	
adjR ^{2(b)}	0.823	0.903	0.988	0.983	
SE	0.624	0.594	0.198	0.234	
a ₀ ^(a)	-3.1241	-2.8226	-2.7602	-2.0973	(5)
lnD	1.2015	1.3250	1.1392	1.1196	
lnH	-0.3935	-0.5683	0.8256	0.5406	
(lnD)(lnH)	0.2429	0.4168	0.2085	0.2560	
adjR ^{2(b)}	0.830	0.918	0.992	0.989	
SE	0.611	0.547	0.165	0.188	
a ₀ ^(a)	-2.6896	-2.7559	-2.8711	-2.1360	(6)
lnA	-0.2015	-0.0320 ^(d)	0.0503	0.0172 ^(d)	
lnD	1.2223	1.3248	1.1317	1.1154	
lnH	-0.3656	-0.5600	0.8211	0.5407	
(lnD)(lnH)	0.2665	0.4206	0.2027	0.2541	
adjR ^{2(b)}	0.833	0.918	0.992	0.989	
SE	0.606	0.547	0.164	0.188	

^(a)The intercept hereafter is adjusted according to logarithmic transformation by Baskerville (1972);
^(b)adjR² is the coefficient of determination, adjusted for the number of variables; ^(c)SE is the standard error of the equation; ^(d) these regression coefficients are not reliable at the level of p = 0.05

Designing the model of aboveground biomass sensitive to climate variables

We propose a model of aboveground biomass at the continental level, combining dendrometric indicators of trees (model (5)) and climate variables as independent variables:

$$\ln P_i = a_0 + a_1(\ln D) + a_2(\ln H) + a_3(\ln D)(\ln H) + a_4[\ln(T+50)] + a_5(\ln PR) + a_6[\ln(T+50)] \cdot (\ln PR) \quad (\text{Eq.7})$$

where T is mean January temperature, °C; PR is mean annual precipitation, mm; $[\ln(T+40)] \cdot (\ln PR)$ is a combined variable that characterizes the common effect of temperature and precipitation. The regression coefficients for all biomass components in model (7) are significant at $p < 0.001$. Since the mean January temperature in high latitudes has a negative value, for its logarithmic transformation in model (7), it is modified as $(T+50)$. The results of the calculation of the models (7) are shown in *Table 3*.

Table 3. Model calculation results (7)

$\ln(Y)^{(1)}$	$a_0^{(2)}$	$\ln D$	$\ln H$	$\frac{(\ln D) \times (\ln H)}{(\ln H)}$	$\ln(T+50)$	$\ln PR$	$\frac{[\ln(T+50)] \times (\ln PR)}{(\ln PR)}$	adjR ²⁽⁴⁾	SE ⁽⁵⁾
$\ln(P_f)$	28.7262	1.2510	-0.4746	0.2452	-7.7748	-5.3644	1.3163	0.847	0.580
$\ln(P_b)$	95.4290	1.3795	-0.6457	0.4143	-27.4814	-15.7630	4.4051	0.925	0.522
$\ln(P_s)$	17.8565	1.1561	0.7954	0.2090	-5.7867	-3.3436	0.9385	0.992	0.162
$\ln(P_a)$	30.6312	1.1461	0.4957	0.2563	-9.1593	-5.3031	1.4839	0.990	0.181

The geometric interpretation of models (7) is obtained by substituting in (7) the average values of D and H taken from *Table 1* (*Figure 2*). As we can see in *Figure 2*, the dependence of all components of the aboveground biomass of equal-sized birch trees on temperatures and precipitation is described by 3D-surfaces of a propeller-shaped form. In cold regions, as precipitation increases, the biomass decreases, but as it moves to warm regions, it is characterized by the opposite trend. As the temperature increases in humid regions, the biomass increases, but as the transition to dry conditions begins to decrease.

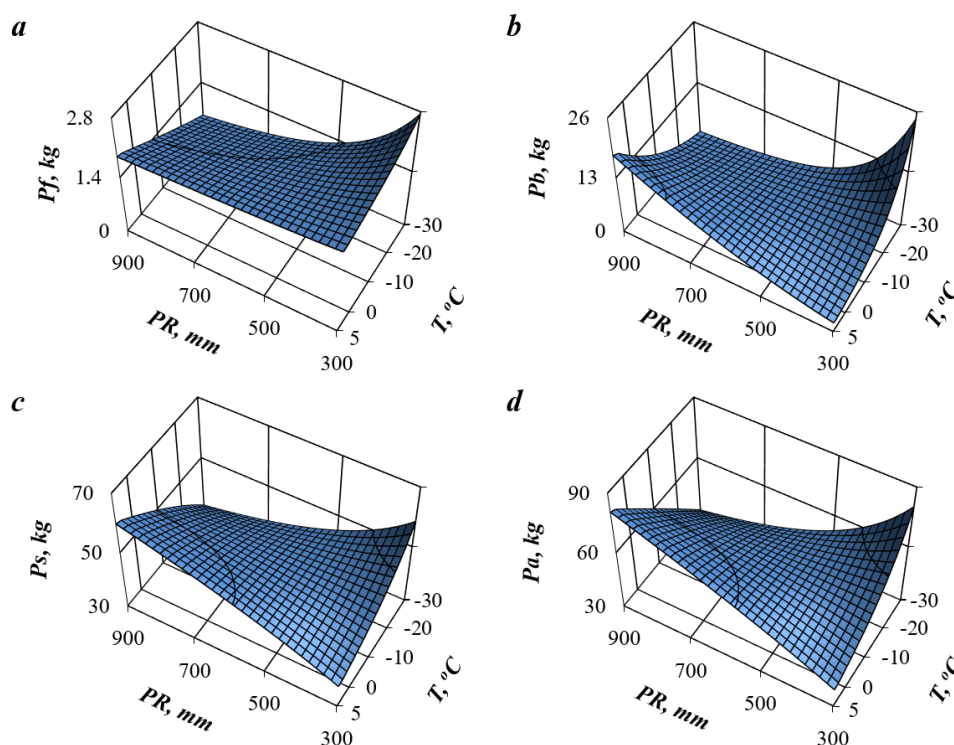


Figure 2. Calculated changes in aboveground birch biomass of trees ($D=13.4$ cm; $H=14.6$ m) according to the model (7) due to the mean January temperature (T) and mean annual precipitation (PR). The designations of the components of the biomass hereafter: a, b, c, d are foliage, branches, stems over bark, and aboveground biomass respectively, kg

Predicting *Betula* spp. biomass change related to climate shifts on the base of the principle of space-for-time substitution

Let us consider the described patterns in a different perspective, implementing the concept of space-time substitution and the principle "What will be happened, if...?". In other words, we will find out how the tree biomass will react if, with constant territorial temperature and precipitation gradients, we assume a temporal temperature change of 1°C or annual precipitation of 100 mm. Taking the first derivatives of the two-factor surfaces presented in *Figure 2*, we obtained the regularities of changes in the biomass at the given increments of temperature and precipitation.

Figure 3 shows the change in tree biomass (Δ , %) with a temperature increase by 1°C in different climatic zones (territorial gradients) characterized by different temperature and precipitation ratios. It is assumed that precipitation changes only geographically, and the temperature as a result of the expected climate change increases by 1°C at different territorial temperature levels, designated as $-30\Delta\dots+5\Delta$. For all components of biomass, a general pattern of the Eurasian scale is obtained: in moisture-rich climatic zones, an increase in temperature with a constant amount of precipitation causes its increase (red areas of the surfaces in *Figure 3*), and in the moisture-deficit zones its decrease (blue areas of the surfaces in *Figure 3*).

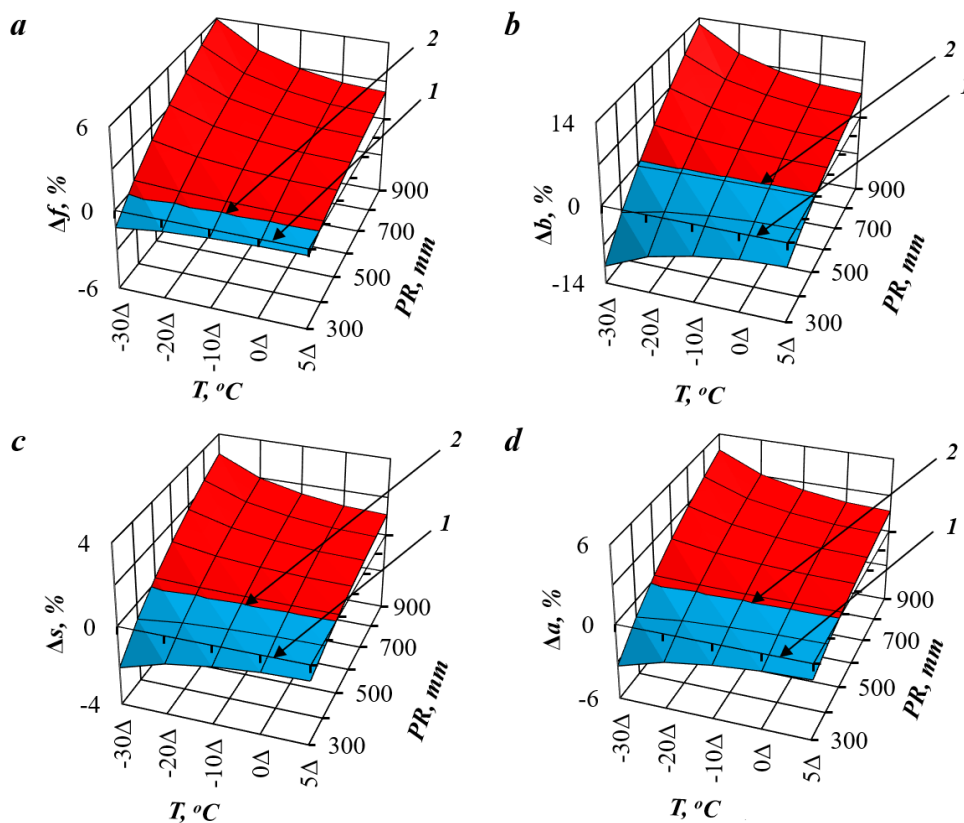


Figure 3. Possible changes in the biomass of trees with the increase in January temperature by 1°C due to the expected climate change at different territorial levels of temperature and precipitation. 1 – the plane corresponding to the zero change in biomass at the expected temperature increase by 1°C; 2 – the line of differentiation of positive and negative changes in biomass at the expected temperature increase by 1°C

Figure 4 shows the change in tree biomass (Δ , %) with the decrease in annual precipitation by 100 mm in different climatic zones. At the same time, it is assumed that the January temperature changes only geographically, and precipitation as a result of climate change decreases by 100 mm at different territorial precipitation levels, designated as -400Δ ... -900Δ . A general transcontinental pattern has been established for the biomass of branches, stem, and aboveground: in warm climatic zones, a decrease in precipitation by 100 mm at a constant average January temperature causes a decrease in the biomass of stems and aboveground (blue area of surfaces), and in cold climatic zones – its increase (red area of surfaces) (Figure 4b,c,d). For foliage biomass, the entire 3D surface is represented by the red zone (Figure 4a), which means that when precipitation decreases by 100 mm in all climatic zones, the foliage biomass increases. But during the transition from cold to warm climatic conditions, the value of this increase decreases, and in the warmest zones (January temperature is 5°C), this reduction in the increment of biomass approaches zero, but does not go to "minus". Thus, the patterns of changes in the biomass of foliage with shifts in temperature and precipitation are somewhat different from the changes in the biomass of other components. The reason may be a more pronounced residual variance in the foliage biomass model due to the fact that interspecific variation in foliage biomass is due not only to climatic factors, but also to the environmental "noise" unaccounted.

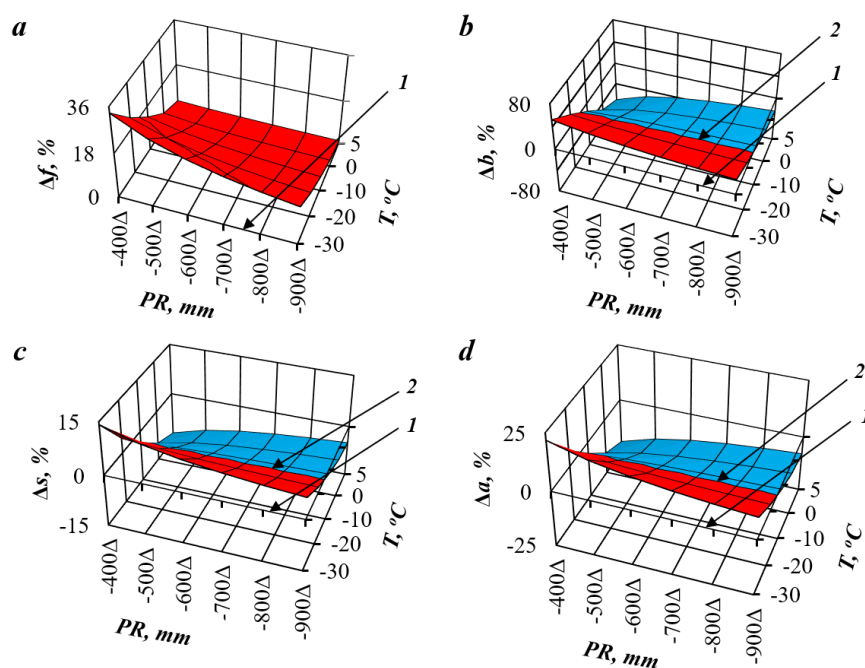


Figure 4. Possible changes in the biomass of trees with a decrease in precipitation due to the expected climate change at different territorial levels of temperature and precipitation. 1 – the plane corresponding to the zero change in biomass with the expected decrease in precipitation by 100 mm; 2 – the line of differentiation of positive (red) and negative (blue) changes in biomass with the expected decrease in precipitation by 100 mm

Thus, both the lack of heat and moisture, and their excess, are manifested as factors limiting the biomass of trees of the genus *Betula* sp. at the transcontinental level.

Today, the results of modeling the responses of forest biomass to global changes in temperature and precipitation are contradictory and characterized by uncertainty in the forecasts of climate-driven dynamics of forest cover (Marcolla et al., 2020). One of the most significant is the contradiction of two possible scenarios. On the one hand, an increase in primary production due to the potential enrichment of the atmosphere with CO₂ and its reclamation effect on vegetation. On the other hand, its decrease due to loss of stability with a sharp reduction in the adaptive time lag (Santini et al., 2014; Sperry et al., 2019; Berdugo et al., 2020). The largest reserves of biomass in the zone of moderately moist forests, depersonalized by species composition and morphological structure of stands, were found at moderately low temperatures and moderately abundant precipitation (Keith et al., 2009). Positive dependences of aboveground biomass on average annual precipitation have been established for the total American continent from Canada in the north to the south of Chile. With the average annual temperature, the relationship of this indicator in humid tropical forests is positive, and in forests of excessive moisture is negative, but statistically insignificant. In general, climatic indicators explain the weak, and in many cases statistically insignificant share of the variability of the biomass of stands (Stegen et al., 2011). In some habitats, elevated temperatures can lead to stress from water deficiency and, consequently, to a decrease in biomass (Wilmking et al., 2004).

We cannot compare the results obtained by us with the available results of biomass forecasting based on simulation models. According to their forecasts, changes in the carbon pool by the end of this century range from -106 to +201 Pg (billion tons). Various scenarios of the Dynamic Global Vegetation Model (LPJ-DGVM) show significant uncertainty about the future carbon storage in terrestrial biota. Thus, even the sign of a change in the carbon pool on the planet is reliably unknown, and we do not fully know whether the biota of the planet is a source or storage of carbon (Schaphoff et al., 2006).

Our results on changes in aboveground tree biomass in two climatic gradients confirm the patterns previously established by Russian researchers at the local and regional levels. A similar pattern was observed earlier at the local level in the swamp forests of the Tomsk region in Siberia, when at maximum amounts of temperatures above 10 °C, equal to 2200 °C, with an increase in precipitation from 400 to 600 mm, the radial growth of stems increases by 30-50%, and at minimum amounts of temperatures (1600 °C) with an increase in precipitation in the same range, the radial growth decreases by 4-9%. Accordingly, at a precipitation level of 400 mm with an increase in the sum of temperatures from 1600 to 2200 °C, the radial growth decreases by 14-20%, and at a precipitation level of 600 mm in the same temperature range, it increases by 14-33% (Glebov and Litvinenko, 1976). According to the results obtained by Molchanov (1976), in the conditions of the North of Eurasia, the air temperature has the greatest influence on the growth of the annual ring, and in the conditions of the southern forest-steppe, precipitation plays the dominant role. A similar propeller-like pattern, sensitive to climate change, was previously identified for the biomass of pine stands (Usoltsev et al., 2019).

These patterns correspond to Liebig's principle of limiting factors (Liebig, 1840). However, Liebig's law of a limiting factor works well in stationary conditions. With rapid changes in limiting factors (for example, air temperature or precipitation), forest ecosystems are in a transitional (non-stationary) state, in which some factors that have not yet been significant may come to the fore, and the final result may be determined by other limiting factors (Odum, 1971).

We used the existing changes in the tree biomass in the territorial climate gradients to predict its possible changes in the assumed temporal gradients of temperature and precipitation. However, the fundamental assumption that the spatial relationship between climate and biomass can be used to predict the temporal trajectories of biological productivity in a changing climate remains largely untested (Veloz et al., 2012). The success of applying the theory of space-for-time substitution in plant ecology depends on the extent to which the ecological conditions that determine the properties of plants in territorial gradients correspond to the future ecological conditions that determine the properties of plants in the temporal gradient (Bjorkman et al., 2018; Bergstrom et al., 2021). Nevertheless, when there is no other way to study ecosystem processes in perspective, the method of spatial-for-time substitution is still quite an acceptable alternative.

Conclusion

On the basis of the database on the aboveground biomass of 1,717 *Betula* spp. trees growing on the territory of Eurasia, formed by the authors, a regression model was developed that includes both denrometric indicators of trees and territorial long-term data on temperature and precipitation as independent variables. The obtained trans-Eurasian regularities are used to predict changes in biomass due to climate shifts based on the theory of space-for-time substitution. The regularities of the Eurasian scale are obtained: in sufficiently moisture-rich climatic zones, an increase in temperature by 1°C with a constant amount of precipitation causes an increase in aboveground biomass, and in water-deficient zones its decrease; in warm climatic zones, a decrease in precipitation by 100 mm with a constant average January temperature causes a decrease in aboveground biomass, and in cold climatic zones its increase.

REFERENCES

- [1] Baskerville, G. L. (1972): Use of logarithmic regression in the estimation of plant biomass. – Canadian Journal of Forest Research 2: 49-53.
- [2] Berdugo, M., Delgado-Baquerizo, M., Soliveres, S., Hernández-Clemente, R., Zhao, Y., Gaitán, J. J., Gross, N., Saiz, H., Maire, V., Lehman, A., Rillig, M. C., Solé, R. V., Maestre, F. T. (2020): Global ecosystem thresholds driven by aridity. – Science 367(6479): 787-790.
- [3] Bergstrom, D. M., Wienecke, B. C., van den Hoff, J., Hughes, L., Lindenmayer, D. B., Ainsworth, T. D., Baker, C. M., Bland, L., Bowman, D. M. J. S., Brooks, S. T., Canadell, J. G., Constable, A. J., Dafforn, K. A., Depledge, M. H., Dickson, C. R., Duke, N. C., Helmstedt, K. J., Holz, A., Johnson, C. R., McGeoch, M. A., Melbourne-Thomas, J., Morgain, R., Nicholson, E., Prober, S. M., Raymond, B., Ritchie, E. G., Robinson, S. A., Ruthrof, K. X., Setterfield, S. A., Sgrò, C. M., Stark, J. S., Travers, T., Trebilco, R., Ward, D. F. L., Wardle, G. M., Williams, K. J., Zylstra, P. J., Shaw, J. D. (2021): Combating ecosystem collapse from the tropics to the Antarctic. – Global Change Biology 27: 1-12.
- [4] Bijak, S. (2010): Tree-ring chronology of silver fir and its dependence on climate of the Kaszubskie Lakeland (Northern Poland). – Geochronometria 35: 91-94.
- [5] Bjorkman, A. D., Myers-Smith, I. H., Elmendorf, S. C., Normand, S., Rüger, N., Beck, P. S. A., Blach-Overgaard, A., Blok, D., Cornelissen, J. H. C., Forbes, B. C., Georges, D., Goetz, S. J., Guay, K. C., Henry, G. H. R., RisLambers, J. H., Hollister, R. D., Karger, D. N., Kattge, J., Manning, P., Prevéy, J. S., Rixen, C., Schaepman-Strub, G., Thomas, H. J. D., Vellend, M., Wilmking, M., Wipf, S., Carbognani, M., Hermanutz, L., Lévesque, E.,

- Molau, U., Petraglia, A., Soudzilovskaia, N. A., Spasojevic, M. J., Tomaselli, M., Vowles, T., Alatalo, J. M., Alexander, H. D., Anadon-Rosell, A., Angers-Blondin, S., Beest, M., Berner, L., Björk, R. G., Buchwal, A., Buras, A., Christie, K., Cooper, E. J., Dullinger, S., Elberling, B., Eskelinen, A., Frei, E. R., Grau, O., Grogan, P., Hallinger, M., Harper, K. A., Heijmans, M. M. P. D., Hudson, J., Hülber, K., Iturrate-Garcia, M., Iversen, C. M., Jaroszynska, F., Johnstone, J. F., Jørgensen, R. H., Kaarlejärvi, E., Klady, R., Kuleza, S., Kulonen, A., Lamarque, L. J., Lantz, T., Little, C. J., Speed, J. D. M., Michelsen, A., Milbau, A., Nabe-Nielsen, J., Nielsen, S. S., Ninot, J. M., Oberbauer, S. F., Olofsson, J., Onipchenko, V. G., Rumpf, S. B., Semenchuk, P., Shetti, R., Collier, L. S., Street, L. E., Suding, K. N., Tape, K. D., Trant, A., Treier, U. A., Tremblay, J.-P., Tremblay, M., Venn, S., Weijers, S., Zamin, T., Boulanger-Lapointe, N., Gould, W. A., Hik, D. S., Hofgaard, A., Jónsdóttir, I. S., Jorgenson, J., Klein, J., Magnusson, B., Tweedie, C., Wookey, P. A., Bahn, M., Blonder, B., van Bodegom, P. M., Bond-Lamberty, B., Campetella, G., Cerabolini, B. E. L., Chapin III, F. S., Cornwell, W. K., Craine, J., Dainese, M., de Vries, F. T., Díaz, S., Enquist, B. J., Green, W., Milla, R., Niinemets, Ü., Onoda, Y., Ordoñez, J. C., Ozinga, W. A., Penuelas, J., Poorter, H., Poschlod, P., Reich, P. B., Sandel, B., Schamp, B., Sheremetev, S., Weiher, E. (2018): Plant functional trait change across a warming tundra biome. – *Nature* 562: 57-80.
- [6] Blois, J. L., Williams, J. W., Fitzpatrick, M. C., Jackson, S. T., Ferrier, S. (2013): Space can substitute for time in predicting climate-change effects on biodiversity. – *Proceedings of the National Academy of Sciences USA* 110: 9374-9379.
- [7] Bloom, A. J., Chapin III, F. S., Mooney, H. A. (1985): Resource limitation in plants - An economic analogy. – *Annual Review of Ecological Systems* 16: 363-392.
- [8] Burian, K. (1970): Produktion und Strahlungsnutzung bei *Helianthus annuus*, *Zea mays* und *Phaseolus vulgaris* während der gesamten Vegetationszeit. – *Sitzungsberichte der Akademie der Wissenschaften mathematisch-naturwissenschaftliche Klasse* 178: 1-35.
- [9] Cárdenas-Pérez, S., Rajabi Dehnav, A., Leszczynski, K., Lubinska-Mielinska, S., Ludwiczak, A., Piernik, A. (2022): *Salicornia europaea* L. functional traits indicate its optimum growth. – *Plants* 11: 1051.
- [10] DeLeo, V. L., Menge, D. N. L., Hanks, E. M., Juenger, T. E., Lasky, J. R. (2020): Effects of two centuries of global environmental variation on phenology and physiology of *Arabidopsis thaliana*. – *Global Change Biology* 26: 523-538.
- [11] Devi, N. M., Kukarskih, V. V., Galimova, A. A., Mazepa, V. S., Grigoriev, A. A. (2020): Climate change evidence in tree growth and stand productivity at the upper treeline ecotone in the Polar Ural. – *Forest Ecosystems* 7: 7.
- [12] Falster, D. S., Duursma, R. A., Ishihara, M. I., Barneche, D. R., FitzJohn, R. G., Vårhammar, A., Aiba, M., Ando, M., Anten, N., Aspinwall, M. J., Baltzer, J. L., Baraloto, C., Battaglia, M., Battles, J. J., Bond-Lamberty, B., van Breugel, M., Camac, J., Claveau, Y., Coll, L., Dannoura, M., Delagrangé, S., Domec, J.-C., Fatemi, F., Feng, W., Gargaglione, V., Goto, Y., Hagihara, A., Hall, J. S., Hamilton, S., Harja, D., Hiura, T., Holdaway, R., Hutley, L. S., Ichie, T., Jokela, E. J., Kantola, A., Kelly, J. W. G., Kenzo, T., King, D., Kloeppe, B. D., Kohyama, T., Komiyama, A., Laclau, J.-P., Lusk, C. H., Maguire, D. A., le Maire, G., Mäkelä, A., Markesteijn, L., Marshall, J., McCulloh, K., Miyata, I., Mokany, K., Mori, S., Myster, R. W., Nagano, M., Naidu, S. L., Nouvellon, Y., O'Grady, A. P., O'Hara, K. L., Ohtsuka, T., Osada, N., Osunkoya, O. O., Peri, P. L., Petritan, A. M., Poorter, L., Portsmouth, A., Potvin, C., Ransijn, J., Reid, D., Ribeiro, S. C., Roberts, S. D., Rodríguez, R., Saldaña-Acosta, A., Santa-Regina, I., Sasa, K., Selaya, N. G., Sillett, S. C., Sterck, F., Takagi, K., Tange, T., Tanouchi, H., Tissue, D., Umehara, T., Utsugi, H., Vadeboncoeur, M. A., Valladares, F., Vanninen, P., Wang, J. R., Wenk, E., Williams, R., Ximenes, F., de Aquino Yamaba, A., Yamada, T., Yamakura, T., Yanai, R. D., York, R. A. (2015): BAAD: a Biomass And Allometry Database for woody plants. – *Ecology* 96: 1445-1445.

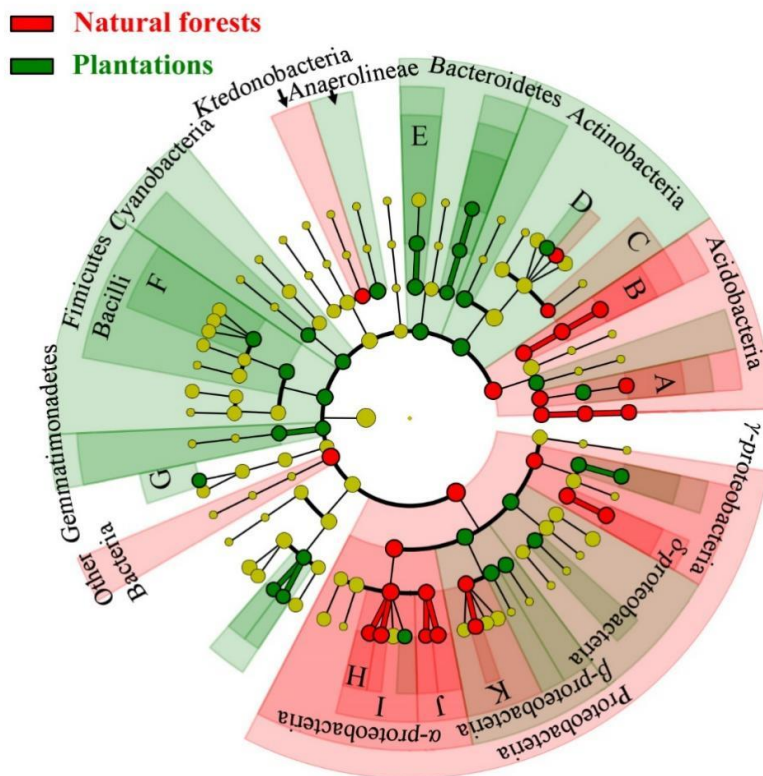
- [13] Fitzpatrick, M. C., Sanders, N. J., Ferrier, S., Longino, J. T., Weiser, M. D., Dunn, R. R. (2011): Forecasting the future of biodiversity: a test of single- and multi-species models for ants in North America. – *Ecography* 34: 836-847.
- [14] Fonti, M. V. (2020): Climatic signal in the parameters of annual rings (wood density, anatomical structure and isotopic composition) of coniferous and deciduous tree species in various natural and climatic zones of Eurasia. – Diss. Doct. Biol. Sci.: 03.02.08. Krasnoyarsk, Siberian Federal University, 45p. (In Russian). (https://research.sfu-kras.ru/sites/research.sfu-kras.ru/files/Avtoreferat_Fonti.pdf).
- [15] Forrester, D. I., Tachauer, I. H. H., Annighoefer, P., Barbeito, I., Pretzsch, H., Ruiz-Peinado, R., Stark, H., Vacchiano, G., Zlatanov, T., Chakraborty, T., Saha, S., Sileshi, G. W. (2017): Generalized biomass and leaf area allometric equations for European tree species incorporating stand structure, tree age and climate. – *Forest Ecology and Management* 396: 160-175.
- [16] Frauendorf, T. C., MacKenzie, R. A., Tingley III, R. W., Infante, D. M., El-Sabaawi, R. W. (2020): Using a space-for-time substitution approach to predict the effects of climate change on nutrient cycling in tropical island stream ecosystems. – *Limnology and Oceanography* 65: 3114-3127.
- [17] Fu, L., Sun, W., Wang, G. (2017): A climate-sensitive aboveground biomass model for three larch species in northeastern and northern China. – *Trees* 31: 557-573.
- [18] Glebov, F. Z., Litvinenko, V. I. (1976): The dynamics of tree ring width in relation to meteorological indices in different types of wetland forests. – *Lesovedenie (Soviet Forest Science)* 4: 56-62.
- [19] Grimm, G. W., Renner, S. S. (2013): Harvesting *Betulaceae* sequences from Gen-Bank to generate a new chronogram for the family. – *Botanical Journal of the Linnean Society* 172: 465-477.
- [20] Hynynen, J., Niemistö, P., Viherä-Aarnio, A., Brunner, A., Hein, S., Velling, P. (2009): Silviculture of birch (*Betula pendula* Roth and *Betula pubescens* Ehrh.) in northern Europe. – *Forestry: An International Journal of Forest Research* 83: 103-119.
- [21] Johnson, E. A., Miyanishi, K. (2008): Testing the assumptions of chronosequences in succession. – *Ecology Letters* 11: 419-431.
- [22] Keith, H., Mackey, B. G., Lindenmayer, D. B. (2009): Re-evaluation of forest biomass carbon stocks and lessons from the world's most carbon-dense forests. – *Proceedings of the National Academy of Sciences of the United States of America* 106(28): 635-640.
- [23] Kosanic, A., Anderson, K., Harrison, S., Turkington, T., Bennie, J. (2018): Changes in the geographical distribution of plant species and climatic variables on the West Cornwall Peninsula (South West UK). – *PLoS ONE* 13: e0191021.
- [24] Laughlin, D. C., Mommer, L., Sabatini, F. M., Bruelheide, H., Kuyper, T. W., McCormack, M. L., Bergmann, J., Freschet, G. T., Guerrero-Ramírez, N. R., Iversen, C. M., Kattge, J., Meier, I. C., Poorter, H., Roumet, C., Semchenko, M., Sweeney, C. J., Valverde-Barrantes, O. J., van der Plas, F., van Ruijven, J., York, L. M., Aubin, I., Burge, O. R., Byun, C., Čušterevska, R., Dengler, J., Forey, E., Guerin, G. R., Hérault, B., Jackson, R. B., Karger, D. N., Lenoir, J., Lysenko, T., Meir, P., Niinemets, Ü., Ozinga, W. A., Peñuelas, J., Reich, P. B., Schmidt, M., Schrod, F., Velázquez, E., Weigelt, A. (2021): Root traits explain plant species distributions along climatic gradients yet challenge the nature of ecological trade-offs. – *Nature Ecology & Evolution* 5(8): 1123-1134.
- [25] Lei, X., Yu, L., Hong, L. (2016): Climate-sensitive integrated stand growth model (CS-ISGM) of Changbai larch (*Larix olgensis*) plantations. – *Forest Ecology and Management* 376: 265-275.
- [26] Liebig, J. (1840): *Die organische Chemie in ihrer Anwendung auf Agricultur und Physiologie*. – Braunschweig: Verlag Vieweg. Deutsches Textarchiv, available at: http://www.deutschestextarchiv.de/liebig_agricultur_1840. Accessed on 26.11.2019.
- [27] Liepa, I. Y. (1980): Dynamics of wood stock: Forecast and ecology. – Riga, Zinatne, 170p. (In Russian).

- [28] Lieth, H. (1975): Modeling the primary productivity of the world. – In: Lieth, H., Whittaker, R. H. (eds.) Primary productivity of the biosphere. New York, Springer-Verlag, pp. 237-263.
- [29] Marcolla, B., Migliavacca, M., Rödenbeck, C., Cescatti, A. (2020): Patterns and trends of the dominant environmental controls of net biome productivity. – *Biogeosciences* 17: 2365-2379.
- [30] Mohan, J. E., Cox, R. M., Iverson, L. R. (2009): Composition and carbon dynamics of forests in northeastern North America in a future, warmer world. – *Canadian Journal of Forest Research* 39: 213-230.
- [31] Molchanov, A. A. (1976): Dendro-climatic fundamentals of weather forecasts. – Moscow, Russia, “Nauka” Publishing House, 168 p.
- [32] Morley, J. W., Batt, R. D., Pinsky, M. L. (2016): Marine assemblages respond rapidly to winter climate variability. – *Global Change Biology* 23: 2590-2601.
- [33] Mugasha, W. A., Eid, T., Bollandås, O. M., Malimbwi, R. E., Chamshama, S. A. O., Zahabu, E., Katani, J. Z. (2012): Allometric models for prediction of aboveground biomass of single trees in miombo woodlands in Tanzania. – *Proceedings of the first Climate Change Impacts, Mitigation and Adaptation Programme Scientific Conference*, pp. 8-17.
- [34] Niu, S., Wang, S., Wang, J., Xia, J., Yu, G. (2020): Integrative ecology in the era of big data. From observation to prediction. – *Science China Earth Sciences* 63: 1-14.
- [35] Odum, E. P. (1971): *Fundamentals of ecology*. – London, Philadelphia, Toronto, W.B. Saunders Company, 574p.
- [36] Paul, K. I., Roxburgh, S. H., Chave, J., England, J. R., Zerihun, A., Specht, A., Lewis, T., Bennett, L. T., Baker, T. G., Adams, M. A., Huxtable, D., Montagu, K. D., Falster, D. S., Feller, M., Sochacki, S., Ritson, P., Bastin, G., Bartle, J., Wildy, D., Hobbs, T., Larmour, J., Waterworth, R., Stewart, H. T. L., Jonson, J., Forrester, D. I., Applegate, G., Mendham, D., Bradford, M., O’Grady, A., Green, D., Sudmeyer, R., Rance, S. J., Turner, J., Barton, C., Wenk, E. H., Grove, T., Attiwill, P. M., Pinkard, E., Butler, D., Brooksbank, K., Spencer, B., Snowdon, P., O’Brien, N., Battaglia, M., Cameron, D. M., Hamilton, S., McAuthur, G., Sinclair, J. (2016): Testing the generality of above-ground biomass allometry across plant functional types at the continent scale. – *Global Change Biology* 22(6): 2106-2124.
- [37] Pickett, S. (1989): Space-for-time substitution as an alternative to long-term studies. – In: Likens, G. E. (ed.) *Long-term studies in ecology: Approaches and alternatives*. New York, Springer, pp. 110-135.
- [38] Qiu, Q., Yun, Q., Zuo, Sh., Yan, J., Hua, L., Ren, Y., Tang, J., Li, Y., Chen, Q. (2018): Variations in the biomass of Eucalyptus plantations at a regional scale in Southern China. – *Journal of Forestry Research* 29(5): 1263-1276.
- [39] Reich, P. B., Luo, Y., Bradford, J. B., Poorter, H., Perry, C. H., Oleksyn, J. (2014): Temperature drives global patterns in forest biomass distribution in leaves, stems, and roots. – *Proceedings of the National Academy of Sciences of the United States of America* 111: 13721-13726.
- [40] Russell, M. B., Domke, G. M., Woodall, C. W., D’Amato, A. W. (2015): Comparisons of allometric and climate-derived estimates of tree coarse root carbon stocks in forests of the United States. – *Carbon Balance and Management* 10: 20.
- [41] Santini, M., Collalti, A., Valentini, R. (2014): Climate change impacts on vegetation and water cycle in the Euro-Mediterranean region, studied by a likelihood approach. – *Regional Environmental Change* 14(4): 1405-1418.
- [42] Sato, H., Kobayashi, H., Delbart, N. (2010): Simulation study of the vegetation structure and function in eastern Siberian larch forests using the individual-based vegetation model SEIB-DGVM. – *Forest Ecology and Management* 259: 301-311.
- [43] Schaphoff, S., Lucht, W., Gerten, D., Sitch, S., Cramer, W., Prentice, I. C. (2006): Terrestrial biosphere carbon storage under alternative climate projections. – *Climatic Change* 74(1-3): 97-122.

- [44] Schepaschenko, D., Shvidenko, A., Usoltsev, V. A., Lakyda, P., Luo, Y., Vasylyshyn, R., Lakyda, I., Myklush, Y., See, L., McCallum, I., Fritz, S., Kraxner, F., Obersteiner, M. (2017): A dataset of forest biomass structure for Eurasia. – *Scientific Data* 4: 1-11. Article 170070.
- [45] Shuman, J. K., Shugart, H. H., O'Halloran, T. L. (2011): Sensitivity of Siberian larch forests to climate change. – *Global Change Biology* 2: 2370-2384.
- [46] Sperry, J. S., Venturas, M. D., Todd, H. N., Trugman, A. T., Anderegg, W. R. L., Wang, Y., Tai, X. (2019): The impact of rising CO₂ and acclimation on the response of US forests to global warming. – *Proceedings of the National Academy of Sciences of the United States of America* 116(51): 25734-25744.
- [47] Stegen, J. C., Swenson, N. G., Enquist, B. J., White, E. P., Phillips, O. L., Jorgensen, P. M., Weiser, M. D., Mendoza, A. M., Vargas, P. N. (2011): Variation in above-ground forest biomass across broad climatic gradients. – *Global Ecology and Biogeography* 20(5): 744-754.
- [48] Tolmachev, A. I. (1962): *Fundamentals of Plant Habitat Theory: Introduction to Plant Community Chorology*. – Leningrad, State University Publishing, 100p. (In Russian).
- [49] Toromani, E., Bojaxhi, F. (2010): Growth response of silver fir and Bosnian pine from Kosovo. – *South-East European Forestry* 1: 20-28.
- [50] Tranquillini, W. (1955): Die Bedeutung des Lichtes und der Temperatur für die Kohlensäureassimilation von *Pinus cembra* - Jungwuchs an einem hochalpinen Standort. – *Planta* 46(2): 154-178.
- [51] Usoltsev, V. A. (2020): Single-tree biomass data for remote sensing and ground measuring of Eurasian forests: digital version. – The second edition, enlarged, Yekaterinburg, Ural State Forest Engineering University; Botanical Garden of Ural Branch of RAS. CD-ROM. Retrieved from: https://elar.usfeu.ru/bitstream/123456789/9647/2/Base1_v2_ob.pdf.
- [52] Usoltsev, V. A., Shobairi, S. O. R., Tsepordey, I. S., Chasovskikh, V. P. (2019): Modelling forest stand biomass and net primary production with the focus on additive models sensitive to climate variables for two-needled pines in Eurasia. – *Journal of Climate Change* 5(1): 41-49.
- [53] Veloz, S., Williams, J. W., Blois, J. L., He, F., Otto-Bliesner, B., Liu, Z. (2012): No-analog climates and shifting realized niches during the late Quaternary: Implications for 21st-century predictions by species distribution models. – *Global Change Biology* 18: 1698-1713.
- [54] Wilmking, M., Juday, G. P., Barber, V. A., Zald, H. S. (2004): Recent climate warming forces contrasting growth responses of white spruce at treeline in Alaska through temperature thresholds. – *Global Change Biology* 10: 1724-1736.
- [55] World Weather Maps (2007): Retrieved from: <https://www.mapsofworld.com/referrals/weather>.
- [56] Zeng, W. S., Duo, H. R., Lei, X. D., Chen, X. Y., Wang, X. J., Pu, Y., Zou, W. (2017): Individual tree biomass equations and growth models sensitive to climate variables for *Larix* spp. in China. – *European Journal of Forest Research* 136: 233-249.
- [57] Zeng, W. S., Chen, X. Y., Pu, Y., Yang, X. Y. (2018): Comparison of different methods for estimating forest biomass and carbon storage based on National Forest Inventory data. – *Forest Research* 31: 66-71.
- [58] Zubairov, B., Heußner, K.-U., Schröder, H. (2018): Searching for the best correlation between climate and tree rings in the Trans-Ili Alatau, Kazakhstan. – *Dendrobiology* 79: 119-130.

Applied Ecology and Environmental Research

International Scientific Journal



VOLUME 20 * NUMBER 4 * 2022

Published: July 30, 2022
<http://www.aloki.hu>
ISSN 1589 1623 / ISSN 1785 0037
DOI: <http://dx.doi.org/10.15666/aecer>